EPHyC 2024

European PhD Hydrogen Conference

Book of Abstracts

March 20 - 22, 2024
Ghent, Belgium

Hydrogen Europe Research

BE-HyFE
Belgian Hydrogen Fundamental Expertise

Edited by:
Ali Nabizada - Antoine Dechany - Bryan Carré - Digvijay Ghogare - Elisa Stendardo
Foteini Lappa - Joren Vanlaere - Lorenzo Vallisa - Maria J. Mendoza - Marie Dejonghe
Mauro Daese - Negar Namazifard - Robbe Jacops - Samuel Jottrand - Sohrab Pahlavan

Organizers

BE-HyFE

BE-HyFE (Belgian Hydrogen Fundamental Expertise) is an academic collaboration project bringing together all Belgian knowledge institutes to join forces in fundamental hydrogen research.

The project groups together 16 PhD's, each of them covering a different aspect of hydrogen, spanning its entire value chain.

The goal of this project is to achieve an academic hydrogen backbone to support the Belgian industry in finding both technological and societal solutions, guaranteeing security and meeting environmental targets.

Hydrogen Europe Research

Hydrogen Europe Research (HER) is an international, non–profit association grouping several universities and research & technology organisations from 29 countries in Europe and beyond. Their members are active within the European hydrogen and fuel cells sector.

HER is a member of the Clean Hydrogen Partnership, follows and discusses European policies, and works to create a hydrogen skills agenda. Its ambition is to enable the development of mature hydrogen technologies to achieve a fully integrated, sustainable, low-carbon energy system.

Hydrogen Europe Research

Sponsors


economie


Bekaert


A
B
C
ANGLO BELGIAN
CORPORATION
Since 1912


fluxys


John
Cockerill


virya
energy


North
Together.
Smarter.
Sea
Port


AGFA
Agfa


ENGIE

Contents

Addressing Legal Challenges in the Deployment of Hydrogen for Industrial Applications

Álvaro Martín Morán[1*1],

[1]THERESA Project PhD researcher at Universitat Rovira i Virgili

Introduction

Hydrogen usage as an energy carrier offers the potential to environmentally revamp industrial sectors traditionally heavily reliant on fossil fuels, often referred to as 'hard to abate' sectors. While the basic use of hydrogen has been known for a long time, today's technical innovation and geopolitical momentum provide the perfect conditions for large-scale hydrogen deployment. Environmental concerns and emission targets are driving the shift towards a carbon-neutral economy [1]. Furthermore, the current geopolitical landscape highlights the importance of strategic autonomy. The use of hydrogen can address both of these concerns, making its deployment a key element to achieve the decarbonization objectives [2].

The generation of hydrogen can take various forms, not all of which are carbon neutral. Currently, numerous opportunities exist for producing clean hydrogen, ranging from electrolysis powered by green electricity to production from waste and biomass. [2] To meet our climate objectives, the focus should be made on carbon neutral hydrogen sources [3].

In contrast to the linear economy, which revolves around production, use, and disposal, the concept of a circular economy emphasizes recycling, reuse, and repurposing of materials. This approach reduces the demand for raw materials without impeding economic growth [4].

Not all impediments for the deployment of a hydrogen economy are technical. Numerous legal barriers hinder the adoption of hydrogen as a more sustainable model [5]. Barriers range from the inadequacy of existing regulations, which often do not align with the unique characteristics of hydrogen, to measures that obstruct the full utilization of this versatile energy carrier [6].

Hydrogen has a dual relationship with industry, as it is both produced and used by industrial processes [7]. Production of hydrogen primarily derives from an industrial process, regardless of it being hydrolysis, steam methane reforming or fermentation [8].

* Corresponding author: alvaro.martin@urv.cat

[1] This work has been carried out within the framework of (i) MSCA THERESA Doctoral Network under the HORIZON-MSCA-2021-DN-01; and within the research group of the Universitat Rovira i Virgili, of which the author is a member, "Territory, Citizenship and Sustainability", recognized as a consolidated research group and supported by the Departament de Recerca i Universitats de la Generalitat de Catalunya (2021 SGR 00162).

Consequently, the regulation governing its production requires different considerations than those essential for subsequent industrial applications [9], such as the production of hydrogen from waste materials or as a byproduct of other processes [10]. Nonetheless, common concerns exist that serve as central issues when addressing the deployment of a hydrogen-based economy [11], particularly in terms of regulations related to transportation and storage [12].

Methodology

This is a legal research work focusing on a legal analysis of the existing regulation. The work aims at retrieving, identifying, and categorizing the current and planned regulation in the matter at European level. The main legal instruments that will be examined are the ones dealing with Hydrogen and the ones relating to the Circular Economy [13].

The justification of examining only elements at EU level comes from the fact that the EU has been very active in the matter and that the EU regulation determines the direction of all the national legislation of its member states. No national transposition of EU law nor international legislation will be examined. However, some pieces of upcoming EU legislation will be analyzed to provide a better understanding of the upcoming issues.

It should be noted that this work will explore the legal barriers for the deployment of a Circular Economy based on the use of hydrogen in the framework of the decarbonisation objectives and the accomplishment of a Just transition [14]. Additionally, the framework of planetary boundaries will be used to justify the necessity of a Circular Economy.

Discussion

The expected outcome of this paper is to produce a map of the current and upcoming regulation governing the use of hydrogen in the framework of the circular economy, such as production of hydrogen from waste like plastics, renewable sources such as biomass or from other industrial processes such as water treatment [10]. This will allow to identify the main bottlenecks of the regulation and the areas where regulation is missing.

The main legal instruments analyzed for the purpose of this work will be the EU strategies for a Climate Neutral Europe **[2]** and the Repower EU plan [3] and the New Circular Economy Action plan [15], along with the current regulation on the gas [16] and electricity directives [17] and the current proposal for new gas and hydrogen Directive [6]. Other relevant documents are the directive on waste management that is also relevant for the Circular Economy [18].

Conclusions

Legal uncertainty and poorly adapted regulation represent one of the main obstacles for the adoption of hydrogen on an industry wide basis, hindering investment and creating a dependence on financial aid for innovation. While technology advances bringing costs of new processes down [10], the regulation needs to be adapted to provide a stable framework.

However, there is some regulatory innovation underway [8]. The pace of innovation may be faster than the legislator and sometimes clash with health and safety regulations or with stablished principles such as precaution.

References

[1] R. Rivas, M. Pansera, L. Antunes and M. Monteiro, “Technological Forecasting & Social Change Socio-technical imaginaries of a circular economy in governmental discourse and among science, technology , and innovation actors : a Norwegian case study”. *Technol. Forecast. Soc. Change* vol. 183, p. 121903, 2022 https://doi.org/10.1016/j.techfore.2022.121903.

[2] European Commission. "Communication from the Commission to the European Parliament, the Council, the European Economic and Social Committee and the Committee of the Regions: A hydrogen strategy for a climate-neutral Europe." July 8, 2020.

[3] European Commission. "Communication from the Commission to the European Parliament, the Council, the European Economic and Social Committee and the Committee of the Regions: REPowerEU Plan”. May 18, 2022.

[4] P. Ekins, T. Domenech, P. Drummond, R. Bleischwitz, N. Hughes and L. Lotti, “The Circular Economy: What, Why, How and Where”, In *Managing Environmental and Energy Transitions for Regions and Cities, Proceedings of the OECD/EC Workshop,* Paris, France, 5 July 2019; OECD: Paris, France, 2019

[5] European Commission. "Commission Staff Working Document: Implementing the Repower EU Action Plan: Investment Needs, Hydrogen Accelerator, and Achieving the Bio-methane Targets." May 18, 2022

[6] European Commission. "Proposal for a Directive of the European Parliament and of the Council on common rules for the internal markets in renewable and natural gases and in hydrogen" (COM (2021) 803 final, 2021/0425(COD)). December 15, 2021

[7] European Commission. "Communication from the Commission to the European Parliament, the Council, the European Economic and Social Committee and the Committee of the Regions: A New Industrial Strategy for Europe." March 10, 2020.

[8] G. Squadrito, G. Maggio and A. Nicita, ”The green hydrogen revolution”, *Renew. Energy*, vol. 216, p. 11904, 2023. https://doi.org/10.1016/j.renene.2023.119041.

[9] “European Commission. "Commission Staff Working Document: Towards Competitive and Clean European Steel." May 5, 2021.

[10] S. Sharma, S. Basu., P.N. Shetti and T.M. Aminabhavi, “Waste-to-energy nexus for circular economy and environmental protection: Recent trends in hydrogen energy”, *Sci. Total Environ.*, vol. 713, p. 136633. 2020

[11] European Commission. "Commission Delegated Regulation (EU) 2023/1184 supplementing Directive (EU) 2018/2001 of the European Parliament and of the Council by establishing a minimum threshold for greenhouse gas emissions savings of recycled carbon fuels and by specifying a methodology for assessing greenhouse gas emissions savings from renewable liquid and gaseous transport fuels of non-biological origin and from recycled carbon fuels." February 10, 2023.

[12] European Commission. "Commission Delegated Regulation (EU) 2023/1184 supplementing Directive (EU) 2018/2001 of the European Parliament and of the Council by establishing a Union methodology setting out detailed rules for the production of renewable liquid and gaseous transport fuels of non-biological origin." February 10, 2023.

[13] T.J. De Römph and J. Cramer, “How to improve the EU legal framework in view of the circular economy”, *J. Energy Nat. Resour*., vol. 38, no. 3, pp. 245-260, 2020. DOI: 10.1080/02646811.2020.1770961

[14] European Parliament and Council. "Directive (EU) 2018/2001 of the European Parliament and of the Council on the promotion of the use of energy from renewable sources." *Official Journal of the European Union*, L 328/82. December 11, 2018.

[15] European Commission. "Communication from the Commission to the European Parliament, the Council, the European Economic and Social Committee and the Committee of the Regions: A New Circular Economy Action Plan." March 11, 2020.

[16] European Parliament and Council. "Directive 2009/73/EC concerning common rules for the internal market in natural gas and repealing Directive 2003/55/EC."
July 13, 2009.

[17] European Parliament and Council. "Directive (EU) 2019/944 on common rules for the internal market for electricity and amending Directive 2012/27/EU." June 5, 2019.

[18] European Parliament and Council. "Directive 2008/98/EC on waste and repealing certain Directives." November 19, 2008.

Advanced characterization of densified cryogenic hydrogen

Lorenzo Vallisa *[1], Delphine Laboureur[1], Maria Teresa Scelzo [2], Michel De Paepe[3]

[1]Department of Environmental and Applied Fluid Dynamics, von Karman Institute for Fluid Dynamics
[2]Aeronautics and Aerospace Department, von Karman Institute for Fluid Dynamics
[3] Department of Electromechanical, Systems and Metal Engineering, Ghent University

Introduction

This work wants to investigate one of the most critical topic related to hydrogen technologies: the improvement of storage efficiency. Due to its very low volumetric energy density [7] it is in fact a challenge to store hydrogen in limited sized tanks in gaseous form. A possible solution to tackle this issue is to densify hydrogen to its slush state: a multi-phase mixture of vapor, liquid and solid crystals near the thermodynamic triple point temperature. At slush state, hydrogen gains a significant 15 % of higher volumetric energy density and 18 % lower enthalpy with respect to the single-phase liquid state, resulting thus in a better resistance against boil-offs and heat losses [2]. With the current limits and safety standards required to run experimental campaign with hydrogen, computational fluid dynamics offers a viable alternative to investigate the physics of slush hydrogen. This research project ambitiously aims at formulating a robust numerical solver able to simulate the complex dynamics of slush hydrogen to optimize the design of storage tanks. Hydrogen at slush state provides non-trivial modelling challenges as crystals are arbitrarily shaped. Their complex geometry in fact strongly influence the exchange of heat between solid and liquid phase and hence the thermal stratification inside the storage tank. The project foresees the realisation of a particle laden Lagrangian-based multi-phase solver not only able to accurately reproduce the particle-fluid thermal and dynamical interaction but also to account for the melting of crystals, given their not trivial geometrical configuration.

Methodology

The presented numerical model is able to resolve the particle-fluid and particle-particle interactions by means of an Immersed Boundary Method (IBM) [5]. The IBM defines the boundary of a solid object immersed in the fluid domain through so called Lagrangian points, entities independent from the grid points where the flow field is solved. An Indicator Function I encodes the surface boundary of the solid object at the fluid grid points, and its values range from 0 (fluid domain) to 1 (solid domain). At the interface cells a Pyramid Decomposition Method, proposed in the work of Zhang [11], is used to compute the local solid volume fraction, transforming hence the Indicator Function I into a Volume of Fluid ϕ field variable, linearly interpolating values across the solid boundary from 0 to 1. According to Fadlun et al. [3] a first-order accurate direct-forcing approach is used to exchange information between the solid and the fluid part, the coupling force is scaled with the ϕ value of the solid volume fraction on the Eulerian grid points:

$$f = \phi \frac{U_P - U_f}{\Delta t} \tag{1}$$

where U_P and U_f are the particle and fluid velocity at fluid grid cell. The momentum equation for incompressible and thermo-buoyant flow is hence re-written to account for the coupling forcing term f:

$$\frac{\partial u}{\partial t} + \nabla(u \otimes u) = -\frac{\nabla p}{\rho_0} - \nu \Delta u + \overline{\rho}(1 + \beta(T - T_{\text{Ref}}))g + \frac{f}{\rho_0} \tag{2}$$

in which the buoyant term $\overline{\rho}(1 + \beta(T - T_{\text{Ref}}))g$ is derived by using the Boussinesq approximation. Equation 2 is solved using a fractional-step approach: an intermediate velocity is firstly computed excluding

*Corresponding author: lorenzo.vallisa@vki.ac.be

contribution of volume force, pressure and density gradients due to buoyancy. Secondly, by enforcing incompressibility, a Poisson equation for pressure is obtained. The final velocity corrected with the resulting pressure gradients. Accuracy and stability are ensured by looping over the pressure computation-prediction step (PISO). Particle dynamics is solved in a semi-implicit way as in the work from Tschigale et al. [9]:

$$u^n = (m_p + m_l)^{-1}(m_p u^{n-1} + \int_L u dV + [\int_{\Omega_P} \rho_f u dV]_{n-1}^n + \Delta t V_P(\rho_P - \rho_f)g) \tag{3}$$

in which the the added-mass integral $[\int_{\Omega_P} \rho_f u dV]_{n-1}^n$ is integrated numerically over the whole particle domain, as shown by Uhlmann [10] to be more stable and accurate. For what concerns the temperature field we solved the thermal energy equations in the entire domain and we exploit the continuity property of the scalar function ϕ to allow for a smooth variation across the particle's boundary of the thermodynamic variables, as already shown in the work of Tryggvason [8]:

$$\frac{DT}{Dt} = -(\alpha_p \phi + \alpha_f(1-\phi))\nabla^2 T \tag{4}$$

where α_p and α_f are respectively the particle and fluid thermal diffusivity. In this work we propose to model highly non-regular surfaces by means of a NURBS algorithm [4]. Given a set of control points tracing the boundary of the particle, NURBS is able to generate a surface interpolating these points through a bi-variate products of B-spline basis functions defined on a set of parametric coordinates. NURBS surfaces are initialized through a set of control points identifying the boundary of the particle.

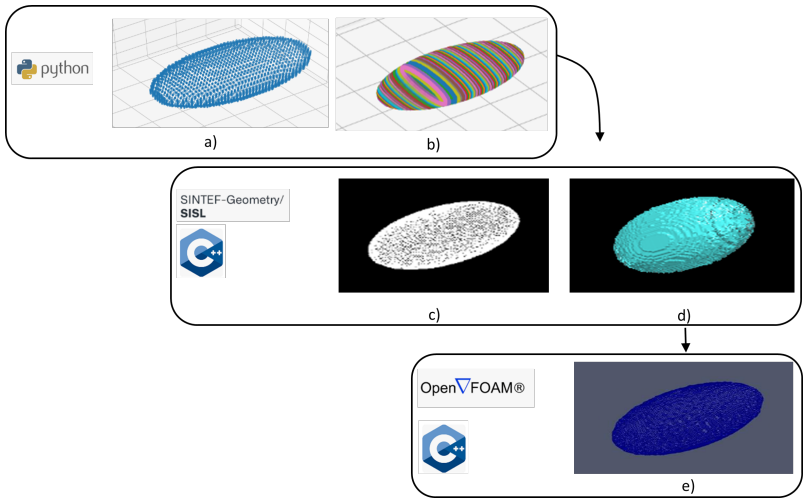

Figure 1: Automatized Input Surface Assembly (AISA) algorithm: a) Parsing a STL file b) Assembling control points for NURBS definition c) Interface for SISL library d) Final surface object. e) Indicator function inside the final solver

This part divides into two main parts: the creation of the surface object and the algorithm interfacing the object with the final indicator function. In the first part, as shown in figure 1, an Automatized Input Surface Assembly (AISA) algorithm is written to parse STL input file containing the 3D coordinates of the boundary points of the solid object. The AISA then uses an efficient approach to reorganize and order the input control points so that they can be used as input variables for the correct parametrization of the NURBS surface. In a second part an innovative Control Point Scan (CPS) algorithm is introduce to correctly assemble the indicator function from the surface object. CPS exploits the introduced NURBS features to identify first the boundary points, and then to correctly distinguish between the internal and the external part of the solid object. The CPS algorithm has been tested to perform well on several different shapes with concave surfaces (figure 2), and it has been proven to over-perform in terms of efficiency the Poisson solver currently used in literature to compute the indicator function (See work of Tryggvason).

Results

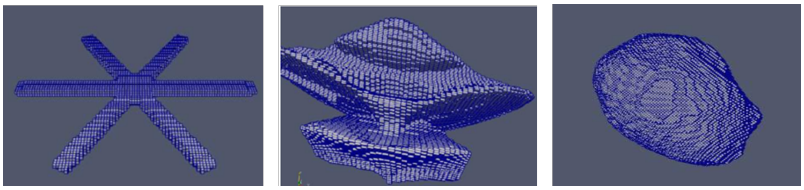

Figure 2: Computation of indicator function performed by the Control Point Scan (CPS) algorithm for different shapes

So far, the implemented numerical model features the isothermal solver for moving particles and the thermo-buoyant solver for static particles have been successfully tested and validated against well-known benchmark cases in literature. For the isothermal solver the validation test case is taken from the work of

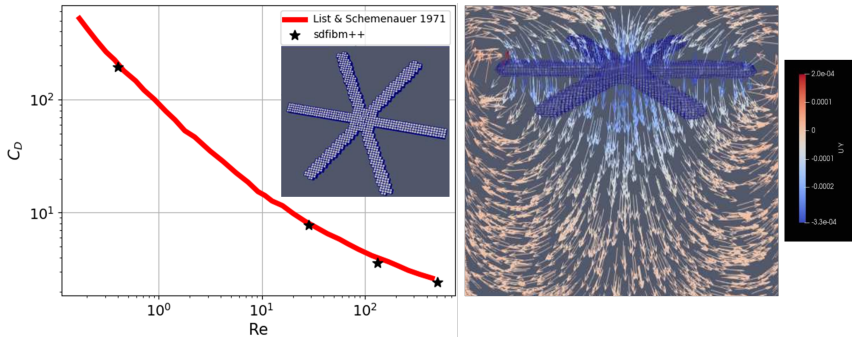

Figure 3: Left: Drag coefficient versus Reynolds correlation for isothermal test-case of free-falling snowflake. Right: Quiver plot of the flow deviated by the falling snowflake

[6],in which the settling velocities of a free-falling snowflake are given for $Re < 600$. The drag coefficient is measured when the force balance between the gravitational force and the drag force is reached:

$$C_D = \frac{2gV_P(\rho_p - \rho_f)}{\rho_f v_T^2 S_p} \tag{5}$$

where v_T is the particle terminal velocity and S_p the cross-sectional area of the particle. To reproduce the above mentioned experimental test-case a uniform tetrahedral meshgrid of size 4d x 6d x 4d has been chosen, where d is the reference length of the geometry defined as the diameter of the circle circumscribed to the particle. It has been proven that the external's domain boundary patches do not interfere with the dynamics of the falling particle. The number of cells of the discretized domain is $4.5e^6$. Results are shown in figure 3. For the validation of the thermo-buoyant flow of a static particle a test case of a flow past a heated elliposidal particle described in the work of Richter [1] (identified as *Elliposid 1*) is considered. The particle has constant and fixed temperature of 125°C in its entire domain, including its surface. The frame of reference is Cartesian and the incoming flow, entirely determined by the inflow, is parallel to the x axis. In the freestream region gradients of velocity and temperature are assumed to be zero, therefore all domain boundaries except inlet and outlet are symmetry boundaries. No buoyancy effect is considered and density, as well as all thermophysical properties, are constant in the whole domain. the domain size is chosen as 30d x 12d x 30d, where d is the sphere-volume equivalent diameter. The number of cells of the uniform tetrahedral mesh is approximately $61e^6$The flow is initially still. At the inlet of the domain, a uniform velocity is set with only the cross-wise component different from zero. At the outlet of the domain, an atmospheric uniform pressure is set. The geometry has been built using over 25000 control points to enable a smooth particle interface.Figure 4 shows the comparison between the reference test case and the present study in terms of Nusselt number and drag coefficient. The overall agreement is within 7.5% of deviation for the drag coefficient and 3.5% deviation for the Nusselt number.

Conclusions

In the present work we presented the main features of the numerical solver we are developing and that we need to correctly reproduce the complex physics of the slush hydrogen in storage tank. The solver

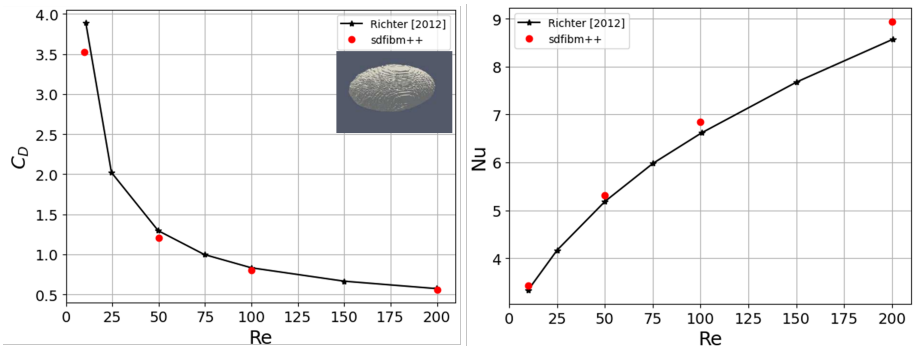

Figure 4: Left: Drag coefficient versus Reynolds correlation for thermo-buoyant test-case of static ellisposid. Right: Nusselt number versus Reynolds correlation

is currently able to simulate particles of complex geometries. The isothermal solver for moving particles and the thermo-buoyant solver for static particles have been validated against well-known experimental benchmarks. Currently, we are working on the improvement of model to accurately simulate fluid-structure interactions for a wide range of Reynolds number and particle-fluid density ratios. Moreover we are finalizing the implementations of a phase change model and its interface with the front tracking method embedded in the numerical solver.

References

[1] P. N. A. Richter. Drag forces and heat transfer coefficients for spherical, cuboidal and ellipsoidal particles in cross flow at sub-critical Reynolds numbers. *International Journal of Heat and Mass Transfer*, 55:1343–1354, 2012.

[2] P. L. C. Sindt. Slush hydrogen flow charachteristics and solid fraction upgrading. *Advances in Cryogenic Engineering*, 1995.

[3] P. J. M.-Y. E. Fadlun, R. Verzicco. Combined immersed-boundary finite-difference methods for threedimensional complex flow simulations. *Journal of Computational Physics*, 161:35–60, 2000.

[4] W. T. L. Piegl. *The NURBS book*. Springer Verlag, 1997.

[5] C. P. M. Lai. An Immersed Boundary Method with Formal Second-Order Accuracy and Reduced Numerical Viscosity. *Journal of computational physics*, 160, 2000.

[6] R. S. R. List. Free-fall behavior of planar snow crystals, conical graupel and small hail. *Atmospheric Science Journal*, 28, 1971.

[7] C. Sindt. A summary of the characterization study of slush hydrogen. *Cryogenics*, 10(5):372–380, 1970.

[8] G. T. S.O. Unverdi. A front-tracking method for viscous, incompressible, multi-fluid flows. *Journal of Computational Physics*, 100:2999–3011, 2007.

[9] J. F. T. Kempe. An improved immersed boundary method with direct forcing for the simulation of particle laden flows. *Journal of Computational Physics*, 231:3663–3684, 2012.

[10] M. Uhlmann. An immersed boundary method with direct forcing for the simulation of particulate flows. *Journal of Computational Physics*, 209:448–476, 2005.

[11] C. Zhang. sdfibm: a signed distance field immersed boundary field based discrete forcing immersed boundary method in OpenFOAM. *Journal of Computational Physics*, 255, 2020.

Advancing PEM Electrolyzers: A Simulation-Centric Approach Supported by Experimental Validation

J. Rauh*[1], J. Wilhelm[1], B. Grabner[1], A. Trattner[1,2]

[1]HyCentA Research GmbH, Graz, Austria
[2]Institute of Thermodynamics and Sustainable Propulsion Systems, Graz University of Technology, Austria

Introduction

The necessary global shift towards sustainable energy sources requires the production of green hydrogen as an alternative to traditional fossil fuels. As a clean and versatile energy carrier, green hydrogen has the potential to decarbonize various sectors, from transportation to industrial processes. However, realizing the promise of large-scale green hydrogen production at competitive prices hinges on the development of electrolysis stacks that are not only efficient but also durable and cost-effective.

Simulations play a crucial role in advancing the development of electrolyzers. However, acknowledging the potential limitations of simulations when standing alone, this dissertation takes a comprehensive approach. It aims not only to enhance current development practices for PEM electrolyzers by integrating simulation tools to answer vital design questions but also to address the need for robust validation. These design questions span various domains, ranging from mechanical considerations such as determining the optimal clamping force to fluid dynamics challenges like achieving a uniform temperature and flow distribution, and electrochemical aspects, including strategies to minimize performance losses in electrolyzers.

Methodology

The types of simulations that are to be improved and validated are a zero-dimensional (0D) general purpose electrolyzer stack model in MATLAB Simulink, 3D Computation Fluid Dynamics (CFD) models in ANSYS Fluent and 3D Finite Element Analysis (FEA) in ANSYS mechanical.

The best way to get experimental data for most of the simulations is through in-situ testing of electrolyzers. For this, a PEM single cell test rig for benchmarking and accelerated stress tests (named BEAST) was developed, which can be seen in figure 1. With a maximum current of 200 A, the test rig can be used to investigate relatively large single cells compared to commercially available single cell test benches. The size was chosen in such a way that effects can be measured more intensively which otherwise are only relevant in stacks, such as unequal distributions of temperature and gas accumulation, pressure drops across the cell and unequal contact forces of the compressed components. The test rig is equipped with its own deionization loop and is suitable for cathode pressures up to 80 bar and temperatures up to 85 °C. Cells can be investigated with electrochemical impedance spectroscopy in the whole current range using a custom-made setup consisting of a 5 Toellner 4 quadrant multiplier power supply and Gamry Load/Power-Supply Interface – LPI 1010 High Voltage. Other measurements implemented that provide necessary data for simulations include the amount of H2 produced, the amount of water produced at the cathode, the H2 in O2 concentration on the anode, the conductivity of the water before the cell, the differential pressure across the cell and temperatures and pressures at several points in the measurement setup.

Using measurement results from the test rig all parameters can be obtained that are required to fit and validate most 0D models. In this dissertation a 0D model was developed in the EU Horizon project Recycalyse, written in *MATLAB Simulink*, that builds upon the models of Marangio [5] and Sartory [7]. A short overview of the model inputs, outputs and internal submodels is shown in figure 2. The 4 coupled submodels calculate the average pressure in the cell, mass transport of gasses and water, the voltage and lastly the average temperature of the cell or stack in an iterative loop. The first three of these models require empirical coefficients obtained from the test results. In the mass-transport model the parameters

*Corresponding author: rauh@hycenta.at

Figure 1: Single cell test bench "BEAST" at HyCentA, with the cell conditioning infrastructure shown on the left image and the Toellner 4 quadrant multipliers with the Gamry LPI 1010 on the right image.

that have to be fitted from experimental results are the gas permeabilities and the water drag coefficient of the membrane. The gas permeabilities of the membrane can be obtained through the measurement of gas concentrations in the product gases, while the water drag coefficient is obtained through measuring the amount of water that is separated on the cathode side. In the voltage model the losses are separated into anodic and cathodic activation losses, anodic and cathodic mass-transport losses, ohmic losses of the membrane and ohmic losses of all electrically conductive components. The measured overvoltage can be assigned to the individual causes through the use of EIS with a study of the Distribution of Relaxation Times (DRT) as described in [4] through which coefficients in each overvoltage model are fitted. The pressure model is fitted using the measured pressure loss over the single cell for different current densities, flow rates and cell temperatures.

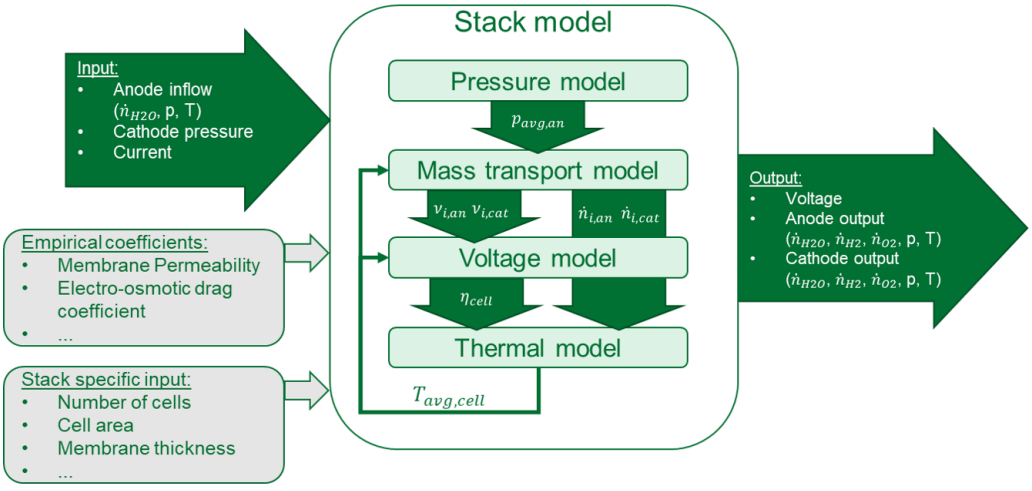

Figure 2: Overview of the 0D PEM electrolyzer model and its inputs and outputs.

For the validation of CFD Simulations, the total pressure loss across the cell is already available from the single cell test rig, but to validate all aspects of the simulation the distribution of temperature and current density inside the cell has to be known too. Since at the beginning of the dissertation no PEM single cell on the market met the necessary criteria for maximum pressure, temperature, and current density, a custom single cell was developed as shown in figure 3. This single cell, when coupled with a segmented current density and temperature measurement device (as for example described in [1]), enables

a validation of the most important aspects of a CFD result. At the current stage of the dissertation, the single cell is currently undergoing initial testing, with subsequent validation of CFD results using the segmented cell measurement device planned as the next step.

An exemplary result of the preliminary (yet to be validated) CFD simulations can be seen in 4. This simulation was done for the anode side only, as for PEM electrolyzers the anode side is of the higher interest here, as this is where the cell is cooled by the water flow while also the oxygen has to be removed. This makes a uniform water flow distribution necessary, which can be quite a challenge when the cell geometry is for example circular [6]. Some crucial parameters that are important for these types of simulation, that can not be tested easily through in-situ testing, are the permeabilities of the porous materials on anode and cathode side. Also, in the simulation flow resistance parameters are required to model the expanded metal meshes that are used instead of a conventional flow field on the anode side, as they are replaced by a porous zone to reduce computational effort [3]. These parameters are obtained in this work by using a custom built material sample fixture to measure the flow resistance at known volume flow rates of the various materials. By placing the material fixture behind a single cell, also 2-phase flow resistance can be measured.

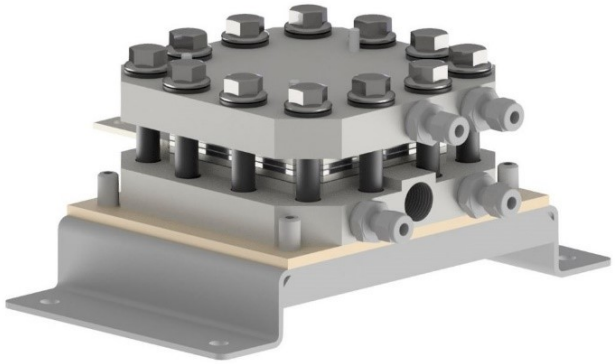

Figure 3: PEM electrolyzer single cell for testing at 35 bars differential pressure.

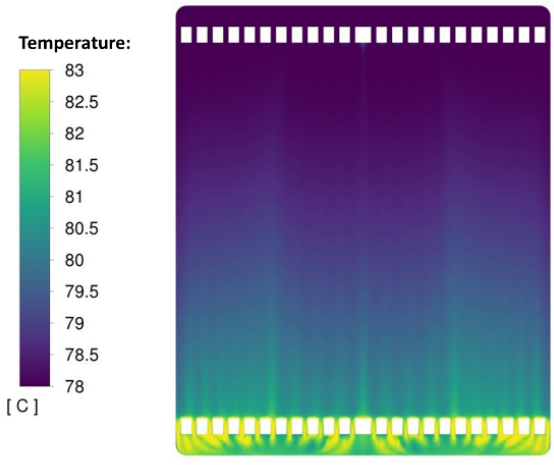

Figure 4: Temperature distribution in a 50 cm^2 PEM electrolyzer cell at 2 A/cm^2, 2.2 V and a water flow rate of 515 ml/min, simulated using *ANSYS Fluent*

The third type of simulation that is looked at in this dissertation is finite element analysis (FEA), which is used to answer mainly structural questions. In PEM electrolyzers the catalyst coated membrane (CCM)

and the gaskets require an optimal individual and uniform compression to ensure good performance and gas tightness. While some laboratory single cells can set the compression of the active layer and the compression of the gaskets individually, in a PEM electrolyzer stack they are usually linked, which means that an increase in clamping force can improve gas tightness, but it may also over-compress the inner components and reduce the lifetime and performance. To find the right size of all components a good methodology is required, as most used materials show non-linear stress-strain behavior, and change their properties over time and also as a function of the operating temperature [8, 2]. To validate such an FEA-based methodology, pressure-sensitive films (PSF) are used to analyze the contact pressure in the cell materials and gaskets. A quantitative evaluation tool written in *MATLAB Simulink* is currently in the validation phase. An evaluated result of this tool can be seen in figure 5, where a Quintech EC-EL-50 electrolyzer cell was compressed according to the manufacturers recommendations. As can be seen from the evaluated image, some areas of the gaskets only see a fraction of the average compressive stress, which indicates a low sealing effect and highlights the need for higher parallelism tolerances in the cell components.

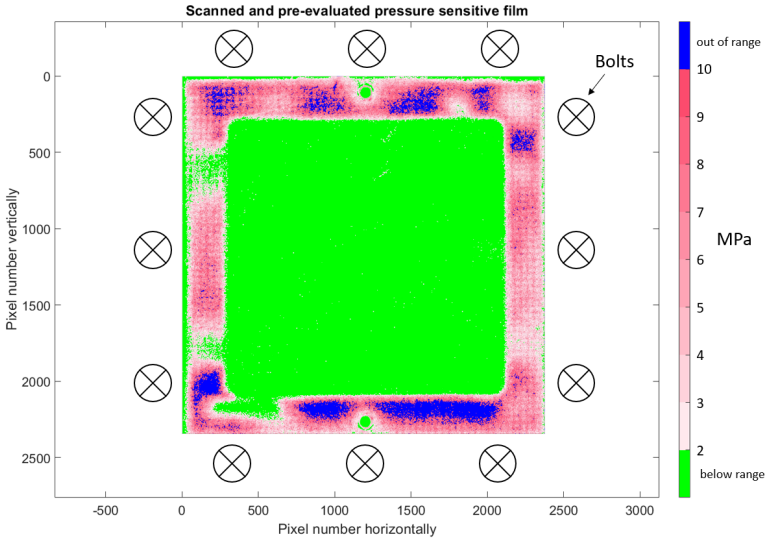

Figure 5: Scanned and evaluated pressure sensitive film LW (2.5 - 10.0 MPa range), compressed in a Quintech EC-EL-50 single cell

Discussion

This dissertation aims to advance the development of proton exchange membrane (PEM) electrolyzers by integrating simulation tools into the development process to address design questions across mechanical, fluid dynamics, and electrochemical domains.

The specially developed PEM electrolyzer test rig, BEAST, together with a single cell containing a segmented current and temperature measurement device, serves as a robust validation platform. Its capacity for measuring effects relevant in stacks, such as temperature and current distribution, product gas compositions and pressure drops, enables the validation of a 0D electrolyzer stack model and the 3D CFD simulations of PEM electrolyzers. Additional material properties required for the CFD simulations are obtained through a custom built flow resistance measurement device.

Furthermore, finite element analysis (FEA) addresses structural questions, especially the necessary thicknesses and material properties for a correct force distribution between sealing materials and inner cell materials. Experimental validation, using pressure-sensitive films and a MATLAB Simulink-based tool for evaluation, offers a quantitative approach for the validation of these finite element simulations.

Conclusions

In conclusion, this dissertation undertakes a comprehensive approach to advance PEM electrolyzer development. While the ultimate goal is to improve the simulation tools for the development of PEM electrolyzers, a strong emphasis is placed on a robust validation strategy. The approaches outlined for

validating individual simulations are currently in the implementation phase. When completed, the next step will be to answer the most important design questions by means of simulations and to find optimization potentials as well as to identify any further gaps that cannot yet be satisfactorily solved in the development.

Acknowledgements

The authors would like to acknowledge the Austrian Research Promotion Agency (FFG), the Climate and Energy Fund, the Federal Ministry of Labour and Economy and the Federal Ministry for Climate Action, Environment, Energy, Mobility, Innovation and Technology of the Republic of Austria for processing and financing this work in the framework of the COMET project HyTechonomy. This work also received funding from the European Union's Horizon 2020 Research and Innovation program under grant agreement no. 861960 ("Recycalyse" project).

References

[1] I. Biswas, D. G. Sánchez, M. Schulze, J. Mitzel, B. Kimmel, A. S. Gago, P. Gazdzicki, and K. A. Friedrich. Advancement of segmented cell technology in low temperature hydrogen technologies. *Energies*, 13(9):2301, 2020.

[2] E. Borgardt, L. Giesenberg, M. Reska, M. Müller, K. Wippermann, M. Langemann, W. Lehnert, and D. Stolten. Impact of clamping pressure and stress relaxation on the performance of different polymer electrolyte membrane water electrolysis cell designs. *International Journal of Hydrogen Energy*, 44(42):23556–23567, 2019.

[3] C. Haas, M.-G. Macherhammer, N. Klopcic, and A. Trattner. Capabilities and limitations of 3d-cfd simulation of anode flow fields of high-pressure pem water electrolysis. *Processes*, 9(6):968, 2021.

[4] Y. Li, Y. Jiang, J. Dang, X. Deng, B. Liu, J. Ma, F. Yang, M. Ouyang, and X. Shen. Application of distribution of relaxation times method in polymer electrolyte membrane water electrolyzer. *Chemical Engineering Journal*, 451:138327, 2023.

[5] F. MARANGIO, M. SANTARELLI, and M. CALI. Theoretical model and experimental analysis of a high pressure pem water electrolyser for hydrogen production. *International Journal of Hydrogen Energy*, 34(3):1143–1158, 2009.

[6] A. C. Olesen, S. H. Frensch, and S. K. Kær. Towards uniformly distributed heat, mass and charge: A flow field design study for high pressure and high current density operation of pem electrolysis cells. *Electrochimica Acta*, 293:476–495, 2019.

[7] M. Sartory, E. Wallnöfer-Ogris, P. Salman, T. Fellinger, M. Justl, A. Trattner, and M. Klell. Theoretical and experimental analysis of an asymmetric high pressure pem water electrolyser up to 155 bar. *International Journal of Hydrogen Energy*, 42(52):30493–30508, 2017.

[8] Y. Zhou, G. Lin, A. J. Shih, and S. J. Hu. Assembly pressure and membrane swelling in pem fuel cells. *Journal of Power Sources*, 192(2):544–551, 2009.

An experimental and numerical investigation of CO2 dilute, oxy-fuel combustion in a reciprocating engine using mixtures of natural gas and hydrogen

M. Daese*[1], F. Contino[2], J. Lacey[3]

[1]Applied Mechanics and Energy conversion (TME), Group T Leuven Campus
[2]Institute of Mechanics, Materials and Civil Engineering (iMMC), UC Louvain
[3]Applied Mechanics and Energy conversion (TME), Group T Leuven Campus

Introduction

The European Green Deal is the EU's answer to address global climate change and its goal is to achieve net-zero emissions of greenhouse gases by 2050 [12]. This necessitates an energy transition towards renewable energy sources, introducing the need for a wide range of storage technologies due to the intermittency of such sources of power generation and the inherent imbalance created between the supply and demand sides. Synthesis of fuels such as hydrogen (H_2), methane (CH_4), ammonia (NH_3) and methanol (CH_3OH) using excess renewable power on the grid (so-called "e-fuels") are possibilities for long term and seasonal storage [11, 8, 19], and is an attractive storage option given the existing gas grid infrastructure. Furthermore, these e-fuels can be produced where renewable energy is abundant and transported across the globe, contributing to one of the cornerstones of electrical grid decarbonization; providing diverse and flexible resources in the energy mix to ensure a smooth energy transition towards renewable energies and to bolster the security of energy supply. One part of this portfolio of diverse power generation options are engine power plants, which are scalable to demand and can provide electrical power from 10 kW up to 20 MW per unit. Due to their high dispatchability and ramping capabilities, engine power plants are the ideal technology to act as peaking or grid stability units. Currently, 30 GW of engine power plant capacity is installed in the EU, which is ∼15% of the current installed wind power across the member states. The share of such power plants is expected to grow in the following decades [1], and therefore carbon neutrality will require these power plants to evolve towards renewable fuels. State-of-the-art reciprocating engines for power generation currently produce undesirable emissions such as CO_2 and NO_x [21]. though the choice of fuel or combustion mode offer possibilities to mitigate or even eliminate such species. A compelling solution to simultaneously decrease the output of both species is with the use of an oxy-fuel reciprocating engine operating with a mix of hydrogen and methane. The use of renewably sourced hydrogen in the fuel blend reduces engine-out CO_2 emissions, oxy-fuel combustion produces an exhaust with a high concentration of CO_2 that is favorable to carbon capture, and the removal of nitrogen in the oxidizer supply eliminates NO_x production. Because of enhanced oxygen concentration in the fuel-oxidizer mixture, dilution is necessary to mitigate excessive in-cylinder temperatures and this diluent can be sourced from recirculated exhaust CO_2 or from other industrial processes if operating with pure hydrogen. Oxy-fuel reciprocating engines featuring CO_2 dilution and a completely renewably-produced fuel mixture could even be net-negative CO_2 emitting, as they would need to source a supply of CO_2 from an exterior system. However to date, there have been limited investigations of such reciprocating engines, and their performance using H_2 or CH_4 fuelling is not well characterized. This study will therefore provide a first-of-its-kind experimental investigation of CO_2 diluted oxy-fuel combustion in a reciprocating engine using low- and zero-carbon intensity gaseous fuels.

Oxy-fuel combustion in reciprocating engines

Oxy-fuel combustion is defined as burning fuel with pure oxygen instead of air, as found in applications such as oxy-acetylene welding. In a reciprocating engine, however, this would lead to temperatures that exceed the mechanical limitations of the engine (2500 K) [22]. To reduce these temperatures, a diluent

*Corresponding author: mauro.daese@kuleuven.be

is introduced in the combustion chamber that displaces N_2, which should ideally be an inert gas. This introduces a trade-off between ideal efficiency and practicality. If efficiency would be the only concern, it is key to select a diluent with a high ratio of specific heats (γ). Ar, for which γ is equal to 1.66, is one such option [6, 4]. As opposed to efficiency, if practicality is the main concern, CO_2, H_2O, O_2 or a mixture thereof are the most interesting options due to its abundant availability. A more practical option is the dilution of O_2 with CO_2, H_2O or a mixture of these species due to their abundant availability. The first stage of this research will focus on methane and hydrogen oxy-fuel combustion diluted with CO_2. When air is replaced with nitrogen-free oxidants, the main impact on the combustion properties can be seen in the adiabatic flame temperature and laminar burning velocity. When the oxidizer has the same concentration of oxygen as air (i.e. 21% O_2 and 21% CO_2 by volume), the laminar burning velocity is reduced due to the lower thermal conductivity and a higher density of CO_2 compared to N_2. CO_2 also has an interaction on the combustion kinetics, which previous research found occurs through the reaction [3]:

$$CO + OH \Leftrightarrow CO_2 + H \tag{1}$$

which reduces the laminar flame speed. In order to match the laminar burning velocity of the CO_2 diluted oxidant with that of air (ca. 39 cm/s), it requires a mixture with nearly 40% oxygen by volume. However, this corresponds to an adiabatic flame temperature of 2400 K, which is 200 K greater than that for methane/air combustion. This introduces the trade-off between excessive temperature and flame stabilization, where a robust CO_2 diluted oxy-combustion process requires at least 30% oxygen by volume [9, 7]. To conclude, the upper and lower limit of CO_2 in the oxidiser mixture will be defined respectively by excessive thermal load on the engine and flame stabilization. In the second stage of this research, hydrogen will be added to the intake mixture to address the reduced combustion stability. Multiple studies have been performed regarding the combustion of methane and hydrogen mixtures in SI engines, but there are limited investigations for oxy-fuel combustion. Hydrogen addition has been demonstrated to increase combustion stability for various equivalence ratios and hydrogen enhancement levels. The main contribution of hydrogen is the reduction of flame development duration, which enhances combustion stability [17, 24, 10]. As previously mentioned, the working fluid mainly consists out of CO_2, which compromises the indicated efficiency (η_i) due to the reduced laminar flame speed and the γ [22, 3, 4, 5]. To minimise this effect, it is important to decrease the CO_2 concentration in the oxidiser mixture as much as possible and consider mixtures of methane and hydrogen, as this could increase the combustion speed and increase η_i. A key goal of this research is to determine the operating conditions with the highest indicated efficiency.

Experimental setup

Experimental tests are performed on a single-cylinder SI engine specifically developed for oxy-fuel combustion. Table 1 contains the main characteristics of the engine and Figure 1 shows a schematic overview of the setup. The test bench is based on a single cylinder Yanmar diesel generator. The cylinder head is adapted to incorporate a pressure sensor, a spark plug and a thermocouple to monitor the temperature. An investigation is conducted to determine the modified compression ratio (C_r) and valve timing required for the engine. Because methane, hydrogen and their blends will be investigated in this research, both the compression ratio and valve timing should be appropriate for all possible mixtures and the pure components. Hydrogen (RON>120) and methane (RON=120) have a high octane number [23, 14], which makes them more knock resistant compared to gasoline. For this reason the compression ratio can be increased, which will aid efficiency [20, 2]. Due to its low ignition energy, hydrogen is prone to pre-ignition and backfire. Valve timing is one of the main parameters to control these phenomena. It was shown that not only the reduction of valve overlap played a crucial role in the development of backfire, but the timing of the intake valve opening as well. To reduce the possibility for recirculation of residual gasses, valve timing is fixed such that there are CAD of valve overlap [13, 16, 15].

Table 1: YANMAR L100V, air-cooled, single-cylinder characteristics.

Engine type	Air cooled, single-cylinder
Make	Yanmar L100V
Displacement [mm^3]	0.4357
Compression ratio	9.8
Bore x stroke [mm]	86 x 75
Connecting rod length [mm]	120.5
Crank radius [mm]	37.5
IVO [CAD]- IVC [CAD]	0 aTDC - 127 bTDC
EVO [CAD]- EVC [CAD]	127 aBDC - 0 bTDC

The in-cylinder pressure is measured by a high frequency piezoelectric AVL GH15D pressure sensor. The signal is amplified by a AVL FlexIFEM 2P2E. The gaseous mass flows are measured and controlled by Brooks Mass Flow Controller (MFC) SLA-585X. The intake and exhaust pressures are measured with absolute piezoelectric KISTLER 4260 transducers. The intake, exhaust and cylinder-wall temperature measurements are done with K-type thermocouples. A constant velocity of 1500 rpm is provided by an electric motor. The torque sensor is a HBM T40B Torque flange mounted between the engine and the electric motor and the crank angle is acquired every 0.1 CAD by a Heidenhain ROD 426 rotary encoder. The acquisition of all the data is done by a National Instruments Compact Rio 9022. Depending on the required O_2 mass flow rate, the oxygen is fed by an oxygen bottle for low mass flow rates, while higher mass flow rates of oxygen are provided by a Pressure Swing Absorption (PSA) oxygen generator Noxerior OP-60 Ecoline. In this machine the purity of oxygen is 95%. In Table 2, a summary of the uncertainty of the instruments used is reported. The adopted methodology for uncertainty analysis has been extensively explained in [18].

Table 2: Equipment uncertainty data summary. FS = Full Scale, PV = Processed Value

MFC (Brooks SLA585X)	Uncertainty
Accuracy	±0.7% PV
Repeatability	±0.2% FS
Temperature zero drift	±0.05% FS/K
Temperature span drift	±0.05% FS/K
Pressure drift	±0.429% PV/bar
Bottles (Air Liquide)	**Purity**
Methane	99.5%
Oxygen	99.995%
CO_2	99.995%
Hydrogen	99.995%
Crank Angle Encoder (Heidenhain ROD 426)	**Uncertainty**
Least Count θ_{LC}	0.1 CAD
TDC positioning	±0.05 CAD
In-cylinder Pressure (AVL GH15D)	**Uncertainty**
Signal amplifier (AVL FlexIFEM 2P2E)	
$Accuracy_{amp}$	±0.01% FS
$Accuracy_{G,amp}$	±0.5% (U95)
Intake & Exhaust Pressure (KISTLER 4260)	**Uncertainty**
Linearity + Repeatability	±0.2% FS
Age drift	±0.1% PV/year
Temperature drift	±1.5% PV

Figure 1: Experimental setup schematic

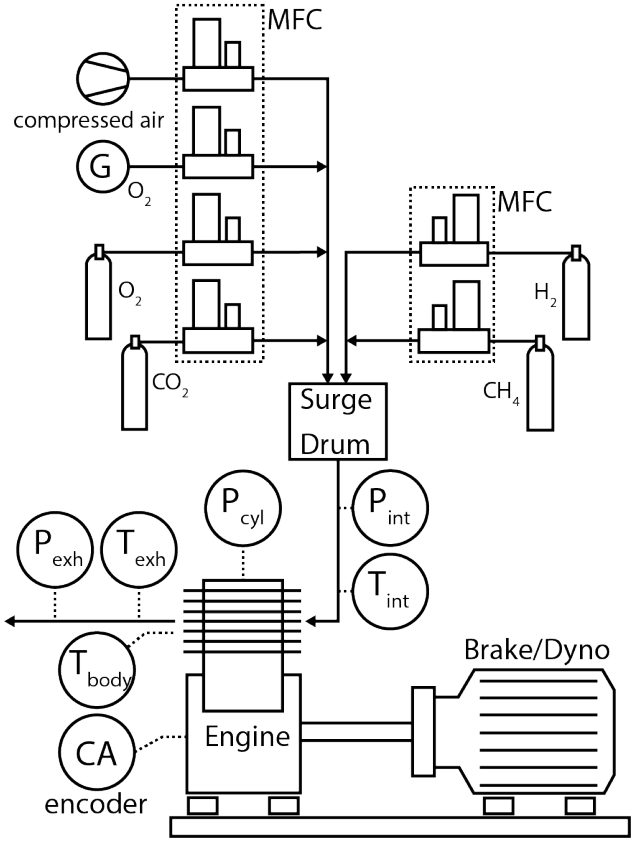

References

[1] E. E. P. P. Association. Engine power plants: A dynamic eu-based manufacturing sector.

[2] J. P. Bhasker and E. Porpatham. Effects of compression ratio and hydrogen addition on lean combustion characteristics and emission formation in a compressed natural gas fuelled spark ignition engine. *Fuel*, 208:260–270, 2017.

[3] A. C. V. Blarigan, R. Seiser, J. Y. Chen, R. Cattolica, and R. W. Dibble. Working fluid composition effects on methane oxycombustion in an si-engine: Egr vs. co2. *Proceedings of the Combustion Institute*, 34:2951–2958, 2013.

[4] A. V. Blarigan, D. Kozarac, R. Seiser, R. Cattolica, J.-Y. Chen, and R. Dibble. Experimental study of methane fuel oxycombustion in a spark-ignited engine. *Journal of Energy Resources Technology*, 136, 3 2014.

[5] A. V. Blarigan, D. Kozarac, R. Seiser, J. Y. Chen, R. Cattolica, and R. Dibble. Spark-ignited engine nox emissions in a low-nitrogen oxycombustion environment. *Applied Energy*, 118:22–31, 4 2014.

[6] P. C. T. D. Boer and J.-F. Hulet. Performance of a hydrogen-oxygen-noble gas engine.

[7] J. A. Caton. The effects of oxygen enrichment of combustion air for spark-ignition engines using a thermodynamic cycle simulation.

[8] V. Dias, M. Pochet, F. Contino, and H. Jeanmart. Energy and economic costs of chemical storage. *Frontiers in Mechanical Engineering*, 6, 5 2020.

[9] M. Ditaranto and J. Hals. Combustion instabilities in sudden expansion oxy-fuel flames. *Combustion and Flame*, 146:493–512, 8 2006.

[10] C. Dong, Q. Zhou, X. Zhang, Q. Zhao, T. Xu, and S. Hui. Experimental study on the laminar flame speed of hydrogen/natural gas/air mixtures. *Frontiers of Chemical Engineering in China*, 4:417–422, 2010.

[11] J. Ferrari. *Renewable fuels for long-term energy storage*, pages 109–138. Elsevier, 2021.

[12] D.-G. for Communication. A european green deal striving to be the first climate-neutral continent, 12 2022.

[13] J. Gao, X. Wang, P. Song, G. Tian, and C. Ma. Review of the backfire occurrences and control strategies for port hydrogen injection internal combustion engines, 1 2022.

[14] G. Genchi and E. Pipitone. Octane rating of natural gas-gasoline mixtures on cfr engine. *SAE International Journal of Fuels and Lubricants*, 7:1041–1049, 11 2014.

[15] J. Lee, K. Lee, J. Lee, and B. Anh. High power performance with zero nox emission in a hydrogen-fueled spark ignition engine by valve timing and lean boosting. *Fuel*, 128:381–389, 7 2014.

[16] K. J. Lee, T. C. Huynh, and J. T. Lee. A study on realization of high performance without backfire in a hydrogen-fueled engine with external mixture. volume 35, pages 13078–13087, 12 2010.

[17] F. Ma, S. Ding, Y. Wang, Y. Wang, J. Wang, and S. Zhao. Study on combustion behaviors and cycle-by-cycle variations in a turbocharged lean burn natural gas s.i. engine with hydrogen enrichment. *International Journal of Hydrogen Energy*, 33:7245–7255, 12 2008.

[18] M. Pochet, H. Jeanmart, and F. Contino. Uncertainty quantification from raw measurements to post-processed data: A general methodology and its application to a homogeneous-charge compression–ignition engine. *International Journal of Engine Research*, 21:1709–1737, 11 2020.

[19] X. Rixhon, G. Limpens, H. Jeanmart, and F. Contino. Taxonomy of the fuels in a whole-energy system. *Frontiers in Energy Research*, 9, 6 2021.

[20] S. Sahoo and D. K. Srivastava. Effect of compression ratio on engine knock, performance, combustion and emission characteristics of a bi-fuel cng engine. *Energy*, 233, 10 2021.

[21] F. L. K. Senecal. *Racing Toward Zero: The Untold Story of Driving Green.* SAE International, 6 2021.

[22] J. R. Serrano, J. Martín, J. Gomez-Soriano, and R. Raggi. Theoretical and experimental evaluation of the spark-ignition premixed oxy-fuel combustion concept for future co2 captive powerplants. *Energy Conversion and Management*, 244, 9 2021.

[23] S. Verhelst, R. Sierens, and S. Verstraeten. A critical review of experimental research on hydrogen fueled si engines, 2018.

[24] R. Zhang, L. Chen, J. Pan, H. Wei, L. Zhou, and C. Liu. Effects of direct-injected hydrogen addition on methane combustion performance in an optical si engine with high compression-ratio. *International Journal of Hydrogen Energy*, 45:3284–3293, 1 2020.

An in-situ cryo-charging method to study low energy trapping of H_2 in metals

J-B. Maillet*[1], G. Da Costa[1], C. Bacchi[1], C. Vaudaulon[1], F. Vurpillot[1]

[1]Univ Rouen Normandie, INSA Rouen Normandie, CNRS, Normandie Univ, GPM UMR 6634, F-76000 Rouen, France

Introduction

The study of hydrogen in Atom Probe Tomography appears as a relevant challenge whether of its low mass, high diffusion coefficient and presence as a residual gas in vacuum chambers generate multiple complications for atom probe investigation [1-5]. Different solutions were proposed in literature like ex-situ charging coupled with cryotransfer [6-7] or H charging at high temperature in a separate chamber [8]. In this study, we propose an alternative route for in-situ H-charging in atom probe derived from a method developed in Field Ion Microscopy by Dudka et al. to study the Helium in-situ implantation damage [9-12] to understand low-energy traps. By applying negative voltage pulse on the specimen in an atom probe chamber under low pressure of H_2, it is demonstrated that high dose of H can be implanted in the range 2-20 nm under the specimen surface. An atom probe chamber was modified to enable direct negative pulse application with controlled gas pressure, pulse repetition rate and pulse amplitude. Using electrodynamical simulations, it is shown that implantation energy is in the range 100 - 1,000 eV generating mild implantation defects. A theoretical depth of implantation was predicted and compared to experiments.

Methodology

Before detailing the methodology, a quick reminder of the Atom Probe Tomography (APT) principles. Under the effect of the high voltage V applied to a metallic sample prepared as sharp needle, an intense electric field F is generated at the apex. This field is proportional to the inverse of the radius of curvature R at the apex of the tip, as shown in the following eq. 1 [13] :

$$F = \frac{V}{k_f R} \quad (1)$$

* Corresponding author: jean-baptiste.maillet@univ-rouen.fr

k_f a field factor (3 to 5), is a slowly varying semi-constant with R [14]. The generated electric field F is around $10 - 60\ V.nm^{-1}$. This high electric field F allow to evaporate atom per atom and analyses a sample at atomic scale in a standard use, resolved in time, mass and position for each atom. Conversely, when a negative pulse voltage is applied to an APT sample, a negative electric field is generated at the apex tip. This electric field generates an electron emission characterized by the density of electrons emitted in A/m² at the apex of the specimen. This density follows an exponential law known today under the name of Fowler-Nordheim [15].

The flux of electron emitted J at the apex depending on the electric field F and the work function of electron. For Nickel, Tungsten and Iron the work function is respectively $\Phi = 5\ eV$, $4.5\ eV$ and $4.4\ eV$ [14]. When we introduce a gas in the chamber analysis, in our case H_2 gas, this emission of electrons can ionize the environment gas in electronic cone emission Figure 1. The gas is positively charged therefore be attracted into sample by the negative polarization and impacted into sample.

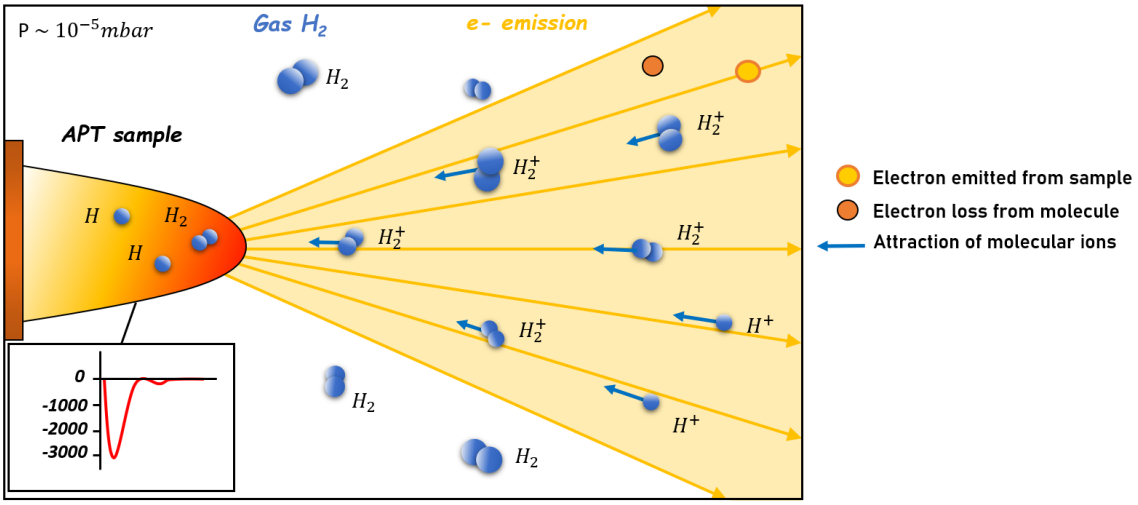

Figure 1: Implantation in-situ of H_2 in chamber analysis in Atom Probe Tomography (APT). These H_2^+ molecules are ionized by the electron emitted from sample and attracted into an APT sample.

Negative pulses are applied to the tip in H_2 gas to implant, then the sample can be analyzed with H charged. Remember that the sample is metallic and at cryogenic temperature (20K < T < 80K) during the process. The trapping behavior of H2 in materials can be studied.

Using Lorentz-2E software [17-18] allows us to obtain the kinetic energies of electrons when they are emitted from the tip when a negative pulse is applied and the kinetic energy of H_2^+ particles when they are attracted and implanted to the APT sample. Using realistic pulse Figure 2a to generate an electric field and the geometry of instrument are modelized to predict the H-charging into an APT metallic sample.

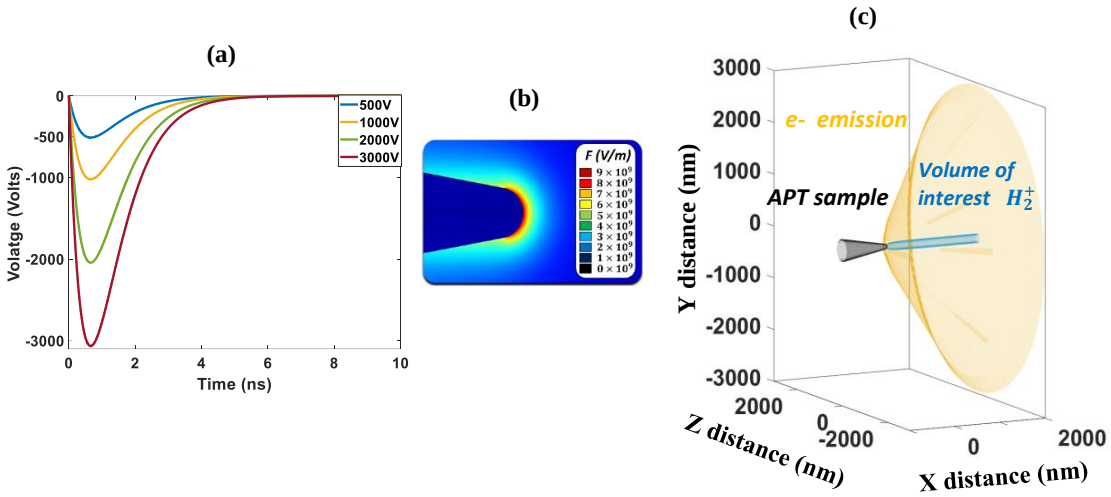

Figure 2: Simulation with Lorentz-2D of negative pulse using for implantation in-situ in APT. The rise time is 1.2 ns and the width is 1.8 ns. Lorentz simulations are carried with the most closed pulse to the real pulse using in APT (a). Generation of electric field at the apex of the tip (b). Simulation of electron emitted from APT sample (yellow) and volume of H_2^+ ions created and implanted in apex sample (blue) (c).

Simulations have been done for different pulse amplitude ($-500V, -1{,}000V, -2{,}000V$ *and* $-3{,}000V$) and we obtain for example the simulation of electronic cone emission from an APT sample in Figure 2c. The average kinetic energy of implanted ions H_2^+ is extracted for different pulse amplitude by considering a lot of parameters (not show here). The average implantation energy considering the proportions for $-1{,}000V$ is around $150eV$, for $-2{,}000V$ *is* $\sim 250eV$ and for $-3{,}000V$ is $\sim 320eV$ as shown in Figure 3a and an example of simulation is show for $-2{,}500V$ on an APT tip in Figure 3b.

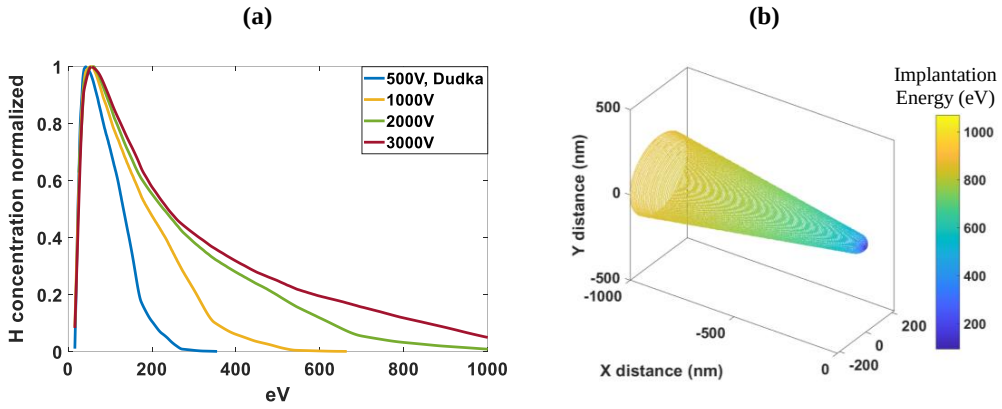

Figure 3: Simulations done with Lorentz-2D to obtain an estimation of implantation energy for different pulse voltage with quantity of ions implanted normalized (a). Implantation energy gradient of H_2^+ particles for a voltage pulse at -2.500V applied on APT sample (b).

Discussions

Some experiments are done in homemade APT on Iron and Nickel pure to compare and verify the theory and the H-charging prediction.

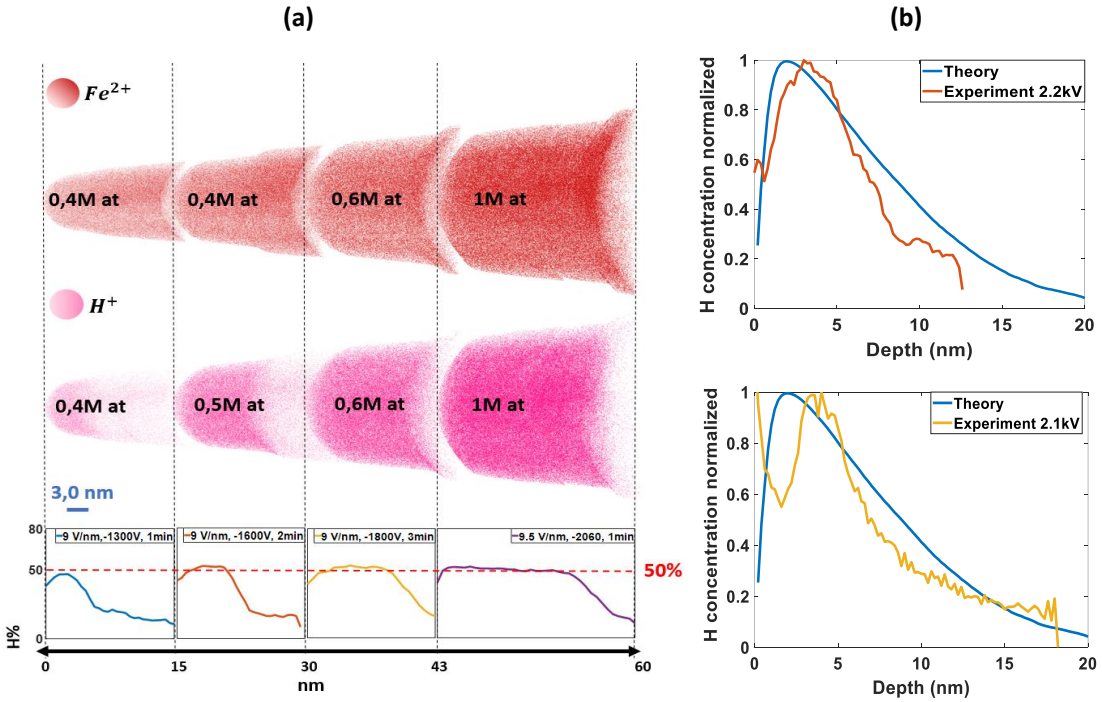

Figure 4: Experiments of in-situ pulsed implantation of hydrogen in Iron sample with their implantation profiles. Each analysis volume is shown with their Fe^{2+} (red) and H^+(pink) ions, the number of atoms analyzed and their implantation profiles and parameters (a). Comparison of normalized implantation profiles with the analytic model developed in Nickel sample case (b).

Figure 4 shows the result of H2 charging at cryogenic temperature in Iron and Nickel sample. Experiments of in-situ implantations of H performed on the same Iron sample, displayed side by side to reconstruct the entire tip to demonstrate how the method works in Figure 4a. For the Nickel sample, implantation profiles are compared to simulation in Figure 4b. The model has good agreement with experiments and can predict the density of H implanted and the depth of implantation. We reach a hydrogen saturation around 50% and 60% inside an Iron and Nickel tip respectively. We observe a slight loss of hydrogen implanted on the first nanometers probably due to desorption. Indeed, this implanted hydrogen is located in the sub-surface of the sample and therefore has greater ease of escaping from the sample. Concerning the implantation depth, it agrees with the model, as does the expected hydrogen density implanted in the sample (not shown here).

Conclusion

We described in this study a method to implant successfully a high dose of H in the first 20 nm of a metallic sample at cryogenic temperature. The goal is to study the diffusive trap of H in different alloys, improving our knowledge of the behavior of H in materials. In situ pulsed implantation allows us to implant a higher dose and energy of implantation than continuous. The method is simple and straightforward. Nevertheless, the good control of many parameters is required. Parameters related to the implantation and the instrument of course but also related to the tip shape. The theory and the experimental are consistent. The implantation profiles are satisfactory, the implantation of H ions in Nickel reaches a depth of 4nm with a significant quantity (100,000at) with up to 10% remaining at 10nm of depth. Pulsed allows to reach a higher negative voltage amplitude than in constant voltage, to ionize a large quantity of ions close to the tip and thus to implant a large quantity in the optical axis of a APT sample with high energy. This in-situ implantation makes it possible to avoid any cryogenic transfer and diffusion of H implanted due to the low temperature process ($20K < T < 70K$) and allows a study on H in materials with a relatively good statistic. This method therefore appears today as a good alternative for the study of H in materials at the atomic scale. In the following study we will study lateral implantation in larger depth with different shank angle and TEM analysis before and after implantation. And we are currently working on in-situ implantation in other materials like Ni-Mo with some grain boundary of molybdenum. The goal is will be to study this method at trapping sites, such as Scandium, Zirconium, grain boundary or dislocations and study the spatial location of H in APT specimen.

References

[1] E. Wimmer *et al.*, « Temperature-dependent diffusion coefficients from *ab initio* computations: Hydrogen, deuterium, and tritium in nickel », *Phys. Rev. B*, vol. 77, nº 13, p. 134305, avr. 2008, doi: 10.1103/PhysRevB.77.134305.

[2] P. Felfer *et al.*, « An Atom Probe with Ultra-Low Hydrogen Background », *Microscopy and Microanalysis*, vol. 28, nº 4, p. 1255-1263, août 2022, doi: 10.1017/S1431927621013702.

[3] G. Sundell, M. Thuvander, et H.-O. Andrén, « Hydrogen analysis in APT: Methods to control adsorption and dissociation of H2 », *Ultramicroscopy*, vol. 132, p. 285-289, sept. 2013, doi: 10.1016/j.ultramic.2013.01.007.

[4] I. E. McCarroll, P. A. J. Bagot, A. Devaraj, D. E. Perea, et J. M. Cairney, « New frontiers in atom probe tomography: a review of research enabled by cryo and/or vacuum transfer systems », *Materials Today Advances*, vol. 7, p. 100090, sept. 2020, doi: 10.1016/j.mtadv.2020.100090.

[5] I. Mouton *et al.*, « Quantification Challenges for Atom Probe Tomography of Hydrogen and Deuterium in Zircaloy-4 », *Microsc Microanal*, vol. 25, nº 2, p. 481-488, avr. 2019, doi: 10.1017/S143192761801615X.

[6] Y.-S. Chen *et al.*, « Observation of hydrogen trapping at dislocations, grain boundaries, and precipitates », *Science*, vol. 367, nº 6474, p. 171-175, janv. 2020, doi: 10.1126/science.aaz0122.

[7] Y.-S. Chen, P. A. J. Bagot, M. P. Moody, et D. Haley, « Observing hydrogen in steel using cryogenic atom probe tomography: A simplified approach », *International Journal of Hydrogen Energy*, vol. 44, nº 60, p. 32280-32291, déc. 2019, doi: 10.1016/j.ijhydene.2019.09.232.

[8] J. Takahashi, K. Kawakami, et Y. Kobayashi, « Origin of hydrogen trapping site in vanadium carbide precipitation strengthening steel », *Acta Materialia*, vol. 153, p. 193-204, juill. 2018, doi: 10.1016/j.actamat.2018.05.003.

[9] A. A. Mazilov, « DETERMINATION OF THE SPECTRA OF ION He AND H2 BOMBARDMENT OF AUTOEMITTER SURFACE ».

[10] O. V. Dudka, V. A. Ksenofontov, A. A. Masilov, et E. V. Sadanov, « Formation of interstitial atoms in surface layers of helium-implanted tungsten », *Tech. Phys. Lett.*, vol. 39, nº 11, p. 960-963, nov. 2013, doi: 10.1134/S1063785013110035.

[11] J. Y. Cavaille et M. Drechsler, « Ion impact on field emitter crystals », *Rev. Phys. Appl. (Paris)*, vol. 12, nº 10, p. 1631-1639, 1977, doi: 10.1051/rphysap:0197700120100163100.

[12] J. Y. Cavaillé et M. Drechsler, « Surface self-diffusion by ion impact », *Surface Science*, vol. 75, nº 2, p. 342-354, juill. 1978, doi: 10.1016/0039-6028(78)90256-X.

[13] E. W. Müller et K. Bahadur, « Field Ionization of Gases at a Metal Surface and the Resolution of the Field Ion Microscope », *Phys. Rev.*, vol. 102, nº 3, p. 624-631, mai 1956, doi: 10.1103/PhysRev.102.624.

[14] W. Lefebvre-Ulrikson, Éd., *Atom probe tomography: put theory into practice*. London: Academic Press, 2016.

[15] J. Paulini, T. Klein, et G. Simon, « Thermo-field emission and the Nottingham effect », *J. Phys. D: Appl. Phys.*, vol. 26, nº 8, p. 1310-1315, août 1993, doi: 10.1088/0022-3727/26/8/024.

[16] J. Hölzl, F. K. Schulte, et H. Wagner, Éd., *Solid surface physics*. in Springer tracts in modern physics, no. 85. Berlin Heidelberg: Springer, 1979.

[17] S. T. Loi, B. Gault, S. P. Ringer, D. J. Larson, et B. P. Geiser, « Electrostatic simulations of a local electrode atom probe: The dependence of tomographic reconstruction parameters on specimen and microscope geometry », *Ultramicroscopy*, vol. 132, p. 107-113, sept. 2013, doi: 10.1016/j.ultramic.2012.12.012.

[18] L. Rousseau *et al.*, « Dynamic Effects in Voltage Pulsed Atom Probe », *Microsc Microanal*, vol. 26, nº 6, p. 1133-1146, déc. 2020, doi: 10.1017/S1431927620024587.

Analysis and Design of the institutional environment for deploying a green hydrogen value chain in the Netherlands

R.J. van 't Veer *[1]

[1] Delft University of Technology, Faculty of Technology, Policy and Management

3rd of October, 2023

Introduction

The increasing global temperatures and adverse effects that are experienced call for a dramatic change in the amount of greenhouse gas emitted with studies indicating a decrease of at least 90% by 2050. The decarbonization of the energy sector has therefore become a stringent topic in national and international efforts to combat climate change [8]. Green hydrogen has the potential to contribute to this decarbonization [29], because it can be produced from renewable energy and does not emit greenhouse gases. Consequently, this hydrogen type has received significant attention among academia, practitioners and policymakers [2]. The value chain of hydrogen can have different configurations since the energy vector can be produced, stored and converted in different ways and forms (e.g. gaseous, liquid [31], but typically consists of the nodes 'source of energy', 'production units', 'storage facilities', 'transportation modes' and 'end use' [1].

The potential of green hydrogen relates to the use of renewable energy sources for the production, rather than fossil fuels from which the currently used grey hydrogen is produced [18]. With green hydrogen the production process can therefore be decarbonized [2, 14]. Hydrogen also has the potential to replace fossil fuels in the process industry and to be used in mobility, built environment and commercial sectors [15, 35]. Thus, green hydrogen has the potential to enhance the sustainability and reliability of the energy system and play an important role in assuring flexibility of the energy system [19]. Accordingly, the European Commission has set a target of 40 GW of green hydrogen production by 2030 [6] and, following the Russian invasion of Ukraine, the production and import of 10 million tonnes of green hydrogen each by 2030 [7]. Also in the Netherlands the potential of green hydrogen has resulted in the goal of an electrolyser capacity of 3-4 GW by 2030 [16] and 15 - 20 GW around 2040 [24]. Besides plans for green hydrogen, several projects are taking place in the Netherlands. Examples are the execution of four pilots on hydrogen use in the built environment [30], the construction of a national hydrogen network [22] and the development of a large-scale hydrogen hub in the Port of Rotterdam [28].

Despite the potential of green hydrogen in decarbonizing the energy system and the formulation of targets on green hydrogen across the EU, the transition to green hydrogen has encountered several barriers, amongst which technical, economic and regulatory challenges. The policies and regulations relating to hydrogen form in many countries a barrier in their efforts to scale up the hydrogen energy system whilst the technologies are ready for implementation [17, 13]. These barriers are for instance regulatory uncertainty due to the lack of a harmonized legislative framework [3] or difficulties in regulatory frameworks from moving disruptive technologies from demonstration projects to large-scale deployment [31]. In other words, conventional 'one-size-fits-all' approaches to regulation might be outdated for sectors in transition, thereby making alternative approaches to regulation potentially more suitable [21].

The scale-up of the hydrogen market is faced with a 'chicken-and-egg' problem [25] where on the demand side businesses interested in using green hydrogen require insight about the expected quantity, price, network operators and tariffs, whereas in terms of supply potential investors require insight into the future demand [23]. Additionally, this impasse in transitioning to green hydrogen is exacerbated by the big cost gap between grey and green hydrogen, resulting decreased interest among producers and consumers [2]. Meanwhile, the expected demand and supply determines the development of infrastructure

*Corresponding author: r.j.vantveer@tudelft.nl

[23]. Overcoming these interdependencies require coordinated action across stakeholders to materialize the full benefit of hydrogen in the transition to green hydrogen systems [15].

Thus, barriers encountered in transitioning to green hydrogen relate to the formal rules of green hydrogen value chains (GHVCs) on the one hand and coordination amongst stakeholders on the other hand. Overcoming these barriers requires gaining an understanding of the institutional framework in which its activities take place [9] and the interaction between the political, techno-economic, market and social dimensions of the hydrogen transition [13]. An institutional framework consists of formal and informal institutions, actors and the governance of a sector [9]. Institutions are defined as widely understood rules, norms or strategies which create incentives for behaviour in repetitive situations [4]. These can either be public policies and laws (formal) or spoken or tacitly understood social norms (informal) [10] and can comprise a single statement or multiple statements [32]. Gaining an understanding of the institutional framework and its institutional framework in the hydrogen transition will provide insight into the sector and potential negative mechanisms [9], thereby contributing to the identification and implementation of adequate policy mechanisms, which are crucial for transparent procedures for national, renewable-based hydrogen plans that support hydrogen supply and demand as well as necessary infrastructure [14, 13].

The conducted research in this PhD seeks to contribute to overcoming these barriers in the hydrogen transition by taking a socio-technological perspective on the transition to GHVCs. It combines the disciplines of law, social sciences and engineering to perform a comprehensive analysis of the influence and design of the institutional framework in achieving a coherent technological and institutional transition to a GHVC. With a socio-technical perspective the green hydrogen value chain is considered as a combination of the social and technical systems involved in making, distributing and using green hydrogen [14]. Using this perspective allows for the analysis of the interactions between the institutional framework and the technical dimensions of the GHVC. As this doctoral research started in January 2023, research results or papers are not yet available. Up to the time of writing this research abstract, the doctoral research consisted of the identification of knowledge gaps and formulation of the approach to be taken to decrease these gaps. In the following sections, the formulated research approach, questions and methods are therefore described.

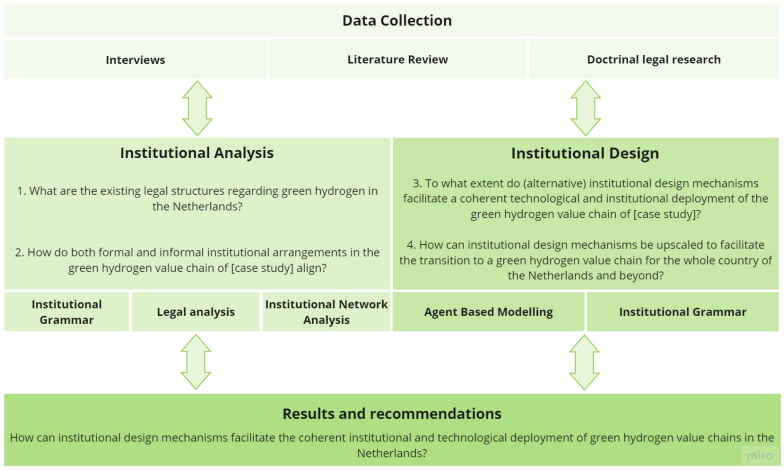

Figure 1: Research approach

Research methods

This research will be applied to a GHVC in the Netherlands that already exists or will be developed. The use of a case study will aid in maintaining a feasible and manageable research scope. Additionally, the research results will be valuable to stakeholders of the chosen GHVC application. In terms of methodology, a synergy between legal, qualitative and quantitative research is proposed. These research steps will build onto each other and will collectively provide insight about the effect and potential design of the institutional framework of a chosen GHVC in the Netherlands. The approach that will be taken in this research is depicted in Figure 1, along with the corresponding research questions and methodologies. This

research is divided into two phases, the institutional analysis and institutional design phase, which will be discussed in the next subsections.

Institutional analysis

This doctoral research commences with gaining an understanding of the institutional framework of a GHVC in the Netherlands that already exists or will be developed. This phase identifies the space in which actions related to green hydrogen can be undertaken and the extent to which alternatives are possible by identifying and analysing (1) the formal institutions and (2) the stakeholders and their informal institutions on the other hand. Legal analysis will be employed to understand how the formal institutions shape and influence the development of the GHVC under analysis, thereby answering research question 1 shown in figure 1. Data will be collected with literature review and a doctrinal legal analysis which entails research into the law (legal acts, regulations, policy guidelines, case law, administrative decisions) and the legal concepts [5].

The stakeholder network of the GHVC and their informal institutions, such as their relationships, agreements and strategies, and the alignment of their formal and informal institutions, will be studied using Institutional Network Analysis (INA) which utilizes interviews for data collection. The approach aids analyzing and visualizing the complexity of the institutional framework of a subject where multiple stakeholders are involved and coordination is required [20].

To visualize the alignment of institutions, we use the Institutional Grammar (IG) which is an analytical tool for assessing the content and structure of institutions. A first step in applying IG is dissecting an institution into its constituting statement(s) [32], which are the shared linguistic constraints or opportunities that prescribe, permit or advise actions or outcomes for actors [4, 33]. The tool enables the analysis of the core elements of institutional statements in a structured manner with a syntax, which aids in identifying common components of institutional statements and establishes the set of components that comprise each type of institutional statement [4, 33]. By analyzing the elements of the institutions identified for the case study GHVC using IG and visualizing them using INA, the alignment of the institutions in the institutional framework will be identified as well as potential voids or overlaps.

Institutional design

In the second phase of the doctoral research the interaction between the institutional and technological dimensions of the GHVC under analysis will be studied by means of agent based modelling (ABM). The methodology is suited for comparing and illustrating before and after situations of a policy implementation [12, 27]. ABM will be used to simulate the future development of the GHVC under the existing and alternative institutional design, thereby providing insight about the extent by which the institutional framework plays a role in the transition to a GHVC and providing insight on potential mechanisms that can be employed to facilitate the coherent technological and institutional development of the GHVC. To integrate the institutions into the ABM, the meta-model "Modelling Agent systems based on Institutional Analysis" (MAIA) introduced by [11] will used as a basis. This framework helps understanding and analyzing social systems where interactions taken place under an institutional structure. It extends and formalizes the concepts of the Institutional Analysis and Development (IAD) framework of [26] and provides a template of concepts to model social systems, particularly focused on the institutional aspects of the system [34].

As Figure 1 shows, Institutional Grammar will also be used in the institutional design phase of the doctoral research. IG will be used to decompose and integrate the institutions of the case study that are identified in the preceding research phase into the Agent Based Model. For exemplary purposes, the concepts of the MAIA framework, which correspond to the structures of the IAD-framework, have been applied to the green hydrogen value chain system in this research and is shown in Figure 2. In the IAD framework "rules-in-use" and "rules-in-form" are used, which in this research respectively refer to informal and formal institutions.

Discussion

The aim of this doctoral research is to show to what extent an institutional framework plays a role in the development of the value chain of hydrogen. Additionally, this research aims to show how the design of the institutional framework can facilitate the coherent technological and institutional development. The research questions will be answered by means of differing methodologies from various disciplines,

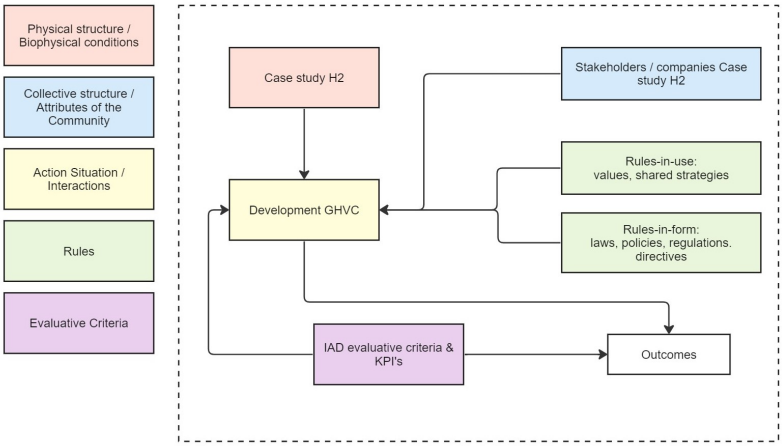

Figure 2: Draft structure of the ABM on the GHVC

thereby analysing the socio-technological system from various perspectives and allowing a comprehensive multi-dimensional understanding. The results are expected to demonstrate that a transition such as that of green hydrogen is not only determined by technological advancements, but that research into this topic should include the social and institutional dimensions. Moreover, this doctoral research seeks to provide insight into potentially effective institutional design mechanisms which can contribute to formulating effective regulatory and legislative approaches prior to the actual materialization of the GHVC. This can decrease the timeline of policy-making and avoid potential ineffective or harmful institutional design mechanisms to be implemented.

Limitations of this doctoral research relate to its focus on the coherence between the institutional and technological system of the GHVC, which infers less attention to the technical specificities related to hydrogen. Moreover, the socio-technical perspective taken in this research is limited to formal and informal institutions and stakeholders within the chosen GHVC whereas the social dimension could also include topics such as public acceptance or ethics. Even though these debates are of great importance, these fall outside of the scope of this doctoral research. As the research is interdisciplinary, it is limited in the depth attributed to each discipline whilst these all could encompass a doctoral research in itself. Lastly, the use of a case study does provide valuable results, also for other GHVCs, but does limit the generalizability of the research results.

Conclusions

Green hydrogen has received significant attention among academia, practitioners and policymakers since the energy carrier has the potential to replace grey hydrogen as well as fossil fuels. Despite the various national plans for the production and use of green hydrogen, both the unsupportive legislative and / or regulatory frameworks and lack of coordination among stakeholders form barriers in the materialization of green hydrogen value chains. Analysis of the institutional framework, which involves the formal rules, the stakeholders and their agreements, norms and behaviour, of a sector aids in understanding potential negative mechanisms for the advancement of that sector. This research therefore adopts an institutional analysis and design approach to analyze the development of a green hydrogen value chain in the Netherlands under the current and alternative institutional frameworks. In the institutional analysis phase will gain an understanding of the institutional framework and the alignment of the institutions applicable to the green hydrogen value chain of the case study. The design phase will identify how the GHVC will develop in the future and how design mechanisms can facilitate the transition the a green hydrogen value chain in the Netherlands. The obtained insights from the proposed research are expected to contribute to the development of robust and supportive regulatory approaches that facilitate the coherent technological and institutional deployment of GHVCs in the Netherlands. This can consequently contribute to achieving a more sustainable energy system, the decrease of greenhouse gas emissions and mitigating climate change.

Acknowledgement

This is research is undertaken at the Delft University of Technology in collaboration with Tilburg University School of Law. Supervision is undertaken by Prof.dr.ir. Zofia Lukszo (TU Delft), Dr. Amineh Ghorbani (TU Delft), Prof.dr. Saskia Lavrijssen (Tilburg University) and Dr. Max Baumgart (Tilburg University). The doctoral research is supported by the Dutch Research Council (NWO) program "HyChain-ESI - Agenda for the emerging hydrogen economy supporting energy system integration".

References

[1] A. Almansoori and N. Shah. Design and operation of a future hydrogen supply chain: Multi-period model. *International Journal of Hydrogen Energy*, 34(19):7883–7897, 2009.

[2] A. H. Azadnia, C. McDaid, A. M. Andwari, and S. E. Hosseini. Green hydrogen supply chain risk analysis: A european hard-to-abate sectors perspective. *Renewable and Sustainable Energy Reviews*, 182(8), 2023.

[3] M. Baumgart and S. Lavrijssen. Exploring regulatory strategies for accelerating the development of sustainable hydrogen markets in the european union. *Journal of Energy Natural Resources Law*, (9):1–30, 2023.

[4] S. E. Crawford and E. Ostrom. A grammar of institutions. *American political science review*, 89(3):582–600, 1995.

[5] N. Duncan and T. Hutchinson. Defining and describing what we do: Doctrinal legal research. *Deakin Law Review*, 17(1):83–119, 2012.

[6] European Commission. 'A hydrogen strategy for a climate neutral Europe'. (Communication) COM(2020)301 final, 2020.

[7] European Commission. 'REPowerEU: affordable, secure and sustainable energy for Europe' (Communication) COM(2022)230 final, 2022.

[8] S. S. Farahani, C. Bleeker, A. van Wijk, and Z. Lukszo. Hydrogen-based integrated energy and mobility system for a real-life office environment. *Applied Energy*, 264, 2020.

[9] R. Fernández-González, F. Puime-Guillén, and M. Panait. Multilevel governance, PV solar energy, and entrepreneurship: the generation of green hydrogen as a fuel of renewable origin. *Utilities Policy*, 79, 2022.

[10] A. Ghorbani. Institutional modelling: Adding social backbone to agent-based models. *MethodsX*, 9, 2022.

[11] A. Ghorbani, P. Bots, V. Dignum, and G. Dijkema. MAIA: A framework for developing agent-based social simulations. *JASSS*, 16(2), 2013.

[12] A. Ghorbani, V. Dignum, and C. M. Jonker. Enhancing ABM into an Inevitable Tool for Policy Analysis. *Policy and Complex Systems*, 1(1), 2014.

[13] J. A. Gordon, N. Balta-Ozkan, and S. A. Nabavi. Socio-technical barriers to domestic hydrogen futures: Repurposing pipelines, policies, and public perceptions. *Applied Energy*, 336, 2023.

[14] S. Griffiths, B. K. Sovacool, J. Kim, M. Bazilian, and J. M. Uratani. Industrial decarbonization via hydrogen: A critical and systematic review of developments, socio-technical systems and policy options. *Energy Research and Social Science*, 80, 2021.

[15] Hydrogen Council. How hydrogen empowers the energy transition. https://hydrogencouncil.com/wp-content/uploads/2017/06/Hydrogen-Council-Vision-Document.pdf, 2017. Accessed: 01-09-2023.

[16] Klimaatakoord. Klimaatakkoord. https://www.klimaatakkoord.nl/documenten/publicaties/2019/06/28/klimaatakk 2019. Acessed: 01-09-2023.

[17] I. Lammers and L. Diestelmeier. Experimenting with law and governance for decentralized electricity systems: Adjusting regulation to reality? *Sustainability*, 9(2), 2017.

[18] T. Lepage, M. Kammoun, Q. Schmetz, and A. Richel. Biomass-to-hydrogen: A review of main routes production, processes evaluation and techno-economical assessment. *Biomass and Bioenergy*, 144, 2021.

[19] L. Li, H. Manier, and M. A. Manier. Hydrogen supply chain network design: An optimization-oriented review. *Renewable and Sustainable Energy Reviews*, 103:342–360, 2019.

[20] B. Mesdaghi, A. Ghorbani, and M. de Bruijne. Institutional dependencies in climate adaptation of transport infrastructures: an institutional network analysis approach. *Environmental Science and Policy*, 127:120–136, 2022.

[21] G. Mete and L. Reins. Governing new technologies in the energy transition – the hydrogen strategy to the rescue? *Carbon and Climate Law Review*, 14(3):210–231, 2020.

[22] Ministry Economic Affairs and Climate. Ontwikkeling transportnet voor waterstof. https://open.overheid.nl/documenten/ronl-5c57a9ba35fa907dcc805ca0da463dc33b036bb8/pdf, 2022. Acessed: 01-09-2023.

[23] Ministry of Economic Affairs and Climate. Kabinetsvisie waterstof. https://open.overheid.nl/documenten/ronl-44c87a40-bac0-42ec-ae91-eb81c87e2186/pdf, 2020. Acessed: 01-09-2023.

[24] Ministry of Economic Affairs and Climate. Nationaal plan energiesysteem. https://www.rvo.nl/onderwerpen/energiesysteem/nationaal-plan-energiesysteem, 2023. Acessed: 22-09-2023.

[25] T. Mäkitie, J. Danebergs, J. Hanson, and E. G. Medbø. Solving the chicken and egg problem in maritime hydrogen value chains in western norway. *TFME NTRANS report*, 21(3), 2021.

[26] E. Ostrom. Background on the institutional analysis and development framework. *Policy studies journal*, 39(1):7–27, 2011.

[27] G. Papachristos. Towards multi-system sociotechnical transitions: why simulate. *Technology Analysis Strategic Management*, 26(9):1037–1055, 2014.

[28] Port of Rotterdam Authority. Highlights annual report 2022 – port of rotterdam authority. https://www.portofrotterdam.com/en/news-and-press-releases/annual-report-2022-making-room-for-transition, 2022. Acessed: 01-09-2023.

[29] C. J. Quarton and S. Samsatli. How to incentivise hydrogen energy technologies for net zero: Whole-system value chain optimisation of policy scenarios. *Sustainable Production and Consumption*, 27:1215–1238, 2021.

[30] Rijksdienst voor Ondernemend Nederland. Aanvullend richtsnoer waterstofpilots in de gebouwde omgeving, eerste versie. https://www.rvo.nl/onderwerpen/richtsnoeren-waterstof, 2022. Acessed: 01-09-2023.

[31] C. B. Robledo, V. Oldenbroek, F. Abbruzzese, and A. J. van Wijk. Integrating a hydrogen fuel cell electric vehicle with vehicle-to-grid technology, photovoltaic power and a residential building. *Applied Energy*, 215:615–629, 2018.

[32] S. Siddiki, T. Heikkila, C. M. Weible, R. Pacheco-Vega, D. Carter, C. Curley, and A. Bennett. Institutional analysis with the institutional grammar. *Policy Studies Journal*, 50(2):315–339, 2022.

[33] S. Siddiki, C. M. Weible, X. Basurto, and J. Calanni. Dissecting policy designs: An application of the institutional grammar tool. *Policy Studies Journal*, 39(1):79–103, 2011.

[34] R. Verhoog, A. Ghorbani, and G. P. Dijkema. Modelling socio-ecological systems with maia: A biogas infrastructure simulation. *Environmental Modelling and Software*, 81:72–85, 2016.

[35] A. Wolf. Establishing hydrogen hubs in europe: An analysis of the european hydrogen landscape. *Centrum fur Europaische Politik*, (1), 2023.

Analysis of copper-based double perovskites as air electrode for the reversible solid oxide cell

K. Machaj[*1,2,3], A. Niemczyk[1,2], P. Winiarz[4], Y. Naumovich[1,2], K. Świerczek[4], R. Kluczowski[5], K. Zheng[4]

[1]Institute of Power Engineering, Department of High Temperature Electrochemical Processes, Mory 8 St., 01-330 Warsaw/Poland
[2]Center for Hydrogen Technologies CTH2, Institute of Power Engineering Augustówka 36 St., 02-981 Warsaw/Poland
[3]Wroclaw University of Science and Technology, Department of Cryogenics and Aerospace Engineering, Wybrzeze Wyspianskiego 27, 50-370 Wroclaw, Poland
[4]AGH University of Science and Technology, Krakow, Poland, Adam Mickiewicz 30 St., 30-059 Cracow/Poland
[5]Institute of Power Engineering, Ceramic Department CEREL, Techniczna 1 St., 36-040 Boguchwała/Poland

*corresponding author: Krystian.machaj@ien.com.pl

Keywords: *solid oxide cells, copper, air electrode, MIEC, rSOC*

Introduction

The significance of hydrogen to the global economy is still increasing. By the end of 2021, more than 20 significant government documents were issued to plan the deployment of hydrogen [1,2]. Crucial is rapid increase of installed capacity of CO2-free hydrogen production plants to meet the predicted demand and ambitious climate-friendly goals. Solid Oxide Electrolysis (SOE) is one of the electrolyser technology being evaluated for widespread implementation in this field. Due to excellent catalytic activity and high mixed ionic-electronic conductivity (MIEC), cobalt-based oxides (perovskite like LSC) are cutting-edge materials for SOC air electrodes [3]. However, the predicted continuous development of the demand in the coming decades (related to the Li-ion batteries market), and the politically unstable location of main cobalt mines causes the high supply risk of cobalt. For that reason, cobalt has been listed as a critical raw material (CRM) by the European Union (EU) since 2020 [4]. In addition, toxicity of this material and the socioeconomic concerns associated with its mining production are further impetuses for development of alternative air electrodes with limited amount of Co. A feasible and economically beneficial alternative to the Co-based air electrodes seem to be Cu-based materials. With the implementation of copper, partial or complete replacement of cobalt is possible. It was demonstrated that rare-earth Cu-based oxides double perovskites have potential for application in reversible solid oxide cells (rSOC).

Material and methods:

The physicochemical features, including structure, stability, and transport properties, of Cu-based double perovskites derived from $ReBa_{0.5}Sr_{0.5}CoCuO_{5+\delta}$ (where Re: Sm, Gd, Pr, Nd) were evaluated. Based on the obtained results – the highest peak power density in the range of 550-750°C (up to 700 mW cm-2 at 750°C) – the $SmBa_{0.5}Sr_{0.5}CoCuO_{5+\delta}$ oxide was chosen for fabrication of the fuel electrode-based cells (size of 5 cm x 5 cm). The electrochemical

* Corresponding author: kystian.machaj@ien.com.pl

investigation of the manufactured SOCs includes the assessment of current density-voltage curves (I-V) and electrochemical impedance spectra (EIS) in the temperature range of 650-700 °C in the rSOC mode. Also, the post-mortem analysis of the pristine and tested cells was performed using SEM and SEM-EDS technique.

Objectives

The main objective of the current study was to compare the performance and characterize the properties of cells that were sintered at various temperatures, ranging from 965 °C down to 925 °C, 900 °C, and 880 °C.

Results and Conclusions

The physical properties of the developed cells have been verified, indicating that the Cu-based oxides with a perovskite-related structure described in this study appear to be well-suited for solid oxide cell applications. The fuel electrode-supported cell with $SmBa_{0.5}Sr_{0.5}CoCuO_{5+\delta}$ as the air electrode sintered at 900°C achieved the current density at thermoneutral voltage ca. 0.4 A cm^{-2} in the SOE mode at 700°C while fueled with 10% H_2 and 90% H_2O (Fig. 1a). At the same temperature in the SOFC mode the same cell fueled with 50% H_2 and 50% H_2O 50% reached maximum power density ca. 150 mW cm^{-2}. The study concluded that cells sintered at 900°C have significantly lower ohmic and polarization (for 900° in range of 1.0-1.6 Ω in SOFC mode and for 925° in range of 2.0-4.5 Ω in SOFC mode, Fig 1b,c) due to minor or lack of migration of strontium and barium, comparing to the observed for electrode sintered at higher temperature (Fig. 1d-f).

a)

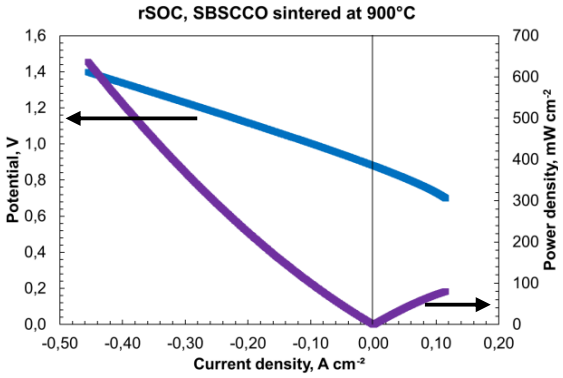

b)

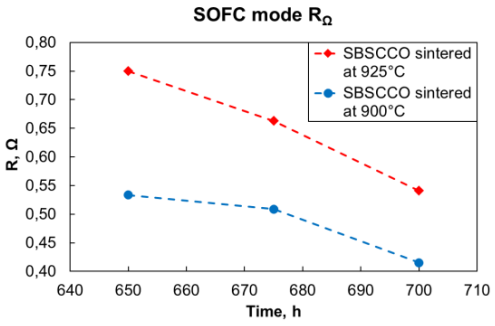

c)

d)

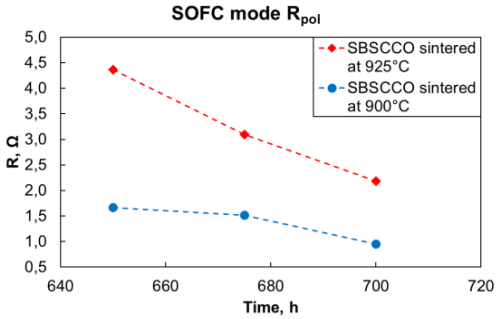

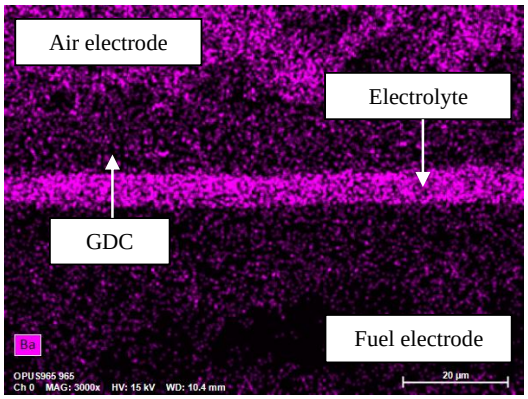

e)

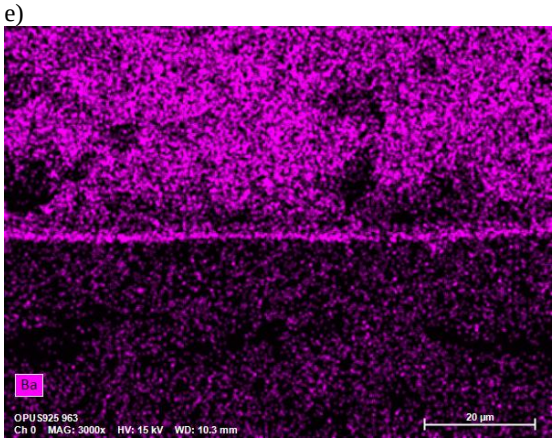

f)

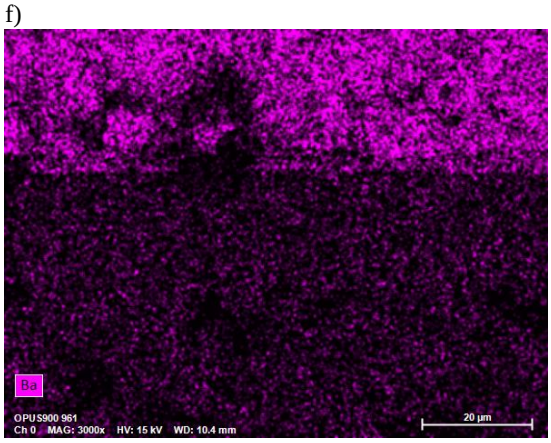

Figure 1. a) rSOC performance for SOFC sintered at 900°C and fueled with with 10% H_2 and 90% H_2O; b) ohmic resistance at SOFC mode for cells sintered at 925°C and 900°C; c) cell sintered at 965° cross-section SEM picture; d) cell sintered at 965°C cross-section map with marked barium; e) cell sintered at 925°C cross-section map with marked barium; f) cell sintered at 925°C cross-section map with marked barium for

Acknowledgment:

This project was financially supported by the National Science Centre, Poland, within project no. 2020/37/B/ST8/02097.

References:

[1] IRENA. Geopolitics of the energy transformation: the hydrogen factor. 2022.
[2] IRENA. Green hydrogen: A guide to policy making. 2020.
[3] Vinoth Kumar R et al., A review on recent progress and selection of cobalt-based cathode materials for low temperature-solid oxide fuel cells, Renewable and Sustainable Energy Reviews 2022;156, doi: 10.1016/j.rser.2021.111985
[4] European Commission. COMMITTEE AND THE COMMITTEE OF THE REGIONS Critical Raw Materials Resilience: Charting a Path towards greater Security and Sustainability 1. n.d.

Analysis of the impact of Multi-Layer Insulation (MLI) thermal degradation on the liquid Hydrogen tank pressurization in fire scenarios

D. Camplese*[1], G.E. Scarponi[1],R. Eberwein[2], F. Otremba[2], V. Cozzani[1]

[1] Alma Mater Studiorum - Università di Bologna, Department of Civil Chemical Environmental and Materials Engineering, via Terracini 28, 40131 Bologna, Italy

[2] Federal Institute for Materials Research and Testing - Bundesanstalt für Materialforschung und -prüfung (BAM), Berlin

Introduction

Hydrogen represents a promising alternative to fossil fuels in the ongoing energy transition [1]. Hydrogen-powered vehicles are already a reality, and their number is expected to increase considerably in the next decade. Among the possible solutions for storing hydrogen in such vehicles, cryogenic tanks with Multi-Layer Insulation (MLI) have emerged as one of the most effective to ensure a high volumetric energy density [2]. To guarantee the long-term preservation of cryogenic conditions and minimal boil-off rates, the heat leakage into cryogenic tanks must be minimized. For this purpose, several superinsulation systems such as vacuum combined with perlite, microspheres, or multi-layer Insulation (MLI) have been developed. MLI systems are composed of several layers of low-emissivity material (radiative layers) interleaved with high-free volume spacers. These are enclosed within the vessel's double-walled shell, working under high-vacuum conditions. The peculiarity of MLI systems is that they have the smallest volume requirement and lowest weight today [3]. However, the incoming widespread of hydrogen-based technologies brought attention to the potential risks related to the hydrogen's high flammability. The potential loss of integrity of this type of equipment might result in extremely dangerous events, such as BLEVEs and Fireballs. One potential scenario that could give rise to this situation is the exposure to an external heat source such as a fire triggered by a road accident. Despite the presence of superinsulation, fire testing outcomes suggest that cryogenic liquid hydrogen tanks fail in a relatively short time [4]. As demonstrated in the tests conducted by Eberwein et al. [5], this is due to the strong degradation of MLI at high temperatures, which leaves the tank unprotected against the fire heat flux. This phenomenon causes a rapid tank self-pressurization which can potentially culminate in the catastrophic failure of the equipment. In this sense, the availability of robust and accurate models to simulate the tank response is of paramount importance to ensure a safe design. For this purpose, several CFD and zone models were developed, which provide satisfactory results for both ambient and pressure tanks [6]. On the other hand, all the thermal models able to simulate the heat flux throughout the MLI (e.g., the one proposed by McIntosh [7]) were developed and validated for normal operative conditions only, not accounting for insulation performance deterioration at high temperatures. This study proposes an innovative modeling approach to simulate the thermal degradation of aluminum-based MLI, which can predict the loss in insulation performances of these systems when subjected to high temperatures as a result of fire exposure. The aim is to provide a tool that can be integrated into CFD and zone models for the simulation of the response of cryogenic liquid tanks to fire exposure. The impact of MLI degradation on the self-pressurization rate of cryogenic liquid hydrogen tank during fire attack is demonstrated through the application of the model to several case studies. Moreover, the study highlighted the influence of MLIs features on the rate of degradation and, consequently, tank self-pressurization.

* Corresponding author: davide.camplese@unibo.it

Methodology

The innovative MLI thermal degradation model proposed subdivides the tank into N+3 nodes, as schematized in Figure 1. Nodes 1 to N are assigned to the MLI radiative layers (one node per each), while nodes Se and Si represent the external and internal shells of the tank, respectively. Finally, liquid hydrogen thermal behaviour is represented by node L,with the aim of simulating the tank self-pressurization rate. The transient heat thermal balance (eq. 1 to 6 in Table 1) is solved for each node to obtain the temperature profile within the insulation system.

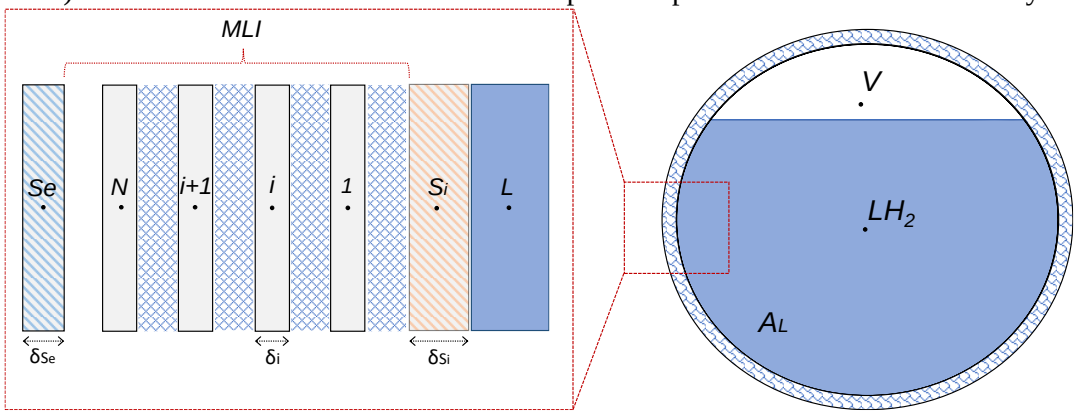

Figure 1. Thermal node schematization of the MLI system.

Table 1. Set of thermal balances used in the model.

Node	Variable	Equation	Eq. N°
Se	T_{Se}	$\delta_{S_e}\rho_{S_e}c_{p\_S_e}\frac{dT_{S_e}}{dt} = \varepsilon_{S_e}\sigma\left(T_{BB\_fire}^4 - T_{S_e}^4\right) - \frac{1}{\left(\frac{1}{\varepsilon_{S_e}}+\frac{1}{\varepsilon_N}-1\right)}\sigma\left(T_{S_e}^4 - T_N^4\right)$	(1)
N	T_N	$\delta_{rl}\rho_{rl}c_{p\_rl}\frac{dT_N}{dt} = \frac{1}{\left(\frac{1}{\varepsilon_{S_e}}+\frac{1}{\varepsilon_N}-1\right)}\sigma\left(T_{S_e}^4 - T_N^4\right) - \mathrm{q}_{rl}^N$	(2)
i	T_i	$\delta_{rl}\rho_{rl}c_{p\_rl}\frac{dT_i}{dt} = \mathrm{q}_{rl}^{i+1} - \mathrm{q}_{rl}^i$	(3)
1	T_1	$\delta_{rl}\rho_{rl}c_{p\_rl}\frac{dT_1}{dt} = \mathrm{q}_{rl}^2 - \mathrm{q}_{rl}^1$	(4)
Si	T_{Si}	$\delta_{S_i}\rho_{S_i}c_{p\_S_i}\frac{dT_{S_i}}{dt} = \mathrm{q}_{rl}^1 - h_L\left(T_{S_i} - T_L\right)$	(5)
L	T_L	$m_L c_{p\_L}\frac{dT_L}{dt} = A_L h_L\left(T_{S_i} - T_L\right)$	(6)
-	P	$P = P^*(T_L)$	(7)

The balance equations in Table 1 assume heat transfer occurs only in the direction normal to the surface of the layer, resulting in a one-dimensional approach. The heat flux between any adjacent layer is expressed according to the classical "layer by layer" model proposed by McIntosh [7], in which three mechanisms of heat transfer contribute to the total heat flux: the thermal radiation between each layer (q_{rad}, eq. 8), the solid conduction ($q_{s,cond}$, eq. 9) and the gas conduction through the spacer ($q_{g,cond}$, eq. 10). Thus, the total heat flux from the i-th radiative layer to the (i-1)-th one is calculated according to eq. 11.

$$q_{rad}^i = \frac{\sigma}{\left(\frac{1}{\varepsilon_i}+\frac{1}{\varepsilon_{i-1}}-1\right)}\left(T_i^4 - T_{i-1}^4\right) \quad (8)$$

$$q_{s,cond}^i = \frac{C_2 f k_s}{D_x}\left(T_i - T_{i-1}\right) \quad (9)$$

$$q^i_{g,cond} = C_1 P_r \theta (T_i - T_{i-1}) \quad (10)$$

$$q^i_{rl} = q^i_{rad} + q^i_{s,cond} + q^i_{g,cond} \quad (11)$$

The same form of the thermal balance is used for each radiative layer, except for the 1-st and the N-th ones asthese face the inner and outer shells, respectively. Since the model assumes the 1-st radiative layer is separated from the inner shell by a single spacer, the thermal balance in node 1 (eq. 5 in Table 1) has to consider the inner shell surface emissivity at one side. On the contrary, only high-vacuum is present between the N-th and the S_e nodes, thus the heat between the external shell and the N-th radiative layer is assumed to be transferred by radiation only in eq. 2. The novelty with respect to the McIntosh model is that the high-temperature degradation of the MLI is considered by assuming that each layer is destroyed when its temperature reaches the melting point of the material (here defined as the degradation temperature, T_{deg}). It is assumed that, when the i-th layer melts, it loses its shape, leaving the underlying layer unprotected. For simplicity, each layer is considered to be entirely and instantaneously destroyed as soon as T_{deg} is exceeded. From the numerical point of view, this behavior is simulated by replacing both the i-th radiative layer and the i-th spacer with a vacuum space of the same thickness. In this way, only radiative heat transfer is considered to take place between the first undamaged layer and the external shell. This procedure allows for reproducing the gradual deterioration of the MLI system with time. The fire scenario is simulated by assuming constant thermal radiation from a constant black body temperature (T_{BB_fire}). Stefan-Boltzmann law is used to calculate the heat fire heat flux entering the shell of the tank is calculated in eq. 1 (Table 1). The tank pressure is assumed to match the saturation pressure (see Eq. 7 in Table 1) at the liquid temperature (T_L), which is obtained from the energy balance to the liquid node (see eq. 6 in Table 1). The nucleate boiling heat transfer coefficient (h_L) is calculated according to Ray [8], assuming the liquid is saturated. Liquid and vapor phases are considered to be in thermodynamic equilibrium and, thus, share the same temperature and pressure. For this reason, the thermal balance for the vapor phase is not solved.

Case study

The proposed aluminum-based MLI degradation model is applied to a typical storage tank used for cryogenic hydrogen-powered vehicles. This is a 0.31 m^3 horizontal cylindrical tank with a length of 1.2 m and an inner diameter of 0.6 m. 80 % of the volume capacity is filled with saturated liquid hydrogen at ambient pressure (T_L = -252.75 °C [9]). Tank materials properties are listed in Table 2 and are assumed constant during the simulation.

Table 2. Properties of the tank's materials.

Property	Symbol	Unit	Tank lading	External shell	Internal shell
Material/Compounds	-	-	Liquid hydrogen	AISI-304	AISI 316L
Density	ρ	kg/m^3	70.9*	7800	7900
Thermal Conductivity	k	W/(m·K)	-	16	15
Heat capacity	cp	J/(kg·K)	9800*	490	500
Emissivity	ε	-		0.9	0.275
Thickness	δ_{Se}/ δ_{Si}	m	-	0.003	0.01

* NIST, NIST Chemistry WebBook [9]

The tank features a typical commercial uniform-density aluminum-based MLI, whose properties are listed in Table 3. The degradation temperature (Tdeg) was set to 660 °C, which is the melting point temperature of the aluminum. The fire scenario considered is a fully engulfing hydrocarbon pool fire for which is assumed a fire black body temperature (T_{BB_fire})

of 871 °C [10]. A set of five case studies is defined to evaluate the influence of MLI presence and degradation on the tank self-pressurization during fire scenarios. In cases A, B and C the MLI degradation model is applied as previously described for a tank featuring the abovementioned MLI. These cases only differ for the number of radiative layers assumed. Specifically, 10, 40, and 80 layers are chosen for cases A, B and C, respectively. These are representative of the number of layers commonly applied for cryogenic tank superinsulation. Such cases are compared to investigate the influence of the radiative layers number on the time of degradation of the MLI, and, consequently, into the self-pressurization rate of the tank in case of fire exposure. Then, two additional cases are also introduced (cases D and E). In case D it is assumed the MLI is never affected by thermal decomposition during fire exposure (even in the case T_i exceeds T_{deg}), in fact keeping all radiative layers intact. In case E the MLI is not present and only high vacuum is considered between the two shells. Table 4 summarizes the simulations performed.

Table 3. MLI material properties.

Property	**Symbol**	**Unit**	**Radiative layer**	**Spacer**
Material	-	-	Aluminum	Glass fiber fleece
Thickness	δ_{rl}/D_x	m	$9\cdot10^{-6}$	$7\cdot10^{-4}$
Density	ρ	kg/m^3	2700	2500*
Thermal Conductivity	k	W/(m·K)	250	0.8*
Heat capacity	c_p	J/(kg·K)	900	-
Relative density	f	-	-	0.017
Emissivity	ε	-	0.04	-
Spacer empirical factor	C_2	-	-	0.0025
Residual gas pressure**	P_r	Pa	$1\cdot10^{-4}$	$1\cdot10^{-4}$

*solid material properties

**air is assumed as residual gas within the MLI

Table 4. List of case studies.

Case study	**Description**	**Nr. of radiative layers**
A	MLI degradation on	10
B	MLI degradation on	40
C	MLI degradation on	80
D	NO MLI degradation	10
E	NO MLI presence in the vacuum chamber	-

In all the cases, the initial temperature profile in each node is set as the steady-state solution obtained considering constant boundary temperatures: a liquid temperature of -252.75 °C (i.e., the saturation temperature of hydrogen at atmospheric pressure) and an outer shell temperature of 25 °C (ambient temperature). This is representative of the system condition prior to fire exposure.

Result and Discussion

The transient temperature evolution within the insulation system and the heat flux through the inner shell of the tank (q_{Si}) obtained for case A are illustrated in Figure 2a. Similar results were obtained for cases B and C, which are omitted for the sake of brevity. The dashed red line depicts the temperature of the external wall (T_{Se}). Starting from the initial value, T_{Se} rapidly approaches the fire temperature. As a result, the temperature of the MLI layer facing the external shell (T_{10}) starts to rise until it reaches T_{deg}. At this point, the layer is degraded and

removed from the simulation. The underneath layers (solid lines) are affected by the external shell temperature increase with a delay that is longer the further the layer is from the fire. It is worth noticing that, apart from the outermost layer, the rate of temperature increment of each radiative layer rises sharply as soon as the overlying layer is destroyed.

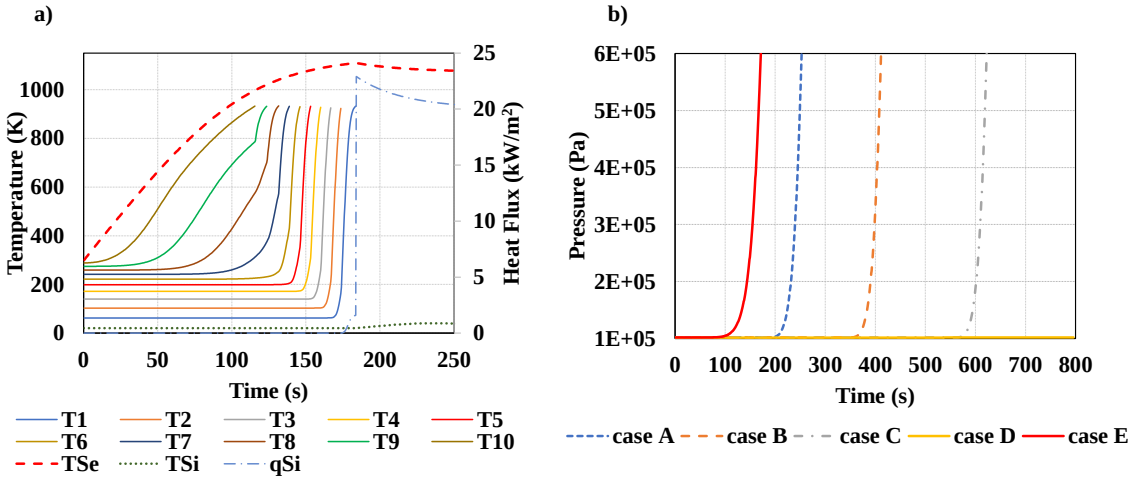

Figure 2. Modeling results of the case studies; (a) transient temperature behavior (primary axis) within MLI and heat flux (secondary axis) through the inner wall of the tank (q_{Si}) for case A; (b) self-pressurization curves of the case studies.

In fact, when the i-th layer vanishes, the (i-1)-th one is suddenly subjected to a significant heat flux coming from the heated external surface. This phenomenon progresses until all the layers are destroyed. In case A, this occurs after 184 s of fire exposure. The dash-dotted blue line depicts the heat flux through the inner wall of the tank. Its value remains close to zero until the temperature of the layer facing the inner shell (T_1) starts to rise, when a slight increase up to 1.6 kW/m^2 is observed. Then, when layer 1 degrades, the inner shell is directly exposed to the hot external wall, and this results in an abrupt increase of the heat flux (up to 23 kW/ m^2). From this moment onwards, the temperature of the inner shell (dotted green line) starts to rise from the steady state value. Since T_{Si} directly affects the heat flow entering the liquid phase (eq. 6 in Table 1), this means that the temperature of the tank lading does not change from the initial value until the entire MLI is destroyed. This demonstrates the protective effect of the MLI on tank lading in terms of delaying the temperature and, consequently, the pressure rise of the liquid hydrogen.

This is also clearly visible by looking at the self-pressurization curves shown in Figure 2b. When the MLI is not in place (case E), the pressure within the tank starts to rise after 100 s as a consequence of the direct exposure to fire heat flux. On the contrary, when the MLI degradation is not considered (case D), the pressure increase over the simulation range is negligible. Such a result is not realistic since it is in contrast with experimental evidences [4]. Regarding the cases in which the MLI degradation is modeled (cases A, B, and C), the pressure trend is similar to case E, but the self-pressurization occurs only once the MLI is completely degraded, resulting in a significant delay with respect to the case in which MLI is not present. Such a delay is the larger the higher the number of layers of the MLI. This behavior is explained by the fact that the total degradation time (t_{td}) increases significantly with the number of layers. For instance, t_{td} varies from 184 s for case A (10 layers) to 560 s for case C (80 layers). Therefore, the MLI presence protects the liquid from the fire “heat wave” until complete degradation occurs, resulting in a delayed pressure growth when compared to scenarios involving tanks not equipped with MLI. These outcomes are also in agreement with what was observed by Eberwein et al. [5]. Moreover, model results suggest that a larger number of layers

should be preferred when designing the MLI system featuring cryogenic liquid hydrogen tanks, since this guarantees longer protection during fire exposure.

Conclusions

The aim of this study was to develop an innovative heat transfer model for aluminum-based MLI under fire exposure conditions in order to investigate the effect of MLI degradation on the pressure build-up within cryogenic liquid hydrogen tanks. The model takes into account the MLI degradation by assuming that a layer is destroyed when it reaches its melting point. The results obtained from the application of such an approach to a realistic case study demonstrate the strong effect of the insulation system degradation on the tank pressurization in fire scenarios. Although by increasing the number of radiative layers of the MLI the self-pressurization of the tank can be significantly delayed, the response to the fire exposure is similar to the one of an unprotected tanks rather than one with an intact insulation system. In fact, in case of MLI deterioration, the insulation system failed within a few minutes, resulting in rapid self-pressurization of the tank. This suggests that further research should be devoted to improving the fire resistance of these systems.

It is worth remarking that the proposed approach assumes a quite simple MLI degradation mechanism, which requires further investigation. However, the analysis of the case studies underscores the necessity of developing models aimed at simulating the response of liquid hydrogen tanks to fire exposure with due consideration to the phenomenon of insulation system degradation. The same is true for manufacturers and regulators willing to ensure the safe design and operation of liquid hydrogen tanks.

References

[1] P. Preuster, A. Alekseev, and P. Wasserscheid, “Hydrogen Storage Technologies for Future Energy Systems,” Annu. Rev. Chem. Biomol. Eng., vol. 8, no. 1, pp. 445–471, Jun. 2017

[2] K. Kunze and O. Kircher, “Cryo-compressed hydrogen storage cryogenic cluster day,” Oxford, Sept., vol. 28, p. 2012, 2012.

[3] L. Edward and L. Filip, “Influence of vacuum level on insulation thermal performance for LNG cryogenic road tankers,” in MATEC Web of Conferences, 2018, vol. 240, p. 1019.

[4] K. Pehr, “Experimental Examinations on the Worst Case Behavior of LH2/LNG Tanks for Passenger Cars,” in Proceedings of the 11th World Hydrogen Energy Conference, Stuttgart, Germany, 1996, pp. 2169–2186.

[5] R. Eberwein, A. Hajhariri, D. Camplese, G. E. Scarponi, V. Cozzani, and F. Otremba, “Insulation materials used in tanks for the storage of cryogenic fluids in fire scenarios,” 2023.

[6] G. E. Scarponi, I. Bradley, G. Landucci, A. M. Birk, and V. Cozzani, “Modelling Pressure Tanks under Fire Exposure: Past Experience, Current Challenges and Future Perspectives,” Chem. Eng. Trans., vol. 90, no. December 2021, pp. 481–486, 2022,

[7] G. E. McIntosh, “Layer by Layer MLI Calculation Using a Separated Mode Equation,” in Advances in Cryogenic Engineering, P. Kittel, Ed. Boston, MA: Springer US, 1994, pp. 1683–1690.

[8] M. S. Ray, “Coulson and Richardson’s Chemical Engineering Volume 6 (Design), by RK Sinnott, Pergamon Press, Oxford, UK (1993). 954 pages. ISBN 0‐08‐041865‐1.” Wiley Online Library, 1994.

[9] NIST, “NIST Chemistry WebBook 69, National Institute for Standards and Technology,” 2019. https://webbook.nist.gov/chemistry/ (accessed Jul. 11, 2023).

[10] C. Anderson, W. Townsend, J. Zook, and G. Cowgill, “The effects of a fire environment on a rail tank car filled with LPG,” 1974.

Assessment of degradation effects of intermittent supply in PEM electrolyzers

D. Botana-Vilanova [*1], P. Ferreira-Aparicio[1], A. Fuerte [1]

[1] CIEMAT, Center for Energy, Environment and Technology Research. Av. Complutense 40. E28040. Madrid. Spain

Introduction

The extensive consumption of fossil fuels in recent decades and up today has caused many environmental problems. The development of technologies to promote the use of clean and renewable energies able to replace fossil fuels has become an urgent issue with the aim of reducing greenhouse gas emissions and achieving carbon neutrality by 2050[1, 2].

Renewable energy sources like wind or solar energies depend on the weather with a naturally intermittent character and highly uneven spatial distribution. Besides, it is not possible to synchronize energy production with demand, so there will be moments when demand cannot meet supply and others where excess production is wasted [3].

Due to this, it is interesting to have mechanisms to store energy at production peaks, energy that can be returned to the electrical grid at times of high demand. The electric power generated by renewable energy can be stored in different ways, one of them using energy carriers like hydrogen.

Water electrolysis is, from a sustainability point of view, one of the best practical methods for hydrogen production on a large scale [4].

Depending on the electrolyte, operating temperatures and ionic transport, electrochemical water splitting (EWS) can be divided in different categories: alkaline water electrolysis (AWE), proton exchange membrane water electrolysis (PEM or PEMWE), anion exchange membrane water electrolysis (AEMWE) and high temperature water electrolysis in solid oxide cells (SOEL) [5, 6].

From the previous categories, PEM electrolysis is one of the most suitable options for its integration with intermittent energy sources. The core of a PEM electrolyzer includes the following components: bipolar plates, porous transport layers and a membrane-electrode assembly. The electrolyte is the polymer membrane separating both electrodes and allowing the pass of protons from one electrode to the other. In most cases, the catalyst layers are deposited on each side of the membrane forming the key component of the cell: the membrane-electrode assembly (MEA). Two porous transport layers (PTL), also called gas diffusion layers (GDL), are sandwiched on both sides of the MEA helping the passage of water and gases to the MEA. Two bipolar plates (BPs), also called flow-field plates, encapsulate the rest of components facilitating transfer of charge, mass, heat and establish contact to the external power supply [5, 7].

The main advantages of a PEM electrolyzer are operation at high current density, high purity hydrogen production, ability to work under a wide range of input power and a compact system design in which high operation pressures are achievable [6, 8].

* Corresponding author: David.Botana@ciemat.es

Some negative aspects are that PEM systems require expensive materials, like precious metals in electrodes or titanium in current collectors and separator plates. In addition, all components of the stack suffer from corrosion problems to a lesser or greater extent due to the combination of acidic regime and the high applied overvoltage.

There are also additional problems derived from its combination with intermittent energy sources. Intermittent renewable energies rarely satisfy the operation requirements of these systems, since they are compelled to operate under a wide fluctuating power range. This will lead repeatedly changes of the electrolyzer temperature and current density from low to high under fluctuating power operation. These changes could contribute to fast degradation of its components.

Furthermore, when an electrolyzer works at low power, the rates at which hydrogen and oxygen are produced (which are proportional to current density) may be lower than the rate at which these gases permeate through electrolyte, and mix with each other. This may create hazardous conditions inside the electrolyzer due the flammability of hydrogen in oxygen. Hydrogen flammability limits in oxygen range from 4.6 vol. % to 93.9 vol. % [1, 2, 9].

The scaling up and bundling of generation plants contribute to largely mitigate the effects of intermittency [2]. There are various strategies to minimize the inconveniences of associating an electrolyzer with a renewable energy source. A possibility for enhancing their durability consists in protecting the electrodes by applying an arbitrary low protection current during shutdown, with the drawback that this solution requires additional power supply [10].

Other type of strategies focus on modifying the material components of the different parts of the electrolyzer with the objectives of making the cost of the stack cheaper, increasing the mechanical and chemical resistance, making corrosion and degradation more difficult, and reducing the permeability of hydrogen through the electrolyte. This approach includes electrodes, the electrolyte, porous transport layers and flow-field and collector plates.

In the case of electrodes, the best strategies are trying to reduce the amount of precious or rare metals necessary, usually Ir or Ru for the anode and Pt for the cathode. Various nanostructures have been proposed to reduce the necessary load of said metals. Alloys of these materials with cheaper metals have also been tested. Diverse attempts have been made to completely dispense precious metals, but, in general, they have had durability problems [5, 6, 8].

These strategies go through two possibilities in the case of the polymeric membrane. The first is continuing with perfluorosulfonic acid (PFSA) type membranes, but improving its behavior through changes in its microstructure or incorporation of diverse fillers: i.e. nanofillers or nanofibers. The second strategy is to replace PFSA membranes with hydrocarbon membranes, which generally have lower hydrogen permeation, but have degradation problems. In both types of membranes, various copolymers are also tested [11–14].

In the case of PTLs, a fundamental factor is the optimization of porosity; high porosity favors the flow of water and gases but decreases the transport of electrons, low porosity reverses the previous effects. On the other hand, the most used material is titanium, which, although it has reasonable resistance to corrosion, is not immune to it, suffering from passivation problems; various coatings are being studied to improve its behavior. Titanium is also used for BP. It presents corrosion problems especially on the anode side, where a surface layer of oxide that increases resistance and thermal conductivity is usually developed. On the cathode side, the presence of hydrogen tends to weaken it. Diverse coatings and cheaper materials such as stainless steel, aluminum or graphite (only for the cathode side) have been investigated as improvement strategies.

The main objective of the research of this work is focused on this last strategy of improving materials and components to increase the durability of PEM electrolyzers operated with intermittent power supply. In a first approach, a commercial single cell PEM electrolyzer will be operated under transitory regimes with variable operation conditions to analyze its behavior. The degradation effects originated by these conditions in the main components will be evaluated.

Initial approach and methodology

The objective of this work is studying the coupling of a PEM type electrolyzer to renewable energy sources, especially wind turbines, and trying to minimize the problems associated with the characteristic intermittency of this kind of energy sources.
To do this, a stack with state-of-the-art components is being evaluated under stationary and transient operation condition in order to study the problems that may arise when it is associated with intermittent energy sources.
For this, different tests are being carried out. In all tests, measurement of voltage and current along with time is required. It would be appropriate to measure other variables such as hydrogen generation, pressure and temperature in order to collect as much information as possible.[15]

1) Start-up test up to nominal power of the electrolyzer.

The objective of the test is acquiring the voltage and current profiles as a function of time, in a start-up under different conditions, until reaching the permanent regime at nominal power. There are two different tests within this category:
1a) Cold start test. The cold start test refers to the initial operation when the device or system is at ambient temperature and pressure. The purpose is determining the period required until the nominal power is reached. At the beginingt of this test, the electrolyzer must have been at complete stop for at least 2 hours at room temperature and pressure. Then, it is turned on and set at the nominal power waiting until reaching the permanent regime at nominal power.
1b) Start-up test from standby conditions. At the beginning of this test, the system must be in standby conditions for at least 1 hour. Then, a nominal power reference is applied, registering the parameters until reaching the permanent regime at nominal power.

2) Stop test from nominal power.

This test aims to know the response of the electrolyzer to a sudden stop from its nominal power. For that, we bring the electrolyzer up to nominal power keeping it for at least one hour in these conditions. Then, we disconnect the source or bring the current to zero waiting for hydrogen production drop to zero.

3) Voltage gap tests.

The objective of the test is determining the response of the electrolyzer to voltage gaps. To do this, the power supply is inhibited for different periods of time and reconnected after these periods. Initially, the electrolyzer is mantained at nominal power for at least 15 minutes. Then, the power supply is disconnected for a variable period of time (1s -5s -30s -60s) and hereunder reconnected again.

4) Current gap tests.

The test consists of lowering the current setpoint in steps to 75%-50%-25%-0% of the maximum available for 60 seconds and returning to the maximum to watch the response of the electrolyzer to current gaps. To do it, the electrolyzer is keeping at maximum current for at least 15 minutes and then the current setpoints are varied for a period of time of 60 seconds returning to 100% of maximum current between each change. The Figure 1 shows the expected behavior:

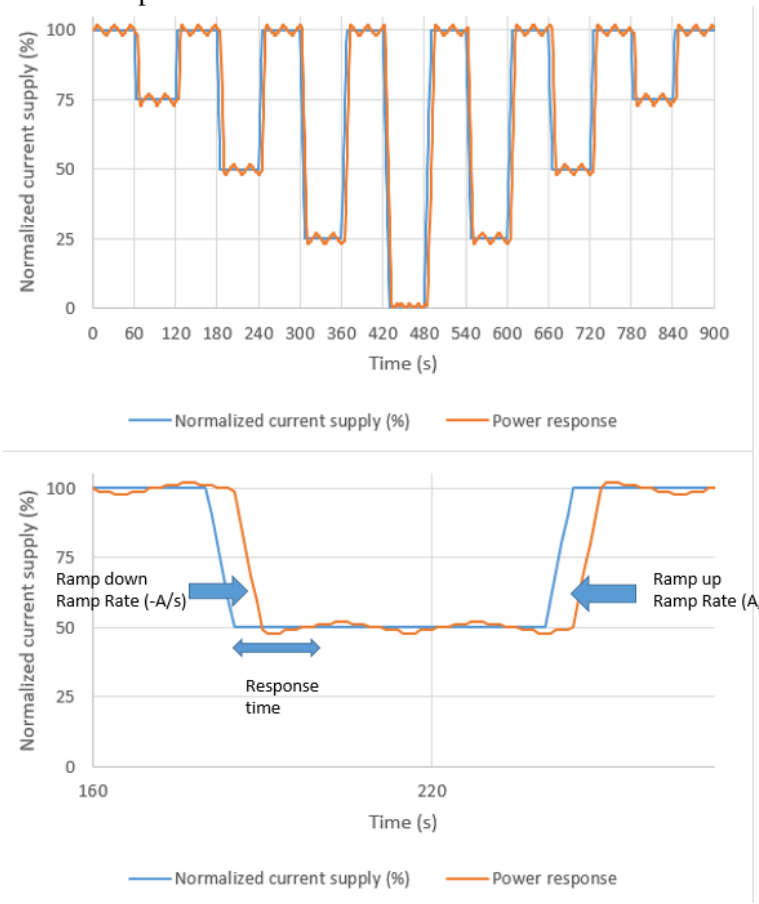

Figure 1. Current gap tests, whole figure (top) and part (below).

5) Tests with steps and current ramps.

The test aims to analyze the dynamic response of the electrolyzer to current steps of different magnitude. It consists of giving slogans of current steps until reaching the permanent regime. From this test, it is possible to make an electrical dynamic model of the electrolyzer [16]. For that, it is necessary to have the electrolyzer in standby state and then give current setpoints in steps (25% - 50% - 75% - 100%) to reach the permanent regime in each setpoint, waiting after that 2 minutes in steady state before moving to the next stage.

6) Tests with a variable electricity generation profile.

The objective of this test is to evaluate the response of the electrolyzer to variable generation (imitating wind production) for a considerable time. The profile data provided for the Figure 2 is taken from the real data of the NED100 wind turbine of the CIEMAT.

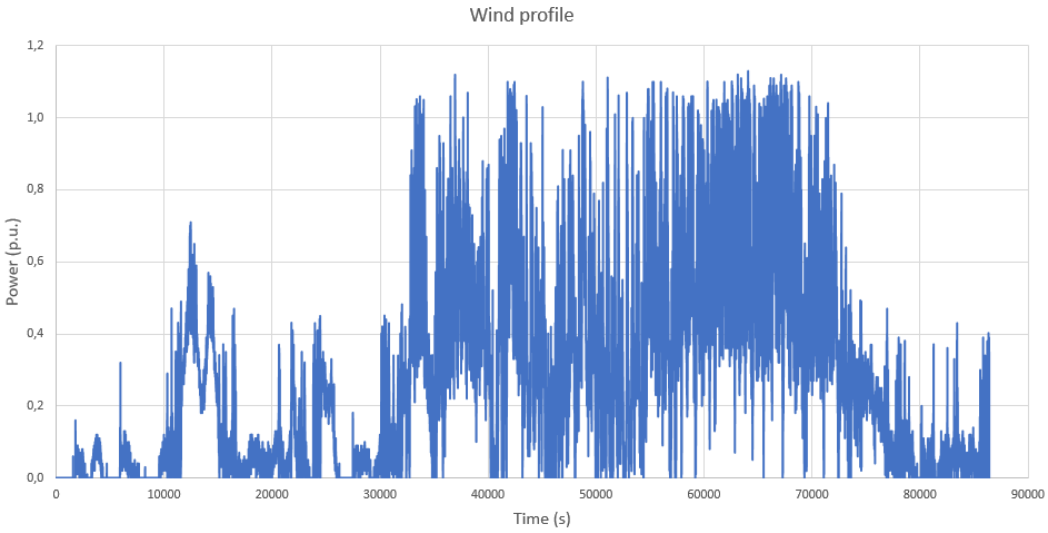

Figure 2. Test with a variable electricity generation profile.

Conclusions

According to the proposed methodology, a single cell electrolyzer is being analyzed after operation under stationary and transient regimes. The postmortem analysis after reducing their performance is expected to provide valuable information about the main deactivation processes reducing the durability of the systems. This study is key to introduce adequate strategies to improve the useful life of components and systems.

References

[1] F. Barbir, "PEM electrolysis for production of hydrogen from renewable energy sources," *Solar Energy*, vol. 78, no. 5, pp. 661–669, May 2005, doi: 10.1016/j.solener.2004.09.003.

[2] H. Kojima, K. Nagasawa, N. Todoroki, Y. Ito, T. Matsui, and R. Nakajima, "Influence of renewable energy power fluctuations on water electrolysis for green hydrogen production," *International Journal of Hydrogen Energy*, vol. 48, no. 12. Elsevier Ltd, pp. 4572–4593, Feb. 08, 2023. doi: 10.1016/j.ijhydene.2022.11.018.

[3] A. Mohammadi and M. Mehrpooya, "A comprehensive review on coupling different types of electrolyzer to renewable energy sources," *Energy*, vol. 158, pp. 632–655, Sep. 2018, doi: 10.1016/j.energy.2018.06.073.

[4] K. Bareiß, C. de la Rua, M. Möckl, and T. Hamacher, "Life cycle assessment of hydrogen from proton exchange membrane water electrolysis in future energy systems," *Appl Energy*, vol. 237, pp. 862–872, Mar. 2019, doi: 10.1016/j.apenergy.2019.01.001.

[5] K. Zhang *et al.*, "Status and perspectives of key materials for PEM electrolyzer," *Nano Research Energy*, vol. 1, no. 3. Tsinghua University Press, Dec. 01, 2022. doi: 10.26599/NRE.2022.9120032.

[6] Y. Chen *et al.*, "Key Components and Design Strategy for a Proton Exchange Membrane Water Electrolyzer," *Small Struct*, vol. 4, no. 6, Jun. 2023, doi: 10.1002/sstr.202200130.

[7] G. Bin Jung, S. H. Chan, C. J. Lai, C. C. Yeh, and J. W. Yu, "Innovative membrane electrode assembly (MEA) fabrication for proton exchange membrane water electrolysis," *Energies (Basel)*, vol. 12, no. 21, Nov. 2019, doi: 10.3390/en12214218.

[8] M. Carmo, D. L. Fritz, J. Mergel, and D. Stolten, "A comprehensive review on PEM water electrolysis," *International Journal of Hydrogen Energy*, vol. 38, no. 12. pp. 4901–4934, Apr. 22, 2013. doi: 10.1016/j.ijhydene.2013.01.151.

[9] M. N. I. Salehmin, T. Husaini, J. Goh, and A. B. Sulong, “High-pressure PEM water electrolyser: A review on challenges and mitigation strategies towards green and low-cost hydrogen production,” *Energy Conversion and Management*, vol. 268. Elsevier Ltd, Sep. 15, 2022. doi: 10.1016/j.enconman.2022.115985.

[10] J. Divisek, J. Mergel, and H. Schmitz, “ADVANCED WATER ELECTROLYSIS AND CATALYST STABILITY UNDER DISCONTINUOUS OPERATION,” 1990.

[11] H. R. Corti, “Polymer electrolytes for low and high temperature PEM electrolyzers,” *Current Opinion in Electrochemistry*, vol. 36. Elsevier B.V., Dec. 01, 2022. doi: 10.1016/j.coelec.2022.101109.

[12] E. J. Park, C. G. Arges, H. Xu, and Y. S. Kim, “Membrane Strategies for Water Electrolysis,” *ACS Energy Letters*, vol. 7, no. 10. American Chemical Society, pp. 3447–3457, Oct. 14, 2022. doi: 10.1021/acsenergylett.2c01609.

[13] S. Adhikari, M. K. Pagels, J. Y. Jeon, and C. Bae, “Ionomers for electrochemical energy conversion & storage technologies,” *Polymer (Guildf)*, vol. 211, Dec. 2020, doi: 10.1016/j.polymer.2020.123080.

[14] H. Nguyen, C. Klose, L. Metzler, S. Vierrath, and M. Breitwieser, “Fully Hydrocarbon Membrane Electrode Assemblies for Proton Exchange Membrane Fuel Cells and Electrolyzers: An Engineering Perspective,” *Advanced Energy Materials*, vol. 12, no. 12. John Wiley and Sons Inc, Mar. 01, 2022. doi: 10.1002/aenm.202103559.

[15] G. Tsotridis and A. Pilenga, “EU harmonised protocols for testing of low temperature water electrolysers,” 2021. doi: 10.2760/58880.

[16] D. Guilbert and G. Vitale, “Dynamic emulation of a PEM electrolyzer by time constant based exponential model,” *Energies (Basel)*, vol. 12, no. 4, Feb. 2019, doi: 10.3390/en12040750.

Behavior of a low-temperature electrolysis technologies under intermittent operation: analysis of the impacts and mitigation strategies

E. Nguyen[1 2*], P. Olivier[1], MC. Pera[2], E. Pahon[3], R. Roche[2]

[1] Engie Lab CRIGEN, 4 rue Joséphine Baker, 93240 Stains, France
[2] Université de Franche-Comté, CNRS, institut FEMTO-ST, FCLAB, F-90000 Belfort, France
[3]UTBM, CNRS, institut FEMTO-ST, FCLAB, F-90000 Belfort, France

Introduction

In recent years, the incorporation of renewable energies into electrolysis systems has been attracting increasing attention from both the scientific community and major industrial stakeholders. This growing interest arises from their critical role in facilitating the shift towards low-carbon and sustainable hydrogen production. Nevertheless, the intermittent nature of renewable energy sources introduces complexity into this integration, affecting various key performance indicators of electrolysis systems [1]. Despite the significant lack of research in this area, especially at industrial scales, there is a prevailing literature consensus that intermittency exerts a substantial impact on the performance of electrolyzers across all levels of system operation [2]–[4]. The analysis and optimization of such intermittent operation are therefore critical steps towards a deeper understanding of the challenges linked to the integration of renewable energies as power sources for electrolysis systems.

This work focuses on the development of tools based on experimental work and modeling to achieve a twofold objective of gaining further insight into the impacts of intermittency on the performance of a 55 kW proton exchange membrane (PEM) electrolyzer and proposing solutions for their mitigation.

Methodology

A test campaign was conducted on a 55 kW PEM electrolyzer to gather preliminary information about the actual system performance when operating under intermittent conditions. In addition, a 0D performance model has been developed in order to simulate its operation of under various load scenarios. Simulation results have been fitted to the experimental polarization curve recorded from the electrolyzer plant. This preliminary step towards model validation is presented in this paper.

1. Experimental tests

The experimental tests were performed on a 55 kW PEM electrolyzer manufactured by ELOGEN. The system consists of a single cylindrical stack made of 48 cells, 600 cm² each, connected in series using bipolar plates. The plant is able to produce 10 Nm^3/h of hydrogen at a nominal current density of 0.8 A/cm^2 and can operate at partial loads ranging from 10% to 100% of its nominal capacity. The Balance-of-Plant (BoP) is divided into two primary areas. The process area is equipped with a multitude of components including purification, cooling

* Corresponding author: emma.nguyen@engie.com

and conditioning units. In this section, an array of regulation loops and sensors is integrated to control the main operation parameters such as temperature, pressure, liquid levels, and gas composition, and to ensure safe operations. Additionally, a utilities area dedicated to electrical units, most notably the AC/DC rectifier, which plays a crucial role in electrical distribution and system power management, is integrated to the system. This area also houses water purification and cooling units. Figure 1 provides an overview of the process flow diagram of the electrolyzer.

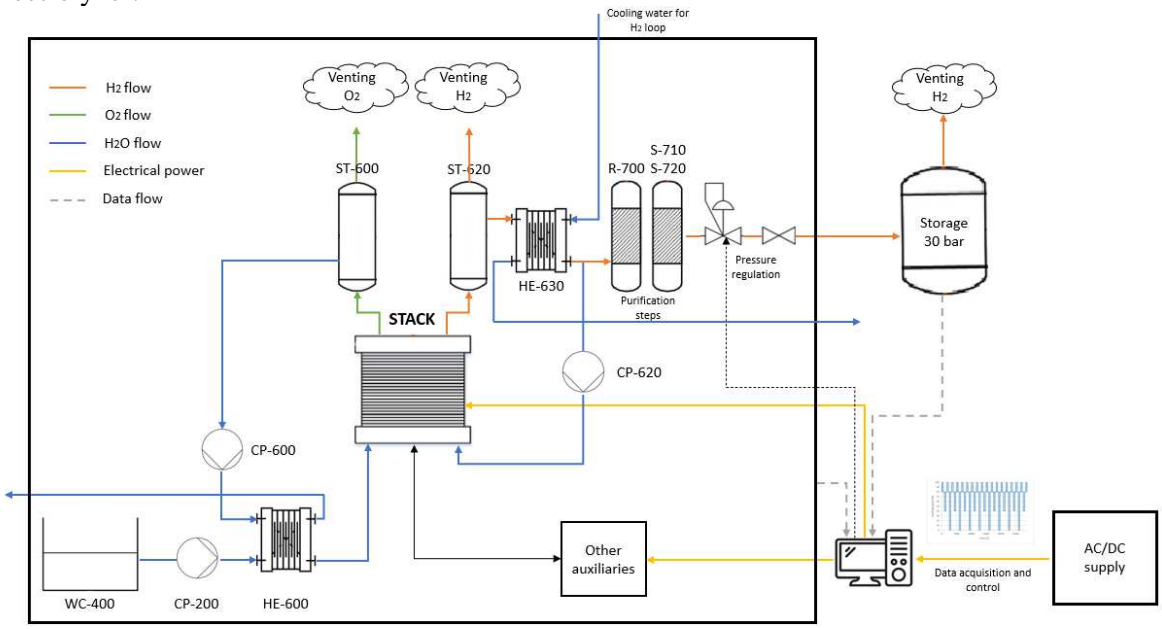

Figure 1: Simplified Process Flow Diagram (PFD) of the electrolyzer

Specifications	ELYTE10
Nominal power (kW)	55
Nominal H_2 flow rate (Nm^3/h)	10
Load range (%)	10 – 100
Max ramp-up (A/s)	10
Stack specific consumption (kWh/Nm^3H_2)	4.3
System specific consumption (kWh/Nm^3H_2)	5.4
Nominal temperature (°C)	63 – 66
H_2 pressure (bar)	30

Table 1: Electrolyzer manufacturer specifications (model ELYTE10 from ELOGEN)

The objectives of the test campaign were twofold. The first one was to establish a solid experimental database regarding the electrolyzer performance under nominal conditions (P=55 kW, T=65°C). This dataset serves a dual purpose: as a benchmark for comparison with other tests and as a means to validate a performance model. The second objective was to test various types of dynamic power profiles based on grid services and renewable energies, in order to quantify the impacts of intermittency on the most relevant performance indicators of the system.

2. Modeling

A lumped and homogeneous 0D approach has been adopted to develop a multiphysic model of the PEM electrolyzer. The main model specificity lies on its ability to estimate the electrolyzer performance and behavior across diverse load scenarios, thereby promoting the incorporation

of renewable and intermittent energy sources, and its scalability to larger-scale electrolyzers. A semi-empirical approach, mostly based on analytical equations and existing works [4]–[7] has been applied to describe the physical behavior of the electrolyzer. At the system level, all Balance-of-Plant components including control loops have been designed in accordance with the manufacturer specifications. At a lower level, three submodels have been developed to capture the fluidic, electrochemical and thermal behavior of the stack. Figure 2 offers a deeper insight into the model structure, the input and output flows of each block, and how they interact with each other.

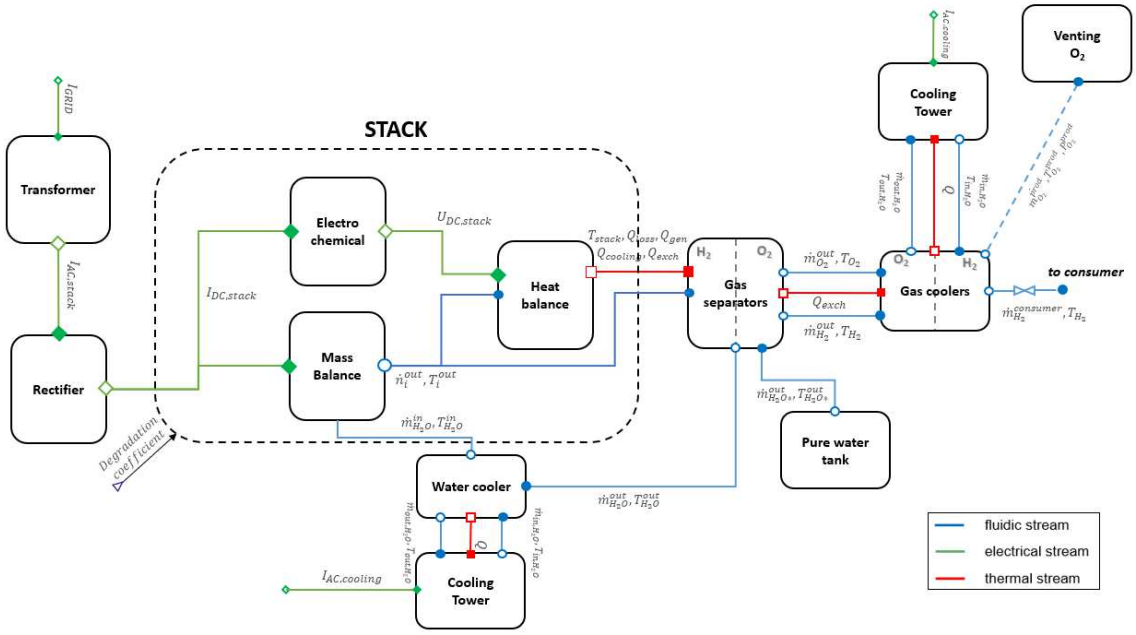

Figure 2: Model Flow Diagram (MFD)

The main assumptions are detailed below:

- Pressure drops are assumed to be low enough to be neglected;
- Temperature distribution is assumed to be uniform within the stack;
- Mass transfers and electrochemical and thermal behavior are assumed to be similar in each cell;
- Diffusion overpotentials are considered negligible at high current densities;
- Two-phase flow issues related to bubble coverage are neglected for the two following reasons: (i) they mainly impact performances at high current densities, (ii) the accurate description of such two-phase issues requires to take into account both time and spatial variations;
- The electrical dynamics of the system are considered to be fast enough to not be taken into account.

Results and discussion

1. Model validation

The analytical equation employed to model the polarization curve has been fitted based on the experimental data recorded from the 55 kW PEM electrolyzer. During this test, the electrolyzer started to operate from a cold state and a constant DC power setpoint was applied at the system

maximum capacity. As depicted in Figure 3, the temperature began to stabilize at 65°C±1°C, approximately 1h after the Beginning-of-Test (BoT). Once thermal equilibrium was achieved, (j,U) data points between 30% and 100% of the system nominal power condition were collected to plot the polarization curve.

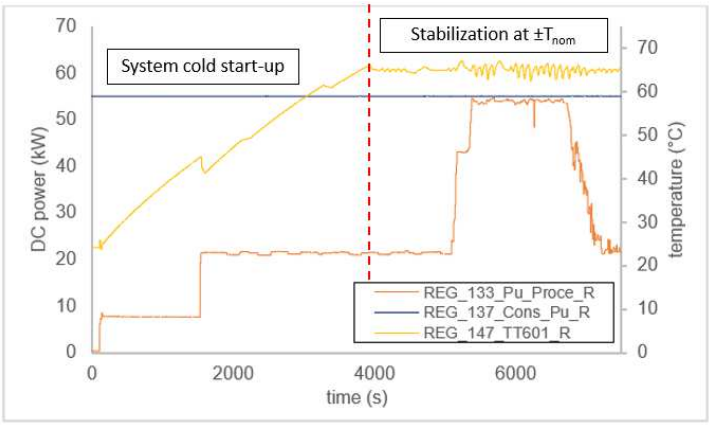

Figure 3: System start-up from cold state to nominal conditions (test performed on 09/15/2022)

A non-linear Generalized Reduced Gradient (GRG) optimization algorithm has been applied to the equation of the polarization curve and provided a satisfactory fitting with a root mean square error of 10^{-3}, as depicted in Figure 4. The three fitted parameters, summarized in Table 2, were then compared to typical value ranges found for PEM technology under the same operating conditions, demonstrating consistent alignment with existing literature data [4]. To illustrate, Biaku et al. [8] reported solutions on the order of 10^{-4} to 10^{-3} for the anode exchange current density and of 10^{-1} for the cathode exchange current density.

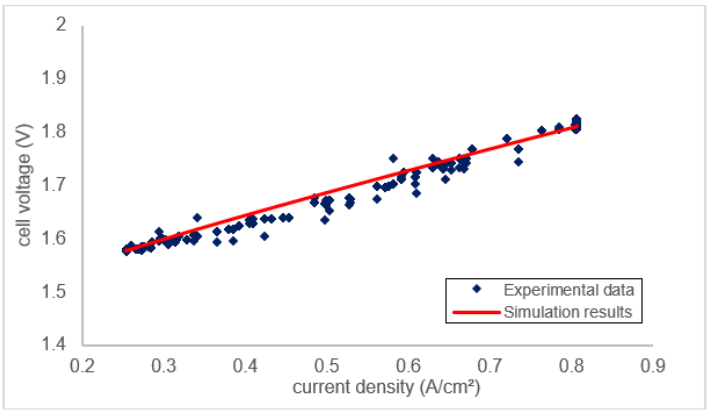

Figure 4: Fitting of the polarization curve at 65°C

Description	Parameter	Value
Anode exchange current density (A/cm²)	i0,an	$1.34*10^{-4}$
Cathode exchange current density (A/cm²)	i0,cat	$8*10^{-1}$
Equivalent ohmic resistance (Ω)	Req	$3.18*10^{-1}$

Table 2: Fitted parameters from the polarization curve equation

The next step of this work will consist in validating the entire model. Once achieved, long-term simulations will be conducted to capture seasonal intermittency, with the goal of defining and testing advanced control strategies and monitoring tools.

2. Experimental results

The same test also served as a benchmark for assessing key performance indicators of the electrolyzer at nominal conditions, including the mean specific consumption at the stack and system levels and the quality of produced hydrogen. An additional test has been performed under dynamic grid conditions and compared to the system baseline performance obtained at nominal conditions and allowed drawing the first outcomes on the impacts of intermittency. The results from these tests are summarized in Table 3.

KPI	Dynamic grid conditions	Steady-state nominal conditions
Stack specific consumption (kWh/Nm^3H_2)	3.924	4.334
System specific consumption (kWh/Nm^3H_2)	7.786	5.784
Amount of O_2 in H_2 (%)	1.058	0.298

Table 3: Performance of the 55 kW PEM electrolyzer under dynamic and steady-state nominal conditions (test performed on 09/15/2022)

Additional dynamic profiles based on grid services and renewable load scenarios will be tested to further refine these first conclusions.

Conclusion

In this paper, a methodology aimed at deepening the level of understanding on intermittency issues was introduced. This approach hinges on the development of a performance model of a system-scale electrolyzer and the implementation of experimental tests designed to evaluate different topologies of intermittent power profiles and deduce relevant outcomes regarding the impacts of intermittency on the performance of electrolyzer systems. Preliminary results from the test campaign have also contributed to the validation of the electrochemical submodel and the calibration of the polarization curve with a high correlation factor. Further tests will be performed in order to validate the entire model and build a strong database on intermittency impacts. This will provide valuable information to develop and test mitigation strategies based on long-term simulations over a large spectrum of intermittent load scenarios.

References

[1] A. Godula-Jopek, *Hydrogen Production*. Wiley, 2015.
[2] J. M. Stansberry et J. Brouwer, « Experimental dynamic dispatch of a 60 kW proton exchange membrane electrolyzer in power-to-gas application », *International Journal of Hydrogen Energy*, vol. 45, nº 16, p. 9305-9316, mars 2020, doi: 10.1016/j.ijhydene.2020.01.228.
[3] A. Weiß, A. Siebel, M. Bernt, T.-H. Shen, V. Tileli, et H. A. Gasteiger, « Impact of Intermittent Operation on Lifetime and Performance of a PEM Water Electrolyzer », *J. Electrochem. Soc.*, vol. 166, nº 8, p. F487-F497, 2019, doi: 10.1149/2.0421908jes.
[4] D. F. Pierre Olivier, « Modélisation et analyse du comportement dynamique d'un système d'électrolyse PEM soumis à des sollicitations intermittentes : Approche Bond Graph », 2016.
[5] P. Olivier, C. Bourasseau, et Pr. B. Bouamama, « Low-temperature electrolysis system modelling: A review », *Renewable and Sustainable Energy Reviews*, vol. 78, p. 280-300, oct. 2017, doi: 10.1016/j.rser.2017.03.099.
[6] W. J. Tiktak, « Heat Management of PEM Electrolysis », p. 80.
[7] F. Z. Aouali, M. Becherif, H. S. Ramadan, M. Emziane, A. Khellaf, et K. Mohammedi, « Analytical modelling and experimental validation of proton exchange membrane electrolyser for hydrogen

production », *International Journal of Hydrogen Energy*, vol. 42, nº 2, p. 1366-1374, janv. 2017, doi: 10.1016/j.ijhydene.2016.03.101.

[8] C. Biaku, N. Dale, M. Mann, H. Salehfar, A. Peters, et T. Han, « A semiempirical study of the temperature dependence of the anode charge transfer coefficient of a 6kW PEM electrolyzer », *International Journal of Hydrogen Energy*, vol. 33, nº 16, p. 4247-4254, août 2008, doi: 10.1016/j.ijhydene.2008.06.006.

Bibliometric analysis of SO_2 Depolarized Electrolyser

Pragya Narayana Prasad*[a], Neha Garg[a], Annukka Santasalo-Aarnio [a]

[a] Department of Mechanical Engineering, Aalto University, Finland

Introduction

Green hydrogen is needed as an energy carrier in the energy transition away from fossil energy sources. For this reason, large quantities of renewable energy-based hydrogen will be required. Most of this will be produced by PEM water electrolyser technology, which has the disadvantage of requiring high overvoltage to break the water molecule into hydrogen and oxygen gas products [1]. If SO_2 is added to the anode, the reaction changes, and SO_2 is oxidized to sulphuric acid, simultaneously producing protons that transport via a Proton exchange membrane (PEM) to the cathode to produce hydrogen. This reaction has the advantage of significantly lower standard potential $E° \sim 0.17$ V compared to conventional water electrolysis $E° \sim 1.23$ V [2]. A bibliometric analysis in the field of Sulphur dioxide Depolarized Electrolyser (SDE) is quite necessary to have a complete overview of the evolution of research in this field. It provides an extensive outlook on the past, present, and prospective research areas along with patterns in citation of the articles [3]. There are many benefits to performing a bibliometric analysis [4]:

1) It helps in improving the quality of future papers by allowing authors to consider the success from the past.
2) It can save time for future authors by helping them identify relevant papers quickly.
3) It reveals information in connection to the field's growth and impact, and the key contributors and publications within that field.

There has been a bibliometric study on hydrogen electrolyser technologies but there is no mention of SDE [5] and this is the first bibliometric analysis for SDE technology. The study stands out in a way that it provides insights on the evolution of the SDE technology, the issues that have been addressed and the future direction for researchers. It illustrates how SDE technology has developed over time, highlighting significant turning points and areas of research interest such as catalyst development, membrane materials, scalability, and cost minimization.

Methodology

The SCOPUS database is a useful tool that provides statistical analysis of the extracted documents by giving data of type of documents published, number of documents per year, source, author, country, subject area, affiliation, and funding sponsor. To map the data obtained based on key words and author contributions, VOSviewer software (version 1.6.18) developed by Van Eck and Waltman [6] was used. The software provides a variety of features to analyze and visualize data obtained from databases like Web of Science, Scopus, and PubMed. It generates maps that can be altered as per the analyzer's key interests and takeaways from the data [7]. The analysis combines the benefits of VOSviewer and Scopus to map the developments in the field of SDE. To better understand the trend of articles published in SDE, it is essential to perform a search on the SCOPUS database. The database yielded 65 articles as of 20th of March 2023. To gather the relevant dataset, the terms "SO_2 depolarized electrolyser", "Oxidation of Gas-Phase SO_2 " and "oxidation of dissolved sulphur dioxide". Different variations of the phrase "SO_2 depolarized electrolyser" were searched for based on a thorough survey of the keywords used in several papers in the data base, along with the variation in language in different parts of the world, for example, "sulphur" maybe be spelled

* Corresponding author: pragya.narayanaprasad@aalto.fi

in different ways. The search resulted in around 120 articles, but each abstract was checked for relevance and filtered to give 65 documents. To create keyword co-occurrences map, the data was retrieved as a comma-separated value (csv.) file and imported to VOSviewer. The data type was chosen as map based on text data, and the csv file was read, followed by choosing the terms to be extracted from title and abstract fields. Further, binary counting was chosen, meaning only the presence of a given term is counted while the number of repetitions within the content is not accounted for. The minimum number of occurrences of a term was set to three times. This filtered 1719 to 158 terms; by default, only 60% of the most relevant terms were selected. Out of the 95 most relevant terms, each term was checked manually for repetitions and relevance and removed accordingly.

Discussion

Based on the data obtained from SCOPUS and VOSviewer mapping tool, the keyword co-occurrences map was created as shown in Figure 1. The clusters are formed by the software based on the keywords' co-occurrences and relevance. The keywords show the infancy of the field of SDE even though the information about SO_2 electrolysis was first published in 1965 [8]. This is also attributed to the number of documents in the field, especially the existence of only one review paper [9]. It may be seen from the map that the three clusters are almost equally sized: the red and green clusters consist of 17 keywords, while the blue cluster comprises of 15 keywords. Mapping the keywords provides insight into the most important research areas focused on. The focus has been on developing a system to increase hydrogen production. The keywords seem to have repeated quite often like “HyS process” and “hybrid sulphur process” or “SO_2 depolarized electrolysis” and “SDE process”. The red cluster focuses on the keywords such as “sulphur”, hys process”, “Proton exchange membrane”, “transport” and “oxygen” that indicate the initial years of development of the SDE.

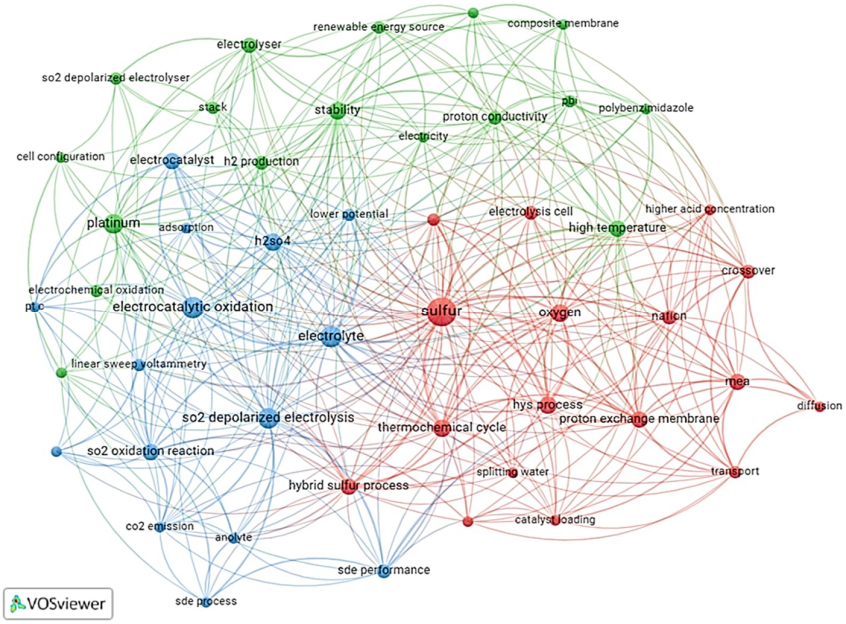

Figure 1: Keyword co-occurrences map: Red cluster- Early SDE Development; Green cluster- Improved Hydrogen Production; Blue cluster- Electrochemical Analysis Focus; the size of the circle indicates the occurrences’ weightage, and the color of the nodes give away the cluster they belong to.

The green cluster focuses on the experimentation to enhance the system for higher H_2 production by increasing stability through changes in cell configuration in the stack and finding the suitable membrane for the SDE. Polybenzindazole has been used in composite membranes

to enhance H_2 production [10, 11]. H_2 production at high temperatures in the range of 110 to 140°C has been reported by Díaz-Abad, Fernández-Mancebo et al. 2022 [10]. SO_2 crossover and its reduction leading to the formation of sulphur can also be interpreted through the link between the keywords “sulphur”, “crossover”, “diffusion” and “transport” in the red cluster [11]. SDE offers a more effective and economical way to produce hydrogen gas, which has the potential to lower CO_2 emissions [12]. The efficiency and the cost of the electrolysis cell can be improved by varying the catalyst loading and design and optimise the electrolysis cells. It has been shown that SDE has the potential to produce hydrogen gas with higher efficiency and lower cost compared to traditional water electrolysis methods [13]. The stability of the cell is an important consideration for the long-term viability of the SDE process [14].

The keywords like “linear sweep voltammetry” and “cyclic voltammetry” find value in the electrochemical aspect of SDE and have been used frequently in articles [15-18]. The connection between H_2SO_4 and electrolyte can represent the requirement of extremely low pH to support the reaction [11, 19]. “Platinum” appears to be used frequently, which can be accounted for by using platinum as the catalyst of the electrocatalytic oxidation of SO_2 and has been found to be one of the best catalysts for SDE [8]. Most of the research has been related to the catalysts, membranes, and cell configuration of the electrolyser. This means that the research horizon needs to broaden in the future to increase the system's efficiency, stability and prevent the formation of sulphur on the cathode. Reducing the cost of the system could also be an important parameter that can be achieved by using non-platinum group metals. The analysis clarifies the existing research in the SDE field and allows research to look for an expansion of the field in the future.

Table 1 Top five most productive countries

Sno.	Country	Number of documents	Citations	Average citations
1	USA	21	467	22.2
2	China	10	70	7
3	South Korea	9	43	4.8
4	Spain	6	42	7
5	Finland	5	54	10.8

To better understand the distribution of research in SDE topographically, the data was analysed using Scopus and a total of 19 countries were identified, out of which the top 5 contributing countries have been listed in Table 1.The USA has published the most documents, contributing 32.3% of the total number of publications, making it the leading country in SDE research with an average citation of 22.2. The large difference in the citation is attributed by the fact that the initial work was done in the USA. Even though China has published 17% of the publications, it has an average citation of 7 which may be attributed by the fact that the publications are quite recent, with seven papers published in 2021-22 and three papers published from 2013-15. On the other hand, the papers published in Finland have higher citations when compared to China, South Korea, and Spain. This shows that the group has studied SDE related phenomena, making it valuable for future researchers and began their research in SDE earlier than the other countries meaning longer periods of citation. Comparing the average citations can be complicated in the case of SDE since majority of the documents have been published recently giving very less time to be cited. South Korea and Spain contributed 14% and 9% of published documents. The self-citations have been excluded from the total number of citations, and the same has been used to calculate the average citations.

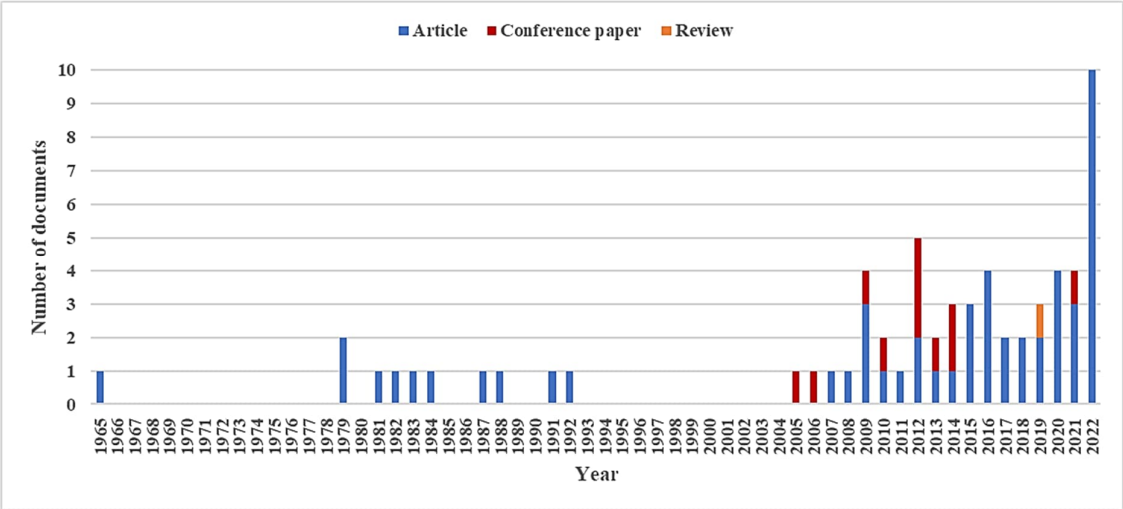

Figure 2 Number of documents by their type published per year.

The year-wise number of publications has been graphically represented in Figure 2. It shows a growing trend in research in SDE and appropriately represents the evolution of the field. The SDE technology wouldn't exist without the research on the electrochemical oxidation of dissolved SO_2 in water to give H_2SO_4 and H^+ ions. The first paper related to the chemistry behind SDE was published in 1965, and the tests were performed using platinum and gold electrodes [8]. The article provided insight into the mechanisms involved in the oxidation of SO2 in two stages: sulphite (SO_3^{2-}) and sulphate (SO_4^{2-}) intermediates formation, followed by the final oxidation of SO_4^{2-} to produce O_2 and H_2SO_4. The effect of pH, temperature, and electrode potential was studied, which showed that the oxidation of SO_2 was pH-dependent, with higher pH values resulting in faster reaction rates and higher efficiency achieved at higher temperatures and more positive electrode potentials [8].

In 1979, the first Hybrid Sulphur (HyS) closed cycle laboratory model and electrolyser was developed [21]. Further, the three main steps in the closed HyS cycle were discussed, along with the use of different concentrations of the electrolytes. Contrary to the findings of Seo and Sawyer in 1965 [8], a higher concentration of sulphuric acid resulted in a higher yield of hydrogen (in opposition to the higher pH requirement in the former case), while the addition of sodium sulphate and sodium bisulphite in the electrolyte improved the stability of the electrolyte and reduced corrosion of the reactor materials [21]. Over the next few years (1980-1983) [13, 22, 23], the articles describe the development of the SDE cell, and the challenges associated with the SDE. This included optimizing the operating parameters like temperature, pressure, and composition of the electrolyte and catalyst material. A reduction of efficiency was observed due to the deposition of sulphur on the surface of the cathode. It was also noted that the current density was relatively low.

In the late 1980s and early 1990s, the focus was on the anodic oxidation of SO_2 by different methods [24-27]. Numerous investigations have shown that SDE may efficiently and economically produce hydrogen gas. The effect of nitrogen oxides on the oxidation of SO_2 was also studied, showing that NO_x blocks the catalyst surface, leading to a partial reduction in the electrocatalytic process rate [28]. SDE's ability to function at very low temperatures and pressures, which lowers the energy needed to produce hydrogen, was seen as one of its main advantages and further work was continued in the 2000s. Interestingly, after 1992, the first paper in the 2000s was published only in 2005. This large gap in the technology development

could be attributed to the availability of funds for SDE related projects. As researchers worked to improve the efficiency and stability of the SDE process, they also explored several catalysts, electrode materials, cell parameters, and different methods of operation [29]. In 2006, Summers and Gorensek proposed a promising option, the potential use of a nuclear reactor to provide the necessary energy to produce green H_2 by the HyS process [30].

After 2010, the primary focus has been on improving the technology, exploring its potential, and overall cost reduction. The development of effective and stable catalysts for the electrochemical reaction that occurs in SDE has been the subject of extensive research [18]. The efficiency of catalysts like platinum, palladium, nickel, and cobalt has been investigated [9]. To increase the efficacy and long-term viability of SDE, researchers have been looking at new materials for the membranes that are employed in the process. An essential component of the commercialization of SDE technology is its scalability. Studies have been done on how to increase the performance of the system on a larger scale by optimizing the design and operational circumstances. To minimize the overall cost of the technology, studies have been done to find ways to lower the cost of materials, boost process efficiency, and improve system design [31].
Only one review paper has been written on SDE technology that focuses on catalysts development for the system. The paper highlights the different anodic catalysts that have been tested for SDE, their advantages and disadvantages, the effect of platinum loading and prospects for development of new catalysts [9]. The authors point out that platinum is the most promising catalyst for the SDE process but most of the tests have been conducted using half-cells or three electrode assemblies using rotating electrodes which means that it is important to test these catalysts in full electrolysers to support the obtained results for scale up of the process.

Conclusions

Using the analysis made, it is possible to create a basis for further research in the field of SDE. This analysis can be used as the first step in the right direction towards the growth and maturity of SDE. There could be several directions:

1. Catalyst development: Due to criticality of noble metals that seem to be most effective for SDE, it would be beneficial to explore alternate catalyst materials even though catalyst development is the most researched area in SDE.
2. Membrane materials: This is the most critical part of the SDE where the SO_2 crossover takes place. This is because SO_2 is absorbed in water and all PEMs work by water transport. Thus, finding a membrane that is proton conductive but does not allow SO_2 to pass through is quite challenging. Finding the right membrane would be the key to long term viability and stability of SDE.
3. Scalability, cost reduction and system optimization: Research efforts should be directed towards minimizing the overall cost of the technology. This could involve finding ways to lower the cost of materials, increase process efficiency, and improve system design. This would mean that the scalability of the process would be enhanced.
4. Addressing sulphur deposition and SO_2 crossover: The reduction of SO_2 at the cathode is one of the most important challenges that needs to be addressed and it is important to consider innovative approaches to mitigate the same.
5. Other approaches: A thorough environmental and economic analysis in the field of SDE would be useful in comparing the SDE with other commercially available electrolyser technologies. Encouraging collaboration among researchers, institutions, and industries to share knowledge and expertise, could potentially lead to innovative breakthroughs in SDE technology as it has in the past.

References

[1] M. A. Lewis, J. G. Masin, and P. A. O'Hare, "Evaluation of alternative thermochemical cycles, Part I: The methodology," *International journal of hydrogen energy*, vol. 34, no. 9, pp. 4115-4124, 2009.

[2] C. Sattler, M. Roeb, C. Agrafiotis, and D. Thomey, "Solar hydrogen production via sulphur based thermochemical water-splitting," *Solar Energy*, vol. 156, pp. 30-47, 2017.

[3] P. N. Prasad and S. Kalla, "Plant-microbial fuel cells-A bibliometric analysis," *Process Biochemistry*, vol. 111, pp. 250-260, 2021.

[4] S. K. Kar, S. Harichandan, and B. Roy, "Bibliometric analysis of the research on hydrogen economy: An analysis of current findings and roadmap ahead," *International Journal of Hydrogen Energy*, 2022.

[5] A. Arsad *et al.*, "Hydrogen electrolyser for sustainable energy production: A bibliometric analysis and future directions," *International Journal of Hydrogen Energy*, 2022.

[6] N. Van Eck and L. Waltman, "Software survey: VOSviewer, a computer program for bibliometric mapping," *scientometrics*, vol. 84, no. 2, pp. 523-538, 2010.

[7] N. J. Van Eck and L. Waltman, "Text mining and visualization using VOSviewer," *arXiv preprint arXiv:1109.2058*, 2011.

[8] E. Seo and D. Sawyer, "Electrochemical oxidation of dissolved sulphur dioxide at platinum and gold electrodes," *Electrochimica Acta*, vol. 10, no. 3, pp. 239-252, 1965.

[9] S. Díaz-Abad, M. Millán, M. A. Rodrigo, and J. Lobato, "Review of anodic catalysts for SO2 depolarized electrolysis for “green hydrogen” production," *Catalysts*, vol. 9, no. 1, p. 63, 2019.

[10] S. Díaz-Abad, S. Fernández-Mancebo, M. A. Rodrigo, and J. Lobato, "Enhancement of SO2 high temperature depolarized electrolysis by means of graphene oxide composite polybenzimidazole membranes," *Journal of Cleaner Production*, vol. 363, p. 132372, 2022.

[11] A. Santasalo-Aarnio, J. Virtanen, and M. Gasik, "SO 2 Carry-over and sulphur formation in a SO 2-depolarized electrolyser," *Journal of Solid State Electrochemistry*, vol. 20, pp. 1655-1663, 2016.

[12] L. Xue, P. Zhang, S. Chen, and L. Wang, "Pt-based bimetallic catalysts for SO2-depolarized electrolysis reaction in the hybrid sulfur process," *International journal of hydrogen energy*, vol. 39, no. 26, pp. 14196-14203, 2014.

[13] P. W. Lu, "Technological aspects of sulfur dioxide depolarized electrolysis for hydrogen production," *International journal of hydrogen energy*, vol. 8, no. 10, pp. 773-781, 1983.

[14] H. R. Colón-Mercado, M. B. Gorensek, C. H. Fujimoto, A. A. Lando, and B. H. Meekins, "High-performance SO2-depolarized electrolysis cell using advanced polymer electrolyte membranes," *International Journal of Hydrogen Energy*, vol. 47, no. 1, pp. 57-68, 2022.

[15] A. H. Dourado *et al.*, "Opportunities and knowledge gaps of SO2 electrocatalytic oxidation for H2 electrochemical generation," *ACS Catalysis*, vol. 9, no. 9, pp. 8136-8143, 2019.

[16] A. Santasalo-Aarnio, A. Lokkiluoto, J. Virtanen, and M. Gasik, "Performance of electrocatalytic gold coating on bipolar plates for SO2 depolarized electrolyser," *Journal of Power Sources*, vol. 306, pp. 1-7, 2016.

[17] S.-K. Lee, C.-H. Kim, W.-C. Cho, K.-S. Kang, C.-S. Park, and K.-K. Bae, "The effect of Pt loading amount on SO2 oxidation reaction in an SO2-depolarized electrolyzer used in the hybrid sulfur (HyS) process," *International journal of hydrogen energy*, vol. 34, no. 11, pp. 4701-4707, 2009.

[18] H. R. Colón-Mercado and D. T. Hobbs, "Catalyst evaluation for a sulfur dioxide-depolarized electrolyzer," *Electrochemistry communications*, vol. 9, no. 11, pp. 2649-2653, 2007.

[19] M. Gasik, J. Virtanen, and A. Santasalo-Aarnio, "Improved operation of SO2 depolarized electrolyser stack for H2 production at ambient conditions," *International Journal of Hydrogen Energy*, vol. 42, no. 19, pp. 13407-13414, 2017.

[20] A. Santasalo-Aarnio, I. Galfi, J. Virtanen, and M. M. Gasik, "New analytical methodology for analysing S (IV) species at low pH solutions by one stage titration method (bichromatometry) with a clear colour change. Could potentially replace the state-of-art-method iodometry at low pH analysis due higher accuracy," *Plos one*, vol. 12, no. 11, p. e0188227, 2017.

[21] G. Parker and L. PWT, "LABORATORY MODEL AND ELECTROLYTES DEVELOPMENT FOR THE SULFUR CYCLE HYDROGEN PRODUCTION PROCESS," 1979.

[22] P. Lu and R. Ammon, "Sulfur dioxide depolarized electrolysis for hydrogen production: development status," *International Journal of Hydrogen Energy*, vol. 7, no. 7, pp. 563-575, 1982.

[23] P. Lu, E. Garcia, and R. Ammon, "Recent developments in the technology of sulphur dioxide depolarized electrolysis," *Journal of Applied Electrochemistry*, vol. 11, no. 3, pp. 347-355, 1981.

[24] S. E. Lyke and S. H. Langer, "Oxidation of Sulfur Dioxide in Sulfur‐Modified Platinum‐Graphite Packed Bed Electrodes," *Journal of the Electrochemical Society*, vol. 138, no. 6, p. 1682, 1991.

[25] J. C. Card, M. J. Foral, and S. H. Langer, "Electrogenerative oxidation of dissolved sulfur dioxide with packed-bed anodes," *Environmental science & technology*, vol. 22, no. 12, pp. 1499-1505, 1988.

[26] E. Matveeva and E. Kasatkin, "ANODIC-OXIDATION OF SULFUR-DIOXIDE ON A PLATINUM-ELECTRODE IN THE PRESENCE OF POTASSIUM-IODIDE-ELECTROCATALYSIS," *SOVIET ELECTROCHEMISTRY*, vol. 20, no. 5, pp. 550-556, 1984.

[27] B. Cho, K. Yun, and I. J. Chung, "A study on the anodic oxidation of iodide‐mediated sulfur dioxide solution," *Journal of the Electrochemical Society*, vol. 134, no. 7, p. 1664, 1987.

[28] P. Iliev, I. Nikolov, T. Vitanov, and E. Budevski, "Influence of nitrogen oxides on the electrocatalytic oxidation of sulphur dioxide," *Journal of applied electrochemistry*, vol. 22, pp. 425-428, 1992.

[29] J. Steimke and T. Steeper, *Generation of hydrogen using electrolyzers with sulfur dioxide depolarized anodes*. American Institute of Chemical Engineers, 2005.

[30] W. A. Summers and M. B. Gorensek, "Nuclear hydrogen production based on the hybrid sulfur thermochemical process," American Nuclear Society, 555 North Kensington Avenue, La Grange Park, IL …, 2006.

[31] A. Lokkiluoto *et al.*, "Novel process concept for the production of H 2 and H 2 SO 4 by SO 2-depolarized electrolysis," *Environment, development and sustainability*, vol. 14, pp. 529-540, 2012.

Breaking the silo's and reducing fragmentation: hydrogen as a catalyst for an integrated legal framework for energy law in the EU

P. Jimenez Casanova*[1], J. Pinto[2]

[1]Universitat Rovira i Virgili, Tarragona Centre for Environmental Law Studies (CEDAT), Spain.
[2]UEF Law School, Center for Climate Change, Energy and Environmental Law, Finland.

Introduction

More than 145 years ago, author Jules Verne wrote of a world where "*water will one day be employed as fuel, that hydrogen and oxygen which constitute it, used singly or together, will furnish an inexhaustible source of heat and light, of an intensity of which coal is not capable*". Today, we see that imagined world emerging. Whilst hydrogen is the most abundant compound in the world, interest in low carbon hydrogen has increased throughout the globe and particularly in the EU since the 2020 covid pandemic and the military invasion in Ukraine in 2021. Hydrogen marks an opportunity for energy security and is a critical element of the energy transition to a low-carbon world, as it has become evident that certain types of hydrogen have the potential to replace natural gas and electricity sourced from fossil fuels in the road to the decarbonization of the energy sector. Its versatility and ability to be produced from renewable energy (and consequently emit no carbon) are some of the reasons for the increased interest, which has seen many nations including hydrogen as an integral part of their decarbonization strategies. As an example of its versatility, hydrogen can be utilized as feedstock, fuel, and as energy storage for either electricity (power-to-power) or gas (power-to-gas) [1].

For the hydrogen economy to take off, a regulatory framework that captures all its potential benefits to several systems such as electricity, gas and transportation is critically needed. However, the current regulatory framework for the energy system is heavily siloed; geared toward regulating one sector with little if any cross-sectoral or integrated elements. The versatile nature of hydrogen, however, requires a holistic approach to regulation, for example, so that hydrogen production relying on electricity can feed the end product into the gas system. The International Renewable Energy Authority (IRENA) has stated that the creation of the hydrogen economy requires a regulatory framework which transcends sectoral boundaries [2].

The future EU energy system is envisaged to be an integrated energy system, as set out in the EU strategy on energy system integration [3]. However, whilst infrastructural and technological integration is indeed a positive step, this must be coupled with legal integration. Some of the critical issues obstructing the development of an integrated energy system, include that the energy sector is largely still regulated independently (for example the separate regulation of electricity and gas); consequently, networks are still planned and managed independently. In addition, there exist discrepancies between the ten-year network development plan (TYNDP) at EU level and national network development plans (NDP) at Member State level, as Member States are not obligated to develop them in certain circumstances.

The current existing, envisaged and burgeoning framework has issues, including that: (i) the regulatory design of the energy sector is still largely based on the traditional market model [4]; and (ii) there is a lack of a legal framework for hydrogen networks, which merely exist in draft

* Corresponding author: paola.jimenez@urv.cat

form and/or requires further elaboration in the future [5]. For these reasons, the research will aim at proposing the legal and policy instruments that are needed for harmonizing the EU legal framework for cross-sectoral integration and for network planning to foster more integration and enabling more flexibility in the EU energy system. Achieving coherence at EU level will axiomatically facilitate Member States to reach the same level of integration and harmonization of their networks. Aspects such as unbundling rules, tariffs, third-party access and network codes to energy and hydrogen systems must be analyzed as these are considered the necessary regulatory conditions for the development of a new competitive market [6].

This research calls for legal system integration in EU energy law and the amalgamation of currently discreet legal regulation of different energy sectors. It also looks to reducing the fragmentation between the EU level and Member State level in this regard. Whilst the broader topic of fragmentation is a large one, the research presented at the conference will be the results from the preliminary research related to finding the lacunas and sources of incoherence and fragmentation.

Methodology

This research will be rooted in the theoretical framework and principles of energy justice, the ‘just’ transition, and the planetary boundaries framework. The reason behind this being that the EU energy planning and regulation should promote and enable a transition into an integrated energy system that is inclusive, fair and within the planetary boundaries. This will ensure that societies function under the safe operating space for humanity. A new study revealed not only that the level of transgression of three of the planetary boundaries previously identified have increased, but also that six out of the nine planetary boundaries have been transgressed [7]. Thus, bolstering the need for energy policy and legislation to be seen through this lens.

The preliminary legal analysis will focus on answering the following research questions:

1. What are the existing EU energy policies promoting the energy transition to net-zero and the integration of renewable energy, including ‘renewable’ hydrogen, and what is the existing legal and regulatory framework at EU level that enables it at a Member State level?

2. Are there any contradictions, gaps, ambiguities, or redundancies between policies and/or secondary legislation that are causing barriers for the deployment of the hydrogen economy on one hand, and achieving the climate goals and the development of a net-zero energy economy in the EU on the other hand?

3. What fragmentation or lack of coherence is found as a result of the aforementioned two queries?

The research will be driven by the need to understand "how to design an integrated hydrogen regulatory and policy framework for the EU which holistically governs hydrogen across its most relevant sectors and avoids fragmentation." Given that the research aims to find a holistic manner to regulate hydrogen in all its necessary contexts, various research methods will be adopted.

The research methods adopted for this will include comparative and 'law in context' approaches to energy law and policy. An element of doctrinal research aimed at ascertaining what the law

and policy is at an EU and Member State level as well as cementing the different contexts to which these legal regimes and policies apply, will also be used. In order to achieve this, first, it will be necessary to identify the cause of the existing network and planning fragmentation in the region and then at country level by adopting a comparative methodology and analyzing specific case studies, such as the Netherlands, Germany and Spain. Thereafter, proposing the legal instruments needed at an EU level that could potentially facilitate and promote more network integration through planning. Consequently, one of the focuses of this research is on hydrogen as the nexus between the electricity, transport and gas sectors and removing the siloed and discreet approach to which these areas of the energy landscape have been regulated to date.

In answering these questions, not only legal analysis of the relevant policies and legislation is necessary, but also literature review and content analysis of reports on the development of a hydrogen economy for creating integrated energy systems. The aim of the preliminary stage of the research is to create a matrix that identifies the gaps, ambiguities, contradictions that could be creating barriers for the development of an integrated energy system through hydrogen.

Discussion

Hydrogen is an energy carrier or a secondary energy source, and not an energy source itself [2]. Resultantly, hydrogen needs to be produced through other forms of energy such as renewable energy in the form of electricity. Therefore, hydrogen is not always necessarily 'green', but rather, this depends on the primary energy source used to produce it. Currently, it is widely produced from fossil fuels [8]. However, renewable energy, derived predominantly from solar and wind have the potential to increase the production of hydrogen from renewable sources and make it 'green'. The push to do so is bolstered by its potential to contribute to the achievement of increasing the overall energy consumption of renewable energy in the EU to 42.5% by 2030 as well the mandatory usage targets of hydrogen in industry and transport set in the new recast Renewables Energy Directive [9]. Another reason for the increased interest and attractiveness of hydrogen relates to its storage potential, which makes it an attractive technology for both the electricity and gas industries as it can provide flexibility (especially in light of the intermittence caused by renewable forms of electricity) [4].

The last five years have seen significant legislative and policy activity at an EU level aimed at climate change mitigation and adaptation and focusing on the energy transition as a way to achieve decarbonization. As a result, the different EU institutions have either published proposals to reform the main secondary legislation or already published the recast of some of them to facilitate the integration of new technologies and energy carriers into the energy system, foster system integration and flexibility. Examples include the 2020 European Green Deal [10], the 2020 EU Hydrogen Strategy [11], 2020 EU Energy System Integration Strategy [12], the 2021 Fit for 55 Package [13], the EU Green Deal Industrial Plan [14], and the recently published Directive (EU) 2023/1791 on energy efficiency [15], the Regulation (EU) 2023/1804 on the deployment of Alternative Fuels Infrastructure [16] and the recast Renewable Energy Directive 2023 [9]. However, as set out earlier, these policies and legal instruments are often siloed, do not speak to one another or have the possibility of creating fragmentation rather than integration. Resultantly, for the 2024 EPHyC Conference that will take place in March 2024, we will present on our preliminary findings consisting of the identification and mapping of all the legal hurdles for integrated energy system planning for the 'Hydrogen Economy' in the EU.

The expected findings of the preliminary stage of the research will consist of identifying the sources of fragmentation in the European energy system. As an example, the recently published Regulation on alternative fuels infrastructure and the recast Renewables Energy Directive already present challenges as well as contradictions between electricity and gas directives. On one hand the Regulation on alternative fuels infrastructure will require investment in transmission lines, gas network infrastructure and storage infrastructure throughout the European transport corridors for the transport of hydrogen, which will require EU and Member States cooperation and planning at an EU and national levels. However, if the expected investment and infrastructure do not happen as expected then it could potentially hinder the industry and transport sector in the compliance of the new mandatory uses of renewable hydrogen for 2030 set in the recast Renewables Energy Directive. Furthermore, a new Directive on the development of the internal markets in renewable and natural gases and in hydrogen is expected to be adopted in the following year.

It will be relevant to analyze these and other policies and legislation and how they reduce or increase fragmentation and achieve an integrated legal approach to achieving a hydrogen economy in the EU.

Conclusion

It is expected that the findings will reveal a lack of a coherent and integrated approach to planning and regulation for the energy sector. Such lack is a barrier for the development of an integrated energy system and the source of fragmentation between EU energy and climate policies and national energy and climate plans, including, but not limited to, the gas, electricity, and transport sectors in the EU. These findings will be relevant to enable further research, consisting of understanding how planning of the energy sector should be regulated and which elements it must contemplate to reach a high level of integration, particularly in the development of hydrogen markets.

Acknowledgements

The authors work within the framework of the Project 101073195, ‘Training for a Hydrogen Economy based Renewable Energy Society in Anthropocene’ (THERESA), funded by the Marie Skłodowska-Curie Actions programme, HORIZON-MSCA-2021-DN-01.

P. Jimenez Casanova is also member of the research group "Territory, Citizenship and Sustainability", recognized as a consolidated research group and funded by the Departament de Recerca i Universitats de la Generalitat de Catalunya (2021 SGR 00162).

References

[1] R. Fleming, "Clean or renewable - hydrogen and power-to-gas in the EU energy law," *Journal of Energy & Natural Resources*, pp. 43-63, 2021.

[2] International Renewable Energy Authority, "Geopolitics of the Energy Transformation: The Hydrogen Factor," Abu Dhabi, 2022.

[3] H. Ishaq, I. Dincer and C. Crawford, "A review on hydrogen production and utilization: Challenges and opportunities," *International Journal of Hydrogen Energy*, vol. 47, no. 62, pp. 26238-26264, 2022.

[4] S. Lavrijssen and B. Vitéz, "Make Hydrogen whilst the sun shines," *CCLR*, no. 4, pp. 266-280, 2020.

[5] R. Fleming, "Hydrogen Networks: Networks of the Future?," in *A Force of Energy*, University of Groningen Press, 2022.

[6] L. Tanase and I. Herrera Anchusteguí, "EU Hydrogen and Decarbonized Gas Market Package: Unbundling, third-party access, tariffs and discounts rules at the core of transport of hydrogen," in *Retos Regulatorios de los Gases Renovables en la Economía Circular*, SSRN, 2023, pp. 1-26.

[7] K. R. e. al, "Earth beyond six of nine planetary boundaries," *Science Advances*, vol. 9, no. 37, pp. 1-16, 2023.

[8] International Energy Agency, "Global Hydrogen Review 2023," IEA, Paris, 2023.

[9] Council of the EU, "European Council," 9 October 2023. [Online]. Available: https://www.consilium.europa.eu/en/press/press-releases/2023/10/09/renewable-energy-council-adopts-new-rules/.

[10] European Commision, "The European Green Deal COM(2019) 640 final," Brussels, 2019.

[11] European Commission, "A Hydrogen Strategy for a Climate-Neutral Europe COM(2020) 301 final," Brussels, 2020.

[12] European Commission, "Powering a climate neutral economy: An EU Strategy for Energy System Integration COM(2020) 299 final," Brussels, 2020.

[13] European Commision, "Fot fro 55: delivering the EU's 2030 Climate Target on the way to climate neutrality," Brussels, 2021.

[14] European Commission, "A Green Deal INdustrial Plan for the Net-Zero Age COM(2023) 62 final," Brussels, 2023.

[15] European Parliament and of the Council, "Directive (EU) 2023/1791 on energy efficiency and amending Regulation (EU) 2023/955 (recast)," 2023.

[16] European Parliament and of the Council, "Regulation (EU) 2023/1804 on the deployment of alternative fuels infrastructure, and repealing Directive 2014/94/EU," 2023.

[17] European Commission, "Powering a climate neutral economy: An EU Strategy for Energy System Integration COM(2020) 299 final," Brussels, 2020.

CFD simulations of electrolyte flow uniformity and recirculation in alkaline water electrolysis cells

K. Van Droogenbroek[1], C. Georgadis[1], J. Proost*[1]

[1]Division of Materials and Process Engineering, Université catholique de Louvain (UCLouvain)
Louvain-la-Neuve, Belgium

Introduction

In the coming years, considerable efforts will have to be made to reduce greenhouse gas emissions to as close to zero as possible in order to limit the increase in global average temperature to 1.5°C, as stated in the Paris Agreement [1]. One way to decarbonize a wide range of sectors – including transport, iron and steel production and chemicals manufacture – is to use green hydrogen as an energy carrier to store and deliver usable and clean energy. Currently, the most mature technology used to produce hydrogen is Alkaline Water Electrolysis (AWE). It uses an alkaline solution, typically KOH between 1 and 6 M, at a temperature in the range 30-80°C, a diaphragm and Ni-based electrodes. This process can be further enhanced in terms of sustainability through the utilization of renewable electricity for conducting electrolysis. The primary hurdle associated with this technology revolves around improving the efficiency and diminishing capital expenditure (CAPEX) of the electrolyzer [2].

Recent experimental studies in our group have shown that it is possible to significantly improve the performance of such alkaline electrolyzers by shifting from traditional gap cells to zero-gap cells, wherein the anodic and cathodic chambers are filled with 3D porous electrodes such as foams and 3D-printed structures [2,3]. The advantage of using such 3D structures is that the available surface area for hydrogen production is much higher. At the same time, increased hydrogen production may lead to stagnant gases trapped in the complex porous channels of the foam. This is the reason why optimised electrolysis cells with forced electrolyte flow have been developed at the lab scale to favor bubble removal. A double elbow configuration was also used in order to guide the flow and enhance its spread throughout the cell, to take advantage of the whole area provided by the 3D electrodes [2].

Efforts have then been made in order to apply the same methodology – i.e. using 3D porous electrodes and forced electrolyte flow – to an industrial scale electrolyzer. Unfortunately, it was impossible to get such low cell voltages as with the lab-scale setup. This is mainly due to the fact that the pilot cells are not optimized for forced electrolyte flow, leading to a non-optimal distribution of the electrolyte and therefore to a poorer performance of the electrolyzer. The aim of this work is to perform Computational Fluid Dynamics (CFD) simulations to assess the behavior of the electrolyte within a pilot cell in order to find some optimal configuration that homogenizes the flow, reduces recirculation of the electrolyte and favors bubble removal.

The main objective of this research is to define parameters – based on a Residence Time Distribution (RTD) analysis – that will allow to compare the performance of different cell configurations. The first parameter will be used to evaluate the level of flow uniformity inside the electrolysis cell while the second one will give an estimation of flow recirculation. Modification of the injection channels as well as the addition of porous media will be considered as options to improve the performance of the electrolyzer.

* Corresponding author: joris.proost@uclouvain.be

Methodology

The geometry of the pilot-scale cathodic chamber considered as a reference configuration for this work is depicted in Figure 1. It consists in a flat cylinder of diameter 20 cm and of thickness 6 mm. The inlet is located at the bottom of the cell and has a diameter of 2 mm while the outlet, at the top, presents a diameter of 3 mm. The electrolyte is a 30 wt% KOH solution at 70°C and its flow is forced at the entrance of the chamber by imposing an inlet flow rate Q_{in} corresponding to an inlet velocity v_{in}. The considered inlet velocities are in the range of 0.3 to 1.9 m/s. The latter is fixed by the applicable maximal power of the pilot pumps.

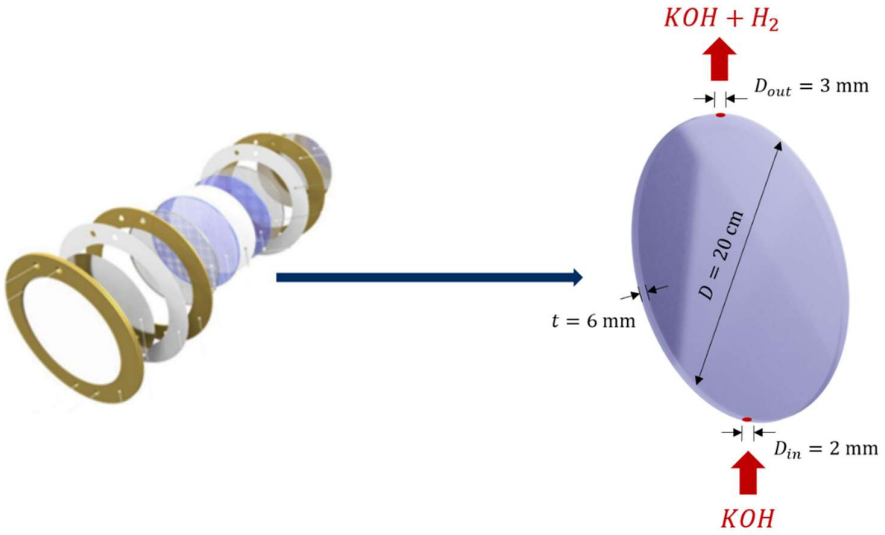

Figure 1: Reference configuration of the cathodic chamber of one single water electrolysis cell

To simulate the electrolyte flow within the cell, the incompressible Navier-Stokes equations for a single-phase flow were solved using the finite volume method implemented in OpenFOAM. The assumption of 2D flow is made since the thickness of the chamber is small compared to its diameter and the k-ω turbulent model is used to account for turbulence. Concerning the addition of porous electrodes within the cell, it is possible to describe explicitly the exact foam geometry based on high-resolution micro-CT (computed tomography) scanned data. Unfortunately, this is highly demanding from a computational point of view. To counter this problem, spatially averaged equations are used to account for porosity, based on the Darcy-Forchheimer law and on the intrinsic and inertial permeabilities of the porous structure [4]. In what follows, two foams will be considered with different characteristic pore sizes a = 450 µm and a =3000 µm, respectively.

In order to assess flow uniformity and recirculation of the flow within the electrolysis cell, two parameters will be defined based on a Residence Time Distribution (RTD) analysis. This method consists in the injection of a tracer at the inlet of a reactor at time $t = 0$ s and in measuring the concentration of tracer at the outlet as a function of time, $C(t)$. This concentration can be determined numerically by solving the convection-diffusion equation [5]. Based on this concentration, it is possible to calculate the RTD function $E(t)$ that gives an indication of the number of fluid elements leaving the reactor after having spent a given time inside it.

The first parameter, aimed at determining flow uniformity and the presence of dead/stagnant zones within the cell, is called the dimensionless time [5] and is defined as the ratio between the mean residence time of the fluid inside the cell of volume V, and the space time, i.e. the time that would be required to fill the whole space available at fixed inlet flow rate:

$$\theta = \frac{t_m}{\tau} = \frac{\int_0^\infty t\, E(t)\, dt}{V/Q_{in}} \; [-]$$

This parameter gives an image of the effective volume used inside the cell. Two cases must be identified here: $\theta < 1$ and $\theta \geq 1$. On the one hand, $t_m < \tau$ and so the mean time spent by the fluid inside the cell is lower than the time required to fill it. In other words, there will be some dead/stagnant zones of low velocity in the cell where no hydrogen will be produced. On the other hand, $t_m \geq \tau$ which means that fluid elements remain in the cell for a time higher or equal to the space time. In this specific case, the electrolyte will have time to homogenize over the whole volume and to fill all the space. In other words, no dead zones are to be expected and the electrolyte will be uniformly distributed over the area provided by the electrodes, enhancing hydrogen production.

Another phenomenon which may occur during hydrogen production inside the porous electrode is the entrapment of hydrogen bubbles inside the domain. For this reason, it is interesting to determine whether the electrolyte goes directly from the inlet to the outlet of the chamber or if it recirculates, leading to poor evacuation of the bubbles. A second parameter is therefore defined to characterize this recirculation phenomenon [6]. It is called the dimensionless variance and it is defined as the ratio between the variance of the RTD function and the square of the mean residence time:

$$\sigma_\theta^2 = \frac{\sigma^2}{t_m^2} = \frac{\int_0^\infty (t - t_m)^2\, E(t)\, dt}{\left(\int_0^\infty t\, E(t)\, dt\right)^2} \; [-]$$

This parameter gives an image of the level of mixing inside the electrolysis cell. When $\sigma_\theta^2 = 0$, it means that there is no mixing of the flow since the RTD function presents no dispersion around the mean residence time. This case corresponds to an ideal plug flow. Next to this, when $\sigma_\theta^2 \geq 0$, some mixing of the flow occurs, which could lead to entrapment of hydrogen bubbles in the cell.

Discussion

The approach described in the previous section has been applied to the reference cell presented in Figure 1. Figure 2.a shows the velocity profile inside the domain for an inlet velocity of 1.5 m/s. As observed, the electrolyte forms a jet stream flow at the entrance of the chamber due to the small inlet diameter compared to the much larger diameter of the cell chamber. This leads to an inhomogeneous distribution of the flow, with some zones that are not flushed by the electrolyte. Computation of the dimensionless time allows to quantify the degree of homogeneity. Its profile as a function of the inlet velocity has been plotted in Figure 2.b. It clearly shows that flow uniformity increases as the inlet flow rate increases (i.e. as θ increases). However, for the range of velocities considered in our pilot, the dimensionless time remains quite low (lower than 0.3) meaning that distribution of the electrolyte is poor. In order to quantify the occurrence of recirculation of the flow, the dimensionless variance has been calculated as shown in Figure 2.c. It appears that σ_θ^2 also increases as v_{in} increases, which

means that a higher flow rate leads to a higher mixing of the flow. This also explains why there are fewer dead zones as the inlet flow rate is increased. Contradictory conclusions arise from these two parameters, since a higher flow rate is desired from a uniformity point of view while lower velocities will generate less recirculation of the flow. For this reason, an optimum needs to be found. Since the dimensionless time remains so low and the dimensionless variance so high (far above 1), new configurations have to be considered in order to improve the performance of the electrolyzer.

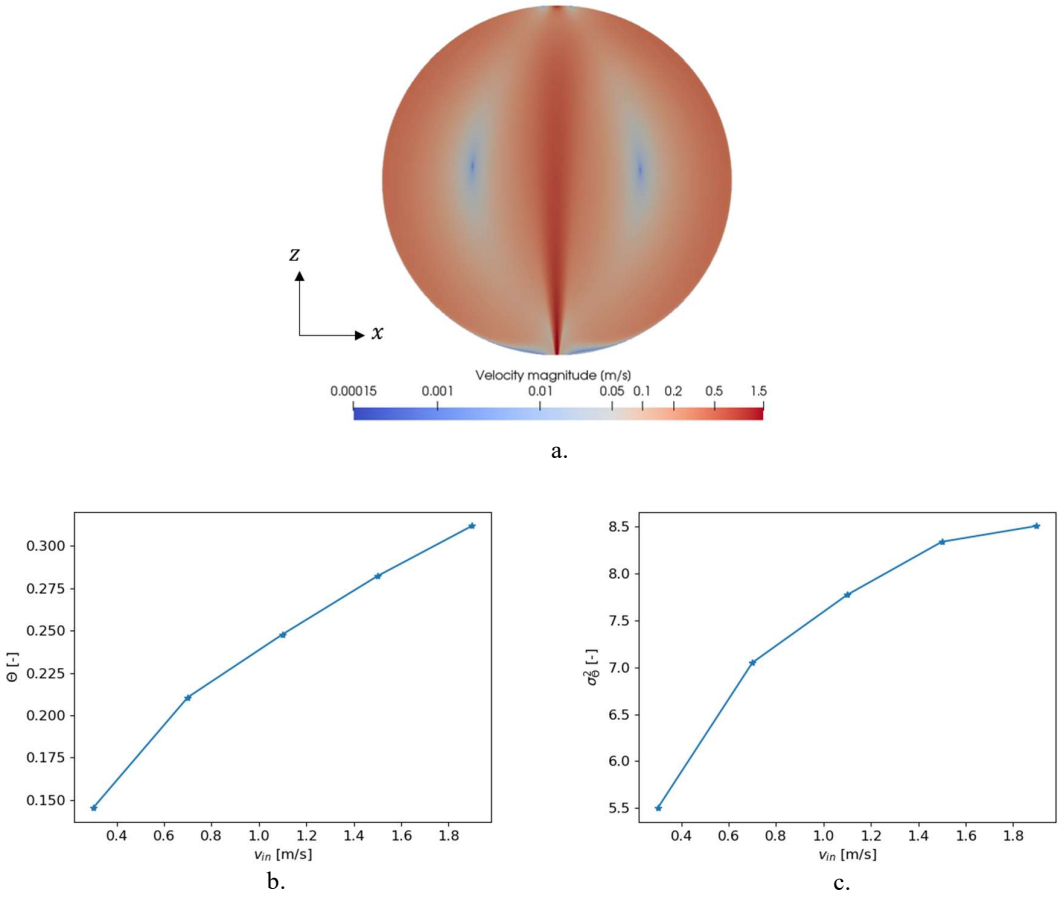

Figure 2: (a) Velocity profile for the reference configuration with v_{in} = 1.5 m/s. (b) Dimensionless time and (c) dimensionless variance as a function of inlet velocity.

At first, since the inlet opening seems to be the critical point in terms of distribution of the flow, different inlet configurations have been studied, such as a bigger inlet diameter (4 mm instead of 2 mm), an inclined inlet (at 45° to the right) and three inlets. The dimensionless times and variances of these three new configurations have been compared to the reference case in Figure 3. Concerning flow uniformity, it appears that increasing the size of the inlet or inclining the inlet channel leads to a lower value of θ. However, increasing the number of inlets clearly lowers the risk of dead zones in the cell. Next to this, the reference configuration and the case with a larger inlet present high dimensionless variances over the velocity range considered, which means that these configurations generate a lot of recirculation. The cells with three inlets or with an inclined inlet are more suited to avoid recirculation of the electrolyte. From these observations, the case with three inlets might be the most suited to improve distribution of the flow while lowering the level of mixing. However, this configuration presents some

disadvantages. The major drawback from a design point of view is that it requires a modification of the cell geometry. Moreover, as observed in Figure 3.a, this solution is not durable. For example, if the number of cells in the electrolyzer increases, the inlet flow rate in one cell will be lower, meaning that the value of θ will decrease significantly. Finally, it is clearly possible to lower recirculation even more to approach the ideal value of $\sigma_\theta^2 = 0$.

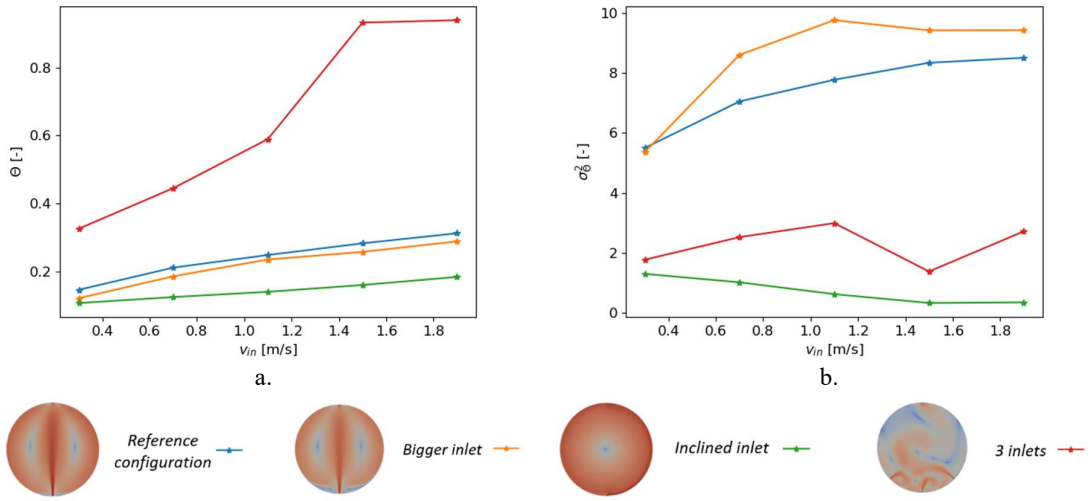

Figure 3: (a) Dimensionless time and (b) dimensionless variance as a function of inlet velocity for different inlet configurations.

To tackle these hurdles, the possibility to add porous structures within the electrolysis cell has been considered in order to better distribute the flow. Figure 4 compares the values of θ and σ_θ^2 for the reference configuration, the case with three inlets and for electrolysis cells filled with foams presenting pore sizes of 450 and 3000 µm.

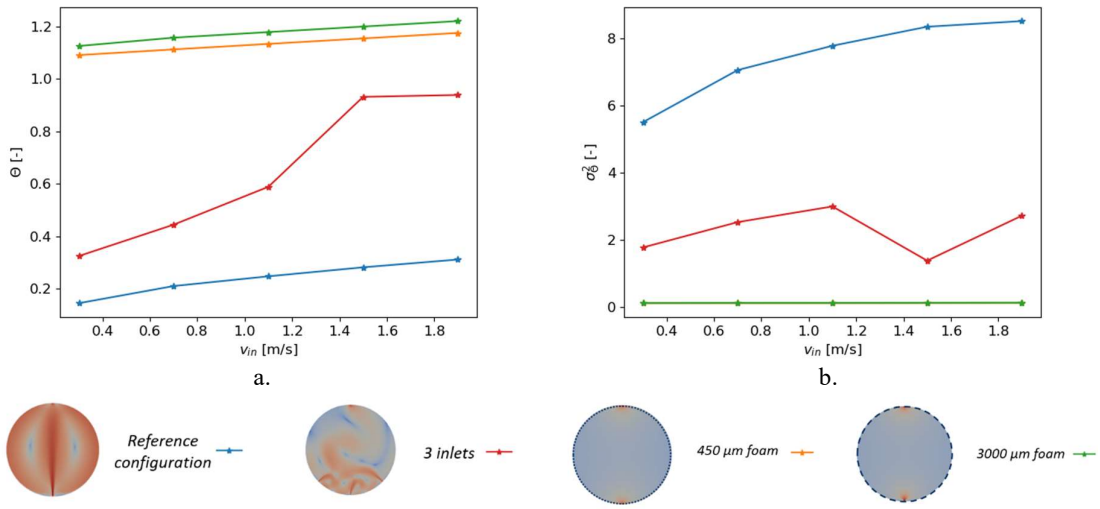

Figure 4: (a) Dimensionless time and (b) dimensionless variance as a function of inlet velocity after the addition of foams in the domain.

Figure 4.a highlights the fact that adding 3D porous structures in the cathodic chamber allows to homogenize the electrolyte distribution over the whole volume of the cell, resulting in a dimensionless time higher than 1. In other words, no dead zones are to be expected, on the contrary to the reference case and the case with 3 inlets. The fact that the 3000 µm foam presents a higher dimensionless time is simply due to the fact that the electrolyte takes more time to go out of the cell since it is more likely to be stuck somewhere within the larger pores. In terms of flow recirculation, the addition of foams helps to lower the value of σ_θ^2 significantly (i.e. close to 0) as observed in Figure 4.b. In this case, both foams present nearly similar results and the curves overlap on the graph. However, the 450 µm foam presents a slightly lower dimensionless variance which confirms the fact that the flow will present a lower risk to recirculate when the porous structure is finer.

Conclusions

In this work, CFD simulations have been used to extract two parameters that allow to quantify flow uniformity and flow recirculation in alkaline water electrolysis cells. The main objective is to find a cell configuration that homogenizes the flow ($\theta \geq 1$) without generating mixing of the electrolyte in the cell ($\sigma_\theta^2 \to 0$). Therefore, an optimum has to be found between these two parameters such that we take advantage of the whole surface area of the electrodes but without getting hydrogen bubbles trapped into the cathodic chamber. As a first step, modifying the inlet channels of the cell seemed to be an interesting solution to improve the performance of the cell. However, significantly better results are obtained by adding porous media inside the cell since it increases the effective volume covered by the electrolyte and it lowers risks of flow recirculation within the chamber. This quantitative analysis is a first step to assess the performance of AWE electrolyzers and it allows to compare different geometries on the same ground. Multiphase modeling will be a further step in the validation of the results that were obtained here.

Acknowledgements

Financial support from the Regional Walloon Project HeCO2 is gratefully acknowledged.

References

[1] United Nations Environment Programme, *Paris Agreement*. [online]. Available: https://wedocs.unep.org/20.500.11822/20830. [Accessed: Sept. 4, 2023].

[2] F. Rocha, R. Delmelle, C. Georgiadis and J. Proost, Effect of pore size and electrolyte flow rate on the bubble removal efficiency of 3D pure Ni foam electrodes during alkaline water electrolysis, *Journal of Environmental Chemical Engineering*, vol. 10, no. 3, p. 107648, Jun. 2022, doi: 10.1016/j.jece.2022.107648.

[3] F. Rocha, R. Delmelle, C. Georgiadis and J. Proost, Electrochemical Performance Enhancement of 3D Printed Electrodes Tailored for Enhanced Gas Evacuation during Alkaline Water Electrolysis, *Advanced Energy Materials*, vol. n/a, no. n/a, p. 2203087, doi: 10.1002/aenm.202203087.

[4] D. Edouard, M. Lacroix, C. P. Huu and F. Luck, Pressure drop modeling on SOLID foam: State-of-the art correlation, Chemical Engineering Journal, vol. 144, no. 2, pp. 299–311, Oct. 2008, doi: 10.1016/j.cej.2008.06.007.

[5] T. Wang, J. Wang, P. Wang, F. Wang, L. Liu and H. Guo, Non-uniform liquid flow distribution in an alkaline water electrolyzer with concave-convex bipolar plate (CCBP): A numerical study, *International Journal of Hydrogen Energy*, Jan. 2023, doi: 10.1016/j.ijhydene.2022.12.203.

[6] E. B. Nauman, 'Residence Time Distributions', in Handbook of Industrial Mixing, John Wiley & Sons, Ltd, 2003, pp. 1–17. doi: 10.1002/0471451452.ch1.

Methanol intermediated catalytic hydrogenation of CO2 to fuels: A critical review

F.Lappa*[1,2], M. Dusselier[1], G. Leonard[2]

[1]Faculty of Bioscience Engineering, Center for Sustainable Catalysis and Engineering, KU Leuven, Belgium
[2] Chemical Engineering Department, University of Liège, Belgium

Introduction

One of the global problems that need to be solved as soon as possible is the environmental pollution. The reduction of greenhouse gases (GHG) emissions is one of the main solutions that the fields of technology and research focus on, and more specifically the reduction of carbon dioxide which is the major GHG (77% of total GHG emissions)[1]. Multiple technologies have been developed targeting this goal by capturing, storing and further converting CO_2 (Carbon Capture and Storage, CCS and Carbon Capture and Utilization, CCU)[1]. CO_2 can be valorized in many ways such as when it is used directly for example in food industry or oil recovery, when biological fixation is used such as for microalgae growth, when mineralization takes place, for instance for direct carbonation and finally through catalytic reduction for example for methanation or the synthesis of chemicals, fuels etc[2].
This work focuses on the last pathway and more specifically on the hydrogenation of CO_2 to the production of fuels. For this process the feed gases are CO_2 and hydrogen. The source of hydrogen is of high importance as the way it is produced could cause extra GHG emissions. Consequently, hydrogen is divided in 5 categories: grey hydrogen, blue hydrogen, brown hydrogen, turquoise hydrogen and green hydrogen which have different carbon footprints[6]–[11]. It should be noted that Green hydrogen could have potentially the lowest footprint but this is highly dependent on the source of electricity (for instance when electricity is produced from nuclear power the emissions are the lowest, followed by wind and solar energy)[8].
Valorizing C1 compounds such as CO and CO_2 to hydrocarbons is possible through 2 main processes that have been developed which are the Fischer-Tropsch (FT) process and the methanol to hydrocarbons (MTH) route[9], [10]. In the FT synthesis, CO is hydrogenated to hydrocarbons directly or CO_2 is first converted to CO through the reverse Water-Gas-Shift (RWGS) reaction and then CO is hydrogenated to targeted products[11]. With the MTH process, methanol is the important intermediate that can be further converted to hydrocarbons. For this purpose, a first step is necessary in order to convert CO or CO_2 to methanol. The CO to methanol route (with syngas) is commercial and catalytic. Starting with CO_2 conversion is off course more interesting from a GHG point of view. Going to fuels from methanol has some advantages compared to the FT synthesis route. First of all, the hydrocarbons produced this way are of a smaller range maximum with 11 carbon atoms while the production of C1 hydrocarbons such as CH_4 is very low. Another important reason is that the selectivity and yield are high increasing the quality of the fuel produced[9]. On the other hand, when combining CO_2 hydrogenation to methanol process with MTG process some difficulties arise (such as limited selectivity and yield) as well. Developing highly effective materials that catalyze this reaction towards certain products selectively and optimizing the reaction conditions are needed in order for this system to be scaled up.

* Corresponding author: foteini.lappa@kuleuven.be

Methodology

CO_2 to fuels through the methanol synthesis route is a catalytic process as it has been mentioned before. Not so much research has been done on this particular, very complex reaction which leads to the demand of a critical comparison between the catalysts and reaction conditions in order to find useful conclusions and optimum conditions.
First of all it must be explained here that the catalysts needed for this reaction are tandem catalysts that consist of a part that converts CO_2 to methanol (usually an oxide) and a second part for the methanol to fuels reaction (usually a zeolite). The conventional system for CO_2 (and CO) to methanol that has been studied is Cu-Zn-Al while recently, In, Zr and Zn-containing oxides are coming to the fore. Such decent methanol synthesis catalysts can be combined with ZSM-5 or other zeolites[12]–[15]. For the purpose of this paper the latest system will be discussed and used for extracting useful information by collecting data from previous works and comparing them in a critical way, leading to conclusions.

Results and Discussion

To start with, it should be mentioned that the groups who have studied this system have, as main product, alkanes C5+ or aromatics in mind, and work with a feed of H_2 and CO_2 of a ratio equal to 3 (H_2/CO_2). The temperature chosen is always higher than 300°C and more specifically 315-340°C. As for the pressure, 30-40 bar is preferred for the system. Different synthesis methods for the oxide have been tested as well as different Si/Al ratios for the ZSM-5, which relates to its acidity. The Gas Hourly Space Velocity (GHSV) applied to the system lays between the range of 1020-9000 ml/gcat/h. As shown in Figure 1, different Si/Al ratios of the zeolite do not influence the conversion of CO_2 as this is mainly performed at the oxide part of the dual catalyst system. On the other hand, this ratio has an effect on the Space Time Yield (STY) of the target fuels which seems to benefit from low ratios (Si/Al=25 shows the highest STY), while a drop is observed for Si/Al=65 and reaching a plateau with further increase. As it is also worth noticing in Figure 1, the main determinator of the space time conversion is the GHSV (of course linked with the nature of the oxide).

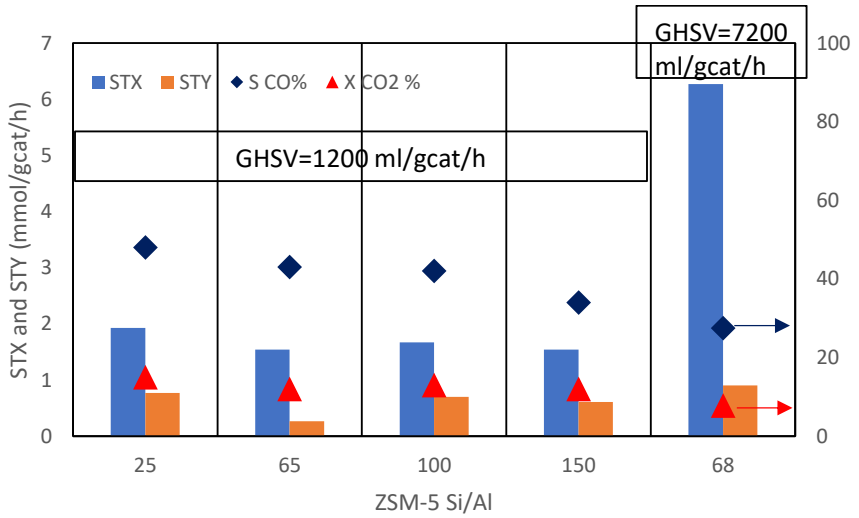

Figure 1. Effect of Si/Al ratio of ZSM-5 zeolite on Space Time Conversion (STX) and Space Time Yield (STY) in a system with dual catalysts physically mixed: ZnZrOx + ZSM-5 Based on data from [12], [13], [14].

Thus, Figure 2 represents the effect of GHSV for the same systems working at 2 different pressures. The main assumption that can be extracted from this comparison is that pressure does not play a major role in STX especially compared to GHSV. However when GHSV is higher, the pressure contributes more to STX because as we can see at 3000 and 3060 ml/g_{cat}/h a big difference is observed. The same behavior is observed for Space Time Yield of fuel-range products even though as it can be seen in Figure 3 there is some data missing.

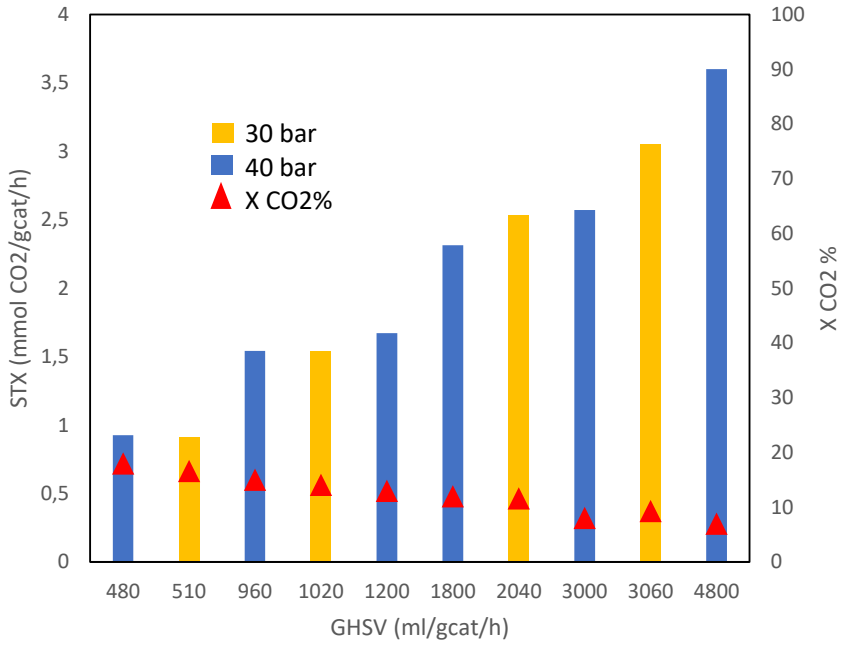

Figure 2. Effect of pressure and GHSV in Space Time Conversion of CO_2 in system ZnZrOx+ZSM-5 [12], [13]

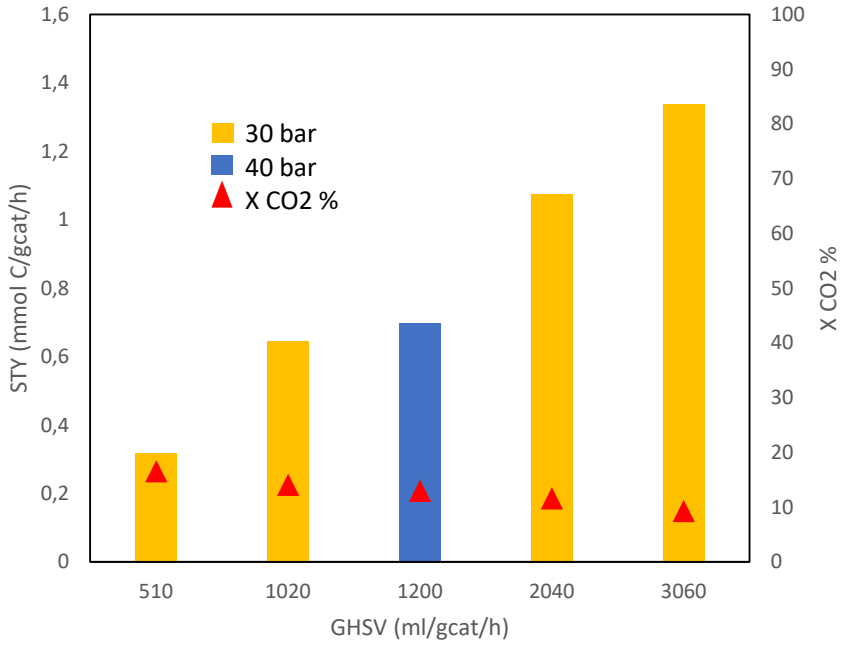

Figure 3. Effect of pressure and GHSV in Space Time Yield in fuel products in system ZnZrOx+ZSM-5 [12], [13]

Conclusions

Based on the preliminary results from this critical review there are some assumptions that can be extracted safely. First of all, the difference in the acidity of the zeolite part, as indicated based on the Si/Al ratio is one of the main contributors for altering the experimental results in the CO_2 conversion to fuels reaction on the part of what happens to the intermediate methanol. Moreover, GHSV plays a crucial role since it is the main way to increase the STX of the CO_2 and at the same time increase the STY of the targeted products. It is important to find an optimum GHSV to work with because increasing the flow has also a negative impact on the conversion of CO_2 with a higher rate compared to the rate of the increase noticed in STYs. In addition, increase of the pressure (30-40) has a slightly positive effect on the system in higher GHSVs. Lower pressures (<20 bar) would lower the conversion of the CO_2/H_2 mixture. However, there is still a lot of research that needs to be done in order to make sure that these assumptions are general conclusion and more contribution is needed towards the study of the mechanism and kinetics of such a complex system. In further work, our research will focus on developing tandem catalysts by improving the zeolites and studying the proximity between the 2 materials (oxide-zeolite), in order to increase the selectivity of gasoline range hydrocarbons and more specifically, C5+ alkanes, while at the same time avoiding the production of aromatics.

References

[1] C. B. Peres, P. M. R. Resende, and L. J. R. Nunes, “clean technologies Advances in Carbon Capture and Use (CCU) Technologies : A Comprehensive Review and CO 2 Mitigation Potential Analysis,” pp. 1193–1207, 2022.

[2] S. Y. Pan, P. C. Chiang, W. Pan, and H. Kim, “Advances in state-of-art valorization technologies for captured CO2 toward sustainable carbon cycle,” *Crit. Rev. Environ. Sci. Technol.*, vol. 48, no. 5, pp. 471–534, 2018, doi: 10.1080/10643389.2018.1469943.

[3] M. Hermesmann and T. E. Müller, “Green, Turquoise, Blue, or Grey? Environmentally friendly Hydrogen Production in Transforming Energy Systems,” *Prog. Energy Combust. Sci.*, vol. 90, no. September 2021, p. 100996, 2022, doi: 10.1016/j.pecs.2022.100996.

[4] T. I. Korányi, M. Németh, A. Beck, and A. Horváth, “Recent Advances in Methane Pyrolysis: Turquoise Hydrogen with Solid Carbon Production,” *Energies*, vol. 15, no. 17, 2022, doi: 10.3390/en15176342.

[5] J. Diab, L. Fulcheri, V. Hessel, V. Rohani, and M. Frenklach, “Why turquoise hydrogen will Be a game changer for the energy transition,” *Int. J. Hydrogen Energy*, vol. 47, no. 61, pp. 25831–25848, 2022, doi: 10.1016/j.ijhydene.2022.05.299.

[6] A. Molina and F. Mondragón, “Reactivity of coal gasification with steam and CO 2,” *Fuel*, vol. 77, no. 15, pp. 1831–1839, 1998, doi: 10.1016/S0016-2361(98)00123-9.

[7] J. Yu, F. J. Tian, M. C. Chow, L. J. McKenzie, and C. Z. Li, “Effect of iron on the gasification of Victorian brown coal with steam: Enhancement of hydrogen production,” *Fuel*, vol. 85, no. 2, pp. 127–133, 2006, doi: 10.1016/j.fuel.2005.05.026.

[8] R. Bhandari, C. A. Trudewind, and P. Zapp, “Life cycle assessment of hydrogen production via electrolysis e a review,” *J. Clean. Prod.*, vol. 85, pp. 151–163, 2014, doi: 10.1016/j.jclepro.2013.07.048.

[9] M. R. Gogate, “Methanol-to-olefins process technology: current status and future prospects,” *Pet. Sci. Technol.*, vol. 37, no. 5, pp. 559–565, 2019, doi: 10.1080/10916466.2018.1555589.

[10] M. L. Hindman, “Methanol to Gasoline technology,” *Proc. Int. Offshore Polar Eng. Conf.*, pp. 38–41, 2013.

[11] Z. Teimouri, N. Abatzoglou, and A. K. Dalai, *Kinetics and selectivity study of fischer-tropsch synthesis to c5+ hydrocarbons: A review*, vol. 11, no. 3. 2021. doi: 10.3390/catal11030330.

[12] Z. Li *et al.*, “Highly Selective Conversion of Carbon Dioxide to Aromatics over Tandem Catalysts,” *Joule*, vol. 3, no. 2, pp. 570–583, 2019, doi: 10.1016/j.joule.2018.10.027.
[13] T. Wang *et al.*, “ZnZrOx integrated with chain-like nanocrystal HZSM-5 as efficient catalysts for aromatics synthesis from CO2 hydrogenation,” *Appl. Catal. B Environ.*, vol. 286, no. January, p. 119929, 2021, doi: 10.1016/j.apcatb.2021.119929.
[14] C. Zhou *et al.*, “Highly Active ZnO-ZrO2 Aerogels Integrated with H-ZSM-5 for Aromatics Synthesis from Carbon Dioxide,” *ACS Catal.*, vol. 10, no. 1, pp. 302–310, 2020, doi: 10.1021/acscatal.9b04309.
[15] P. Gao *et al.*, “Direct conversion of CO2 into liquid fuels with high selectivity over a bifunctional catalyst,” *Nat. Chem.*, vol. 9, no. 10, pp. 1019–1024, 2017, doi: 10.1038/nchem.2794.

Can a non-dimensional Multi-Zone model predict hydrogen distribution during indoor releases?

J. Vanlaere*[1,2,3], J. Blondeau[2,3], P. Hendrick[1,3]

[1]Aero-Thermo-Mechanics Laboratory, Université libre de Bruxelles, Avenue F.D. Roosevelt 50, 1050 Brussels, Belgium
[2]Thermo and Fluid Dynamics (FLOW), Faculty of Engineering, Vrije Universiteit Brussel, Pleinlaan 2, 1050 Brussels, Belgium
[3]Brussels Institute for Thermal-fluid Systems and Clean Energy (BRITE), Université libre de Bruxelles (ULB) and Vrije Universiteit Brussel (VUB), Belgium

Introduction

This extended abstract discusses the prediction of hydrogen distribution within an enclosure following a plume-like release. Prior research has examined hydrogen distribution during and after such releases in both buoyancy and momentum-dominated scenarios. Upon reviewing these studies, it becomes apparent that a limited set of variables defines this physical system. To address this, a dimensional analysis based on Buckingham's Π-theorem is proposed to derive dimensionless numbers of interest. A non-dimensional approach allows to compare datasets of similar problems with various dimensions. This work extends the findings originally presented at the International Conference on Hydrogen Safety 2023 [1].

The distribution is mainly driven by three phenomena; diffusion, momentum and bouyancy. Diffusion is neglected as previously proposed by Worster et Huppert [2]. When momentum is small with respect to bouyancy, a specific filling process can be observed called filling box. It results in a vertical distribution of hydrogen where the heighest concentration appears near the ceiling. Concentration of hydrogen decreases further from the ceiling. When momentum becomes larger with respect to buoyancy, more mixing will be present. As a result, a more homogeneous distribution of hydrogen can be observed. The relation between momentum, buoyancy and volume is typically expressed using the Richardson number of the problem.

$$\mathrm{Ri_v} = \frac{\sqrt[3]{V} \cdot g'}{u_0^2} \tag{1}$$

$$g' = g \cdot \frac{\rho_\mathrm{a} - \rho_0}{\rho_0} \tag{2}$$

where V - volume of the enclosure, m^3; u_0 - release velocity at the orifice, $\mathrm{m\,s^{-1}}$; g' - reduced gravity, $\mathrm{m\,s^{-2}}$; g - gravitational constant, $\mathrm{m\,s^{-2}}$; ρ_a - density of the surrounding air, $\mathrm{kg\,m^{-3}}$; and ρ_0 density of the bouyant gas at the orifice, $\mathrm{kg\,m^{-3}}$.

This study addresses a fundamental problem, focusing on a parallelepiped enclosure with a floor-level ventilation opening. This last assumption is required to consider the problem as isobaric. Hydrogen is released at a constant velocity for a predetermined duration, and the hydrogen mole fraction is calculated at various points within the enclosure. Figure 1 shows a schematical representation of the domain. In a prior study by the same author [1], it was assumed that both the release velocities and orifice diameters were of a similar order of magnitude, resulting in buoyancy dominanated flow in all cases. Consequently, the Richardson number was excluded from the dimensional analysis. This abstract proposes an adapted dimensional analysis that accounts for both momentum and buoyancy as separate factors. Four distinct dimensional scenarios are modeled, where the geometrical attributes and release characteristics are defined by dimensional parameters like length and volumetric flow rate. A dimensionless scenario is defined by a set of dimensionless numbers, and multiple dimensional scenarios can correspond to the same dimensionless scenario. The scenarios studied in this work all have the same dimensionless characteristics,

*Corresponding author: joren.vanlaere@ulb.be

which are selected based on experimental and numerical work by Brzezinska [3].

To model these four scenarios, we employ the Multi-Zone model introduced by Johansson et Runefors [4]. The Multi-Zone model divides the domain into multiple zones. Each zone uses specific models to solve species distribution over time. Details of these different models are provided in [4]. It's important to note that the Multi-Zone model is a recent release, still undergoing further development and validation. Validation is not provided in this abstract, however, the model was previously validated based on the results of Brzezinska [3] by Johansson et Runefors [5].

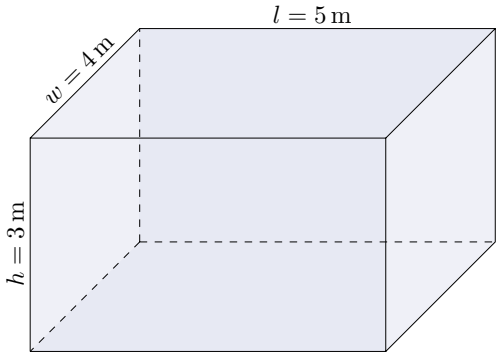

Figure 1: Schematic representation of one of the domains considered in this work. In the Multi-Zone model length, width and height will be divided into 5 by 5 by 10 zones respectively.

Methodology

Based on Cleaver et al.'s work [6] dimensional, functional parameters were selected. To incorporate momentum, the volumetric flow rate was replaced with release velocity and orifice diameter. A dimensional analysis, following Buckingham's approach [7], was then performed to derive a relevant set of dimensionless numbers. Four dimensional cases were modeled and solved using the Multi-Zone model proposed by Johansson et Runefors [4]. One of the dimensional scenarios was validated based on the experimental and numerical work of Brzezinska [3]. Validation is not presented in this extended abstract. As previously mentioned, even though the four scenarios differ dimensionally, they share the same dimensionless characteristics. The results are post-processed, presented and discussed in this extended abstract.

Theory

A dimensional analyis based on Buckingham's Π-theorem has been carried out. The release velocity u_0, the orifice diameter d_0 and the reduced gravity g' are included in the analysis to account for volume flux, momentum flux and buoyant flux. The reduced gravity originates from the Boussinesq approximation that states that differences in density do not influence the system, except for the bouyancy term g'. The details of the dimensional analysis are not provided here, the reader is referred to [7] and [1]. The main idea of Buckingsham's Π-theorem can be stated as follows: If a system is described by a set of n functional parameters containing m primary dimensions, then a set of $n - m$ dimensionless parameters is sufficient to describe the problem. For the release of a buoyant gas, like hydrogen, in a (semi-)closed space where momentum should be accounted for, the following set of functional parameters is proposed:

$$f\left(\chi_{\mathrm{H_2}}, t, u_0, d_0, g', l, w, h, h_0, h_\mathrm{d}, A_\mathrm{vent}\right) = 0 \tag{3}$$

where $\chi_{\mathrm{H_2}}$ - mole fraction of hydrogen, /; t - time, s; u - velocity, $\mathrm{m\,s^{-1}}$; d_0 - diameter of the release orifice, m; g' - reduced gravity, $\mathrm{m\,s^{-2}}$; l - length of enclosure, m; w - width of enclosure, m; h - height of enclosure, m; h_0 - height of release, m; h_d - height of measurement, m; A_vent - ventilation surface area, $\mathrm{m^2}$. A non-dimensional description of the same problem is derived from the dimensional analysis:

$$\Psi\left(\chi_{\mathrm{H_2}}, \frac{l}{h}, \frac{w}{h}, \frac{d_0}{h}, \frac{h_0}{h}, \frac{h_\mathrm{d}}{h}, \frac{A_\mathrm{vent}}{h^2}, \frac{u_0 \cdot t}{h}, \frac{h \cdot g'}{u_0^2}\right) = 0 \tag{4}$$

The problem's Richardson number is typically formulated as in Equation 1. However, in this work we chose to use the following, equivalent expression based on the selected parameters of interest:

$$\mathrm{Ri_v} = \frac{h \cdot g'}{u_0^2} \tag{5}$$

Dimensionless time t^* and dimensionless height above the ground h_d^* are defined as:

$$t^* = \frac{u_0 \cdot t}{h} \tag{6}$$

$$h_\mathrm{d}^* = \frac{h_\mathrm{d}}{h} \tag{7}$$

Models

To reduce the number of dimensions involved in the analysis, limited simplifications were brought to the scenario investigated by Brzezinska [3], which corresponds to one of the four dimensional scenarios simulated here. It is important to note that the experimental setup used in their study does not precisely resemble a theoretical parallelepiped. In addition, the release orifice in the experiment is not perfectly centered, but approximated as such in the model. Hydrogen is released from the orifice at a velocity of $130\,\mathrm{m\,s^{-1}}$ for 50 s. Subsequently, the release is halted, yet the calculation continues for an additional 150 s. The enclosure is not entirely sealed; this is approximated in the model by incorporating a ventilation surface near the floor, with an area of $0.1\,\mathrm{m^2}$, as proposed by Johansson et Runefors [5]. The dimensionless numbers used in this study were derived for this streamlined case, and were kept constant for the three other dimensional cases. Johansson et Runefors [4] divided the domain into 3 by 3 by 10 zones. For this research, a grid dependence analysis was conducted, leading to the domain being divided into 5 by 5 by 10 zones. It's worth noting that the Multi-Zone model only accepts natural numbers as input for the geometry. Therefore, parameters cannot be downscaled from the initial scenario. Table 1 provides a summary of the key dimensional (blue) and dimensionless (red) parameters for these four scenarios.

Table 1: Details on the four scenarios. The first one is based on the work of Brzezinska [3]. Dimensional parameters are presented in blue, dimensionless numbers in red.

	l [m]	b [m]	h [m]	A_vent [$\mathrm{m^2}$]	d [m]	u_0 [$\mathrm{m\,s^{-1}}$]	t_stop [s]	$\mathrm{Ri_v}$	t^*_stop
Scenario 1	4	5	3	0.01	0.02	130	50	0.00086	2167
Scenario 2	8	10	6	0.08	0.04	180	72	0.00090	2160
Scenario 3	12	15	9	0.27	0.06	225	87	0.00086	2175
Scenario 4	16	20	12	0.64	0.08	256	101	0.00089	2155

Results & Discussion

Figure 2 presents the data as a function of vertical distance above the floor (h_d) on the top graph, and the dimensionless distance above the floor (h_d^*) on the bottom graph. The data is calculated far from the plume at the end of the release phase. The influence of utilizing dimensionless numbers becomes apparent, as the top graph illustrates four datasets with distinct characteristics, while the bottom graph showcases the substantial similarity among the data.

Figure 3 shows the extent of similarity among the four datasets. The deviation of hydrogen mole fraction is measured at each dimenionless height h_d^*. The relative difference predominantly remains within 0.25 (25%) of scenario 1 for the majority of the data. However, at lower values, the relative difference surpasses the limits of the figure. Figure 2 shows that the relative discrepancy locally reaches more than 150 % at dimensionless heights lower than 0.2. This is due to the low absolute value of the concentration at this elevation, especially for the reference scenario.

Figure 4 show the change in distribution over time. The four datasets are computed in zones sharing a consistent non-dimensional location, situated at the sixth vertical layer out of a total of ten layers and located at a substantial distance from the plume. By comparing the dimensional and non-dimensional

results, the similarity between the datasets becomes apparent even if the relative discrepancies are non-negligible. It shows that the datasets are not only similar at one certain value of t^*, but remain similar during the range of dimensionless time studied in this work.

Although they could be deemed reasonable for safety applications where sufficient margins can be applied, the observed discrepancies between the non-dimensional results limit the generalization power of this approach combined to the Multi-Zone model proposed by [4]. This can result from two distinct causes: or the non-dimensional analysis is not complete, or the validity of the Multi-Zone model is limited to specific dimensional conditions.

Further investigation is required to ascertain if all functional parameters have been encompassed in the current analysis. For example, the Reynolds number might influence mixing, resulting in higher concentrations in the lower regions. In parallel, the Multi-Zone model could be further validated or refined through additional experimental and numerical results.

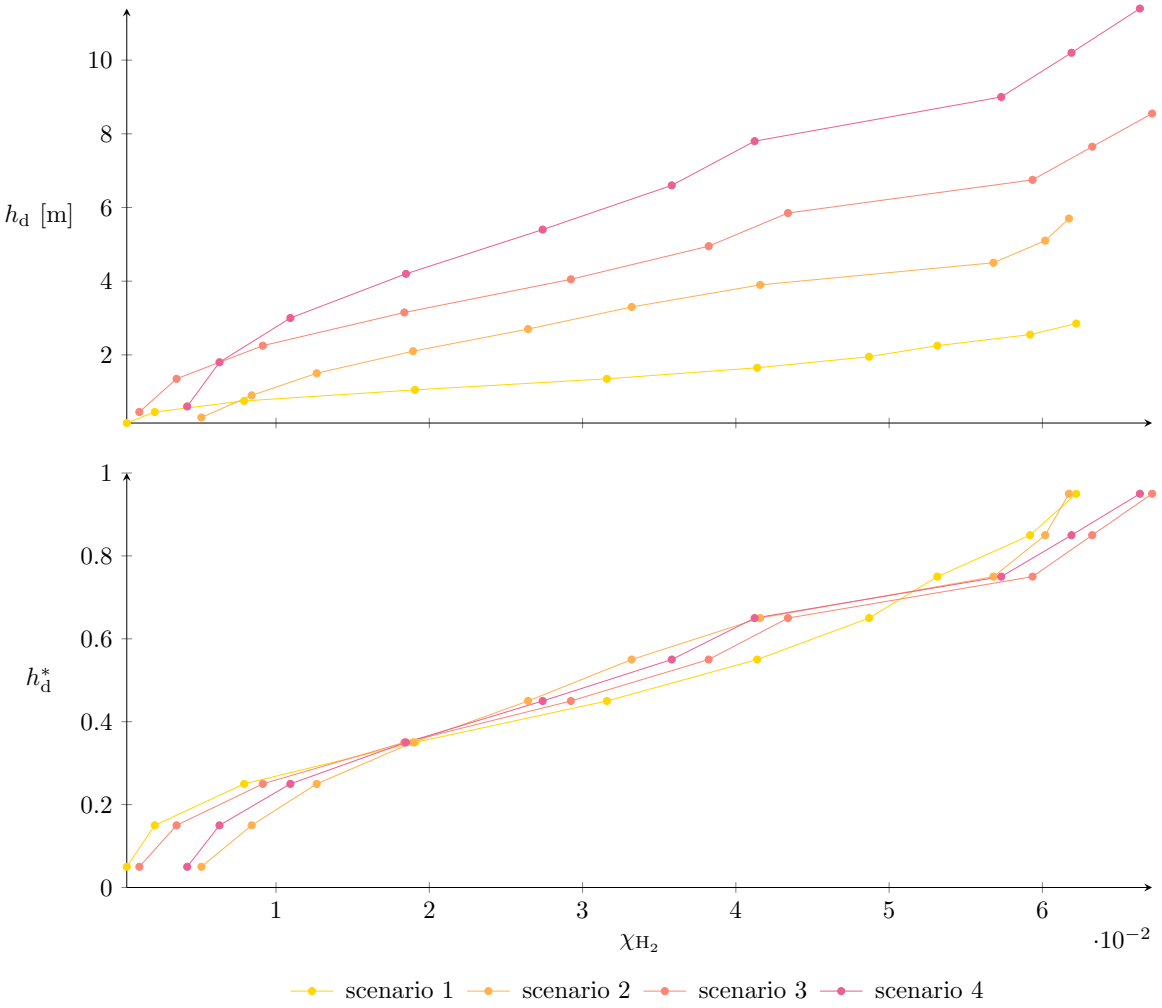

Figure 2: Vertical distribution of hydrogen at t^*_stop, measured as hydrogen mole fraction (χ_{H_2}). Upper graph uses the measuring height h_d on the vertical axis. In the lower graph dimensionless measuring height h^*_d is used.

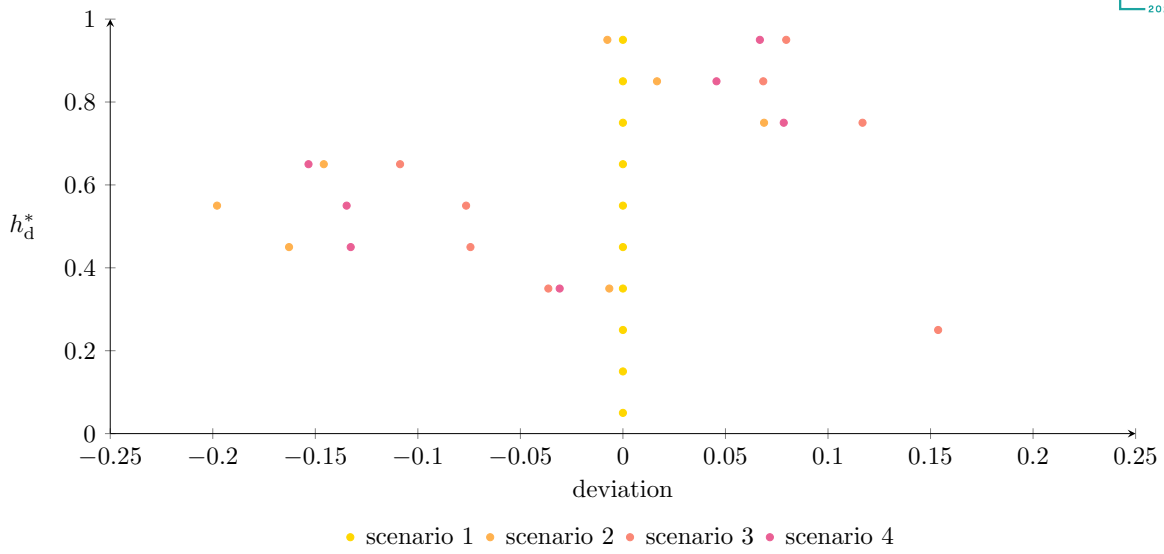

Figure 3: Deviation of χ_{H_2} compared to scenario 1, as a function of non-dimensional height h_{d}^*. For scenario 1 experimental and numerical result are available in [3].

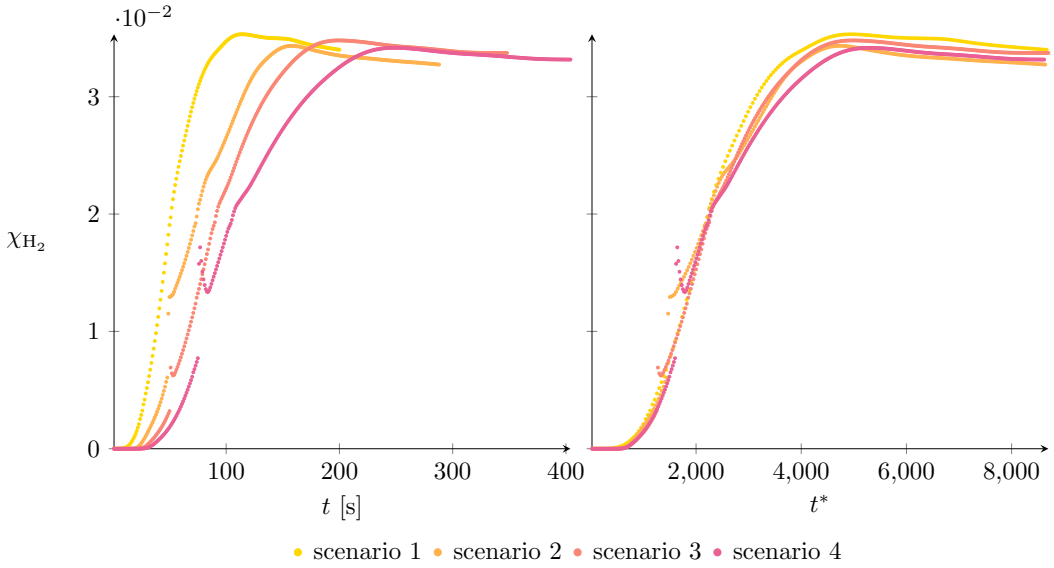

Figure 4: Time series of hydrogen mole fraction, measered at a location far from the plume in the sixth vertical layer out of ten. On the left graph as a function of time (t). On the right graph as a function of dimensionless time (t^*).

Conclusion

A dimensional analysis on an indoor release of hydrogen based on Buckingham's Π-theorem is discussed, building upon prior research by Vanlaere et al. [1]. In the presented scenarios, momentum takes on a more significant role and has thus been integrated into the dimensional analysis. Four distinct dimensional scenarios were modeled using the Multi-Zone model introduced by Johansson et Runefors [4]. Our results show the similarity of the non-dimensional concentration profiles obtained for several, dimensional cases of indoor releases of hydrogen, modeled with the Multi-Zone approach. However, the predicted hydrogen concentrations exhibits non-negligible discrepancies. Further works should be carried out to investigate the completeness of the dimensional analysis for such a case, and the validity of the Multi-Zone approach for broader conditions than those for which it has been validated.

References

[1] Joren Vanlaere, Patrick Hendrick, and Julien Blondeau. A non-dimensional surrogate model of stratified filling during indoor, plume-like hydrogen releases [paper presentation]. In *International Conference on Hydrogen Safety*, Quebec, 2023.

[2] M. Grae Worster and Herbert E. Huppert. Time-dependent density profiles in a filling box. *Journal of Fluid Mechanics*, 132:457–466, 1983.

[3] Dorota Brzezińska. Hydrogen Dispersion and Ventilation Effects in Enclosures under Different Release Conditions. *Energies*, 14(13):4029, 7 2021.

[4] Nils Johansson and Marcus Runefors. MZ-gas: A multi-zone model for calculating hydrogen concentrations in an enclosure, 6 2023.

[5] Marcus Runefors and Nils Johansson. A Multi-Zone Model for Hydrogen Accumulation and Ventilation in Enclosures. In *International Conference on Hydrogen Safety*, Quebec, 2023.

[6] R.P. Cleaver, M.R. Marshal, and P.F. Linden. The build-up of concentration within a single enclosed volume following a release of natural gas. *Journal of Hazardous Materials*, 36(3):209–226, 3 1994.

[7] E. Buckingham. On Physically Similar Systems; Illustrations of the Use of Dimensional Equations. *Physical Review*, 4(4):345–376, 10 1914.

Can floating wind accelerate EU & UK renewable hydrogen targets with US Inflation Reduction Act influenced tax credits?

Omar S. Ibrahim [*1,2], Matthew Kotarbinski [3], Shane McDonagh[4], Cian Desmond [5], Jerry D. Murphy[1]

[1]University College Cork, Cork, Ireland
[2]ORE Catapult, Glasgow, United Kingdom
[3]National Renewable Energy Laboratory (NREL), Golden, United States
[4]International Energy Agency, Paris, France
[5]ESB, Dublin, Ireland

Introduction

In response to national targets aimed at increasing renewable energy, especially in the context of floating offshore wind, and considering the global projections for expanding clean hydrogen [1], it is essential to evaluate optimal pathways and systems. This evaluation focuses on the integration of high-capacity factor floating offshore wind with hydrogen production. The EU recently doubled the 2030 target to 10 million tonnes (circa. 57 GW) of domestic renewable hydrogen [2]. The UK recently doubled their ambition up to 10 GW of low-carbon hydrogen production capacity by 2030, with at least half to be produced through electrolysis [3]. On the other hand, floating offshore wind is set for significant expansion with approximately 80% of the world's offshore wind resource potential in waters deeper than 60 metres [4], where bottom-fixed wind turbines are less feasible. The continued growth of the hydrogen economy is necessary to effectively decarbonise particular sectors including heavy transport, steel, ammonia and methanol production. More recently, the role of hydrogen is perceived to be a key catalyst as a natural gas replacement due to the various global supply chain sensitivities, including the war in Ukraine and the associated reduction of fossil fuel dependency and supply from Russia. Leveraging the potential of offshore wind is believed to be a significant contributor to unlocking this projected clean hydrogen expansion.

Methodology

This study investigates how adapting a timely sensitive policy incentives scheme as the US inflation reduction act (IRA), in both the EU and the UK regions could assist in reducing deployment barriers to meet their clean hydrogen targets. The 45V "Credit for production of clean hydrogen" [5] is a key IRA incentive that has been identified for this analysis. The study aims to understand how much the forecasted range of levelised cost of hydrogen (LCoH) from floating wind are affected by applying a similar support mechanism from 2030-2040. This analysis aims to contribute to the achievement of both the EU and UK renewable hydrogen targets. In present time, dedicated floating wind farms for hydrogen production are not clear in any of the two regions' roadmaps. However, this analysis aims to gain insights if introducing a similar tax credits approach could serve as a potential motivator for relevant stakeholders develop dedicated floating wind farms for hydrogen production.

The introduction of IRA tax credits aims to overcome barriers to clean energy deployment. This includes lowering the costs of clean energy and related products, reducing emissions to achieve decarbonization goals, and providing incentives for newly commissioned renewable energy plants. These plants are to be eligible for specific tax credit percentages, potentially up to 100%. This approach is designed to expedite the development of projects, ensuring their

* Corresponding author: oibrahim@ucc.ie

timely completion to meet national targets. The analysis particularly targets domestic green hydrogen production in both regions at potential floating wind sites. The generic techno-economic assessments (TEAs) of floating wind-to-hydrogen systems from an earlier piece of work are used as the base case scenario for this study. Three levelised cost of energy (LCoE) scenarios were considered; best, average and worst cases. This consequently dictated three levels of LCoHs forming a range of values as base policy scenarios for this work.

Discussion

The analysis has an emphasis on adapting the approach for a large-scale hydrogen production outside the US, with a different proposal for the bonus tax credits component. The study explores three main policy scenarios for the LCoH. First, the ‘no tax credits’scenario, which provides a technological, cost, and performance baseline for the use-cases. Second, the ‘base tax credits’ scenario, which includes the full 100% credit values however not including any potential bonus credits or any credit multiplier known as the Prevailing Wage and Apprenticeship (PWA) requirement. Third, the ‘maximum tax credits’ scenario, which reflects the full 100% credit values in addition to bonus credits and credit multiplier.

Conclusions

The study concludes a sensitivity analysis reaching an adapted credit multipliers proposal in the context, with a different bonus tax credits scheme. Conclusions also include estimates of the projected scale of dedicated floating wind to hydrogen in both the EU and the UK.

References

[1] IEA. Global Hydrogen Review 2022. Paris: 2022. https://doi.org/10.1787/39351842-en.
[2] European Commission. REPowerEU: A plan to rapidly reduce dependence on Russian fossil fuels and fast forward the green transition 2022:1–11.
[3] HM Government. Hydrogen Net Zero Investment Roadmap The UK is leading the charge towards a net zero , nature-positive future. 2023.
[4] Ibrahim OS, Singlitico A, Proskovics R, Mcdonagh S, Desmond C, Murphy JD. Dedicated large-scale floating offshore wind to hydrogen : Assessing design variables in proposed typologies. Renew Sustain Energy Rev 2022;160:112310. https://doi.org/10.1016/j.rser.2022.112310.
[5] U.S. government. §45V. Credit for production of clean hydrogen 2022. https://uscode.house.gov/view.xhtml?req=granuleid:USC-prelim-title26-section45V&num=0&edition=prelim (accessed July 5, 2023).

Catalysts on Top? Importance of the final layer of a catalyst on OER performance using Ni-Fe catalysts deposited by ALD

R. Blomme*[,1], R. Ramesh[1] and J. Dendooven[1]

[1]Conformal Coating of Nanostructures (CoCooN), Department of Solid State Sciences, Ghent University, 9000 Ghent, Belgium

Introduction

In achieving the global dream of a sustainable future, the development of new and alternative methods to generate electricity are of high importance. Current renewable energy sources are mainly dependent on the sun and wind, and are thus very unpredictable. To achieve a reliable energy supply overall, we need to be able to store clean energy for extended periods of time to compensate for unfavorable weather conditions or sudden surges in energy demand.

One way to store energy is by generating H_2-gas, which has several interesting advantages as an energy carrier molecule. It has a very high energy density, is multifunctional as feedstock or an energy carrier and it is not a greenhouse gas itself. However, the production efficiency of green H_2 still needs optimization before it can be adopted on a global scale. Electrochemical water splitting is primarily hindered by the sluggish kinetics of the oxygen evolution half-reaction (OER) of the process. This involves a transfer of four electrons, each with its own intermediary product(s) requiring catalysis, resulting in a significant overpotential[1].

Atomic layer deposition (ALD) could be an interesting technique in the research, development and possibly production of such OER catalytic materials. This technique is suited to deposit thin films in a controlled layer-by-layer manner with dimension control up to the Angström level. In this development, transition metals could be interesting catalyst candidates due to their availability and pricing over traditional OER catalysts based on noble metals [2]. Both oxides and phosphate variants have been explored; the latter occasionally outperforming the former[3][4].

Nickel has been shown to be one of the more OER-active transition metals, and doping or combining it with iron seems to further increase its performance [5]. Inspired by these results, ALD was used in this work to deposit and finetune the properties of a Ni-Fe ternary phosphate for its use as an OER-catalyst material. This material was deposited by alternating ALD cycles of Ni- and Fe-phosphate (denoted here as NiPO and FePO) based on previous works of Rongé et al.[6] and Henderick et al.[7].

* Corresponding author: rpblomme.blomme@ugent.be

Methodology

Using ALD a set of Ni-Fe mixed metal phosphates were deposited on Ni-PVD substrates a and tested in a rotating-disc electrode (RDE) set-up. The effects of changing certain parameters such as composition, thickness and ALD-sequence on the performance of the sample for OER catalysis were observed and compared.

Discussion

Results indicated that compositions with high nickel and low iron content performed best. Within the samples deposited with a 4 to 1 nickel to iron ALD ratio the better performing materials were the ones where the iron ALD cycle was deposited last (Fig 1).

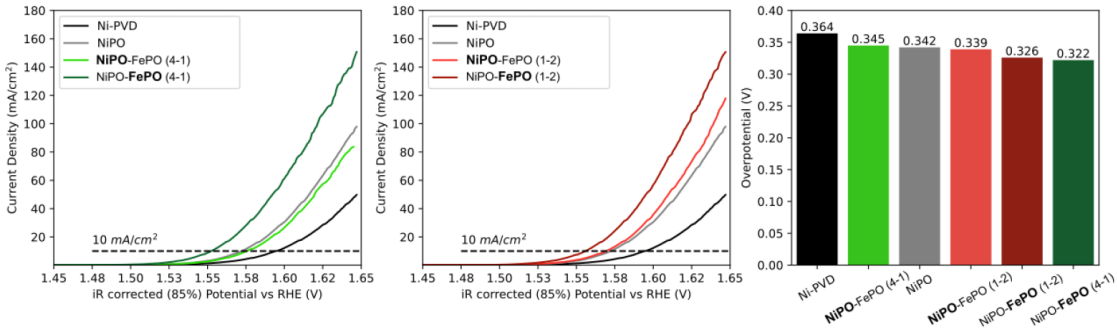

Figure 1: Overview of the results of changing both composition and ALD sequence on the performance of the materials. Largest effects seems to be originating from the species present on the surface of the deposited material.

Also the thickness of the material played a significant role in the performance of the material, as thickness increased up to 160 nm the performance of the material increased accordingly.

Conclusions

The results of this explorative work in the use of ALD for the development of OER catalytic materials indicate that it is a promising technique due to the precise control that can be exerted over both the thickness and composition of the material. Specifically the option to exert high control over the surface of the catalyst can be a big asset in researching catalytic materials.

References

[1] X. Xie, Adv. Funct. Mater., **32**, 2110036 (2022)
[2] C.C.L. McRory,J. Am. Chem. Soc., **137**, 13, 4347–4357 (2015)
[3] J. Rongé, Nanoscale Adv., **1**, 4166-4172 (2019)
[4] R. Zhang, ACS Catal., **11**, 5, 2774–2785 (2021)
[5] F. Diongini, Adv. Energy Mater., **6**, 1600621(2016)
[6] T. Dobbelaere, Chem. Mater., **28**, 10, 3435-3445(2016)
[7] L. Henderick, Dalton Trans., **51**, 2059(2022)

Cathode catalyst layer transport limitations inside the PEM fuel cell

T. Servais*, N. Job

Department of Chemical Engineering - NCE (Nanomaterials, Catalysis, Electrochemistry), University of Liège, 4000 Liège, Belgium

Introduction

The proton exchange membrane (PEM) fuel cell is a promising alternative to current energy converters that rely on fossil fuels. Its valuable qualities, including durability, ability to operate at low temperatures, and compactness, could make it the future of power sources. In addition, the PEM fuel cell does not produce pollutants, only water as a by-product. Despite these advantages, the PEM fuel cell is not yet fully commercialized due to its high manufacturing cost, which is partly due to the use of platinum as a catalyst for chemical reactions [1,2].

The PEM fuel cell is an electrochemical device that converts chemical energy into an electric current. Like a battery, it functions through a set of redox reactions separated by an electrolyte, the proton exchange membrane. However, H_2 at the anode and O_2 at the cathode have to be fed continuously to produce the electric energy. In addition, platinum (Pt) must be added to the electrodes to catalyze the electrochemical reactions. To reduce the manufacturing cost of the PEM fuel cell, the amount of platinum is usually minimized by dispersing it as nanometer-sized particles onto a conductive carbon support; the obtained catalysts are used to manufacture the catalyst layers on both sides of the PEM. This structure provides a high surface area for the catalyst but requires that the chemical reactants can access each catalyst particle. While the carbon conducts electrons, the pores of the support supply other chemical species. Gas reactants diffuse in the carbon structure and an ionomer network is built inside the pores to provide a pathway for the protons between the PEM and the catalyst. This network is obtained using a polymer similar to that used in the PEM.

In open circuit, the voltage of the cell can be calculated using the Nernst equation. However, when a current is produced, three different voltage drops, or overpotentials η, are observed (Eq. 1), corresponding to energy losses.

$$\eta = \eta_{k} + \eta_{ohm} + \eta_{diff} \quad (1)$$

The voltage of the PEM fuel cell is lowered by η_k due to the energy required to activate the chemical reactions. As the current increases, the transport of electrons and ions through the ionomer and carbon support becomes a limiting factor (η_{ohm}), causing a linear decrease in cell voltage following Ohm's law. At larger currents, the reaction rate becomes faster than the

* Corresponding author: tom.servais@uliege.be

supply of gas reactants, which results in a further decrease in cell voltage due to the diffusion of gas through the electrode to the active sites (η_{diff}). While the activation energy is intrinsic to the chemical reactions and the choice of catalyst, the overpotentials linked to the transport of charges and the diffusion of gas reactants are influenced by the electrode structure. However, these voltage losses are often seen as "black boxes," making it difficult to determine the limiting phenomena in the process.

Methodology

The goal of this project is to investigate the causes of performance limitations of the cathode catalyst layer of PEM fuel cells. To quantify the transport properties and parameters of the fuel cell, electrochemical impedance spectroscopy [3,4] and limiting current [5-7] methods are often used in the literature. In this paper, various catalyst layer architectures will be considered to distinguish between ion, electron, and oxygen transport. The project will explore different configurations where catalyst particles are only present in certain areas of the catalyst layer. The diffusion and conductivity properties will then be retrieved by analyzing the polarization curves exhibited by the electrode configurations.

Figure 1 illustrates two different catalyst distributions of interest. In (a), the catalyst is situated near the membrane, so the distance for protons to cross is short. However, oxygen must diffuse across the entire catalyst layer to reach the active sites, and electrons have a longer distance to travel to reach platinum. In contrast, the distribution of catalyst in (b) has the opposite effect on chemical species. Protons must conduct across the full width of the catalyst layer *via* the ionomer network. However, the diffusion process that channels oxygen to the active sites is shorter, and electrons do not need to cross the entire catalyst layer to reach Pt.

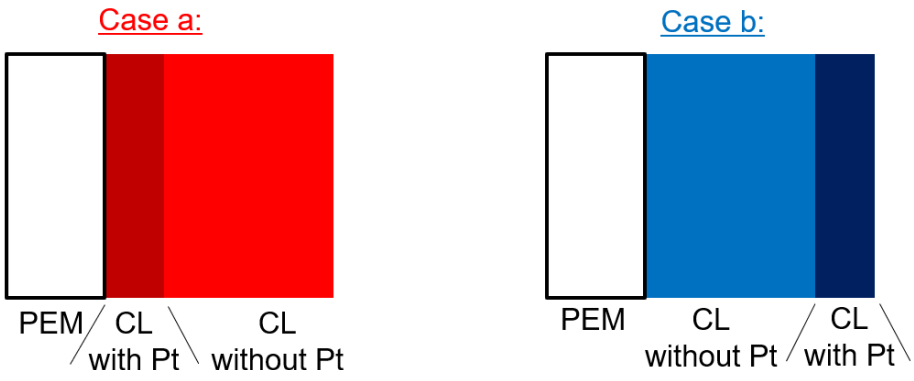

Figure 1: Cathode catalyst layers (CL) configurations considered.

Two inks were prepared to manufacture either active or inactive sublayers on top of each other. The catalyst powder used for active layers is made of 50 wt.% Pt on carbon black Ketjenblack EC-300J purchased at Premetek while the inactive layer is made of Ketjenblack EC-300J alone. An ionomer/carbon ratio of 0.8 was selected, and the solvent was a mix of water and isopropyl alcohol. Their weight ratio was fixed at 1.3 to prevent combustion of isopropyl alcohol, especially when contacted with Pt and carbon. Ionomer was added to the

mixture by incorporating Nafion® D2021. The complete composition of the ink was as follows: 1.1 wt.% of C, 53.8 wt.% of MilliQ water, 4.9 wt.% of Nafion® D2021, and 41.2 wt.% of isopropyl alcohol. It is important to note that this composition is expressed in terms of C and not Pt/C. Therefore, the amount of Pt/C catalyst must be adjusted to meet this composition, depending on the Pt content. This means that the volume of Pt is ignored, as it accounts for a negligible portion of the ink volume due to its high density.

To form the catalyst layers on both sides of the PEM, the spray deposition technique was used, which involved a nozzle connected to a robotic arm in a container. A plate with a controllable temperature was put in the container to evaporate the solvents of the sprayed ink. An aluminum mask with a square hole of 5 cm x 5 cm was placed on top of Nafion® NRE-212 membranes to cover the appropriate area. The deposition size (25 cm^2) was limited by the available cells and test bench in the laboratory. The nozzle of the spray was fed by air, and the outlet relative pressure was set at 0.4 MPa. A syringe pump was used to control the ink flow rate at 0.3 mL min^{-1} for atomization. Forty sublayers were required to spray catalyst layers of 10 µm. The Pt loading for the anode side was 0.33 mg cm^{-2} (full active layer) while it was 0.066 mg cm^{-2} at the cathode as the active layer is five times smaller.

The membrane-electrodes assemblies (AMEs) were made by adding gas diffusion layers (Freudenberg H23C6) on both electrodes. After hot pressing at 403 K with a force of 30 kN for 3 min, the assemblies were then clamped in cells by applying a 8-Nm torque. The fuel cells were conditioned on the test bench by imposing a constant voltage of 0.6 V. The flowrates supplied during the experiments were 400 mL min^{-1} of H_2 at the anode and 1000 mL min^{-1} of air at the cathode. The relative humidity was maintained at 100% at both electrodes. Every 10 min during conditioning, electrochemical impedance spectroscopy (EIS) was performed to check the high frequency resistance and thus, evaluate the humidification of the membrane electrode assemblies. To assess the performance of the fuel cells during stabilization, a polarization curve is carried out every 30 min. This procedure was repeated during one day which is enough for chronoamperometry, EIS and polarization curve to simultaneously stabilize. It has to be noted that a cyclic voltammetry with nitrogen flushed at the cathode is performed at the start and end of the conditioning day to determine the active surface area.

Five different cathode electrode configurations were characterized for this project. Table 1 summarizes different parameters related to these electrodes. The active parts of these electrodes have a thickness of 2 µm for each configuration.

Table 1: Summary of the different cathode electrode configurations envisaged in this project.

Name	**Thickness** [µm]	**Structure**
a	10	Active layer close to the membrane
b	10	Active layer away from the membrane
b2	18	Active layer away from the membrane
c	2	Active layer only
d	10	Active layer in between two identical inactive layers

Discussion

Figure 2 shows the polarization curves after stabilization for cathode catalyst layers in the configurations (a) and (b). This graph also displays the resulting curve for the configuration (c) which is just a thin active layer of 2 µm, one fifth of the thickness of the (a) and (b) electrodes. The poor performance exhibited by the case (b) indicates the large impact of proton resistivity on the performance of the electrode structure. Indeed, the only difference between (b) and (c) is the inactive layer between the membrane and the 2-µm active layer. On the contrary, the electrode in case a produces a slightly larger current than the case (c). The inactive layer in this configuration seems to play a beneficial role. The larger electrode volume could improve the water management. In Figure 3, the (a) and (b) configurations are now compared with case (d). In this electrode, the 2-µm active layer is now in between two 4-µm inactive layers to make the same electrode thickness as the configurations (a) and (b). As expected, the polarization curve for case (d) is better than the case (b) but worse than (a), confirming the impact of proton resistivity.

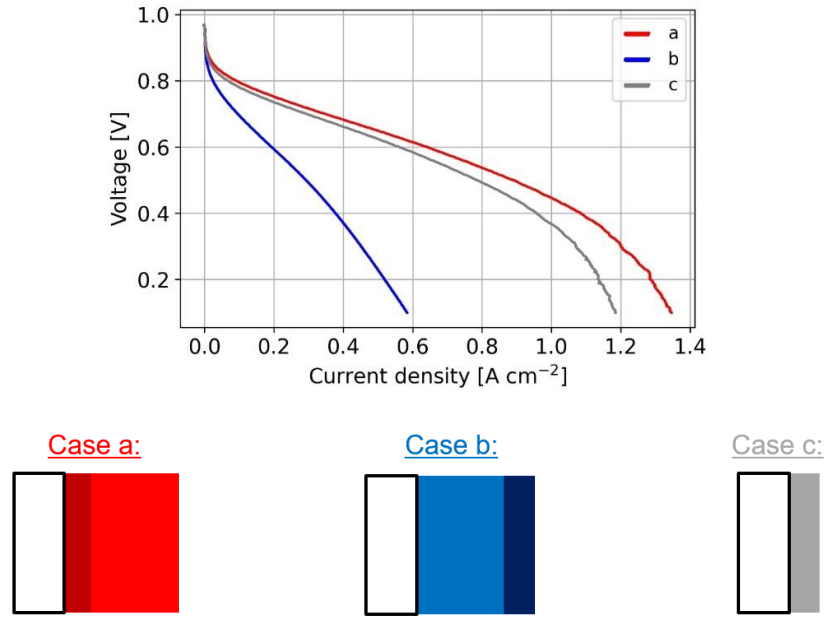

Figure 2: Polarization curves for cathode catalyst layers configurations a, b and c.

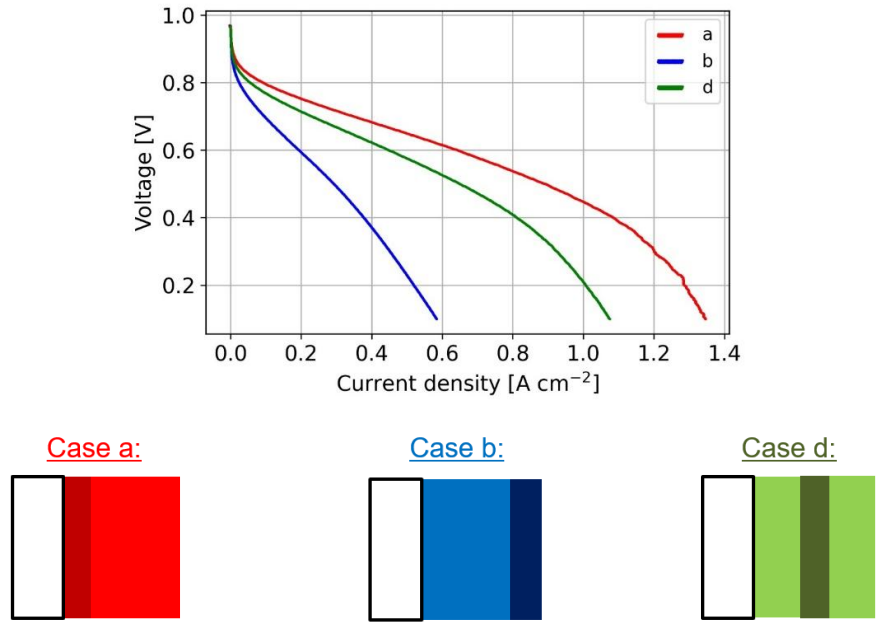

Figure 3: Polarization curves for cathode catalyst layers configurations a, b and d.

Now that the large impact of proton conductivity is known in the case of this electrode formulation, the proton resistivity can be quantified using the active/inactive layers. Figure 4 displays the polarization curves for cases (b) and (c) that were already mentioned in the previous graphs. Concerning case (b2), the inactive layer next to the membrane is twice the thickness of the case (b) (16 µm) while maintaining the same active layer. What differentiates these three electrodes is the path that protons have to cross to reach the active sites. It means that the polarization curves are only different by a resistance factor at low current, when no diffusion overvoltage occurs. By applying a linear factor to the curves, the value of resistance of these inactive layers can be retrieved and the proton resistivity computed is: 525±75 Ω cm.

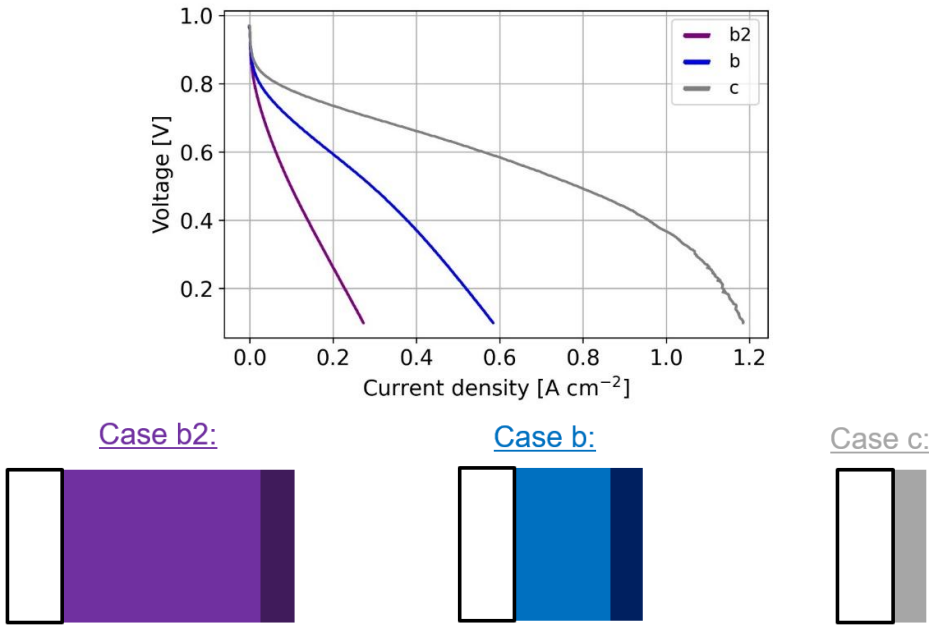

Figure 4: Polarization curves for cathode catalyst layers configurations b2, b and c.

Conclusions

This experimental project aims at determining the limitation arising from the cathode catalyst layer. Catalyst layers were prepared using robotic spray ink deposition and were then characterized *in situ*. After conditioning, the analysis was focused on the polarization curves. Five different configurations of catalyst layers involving active and inactive areas were considered to distinguish between proton, electron and oxygen transports in the layer structure. The proton resistivity was found to be the main source of overvoltage in the cathode catalyst layer, the oxygen and electric transports having nearly no impact in the case of the chosen electrode formulation. Finally, a value of proton resistivity was found by taking advantage of the active/inactive layers architectures.

This project will then focus on the modeling of the polarization curves and the electrochemical impedance spectroscopy curves using a 1D model. In the meantime, the carbon black used in the catalyst layer will be replaced by a nanostructured carbon, *i.e.* a carbon xerogel, which will deeply modify its transport properties. Indeed, the pore texture of this material can be tuned by slightly changing the synthesis procedure, and the electrical conductivity will depend on the particle size. This will allow to obtain properties much different from carbon-black based catalytic layers and highlight different transport phenomena.

References

[1] N. Guerrero Moreno, M. Cisneros Molina, D. Gervasio, and J. F. Perez Robles, “Approaches to polymer electrolyte membrane fuel cells (PEMFCs) and their cost”, *Renewable and Sustainable Energy Reviews*, vol. 52, pp. 89-906, 8 2015.

[2] O. Z. Sharaf and M. F. Orhan. “An overview of fuel cell technology”. *Fundamentals and applications, Renewable and Sustainable Energy Reviews*, vol. 32, pp. 810-853, 4 2014.

[3] T. V. Reshetenko et al. “Systematic studies of the gas humidification effects on spatial PEMFC performance distributions”, *Electrochemical Acta 69*, pp. 220-229, 2012.

[4] T. Gaumont et al. “Measurement of protonic resistance of catalyst layers as a tool for degradation monitoring”, *International Journal of Hydrogen 42*, pp. 1800-1812, 2017.

[5] D.R. Baker et al. “Measurement of Oxygen Transport Resistance in PEM Fuel Cells by Limiting Current Methods”, *Journal of the Electrochemical Society 156*, pp. B991-B1003, 2009

[6] C.Wang et al. “The Experimental Measurement of Local and Bulk Oxygen Transport Resistances in the Catalyst Layer of Proton Exchange Membrane Fuel Cells”, *The journal of Physical Chemistry Letters 8*, pp. 5848-5852, 2017

[7] Y. V. Yakovlev et al.: “Ionomer content effect on charge and gas transport in the cathode catalyst layer of proton-exchange membrane fuel cells”, *Journal of Power Sources 490*, 2021

Challenges Related to the Application of Hydrogen Fuel Cells in Unmanned Aerial Vehicles

J. Mus*[1] and F. Buysschaert[1]

[1]KU Leuven, Department of Mechanical Engineering, Div. TME, Bruges Campus

1 Introduction

Unmanned Aerial Vehicles (UAVs) have revolutionised the aircraft industry. Currently, the applications and sectors in which they are deployed keep increasing [2]. Unlike other aerial vehicles, UAVs offer higher flexibility, are easier to deploy, and are cheaper [11]. Examples of areas in which UAVs are mainly deployed are goods delivery, inspection, agriculture, monitoring and wireless communication [1]. It is expected that the drone market will keep growing. Fortune Business published a recent market report (2023) and expects a compound annual growth rate (CAGR) of 25.82% between 2023 and 2030 [5].

The popularity of electric-powered UAVs is increasing, as systems relying on combustion engines have lower efficiencies and emit greenhouse gases [22]. The overwhelming evidence of climate change's impact calls for urgent action. Rising temperatures, melting ice caps, forest fires and extreme weather events are already affecting the global population [9]. Other advantages of electric-powered UAVs are a low thermal signature, quieter operation, and an easier-to-control powertrain [8]. However, combustion engines typically use conventional liquid fuels, characterised by a higher gravimetric energy density compared to batteries [4]. Therefore, electric UAVs powered by batteries typically have lower endurance [11] and suffer long charging times [1, 15].

According to the literature [3, 6, 22], FCs have the potential to increase the endurance and payload of electric UAVs significantly. This is thanks to their high conversion energy, and the high gravimetric energy density of hydrogen [12, 17]. A long endurance and high payload UAV combined with the advantages of electric propulsion could open opportunities for broader applications and new markets [15]. However, there are several challenges related to applying FCs in UAVs. This abstract aims to address these challenges and unveils ideas to overcome them, which will be the research direction. First, the FC operating principle is discussed, and different FC types are compared to understand the best option for UAVs. After that, the major limitations of FCs are discussed and then linked to challenges for UAV implementation. As the research is still in its initial stages, the current ideas for a methodology to overcome these challenges are briefly discussed. Afterwards, the limitations and threats to validity are unveiled in the discussion section. To conclude, the following steps and goals of this research are discussed.

2 Fuel Cells for UAVs

FCs convert hydrogen and oxygen, usually from air, into water through redox reactions, as the molecules can achieve a lower energy state. This spontaneous process converts chemical energy into electricity and heat, characterised by a high efficiency of around 40-60% [17]. The basic operating principle and chemical reactions taking place in a FC are shown in figure 1. Hydrogen is fed at the anode and splits into two protons and electrons, which will take a different path to reach the cathode, where the reaction continues. The protons transfer via a membrane, while the electrons go through an external circuit. At the cathode, everything is combined with oxygen to form water. The proton conducting membrane is sandwiched between the anode and cathode electrode, forming the membrane electrode assembly (MEA). The electrodes typically consist of a porous gas diffusion layer and a catalyst to facilitate the reactions. Different types of FCs exist, usually determined by the type of proton conducting membrane. The different FC types considered for UAVs are discussed below. A single-cell FC typically generates a maximum current of 1-1.5 A/cm^2, corresponding to about 0.6 V under load circumstances. To increase the voltage, multiple cells are combined in a series configuration to form FC stacks [12, 17].

*Corresponding author: jorben.mus@kuleuven.be

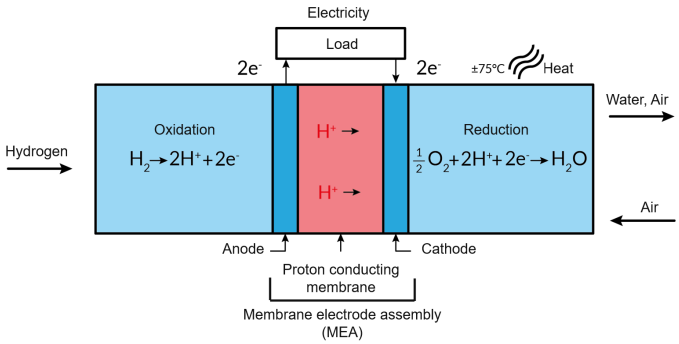

Figure 1: FC operating principle. Adapted from [17].

Both batteries and FCs are electrochemical energy systems that convert chemical energy into electricity [12]. The main difference is the containment of the chemical energy, which is stored in the active material for batteries [13]. FCs, by contrast, are fueled by hydrogen, which enables quick refuelling compared to the slower battery recharging process. Furthermore, FCs provide a greater gravimetric energy density thanks to the fuel they use [17]. Different FC types exist and are briefly discussed in terms of their suitability for UAV implementation. The literature considers three different types, namely solid oxide fuel cells (SOFCs), polymer electrolyte membrane fuel cells (PEMFCs) and direct methanol fuel cells (DMFCs) [21]. These different types are compared regarding their modes of functioning, advantages, and limitations to assess the practicality of UAV implementation. Table 1 summarises each FC type's key characteristics.

Table 1: Comparison of fuel cell types for UAVs [23]

Type	Fuel	Efficiency [%]	Temperature [°C]	System Specific Power [Wkg^{-1}]
PEMFC	Hydrogen	40-60	30-100	>150
DMFC	Methanol	20-30	20-90	>50
SOFC	Hydrocarbons	30-50	500-1000	>100

SOFCs operate between 600-1000°C and are categorised as high-temperature FCs. This makes it possible to use traditional liquid fuels instead of pure hydrogen [16]. These fuels are more affordable and easier to handle than pure hydrogen, but SOFCs using them emit greenhouse gases [21]. Other problems are long warm-up times and challenges related to mechanical and thermal stability [16]. Therefore, the literature [6, 21, 23] concludes that high-temperature FCs are not ideal for UAVs and are better suited for stationary applications [16].

PEMFCs rely on pure hydrogen as fuel and thus do not emit greenhouse gases [12]. Their operating temperature range of 30-100 °C is more favourable for UAVs. Compared to other types of FCs, PEMFCs have a higher power density and respond better to transient load changes [6]. The use of methanol as fuel in DMFCs is their most significant advantage over PEMFCs, their composition is very similar. Relying on methanol instead of pure hydrogen results in easier handling and storage while offering a better volumetric energy density [21]. Disadvantages are a considerably lower efficiency due to methanol crossover and lower kinetics. Moreover, the lower specific power of DMFCs also implies that PEMFCs are a superior choice [6].

In summary, according to the literature, PEMFCs running on pure hydrogen are currently the most promising and widely used option for powering UAVs [6, 21, 23]. However, there are limitations to the use of fuel cells. These limitations are briefly outlined below and serve as a basis for discussing their potential impact on UAVs in the next section.

First, pure hydrogen storage and handling introduce complexities, and the lack of infrastructure is also a disadvantage [7]. This issue can be addressed by utilising FC types that can accept fuels besides pure hydrogen [1]. However, as discussed, PEMFCs are still considered to be the best option for UAVs, and the drawbacks related to hydrogen won't be considered in this research. Second, FCs typically have a low maximum power output due to their limited power density in relation to their mass [6]. Third, the efficiency decreases significantly at high power outputs compared to at low currents. In addition, high currents cause a considerable drop in voltage, resulting in an unstable voltage output which can be unsuited for powertrains [21]. Fourth, FCs have a slow dynamic response due to electrochemical reaction delay and Balance of Plant (BoP) systems, present to support functions like FC cooling and reactant

delivery [6, 21]. Fifth, FC degradation can significantly reduce power output, which can be reversible or irreversible. FC lifetime and durability are seen as key challenges in FC commercialisation [20]. According to the literature, important causes of degradation are operating time [20], harsh ambient conditions in which the FC is operated [6], noisy and continuously high power demands [20] and impurities that can poison the FC, as for example, air impurities such as NaCl, NOx, CO,... [19].

3 Methodology

After presenting the opportunities for implementing FCs in UAVs, the focus shifts to the challenges and proposed methodology to overcome them. This section examines how the discussed drawbacks of FC technology can impact the performance of FC UAVs. As the research is still in its early stages, a complete methodology to cope with these challenges will not be discussed. Therefore, each challenge will be discussed briefly and linked to the current idea and considered methods to solve it.

As discussed, FCs generally suffer from limited power density and slow dynamics [21]. In UAVs purely relying on FCs, this is expressed by having a lower power output combined with poor performance when exposed to noisy power profiles. As a result, the UAV's maximum speed, payload capacity, flying altitude and climbing rate will be affected [6, 23]. In addition, the FC will degrade faster due to the higher power output and fluctuating power patterns [20]. Therefore, UAVs solely relying on FCs are generally not the best idea due to affected flight characteristics and limited FC lifetime. As a result, FCs are often integrated with other energy systems to create hybrid systems that combine their advantages [6, 21, 22, 23]. This is summarised in a Ragone plot shown in figure 2, which compares energy systems in terms of gravimetric energy density and power density. As already discussed, FCs offer a great gravimetric energy density as hydrogen is used, but they suffer from low power density, which is undesirable for UAVs. The frequently considered energy systems to support FCs in UAVs are briefly discussed below. Special attention is given to the methodology and future work in addressing the challenges of hybrid system design.

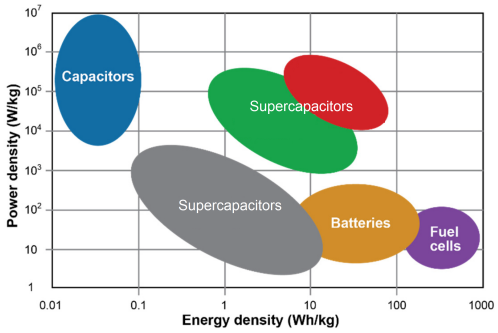

Figure 2: Ragone plot to compare different energy systems. Adapted from [18].

Most UAVs rely on lithium-based batteries, either Li-ion or Li-polymer, as they score well in terms of energy and power density [23]. Using Li-batteries to support FCs in the UAV hybrid system is already widely studied [21]. Batteries serve three main functions in hybrid FC systems for UAVs. First, they help provide the propulsion system with a constant output voltage as, compared to FCs, the voltage is less dependent on the load current [23]. Second, by supporting the FC during high-power demanding flight phases, such as take-off, batteries can improve the power density of the system. Afterwards, the FC can recharge the battery, for instance, during the cruise phase [22]. Third, batteries can assist in stabilising the power demand of the FC to increase lifetime [3].

DC-DC converters allow power source management and determine the hybrid system layout by making different voltage sources compatible. Systems that do not have DC-DC converters are called direct hybrid systems and are classified as passive. Indirect hybrid systems are managed by energy management strategies to improve their efficiency and reliability [6].

The combination of the FC and battery is most common in the hybrid system literature. However, other energy systems are also considered. Solar cells covering the wings of the UAV are seen as a great option to increase the endurance of UAVs operated during daylight. Figure 2 also shows that (super)capacitors are a great option to improve the power density of the hybrid system. In addition, the dynamic response to fluctuating power profiles can also be enhanced by employing (super)capacitors [21, 23].

Designing a UAV hybrid system that balances cost, weight, endurance, payload, and flying behaviour can be challenging. The current literature lacks information on how to design hybrid systems regarding which combination is needed, the best layout, dimensioning the energy systems and selecting the appropriate characteristics. Therefore, this research aims to develop a tool that can assist in designing hybrid systems for UAVs by proposing optimised layouts for different inputs, such as expected endurance, maximum weight, mission profile, etc... This also enables the user to simulate the feasibility of performing a specific mission using a hybrid FC UAV.

In addition, UAVs are often designed to fly in various environments and timeframes. For example, a UAV for inspection purposes is expected to perform well during summer and winter. As discussed, the performance of FCs can be highly affected by degradation. The remaining of this section highlights the connection between the expected performance of FC UAVs and the impact of FC degradation.

FCs for UAVs are generally open cathode types, meaning that unconditioned air is drawn for the cathode reactions and FC cooling. This makes the FC lighter, as BoP systems such as humidifiers and compressors are not present. However, open cathode FCs are also more exposed to ambient conditions. As a result, the power output of the FC can be highly affected by ambient conditions, as for example, air temperature and air humidity [6, 10]. Therefore, the flying characteristics and endurance of FC UAVs can be influenced by where and when the UAV is flown. It could be useful to consider this and adjust the hybrid system layout based on the expected ambient conditions. Currently, a test bench is being constructed to evaluate the impact of ambient conditions on open cathode FCs. As discussed, contaminated environments can also lower FC power output by, for example, catalyst deactivation [19]. Operating a FC UAV in harsh conditions can significantly shorten its lifespan. This can be important for UAVs operated in these environments, like offshore inspection UAVs. In some cases, it could even be impractical to deploy a FC UAV due to the harsh environments or a different hybrid system composition should be considered.

The ambient conditions and presence of impurities can vary depending on the location and timing of the flight mission [14]. Therefore, when designing hybrid systems, it could be important to consider degradation due to its influence on the system's performance. This is already mentioned in the literature but not elaborated. Therefore, this research aims to assess if ambient conditions and impurities affect the feasibility of FC UAVs and whether this influences hybrid system design. Therefore, PEMFC performance will be studied via modelling and simulation. This could then be linked to the proposed hybrid system design tool.

4 Discussion

This section will briefly discuss, due to the initial stage of the research, potential challenges that may arise. Regarding the hybrid system design tool, gathering realistic flight profiles and information about the UAV, such as mass and endurance, might be difficult. In addition, manufacturers do not frequently share FC performance characteristics. Additionally, building test benches for open cathode FCs can be expensive, especially if one wants to modify ambient conditions or introduce impurities to study degradation. Modelling and simulations are helpful but introduce threats to validity that require extensive study.

5 Conclusion

It is clear that the literature considers implementing FCs in UAVs as an interesting opportunity to achieve long endurance, high payload electric flights. However, several challenges must be addressed to go from the demonstrator phase to commercialisation. The most important ones were discussed in this abstract. One key aspect is the development of a tool to aid in hybrid system design for UAVs based on the UAV requirements. Optimising the UAV hybrid system is lacking in the literature as the current trend focuses on optimised energy management. In addition, studying the influence of ambient conditions and degradation on FCs is necessary to determine whether including this in the hybrid system design is useful. The goal of this study is to help evaluate the feasibility of hydrogen FC UAVs regarding lifespan, ambient conditions influence, and UAV requirements for deployment in various applications and environments. The following steps are developing the discussed tool and setting up models. An update on the research status will be provided in the future and the first results will be unveiled. This pertains to discussing the test bench, presenting the initial results of the hybrid system dimensioning tool, and elaborating on the strategy for developing the models to assess the impact of ambient conditions and degradation.

References

[1] M. N. Boukoberine, Z. Zhou, and M. Benbouzid. A critical review on unmanned aerial vehicles power supply and energy management: Solutions, strategies, and prospects. *Applied Energy*, 255:113823, 2019.

[2] V. Chamola, P. Kotesh, A. Agarwal, Naren, N. Gupta, and M. Guizani. A comprehensive review of unmanned aerial vehicle attacks and neutralization techniques. *Ad Hoc Networks*, 111:102324, 2021.

[3] T. Donateo, A. Ficarella, L. Spedicato, A. Arista, and M. Ferraro. A new approach to calculating endurance in electric flight and comparing fuel cells and batteries. *Applied Energy*, 187:807–819, 2017.

[4] M. Fischer, M. Werber, and P. V. Schwartz. Batteries: Higher energy density than gasoline? *Energy Policy*, 37(7):2639–2641, 2009.

[5] Fortune Business Insights. Commercial drone market, 2023. Business Report ID:FBI102171.

[6] A. Gong and D. Verstraete. Fuel cell propulsion in small fixed-wing unmanned aerial vehicles: Current status and research needs. *International Journal of Hydrogen Energy*, 42(33):21311–21333, 2017.

[7] J. Hoelzen, D. Silberhorn, T. Zill, B. Bensmann, and R. Hanke-Rauschenbach. Hydrogen-powered aviation and its reliance on green hydrogen infrastructure – review and research gaps. *International Journal of Hydrogen Energy*, 47(5):3108–3130, 2022. Hydrogen Energy and Fuel Cells.

[8] D. Joshi, D. Deb, and S. M. Muyeen. Comprehensive review on electric propulsion system of unmanned aerial vehicles. *Frontiers in Energy Research*, 10, 2022.

[9] A. Kumar, S. Nagar, and S. Anand. 1 - climate change and existential threats. In S. Singh, P. Singh, S. Rangabhashiyam, and K. Srivastava, editors, *Global Climate Change*, pages 1–31. Elsevier, 2021.

[10] J. C. Kurnia, B. A. Chaedir, A. P. Sasmito, and T. Shamim. Progress on open cathode proton exchange membrane fuel cell: Performance, designs, challenges and future directions. *Applied Energy*, 283:116359, 2021.

[11] S. A. H. Mohsan, M. A. Khan, F. Noor, I. Ullah, and M. H. Alsharif. Towards the unmanned aerial vehicles (uavs): A comprehensive review. *Drones*, 6(6), 2022.

[12] R. O'Hayre, S.-W. Cha, W. Colella, and F. B. Prinz. Chapter 1: Introduction. In *Fuel Cell Fundamentals*, chapter 1, pages 1–24. John Wiley & Sons, Ltd, 2016.

[13] K. Reddy, V. Mudgal, and T. Mallick. Review of latent heat thermal energy storage for improved material stability and effective load management. *Journal of Energy Storage*, 15:205–227, 2018.

[14] M. Schröder, F. Becker, J. Kallo, and C. Gentner. Optimal operating conditions of pem fuel cells in commercial aircraft. *International Journal of Hydrogen Energy*, 46(66):33218–33240, 2021.

[15] H. Shakhatreh, A. H. Sawalmeh, A. Al-Fuqaha, Z. Dou, E. Almaita, I. Khalil, N. S. Othman, A. Khreishah, and M. Guizani. Unmanned aerial vehicles (uavs): A survey on civil applications and key research challenges. *IEEE Access*, 7:48572–48634, 2019.

[16] M. Singh, D. Zappa, and E. Comini. Solid oxide fuel cell: Decade of progress, future perspectives and challenges. *International Journal of Hydrogen Energy*, 46(54):27643–27674, 2021.

[17] C. Spiegel. Chapter 1: An introduction to fuel cells. In *Designing and Building Fuel Cells*, pages 1–14. McGraw-Hill Professional, 2007.

[18] V. Vandeginste. A review of fabrication technologies for carbon electrode-based micro-supercapacitors. *Applied Sciences*, 12(2), 2022.

[19] L. Vichard, F. Harel, A. Ravey, P. Venet, and D. Hissel. Degradation prediction of pem fuel cell based on artificial intelligence. *International Journal of Hydrogen Energy*, 45(29):14953–14963, 2020.

[20] L. Vichard, N. Y. Steiner, N. Zerhouni, and D. Hissel. Hybrid fuel cell system degradation modeling methods: A comprehensive review. *Journal of Power Sources*, 506:230071, 2021.

[21] B. Wang, D. Zhao, W. Li, Z. Wang, Y. Huang, Y. You, and S. Becker. Current technologies and challenges of applying fuel cell hybrid propulsion systems in unmanned aerial vehicles. *Progress in Aerospace Sciences*, 116:100620, 2020.

[22] C. Xiao, B. Wang, D. Zhao, and C. Wang. Comprehensive investigation on lithium batteries for electric and hybrid-electric unmanned aerial vehicle applications. *Thermal Science and Engineering Progress*, 38:101677, 2023.

[23] C. Zhang, Y. Qiu, J. Chen, Y. Li, Z. Liu, Y. Liu, J. Zhang, and C. S. Hwa. A comprehensive review of electrochemical hybrid power supply systems and intelligent energy managements for unmanned aerial vehicles in public services. *Energy and AI*, 9:100175, 2022.

Combustion Behavior of Carbon-Free Fuels for Large Engines

M. Klawitter*[1], C. Gößnitzer[2], G. Pirker[2], A. Wimmer[1,2], S. Wüthrich[3], K. Herrmann[3]

[1]Institute of Thermodynamics and Sustainable Propulsion Systems, Graz University of Technology, Graz, Austria

[2]LEC GmbH (Large Engines Competence Center), Graz, Austria

[3]Institute of Thermal and Fluid Engineering, University of Applied Sciences Northwestern Switzerland, Windisch, Switzerland

Introduction

Global warming is on a pathway of about +3 °C compared to preindustrial times, if the current measures to counteract are considered [1]. This would lead to the collapse of ecosystems, a further loss in biodiversity, an increase in extreme weather events, and an overshooting of irreversible climate tipping points, which leads to further global warming [2]. Thus, near-term measures to reduce humankind's greenhouse gas emissions to net zero have to be implemented on a political, societal, and technical level. Focusing on the technical level, the energy demand for mobility and transportation is a main driver of CO_2 emissions. Since the energy demand for this sector is projected to rise in the foreseeable future, there is a strong need for new energy carriers with reduced global warming potential. Regarding the large engines sector, the IPCC is recommending ammonia and hydrogen from renewable sources as promising fuels for shipping in their latest report on the mitigation of climate mitigation [3]. Ammonia can serve as a hydrogen carrier with a higher volumetric energy density than hydrogen combined with a low carbon intensity. Still, its properties to be used as a fuel are challenging and have to be explored thoroughly.

The present PhD project investigates the combustion behavior of alternative fuels for large engines. For this, the aforementioned fuels ammonia and hydrogen are considered due to their carbon-free nature and their applicability in large engines. Experimental studies are performed to investigate the combustion behavior of the fuels under fundamental and engine-relevant conditions. The experimental results serve as a base for the validation of simulation models, which capture the particular characteristics of the new fuels. An experimental-numerical methodology is being developed to predict the combustion behavior of the new fuels and thereby reduce the required experimental efforts. This helps reduce the time to implement the new fuels into the fleet, and thereby speed up the mitigation of greenhouse gases from all sectors using large engines.

Methodology

To investigate the combustion behavior of new fuels, characteristic parameters have to be determined in fundamental experiments. The laminar burning velocity (LBV) is an intrinsic property of fuels, governing the combustion efficiency and stability. Therefore, it is also a main input parameter for flame propagation modeling. To experimentally determine the LBV of different fuel mixtures, optical investigations of spherically propagating flames under quasi-isobaric conditions have been performed on a constant volume combustion chamber [4], see Figure 1a). Applying Schlieren imaging, the flame propagation is captured with a high-speed camera. The LBV is derived by extrapolating the gathered flame propagation to an unstretched

* Corresponding author: klawitter@ivt.tugraz.at

flame and calculating the flame speed of the unburnt gas from the burnt gas by applying mass continuity.

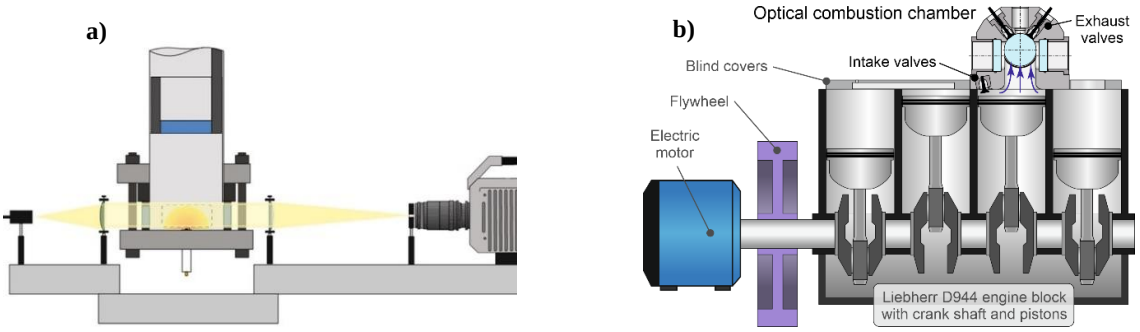

Figure 1: Experimental setup of test rigs used with optical access a) Rapid compression machine as constant volume combustion chamber [4] b) Optical test rig Flex-OeCoS [5]

While knowledge of the laminar flame behavior of new fuels is the fundament of their characterization, investigating the behavior under turbulent conditions is of the highest importance for the application of those fuels in internal combustion engines. Special attention has to be brought to the flame-turbulence interaction for hydrogen and ammonia-hydrogen mixtures because of the strong differential diffusion of those fuel mixtures. This particular characteristic causes an increase in the response of the flame speed to turbulence intensity and has to be appropriately captured by flame models. To this end, optical investigations of turbulent flame propagation under application-relevant conditions have been performed on the optical research engine test rig "Flex-OeCoS" [5], see Figure 1b). Similar to the laminar investigations, the flame propagation has been captured with a high-speed Schlieren imaging setup. The apparent flame propagation speed is based on the projected flame area growth over time. The thermodynamic conditions in the combustion chamber are characterized by fine wire thermocouple measurements and in-cylinder pressure measurements [6] as well as heat release rate calculations [7, 8]. The flow and turbulence conditions are characterized by high-speed particle image velocimetry (PIV) measurements [5].

Discussion

Laminar flame propagation

The results of the laminar flame propagation have been published and presented in [4, 9]. The investigated fuel is a gas mixture representing partially dissociated (or "cracked") ammonia, which contains ammonia itself, hydrogen, and nitrogen. The hydrogen serves as a combustion promoter to improve the poor combustion behavior of ammonia. In engine applications, a part of the ammonia can be dissociated into hydrogen and nitrogen upstream of the engine. The measurements are conducted for cracking ratios of $\gamma = [10\% - 40\%]$, equivalence ratios of $\varphi = [0.7 - 1.3]$, and initial conditions of

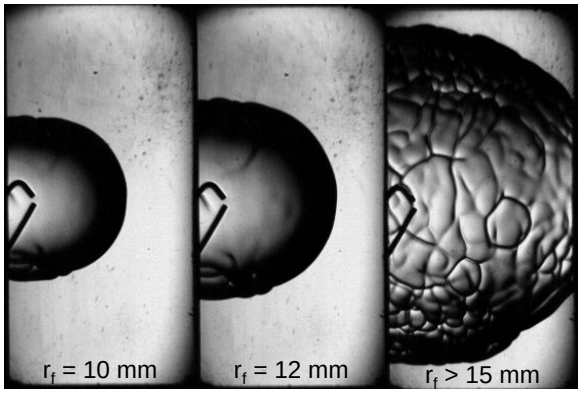

Figure 2: Schlieren image sequence of flame propagation of $NH_3/H_2/N_2$/air mixture; γ = 40%, φ = 0.9, T_0 = 298 K, p_0 = 5 bar; onset of instabilities visible for flame radii > 15 mm [4]

p_0 = [1 – 10 bar] and T_0 = 298 K. The results are compared to the results of methane, which serve as a baseline.

The outwardly spherical propagation of a lean $NH_3/H_2/N_2$/air flame with a cracking ratio of γ = 40% and p_0 = 5 bar is depicted in Figure 2. Within the evaluation range of r_f < 12 mm, the flame surface is assumed to be unwrinkled and thereby evaluable for the LBV. For larger flame radii, the onset of instabilities is visible by the strong wrinkling. These instabilities are caused by differential diffusion of the fuel mixture and mainly the contained hydrogen. This is represented by an effective Lewis number of the mixture below unity. For cases with a higher cracking ratio, a leaner fuel/air mixture, or a higher pressure, the LBV cannot be evaluated due to the onset of instabilities within the evaluation range.

Figure 3 a) shows the results of the LBV of $NH_3/H_2/N_2$/air flames for an equivalence ratio and pressure variation at T_0 = 298 K and a cracking ratio γ = 40 %. The LBV is peaking in the stoichiometric to slightly rich area and is decreasing over increasing pressure, as expected. In comparison to the literature results of Mei et al [10], an overestimation of the LBV can be observed in the lean area. Consulting the experimental Markstein Length, an underestimation of the stretch sensitivity of the flame front can be found as the source of the deviation, which is caused by a low and narrow evaluation range of the present test rig (6 mm < r_f < 12 mm). To compare the LBV of cracked NH_3 flames to CH_4 flames, CH_4 flame results have been gained performing reaction kinetic calculations in Cantera using the GRI 3.0 mechanism [11, 12]. While the equivalence ratio effect is similar for both fuels in the lean area, it is less pronounced for cracked NH_3 in the rich area. This is caused by the peak LBV of the admixed H_2 in the rich area (ϕ = 1.6 – 1.8).

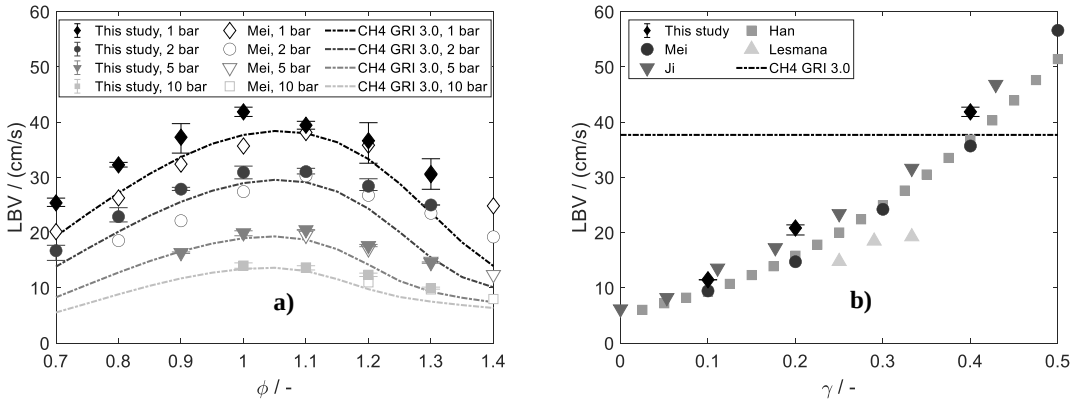

Figure 3: Laminar burning velocity of $NH_3/H_2/N_2$/air flames and CH_4/air flames at T_0 = 298 K [4] a) Equivalence ratio and pressure variation, γ = 40 %; Mei et al [10], GRI 3.0 [11] b) Cracking Ratio variation, p_0 = 1 bar, φ = 1.0; Mei et al. [10], Ji et al. [13], Han et al. [14], Lesmana et al. [15], GRI3.0 [11]

Figure 3 b) presents a comparison of the LBV results of the present study and literature results for a cracking ratio variation at T_0 = 298 K, p_0 = 1 bar, and φ = 1.0 [10, 13–15]. All results agree in a nonlinear increase of LBV for an increasing cracking ratio. This illustrates that the accelerating effect of additional hydrogen dominates over the decelerating effect of additional nitrogen in the fuel mixture. Considering the general large deviations in flame speed measurements of experimental results in the literature, a good agreement of the current results with the displayed literature results can be found, despite the limitations of the test rig. Compared to the reaction kinetic results for CH_4 flames under the same conditions, a cracking ratio of 35 - 40% is required to reach similar burning velocities, dependent on the considered source.

Turbulent flame propagation

The experiments of the turbulent flame propagation are currently being evaluated. The presented results are to be considered “work in progress” and will be published at a later time. The investigated fuel mixtures are NH_3 and cracked NH_3 and are compared to reference measurements of CH_4. The measurements are conducted for mixtures with cracking ratios of γ = [0%, 3%, 7%, 10%], equivalence ratios of φ = [0.60 – 1.20], and boundary conditions of p_c = [40, 70, 100 bar], n = [400, 600, 800, 1000 min^{-1}], ignition timing = -15°CA and T_{in} = 100°C for NH_3 and cracked NH_3 and T_{in} = 50°C for CH_4. The flame propagation for γ = 10%, ϕ = 1.00, n = 600 /min, p_c = 70 bar, and T_{in} = 100 °C is depicted in Figure 4, represented by an overlay of the Schlieren images and the detected flame area and contour. The flame shape is close to spherical in the given exemplary combustion cycle but can vary strongly from this shape due to the flow conditions in the combustion chamber. The flame-turbulence interaction is apparent by the small-scale winkled flame front.

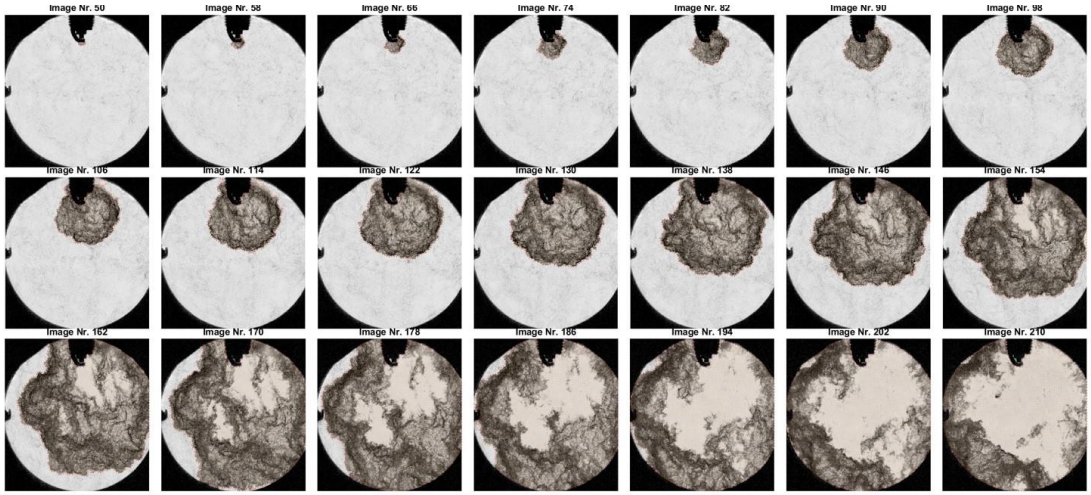

Figure 4: Overlay of Schlieren image sequence and detected area and contour of flame propagation of $NH_3/H_2/N_2$/air mixture; γ = 10 %; φ = 1.00, n = 600 min^{-1}, p_c = 70 bar, T_{in} = 100 °C

The preliminary results indicate an increase in flame propagation for increasing turbulence intensity for all fuel mixtures. The turbulence intensity is controlled by the engine speed and has been characterized in previous PIV measurements [5]. Pure NH_3 performs comparatively better under engine-relevant conditions than under laminar, quiescent conditions. The partial NH_3 cracking of up to γ = 10% effects a further significant increase in flame speed. The partially cracked NH_3 reaches similar flame speeds and combustion stability to CH_4. For lean cases, the effect of turbulence on NH_3 and cracked NH_3 flames is stronger compared to CH_4. This is caused by thermodiffusive instabilities accelerating the flame propagation, occurring for mixtures with effective Lewis numbers below unity.

Conclusions

Ammonia and hydrogen have great potential as fuels for large engines to reduce the greenhouse gas emissions of the transportation and energy sectors. While ammonia is an excellent carbon-free hydrogen carrier, its combustion behavior remains a challenge for implementation as a fuel. The combustion behavior of ammonia and cracked ammonia mixtures has been investigated experimentally under fundamental and engine-relevant

conditions. The necessity of the performed experiments becomes apparent by observing the laminar and turbulent flame characteristics to differ strongly from conventional fuels. Because of the very low laminar burning velocity of ammonia, a cracking ratio of 35 - 40% - and thereby a significant addition of hydrogen - is required to reach the same LBV as methane under laminar conditions. Additionally, even with low amounts of hydrogen added, the flame surface is exposed to instabilities already at rather low pressures, speeding up the flame propagation.

In contrast, the investigations under turbulent, engine-relevant conditions expose a better performance of ammonia and cracked ammonia mixtures than expected from laminar results. With a comparatively low cracking ratio of $\gamma = 10\%$, the combustion gives satisfactory results regarding flame propagation and operation stability. This can be explained, inter alia, by the particular diffusion behavior of ammonia and especially hydrogen. The expectedly low required cracking ratios could be feasible for an on-board cracking process in maritime applications, possibly powered only by the waste heat of the combustion process.

Based on these experimental results, simulation models for laminar, turbulent, and application-oriented conditions will be reevaluated and adapted to reliably predict the combustion behavior of those new fuels. These simulation models enable a fast development process of large engines running on carbon-free fuels. Thereby, precious time can be saved on the track of net-zero greenhouse gas emissions, to prevent the crossing of the planetary boundaries at risk.

References

[1] IPCC, “Climate Change 2021: The Physical Science Basis: Contribution of Working Group I to the Sixth Assessment Report of the Intergovernmental Panel on Climate Change,” 2021.

[2] IPCC, “Climate Change 2022: Impacts, Adaptation and Vulnerability: Working Group II contribution to the Sixth Assessment Report of the Intergovernmental Panel on Climate Change,” 2022.

[3] IPCC, “Climate Change 2022: Mitigation of Climate Change: Working Group III contribution to the Sixth Assessment Report of the Intergovernmental Panel on Climate Change,” 2022.

[4] G. Pirker, M. Klawitter, A. Ramachandran, C. Gößnitzer, A. Tilz, and A. Wimmer, “Characterization of future fuels using an optically accessible rapid compression machine,” *30th CIMAC World Congress*, 2023.

[5] B. Schneider *et al.*, “The Flex-OeCoS—a Novel Optically Accessible Test Rig for the Investigation of Advanced Combustion Processes under Engine-Like Conditions,” *Energies*, vol. 13, no. 7, p. 1794, 2020, doi: 10.3390/en13071794.

[6] S. Wüthrich, D. Humair, K. Herrmann, and A. Bertola, “Enhanced instrumentation of an optical research engine with unique combustion chamber,” *14th Int. AVL Symposium on Propulsion Diagnostics*, 2020.

[7] S. Wüthrich, P. Cartier, P. Süess, B. Schneider, P. Obrecht, and K. Herrmann, “Optical investigation and thermodynamic analysis of premixed ammonia dual-fuel combustion initiated by dodecane pilot fuel,” *Fuel Communications*, vol. 12, p. 100074, 2022, doi: 10.1016/j.jfueco.2022.100074.

[8] K. Herrmann, S. Wüthrich, P. Cartier, P. Süess, R. de Moura, and G. Weisser, “Initial investigations into ammonia combustion at conditions relevant for marine engines,” *30th CIMAC World Congress*, 2023.

[9] M. Klawitter, C. Gößnitzer, A. Tilz, G. Pirker, and A. Wimmer, “Partially Dissociated Ammonia as a Fuel: Experimental Study on Laminar Flame Characteristics of Premixed

NH3/H2/N2/Air Mixtures," 2nd Symposium on Ammonia Energy. Orleans, France, Jul. 11 2023.

[10] B. Mei, J. Zhang, X. Shi, Z. Xi, and Y. Li, "Enhancement of ammonia combustion with partial fuel cracking strategy: Laminar flame propagation and kinetic modeling investigation of NH3/H2/N2/air mixtures up to 10 atm," *Combustion and Flame*, vol. 231, p. 111472, 2021, doi: 10.1016/j.combustflame.2021.111472.

[11] Gregory P. Smith *et al.*, *GRI-MECH 3.0*. [Online]. Available: http://www.me.berkeley.edu/gri_mech/

[12] D. G. Goodwin, R. L. Speth, H. K. Moffat, and B. W. Weber, *Cantera: An Object-oriented Software Toolkit for Chemical Kinetics, Thermodynamics, and Transport Processes*: Zenodo, 2021.

[13] C. Ji, Z. Wang, Du Wang, R. Hou, T. Zhang, and S. Wang, "Experimental and numerical study on premixed partially dissociated ammonia mixtures. Part I: Laminar burning velocity of NH3/H2/N2/air mixtures," *International Journal of Hydrogen Energy*, vol. 47, no. 6, pp. 4171–4184, 2022, doi: 10.1016/j.ijhydene.2021.10.269.

[14] X. Han, Z. Wang, Y. He, Y. Zhu, R. Lin, and A. A. Konnov, "Uniqueness and similarity in flame propagation of pre-dissociated NH3 + air and NH3 + H2 + air mixtures: An experimental and modelling study," *Fuel*, vol. 327, p. 125159, 2022, doi: 10.1016/j.fuel.2022.125159.

[15] H. Lesmana, M. Zhu, Z. Zhang, J. Gao, J. Wu, and D. Zhang, "Experimental and kinetic modelling studies of laminar flame speed in mixtures of partially dissociated NH3 in air," *Fuel*, vol. 278, p. 118428, 2020, doi: 10.1016/j.fuel.2020.118428.

Comparing the Activity of NiFe Catalysts for H_2O_2 Decomposition and Electrocatalytic Water Splitting

N. K. Varghese*[1], M. Boccia[2], V. Marzocchi[2], M. Pagliero[1], A. Comite[1]

[1]University of Genoa, Genoa, Italy
[2]H_2 Energy SRL, Pizzighettone, Cremona, Italy

Introduction

Climate change is not a distant threat anymore, it's the pressing reality of our fragile planet that requires immediate action, not tomorrow, but today [1]. Thus, cutting down on fossil fuels is necessary for the very survival of humankind. Hydrogen provides a perfect solution and stands as a potential game-changer in the quest for sustainable and clean energy sources [2, 3]. Hydrogen is gaining momentum as a fuel of the future because of it significantly reduces CO_2 emissions, has high energy density and versatility, storage and grid stability and can be integrated easily with renewable energy [4].

Despite these benefits, challenges remain. The hydrogen production process can be energy-intensive, and most hydrogen currently produced is "grey hydrogen" i.e., it comes from natural gas in a process that releases carbon dioxide [2]. In the burgeoning landscape of sustainable energy and environmental remediation, the exploration of efficient and versatile catalysts stands as a paramount focus. The transition from carbon-intensive energy sources to cleaner alternatives hinges on breakthroughs in electrochemical technologies, of which catalysis is a core component. Among these, the electrochemical splitting of water—wherein water is decomposed into its constituent hydrogen and oxygen gases—is recognized as a critical pathway for generating hydrogen, a clean and renewable energy vector. Concurrently, in the realm of environmental technologies, the decomposition of hydrogen peroxide is a vital reaction, aiding in wastewater purification and other decontamination processes [2, 4, 5].

At the heart of these reactions lies the NiFe class of catalysts, which have garnered significant attention due to their promising catalytic performances, cost-effectiveness, and relative abundance. These bimetallic catalysts, leveraging the synergistic properties of nickel and iron, have showcased their prowess, particularly in the oxygen evolution reaction (OER) segment of water splitting. However, their potential does not stop there. Recent forays into their applicability for hydrogen peroxide decomposition reveal another exciting avenue for exploration.

This work seeks to bridge the knowledge gap between the two distinct, yet interrelated, applications of NiFe catalysts: in the OER reaction and hydrogen peroxide decomposition. By juxtaposing their performance, mechanisms, and stability in both reactions, we aim to present a holistic understanding that could be pivotal for future innovations in clean energy production and environmental protection.

Rationale

The main rationale behind the study is to understand the mechanistic insights and reaction pathways. The OER and H_2O_2 decomposition reactions, though different in nature, share certain intermediate steps and mechanistic nuances [6, 7].

*Corresponding author: neethu.kochukunnel.varghese@edu.unige.it

Let us now go into the details of the reaction mechanism [8, 9]. The Adsorbate Evolution Mechanism is a 4-step-reaction process with 3 reaction intermediates (*OH, *O, *OOH). The binding energy between the intermediates and the catalytic active site determines the rate of the reaction.

Step 1: M + OH- → M-OH + e-

Step 2: M-OH + OH-→ M-O + H_2O + e-

Step 3: M-O + OH-→ M-OOH + e-

Step 4: M-OOH + OH-→ M + O_2 + H_2O + e-

The creation of O* and *OOH are the pivotal steps in the reaction process and the magnitude of difference between the free energy of these species is indicative of its OER activity. The G*O-G*OOH values vs the overpotential show a volcanic distribution and, according to the Sabatier principle, an intermediate value of G*O-G*OOH is preferred. The catalytic activity is found to be maximum at G*O-G*OOH value of 1.6 eV.

The decomposition of the hydrogen peroxide on Fe^+ ions is found to have involvement of the intermediates *OH, *O, *OOH [6, 7]. So a comparative study will help elucidate the similarities and differences in the reaction pathways when catalyzed by NiFe. This could lead to improved catalyst designs by exploiting the favorable features from each reaction. NiFe catalysts have demonstrated promising catalytic performance in both OER and H_2O_2 decomposition. By comparing their activity in both reactions, we can derive insights into the versatility of these catalysts, potentially unlocking new applications or opportunities for optimization. In addition to that both the OER and hydrogen peroxide decomposition reactions impose oxidative and reductive stresses on catalysts. By exposing NiFe catalysts to both environments, this study can provide valuable insights into the durability, longevity, and possible degradation pathways of these materials. This is crucial for commercial applications where catalyst stability often dictates the lifespan and maintenance costs of the devices.

In light of these rationales, our study aims to comprehensively evaluate and compare the activity of NiFe catalysts in both the OER and hydrogen peroxide decomposition reactions. Through this analysis, we hope to expand our understanding of the fundamental processes at play and promote the development of more effective and versatile catalytic systems.

Methodology

To achieve a comprehensive understanding of the activity of NiFe catalysts in hydrogen peroxide decomposition and the oxygen evolution reaction (OER), we synthesised a range of NiFe catalysts using chemical reduction method with $NaBH_4$ [10], with multiple Ni to Fe ratios. These catalysts were supported on both cerium oxide (CeO_2) and zirconium dioxide (ZrO_2) substrates, selected for their known stability and conductivity properties. This variety of catalysts allowed for a robust investigation into the influence of metal ratios and the nature of support on the catalytic activity. The catalysts were characterized using X-ray diffraction (XRD), scanning electron microscopy (SEM), and Brunner-Emmett -Teller (BET) method to characterize the crystal structure, morphology, and surface properties of the catalysts, respectively.

The catalytic activity of the NiFe catalysts were then evaluated for hydrogen peroxide decomposition. The decomposition rate of H_2O_2 in the presence of the synthesized NiFe catalysts is assessed through volumetric measurements. 200 mg of catalysts and a 100 mL solution of 0.3 M H_2O_2 solution were kept in Büchner flask and the volume of O_2 evolved was measured every three minutes.

The OER catalytic activity is measured by conducting electrochemical tests using a three-electrode setup. Linear sweep voltammetry (LSV) is employed to determine the OER onset potential and overall activity [11]. Electrochemical impedance spectroscopy (EIS) will provide insight into the charge transfer resistance at the catalyst interface [12].

The catalysts were analyzed for stability and degradation studies by subjecting them to prolonged reaction conditions for both H_2O_2 decomposition and OER to assess their durability. Post-reaction characterizations are conducted using XRD and SEM to detect any structural or morphological changes in the catalysts. Inductively coupled plasma mass spectrometry (ICP-MS) is used to detect any leaching of the metal components. Infrared (IR) spectroscopy is employed to identify and monitor possible intermediates or adsorbed species during both reactions.

This multifaceted methodology aims to provide a rigorous and thorough analysis of NiFe catalysts in the context of both hydrogen peroxide decomposition and OER, ultimately contributing to the advancement of catalytic systems in these domains.

Discussion

The in-depth examination of NiFe catalysts' activity in hydrogen peroxide decomposition and the oxygen evolution reaction (OER) offers an avenue to bridge two critical areas in electrochemistry and catalysis. Several pertinent observations and implications emerge from this study:

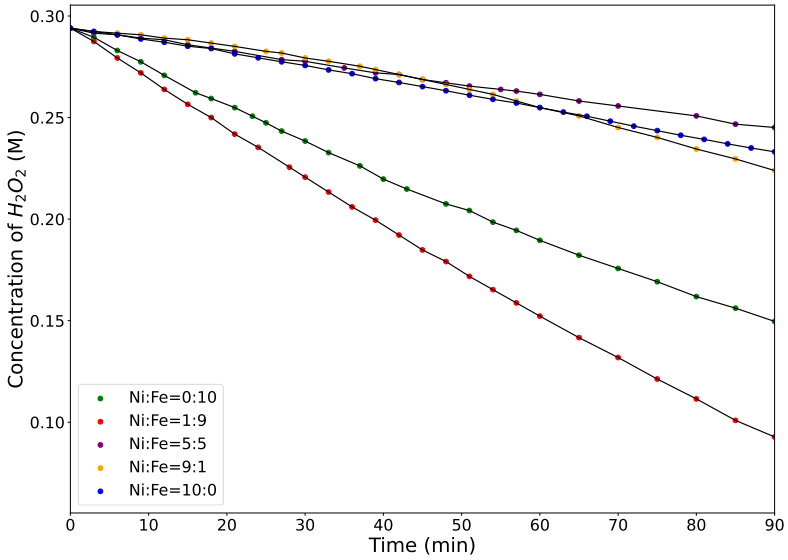

Figure 1: H_2O_2 decomposition rates for NiFe catalysts with different Ni:Fe ratios

Our initial findings suggest that NiFe catalysts with a Ni:Fe ratio of 1:9 are optimal for hydrogen peroxide decomposition (Fig. 1). The study highlights the importance of the Ni:Fe balance in optimizing performance. These catalysts showed an impressive level of activity during hydrogen peroxide decomposition studies, indicating their potential as highly efficient OER catalysts; a subject of current research. While NiFe catalysts potentially exhibit promising performance in both hydrogen peroxide decomposition and OER, the extent of their activity can differ based on the specific reaction. Factors such as electronic structure, binding energies, and the microenvironment of active sites play a determining role in catalytic efficiency. It's intriguing to note the influence of Ni:Fe ratios in these dynamics, emphasizing the importance of achieving the right balance for optimal performance in each reaction. The presence of iron, known for its ability to facilitate the formation of stable metal-oxygen bonds, might offer clues in enhancing the robustness of these bimetallic catalysts. Insights from the mechanistic study could indicate that certain intermediate states or adsorbed species are common or analogous across the two reactions. This shared mechanistic behavior underscores the versatility of NiFe catalysts. However, the energy barriers and reaction kinetics might differ, elucidating the distinctive challenges faced in each process. Also beyond the realm of academic interest, the dual utility of NiFe catalysts in both OER and hydrogen peroxide decomposition positions them as economically viable materials. By minimizing the need for multiple specialized catalysts, industries can achieve more streamlined, cost-effective processes,

especially considering the relative abundance and low cost of nickel and iron. Feedback from the optimization phase underscores the adaptability of NiFe catalysts. Post-treatment techniques, doping agents, or support materials can notably enhance activity, suggesting a broad design space for researchers and engineers to explore.

Conclusions

In this study of NiFe catalysts for hydrogen peroxide decomposition and the oxygen evolution reaction (OER), we systematically examined several variables to understand their performance and properties. By synthesizing catalysts with varied Ni:Fe ratios, morphologies, and support materials, we delineated the impact of these parameters on catalytic activity. The catalysts were characterized using XRD, SEM, and BET and it provided detailed insights into the catalysts' crystal structures, morphologies, and surface properties.

The catalytic activity assessments showed the efficiency of the synthesized NiFe catalysts in hydrogen peroxide decomposition and their potential in OER applications. The durability and stability of the catalysts were assessed by subjecting the catalysts to prolonged reaction conditions.

In summary, this research offers a systematic and thorough analysis of NiFe catalysts in hydrogen peroxide decomposition and OER. The findings, grounded in empirical evidence and rigorous analysis, contribute significantly to the field of catalysis, emphasizing the relevance and potential of NiFe catalysts in these reactions.

References

[1] Hans O Pörtner, Debra C Roberts, Helen Adams, Carolina Adler, Paulina Aldunce, Elham Ali, Rawshan Ara Begum, Richard Betts, Rachel Bezner Kerr, Robbert Biesbroek, et al. Climate change 2022: impacts, adaptation and vulnerability. Technical report, IPCC, 2022.

[2] Alexandra M Oliveira, Rebecca R Beswick, and Yushan Yan. A green hydrogen economy for a renewable energy society. *Current Opinion in Chemical Engineering*, 33:100701, 2021.

[3] Alfredo Ursua, Luis M Gandia, and Pablo Sanchis. Hydrogen production from water electrolysis: current status and future trends. *Proceedings of the IEEE*, 100(2):410–426, 2011.

[4] Naiying Du, Claudie Roy, Retha Peach, Matthew Turnbull, Simon Thiele, and Christina Bock. Anion-exchange membrane water electrolyzers. *Chemical Reviews*, 122(13):11830–11895, 2022.

[5] Dongguo Li, Andrew R Motz, Chulsung Bae, Cy Fujimoto, Gaoqiang Yang, Feng-Yuan Zhang, Katherine E Ayers, and Yu Seung Kim. Durability of anion exchange membrane water electrolyzers. *Energy & Environmental Science*, 14(6):3393–3419, 2021.

[6] Regina CC Costa, MFF Lelis, LCA Oliveira, JD Fabris, JOSÉ D Ardisson, RRVA Rios, CN Silva, and RM Lago. Novel active heterogeneous fenton system based on fe3- xmxo4 (fe, co, mn, ni): the role of m2+ species on the reactivity towards h2o2 reactions. *Journal of hazardous materials*, 129(1-3):171–178, 2006.

[7] Paula M Gómez-Largo, Carlos D Miranda, Alejandra C Villagrán-Olivares, Carlos A López, and Bibiana P Barbero. Study of cobalt-iron mixed oxides and catalytic behavior for decomposition of hydrogen peroxide. *Molecular Catalysis*, 530:112639, 2022.

[8] Emmanuel Zoulias, Elli Varkaraki, Nicolaos Lymberopoulos, Christodoulos N Christodoulou, and George N Karagiorgis. A review on water electrolysis. *Tcjst*, 4(2):41–71, 2004.

[9] Emiliana Fabbri and Thomas J Schmidt. Oxygen evolution reaction—the enigma in water electrolysis, 2018.

[10] Emily Cossar, Kushagra Agarwal, Vu Bao Nguyen, Reza Safari, Gianluigi A Botton, and Elena A Baranova. Highly active nickel–iron nanoparticles with and without ceria for the oxygen evolution reaction. *Electrocatalysis*, 12(5):605–618, 2021.

[11] Koichi Tokuda, Hiroaki Matsuda, et al. Linear sweep and cyclic voltammetry for electrocatalysis at modified electrodes with very thin films. *Journal of electroanalytical chemistry and interfacial electrochemistry*, 199(1):69–79, 1986.

[12] Alexandros Ch Lazanas and Mamas I Prodromidis. Electrochemical impedance spectroscopy - a tutorial. *ACS Measurement Science Au*, 2023.

Correlative microscopy for nanoscale imaging of hydrogen-materials interaction: an in-situ approach based on SIMS

Athira Suresh Kumar[1,2]*, Tom Wirtz[1], Santhana Eswara[1],

[1.] Advanced Instrumentation for Nano-Analytics (AINA), MRT Department, Luxembourg Institute of Science and Technology (LIST), Belvaux, Luxembourg
[2] University of Luxembourg, 2 Avenue de l'Université, L-4365, Esch-sur-Alzette, Luxembourg

Introduction

With the increasing global energy demands and depleting fossil fuel reserves, the world economy is now setting stronger goals towards production, transport and storage of green hydrogen which is an ideal renewable energy carrier for future[1]. While diffusible hydrogen in many materials degrades its performance and durability, hydrogen trapped in deep traps can reduce embrittlement and may pave the way towards development of solid-state hydrogen storage materials. In this scenario, understanding hydrogen interaction with materials at the nanoscale is crucial to develop sustainable, safe, and strong materials for hydrogen storage and transport. Hydrogen in materials introduces a series of microstructural, chemical, and electronic changes in materials at micro to nanoscales and no single technique can fully reveal the entire process [1]. Correlative microscopy integrates multiple characterization techniques to provide a comprehensive insight into local hydrogen-material interaction at the nanoscale [1].

Methodology

Direct imaging of hydrogen in solid materials with nanometer scale lateral resolution is challenging with most conventional microscopic techniques. A solution to this can be Secondary Ion Mass Spectrometry (SIMS), which is a high sensitivity analytical technique that can detect all elements (and isotopes) of the periodic table including hydrogen at sub 20 nm lateral resolution [2]. Our group, at LIST, have developed a prototype focused ion beam (FIB) −scanning electron microscope (SEM) -SIMS instrument (FIB-SEM-SIMS) which is based on an in-house developed double-focusing magnetic sector mass spectrometer with a continuous focal plane detector attached to a commercially available high vacuum dual-beam FIB-SEM which uses a liquid metal $^{69}Ga^{+}$ ion source [2]. This instrument combines the merits of electron microscopy with SIMS imaging to obtain structural and chemical information over the same region of interest in hydrogen containing samples.

Moving forward, we have also developed an in-situ electrochemical charging holder which can perform electrochemical hydrogen charging of samples inside the FIB-SEM-SIMS instrument to account for the loss of hydrogen diffusing out of the sample while performing the measurements. It consists of an electrolyte compartment which can hold around 600 µl of electrolyte. The sample is machined in the form of a lid to the electrolyte compartment, so that only one surface of the sample comes in direct contact with the electrolyte and the top surface of the lid to which hydrogen diffuses through the material will be clean for analysis purposes. Figure 1 illustrates the in-situ electrochemical charging set up.

*Corresponding author: athira.kumar@list.lu

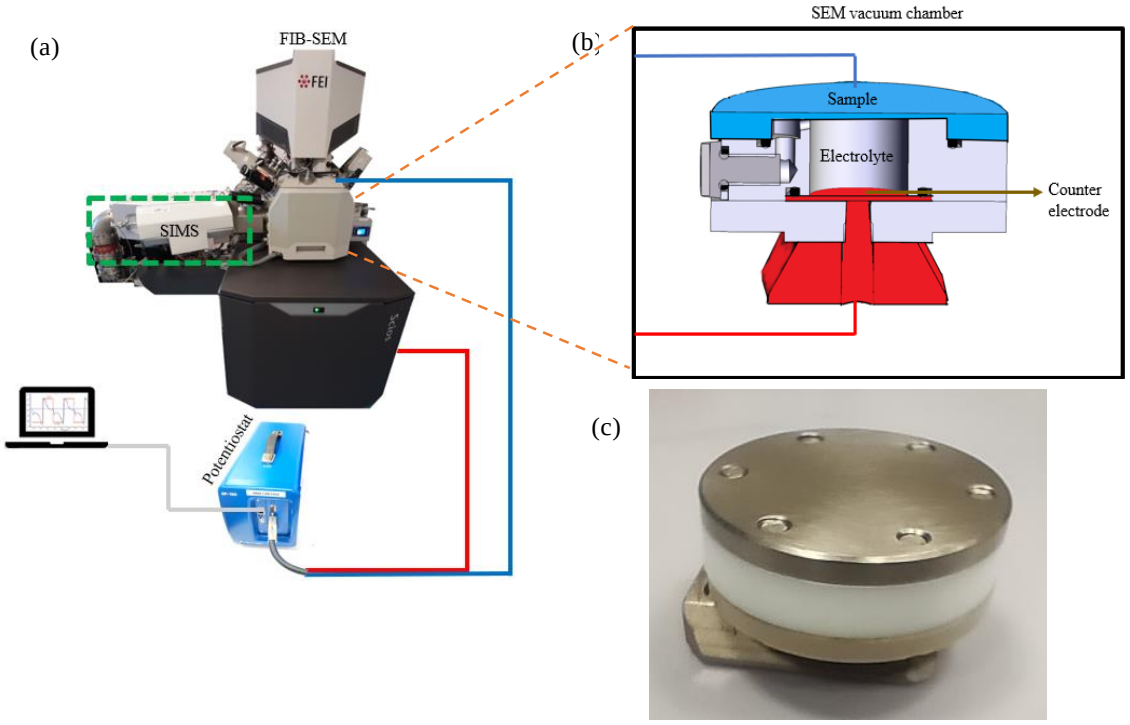

Figure 1. (a) Schematic of the FIB-SEM-SIMS instrument. A potentiostat (Biologic SP-150) is used to provide the sample bias with respect to stage for electrochemical charging using in-situ electrochemical charging holder (b) Cross sectional view of the in-situ sample holder. Inside the SEM vacuum chamber, the lid (sample) will be biased negatively(blue), and the counter electrode will be biased positively(red) (c) The in-situ electrochemical charging holder.

Discussion

The in-situ electrochemical charging holder is used for charging different samples inside FIB-SEM-SIMS to obtain elemental maps of hydrogen in materials which can aid hydrogen embrittlement studies and the identification of suitable materials for hydrogen storage. Ti-6Al-4V, a dual phase Titanium alloy, is an interesting material to start with, as it is well known for its specific strength and mechanical characteristics and has wide ranging aerospace, industrial and biomedical applications [3]. In hydrogen environment, this alloy absorbs large amount of hydrogen leading to hydride formation and gradual failure due to hydride embrittlement [4]. In-situ SIMS analysis of the sample using the electrochemical charging holder inside FIB-SEM-SIMS can track the hydrogen distribution in the sample in course of time. It can also help in identifying preferential nucleation sites of hydrides in the material and can track its growth in time. As a first step to this, electrochemical charging of Ti-6Al-4V samples has been performed inside a beaker and hydrogen maps of the sample was obtained before and after hydrogenation as shown in figure 2. The experiment was repeated using the sample holder outside the instrument for testing purposes before introducing it into the vacuum environment. SIMS images correlated with corresponding SEM images yielded interesting information on hydrogen distribution and hydride nucleation in the material. The FIB-SEM-SIMS instrument was also used to map hydrogen in Titanium Carbide and Vanadium Carbide precipitates in ex-situ gaseous hydrogen charged ferritic steel samples. The SIMS images obtained were correlated with SEM images of the precipitates and preferential hydrogen trapping sites were located for both the precipitates.

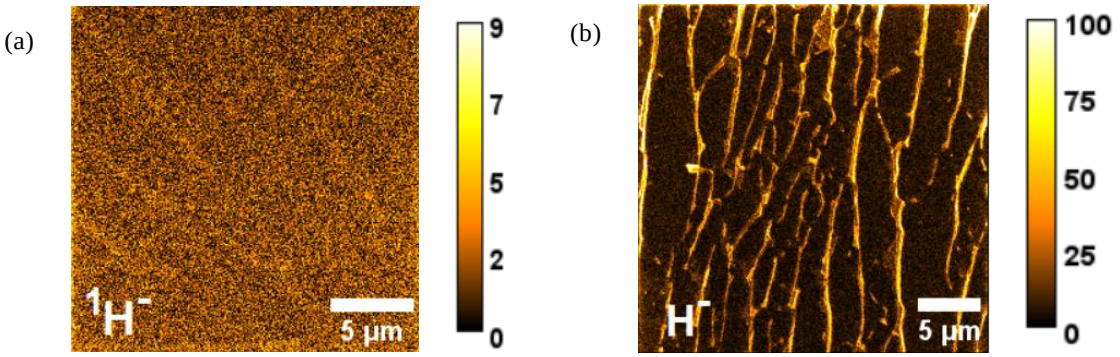

Figure 2: Hydrogen maps of Ti-6Al-4V sample obtained using SIMS imaging (a) before hydrogenation (b) after ex-situ electrochemical hydrogen charging at a current density of 0.5 mA/cm^2 in 5 wt% H_2SO_4. Both images employ a beam current of 100 pA and dwell time of 3ms per pixel. Both the SIMS images have 256 X 256 resolution over a field of view (a) 21µm x 21µm (b) 28µm x 28µm

Conclusions

To compensate the loss of hydrogen due to diffusion from samples during analysis, an in-situ electrochemical charging holder was designed to perform in-situ hydrogen charging of samples in the FIB-SEM-SIMS instrument. With the case studies, we introduce the design, capabilities and challenges of the in-situ charging holder and the FIB-SEM-SIMS instrument in SIMS based correlative microscopy to directly visualize hydrogen-metal interactions with nanoscale lateral resolution.

References

[1] D. Andersen *et al.*, "Correlative high-resolution imaging of hydrogen in Mg2Ni hydrogen storage thin films," *Int J Hydrogen Energy*, vol. 48, no. 37, pp. 13943–13954, Apr. 2023, doi: 10.1016/j.ijhydene.2022.12.216.

[2] O. De Castro *et al.*, "Magnetic Sector Secondary Ion Mass Spectrometry on FIB-SEM Instruments for Nanoscale Chemical Imaging," *Anal Chem*, vol. 94, no. 30, pp. 10754–10763, Aug. 2022, doi: 10.1021/acs.analchem.2c01410.

[3] L. Deconinck, T. Depover, and K. Verbeken, "The mechanism of hydride formation during electrochemical hydrogen charging of Ti–6Al–4V," *Materials Today Sustainability*, vol. 22, Jun. 2023, doi: 10.1016/j.mtsust.2023.100387.

[4] J. Kim, E. Plancher, and C. C. Tasan, "Hydrogenation-induced lattice expansion and its effects on hydrogen diffusion and damage in Ti–6Al–4V," *Acta Mater*, vol. 188, pp. 686–696, Apr. 2020, doi: 10.1016/j.actamat.2020.02.029.

Cost Optimal Design of Electrochemical Hydrogen Production Systems Powered by CSP/PV Hybrid Power Plants

A. Rosenstiel*[1,2], N. Monnerie[1], M. Roeb[1], C. Sattler[1,2]

[1]Deutsches Zentrum für Luft- und Raumfahrt, Institute of Future Fuels, Köln, Germany
[2]Faculty of Mechanical Engineering, RWTH Aachen University, Aachen, Germany

Introduction

In a climate-neutral global energy system, fossil fuels could be replaced by green hydrogen and hydrogen derivatives produced in regions with favorable conditions for renewable energy [1]. The Earth's sunbelt is one of the most promising regions in this context due to the enormous potential for solar energy and the availability of unused land [2].
However, electrochemical hydrogen production using solar energy is a challenge. With photovoltaics (PV), it is possible to provide electricity at attractive prices, but only during the day and with fluctuations. Since electricity storage with batteries is too expensive to ensure a continuous power supply, an electrolysis system powered exclusively by PV operates with relatively low full-load hours and also requires electricity for standby operation. This leads to lower system efficiency and increases the cost of the hydrogen produced.

This work therefore proposes combining photovoltaics with concentrated solar power (CSP) and thermal energy storage (TES) to operate an electrochemical hydrogen production plant. In this concept, the PV system generates electricity depending on the momentary solar radiation. In the CSP plant, a working fluid (molten salt) is heated in a receiver at the top of a solar tower and stored in a hot storage tank. From there, hot molten salt can be extracted as needed to transfer heat to a steam cycle that drives a steam turbine connected to a generator.

Thereby, the CSP electricity production can be adapted to the demand [3] and, together with photovoltaics, a very continuous power supply can be achieved. Such a CSP/PV hybrid power plant has further synergies: PV electricity can cover the CSP auxiliary power consumption and excess PV electricity can also be stored as thermal energy. If such hybrid solar energy systems are to be used for electrochemical hydrogen production, they offer a wide variety of operating modes and system configurations. Previous work has focused on the techno-economic evaluation of CSP/PV systems based on existing plant designs. The studies did not include a detailed energy system analysis of CSP/PV and electrolyzer combinations [4, 5].
The search for the best configuration that leads to the lowest levelized cost of hydrogen (LCOH) is a complex optimization problem that is addressed in this work. Therefore, a techno-economic energy system and optimization model is developed. This model includes an operational strategy and is able to determine the ideal scaling of the individual process units. The study shows that a combination of PV and CSP is a promising concept for large-scale solar hydrogen production that can lead to lower hydrogen production costs than using either technology alone. The advantages of these CSP/PV hybrid systems become particularly clear when a continuous supply of hydrogen is beneficial, for example when hydrogen production is coupled with a hydrogen liquefaction process or synthetic fuel production.

* Corresponding author: andreas.rosenstiel@dlr.de

Methodology

In order to determine the cost-optimized design of a CSP/PV powered stand-alone electrochemical hydrogen production plant, we developed an energy system model, which is illustrated in Figure 1. In the CSP plant, so-called heliostats concentrate the solar radiation on a receiver at the top of a solar tower and thereby heat a working fluid (molten salt), which is stored in a hot storage tank. From there, the hot molten salt can be extracted as required to transfer the heat to a steam cycle that drives a steam turbine connected to a generator. An alkaline (AEL) electrolyzer system can now be operated with the electricity generated in the steam cycle and in the PV system. If there is a surplus of PV electricity, this electricity can be supplied to an electric heater to heat the molten salt which is then also stored in the thermal energy storage. We have implemented an operational strategy algorithm for the optimal interaction between PV, CSP and the AEL electrolysis system. The operating strategy includes the utilization of the PV electricity surplus in a cascade that first covers the auxiliary consumption of all processes and only stores the remaining surplus electricity as heat. By incorporating techno-economic data, the model is able to determine cost-optimal system designs based on a global optimization algorithm. Figure 1 shows the six optimization variables considered for plant design. Each optimization variable is a characteristic design variable for one of the process units. The nominal receiver power $P_{CSP,Rec}$ is the design variable of the CSP part. This parameter represents the concentrated solar power that reaches the receiver at a DNI of 900 W/m^2. Other design variables are: the PV peak power ($P_{PV,Peak}$), the nominal power of the AEL system P_{AEL}, the nominal power of the steam turbine P_{Turb}, the nominal power of the electric heater $P_{Heater,el}$ and the capacity of the thermal energy storage C_{TES}. The general approach to optimizing the power plant design is to minimize the levelized cost of hydrogen (LCOH) as a function of these six optimization variables:

$$\mathrm{MIN}(LCOH) = f(P_{CSP,Rec}, P_{PV,Peak}, P_{AEL}, P_{Turb}, C_{TES}, P_{Heater,el}) \quad (1)$$

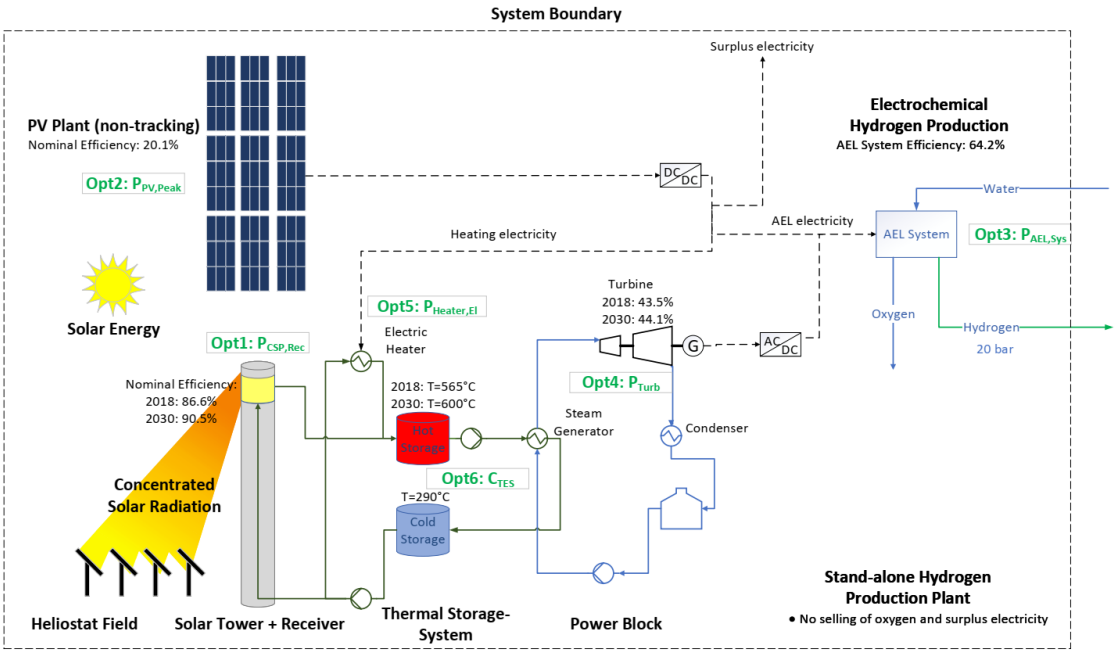

Figure 1. Schematic of the proposed stand-alone solar hydrogen production plant. An alkaline electrolyzer system (AEL) powered by a CSP/PV hybrid power plant. The six variables for optimizing the plant are highlighted in green[6].

Discussion

Figure 2 illustrates various possible operating modes for solar hydrogen production in a period with good solar irradiation. P_{AEL} is here the inlet power of the electrolyzer system. In addition, the electricity supply from the photovoltaic system (P_{PV}), the electricity generated by the steam turbine (P_{Turb}) and the electricity supply to the electric heater ($P_{Heater,el}$) are shown. In the reference case, a system powered exclusively by PV (a), electrochemical hydrogen production is only operated during the day. Due to the standby mode, hydrogen production starts immediately when the PV field supplies the minimum load of the elctrolyzer system. The techno-economic optimization leads to an oversized PV system. This leads to higher full load hours for the electrolyzer, but also to surplus electricity production. The second plot (b) is a CSP/PV powered AEL plant with an oversized PV system, which leads to fluctuating hydrogen production. At night, the electricity is supplied by the steam turbine. The electrolyzer system has a higher rated output and is operated at its maximum load by the PV system during the day. In the design of the third system (c) a constant hydrogen production was achieved by limiting the maximum AEL system power to 150 MW_{el}, a typical power output of a CSP tower system.

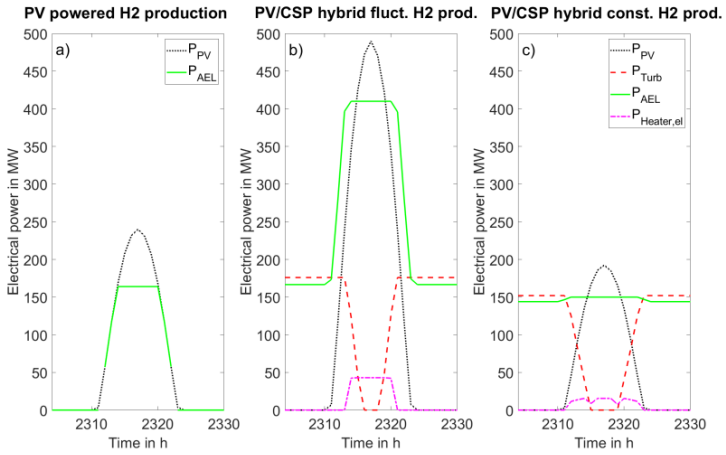

Figure 2. Comparison of different operating concepts for solar hydrogen systems for a day with good solar irradiation. (a) Exclusively PV-powered H_2 production; (b) CSP/PV-powered fluctuating H_2 production; (c) CSP/PV-powered constant H_2 production [6].

Which of these operating modes and system configurations lead to the lowest LCOH strongly depends on the cost assumptions used for the techno-economic optimization. If the investment costs for PV are low compared to CSP, the PV-dominated systems (a) and (b) may be the best options. Decreasing costs for CSP lead to a more continuous operation of the electrolyzer as in (c). In future work, a detailed sensitivity analysis will be carried out to investigate the influence of the cost assumptions used and to identify the most important influencing factors. It is also investigated how the coupling with other processes affects the results. For example, when hydrogen production is coupled with a synthetic fuel production process such as an e-methanol plant. In this case, the synthesis process can be operated more economically with a continuous supply of hydrogen, electricity and often also thermal energy, which favors a system of type c) in Figure 2.

Conclusions

In this study, we have developed an energy system model for an electrochemical hydrogen production plant powered by a combination of PV and CSP. The energy system includes a thermal energy storage system and an electric heater that can be used to store excess electricity as heat. We have implemented an operational strategy algorithm for the optimal interaction of PV, CSP and an alkaline (AEL) electrolyzer system. The operating strategy includes the utilization of the PV electricity surplus in a cascade, which initially covers the auxiliary consumption of the processes and only stores the remaining surplus as heat.
The plant optimizations carried out indicate that it may be advantageous to use such CSP/PV hybrid systems with heat storage to operate electrochemical hydrogen production at locations with high solar irradiation. Depending on the location and cost assumptions, this can lead to more full load hours of the electrolyzer and lower costs for hydrogen compared to a system powered solely by photovoltaics.
The advantages of these hybrid systems become particularly clear when hydrogen production is coupled with other processes, such as hydrogen liquefaction for hydrogen transportation or a fuel synthesis process, such as a methanol production plan. In this case, continuous hydrogen production leads to lower investment costs for subsequent process steps, as over-scaling of process equipment and the need for hydrogen storage is reduced. This effect will be investigated in more detail in the following studies. In addition, the influence of cost assumptions will be examined in a detailed sensitivity analysis and described with characteristic key parameters.

References

[1] IEA, *Global Hydrogen Review 2022: License: CC BY 4.0*. Paris, 2022. [Online]. Available: www.iea.org/reports/global-hydrogen-review-2022
[2] F. Trieb, C. Schillings, M. O'Sullivan, T. Pregger, and C. Hoyer-Klick, *Global Potential of Concentrating Solar Power. Solar Paces Conference 2009.* Berlin.
[3] D. Benitez *et al.*, "Solarthermische Kraftwerke. Wärme, Strom und Brennstoffe aus konzentrierter Sonnenenergie.," Deutsches Zentrum für Luft- und Raumfahrt e.V. (DLR), Institut für Solarforschung, Köln (D), 2021.
[4] F. I. Gallardo, A. Monforti Ferrario, M. Lamagna, E. Bocci, D. Astiaso Garcia, and T. E. Baeza-Jeria, *A Techno-Economic Analysis of solar hydrogen production by electrolysis in the north of Chile and the case of exportation from Atacama Desert to Japan*.
[5] C. Hernández Moris, M. T. Cerda Guevara, A. Salmon, and A. Lorca, *Comparison between Concentrated Solar Power and Gas-Based Generation in Terms of Economic and Flexibility-Related Aspects in Chile*.
[6] A. Rosenstiel, N. Monnerie, J. Dersch, M. Roeb, R. Pitz-Paal, and C. Sattler, "Electrochemical Hydrogen Production Powered by PV/CSP Hybrid Power Plants: A Modelling Approach for Cost Optimal System Design," *Energies*, vol. 14, no. 12, 2021, doi: 10.3390/en14123437.

Current State and Deficiencies of the Regulatory Framework for Low Carbon Hydrogen in the European Union

A. Nils Bruch*[1]

[1]A. Institute of Political Science, Technical University Darmstadt, Germany

Introduction

Renewable hydrogen is necessary for the decarbonization of sectors that are difficult to electrify, such as industry and aviation, and as a storage medium for surplus electricity from renewable sources [1]. The production of hydrogen on a fossil fuel basis has been the dominant production method, but renewable hydrogen has gained considerable relevance in the energy and climate policy debate in recent years. But so far, no significant amounts of renewable hydrogen were produced, as the market ramp-up is still in an early stage [2, 3, 4]. To push the emergence of a market, the European Union adopted a hydrogen strategy as part of the Fit-for-55 package and detailed framework conditions are being created to promote a sustainable and effective hydrogen economy [5]. The regulation of hydrogen in context of decarbonization is particularly challenging due to its novelty and complexity [6]. Hydrogen-related issues have to be integrated in the existing framework and new legislation has to be developed to fill in regulatory gaps and provide a coherent approach to hydrogen. The task of developing a coherent EU framework is complicated by varying regulatory needs and challenges for renewable and low carbon hydrogen. Low carbon hydrogen can be produced by a variety of production methods using different energy sources. These include the production of low carbon hydrogen on the basis of natural gas with subsequent carbon capture and storage (CCS) and carbon capture and utilization (CCU), but also the use of nuclear energy to power water electrolysis. While low carbon hydrogen is not produced with renewable sources, its greenhouse gas (GHG) emissions can be significantly lower than conventional fossil-based production. Therefore, the use of low carbon hydrogen is considered by some actors as a way of accelerating the market ramp-up by providing more hydrogen supply for offtakers and paving the way for a renewable hydrogen economy.

While the development of infrastructure and market design are important topics that need to be addressed on the regulatory level, the development of a framework for the production and import of low carbon hydrogen that supports decarbonization and does not place renewable hydrogen at a disadvantage is the center of this analysis. While the EU's main objective is to produce and import renewable hydrogen, low carbon hydrogen will also play a role, even if it's only during a transitional period to satisfy the demand that cannot be covered until more capacities for renewable hydrogen are build. The central challenge is to guarantee that the domestically produced and imported hydrogen, both renewable and low carbon, is contributing to GHG emission savings and consequently contributes to the decarbonization, while simultaneously providing enough hydrogen to satisfy demand and make the market ramp-up in the European Union possible. With the adoption of the Commission Delegated Regulation (EU) 2023/1184 of the second Renewable Energy Directive 2018/2001 (REDII) regarding requirements for the production of renewable fuels of non-biological origin (RFNBOs), the framework for renewable hydrogen is in an advanced phase. Yet, the regulatory framework for low carbon hydrogen is still in development. As low carbon hydrogen production requires

* Corresponding author: bruch@pg.tu-darmstadt.de

investments in fossil fuel technology, it carries the risk of creating fossil lock-ins or stranded assets. Therefore, special consideration must be given to a regulatory framework that ensures a positive contribution to achieve climate neutrality and the development of a level playing field between renewable and low carbon hydrogen.

Methodology

In this context, the following analysis of the EU regulatory framework for low carbon hydrogen will have three objectives:

- Outline the existing regulatory framework for low carbon hydrogen production and imports
- Identify deficiencies of the existing regulatory framework in the form of regulatory gaps and incoherencies
- Propose recommendations with regard to measures that could address those deficiencies to develop a coherent regulatory framework

These three objectives will be addressed in each section of the analysis, focusing on different elements of the regulatory framework. This will be done by a detailed examination of the current EU legislation relevant for these different types of low carbon hydrogen, including the most important directives, regulations, tertiary legislation, initiatives and acts still in the legislative process.

In the second section, the current and future role of low carbon hydrogen is outlined and compared to the EUs strategic approach towards hydrogen. In the third section, the detailed provisions on definitions are outlined and the integration of low carbon hydrogen in the target structure for hydrogen is examined. The fourth section covering detailed requirements of low carbon hydrogen production will be structured around the different production methods, namely gas-based production with CCS, gas-based production with CCU and production using nuclear energy. This allows a nuanced view on the peculiar challenges of each production method for the regulatory framework, especially in regards to guaranteeing GHG emission reductions throughout the entire production cycle. As hydrogen imports into the EU will play a significant role to secure supply in the future, the analysis of domestic low carbon hydrogen production is followed by an assessment of the EU framework for hydrogen imports in the fifth section. In the first subsection, the lacking strategic approach to low carbon hydrogen imports is outlined and recommendations are formulated to integrate low carbon hydrogen in the proposed Union strategy for imported and domestic hydrogen. The second subsection covers the implication of the detailed requirements for domestic low carbon hydrogen production for imported hydrogen and what matters to achieve a level playing field between domestic and third-country producers. The third subsection then discusses, if the European Hydrogen Bank can be a central initiative for a robust governance of low carbon hydrogen imports. In the concluding section, a table summarizing the issues, deficits and recommendations is provided.

Discussion

The analysis outlined the need for a more comprehensive approach of the European Union towards low carbon hydrogen. While the ultimate objective is the rapid development of a renewable hydrogen economy, low carbon hydrogen is already being produced in the EU and in third countries with the objective to be exported into the European Union. While key

elements of the regulatory framework have been adopted or are in the legislative process, regulatory gaps and incoherencies are still present.

Figure 1 illustrates factors to be considered in a regulatory framework for gas-based low carbon hydrogen production. It covers the upstream, midstream and downstream emissions and which respective legislation can be linked with the delegated acts of the Gas and Hydrogen Markets Directive to guarantee the proposed 70% greenhouse gas emission savings.

The upstream emissions consist of methane leakages during gas production, as well as transport and distribution of natural gas. These leakages will be covered under the Methane Regulation after it passes the legislative process. The provisions set for leakages under the Methane Regulation can then be linked to the central methodology for the calculation of GHG emission savings required under the Gas and Hydrogen Markets Directive, that is also still in the legislative process. Downstream emissions are mainly composed of CO2 leakages occurring during transport and distribution of CO2, leakages of storage sites or re-emissions at the lifetime end of products produced with captured carbon. CO2 transport and distribution, as well as storage is covered under the CCS Directive and these provisions can be linked to the methodology of the Gas and Hydrogen Markets Directive. But an EU framework for carbon capture and utilization is not existent. As low carbon hydrogen production facilities transferring the captured CO2 for use in other industrial processes or products are already operating, the risk of re-emission is imminent, wherefore the lack of rules for CCU is a major regulatory gap to be closed. While the proposed Carbon Removal Certification Regulation does not cover the utilization of non-biogenic carbon, it can still be used as a blueprint to develop provisions for carbon of fossil origin that is stored in products.

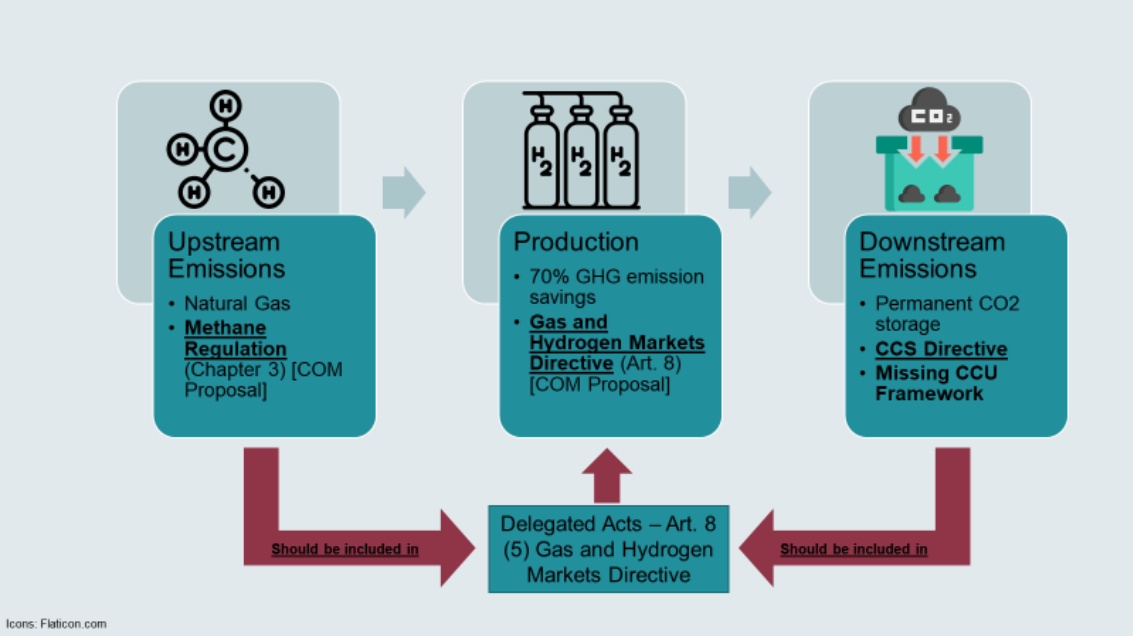

Figure 1: Proposal for a Regulatory Framework of Gas-Based Low Carbon Hydrogen Production

While nuclear-based hydrogen also falls under the umbrella of low carbon hydrogen, the energy sources and production methods differ significantly. Therefore, the regulatory framework needs to be adjusted to the peculiar challenges of nuclear power and be coherent with renewable hydrogen production to ensure a level playing field in the EU hydrogen market. The requirements of additionality, temporal correlation and geographical correlation were

introduced for renewable hydrogen production, but the introduction of similar requirements for nuclear hydrogen production should be discussed to prevent negative impacts on the electricity system and disadvantages for renewable hydrogen production. While the rules for temporal and geographical correlation can be transferred to nuclear hydrogen production, additionality needs to be adjusted to the properties of NPPs and nuclear electricity production. An additionality rule imposing that only new capacities can be used for nuclear hydrogen production is unfeasible, therefore the requirements should be adjusted to ensure the use of nuclear power for hydrogen production has no negative impacts on electricity prices, electricity supply for other sectors and does not trigger additional fossil electricity generation. Furthermore, equal rules for the eligibility of financial support for installations generating electricity for hydrogen production have to be developed.

In summary, the regulatory framework for gas-based low carbon hydrogen needs to be focused on capturing all points in the production lifecycle where the GHG emissions reduction target could be compromised. For nuclear-based hydrogen production, the challenges of the regulatory framework consist of the prevention of disadvantages for renewable hydrogen production.

Conclusions

While low carbon hydrogen is already produced in the European Union and different import agreements have been signed, a strategic approach guaranteeing long-term emission reductions and the prevention of fossil lock-ins is lacking. Still, a variety of policies relevant for low carbon hydrogen is already in force or in the legislative process. Regulatory instruments in the form of definitions and targets exist or are discussed in the ongoing legislative process. The different legislative acts form a fragmented framework of low carbon hydrogen definitions with varying eligibility for EU targets depending on the sector.

The proposed Gas and Hydrogen Markets Directive has the potential to align the fragmented framework as the central legislation for low carbon hydrogen and ensure long-term impacts on greenhouse gas emission reductions. The proposal sets up the requirement of a 70% greenhouse gas (GHG) emission savings threshold to be achieved during the production. To achieve comprehensive impacts on decarbonization, it is recommended that the forthcoming methodology for the calculation of emission savings should include upstream, midstream and downstream emissions and take into account differences of the production methods. The integration of lifecycle emissions into the regulatory framework can be realized by linking existing legislation with the requirements of low carbon hydrogen production. Nevertheless, some factors are not covered by EU legislation and display regulatory gaps to be closed.

To ensure sufficient GHG emission reductions during the production of gas-based low carbon hydrogen, it is recommended to cover upstream emissions (e.g. methane leakages) by linking the provisions of the Methane Regulation to the requirements of low carbon hydrogen. In the case of subsequent carbon capture and storage (CCS), the provisions set out in the CCS Directive should be linked to the calculation of GHG emission reductions of low carbon hydrogen to ensure permanent storage of CO2 with strict monitoring and reporting obligations to prevent leakages. Major regulatory gaps are identified for carbon capture and utilization (CCU), for example when captured carbon is being stored in products or used in industrial processes. In this case, it is recommended to extend the regulatory framework to ensure carbon utilization leads to emission mitigation instead of a temporal shift of emissions. While the

proposed Carbon Removal Certification Framework does not cover non-biogenic CO_2, it could be used as a foundation for a CCU regulatory framework.

Low carbon hydrogen also includes the production of hydrogen using nuclear energy. It is recommended to include upstream emissions from mining and processing of materials in the calculation of GHG emission reductions. But more importantly, the regulatory framework needs to be adjusted to the peculiar challenges of nuclear power and be coherent with renewably hydrogen production to ensure a level playing field in the EU hydrogen market. The requirements of additionality, temporal correlation and geographical correlation were introduced for renewable hydrogen production and the development of similar requirements that prevent negative impacts of nuclear hydrogen production on the electricity system and disadvantages for renewable hydrogen production should be discussed. While the rules for temporal and geographical correlation can be transferred, additionality needs to be adjusted to the properties of nuclear electricity production. An additionality rule imposing that only new capacities can be used for nuclear hydrogen production is unfeasible, therefore the requirements should be adjusted to ensure the use of nuclear power for hydrogen production has no negative impacts on electricity prices, electricity supply for other sectors and does not trigger additional fossil electricity generation. Furthermore, equal rules for the eligibility of financial support for installations generating electricity for hydrogen production have to be developed.

As low carbon hydrogen will be imported from third-countries into the European Union, it is recommended to introduce a strategic approach and measures to safeguard similar standards that ensure actual GHG emission reductions are achieved. Complementary to the Carbon Border Adjustment Mechanism, the European Hydrogen Bank has the potential to be the central institution to lay down a strategic approach to low carbon hydrogen imports, manage the approval of certification schemes and monitor compliance with the detailed requirements.

References

[1] A.M. Ferrario, V. Cigolotti, A.M. Ruz, F. Gallardo, J. García, G. Monteleone, “Role of Hydrogen in Low-Carbon Energy Future”, in Technologies for Integrated Energy Systems and Networks, G. Graditi and M. Somma, Ed. Weinheim: Wiley-VCH, 2022, pp. 71-104, doi: 10.2843/249013.

[2] IRENA, “Hydrogen: A renewable energy perspective”, Abu Dhabi: IRENA, 2019, https://www.irena.org/publications/2019/Sep/Hydrogen-A-renewable-energy-perspective.

[3] Hydrogen Europe, “Clean Hydrogen Monitor 2022“, 2022, https://hydrogeneurope.eu/wp-content/uploads/2022/10/Clean_Hydrogen_Monitor_10-2022_DIGITAL.pdf.

[4] D. Tarvydas, “The role of hydrogen in energy decarbonization scenarios”, JRC Technical Report, JRC131299, Luxembourg: Publications Office of the European Union, 2022, https://publications.jrc.ec.europa.eu/repository/handle/JRC131299.

[5] European Commission, “A hydrogen strategy for a climate-neutral Europe”, COM(2020) 301 final, Brussels: European Commission, 08.07.2020, https ://eur-lex.europa.eu/legal-content/EN/TXT/PDF/?uri=CELEX:52020DC0301&from=EN.

[6] M. Janautre, “Renewable Hydrogen – Renewable Energy and Renewable Hydrogen APAC Markets Policies Analysis”, Wiesbaden: Springer Gabler, https ://doi.org/10.1007/978-3-658-32642-5.

Development of a Redox Material Assembly for Solar Thermochemical Fuel Production

L. Thomas*[1], S. Brendelberger[1], C. Sattler[1,2]

[1]German Aerospace Center (DLR), Institute of Future Fuels
[2]RWTH Aachen, Chair for Solar Fuel Production

Introduction

For the production of green hydrogen, a two-step thermochemical reduction-oxidation (redox) cycle can be implemented in a solar power plant. Therein, solar radiation is concentrated by a heliostat field onto the receiver-reactor on top of a solar tower in order to provide high temperature heat for a thermochemical reaction. In the first endothermic step of the cycle, a redox material (e.g. CeO_2) is reduced at high temperatures ($T_{red} \geq 1400$ °C) and low oxygen partial pressures ($p_{O_2} \leq 10$ mbar). In the second exothermic step the reduced redox material is cooled down ($T_{ox} \leq 1000$ °C) and brought into contact with an oxidizer (H_2O / CO_2), producing H_2 / CO and returning to its initial oxidized state. This cyclic process presents a sustainable production pathway for green hydrogen or syngas for various applications.
The state-of-the-art receiver-reactor design consists of one reactor cavity with a windowed aperture as an interface for concentrated solar radiation [1]. The redox material in form of reticulated porous ceramic elements is assembled at the inner cavity walls, allowing a direct irradiation. This reactor concept operates in batch mode, where the entire reactor needs to be cycled between reduction and oxidation conditions (temperature and pressure swing). The temperature increase between each oxidation and reduction step consumes a large fraction of the solar energy input and thereby reducing the overall process efficiency [2].
In order to address amongst others this limitation and to obtain a more efficient H_2 / CO production, a novel receiver-reactor concept was proposed [3]. The main feature of the new R2Mx design is the spatial and technical separation of the receiver-reactor for reduction from the oxidation reactor (Figure 1). The redox material is mounted onto vertical transport units, allowing it to be moved between the hot receiver-reactor cavity for reduction and the colder oxidation reactor for re-oxidation and fuel production. This approach allows to have a continuous on-sun operation, as the receiver-reactor does not need to be cooled down for oxidation. Furthermore, the setup facilitates the incorporation of a heat recovery system between the two reaction zones to further improve the process efficiency.
For the innovative R2Mx concept it is necessary to develop a new key component, the redox material assembly (RMA). An RMA primarily consists of the structured redox material and the thermal insulation towards the transport unit. The development of the RMA within the technical boundary conditions given by the R2Mx design is the main goal of this work.

* Corresponding author: louis.thomas@dlr.de

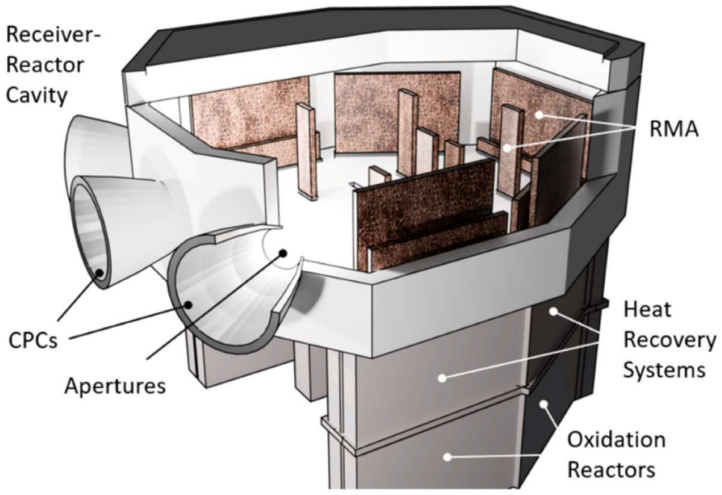

Figure 1: MW scale vision of the R2Mx concept featuring a separated Receiver-reactor cavity for reduction and oxidation reactors for oxidation with several movable redox material assembly (RMA) units [3].

Methodology

For the optimization of the RMA a numerical model is being developed. The model simulates the heat transfer, especially via thermal radiation, between the RMA and its environment and within the RMA itself. Further simulation tasks include the modeling of fluid dynamics and redox reactions during oxidation.
For the R2Mx design a proof-of-concept test rig is currently in development, featuring separate reduction and oxidation reactors and a transport unit for moving the RMA. The test rig will provide experimental data to validate and improve the numerical model, allowing the development of an optimized RMA for solar thermochemical fuel production.

Discussion

The different boundary conditions and simulated characteristics represent the changing reactor environments during cyclic operation between reduction and oxidation reactor cavities. This allows to better understand and improve the design of the RMA and the redox structure. The modeling approach and simulation results will be presented and discussed.

Conclusions

It is expected, that the numerical model will help to predict and assess the performance of different RMA designs under cyclic operation. Based on these results, overall process efficiency and solar thermochemical fuel production can be optimized by utilizing an improved RMA design. Due to the early stage of the work no final conclusions will be available.

References

[1] S. Zoller, E. Koepf, D. Nizamian, M. Stephan, A. Patané, P. Haueter, M. Romero, J. González-Aguilar, D. Lieftink, E. d. Wit and Brendelberger, "A solar tower fuel plant for the thermochemical production of kerosene from H2O and CO2," *Joule,* pp. 1606-1616, 2022, DOI: 10.1016/j.joule.2022.06.012.

[2] S. Zoller, E. Koepf, P. Roos and A. Steinfeld, "Heat Transfer Model of a 50 kW Solar Receiver–Reactor for Thermochemical Redox Cycling Using Cerium Dioxide," *Journal of Solar Energy Engineering,* 2019, DOI: 10.1115/1.4042059.

[3] S. Brendelberger, P. Holzemer-Zerhusen, E. Vega Puga, M. Roeb and C. Sattler, "Study of a new receiver-reactor cavity system with multiple mobile redox units for solar thermochemical water splitting," *Solar Energy,* pp. 118-128, 2022, DOI: 10.1016/j.solener.2022.02.013.

Development of a computational tool to assess the hydrogen demand-supply ratio within a hydrogen valley environment

F. Del Mondo*[1], D. Pivetta[1]

[1]Department of Engineering and Architecture, University of Trieste, Via Valerio 10, 34127 Trieste, Italy

Introduction

Hydrogen valleys are considered as regional ecosystems that link hydrogen production, transportation, and various end uses such as mobility or industrial feedstock [1].
In the context of developing a large hydrogen economy, many barriers are identified across the hydrogen value chain, starting from the availability of renewable sources to the hydrogen end-use or distribution.
Several studies in literature [2]–[4] identify issues including policy and regulatory uncertainty, technological and commercial risk, production costs, lack of infrastructure, distribution and storage constraints, and lack of market structure. For example, authors in [2], found that the Australia's large production and cost-competitive green hydrogen will offer competitive advantages over the other exporters but must increase the hydrogen demand through potential strategic partnership in Europe nations. The development of hydrogen economy in Brazil in [3] underline that the government should establish long-term policy framework aimed at the increment of private investors, stimulating market demand, develop standards and regulations to eliminate market expansion barriers, and enhancing support for research and development. The study reported in [4] analyse the collected information by written questionnaires and interviews of experts of almost all European countries. Based on the survey findings, the recommended strategy for harnessing the potential of hydrogen involves a top-down approach. In this approach, stakeholders, experts, academics, and industrial leaders play a crucial role in communicating to decision-makers at local and national government levels the potential of hydrogen in the current and future energy landscape. This approach serves the dual purpose of facilitating greater integration of variable renewable energy sources into the energy market and reducing greenhouse gas emissions to enhance sustainable mobility.
A study reported in [5] highlights the uncertainties in matching of supply-demand coordination that, a progressive implementation of hydrogen end-use applications, will require for hydrogen production, storage, transportation, and distribution across multiple sectors.
The distribution and transportation of hydrogen pose challenges, with efficiency losses of approximately 42% when converting it from a gas to a liquid form [6]. Additionally, the costs for end users can range from 0.45 €/kg to 2.7 €/kg for gaseous hydrogen, depending on the transported quantity and travel distance [7].
A large-scale hydrogen economy evaluated in [8] analyse the highway distribution network among 15 production sites in Germany and the 9,683 refuelling stations planned for development by 2050. In addition to the economic evaluation of the optimal hydrogen energy carrier for transportation based on the covered distance during the transport phase, a twofold per day increase in trucks on the roads is identified. The study raises concerns about the suitability of German highway infrastructure highlighting the need to provide a dedicated pipeline infrastructure.

*Corresponding author: federico.delmondo@dia.units.it

The study presented in [9] explores various distribution methods, including pipelines and gas or liquid truck delivery. Results shown that gas truck delivery is well-suited for small facilities and limited demand, liquid delivery is optimal for transporting over long distances and for moderate demand, while pipeline delivery is most efficient in densely populated areas with high hydrogen demand. According to Yang and Ogden [9], the selection of the most economical supply method will be determined by the unique geographical and market attributes, including factors like the number of demand centers, requested demand, and market reach.

From the literature analysis, it is worth noticing that a hydrogen delivery network is essential to match supply and demand, both within and outside a hydrogen valley, by considering distribution area characteristics and end-user demand.

The North Adriatic Hydrogen Valley (NAHV) project, started in September 2023 and funded also by the Horizon Europe scheme, is a transnational initiative encompassing the Friuli Venezia Giulia region in Italy, Croatia and Slovenia. The project aims to developing 17 pilot projects distributed across the three territories with the goal of an annual green hydrogen production of at least 5000 tons per year [10]. Considering the presence of facilities of varying sizes within the NAHV, a management system that consider the variability in hydrogen production and consumption can play a crucial role in establishing a robust and optimized distribution system.

The project aims to be a starting point for the development of a more extensive hydrogen ecosystem in the three territories. In addition, potential import and export of hydrogen could be consider in the future, thanks also to the strategic position of the three countries in Eastern Europe and with the easy access to ship trade channels.

The establishment of hydrogen optimized distribution and supply system is essential to ensure a suitable economic alignment between hydrogen suppliers and consumers. Even more, in a long-term prospective, this will be necessary for considering the entering of other new hydrogen suppliers and end-users and to allow the effective and viable development of a more extensive hydrogen-based economy.

To contribute to this framework this work propose the development of an advanced computational tool able to optimally manage the relationship between hydrogen supply and demand, considering the available hydrogen production, distribution and use technologies and their optimal integration in a hydrogen ecosystem.

Methodology

Fig. 1 represents a simplified schematic of the routes considered for the hydrogen exchange within the NAHV. The squares identify the location of testbed while the arrows the exchange of hydrogen between the facilities. Hydrogen is supposed to be transported both as liquefied or gas form and also the development of dedicated pipeline is considered for hydrogen distribution.

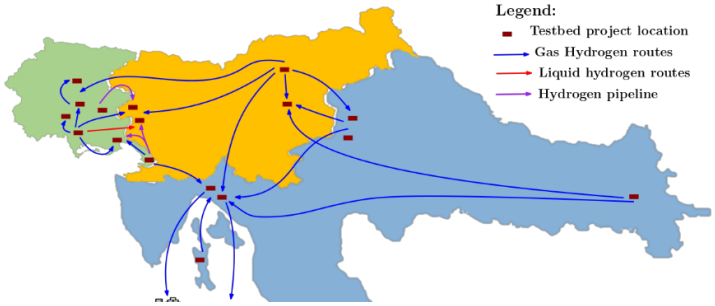

Figure 1: Hydrogen exchange scheme within NAHV region.

This study is based on the optimization tools previously developed in [11, 12] .These tools aim at analysing the potential use of hydrogen for the decarbonization of industrial port areas. Similarly, to industrial port areas, HV can be considered as complex systems where both industry and mobility hydrogen demand are required. In these areas, a proper management system of hydrogen incoming and outgoing flows is needed to assess the optimal distribution for the different end users. The NAHV project encompass 17 pilot facilities distributed over the macro-region each with its own characteristics as for example electrolyser and storage capacity, and the quantities of hydrogen produced and/or consumed. A new version of model [11, 12] is proposed here for conducting technical and economic assessments of the hydrogen distribution network. A multi-objective approach is adopted through a Mixed-Integer Linear Programming (MILP) algorithm to concurrently optimize techno-economic and environmental objective functions.

A generic testbed can encompass hydrogen production, followed by its on-site utilization (or distribution), or alternatively, hydrogen can be imported into the pilot facility for subsequent utilization, as depicted in Fig. 2.

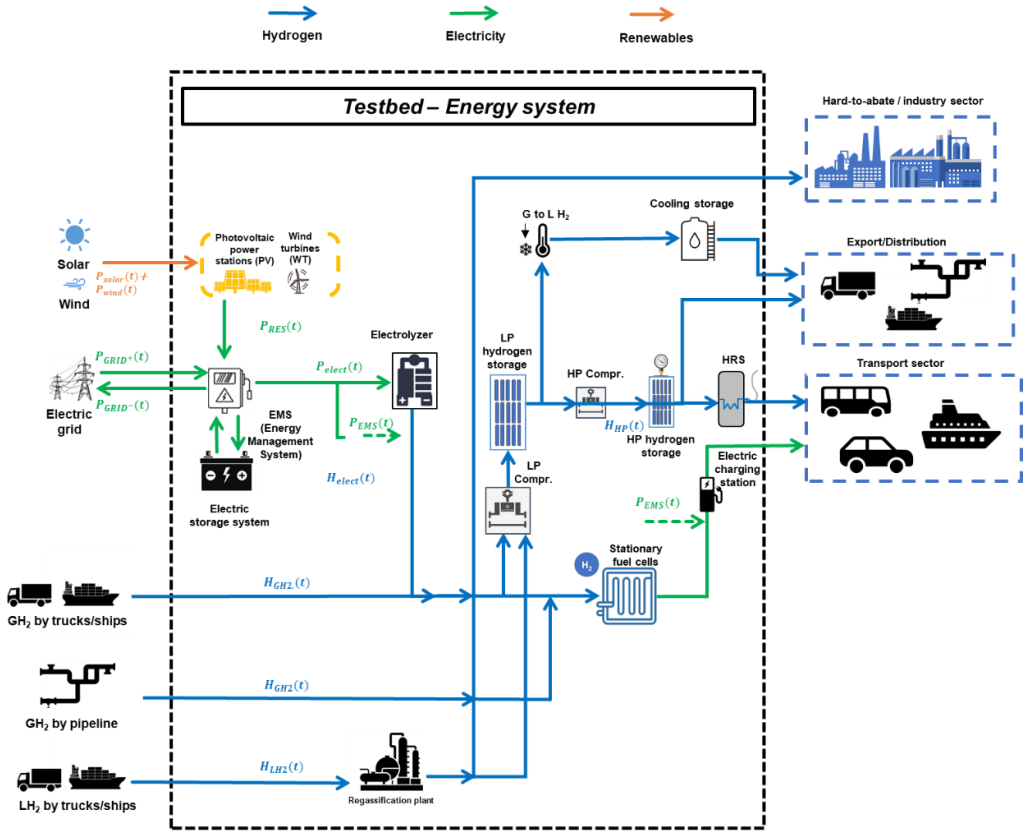

Figure 2: Model encompassing all the possible iterations that can occur within a testbed in the NAHV scenario.

In the schematic in Fig. 2, arrows of different colour identify the flows of H2 (blue lines), electric power (green lines) and solar/wind power (yellow lines). Dashed lines mark the whole system boundaries (black dashed lines), the H2/energy user (or distribution) units (blue dashed lines), and the available renewable sources (yellow dashed lines).

Describing Fig.2 from the top left corner the solar and wind energy resources at the chosen pilot facility can be described by the Photo Voltaic (PV) power plant and Wind Turbines (WT), respectively.
The energy flows for the electrolyser, when the testbed includes a hydrogen production facility, are managed by a management system which provides energy to the electrolyser from two sources: electric grid or from Renewable Energy Sources (RES) depending on its availability. When there is a surplus of renewable energy production, the management system either stores the excess energy in the battery, up to its storage capacity, or feeds it into the electric grid
In another scenario, the hydrogen is supposed to be imported into the testbed through a pipeline or through a logistic hydrogen distribution network of trucks and ships.
The H2/energy user (or distribution) units (blue dashed lines) includes the hydrogen demand for industries, the hydrogen demand for distribution and the hydrogen demand for transport sector.
In case of hydrogen distribution, a possible gaseous to liquid transformation of hydrogen is considered, while, in case of hydrogen utilization in transport sector a high-pressure storage or a power electric generation via fuel cell is assessed. A generic NAHV testbed thus defined is considered and a computational tool encompassing different hydrogen production scenarios, storage and distribution type will be developed. The model aims to determine the technical and economic aspects related to the distribution infrastructure within a hydrogen facility.

Discussion

A computational tool of a hydrogen pilot facility could allow a better use of available renewable energy and reduce the effect of mismatching the supply and hydrogen demand as well as considering the technical and economic aspects of hydrogen distribution.
Numerical models defining each sites of production, storage and use of hydrogen could be integrated into a whole hydrogen valley plants management system interconnecting all pilot facilities ensuring supply\demand digital infrastructure.
The modelling and optimization approach adopted in this study is well adaptable to other hydrogen ecosystems with different sizes and geographical locations, making it a versatile computational tool for addressing the specific characteristics of different regions.

Conclusions

The Hydrogen Valleys ecosystems often cover wide geographical areas, with hydrogen produced in different hubs and either used on-site or distributed from production facilities.
The North Adriatic Hydrogen Valley (NAHV) project, started in September 2023, is a transnational H_2 valley encompassing the Friuli Venezia Giulia region in Italy, Croatia, and Slovenia. The project's objective is to establish 17 pilot initiatives across these territories, aiming to produce at least 5000 tons of green hydrogen annually.
Within the NAHV environment, the development of an optimized hydrogen distribution and supply system is considered fundamental to achieve economic alignment between hydrogen suppliers and consumers.
A generic testbed is modelled by using a Mixed-Integer Linear Programming (MILP) algorithm system to provide the optimal match between hydrogen production (or supply) and demand within the pilot facility. The testbed model, defined through its own value-chain characteristic, is integrated inside a computational tool to assess the uncertainties in matching of supply-demand and to evaluate the technical and economic aspects of hydrogen distribution.

A computational tool including all hydrogen production, storage and use sites within a hydrogen valley will be developed in future to allow the definition of a digital supply/demand infrastructure.

An efficient design of the hydrogen distribution network not only leads to cost reduction but also supports the overarching goal of reducing carbon emissions, aligning with the broader sustainability objectives of the hydrogen industry.

References

[1] Fuel Cells and Hydrogen 2 Joint Undertaking, U. Weichenhain, M. Kaufmann, and A. Benz, "Hydrogen valleys – Insights into the emerging hydrogen economies around the world," *Publ. Off.*, 2021, doi: https://data.europa.eu/doi/10.2843/133091.

[2] S. K. Kar, A. S. K. Sinha, R. Bansal, B. Shabani, and S. Harichandan, "Overview of hydrogen economy in Australia," *WIREs Energy Environ.*, vol. 12, no. 1, Jan. 2023, doi: 10.1002/wene.457.

[3] C. Chantre *et al.*, "Hydrogen economy development in Brazil: An analysis of stakeholders' perception," *Sustain. Prod. Consum.*, vol. 34, pp. 26–41, Nov. 2022, doi: 10.1016/j.spc.2022.08.028.

[4] D. Astiaso Garcia, "Analysis of non-economic barriers for the deployment of hydrogen technologies and infrastructures in European countries," *Int. J. Hydrogen Energy*, vol. 42, no. 10, pp. 6435–6447, Mar. 2017, doi: 10.1016/j.ijhydene.2017.01.201.

[5] F. Eljack and M.-K. Kazi, "Prospects and Challenges of Green Hydrogen Economy via Multi-Sector Global Symbiosis in Qatar," *Front. Sustain.*, vol. 1, Jan. 2021, doi: 10.3389/frsus.2020.612762.

[6] J. T. Hinkley, A. R. Heenan, A. C. S. Low, and M. Watson, "Hydrogen as an export commodity – Capital expenditure and energy evaluation of hydrogen carriers," *Int. J. Hydrogen Energy*, vol. 47, no. 85, pp. 35959–35975, Oct. 2022, doi: 10.1016/j.ijhydene.2022.08.192.

[7] A. Lahnaoui, C. Wulf, H. Heinrichs, and D. Dalmazzone, "Optimizing hydrogen transportation system for mobility via compressed hydrogen trucks," *Int. J. Hydrogen Energy*, vol. 44, no. 35, pp. 19302–19312, Jul. 2019, doi: 10.1016/j.ijhydene.2018.10.234.

[8] M. Reuß, P. Dimos, A. Léon, T. Grube, M. Robinius, and D. Stolten, "Hydrogen Road Transport Analysis in the Energy System: A Case Study for Germany through 2050," *Energies*, vol. 14, no. 11, p. 3166, May 2021, doi: 10.3390/en14113166.

[9] C. YANG and J. OGDEN, "Determining the lowest-cost hydrogen delivery mode," *Int. J. Hydrogen Energy*, vol. 32, no. 2, pp. 268–286, Feb. 2007, doi: 10.1016/j.ijhydene.2006.05.009.

[10] NAHV, "NAHV's objectives and ambition." https://www.nahv.eu/our-ambition/ (accessed Oct. 06, 2023).

[11] D. Pivetta, A. Tafone, S. Mazzoni, A. Romagnoli, and R. Taccani, "A multi-objective optimization approach for the design of alternative port energy systems in tropical region," *ECOS 2023, Las Palmas Gran Canar. 25-30 June 2023, Spain*, 2023.

[12] D. Pivetta *et al.*, "Optimal decarbonization strategies for an industrial port area by using hydrogen as energy carrier," *Int. J. Hydrogen Energy*, Sep. 2023, doi: 10.1016/j.ijhydene.2023.07.008.

Development of a new generation of PEM electrolysis cells - Novel CCMs for high-pressure application

E. Suntinger*[1], K.Treusch[1], B. Grabner[1], A. Trattner[1,2]

[1]HyCentA Research GmbH, Graz, Austria
[2]Institute of Thermodynamics and Sustainable Propulsion Systems, Graz University of Technology, Graz, Austria

Introduction

Global hydrogen demand is continuously increasing, especially in sectors such as transportation, steel manufacturing and minerals processing. With currently more than 95 % of the hydrogen produced being “grey” hydrogen from mainly coal gasification or steam methane reforming, producing “green” hydrogen from water electrolysis (WE) using renewable electricity is a crucial step on the path towards carbon neutrality.[1], [2]

Alkaline electrolyte water electrolysis (AELWE) is the most mature electrolysis technology and has been employed for hydrogen production for decades. However, due to the long response time of the system, AELWE offers limited suitability for coupling with intermittent renewable energy sources. Proton exchange membrane water electrolysis (PEMWE) is a less mature but more advanced technology with better dynamic behaviour – meeting the requirements for integration into a renewable energy system. Additional advantages of PEMWE include higher current densities, more compact design, better conversion efficiencies and hydrogen purity of up to 99.999 %.[1], [2]

The urgently required scale-up of PEMWE to gigawatt scale is limited by expensive cell materials and thus high investment costs. State-of-the-art (SoA) PEM electrolysers use perfluorosulphonated acid (PFSA) membranes paired with Pt/C and Ir/IrO_2 catalysts on the cathode and anode, respectively. In an effort to reduce costs to < 2 €/kg H_2, research is put into reducing the oxygen evolution reaction (OER) catalyst loading on the anode side while maintaining long durability, good electrical conductivity, and thus, high hydrogen production rates. Moreover, with current Ir loadings of 1-3 mg/cm^2, the earth’s Ir availability could be exceeded in the near future. Regarding membranes, the trend goes towards developing thinner membrane materials or alternatives, such as sulphonated hydrocarbon-based membranes, addressing environmental concerns about fluorine chemistry.[1], [2]

Methodology

In the course of this dissertation, a new generation of PEM electrolysis cells will be developed and scaled into a 5 kW stack, with the goal of increasing lifetime and reducing costs. This is approached by material benchmarking state-of-the-art PEMWE cell components and gaining an in-depth understanding of degradation mechanisms. Material characterisation will be done by polarisation curves, electrochemical impedance spectroscopy (EIS), rotating disc electrode (RDE) and SEM imaging. Further analyses of interactions between different cell components shall lead to identifying possible

* Corresponding author: suntinger@hycenta.at

performance improvement areas and developing an optimised membrane electrode assembly (MEA) and possible cell configurations.

The target area of improvement is set to reduce catalyst loading – catalyst-coated membranes (CCM) from different manufacturing processes will be evaluated in a single-cell test setup. Using alternative polymers, either based on hydrocarbon structure or a short side chain (SSC), PFSA and low-iridium catalysts for the OER will be tested. The optimised single-cell configuration is scaled up to a 5 kW stack with an efficiency of 70 % and possible operation at an output pressure of up to 80 bar. A sophisticated testing plan for long-term testing and accelerated stress tests (ASTs) based on Design of Experiment (DoE) is developed and is applied for lifetime and state of health monitoring.

Discussion

In the PEM electrolysis cell, the overall reaction is split into two half-reactions: the oxygen evolution reaction (OER) on the anode side (eq. 1) and the hydrogen evolution reaction (HER) on the cathode side (eq. 2). The HER has fast reaction kinetics - SoA HER Pt/C catalysts perform efficiently at loadings of 0.3 mg/cm^2 and, therefore, do not represent a focus area of research emphasis. The OER reaction kinetics is substantially slower. The cathode activation is the rate-determining step and a significant contributor to the activation overpotential. Therefore, intensive research on OER catalysts is crucial to increase overall performance and decrease costs. Providing both strength and stability, SoA OER catalysts mostly use IrO_2 at loadings of 1-3 mg/cm^2, accounting for approximately 8 % of overall stack costs. Previously investigated low-iridium catalysts stabilised by support materials such as carbides, nitrides, and transition metals, such as $SrIrO_3$, show promising mass activity but insufficient stability.[1], [3], [4]

anode $$H_2O \xrightarrow{Ir/IrO_2} 2H^+ + \frac{1}{2}O_2 + 2e^- \quad \text{(eq. 1)}$$

cathode $$2H^+ + 2e^- \xrightarrow{Pt/C} H_2 \quad \text{(eq. 2)}$$

total $$H_2O \rightarrow H_2 + \frac{1}{2}O_2 \quad \text{(eq. 3)}$$

The solid electrolyte (membrane) separates the OER from the HER – protons from decomposed water molecules at the anode migrate through the membrane to the cathode, where they are reduced to hydrogen. Thinner membranes have lower ohmic losses and, thus, are more efficient. However, with decreasing membrane thickness, hydrogen crossover increases. Crossover provides a substantial safety risk and leads to the formation of peroxide and free radicals. It creates a potentially explosive environment and damage delt by peroxides and radicals could require replacing the whole stack prematurely resulting in drastically higher overall system costs. PFSA membranes can be classified as long side chain (LSC) and short side chain (SSC). SoA membranes are LSC, such as Nafion. However, SSC provide the advantage of decreasing the polymer's equivalent weight at the same number of ion conducting units, resulting in a better ion exchange capacity. At the same time, improved mechanical stability leads to less hydrogen crossover and overall improved lifetime. A typical SSC PEM in fuel cells is Aquivion, showing improved hydrogen crossover and even allowing operating temperatures above 90 °C. PFSA membranes account for approximately 5 % of overall stack costs.[1], [2], [5]

Conclusions

SoA PEM electrolysers operate at current densities of up to 3 A/cm^2 for an expected ideal lifetime up to 100.000 h. Their short response time enables an integration into intermittent renewable energy sources. However, intermittent energy supply accelerates degradation, such as membrane thinning and dissolution of the OER catalyst. Ir loadings are targeted to well below 1 mg/cm², stressing again the need to develop mechanically stable low-iridium catalysts. Conventional LSC PFSA membranes are prone to membrane thinning and hydrogen crossover, proposing a substantial safety risk and driving up overall system costs due to insufficient lifetime. Promising membrane types are SSC PFSA, which are less prone to hydrogen crossover. To achieve the production cost target of < 2 €/kg H_2, it is crucial to put research emphasis on reducing the OER catalyst loading and increasing overall lifetime by improving the membrane.[1]–[5]

References

[1] K. Zhang *et al.*, "Status and perspectives of key materials for PEM electrolyzer," *Nano Research Energy*, vol. 1, p. e9120032, Dec. 2022, doi: 10.26599/NRE.2022.9120032.

[2] P. Shirvanian and F. van Berkel, "Novel components in Proton Exchange Membrane (PEM) Water Electrolyzers (PEMWE): Status, challenges and future needs. A mini review," *Electrochem commun*, vol. 114, p. 106704, May 2020, doi: 10.1016/j.elecom.2020.106704.

[3] G. Jiang *et al.*, "Low-Loading and Highly Stable Membrane Electrode Based on an Ir@WO $_x$ NR Ordered Array for PEM Water Electrolysis," *ACS Appl Mater Interfaces*, vol. 13, no. 13, pp. 15073–15082, Apr. 2021, doi: 10.1021/acsami.0c20791.

[4] E. J. Park, C. G. Arges, H. Xu, and Y. S. Kim, "Membrane Strategies for Water Electrolysis," *ACS Energy Lett*, vol. 7, no. 10, pp. 3447–3457, Oct. 2022, doi: 10.1021/acsenergylett.2c01609.

[5] E. Kuhnert, V. Hacker, and M. Bodner, "A Review of Accelerated Stress Tests for Enhancing MEA Durability in PEM Water Electrolysis Cells," *Int J Energy Res*, vol. 2023, pp. 1–23, Feb. 2023, doi: 10.1155/2023/3183108.

Digital Sensors Twin for the Hydrogen Refueling Station Application

Raduan Sarif [*1], Carlo Tiebe[2], Marc Reichenbach[3]

[1, 2] Federal Institute for Materials Research and Testing, Berlin, Germany
[3] Brandenburg University of Technology Cottbus–Senftenberg, Cottbus, Germany

Introduction

A hydrogen refueling station (HRS) is a complex unit consisting of various devices that interact with each other and simultaneously have significant interactions with the external atmosphere and environmental influences. The fundamental risks of HRS include burning, fire, explosion, overpressure, temperature risk, hydrogen flow, and possible adverse effects on human health from close contact or exposure. It must incorporate measurement techniques to lower the risk of fire, explosion, deflagration, and pressure waves to a manageable level. Several regulations, codes, and standards apply to the design, construction, and operation of hydrogen refueling stations, constantly being updated, and revised as new technologies and practices emerge. Overall, to enhance safety and ensure the proper application of the fueling protocol, several technology solutions are necessary to monitor the total process status data of the HRS.

Statistical process control (SPC) is a set of statistical tools and techniques to monitor and control industrial processes. A digital twin (DT) is one type of SPC that can improve process efficiency, increase productivity, and improve quality control of industries[1, 2]. It can be defined as a virtual dynamic representation of a physical space connected to it over the entire lifecycle for bidirectional information and data exchange. The physical space automatically transfers information to the virtual space during the whole process lifecycle. The virtual space instead identifies the improvements, control demands, or predictions and sends them back the data to the real space for improvements; data exchange is an automatic process. A digital twin provides live or near real-time information to proactively improve, optimize, and transform the process operation using emerging technologies like the Internet of Things (IoT), Big Data, edge computing, machine learning, and predictive analytics. In tackling the challenges of HRS, a DT would be an appropriate solution to optimize and validate the process management of hydrogen fueling stations. It will help with HRS real-time monitoring, leakage detection, future condition prediction, optimization, indirect carbon emissions reductions, and maintenance. HRS is the real space for this project, and the IoT, software simulation, data analytics, and data cloud are the virtual space [3, 4]. Different types of sensors are deployed on the physical space (HRS) for the various parameters for the comprehensive information, such as ambient temperature, hydrogen fuel temperature, pressure, and vehicle tank fuel temperature. All the information is sent to the virtual space through the data cloud to analyze the performance issues and generate possible improvements in data, for instance, maintenance, leak detection, and indirect carbon emissions reductions. Virtual space can give feedback data on the demand for physical space. Digital twins for hydrogen refueling stations are shown in Figure 1.

This analytical overview is the initial study in developing the digital sensors twin for the hydrogen refueling station. The research includes a comprehensive analysis of the current literature, refueling protocol, standards, mathematical model, simulation model, and trends in digital twins and H_2 technologies. Furthermore, this study has explored the various HRS attributes, such as leakage, temperature, pressure, and hydrogen flow, and identified different use cases of the hydrogen fuel station to build a digital sensor twin. Various real gas equations, such as the Van der Waals and Able-Noble equation of state (EOS), are applied to analyze the key factors and parameters affecting hydrogen and the MATLAB simulation model to validate

* Corresponding author: Raduan.Sarif@bam.de

the key elements and parameters. This study also focuses on identifying and addressing research gaps in hydrogen technology, contributing to advancing hydrogen infrastructure, and supporting the global transition to cleaner energy solutions. The many forms of analytical questions that will emerge from this research are as follows:

- How can digital twin technology be an effective solution for hydrogen refueling stations (HRS) to enhance safety, efficiency, and overall operation?
- What is the appropriate gas equation to analyze the H_2 in a refueling station?
- What would be the optimal use case for the DT?

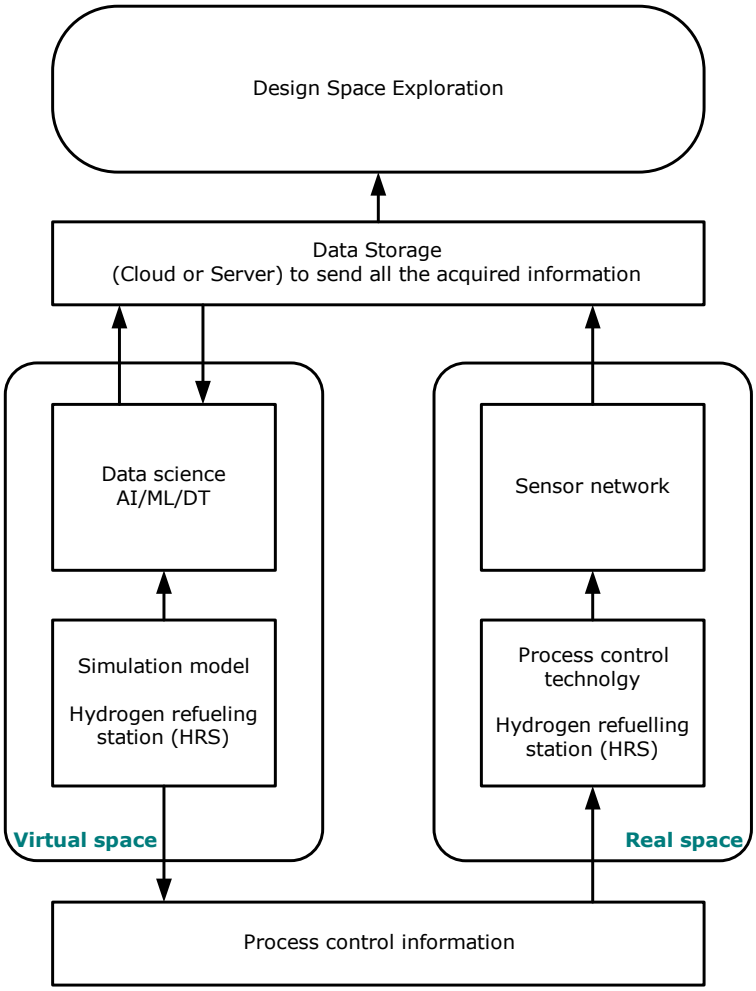

Figure 1: Digital sensor twin for hydrogen applications.

Methodology

Based on the standards SAE J2601 [5] and ISO 19880-1:2020 [6], the Fueling protocol process limits for light-duty vehicle dispensing systems. During the fueling process, the dispensing system shall meet the following fueling protocol limits or terminate the fueling within 5 seconds. There are some selected use cases, and their protocol limits are discussed below in Table 1.

Table 1: Selected use case for the digital twin.

	Sensor's name	Criteria	Fuelling limits
Temperature	1. Ambient temperature sensor	Ambient temperature/ environmental temperature of the operation	-40 °C< t_{amb} < 50 °C
Pressure	2. Pressure Sensor (p_1)	The dispenser fuel pressure	70 MPa < p_1 <87.5 MPa
	3. Pressure Sensor (p_2)	Vehicle tank starting pressure monitoring	<0.5 MPa < p_2 < 35MPa
	4. Pressure Sensor (p_3)	Vehicle tank starting pressure monitoring	<0.5 MPa <p_3 < 70 MPa
Temperature	5. Temperature sensor (t_1)	Fuel delivery temperature (at the dispenser breakaway)	-40 °C < t_1 < -17.5 °C
	6. Temperature sensor (t_2)	Vehicles Compressed Hydrogen Storages System (CHSS) Temperature	t_2 < 85 °C
Gas flow	7. Flow meter (q_{H2})	Fuel flow rate (mass flow rate)	q_{H2} < 60 g/s

Analyzing hydrogen flow and its thermodynamic behavior is essential for validating simulation models and ensuring compliance with H_2 fueling standards. The laws of thermodynamics dictate that as hydrogen gas is compressed, it gains thermal energy and warms up, and conversely, it cools down upon release. The significant feature of compressed hydrogen is that it is stored as energy; therefore, instead of being an ideal gas, hydrogen must be handled as a real gas. The following is the Van der Waals [7] is considered more applied for the real gas in equation (1):

$$\left(p+a\left(\frac{n}{V}\right)^2\right)(V-nb) = nRT \qquad (1)$$

Where pressure p / Pa, molar amount n / mol, volume V / m^3, temperature T / K, and the vdW-parameters a / bar·L^2/mol^2 and b/ L/mol

These alternative equations often account for complexities that the vdW equation doesn't fully address, especially at extreme conditions or for specific gases. Examples Noble-Abel, I. A. Johnston [8] published 2005 the Able-Noble equation; this equation is used for real-gas

considerations in hydrogen technologies, e. g. D. Molkov [9, 10]. These equations are crucial in accurately predicting and analyzing hydrogen behavior in different scenarios, aiding advancements in hydrogen-related technologies and applications. The Noble-Abel equation of state has already been defined in the introduction as (2):

$$p = Z\rho R_{H2} \quad (2)$$

Where p is the gas pressure in Pa, R_{H2} is the specific hydrogen gas constant = $4124.3 \frac{J}{kg\ K}$ Z the compressibility factor, Z is calculated with equation (3)

$$Z = \frac{1}{1-b\rho} \quad (3)$$

Where b is the co-volume $7.69 \cdot 10^{-3}$ m³/kg [10].

Discussion

Different major thermodynamic events cause a fast temperature to rise during filling. Figure 2 (a & b) shows the temperature and the pressure range; Figure 3 (a & b) shows an operating window for the dispensing unit and CHSS based on the vDW.

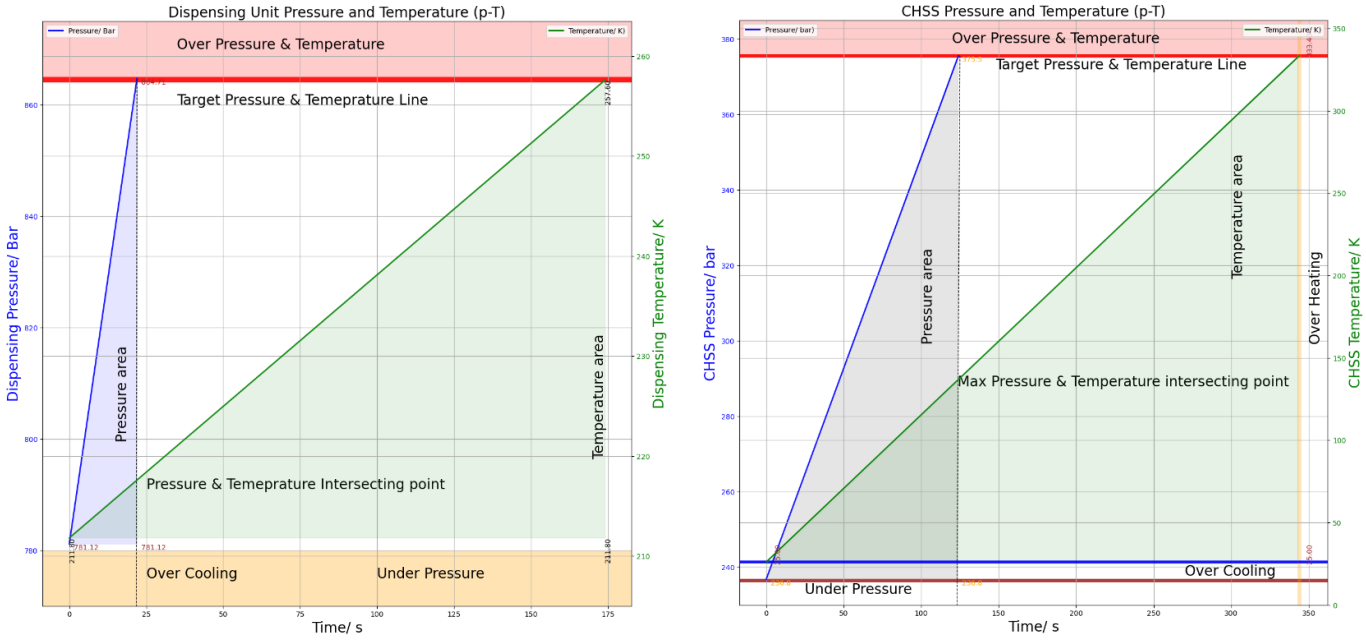

(a) (b)

Figure 2: Temperature & pressure range based on vDW equation (a) dispensing unit (b) CHSS.

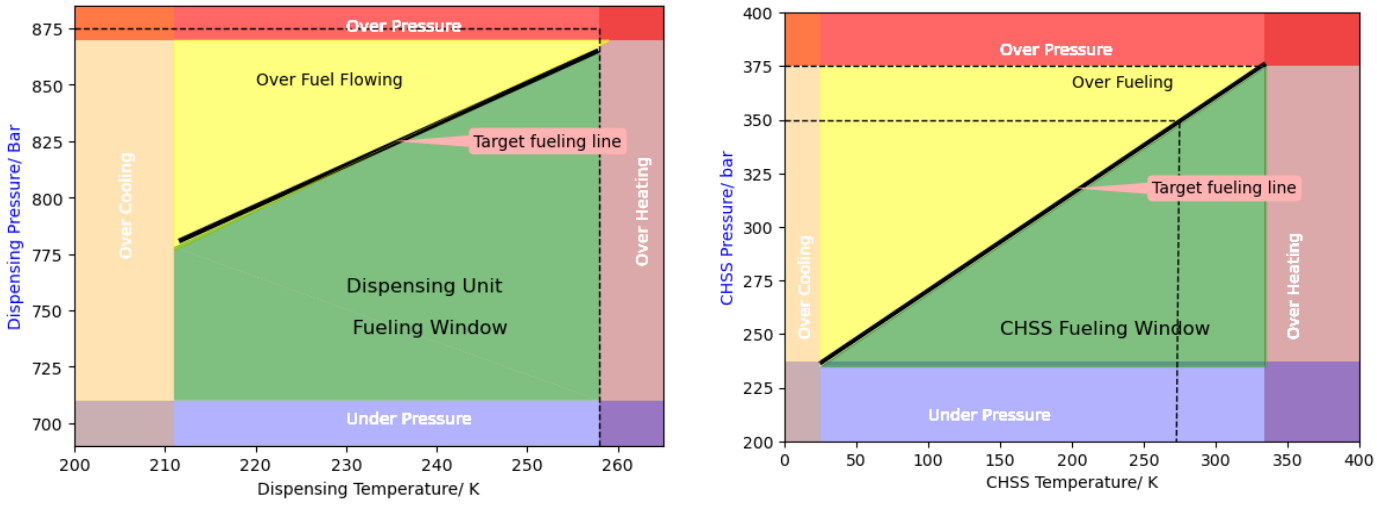

(c) (d)

Figure 3: Calculated Operating limits based on vDW (c) dispensing unit (d) CHSS.

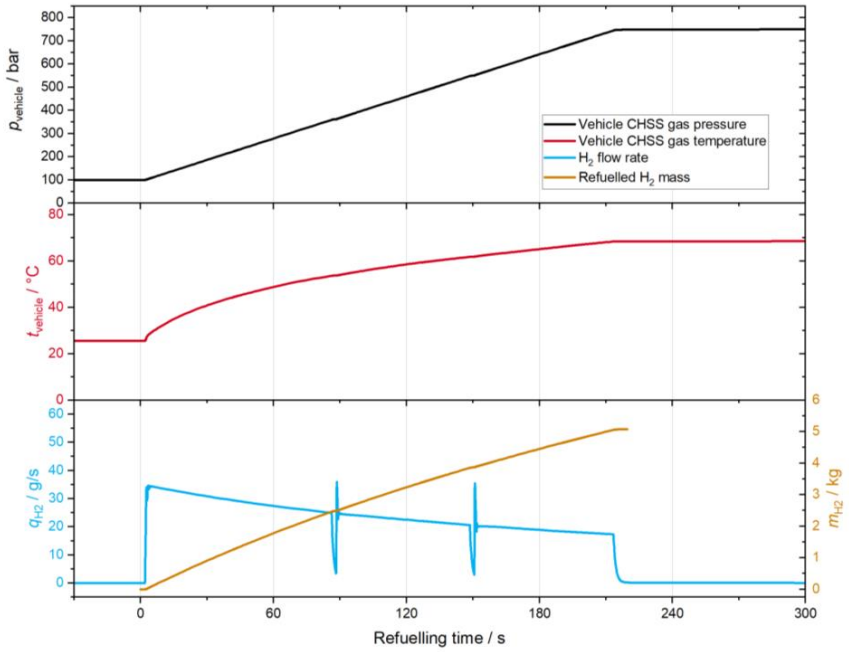

Figure 4: Results from the MATLAB simulation.

According to the Van der Waals equation, the 2a for dispensing unit temperature ranges from 233.15 K to 256.15 K; the computed maximum pressure is 884.71 bar, whereas ISO and SAE require 875 bar. Likewise, the highest estimated temperature is 257.60 K, whereas the pressure range was between 700 and 875 bars. The estimated minimal temperature was substantially less than the ISO and SAE standards (233.15 K). Besides in 2b, the predicted maximum pressure for the 350 bar light cars was 375.5 bar, with the selected temperature range of 233.15 K to 358.15 K. Nevertheless, the highest temperature calculated output was 333.43 K, although

it is advised that it be 358.15 K; the pressure range was chosen to be 5 bars to 350 bars. In Figure 5, the hydrogen fueling process in the CHSS MATLAB simulation, the initial pressure was 100 bar, which significantly increased to 745 bar post-fueling. The temperature during this process peaked at 341.75 K. The mass flow rate of hydrogen varied from 35 g/s to 18 g/s during the fueling, with a notable decrease as the pressure increased. The total amount of hydrogen fueled amounted to approximately 5.5 kg. This research demonstrates temperature and pressure analysis based on vDW for H_2 as real gas, where for vDW and MATLAB simulation, CHSS pressure was considered 350 bar and 700 bar. Although this estimation is not optimal for hydrogen fueling stations; for more appropriate results in the future, this study will use the Abole Nobel equation by considering molecular size, shape, and intermolecular forces. Above all, the graphical visualization and the vDW and MATLAB simulation yield similar results for temperature and pressure rising, which could be an optimal use case for the digital twin.

Conclusions

In summary, this analytical study initiates the development of a digital twin of hydrogen fueling station. The existing literature, refueling protocols, and mathematical and simulation models were thoroughly analyzed to accomplish these studies. Real gas equations like the Van der Waals equations were employed to analyze hydrogen behavior and investigate critical factors and parameters. The MATLAB simulation model was used to validate these essential parameters. This study has focused on current knowledge and the research gaps within hydrogen technology for further advancements in hydrogen infrastructure. Further analysis will apply the Abel-Noble alternative real gas equation to analyze hydrogen-associated parameters precisely. These parameters will be subsequently validated through MATLAB simulations based on P&ID. Overall, this project aims to assist in the creation of a robust and reliable digital twin for hydrogen applications, promoting the widespread adoption of hydrogen fuel as a sustainable alternative energy.

References

[1] "NAMUR -Interessengemeinschaft Automatisierungstechnik der Prozessindustrie Technologie-Roadmap „Prozess-Sensoren 2027+“," *NAMUR - Roadmap*, 2021-11, doi: https://www.namur.net/fileadmin/media_www/Dokumente/Roadmap_Prozesssensoren_2027.pdf.

[2] T. Tauchnitz, *NAMUR Open Architecture (NOA) - Das Konzept zur Öffnung der Prozessautomatisierung*. Essen: Vulkan-Verlag GmbH, 2021.

[3] M. Attaran and B. G. Celik, "Digital Twin: Benefits, use cases, challenges, and opportunities," *Decision Analytics Journal*, p. 100165, 2023.

[4] A. Mohsen and C. Gokhan, "Digital Twin: Benefits use cases challenges and opportunities [J]," *Decision Analytics Journal*, vol. 6, no. 1, pp. 111-123, 2023.

[5] "SAE-J2601-The-Worldwide-Standard-for-Hydrogen-Fueling-Stations.pdf." [Online]. Available: https://www.sae-j2601.com/wp-content/uploads/2021/01/SAE-J2601-The-Worldwide-Standard-for-Hydrogen-Fueling-Stations.pdf.

[6] "ISO 19880-1:2020(en), Gaseous hydrogen — Fuelling stations — Part 1: General requirements." [Online]. Available: https://www.iso.org/obp/ui/#iso:std:iso:19880:-1:ed-1:v1:en.

[7] P. Atkins and J. de Paula, *Physical Chemistry*. Oxford University Press, 2006.

[8] I. A. Johnston, "The Noble-Abel equation of state: thermodynamic derivations for ballistics modelling," 2005, doi: https://apps.dtic.mil/sti/pdfs/ADA454209.pdf.

[9] V. Molkov, M. Dadashzadeh, and D. Makarov, "Physical model of onboard hydrogen storage tank thermal behaviour during fuelling," *International Journal of Hydrogen Energy*, vol. 44, no. 8, pp. 4374-4384, 2019, doi: 10.1016/j.ijhydene.2018.12.115.

[10] V. Molkov, *Fundamentals of Hydrogen Safety Engineering I*. bookboon.com, 2012.

Dynamic modeling of alkaline electrolyzers for diagnostic purposes

V. Pignataro*[1], L. Ferrari[1],

[1]Department of Energy, Systems, Territory and Construction Engineering, University of Pisa, Pisa, Italy

Introduction

Despite global warming becoming a central topic for the scientific community, the persistent massive use of fossil fuels for power generation leaves room for uncertainty regarding the future energy policies of nations. However, the interest in using hydrogen as an energy carrier is increasing, paving the way for future scenarios in which it could play a significant role in daily life. Nevertheless, decarbonization objectives leave no room for fossil fuels, thus making the production of hydrogen from renewable energy sources (green hydrogen) the only conceivable solution. In particular, alkaline electrolysis is the prevailing technology for green hydrogen production due to its maturity.
Several models for simulating the operation of alkaline electrolyzers are available in the literature [1]–[4]. However, these models do not take into account that the performance of real electrolyzers can be compromised by malfunctions and failures. Until now, the industrial use of alkaline electrolyzers has been limited to stationary applications (e.g., chemical industry and jewelry production). However, today, the energy and industrial landscape are undergoing a radical transformation due to a massive integration of renewable energy sources. This results in a significant variation in the operating conditions of alkaline electrolyzers, making them more susceptible to fluctuations, transient operation, shutdowns, and, consequently, degradation and reduced lifespan. For these reasons, companies like McPhy Energy [5], which co-funds this doctoral project, shifted their focus towards the dynamic modeling of electrolyzers that will enable more reliable monitoring of electrolyzer performance to optimize their efficiency and lifespan.
The main objectives of this study are:

- Development of a transient model for an electrolyzer of interest.
- The development of a fault detection and identification algorithm based on the developed model.
- The application of the diagnostic tool to real case applications.

Methodology

This research project started with the Matlab modeling of a 3MW alkaline electrolyzer, using the study by Sakas et al. [6] as a reference. However, in this model, an ON-OFF temperature control to prevent overheating of the stack, and an ON-OFF liquid level control to prevent excessive filling or emptying of gas-liquid separators were integrated. In Fig.1 there is a schematic representation of the model [7].
This model, similar to those found in the literature, simulates the ideal behavior of an alkaline electrolyzer. However, real electrolyzers, like any complex technological system, are liable to failures and malfunctions that necessitate corrective actions by operators. For

* Corresponding author: valeria.pignataro@phd.unipi.it

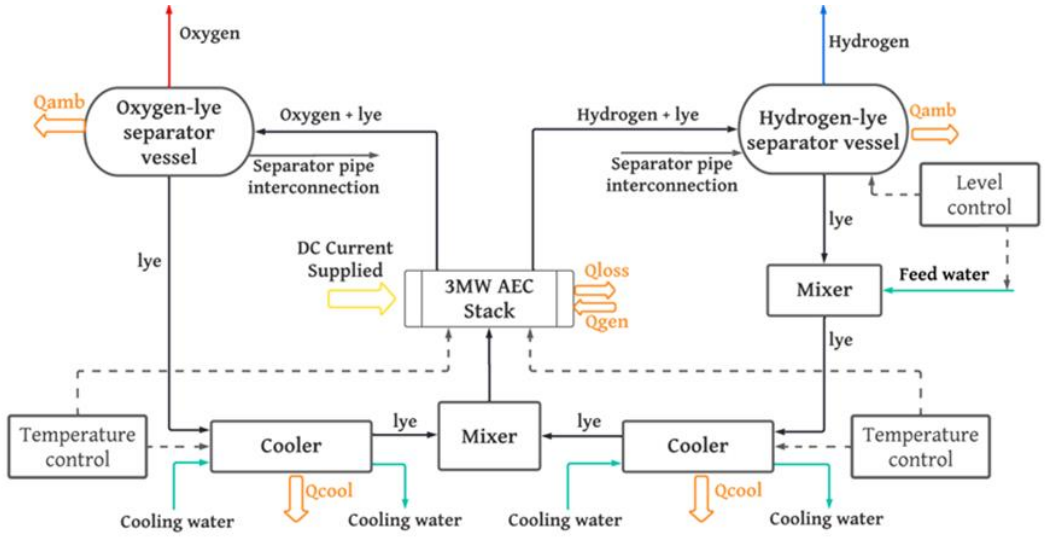

Figure 1: Alkaline water electrolyzer plant process diagram [7].

this reason, the above-mentioned model will be scaled and adapted by considering a McPhy Piel H-15 Hydrogen Generator. The main characteristics of this electrolyzer are provided in Table 1.

The stack modeling will be implemented using the MATLAB/Simulink software [8], and the curve fitting of the parameters of the electrochemical model will be done according to [1]. Subsequently, the dynamic modeling of the electrolyzer will be carried out in MATLAB/Simscape using parameters from a real device. Finally, the model will be validated against measured data.

Pressure [bar]	Hydrogen production nominal flowrate [Nm^3/h]	Oxygen production nominal flowrate [Nm^3/h]	Nominal power [kW]
8	10	5	60

Table 1: McPhy Piel H-15 Hydrogen Generator operating parameters.

In Fig.2 and Fig.3 a draft of the stack model and electrolyzer model, respectively, is done.

At the end of the modeling phase, the validated model will serve as a basis for the application of machine learning principles to detect and identify potential faults of a real machine. To this purpose, data collected from the electrolyzer sensors will be used to train machine learning models, such as artificial neural networks and regression algorithms, to identify patterns associated with faults.

Once “instructed”, these models can be used for real-time monitoring of the electrolyzer performance.

Expected results

The aim of this study is to obtain a dynamic model that accurately simulates the behavior of an alkaline electrolyzer. Initially, the modeling will be conducted using a McPhy Piel H-15 machine as a reference, and subsequently, the model will be adaptable to different-sized machines.

Furthermore, the application of machine learning models for the analysis and interpretation of data collected from alkaline electrolyzers will offer a promising solution to enhance

prediction accuracy and strengthen the performance monitoring of alkaline electrolyzers, enabling timely corrective maintenance, and, thus, ensuring extended durability and reliability of the electrolyzer.

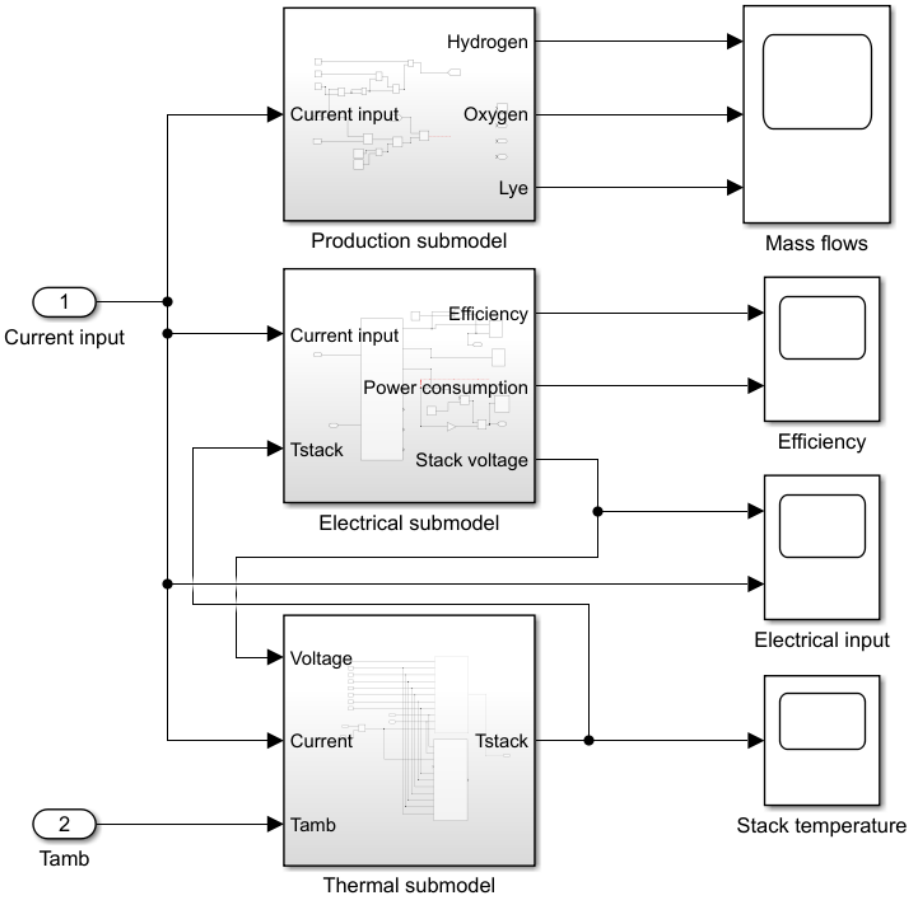

Figure 2: MATLAB/Simulink stack model.

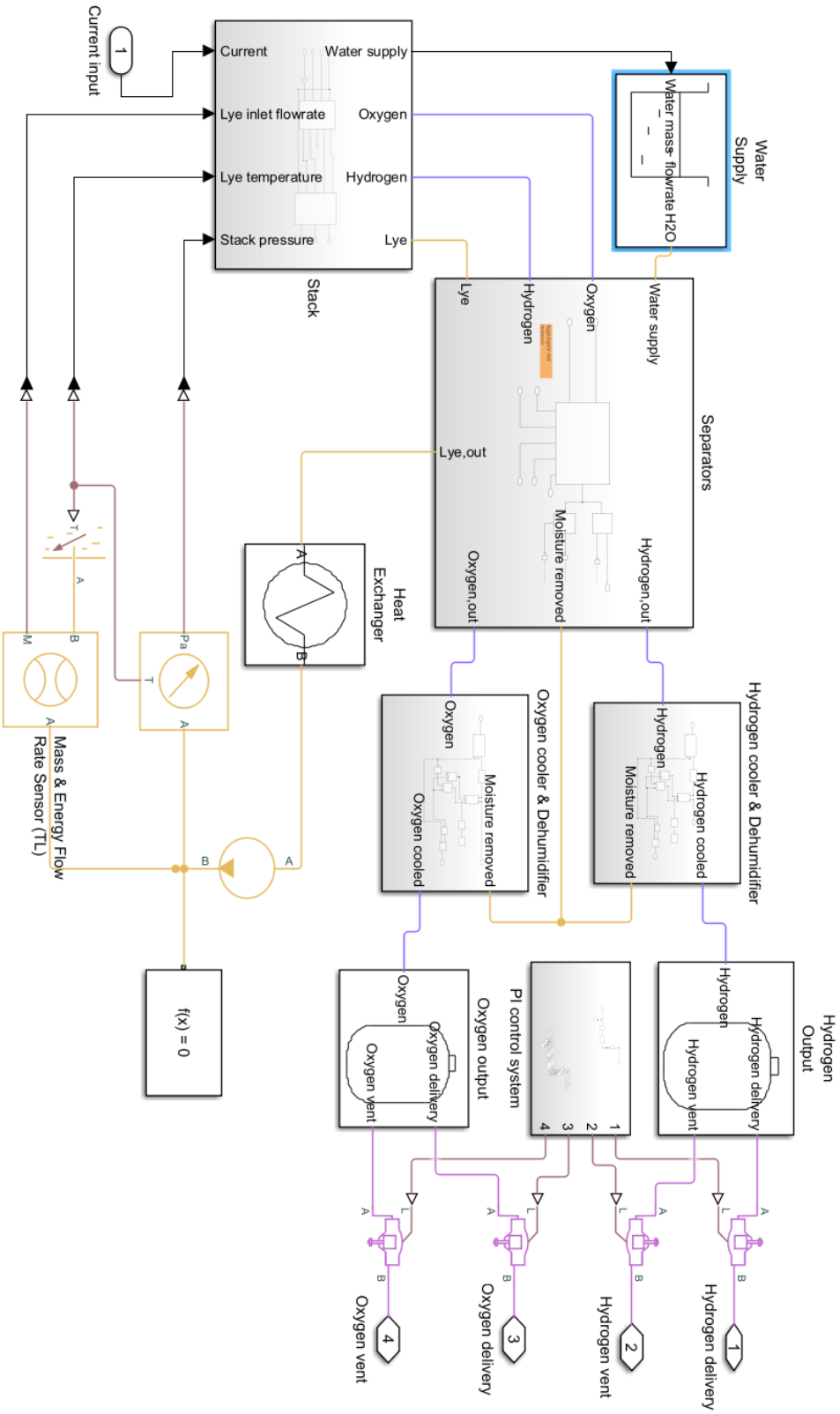

Figure 3: MATLAB/Simscape electrolyzer model.

References

[1] Ulleberg I. Modeling of advanced alkaline electrolyzers: a system simulation approach. Int J Hydrogen Energy, vol. 28, 2003, p. 21-3. https://doi.org/10.1016/S0360-3199(02)00033-2.

[2] E. Amores, J. Rodríguez, and C. Carreras, “Influence of operation parameters in the modeling of alkaline water electrolyzers for hydrogen production,” in *International Journal of Hydrogen Energy*, Elsevier Ltd, Aug. 2014, pp. 13063–13078. doi: 10.1016/j.ijhydene.2014.07.001.

[3] M. Sánchez, E. Amores, D. Abad, C. Clemente-Jul, and L. Rodríguez, “Development and Experimental Validation of a Model to Simulate an Alkaline Electrolysis System for Production of Hydrogen Powered by Renewable Energy Sources,” in *Smart Innovation, Systems and Technologies*, Springer Science and Business Media Deutschland GmbH, 2019, pp. 358–368. doi: 10.1007/978-3-030-22964-1_40.

[4] M. Sánchez, E. Amores, L. Rodríguez, and C. Clemente-Jul, “Semi-empirical model and experimental validation for the performance evaluation of a 15 kW alkaline water electrolyzer,” *Int J Hydrogen Energy*, vol. 43, no. 45, pp. 20332–20345, Nov. 2018, doi: 10.1016/j.ijhydene.2018.09.029.

[5] “McPhy Energy role in French Power-to-Gas GRHYD programme,” *Fuel Cells Bulletin*, vol. 2014, no. 2, pp. 9–10, Feb. 2014, doi: 10.1016/S1464-2859(14)70054-9.

[6] G. Sakas, A. Ibáñez-Rioja, V. Ruuskanen, A. Kosonen, J. Ahola, and O. Bergmann, “Dynamic energy and mass balance model for an industrial alkaline water electrolyzer plant process,” *Int J Hydrogen Energy*, vol. 47, no. 7, pp. 4328–4345, Jan. 2022, doi: 10.1016/j.ijhydene.2021.11.126.

[7] V. Pignataro, A. Liponi, E. Bargiacchi, and L. Ferrari, “Dynamic modeling of a power-to-gas system for green methane production from wind energy,” in *36th international conference on Efficiency, Cost, Optimization, Simulation and environmental impact of energy systems, ECOS23*, 2023.

[8] M. Maruf-ul-Karim and M. T. Iqbal, "Dynamic modeling and simulation of alkaline type electrolyzers," *2009 Canadian Conference on Electrical and Computer Engineering*, St. John's, NL, Canada, 2009, pp. 711-715, doi: 10.1109/CCECE.2009.5090222.

EHC - Electrochemical Hydrogen Compression or Efficient Humidification Counts

M. Richter*[1], C. Keuschnigg[1], B. Grabner[1], F. Winkler[1], A. Trattner[1,2]

[1]HyCentA Research GmbH, Graz, Austria
[2]Graz University of Technology, Institute of Thermodynamics and Sustainable Propulsion Systems, Graz, Austria

October 11, 2023

Introduction

Electrochemical hydrogen compressors (EHC) have the potential to overcome current drawbacks of established mechanical compression technologies regarding noise, vibrations, gas quality and energy demand for low input pressures [4, 10]. Nevertheless, significant hydrogen back-permeation at elevated pressure gradients and uneven humidification of the membrane remain major challenges reducing the overall efficiency of the EHC [3, 9] This research aims to define appropriate operating conditions for electrochemical compressors and separators by means of 0D-electrochemical and computational fluid dynamics (CFD) simulations. In addition, the simulation results will be validated via extensive testing on a developed single-cell and short-stack testbench. Various materials (membranes, gas diffusion layers, catalysts) and cell designs shall be investigated to tackle current limitations of the technology [1, 6]. The main advantages and drawbacks of the technology are summarized in Table 1.

Table 1: Advantages and drawbacks of EHC-technology from current perspective [1, 2, 5, 6, 7, 10]

Advantages	Drawbacks
Noise and vibration-free operation, enables hydrogen refueling stations in populous urban areas	TRL for industrial scale systems is generally low (5−7)
Simple structure and generally low maintenance efforts compared to mechanical compressors	Significant back-permeation of hydrogen at high differential pressures
No lubricants required and no risk of corresponding impurities entering the product gas	No educt or product water and hence critical water management to ensure a durable & efficient operation
High efficiencies and less required stages for low input pressures (< 3 kWh/kg for compression from 1 to 100 bar)	Low efficiencies (> 6 kWh/kg) in unsuitable operating ranges (low humidity, high current densities)
Modular and flexible technology, can be stepwise extended starting with a small system until reaching the final design throughput	Due to low current densities for high efficiencies, big footprints and high number of stacks required for high throughput
Possible purification of gas mixtures or hydrogen transported in repurposed natural gas grid	Sensitive to specific critical impurities in gas mixtures (CO, CO_2, H_2S, HCl)
Manufacturing and research synergies with electrolysers and fuel cells	Current costs for high flow rates due to high membrane costs generally high

*Corresponding author: richter@hycenta.at

Methodology

This work covers the entire development process of an electrochemical hydrogen compressor. A 0D-thermodynamical simulation model was built up to perform a general benchmarking of the technology and investigate cell overvoltage shares. By carrying out 3D-CFD simulations of the anode of the cell, special focus is set on the humidification and water management of the cell. The boundary conditions (BC) for the 3D-CFD-model implemented in ANSYS Fluent are illustrated in Figure 1.

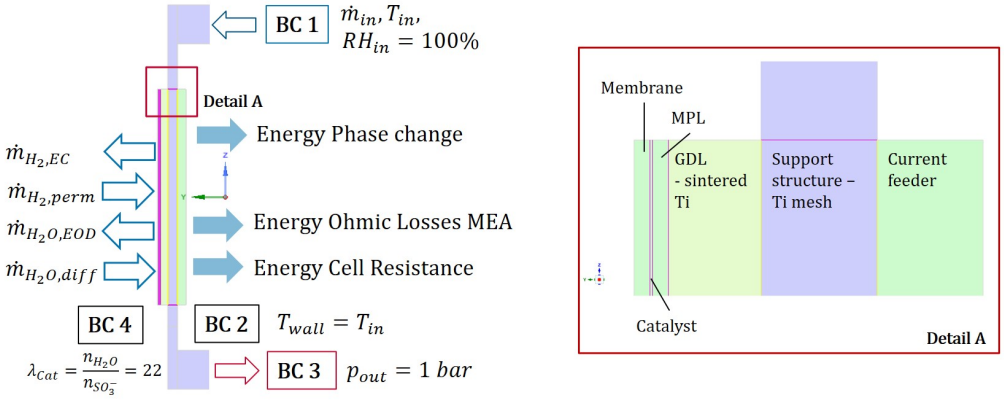

Figure 1: Boundary conditions for 3D-CFD-model of EHC-anode

The cell layers, material data and geometries are identical to the single-cell prototype with a circular active area of 20 cm^2, shown in Figure 2a. Hyperstochiometric saturated hydrogen is supplied at the anode inlet and distributed over the active area via expanded Ti meshes, a sintered Ti gas diffusion layer (GDL) and a carbon based microporous layer (MPL). The membrane electrode assembly (MEA) comprises Nafion®117 with a symmetric coating of 0.55 mg Pt/cm^2. The relevant mass flows through the membrane including protonic transport $\dot{m}_{H_2,EC}$, H_2 back-permeation $\dot{m}_{H_2,perm}$, electroosmotic drag $\dot{m}_{H_2O,EOD}$ and H_2O back-diffusion $\dot{m}_{H_2O,diff}$ are implemented via sources and sinks in the catalyst layer of the model. Due to the high pressure and oversaturated conditions on the cathode side, liquid water is present there and a water content of the MEA λ_{cat} of 22 is assumed acc. to [11]. If the MEA is in contact with saturated gas, the maximum value corresponds to 14. The influences of operating temperature and stochiometric ratio on cell voltage U_{cell}, water content of the MEA, faraday efficiency η_F and isothermic efficiency η_T are investigated by a variation of T_{in} between 60 and 90 $°C$ and the stochiometric ratio λ between 1.5 and 20. Faraday and isothermic efficiency for the EHC are defined acc. to Equation 1 and Equation 2, respectively.

$$\eta_F = \frac{\dot{n}_{H_2,net}}{\dot{n}_{H_2,EC}} = \frac{\dot{n}_{H_2,EC} - \dot{n}_{H_2,perm}}{\dot{n}_{H_2,EC}} \tag{1}$$

$$\eta_T = \frac{w_{ideal}}{w_{actual}} = \frac{\dot{n}_{H_2,net} RT \ln \frac{p_{cat}}{p_{an}}}{U_{cell}(2F\dot{n}_{H_2,EC})} \tag{2}$$

In addition to the theoretical assessment, the single-cell prototype will be tested on the developed testbench shown in Figure 2b. On the anode supply side, hydrogen is humidified in a heated bubbler before entering the cell. Humidity, pressure and temperature of the anode inlet and outlet are measured. The anode outlet gas is further passing a condensate filter and silica gel before entering the vent line. On the high-pressure side, the desired output pressure is set via a back-pressure regulator. The compressed hydrogen flow is measured downstream at atmospheric pressure. The testbench further features a connection to the existing gas analysis laboratory at the facilities of HyCentA. With the available mass-spectrometry (MS) and the Fourier-transform infrared spectroscopy (FTIR), a comprehensive impurity analysis with detection limits of single-digit ppb-values is applicable. This is of major importance for the scheduled test runs with mixed gases (including N_2, CH_4 and natural gas).

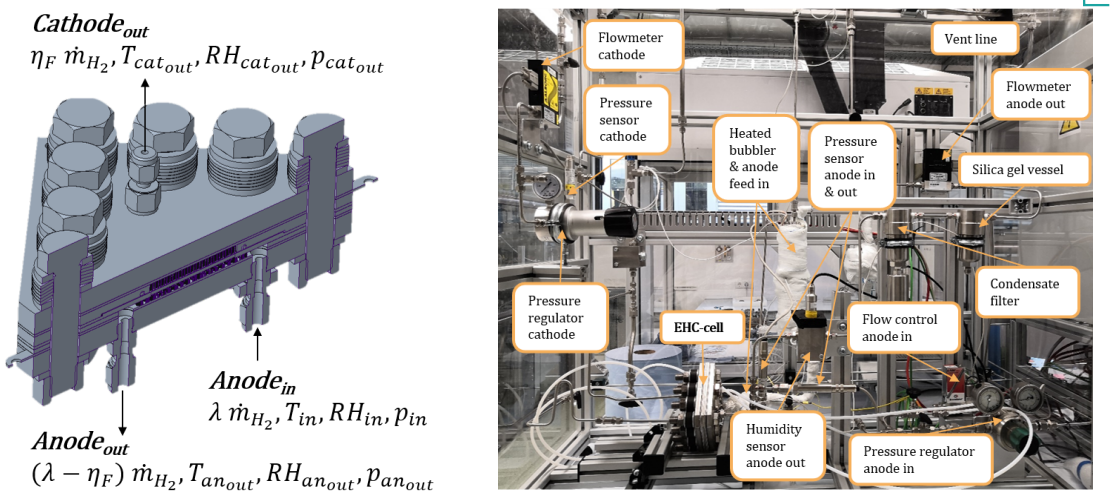

(a) (b)

Figure 2: EHC single-cell prototype (a) and testbed for single-cell and short stack testing (b)

Discussion

The obtained results of the 3D-CFD simulations are discussed in the following. In Figure 3a, the required stochiometric ratio for a complete humidification of the membrane is depicted for various temperatures, considering an electroosmotic drag coefficient of 0.9 [9]. At atmospheric pressure, λ of 0.7 to 13 are required to absorb sufficient water in the humidified gas stream. At common output pressures of electrolysers >30 bar, λ of 80−480 would be required if the humidification is exclusively realised via the input gas stream. At higher temperatures, a significantly higher amount of water can be transported into the cell leading to a higher water content of the membrane, compare Figure 3b. Nevertheless, at T=90°C and λ=1.5, some parts of the anode side suffer from hydrogen depletion resulting in a lower water absorption capacity. This leads to an oversaturation and condensation of the water vapor at the edges of the active area.

Insufficient humidification at lower λ and T results in high cell voltages, shown in Figure 4. Especially below 70°C, the voltage increases disproportionately with higher current densities >0.3 A/cm^2 and lower λ. In contrast, the voltage increase is relatively independent from λ for T=80−90°C. The resulting voltages at higher current densities are generally very high in relation to the theoretically required Nernst voltages. Dehumidification, poor electrical conductivity or too thick membranes are the dominant factors

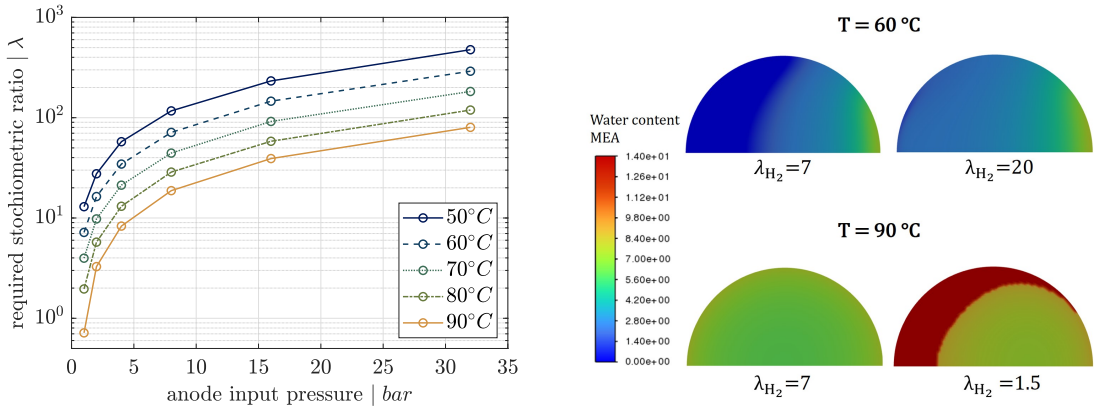

(a) (b)

Figure 3: Required stochiometric ratios λ for electroosmotic drag at $i = 0.66$ A/cm^2 (a) and anodic water content of MEA for compression of 1 to 100 bar at $T = 60°C$ and $T = 90°C$ and different λ.

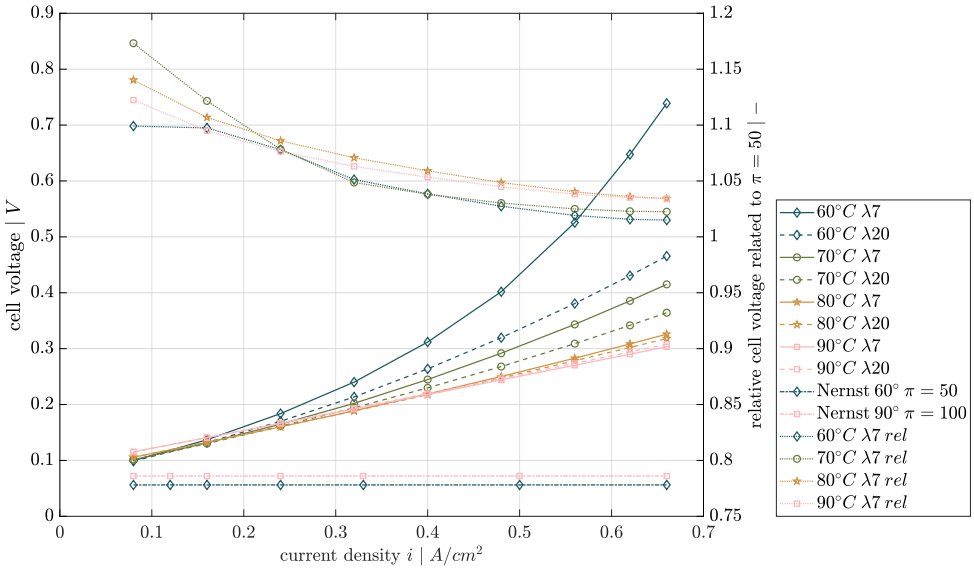

Figure 4: Simulation results for cell voltages for a compression ratio π=100 over current density i as function of gas temperature T and stochiometric ratio λ. The relative voltages compared to a compression ratio π=50 are depicted on the secondary y-axis.

for these overvoltages. However, the results are comparable to the experimental results in literature [8].

In Figure 5, the corresponding isothermic efficiencies are plotted for a compression of 1 to 100 bar (π=100) and related to a compression to 50 bar (π=50). The dashed vertical line at 0.16 A/cm^2 separates the areas where the back-diffusion coefficient D or the membrane resistance R are the dominant factors for the EHC-performance. In the very low range, the back-diffusion, illustrated in Figure 6a, is dominating for high temperatures and thus the efficiency for a compression to 100 bar drops to 50−85% of a compression to 50 bar. Nevertheless, over 0.4 A/cm^2 the performance of a compression to 100 bar is superior, regardless of temperature or stochiometric ratio. The occurring membrane resistance could be reduced by thinner membranes, as long as they withstand the targeted pressure difference, and an improved humidification.

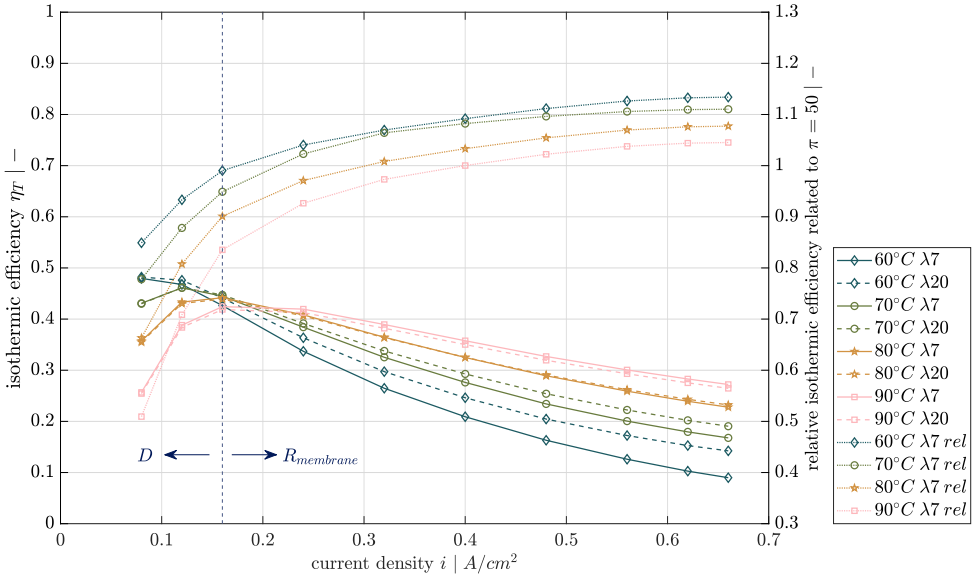

Figure 5: Simulated isothermic efficiencies for a compression ratio π=100 and relative values compared to π=50 as function of gas temperature T and stochiometric ratio λ.

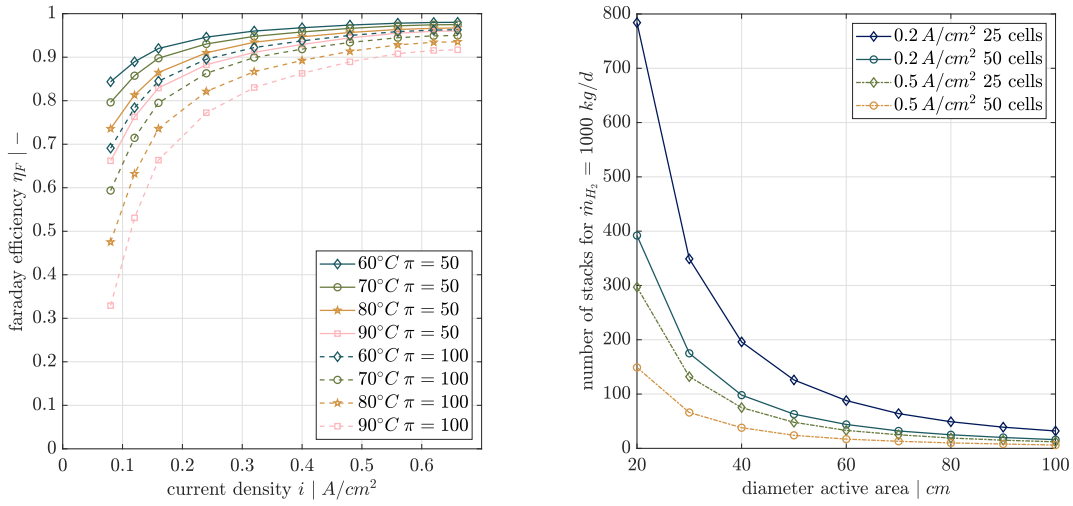

(a) (b)

Figure 6: Calculated faraday efficiencies as function of gas temperature T and compression ratio π (a). The resulting required number of EHC stacks for compression of $\dot{m}_{H_2}$= 1000 kg/d depending on active area, current density i and number of cells per stack are shown in (b).

Compared to electrolysis cells and fuel cells, the achievable efficiencies drop even more with increasing current densities due to the one order of magnitude lower Nernst voltage of the EHC. Consequently, EHC cells should be operated at low current densities or high efforts have to be made to significantly reduce inner cell resistances for higher current density operations.

Sdanghi et al. found out that electrochemical compressors are already very cost competitive at low flow rates and low-pressure applications up to 100 bar with investment costs of <1700 $/(kg/d) compared to 2300 $/(kg/d) for mechanical compressors [10]. However, for higher flow rates the current density limitations for an efficient operation lead to a high number of stacks and thus high investment costs. In Figure 6b, the required number of EHC-stacks for compressing 1000 kg H_2/d is shown as function of the active area, the number of cells per stack and the current density i. With an active area of 0.28 m^2 (d = 60 cm), 25 cells per stack and 0.2 A/cm^2 88 stacks are required. The resulting energy demand for a compression from 1 to 100 bar amounts to 3 kWh/kg. Increasing the current density of these stacks to 0.5 A/cm^2 leads to a reduction to 33 stacks, but an energy demand increase to roughly 7.5 kWh/kg.

Conclusions

A broad roll-out of the electrochemical hydrogen compression technology requires addressing numerous research questions. Based on the conducted technology evaluation via 3D-CFD-simulations, literature research and initial proof-of-concept tests with the single-cell prototype, the following research priorities are derived. These tasks will be tackled within the progression of the research projects.

- Investigation of suitable anode flow-field designs in order to enable a homogeneous humidification of the membrane (defined flow-fields vs. expanded metal mesh).
- Applicable humidification concepts for different input pressures including exclusive humidification via humidified input gas stream and direct injection of liquid water.
- Development of advanced membranes for EHC-applications to enhance the water retention and lower the diffusivity for reduced hydrogen back-permeation. Further, thinner but durable membranes are beneficial to reduce the ohmic resistance of the cell and improve overall efficiencies.
- Coating of cell components (GDL, MPL, bipolar plates) with highly conductive materials (e.g. TiN) and reduction of individual component layers to minimize contact areas and resistances.
- Reduce Pt-content and hence costs and environmental footprint, without significantly affecting the overall performance.

- Suitable selection of catalysts for purification purposes with similar performance to Pt but lower vulnerability to sulphuric and chloride compounds as well as CO.
- Identification of beneficial operating modes to enable a long-term durability of the MEAs and achieve high compression and purification efficiencies.
- Better understanding of the transport mechanisms within the cell by means of single-cell tests with electrochemical impedance spectroscopy (EIS)-measurements and segmented cell testing devices. The segmented cell measurement enables detections of local gas starvation phenomena and thus high occurring voltages. These high voltages may lead to carbon corrosion effects.
- Development of multi-stage design, durable sealing solutions and operation concept for high-pressure operation of several hundred bars.
- Techno-economic and environmental assessment of most promising EHC application scenarios.

Acknowledgements

The authors would like to acknowledge the Austrian Research Promotion Agency (FFG), the Climate and Energy Fund, the Federal Ministry of Labour and Economy and the Federal Ministry for Climate Action, Environment, Energy, Mobility, Innovation and Technology of the Republic of Austria for processing and financing this work in the framework of the COMET project HyTechonomy and the lighthouse project move2zero.

References

[1] Y. Aykut and A. Bayrakçeken Yurtcan. Catalyst development for viability of electrochemical hydrogen purifier and compressor (ehpc) technology. *International Journal of Hydrogen Energy*, 47(45):19619–19632, 2022.

[2] Y. Aykut and A. B. Yurtcan. The role of the ehc system in the transition to a sustainable energy future: A review. *International Journal of Hydrogen Energy*, 48(60):23089–23109, 2023.

[3] A. Chouhan, B. Bahar, and A. K. Prasad. Effect of back-diffusion on the performance of an electrochemical hydrogen compressor. *International Journal of Hydrogen Energy*, 45(19):10991–10999, 2020.

[4] G. N. B. Durmus, C. O. Colpan, and Y. Devrim. A review on the development of the electrochemical hydrogen compressors. *Journal of Power Sources*, 494:229743, 2021.

[5] H. Hydrogen. Hyet group — hyet hydrogen, 15.02.2023.

[6] D. Marciuš, A. Kovač, and M. Firak. Electrochemical hydrogen compressor: Recent progress and challenges. *International Journal of Hydrogen Energy*, 47(57):24179–24193, 2022.

[7] S. Mrusek, M. Blasius, F. Morgenroth, S. Thiele, and P. Wasserscheid. Hydrogen extraction from methane-hydrogen mixtures from the natural gas grid by means of electrochemical hydrogen separation and compression. *International Journal of Hydrogen Energy*, 2023.

[8] J. L. Pineda-Delgado, A. U. Chávez-Ramirez, C. K. Gutierrez B, S. Rivas, C.-R. Marisela, R. de Jesús Hernández-Cortes, J. A. Menchaca-Rivera, and J. F. Pérez-Robles. Effect of relative humidity and temperature on the performance of an electrochemical hydrogen compressor. *Applied Energy*, 311:118617, 2022.

[9] G. Sdanghi, J. Dillet, S. Didierjean, V. Fierro, and G. Maranzana. Feasibility of hydrogen compression in an electrochemical system: Focus on water transport mechanisms. *Fuel Cells*, 20(3):370–380, 2020.

[10] G. Sdanghi, G. Maranzana, A. Celzard, and V. Fierro. Review of the current technologies and performances of hydrogen compression for stationary and automotive applications. *Renewable and Sustainable Energy Reviews*, 102:150–170, 2019.

[11] T. E. Springer, T. A. Zawodzinski, and S. Gottesfeld. Polymer electrolyte fuel cell model. *Journal of The Electrochemical Society*, 138(8):2334–2342, 1991.

Economic assessment of current and emerging electrolysis technologies

F. Romano*[1], M. Minutillo[2,4], V. Cigolotti [3,4], E. Jannelli [1,4]

[1]Department of Engineering, University of Naples Parthenope, Naples, Italy
[2]Department of Industrial Engineering, University of Salerno, Fisciano, Italy
[3]ENEA - Italian National Agency for New Technologies, Energy and Sustainable Economic Development, Naples, Italy
[4]ATENA Future Technology, Naples, Italy

Introduction

In 2019, the European Commission presented a road map to make Europe the first climate-neutral continent by 2050. To comply with this constraint, the transition toward low/zero-carbon fuels is necessary[1]. Great attention is given to the hydrogen that plays a key role in sectors that are hard to decarbonize such as heavy industry, shipping, aviation and heavy transport sectors. Hydrogen is a very versatile gas because it can store large volumes of energy for a long time and work with the electricity grid to cope with the intermittence of renewable energy sources such as wind and solar. However, this energy carrier must be produced. The H_2 production methods, based on fossil fuels, are economically advantageous thanks to scale economies and reasonable fossil fuel prices, but they cause tons of CO_2 emissions. On the other hand, water electrolysis technology (if powered by renewable electricity) is considered the alternative solution to produce green hydrogen. Depending on the electrolyte, the operating temperatures and pressures, different types of electrolyzers are distinguished: the Anion Exchange Membrane Water Electrolyzers (AEMWE), the Alkaline Water Electrolyzers (AWE), the Proton Exchange Membrane Water Electrolyzers (PEMWE), the Solid Oxide Electrolyzers Cell (SOEC) and the Proton Conducting Ceramic Electrolyzers (PCCEL). AEMWE is still in the early research and development stage. It operates in an alkaline medium by allowing the use of low-cost transition metal catalysts. AWE is widely employed in industry due to its commercial maturity, despite it works at low current density and low operating temperature. PEMWE operates at low temperatures and works at a high power density. It is used for small-scale applications. The SOEC technology is the least mature. Currently, this electrolyzer is only demonstrated on a laboratory scale, although some current demonstration projects have already reached 1 MW. SOEC operates at higher temperatures that allow to improve the efficiency of the cell but cause premature degradation of the stack. Finally, PCCEL is a novel technology that works at intermediate operating temperatures with good efficiency [2]–[4]. In order to support the exploitation of hydrogen production from the electrolysis process, it is important to analyze the economic feasibility of these technologies. In this paper, an economic assessment of the AWE, the PEMWE and the SOEC technologies is carried out by estimating the levelized cost of hydrogen (LCOH) in different time scenarios (2023-2050).

Methodology

The evaluation of LCOH for the AWE, the PEMWE and the SOEC electrolyzers is carried out by applying Eq. 1, as suggested in ref. [5].

* Corresponding author: fabiana.romano001@studenti.uniparthenope.it

$$LCOH = \frac{CRF \cdot (C_{FC} + \sum_{n=0}^{N-1} C_{O\&M,n,annualized} + \sum_{n=t}^{N-1} C_{rep,t,annualized} - \sum_{n=0}^{N-1} R_{O2,n,annualized})}{m_{H_2,annual}} \quad (1)$$

where CRF is the capital recovery factor expressed as a function of the real interest rate (I_r) and the lifetime (N) of the electrolysis system. It is calculated as in the Eq. 2 [5].

$$CRF = \frac{I_r \cdot (1 + I_r)^N}{(1 + I_r)^N - 1} \quad (2)$$

In this study, CRF, based on N and I_r equal to 20 years and 1%, respectively, is 0.06. In Eq. 1 the terms C_{FC}, $C_{O\&M,n,annualized}$ and $C_{rep,t,annualized}$ are the total fixed capital cost, the annual present values of the operating and maintenance (O&M) costs and the annual present values of the replacement costs, respectively. It is important to note that the annualization of the replacement costs is carried out by assuming *t* as the years in which the replacement of components is suggested. Moreover, $R_{O2,\mathrm{n,annualized}}$ is the revenue obtained from selling oxygen and the $m_{H_2,annual}$ is the annual hydrogen production. The total fixed capital cost is the total cost of the system ready for the start-up. This means that, to estimate this cost, it is needed to consider the capital expenditures $(CAPEX)$ of electrolysis system and the other costs related to all technical and engineering equipment such as equipment erection, piping, instrumentation and control, electrical, civil, structures and buildings, lagging, paint, materials, offsites, contingencies, design and engineering. Thus, C_{FC} is given as a function of CAPEX and the other costs expressed as factors of the equipment costs. Taking into account the estimation method of Sinnott and Towler [6], it is calculated as in Eq. 3.

$$C_{FC} = CAPEX \cdot \sum cost\ factors \quad (3)$$

As suggested in ref. [6], the total cost factors for this kind of technology can be assumed equal to 6.8. To estimate $C_{O\&M,n,annualized}$, $C_{rep,t,annualized}$ and $R_{O2,\mathrm{n,annualized}}$, the following Eq. 4-6 are applied [5]:

$$C_{O\&M,n,annualized} = \frac{C_{O\&M}}{(1 + I_r)^n} \quad (4)$$

$$C_{rep,t,annualized} = \frac{C_{rep}}{(1 + I_r)^t} \quad (5)$$

$$R_{O2,n,annualized} = \frac{p_{O2} \cdot m_{O2,n}}{(1 + I_r)^n} \quad (6)$$

$C_{O\&M}$, C_{rep}, p_{O2} and $m_{O2,n}$ are the annual O&M costs, the replacement costs, the specific price of the sold oxygen and the annual amount of the produced oxygen, respectively. In Table 1 are reported the parameters used to calculate these costs and revenues.

Table 1. Input data applied for the selected electrolyzers in the 2023-2050 scenarios.

Parameters	**Value**		**Ref.**
Time Scenario	**2023**	**2050**	
O&M costs			
Electrolyzer	3% of C_{FC}/y	3% of C_{FC}/y	[7]
BoP	3% of C_{FC}/y	3% of C_{FC}/y	[7]
Deionized Water	0.01 €/kg	0.01 €/kg	[8]

Electricity*	100 €/MWh (EU)	70 €/MWh (EU)	[9], [10]
Salary**	33,649 € full-time	33,649 € full-time	[8]
Replacement costs			
Electrolyzer replacement	35% of $CAPEX$/y	35% of $CAPEX$/y	[7]
Revenue			
Oxygen sold	0.13 €/m^3	0.13 €/m^3	

*The electrolyzers are connected to the grid.
**The labor cost is calculated based on the assumption that one full-time worker is employed.

In order to calculate LCOH, the techno-economic data of the selected electrolysis system are taken from IRENA [11]. These data are summarized in Table 2.

Table 2. The techno-economic data of electrolyzers in the 2020-2050 scenarios [11].

Parameters (average values)	**AWE**		**PEMWE**		**SOEC**	
Time Scenario	**2020**	**2050**	**2020**	**2050**	**2020**	**2050**
Stack unit size (MW)	1	10	1	10	0.005*	0.2
Stack Electrical consumption (kWh/kg H_2)	56.5	42	56.5	42	42.5	35
System Electrical consumption (kWh/kg H_2)	64.0	45	66.5	45	45.0	40
H_2 production (kg/h)	17.7	23.8	17.7	23.8	23.5	28.6
O_2 production (kg/h)	142.0	190.0	142.0	190.0	188.0	229.0
H_2O utilization (kg/h)	177.0	238.1	177.0	238.1	235.3	285.7
Stack CAPEX (€/kW)	248.4	92.0	368.0	92.0	1,840**	184.0
System CAPEX (€/kW)	441.6	92.0	598.0	92.0	-	92.0

* This size is not significant on an industrial scale, but currently, these data are only available.
** The CAPEX of the SOEC system is not reported by IRENA; for this reason, in this study, the analysis is carried out by considering only the CAPEX of the SOEC stack.

Since CAPEX is referred to 2020, the conversion factor inherent to Chemical Engineering Plant Cost Indices ($CEPCI$) is applied, as illustrated in eq. 7. [12]

$$C_{FC,2022} = C_{FC,2020} \cdot \frac{CEPCI_{2022}}{CEPCI_{2020}} \tag{7}$$

The values of CEPCI 2022 and CEPCI 2020 are equal to 813.0 and 596.2, respectively [13]. According to these data, the terms of these equations are calculated, as summarized in Table 2.

Table 2. The total costs and revenue of electrolyzers in the current and future scenario.

Parameters	**AWE**		**PEMWE**		**SOEC**	
Time Scenario (y)	**2023**	**2050**	**2023**	**2050**	**2023**	**2050**
C_{FC} (k€)	6,404.8	1,252.5	8,966.4	1,252.5	17,078.9	1,878.7
$C_{O\&M,\ annualized}$ (k€)	20,906.1	12,575.5	22,955.7	12,575.5	25,751.6*	13,712.8*
$C_{rep,\ annualized}$ (k€)	212.6	28.5	312.1	28.2	5,582.5	58.4
$R_{O2,\ annualized}$ (k€)	1,881.5	2,531.1	1,881.5	2,531.1	2,501.3	3,037.3
$H_{2\ production,\ annual}$ (kg/y)	141,592.9	190,476.2	141,592.9	190,476.2	188,235.3	288,571.4

*The costs of the heat source for the SOEC electrolyzer are not considered because it has been paired with a plant that generates high-temperature waste heat as a by-product and, therefore, useful for supplying the SOEC.

It is noticed that the costs of electrolysis systems will reduce drastically in the coming years; in fact, in the 2050 scenario, the total fixed capital costs will decrease until to 90% thanks to the design simplification and less expensive materials utilization. The O&M costs will be

cut until to 50% due to the stack efficiency improving and, as a consequence, to a lower electricity consumption. Finally, the replacement costs will also decrease (more than 90%) because the system lifetime will increase.

Discussion

This study aims to evaluate and compare LCOH for different electrolysis system technologies by also considering a future cost scenario.

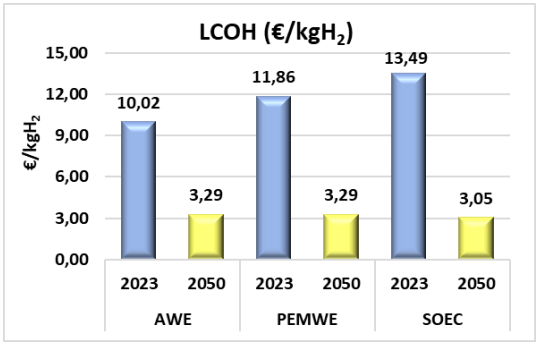

Figure 1. LCOH comparison for 2023-2050 scenarios.

Figure 1 shows the results of this analysis in terms of LCOH for 2023 and 2050 scenarios. In 2023, the calculated LCOH values are 10.02 €/kg, 11.86 €/kg and 13.49 €/kg for the AWE system, the PEMWE system and the SOEC unit, respectively. At 2050, the expected LCOH values are substantially reduced; they are 3.29 €/kg for the AWE and PEMWE systems and 3.05 €/kg for the SOEC system.

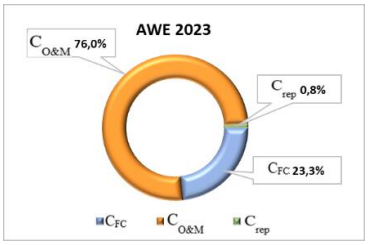

AWE Sharing costs in the 2023 scenario.

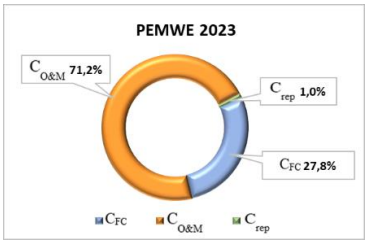

PEMWE Sharing costs in the 2023 scenario.

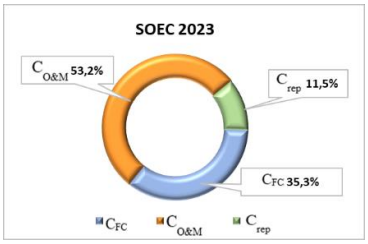

SOEC Sharing costs in the 2023 scenario.

Figure 2. The sharing costs of the electrolyzers in the 2023 scenario.

In Figure 2, the incidence of each item cost on LCOH calculation is illustrated for each electrolysis system (2023 scenario). It is observed that the O&M costs affect the LCOH by about 76.0% for the AWE system, 71.2% for the PEMWE system and 53.2% for the SOEC unit; thus, it can be underlined that the O&M costs have the greatest impact on the LCOH value. This result mainly depends on the electricity cost that has an incidence equal to 79% for the AWE system, 75% for the PEMWE system and 60% for the SOEC unit.

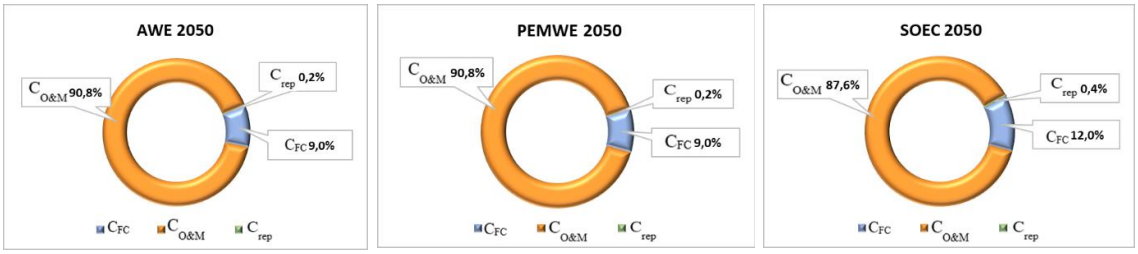

AWE Sharing costs in the 2050 scenario.

PEMWE Sharing costs in the 2050 scenario.

SOEC Sharing costs in the 2050 scenario.

Figure 3. The sharing costs of the electrolyzers in the 2050 scenario.

Figure 3 shows the cost incidence in 2050. It is worth noting that the O&M costs are still too high compared to the other cost items. Also in this case, the cost of electricity has the greatest impact with respect to the other costs even if this cost is assumed equal to 70 €/MWh EU as suggested in ref. [10]. In particular, the electricity cost has an incidence on the O&M cost of 87% for the AWE and PEMWE systems and 85% for the SOEC system.

Conclusions

This study proposes a preliminary analysis focused on the evaluation of LCOH for different water electrolysis technologies by considering the current scenario and the future scenario. In the current scenario (2023), the LCOH values for the AWE, the PEMWE and the SOEC systems are very high (in the range of 10 – 13 €/kg) and far from the values desired for the hydrogen production cost (2 - 3 €/kg) that would make it competitive with current fossil fuels. In the 2050 scenario, the SOEC technology seems to have become the most competitive with an LCOH close to 3 €/kg (this value is close to the expected hydrogen production cost in the EU in 2050). In conclusion, with respect to the technical literature on LCOH calculation, in this study, a more detailed cost estimation based on both the cost escalation and the Sinnott and Tower method, is performed. For this reason, the LCOH values in 2023, although high, reflect the current technological situation as closely as possible. For 2050, despite the application of a more rigorous costing methodology, the obtained results are only indicative because many of the considered costs are highly susceptible to continuous variation, such as the cost of electricity.

Acknowledgment

PROTOSTACK project (n.101101504) has received support from the European Union's Horizon 2020 Research and Innovation Program, Hydrogen Europe and Hydrogen Europe Research.

References

[1] "REPORT FROM THE COMMISSION TO THE EUROPEAN PARLIAMENT." Accessed: Sep. 20, 2023. [Online]. Available: https://eur-lex.europa.eu/legal-content/IT/TXT/PDF/?uri=CELEX:52021DC0962&from=EN

[2] S. Shiva Kumar and H. Lim, "An overview of water electrolysis technologies for green hydrogen production," *Energy Reports*, vol. 8. Elsevier Ltd, pp. 13793–13813, Nov. 01, 2022. doi: 10.1016/j.egyr.2022.10.127.

[3] O. Schmidt, A. Gambhir, I. Staffell, A. Hawkes, J. Nelson, and S. Few, "Future cost and performance of water electrolysis: An expert elicitation study," *Int J Hydrogen Energy*, vol. 42, no. 52, pp. 30470–30492, Dec. 2017, doi: 10.1016/j.ijhydene.2017.10.045.

[4] M. Chatenet *et al.*, “Water electrolysis: from textbook knowledge to the latest scientific strategies and industrial developments,” *Chemical Society Reviews*, vol. 51, no. 11. Royal Society of Chemistry, pp. 4583–4762, May 16, 2022. doi: 10.1039/d0cs01079k.

[5] A. Perna, E. Jannelli, S. Di Micco, F. Romano, and M. Minutillo, “Designing, sizing and economic feasibility of a green hydrogen supply chain for maritime transportation,” *Energy Convers Manag*, vol. 278, Feb. 2023, doi: 10.1016/j.enconman.2023.116702.

[6] G. Towler *et al.*, “CHEMICAL ENGINEERING DESIGN Principles, Practice and Economics of Plant and Process Design,” 2008. [Online]. Available: http://elsevier.com

[7] R. Hancke, T. Holm, and Ø. Ulleberg, “The case for high-pressure PEM water electrolysis,” *Energy Convers Manag*, vol. 261, Jun. 2022, doi: 10.1016/j.enconman.2022.115642.

[8] D. Jang, J. Kim, D. Kim, W. B. Han, and S. Kang, “Techno-economic analysis and Monte Carlo simulation of green hydrogen production technology through various water electrolysis technologies,” *Energy Convers Manag*, vol. 258, Apr. 2022, doi: 10.1016/j.enconman.2022.115499.

[9] “Electricity prices in Europe fell significantly in January 2023. https://gmk.center/en/posts/electricity-prices-in-europe-fell-significantly-in-january-2023/.”

[10] “EU Energy Outlook to 2060. https://energypost.eu/eu-energy-outlook-to-2060-how-will-power-prices-and-revenues-develop-for-wind-solar-gas-hydrogen-more/ .”

[11] I. Renewable Energy Agency, *Making the breakthrough: Green hydrogen policies and technology costs*. 2021. [Online]. Available: www.irena.org

[12] S. Pratschner, F. Radosits, A. Ajanovic, and F. Winter, “Techno-economic assessment of a power-to-green methanol plant,” *Journal of CO2 Utilization*, vol. 75, Sep. 2023, doi: 10.1016/j.jcou.2023.102563.

[13] “Chemical Engineering Plant Cost Index. https://personalpages.manchester.ac.uk/staff/tom.rodgers/Interactive_graphs/CEPCI.html?reactors/CEPCI/index.html.”

Effect of bias voltage and process temperature on the properties of carbon-based thin films as bipolar plate coating

M. Steinhorst*[1,2]

[1]Fraunhofer Institute for Material and Beam Technology IWS, Dresden & Dortmund, Germany
[2]Institute for Material Science IfWW, TUD Dresden University of Technology, Dresden, Germany

Introduction

Hydrogen is a key to a climate-neutral economy and in this context polymer electrolyte fuel cells (PEMFC) are an excellent choice for long-distance mobility. The bipolar plate (BPP) is a crucial component in PEMFC because it is responsible for various functions [1, 2]. Certain requirements including manufacturability, electrochemical stability, electrical conductivity as well as mechanical strength must be achieved [2, 3]. Considering the necessity of a wider application of fuel cells, metallic bipolar plates exhibit some important advantages compared to graphite or composites which are the mechanical properties, good volume-to-weight ratio and relative low costs [4,5]. Austenitic stainless steel (grade 1.4404 or 316L) is a highly attractive option because of its good combination of properties [6,7]. However, the electrical and electrochemical properties need to be improved to guarantee a high electrical performance and to withstand the harsh fuel cell environment and by this extended operational life time [5,8]. As surface modification for metallic BPP, a large variety of thin film coatings have been and still under investigation [9]. Extensive work has been conducted over the past years to develop various types of carbon thin films [10–17]. Here, carbon-based coatings exhibit promising properties because of the superior electrical conductivity, good adhesion and corrosion resistance. However, in most studies magnetron sputtering system is employed which has the drawbacks of a relatively low deposition rate and efficiency [18].

In my thesis, I study the impact of the process parameters temperature, pressure and bias voltage on the microstructure, interfacial contact resistance (ICR) and corrosion resistance of carbon-based coatings. The aim is to better understand the corresponding relationships and by this to improve or optimize the deposition process for a future up-scaling. For the experiments, I use the cathodic arc deposition technique which has beneficial characteristics such as a high deposition rate, high ion energy, good efficiency as well as low costs [18–20]. The ion energy is an important characteristic since it can considerably affect the layer growth and consequently the resulting microstructure and properties as shown by A. Anders [21] for energetic deposition techniques. Via a negative bias voltage applied to the substrate the ion energy can be increased [19, 22]. Another important parameter is the process temperature which mainly influences the adatom mobility and by this the growth of a PVD coating [21, 22].

In this paper, I want to focus on the results of the experiment series regarding the process temperature and bias voltage. The presented results partly base on my publication in AMPC [23] and ACS Appl. Mater. Interfaces [24].

Methodology

Austenitc (SS316L) stainless steel of 0.1 mm thickness was used as substrate material and cleaned with distilled water, isopropanol and then dried with nitrogen. In two experiment series various carbon-based coatings with different carbon top layer variants were deposited by cathodic arc evaporation. The base pressure was set at 10^{-4} Pa. All coatings have the same metallic interlayer. In first study, four carbon top layer variants were deposited at negative bias voltages between 900 V and 1 V. Process temperature of 300 °C and pressure of 10^{-1} Pa were kept constant. In the second series, the process temperature during the carbon deposition was varied between 300 °C and 100 °C while the bias voltage and pressure were set at 900 V and 10^{-1} Pa, respectively.

*Corresponding author: maximilian.steinhorst@iws.fraunhofer.de

For the structural analysis, Raman spectroscopy as well as transmission electron microscopy were used. Raman spectra were recorded between 900 and 1850 cm^{-1} by a Renishaw inVia with an excitation laser of 514 nm wavelength. Evaluation of the spectra was done by fitting the D peak and G peak with a Lorentzian and a Breit-Wigner-Fano function, respectively. A Joel JEM-F200 TEM was used for cross-section observations of the microstructure at 200 kV. Cross-section preparation was done via focused ion beam (FEI Helios 660 Dual-Beam SEM/FIB) using a platinum/carbon (Pt/C) plus an iridium (Ir) coating as protective layers.

The interfacial contact resistance was measured according to the procedure of Wang et al. [25]. The measurement setup includes a tensile tester with two gold-plated copper blocks for applying the compaction force and an ohmmeter attached to the copper blocks for measuring the resistance. The specimen is placed with two GDL sheets (Freudenberg H14) between the copper blocks and the resistance of the assembly is measured at a compaction force of 150 N cm^{-2}. With the contact resistance of one GDL, the contact resistance of the coated sample can be calculated.

To analyze the corrosion resistance, potentiodynamic polarization tests in 0.5 M H_2SO_4 solution at room temperature and 80 °C were conducted. The open circuit potential was recorded for 1 h prior the polarization measurement. As measurement parameters, a potential range of -0.5 to 1.5 V vs. standard hydrogen electrode (SHE) at a scan rate of 0.001 V s^{-1} was set. A Metrohm Autolab PGSTAT302N potentio-/galvanostat and a three-electrode setup including a graphite rod as counter electrode, a Ag/AgCl reference and the sample as working electrode were the measurement setup. Via Tafel plot analysis, using the Metrohm software Nova 2.1.5, the corrosion current density j_{corr} as well as polarization resistance R_p were determined.

Results and Discussion

In figure 1 the Raman spectra of the carbon top layer variants are depicted. In general, carbon exhibits two peaks, namely D peak at 1350 cm^{-1} and G peak at 1580-1600 cm^{-1}. For the bias voltage variation, an evolution from nearly equal pronounced D and G peaks (900 V and 600 V) to a more pronounced G peak (1 V) can be seen. The decrease of the D peak height can be attributed to increased long-range ordering and less fine structures due to fewer six-fold carbon rings [26, 27]. In the case of the process temperature, such an evolution is not visible. Here, the 300 °C and 100 °C sample exhibit comparable spectra with two distinct peaks. Compared to that, the 200 °C has a very broad spectrum indicating a different structure.

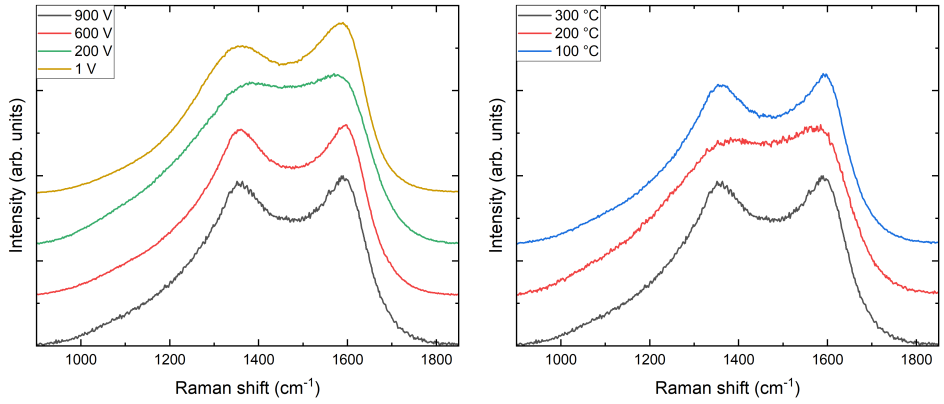

Figure 1: Raman spectra of the coated samples with carbon top layers deposited at different bias voltages (left) and process temperatures (right).

Figure 2 and figure 3 present the TEM cross-section images of the deposited coatings depending on the bias voltage and process temperature during the carbon deposition, respectively. In each case the Cr interlayer is between 15 and 20 nm. Because of the decreasing bias voltage a structural change from a mostly perpendicular graphite layers (see figure 2a) towards a more disordered (see figure 2b and c) and eventually amorphous structure (see figure 2d) can be observed. The visible disorder for the 600 V and 200 V carbon layer can be described as distortions in the form of clusters or diversions in the growth direction. The carbon layer thickness increases from approximately 10 nm at 900 V to 95 nm at 1 V. This can be attributed to self-sputtering due to high kinetic energies of the impinging ions at a high bias voltage.

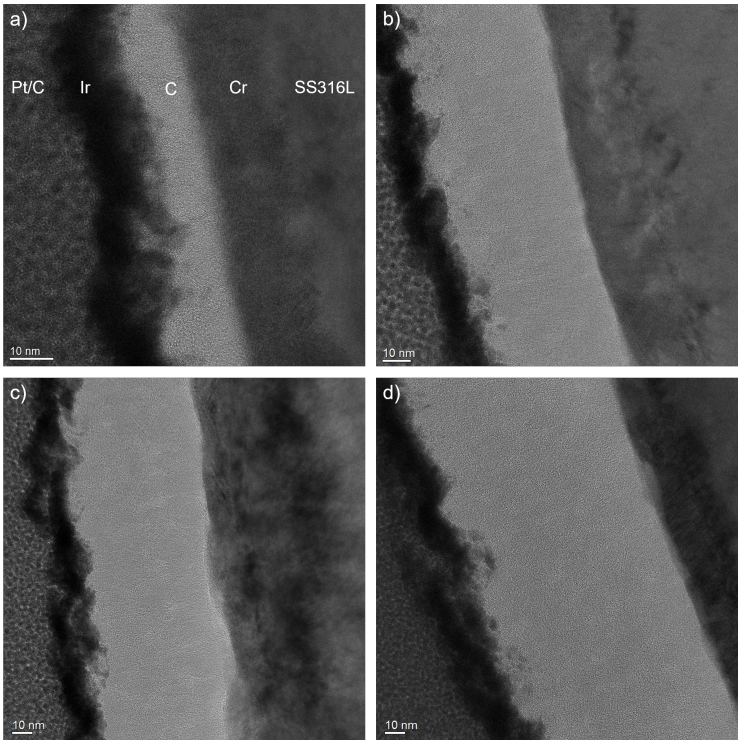

Figure 2: TEM images of coated samples with a carbon top layer deposited at a) 900 V, b) 600 V, c) 200 V and d) 1 V bias voltage.

The carbon top layer deposited at 200 °C has clearly graphitic layers but often oriented in round shaped form (see figure 3). Furthermore, the layer thickness is increased, although the bias voltage is as high as for the 300 °C. Both indicates a changed growth mechanism of the carbon layer compared to the 300 °C. The TEM analysis of the 100 °C is in progress.

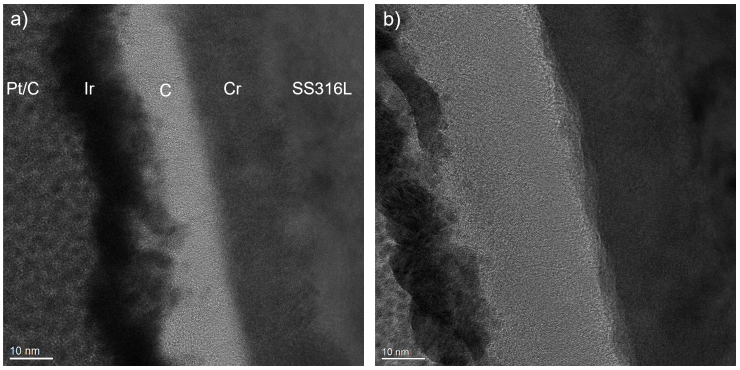

Figure 3: TEM images of coated samples with a carbon top layer deposited at a) 300 °C and b) 200 °C process temperature.

The contact resistance depending on the compaction force is shown in figure 4. A compaction force of 150 Ncm^{-2} corresponds to the defined force of 138 Ncm^{-2} by the DOE [3]. From 50 to 150 Ncm^{-2} the ICR is significantly reduced because of the increased contact area between the GDL and the specimen. The bias voltage during the carbon deposition greatly affects the electrical resistance. At the lower compaction force, the coatings with the 900 V and 600 V carbon top layer already achieve very low ICR values around 2.5 $m\Omega\ cm^2$. The 200 V sample exhibits slightly higher resistance values at both compaction forces. Due to disordered parts in the structure, the electrical conductivity might be reduced (see figure 2). The 1 V sample has the highest ICR which is likely attributed to the amorphous structure.

Regarding the effect of the process temperature, it can be concluded that there are only small differences. However, the sample with a carbon top layer deposited at 200 °C has the highest resistance values. All in all, the different carbon top layer variants are highly conductive.

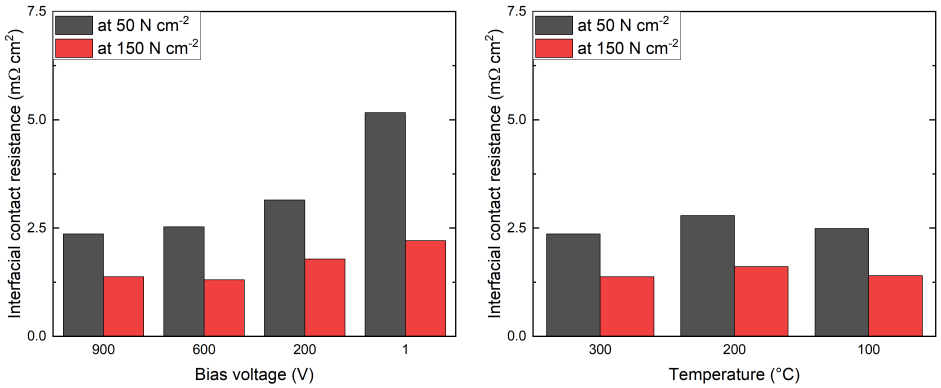

Figure 4: Interfacial contact resistance values of the coated samples with a carbon top layer deposited at 900 V, 600 V, 200 V, and 1 V bias voltage (left) and at 300 °C and 200 °C (right).

Based on the potentiodynamic polarization curves (not shown here) important corrosion key figures, namely corrosion current density j_{corr} and polarization resistance R_{p}, were determined via Tafel plot analysis. Figure 5 shows the dependency of these key figures on the bias voltage (left) and process temperature (right). From 900 V to 200 V j_{corr} decreases, thus, the coatings are more corrosion resistant. Consequently R_{p}, which corresponds to the corrosion resistance, decreases as well. The 600 V and 200 V samples exhibit excellent corrosion properties and both still have a low layer thickness. The increase in the corrosion resistance, compared to the 900 V sample, might be attributed to the increasing layer thickness. However, the 1 V with the thickest coating thickness has the worst properties. A possible explanation is the amorphous structure. In the case of the process temperature, the sample with the 200 °C carbon top layer achieves the best properties. A thickness effect can be responsible, but the 100 °C with likely a thicker carbon top layer, achieves a significantly lower R_{p}. Hence is much less inert or stable in the electrolyte. The microstructural analysis by TEM should give more insight. Also, considering that the Raman characteristics are comparable to the 300 °C which exhibits better properties. Moreover, measurements at an electrolyte temperature of 80 °C (not shown here) revealed that the corrosion current density increases by approximately one order of magnitude.

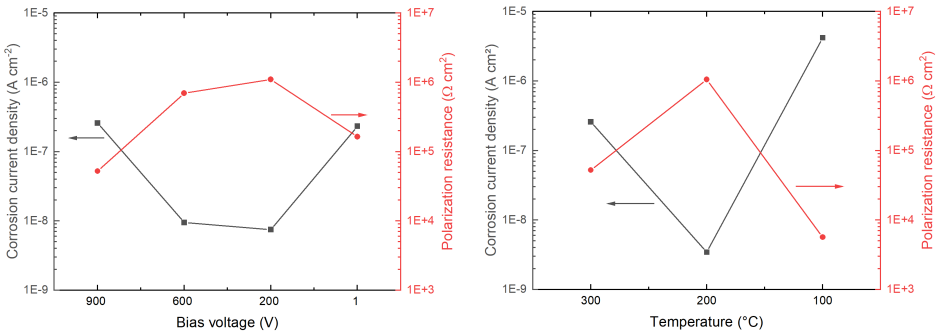

Figure 5: Corrosion key figures of the coated samples with a carbon top layer deposited at 900 V, 600 V, 200 V, and 1 V bias voltage (left) and at 300 °C and 200 °C (right).

Conclusion

In total seven multi layer coatings consisting of a metallic interlayer and a carbon top layer deposited at either different bias voltages or different process temperatures were prepared by cathodic arc evaporation. Hereby, the influence of the deposition parameters on relevant properties were investigated. Therefore

TEM analysis, Raman spectroscopy, interfacial contact resistance measurements and potentiodynamic polarization tests in 0.5 M H_2SO_4 were used. The bias voltage can considerably affect the microstructure, ranging from graphite-like to amorphous. It has a relatively small effect on the contact resistance, but therefore, a great influence on the electrochemical properties. There are only small difference between the 600 V and 200 V samples, both exhibiting a corrosion current density around 10^{-8} Acm^{-2}. The results of the temperature variation show that the contact resistance is only negligibly affected. Equivalent to the bias voltage, the main influence is on the electrochemical properties. Here, the sample with a carbon top layer deposited at 200 °C exhibit the best characteristics with the high polarization resistance among the samples. This sample also exhibits a clearly different microstructure in the TEM cross-section. A thickness effect is possible in both studies, however, the results indicate that the microstructure also has an essential impact on the properties.

In conclusion, the coatings exhibit an excellent electrical conductivity and good corrosion resistance which renders them as suitable option as bipolar plate surface modification. The deposition process can be improved in terms of the bias voltage and process temperature which is beneficial for a future production of coated bipolar plates. For a future study, the combination of the most suitable parameters to further optimize the process is planned.

Acknowledgements

This work was partly supported by the public funded project miniBIP II (reference no.: 03ETB007B) and the Fraunhofer internal research project HOKOME. M. Steinhorst acknowledges Mr. D. Pohl, from the Dresden Center for Nanoanalysis, for the support with the TEM investigations.

References

[1] L. Carrette, K. Friedrich, and U. Stimming, "Fuel cells: Principles, types, fuels, and applications," *ChemPhysChem : a European journal of chemical physics and physical chemistry*, vol. 1, p. 162—193, 2000.

[2] P. Mohr, *Optimierung von Brennstoffzellen-Bipolarplatten für die automobile Anwendung.* PhD thesis, University Duisburg-Essen, 2018.

[3] Hydrogen and F. C. T. Office, "Hydrogen and fuel cell technologies office multi-year research, development, and demonstration plan," tech. rep., U.S. Department of Energy, Washington D.C., 2017.

[4] Y. Song, C. Zhang, C. Ling, M. Han, R. Yong, D. Sun, and J. Chen, "Review on current research of materials, fabrication and application for bipolar plate in proton exchange membrane fuel cell," *International Journal of Hydrogen Energy*, vol. 45, pp. 29832–29847, 2020.

[5] Q. Liu, F. Lan, C. Zeng, J. Chen, and J. Wang, "A review of proton exchange membrane fuel cell's bipolar plate design and fabrication process," *Journal of Power Sources*, vol. 538, p. 231543, 2022.

[6] H. Tawfik, Y. Hung, and D. Mahajan, "Metal bipolar plates for PEM fuel cell—a review," *Journal of Power Sources*, vol. 163, pp. 755–767, 2007.

[7] Z. Xu, D. Qiu, P. Yi, L. Peng, and X. Lai, "Towards mass applications: A review on the challenges and developments in metallic bipolar plates for PEMFC," *Progress in Natural Science: Materials International*, vol. 30, pp. 815–824, 2020.

[8] D. Papadias, R. Ahluwalia, J. Thomson, H. Meyer, M. Brady, H. Wang, J. Turner, R. Mukundan, and R. Borup, "Degradation of SS316L bipolar plates in simulated fuel cell environment: Corrosion rate, barrier film formation kinetics and contact resistance," *Journal of Power Sources*, vol. 273, pp. 1237–1249, 2015.

[9] S. Chauhan and S. Ponkshe, "A review of coated metallic bipolar plates for proton exchange membrane fuel cell PEMFC," in *WCX SAE World Congress Experience*, 2022.

[10] Y. Park, H. Myung, J. G. Han, and B. Hong, "The electrical and structural properties of the hydrogenated amorphous carbon films grown by close field unbalanced magnetron sputtering," *Thin Solid Films*, vol. 482, pp. 275–279, 2005. EMRS 2004, Symposium J.

[11] Y. Show, "Electrically conductive amorphous carbon coating on metal bipolar plates for PEFC," *Surface and Coatings Technology*, vol. 202, pp. 1252–1255, 2007.

[12] H. Husby, O. Kongstein, A. Oedegaard, and F. Seland, "Carbon-polymer composite coatings for PEM fuel cell bipolar plates," *International Journal of Hydrogen Energy*, vol. 39, pp. 951–957, 2014.

[13] W. Mingge, L. Congda, T. D. A. C. Guohai, W. Donghui, Z. Haifeng, Z. Dong, and W. Aiying, "Effects of metal buffer layer for amorphous carbon film of 304 stainless steel bipolar plate," *Thin Solid Films*, vol. 616, pp. 507–514, 2016.

[14] R. Hu, J. Tang, G. Zhu, Q. Deng, and J. Lu, "The effect of duty cycle and bias voltage for graphite-like carbon film coated 304 stainless steel as metallic bipolar plate," *Journal of Alloys and Compounds*, vol. 772, pp. 1067–1078, 2019.

[15] M. Havigh, A. Hubin, and H. Terryn, "Assessment of carbon-titanium multilayer coatings on aluminum as bipolar plates in PEM fuel cells," *Journal of the Electrochemical Society*, vol. 168, p. 061503, 2021.

[16] I. Alaefour, S. Shahgaldi, J. Zhao, and X. Li, "Synthesis and ex-situ characterizations of diamond-like carbon coatings for metallic bipolar plates in PEM fuel cells," *International Journal of Hydrogen Energy*, vol. 46, pp. 11059–11070, 2021.

[17] Y. L. Su, W. H. Kao, and G. Y. Chang, "Tribological, anti-corrosion, and electrical conductivity properties of crcx coatings deposited on stainless steel 316l and used as metal bipolar plates for fuel cells," *Journal of Materials Engineering and Performance*, vol. 32, p. 3739–3754, 2023.

[18] J. Vetter, J. Mueller, and G. Erkens, "Domino platform: PVD coaters for arc evaporation and high current pulsed magnetron sputtering," *IOP Conference Series: Materials Science and Engineering*, vol. 39, p. 012004, 2012.

[19] A. Anders, "A review comparing cathodic arcs and high power impulse magnetron sputtering (HiPIMS)," *Surface and Coatings Technology*, vol. 257, pp. 308–325, 2014.

[20] A. v. K. J. T. Gudmundsson, A. Anders, "Foundations of physical vapor deposition with plasma assistance," *Plasma Sources Science and Technology*, vol. 31, p. 083001, 2022.

[21] A. Anders, "A structure zone diagram including plasma-based deposition and ion etching," *Thin Solid Films*, vol. 518, pp. 4087–4090, 2010.

[22] D. Mattox, *Handbook of Physical Vapor Deposition (PVD) Processing*. William Andrew, Elsevier, 2 ed., 2010.

[23] M. Steinhorst, M. Giorgio, T. Roch, and C. Leyens, "Influence of deposition temperature on the electrical and electrochemical properties of carbon-based coatings for metallic bipolar plates, prepared by cathodic arc evaporation," *Advances in Materials Physics and Chemistry*, vol. 12, pp. 47–57, 2022.

[24] M. Steinhorst, M. Giorgio, T. Roch, and C. Leyens, "Bias voltage dependency of structural and bipolar plate-related properties of cathodic arc-deposited carbon-based coatings," *ACS Applied Materials & Interfaces*, vol. 15, p. 51704–51712, 2023.

[25] H. Wang, M. Sweikart, and J. Turner, "Stainless steel as bipolar plate material for polymer electrolyte membrane fuel cells," *Journal of Power Sources*, vol. 115, pp. 243–251, 2003.

[26] A. Afshar, M. Yari, M. M. Larijani, and M. Eshghabadi, "Effect of substrate temperature on structural properties and corrosion resistance of carbon thin films used as bipolar plates in polymer electrolyte membrane fuel cells," *Journal of Alloys and Compounds*, vol. 502, pp. 451–455, 2010.

[27] Y. Wang, H. Li, L. Ji, F. Zhao, Q. Kong, Y. Wang, X. Liu, W. Quan, H. Zhou, and J. Chen, "Microstructure, mechanical and tribological properties of graphite-like amorphous carbon films prepared by unbalanced magnetron sputtering," *Surface and Coatings Technology*, vol. 205, pp. 3058–3065, 2011.

Effect of porosity on the mechanical properties of 316L processed by powder bed fusion after gaseous hydrogen charging

Ali Nabizada*[1], Lisa Claeys[1], Pascal J. Jacques[2], Tom Depover[1], Kim Verbeken[1]

[1] Ghent University, Department of Materials, Textiles and Chemical Engineering, Research group of Sustainable Materials Science, Ghent, Belgium
[2] UCLouvain, Institute of Mechanics, Materials and Civil Engineering (IMMC), IMAP, Louvain-la-Neuve, Belgium

Introduction

Hydrogen has received significant attention as a viable alternative energy carrier in response to the growing environmental challenges associated with fossil fuels [1]. In the context of direct hydrogen exposure, structural metals, particularly austenitic stainless steels (ASSs) such as type 316 L, have been recognized for their ability to withstand hydrogen embrittlement (HE) with limited degradation in mechanical performance. Nonetheless, annealed 316L, characterized by a face-centered cubic structure, exhibits relatively low strength, rendering it less suitable for applications involving elevated pressures within hydrogen-rich environments [2]. The rise of additive manufacturing (AM) technologies, which entails the layer-by-layer deposition of molten metals to create intricate components, has sparked considerable research interest. Components produced via additive manufacturing exhibit distinct mechanical properties owing to variations in microstructure, texture, and surface characteristics when compared to conventionally manufactured (CM) counterparts. Generally acknowledged is the fact that AM 316L shows higher yield and tensile strengths than CM 316L when tested in ambient air [3]. However, the mechanical behavior of AM 316L in the presence of hydrogen remains uncertain. Furthermore, the AM manufacturing process is susceptible to the formation of porosities that can significantly influence the macroscopic performance of AM 316L [4]. To enhance mechanical properties and mitigate the risk of catastrophic failures stemming from HE, or in other words, to enhance HE resistance, it is imperative to investigate the influence of porosity in presence of hydrogen. Understanding hydrogen diffusivity and hydrogen trapping mechanisms in materials containing porosity is also pivotal in elucidating their HE mechanisms [5]. An effective method involves the utilization of Scanning Electron Microscopy (SEM) in conjunction with ex-situ tensile tests to characterize mechanical properties and establish correlations with the microstructure. This approach will facilitate the optimization of AM 316L performance within hydrogen-rich atmospheres. Consequently, the aim of current study is investigating the impact of porosity on hydrogen embrittlement behavior of powder bed fusion printed 316L.

Methodology

In this research, we adhered to standard printing parameters for the fabrication of Powder Bed Fusion (PBF) 316L components, employing a laser power of 200 W, a scan speed of 1400 mm/s, a layer thickness of 50 µm, and a hatch spacing of 100 µm. A comprehensive analysis was conducted to compare specimens subjected to hydrogen exposure and those left unchanged. The introduction of hydrogen into the specimens was achieved through gaseous charging at 130 bar pure H_2 gas, maintained at a temperature of 250°C for a duration of 7 days. The assessment of hydrogen absorption behavior was carried out employing Thermal Desorption Spectroscopy (TDS). The density of the LPBF specimens was determined utilizing the hydrostatic weighing method under ambient conditions. Concurrently, the extent of

* ali.nabizada@ugent.be

porosity within the specimens was quantified through the application of Archimedes' principle and Backscatter Electron image analysis. The mechanical behavior of the material was evaluated through ex-situ tensile testing along the building direction at room temperature performed on a Tinius Olsen 50ST machine for both uncharged condition and after exposure to hydrogen. The prescribed constant extension rate was set at 0.06 mm/min, corresponding to a strain rate of 10^{-4} s^{-1} and the specimens had gauge dimensions of 10x4x1mm³. Furthermore, Scanning Electron Microscopy (SEM) analysis was conducted utilizing a FEI Quanta 450 microscope equipped with a field emission gun for microstructural characterization.

Results

The analysis of the experimental TDS data involved the use of a numerical 1D diffusion model based on Fick's laws. The results of these simulations, specifically the dissolved hydrogen content (C_t) and the hydrogen diffusion coefficient at room temperature (D_{RT}), are presented in Table 1. Figure 1a displays Backscatter Electron (BSE) images, revealing the presence of spherical pores and layer voids within the as-built PBF 316L. The fraction of porosity, as determined through BSE image analysis, stands at 0.91%, a value closely aligned with that obtained via the hydrostatic weighing method (1.03%). Uniform specimen thicknesses were employed for both TDS and tensile testing samples. Figure 1b represents engineering stress-strain curves. Table 2 indicates the average yield strength (YS), ultimate tensile strength (UTS), and strain at fracture (%El) for both uncharged and hydrogen-charged conditions, along with their corresponding standard deviations. Figures 2a and 2b depict the fracture surfaces of specimens subjected to tensile testing without and with hydrogen exposure, respectively. Consequently, the study examined hydrogen-assisted cracking on the normal surfaces of the tensile-tested specimens for both uncharged and hydrogen-charged conditions. The cracks observed were oriented perpendicular to the loading direction, which the fracture surfaces presented in Figures 2c and 2d.

Table 1: Averaged hydrogen content C_t of specimen charged at 250°C and 130 bar for 7 days and hydrogen diffusion coefficient D at room temperature (RT)

	$D_{RT}(m^2/s)$	C_t (wppm)
PBF 316L	8.21E-17	76.03

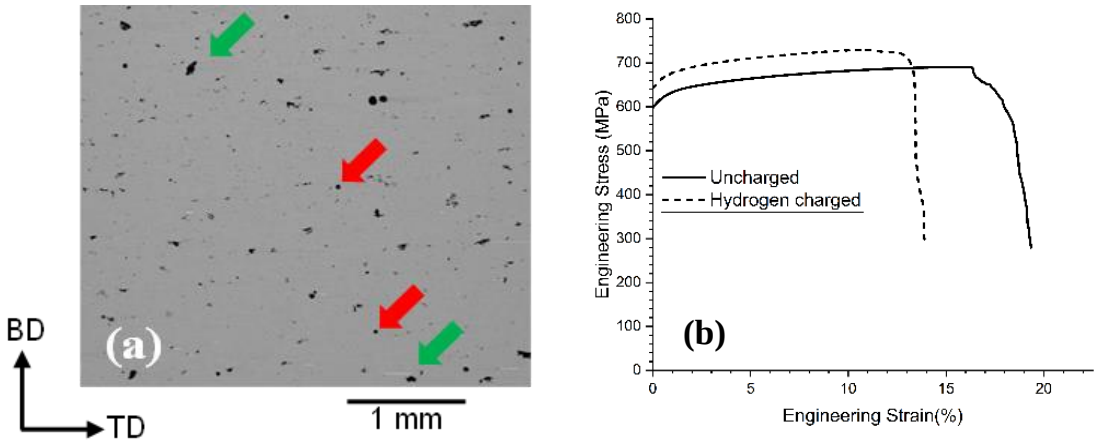

Figure1. (a) SEM-BSE micrograph of PBF 316L, red and green arrows show spherical and keyhole pores, respectively (b) Engineering Stress-Strain curves of tensile test performed at $10^{-4}s^{-1}$ in uncharged and hydrogen charged condition.

Table 2: Average yield strength (YS), ultimate tensile strength (UTS) and total elongation (%EI) of tensile test performed at $10^{-4}s^{-1}$ in uncharged and hydrogen charged condition.

	YS (MPa)	UTS(MPa)	%EI
Uncharged	598±8.4	690±7.3	19.35±0.9
Charged	642±14.0	730±5.8	13.99±0.7

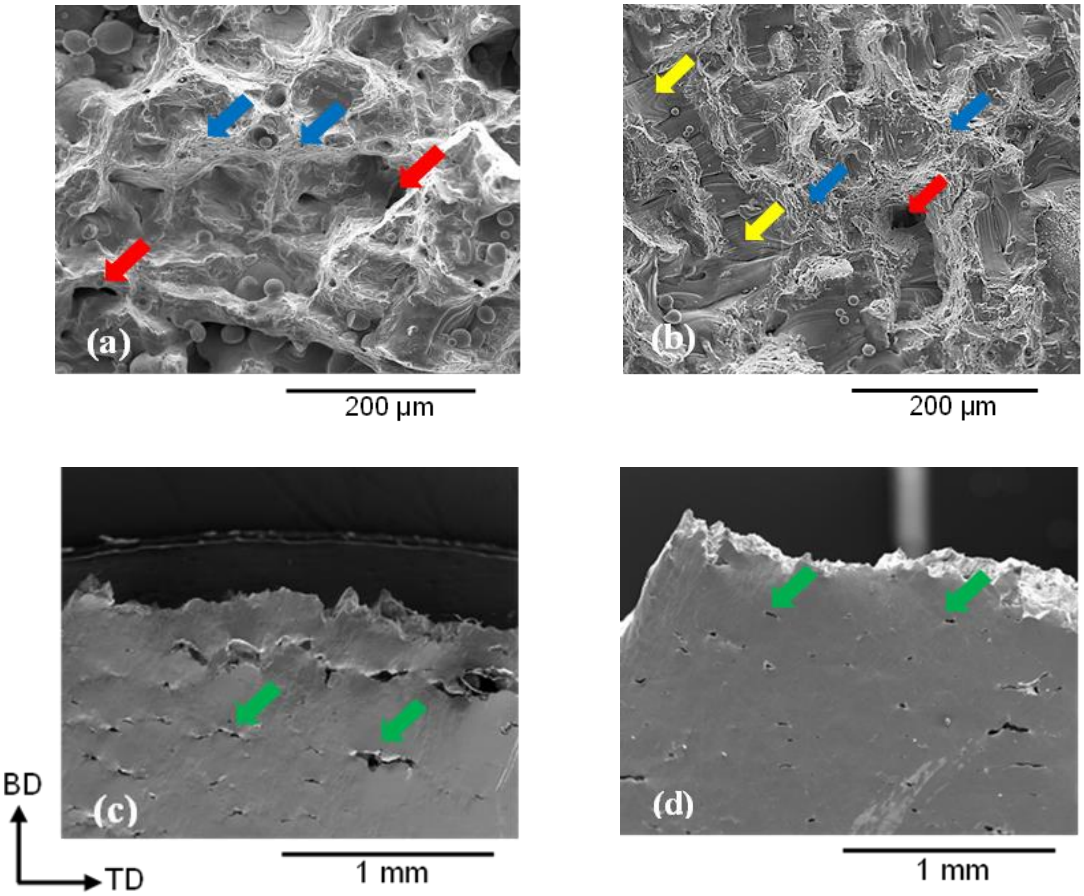

Fig 2. SE images of characteristic fracture surface and normal surface appearance when tested at $10^{-4}s^{-1}$: (a and c) uncharged, (b and d) hydrogen charged PBF 316L. Red, blue, yellow, and green arrows point to pores, dimples, facet like features, and secondary cracks, respectively.

Discussion

The presence of internal defects within Additive Manufacturing (AM) materials aligns with expectations established in the existing literature. Liverani et al. [6] discussed three primary categories of internal defects, which include: (i) binding defects, (ii) spherical pores, and (iii) keyhole pores. Binding defects originate from the incomplete fusion of powder particles at the local level, while spherical voids are predominantly associated with the entrapment of gases. Keyhole pores, on the other hand, are typically situated at the boundaries of melt pools and emerge due to elevated residual stresses generated by rapid cooling, thus promoting crack formation and the development of voids. It is worth noting that all three varieties of internal defects were also observed in the current material. LPBF 316L exhibited a relatively high yield strength but limited work hardening, leading to an ultimate tensile strength (UTS) level of 690

MPa. The presence of pores and internal defects, which are characteristic of LPBF processes, tends to restrict the ductility of LPBF 316L compared to CM counterparts. These internal defects act as stress concentration sites, triggering damage nucleation or contributing to the growth of ductile voids. Upon the introduction of hydrogen into the specimens, both the yield strength and ultimate tensile stress exhibited an increase. This strengthening effect of hydrogen stems from its impact on solid solution strengthening, slip planarity, and pinning of dislocations. To evaluate the embrittling influence of hydrogen, an average embrittlement index was calculated based on the strain at fracture for reference tests and hydrogen precharged tests, as outlined in Equation 1. This approach enables a qualitative assessment of the susceptibility to HE.

$$\text{HE index} = \frac{\%\text{El}_{\text{uncharged}} - \%\text{El}_{\text{charged}}}{\%\text{El}_{\text{uncharged}}} \qquad \text{Equation 1}$$

The HE Index for PBF 316L was determined to be 27.7%. Hydrogen could primarily localized within pores, which functioned as reversible traps at room temperature [5]. These pores, acting as sites of stress concentration, in conjunction with the accumulated hydrogen content, trigger hydrogen embrittlement within the charged specimen. The fracture surface of the uncharged specimen exhibited characteristics of a ductile fracture, featuring the presence of dimples, pores, and unmelted particles. During the tensile test, the coalescence of pores and voids accelerated the fracture process, impeding the growth of dimples and thereby limiting the extent of ductility. In contrast, the hydrogen-charged sample also displayed a ductile fracture surface, but with three notable differences. Firstly, the fraction and size of dimples were smaller than those observed in the uncharged condition, indicating reduced dimple growth during straining. Secondly, the presence of facet-like features, including ungrown voids and an absence of plastic deformation, suggested a brittle mode of fracture. Finally, there was less coalescence of pores, a phenomenon also observed on the corresponding normal surface image, where the size of secondary cracks in the uncharged specimen exceeded that in the charged specimen. Crack initiation and propagation predominantly occurred within the pores and voids.

Conclusions

The impact of porosity on the mechanical characteristics of PBF manufactured 316L stainless steel, both in the presence and absence of hydrogen, was examined through constant strain rate tensile test and SEM. Specimens subjected to hydrogen charging exhibited elevated values for the yield strength and ultimate tensile stress in comparison to their non-hydrogen-charged counterparts. This is attributed to the influence of hydrogen on the mechanisms responsible for strengthening the material. The pores, as reversible hydrogen traps, facilitated hydrogen embrittlement (HE) in the tested material, leading to a reduction in fracture strain. Both the non-hydrogen-charged and hydrogen-charged specimens displayed a combination of brittle and ductile fracture characteristics, resulting from the coalescence of voids and pores. However, the uncharged material exhibited notably larger dimples and secondary cracks in comparison to the hydrogen-charged condition, which can be ascribed to the phenomenon of hydrogen-induced ductility loss.

Acknowledgement

The authors would like to acknowledge the financial support of the Energy Transition Fund via the BE-HyFE project. The research was also supported by FWO (senior postdoctoral fellow project number 12ZO420N) and the special research fund (BOF) of Ghent University (grant BOF15/BAS/062 and BOF20/BAS/121) for the used equipment.

References

[1] H. J. Undertaking, “Hydrogen roadmap Europe: a sustainable pathway for the European energy transition,” 2019.

[2] T. Michler, C. San Marchi, J. Naumann, S. Weber, and M. Martin, “Hydrogen environment embrittlement of stable austenitic steels,” *Int J Hydrogen Energy*, vol. 37, no. 21, pp. 16231–16246, 2012.

[3] W. E. Frazier, “Metal additive manufacturing: a review,” *J Mater Eng Perform*, vol. 23, pp. 1917–1928, 2014.

[4] D. Yang *et al.*, “Influence of porosity on mechanical and corrosion properties of SLM 316L stainless steel,” *Applied Physics A*, vol. 128, pp. 1–9, 2022.

[5] A. Yaktiti, A. Dreano, J. F. Carton, and F. Christien, “Hydrogen diffusion and trapping in a steel containing porosities,” *Corros Sci*, vol. 199, p. 110208, 2022.

[6] E. Liverani, S. Toschi, L. Ceschini, and A. Fortunato, “Effect of selective laser melting (SLM) process parameters on microstructure and mechanical properties of 316L austenitic stainless steel,” *J Mater Process Technol*, vol. 249, pp. 255–263, 2017.

Effects of hydrogen on fatigue properties of austenitic stainless steels at low temperature

Romain Chochoy*[1], Pierre Osmond[2], Denis Bertheau[1], Guillaume Benoit[1], Daniella Guedes Sales[2], Gouenou Girardin[2], Gilbert Hénaff[1]

[1]Institut P' UPR 3346 CNRS – ENSMA – Université de Poitiers, Téléport 2, 1 avenue Clément Ader, 86961 Futuroscope Chasseneuil cedex, France

[2]Cetim, 74 route de la Jonelière – CS 50814, 44308 Nantes Cedex 3, France

Introduction

The design of liquid hydrogen tanks requires a thorough understanding of the factors influencing fatigue crack initiation and propagation at cryogenic temperatures in materials used in hydrogen environments. In the case of austenitic stainless steels, it is well-established that hydrogen embrittlement (HE) is characterized by a loss of ductility in tension, with a maximum embrittlement occurring at approximately 190 K, and a vanishing effect at very low temperatures [1]. Figure 1 illustrates the influence of temperature on HE in different grades of steel under monotonic tensile loading. Below a temperature of approximately 150K, no HE is noticeable. It can be hypothesized that below 190K, hydrogen diffusion is significantly slowed down, possibly even halted below 150K [2]. These results suggest that below 200K, HE is controlled by hydrogen diffusivity within the material, while above this temperature, martensitic transformation governs HE.

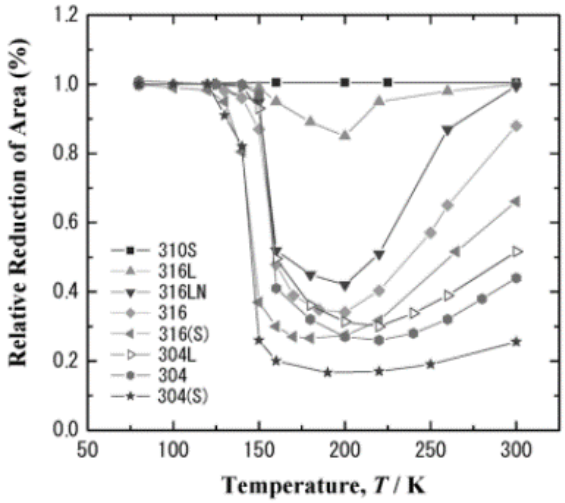

Figure 1: Effect of temperature on air reduction on various stainless steels under 1.1 MPa of hydrogen and helium [3]

Indeed, at low temperatures, the austenitic phase can transform into a more stable phase, namely martensite. Molnár et al. [4] demonstrated in a 316L steel the correlation between the increase in stacking fault energy and the rise in the exposure temperature from 25°C to 500°C. It appears that martensitic transformation occurs for intrinsic stacking fault energies less than 18 mJ/m^2 [5]. However, Caskey [2] shows that the loss of ductility in the presence of hydrogen is not uniquely correlated with the martensitic transformation rate.

More generally, the literature indicates that it is not justified to investigate HE below 150K to observe HE phenomena. These fatigue tests were conducted under gaseous hydrogen, which implies that only the effect of external hydrogen was taken into account. Concerning

* Corresponding author: romain.chochoy@ensma.fr

high cycle fatigue properties in hydrogen environment, literature suggests that the impact on the high cycle fatigue strength would be much more limited [6]. However, only a limited amount of results is available, and of the effect of hydrogen environment on fatigue damage mechanisms is unclear. Therefore, the work presented here aims to assess the influence of hydrogen on the high-cycle fatigue resistance of austenitic stainless steels in a hydrogen environment within the temperature range of 20K to 300K.

Two grades of austenitic stainless steels were selected, namely 304L and 316L. Due to differences in stacking fault energy, these two grades of steels are expected to have varying proportions of martensitic transformation at low temperatures under fixed loading conditions, which may influence sensitivity to HE.

The first step of this work consisted in the determination of the fatigue resistance of these grades in air at room temperature. The second step was concerned by the influence of temperature in the range of -83°C to 100°C. Finally, the fatigue strength is evaluated in hydrogen gas at various temperatures. The initial results of this study will be presented in this paper.

Methodology

The materials used in this study are two grades of austenitic stainless steel (type 304L stainless steel and 316L stainless steel). Table 1 shows the chemical compositions and Table 2 presents the tensile properties determined at room temperature.

Table 1: Chemical compositions of 304L and 316L stainless steel (wt%)

		Fe	C	Mn	P	S	Si	Cu
304L	Concentration (%m)	70,6	0,024	1,88	0,034	0,001	0,328	0,363
316L		68,2	0,023	1,84	0,036	0,001	0,328	0,345
		Ni	Cr	Mo	Nb	Ti	N	Co
304L	Concentration (%m)	8,08	18,1	0,403	0,003	0	0,100	0,152
316L		10,0	17,0	2,01	0,013	0,004	0,036	0,157

Table 2: Tensile properties of 304L and 316L stainless steel used in this study

	UTS (MPa)	R0,2% (MPa)	A%	Z%
304L	700	336	90	64
316L	620	290	91	61

Tensile tests were conducted at room temperature with a strain rate of 10^{-3} s^{-1} until failure. To assess the test repeatability, two tests per rolling orientation (0° and 90°) were conducted. Figure 2 shows the change in martensite content with total strain measured for each alloy during tensile test. Two analysis techniques are used, Feritscope® and X-ray diffraction (DRX). Notable differences are observed between the results obtained with these two techniques. Further analysis is planned to precisely evaluate the percentage of martensite transformed as a function of deformation.

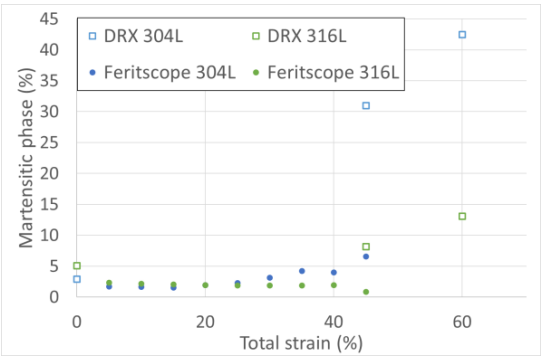

Figure 2: Measurement of martensite content using XRD and Feritscope®

Cylindrical test specimens were machined for fatigue testing and polished to achieve a mirror-like surface finish, with an arithmetic mean roughness (R_a) of less than 0.02 µm.

The fatigue tests were performed using a load ratio of 0.1, at a frequency of 10 Hz, at temperature ranging between -120°C and 100°C either in laboratory air or in a hydrogen gas environment (1,5 MPa). Fatigue tests were performed until total failure of specimens or run-out at two million of cycles. For the tests in hydrogen, gas pressure was set at 1,5 MPa of dihydrogen in order to assess the impact of external hydrogen on fatigue strength.

Observations of fracture surfaces were conducted on fractured specimens to assess damage mechanisms and their sensitivity to the presence of hydrogen.

Results & Discussion

Fatigue behaviour at different temperature

The fatigue resistance in air has been studied at various temperatures to evaluate cyclic behaviour under typical load-controlled R=0,1 fatigue loadings and resulting fatigue strengths. The objective was to establish reference data to be later compared to the results in hydrogen gas at the same temperatures.

Due to the positive mean stress, a ratchetting deformation appears during the fatigue life. This deformation might require a special attention as, at low temperatures, the accumulation of plastic deformation can induce the formation of martensite, which is likely to alter the mechanisms of crack initiation and propagation in a hydrogen environment. Figure 3 shows typical behaviour obtained during fatigue test on 316L at -83°C, 25°C and 100°C. The mean strain is obtained by considering the mean strain values collected during each loading cycle. Furthermore, the progressive deformation rate is obtained by deriving the mean strain with respect to the number of cycles.

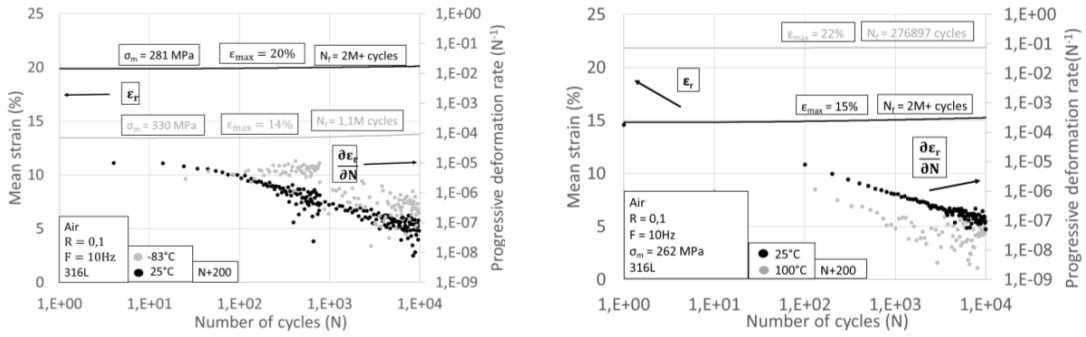

Figure 3: Evolution of average ratchetting deformation and progressive deformation rate as a function of the number of cycles based on temperature for 316L (comparison of behaviour at room temperature compared to -83°C and 100°C)

The preliminary results indicate that for a given stress amplitude, at -83°C, the mean deformation at failure is lower compared to the test conducted at 25°C, while the ratchetting deformation rate is higher. At 100°C, the final average deformation is higher than room temperature, and the ratchetting deformation rate is similar compared to the test conducted at 25°C.

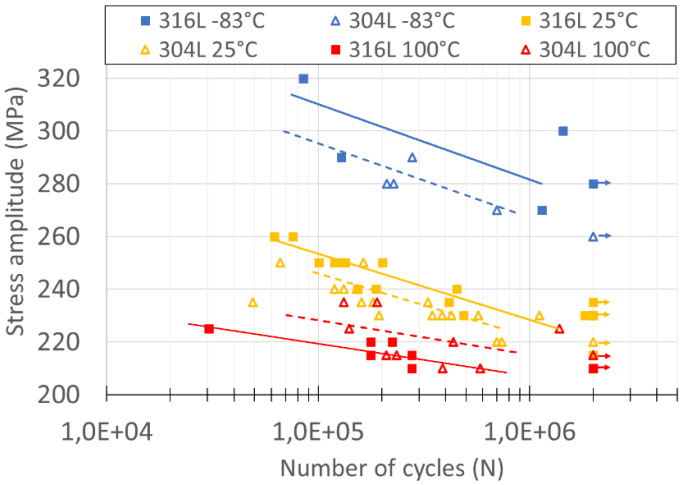

Figure 4: S-N curve for 316L and 304L at 3 different temperatures

Figure 4 shows the S-N curves for 316L and 304L at the three temperatures namely 100°C, 25°C, and -83°C. It appears that the lower the temperature, the higher the life is for a given stress amplitude. The temperature dependence of the fatigue strength of the two materials seems to be similar. Fatigue tests at -83°C in air are currently in progress.

As mentioned earlier, martensitic transformation appears to play a role in hydrogen embrittlement. Therefore, it is important to be able to assess the amount of martensite transformed during tensile tests. Initially, only the amount of martensite transformed during monotonic tensile tests was studied. Quantification of martensite during and after cyclic tensile tests is currently in progress.

Subsequently, martensite measurements will be conducted for each experimental condition at various temperatures under both air and hydrogen environments.

Fatigue behaviour in hydrogen gas at room temperature

Figures 5a and 5b describes the deformation variation as a function of the number of cycles in both materials, at room temperature, in air, and in hydrogen gas with the same stress amplitude. The ratchetting deformation is also represented, so as to assess the progressive deformation rate as a function of the number of cycles. The initial results appear to suggest no hydrogen effect on the ratchetting behaviour. This result is explainable by the fact that hydrogen does not have sufficient time to diffuse deeply into the material.

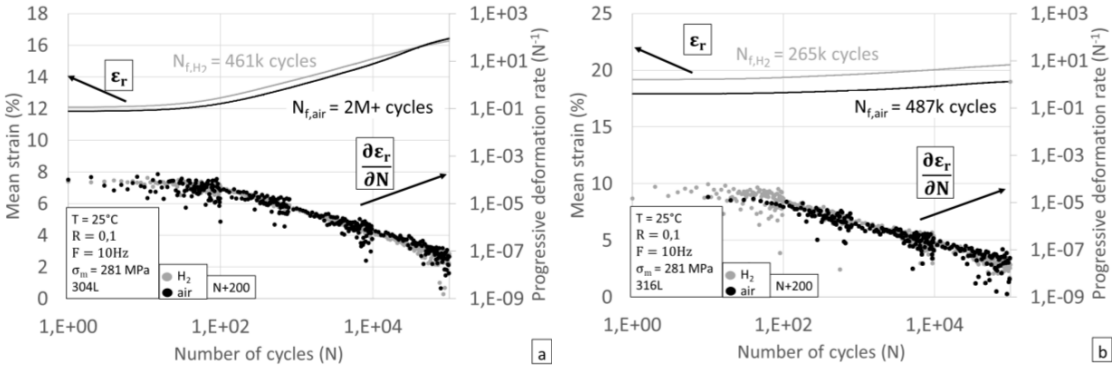

Figure 5: Evolution of average ratchetting deformation and progressive deformation rate as a function of the number of cycles for 304L (a) and 316L (b) in air and hydrogen

Figure 6 shows the fatigue lives in air and in hydrogen gas for the two grades at room temperature. It appears that, the exposure to hydrogen gas does not significantly affect the fatigue life.

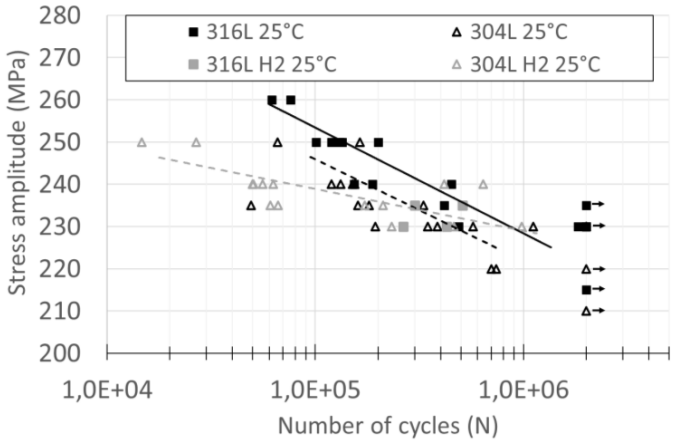

Figure 6: S-N curve for 316L and 304L in air and hydrogen at room temperature

The fracture surfaces (Figure 7) indicate a difference in the maximum crack depth at the end of the stable propagation stage between exposure to air (1,47 mm) and to gaseous hydrogen (1,90 cm). To validate this point, a statistical study comparing these parameters is currently underway. Additionally, several specimens fractured as a result of crack initiation at inclusion-type defects during hydrogen gas exposure. Further in-depth analyses are currently under progress to identify the composition of these inclusions.

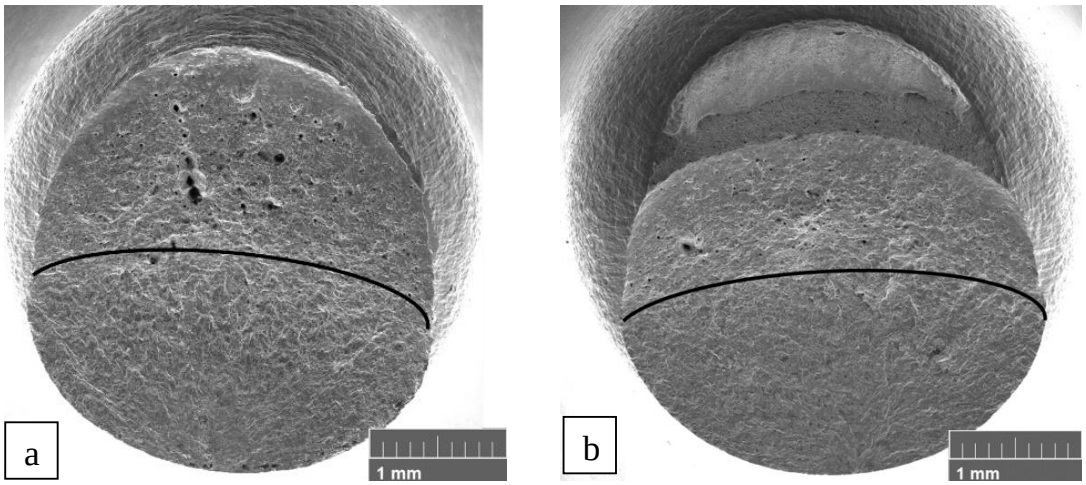

Figure 7: SEM image of fracture surfaces for 304L under air (a) and under hydrogen (b) tested at the same stress amplitudes. The black line allows the distinction between the stable propagation zone (lower region) and the abrupt rupture zone (upper region).

The initial results indicate that in gaseous hydrogen, at room temperature, and for an identical mechanical load, the crack front is more extensive, and the propagation distance is greater than in the case of exposure to air.

Conclusions and future work

The preliminary results of tests conducted so far at 100°C, 25°C and -83°C in ambient air indicate the presence of a ratchetting effect leading to a significant accumulation of plastic deformation, which could potentially contribute to the formation of martensite on the order of

a few percent at room temperature [7]. This phase would promote the susceptibility to HE (Hydrogen Embrittlement). Since 316L stainless steel is more stable than the 304L grade, we can assume that 304L is more sensitive to hydrogen embrittlement effects. This will need to be confirmed by studying the fatigue behaviour in low-temperature hydrogen exposure.

Prior to testing in low-temperature hydrogen conditions, it is necessary to characterize the fatigue resistance of the studied grades at these temperatures in an inert environment. This includes evaluating the transformed martensite rate (especially as a function of the ratchetting effect) and describing the damage mechanisms related to temperature reduction.

As concerns tests in hydrogen, little or no significant effect on endurance and fatigue behaviour has been observed at room temperature. However, further analysis is planned, including the examination of fracture surface morphology and martensite quantification after fracture. Phenomena occurring at temperatures above and below the maximum embrittlement temperature will be investigated so as to identify the role of various factors (martensitic transformation and hydrogen diffusivity).

The effect of hydrogen on fatigue crack initiation has not yet been established, therefore, this aspect will be studied further in the course of this study, especially for low stress levels. One hypothesis is that in the absence of crack initiation or slip emergence at the surface, hydrogen may not penetrate into the material, presumably partly due to the presence of the native oxide layer. Therefore, a special attention will be paid to the stability of this oxide layer under cyclic loading. To assess the impact of internal hydrogen, fatigue tests will be conducted on precharged materials.

References

[1] “Hydrogen embrittlement evaluation in tensile properties of stainless steel at cryogenic temperatures”, doi: 10.1063/1.2900335

[2] “Hydrogen compatibility handbook for stainless steels”, doi: 10.2172/5906050

[3] “Effect of temperature on hydrogen environment embrittlement of type 316 series austenitic stainless steels at low temperatures”, doi: 10.2320/jinstmet1952.67.9_456

[4] “Effect of temperature on the stacking fault energy and deformation behaviour in 316L austenitic stainless steel”, doi: 10.1016/j.msea.2019.05.079

[5] “Twinning and martensite in a 304 austenitic stainless steel”, doi: 10.1016/j.msea.2012.05.080

[6] “Hydrogen environment embrittlement evaluation in fatigue properties of stainless steel SUS304L at cryogenic temperatures”, doi: 10.1063/1.3402310

[7] “Effects of strain state and strain rate on deformation-induced transformation in 304 stainless steel: Part I. magnetic measurements and mechanical behavior”, doi: 10.1007/BF02644427

Electrocatalysts for Oxygen Evolution Reaction in Seawater Electrolysis

Caillean Convery*[1], Mohamed Mamlouk[1]

[1] School of Engineering, Newcastle University, Newcastle, NE1 7RU, United Kingdom

Introduction

In order to help combat the current climate crisis, alternate cleaner fuel sources are required. When utilized, they should release less/no environmentally harmful emissions when compared to the CO_2 emitted when fossil fuels are combusted (80% of energy worldwide current produced utilizing fossil fuels[1]).

One such alternate fuel source that could be used is hydrogen gas [2]. When hydrogen is reacted (either combusted or used in a fuel cell) with oxygen it produces water and energy. This demonstrates that hydrogen, when used as a fuel source doesn't produce any environmentally harmful products. However, we need to consider sustainable methods to produce hydrogen. One such method is through water electrolysis and if renewable energy used for the electrolysis the produced hydrogen is termed green hydrogen. Green hydrogen, however only accounts for less 5% of world production with the majority been produced from methane steam reforming producing emitting CO_2 during the process [3]. This mainly due to high capital costs of electrolyzers partly caused by use of precious metal catalysts.

It is therefore vital that methods are found by which it is possible to produce green hydrogen (hydrogen not produced using energy derived from fossil fuels) or blue hydrogen where any produced CO2 is captured and stored. Electrolysis of water (reaction 5) generates hydrogen (through the hydrogen evolution reaction, HER, reactions 1 & 2) and oxygen (through oxygen evolution reaction, OER, reactions 3&4) [3]. Water electrolysis has been studied since the 18th century [4]. However, it has largely been carried out in freshwater/deionized water. With freshwater shortages caused by climate change, there is a drive to use alternative water sources. If seawater could be utilized as the fuel source, then this would open up the use of an abundant fuel source to be used with minimal pre-treatment [5].

* Corresponding author: c.a.convery2@newcastle.ac.uk

$$\text{Cathodic reaction (neutral/acidic pH): } 2H^+ + 2e^- \rightleftharpoons H_2 \; E^0_{cathode} = 0\ V \quad (1)$$

$$\text{Cathodic reaction (alkaline pH): } 2H_2O + 2e^- \rightleftharpoons H_2 + 2OH^- \; E^0_{cathode} = -0.83\ V \quad (2)$$

$$\text{Anodic reaction (neutral/acidic pH): } 2H_2O \rightleftharpoons O_2 + 4H^+ + 4e^- \; E^0_{anode} = 1.23\ V \quad (3)$$

$$\text{Anodic reaction (alkaline pH): } 4OH^- \rightleftharpoons O_2 + 4H_2O + 4e^- \; E^0_{anode} = 0.4\ V \quad (4)$$

$$\text{Full cell reaction: } 2H_2O \rightleftharpoons O_2 + 2H_2 + 4e^- \; E^0_{cell} = -1.23\ V \quad (5)$$

Seawater electrolysis (SWE) offers its own set of challenges that must be overcome before it can be widely utilized as a source for hydrogen production. On the cathodic side, any OH^- produced can precipitate into metal hydroxides when it reacts with metal cations present in seawater and poison the surface of the electrode [6]. The main focus of this research is however associated with the anodic side reactions. Thes arise from the presence of NaCl in seawater, in particular that chloride oxidation (CO, reaction 6) competes with OER at the anode as well as the corrosion chemistry which can arise from the presence of the chloride anion, damaging the anode material and therefore, limiting the efficiency of the cell [7].

$$2Cl^- \rightarrow Cl_2 + 2e^- \; E^0 = 1.36\ V \quad (6)$$

So, stable, selective (towards OER) and active catalysts are required to overcome these problems. The presence of chloride and neutral to acidic pH at the anode can also lead to corrosion of the electrode substrate, leading to loss of activity, so as part of this project substrates for catalysts will also be studied. A variety of catalysts have already been reported throughout literature looking at the anodic reactions associated with seawater electrolysis. Some of the catalysts that have demonstrated promise are multi-metallic layered hydroxides, for example, NiFe layered hydroxides (1.413 V @ 10 mA cm^{-2}) and NiCoFe layered hydroxides (1.5 V @ 10 mA cm^{-2}) have demonstrated promising performances for OER [8] . Whilst these catalysts show promise they, along with others, are tested in alkaline conditions in order to minimize the effect of CO on the activity of OER (as alkaline conditions maximize the thermodynamic potential difference between OER and CO [8]). When neutral conditions are considered for SWE the CO reaction is a more prevalent obstacle, due to these other methods have been explored in order to obtain systems that are selective towards OER, one such method is introducing a blocking layer. One material which has been identified as a blocking layer is MnO2 which has demonstrated a selectivity towards OER over CO in SWE

[9]. This material allows for only H_2O/OH^- to pass to the catalyst/anodic material and therefore, can lead to the possibility to limit any chlorine chemistry which could occur at the anode.

Methodology

Synthetic MnO_2 was created using a hydrothermal method that was taken from literature [10] in order to synthesize three different morphologies of the MnO_2 electrocatalyst in order to study if the morphology has an effect on the catalytic activity of the electrocatalyst or the activity of the material.

Figure 1 - hydrothermal reactor for synthesizing catalyst

The characterization techniques that were employed during the research project will include both SEM and XRD in order to determine the crystallographic phase as well as the discrete morphology of each synthetic material.

Following synthesis and physical characterization methods, electrochemical methods will then be used in order to determine the catalytic activity of the synthesized materials. All techniques thus far have been carried out utilizing a three-electrode setup (figure 2) with different substrates used as the working electrode, with Pt coated titanium and a real hydrogen electrode (RHE) used as the counter and reference electrode respectively. Different substrates were investigated for the working electrode in order to determine a suitable substrate for the electrocatalysts as some substrates are not suitable for use in saline environments due to susceptibility to corrosion. The electrolytes utilized in these experiments were 0.1 M KOH and 0.1 M NaCl.

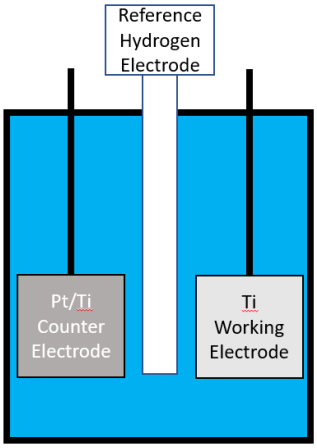

Figure 2 - Three electrode setup for analyzing the synthesized materials with Ti foil used as the example working electrode material.

Discussion

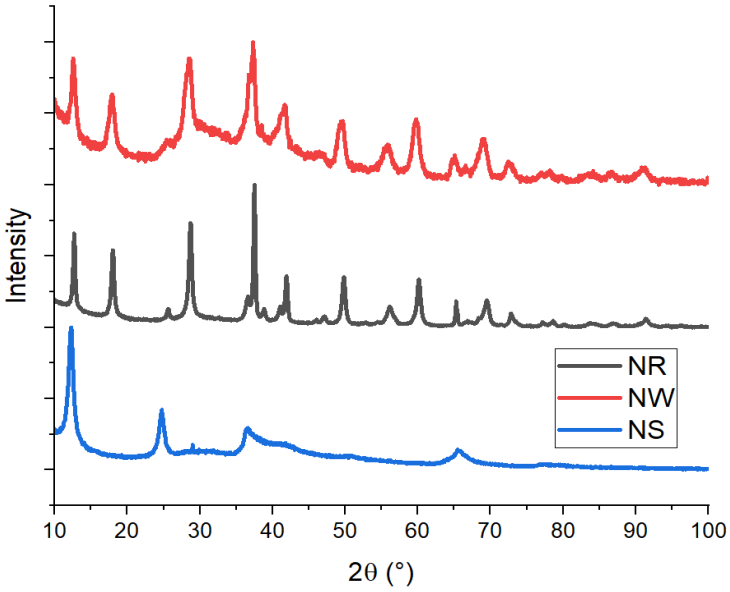

Figure 3 - XRD results of the synthesized materials with their labeling for their respective morphologies NW (nanowires), NR (nanorods) and NS (nanosheet)

Firstly, in order to determine the morphologies and crystallographic nature of the synthesized MnO2 catalyst X-ray diffraction and scanning electron microscopy were utilized.

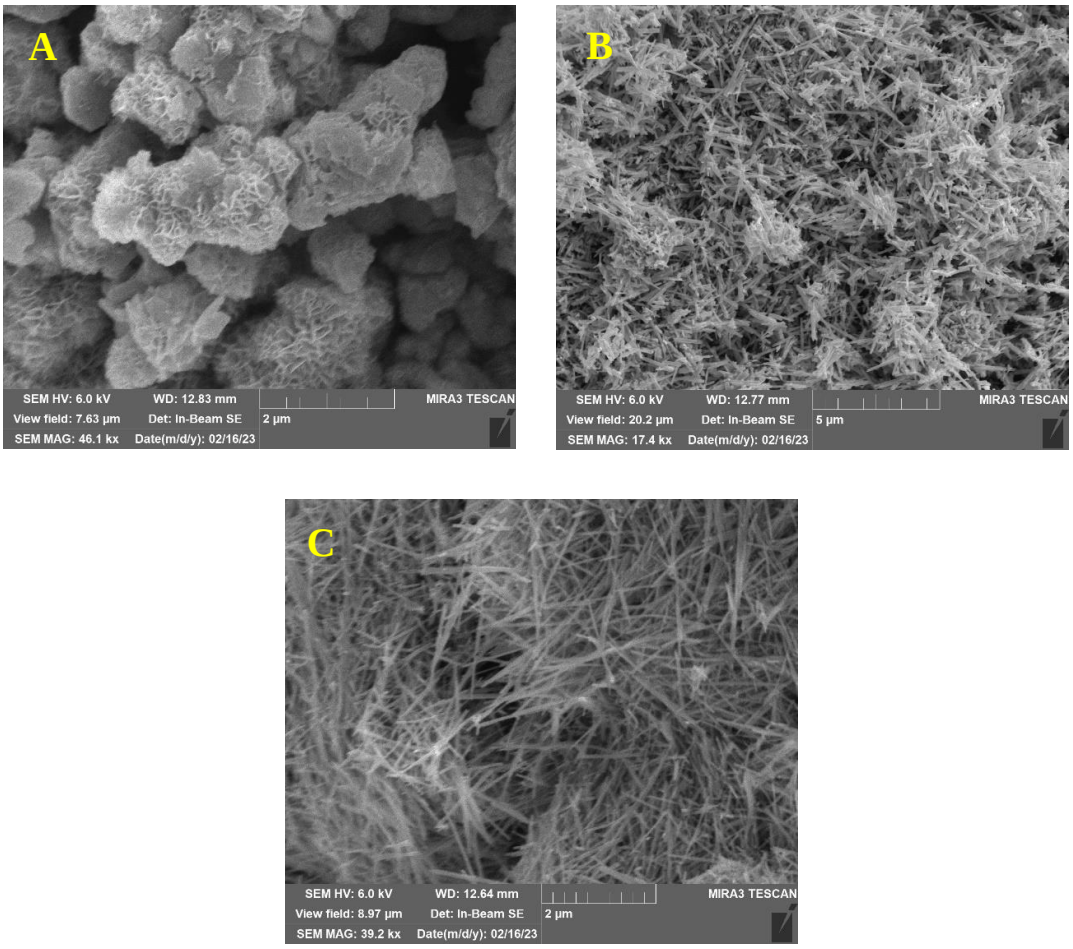

Figure 4 - SEM results of the 4 materials, A-NS, B-NR and C - NW

The materials phases were then determined using an XRD library database found in the following paper [11]. The materials were determined to be two alpha phase materials (NR and NW) and one delta phase material (NS).

The electrochemical results of these materials and substrates are still to be processed but would be ready for display in March.

Conclusions

In conclusion in order to test electrocatalysts to find a suitable material to use as a selective electrocatalyst for OER in seawater electrolysis, three MnO_2 materials have been synthesized and partially characterized and are awaiting electrochemical testing.

References

[1] "Fossil Fuels | EESI." Accessed: Dec. 05, 2022. [Online]. Available: https://www.eesi.org/topics/fossil-fuels/description

[2] H. Ishaq, I. Dincer, and C. Crawford, "A review on hydrogen production and utilization: Challenges and opportunities," Int J Hydrogen Energy, vol. 47, no. 62, pp. 26238–26264, Jul. 2022, doi: 10.1016/J.IJHYDENE.2021.11.149.

[3] P. Nikolaidis and A. Poullikkas, "A comparative overview of hydrogen production processes," Renewable and Sustainable Energy Reviews, vol. 67, pp. 597–611, Jan. 2017, doi: 10.1016/J.RSER.2016.09.044.

[4] G. Chisholm and L. Cronin, "Chapter 16 - Hydrogen From Water Electrolysis," Storing Energy, pp. 315–343, 2016, doi: 10.1016/B978-0-12-803440-8.00016-6.

[5] S. Dresp, F. Dionigi, M. Klingenhof, and P. Strasser, "Direct electrolytic splitting of seawater: Opportunities and challenges," ACS Energy Letters, vol. 4, no. 4. American Chemical Society, pp. 933–942, Apr. 12, 2019. doi: 10.1021/acsenergylett.9b00220.

[6] S. Zhang, Z. Liu, D. Chen, Z. Guo, and M. Ruan, "Oxygen vacancies engineering in TiO2 homojunction/ZnFe-LDH for enhanced photoelectrochemical water oxidation," Chemical Engineering Journal, vol. 395, Sep. 2020, doi: 10.1016/J.CEJ.2020.125101.

[7] G. Liu, Y. Xu, T. Yang, and L. Jiang, "Recent advances in electrocatalysts for seawater splitting," Nano Materials Science, 2021, doi: 10.1016/J.NANOMS.2020.12.003.

[8] F. Dionigi, A. Pawolek, A. Gliech, and P. Strasser, "Design Criteria, Operating Conditions, and Nickel-Iron Hydroxide Catalyst Materials for Selective Seawater Electrolysis", doi: 10.1002/cssc.201501581.

[9] A. Sivanantham and S. Shanmugam, "Nickel selenide supported on nickel foam as an efficient and durable non-precious electrocatalyst for the alkaline water electrolysis," Appl Catal B, vol. 203, pp. 485–493, 2017, doi: 10.1016/j.apcatb.2016.10.050.

[10] X. Wang and Y. Li, "Selected-Control Hydrothermal Synthesis of r-and-MnO 2 Single Crystal Nanowires," 2002, doi: 10.1021/ja0177105.

[11] G. Gupta, K. Selvakumar, N. Lakshminarasimhan, S. Murugesan, S. Kumar, and M. Mamlouk, "The effects of morphology, microstructure and mixed-valent states of MnO 2 on the oxygen evolution reaction activity in alkaline anion exchange membrane water electrolysis," J Power Sources, vol. 461, p. 228131, 2020, doi: 10.1016/j.jpowsour.2020.228131.

Electrochemical Dealloying of Bimetallic Oxygen Reduction Reaction Catalysts: A Comprehensive Analysis

A. Mohandas Sandhya, Athira Lekshmi*[1], B. Martos, Valentín Briega[2], C. Cherevko, Serhiy[2], D. Matolínová, Iva[1], E. Khalakhan, Ivan[1]

[1] Charles University, Faculty of Mathematics and Physics, Prague, Czech Republic

[2] Helmholtz Institute Erlangen-Nürnberg (IEK-11), Germany

Introduction

One of the most promising possibilities to lead the transition from energy production techniques based on fossil fuels to zero-emission technologies is Proton Exchange Membrane Fuel Cell (PEMFC). However, large-scale deployment of PEMFC is still constrained due to several shortcomings, among which high cost of the cathode catalyst and its stability are the most prominent ones. Due to their enhanced specific and mass oxygen reduction reaction (ORR) activity at lower metal loadings, platinum-based alloys stand out among the most examined catalysts as the preeminent candidates for replacing pure platinum cathode catalysts. Exploring Pt alloys with late transition metals including Fe, Co, Cu, Ni etc. has been the focus of substantial study for more than 20 years [1-6]. In addition, recent years have seen the emergence of a new family of catalytic materials that combine Pt with lanthanide metals like La, Ce, Gd etc. as well as early transition metals such as Y [7,8] or Sc [9].

Nevertheless, despite many advantages such alloys were found to be more prone to degradation in comparison to monometallic platinum. A major factor contributing to fuel cell degradation is the dissolution of cathode catalyst at the operating potentials followed by secondary catalyst degradation processes such as Ostwald ripening or coalescence [10-12], which will eventually decrease its active surface area and thus fuel cell performance. The Pt dissolution itself is a multifaceted process, impacted by various parameters, which has been extensively investigated [13-19] but dissolution process of alloys is intricately complex given by the preferential dissolution of non-noble metals. Hence, monitoring of dynamic dissolution behavior and dealloying of the bimetallic catalysts is of utmost importance to describe the entire chain of interconnected degradation mechanisms and formulate a comprehensive model of catalyst degradation that will help to develop a corresponding mitigation strategy leading toward a more robust catalyst.

This investigation aims to comprehensively analyze the dissolution tendencies and disparities exhibited by three distinct bimetallic catalysts of platinum-copper (PtCu), platinum-cobalt (PtCu) and platinum-yttrium (PtY) prepared by the magnetron co-sputtering technique. This was performed mainly using the scan fluid cell coupled with inductively coupled plasma spectroscopy (SFC-ICP-MS) technique. This study explores the dissolution of these bimetallic catalysts during electrochemical cycling at a wide range of potentials focusing on the oxygen reduction reaction (ORR) potential range and investigating different compositional variations. The work further explores the progressive evolution of catalysts in terms of their morphology and composition following the dealloying process, hence uncovering the trend that can guide the future design of more stable materials.

Methodology

* Corresponding author: mailmeathira96@gmail.com

Sample preparation

Pt bimetallic alloys were methodically deposited onto glassy carbon substrates utilizing magnetron co-sputtering via two circular TORUS magnetrons (Kurt J Lesker). These magnetrons were positioned at a 45^0-angle relative to the substrate and were employed alongside dual targets as shown in figure 1. The deposition chamber was pre-evacuated prior to deposition to attain a pressure of 2 x 10^{-4} Pa. The sputtering process was carried out in DC mode within an Ar atmosphere of 2.6 Pa pressure which we optimized in our previous work [20]. By manipulating the applied power on Pt target and the corresponding metal targets, Pt-M alloys of diverse compositions were proficiently deposited.

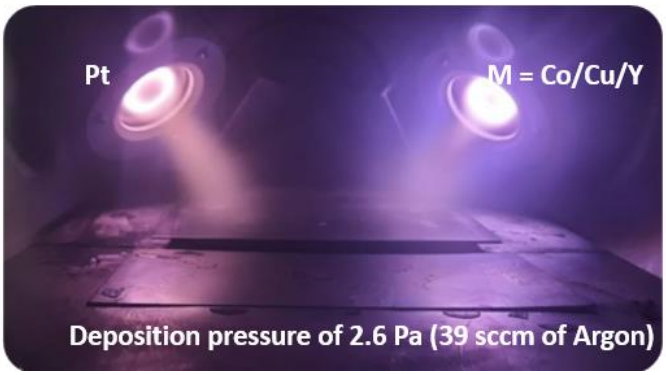

Figure 1: Preparation of Pt bimetallic alloys by magnetron co-Sputtering

Sample Characterization

Scan Fluid Cell coupled with Inductive Coupled Plasma Mass Spectrometry

The setup consists of a V-shaped electrochemical scanning flow cell (SFC) outlet directly hyphenated to the ICP-MS sample introduction mechanism. Thus, dissolved metal ions in SFC are carried downstream and measured by ICP-MS while electrochemical reactions occur on the working electrode (Figure 2) and hence cyclic voltammograms and dissolution spectrograms for the sample in an acidic electrolyte is measured simultaneously [21]. The experimental setup involved the utilization of a saturated Ag/AgCl electrode (Metrohm) as the reference electrode, while a glassy carbon rod (HTW Sigradur G) served as the counter electrode. The contact area of the working electrode was estimated to be around 1.1 mm^2. The electrolyte used in the experiment, 0.1M $HClO_4$ was freshly generated by combining 70% Perchloric acid (Suprapur, Merck) with ultra-pure water (Milli-Q IQ 7000 Merck). The electrolyte was then flowed at a rate of approximately 200 µL/min while continuously purging with argon gas. The dissolution was monitored on a NexION 300X (Perkin Elmer) via calibration from solutions of platinum (Pt), copper (Cu), cobalt (Co) and yttrium (Y) (at concentrations of 0, 0.5, 1.0, 5.0 µg/L respectively, Certipur Merck) while 10 µg/L of ^{187}Re for ^{195}Pt, 10 µg/L of ^{74}Ge for ^{63}Cu and ^{59}Co, and 10 µg/L of ^{45}Sc for ^{89}Y were utilized as internal standards.

The electrochemical protocol was initiated with an activation procedure during which the sample is held at a potential of 0.05 V_{RHE} for 5 minutes. Subsequently, the initial electrochemical cycling is conducted within a potential range of 0.05 to 0.8V_{RHE} at a scan rate of 5 mV/s. After each cycling, the contact is repositioned to a different spot on the sample.

After the similar activation protocol on each spot, electrochemical cycling is carried out to different upper potential limits (UPLs) of 1, 1.2, 1.5 V_{RHE} respectively and the dissolution spectra of each metal is recorded simultaneously.

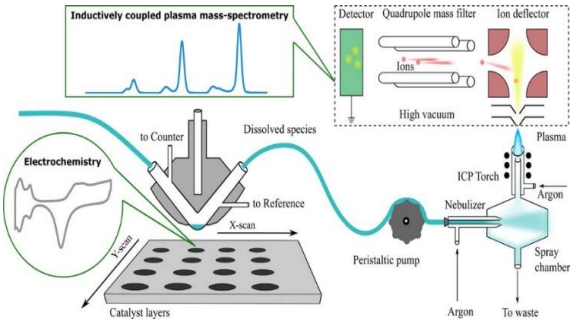

Figure 2: A simplified scheme showing the basic operational principles of SFC-ICP-MS [20]

Results and discussion

Herein, the discussion will be focused on a specific composition (Pt_3M) of all the alloys as well as monometallic platinum cycled to an UPL of 1.5 V_{RHE}. Figure 3b illustrates the different dissolution tendencies of the less noble metals derived from bimetallic alloys namely Pt_3Co, Pt_3Cu and Pt_3Y when cycled from 0.05 to 1.5 V_{RHE} which simulates the most severe conditions in real fuel cell device, and on the other hand Figure 3a depicts the simultaneous dissolution of platinum from the corresponding alloys as well as monometallic platinum.

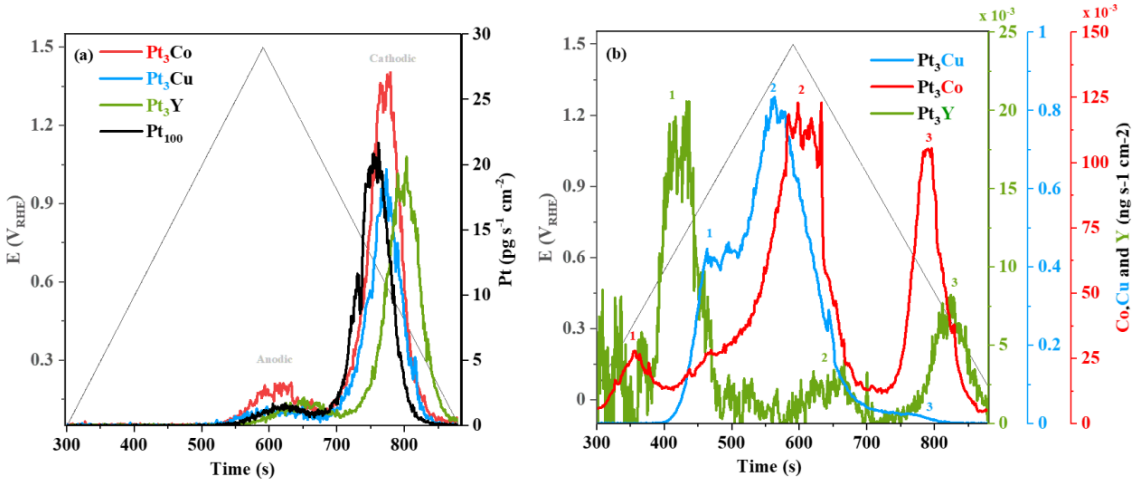

Figure 3: Dissolution spectra of (a) Pt from Pt_3M (M= Co, Cu, Y) and of pure Pt and (b) Co, Cu, Y from Pt_3M (M= Co, Cu, Y) during electrochemical dissolution to UPL 1.5 V_{RHE}

Pt dissolution spectra in Figure 3a show two well resolved peaks for all investigated samples which are known as anodic and cathodic dissolution peaks [13]. Anodic dissolution peak occurs during the transition of platinum from metal to oxide during anodic potential scan whereas cathodic dissolution is related to subsequent oxide reduction during cathodic scan. The peaks shape and intensities are comparable for all investigated samples.

Figure 3b represents respective dissolution of the less noble metals during the anodic and cathodic polarizations. All alloys show two different dissolution peaks during the anodic polarization. The former (peak 1) can be accounted for dissolution of the metal from the surface and sub-surface regions of the alloy which leads to catalyst dealloying. The latter (peak 2) is triggered by corresponding anodic dissolution of platinum. The cathodic dissolution (peak 3)

of these metals is stimulated solely by the cathodic dissolution of platinum which exposes alloying metal from the bulk leading to its enhanced dissolution. Similar dissolution profiles of Co and Cu have been reported before [22,23].

It can be clearly seen in Figure 3a that the dissolution spectra of Pt exhibit peak shifts in the presence of less noble metals with respect to that of monometallic Pt. This shift can be attributed to multiple factors such as changes in the electrocatalytic property, cohesive energy, and oxygen adsorption energy due to the alloy formation, which in turn can affect its dissolution properties [24]. Similarly alloying influence less noble metals like Co, Cu and Y which alter their dissolution with respect to their monometallic counterpart [25] and exhibit different dissolution peak potentials with respect to each other.

Further experiments were carried out for all the other compositions of the Pt bimetallic alloys (PtM and PtM_3) and at different potential ranges from 0.05 to 0.8,1.0 and 1.2 V_{RHE} which simulate different operation regimes of real fuel cell device.

Conclusions

PtCo, PtCu, and PtY catalysts with different compositions were prepared by means of magnetron sputtering and dissolution of constituent elements during potential cycling was probed using online ICP-MS technique. The dissolution tendencies of the less noble metals from different bimetallic catalysts showed contrasting behavior with each other. All these studies were also supported by the morphological and compositional evolution of these catalysts observed via scanning electron microscopy and energy dispersive Xray spectroscopy (EDX) respectively and more interpretations of the above results are going on.

It is expected that the results acquired from this study can offer valuable insights into the process of dissolution of less noble metal and dealloying mechanisms in platinum bi-metallic catalysts within the operational potential range of the fuel cells and the findings may contribute significantly to the existing knowledge on the durability and performance of fuel cell catalysts.

References

[1] X. Xie, A.L. Mohandas Sandhya, L. Piliai, Mykhailo Vorokhta, I. Matolínová, and I. Khalakhan, “Surface compositional dynamics in a PtNi bimetallic alloy under simulated operational conditions: Electrochemical and NAP-XPS Study,” *Applied Catalysis B-environmental*, vol. 325, pp. 122328–122328, May 2023, doi: https://doi.org/10.1016/j.apcatb.2022.122328.

[2] B. G. Pollet, S. S. Kocha, and I. Staffell, “Current status of automotive fuel cells for sustainable transport,” *Current Opinion in Electrochemistry*, vol. 16, pp. 90–95, Aug. 2019, doi: https://doi.org/10.1016/j.coelec.2019.04.021.

[3] G. Ercolano, F. Farina, L. Stievano, D. J. Jones, J. Rozière, and S. Cavaliere, “Preparation of Ni@Pt core@shell conformal nanofibre oxygen reduction electrocatalysts via microwave-assisted galvanic displacement,” Catalysis Science & Technology, vol. 9, no. 24, pp. 6920–6928, Jan. 2019, doi: https://doi.org/10.1039/c9cy01514k.

[4] D. Wang *et al.*, “Structurally ordered intermetallic platinum–cobalt core–shell nanoparticles with enhanced activity and stability as oxygen reduction electrocatalysts,” *Nature Materials*, vol. 12, no. 1, pp. 81–87, Oct. 2012, doi: https://doi.org/10.1038/nmat3458.

[5] L. Liu, H. Liu, X. Sun, C. Li, and J. Bai, “Efficient electrocatalyst of Pt–Fe/CNFs for oxygen reduction reaction in alkaline media,” *International Journal of Hydrogen Energy*, vol. 45, no. 30, pp. 15112–15120, May 2020, doi: https://doi.org/10.1016/j.ijhydene.2020.03.243.

[6] A. Pavlets, Ilya Pankov, and A. A. Alekseenko, “Electrochemical Activation and Its Prolonged Effect on the Durability of Bimetallic Pt-Based Electrocatalysts for PEMFCs,” *Inorganics (Basel)*, vol. 11, no. 1, pp. 45–45, Jan. 2023, doi: https://doi.org/10.3390/inorganics11010045.

[7] J. Greeley *et al.*, “Alloys of platinum and early transition metals as oxygen reduction electrocatalysts,” *Nature Chemistry*, vol. 1, no. 7, pp. 552–556, Oct. 2009, doi: https://doi.org/10.1038/nchem.367.

[8] R. Brown *et al.*, “Unraveling the Surface Chemistry and Structure in Highly Active Sputtered Pt_3Y Catalyst Films for the Oxygen Reduction Reaction,” *ACS Applied Materials & Interfaces*, vol. 12, no. 4, pp. 4454–4462, Dec. 2019, doi: https://doi.org/10.1021/acsami.9b17817.

[9] C. A. Campos-Roldán, D. J. Jones, J. Rozière, and S. Cavaliere, “Platinum-Rare Earth Alloy Electrocatalysts for the Oxygen Reduction Reaction: A Brief Overview,” *Chemcatchem*, vol. 14, no. 19, Aug. 2022, doi: https://doi.org/10.1002/cctc.202200334.

[10] J. C. Meier *et al.*, “Design criteria for stable Pt/C fuel cell catalysts,” *Beilstein Journal of Nanotechnology*, vol. 5, no. 1, pp. 44–67, Jan. 2014, doi: https://doi.org/10.3762/bjnano.5.5.

[11] I. Martens, Raphaël Chattot, and Jakub Drnec, “Decoupling catalyst aggregation, ripening, and coalescence processes inside operating fuel cells,” *Journal of Power Sources*, vol. 521, pp. 230851–230851, Feb. 2022, doi: https://doi.org/10.1016/j.jpowsour.2021.230851.

[12] F.-Y. Chen, Z.-Y. Wu, Z. Adler, and H. Wang, “Stability challenges of electrocatalytic oxygen evolution reaction: From mechanistic understanding to reactor design,” *Joule*, vol. 5, no. 7, pp. 1704–1731, Jul. 2021, doi: https://doi.org/10.1016/j.joule.2021.05.005.

[13] A. A. Topalov *et al.*, “Dissolution of Platinum: Limits for the Deployment of Electrochemical Energy Conversion?,” *Angewandte Chemie*, vol. 51, no. 50, pp. 12613–12615, Nov. 2012, doi: https://doi.org/10.1002/anie.201207256.

[14] D. J. S. Sandbeck *et al.*, “Particle Size Effect on Platinum Dissolution: Considerations for Accelerated Stability Testing of Fuel Cell Catalysts,” *ACS Catalysis*, vol. 10, no. 11, pp. 6281–6290, May 2020, doi: https://doi.org/10.1021/acscatal.0c00779.

[15] S. Cherevko, N. Kulyk, and K. J. J. Mayrhofer, “Durability of platinum-based fuel cell electrocatalysts: Dissolution of bulk and nanoscale platinum,” *Nano Energy*, vol. 29, pp. 275–298, Nov. 2016, doi: https://doi.org/10.1016/j.nanoen.2016.03.005.

[16] S. Cherevko *et al.*, “Dissolution of Platinum in the Operational Range of Fuel Cells,” *ChemElectroChem*, vol. 2, no. 10, pp. 1471–1478, May 2015, doi: https://doi.org/10.1002/celc.201500098.

[17] S. Cherevko, A. R. Zeradjanin, A. A. Topalov, N. Kulyk, I. Katsounaros, and K. J. J. Mayrhofer, “Dissolution of Noble Metals during Oxygen Evolution in Acidic Media,” *ChemCatChem*, vol. 6, no. 8, pp. 2219–2223, Jul. 2014, doi: https://doi.org/10.1002/cctc.201402194.

[18] P. P. Lopes, Dusan Strmcnik, Dusan Tripkovic, J. G. Connell, V. R. Stamenkovic, and N. M. Markovic, “Relationships between Atomic Level Surface Structure and Stability/Activity of Platinum Surface Atoms in Aqueous Environments,” vol. 6, no. 4, pp. 2536–2544, Mar. 2016, doi: https://doi.org/10.1021/acscatal.5b02920.

[19] P. P. Lopes *et al.*, “Dynamics of electrochemical Pt dissolution at atomic and molecular levels,” vol. 819, pp. 123–129, Jun. 2018, doi: https://doi.org/10.1016/j.jelechem.2017.09.047.

[20] A.L. Mohandas Sandhya *et al.*, “Tuning the morphology of sputter-deposited platinum catalyst: From compact layers to dispersed nanoparticles,” *Surfaces and Interfaces*, vol. 40, pp. 103079–103079, Aug. 2023, doi: https://doi.org/10.1016/j.surfin.2023.103079.

[21] O. Kasian, S. Geiger, K. J. J. Mayrhofer, and S. Cherevko, “Electrochemical On-line ICP-MS in Electrocatalysis Research,” *The Chemical Record*, vol. 19, no. 10, pp. 2130–2142, Dec. 2018, doi: https://doi.org/10.1002/tcr.201800162.

[22] M. Gatalo *et al.*, “Comparison of Pt–Cu/C with Benchmark Pt–Co/C: Metal Dissolution and Their Surface Interactions,” *ACS Applied Energy Materials*, vol. 2, no. 5, pp. 3131–3141, Apr. 2019, doi: https://doi.org/10.1021/acsaem.8b02142.

[23] A. A. Topalov, S. Cherevko, A. R. Zeradjanin, J. C. Meier, I. Katsounaros, and K. J. J. Mayrhofer, “Towards a comprehensive understanding of platinum dissolution in acidic media,” Chem. Sci., vol. 5, no. 2, pp. 631–638, 2014, doi: https://doi.org/10.1039/c3sc52411f.

[24] M. Schalenbach *et al.*, “Nickel-molybdenum alloy catalysts for the hydrogen evolution reaction: Activity and stability revised,” *Electrochimica Acta*, vol. 259, pp. 1154–1161, Jan. 2018, doi: https://doi.org/10.1016/j.electacta.2017.11.069.

[25] F. D. Speck, A. Zagalskaya, V. Alexandrov, and S. Cherevko, “Periodicity in the Electrochemical Dissolution of Transition Metals,” *Angewandte Chemie International Edition*, vol. 60, no. 24, pp. 13343–13349, May 2021, doi: https://doi.org/10.1002/anie.202100337.

Electrolysis induced simultaneous hydrogen and ammonia production from high concentration urea solutions

J.C. Chmielarz[1,2], T. Morawietz[*1,3], K.A. Friedrich [1,2]

[1]Institute of Engineering Thermodynamics, German Aerospace Center (DLR), Pfaffenwaldring 38/40, 70569, Stuttgart, Germany
[2]Institute for Building Energetics, Thermotechnology and Energy Storage (IGTE), University of Stuttgart, Pfaffenwaldring 31, 70569, Stuttgart, Germany
[3]Faculty of Science, Energy and Building Services, Esslingen University of Applied Sciences, Kanalstraße 33, 73728, Esslingen am Neckar, Germany

Introduction

The driving force of research in this area is fueled by the environmental impact of NOx pollution, caused by the transport sector emissions. In particular, diesel engine exhaust gasses are a major contributor, amounting to over 50 % to the total NOx emissions [1]. Despite growing efforts in legislation [2] and technology advancements for NOx aftertreatment [3], the so-called cold start remains a concern that has not yet been addressed sufficiently. The problem is especially prominent during the running of a cold engine, when the passenger car emits approximately 10 - 18 times more NOx than it is foreseen as per Euro6 limit [4]. This is directly caused by the operating temperatures of the exhaust gas aftertreatment (EGA) of the NOx selective catalyst (SC). Currently, the NOx conversion happens at temperatures between 200 - 400 °C [5], often not reached during urban driving conditions. To lower the SC effective temperature range below 200 °C, and simultaneously increase the catalyst NOx conversion rate, we propose implementing a small, onboard electrolyzer, supporting the EGA with H2-deNOx system, enabling efficient SC operation between approximately 100°C and 200°C. Our solution aims to produce both ammonia and hydrogen that would be mixed in with the exhaust gasses at specific points of the catalyst units, to aid NOx emission reduction during cold engine periods e.g. congested city driving. The working principle of H2-deNOx is shown in Figure 1.

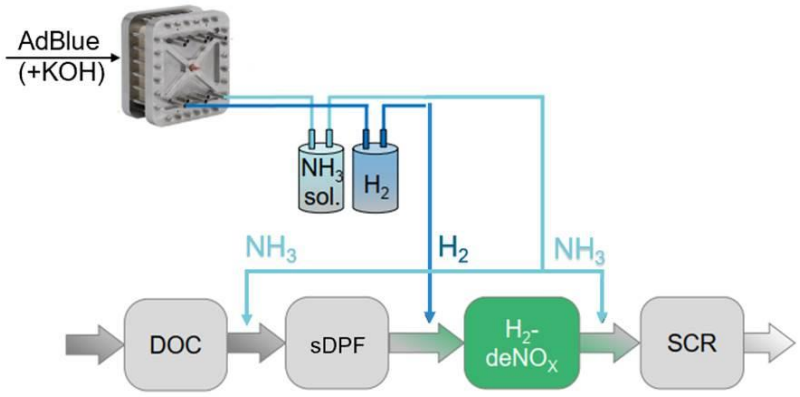

Figure 1. Schematic of the H2-deNOx system integration into the existing exhaust gas aftertreatment line.

The objective of this research is to simultaneously produce hydrogen and ammonia via electrolysis of high concentration urea solutions. The most straightforward option for the

* Corresponding author: tobias.morawietz@dlr.de

electrolyte is an already existing source of urea rich solution in the car - diesel exhaust fluid (DEF), also known as AdBlue.

A vast majority of the research in the urea electrolysis sector is focused on hydrogen production from low urea concentration e.g. wastewater, due to overpotential reduction compared to water electrolysis [6] [7]. However, the urea oxidation reaction leads to nitrogen and carbon-dioxide production at the anode, whereas in our case, we aim for a pathway to create ammonia. The feasibility of urea hydrolysis to ammonia has been first reported by G. Botte et.al., in 2015, where they introduced a novel electrochemically induced method for ammonia synthesis from urea (eU2A) [8]. Later, in 2017, they proposed the responsible electrochemical mechanisms of eU2A and pointed out that catalyst conversion from Ni^{2+} to Ni^{3+} directly enables the urea hydrolysis reaction [9]. These findings establish a foundation for investigating electrochemically induced production of ammonia from urea.

Methodology

After conducting literature research, the main boundary conditions were identified. Specifically, it was found that a Nickel-based anode catalyst is required for urea decomposition into ammonia, and the OH^- transfer must be provided, which can be facilitated through the use of an AEM. Another viable method for generating ammonia via urea electrolysis supported hydrolysis involves the use of a bipolar membrane. Layering membrane electrode assemblies consisting of a proton exchange membrane and an anion exchange membrane might offer a promising approach to investigate as a competing technique against an AEM electrolyzer, with the aim of diminishing the overpotential of water splitting. Additionally, ammonia production is influenced by parameters such as temperature, voltage of the cell, and the pH of the electrolyte. We will methodically elucidate each step involved in creating a functioning cell that produces sufficient amounts of ammonia and hydrogen for use in the NOx selective catalyst.

Initially, we carried out catalyst screening using a rotating disc electrode (RDE) setup for specific Ni-based catalysts with different electrolytes at room temperature. The catalyst inks consistently contained 20 wt.% of Nafion ionomer to ensure proper particle binding, however, solvent ratios were adjusted, when required, for optimal catalyst dispersion. The samples were electrochemically analysed under nitrogen purging conditions in pure AdBlue, AdBlue + 0.1 M KOH, AdBlue + 1 M KOH, and 1 M KOH.

Subsequently, we focused on electrode preparation and its implications for the cell performance. The electrodes were prepared via airbrush spraying of the catalyst ink and its deposition on either a membrane, creating a catalyst coated membrane (CCM), or on a porous substrate, making a catalyst coated substrate (CCS). It needed to be recognised, that when creating a CCM on an AEM, the temperature during spraying had to be close to atmospheric, to prevent the ionomer degradation. This led to alcohol-based ink compositions with low water content allowing for faster evaporation and preventing the membrane swelling. Moreover, further parameters of electrode preparation had to be investigated, such as ink water content, catalyst deposition temperature, hot pressing, ionomer content at the anode and cathode, and lastly ionomer layering in the catalyst layer. All these parameters have a direct impact on performance, creating different catalyst nanostructures.

In order to qualitatively compare the performance of prepared electrodes, a single cell electrolysis testbench was used with an active surface area of 4 cm^2. For this, all testbench operating parameters like temperature and flow were fixed, only the working electrolyte could be replaced. Additionally, only standard (reference at DLR) stainless steel components were used for the bipolar plates and PTLs, Spectacarb 2050A-1050 carbon paper was used on the

cathode side of the membrane electrode assembly (MEA), and a nickel sintered metal fibre felt from Bekaert type 2Ni06-020 was used on the anode side of the MEA. All reference cells had been compressed with the same torque allowing comparability. For further standardisation purposes, we created cell activation protocols and defined specific points for representable performance measurements. This way optimum ink loading and electrode preparation techniques were defined. The same methodology was used for a comparative performance measurements of additional cell functional elements such as AEM kind and thickness (various companies), BPP material, PTL structure and material. The existing setup was enhanced by a reference hydrogen electrode (RHE) – 3 electrode setup, allowing for a separate electrochemical characterisation of cell' anode and cathode. The aim of such analysis is to define the influence of the anodic and cathodic catalysts independently.

As previously mentioned, a bipolar membrane (BPM) can be employed in a urea electrolyser to produce ammonia and hydrogen. Based on the anode MEA results from the AEM characterisation, and the PEM water electrolysis state of the art for cathode, we will try to optimise the interlayer. For a comparative BPM characterisation, a single cell setup will be employed again. Finally, to compare the viability of BPM against AEM urea electrolyser, the most promising cell setups will be further optimised individually by controlling the anode and cathode electrolyte flow as well as setting the maximum possible compression (functional materials dependent). Additionally, we will use a differential electrochemical mass spectrometry (DEMS) technique to link the performance results with ammonia production capabilities of promising cells.

Discussion

Through RDE tests, we discovered that pure Nickel is an extremely active catalyst for pure AdBlue. This was also observed in the single cell electrolysis testbench with nickel functional components. Nevertheless, after the cell was disassembled, it became apparent that nickel oxidation had occurred not only at the catalyst but also on the anode PTL and anode BPP, resulting in erosion marks and structural damage of the cell. The findings suggest that for pure AdBlue operation, nickel components should be avoided within the electrolysis cell, and instead stainless steel could be used. However, if KOH is added to the electrolyte, significant prevention of nickel oxidation of the anode side BPP and PTL is observed in solutions starting from 0.1 M KOH + AdBlue. Furthermore, NiFe catalysts demonstrate superior performance in comparison to Ni catalysts once the pH level is raised above ca. 9 pH (AdBlue) to ca. 13 pH.

Due to the corrosive nature of potassium hydroxide, it is advisable to avoid high concentrations of the substance in the final use case. One potential solution is the implementation of a bipolar membrane, which could reduce the concentration of potassium hydroxide without compromising the current density. Another option could be to use an immobilised KOH electrolyte, such as a poly gel electrolyte [10]. This method offers inherent system safety benefits and is therefore a viable option to consider.

In addition, the single cell tests performed in a three-electrode setup have revealed that high overpotential stems from both the anode and the cathode. Therefore, making it necessary to optimise the cathode membrane-electrode assembly, including catalyst selection. To date, we have compared the platinum-based catalyst with NiFe or MoCa, with the latter displaying best performance so far. It is possible that platinum-based hydrogen evolving catalyst for urea electrolysis may not be the most effective choice. In forthcoming studies, we will assess the activity and stability of selected cathode catalysts.

Conclusions

The trend toward powertrain hybridization lowers engine temperatures and increases cold-running characteristics, making it unsuitable for exhaust aftertreatment with existing SCR-systems. To counteract this, the introduction of an onboard electrolyzer capable of producing hydrogen and ammonia is proposed. Via a H2-deNOx, the conversion of NOx to N2 and water can be performed at temperatures as low as 80 °C. This technology foresees the use of DEF as a urea-rich electrolyte, providing a safe and energy-efficient solution that can be easily integrated into existing exhaust lines. In addition, deposits are counteracted by the non-direct injection of DEF.

The initial single cell results show a high overvoltage originating from both the anode and cathode reactions, as well as a rapid degradation rate that depends on the electrolyte and operating conditions. Based on the research results at the MEA and cell levels, a number of improvements are proposed and will be investigated experimentally in the future. Consequently, further performance improvement should be pursued, as well as the development of an operation strategy aimed at stable operation. In addition, the use of the bipolar membrane for hydrogen and ammonia production from urea has been successfully investigated. Future steps of BPM optimization will include interlayer design and AEM-PEM assembly techniques. Functional BPM would allow reduction of KOH concentration.

References

[1] International Energy Agency, „Emissions of Nitrogen oxyde (NOx) by sector and scenario, 2015 and 2040,“ 2018. [Online]. Available: : https://www.iea.org/data-and-statistics/charts/emissions-of-nitrogen-oxyde-nox-by-sector-and-scenario-2015-and-2040, IEA. Licence: CC BY 4.0.

[2] European Comission, „Commission proposes new Euro 7 standards to redue pollutant emissions from vehicles and improve air quality,“ 10 Nov. 2022. [Online]. Available: https://ec.europa.eu/commission/presscorner/detail/en/ip_22_6495..

[3] B. Choi, K. Lee and G. Son, “Review of Recent After-Treatment Technologies for De-NOx Process in Diesel Engines.,” *Int.J Automot. Technol. 21,* p. 1597–1618, 2020.

[4] C. Weber, I. Sundvor and E. Figenbaum, “Comparison of regulated emission factors of Euro 6 LDV in Nordic temperatures and cold start conditions: Diesel- and gasoline direct-injection,” *Atmospheric Environment, vol. 206,* pp. 208-217, 2019.

[5] V. Praveena and M. L. J. Martin, “A review on various after treatment techniques to reduce NOx emissions in a CI engine,” *Journal of the Energy Institute, vol. 91, issue 5,* pp. 704-720, 2018.

[6] X. Sun und R. Ding, „Recent progress with electrocatalysts for urea electrolysis in alkaline media for energy-saving hydrogen production,“ *Catal. Sci. Technol.,* pp. 10, 1567-1581, 2020.

[7] K. S. Anuratha, M. Rinawati, T.-H. Wu, M.-H. Yeh and J.-Y. Lin, “Recent Development of Nickel-Based Electrocatalysts for Urea Electrolysis in Alkaline Solution,” *Nanomaterials, vol. 12, no. 17,* p. 2970, Aug. 2022.

[8] F. Lu and G. Botte, “Electrochemically Induced Conversion of Urea to Ammonia,” *ECS Electrochemistry Letters 4 E5,* 2015, DOI 10.1149/2.0041510eel.

[9] F. Lu and G. Botte, “Understanding the Electrochemically Induced Conversion of Urea to Ammonia Using Nickel Based Catalysts,” *Electrochimica Acta, Vol. 246,* pp. 567-571, 2017.

[10] R. L. King and G. G. Botte, “Hydrogen production via urea electrolysis using a gel electrolyte,” *Journal of Power Sources, Volume 196, Issue 5,* pp. 2773-2778, 1 March 2011.

Electrospinning of polybenzimidazoles: a new approach for the obtainment of non-fluorinated membranes for Fuel Cells applications

Emmanuel De Gregorio [*1,2], Carlo De Luca[3], Alessio Occhicone[2], Giuseppina Roviello[2], Claudio Ferone[2], Oreste Tarallo[3], Viviana Cigolotti[1], Elio Jannelli[2], Luis Alexander Hein[4], Alfonso Pozio[1]

[1] Laboratory for Energy Storage, Batteries and Hydrogen Production and Utilization Technologies, Department of Energy Technologies and Renewable Sources, ENEA—Italian National Agency for New Technologies, Energy and Sustainable Economic Development

[2] University of Naples "Parthenope", Department of Engineering, Centro Direzionale, Isola C4, 80143 Naples, Italy

[3] University of Naples "Federico II", Department of Chemical Sciences, Complesso Universitario di Monte Sant'Angelo, 80126 Naples, Italy

[4] NANOFABER srl, Via Anguillarese 301, 00123, Roma

Introduction

High-temperature fuel cells, HTFCs, membranes mainly consist of polybenzimidazoles (PBI), a basic polymer characterised by an aromatic structure and the presence of a aminated group, which is mainly involved in the proton conduction mechanism. The synthesis reaction for this material was developed in the 1960s and consists of a condensation polymerization process between 3,3'-diaminobenzidine and terephthalic acid. Over the past 10 years, PBI has been widely studied and used due to its ability to interact with strong acids [1]. For this reason, PBI membranes are generally 'doped' with appropriate molecules and/or fillers in order to achieve better performance than Low Temperature Fuel Cells (LTFCs) materials. The impregnation of PBI in phosphoric acid (PA) is the technique mainly used for HTFCs as it makes the material ductile and highly conductive. The acid serves as a proton carrier, facilitating the proton hopping within the membrane, which is crucial for the functioning of the cell [2]. Nowadays, PBI is commercially available as a membrane obtained by a cast solvent method. However, solution-cast phosphoric acid-doped PBI proton exchange membranes have some disadvantages that can negatively affect their long-term durability and performance, including (a) high acid adsorption, which can lead to swelling reducing mechanical stability [1]; (b) a difficult production process, as solution casting requires hazardous solvents and careful control of the production and drying processes to achieve a uniform thickness; (c) mechanical fragility. In order to contribute to the development of efficient and durable phosphoric acid-doped PBI-based Proton Exchange Membranes (PEM) with improved performances, in this contribution we want to explore the characteristics and properties of membranes obtained using the electrospinning technique.

Corresponding author: emmanuel.degregorio001@studenti.uniparthenope.it

These new electrospun membranes could provide several advantages compared to those obtained by solvent casting. In particular, electrospinning could allow precise control of membrane morphology and thickness: by adjusting parameters such as polymer concentration, solvent composition, and electrospinning conditions, the membrane's fiber diameter, pore size, and overall structure can be tailored to specific requirements. Moreover, electrospun membranes could offer a significantly larger surface area compared to conventional casting methods, thus facilitating the impregnation and retention of phosphoric acid, which is essential for the proton conduction mechanism. Finally, electrospinning will allow the creation of a highly interconnected network of ultrafine fibres, typically in the nanometer range [3]. This will result in a high surface area-to-volume ratio, which will promote efficient proton conduction through the membrane. This morphology will also result in improved mechanical properties of the material, as the fibrous structure, with aligned and/or interconnected fibres, will provide high tensile strength and good flexibility, ensuring the integrity of the membrane during operation. Starting from these materials, it is possible to develop a mathematical Design of Experiment (DOE) model from which a correlation between the various electrospinning parameters could be noticed, selecting the most influential one in the entire process. This model can be coupled with an Analysis of Variance (ANOVA regression), which gives a clear idea of which factors most affect the production of these materials.

Methodology

Electrospinning is an electro-fluid-dynamic process in which a drop of liquid is electrified to generate a jet which, subjected to various stretching processes, is stretched to generate fibers. A classic experimental setup for electrospinning tests includes a high-voltage power supply, a syringe pump, an ejector (usually a hypodermic needle with a blunt tip) and a conductive collector. The power supply can be either a direct current or an alternating current. During electrospinning, the liquid is extruded from the needle to produce a pendant drop as a result of surface tension. Upon electrification, the electrostatic repulsion between surface charges having the same sign deforms the droplet into a Taylor cone, from which a charged jet is ejected. The jet initially develops in a straight line and then undergoes vigorous lashing movements due to bending instabilities. As the jet is stretched into finer diameters, it rapidly solidifies, leading to the deposition of solid fibers on the manifold. In general, the electrospinning process can be divided into four consecutive stages:

- Electrification of the liquid droplet and formation of the Taylor cone;
- Extension of the charged jet along a straight line;
- Thinning of the jet in the presence of an electric field and growth of the electric bending instability (whipping instability);
- Solidification and collection of the jet as solid fibers on a manifold [4].

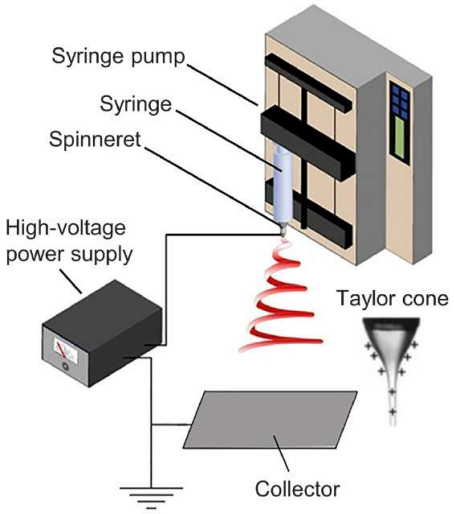

Figure 1 - Experimental setup of the electrospinning technique

Polybenzimidazole (poly-[2,2-(m-phenylene)-5,5-bibenzimidazole]) (PBI) based membranes have received wide attention, as they are capable of increasing temperature tolerance compared to materials conventionally used in PEM Fuel Cells systems; this is due to the excellent chemical and thermal stability of PBI. The fabrication of electrospun PBI nanofibres was first reported by Kim et al. [5] and, over the past few years, has been improved and further implemented. Specifically, the effect of polymer concentration and process parameters on the morphology and size of PBI nanofibres has been examined. Through a software elaboration, it was possible to define the mathematical model that most closely matched the experimental data. Starting from this model, it was possible to understand the main interactions between the different factors.

Discussion

Starting from a commercial PBI solution (S26, PBI Product©, Charlotte, US), several polymer solutions have been obtained at different concentrations by dilution in dimethylacetamide (DMAc). The modulation of operating parameters such as voltage, flow rate, needle-collector distance, temperature, and relative humidity (RH) made it possible to obtain several membrane specimens, whose morphology was studied by Scanning Electron Microscopy (SEM) (Fig.2).

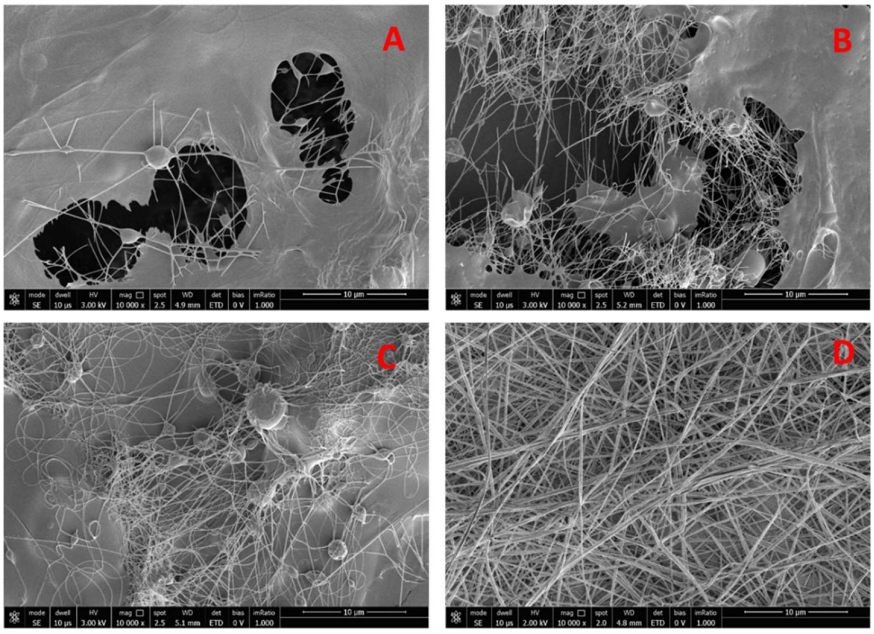

Figure 2 – Nano fibrous structure evolution by varying Voltage (V), Temperature (T) and Humidity (RH): A) V= 20kV; T=25°C; RH=36% - B) V= 15kV; T= 35°C; RH=25% - C) V=20 kV; T= 40 °C; RH= 26% - D) V=20 kV; T=45 °C; RH=20%

The performed tests, despite being very preliminary, already show the influence of the explored operating parameters on the structure of the membrane. It is possible to note a strong correlation between the morphological characteristics of the membranes and the temperature and humidity at which the experiment was conducted. At room temperature (25°C) and humidity (36%), PBI does not present a well-defined fibrous structure, indeed, the polymer chains are agglomerated in clusters due to poor evaporation of the solvent. Instead, tests carried out at higher temperatures (between 35 and 45 °C) and variable humidity (20-26%) show an incipient fibrous structure with fiber diameters varying in the nanometer range. However, a discontinuous structure is evident, which can be attributed to the high viscosity of the polymer solution and, consequently, the different behavior of the fluid in the electrification process.

It is worth pointing out that from a preliminary DOE analysis, it is already possible to identify the main parameters influencing the electrospinning process. In Figure 3a, the interaction between temperature and humidity is visible from the intersection of the straight line referring to the effects derived from the developed mathematical model. This model was made starting from the SEM images of the samples and presents as output the average fiber diameter obtained for each test. Figure 3b shows the quasi-linear trend for the residual distribution of our model as a function of probability. The good agreement between the experimental data and the model's calculated ones returns an R^2 close to unity, defining a good correlation between the various factors. Hence, increasing temperature and varying humidity allow the obtainment of a fibrous structure, which can be further improved through optimization of the operating parameters.

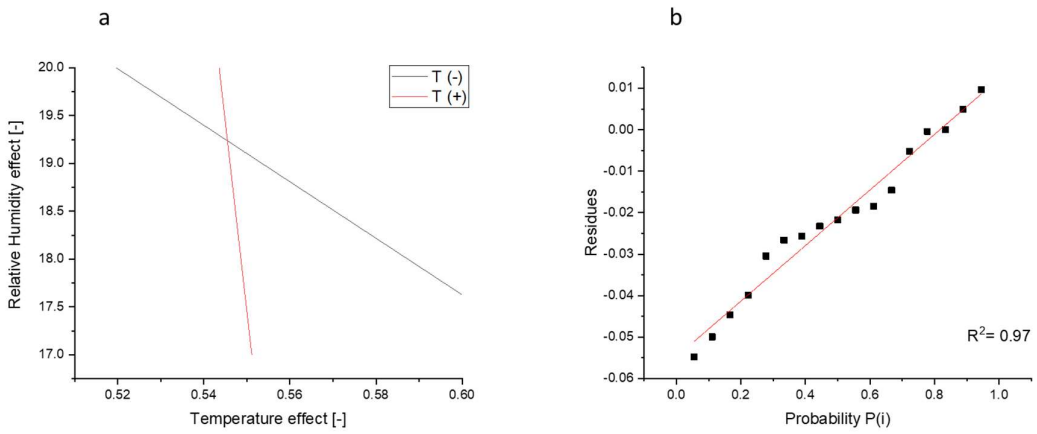

Figure 3 –Influence of temperature and humidity (a) and residue distribution (b)

Conclusions

A preliminary DOE analysis aimed at understanding the main parameters influencing the electrospinning process has been performed. Further optimization of the experimental conditions for the obtainment of PBI fibers will be performed by using the DOE approach and the ANOVA statistical regression, to identify the main process parameters that influence the chemical and morphological characteristics of the desired material. Afterwards, the resulting materials will be doped with phosphoric acid and their electrochemical properties will be tested through proton conductivity and impedance analysis (EIS), comparing their performance with that of commercially used PBI membranes.

References

[1] «EFFECT OF CELL SIZE IN METAL FOAM INSERTED TO THE AIR CHANNEL OF POLYMER ELECTROLYTE MEMBRANE FUEL CELL FOR HIGH PERFORMANCE»,

doi: ttps://doi.org/10.1016/j.renene.2017.08.085

[2] «ELECTROSPINNING OF NANOFIBERS: REINVENTING THE WHEEL»,

doi: https://doi.org/10.1002/adma.200400719

[3] «CO TOLERANCE IN PBI/H_3PO_4 POLYMER ELECTROLYTE FUEL CELLS»,

doi: 10.1149/200231.0440PV

[4] «ADVANCES IN THREE-DIMENSIONAL NANOFIBROUS MACROSTRUCTURES VIA ELECTROSPINNING»,

doi: https://doi.org/10.1016/j.progpolymsci.2013.06.002

[5] «FUEL CELL MEMBRANE CHARACTERIZATIONS»,

doi: https://doi.org/10.1080/15583724.2015.1011275

[6] «FABRICATION AND CHARACTERIZATION OF CROSS-LINKED POLYBENZIMIDAZOLE BASED MEMBRANES FOR HIGH TEMPERATURE PEM FUEL CELLS»,

doi: https://doi.org/10.1016/j.electacta.2017.05.111

[7] «A COMPREHENSIVE REVIEW OF PBI-BASED HIGH TEMPERATURE PEM FUEL CELLS»,

doi: https://doi.org/10.1016/j.ijhydene.2016.09.024

Energetic, Environmental, and Material Criticality Evaluation of Hydrogen Production via Water Electrolysis

Elke Schropp[1] and Matthias Gaderer[1]

[1] Technical University of Munich, Professorship of Regenerative Energy Systems, Schulgasse 16, 94315 Straubing, Germany

Introduction

Climate change is considered one of the most pressing issues facing humanity today. In order to limit climate change, several measures have been taken and green technologies have evolved and developed in the recent decades. One technology that is attracting a lot of interest due to its promising potential to help limit climate change is hydrogen production based on electrolytic water splitting. The importance of electrolytic hydrogen production from water is emphasized by the targets set out in the European Hydrogen Strategy (EHS): as hydrogen via water electrolysis is seen as crucial for carbon neutrality in 2050, 6 GW of water electrolysis capacity is to be installed in the European Union by 2024 and 40 GW by 2030 [1].
Since the first successful attempts at electrolytic water splitting in 1789 [2], many different electrolysis processes have evolved, of which the four technologies shown in Figure 1 are considered the most important.

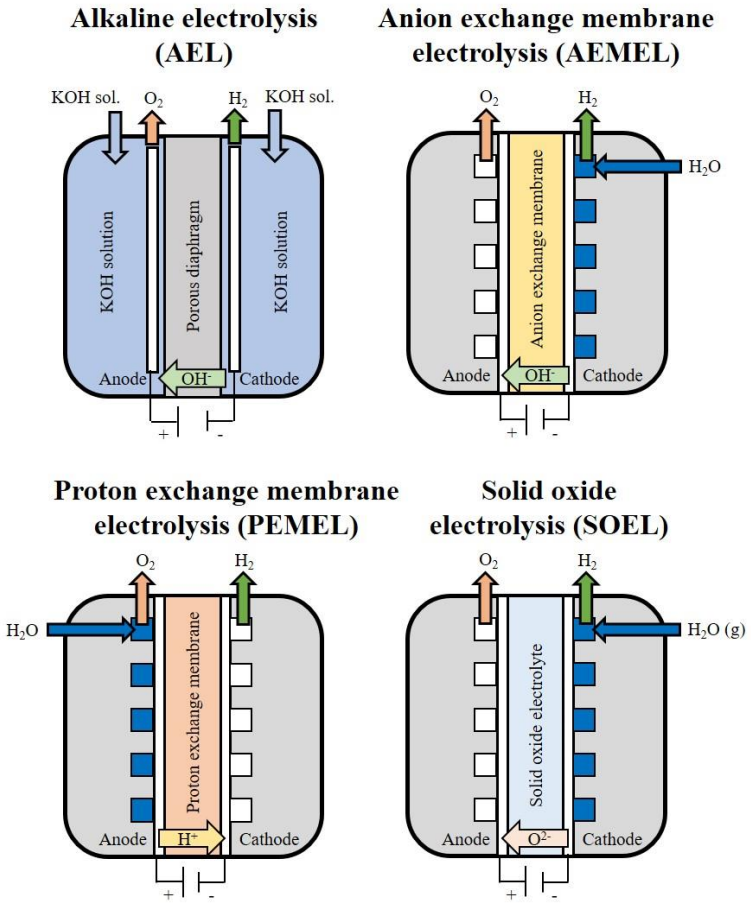

Figure 1: Schematic structure of alkaline electrolysis (AEL), anion exchange membrane electrolysis (AEMEL), proton exchange membrane electrolysis (PEMEL), and solid oxide electrolysis (SOEL); adapted from [2]

These technologies differ in electrolytes, separators, operating temperature and pressure, efficiency, material and more aspects [2]. As mentioned before, the target behind hydrogen production via water electrolysis is to help limit climate change. To achieve this, water electrolysis technologies should produce hydrogen with the least possible impact on climate change. In addition, other environmental impact categories, such as ozone depletion and acidification, must also be considered to avoid burden shifting. To evaluate the main water electrolysis technologies in terms of their holistic environmental performance, a life cycle assessment approach is applied. Due to the transition of the energy supply from a fossil fuel dependent to a materials dependent system, concerns about material criticality are being raised [3]. Therefore, in addition to the environmental performance, the material criticality performance will play an important role in whether or not a technology will prevail.

Methodology

In order to compare different hydrogen production technologies based on water electrolysis in terms of energetic, environmental, and material criticality concerns, assessment methods are introduced in the following section. Finally, the multi-criteria optimization aims to find the most promising technology regarding the afore mentioned criteria, i. e. energy, environment, and material criticality.

1. Energetic Simulation via Mathematical Modeling

Mathematical modeling is a crucial tool to understand the physicochemical processes taking place in water electrolysis cells [4]. Understanding the processes within the electrolysis cell provides the opportunity to analyze the impacts of various parameters, e.g. operating temperature and pressure, on the cells behavior and to optimize energy management, operation conditions, as well as cell shape and size accordingly [5, 6]. From an electrochemical point of view, the behavior of a cell is described by the current-voltage characteristics, where the cell voltage (E_{cell}) is defined as [7]:

$$E_{cell} = E_{rev} + \eta_{act} + V_{ohm} + \eta_{diff}$$

The reversible cell potential (E_{rev}) is the minimum voltage that must be applied to the cell in order to perform electrochemical water splitting, the activation overpotential (η_{act}) represents the activation energies that must be overcome to start the hydrogen evolution reaction and oxygen evolution reaction, respectively, the ohmic voltage losses (V_{ohm}) are caused by electrical resistances of the different cell components, and the diffusion potential (η_{diff}) results from mass transport limitations [7]. These mechanisms define the current-voltage characteristics of the cell and are functions of several parameters, like temperature, pressure, current density, cell configuration, and material characteristics. Such mathematical models are being developed for the major electrolysis technologies to allow evaluation and optimization of operation and comparison of the operating characteristics of the different technologies.

2. Life Cycle Assessment

The aim of the life cycle assessment (LCA) methodology is to assess the environmental impacts of a product along its entire life cycle. This methodology is outlined in DIN EN ISO standards 14040 and 14044 [8, 9] and, according to these standards, comprises four steps: (i) goal and scope definition, (ii) inventory analysis, (iii) impact assessment, and (vi) interpretation. While many different LCA approaches have evolved in the recent years, this work focuses on the prospective life cycle assessment (pLCA) approach. The pLCA method's target is to assess

emerging technologies that are at an early stage of development in order to provide data on the potential environmental impacts in a more distant future when a higher level of technology readiness has been achieved [10]. Due to the immaturity of large-scale hydrogen production technologies and the forward-looking approach, the pLCA's complexity is different compared to conventional LCA, which takes a retrospective view on systems [11]. Concerns associated with pLCA are, for example, lack of data and inherent uncertainties of the technology's development. Nonetheless, insights into the environmental impacts of technologies in early development phases are crucial because these phases have the most degrees of freedom in development [12] and thus the greatest leverage to avoid potential unintended impacts [13].

3. Material Criticality Assessment

In general, material criticality assessment (MCA) evaluates the probability of a supply disruption of a material and the vulnerability of an economic system to this disruption [14]. Due to the transition from a fossil fuel-intensive to a material-intensive energy system, MCA recently attracts wide attention [3]. The growing interest leads to the development of a variety of methodologies and indicators that encompass different assessment levels, temporal scopes, materials, and further aspects such as geopolitical and social concerns. A closer look at the different assessment levels shows that the criticality score of a product, technology, company, country or region, or at a global level can be evaluated using MCA [14].
In this work, the material criticality is assessed using a product-level MCA approach, as it provides information that can guide product development and material selection towards lower criticality [15]. The two product-level MCA methods considered are:

(i) SH2E criticality indicator based on the European Commission MCA framework [16] and developed in the SH2E project [17]: This methodology aims to assign a "unitary supply risk" factor to each material included in the European list of critical raw materials [16], incorporating domestic production as a factor to reduce the supply risk.

(ii) GeoPolRisk Midpoint indicator developed by Gemechu et al. [18] and refined by Santillán-Saldivar et al. [19]: In this method, the supply risk potential of materials is represented in monetary units.

4. Multi-Criteria Optimization

The preceding assessments, i.e. energetic simulation, pLCA, and MCA, provide information on the energetic, environmental, and criticality performance of different electrolysis technologies. Although the results of the technologies in each assessment can be easily compared, a comparison of the individual assessments does not necessarily lead to an overall conclusion which technology is the best in a considered case. A common approach to define the best technology, i.e. the optimum, is to introduce weighting factors for the different objectives in order to sum up the results to a single value that can be subsequently optimized. However, this approach makes it necessary to decide for a set of weighting factors beforehand. Since the choice can be made in many different ways, different sets of weighting factors should be studied in terms of their effects on the results, which makes this approach empirical and iterative in practice. As a result, efforts have been made to develop more systematic and efficient algorithms, multi-purpose numerical tools, and other methods to determine optimal solutions [20].

Discussion

For the four main electrolysis technologies, i.e. AEL, AEMEL, PEMEL, and SOEL, the before mentioned assessments are carried out. The mathematical modeling of the electrolysis technologies provides information on the electrochemical behavior and the current-voltage characteristics, which allows for statements on the efficiency of each technology in certain operation modes and an optimization of operation. Based on this, conclusions can be drawn as to which technology is most efficient in a particular required operation mode, e.g. for space-constrained applications at the highest current densities. However, it is assumed that different technologies are advantageous for different operational conditions and requirements. Aspects that are expected to affect the choice of technology are, for example, the availability of waste heat, the flexibility requirements, the space offer, and safety requirements. Nonetheless, apart from technical aspects, environmental and material criticality effects must be considered in the choice of the most appropriate electrolysis technology in a particular operation mode. These aspects are evaluated using the pLCA and the MCA approach. With the help of pLCA not only the environmental impacts in terms of global warming are assessed, but also a variety of other categories such as ozone layer depletion, water use, and land use are considered. For most categories, the pLCA results show a strong correlation with the impacts associated with the electricity that is fed to the electrolysis. This means that the environmental impacts of hydrogen production based on water electrolysis are strongly dominated by the electricity required for the operation even if it will be operated with renewable energy. However, such a future-oriented pLCA approach incorporates high uncertainty due to many future unknowns, such as the technological development of both electrolysis and electrical power systems. Thus, the evaluation of different scenarios, e.g. representing low, moderate, and high hydrogen market penetration, could give broader insights into potential future developments and their environmental implications. Concerns about material criticality currently exist primarily in the context of PEMEL, as this technology relies on the use of platinum group metals (PGMs), which are now considered particularly critical. Considering a huge expansion of water electrolysis, it is questionable whether PEMEL is the technology of choice, as a massive expansion of PEMEL would be accompanied by a huge increase in PGM demand. This could lead to sharply rising prices, which in turn would make the PEMEL less attractive or would result in a substitution of materials, which would affect the technical performance. However, the material criticality is assessed based on material supply chain as they are nowadays. For a future perspective, information on the future supply situation, e.g. additional supplying countries, changed political situations in the supplying countries, and price development, of the different materials are required. A prospective MCA would be subject to such a high degree of uncertainty that this approach is not being pursued at this time. Another aspect that affects material criticality is recycling of materials as it reduces criticality, in general.

As the brief discussion on results shows, there are several criteria that influence the choice of an optimal electrolysis technology under certain circumstances and that there is not one technology that provides best performance in all considered assessments. Thus, the aim of the multi-criteria optimization is to find the optimum technology, i.e. the technology that provides best comprise considering the before generated energy-, environment- and material criticality-related findings for particular situations. However, depending on the results obtained by the before described assessments, the method for handling the multiple criteria must thoroughly be chosen. Basically, there are two opposing aspects that affect the choice of a method: informative value and computational effort. Considering the intended statements, the method that represents the best compromise between these two aspects must be found. Finally, this allows for statements on which technology is the best considering energetic, environmental, and material criticality belongings under given circumstances.

Conclusions

Hydrogen production based on water electrolysis is considered a key technology in limiting global warming. However, various types of water electrolysis have developed in recent decades, with AEL, AEMEL, PEMEL, and SOEL being the most important technologies today. None of these technologies has yet gained market dominance, and the trend toward any of them is not yet foreseeable. Thus, in this work the four named technologies are evaluated in terms of their energetic, environmental, and material criticality performance. It is not expected that one of these technologies will perform best for all criteria, which is why different technologies represent the optimal solution under different preconditions and requirements. In order to unleash the full potential of each technology, it must be used under suitable conditions. This work presents the respective operation modes with best energetic, environmental, and material-criticality performance for the named technologies. Furthermore, the work shows that the use of certain electrolysis technologies should be avoided under certain circumstances due to unfavorable energetic, environmental, or material-criticality properties. Nonetheless, there are ways to use the different water electrolysis technologies for hydrogen production in such a way that a significant contribution to climate neutrality in 2050 can be expected.

References

[1] European Commission, "Communication from the commission to the European parliament, the council, the European economic and social committee and the committee of the regions: A hydrogen strategy for a climate-neutral Europe," Brussels, 2020. Accessed: Apr. 17 2023. [Online]. Available: https://eur-lex.europa.eu/legal-content/EN/TXT/PDF/?uri=CELEX:52020DC0301&from=EN

[2] M. Chatenet *et al.*, "Water electrolysis: from textbook knowledge to the latest scientific strategies and industrial developments," *Chemical Society reviews*, vol. 51, no. 11, pp. 4583–4762, 2022, doi: 10.1039/D0CS01079K.

[3] International Energy Agency, *The Role of Critical Minerals in Clean Energy Transitions*: OECD, 2021.

[4] L. An, T. S. Zhao, Z. H. Chai, P. Tan, and L. Zeng, "Mathematical modeling of an anion-exchange membrane water electrolyzer for hydrogen production," *International Journal of Hydrogen Energy*, vol. 39, no. 35, pp. 19869–19876, 2014, doi: 10.1016/j.ijhydene.2014.10.025.

[5] *33rd European Symposium on Computer Aided Process Engineering*: Elsevier, 2023.

[6] S. Hu *et al.*, "A comprehensive review of alkaline water electrolysis mathematical modeling," *Applied Energy*, vol. 327, p. 120099, 2022, doi: 10.1016/j.apenergy.2022.120099.

[7] A. Gomez Vidales, N. C. Millan, and C. Bock, "Modeling of anion exchange membrane water electrolyzers: The influence of operating parameters," *Chemical Engineering Research and Design*, vol. 194, pp. 636–648, 2023, doi: 10.1016/j.cherd.2023.05.004.

[8] *Environmental management - Life cycle assessment - Principles and framework: ISO 14040:2006*, 14040, International Organization for Standardization, 2006.

[9] *Environmental management - Life cycle assessment - Requirements guidelines: ISO 14044:2006*, 14044, International Organization for Standardization, 2018.

[10] R. Arvidsson *et al.*, "Environmental Assessment of Emerging Technologies: Recommendations for Prospective LCA," *Journal of Industrial Ecology*, vol. 22, no. 6, pp. 1286–1294, 2018, doi: 10.1111/jiec.12690.

[11] S. M. Moni, R. Mahmud, K. High, and M. Carbajales‐Dale, "Life cycle assessment of emerging technologies: A review," *Journal of Industrial Ecology*, vol. 24, no. 1, pp. 52–63, 2020, doi: 10.1111/jiec.12965.

[12] N. Thonemann, A. Schulte, and D. Maga, "How to Conduct Prospective Life Cycle Assessment for Emerging Technologies? A Systematic Review and Methodological Guidance," *Sustainability*, vol. 12, no. 3, p. 1192, 2020, doi: 10.3390/su12031192.

[13] S. A. Miller and G. A. Keoleian, "Framework for analyzing transformative technologies in life cycle assessment," *Environmental science & technology*, vol. 49, no. 5, pp. 3067–3075, 2015, doi: 10.1021/es505217a.

[14] D. Schrijvers *et al.*, "A review of methods and data to determine raw material criticality," *Resources, Conservation and Recycling*, vol. 155, p. 104617, 2020, doi: 10.1016/j.resconrec.2019.104617.

[15] A. Cimprich *et al.*, "Raw material criticality assessment as a complement to environmental life cycle assessment: Examining methods for product‐level supply risk assessment," *Journal of Industrial Ecology*, vol. 23, no. 5, pp. 1226–1236, 2019, doi: 10.1111/jiec.12865.
[16] European Commission, "Study on the Critical Raw Materials for the EU 2023 - Final Report," 2023. Accessed: Apr. 26 2023. [Online]. Available: https://single-market-economy.ec.europa.eu/system/files/2023-03/Study%202023%20CRM%20Assessment.pdf
[17] E. Bargiacchi *et al.*, "D2.2 Definition of FCH-LCA guidelines: SH2E project," 2022.
[18] E. D. Gemechu, C. Helbig, G. Sonnemann, A. Thorenz, and A. Tuma, "Import-based Indicator for the Geopolitical Supply Risk of Raw Materials in Life Cycle Sustainability Assessments," *Journal of Industrial Ecology*, vol. 20, no. 1, pp. 154–165, 2016, doi: 10.1111/JIEC.12279.
[19] J. Santillán-Saldivar, E. Gemechu, S. Muller, J. Villeneuve, S. B. Young, and G. Sonnemann, "An improved resource midpoint characterization method for supply risk of resources: integrated assessment of Li-ion batteries," *Int J Life Cycle Assess*, vol. 27, no. 3, pp. 457–468, 2022, doi: 10.1007/s11367-022-02027-y.
[20] M. Bortz *et al.*, "Multi-criteria optimization in chemical process design and decision support by navigation on Pareto sets," *Computers & Chemical Engineering*, vol. 60, pp. 354–363, 2014, doi: 10.1016/j.compchemeng.2013.09.015.

Enhanced Hydrogen Storage in Modified Carbon Nanotubes: A first-principles study

Shima Rezaie*[1], Azahara Luna-Triguero[2]

[1]Energy Technology, Department of Mechanical Engineering, Eindhoven University of Technology, P.O. Box 513, 5600 MB Eindhoven, The Netherlands.
[2]Eindhoven Institute for Renewable Energy Systems (EIRES), Eindhoven University of Technology, PO Box 513, Eindhoven 5600 MB, The Netherlands.

Introduction

The increase in global energy demand along with the pollution caused by the use of fossil fuels has sent a clear message to use a clean and renewable energy source. The use of hydrogen gas along with other renewable energy sources such as solar and wind energy is the most promising way to provide sufficient energy [1]–[3]. Hydrogen is the most abundant element on earth, which can achieve a maximum efficiency of about 65% in fuel cells. This amount is higher than gasoline (22%), diesel (45%) and other fossil fuels. In addition, hydrogen is a non-toxic energy source that does not emit any CO_2 upon combustion. Water vapor and heat are the only byproducts of burning hydrogen [4].
The most significant limitation of using hydrogen is finding a safe and cheap way to store hydrogen gas. Among all proposed methods for storing hydrogen gas, using nanomaterials as a substrate for storing hydrogen molecules is the most promising method [5], [6]. Although different kinds of nanomaterials, such as metal-organic frameworks, zeolites, and covalent organic frameworks, have been used for hydrogen storage applications, they have failed to meet the expectations of the Department of Energy of US (DOE) [7]–[10]. In this regard, carbon nanotubes (CNTs) have been used for hydrogen storage applications due to their unique properties such as large surface area, lightweight, and the ability to work at room temperature [11]–[13]. The most important problem of CNTs is the weak interaction between hydrogen gas and the surface of CNTs. In general, CNTs are not able to adsorb hydrogen molecules in the range defined by the DOE (0.15-0.6 eV). Surface modification of these amazing structures can solve the problem of weak binding energy [14]–[16].
In the present work, surface modification of CNTs with different types of impurities has been investigated as a promising method for solving the hydrogen storage problem of CNTs. Using impurities not only solved the binding energy problem but also increased the gravimetric capacity to the value defined by the DOE (5.5 wt%).

Methodology

First principle density functional theory (DFT) implemented in the SIESTA package is used to perform the simulations [17]. The exchange-correlation energy is calculated using the generalized gradient approximation (GGA) formulated by Perdew-Burke-Ernzerhof (PBE) [18]. The Troullier-Martins norm-conserving pseudo-potentials are used to describe the potential of atomic cores and related core electrons with valence electrons. The basis wave functions are expanded over a set of numerical atomic orbitals (NAOs) at the level of

* s.rezaie@tue.nl

double-ζ plus polarization (DZP). The Hellmann-Feynman theorem is used for all atomic relaxation coordinates by minimizing the forces on individual atoms down to less than 0.03 eV/Å. The van der Waals interaction has been considered through the Grimme dispersion potential. Moreover, real space mesh cut-off energy of 150 Ry is chosen. The Brillouin zone is sampled by a 4×4×4 k-points grid under the Monkhorst-pack scheme.
The average binding energy per hydrogen molecule has been calculated using Eq. (1):

$$E_b\,(H_2) = \left[\frac{E_{tot(doped-CNT)} + E_{tot(iH_2)} - E_{tot((doped-CNT)+iH_2)}}{i}\right], \quad (1)$$

where $E_{tot(doped-CNT)}$ is the total energy of the host structure per unit cell, $E_{tot(iH_2)}$ denotes the total energy of *i* hydrogen molecules, $E_{tot((doped-CNT)+iH_2)}$ indicates the total energy of the i adsorbed hydrogen molecules on the surface of the doped carbon nanotube per unit cell.
Mulliken charge transfer analysis is used to calculate the charge transfer between hydrogen molecules and the surface of doped-CNT:

$$q_t = q_{(ads-H_2)} - q_{(iso-H_2)}, \quad (2)$$

where $q_{(ads-H_2)}$ indicates the total charge of the adsorbed hydrogen molecule and $q_{(iso-H_2)}$ is the total charge of the isolated hydrogen molecule.
Moreover, Van 't Hoff's equation is used to calculate the desorption temperature of hydrogen molecules on the surface of nAu-CNT [19]:

$$T_d = \frac{E_{ads}}{k_B}\left(\frac{\Delta S}{R} - \ln p\right)^{-1}, \quad (3)$$

where E_{ads}, k_B, ΔS, R, and p represent the average adsorption energy per hydrogen molecule, the Boltzmann constant, the experimentally reported standard molar entropy change at 298 K [70], the gas constant, and the atmospheric pressure, respectively.
In addition, the following equation is applied to compute gravimetric storage capacity of doped-CNT:

$$wt\ \% = \frac{i\,W_{H_2}}{i\,W_{H_2} + W_{(doped-CNT)}} \times 100, \quad (4)$$

here i is the number of adsorbed hydrogen molecules, W_{H_2} the molecular weight of the hydrogen molecule, and $W_{(doped-CNT)}$ is the molecular weight of the doped-CNT.

Discussion

1- Since pure CNTs cannot meet DOE's expectations for hydrogen storage applications, modification of these amazing structures has been introduced as an effective method to improve the performance of CNTs for hydrogen storage applications. Initially, about 29 different impurities are added to the surface of single and double-walled CNTs. After the relaxation of the doped CNTs structures, the binding energy between different impurities and the surface of single and double-walled CNTs has been calculated (Figure 1 (a) and (c)). The purple region shows the acceptable range of binding energy (above 0.5 eV) of different impurities to the surface of CNTs. In the second step, a hydrogen molecule has been added to the doped single and double-walled CNTs. The

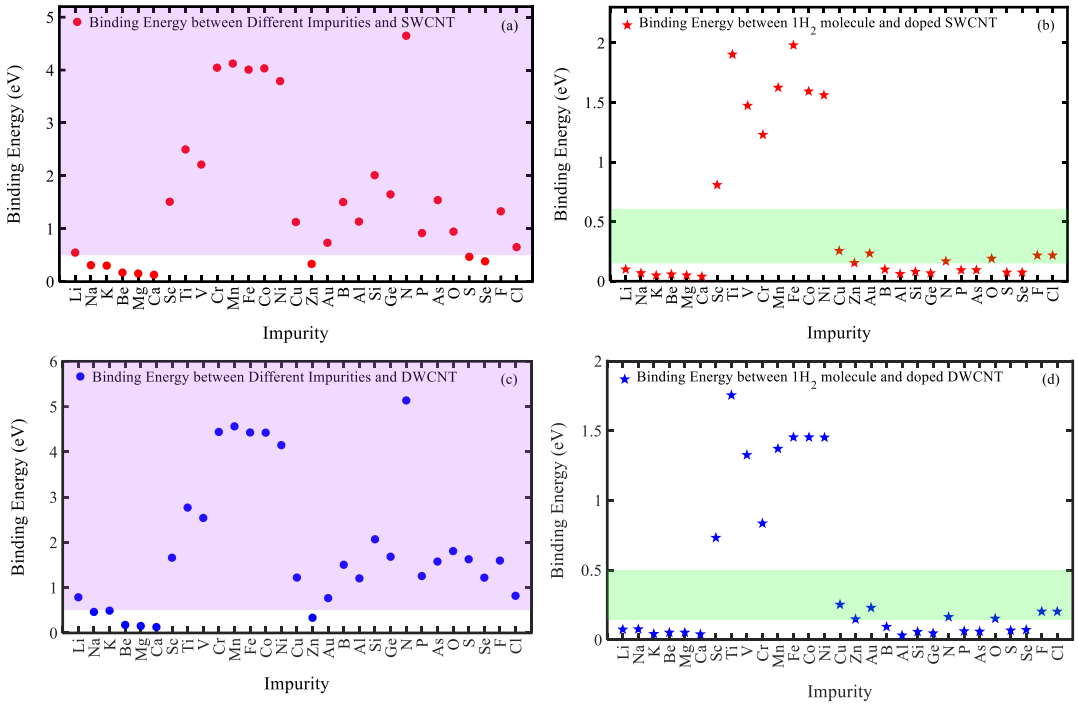

Figure 1: (a), (c) Binding Energy between different impurities and the surface of single and double-walled CNT. (b), (d) Binding energy between a hydrogen molecule and the surface of doped single and double-walled CNT.

binding energy between a hydrogen molecule and the surface of doped CNTs has been shown in Figure 1 (b) and (d). The green region shows the acceptable range for hydrogen binding energy defined by the DOE (between 0.15 to 0.6 eV). Among all impurities, amazing results have been obtained by adding copper and gold to the surface of CNTs. Therefore, these two impurities have been deeply investigated to earn as much information as needed.

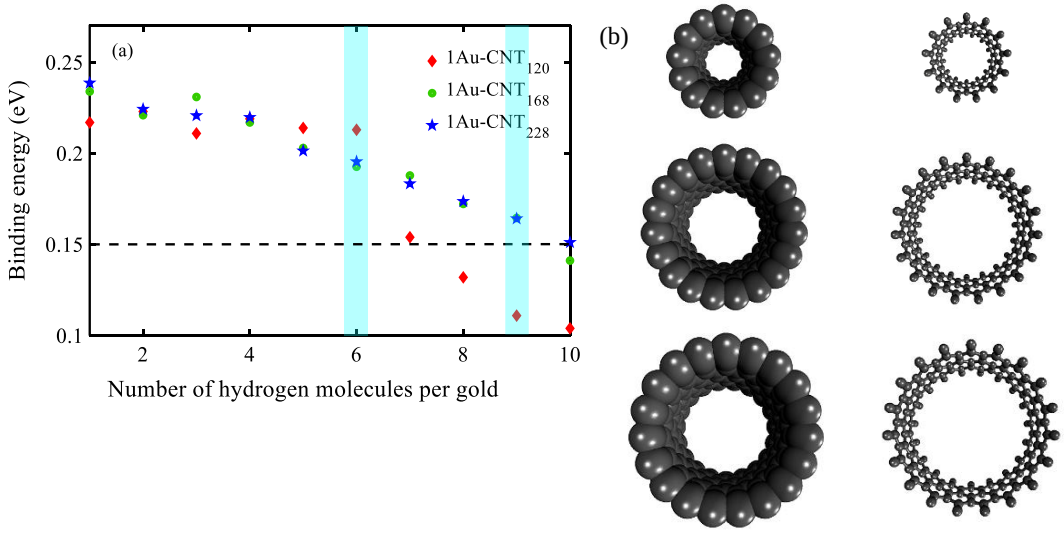

Figure 2: (a) Binding energy between hydrogen molecules and the surface of 1Au-CNTs (dashed line: the lower boundary of binding energy as defined by DOE). (b) Schematic representation of three zigzag CNT nanostructures.

2- Schematic representation of zigzag CNTs along with binding energies between hydrogen molecules and the surface of doped-CNTs are shown in Figure 2 and Figure 3.

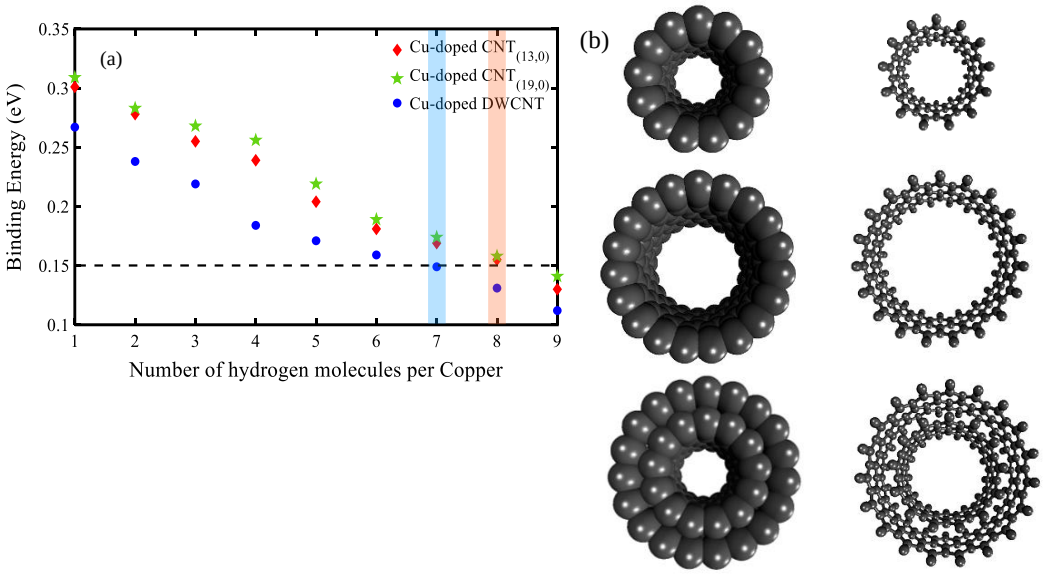

Figure 3: (a) Binding energy between hydrogen molecules and the surface of 1Cu-CNTs (dashed line: the lower boundary of binding energy as defined by DOE). (b) Schematic representation of three zigzag CNT nanostructures.

3- The distribution of charge in pure, doped CNT, and doped CNT after the adsorption of eight hydrogen molecules has been shown in Figure 4. As shown in Figure 4, the charge is uniformly distributed in pure CNT. After adsorbing eight hydrogen molecules to the surface of the doped CNT, the distribution of charge is completely changed, especially around the doping.

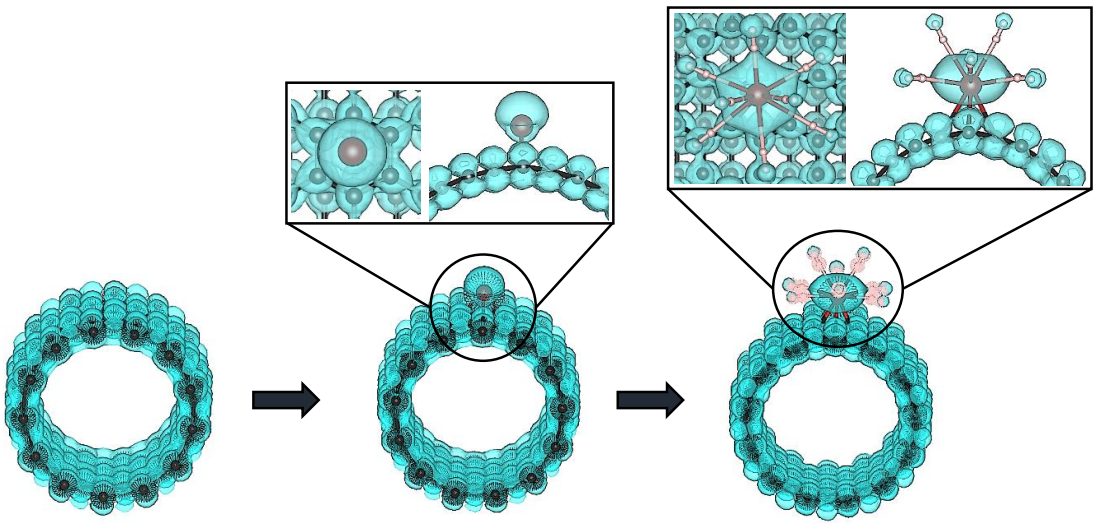

Figure 4. LDOS of pure, doped, and doped $CNT_{(13,0)}$ after adsorbing eight hydrogen molecules.

Conclusions

In the present work, the effect of adding doping to the surface of CNTs on hydrogen storage properties has been investigated using density functional theory (DFT). The calculation results show that the addition of gold and copper impurities to the surface of CNTs creates empty states on the surface of these structures that can be filled by electrons and enhance the adsorption of hydrogen.

References

[1] S. Sharma, S. Basu, N. P. Shetti, and T. M. Aminabhavi, "Waste-to-energy nexus for circular economy and environmental protection: Recent trends in hydrogen energy," *Science of the Total Environment*, vol. 713, Apr. 2020, doi: 10.1016/j.scitotenv.2020.136633.

[2] J. O. Abe, A. P. I. Popoola, E. Ajenifuja, and O. M. Popoola, "Hydrogen energy, economy and storage: Review and recommendation," *International Journal of Hydrogen Energy*, vol. 44, no. 29. Elsevier Ltd, pp. 15072–15086, Jun. 07, 2019. doi: 10.1016/j.ijhydene.2019.04.068.

[3] D. J. Durbin and C. Malardier-Jugroot, "Review of hydrogen storage techniques for on board vehicle applications," *International Journal of Hydrogen Energy*, vol. 38, no. 34. pp. 14595–14617, Nov. 13, 2013. doi: 10.1016/j.ijhydene.2013.07.058.

[4] S. Niaz, T. Manzoor, and A. H. Pandith, "Hydrogen storage: Materials, methods and perspectives," *Renewable and Sustainable Energy Reviews*, vol. 50. Elsevier Ltd, pp. 457–469, May 30, 2015. doi: 10.1016/j.rser.2015.05.011.

[5] R. Kumar, A. Khan, A. M. Asiri, and H. Dzudzevic-Cancar, "Preparation methods of hydrogen storage materials and nanomaterials," in *Nanomaterials for Hydrogen Storage Applications*, Elsevier, 2021, pp. 1–16. doi: 10.1016/b978-0-12-819476-8.00002-5.

[6] M. Hirscher *et al.*, "Materials for hydrogen-based energy storage – past, recent progress and future outlook," *J Alloys Compd*, vol. 827, Jun. 2020, doi: 10.1016/j.jallcom.2019.153548.

[7] S. H. Sang, H. Furukawa, O. M. Yaghi, and W. A. Goddard, "Covalent organic frameworks as exceptional hydrogen storage materials," *J Am Chem Soc*, vol. 130, no. 35, pp. 11580–11581, Sep. 2008, doi: 10.1021/ja803247y.

[8] K. Suresh, D. Aulakh, J. Purewal, D. J. Siegel, M. Veenstra, and A. J. Matzger, "Optimizing Hydrogen Storage in MOFs through Engineering of Crystal Morphology and Control of Crystal Size," *J Am Chem Soc*, vol. 143, no. 28, pp. 10727–10734, Jul. 2021, doi: 10.1021/jacs.1c04926.

[9] J. Ren, N. M. Musyoka, H. W. Langmi, M. Mathe, and S. Liao, "Current research trends and perspectives on materials-based hydrogen storage solutions: A critical review," *International Journal of Hydrogen Energy*, vol. 42, no. 1. Elsevier Ltd, pp. 289–311, Jan. 05, 2017. doi: 10.1016/j.ijhydene.2016.11.195.

[10] N. P. Stadie, J. J. Vajo, R. W. Cumberland, A. A. Wilson, C. C. Ahn, and B. Fultz, "Zeolite-templated carbon materials for high-pressure hydrogen storage," *Langmuir*, vol. 28, no. 26, pp. 10057–10063, Jul. 2012, doi: 10.1021/la302050m.

[11] M. Mohan, V. K. Sharma, E. A. Kumar, and V. Gayathri, "Hydrogen storage in carbon materials—A review," *Energy Storage*, vol. 1, no. 2, p. e35, Apr. 2019, doi: 10.1002/est2.35.

[12] K. Kajiwara, H. Sugime, S. Noda, and N. Hanada, "Fast and stable hydrogen storage in the porous composite of MgH2 with Nb2O5 catalyst and carbon nanotube," *J Alloys Compd*, vol. 893, Feb. 2022, doi: 10.1016/j.jallcom.2021.162206.

[13] S. ullah Rather, "Preparation, characterization and hydrogen storage studies of carbon nanotubes and their composites: A review," *International Journal of Hydrogen Energy*, vol. 45, no. 7. Elsevier Ltd, pp. 4653–4672, Feb. 07, 2020. doi: 10.1016/j.ijhydene.2019.12.055.

[14] J. P. Paraknowitsch and A. Thomas, "Doping carbons beyond nitrogen: An overview of advanced heteroatom doped carbons with boron, sulphur and phosphorus for energy applications," *Energy and Environmental Science*, vol. 6, no. 10. pp. 2839–2855, Oct. 2013. doi: 10.1039/c3ee41444b.

[15] A. Muhulet, F. Miculescu, S. I. Voicu, F. Schütt, V. K. Thakur, and Y. K. Mishra, "Fundamentals and scopes of doped carbon nanotubes towards energy and biosensing applications," *Materials Today Energy*, vol. 9. Elsevier Ltd, pp. 154–186, Sep. 01, 2018. doi: 10.1016/j.mtener.2018.05.002.

[16] P. Liu, J. Liang, R. Xue, Q. Du, and M. Jiang, “Ruthenium decorated boron-doped carbon nanotube for hydrogen storage: A first-principle study,” *Int J Hydrogen Energy*, vol. 44, no. 51, pp. 27853–27861, Oct. 2019, doi: 10.1016/j.ijhydene.2019.09.019.
[17] J. M. Soler *et al.*, “The SIESTA method for ab initio order-N materials simulation,” 2002.
[18] J. P. Perdew, K. Burke, and M. Ernzerhof, “Generalized Gradient Approximation Made Simple,” 1996.
[19] S. Hu, Y. Yong, Z. Zhao, R. Gao, Q. Zhou, and Y. Kuang, “C7N6 monolayer as high capacity and reversible hydrogen storage media: A DFT study,” *Int J Hydrogen Energy*, vol. 46, no. 42, pp. 21994–22003, Jun. 2021, doi: 10.1016/j.ijhydene.2021.04.053.

Environmental impact of manufacturing and end-of-life phase of PEMFC for ecodesign purposes

J. Gramc[1], R. Stropnik[1], J. Dufour[2], M. Mori[1*]

[1]University of Ljubljana, Faculty of Mechanical Engineering, Aškerčeva 6, Ljubljana, SI-1000, Slovenia
[2]IMDEA Energy, Systems Analysis Unit, E-28935 Móstoles, Spain

Introduction

Global warming is one of the greatest challenges facing humanity. Anthropogenic actions have led to a significant increase in greenhouse gas (GHG) emissions, which are blamed for climate change [1]. Total global CO_2 emissions from energy combustion and industrial processes reached a new high of 36.8 Gt CO_2 in 2022, increasing by 0.9% compared to the year 2021 [2]. The effects of historically high GHG are devastating in many cases. Global warming is directly or indirectly responsible for increases in the frequency and intensity of droughts and heat waves, as well as flooding, salinization, and freezing stress [3]. In response to climate change, the European Union (EU) has adopted the European Green Deal, which aims to reduce net GHG emissions by at least 55% by 2030 and achieve carbon neutrality by 2050 [4].

Hydrogen has great potential as an energy carrier for all applications that replace fossil fuels. The EU has recognized this potential of hydrogen and is planning extensive investments in fuel cells and hydrogen technologies (FCH). The European Commission aims to produce 10 million tons of renewable hydrogen and import 10 million tons by 2030 [5]. Proton exchange membranes (PEM) and solid oxide cells (SOC) are the most promising FCH technologies for hydrogen utilization. Given the expected rapid commercialization of FCH technologies, it is important to consider ecodesign guidelines, especially for the manufacturing and end-of-life (EoL) phases. Ecodesign guidelines for FCH products are being developed as part of the ongoing EU project eGHOST [6]. For the PEMFC, four product concepts are developed simulating the expected development in the future with the implementation of the ecodesign guidelines. For each product concept, a life cycle assessment (LCA) study is developed, and environmental impacts are assessed.

Methodology

Ecodesign methodology [7] is used to develop product concepts. The goal of ecodesign is to reduce the environmental impact as much as possible without reducing the quality of the product or changing its functionality [8]. Ecodesign measures address different product levels: (i) at the product component level by selecting environmentally friendly materials and/or reducing material use, (ii) at the product structure level by optimising production techniques, optimising the distribution system, and reducing impacts during the use phase, and (iii) at the product system level by optimising the life cycle and optimising the EoL system. The focus of the study is on the manufacturing and EoL phases, so only ecodesign measures at the product component and product system levels are implemented for product concept development. Based on the ecodesign measures, the following product concepts were developed for PEMFC: (i) short-term concept, (ii) long-term concept, (iii) optimistic

* Corresponding author: mitja.mori@fs.uni-lj.si

concept, and (iv) disruptive concept. The product concepts are compared with the base case concept:

- **The base case concept** represents the current state of manufacturing and EoL treatment of PEMFC. Only virgin materials are used in the manufacturing phase and there is no closed-loop recycling or component reuse in the EoL phase. In the EoL phase, the PEMFC stack is broken down into its components. For components made of common and easily recyclable materials (steel, copper, plastic), an open recycling loop is considered. Other components are landfilled or incinerated, including membrane electrode assembly (MEA), which is made of platinum (Pt). There is no recycling of Pt.
- **The short-term concept** envisions some technological advances in FCH technologies that will reduce the mass of some components used in PEMFC. We have considered a reduction in the thickness of the bipolar plates, the gas diffusion layer, the Pt loading, and the Nafion membrane. In addition, the power-to-weight ratio will be increased (less material per power). In the EoL phase, a closed loop of Pt recycling is considered. Therefore, 30% of virgin Pt is replaced by recycled Pt in the manufacturing phase. The Pt recycling process is implemented in an aggregated form in the LCA model, based on the results of the EU partnering project BEST4Hy [9], where the recycling of Pt and Nafion is performed at a laboratory scale using current and novel recycling technologies. Furthermore, a 30% reuse of end plates is assumed.
- For each product concept, technological advancement of FCH technologies is foreseen. In the **long-term concept**, the reduction of bipolar plates, gas diffusion layer, Pt loading, and Nafion membrane is considered due to further thickness reduction. The power-to-weight ratio will also be further increased. In the EoL phase, an additional 30% reuse of the bipolar plates is assumed.
- In the **optimistic concept**, an additional reduction in the thickness of the bipolar plates, the Pt loading, and the Nafion membrane is made while increasing the power-to-weight ratio. In the EoL phase, it is assumed that the Pt recycling process is further developed and not only is the Pt recycling rate increased to 70%, but also Nafion recycling (30%) is included. The percentage of bipolar plates reused has also increased to 67%.
- In the **disruptive concept**, the thickness of bipolar plates and gas diffusion layer is further reduced while the power-to-weight ratio is increased. In the EoL phase, the recycling rates of Pt and Nafion are increased to 95% and the rate of reused bipolar plates is increased to 80%. In addition, closed-loop recycling of copper (from current collectors) is considered at a rate of 80%.

For the environmental LCA, a standardised methodology is used according to ISO standards 14040 [10] and 14044 [11]. The functional unit in the study is a piece of 48 kW_{el} PEMFC stack with 48 kW electrical power used for passenger transportation in a light vehicle, without Balance of Plant components. The electrical output of the PEMFC increases with each subsequent product concept, but the life cycle inventory is normalised to the functional unit of 48 kW_{el}. The scope of the study includes the manufacturing and EoL phases, the use phase is excluded from the study. The environmental impacts are assessed using the Environmental Footprint 3.1 assessment methodology. The study considers only the following impact categories: Climate Change, Acidification, Eutrophication – Terrestrial, Eutrophication – Aquatic Freshwater, Eutrophication – Aquatic Marine, Resource Use – Minerals and Metals, and Resource Use – Energy Carriers. The selected impact categories

are consistent with the guidance provided in one of the key documents for LCA of FCH technologies, the HyGuide [12].

Results and discussion

The results of the environmental LCA are shown in Figure 1. The results of each environmental impact category considered are presented in a separate diagram. The environmental impacts are divided into three life cycle phases (manufacturing phase, reuse and circular economy-closed loop recycling, and end-of-life phase) and an additional category “avoided impacts” that represents the potential of avoided environmental impacts due to open-loop recycling. Recycled materials in open loops enter the free market and are used in other applications, reducing their environmental impacts due to the substitution of virgin materials, which generally have higher environmental impacts. “Reuse and closed-loop recycling" processes could be included in both the manufacturing and EoL phases of the life cycle since the EoL treatment and the manufacturing of the materials occur in the same process.

As shown in Figure 1, the base case has the highest impacts (with and without the avoided impacts) for each impact category except eutrophication – freshwater, where the environmental impacts are higher in the short-term case (and in the long-term and optimistic case when the avoided impacts are included) due to the high environmental impacts of the Pt recycling process, the low environmental impacts of virgin Pt production, and the high environmental impacts of virgin glass fibre reinforced thermoplastic production. In the short-term case, there is a 19% increase in freshwater eutrophication without considering avoided impacts. Other product concepts have lower environmental impacts, 25% in the long-term case, 33% in the optimistic case and 52% in the disruptive case.

In other impact categories, each product concept has lower environmental impacts than the previous one. For the short-term case, the reductions in environmental impact range from 31% (climate change and resource use – fossils) to 60% (acidification); for the long-term case, from 51% (resource use – fossils) to 66% (acidification); for the optimistic case between 73% (resource use – fossils) and 90% (acidification), and for the disruptive case between 83% (resource use – fossils) and 97% (acidification and resource use – minerals & metals). The reductions for the climate change category, which is the most important, are 31% for the short-term case, 52% for the long-term case, 74% for the optimistic case, and 85% for the disruptive case.

There is also a step increase in avoided impacts from the base case to the short-term case due to the Pt recycling. The Pt recycling process has a higher recycling rate than the usage rate of recycling Pt in the short-term concept, therefore some Pt goes to the free market. Because virgin Pt production has high environmental impacts in all considered impact categories except eutrophication – freshwater, avoided impacts are much higher as in the base case, where there is no Pt recycling. With each following product concept (long-term, optimistic, and disruptive) avoided impacts are lower since the rates of recycling materials are higher (less material goes to the open-loop) and the masses of materials are lower in the PEMFC stack.

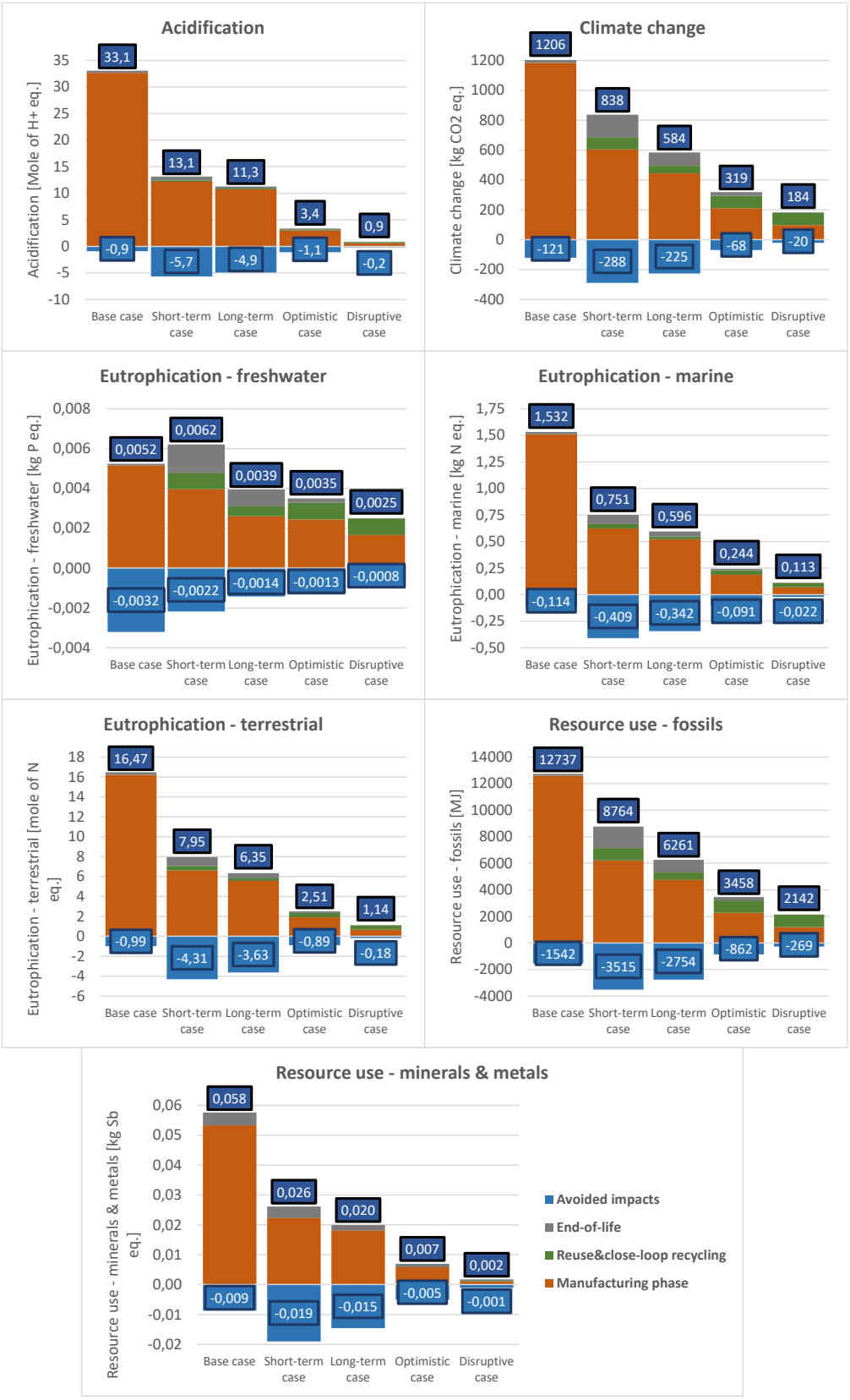

Figure 1: Environmental impacts for each impact category

Relative comparisons between different environmental impact categories with and without avoided impacts are shown in Figure 2. Environmental impacts for the base case represent reference point (100%). In the scenario without avoided impacts, the reductions are clear for each subsequent product concept. In the scenario with avoided impacts, the results are somewhat skewed because the relative reductions between the base case and the product concepts are greater for each impact category, except for Eutrophication – Freshwater, which not only has smaller reductions, but the environmental impacts of the product

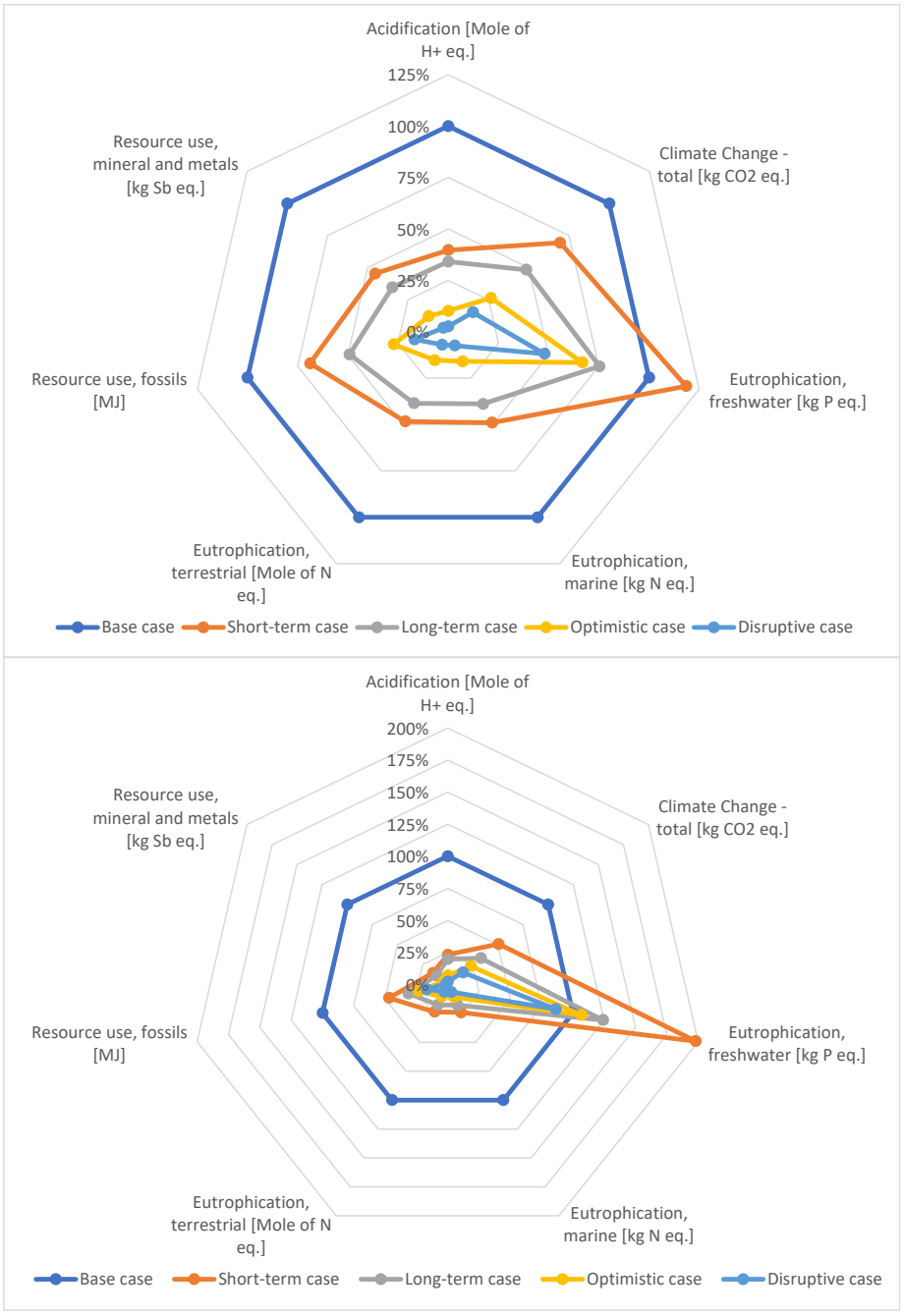

Figure 2: Relative environmental impacts without avoided impacts (up) and with avoided impacts (down)

concepts are greater than the environmental impacts of the base case. In this scenario, only the disruptive case has lower eutrophication – freshwater than the base case. The relative difference between the base case and the product concepts is greater with avoided impacts, and the relative differences between the product concepts are also smaller than without avoided impacts.

Conclusions

The study shows the environmental benefits of implementing ecodesign product concepts for the PEMFC stack. In each environmental impact category considered, the impacts for the product concepts are lower than in the base case, except for the impact category Eutrophication – Freshwater, where the impacts are 19% higher in the short-term case due to the Pt recycling process. Environmental impacts are reduced between 31% and 60% in the short-term case and between 51% and 66% in the long-term case. The reduction in climate change is 31% and 52% in the short and long term, respectively. The largest contribution to environmental impact comes from the manufacturing phase. The end-of-life phase has a much smaller impact but can significantly reduce the environmental impact if the components are reused or recycled.

This work was conducted under the eGHOST project funded by the Fuel Cells and Hydrogen 2 Joint Undertaking (now Clean Hydrogen Partnership) under Grant Agreement No. 101007166 and the Best4Hy project funded by the Fuel Cells and Hydrogen 2 Joint Undertaking (now Clean Hydrogen Partnership) under Grant Agreement No. 101007216. This Joint Undertaking is supported by the European Union's Horizon 2020 research and innovation programme, Hydrogen Europe and Hydrogen Europe Research.

References

[1] Intergovernmental Panel on Climate Change, “Climate Change 2021: The Physical Science Basis,” 2021.
[2] International Energy Agency – Global Hydrogen Review 2022, https://www.iea.org/reports/global-hydrogen-review-2022/executive-summary (accessed August 30, 2023)
[3] S. I. Zandalinas, F. B. Fritschi, and R. Mittler, “Global Warming, Climate Change, and Environmental Pollution: Recipe for a Multifactorial Stress Combination Disaster,” *Trends in Plant Science*, vol. 26, 2021. doi: 10.1016/j.tplants.2021.02.011.
[4] European Commission, “The European Green Deal,” 2019.
[5] European Commission, “A hydrogen strategy for a climate-neutral Europe,” 2020.
[6] Project – eGHOST, https://eghost.eu/ (accessed August 30, 2023)
[7] European Parliament, Ecodesing and Energy Labelling – Framework Directives (2009)
[8] J.C. Brezet, C.G. Van Hemel, Ecodesign: a promising approach to sustainable production and consumption, United Nations Environment Programme, 1997
[9] Project – BEST4Hy, https://best4hy-project.eu/ (accessed July 27, 2023)
[10] International Organisation for Standardisation. ISO 14040: environmental management - life cycle assessment - principles and framework. 2006. 2006.
[11] International Organisation for Standardisation. ISO 14044: environmental management - life cycle assessment - requirements and guidelines. 2006. 2006.
[12] Masoni P, Zamagni A. Guidance document for performing LCAs on fuel cells and hydrogen technologies. FC-HyGuide); 2011.

Evaluation of start-up and shutdown protocols for high-temperature proton exchange membrane fuel cells concerning their impact on degradation

Filip Todorovski[1], Mihael Sekavčnik[1], Mitja Mori[1], Andrej Lotrič*[1]

[1]Laboratory of Heat and Power, Faculty of Mechanical Engineering, University of Ljubljana, Ljubljana, Slovenia

Introduction

The European Union (EU)'s push for renewable energy sources is motivated by a combination of environmental, economic, energy security, and geopolitical reasons. By reducing greenhouse gas emissions from the energy sector and promoting low-carbon energy systems, the EU is taking concrete steps towards a more sustainable and climate-resilient future. In addition, the EU has a very ambitious target of reducing net greenhouse gas emissions by at least 55 % by 2030 compared to 1990 levels. [1].

Fuel cells are efficient energy conversion systems that transform hydrogen's chemical energy, derived from various sources including renewables, into electricity, offering compact size, quiet operation, and a reduced environmental footprint, particularly during operation. Proton exchange membrane fuel cells (PEMFCs) find wide applications in transportation, stationary power generation, and portable electronics, with advantages like rapid start-up and high power density. Recent focus has shifted to high-temperature (HT) PEMFCs using polybenzimidazole (PBI) membranes doped with phosphoric acid (PA) as a promising clean energy solution. Differing from its low temperature counterpart (LT-PEMFC), the HT-PEMFC offers notable advantages.

Primarily, operating at temperatures exceeding 120 °C with the specified electrolyte simplifies water management by eliminating liquid water during operation. This allows for dry supply gases, preventing flooding of the active area, as water on the cathode side is produced in a gaseous state [2]–[6].

Operating in the temperature range of 120 – 200 °C in HT-PEMFCs offers the benefit of accelerated electrochemical reactions, enhancing reaction kinetics and producing valuable waste heat for applications like heating or cogeneration, thereby boosting the overall system's efficiency and versatility [2]–[6].

A critical advantage of operating at higher temperatures in HT-PEMFCs is their robust tolerance to impurities in hydrogen fuel, allowing the use of less pure sources like reformed natural gas or biofuels with CO poisoning up to 30,000 ppm and sulfur contamination up to 20 ppm. In comparison, LT-PEMFCs have stricter limits (30 ppm for CO and less than 10 ppm for sulfur), making HT-PEMFCs more suitable for a compact system configuration without requiring gas cleaning or humidification [7].

Despite some advantages, HT PEMFCs face several challenges, including accelerated degradation due to higher operating temperatures and faster degradation during cyclic modes of operation such as load cycles [8], potential cycles [9], thermal cycles, and start/stop cycles, which may worsen their overall degradation and lead to reduced efficiency and shorter lifetime [7], [10], [11].

* Corresponding author: andrej.lotric@fs.uni-lj.si

Methodology

Theoretical background

Recognizing that the degradation of HT-PEMFCs involves various factors (including carbon corrosion, various mechanisms leading to reduction of the Pt surface area, catalyst support depletion, and dehydrophobization), evaluation of the carbon corrosion rate is seen as a valuable means of collecting data on accelerated degradation that is comprehensive in the wider context of HT-PEMFC applications.
During the start-stop cycles, fuel starvation or reverse current lead to temporary increases in the local cathode potential, resulting in an exponential increase in carbon corrosion. In phosphoric acid systems, graphitized carbons are the standard choice due to their resistance to corrosion in high temperature acidic environments. The creation of oxygen-containing surface groups acts as an intermediary step in carbon oxidation to carbon dioxide, influenced by variables like time, temperature, and voltage potential. The interplay of various surface oxides can significantly affect the balance of catalytic oxide species on the carbon surface, potentially leading to electrical isolation, heightened hydrophilicity in the catalyst layer, and a diminished connection between the carbon support and catalyst particles. Complete oxidation of carbon to CO_2 results in the loss of the Pt active surface, changes in the pore structure and morphology of the catalyst layer, and dehydrophobization effects on the remaining catalyst support. This phenomenon can be attributed to the observation that the corrosion of the carbon support leads to thinning of the cathode, which is characterized by a decrease in the cathode electrode material and void volume, which in turn increases the resistance to oxygen diffusion [8], [12].
In a PBI membrane doped with PA, only two acid molecules per PBI repeating unit directly interact with the basic pyridnic nitrogen of PBI. It can, therefore, be expected that the bulk of this phosphoric acid is more or less mobile within the molecular pores of the membrane. Their mobile nature makes it difficult to fix them to the membrane or the electrodes and they can migrate from the membrane and the catalyst layer to other components of the cell, or even out of the fuel cell, causing performance decay [13], [14].
For these technologies to be feasible for commercial use, it is essential to meet specific sustainability requirements, which remains a development challenge for some potential HT-PEMFC applications. The US Department of Energy (DOE) has recommended approximately 40,000 hours of operation for stationary applications and 8,000 hours as 2028 target, requiring minimal performance degradation [15]. Component degradation has a significant impact on fuel cell performance and lifetime, making it critical to optimize operational parameters, especially during start/stop events, and to understand key performance factors and degradation mechanisms.

Experimental setup

The membrane-electrode assembly (MEA) with an active area of 50 cm^2 will be tested in the Laboratory for Heat and Power at the Faculty of Mechanical Engineering of the University of Ljubljana. The tests will be performed on a dedicated test station for PEMFCs manufactured by Greenlight Innovation (Canada). This test station, as shown in figure 1, offers precise control of critical parameters including fuel cell temperature, gas inlet temperature, anode and cathode pressure, gas flow rate, gas humidity, anode and cathode gas stoichiometry, and load current of the FC. To achieve and maintain the desired operating temperature, we use a Huber Ministat 240 oil system, which can heat or cool the fuel cell

system. In addition, a 230 VAC cooling fan can be installed to speed up the cooling process of the fuel cell.

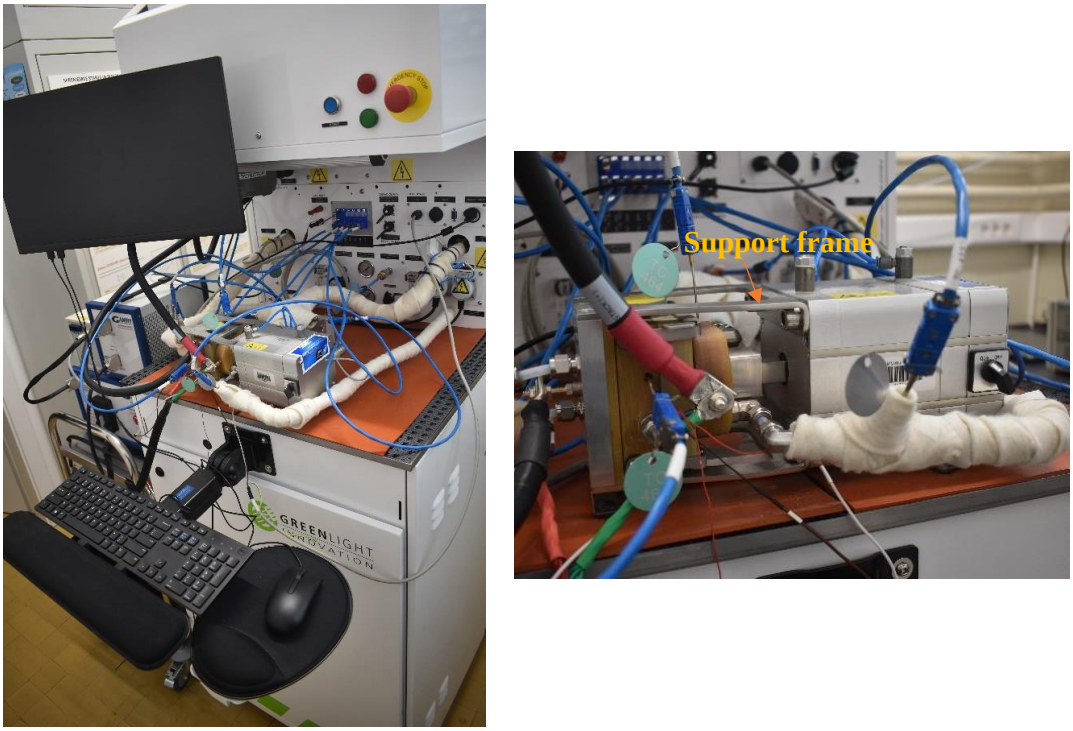

Figure 1: Left: Greenlight Innovation G60, right: assembled cell, clamped in the compression unit and connected to the test station

Greenlight Innovation's Emerald software controls the G60 test station, managing operating conditions, recording set values, and logging measured parameters. The Gamry reference 3000 device characterizes the internal resistance of the fuel cell, with manual or fully automated capabilities, including configuration and data logging, accessible through a graphical user interface or scripts developed using the Emerald Xcue Editor.

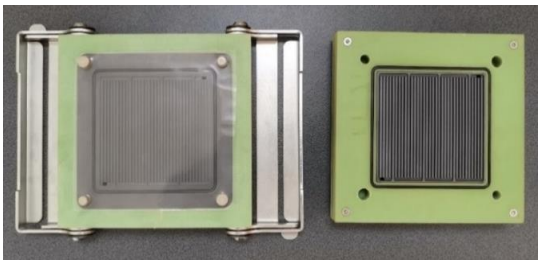

Figure 2: Fixture unit and graphite flow field plates

For start-up and shutdown experiments, single MEAs will be tested - consisting of two gas diffusion electrodes (GDEs), one attached per each side of the proton exchange membrane - and such assembly is rigidly fixed inside the cell compression unit. The MEAs with an active area of 50 cm^2 will be used and they were produced by BASF production method. The production process of these PBI membranes involves a sol-gel method where polyphosphoric acid (PPA) in PBI-PPA solutions is hydrolyzed to PA during the film casting process. This results in membranes with a higher PA concentration in the structure, with up to 70 PA molecules per PBI repeating unit. These membranes exhibit impressive

ionic conductivity reaching up to 0.26 S/cm at 200 °C, along with improved mechanical properties at elevated temperatures [16].

The GDEs inside the PBI MEAs consist of a macroporous carbon fiber fabric substrate approximately 400 μm thick and a catalyst layer approximately 30–50 μm thick deposited on the macroporous substrate using an automated process. These resulting GDLs have a total catalyst loading of 1.8 mg/cm^2 total Pt. The catalyst layers have a porous structure with a diverse composite morphology containing a mixture of platinum on carbon Vulcan XC 72 (C/Pt) and polytetrafluoroethylene (PTFE) as a binder. The C/Pt matrix consists of carbon grains in the range of 20–40 nm, which form agglomerates of size 200–400 nm [16].

The qCf FC50/125 liquid-cooled cell compression unit produced by balticFuelCells consists of two primary elements: a fixture cell (figure 2) and a support frame (figure 1). Inside the cell fixture are graphite flow field plates with a design of seven parallel channels in a tortuous configuration. Meanwhile, the support frame includes a pneumatic cylinder that can apply a wide range of clamping pressures that can be adjusted according to the supplied air pressure. In addition, the cell compression unit includes coolant loops that facilitate external temperature control of the cell, a process managed by the test station's coolant loop.

Discussion

Various authors employ diverse start-stop protocols to assess carbon corrosion, phosphoric acid leaching, and stress degradation. These protocols are conducted at varying temperatures, such as 160 °C [12], [17]–[20], 180 °C [21], and 200 °C [22], with the number of cycles (20 [18], 50 [20], 100 [22], 157 [21], 1562 [12], [17] and 60 daily, three times per week [19]) adjusted based on the observed process and the analysis's specific objectives.

EIS spectra and polarization curve measurements will be used to monitor the performance of the 50 cm^2 MEA over 200 start-stop cycles. EIS is chosen because it allows impedance spectra to be recorded without changing operating conditions, and EIS measurements will be taken after every 10 cycles before continuing with polarization measurements. To evaluate the results, we will compare the experimental data with previous research conducted by Mlakar et al. [3] with a similar experimental configuration.

In line with recommendations from previous researchers [3], [8], [11], [17], [23]–[26], various break-in procedures will be employed to achieve improved operational characteristics and reach the beginning-of-life reference state, before conducting start/stop cycling.

Creating procedures to simulate real-world commercial FC systems during start-up and shut-down is essential because these protocols activate degradation mechanisms including carbon support corrosion, phosphoric acid leaching and vaporization, as described in the introduction. Extreme conditions can impair these processes, resulting in a decline in FC performance. For a thorough evaluation, it is crucial to collect substantial experimental data.

A similar accelerated stress test protocol as described in [3] will be used to test HT-PEMFC. The method outlined in table 1 will be used as an initial step to improve and automate start-stop cycling protocol, as it mimics the start-up and shut-down procedure of conventional HT PEMFC systems. The entire protocol was performed using the stoichiometric ratio mode and set to 1.25 H_2 and 2.5 air. Except for step 2, where the H_2 reactant was flushed in at a flow rate of 0.222 NL/min for 5 s, and step 10, the air flow was stopped and the H_2 flow rate was set to at least 0.078 NL/min for 10 min.

The next goal is reaching reliable and repeatable measurements as the protocol shown in table 1 will be used as a reference case. Based on the results and findings in the reference case, the start-stop protocol will be modified with the aim of reducing the degradation rate caused by repeated start-ups and shut-downs.

Table 1: Start-up and shut-down cycle by steps [3]

Order	Step	Temperature °C	Current density A/cm^2
1	Heating up	0→120	0
2	Fuel flush for 5 sec	120	0
3	Heating up	120→160	0.1
4	Load time = 30 min	160	0.4
5	EIS measurements	160	0.4
6	Polarization curve	160	→maximal current density
7	Load time = 15 min	160	0.4
8	Cooling down	160→120	0.1
9	Stop air flow, 10 sec	120	0.05
10	Consume H_2 for 10 min	120	0.01
11	Cooling down	120→< 50	If U > 0.5 V, set q to 0.01 A/cm^2

Conclusions

The primary objective of this PhD research is to test PBI/H_3PO_4 based HT-PEMFCs using a specific start-stop procedure. To monitor the performance of the 50 cm^2 MEA, measurements of EIS spectra and polarization curves will be performed. The purpose of this testing is to gather practical data on the degradation of HT-PEMFC MEAs when exposed to frequent start-ups and shut-downs. Start-stop testing will be performed at specified operating points for a predetermined number of cycles. The AST protocol for these start-stop tests will be based on the findings of previous researchers, an extensive literature review, and considering the limitations of the experimental setup. Based on the results and findings, established in a reference start-stop protocol, modifications will be implemented with the aim of reducing the degradation rate.

References

[1] "REGULATION (EU) 2021/1119 ESTABLISHING THE FRAMEWORK FOR ACHIEVING CLIMATE NEUTRALITY AND AMENDING REGULATIONS (EC) No 401/2009 and (EU) 2018/1999 ('EUROPIAN CLIMATE LAW')," *Official Journal of the European Union*, 2021.

[2] A. Lotrič, M. Sekavčnik, A. Pohar, B. Likozar, and S. Hočevar, "CONCEPTUAL DESIGN OF AN INTEGRATED THERMALLY SELF-SUSTAINED METHANOL STEAM REFORMER - HIGH-TEMPERATURE PEM FUEL CELL STACK MANPORTABLE POWER GENERATOR," *Int J Hydrogen Energy*, vol. 42, no. 26, pp. 16700–16713, Jun. 2017, doi: 10.1016/j.ijhydene.2017.05.057.

[3] N. Mlakar *et al.*, *EVALUATION OF PERFORMANCE DEGRADATION OF HIGH TEMPERATURE PROTON EXCHANGE MEMBRANE FUEL CELLS USING A SIMPLE START-STOP TESTING PROTOCOL*.

[4] Q. Meyer, C. Yang, Y. Cheng, and C. Zhao, "OVERCOMING THE ELECTRODE CHALLENGES OF HIGH-TEMPERATURE PEM FUEL CELLS," *Electrochemical Energy Reviews*, vol. 6, no. 1. Springer, Dec. 01, 2023. doi: 10.1007/s41918-023-00180-y.

[5] J. Zhang *et al.*, "HIGH TEMPERATURE PEM FUEL CELLS," *Journal of Power Sources*, vol. 160, no. 2 SPEC. ISS. Elsevier, pp. 872–891, Oct. 06, 2006. doi: 10.1016/j.jpowsour.2006.05.034.

[6] Q. Li, Z. Liu, Y. Sun, S. Yang, and C. Deng, "A REVIEW ON TEMPERATURE CONTROL OF PEM FUEL CELLS," *Processes*, vol. 9, no. 2. MDPI AG, pp. 1–21, Feb. 01, 2021. doi: 10.3390/pr9020235.

[7] M. Zhou *et al.*, "MODELING THE PERFORMANCE DEGRADATION OF HIGH TEMPERATURE PEM FUEL CELL," *Energies (Basel)*, vol. 15, no. 15, Aug. 2022, doi: 10.3390/en15155651.

[8] J. Li, L. Yang, Z. Wang, H. Sun, and G. Sun, “DEGRADATION STUDY OF HIGH TEMPERATURE PEM FUEL CELL UNDER START/STOP AND LOAD CYCLING CONDITIONS,” *Int J Hydrogen Energy*, vol. 46, no. 47, pp. 24353–24365, Jul. 2021, doi: 10.1016/j.ijhydene.2021.05.010.

[9] V. Bandlamudi, P. Bujlo, V. Linkov, and S. Pasupathi, “THE EFFECT OF POTENTIAL CYCLING ON HIGH TEMPERATURE PEM FUEL CELL WITH DIFFERENT FLOW FIELD DESIGNS,” *Fuel Cells*, vol. 19, no. 3, pp. 231–243, Jun. 2019, doi: 10.1002/fuce.201800127.

[10] E. Wallnöfer-Ogris, F. Poimer, R. Köll, M.-G. Macherhammer, and A. Trattner, “MAIN DEGRADATION MECHANISEMS OF PEM FUEL CELL STACK - MECHANISMS, INFLUENCING FACTORS, CONSENQUENCES, AND METIGATION STRATEGIES,” *Int J Hydrogen Energy*, Jul. 2023, doi: 10.1016/j.ijhydene.2023.06.215.

[11] A. Kregar, G. Tavčar, A. Kravos, and T. Katrašnik, “PREDICTIVE SYSTEM-LEVEL MODELING FRAMEWORK FOR TRANSIENT OPERATION AND CATHODE PLATINUM DEGRADATION OF HIGH TEMPERATURE PEM FUEL CELLS.”

[12] A. Kannan, J. Kaczerowski, A. Kabza, and J. Scholta, “OPERATION STRATEGIES BASED ON CARBON CORROSION AND LIFETIME INVESTIGATIONS FOR HT-PEMFC STACKS,” *Fuel Cells*, vol. 18, no. 3, pp. 287–298, Jun. 2018, doi: 10.1002/fuce.201700096.

[13] S. S. Araya *et al.*, “A COMPREHENSIVE REVIEW OF PBI-BASED HT-PEMFC,” *International Journal of Hydrogen Energy*, vol. 41, no. 46. Elsevier Ltd, pp. 21310–21344, Dec. 14, 2016. doi: 10.1016/j.ijhydene.2016.09.024.

[14] “ETH LIBRARY PSI ELECTROCHEMISTRY LABORATORY - ANNUAL REPORT”, doi: 10.3929/ethz-a-007047464.

[15] “HYDROGEN STORAGE TEHNOLOGIES ROADMAP FUEL CELL TECHNICAL TEAM ROADMAP,” 2017. [Online]. Available: www.uscar.org.

[16] V. Gurau and E. S. de Castro, “PREDICTION OF PERFORMANCE VARIATION CASUED BY MANUFACTURING TOLERANCE AND DEFECTS IN GDE OF PA-DOPED PBI BASED HIGH-TEMPERATURE PEM FUEL CELLS,” *Energies (Basel)*, vol. 16, no. 3, Mar. 2020, doi: 10.3390/en13061345.

[17] A. Kannan, A. Kabza, and J. Scholta, “LONG TERM TESTING OF START/STOP CYCLES ON HIGH TEMPERATURE PEM FUEL CELL STACK,” *J Power Sources*, vol. 277, pp. 312–316, Mar. 2015, doi: 10.1016/j.jpowsour.2014.11.115.

[18] J. Büsselmann, M. Rastedt, V. Tullius, K. Yezerska, A. Dyck, and P. Wagner, “Evaluation of HT-PEM MEAs: Load cycling versus start/stop cycling,” *Int J Hydrogen Energy*, pp. 19384–19394, Jul. 2019, doi: 10.1016/j.ijhydene.2018.07.181.

[19] M. Rastedt, F. J. Pinar, N. Pilinski, A. Dyck, and P. Wagner, “Effect of Operation Strategies on Phosphoric Acid Loss in HT-PEM Fuel Cells,” *ECS Trans*, vol. 75, no. 14, pp. 455–469, Aug. 2016, doi: 10.1149/07514.0455ecst.

[20] J. Li, L. Yang, Z. Wang, H. Sun, and G. Sun, “Degradation study of high temperature proton exchange membrane fuel cell under start/stop and load cycling conditions,” *Int J Hydrogen Energy*, vol. 46, no. 47, pp. 24353–24365, Jul. 2021, doi: 10.1016/j.ijhydene.2021.05.010.

[21] C. Hartnig and T. J. Schmidt, “Simulated start-stop as a rapid aging tool for polymer electrolyte fuel cell electrodes,” *J Power Sources*, vol. 196, no. 13, pp. 5564–5572, Jul. 2011, doi: 10.1016/j.jpowsour.2011.01.044.

[22] J. O. Leader, Y. Yue, M. R. Walluk, and T. A. Trabold, “Voltage degradation of high-temperature PEM fuel cells operating at 200 °C under constant load and start-stop conditions,” *Int J Hydrogen Energy*, vol. 47, no. 43, pp. 18820–18830, May 2022, doi: 10.1016/j.ijhydene.2022.04.067.

[23] T. Søndergaard *et al.*, “CATALYST DEGRADATION UNDER POTENTIAL CYCLING AS AN ACCELERATED STRESS TEST FOR PBI-BASED HT-PEMFC - EFFECT OF HUMIDIFICATION,” *Electrocatalysis*, vol. 9, no. 3, pp. 302–313, May 2018, doi: 10.1007/s12678-017-0427-1.

[24] F. Javier Pinar, M. Rastedt, N. Pilinski, and P. Wagner, “EFFECT OF IDLING TEMPERATURE ON HIGH TEMPERATURE PEM FUEL CELL DEGRADATION UNDER SIMULATED START/STOP CYCLING,” *Int J Hydrogen Energy*, vol. 41, no. 42, pp. 19463–19474, Nov. 2016, doi: 10.1016/j.ijhydene.2016.05.091.

[25] J. Kim, M. Kim, B. G. Lee, and Y. J. Sohn, “DURABILITY OF HIGH TEMPERATURE PEM FUEL CELLS IN DAILY BASED START/STOP OPERATION MODE USING REFORMATED GAS,” *Int J Hydrogen Energy*, vol. 40, no. 24, pp. 7769–7776, Jun. 2015, doi: 10.1016/j.ijhydene.2014.12.122.

[26] S. S. Araya, S. Thomas, A. Lotrič, S. L. Sahlin, V. Liso, and S. J. Andreasen, “Effects of impurities on pre-doped and post-doped membranes for high temperature PEM fuel cell stacks,” *Energies (Basel)*, vol. 14, no. 11, Jun. 2021, doi: 10.3390/en14112994.

Experimental and Numerical Investigation of a Diffusion Burner with CO2 Dilute Oxy-Combustion of Natural Gas and Hydrogen

N. Jouret*[1], J. Lacey[1], A. Ba [2]

[1] Toegepaste Mechanica en Energieconversie (TME), Campus Groep T, KU Leuven
[2] Air Liquide Technology Center, Brussels

Introduction

Reducing GHG emissions is a significant challenge for energy-intensive industries with high temperature processes such as those used for the production of glass and steel. Oxy-fuel combustion is an efficient means to reduce GHG emissions from conventional air combustion, where the oxidiser for the combustion process is a supply of pure oxygen instead of air (~80% nitrogen by volume). Oxy-fuel combustion enables high efficiency with fuel savings by reducing the thermal balance of nitrogen and reducing the heat loses from the exhaust gases as consequence of the lower flue gas flow[1,2]. Because there is no nitrogen present in the oxidiser, oxy-fuel combustion presents the advantage to increase the CO_2 concentration in exhaust gas that is more amenable to Carbon Capture and Sequestration (CCS) as post-combustion CO_2 reduction [3]. The absence of nitrogen in the oxidizer stream enables also a drastic reduction of Nitrogen Oxide (NOx) emissions.

Another method to decarbonize carbon-intensive industrial processes is with so-called “green” hydrogen generated by means of water electrolysis with renewable electricity. Hydrogen is considered as a promising candidate to decarbonize the gas supply by displacing methane with zero-carbon hydrogen [4]. Oxy-fuel combustors connected to a hydrogen-enriched NG supply are expected to experience sufficient combustion stability due to the enhanced flame propagation provided by the addition of hydrogen to the fuel blend [5,6]. However, introducing hydrogen into the natural gas supply would have several impacts on NG oxy-combustors, including increasing flame speed and temperature, both of which could have deleterious effects on the combustor hardware.

In order to mitigate excessive temperatures and potential mechanical damage, CO_2 and H_2O dilution of the oxidiser supply are viewed as potential solutions. As these species are both inert with respect to the combustion process and possess high specific heats, they induce both a chemical and thermal quenching effect on the flame, effectively reducing flame temperatures. H_2O-dilution is practically easier to implement as it uses commonly available water, but presents the disadvantages of increased risk of metal corrosion and higher heat losses in the exhaust gases. In contrast, CO_2-dilution is more complex to source, but presents the advantage of lowering the corrosion risk and avoiding the condensing issues in the exhaust gases [7,8].

* Corresponding author: nicolas.jouret@kuleuven.be

Oxy-fuel combustion in industrial furnaces

Over the last two decades, Air Liquide has acquired extensive industrial experience of full oxy-combustion for the glass, metals, cement and waste treatment industries. This extensive expertise and scientific knowledge have been used to develop an innovative oxy-burner technology for a large range of fossil fuels [9].

Air Liquide has developed a prototype, coaxial burner for pure H_2 with a capacity of 100 kW. Hydrogen is injected centrally while the oxidiser (air or oxygen) is injected on the periphery of the burner. A series of tests have been carried out to evaluate the full range of the burner, the impact of the momentum flux ratio and the change in radiant fraction as a function of the residence time. It has been observed that the radiative fraction of hydrogen jet flames decreases when compared to other hydrocarbon flames. The main reason is the absence of CO_2 radiation bands within hydrogen flames.

Because radiative heat transfer plays an integral role in high temperature industrial processes, CO_2-dilution is considered as a potential method to improve the radiation properties of hydrogen flames. As previously mentioned, this dilution also has the additional benefit of avoiding excessive flame temperatures during the oxy-combustion process. Therefore, the goal of this research is to investigate the impact of CO_2-dilution on the behavior of H_2-enriched, natural gas oxy-flames and the characterization of the radiative heat transfer of such flames. Combustion experiments will be conducted on a 15kW burner (i.e. a scaled-down version of the Air Liquide burner) with H_2-enriched natural gas at the fuel side and CO_2-diluted oxygen at the oxidiser side (oxy-combustion). In parallel, simplified numerical models will be developed to investigate the chemical reaction paths and the radiative heat transfer of the flames.

Experimental setup

Experimental tests will be performed in an octagonal combustion chamber made of quartz walls, with a diameter and a length of 255 and 650 mm respectively. The burner is installed in the bottom with the flame burning upward, and the combustion products pass through the annular section that is formed by the octagon. The setup runs under atmospheric pressure conditions. A picture of the combustion chamber is shown on Figure 1a.

K. Vanoverberghe [10] has used this experimental combustion chamber to investigate the flow, turbulence and combustion behavior of premixed swirling jet flames burning natural gas with air. In the frame of the current research activities, a new burner has been developed to burn H_2-enriched natural gas with CO_2-diluted oxygen as oxidiser. The burner is depicted on Figure 1b (3D view) and 1c (Section).

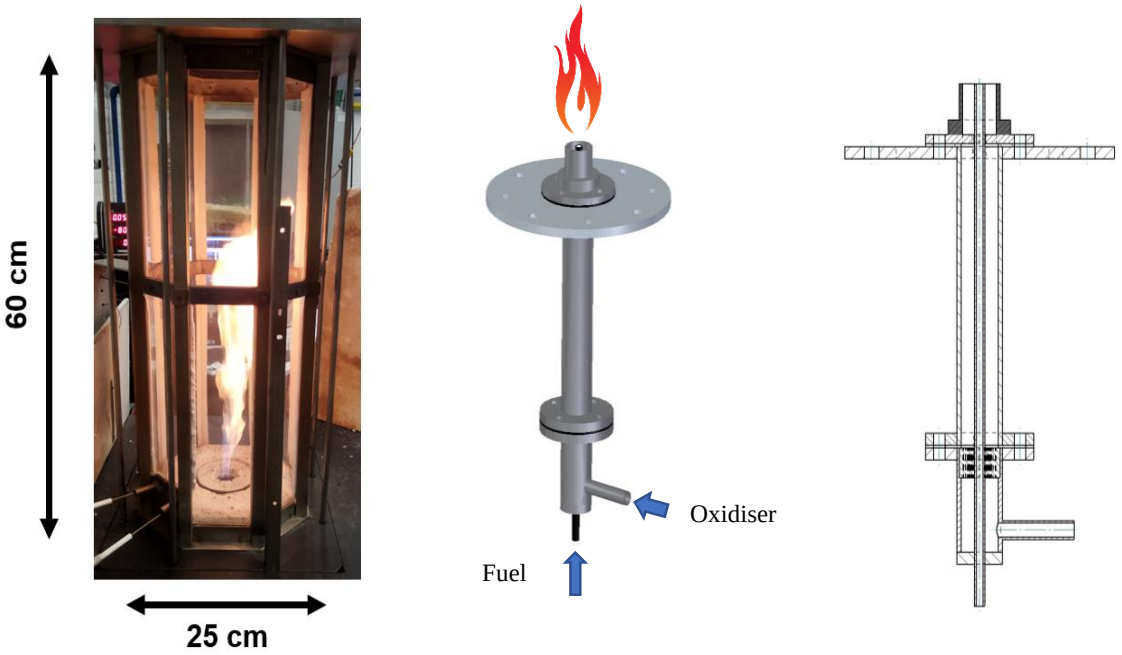

Figure 1: Combustion Chamber (a) - Burner 3D view (b) and Burner Section view (c)

During experiments, key operational parameters will be changed, namely the H_2-concentration at the fuel side, the CO_2-dilution ratio in the oxidiser and the oxidiser temperature as described in Table 1. A flame stability map will be determined by varying the operational parameters within the predefined range. In particular the flame blowout limits will be assessed for high CO_2-dilution rates.

Table 1 : Operating parameters

	min	Max
Hydrogen percentage in Natural gas	0%	100%
CO_2-dilution rate in the oxidiser flow	50%	85%
Oxidiser preheating	20°C	300°C

The combustion chamber is equipped with several sensors to continuously monitor the flame. The gaseous mass flows are measured and controlled by Brooks Mass Flow Controllers (MFC) model SLA-585X. The exhaust gas composition (O_2, CO, CO_2, NO_x, unburned hydrocarbons) is measured at the outlet of the combustor using a flue gas analyser STENHØJ SGA 400 for low CO_2 concentration while high CO_2 will be monitored with a gas analyser Fuji electric NDIR type infrared gas analyser. For safety purpose, a flame detection system, the Flamonitec KLC 10, is installed to assure the safe operation of the burner.

The flame position and shape will be assessed based on OH*-chemiluminescence using a high-speed camera Photron, a UV lens Nikon, a Hamamatsu image intensifier and 310 nm bandpass filter.

The radiative heat transfer will be experimentally investigated by use of 3 measuring devices: flame emission spectroscopy, heat flux sensors and thermocouples. The spectral distribution of radiation is measured with a flame emissions spectrometer from Ocean Insight. The spectrum range considered in this research is the UV and visible (200-775 nm). Fiber optics will be used to collect the light and guide it to the spectrometer. The heat flux will be measured with a Gardon gauge water-cooled, high heat flux sensor. The sensor is equipped with a sapphire window to measure radiative heat flux only, and not convective heat flux. Probe access via small sealable holes in one quartz window allows for the measurement of the temperature field in the combustion chamber using a fine wire thermocouple.

Numerical investigation

In parallel to the experiments, a simplified numerical investigation will be performed to analyse flame characteristics and the radiative heat transfer. The flame reaction zone will be modelled using a Chemical Reactor Network (CRN) composed of 3 zones (Figure 2b) [11,12,13]. The Jet Expansion Zone (JEZ), representing the core of the flame, is a region of high axial velocity with initial entrainment of fluid from the ERZ, the External flue gas Recirculation Zone. The ERZ is a zone confined between the flame and the walls where hot exhaust gases are recirculated to the burner head. Finally the DownStream Zone (DSZ) is the zone located downstream of the flame, where the exhaust gases are leaving the combustion chamber. The physical characteristics (length, angle, ...) of the zones will be determined based on the experimental results. The JEZ zone will be associated with a Plug Flow Reactor (PFR) while ERZ and DSZ zones are associated to Perfect Stirred Reactor (PSR) as illustrated on Figure 2c [11,12,13].

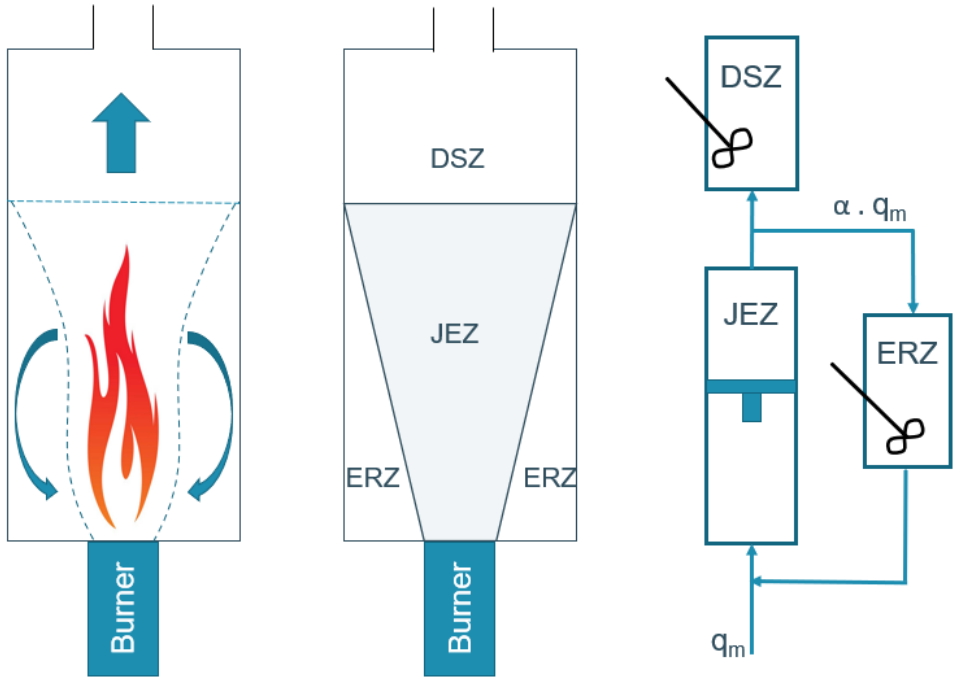

(a) (b) (c)

Figure 2: Combustion Chamber (a) – Flame reaction zones (b) - Chemical Reactor Network (c)

A simplified numerical heat transfer model will be developed using a constant absorption coefficient based on experimental observation (heat flux and spectral composition). A grey gas radiation behavior is considered so that only one Radiative heat Transfer Equation (RTE) has to be solved [14]. The experimental data will be used to define the correlation for the CO_2 and H_2O emissivity in frame of radiative heat transfer (in a similar way of the Hottel charts). The Hottel's zonal method will be implemented, as it the most widely used method for calculating radiation heat transfer in practical engineering systems. The surface and the volume of the combustion chamber is divided into a number of zones, each of which is assumed to have a uniform distribution of temperature and radiative properties [15].

References

[1] J. Caudal, Oxy-hydrogen based combustion for energy-intensive glass melting, TOTEM IFRF, France, 2022.

[2] J. von Schéele, Oxyfuel combustion with hydrogen in the steel, non-ferrous, and glass industries, TOTEM IFRF, France, 2022.

[3] X. Huang, J. Guo, Z. Liu and C. Zheng, Chapter 1 - Opportunities and challenges of oxy-fuel combustion, Editor(s): C. Zheng and Z. Liu, Oxy-fuel combustion, Academic Press, 2018.

[4] A. van Wijk and J. Chatzimarkakis, Green hydrogen for a European green deal A 2x40 GW Initiative, Hydrogen Europe, 2020.

[5] M. Näslund, Combustion control in domestic gas appliances - Fuel gases containing hydrogen, Project report, Danish Gas Technology Centre, Hørsholm, 2014.

[6] K. Altfeld and D. Pinchbeck, Admissible hydrogen concentrations in natural gas systems, Gas for Energy, 3, 36-47, 2013.

[7] L. Cai, C. Zou, Chapter 15 - Oxy-steam combustion, Editor(s): C. Zheng and Z., Oxy-fuel combustion, Academic Press, 2018.

[8] S. Seepana and S. Jayanti, Steam-moderated oxy-fuel combustion, Energy Conversion and Management, Volume 51, Issue 10, 1981-1988, 2010.

[9] D. Cieutat, I. Sanchez-Molinero, R. Tsiava, P. Recourt, N. Aimard and C. Prébendé, The oxy-combustion burner development for the CO2 pilot at Lacq, Energy Procedia, 1, 519-526, 2009.

[10] K. Vanoverberghe, Flow, turbulence and combustion of premixed swirling jet flames. PhD thesis, KULeuven, 2004.

[11] L. Pedersen, P. Breithauptb, K. Dam-Johansen, and R. Weber, Residence time distributions in confined swirling flames, Combustion science and technology, 127:1-6, 251-273, 1997.

[12] R. Monaghan and M. Ghoniem, A dynamic reduced order model for simulating entrained flow gasifiers Part I: Model development and description, Fuel 91, 61–80, 2012.

[13] L.S. Pedersen, P. Glarborg, K. Dam-Johansen, P. W. Hepburn and G.Hesselmann, A chemical engineering model for predicting no emissions and burnout from pulverised coal flames, Combustion Science And Technology, 132:1-6, 251-314, 1998.

[14] V. Becher, A. Goanta and H. Spliethoff, Validation of spectral gas radiation models under oxyfuel conditions. Part C: Validation of simplified models, International Journal of Greenhouse Gas Control 11, 34-51, 2012

[15] R. Viskanta and M. P. Mengüç, Radiation heat transfer in combustion systems, Prog. Energy Combustion Science, Vol 13, pp. 97-160, 1987.

Filament wound composite tanks for pressurized hydrogen storage: Novel predictive simulation models and testing methods.

M. Hondekyn*[1], W. Van Paepegem[1]

[1]Dept. of Materials, Textiles and Chemical Engineering, Ghent University (UGent), Belgium

Keywords

Composite pressure vessels, hydrogen storage, damage modelling, mechanics of composites

Introduction

In the context of transitioning towards net zero GHG emissions by 2050, it is crucial to achieve emission reduction in the transport sector, given that this sector is responsible for 23% of the global CO2 emissions [1]. Electrification of vehicles is regarded as the best method to reach this goal, as long as the electricity is produced using low-carbon renewable energy sources. For light and medium-duty vehicles, lithium-ion batteries are the fastest and most cost-effective option to achieve electromobility. However, batteries are less suitable for long-haul and heavy-duty transport, due to their higher power and capacity requirements. For these applications, hydrogen fuel cells are more promising to achieve emission reduction, especially if hydrogen is produced with renewable electricity. Indeed, hydrogen has a very high gravimetric energy density, and offers much faster refuelling than recharging batteries. However, its volumetric energy density at standard temperature and pressure is significantly lower than most other fuels. Hence, hydrogen storage requires either extremely high working pressures of 700 bar, or liquefication at -253°C to increase its density. As the liquefication process is notably expensive and energy intensive, it is only considered for aerospace applications, while pressurizing is the accepted solution for most other transport applications (trucks, buses, ships, …).

Storage of gaseous hydrogen at 700 bar is typically done in type IV composite pressure vessels (Figure 1), which consist of a polymer liner to ensure hydrogen impermeability, a composite overwrap which bears most of the load, and a metallic boss for refuelling operations. In contrast to types I, II and III, which are mainly composed of metal, type IV offers a higher strength-to-weight ratio, a better controlled burst failure, an improved fatigue and corrosion resistance, and less hydrogen-embrittlement complications.

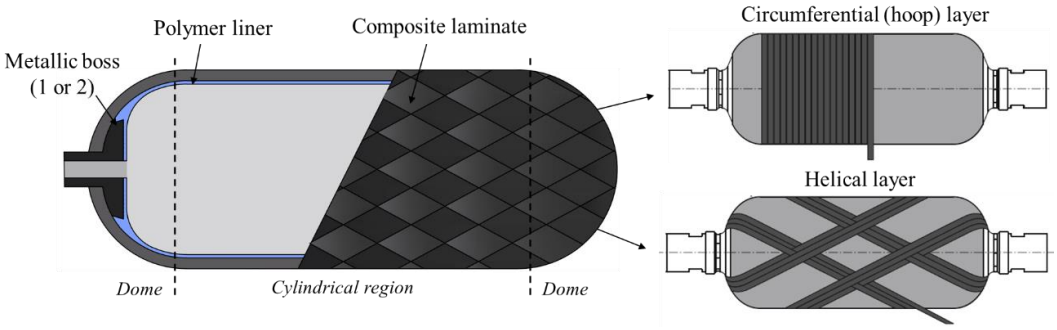

Figure 1: Composition of type IV pressure vessel, with the composite overwrap consisting of hoop layers in the cylindrical part, and helical layers covering the complete tank.

* Corresponding author: marie.hondekyn@ugent.be

Nevertheless, the storage of hydrogen gas at 700 bar poses stringent requirements on the design and safety of the pressure vessels. Numerical simulations and experimental testing are useful tools to understand how failure can be prevented, and how damage initiation and propagation takes place. However, the models used in the industry are based on assumptions which are too simplified to fully comprehend the failure mechanisms, and testing is commonly done at full-scale, which is very expensive and time intensive. Additionally, simulation models in literature focus predominantly on burst failure in the cylindrical region of the tank [2]–[6], often neglect out-of-plane stresses and/or delamination [3], do not properly include the winding angles [4], and do not incorporate the influence of manufacturing defects [2]–[6]. Thus, these simulation models can only partially capture the damage processes, while a clear gap in understanding failure mechanisms in hydrogen pressure vessels remains, especially in fatigue.

Methodology

This research aims to overcome these gaps in the state-of-the-art by developing an analytical, numerical, and experimental framework to acquire a deeper understanding of failure initiation and propagation in type IV composite pressure vessels. In particular, it is focused on fatigue failure, which is caused by cyclic filling and emptying of the tank, and burst failure.

In the *analytical framework*, a tool is developed to make quick estimations on the required wall thickness and optimal fibre angles of the composite laminate. Typically, preliminary design of composite pressure vessels is done with netting theory, which assumes that the fibres support all the internal pressure and neglects the effect of the matrix. In this research, a more precise analytical model will be developed that also incorporates the matrix and is based on the classical lamination theory in cylindrical and spherical coordinates.

The *numerical framework* concentrates on simulations of the tank under burst and fatigue loading, in which both intra- and interlaminar damage is included. Ply cracking, fibre fracture and delamination are the main failure modes that should be incorporated in these types of simulations. Indeed, early ply cracking in fatigue, delamination in the dome region and insufficient exploitation of the carbon fibre strength have already been observed experimentally. In addition, defects can arise during manufacturing, such as fibre volume variations, voids between the plies, and thermal stresses due to cooling after post-curing (Figure 2). These manufacturing defects will also be included in the simulation models, and their impact on burst and fatigue failure will be assessed.

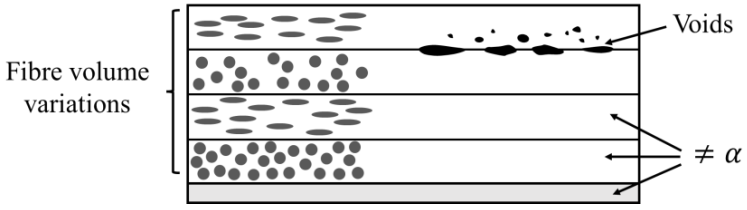

Figure 2: Schematic overview of the most important manufacturing defects in composite pressure vessels.

In the *experimental framework*, input and validation data will be acquired for the models, which involves both burst and fatigue loading data, and statistical data to include the manufacturing defects in the models. Furthermore, it is targeted here to develop representative small-scale coupon tests that can replace full-scale testing which is now the practice in the industry.

Discussion

First, it is anticipated that out-of-plane stresses should be included in the simulation models in order to reproduce damage initiation and propagation correctly. More specifically, this research hopes to demonstrate that the transverse shear stresses in the dome region are essential in the process of fatigue failure. Indeed, due to the high working pressure in the tank, extremely large forces act on the dome region which can lead to significant transverse shear stresses given the high thickness of the composite laminate. For example, at a nominal working pressure of 700 bar, the axial force working on the dome is equal to 3.4 MN (Figure 3). It is predicted here that these transverse shear stresses are responsible for the experimentally observed delaminations in the dome region. This is a huge innovation with respect to present models, which often neglect out-of-plane stresses and focus only on burst failure in the cylindrical region.

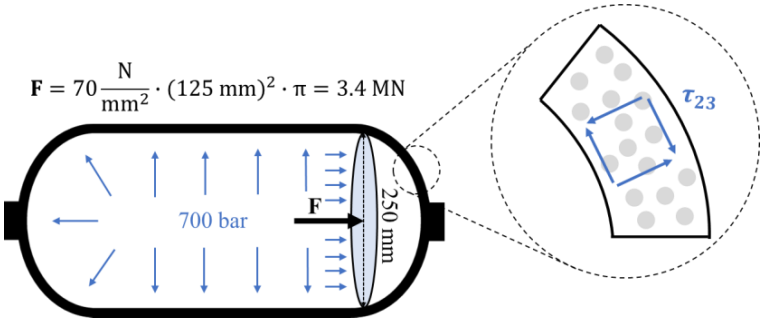

Figure 3: Schematic drawing of the development of transverse shear stresses in the tank.

Furthermore, this research aims to understand the influence of manufacturing defects on damage initiation and propagation in hydrogen pressure vessels. First, it is targeted to integrate the effect of both fibre volume variations and voids in the tank. It can be understood that during filament winding of the helical and hoop layers (Figure 1), the inner layers experience a stronger compaction compared to the outer layers, resulting in higher fibre volume fractions, and therefore altered axial strengths in the innermost layers. In addition, the reduced amount of resin between the carbon fibres in this region leads to stress concentrations, which results in decreased transverse tensile and shear strengths. Moreover, the higher volume fraction of resin in the outer layers makes this region more susceptible to porosity. Previous observations have shown that these voids are typically flattened and are located between plies (Figure 2). Secondly, it is expected that thermal stresses will arise in the tank after post-curing, since the coefficients of thermal expansion are different for the liner, epoxy, carbon fibre and metal boss.

Lastly, it is intended that the developed models will yield a more complete understanding of the complex stress state of the tank, which will allow for the design of representative small-scale coupon tests which can mimic the different stress states. In the ideal scenario, a complete tank could be cut into different pieces on which different tests could be performed, instead of using a complete tank for one single burst or fatigue test.

Conclusions

This research wants to produce a better comprehending of damage initiation and propagation of type IV composite pressure vessels subjected to burst and fatigue loading. For this, it is counted on the development of more accurate and inclusive analytical and numerical models with respect to the-state-of-the-art. Moreover, the complex stress state of the tank is aimed to be reproduced by designing representative small-scale coupon tests.

References

[1] P. R. Shukla, J. Skea, and R. Slade, ‘Working Group III Contribution to the Sixth Assessment Report of the Intergovernmental Panel on Climate Change’.

[2] M. Nebe, A. Soriano, C. Braun, P. Middendorf, and F. Walther, ‘Analysis on the mechanical response of composite pressure vessels during internal pressure loading: FE modeling and experimental correlation’, *Composites Part B: Engineering*, vol. 212, p. 108550, May 2021, doi: 10.1016/j.compositesb.2020.108550.

[3] B. Magneville, B. Gentilleau, S. Villalonga, F. Nony, and H. Galiano, ‘Modeling, parameters identification and experimental validation of composite materials behavior law used in 700 bar type IV hydrogen high pressure storage vessel’, *International Journal of Hydrogen Energy*, vol. 40, no. 38, pp. 13193–13205, Oct. 2015, doi: 10.1016/j.ijhydene.2015.06.121.

[4] J. P. Berro Ramirez, D. Halm, J.-C. Grandidier, S. Villalonga, and F. Nony, ‘700 bar type IV high pressure hydrogen storage vessel burst – Simulation and experimental validation’, *International Journal of Hydrogen Energy*, vol. 40, no. 38, pp. 13183–13192, Oct. 2015, doi: 10.1016/j.ijhydene.2015.05.126.

[5] D. Leh, P. Saffré, P. Francescato, R. Arrieux, and S. Villalonga, ‘A progressive failure analysis of a 700-bar type IV hydrogen composite pressure vessel’, *International Journal of Hydrogen Energy*, vol. 40, no. 38, pp. 13206–13214, Oct. 2015, doi: 10.1016/j.ijhydene.2015.05.061.

[6] M. Nebe, A. Johman, C. Braun, and J. M. J. F. van Campen, ‘The effect of stacking sequence and circumferential ply drop locations on the mechanical response of type IV composite pressure vessels subjected to internal pressure: A numerical and experimental study’, *Composite Structures*, vol. 294, p. 115585, Aug. 2022, doi: 10.1016/j.compstruct.2022.115585.

Flame acceleration and DDT of homogeneous premix hydrogen-air mixture in obstructed channel: A numerical study using OpenFOAM

Petar Bosnic*[1], Mathias Henriksen[2], Knut Vågsæther [3]

[1,2,3] University of South-Eastern Norway

Introduction

Accidental explosions are one of the main risks associated with using hydrogen systems and can result in significant financial losses, harm, or even death. Therefore, it is crucial to understand the physics of these explosions to implement correct safety measures. Large-scale tests are costly in terms of time, money, and resources. Thus, in performing safety assessments, Computational Fluid Dynamics (CFD) can be used as a prevalent tool for predicting the outcomes of gas explosions, offering a cost-effective and efficient approach. Most accidental releases of flammable gases and vapor do not find an ignition source, while those that do ignite mainly result in deflagrations that generate low to moderate overpressure. However, under some circumstances, a slow deflagration can transfer to a fast deflagration that accelerates to a critical velocity. Turbulence influences the propagating laminar flame sheet by inducing wrinkling and stretching, thereby expanding the flame's surface area. This phenomenon accelerates the flame speed and facilitates the transition from deflagration to detonation (DDT). This sequence can be succeeded by a propagating detonation, that rapidly consumes the remaining combustible cloud, resulting in the most catastrophic accident conceivable [1], [2].
In the present work, a 2D numerical study of flame acceleration and DDT in a fuel-rich homogeneous hydrogen-air mixture in an obstructed channel has been conducted. The solver blastXiFoam developed on the OpenFOAM platform by Synthetic Applied Technologies, developers of the open-source blastFoam library [3], has been benchmarked against an experimental study conducted by Gaathaug A.V. et al. [4], [5]. blastXiFoam solver is an extension of the standard OpenFOAM XiFoam solver, a transient solver for compressible premix combustion with turbulence modeling. The main difference is that the flux schemes implemented in the blastFoam solver are used to transport the conserved quantities in blastXiFoam. In the context of blastXiFoam, an approach employing an approximate Riemann solver, such as the HLLC (Harten-Lax-van Leer-Contact) commonly used by other specialized codes for capturing precise shock propagation that better describes a shock-flame interaction [2], [6], is implemented. The blastFoam user guide is recommended to further explain the methods implemented in the code and all the available options [3].
This paper is organized as follows: firstly, the theoretical background of the governing equation used for reactive, compressible flow, turbulence modeling and premix combustion model is presented. Next, numerical methods and numerical setup used in the simulation are described. The last section is dedicated to numerical results with discussion and outlined conclusions.

Conservation Equations Governing Combusting Flow

This section briefly introduces the conservation equations for reacting flows, turbulence modeling and the premix turbulent combustion model. The governing equation for reactive flow is used in the following form (continuity and momentum equations are the same for the reactive and non-reactive flow, but it should be noted that density in combusting flow is a variable dependent on pressure, temperature and species concentration [7]):

* Corresponding author: Petar.Bosnic@usn.no

Continuity equation (combustion does not generate mass):

$$\frac{\partial \rho}{\partial t} + \frac{\partial}{\partial x_i}(\rho u_i) = 0 \quad (1)$$

Conservation of momentum:

$$\frac{\partial}{\partial t}(\rho u_i) + \frac{\partial}{\partial x_i}(\rho u_i u_j) = -\frac{\partial p}{\partial x_i} + \frac{\partial \tau_{ij}}{\partial x_i} + F_i \quad (2)$$

Where τ_{ij} is the viscous stress tensor, and F_i is the body force (which includes gravity).
The energy equation plays a crucial role in reactive flows and can be treated in terms of the absolute enthalpy formulation or the internal energy formulation. Following is the absolute enthalpy formulation, where K is the specific kinetic energy, and P is the thermodynamic pressure (absolute). In this formulation, no chemical heating source is added since absolute enthalpy h_a already contains the chemical enthalpy.

$$\frac{\partial}{\partial t}(\rho h_a) + \frac{\partial}{\partial x_i}(\rho u_i h_a) + \frac{\partial}{\partial t}(\rho K) + \frac{\partial}{\partial x_i}(\rho u_i K) = \frac{\partial P}{\partial t} + \frac{\partial}{\partial x_i}\left[\left(\frac{\mu}{Pr} + \frac{\mu_t}{Pr_t}\right)\frac{\partial h_a}{\partial x_i}\right] \quad (3)$$

The Reynolds-averaged Navier-Stokes (RANS) k-omega SST turbulence model with wall functions was used in this simulation. The turbulence modeling is crucial for accurately predicting scalar transport and the interaction between turbulence and flame. The equations governing the turbulence model introduced by Menter can be found in [8].
The following section discusses the formulation of the transport equation used by flame-wrinkling turbulent combustion mode. When modeling premix turbulent combustion phenomena, the interaction between turbulence and chemical reactions needs to be solved. Different combustion models have been developed and tested to solve this interaction, such as the eddy breakup model, the eddy dissipation concept, turbulent flame speed closure, the coherent flamelet model and the algebraic flame surface wrinkling model, to name a few [9]. In the current numerical study, since the chemical reaction of hydrogen-air mixtures happens much faster than the turbulent fluctuations in the gas, the region where the concentration of chemical species changes significantly is small compared to the entire domain. Therefore, it is valid to approximate the transport equation of every individual species with a single transport equation for the progress variable [10].
OpenFOAM solver XiFoam uses a flame-wrinkling turbulent combustion model developed by Weller H. G. et al. [11]. The model uses the laminar-flamelet approach to create a set of transport equations that describe the complex combustion process. Flamelet modeling of premixed turbulent flame through the Bray-Moss-Libby (BML) theory involves tracking a progress variable c for a global reaction. The BML model's fundamental premise is that the product can exist in one of three states in a premixed turbulent flame: an unreacted state with c = 0, a completely reacted state with c = 1, or an intermediate state with varying degrees of reactiveness. A progress variable c can be defined by quantities such as temperature or reactant mass fraction that is bounded by a single value in the burned gas (b) and the fresh gas (f) [12].

$$c = \frac{T - T_f}{T_b - T_f} \quad (4)$$

Weller's combustion model [11] instead of solving for progress variable c, solves a transport equation for the density-weighted mean reaction regress variable b.

$$b = 1 - c \tag{5}$$

$$\frac{\partial}{\partial t}(\rho b) + \nabla \cdot (\rho \boldsymbol{u} b) - \nabla \cdot \left(\frac{\mu_t}{S_{c_t}} \nabla b + \rho \alpha \right) = - \rho_u S_u \Xi |\nabla b| \tag{6}$$

A detailed description of the transport equation and flame wrinkling factor Ξ (Xi) can be found in [9], [11], [13].

Numerical Setup

The experimental setup used in this study is based on experiments conducted by Gaathaug A. V. et al. [4], [5]. The gas mixture under study was a homogeneous blend of hydrogen and air, with a hydrogen concentration of 35 vol% (σ=1.1). The investigated geometry was a 3 m long channel with a 0.1 x 0.1 m^2 square cross-section, where one end was closed, and the other end was open to the atmosphere. A single obstacle was placed 1m from the close end (creating an 84% blocked ratio) while the mixture was ignited at the close end. Figure 1 illustrates a 2D representation of the experimental configuration employed in this numerical simulation, including a schematic illustration of flame front propagation and positions of 3 pressure sensors.

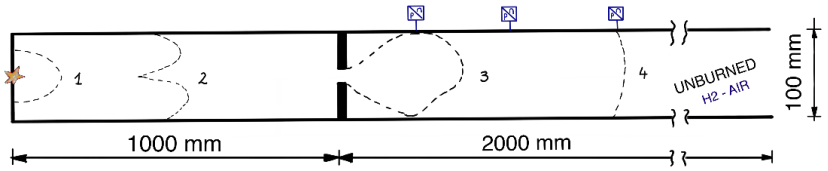

Figure 1: Experimental configuration (the change from laminar to turbulent deflagration occurs in Regions 1-3, while detonation occurs in Region 4)

The resolution of the 2D mesh is 1 mm per square cell, which comprises 299 160 orthogonal hexahedral elements with an aspect ratio of 1. In this study, the mesh independence study was not carried out, but the chosen mesh size was based on previous numerical studies of FA and DDT with similar setups [2], [4], [14]. One can contact the corresponding author for the list of boundaries and initial conditions defined in the simulation.

An essential part of modeling premix combustion using blastXiFoam is the calculation of the thermophysical and transport properties of the unburnt/burnt mixtures. The OpenFOAM blastXiFoam solver requires the definition of the Sutherland law to calculate dynamic viscosity and JANAF table coefficients for C_p. In this study, the thermophysical and transport properties of the gas mixture were obtained using the open-source code *mech2Foam* developed by Henriksen M. et al. [15]. *mech2Foam* code uses Cantera in its subroutine to calculate the mole weights, NASA polynomial coefficients, and Southerland coefficients. Code requires specification of initial parameters, such as the fuel and oxidizer composition, the initial pressure, temperature, and reaction mechanism (as GRI-Mech). Furthermore, in the simulation, combustion properties are defined by the Gulders formulation, which is used to calculate the laminar flame speed. Users must define the fuel and its corresponding Gulder coefficients for laminar flame speed computation to utilize the Gulders formulation; these coefficients are generated by *mech2Foam*. When defining XiModel, the model for flame wrinkling Xi (Ξ), algebraic formulation is used.

The governing equations in OpenFOAM were solved with the collocated finite volume method (FVM). HLLC Riemann solver is used to calculate numerical fluxes. The explicit Euler method

with first-order accuracy was employed for the time discretization. For gradient discretization, the least-square cell-based method with a gradient limiter was utilized to prevent oscillations. The convective terms were discretized using a first-order accurate limited linear scheme, where the amount of upwind can be controlled by a blending coefficient between 0 and 1, where one strongly limits the unwinding, and zero is a pure linear scheme. The diffusive terms were discretized using a second-order cantered differences scheme. The time step interval was chosen using an adaptive method that limited the CFL number to 0.5.

Results and discussion

This section discusses the numerical results and is divided into two main sections, which are the flame propagation before and after the obstacle. The first part of the discussion will be regarding Figure 2. The initial phase of the explosion involves the propagation of a laminar flame, which moves at a speed determined by the laminar burning velocity and the density difference across the flame front. The tulip flame that can be seen at 9 ms is caused by baroclinic instability influenced by the reflection of pressure waves of the obstacle. This is also why we observed fluctuations in the velocity and pressure plot. However, the laminar flame propagation phase is relatively short-lived and is soon succeeded by a "wrinkled" flame phase. In most accidental explosions, this wrinkled flame phase can persist over considerable distances of flame propagation. Consequently, it holds greater significance than the initial laminar phase. Due to the expansion in the flame area and thus the burning rate, the flame propagation speed in the wrinkled flame can be several times higher than in the laminar flame. As a result of turbulence generated by obstacles or boundary layers, the wrinkled flame eventually evolves into a turbulent flame brush. This transformation leads to further flame acceleration due to the increased surface area of the laminar flamelets within the flame brush.

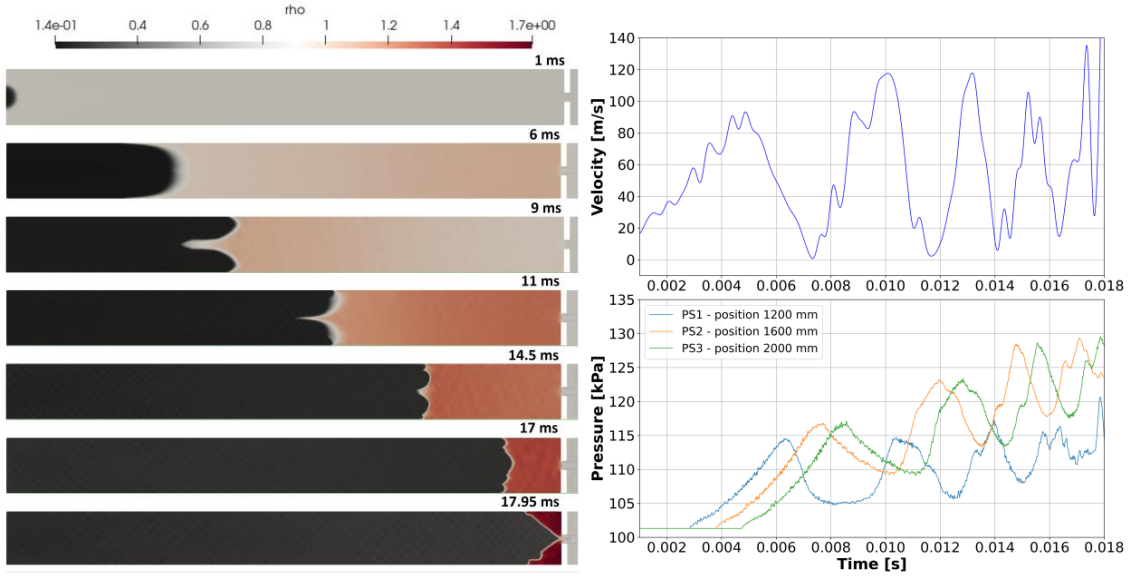

Figure 2: Flame acceleration in first 1 m of channel before obstacle and velocity/pressure plot

Following, we examine Figure 3, which illustrates a jet flame as it exits the first half of the chamber through the obstacle. The pressure gradient, a common way to visualize supersonic flows, is shown in the left picture. The reader will have an easier time visualizing the reaction zone between the approaching detonation wave and the flame front due to the red line's representation of the flame front. Numerical results show that the jet flame creates a weak shock after exiting the obstacle. In the zone between the jet flame front and weak shock on the

upper side, a local hot spot occurs and creates a local "explosion." The local "explosion" occurs in the jet due to the high turbulence levels and large velocity gradients, which generate shock waves. The reflection of these shock waves at the walls forms Mach-reflections where the reactant gas temperature increases to cause a DDT.

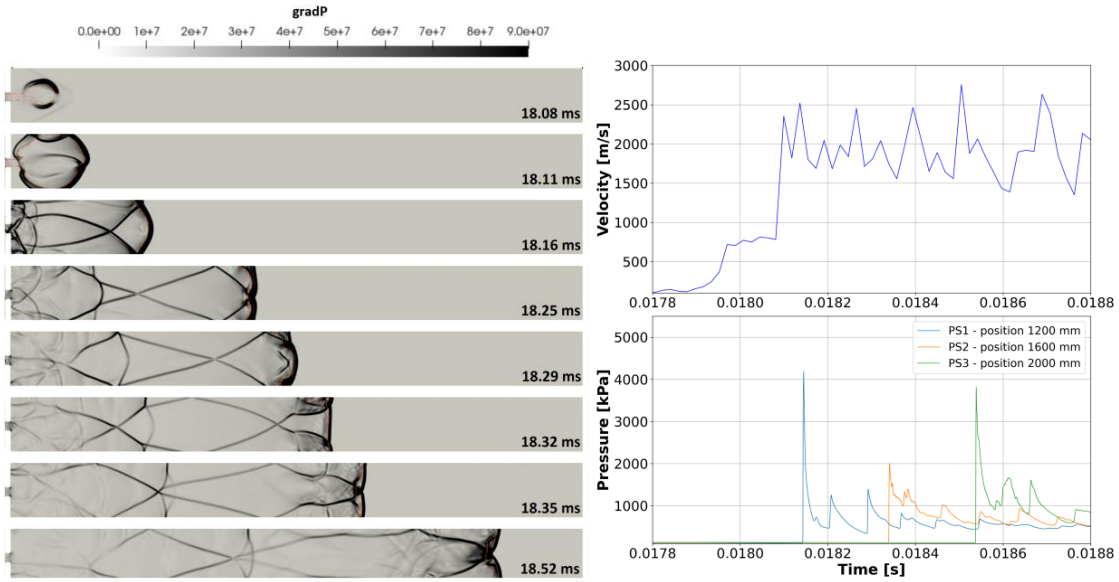

Figure 3: Detonation initiation and propagation after the obstacle and velocity/pressure plot

Compared to the experiments in [4] and [5], the numerical solution shows great agreement with the prediction of overpressure and velocity speeds of the flame front. Moreover, both experiments and simulations observed that the blast from an explosion at one wall can initiate an explosion at the other wall. Numerical results show the underlying physic of flame in the deflagrating regime with the transition to detonation, where the mechanism of detonation as a shock wave, reaction zone, detonation front, transverse detonation wave and reflected pressure wave with shock focusing can be observed. On the other hand, in experiments, DDT occurs further on in the channel after exiting the obstacle, and it is initiated by a local "explosion" far behind the leading edge of the flame. The flame-jet interaction in the simulation causes the reaction rate to increase unrealistically fast, leading to earlier detonation onset. Further understanding of the reaction rate switch in blastXiFoam and enhancements in the numerical approach (higher order numerical schemes) will be pursued in subsequent work.

Summary and Conclusions

This study utilizes the blastXiFoam solver on the OpenFOAM platform to study flame dynamics, focusing on flame acceleration and Deflagration to Detonation Transition (DDT) of premix homogeneous hydrogen-air mixture within an obstructed channel. The flame-wrinkling combustion model with the HLLC scheme, for accurate shock capturing, is used. Results demonstrate the evolution from laminar to wrinkled flames, emphasizing baroclinic instabilities and turbulence's pivotal role in flame acceleration. The wrinkled flame ultimately transforms into a turbulent flame brush, significantly accelerating flame propagation. Moreover, the study reveals intricate flame behaviors after an obstacle, showcasing the potential for local "explosions" that may lead transition to detonation when reaching the wall. Numerical studies show good agreement with experiments regarding overpressure and flame front velocity predictions. DDT occurs in the numerical analysis, but the underlying mechanism of initiation and position in the channel differs from experimental observations. In

conclusion, this research helps us to better understand hydrogen explosion in confined obstructed spaces, and the numerical methods used to solve governing equations of combusting flow, therefore offering a foundation for enhanced safety studies.

Acknowledgements: This publication has been produced with support from the HYDROGENi Research Centre (hydrogeni.no), performed under the Norwegian research program FMETEKN. The authors acknowledge the industry partners in HYDROGENi for their contributions and the Research Council of Norway (**333118**).

References

[1] E. S. Oran, G. Chamberlain, and A. Pekalski, 'Mechanisms and occurrence of detonations in vapor cloud explosions', *Prog. Energy Combust. Sci.*, vol. 77, p. 100804, Mar. 2020, doi: 10.1016/j.pecs.2019.100804.

[2] F. Ettner, K. G. Vollmer, and T. Sattelmayer, 'Numerical Simulation of the Deflagration-to-Detonation Transition in Inhomogeneous Mixtures', *J. Combust.*, vol. 2014, pp. 1–15, 2014, doi: 10.1155/2014/686347.

[3] Synthetik Applied Technologies, 'blastFoam Version 6.0'. https://github.com/synthetik-technologies/blastFoam

[4] A. V. Gaathaug, K. Vaagsaether, and D. Bjerketvedt, 'Experimental and numerical investigation of DDT in hydrogen–Air behind a single obstacle', *Int. J. Hydrog. Energy*, vol. 37, no. 22, pp. 17606–17615, Nov. 2012, doi: 10.1016/j.ijhydene.2012.03.168.

[5] D. Bjerkedvedt, A. V. Gaathaug, and K. Vaagsaether, 'Front Tracking of DDT from Ultra-high Speed Video Films', presented at the 25th ICDERS, Leeds, UK, 2015.

[6] R. Khodadadi Azadboni, J. X. Wen, and A. Heidari, 'Numerical Modeling of Flame Acceleration and Transition from Deflagration to Detonation Using OpenFOAM®', in *OpenFOAM®*, J. M. Nóbrega and H. Jasak, Eds., Cham: Springer International Publishing, 2019, pp. 357–372. doi: 10.1007/978-3-319-60846-4_26.

[7] H. K. Versteeg and W. Malalasekera, *An introduction to computational fluid dynamics: the finite volume method*, 2nd ed. Harlow, England ; New York: Pearson Education Ltd, 2007.

[8] F. R. Menter, 'Two-equation eddy-viscosity turbulence models for engineering applications', *AIAA J.*, vol. 32, no. 8, pp. 1598–1605, Aug. 1994, doi: 10.2514/3.12149.

[9] H. Kutkan and J. Guerrero, 'Turbulent Premixed Flame Modeling Using the Algebraic Flame Surface Wrinkling Model: A Comparative Study between OpenFOAM and Ansys Fluent', *Fluids*, vol. 6, no. 12, p. 462, Dec. 2021, doi: 10.3390/fluids6120462.

[10] A. Karanam, P. K. Sharma, and S. Ganju, 'Numerical simulation and validation of flame acceleration and DDT in hydrogen air mixtures', *Int. J. Hydrog. Energy*, vol. 43, no. 36, pp. 17492–17504, Sep. 2018, doi: 10.1016/j.ijhydene.2018.07.108.

[11] H. G. Weller, G. Tabor, A. D. Gosman, and C. Fureby, 'Application of a flame-wrinkling les combustion model to a turbulent mixing layer', *Symp. Int. Combust.*, vol. 27, no. 1, pp. 899–907, Jan. 1998, doi: 10.1016/S0082-0784(98)80487-6.

[12] C. K. Law, *Combustion Physics*. Cambridge University Press, 2006.

[13] G. Tabor and H. G. Weller, 'Large Eddy Simulation of Premixed Turbulent Combustion Using Flame Surface Wrinkling Model', *Flow Turbul. Combust. Former. Appl. Sci. Res.*, vol. 72, no. 1, pp. 1–28, 2004, doi: 10.1023/B:APPL.0000014910.06345.fb.

[14] K. Vaagsaether, V. Knudsen, and D. Bjerketvedt, 'Simulation of flame acceleration and DDT in H2H2-air mixture with a flux limiter centered method', *Int. J. Hydrog. Energy*, vol. 32, no. 13, pp. 2186–2191, Sep. 2007, doi: 10.1016/j.ijhydene.2007.04.006.

[15] M. Henriksen, K. Vaagsaether, J. Lundberg, S. Forseth, and D. Bjerketvedt, 'Simulation of a premixed explosion of gas vented during Li-ion battery failure', *Fire Saf. J.*, vol. 126, p. 103478, Dec. 2021, doi: 10.1016/j.firesaf.2021.103478.

Fluidization for improved hydrogen release from LOHC – A combined computational and experimental approach.

L. Van Hoecke[*1,2], N.B. Kummamuru[1,2], P. Perreault[1,2]

[1] University of Antwerp, Department of Bioscience Engineering, Sustainable Energy Air and Water Technology, Groenenborgerlaan 171, 2020 Antwerpen, Belgium
[2] University of Antwerp, Blue App, Olieweg 97, 2020 Antwerp Belgium

Introduction

One of the main hurdles in the large-scale roll-out of a hydrogen-based economy is efficient storage of the hydrogen gas. For current – comparably small – applications the use of hydrogen gas tanks provides sufficient storage, but on a large industrial scale the low storage capacity of these hydrogen gas tanks, often only about 2 wt.% for metallic tanks is insufficient. Considering (intercontinental) transport, the use of hydrogen gas tanks becomes even more problematic. Cryogenic storage of hydrogen is more efficient on a mass and volume based, but the low temperatures required to liquify hydrogen (20 K) place a large energy penalty on the system. Large scale handling of cryogenic liquids like LNG has become more standard practice but is still a lot less efficient than handling and transport of liquids. It is on this advantage that Liquid Organic Hydrogen Carriers (LOHC) are trying to capitalize. LOHC are organic carrier molecules that can store hydrogen by hydrogenation reactions, the molecule then becomes a charged carrier, which is a stable liquid product that can be stored at room temperature and ambient pressure. In this work we focus on the molecule dibenzyltoluene (DBT) which is able to store 6.2 wt.% of hydrogen or 56 g L-1, at ambient conditions and exists as a colorless inflammable liquid with a viscosity roughly double that of water. The charged LOHC molecule is called perhydro-dibenzyltoluene or H_{18}DBT. Via a chemical dehydrogenation step, the hydrogen can be released from this molecule, and the original DBT carrier can be reused for subsequent hydrogen storage steps, with minimal losses (<0.1 wt.%) of the carrier material in the entire cycle.[1]

The current oil-based industry is well adapted to transport and store this LOHC molecule, as ships, pipelines, storage tanks and trucks already exist to transport (crude) oil. There are two larger challenges with the use of this molecule. Firstly, the spend carrier has to be brought back to hydrogenation plants, so there needs to be an additional transport cycle in comparison with fossil fuels. Secondly, the dehydrogenation step is highly endothermic (Δ H_R^0$\approx$ 65 kJ mol-1H2) and requires an energy flux of around 570 K for hydrogen to be released in the presence of a heterogenous catalyst (usually Pt/Al2O3).[2] It is on this process that my PhD focusses to make this process as efficient as possible, to minimize energy loss in this step. The strategy that we chose was to investigate the use of fluidization of the catalyst beads. This has a twofold purpose, not only is the fluidization beneficial for the heat transfer of the liquid to the catalyst surface (which cools down due to the endothermic nature of the process), it also helps in the removal hydrogen from the catalytic surface due to the shear stress induced by liquid and solid movement. The volume expansion upon hydrogen release from the liquid is huge, theoretically, 1 mL of H_{18}DBT can yield up to 650 mL of hydrogen gas.[3] This volume expansion causes catalyst dewetting, which lowers the efficiency of the process, since hydrogen is only

* Corresponding author: laurens.vanhoecke@uantwerp.be

being released upon contact of the LOHC liquid with the catalyst surface. Efficient removal of hydrogen is thus a key step to improve the process. [4]

The efficiency of hydrogen removal is studied throughout this PhD via both a computational and experimental method. Firstly, I studied with a cold flow setup the concept of a swirling fluidized bed reactor, which uses a centrifugal field to aid in the removal of hydrogen from the catalyst surface. This was done via combined CFD simulations and validation experiments in our 25 L cold flow mock-up system. Next, I investigated several possible settings in our simulation for three phase fluidization systems, to have more accurate liquid – gas – solid simulations. These simulations were compared to an in house created 2D – fluidized bed reactor characterized using image analysis techniques, including Particle Image Velocimetry (PIV), Particle Tracking Velocimetry (PTV) and Digital Image Analysis (DIA). Thirdly, I programmed a custom chemical source term to study the hydrogen release from LOHC, which allows us to simulate the hydrogen release rate from the catalyst using a Eulerian – Eulerian approach. This should lead to CFD simulations to design new reactors for improved hydrogen release from H_{18}DBT**.**

Methodology

CFD simulations conducted in this work were conducted using the opensource CFD software program OpenFOAM, both version 8 and version 11 have been used. The multiphase nature of the simulation and especially the nature of the dense particle bed pushed us towards the use of Eulerian - Eulerian solvers, called multiphaseEulerFoam (version 8) or the multiphaseEuler solver module in version 11. The turbulent nature of the flows were modeled using the kOmegaSST model, from Menter. [5] The particle behavior was described by using the kinetic theory of granular flow (KTGF).

Two different source term approaches have been used in this work. For cold flow analysis, a general mass-based source term has been used that generates gas, inside a set control volume (i.e., a cellZone, in OpenFOAM terms). To mimic the release of hydrogen during the reaction of H_{18}DBT a custom-made source term was programmed whereby the hydrogen release rate depended on the amount of catalyst present inside each cell of the mesh. This approach was used since there is currently no solver in the OpenFOAM framework that allows for heterogenous catalytic reactions of liquid phase flows. The custom-made source term is based on existing mass-based source terms. Although, mass-based source terms often suffer from stiffness in the initial solution, the low mass flux of hydrogen compared to the liquid/solid mass keeps this effect minimal. Due to the computationally complex nature of the three-phase system, Courant numbers during the simulation are always kept below 0.1, which furthers reduced the stiffness induced by the hydrogen source term.

Three image analysis techniques were used: PIV, PTV and DIA, to study the behaviour of cold flow liquid – gas – solid systems. For the PIV a PCO Panda 26 DS sCMOS Camera has been used, combined with a Rodagon 35 lens. The Matlab extension PIVlab [6] has been used for image postprocessing. The PTV and DIA relied on images taken using a Sony Cybershot camera with a 9.1 Megapixel camera, image analysis was done with the opensource software package imageJ and the trackMate extension, [7] after a pre-processing step in Matlab to generate binary black and white images.

Discussion

In this PhD thesis the first section that was studied was the use of a swirling fluidized bed reactor for the dehydrogenation reaction of H_{18}DBT. This new reactor concept was studied via a cold-flow mockup study. Instead of using H_{18}DBT, H_2 and Al_2O_3 catalysts, a system with similar hydrodynamic properties was used with water, Ar, and glass beads as the catalyst to keep Reynolds and Stokes numbers similar to those expected in a reactive system.

Figure 1 depicts the operation of this new swirling fluidized bed reactor. Liquid is inserted via the bottom two inlet regions, gas in this cold flow mockup was injected via a gas diffuser placed in the center of the reactor bottom plate. On Figure 1, it shows that the beads do no fluidize when there is no gas generation. With gas flow enabled the catalyst bed was agitated by the combined liquid and gas flow. The movement of the particles showed a rotational pattern that followed closely the pattern of the liquid movement near the walls. There was a positive slip velocity of the liquid exerted on the glass beads which in reactive mode would enhance the gas removal from the catalyst surface. One of the main goals of this reactor design. [8]

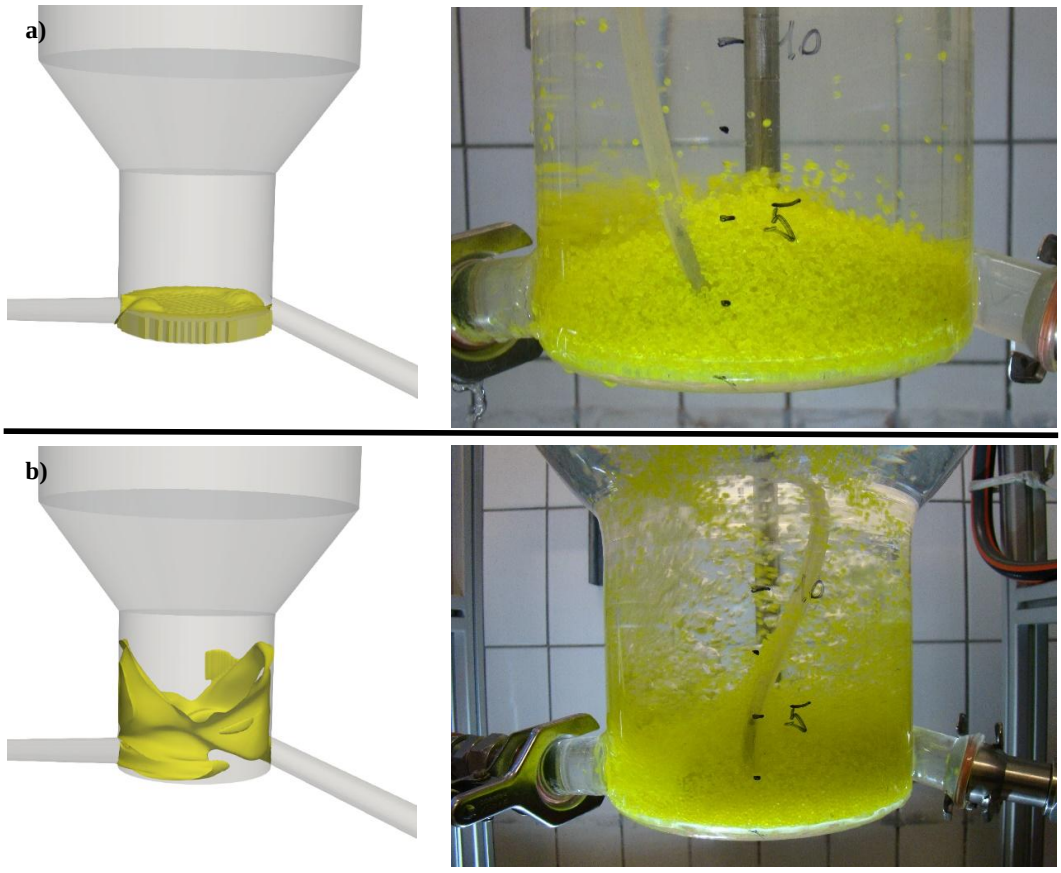

Figure 1 Comparison between simulations and experiments. a) Reactor operation without gas flow, showing little to no movement of the solid bed. b) Reactor operation with 50 LPM of water and 10 LPM gas flow, showing the fluidization of the glass beads (painted in yellow for better visualization). The cut-off value for the CFD – contour plot of the volume fraction of the solids was set to 0.15.

From the results on Figure 1, it was observed that the CFD simulation was not successful in capturing the exact bed height that was achieved in the swirling fluidized bed reactor. To deal with this, an improvement to the interphase exchange models (especially drag models) required for solving the liquid – gas – solid momentum equations was proposed. To investigate the use of improved drag models, image analysis was used to study a pseudo – 2D fluidized bed reactor. And compare the results to CFD simulations. Operation of the fluidized bed reactor can be seen on: https://youtu.be/X9Qnug7ixHY . The selection of improved interphase exchange parameters for the pseudo-2D fluidized bed was able to obtain an estimation of the observed bed height withing a deviation of less than 1 mm, analyzed using DIA. By using PTV, it was attempted to track the particle movements throughout the bed, by the use of black tracer particles, a snapshot of these particle trajectories is shown on Figure 2. From this image it is clear that the movement of the particles is very chaotic. However, the CFD snapshot shows three clear regions, a recirculation area near the bottom of the bed. A downcomer region near the walls of the reactor and an upwards moving center region. These dominant trajectories, especially those close to the wall can also be seen on the particle tracking results. Velocities obtained from both the PTV and CFD images were in the same order of magnitude, 0.05 m s^{-1}. The recirculation area at the bottom of the reactor, which has a more constant dominant flow profile than the rest of the bed will be studied using PIV. Ultimately, the simulations settings will be compared based on three different aspects, the prediction of the particle bed height, the prediction of the velocity magnitude of downwards moving particles near the wall, and the height and velocity within the recirculation zone. The drag models of Schiller and Naumann; Ishii and Zuber; Tomiyama; Syamlal and O'Brien; and that of Lin will be compared for the accuracy in the liquid – gas – solid system.

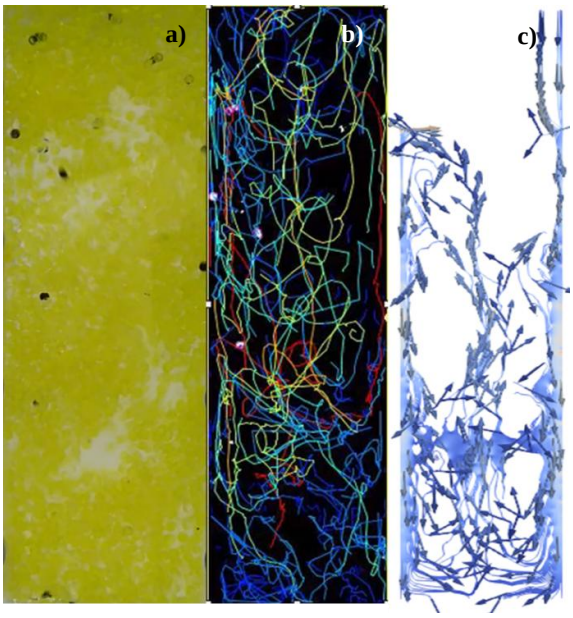

Figure 2 Image analysis of the liquid - gas - solid pseudo- 2D fluidized bed reactor. a) the unprocessed image, b) the particle trajectories analyzed by PTV, c) the processed CFD images of the dominant particle trajectories.

Ultimately, the goal of this research is to obtain CFD simulations that are capable of capturing liquid – gas – solid interactions with a high accuracy which is required to simulate the dehydrogenation reaction of H_{18}DBT. Using a source term approach to mimic

the hydrogen evolution of the H_2 gas from the catalyst particles. This would then in turn allow for simulations to improve the reactor geometry, specifically the geometry shown in Figure 1, to improve the power density of the dehydrogenation system.

Conclusions

The goal of this PhD is to improve the reactor design for the dehydrogenation reaction of H_{18}DBT by fluidization of the catalyst particles to improve mass and heat transfer. This will be done so by a CFD approach to be able to evaluate various parameters for improved fluidization behavior. However, the CFD framework for liquid – gas – solid simulations is not yet completely understood which is why an initial study was required on the simulation settings for liquid – gas – solid fluidized beds. The results of these simulations when compared to image analysis techniques (PIV, PTV, DIA) were promising and from initial analysis it shows that there is a general comparability between the image analysis results and those of the CFD simulation. This will feed, in the future, new CFD simulations that can be used for improved reactor design for dehydrogenation reactors of H_{18}DBT.

References

1. Van Hoecke, L., et al., *Challenges in the use of hydrogen for maritime applications.* Energy & Environmental Science, 2021. **14**(2): p. 815-843.
2. Perreault, P., et al., *Critical challenges towards the commercial rollouts of a LOHC-based H2 economy.* Current Opinion in Green and Sustainable Chemistry, 2023: p. 100836.
3. Modisha, P.M., et al., *The Prospect of Hydrogen Storage Using Liquid Organic Hydrogen Carriers.* Energy & Fuels, 2019. **33**(4): p. 2778-2796.
4. Solymosi, T., et al., *Nucleation as a rate-determining step in catalytic gas generation reactions from liquid phase systems.* Science Advances, 2022. **8**(46).
5. Menter, F.R., *Two-equation eddy-viscosity turbulence models for engineering applications.* AIAA Journal, 1994. **32**(8): p. 1598-1605.
6. Thielicke, W. and R. Sonntag, *Particle Image Velocimetry for MATLAB: Accuracy and enhanced algorithms in PIVlab.* Journal of Open Research Software, 2021.
7. Ershov, D., et al., *TrackMate 7: integrating state-of-the-art segmentation algorithms into tracking pipelines.* Nature Methods, 2022. **19**(7): p. 829-832.
8. Van Hoecke, L., et al., *Intensified swirling reactor for the dehydrogenation of LOHC.* International Journal of Hydrogen Energy, 2023.

From Grey to Green: The Impact of Hydrogen Source on SAF's Climate Benefits

V. Ballal*[1], F. Cherubini [1], M.D.B. Watanabe[1]

[1] Industrial Ecology Program, Department of Energy and Process Engineering, Norwegian University of Science and Technology (NTNU), Trondheim, Norway

Introduction

The aviation sector is a significant contributor, responsible for approximately 4% of total greenhouse gas (GHG) emissions in Europe [1], [2]. Given its heavy reliance on fossil fuels and the complex search for alternatives, it poses a formidable challenge in terms of emissions mitigation [3], [4]. To align with the goal of achieving climate neutrality by 2050, the European Union (EU) has set ambitious targets to reduce emissions from the transport sector by 90% by 2050, with an interim target of a 55% reduction by 2030 [5]. These targets encompass the daunting task of curbing emissions from the aviation sector.

Sustainable Aviation Fuels (SAF) are a vital component of the EU's strategy. SAF, often referred to as drop-in alternative fuels, are produced from renewable and low-carbon feedstocks, including non-food biomass, advanced biofuels from agriculture and forestry residues or through synthetic processes that capture and utilize carbon dioxide (CCU) to create fuels [6]. Synthetic fuels or e-fuels, are a subset of CCU, created by combining captured carbon and hydrogen. In the case of e-fuels, hydrogen is produced via the electrolysis of water, primarily powered by renewable electricity, commonly known as 'Green hydrogen'. The Green hydrogen pathways investigated in this study can also be referred to as e-fuels. However, hydrogen can also be sourced from steam methane reforming of natural gas, with or without carbon capture and storage (CCS), resulting in 'Blue' and 'Grey' hydrogen, respectively. Drop-in synthetic fuels share characteristics with fossil jet fuels, such as high energy density, ease of storage and transport, and combustibility. Moreover, they can have lower carbon footprints, making them sustainable and fitting replacements for fossil jet fuels [6].

In response to the mitigation challenges and goals, the European Union has introduced the ReFuelEU Aviation initiative to promote GHG emission reductions and the use of SAF. This initiative mandates a progressive increase in the use of SAF, commencing in 2025. The obligation starts at 2% usage in 2025, rising to 6% by 2030 and a more substantial 20% by 2035, with a gradual increase to 70% by 2050. These targets encompass specific sub-mandates for synthetic aviation fuels, ranging from 1.2% usage in 2030 to 5% by 2035 and a significant 35% by 2050 [6].

While numerous feedstocks and processes contribute to Sustainable Aviation Fuels (SAF), our study's primary focus is on assessing synthetic drop-in aviation fuels. We specifically examine different hydrogen sources (Green, Blue, and Grey) and sources of captured carbon (Atmospheric, Biogenic, and Fossil). A graphical summary is shown in Figure 1. It's worth noting that previous studies [7], [8] have explored the climate impacts of e-fuels for aviation primarily concerning variations in carbon sources with limited emphasis on hydrogen production variability or the electricity for hydrogen production is drawn from the grid.

* Corresponding author: vedant.p.ballal@ntnu.no

This study aims to provide explicit insights into how the choice of hydrogen source (Green, Blue, or Grey) directly influences the climate impact of synthetic fuels, particularly in the context of their use as SAF in Europe. Furthermore, we investigate how these impacts might change under various policy scenarios, considering socio-economic and infrastructure changes. This comprehensive approach enhances our understanding of the complex factors affecting the sustainability of aviation fuels in the European context.

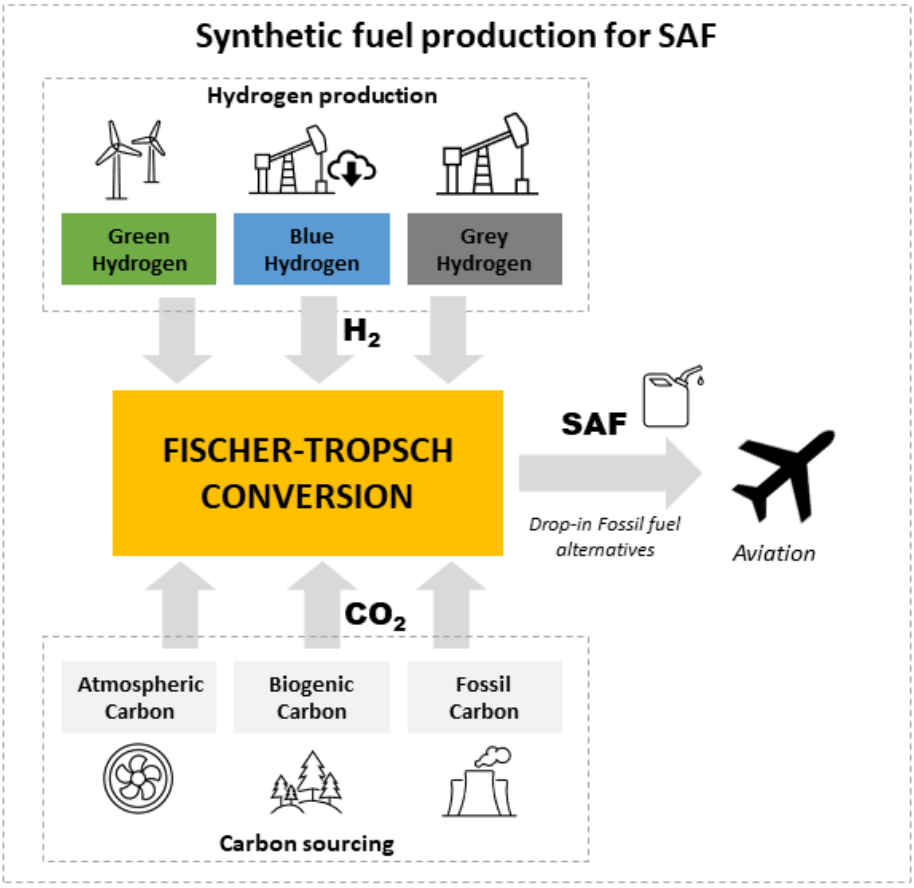

Figure 1: Graphical Summary of Synthetic fuel production for SAF

Methodology

1. Technological Assessment

A comprehensive technological assessment has been meticulously undertaken to scrutinize the production pathways of Sustainable Aviation Fuels (SAF). This assessment entails a thorough analysis encompassing material and energy requirements, process efficiencies, and the Technological Readiness Levels (TRLs) associated with the diverse technologies and processes engaged in the conversion process.

In its entirety, our study investigates nine distinct SAF production pathways. These pathways are the combination of three carbon sources—namely atmospheric, biogenic, and fossil—with three different hydrogen production methods: electrolysis powered by a renewable energy source- off-shore wind energy (green hydrogen), steam methane reforming without Carbon

Capture and Storage (CCS) (grey hydrogen), and steam methane reforming integrated with CCS (blue hydrogen).

To accomplish the transformation of intermediate synthetic gas into a liquid fuel useful for aviation purposes, we employ a thermochemical Fischer-Tropsch conversion process. This comprehensive approach enables us to explore, evaluate, and compare the full spectrum of SAF production possibilities, accounting for the variability in carbon and hydrogen sources while assessing their technological readiness and operational efficiency.

2. Climate Impact Assessment

To assess the climate impacts comprehensively, we adopt a "Well-to-Wake" life cycle perspective. This approach takes into account all phases of the fuel's life cycle, including production, distribution from the plant to the airport, and the combustion stage. In our evaluation of emissions contributors, we encompass the Near-term Climate Forcers (NTCFs) in addition to the Well-Mixed greenhouse gasses (WMGHGs). NTCFs, comprising CO (carbon monoxide), SOx (sulfur oxides), NOx (nitrogen oxides), Volatile Organic Compounds (VOCs), Black and Organic carbons, as well as contrails (generated during the combustion phase in jet engines) have a shorter life span but may have a significant heating or cooling effect contributing to the climate change impacts [9]. The cumulative climate impacts are expressed in terms of Global Warming Potential over a 100-year time horizon (GWP100). Furthermore, we conducted a comparative assessment of the climate impacts of various SAF pathways against those of conventional fossil jet fuel.

In forecasting future climate impacts, we will conduct a prospective life cycle assessment, factoring in anticipated technological advancements and socio-economic changes within the overarching systems. We consider two distinct policy scenarios, each with differing levels of commitment to climate change mitigation. The first scenario represents a business-as-usual trajectory with no stringent climate policies in place. The second scenario aligns with a proactive climate policy framework consistent with the Nationally Determined Contributions (NDCs) in accordance with the Paris Agreement's objectives. This dual approach allows us to evaluate the potential future climate implications of SAF pathways under varying policy contexts. In the latter stages of our research, we will perform an uncertainty analysis. This analysis will consider fluctuations in key parameters such as transport distances, uncertainties in the characterization factors of involved species contributing to climate impacts, and the efficiency of the conversion processes.

Preliminary and Expected Results

Our initial findings suggest that within the context of green hydrogen pathways—where renewable electricity (off-shore wind) is employed for electrolysis—the climate impacts span a range of 62 to 146 gCO_2 eq. MJ^{-1}. This range encompasses synthetic fuel pathways that incorporate the different carbon sources considered.

In the case of biogenic and atmospheric carbon pathways, both coupled with green hydrogen, similar climate impacts are observed. These pathways offer substantial mitigation potential, with emissions reductions of approximately 54% and 56%, respectively, compared to conventional fossil jet fuel. Conversely, the fossil carbon pathway exhibits slightly higher climate impacts relative to fossil jet fuel, registering at 146 gCO_2 eq. MJ^{-1}, as opposed to the latter's 141.6 gCO_2 eq. MJ^{-1}. While omitting the Near-term Climate Forcers (NTCFs), which

are not part of the EU policy considerations, it becomes feasible to attain substantial mitigation benefits for the non-fossil carbon sources. These benefits may reach as high as 81-85%. However, it's worth noting that the impacts of pathways based on fossil carbon sources continue to surpass those associated with conventional jet fuels.

In terms of the contributors to these climate impacts, contrail formations during the combustion stage are the dominant factors for both the biogenic and atmospheric carbon pathways. For the fossil carbon pathway, the primary contributor is the re-emission of fossil CO2 during the combustion stage, following its capture during the fuel production phase. This re-emission significantly elevates the pathway's overall impact, with contrails also playing a noteworthy role. A visual representation of these contributing factors is provided in Figure 2.

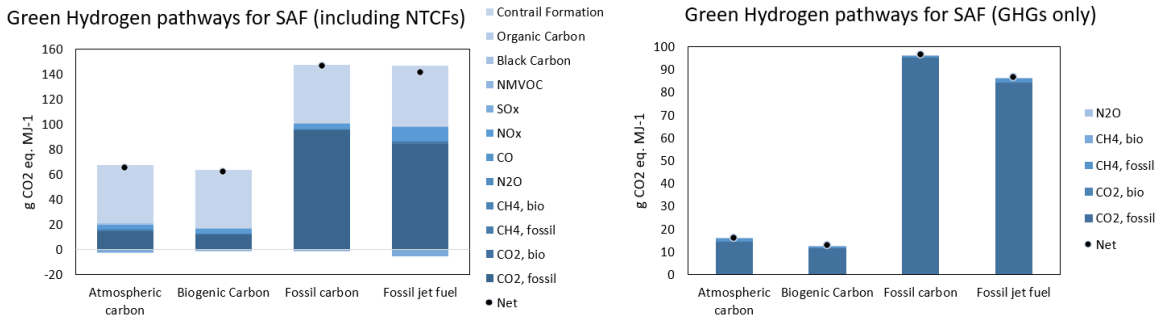

Figure 2: Contribution of different species towards the climate impact of Green Hydrogen pathway synthetic fuels for SAF.

While we anticipate that the climate impacts of blue hydrogen and grey hydrogen pathways will likely surpass those of green hydrogen, it is also of considerable interest to assess the role of carbon capture and storage (CCS) in blue hydrogen. This analysis will provide valuable insights into the extent of CCS's influence on the overall climate impact and mitigation potential.

Furthermore, we anticipate that as we factor in future socio-economic and technological advancements, especially in the context of evolving infrastructure aligned with Nationally Determined Contributions (NDCs), the climate impacts of all pathways are poised to decrease. This decrease should translate into more substantial mitigation benefits when compared to conventional fossil jet fuel.

Conclusions

In conclusion, our study highlights the importance of optimizing synthetic fuel production, particularly for Sustainable Aviation Fuels (SAF) in Europe, to maximize climate benefits. These findings also hold broader implications for hydrogen and hydrogen-based fuel production due to their increasing demand across various applications. As we strive to reduce greenhouse gas emissions and transition to a sustainable energy landscape, understanding how to produce low-carbon fuels efficiently is crucial.

Our research underscores the significance of factors such as green hydrogen, background infrastructure, technology advancements, and supportive policies in scaling up synthetic hydrogen-based fuel production. These insights can guide policymakers, industry stakeholders, and innovators in advancing the infrastructure for large-scale hydrogen-based fuel production, fostering a cleaner and more sustainable future while driving innovation and economic growth.

References

[1] I. Tiseo, “EU CO2 emissions from commercial passenger flights 2013-2019,” Statista. Accessed: Oct. 10, 2023. [Online]. Available: https://www.statista.com/statistics/1237688/eu-commercial-aviation-co2-emissions-by-type/.

[2] I. Tiseo, “Total greenhouse gas emissions in the European Union 1990-2021,” Statista. Accessed: Oct. 10, 2023. [Online]. Available: https://www.statista.com/statistics/780410/total-greenhouse-gas-emissions-european-union-eu/.

[3] S. J. Davis *et al.*, “Net-zero emissions energy systems,” *Science*, vol. 360, no. 6396, p. eaas9793, 2018, doi: 10.1126/science.aas9793.

[4] F. Ueckerdt, C. Bauer, A. Dirnaichner, J. Everall, R. Sacchi, and G. Luderer, “Potential and risks of hydrogen-based e-fuels in climate change mitigation,” *Nat. Clim. Chang.*, vol. 11, no. 5, pp. 384–393, May 2021, doi: 10.1038/s41558-021-01032-7.

[5] European Commission, Directorate-General for Climate Action, “COMMUNICATION FROM THE COMMISSION TO THE EUROPEAN PARLIAMENT, THE COUNCIL, THE EUROPEAN ECONOMIC AND SOCIAL COMMITTEE AND THE COMMITTEE OF THE REGIONS Stepping up Europe’s 2030 climate ambition Investing in a climate-neutral future for the benefit of our people.” European Commission, Sep. 17, 2020. Accessed: Oct. 05, 2023. [Online]. Available: https://eur-lex.europa.eu/legal-content/en/ALL/?uri=CELEX:52020DC0562.

[6] European Commission, “REGULATION OF THE EUROPEAN PARLIAMENT AND OF THE COUNCIL on ensuring a level playing field for sustainable air transport (ReFuelEU Aviation).” THE EUROPEAN PARLIAMENT AND THE COUNCIL OF THE EUROPEAN UNION, Sep. 13, 2023. Accessed: Oct. 10, 2023. [Online]. Available: https://www.consilium.europa.eu/en/press/press-releases/2023/10/09/refueleu-aviation-initiative-council-adopts-new-law-to-decarbonise-the-aviation-sector/.

[7] V. Ballal, O. Cavalett, F. Cherubini, and M. D. B. Watanabe, “Climate change impacts of e-fuels for aviation in Europe under present-day conditions and future policy scenarios,” *Fuel*, vol. 338, p. 127316, Apr. 2023, doi: 10.1016/j.fuel.2022.127316.https://www.iea.org/reports/global-energy-review-2021.

[8] D. Freire Ordóñez, T. Halfdanarson, C. Ganzer, N. Shah, N. M. Dowell, and G. Guillén-Gosálbez, “Evaluation of the potential use of e-fuels in the European aviation sector: a comprehensive economic and environmental assessment including externalities,” *Sustainable Energy Fuels*, vol. 6, no. 20, pp. 4749–4764, 2022, doi: 10.1039/D2SE00757F.

[9] Intergovernmental Panel On Climate Change, *Climate Change 2021 – The Physical Science Basis: Working Group I Contribution to the Sixth Assessment Report of the Intergovernmental Panel on Climate Change*, 1st ed. Cambridge University Press, 2023. doi: 10.1017/9781009157896.

Fuel cell and NiMH accumulator power supply for electric vehicles

D.Boychev*, J.Iliev, K.Petrov

Institute of electrochemistry and energy systems "Academician Evgeni Budevski" – BAS, Acad. Georgi Bonchev Str., Block 10, 1113 Sofia, Bulgaria

Introduction

The electric vehicles (EV) need to provide power for the vehicle under all kinds of road conditions and driving modes. The energy consumption depends on several different factors as mass of vehicle, road type, moment acceleration which are independents of each other. In Fig. 1 is shown example of power consumption taken of urban cycle of vehicle with mass 1600 kg – [1]

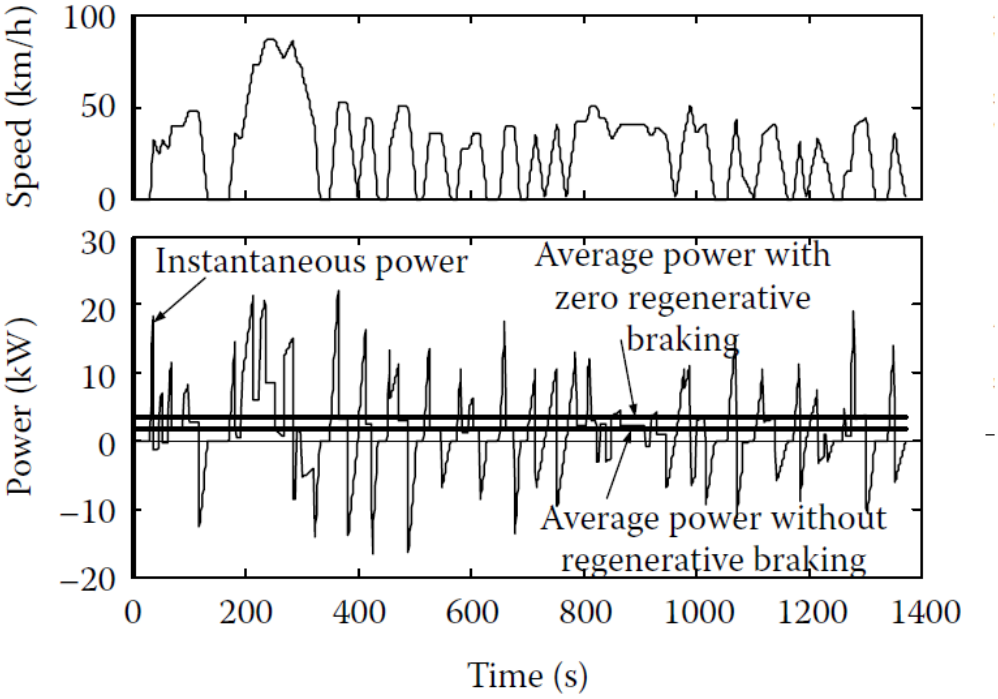

Figure 1 Power consumption taken from urban cycle

It can be seen that the power consumption is extremely dynamic. In general case the average value of the required energy can be found as:

$$E_{EV} = \frac{1}{T}\int_0^T P(t)\,dt \qquad (1)$$

Were E_{EV} is energy, required for traction drive, T is cycle duration, t is time

*Corresponding author: d.boychev@iees.bas.bg

Also, there is a big difference between maximal and minimal consumption. More over electric vehicles needs to have regenerative braking so that the kinetic energy of the moving vehicle can be captured and stored in battery for future use. One of the basic questions for EV construction is what kind of power source has to be chosen? The battery is the ideal power source on the primary point of view. But relatively long time of charging makes it not attractive. Another opportunity is using a fuel cell. It can be charged quickly, but in this case the power source will be not effective in moment of strong acceleration. More over the regenerative braking system can not be realized. So the more suitable design of energy source for EV is the combination between fuel cell and battery, e.g. hybrid power supply system – [2]. A functional scheme is shown in fig. 2

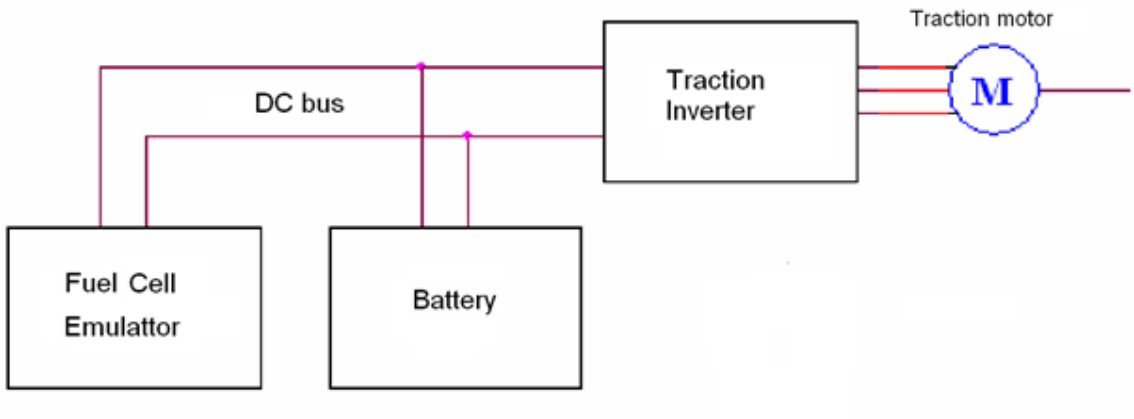

Figure 2: Functional scheme of combine power supply for traction drive

Thus the advantages of the two kinds of power sources can be combined.

Methodology

In this work LMS method of numerical calculation for emulating volt-ampere characteristic is used. More over mathematical methods are used for particularly designing the modules of an experimental setup, and after that realizing it, e.g. fuel cell emulator and battery management system.

Discussion

In the current work it is considered a combined power supply for traction drive inverter composed of fuel cell and NiMH battery. Both power sources are connected to the direct current bus (DCB), which powers the traction inverter, as shown in fig.1. The battery module is realized using real stack of 20 NiMH batteries, type SC3000 mAh, connected in series. The fuel cell is stimulated by emulator, which is realized especially for the purpose of the current work. This particular design was chosen for the implementation of the combined power source in order to achieve more flexibility in order to adjust the fuel cell parameters. A

functional scheme of the emulator is shown in fig.3. The digital part, which includes reference generator and lookup table, is made by using PIC microcontroller architecture. Software is made in assembly language. All another modules – PID regulator, output stage and instrumental amplifier are analog.

The emulator is supplied from public power grid. Power supply module is constructed by using half bridge inverter – [3].

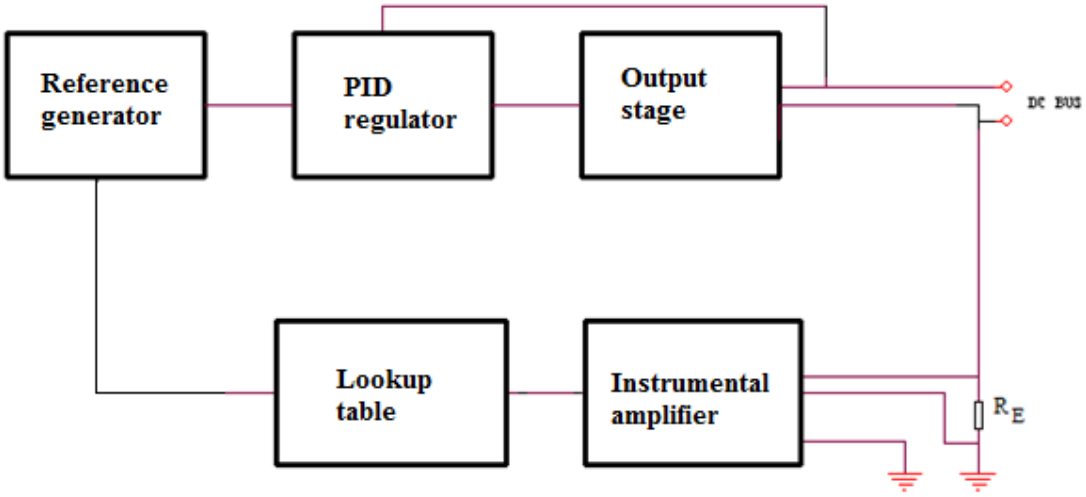

Figure.3: Functional scheme of fuel cell emulator

The power consumption of traction inverter is emulated by programmable current generator, realized for the needs of another task.

The fuel cell volt-ampere characteristic (VAH) – [4-6] is modeled using piecewise linear approximation. Each piecewise line connects two neighbor measurement points. For each measurement value of the load current corresponding reference signal for the regulator. It is done by using lookup table. The load current is measured by etalon resistor Re. Obtained voltage signal is amplified by using instrumental amplifier. The regulator realizes PID law of regulation. The components of regulator - proportional coefficient K_p, integrated constant K_i and differential constant K_d are tuned by using classical Ziegler-Nichols method – [7-9]. The feedback is output voltage, taken from the output terminals and the reference corresponds to the load current.

Conclusions

Power consumption of traction inverter depends on different factors which have no correlation. For this reason the power, respectively energy consumption is extremely dynamic. The combination of fuel cell and NiMH battery is suitable design for powering traction drive inverters. Unfortunately it is very difficult to determine the parameters for required fuel cell and battery. For each case of electric vehicle type the optimal ratio between power of fuel cell and battery will be different.

Future work

In the thus constructed experimental setup will be added super capacitor, connected to the DC bus. Then the same experiments will be made and any optimization tasks relatively to the energy efficiency for the complex power module.

References

[1] Ehsani M, Gao Y, Emadi A (2010) Modern electric, hybrid electric, and fuel cell vehicles: fundamentals, theory and design, 2nd edn. CRC, London
[2] Ouyang, Q.;Wang, F.; Chen, J.; Li, X. Power management of PEM fuel cell hybrid systems. In Proceedings of the 33rd Chinese Control Conference, Nanjing, China, 28–30 July 2014; pp. 7082–7087.
[3] Broun Mary, Power Supply Cook book, Newness Oxford University, 2004.
[4] Chavan SL, Talange DB. Modeling and performance evaluation of PEM fuel cell by controlling its input parameters. Energy 2017;138:437e45.
[5] Fardoun AA, Hejase HA, Al-Marzouqi A, Nabag M. Electric circuit modeling of fuel cell system including compressor effect and current ripples. Int J Hydrogen Energy 2017;42(2):1558e64.
[6] Saadi A, Becherif M, Hissel D, Ramadan H. Dynamic modeling and experimental analysis of PEMFCs: a comparative study. Int J Hydrogen Energy 2017;42(2):1544e57.
[7] D. Bogdan, Popescu M., C. Patrascioju, PID controller optimal tuning, 8th International Conference on Electronics, Computers and Artificial Intelligence (ECAI), 23.02. 2016
[8] Hang Wu, Weihua Su, PID controllers: Design and tuning methods, 9th IEEE Conference on Industrial Electronics and Applications, 09-11 June 2014
[9] Kumar A., Maila De, Effectiveness of Zeigler-Nicholas Method Based Parameter Tuning of Virtual Synchronous Generator for LFC in Low Inertia Islanded Microgrid, IEEE Delhi Section Conference (DELCON), 11-13 February 2022.

Fuelling Tomorrow:

Developing a Normative Regulatory Framework for the adoption of Clean Hydrogen in Heavy-Duty Powertrains

Kelsey Pailman

University of Groningen
EU Marie Skłodowska-Curie Actions: Training for a Hydrogen Economy based Renewable Energy Society in the Anthropocene (THERESA) Project

Introduction

The transport industry accounts for a quarter of the European Union's greenhouse gas (GHG) emissions and is the central cause of air pollution within cities [1]. Today, approximately 42% of the EU's diesel consumption in road transport is from heavy duty trucks and busses [2]. The aviation industry is similarly powered by petroleum fuels such as jet fuel produced from refined kerosene and in certain instances aviation gasoline (Avgas), a residual aviation fuel blended with lead [3]. Furthermore, in the maritime industry, more than 95% of ships today run on internal-combustion engines fuelled by various petroleum products [4]. To reach climate neutrality by 2050, a 90% reduction in transport emissions is required [5]. A key pillar of the European Green Deal is therefore the acceleration of a shift to sustainable mobility by increasing the production and deployment of sustainable alternative transport fuels [6]. In line with the European Green Deal, the EU Hydrogen Strategy identifies the use of hydrogen in hard-to-abate transport sectors as a means of decarbonising the sector. In particular, the EU Hydrogen Strategy identifies heavy-duty trucks, trains as well as maritime and aviation sector as early adopters of hydrogen [1]. The question arises as to the role regulation, and more specifically what type and extent of regulation, would be appropriate in facilitating this adoption in the heavy-duty transport sector.

This paper therefore seeks to develop a normative regulatory framework through which legal barriers and opportunities for the use of clean hydrogen in heavy-duty transportation (i.e. in powertrains for road, maritime and aviation sectors) can be assessed. Leenes' "Regulating Technology (Development) Model" (**RTD Model**) is utilised to identify the appropriateness of regulatory intervention in this context [7]. The paper concludes by identifying three pillars through which the need and extent of regulatory intervention can be evaluated namely: 1) certainty as to the standardisation of fuel compositions, quality and safety in hydrogen transport fuels 2) cohesiveness of existing legal frameworks in electricity, gas and transport sectors across the hydrogen value chain and 3) presence of appropriate fiscal/economic incentives to facilitate the uptake of hydrogen amongst key industry players in the heavy-duty transport sector.

Methodology

To develop a normative framework governing the use of hydrogen in the heavy duty transport industry, a desktop literature review will be undertaken, in terms of which existing literature on the matter will be assessed in the context of identifying gaps in the current EU regulatory framework. In particular, Leenes' RTD Model will be applied to hydrogen in the context of the heavy-duty transport sector. According to the RTD Model (illustrated in Figure 1 below), a

three stage approach can be applied when determining whether regulatory intervention is necessary for a new technology, and if so, the type of regulatory intervention that would be appropriate in light of the issues and context surrounding the technology [7]. The observations and gaps identified in the literature review will be used to develop a normative regulatory framework following the RTD Model for the use of hydrogen in heavy-duty transport industries.

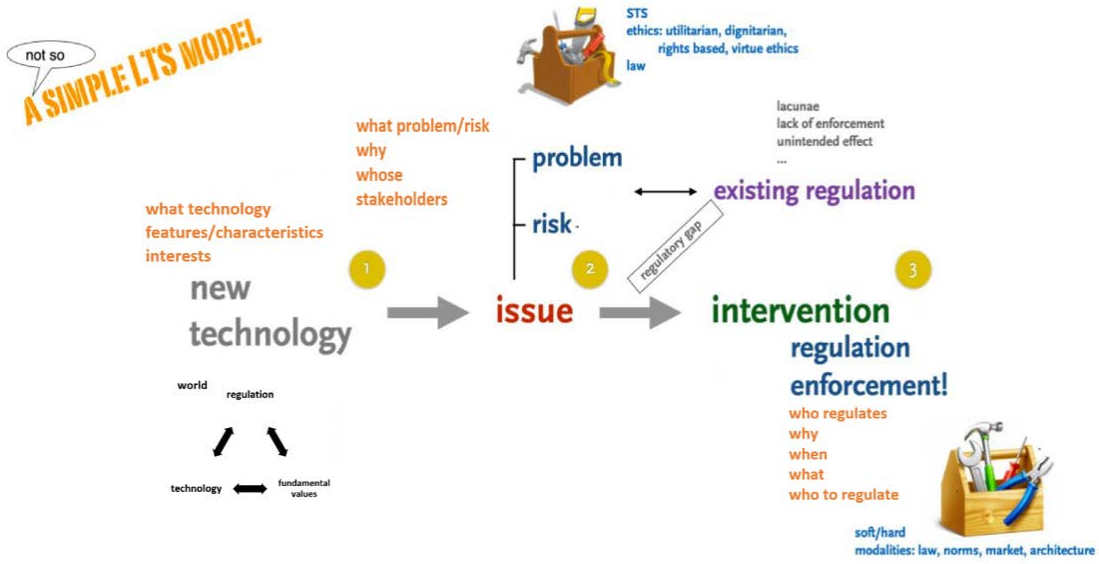

Figure 1: Ronald Leenes Regulating Technology (Development) Model

In step 1 of the RTD Model, the new technology i.e. the use of hydrogen in heavy-duty transportation will be identified and discussed. Here, more than merely identifying the type of technology, a socio-technical lens will be employed in terms of which the relevant characteristics and interests evoked by the technology are analysed. Once step 1 is complete, in step 2, the issues raised by the new technology will be assessed, such as potential and inherent risks that may be present as a result of the new technology. Here, the current law governing the new technology in the electricity, gas and transport sectors must also be evaluated in light of the issues/risks identified. Lastly, if from step 2 a gap in the regulation is identified, in step 3, regulatory intervention may be considered. In respect of step 3, Leenes notes that there are three widely common understandings of what constitutes regulation. Firstly, regulation may be construed as rules established and implemented by the State. Secondly, regulation can be considered as any kind of State intervention, irrespective of the form that that such intervention may take. Lastly, regulation may be considered to be any way of social control or influence which has an impact on the behaviour of others. The third understanding of regulation is the most broad, as it can encapsulate both state and self-governance.

While this paper focuses on steps 1 and 2, step 3 will be the subject of further research on this topic in order to provide recommendations on the extent and kind of regulatory intervention that would be appropriate in the context of hydrogen (fuelled) heavy-duty powertrains.

Discussion

The role that regulation plays in the development of "new technologies" has been an emerging field of research, particularly given the pace at which new innovations are developing in our current point in history [7]. Hydrogen, as an energy carrier, cannot be considered "new" as it has been used for centuries in a number of applications, for example in ammonia for fertilisers and in refineries to produce petroleum products [8]. However, what can be considered novel, is the emerging ways in which hydrogen can be produced, as well as its use in a variety of new applications. According to the International Energy Agency [8], as of 2021, 62% of global hydrogen production is considered "grey" in that it is produced from natural gas without carbon capture utilisation and storage (CCUS). Furthermore, unabated coal (known as "brown/ black" hydrogen) accounted for 21% of the global hydrogen production. These figures can be contrasted with hydrogen produced by renewable energy through the process of electrolysis ("green hydrogen"), which only accounts for 0.1% of the global hydrogen production today.

Notwithstanding the dominance of fossil fuels in the production of hydrogen, the landscape is increasingly changing, with green hydrogen anticipated to play a prominent role in global hydrogen production, particularly as a result in decreasing costs of renewable energy [8]. Moreover, in the context of the use of hydrogen in the transport industry in particular, while novel applications for hydrogen in heavy industry and long-distance transport constitute less than 0.1% of global hydrogen demand today, it is anticipated to account for one-third of global hydrogen demand by 2030 [9]. Furthermore, considering a broad definition of technology as "changes in products, devices, processes and practices" [10], it then becomes important to develop a normative framework to ascertain the role that regulation, if any and to what extent, will play in light of this "new technology" i.e. the use of clean hydrogen in heavy duty transport industries. This framework can be assessed, in light of Leenes' RTD Model, as discussed above.

When applying step 1 of the RTD model to hydrogen, it is evident that hydrogen can be produced in different ways and for different purposes. It can be noted that the European Union is increasingly steering away from defining hydrogen by colour [11], but rather it uses terminology such as "clean hydrogen", "renewable hydrogen" (which entails green hydrogen) as well as "low-carbon hydrogen" (which may cover blue hydrogen as well as "pink/purple" hydrogen produced through nuclear power). With respect to the use of hydrogen in heavy-duty powertrains, hydrogen can either be combusted and blended with existing fuels or used in a fuel cell to power new powertrains [12].

When evaluating step 2, identifying issues and risks, two key broad issues were identified in a recent report by Green Planet: 1) existing legislation not providing sufficient room to label all renewable hydrogen "green" 2) insufficient standardisation in respect of fuel quality implementation and monitoring [13]. While these risks were identified in the context of the Netherlands, it can be widely applied to other member states. As noted by Fleming for example, the Fuel Quality Directive (FQD) currently covers "renewable liquid and gaseous transport fuels from non-biological origin" which includes hydrogen produced in the process of electrolyses but does not include hydrogen produced from bio-mass [11]. The FQD furthermore provides for the monitoring, reporting and verification of the fuels covered in the directive in each member state, however, as noted in the report by Green Planet, certain member states do not have regulatory authorities overseeing compliance with the International Organization for

Standardization (ISO) requirements for fuel quality [13]. Another key issue is whether the current legislation in the electricity, gas and transport sectors, are effectively cohesive in governing the use of hydrogen in the transport sector. This raises the concept of "sector coupling" or "sector integration" which is important in the context of "Power-to-Hydrogen" technologies which involve both the electricity sector as well as the gas sector [11]. At present, these two sectors are regulated separately at an EU level, and therefore it will be important to assess whether the current regulation provides a seamless regulatory framework for the use of hydrogen in the heavy-duty transport sector. Lastly, given that heavy-duty transport industries are the key stakeholders in considering the implementation of hydrogen as an alternative fuel, it will be important to assess whether there are sufficient fiscal/economic incentives in place in order for such stakeholders to switch from their current fuel supply [14]. Only once the above issues are analysed, can step 3 be considered, i.e. whether regulatory intervention is necessary, and if so which intervention would be appropriate.

Conclusions

In light of the above, to evaluate the role regulation should play in the use of hydrogen in the heavy-duty transport sector, it is proposed that the current regulatory framework be assessed through three pillars namely: 1) certainty as to the standardisation of fuel compositions, quality and safety in hydrogen transport fuels; 2) cohesiveness of existing legal frameworks in electricity, gas and transport sectors across the hydrogen value chain; and 3) presence of appropriate fiscal/economic incentives to facilitate the uptake of hydrogen (fuelled) heavy-duty powertrains amongst key industry players (**H2 HDP Regulation Evaluation Framework**). The pillars of the framework are summarised in figure 2 below:

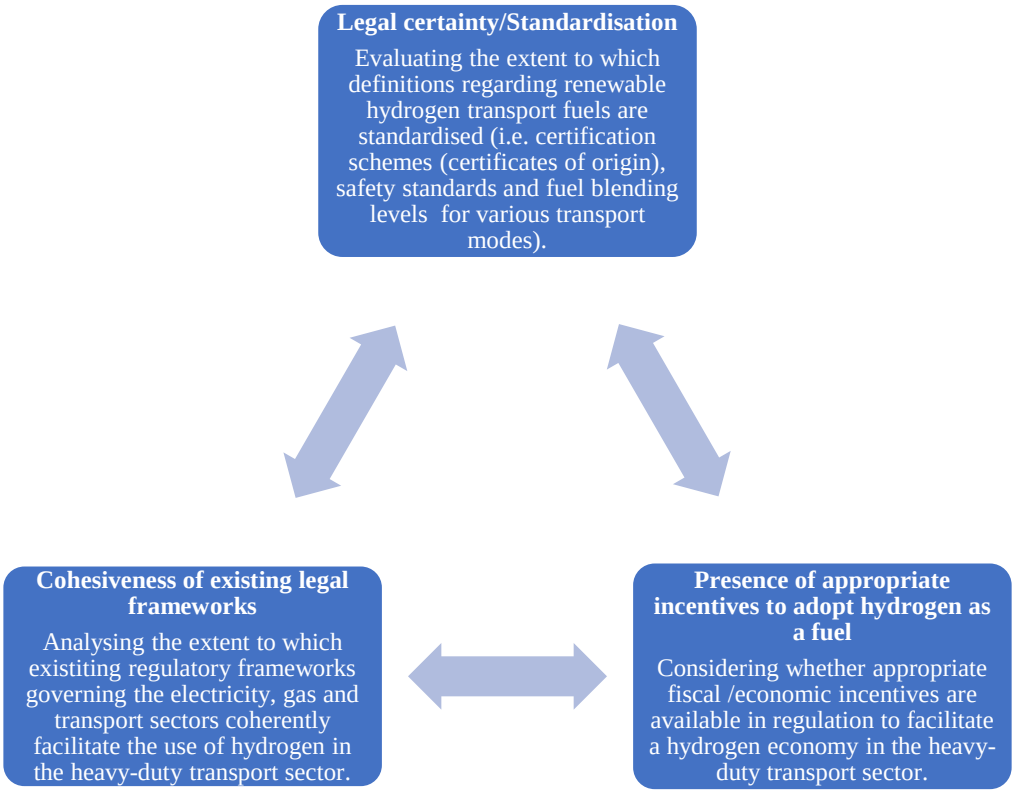

Figure 2: H2 HDP Regulation Evaluation Framework

While this research is still in its initial stages, the H2 HDP Regulation Evaluation Framework will be applied in further research first at an EU level and then to selected individual member states in order to evaluate the regulatory intervention necessary to create a hydrogen economy in the context of the heavy-duty transportation industry.

It is predicted that “the pacing problem” will be a key regulatory hurdle that will need to be overcome in the context of the regulation of hydrogen use in heavy-duty transportation industries More generally, the pacing problem refers to the fact that technological innovations are developing at a faster pace than regulatory frameworks, resulting in regulation being reactionary rather than proactive in setting norms and standards regulating human behaviour and practices [15]. Similarly, a “chicken and egg” dilemma can arise in the context of the pacing problem, whereby the law can be used as a means of facilitating the adoption of certain behaviours/practices, while at the same time is informed by the adoption of such behaviours/practices itself. In the context of hydrogen, the pacing problem is present given that the deployment of hydrogen fuel-cells in transportation and combustion of hydrogen in existing powertrains is already underway, notwithstanding the absence of a dedicated regulatory framework. Furthermore, the “chicken and egg” dilemma arises given that, while these activities are already occurring , the hydrogen fuel market is not yet mature and may require regulatory intervention to facilitate increased adoption. This will inevitably involve regulation having to “anticipate” an appropriate legal and fiscal framework without the market being fully in place. A question also arises as to what constitutes effective regulation, and whether self-regulation may, in some instances, be more appropriate than state imposed regulation. Further research will therefore assess various kinds of regulation that may be appropriate in overcoming the above regulatory hurdles.

References

[1] European Commission, EU strategy on hydrogen (COM/2020/301*)*, Brussels, 2020.

[2] Transport & Environment, "Addressing the Heavy-Duty Climate Problem: Why all new freight trucks and buses need to be zero-emission by 2035," September 2022.

[3] European Commission, "European Alternative Fuels Observatory: Alternative Fuels used for Aviation," [Online]. Available: https://alternative-fuels-observatory.ec.europa.eu/transport-mode/aviation/alternative-fuels-for-aviation. [Accessed October 2023].

[4] Mærsk Mc-Kinney Møller Center for Zero Carbon Shipping, Global Maritime Forum, Global Centre for Maratime Decarbonisation "The Shipping Industry's Fuel Choices on the Path to Net Zero,", 2023.

[5] European Commission, "Sustainable & Smart Mobility Strategy," Brussels , 2021.

[6] European Comission, "Communication and roadmap on the European Green Deal," Brussels, 2020.

[7] R. Leenes, "Regulating New Technologies in Times of Change," in *Regulating New Technologies in Uncertain Times* , vol. 32, L. Reins, Ed., The Hague, Springer , 2019.

[8] International Energy Agency, "Global Hydrogen Review 2023," 2023.

[9] International Energy Agency, "Hydrogen," [Online]. Available: https://www.iea.org/energy-system/low-emission-fuels/hydrogen. [Accessed October 2023].

[10] A. Grübler, N. Nakićenović, D.Victor "Dynamics of energy technologies and global change," *Energy Policy*, vol. 27, no. 5, 1999 (https://doi.org/10.1016/S0301-4215(98)00067-6).

[11] R. Fleming, "The Hydrogen Revolution and Natural Gas," in *The Palgrave Handbook on Natural Gas and Global Energy Transitions* , Palgrave MacMillan , 2022, pp. 123-140.

[12] M. L. Wright, A. C. Lewis, "Decarbonisation of heavy-duty diesel engines using hydrogen fuel: a review of the potential impact on NOx emissions," *Environmental Science:*, vol. 2, 2022, pp.852-866 (DOI: 10.1039/d2ea00029f).

[13] Green Planet, "Hydrogen Applications in Heavy-Duty Transportation," HEAVENN Report, 2021.

[14] N. Schneider, I.R Skov, "Incentive structures for power-to-X and e-fuel pathways for transport in EU," *Energy Policy*, 2022 (https://doi.org/10.1016/j.enpol.2022.113121).

[15] G. E. Marchant, B. R. Allenby, Joseph Herkert Ed. "The Growing Gap Between Emerging Technologies and Legal-Ethical Oversight: the Pacing Problem,", Springer , 2011.

Germany's Hydrogen Ramp-Up in industrial Hydrogen-Hubs: Ecological Potential through regional Synergy Effects

M. Schmid*[1]

[1]Institute for Industrial Ecology (INEC), Pforzheim University, Tiefenbronner Str. 65, D-75175 Pforzheim

Introduction

Various studies show the indispensability of using green hydrogen to achieve a climate-friendly and low greenhouse gas emitting society. Due to its favorable storage properties and wide range of application, hydrogen will contribute to increasing the flexibility of the energy system and thus to the integration of renewable energies. On the one hand, hydrogen can be produced during periods of abundant renewable energy and reconverted into electricity when renewable energy is scarce. On the other hand, hydrogen and its derivatives are predestinated to use in hard to abate sectors. Moreover, the utilization of green hydrogen can serve as a substitute for the currently employed greenhouse gas intensive (grey) hydrogen that acts as a feedstock for various chemical products and processes. Consequently, the ramp-up of a green hydrogen economy is urgently needed.

The green hydrogen ramp-up in Germany is planned within the framework of the National Hydrogen Strategy [1]. This strategy anticipates a hydrogen demand of 95-130 TWh and aims to achieve a total domestic installed electrolysis capacity of 10 GW by 2030. The remaining hydrogen demand of about 50-70 % needs to be covered by imports. In a meta-study, Merten et al. [2] compare potential hydrogen imports to Germany versus domestic hydrogen production options. The authors remark that the investment risks within the assumed export countries as well as their own needs for hydrogen and renewable energies stay frequently neglected. Hence, Merten et al. conclude that the economic attractiveness of domestic hydrogen production is greater than commonly believed. Furthermore, Eckl et al. [3] calculate for an exemplary site in Southern Germany an approximate cost parity between imported and domestically produced hydrogen by utilizing the waste heat generated during hydrogen production.

Numerous total cost minimizing energy system models are employed to investigate the German and European future hydrogen production, usage, transport and underlying system design. Thereby, results for Germany show a high electrolysis and thus hydrogen production concentration in Germany's North (i. a. [4]). In this context, Merten et al. [2] remark that various studies focus the supply side, while already existing industrial demand in southern Germany and their corresponding green hydrogen ramp-up potential remains unconsidered. In addition, concluding their own analysis, Sauer et al. [5] recommend more in-depth research on industrial hydrogen-hubs, as such networks can be beneficial from both economic and environmental perspectives. Regional hydrogen networks of this kind are able to utilize occurring couple products and potential regional synergy effects. This can lead to resource efficiency, faster decarbonization and financial benefits.

Besides the above-mentioned findings related to a "central" hydrogen production in Northern Germany, there are suggestions promoting the establishment of a more "decentralized" hydrogen and overall energy system. These proposals are justified on the grounds of broader public participation – keyword *prosuming* – and the resulting gains in acceptance [6].

* Corresponding author: marco.schmid@hs-pforzheim.de

Furthermore, according to Kendziorski et al. [7] previous studies on the optimal design of the future overall energy system underly the limitation that not all system components are considered adequately. In concrete terms, this means that existing energy system models usually neglect expansion and operating costs of transmission infrastructure or consider them solely in downstream iteration loops. Recent studies, that are tackling this limitation, show for the concept of a more decentralized energy system no or just little higher (< +10 %) total overall system costs ([7], [8]). Neumann et al. [8, p. 19] summarize their results as follows: "[These findings] should enable policymakers to choose from a wide range of compromise energy system designs with low cost but higher acceptance."

Research Gap

In summary, a triad of interrelated topics crystallizes based on the keywords (1) hydrogen import vs. self-generation, (2) industrial hydrogen-hub and (3) centralized vs. decentralized energy and hydrogen system. Although the transformation process of the energy system and the ramp-up of a green hydrogen economy has for reasons of urgency already begun, there is no conclusive and generally valid solution, neither for the individual topics nor holistically. Indeed, there are proposed solutions from national and pan-European studies. Nevertheless, questions remain about the financial and ecological potential of close to industry hydrogen production and the utilization of resulting couple products within regional value chains. Such details are inherently difficult to implement in large-scale models. Furthermore, stakeholders do not inevitably follow the results of politico-economically optimizing models. They rather pursue their own strategies and interest, for instance due to an anticipated postponed access to the hydrogen grid. Such regionally limited and stakeholder specific efforts are also difficult to represent in large-scale models. However, regarding political support for the hydrogen ramp-up, the consideration of these regional stakeholders and their projects is highly relevant since the hydrogen ramp-up must be realized on their very level.

Research Question

By answering the research question "How can decentral industrial hydrogen-hubs in inland regions with little renewable energies contribute techno-economically and ecologically to the decarbonization of entire regions and (how) can this potential be leveraged?", the PhD project is to address mentioned research gaps and thus helps to optimize the German green hydrogen ramp-up. The research question shall be answered by shedding light on it from four different perspectives:

1. Is there an economically self-supporting state of an industrial hydrogen-hub producing its own hydrogen in a renewable energy scarce region?
2. What is the ecological potential of such an industrial hydrogen-hub in a renewable energy scarce inland region?
3. Are there differences between a myopic and perfect foresight approach establishing an industrial hydrogen-hub?
4. How will industrial hydrogen-hubs currently emerging in Southern Germany develop and influence each other as the hydrogen market ramps up?

Methodology

To answer the raised questions, mainly the methodology of energy system modeling and life cycle assessment (LCA) will be applied. Energy system modeling as a sub-discipline of

"electricity market models" [9, p. 18] is situated within the domain of linear optimization and contributes to informed decision-making in investment planning. Thereby, the conventional objective function is the minimization of overall system costs, mostly under consideration of specific emission reduction targets, e. g. CO_2 or NO_x [10].
Given the growing awareness regarding the necessity for a sustainable future and considering the complexity of "sustainability", there emerge requirements for energy system models associated with multi-criteria decision support. Consequently, for instance Naegler et al. [11] integrate social factors into their analysis of future energy systems while Finke and Bertsch [12] additionally consider the degree of self-sufficiency. Focusing on the different environmental impacts of energy systems, the methodology of LCA is particularly suitable for multi-criteria analysis.
LCA is the quantification and analysis of environmental impacts throughout the entire lifecycle of a product, service, technology, or system. Thereby, the aim usually is to support decision-making processes toward a more ecological and sustainable future. To analyze different environmental impacts, LCA makes use of different end- and midpoint indicators, so called (environmental) impact categories. The procedure for LCA is standardized within the two international norms DIN EN ISO 14040 and 14044. Conventional LCAs follow a retrospective approach, namely considering already existing products and technologies. However, to evaluate emerging technologies and systems in terms of their environmental impacts, also future trends (such as a less greenhouse gas intensive energy system) need to be recognized. Hence, future oriented, so called prospective LCAs have been developed in recent years (i. a. [13], [14]).
In the context of multi-criteria decision support, it becomes more and more common to combine such (prospective) LCAs or predefined midpoint indicators with energy system models. Most often, LCA is coupled with the energy system model subsequent to the cost minimizing optimization process. By this approach, many investigations proof the spatial, temporal and systemic shift of environmental burdens associated with the transformation of the energy system (i. a. [15], [16]). These interrelations are also known as *water-energy-land-* or *resource-energy* nexus.
Against this background, more holistic optimization approaches are currently emerging. These approaches already take various environmental impacts into account during the optimization process. For instance, Junne et al. [17] incorporate greenhouse gas emissions into their objective function and compute a Pareto front to emphasize the conflict between minimal system costs and minimal greenhouse gas emissions. Furthermore, Reinert et al. [18] implement the complete LCA procedure into the open-source energy system model *SecMOD* and such create the possibility to optimize the energy system for various minimal environmental impacts. Vandepaer et al. [19] integrate several midpoint indicators into their energy system model's objective function and apply it to the Swiss energy system, while Finke and Bertsch [12] include the indicators CO_2 emissions and self-sufficiency in addition to system costs in the objective function of their open-source energy system model *Backbone*. Finke and Bertsch emphasize, that the inclusion of further indicators, as for instance other environmental impacts, can be done easily. One of the first open-source bottom-up energy system models able to include entire LCAs within its objective function is the **L**ife Cylce **A**ssessment based **EN**ergy **D**ecision Support Tool (LAEND) of Tietze et al. [20]. Thereby, Tietze et al. connect the **o**pen **e**nergy **m**odelling **f**ramework oemof [21] with the LCA software openLCA and thus create the possibility to optimize the system for 16 different environmental impact categories in addition to system costs. Furthermore, LAEND provides the option to use normalization and weighting factors of the Environmental Footprint

impact assessment method. This enables to determine the optimal system design, considering all mapped environmental impacts simultaneously.

Execution of PhD project

Within the scope of the PhD project, the modeling tool LAEND shall be applied. Advantages of LAEND are, besides its open-source availability, its high flexibility (Excel is used as an user interface), LAEND's focus on residential quarters (keyword decentrality) and hence its ability to depicture energy system technologies precisely. Furthermore, LAEND already includes LCA data of important energy sector technologies. Disadvantages are the missing integration of material flows (keyword sector coupling), the myopic optimization approach and the missing ability of spatial differentiation. However, the underlying framework oemof already provides remedies for these drawbacks. These will be used to further develop LAEND to answer the research question.
To be able to answer the research question, the PhD project will concentrate on an exemplary region, wherefrom generalizing conclusions and recommendations will be drawn. The exemplary region will be the south-western area of Baden-Wurttemberg (Southern Germany). A chemical production network situated there anticipates a postponed linking to an interregional hydrogen pipeline grid. Furthermore, a number of additional hydrogen hubs are currently emerging both within and near this region. These hubs will be analyzed as part of the fourth sub-research question, outlined below. As a result, in addition to the general conclusions and political recommendations, the practical application of this research will be of great significance in this area.
To answer the sub-research questions and consequently the main research question, the PhD project shall be carried out as follows:

1. Is there an economically self-supporting state of an industrial hydrogen-hub producing its own hydrogen in a renewable energy scarce region?
   Each project in practice becomes more realistic to be realized if it is economically self-supporting. This is why the ideal design of a self-generating industrial hydrogen-hub is investigated under consideration of several techno-economic synergy effects. In concrete terms, this means that several hydrogen generation technologies including the utilization of their waste heat as well as heat-, electricity- and hydrogen storages in combination with volatile renewable energies are considered.
2. What is the ecological potential of such an industrial hydrogen-hub in a renewable energy scarce inland region?
   In consideration of the present multiple ecological crises [22], in addition to being economically feasible, the development of a hydrogen-hub must add ecological value. Therefore, the ecologically ideal design of an industrial hydrogen-hub will be determined. From this, it shall be derived how the area of conflict between a purely economic and purely ecological point of view can be solved.
3. Are there differences between a myopic and perfect foresight approach establishing an industrial hydrogen-hub?
   Besides the assumed area of conflict between a purely economic and a purely ecological optimized hub design, an area of conflict between a commercial and a politico-economic establishment approach is to be expected. By this, I mean for instance different temporal observation horizons (in the context of energy system modeling: myopic vs. perfect foresight), discount rates or spatial observation horizons. Alongside answering the sub-

research question, potential policy suggestions for resolving such an area of conflict shall be concretized, if possible.

4. How will industrial hydrogen-hubs currently emerging in Southern Germany develop and influence each other as the green hydrogen market ramps up?
   The fourth sub-research question aims to broaden the previous scope of investigating a single hub to examining multiple hubs and how they interact optimally with each other. Subject of own expectations is that currently emerging decentralized hydrogen hubs will engage in trading, merge, or dissolve as a result of an established hydrogen pipeline infrastructure. The assumed future expansion of each individual hub (specifically: the moment from which they can trade with each other) needs to be specified exogenously and their interaction will then be optimized from a techno-economic and ecological point of view. With the aid of various scenarios, an insight into expectable developments will be generated. If possible, in this way necessary political frameworks for achieving desired hub developments shall be derived.

Discussion & Conclusions

As the PhD project is still in its early stages, there are no results for discussion yet. Nevertheless, initial computations show promising results toward the establishment of a self-producing industrial hydrogen hub from the point of view of minimal system costs. However, given the huge demand for renewable energy, these results are not yet valid and further refinement is needed both before and after the conference.

References

[1] BMWK, “Fortschreibung der Nationalen Wasserstoffstrategie,” 2023.
[2] F. Merten *et al.*, “Bewertung der Vor- und Nachteile von Wasserstoffimporten im Vergleich zur heimischen Erzeugung - Update,” Wuppertal Institut; DIW Econ, 2021.
[3] F. Eckl, L. Eltrop, A. Moita, and R. Costa Neto, “Techno-economic evaluation of two hydrogen supply options to southern Germany: On-site production and import from Portugal,” *International Journal of Hydrogen Energy*, vol. 47, no. 60, pp. 25214–25228, Jul. 2022, doi: 10.1016/j.ijhydene.2022.05.266.
[4] B. Lux *et al.*, “The role of hydrogen in a greenhouse gas-neutral energy supply system in Germany,” *Energy Conversion and Management*, vol. 270, p. 116188, Oct. 2022, doi: 10.1016/j.enconman.2022.116188.
[5] A. Sauer *et al.*, “I-H2-Hub-BW. Voruntersuchung: Dezentrale Wasserstofferzeugung und -nutzung im industriellen Umfeld Baden-Württembergs,” Fraunhofer IPA; sphera; Prognos, 2022.
[6] acatech, Leopoldina, and Union der Deutschen Akademien der Wissenschaften, Eds., *Zentrale und dezentrale Elemente im Energiesystem - Stellungnahme*. in Schriftenreihe zur wissenschaftsbasierten Politikberatung. Halle (Saale), 2020.
[7] M. Kendziorski, L. Göke, C. Von Hirschhausen, C. Kemfert, and E. Zozmann, “Centralized and decentral approaches to succeed the 100% energiewende in Germany in the European context – A model-based analysis of generation, network, and storage investments,” *Energy Policy*, vol. 167, p. 113039, Aug. 2022, doi: 10.1016/j.enpol.2022.113039.
[8] F. Neumann, E. Zeyen, M. Victoria, and T. Brown, “The potential role of a hydrogen network in Europe,” *Joule*, p. S2542435123002660, Jul. 2023, doi: 10.1016/j.joule.2023.06.016.

[9] D. Möst, W. Fichtner, and A. Grunwald, *Energiesystemanalyse*. in Workshop Energiesystemanalyse Karlsruhe. Karlsruhe#, 2009.
[10] H.-K. Ringkjøb, P. M. Haugan, and I. M. Solbrekke, "A review of modelling tools for energy and electricity systems with large shares of variable renewables," *Renewable and Sustainable Energy Reviews*, vol. 96, pp. 440–459, Nov. 2018, doi: 10.1016/j.rser.2018.08.002.
[11] T. Naegler *et al.*, "Integrated Multidimensional Sustainability Assessment of Energy System Transformation Pathways," *Sustainability*, vol. 13, no. 9, p. 5217, May 2021, doi: 10.3390/su13095217.
[12] J. Finke and V. Bertsch, "Implementing a highly adaptable method for the multi-objective optimisation of energy systems," *Applied Energy*, vol. 332, p. 120521, Feb. 2023, doi: 10.1016/j.apenergy.2022.120521.
[13] A. Mendoza Beltran *et al.*, "When the Background Matters: Using Scenarios from Integrated Assessment Models in Prospective Life Cycle Assessment," *Journal of Industrial Ecology*, vol. 24, no. 1, pp. 64–79, 2018, doi: 10.1111/jiec.12825.
[14] R. Sacchi *et al.*, "PRospective EnvironMental Impact asSEment (premise): A streamlined approach to producing databases for prospective life cycle assessment using integrated assessment models," *Renewable and Sustainable Energy Reviews*, vol. 160, p. 112311, May 2022, doi: 10.1016/j.rser.2022.112311.
[15] N. Baumgärtner *et al.*, "Life-Cycle Assessment of Sector-Coupled National Energy Systems: Environmental Impacts of Electricity, Heat, and Transportation in Germany Till 2050," *Front. Energy Res.*, vol. 9, p. 621502, Apr. 2021, doi: 10.3389/fenrg.2021.621502.
[16] K. Volkart, C. L. Mutel, and E. Panos, "Integrating life cycle assessment and energy system modelling: Methodology and application to the world energy scenarios," *Sustainable Production and Consumption*, vol. 16, pp. 121–133, Oct. 2018, doi: 10.1016/j.spc.2018.07.001.
[17] T. Junne, K.-K. Cao, K. K. Miskiw, H. Hottenroth, and T. Naegler, "Considering Life Cycle Greenhouse Gas Emissions in Power System Expansion Planning for Europe and North Africa Using Multi-Objective Optimization," *Energies*, vol. 14, no. 5, p. 1301, Feb. 2021, doi: 10.3390/en14051301.
[18] C. Reinert *et al.*, "SecMOD: An Open-Source Modular Framework Combining Multi-Sector System Optimization and Life-Cycle Assessment," *Front. Energy Res.*, vol. 10, p. 884525, Jun. 2022, doi: 10.3389/fenrg.2022.884525.
[19] L. Vandepaer, E. Panos, C. Bauer, and B. Amor, "Energy System Pathways with Low Environmental Impacts and Limited Costs: Minimizing Climate Change Impacts Produces Environmental Cobenefits and Challenges in Toxicity and Metal Depletion Categories," *Environ. Sci. Technol.*, vol. 54, no. 8, pp. 5081–5092, Apr. 2020, doi: 10.1021/acs.est.9b06484.
[20] I. Tietze, L. Lazar, H. Hottenroth, and S. Lewerenz, "LAEND: A Model for Multi-Objective Investment Optimisation of Residential Quarters Considering Costs and Environmental Impacts," *Energies*, vol. 13, no. 3, p. 614, Feb. 2020, doi: 10.3390/en13030614.
[21] S. Hilpert, C. Kaldemeyer, U. Krien, S. Günther, C. Wingenbach, and G. Plessmann, "The Open Energy Modelling Framework (oemof) - A new approach to facilitate open science in energy system modelling," *Energy Strategy Reviews*, vol. 22, pp. 16–25, Nov. 2018, doi: 10.1016/j.esr.2018.07.001.
[22] K. Richardson *et al.*, "Earth beyond six of nine planetary boundaries," *Sci. Adv.*, vol. 9, no. 37, p. eadh2458, Sep. 2023, doi: 10.1126/sciadv.adh2458.

Green Hydrogen from the MENA region: Location factors and boundary conditions

A. Alexander Leuthold[*1], B. PD Dr. Peter Viebahn[2], C. Dr. Julia Terrapon-Pfaff[3], D. Dr. Sascha Samadi[4]

[1]A. Wuppertal Institut für Klima, Umwelt, Energie gGmbH
[2]B. Wuppertal Institut für Klima, Umwelt, Energie gGmbH
[3]C. Wuppertal Institut für Klima, Umwelt, Energie gGmbH
[4]D. Wuppertal Institut für Klima, Umwelt, Energie gGmbH

Introduction

Human well-being depends on a global turnaround towards a profound and rapid reduction of greenhouse gas emissions in all sectors according to the sixth IPCC [1] report. To achieve net zero carbon emission targets, hydrogen has been recognized as a key energy carrier and feedstock. The molecule can be produced by water electrolysis or steam cracking of fossil resources. While the latter is the predominant process in industry, only water electrolysis powered by renewable energy can serve as a truly low carbon and sustainable production route [2]. Therefore, several industrialized countries have announced hydrogen strategies that project the large-scale use of green hydrogen. However, production potentials for green hydrogen strongly correlate to the potentials for renewable energy, which are distributed unevenly throughout the world [3].

The MENA region has abundant renewable energy resources and locations that are suitable for hydrogen production at relatively low costs. Therefore, countries within the region are recognized as potential hydrogen exporters [4]. Furthermore, the prospects of a green hydrogen market have attracted the attention of several political leaders within the MENA region and worldwide. However, the abilities to establish a green hydrogen industry and become a key hydrogen exporter in the future might differ from country to country.

The focus of this PhD thesis is the analysis of factors and boundary conditions that facilitate or impede the establishment of a green hydrogen industry in a certain country by considering political, socioeconomic and technical factors.

Previous studies have assessed the potential for green hydrogen production and/or export of different countries in the MENA region [5]–[8]. The researchers have mainly focused on the techno-economic aspects of hydrogen production. Some studies also consider social and political factors. Nevertheless, those factors have not been analyzed comprehensively and in depth and hence it remains unclear which factors are decisive for the establishment of a hydrogen economy in a country. Furthermore, previous studies have not systematically taken the preferences of actors into account, which are able to influence or make location decisions for hydrogen projects.

* Corresponding author: alexander.leuthold@wupperinst.org

Methodology

The starting point of this thesis is an extensive literature review on location factors and boundary conditions, potentially relevant for the attraction of a hydrogen industry. In a second step, announced hydrogen projects in the MENA region are analyzed and involved actors are identified to investigate their perspectives on the relevance of the previously identified factors and boundary conditions. To this end, qualitative interviews and content analysis are applied. The outcome of this part of the research is a rated list of location factors and boundary conditions (screening tool) that can be used to assess the potential of a country for hydrogen production and export. In a next step, the screening tool is tested in two case studies in two different countries within the MENA region. The goals of the case studies are on the one hand to test the application of the screening tool in practice and on the other hand to gather data and asses the two countries.

Conclusion

This thesis will allow policymakers, researchers and stakeholders to consider and evaluate the various factors, decisive for the establishment of a hydrogen economy and thereby support informed decisions for a decarbonized energy system.

References

[1] IPCC, 'Climate Change 2022: Impacts, Adaptation and Vulnerability. Contribution of Working Group II to the Sixth Assessment Report of the Intergovernmental Panel on Climate Change', Cambridge, 2022.

[2] A. Ajanovic, M. Sayer, and R. Haas, 'The economics and the environmental benignity of different colors of hydrogen', *Int. J. Hydrog. Energy*, vol. 47, no. 57, pp. 24136–24154, 2022.

[3] International Energy Agency, 'Global Hydrogen Review 2022', OECD Publishing, Paris, 2022. [Online]. Available: https://www.iea.org/reports/global-hydrogen-review-2022

[4] P. Viehbahn *et al.*, 'Zusammenfassung des Ergebnisberichts des Projekts MENA-Fuels von Wuppertal Institut, Deutschem Zentrum für Luft- und Raumfahrt (DLR) und Institut für ZukunftsEnergie- und Stoffstromsysteme (IZES) an das Bundesministerium für Wirtschaft und Klimaschutz (BMWK)', Wuppertal, Stuttgart, Köln, Saarbrücken, 2022. [Online]. Available: https://wupperinst.org/fa/redaktion/downloads/projects/MENA-Fuels_Synthesebericht_Zusammenfassung_de.pdf

[5] G. Brändle, M. Schönfisch, and S. Schulte, 'Estimating long-term global supply costs for low-carbon hydrogen', *Appl. Energy*, vol. 302, p. 117481, Nov. 2021, doi: 10.1016/j.apenergy.2021.117481.

[6] E. Jalbout, L. Genge, and F. Muesgens, 'H2Europe: an analysis of long-term hydrogen import-potentials from the MENA region', in *2022 18th International Conference on the European Energy Market (EEM)*, 2022, pp. 1–7. doi: 10.1109/EEM54602.2022.9921055.

[7] L. Sens, Y. Piguel, U. Neuling, S. Timmerberg, K. Wilbrand, and M. Kaltschmitt, 'Cost minimized hydrogen from solar and wind – Production and supply in the European catchment area', *Energy Convers. Manag.*, vol. 265, p. 115742, Aug. 2022, doi: 10.1016/j.enconman.2022.115742.

[8] D. Franzmann *et al.*, 'Green hydrogen cost-potentials for global trade', *Int. J. Hydrog. Energy*, May 2023, doi: 10.1016/j.ijhydene.2023.05.012.

H2 molecules: the complete supply chain in the current context of the energy transition

Q. Crabbé*[1], P. Hendrick[1]

[1] Université libre de Bruxelles (ULB), Aero-Thermo-Mechanics (ATM)

Introduction

In the energy transition perspectives, the objective is to achieve carbon neutrality in 2050. The electrification of industrial processes is underway, however high temperature industrial processes are not easy to be electrified and therefore the use of synthetic molecules is most probably mandatory.

This thesis, related to the Hephaïstos project, is carrying out a comprehensive study on the impact that transformations can have on the electricity and gas transmission network and on Belgium's energy supply from the import and the local production of synthetic molecules that are useful for the requested technical processes.

The work focuses on the analysis of the complete hydrogen molecules supply chain and the security of supply. The research attempts to provide a critical overview of hydrogen production, the need for hydrogen molecules at Belgian and European level and hydrogen transport and storage technologies to understand the impact of all these parameters on the final molecule cost and the TCO (Total Cost of Ownership) for different applications.

Methodology

The first step is to understand the hydrogen supply chain and therefore to know who the different producers are and where are they located, with a clear distinction between import and local production.

We need to understand the different production technologies, the interest or not of still using blue hydrogen, the importance or not of white hydrogen/pink hydrogen, the interest of ammonia, methanol and e-CH4, the importance of hydrogen purity before transport and after transport, the influence of H2 pressure, the understanding of hydrogen compression systems, of hydrogen transportation solutions, even the interest of liquid hydrogen (LH2), …

Then we must study the demand for hydrogen on the Belgian territory, understand the needs of potential customers, establish a prioritization list of these customers and analyze their cost objectives and limitations. This must be done for industry, mobility and buildings.

Finally, the objective of the research is to understand the impact of all these parameters on the final price/cost of hydrogen at the consumer level, with import and/or local production.

Discussion

* Quentin.Crabbe@ulb.be

Figure 1 shows an example of the complete hydrogen molecules supply chain, which must certainly be completed and that must be fully analyzed and parametrized, considering (on land or from the sea) import and/or local (national) production.

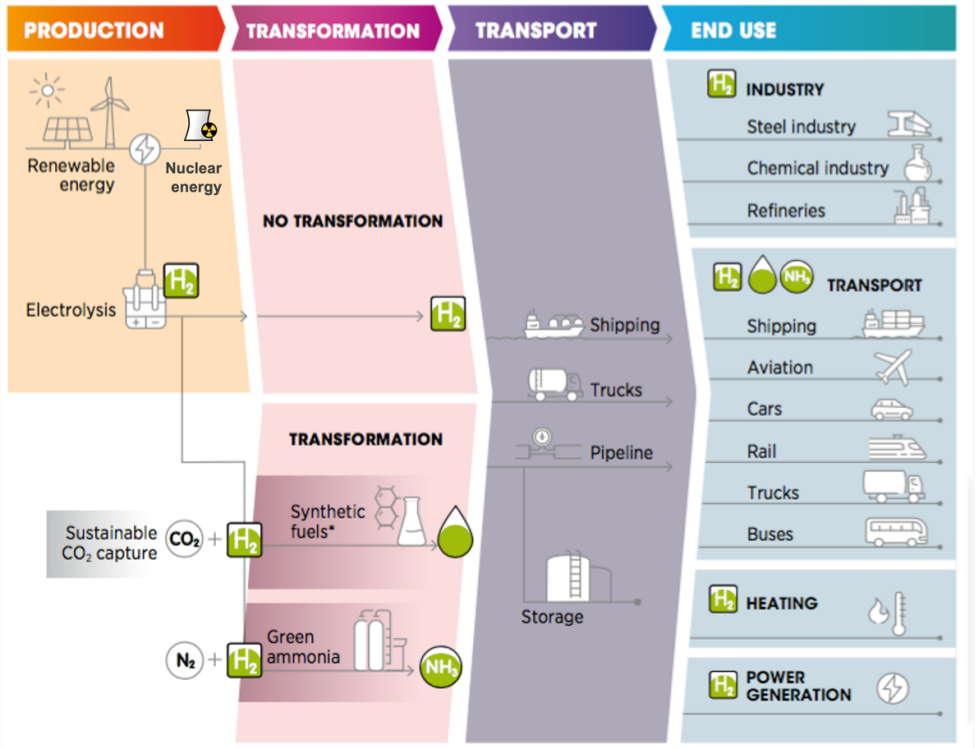

Figure 1 - An example of the complete hydrogen molecules supply chain (inspired from IRENA, Green Hydrogen, A guide of policy making *[1]*)

Conclusions

Using a software environment like GAMS, the analysis and the full quantification of the complete hydrogen molecules supply chain will be made possible. That will deliver an answer to the objective of obtaining the final price/cost of hydrogen at the end-consumer level in Belgium, with sea/land imports and/or local production.

References

[1] International Renewable Energy Agency, "Green Hydrogen : A guide to policy making," 2020.

[2] M. Robinius, S. Cerniauskas, R. Madlener, C. Kockel, A. Praktiknjo and D. Stolten, "The Palgrave Handbook of International Energy Economics," in *Economics of Hydrogen*, Palgrave Macmillan, 2022, pp. 75-102.

[3] European Hydrogen Backbone, "A european hydrogen infrastructure vision covering 28 countries," 2022.

[4] International Energy Agency, World Energy Outlook, 2023.

[5] M. Dejonghe, "Hydrogen: a deus ex machina for today's energy crisis," Ghent, 2023.

High Entropy Oxides for green hydrogen production from anion exchange membrane (AEM) seawater electrolyzer

Praveen Kumar Selvam, Muhammad Sohail Riaz, Pau Farràs Costa*

School of Biological and Chemical Sciences, University of Galway, Galway, Ireland, H91 TK33

Introduction

One of the promising ways of producing green hydrogen is seawater electrolysis by anion exchange membrane (AEM) electrolyzer. Plenty of seawater (97%) is available in our world, which can produce hydrogen for the long term and at a low cost. Nevertheless, seawater also has many challenges [1]–[3]. In particular, the overall reaction is influenced by the free energy of hydrogen adsorption, and the hydroxide precipitation in the cathode compartment blocks the electrode-electrolyte interface. Meanwhile, the chlorine evolution in the anode corrodes the anodic compartment, hindering the efficient production of hydrogen gas. Hence, to increase the rate of the hydrogen evolution reaction (HER), the catalysts should have the hydrogen adsorption energy close to zero.

Similarly, highly conductive, anti-corrosive, and stable electrocatalysts are urgently required to overcome the challenges in the oxygen evolution reaction (OER) compartment and mitigate corrosion issues. Recently, high entropy oxides (HEO) are a class of materials formed by a combination of five or more metal doped with non-metals that will alter the entropy of the material and subsequently shows exceptional catalytic property, high conductivity, and high stability[4]–[7]. Here, we report high entropy oxide nanoparticles as bifunctional electrocatalysts for HER and oxygen evolution reactions (OER). The synthesized materials were characterized using powder X-ray diffraction (PXRD), scanning electron microscopy (SEM), transmission electron microscopy (TEM), and Raman spectroscopy to confirm the material formation. Further, the synthesized catalysts were coated on the Ni foam and Ti fiber felt for HER and OER, respectively. The ex-situ characterized using linear sweep voltammetry (LSV) and chronopotentiometry, impedance studies in simulated alkaline seawater.

*Corresponding author: pau.farras@universityofgalway.ie

Further, Membrane Electrode Assembly (MEA) was fabricated and assembled in a single-cell anion exchange membrane seawater electrolyzer. Full-cell studies, including polarization curves, hydrogen production rates, and the stability of the electrocatalysts, were carried out on the assembled MEA. Followed by designing a dynamic electrolyzer that achieves an industrially required current density of 1 A cm^{-2} at low overpotential (1.8 V) in saline or alkaline saline. These research findings will enable us to move from a laboratory-scale single-cell to a multi-stack electrolyzer to commercialize and improve the environment.

Methodology

High entropy oxides ($Ni_{0.2}Fe_{0.2}Cr_{0.2}Cu_{0.2}Mn_{0.2}O_x$) can be synthesized by the co-precipitation technique would be a facile and scalable technique. Typically, five metal nitrides with equimolar composition were added in deionized water and placed for stirred well in the magnetic stirrer. 1M KOH is added drop by drop as a reducing agent to form high entropy hydroxide precipitates by adjusting the pH to 10. The solution is kept stirring for 12 hrs. Furthermore, the supernatant solution is removed, and the precipitate is centrifuged several times with deionized water and ethanol. Then, the precipitate is dried at 60 ℃ for 12 hrs and calcinated at 500 ℃ for 2 h to obtain $Ni_{0.2}Fe_{0.2}Cr_{0.2}Cu_{0.2}Mn_{0.2}O_x$ (HEO) nanoparticles.

Discussion

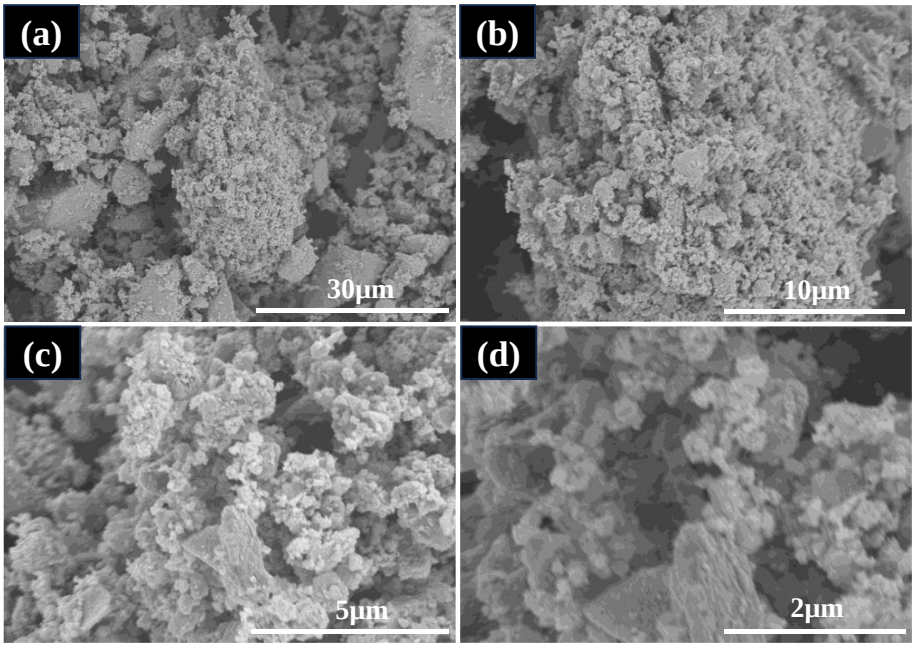

Fig.1 (a-d) SEM images of the synthesized $Ni_{0.2}Fe_{0.2}Cr_{0.2}Cu_{0.2}Mn_{0.2}O_x$

The Fig 1 (a-d) shows the SEM image of the synthesized HEO. It is observed that the synthesized materials are spherical, and the size of the particles is homogeneous.

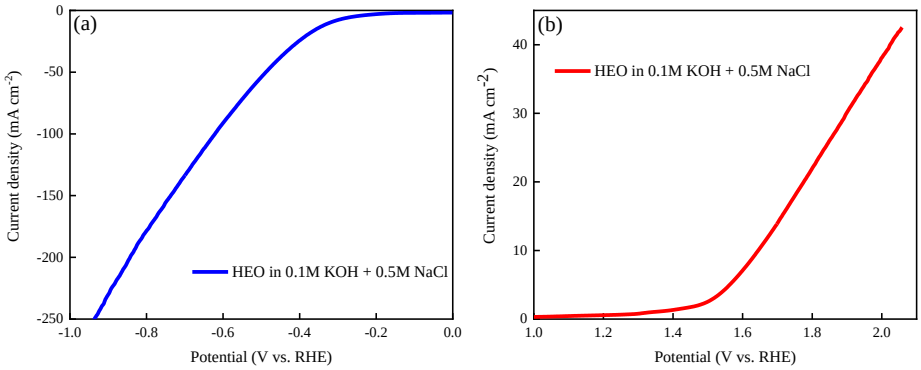

Fig. 2(a) and (b) HER and OER activity of HEO in 0.1M KOH+0.5M NaCl

The synthesized HEO nanoparticles are coated on Ni foam, and Ti felt for cathode and anode to evaluate the electrocatalytic activity. Figures 2(a) and 2(b) show that the electrocatalysts could achieve 10 mA cm^{-2} at 321 mV and 416 mV for HER and OER in 0.1M KOH+0.5M NaCl, respectively.

Conclusions

The $Ni_{0.2}Fe_{0.2}Cr_{0.2}Cu_{0.2}Mn_{0.2}O_x$ (HEO) was synthesized successfully and characterized with various techniques. This electrocatalyst is an exceptional bifunctional catalyst that is appropriately nanostructured to exhibit the current density of 10 mA cm^{-2} at a very low overpotential of 321 mV and 416 mV in HER and OER, respectively. Further, the MEA was fabricated with the synthesized catalysts and assembled in the single-cell electrolyzer; the testing is in progress. These research findings would uphold the possibilities of highly efficient green hydrogen production at low cost, sustainably, for the long term.

Acknowledgments

The authors acknowledge the ANEMEL Project funded by the Horizon Europe (European Innovation Council) Grant agreement 101071111.

References

[1] J. Li, J. Sun, Z. Li, and X. Meng, 'Recent advances in electrocatalysts for seawater splitting in hydrogen evolution reaction', *International Journal of Hydrogen Energy*, vol. 47, no. 69. Elsevier Ltd, pp. 29685–29697, Aug. 12, 2022. doi: 10.1016/j.ijhydene.2022.06.288.

[2] S. Feng *et al.*, 'Recent progress in seawater electrolysis for hydrogen evolution by transition metal phosphides', *Catal Commun*, vol. 162, no. December 2021, p. 106382, 2022, doi: 10.1016/j.catcom.2021.106382.

[3] E. Asghari, M. I. Abdullah, F. Foroughi, J. J. Lamb, and B. G. Pollet, 'Advances, opportunities, and challenges of hydrogen and oxygen production from seawater electrolysis: An electrocatalysis perspective', *Curr Opin Electrochem*, vol. 31, p. 100879, 2022, doi: 10.1016/j.coelec.2021.100879.

[4] S. Praveen Kumar, P. C. Sharafudeen, and P. Elumalai, 'High entropy metal oxide@graphene oxide composite as electrocatalyst for green hydrogen generation using anion exchange membrane seawater electrolyzer', *Int J Hydrogen Energy*, Jun. 2023, doi: 10.1016/j.ijhydene.2023.06.121.

[5] D. Wang *et al.*, 'Low-temperature synthesis of small-sized high-entropy oxides for water oxidation', *J Mater Chem A Mater*, vol. 7, no. 42, pp. 24211–24216, 2019, doi: 10.1039/c9ta08740k.

[6] J. Dąbrowa *et al.*, 'Synthesis and microstructure of the (Co,Cr,Fe,Mn,Ni)3O4 high entropy oxide characterized by spinel structure', *Mater Lett*, vol. 216, pp. 32–36, Apr. 2018, doi: 10.1016/j.matlet.2017.12.148.

[7] S. Jiang *et al.*, 'Amorphous High-entropy Non-precious metal oxides with surface reconstruction toward highly efficient and durable catalyst for oxygen evolution reaction', *J Colloid Interface Sci*, vol. 606, pp. 635–644, Jan. 2022, doi: 10.1016/j.jcis.2021.08.060.

High surface area nickel electrodes for alkaline water electrolysis

Hsin-Yu Chen*[1,2], Matheus de Groot[1,2]

[1]Department of Chemical Engineering and Chemistry, Sustainable Process Engineering Group, Eindhoven University of Technology, P.O. Box 513, Eindhoven, 5600 MB, The Netherlands
[2]Eindhoven Institute for Renewable Energy Systems, Eindhoven University of Technology, PO Box 513, Eindhoven 5600 MB, the Netherlands

Introduction

Green hydrogen has gained significant interest as an environmentally friendly energy carrier to meet the global energy demand and to achieve an eco-friendly fuel economy. Alkaline water electrolysis (AWE) is a well-established and widely-used technology for hydrogen production. Primarily because of the use of nickel-based electrode instead of precious metals like platinum or iridium, the overall components costs are low compared to competing technologies [1]. However, one of the challenges of nickel electrodes is their low electrocatalytic activity in alkaline environment. To improve performance, high surface area nickel (Raney-Ni) coatings can be used to decrease overpotentials [2]. Yet, commercial use of these coatings is still mostly limited to electrolyzers operating at low current densities (< 0.5 A cm^{-2}) and the question is whether these coatings also will show a good and stable performance when operated at high current densities (>1 A cm^{-2}), when mass transport limitations in the porous coatings might occur [3].

Methodology

This work focuses on synthesis, characterization, and performance measurement of Raney-Ni as a coating material in a three-electrode setup (Figure1) and a flow cell (Figure 2). It involves synthesis of the materials, and an investigation of the impact of morphology, pore size distribution and thickness on electrolysis performance. Synthesized materials are also analyzed via microscopy techniques such as Scanning Electron Microscope (SEM).

* Corresponding author: h.y.chen1@tue.nl

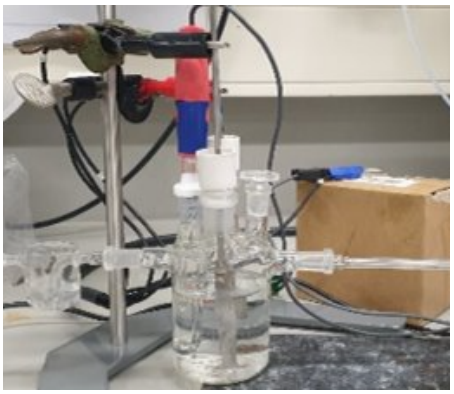

Figure 1.Three-electrode cell setup for electrodeposition

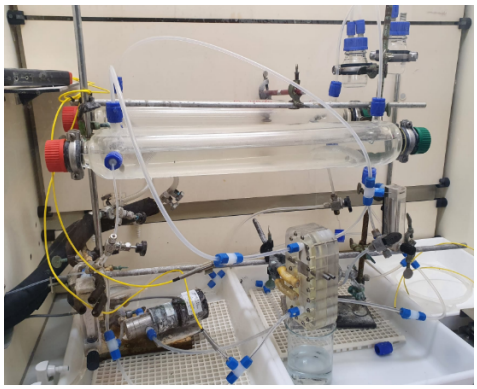

Figure 2. Alkaline water electrolyzer setup

Electroplating of Raney Nickel

All procedures were conducted in a three-electrode cell shown in Figure 1. In this three-electrode cell configuration, two 1cm x 1cm nickel perforated plates are used as counter electrode (anode) and working electrode (cathode).

Before electroplating, the electrodes were degreased in nitric acid solution for 5-10 min, followed by ultrasonically treatment with isopropanol for 20 minutes to remove impurities that might be on the surface of nickel perforated plates. Pretreated electrodes were then placed into the three-electrode cell containing modified Watt's bath consisting of $NiSO_4 \cdot 6H_2O$, $NiCl_2 \cdot 6H_2O$, H_3BO_3 and $ZnCl_2$ and were electroplated at constant current densities controlled by a direct current (DC) power supply [4]. A bubbler containing 4M KOH is connected to the cell to capture any generated chlorine gas.

To create high surface area electrodes, the synthesized NiZn electrodes were leached according to the procedure described in Gannon et al [4]. The leaching was done using 6M NaOH solution at 50 °C for 48h until bubbles stopped forming.

Three-Electrode experiments

All three electrode cell experiments were conducted on an Ivium potentiostat, connected to a three-electrode cell shown in Figure 1. The working electrode (WE) was electroplated 1cm x 1cm nickel perforated plates, the counter electrode (CE) was nickel mesh, and the reference electrode (RE) was reversible hydrogen electrode. 6M KOH with addition of 50 µM Iron(III) was the electrolyte used in this setup.

Measurements included Cyclic Voltammetry (CV), Electrochemically Active Surface Area (ECSA), Chronopotentiometry and Electrochemical Impedance Spectroscopy (EIS). Ohmic resistance was also determined using Electrochemical Impedance Spectroscopy (EIS) to determine IR-corrected overpotentials. Electrochemical Impedance Spectroscopy (EIS) in this work was also used to distinguish ohmic resistance, charge transfer resistance and mass transport.

Flow Cell measurements

The flow cell shown in Figure 2 was subsequently used to measure the performance of the full cell. A flow cell is composed of two electroplated Raney nickel electrodes as cathode and anode, and a Zirfon diaphragm consists of an open mesh poly-phenylene sulfide, which is coated with a mixture of a polymer and zirconium oxide (ZrO_2). The electrolyte used for the flow cell was the same as for the three-electrode cell measurement (6M KOH together with 50 µM Iron(III)). Measurements including Cyclic Voltammetry (CV), Electrochemically Active Surface Area (ECSA), Chronopotentiometry and Electrochemical Impedance Spectroscopy (EIS) were performed.

Results and Discussion

The synthesized Raney nickel electroplated electrodes showed significantly higher surface area in ECSA measurement compared to bare nickel electrode, which is aligned with the literature [2]. These results correlated well with SEM images where the three-dimensional appearance demonstrated much larger surface area compared to bare nickel electrode.

In polarization curves, the electroplated Raney nickel electrodes showed a large reduction in overpotential in HER reaction compared to a bare nickel electrode. This is asrcribed to the larger surface area of Raney nickel, causing faster reaction rates. However, in OER reaction, this effect was more limited. Hence, more research has to be done to probe into the phenomenon. It is worth noting that adding 50 µM Iron(III) into 6M KOH alkaline solution showed a significant impact on the performance of electrodes in alkaline water electrolysis as shown in literature [5].

Conclusions

The high surface area Raney nickel coating electrodes were successfully synthesized using electroplating method. Preliminary results tested in three-electrode setup and flow cell showed that the electroplated Raney nickel electrodes showed enhanced activity toward hydrogen evolution reaction (HER) in alkaline solution, due to its high porosity and large surface area. However, the performance toward oxygen evolution reaction (OER) in alkaline solution was more limited. Since Raney nickel is mechanically fragile due to its high porosity, future research can be done on the prevention of delamination of the coatings from the substrate under operating conditions.

References

[1] W. Kuckshinrichs, T. Ketelaer, and J. C. Koj, "Economic analysis of improved alkaline water electrolysis," Frontiers in Energy Research, vol. 5, 2017. doi:10.3389/fenrg.2017.00001

[2] F. Razmjooei et al., "Improving plasma sprayed Raney-type nickel–molybdenum electrodes towards high-performance hydrogen evolution in alkaline medium," Scientific Reports, vol. 10, no. 1, 2020. doi:10.1038/s41598-020-67954-y

[3] H. G. Xu et al., "Rational design of hydrogen evolution reaction electrocatalysts for commercial alkaline water electrolysis," Small Structures, vol. 4, no. 8, 2023. doi:10.1002/sstr.202200404

[4] W. J. F. Gannon and C. W. Dunnill, "Raney Nickel 2.0: Development of a high-performance bifunctional electrocatalyst," Electrochimica Acta, vol. 322, p. 134687, 2019. doi:10.1016/j.electacta.2019.134687

[5] T. X. Nguyen, Z.-T. Huang, and J.-M. Ting, "Iron-concentration adjusted multi-metal oxides for optimized oxygen evolution reaction performance," Applied Surface Science, vol. 570, p. 151160, 2021. doi:10.1016/j.apsusc.2021.151160

How hydrogen impacts the performance of gas turbines of different sizes

Maria Jose Mendoza Morales*[1, 2], Julien Blondeau[2], Ward De Paepe[1]

[1]Thermal Engineering and Combustion Unit, Faculty of Engineering, Université de Mons (UMONS), Rue de l'Epargne 56, 7000 Mons, Belgium
[2]Thermo and Fluid Dynamics (FLOW), Faculty of Engineering, Vrije Universiteit Brussel (VUB), Pleinlaan 2, 1050 Brussels, Belgium

Introduction

In the future energy scenario, the balance of the electricity grid will become more complex, primarily owing to the increased share of variable renewable energy (VRE). Consequently, it is imperative to establish mechanisms capable of effectively adapting to the power demand. When there is an excess of solar and wind energy production, surplus power should be translated into energy storage solutions. Conversely, during periods of insufficient sun and wind, dispatchable energy means should be available to meet the demand while ensuring that carbon emissions remain minimal. Hydrogen, as an energy carrier can serve both scenarios: as a long-term and large-scale energy storage [1] and as fuel for power production facilities. In this context, hydrogen-fired gas turbines (GT) will likely have a place in the electricity system due to their operational flexibility and dispatchability. Öberg et al. [2] explored the competitiveness of hydrogen-fueled gas turbines in future energy systems, finding out that hydrogen-fueled gas turbines are highly competitive in systems with minimal acceptance of CO_2 emissions. However, in scenarios projected between 2040 and 2050, which still display tolerance for CO_2 emissions, blends ranging from 30% to 77% by volume appear to be more competitive. Nevertheless, the discussion around the use of hydrogen in gas turbines not only involves the hardware technological challenge, including combustion, compression, and storage but also the availability of low-carbon hydrogen. Gülen et al. [3] estimates that producing H_2 to co-fire at 30 vol.-% a combined cycle gas turbine (CCGT) with a capacity factor of 60% corresponds to a 7% of the US curtailment in 2020. It means that the capacity production of green hydrogen (or zero-carbon hydrogen) is somewhat limited to smaller amounts, making small industrial and aero-derivative gas turbines more interesting to be fired with hydrogen than heavy-duty CCGT. Concurrently, larger gas turbines exhibit higher efficiencies, rendering them highly attractive assets. As a result, it is expected that a fleet made of GTs of various sizes for different purposes will be the reality. So, in this work, by analyzing the thermodynamic cycle of these systems, we aim to determine the advantages of using one gas turbine over another based on their performance.

In the early 1980 Tsujikawa and Sawada [4, 5, 6] investigated different configurations of liquid hydrogen-fueled gas turbines, identifying improvements on thermal efficiency and power output. In 2005, Chiesa et al. [7] discussed the impact of hydrogen on the cycle of a gas turbine conceived for methane combustion. They state that the change in fuel implies an off-design operation of the gas turbine, making the matching of the components essential for the modeling. More recently, Arsalis [8] assessed the impact of hydrogen on an industrial gas turbine and estimated the positive impact on the exergetic efficiency, and Lopez-Ruiz et al. [9] analyzed the thermodynamic performance of a regenerative gas turbine, supporting Arsalis's conclusion on the positive impact of hydrogen. Bexten et al. analyzed a hydrogen-fired gas turbine with external exhaust gas recirculation (EGR). They observed a lower impact on efficiency for the hydrogen-fired gas turbine than for the methane one when EGR is at ambient temperature but the opposite for the EGR at high temperature. Thus, the research shows that hydrogen seems to have a rather positive impact in terms of performance. However, a comprehensive and detailed analysis of the evolution of the thermodynamic performance of the different types of gas turbines is missing. For this reason, we decided to investigate the impact of hydrogen on the thermodynamic performance of gas turbines of different sizes to contribute to the discussion about the use of this fuel.

Throughout this extended abstract, we discuss the modeling of three different gas turbines and subsequently assess the influence of hydrogen on their performance. We have selected a heavy-duty gas turbine,

*Corresponding author: mariajose.mendozamorales@umons.ac.be

based on a simple Brayton cycle, an aero-derivative gas turbine with a single spool and a free turbine, and finally, a micro gas turbine (mGT) based on a recuperative Brayton cycle. In the methodology section, we provide a comprehensive explanation of the construction of each of these models and detail the modifications required for hydrogen combustion. Subsequently, we discuss why hydrogen impacts each of these systems differently and comment on other factors that must be considered for further analysis.

Methodology

All the models in this paper have been built using Aspen Plus, a software widely used in the industry for process simulation. The thermodynamic model for property calculation is the Redlich-Kwong-Soave cubic equation of state with the Boston-Mathias alpha (RKS-BM) for all the gas streams, as Aspen Plus recommends it for high-pressure - high-temperature systems. The three models are based on the Brayton cycle principle, where atmospheric air is compressed, followed by combustion to attain elevated temperatures. Subsequently, these high-temperature, high-pressure gases are expanded in a turbine to produce electricity thanks to a generator. However, each system possesses distinct characteristics.

The degrees of freedom of a gas turbine depend on its design and complexity but the control of simple GT for power generation is limited to the fuel flow, the airflow, and the rotational speed. The fuel\air ratio entering the combustion chamber defines the turbine inlet temperature (TIT), which, in turn, based on the Carnot efficiency, defines the thermal efficiency for the same operating conditions. However, the TIT is usually not available in the performance sheet of the original equipment manufacturers (OEM), while the turbine outlet temperature (TOT) is. For this reason, we decided to control the fuel flow to maintain the same TOT in the three cases.

A gas turbine operates as a fixed-volume machine at a constant rotational speed. Thus, to adjust the volume flow, it is necessary to control the rotational speed or modify the inlet section, which is made possible by the presence of inlet guide vanes (IGV). However, the possibility to control the rotational speed of the turbine depends on the size of the equipment. The largest machines are designed to run at constant rotational speed but the existence of IGVs, allows the operators to adapt the output of the machine by changing their position. Some smaller systems, like industrial and aero-derivative run at different speeds and have IGVs. While in the case of mGTs, it is the rotational speed that is controlled to fit the needs of the user.

The heavy-duty gas turbine is based on the performance of the GE 7HA.02. The GE HA series is the fastest-growing fleet in the world, so we considered this model to be representative of this range. As shown in Fig. 1, a single turbine generates the power to drive the compressor and the generator. The matching of the compressor and the turbine for the off-design operation is made by the assumption that the turbine is choked and therefore the swallowing capacity is constant. The cooling flows are simulated as a fraction of the compressed air that is then mixed with the combustion products, reducing the temperature at the inlet of the turbine. The rotational speed of heavy-duty GTs is fixed by the grid at 3000 or 3600rpm limiting the degrees of freedom to operate them and it is assumed that the IGVs are completely open. So in this case, only the fuel flow is controlled to keep the TOT. The GT produces 344MW of electricity with a thermal efficiency of 41.7% at ISO conditions and the model was previously validated in [10].

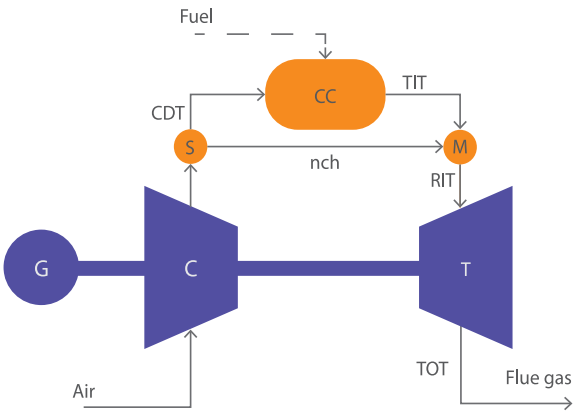

Figure 1: Heavy-duty gas turbine model with nonchargeable cooling flows based on the GE 7HA.02.

In the case of the aero-derivative gas turbine, we have selected the GE-LM2500 which produces 33MW with a thermal efficiency of 38.6%. The GE-LM2500 is one of the well-known power generators in the

industry with over 120 million operating hours [11] and thus an interesting engine to assess. This model at ISO conditions and full load has been validated against actual data available in Thermoflex. The way of modeling changes from the heavy-duty gas turbine because there are two turbines in series as depicted in Fig 2. The high-pressure turbine (HPT) generates the power to drive the compressor while the power turbine (PT) drives the generator to produce electricity. It is assumed that the PT is choked, limiting the HPT in terms of pressure ratio while the rotational speed of the gas generator is controlled to maintain the matching between the HPT and the compressor. Adjusting the rotational speed enables us to navigate within the compressor's performance map and match it to the desired operational point. In short, for the off-design operation, the HPT needs to produce the power to drive the compressor while keeping its pressure ratio constant.

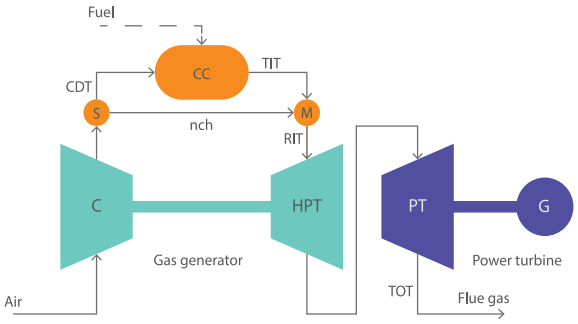

Figure 2: Aeroderivative gas turbine model with nonchargeable cooling flows based on the GE LM2500.

The Turbec T100 was used as a reference for the mGT model. It produces 100kW of power and has an efficiency of 28.85%. The model was validated using both the manufacturer's data, but also experimental data available from previous tests performed in our research group [12]. For this GT, the modeling differs from the simple Brayton cycle because a heat exchanger is placed between the compressor and the combustion chamber to recover heat from the exhaust gases and increase the efficiency of the system as shown in Fig. 3. The TIT is limited because the turbine blades are made of metal and due to size constraints, there are no cooling flows. This, in conjunction with lower component efficiency, results in a reduction in the thermal efficiency of the system. As well as for the heavy-duty, the matching of the compressor and the turbine is done by the assumption of the choke condition at the inlet of the turbine. However, as the scale of the GT is much smaller, the rotation speed can be easily modified to generate the power needed by the user giving more flexibility. Thus, two cases are considered for the mGT: (1) TOT and rotational speed constant and (2) TOT and power output constant.

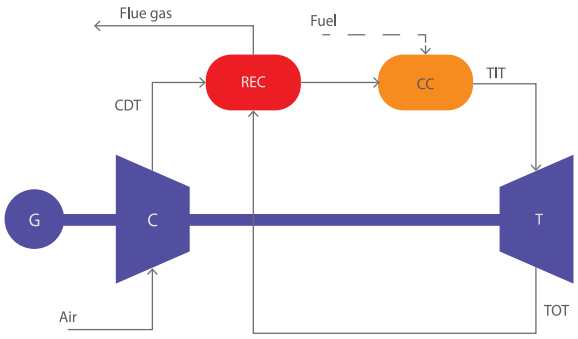

Figure 3: mGT model based on the Turbec T100.

Discussion

When comparing all the configurations it can be concluded that increasing the hydrogen fraction has a positive impact on every one of them in terms of efficiency and power output when operating the gas turbines for a constant TOT. As illustrated in Fig. 4 the power produced by the aero-derivative displays a higher relative increase of 9% compared to 6.5% for the heavy-duty and 3.2% for the mGT. Contrastingly, in terms of efficiency (Fig. 6), the heavy-duty GT shows a higher relative increase of

3.2%, while the aero-derivative exhibits a smaller increase of 2.5%. The mGT shows smaller gains for the two scenarios that were studied, the power constant case being the least advantageous with a 0.9% relative efficiency increase.

The increase in power output and efficiency is due to multiple factors. As Chiesa et al. [7] explains, the change in the composition of the flue gases modifies the enthalpy change in the turbine, while the difference in lower heating value implies a decrease in mass flow rate. In the case of the heavy-duty gas turbine and the mGT, the air mass flow entering the system slightly decreases (and could even be considered constant) while due to hydrogen combustion, the amount of water vapor in the flue gases increases. This has as a consequence an increase in the specific heat capacity (Cp) and the heat capacity ratio (γ) of the combustion products, translating into more power generated by the turbine despite the decrease in mass flow rate.

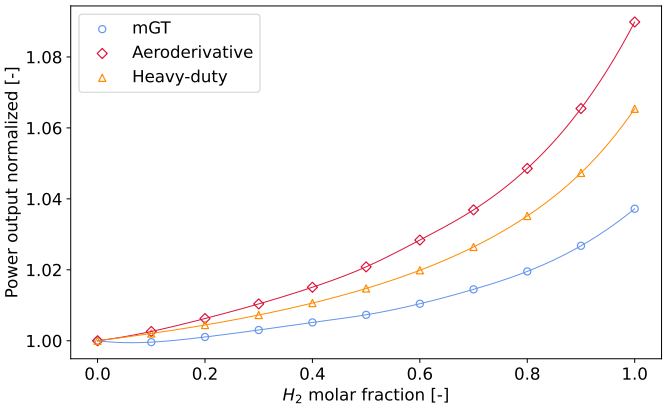

Figure 4: Hydrogen has a higher impact on the aero-derivative gas turbine power output.

The case of the aero-derivative is slightly different. The air mass flow entering the gas turbine increases due to the control to match the compressor and the turbine. The Cp of the combustion products increases with a higher hydrogen fraction, as well as γ. The TIT increases and so does the temperature at the outlet of the HPT. Additionally, the outlet pressure of the HPT increases because the compression ratio also increases, while the pressure ratio of the HPT is constant, resulting in gases with higher enthalpy at the inlet of the power turbine. Finally, with the increase of the flue gases mass flow rate and a higher enthalpy available at the inlet of the power turbine, the GT delivers more power.

The gain in efficiency is a consequence of the increase in power output, but it does not translate directly as the heat input also increases in most cases. Due to temperature controls (TOT in this case) and a higher excess of air for a bigger hydrogen fraction, the required thermal input increases, except in the case of the mGT at constant power as shown in Fig. 5. For the aero-derivative, despite producing more relative power than the heavy-duty, the excess of air is higher resulting in more need for heat to maintain the TOT constant.

In the case of constant power and TOT of the mGT, the enthalpy drop variation due to the composition of flue gases plays an important role. The TIT decreases and so does the heat input rate, resulting in a higher efficiency despite constant power output.

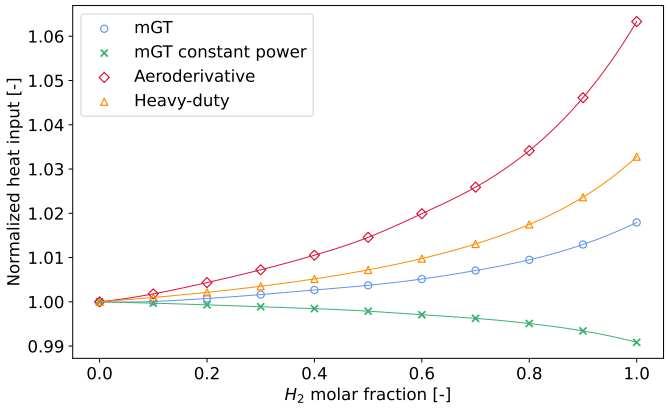

Figure 5: The heat input increases to maintain the TOT, but as the mGT case 2 is limited to producing the same amount of power, the higher Cp of flue gases allows to not increase the heat input.

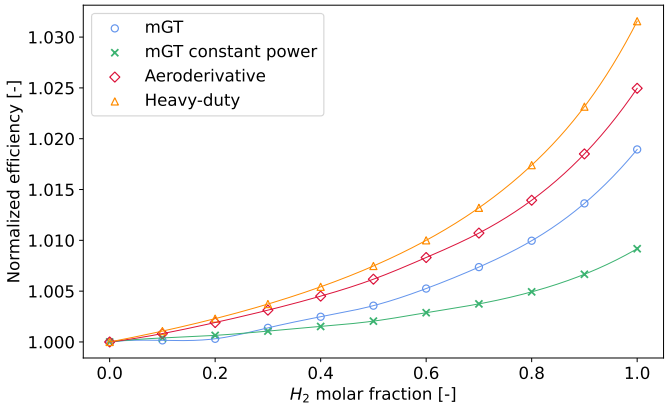

Figure 6: The heavy-duty gas turbine seems to get more advantage from hydrogen in terms of efficiency.

Conclusion

This paper explores the influence of hydrogen on the performance of gas turbines of different sizes. It assesses the overall positive impact on each gas turbine's performance while highlighting distinctions between them. Notably, heavy-duty gas turbines appear to excel in terms of efficiency, whereas aeroderivative models exhibit advantages in power output. The simulations have been done only for the TOT constant, but other control parameters, like IGV control, must be evaluated to have a broader comprehension of the different operating points. However, the comparison in terms of efficiency and power output is not enough to establish the competitiveness of each system within a larger framework.

Acknowledgments

This research is part of the BE-HyFE project, which is a Belgian academic collaboration project, funded by the federal Energy Transition Fund by FPS Economy. More information on www.behyfe.be.

References

[1] Ferdi Schüth. Energy Storage Strategies. In Schlögl; Robert, editor, *Chemical Energy Storage*. De Gruyter, 2nd edition edition, 2022.

[2] Simon Öberg, Mikael Odenberger, and Filip Johnsson. Exploring the competitiveness of hydrogen-fueled gas turbines in future energy systems. *International Journal of Hydrogen Energy*, 2022.

[3] S. Can Gülen, Raj Singh, and Pritam Banerjee. Hydrogen and Gas Turbines – A Rational Approach. In *Proceedings of ASME Turbo Expo 2023*, Boston, 2023. ASME.

[4] Yoshiharu Tsujikawa and Teruo Sawada. On the Utilization of Hydrogen as a Fuel for Gas Turbine : 1st Report, On the Utilization of Low Temperature Exergy of Liquid Hydrogen. *Bulletin of JSME*, 1980.

[5] Y Tsujikawa and T Sawada. Analysis of a gas turbine and steam turbine combined cycle with liquefied hydrogen as fuel. *International Journal of Hydrogen Energy*, 1982.

[6] Y Tsujikawa and T Sawada. Characteristics of hydrogen-fueled gas turbine cycle with intercooler, hydrogen turbine and hydrogen heater. *International Journal of Hydrogen Energy*, 1985.

[7] Paolo Chiesa, Giovanni Lozza, and Luigi Mazzocchi. Using hydrogen as gas turbine fuel. *Journal of Engineering for Gas Turbines and Power*, 2005.

[8] Alexandros Arsalis. Thermodynamic modeling and parametric study of a small-scale natural gas/hydrogen-fueled gas turbine system for decentralized applications. *Sustainable Energy Technologies and Assessments*, 2019.

[9] Gontzal Lopez-Ruiz, Joseba Castresana-Larrauri, and Jesús María Blanco-Ilzarbe. Thermodynamic Analysis of a Regenerative Brayton Cycle Using H2, CH4 and H2/CH4 Blends as Fuel. *Energies*, 2022.

[10] Maria José Mendoza Morales, Antoine Verhaeghe, Laurent Bricteux, Julien Blondeau, and Ward De Paepe. Is blue hydrogen a better alternative than post-combustion carbon capture for combined cycle gas turbines? a thermodynamic point of view. In *Proceedings of ASME Turbo Expo 2023*, Boston, 2023. ASME Turbo Expo.

[11] GE Gas Power. LM2500 - Aeroderivative gas turbine datasheet. Available at https://www.ge.com/gas-power/products/gas-turbines/lm2500.

[12] Ward De Paepe, Marina Montero Carrero, Simone Giorgetti, Alessandro Parente, Svend Bram, and Francesco Contino. Exhaust Gas Recirculation on Humidified Flexible Micro Gas Turbines for Carbon Capture Applications. In *Volume 3: Coal, Biomass and Alternative Fuels; Cycle Innovations; Electric Power; Industrial and Cogeneration; Organic Rankine Cycle Power Systems*. American Society of Mechanical Engineers, 2016.

Hydrogen Economy in Middle East and North Africa: Powerful actors and projections of risks and opportunities in the media discourse

Fabio Schojan[1*1, 2]

[1] Junior Researcher at Wuppertal Institut für Klima, Umwelt, Energie gGmbH
[2]PhD Candidate at University of Agder, Norway

Introduction

The European Union and its member states outlined in the past three years plans [1]– [3] how to decarbonize their economies, achieving climate-neutrality in heavy-industries and transport and transitioning from fossil fuels towards renewable energy altogether until 2050. This energy carrier, which is supposed to drive the decarbonization, can be produced through different ways: Electrolysis of water through renewable energy sources (Green Hydrogen), carbon capture of hydrocarbons (blue hydrogen) and steam reforming of natural gas (grey hydrogen). The plans of the EU and in particular the German government point out particular interest to fuel their economies with preferably 'green hydrogen', but parallelly remaining open for other colors of the hydrogen production scheme. Regardless of the color, there exists bipartisan agreement to import up to 70% of the required amount of hydrogen in 2030 from other parts of the world, pointing to the Middle East and North Africa (MENA) as potential suppliers [2].

Three implicit facts stand out here: First, there is no large-scale 'green hydrogen economy' existing in the region yet, hence grey and blue hydrogen might still play a role in the meantime although not considered sustainable at all [4]. Second, there is much attention in the discourse drawn on the EU perspective to fulfil political and developmental goals and less MENA region how the hydrogen economy will actually evolve based on the political goals of the governments in the region. The region might play a significant role for hydrogen exports to the EU, while pursuing own developmental and political goals as well as committing to climate targets, indicating an unequal balance of priorities. Therefore, it is particularly important to extend the narrow view away from European developmental plans towards the MENA region, as the development of the hydrogen economy in Middle East and North Africa will account in the overall view on the sustainability of imports towards the EU and member countries. Third, contemporary plans in MENA countries to facilitate a hydrogen economy for domestic use and export purposes towards the EU are currently underway due to the local availability of abundant renewable and still significant fossil energy sources which poses a necessary condition for the production of hydrogen [5]. This development will make some countries and in particular actors in the MENA region a powerful driver of an impactful global energy transition that puts a new 'energy regime' of power in place. To further describe this 'regime', I will use the Foucauldian term 'dispositive' to embrace the structure of politics, economy and society in the Middle East and North Africa that has evolved in the past 'regime' of fossil fuels and which will face the energy transition towards the hydrogen economy.

This opens up the general question how the discourse on the hydrogen economy in the MENA region is constructed, based on an assessment of powerful actors and possible risks and

[1*] Corresponding author: fabio.schojan@uia.no ; fabio.schojan@wupperinst.org

opportunities of this transition. Considering the pressuring political agenda to achieve climate-neutrality at all costs [6] and also a predominance of positive outlooks in the media discourse, the contrasting juxtaposition of risks and opportunities needs to be further analysed. Therefore, the aim is to analyse the contemporary media discourse of the hydrogen economy plans in the MENA region to answer the following research question:
Which actors are directly affected or indirectly affected by the development of a green hydrogen economy and which opportunities and risks are discussed in the media discourse in the MENA region?

Relevance

This research paper contributes to two identified research gaps among research on the hydrogen economy. First, contemporary research on the facilitation of a hydrogen economy puts emphasis mainly on techno-economic aspects, economic growth projections [7]–[9] and normative assessments focusing, for example, on environmental and social justice under the framework of 'just transition' [10]. None of these publications have considered the influence of power relationships executed by actors and how they construct the discourse on the current development of the hydrogen economy. Cha and Pastor [11] acknowledged the significant influence of power relations in the case of 'just transitions', therefore it remains also an open question whether certain actors execute more power on the energy transition towards hydrogen than others. Avelino [12] understands any form of sustainability transition as powerful discourse driven by actors, standing in relationship to each other and executing power. Scoones [13, p. 309] considers transformations, particularly in the case of sustainability, as a construct of '…networks, alliances, and coalitions and connect diverse actors - including state and business actors, scientific-technical elites and citizens movements'. Therefore, closer observation of actors and power relationships will disclose which interests drive the contemporary discourse on the upcoming hydrogen economy.

Second, considering the failure of previous attempts to establish a hydrogen economy in the 2000s and strong current political advocacy towards hydrogen production to achieve climate neutrality [14], tangible evidences and assessments of possible risks and opportunities how the hydrogen economy will evolve are currently missing. In particular risks are mostly downplayed, as the economic perceptions are based on perceptions of growth, while environmental or even social risks are being raised by NGOs and research organizations at the same time. This divergency is in need for further tangible analysis. As Beck [15] has raised the term of 'global risk society' the perspectives on risks need to be further analysed, as they represent an important by-product of any modernization process and society needs to respond to it at a given time when crisis occur. It should be no doubt that a large-scale hydrogen economy in the MENA region will be prone to certain risks, as it has also been the case during the 'regime' of fossil fuels exportation in terms of geopolitics, society and economics.

Main Focus of the research paper

The aim of this paper is to give a better understanding of the current media discourse on the upcoming development of a hydrogen economy in the MENA region, focusing on relevant influential actors and power relationships as well as identifying risks and opportunities based on statements, narratives and storylines. When perceiving the transition towards renewable energy, particularly using hydrogen as energy carrier for renewables, as a dynamic process of

'revealing' [16] then I am asking at first: who is transitioning?[2] Answering this question through the following methodology will reflect itself in a disposition of actors and power relationships to be considered in the assessment on risks and opportunities of the energy transition towards a hydrogen economy in the MENA region. It will eventually provide indications on the perspectives from governments of the MENA region how the hydrogen economy is portrayed as a vision until 2030 and beyond.

Methodology

In order to conduct the discourse analysis, the research will use a selection of maximally 20 news articles in the timeframe 2019-2022 from each country in the MENA region. According to Carvalho [17] newspaper articles are highly relevant sources to understand how certain realities are constructed. The news articles will be analysed through a content analysis inspired by a method proposed by Hajer [18], [19] and Dryzek [20] on environmental discourses. Both are equally adapting Foucauldian approaches to discourse, understanding it as an ensemble of practices, objects, statements and images that are regulated by a set of rules [21]. This means, to identify how a certain topic or issue is constructed as well as its basic entities, components and storylines of the discourse. Particular application of those methods inspired by Hajer and Dryzek have been conducted by Doulton and Brown [22] and Machin [23]to analyse environmental modernization and climate change discourses and make sense of their storylines and basic entities. The approach to analyse storylines and how they are constructed in the discourse will be applied here by using the software MAXQDA to code the different news articles to give better understanding of the hydrogen discourse among MENA countries. This will be done based on the using the following categories: Actors and Objects, Storylines on Risks and Opportunities.

The following outline of the research approach is adapted from similar analytical frameworks on how to conduct discourse analysis of texts from [17] and [20]:

1. Selecting the 'corpus' of texts, in this case maximally 20 news articles about the development of the hydrogen economy in the timeframe 2019-2022 from each MENA country (Algeria, Bahrain, Egypt, Iran, Iraq, Israel, Jordan, Kuwait, Lebanon, Libya, Morocco, Mauritania, Oman, Qatar, Saudi Arabia, Syria, Tunisia, UAE and Yemen). If possible, media content from each country's official news agency Unfortunately, not all media landscapes of those MENA countries deliver the same quantity and quality of coverage on the hydrogen economy. Therefore,
2. Comparative reading of the news articles in order to provide an initial impression of the argumentative setting on the discursive perceptions on the hydrogen economy.
3. Reducing the number of MENA countries depending on the availability of media sources. A minimum number of five media articles will be used us lower threshold. . .
4. Screening of the news articles by using the software MAXQDA. Through automated searching of the term 'Hydrogen' and marking the corresponding paragraphs where the term shows up.
5. Analysing and coding the marked paragraphs on actors and objects to identify power relationships in the facilitation process of the hydrogen economy of each MENA country.

[2] See research question

6. Analysing and coding the marked paragraph on storylines about 'risks' or 'opportunities' of the green hydrogen economy in relation to the previously identified actors and objects within the paragraphs.
7. Summarizing all identified codes for actors, objects and storylines into groups to give an improved overview on the results. For instance,
8. Summarizing the results from the accumulated data across all MENA countries and highlighting differences in terms of power relationships and storylines about risks and opportunities to provide tangible results for understanding better the hydrogen discourse.

Conclusions

Preliminary results of the analysis already indicate the following characteristics of the media discourse on the hydrogen economy in the MENA region

1. Some countries do not have a relevant media discourse (Syria, Lebanon, Yemen, Iraq)
2. Other MENA countries have a media discourse on the hydrogen economy, but in an entirely different context (Iran; chemical engineering reports from gas industry), the own country size is acknowledged as too small for large-scale projects (Kuwait & Bahrain) or contemporary political crisis overshadow the feasibility of hydrogen projects (Libya)
3. The remaining MENA countries (Mauritania, Morocco, Algeria, Egypt, Saudi-Arabia, Oman, UAE, Qatar, Israel and Jordan) show in their hydrogen media discourse many similarities with national relevant topics from politics, economy and society in their storylines and depiction of risks and opportunities. For instance, below two findings from Israel and Egypt:

Table 1: Hydrogen Discourse in Egyptian media ranked according to frequency of codes

Actors	Risks	Opportunities	Storylines
1.Government/President	1.Domestic Energy Needs	1.Sustainable Energy	1.The Government is driving the domestic hydrogen economy
2.Suez Canal	2.Water	2.Investment	2. Egypt offers beneficial conditions for a hydrogen hub and production and will lead the field internationally
3.Europe/EU	3.Institutional challenges	3.Environment/Climate	3. Egypt will benefit in environment, society and economy

Table 2: Hydrogen Discourse in Israeli media ranked according to frequency of codes

Actors	Risks	Opportunities	Storylines
1.Israeli Start-ups	1.Political Situation	1.Technical Innovation	1.Domestic Innovation will push hydrogen application
2.Research/ Science/Universities	2.Market Competition	2.International Cooperation	2. Hydrogen economy will foster international partnership in the region (Egypt, Jordan, Saudi-Arabia)
3.Morocco (Government)	3.Water supply & Land	3.Decarbonisation	3. Israel will serve as hydrogen hub for the fuel of the future
4.Transportation, Mobility &Industries		4.Investment	

Final conclusions of the research will be made as soon as the research paper is finalized, which is expected to happen in the first quarter of 2024.

References

[1] BMWi, 'Die Nationale Wasserstoffstrategie'. Bundesministerium für Wirtschaft und Energie (BMWi), Jun. 2020.

[2] BMWK, 'Fortschreibung der Nationalen Wasserstoffstrategie'. Bundesministerium für Wirtschaft und Klimaschutz (BMWK), Jul. 2023.

[3] European Commission, 'COMMUNICATION FROM THE COMMISSION TO THE EUROPEAN PARLIAMENT, THE COUNCIL, THE EUROPEAN ECONOMIC AND SOCIAL COMMITTEE AND THE COMMITTEE OF THE REGIONS - A hydrogen strategy for a climate-neutral Europe'. Jul. 08, 2020. [Online]. Available: https://eur-lex.europa.eu/legal-content/EN/TXT/?uri=CELEX:52020DC0301

[4] R. W. Howarth and M. Z. Jacobson, 'How green is blue hydrogen?', *Energy Sci Eng*, vol. 9, no. 10, pp. 1676–1687, Oct. 2021, doi: 10.1002/ese3.956.

[5] J. Terrapon-Pfaff and S. R. Ersoy, 'Sustainable transformation of energy systems in MENA countries : comparative report', Friedrich-Ebert-Stiftung, Amman, 2022.

[6] M. Corporate Europe Observatory, Food and Water Action Europe, and Re:Common, Eds., 'The Hydrogen Hype: Gas Industry Fairy Tale or Climate Horror Story - The European Commission and its quest to let the gas industry write the book on hydrogen in Europe'. Dec. 2020.

[7] I. E. A. IEA, 'The Future of Hydrogen - Seizing today's opportunities', p. 203, Jun. 2019.

[8] M. Ludwig *et al.*, 'The Green Tech Opportunity in Hydrogen', BCG Global. Accessed: Apr. 21, 2022. [Online]. Available: https://www.bcg.com/publications/2021/capturing-value-in-the-low-carbon-hydrogen-market

[9] McKinsey & Company, 'Hydrogen Insights - A perspective on hydrogen investment, market development and cost competitiveness'. Feb. 2021.

[10] F. Müller, J. Tunn, and T. Kalt, 'Hydrogen justice', *Environ. Res. Lett.*, Oct. 2022, doi: 10.1088/1748-9326/ac991a.

[11] J. M. Cha and M. Pastor, 'Just transition: Framing, organizing, and power-building for decarbonization', *Energy Research & Social Science*, vol. 90, p. 102588, Aug. 2022, doi: 10.1016/j.erss.2022.102588.

[12] F. Avelino, 'Power in Sustainability Transitions: Analysing power and (dis)empowerment in transformative change towards sustainability: Power in Sustainability Transitions', *Env. Pol. Gov.*, vol. 27, no. 6, pp. 505–520, Nov. 2017, doi: 10.1002/eet.1777.

[13] I. Scoones, 'The Politics of Sustainability and Development', *Annu. Rev. Environ. Resour.*, vol. 41, no. 1, pp. 293–319, Nov. 2016, doi: 10.1146/annurev-environ-110615-090039.

[14] V. Vaitheeswaran, 'Hydrogen hype is rising again—will this time be different?', *The Economist*, Nov. 14, 2022. Accessed: Dec. 19, 2022. [Online]. Available: https://www.economist.com/the-world-ahead/2022/11/14/hydrogen-hype-is-rising-again-will-this-time-be-different
[15] U. Beck, *Risikogesellschaft: auf dem Weg in die Moderne*, Einmalige Sonderausg. in Edition Suhrkamp, no. 3326. Frankfurt am Main: Suhrkamp, 1996.
[16] M. Heidegger, *The question concerning technology, and other essays*. New York: Garland Pub, 1977.
[17] A. Carvalho, 'Discourse Analysis and Media Texts: a Critical Reading of Analytical Tools', presented at the International Conference on Logic and Methodology, Köln, 2000.
[18] M. A. Hajer, *The politics of environmental discourse: ecological modernization and the policy process*. Oxford : New York: Clarendon Press ; Oxford University Press, 1995.
[19] M. A. Hajer, 'Doing Discourse Analysis: Coalitions, Practices, Meaning', in *Words matter in policy and planning: discourse theory and method in the social sciences*, M. van den Brink and met, Eds., Utrecht: Koninklijk Nederlands Aardrijkskundig Genootschap : Netherlands Graduate School of Urban and Regional Research, 2006.
[20] J. S. Dryzek, *The politics of the earth: environmental discourses*, 2nd ed. Oxford ; New York: Oxford University Press, 2005.
[21] M. Foucault, *The archaeology of knowledge*. New York, NY: Pantheon Books, 1982.
[22] H. Doulton and K. Brown, 'Ten years to prevent catastrophe?', *Global Environmental Change*, vol. 19, no. 2, pp. 191–202, May 2009, doi: 10.1016/j.gloenvcha.2008.10.004.
[23] A. Machin, 'Changing the story? The discourse of ecological modernisation in the European Union', *Environmental Politics*, vol. 28, no. 2, pp. 208–227, Feb. 2019, doi: 10.1080/09644016.2019.1549780.

Hydrogen Mobility Transition: How it affects the society and how to secure policy consistency

Jina Cheon

University of Leeds

Introduction

Hydrogen energy has been in limelight with its potential to reduce Green House Gas (GHG) emissions while being a means of strengthening energy security. The world has witnessed growing interests of countries in hydrogen applications including hydrogen mobility. The countries focusing on hydrogen energy can be divided into hydrogen producer, hydrogen end-user or both. Among countries which endeavour to promote hydrogen applications, there are meaningful numbers of countries concentrating on increasing the number of Hydrogen Fuel Cell Vehicles (HFCVs) on the road as a part of hydrogen mobility. Given the crucial role of transport sector in reducing emission for decarbonisation, there is a need to activate the transition to environmentally benign vehicles including so called green mobility[1].

According to the IEA Technology Collaboration Programme on Advanced Fuel Cells[2], as of the end of 2022, more than 70,000 units of HFCVs are on the road with 1000 Hydrogen Refuelling Stations(HRSs) worldwide. This demonstrates the meaningful growth in hydrogen mobility market as the result of significant technological advancement in HFCVs along with the governmental efforts of Asian countries such as China, South Korea and Japan as well as the US and European countries[3].

However, as the IEA comments on the Global Hydrogen Review 2022, hydrogen energy is still in the nascent stage. In addition to technological sophistication, there are other aspects to consider. Securing policy consistency and public acceptance can be the ones to focus for hydrogen mobility transition. Hydrogen mobility policies falls under long term energy and environmental policies. This can bring uncertainty about prospects for implementation. Since hydrogen mobility policy affects daily lives of people, policy consistency holds significance in terms of expelling uncertainty to attract industry's interests and raising public acceptance. In this regard, a socio-technical approach to analyse hydrogen transitions can help to identify and examine factors affecting policy consistency [4].

There is limited research to date which analyses hydrogen mobility from a socio-technical perspective. Those studies focus on a few Western countries. Given the countries interested in hydrogen transitions are not only advanced countries but also developing countries, countries take different strategies for hydrogen transitions, raising the necessity of taking socio-technical perspectives for non-Western countries. To this end, this paper extends the socio-technical approach to analyse policy consistency in hydrogen mobility transition in South Korea, a country whose feature of government system differs in this respect to those Western countries previously studied.

Under this circumstance, this research aims at applying socio technical transition and ideal governance framework to hydrogen mobility transition to raise public acceptance and secure policy consistency. Two objectives are set to achieve the aims, which are 1) investigate

which tools and theories from liberal democracies could be effective in analysing hydrogen mobility transition of the non-liberal countries and 2) explore how the result of this research could be a reference for other countries including European countries.

With the recognition of developments on hydrogen mobility as a social phenomenon, this research adopts Multi-level Perspective (MLP) elaborated by Geels [5]. This is to analyse the newly emerging technology with niche, regime and landscape perspectives to figure out whether the new technology is innovate enough to create niche, destabilise existing regime and shift the landscape in a sustainable manner [6]. However, only with MLP, tensions can be identified but it would be restricted to resolve challenges. As Geels[7] has pointed out, an open-type inclusive governance framework should be explored to compensate the limit.

In terms of having different administrative system compared to liberal democracies, South Korea is under the influence of Confucianism and top-down approach. This aspect makes South Korea be a meaningful venue to apply MLP and governance originated from the liberal west. In other words, this will contribute to narrow the gap in introducing Western theories on non-Western countries academically while inferring aspects of practically and effectively applying theories from the west to other countries.

Moreover, figuring out appropriate governance framework holds significance in terms of smooth hydrogen mobility transition. There has been research on Strategic Niche Management (SNM) which could be translated into reflexive governance to understand how SNM could be coordinated with MLP[8, 9]. However, Geels did not name one certain governance framework when refuting the criticisms with credible methods to compensate the limits. This reflects the perspective that the tools and theories assessing the social world could be modified in line with the culture and political system of the target region. Against this backdrop, this research consider adaptive governance which could reflect top-down approach[10].

Among Asian countries, which are standing at the forefront to promote hydrogen vehicles and related infrastructure for hydrogen mobility transition[2], this research takes South Korea to explore the developments on hydrogen mobility transition by adopting MLP and adaptive governance to smoothly facilitate the hydrogen mobility transition for hydrogen economy. The purpose of this case study is to verify the effectiveness of adopting MLP and adaptive governance in South Korea. It can also identify whether the South Korean case could be a reference to other countries in transitioning to hydrogen mobility for hydrogen economy.

To briefly explain, South Korean government has expressed its strong willingness to promote hydrogen mobility transition as a pathway towards hydrogen economy since the announcement of hydrogen roadmap in 2019[11]. However, when comparing the plan to actual progress, much effort is needed to achieve the goal. In the case of HRSs, regulations and opposition of the residents due to hydrogen-induced accidents have been a hurdle to overcome. Under this circumstance, analysing this situation with MLP and applying adaptive governance to resolve challenges would be meaningful in terms of raising public acceptance that could be a basis for securing policy consistency.

In summary, the approaches and philosophies of analysing social world are originated from liberal democracies in the West and South Korea takes different stance in terms of the administrative structure oriented to bureaucracy or top-down approach under the influence

of Confucianism like other Asian countries such as China and Japan[12]. This raises the concern over whether it is effective and sustainable to directly apply theories from Western countries[13]. That is, this situation calls for the necessity of investigating this perspective to consider the culture and system of non-Western countries.

Given the urgency of promoting hydrogen vehicles for decarbonisation, countries involved in this effort are required to accelerate the process of hydrogen mobility transition regardless of Western countries or non-Western countries. The process of exploring this aspect, analysing the social phenomenon on hydrogen mobility transition and figuring out ways to address issues of public awareness and policy consistency could be a reference to other countries for smooth transition to hydrogen mobility.

Methodology

To achieve the objectives elaborated on Introduction, qualitative research is conducted in line with the philosophy of pragmatism that combines inductive reasoning and deductive reasoning under the constructivism[14, 15]. In detail, literature review and data analysis from various sources including document and interview have been carried out to collect empirical data under the theoretical basis. This process is linked to triangulation which could raise the credibility, trustworthy, rigor and quality of this research[16].

When it comes to data collection process, the researcher has conducted literature review to identify theoretical and epistemological aspects of hydrogen transition as a first step. Document analysis on publishments of International Organisations such as IEA, Hydrogen Council, IPHE and IRNEA is followed to understand the global trend on hydrogen transition. The analysis scope is narrowed down to documents, reports and news articles related to South Korea to specifically figure out the status of South Korea in terms of its efforts in activating hydrogen mobility transition for hydrogen economy. With literature review and document analysis, the researcher can achieve knowledge and background information to be an observer and interpreter of the social phenomenon on hydrogen mobility transition.

The interviews that the researcher conducted are categorized into three, the interview with the global experts, the interview with the public officials in South Korea and the interview with the public in South Korea[17]. For the portfolio of the global experts, the researcher tried to diversify the experts from various countries including the US, Canada, Germany, Netherland and the UK who are researching in various fields such as transport, transition theory, policy analysis, governance and urban planning. Among them, three interviewees have an in-depth knowledge in governance efforts, hydrogen mobility related policies and industrial aspects of hydrogen mobility in South Korea.

The interview with the public officials is to listen the developing stories of hydrogen mobility transition in South Korea, challenges during the process and solutions to secure policy consistency. Meanwhile, the interview with the public is to understand whether the public is aware of the endeavour of the government along with their thoughts and opinions on hydrogen vehicles and HRSs. In total, the researcher has interviewed 30 interviewees.

The collected data in line with this process is analysed with thematic analysis[18]. The repeated analysing process will be a set of inductive and deductive reasoning by coding and

decoding the contents of the data. During this process, MLP with niche creation, regime destabilisation and landscape change can be analysed. In addition, the potential of adaptive governance which could consider target country's culture and system with learning by doing process is investigated. This is to figure out ways to raise the public awareness and acceptance to keep policy consistency. This will eventually expel the uncertainty on hydrogen mobility related policies and attract industrial investment while activating hydrogen mobility in an efficient and sustainable manner. Moreover, the research result could be led to the coordination between top-down and bottom-up approach to facilitate the international cooperation for hydrogen mobility transition by referring to the case study.

Results

This research applies a tool of socio technical transition and a governance framework to hydrogen mobility transition. It is to explore the influence of new technology introduction for decarbonisation in mobility sector and figure out how to secure policy consistency amid contradicting opinions of the public on the hydrogen energy. With literature review and data analysis including documents, reports, grey literature, news articles and interviews, this research has concluded that the combination of MLP and adaptive governance could be the most appropriate method to understand the situation and investigate ways to move forward in an efficient and sustainable manner. In addition to this general conclusion, the case study of South Korea could imply lessons to take that certain modifications are required when taking different approach under the same theory. In this regard, the South Korean case has a potential to be a reference to other countries with valid analysis on hydrogen mobility transition in South Korea. It also indicates the ways to raise public awareness for policy consistency to solidly enable hydrogen mobility transition.

Discussion

This research aims at answering the two research questions, which are 1) Is it reliable to directly apply theories from the liberal West to top-down oriented countries for hydrogen mobility transition? And 2) How to validate the reference-ability? This research is not only focusing on applying theories and tools from liberal democracies to Asian countries with Confucian values and top-down approach but also trying to understand the whole process so that it could be applied to other non-Western or non-liberal countries.

To this end, the features of MLP and adaptive governance have been reviewed to understand how this could be coordinated with top-down oriented country for hydrogen mobility transition. Other points to discuss are how tensions and challenges could be identified with MLP and how adaptive governance could be combined to overcome the challenges to secure policy consistency by raising the public awareness.

The discussed point can be a basis for analysing the sustainability and effectiveness of applying MLP and adaptive governance, which leads the discussion point to move on the possibility of being a reference for other countries striving to facilitate hydrogen mobility transition. The other perspective to discuss is the importance of government role in the initial stage indicated in the document analysis. To speed up the hydrogen mobility transition for carbon neutrality, governmental intervention would be meaningful. In other words, South Korean case could convey interesting messages to liberal democracies in terms of governmental leadership.

The world is working together by establishing Hydrogen council and IPHE. Moreover, international organisations such as IEA and IRNEA highlight the importance of international cooperation. Accordingly, it would be worthy to analyse whether this research could lay a foundation for effective international cooperation to facilitate hydrogen economy with hydrogen mobility transition.

Conclusions

When BMW announced the launch of a pilot project on developing hydrogen passenger car, the company explains about the potential of scaling up hydrogen vehicles with clean hydrogen. It also points out the needs to develop HFCVs in consideration of certain regions that are hard to install enough EV charger[1]. This infers the necessity of diversifying the types of green mobility in addition to EVs. Under this circumstance, it would be reasonable to comment that there has been a significant development in hydrogen mobility with the advancement of the related technologies and governmental leadership.

Even though the countries' scheme and approach are varied, the goal could be the same which will be activating and materialising hydrogen economy. The countries set their strategies and schemes in line with their situation. The South Korean case has demonstrated various perspectives. The government is trying to lead the efforts of hydrogen transition by focusing on hydrogen mobility first. With the hydrogen cities[2], the government endeavours the convergence of hydrogen technologies by expanding the application scope to power generation and district heating. So far, all processes are led by the government. For a genuine progress toward hydrogen economy, it is time to consider how to effectively hand over the leadership to private sector while raising public acceptance.

Qualitative research analyses the social world which has kept changing. In the case of hydrogen mobility transition, it has been evaluated that there is a need of attracting the attentions of the public on the hydrogen vehicles and related infrastructure. To this end, securing the policy consistency in hydrogen mobility will let public trust government. This will eventually raise public acceptance and expel uncertainties for industries to invest in hydrogen applications. When it comes to the case study in South Korea, it is true that the new administration has changed views and strategies. However, it can be adaptively reflected in the hydrogen mobility transition so South Korea can continue the journey for hydrogen economy.

So far, this research has identified the viability of combining MLP and adaptive governance to resolve challenges and find solution. During this process, ways of improving policy consistency and public acceptance are reviewed. Moreover, the feasibility of applying this combination is explored and it could be concluded that theories originated from bottom-up oriented countries can be applied to a top-down oriented country under the condition that the culture and uniqueness of the target countries is considered. The whole process leads to the credibility of referring this case study to other countries.

[1] https://www.press.bmwgroup.com/global/article/detail/T0408839EN/bmw-group-brings-hydrogen-cars-to-the-road:-bmw-ix5-hydrogen-pilot-fleet-launches?language=en, https://www.telegraph.co.uk/business/2023/03/15/bmw-make-hydrogen-fuelled-cars-admits-evs-wont-work-everyone/

[2] https://energynews.biz/creation-of-6-hydrogen-cities/#:~:text=From%20the%20next%20year%2C%20Pyeongtaek,billion%20won%20for%20local%20expenses).

Each country adopts strategies and schemes by considering its industrial situation so the starting point for hydrogen journey could be different. While each country strives to activate the hydrogen economy, hydrogen applications will be interlocked each other for the hydrogen economy. Against this backdrop, this research can imply certain aspect to benchmark while implying further study such as the meaning of international cooperation for hydrogen economy.

References

[1] "SCENARIO-BASED ELECTRIC BUS OPERATION: A CASE STUDY OF PUTRAJAYA, MALAYSIA", A SUSTAINABLE PATHWAY FOR THE EUROPEAN ENERGY TRANSITION HYDROGEN ROADMAP EUROPE", doi: 10.1016/j.ijtst.2017.09.002.

[2] "DEVELOPMENT OF FUEL CELL VEHICLES IN ROAD TRANSPORT AND THE EXPANSION OF THE HYDROGEN REFUELLING STATION NETWORK", doi: 10.3390/en15144975

[3] "ADVANTAGES AND TECHNOLOGICAL PROGRESS OF HYDROGEN FUEL CELL VEHICLES", doi: 10.3390/wevj14060162

[4] "SOUTH KOREAN EFFORTS TO TRANSITION TO A HYDROGEN ECONOMY", doi: 10.1007/s10098-020-01936-6

[5] "REGIME RESISTANCE AGAINST LOW-CARBON TRANSITIONS: INTRODUCING POLITICS AND POWER INTO THE MULTI-LEVEL PERSPECTIVES", doi: 10.1177/0263276414531627

[6] "THE SOCIO-TECHNICAL DYNAMICS OF LOW-CARBON TRANSITIONS", doi: 10.1016/j.joule.2017.09.018

[7] "SOCIO-TECHNICAL TRANSITIONS TO SUSTAINABILITY: A REVIEW OF CRITICISMS AND ELABORATIONS OF THE MULTI-LEVEL PERSPECTIVE", doi: 10.1016/j.cosust.2019.06.009

[8] "STRATEGIC NICHE MANAGEMENT AND SISTAINABLE INNOVATION JOURNEYS: THEORY, FINDINGS, RESEARCH AGENDA, AND POLICY", doi: 10.1080/09537320802292651

[9] "REGIME SHIFTS TO SUSTAINABILITY THROUGH PROCESSES OF NICHE FORMATION: THE APPROACH OF STRATEGIC NICHE MANAGEMENT", doi: 10.1080/09537329808524310

[10] "ADAPTIVE AND REFLEXIVE GOVERNANCE: THE LIMITS OF ORGANIZED DECENTRALIZATION", doi: 10.1177/0959680105057215

[11] "KOREA HYDROGEN ECONOMY ROADMAP 2040"

[12] "CONFUCIANISM AND DEMOCRATIZATION IN EAST ASIA"

[13] "ENABLING SUSTAINABILITY TRANSITIONS IN ASIA: THE IMPORTANCE OF VERTICAL AND HORIZONTAL LINKAGES", doi: 10.1016/j.techfore.2008.03.022

[14] "READING AND UNDERSTANDING QUALITATIVE RESEARCH", doi: 10.1007/s10465-016-9219-z

[15] "PRAGMATISM AS A RESEARCH PARADIGM AND ITS IMPLICATIONS FOR SOCIAL WORK RESEARCH", doi: 10.3390/socsci8090255

[16] "TRIANGULATION IN SOCIAL RESEARCH: QUALITATIVE AND QUANTITATIVE METHODS CAN REALLY BE MIXED"

[17] "UNSATISFACTORY SATURATION: A CRITICAL EXPLORATION OF THE NOTION OF SATURATED SAMPLE SIZES IN QUALITATIVE RESEARCH", doi: 10.1177/1468794112446106

[18] "THEMATIC ANALYSIS: STRIVING TO MEET THE TRUSTWORTHINESS CRITERIA", doi: 10.1177/1609406917733847

[19] "GLOBAL HYDROGEN REVIEW 2022", https://www.iea.org/reports/global-hydrogen-review-2022

Hydrogen Storage Capacity of Freeze Cast Microporous Monolithic Composites

Catherine Butler*[1], Timothy J Mays[2], Christopher R Bowen[1]

[1]Department of Mechanical Engineering, University of Bath, Claverton Down, Bath BA2 7AY, UK,
[2] Department of Chemical Engineering, University of Bath, Claverton Down, Bath BA2 7AY, UK

Introduction

Low carbon hydrogen is a highly effective clean energy carrier due to its high gravimetric energy density (Higher Heating Value (HHV) of 142 MJ kg^{-1}) and, when it is oxidised to yield power and heat, the only material product is water. However, hydrogen has a low volumetric energy density (< 14000 MJ m^{-3} under any condition) which requires heavy and complex storage tanks when stored as a high-pressure gas (70 MPa, 298 K) or low temperature liquid (< 1.6 MPa, 20 K). A potential solution to this challenge is to use highly porous solid materials as adsorbent tank inserts, or liners, which allow storage capacity to be increased, or the pressure decreased for the same mass of fuel [1] (Figure 1).

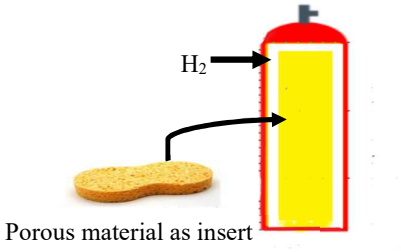

Figure 1: Schematic of tank and adsorbent consolidated composite insert

This increase in performance is due to hydrogen being stored more densely on the surface of the material by physisorption, which is reversible and does not require a significant energy input to desorb the hydrogen. Adsorption or physisorption occurs due to weak attractive forces, known as Van der Waals, between molecules of a fluid, in this case hydrogen gas and a solid adsorbent. The gas molecules stick to the surface of the adsorbent and are more densely stored than in the bulk gas. The amount of gas adsorbed increases approximately linearly with surface area [15]. High surface area materials such as metal organic frameworks (MOFs), activated carbons, porous aromatic frameworks (PAFs), and zeolites have been previously investigated for hydrogen storage [1-5]. In addition to the high surface area, the pore size has been shown to affect the hydrogen storage capacity of these materials, with pores of dimensions 0.6 - 0.7 nm being optimal [6]. As a result, microporous materials (pore widths < 2 nm) are the most appropriate for storing hydrogen and demonstrate uptakes that are sufficient to meet the system guidelines set by US Department of Energy (DoE) for light duty fuel cell vehicles (5.5 wt.% [7]). However, this level of storage includes the mass of the storage system as a whole, and not only the material itself.

* Corresponding author: enmcjb@bath.ac.uk

Work published to date has primarily focused on the hydrogen uptake of a range of highly microporous materials [1-5]; however, these are particulate and their incorporation into storage tanks can lead to fouling, as well as complex handling and safety issues. To date, little has been published on forming such storage materials into usable geometries with sufficient hydrogen storage and mechanical, and thermal properties to withstand tank conditions. A potential material to form into a usable geometry is the Polymer of Intrinsic Microporosity 1 (PIM-1). This has good processability as well as reasonable hydrogen storage capacity due to its constrained spirocentre that prevents polymer chains packing efficiently, and creates pores of up to 2 nm in width [8]. The surface area of the materials is, however, limited to approximately 700 m^2 g^{-1} [8] compared to materials such as activated carbons, which can store up to four times as much hydrogen [9]. However, divided carbon materials can present handling and processing issues. The potential to combine the processability of PIM-1 with the high storage capacity of activated carbon provides a route to exploit the advantages of each material. Generally, polymer forming is dependent upon whether the polymer is a thermoset or thermoplastic, however, PIM-1 does not readily fit into one of these categories, meaning traditional methods are challenging. The solution processability of PIM-1 has been demonstrated widely for planar films but forming 3D structures and monoliths has been studied to a limited extent. One study attempted 3D printing of PIM-1, where polymer fibres formed from a tetrahydrofuran (THF) solution were overlayed in a crisscross pattern [16]. This process is currently at a low technology readiness level and is not ready to be used industrially. An alternative process identified from the literature; is freeze casting. Neville et al. [11] recently developed a method for freeze casting PIM-1 with an activated carbon filler. Freeze casting is a well-established method that typically uses a suspension of solid particles, with water as the solvent. Porosity is developed in freeze cast materials as a result of the expulsion of solid particles from the solvent freeze front. The solvent is then removed by sublimation, using freeze drying, which leaves the structure of the frozen material intact [10]. However, for PIM-1 to be freeze cast, it must be dissolved in a solvent, such as chloroform, to form a solution which is subsequently frozen and is different to the established method of freezing a suspension, where particles are expelled from the freezing front.

We follow the method of Neville et al. [11] to produce monolithic structures of PIM-1, and composite monoliths of PIM-1 doped with activated carbons of MSC-30, and MSC-30SS. Both MSC-30 and MSC-30SS are carbon-based materials, where MSC-30SS has a small particle size (5 μm) compared to the larger sized MSC-30 (60 – 150 μm).

Methodology

Three monoliths were manufactured following freeze casting methods by Neville et al. [11], where powdered PIM-1 material was dissolved in chloroform to form a solution which was stirred at 300 rpm and 20°C for one hour. A pre-prepared elastic resin cylindrical mould, was frozen using liquid nitrogen. The chloroform solution was poured into the frozen mould (77 K) and left for 20 minutes (Figure 2). It was then placed into a vacuum flask and transferred to a freeze drier and left for 24 hours. The chloroform was removed by sublimation, leaving the solid structure behind. The structure was removed from the mould. The monoliths comprised of:

(i) 2 g PIM-1, 10 ml chloroform; this is termed the PIM-1 monolith
(i) 1.6 g PIM-1, 0.4 g (20 wt.%) MSC-30, 10 ml chloroform; this is termed the PIM-1 MSC-30 monolith
(i) 1.6 g PIM-1, 0.4 g (20 wt.%) MSC-30SS, 10 ml chloroform; this is termed the PIM-1 MSC-30SS monolith

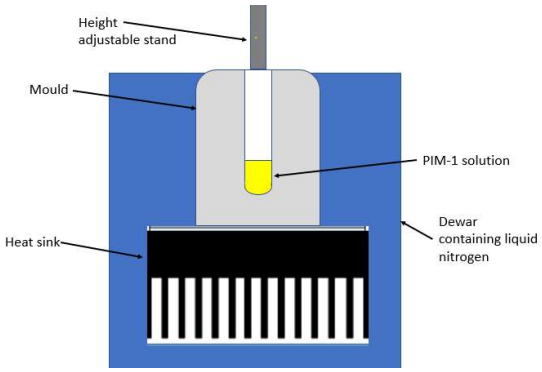

Figure 2: Schematic of non-directional freeze casting

X-ray Computed Tomography (CT) was used as a non-destructive evaluation technique to examine the internal structure of the monoliths (Figure 3).

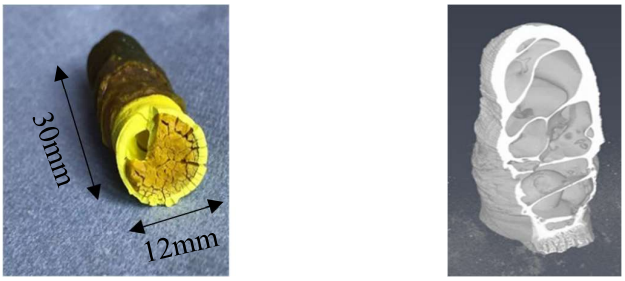

a) b)

Figure 3: Freeze cast monolith a) as manufactured b) XRCT scan

Nitrogen adsorption analysis at 77 K was carried out for relative pressures $p / p^0 = 0.05$ - 0.3 [13] to determine the Brunauer-Emmett-Teller (BET) surface area of the materials. Hydrogen adsorption experiments at low pressure (up to 0.1 MPa) were carried out to compare the hydrogen storage capability at these conditions. The hydrogen data were fit to the Tóth isotherm to estimate the total storage capacity [14].

Discussion

We demonstrate that highly adsorbent 3D structures that will be termed monolithic composites, which consist of a matrix of PIM-1 filled with activated carbons (MSC-30 or MSC-30SS) can be manufactured by a freeze casting method. The composite monoliths generally follow a rule of mixtures in terms of hydrogen storage capacities of the matrix and filler, thereby providing a route for the design of these materials. The experimental isotherm data for the monoliths fitted well to the Tóth isotherm (Figure 4), which allowed their maximum storage capacity to be predicted.

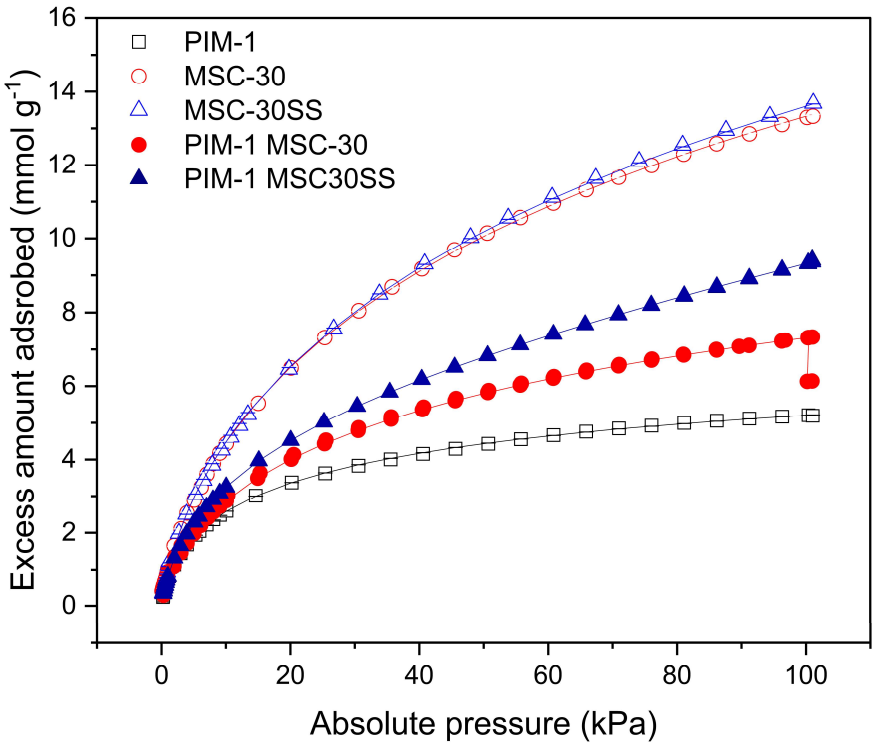

Figure 4: Hydrogen isotherms for PIM-1, MSC-30 and MSC-30SS powders and monoliths
Hollow symbols represent powders, filled symbols represent monoliths. Symbols represent experimental data, lines represent fitting to Tóth isotherm

Conclusions

It is demonstrated that under certain conditions, adsorption can store a greater mass of hydrogen than using compression alone at the same pressure and temperature. The effect of concentration and temperature on the properties of the monolith when using a directional freeze casting method is presented, which demonstrated the potential to tailor the monoliths structure for desired properties.

Acknowledgements

I would like to thank my Academic Supervisors Professor Chris Bowen and Professor Tim Mays for their generous support.

I am also grateful to GKN Aerospace for their funding, as well as the guidance provided through my Industrial Supervisors, Dr Dan Graham and Vijay Sahadevan.

I would like to thank Hugh Davies, George Neville, Dr Rajan Jagpal, Joe Paul-Taylor, and Lawrence Shere for their continued support in the experiments that are undertaken. I would also like to thank John Noble for his help and support in the modelling work.

References

[1] Tian, M. *et al*, Nanoporous polymer-based composites for enhanced hydrogen storage, Adsorption, 2019, **25**(4): p. 889--901.

[2] Rochat, S. *et al*, Hydrogen storage in polymer-based processable microporous composites, Journal of Materials Chemistry A, 2017, **5**(35): p. 18752--18761.

[3] Alcaniz-Monge, J. *et al*, Upper limit of hydrogen adsorption on activated carbons at room temperature: A thermodynamic approach to understand the hydrogen adsorption on microporous carbons, Microporous and Mesoporous Materials, 2008, **112**(1-3): p. 510--520.

[4] Hirscher, M. *et al*, Materials for hydrogen-based energy storage, past, recent progress and future outlook, Journal of Alloys and Compounds, 2020, **827**, 153548.

[5] Purewal, J. *et al*, Estimation of system-level hydrogen storage for metal-organic frameworks with high volumetric storage density, International Journal of Hydrogen Energy, 2019, **44**(29): p. 15135--15145.

[6] Ting, VP. *et al*, Direct Evidence for Solid-like Hydrogen in a Nanoporous Carbon Hydrogen Storage Material at Supercritical Temperatures, ACS Nano, 2015, **9**(8): p. 8249-8254.

[7] Target Explanation Document: Onboard Hydrogen Storage for Light-Duty Fuel Cell Vehicles. Accessed March 2023. https://www.energy.gov/sites/default/files/2017/05/f34/fcto_targets_onboard_hydro_storage_explanation.pdf

[8] Budd, PMG. *et al*, Polymers of intrinsic microporosity (PIMs): robust, solution processable, organic nanoporous materials, Chem. comm, 2004, p. 230--231.

[9] Jorda-Beneyto *et al*, Hydrogen storage on chemically activated carbons and carbon nanomaterials at high pressures, Carbon, 2007, **45**(2): p. 293--303.

[10] Deville, S, Freezing Colloids: Observations, Principles, Control, and Use, Applications in Materials Science, Life Science, Earth Science, Food Science, and Engineering, 2017, Springer.

[11] Neville, G. *et al*, Freeze casting of porous monolithic composites for hydrogen storage, Materials Advances, 2022, **3**(24**)**: p. 8805--9120

[12] Ahmed, A. *et al*, Aligned macroporous monoliths with intrinsic microporosity via a frozen-solvent-templating approach, Chemical Communications, 2015, **51**(9): p. 1717--1720.

[13] Roquerol, J. *et al*, Is the BET equation applicable to microporous adsorbents. Studies in Surface Science and Catalysis, Elsevier, Amsterdam and Oxford, 2007, **160**: p. 49-56.

[14] Vasanth Kumar, K. *et al*, A site energy distribution function from Toth isotherm for adsorption of gases on heterogeneous surfaces, Phys. Chem. Chem. Phys, 2011, **13**: p. 5753-5759.

[15] Broom, D.P., et al., Concepts for improving hydrogen storage in nanoporous materials. International Journal of Hydrogen Energy, 2019. 44(15): p. 7768--7779.

[16] Zhang F *et al*, Solution-Based 3D Printing of Polymers of Intrinsic Microporosity, Macromolecular Rapid Communications, 2018, 39, 1800274.

Hydrogen embrittlement in pipeline girth welds via experiments at different length scales

L. De Pue*[1], Jubica[2], L. Claeys[2], T. Depover[2], S. Hertelé[1], K. Verbeken[2], W. De Waele[1]

[1]Ghent University, Department of ElectroMechanical, Systems and Metal Engineering, Soete Laboratory, Belgium

[2]Ghent University, Department of Materials, Textiles and Chemical Engineering, Sustainable Materials Science, Belgium

Introduction

As part of the European Green Deal, Europe is focusing on a clean energy transition to reduce greenhouse gas emissions [1]. To accomplish the objectives, a hydrogen infrastructure will play a key role. To reach the ambition goal of creating a 31 500km hydrogen grid in Europe by 2030, repurposing existing natural gas pipelines will be essential for the hydrogen transport and storage in this framework [2]. However, pipeline steels are susceptible to hydrogen embrittlement, i.e. hydrogen reduces their ductility and fracture toughness [3–6]. Within the ETF-HyFit-project, the fitness-for-purpose of those existing pipelines is being investigated.

A pipeline grid is built out of sections of pipes which are welded together. The Heat-Affected Zone (HAZ) of these girth welds experienced high temperatures and temperature gradients that transformed their microstructure, changed the related mechanical properties and introduced residual stresses. Due to those changes, the HAZ may be more susceptible for cracking. Since the HAZ is a small region with highly variable microstructure, it is difficult to properly target a specific microstructure during mechanical testing. Therefore, a specific microstructure representative for the HAZ is created using thermal simulations allowing to evaluate the mechanical performance of the microstructure of interest using macroscopic mechanical testing.

Through experimental work, the susceptibility of the materials to hydrogen embrittlement is investigated. The aim of this work is to screen and provide calibration and validation input to a numerical model. Given that fracture toughness is prone to size-effects, the lab-scale tests will be upscaled towards component-scale tests.

Methodology

Of a longitudinal welded pipe, the HAZ of a L485MB pipeline steel is examined with lab-scale, notched tensile specimens oriented parallel to the pipe axis and crossing the girth weld. Because of the large variations in the HAZ, the specimens were heterogeneous with different microstructures and contained base material as well as weld material, adjacent to the HAZ. In the first approach, illustrated in Fig. 1, the goal was to position the centre of the notch in the HAZ. As such, the smallest section triggers this zone with the highest triaxial stresses. In the second approach, illustrated in Fig. 2, a microstructure of the HAZ was thermally simulated, and is referred to as Simulated Heat-Affected Zone (SHAZ). The HAZ consists of different microstructures that vary along the distance from the weld. In this research, the microstructure closest to the weld fusion line, which is defined by its coarse grain microstructure, is chosen to simulate. This is achieved by giving the base material a heat treatment, similar to the temperature cycle it experiences during welding, making use of a thermal-mechanical weld simulation. The thermal cycle reached a peak temperature of 1350°C with a heating rate of 500°C/s and cooled down from 800°C to 500°C in 20.5s. The hardness of the achieved microstructure had a mean value of 254HV1 with a standard deviation of 9HV1 over an area of 1x1cm^2.

The tensile tests were performed using a notched round bar (NRB) specimens with a notch radius of 6mm and a minimum diameter of 6mm in the notch. For each material and for both conditions, with and without hydrogen charging, three tests were executed. The specimens were electrochemically pre-charged

*Corresponding author: laura.depue@ugent.be

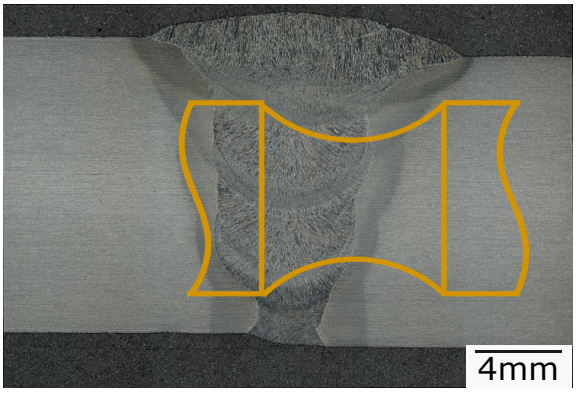

Figure 1: Positioning of the notch in HAZ

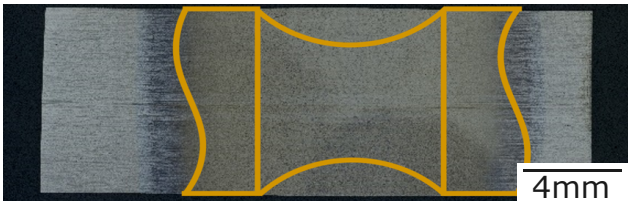

Figure 2: Simulated microstructure of HAZ, SHAZ

with hydrogen. The charging took 18 hours in 0.5M H_2SO_4 containing 1 g/l thiourea at 0.8 mA/cm². After charging, the specimens were stored in liquid nitrogen to avoid hydrogen effusion at that stage. The total time in air before the start of the tensile test was limited to 7 minutes to keep hydrogen effusion within an acceptable limit. The tensile tests were performed ex-situ, i.e. the specimens were charged in advance and tested in air. The strain rate was based on the recommendations in ISO 6892-1:2016 and resulted in crosshead speeds of 0.135 mm/min. Using image analysis, the area reduction was measured to calculate the hydrogen embrittlement index.

Results and Discussion

The force-elongation curves are illustrated in Fig. 3 and Fig. 4. For both materials, a loss in ductility is captured when hydrogen was introduced into the material while the maximum force appeared unaffected.

The HAZ-specimens of the first approach delivered consistent results when the tests were executed without being hydrogen-charged. When hydrogen charged, the results showed more scatter. Analysis of the fracture surfaces revealed that imperfections which are inherent to weldments play a role in this variation. Cross-sectional characterization demonstrated that multiple microstructure contributed to the fracture process, as well the base material, HAZ as the weld material. As such, it was difficult to draw conclusions of the hydrogen susceptibility of purely the HAZ-microstructure. But it revealed the complexity of different aspects that play a role around the weld as it is in reality.

The SHAZ delivered in both conditions consistent results as it was aimed. This is related to the homogeneous microstructure and the lack of weldment imperfections. On the fracture surfaces, inclusions were the origin of a circular zone with quasi-cleavage surrounded by a ductile fracture surface. Those inclusions are inherent to the base material and uniformly spread over all the specimens which can explain why they didn't cause scattered results.

Conclusions and outlook

In this work the hydrogen embrittlement sensitivity of the HAZ of L485MB pipeline steel was examined with two approaches. In the first approach, the specimens were taken directly from the welded material, HAZ. In the second, the microstructure was obtained by a heat treatment on the base material, SHAZ. On the one hand, making use of the SHAZ led to more consistent results which are more suitable for the calibration of a numerical model. But on the other hand, it left out other aspects that also can

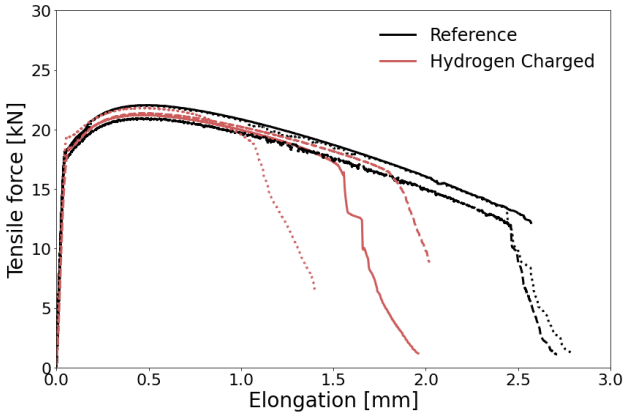

Figure 3: Force-Elongation curves of the HAZ

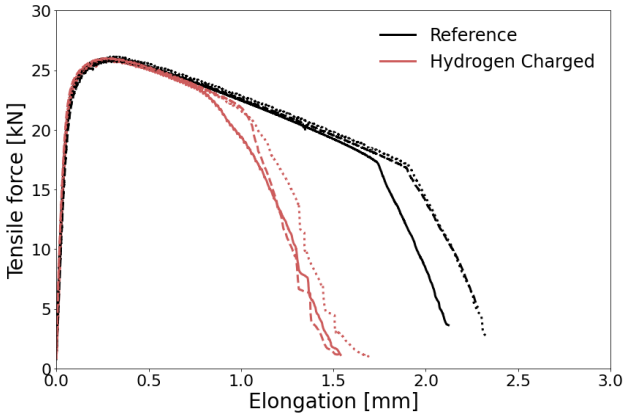

Figure 4: Force-Elongation curves of the SHAZ

have an influence on the hydrogen embrittlement in that region. In a pipeline the different materials and microstructures interact with each other, internal stresses are present in the weldments, imperfections might influence the behaviour and size is different than experimented in the lab.

Besides the determination of the susceptibility of the materials to hydrogen, the results of the lab-scale tests are used to calibrate an in-house developed numerical model. Making use of up-scaled tests will make use able to validate and improve the numerical model and define the suitability of the current acceptability criteria for hydrogen environments.

Acknowledgements

This work is made possible thanks to J. Sietsma, E. Offerman and H. Hofman of TUDelft for the technical contribution and their experience with heat treatments. The preparations and the experiments are carried out in collaboration with H. Cromheeke. The financial support of the 'Energietransitiefonds' of the Belgian FOD Economie and Fluxys for the HyFit- and HySource-project is gratefully acknowledged.

References

[1] European Commission, "Energy and the green deal," 2019, url: https://commission.europa.eu/strategy-and-policy/priorities-2019-2024/european-green-deal/energy-and-green-deal.

[2] EHB Initiative, "European hydrogen backbone: Implementation roadmap - cross border projects and costs update," Tech. Rep., 2023, url: https://ehb.eu/.

[3] R. P. Gangloff and B. P. Somerday, Eds., *Gaseous Hydrogen Embrittlement of Materials in Energy Technologies. Mechanisms, Modelling and Future Development*, ser. Woodhead Publishing Series in Metals and Surface Engineering. Woodhead Publishing, 2012, vol. 2.

[4] Y. H. Lee, H. M. Lee, Y. I. Kim, and S. H. Nahm, "Mechanical degradation of api x65 pipeline steel by exposure to hydrogen gas," *Metals and Materials International*, vol. 17, pp. 389–395, 2011.

[5] N. E. Nanninga, Y. S. Levy, E. S. Drexler, R. T. Condon, A. E. Stevenson, and A. J. Slifka, "Comparison of hydrogen embrittlement in three pipeline steels in high pressure gaseous hydrogen environments," *Corrosion Science*, vol. 59, pp. 1–9, 2012.

[6] T. T. Nguyen, N. Tak, J. Park, S. H. Nahm, and U. B. Beak, "Hydrogen embrittlement susceptibility of x70 pipeline steel weld under a low partial hydrogen environment," *International Journal of Hydrogen Energy*, vol. 45, pp. 23 739–23 753, 2020.

Hydrogen infrastructure planning optimisation towards heat decarbonisation

Margarita E. Efthymiadou[1], Vassilis M. Charitopoulos[1], Lazaros G. Papageorgiou *[1]

[1]The Sargent Centre for Process Systems Engineering, Department of Chemical Engineering,University College London (UCL), Torrington Place, London WC1E 7JE, UK

Abstract

Towards Net-Zero, emission targets are set globally to reduce environmental footprint and adverse climate change impacts. The UK has introduced legislation and measures to achieve Net-Zero goal. Consequently, the exploitation of alternative end-use heat technologies, which are coupled with low-carbon pathways and energy carriers, are required. In this study, we propose a multi-period, spatially-explicit Mixed-Integer Linear Programming (MILP) optimisation framework for hydrogen infrastructure. Hydrogen system consists of production, storage and transmission investments as well as CO_2 capture and storage. The goal of the mathematical model is total cost minimisation accounting for investment and operational decisions. The proposed work includes dual temporal resolution: 5-year steps 2035- 2050 and typical days with hourly resolution. To enhance the computational performance of the studied model, we developed a hierarchical solution approach that results in near-optimal solutions while reducing the solution time by an order of magnitude. From model results, important insights can be obtained for the pathway to a low-carbon heat sector.

Introduction

Global temperature increased by almost 1 ℃ from mid-1970 mainly due to the rising concentration of greenhouse gases in the atmosphere [7]. At COP in Paris 2015, the Parties of United Nations Framework Convention on Climate Change [19] reached an agreement to deal with climate change and intensify the actions for a low-carbon future. Towards Net Zero, the UK has set the goal of greenhouse gases emissions reduction of 68% from 2019 to 2035 [6]. Heating sector accounts for one third of the total UK's emissions while residential heating is responsible for 17% of the carbon footprint mainly due to gas boilers [13]. Therefore, the pathway to energy decarbonisation requires environmentally friendly policies, which support the introduction of low-carbon energy carries and new end-use technologies. Concerning the heat sector, the UK government has made several commitments to achieve heat decarbonisation allocating over £1 billion to support them [11]. Among other alternatives, hydrogen play is a key element in the future energy mix either with its direct use in hydrogen boilers or as an efficient storage carrier for renewable electricity production. In both cases, new infrastructure networks connecting supply to demand are required and thus, a novel modelling tool for hydrogen supply chain is essential to investigate design decisions and what-if analysis scenarios for hydrogen infrastructure.

Over the last decade, supply chain optimisation of hydrogen has received an increasing interest from the PSE community. One of the first infrastructure planning optimisation models was developed by Hugo et al. [12] using a multi-objective optimisation approach. An MILP spatially-explicit framework for hydrogen transportation demand infrastructure design was proposed by Almansoori and Shah [2]. Based on this work, Guillien-Gosalbez et al. [9] introduced a bi-criterion model which examines the minimisation of system cost and environmental impact of the system simultaneously. Agnolucci et al. [1] introduced SHIPmod, a spatially-explicit multi-period MILP framework, which included Carbon Capture and Storage (CCS). SHIPmod was extended by adding hydrogen and CO_2 pipelines for regional transmission by Moreno-Benito et al. [14]. The role of oxygen as a by-product of hydrogen production for transportation fuel was examined by Ogumerem et al. [16]. Sunny et al. [18] and Samsatli and Samsatli [17] investigated the role of hydrogen in heat decarbonisation. Moreover, He et al. [10] proposed a snapshot spatial model

*Corresponding author: l.papageorgiou@ucl.ac.uk

which determines the least-cost hydrogen planning for multiple end-uses. Stochastic approaches for hydrogen supply chains have been studied by Almansoori and Shah [3] Camara et al. [5] and Ochoa-Bique et al. [4]. This work focuses on the development of an optimisation-based framework for hydrogen infrastructure planning while its applicability is demonstrated through a case study for residential hydrogen heat demand in Great Britain. Moreover, the proposed framework includes 5-year bins and representative days with hourly resolution in each year bin to define both planning and operating decisions.

Problem statement

The investigated problem in this work can be stated as follows:

Given:

- H_2 heating demand and renewables (wind,solar) availability in each region, year, cluster and hour,
- capital and operating costs for production technologies, storage sites, hydrogen and CO_2 pipelines and road transportation modes,
- minimum and maximum capacity and ramp rates as well as the lifetime of production plants and storage sites,
- minimum and maximum flowrate in pipelines,
- capacity of H_2 caverns and CO2 reservoirs,
- H_2 import price,
- carbon tax and capture rates for CO_2 emissions as well as CO_2 emission targets

Determine the optimal:

- location and capacity of production technologies, storage sites and renewable farms,
- H_2 production and storage rate in each region, year, cluster and hour,
- H_2 and CO_2 transmission investments between regions,
- H_2 and CO_2 flowrates between regions in year, cluster and hour,
- electricity generation for water electrolysis of renewables (wind, solar)
- H_2 import rates in each year, cluster and hour

So as to minimise the total system cost subject to CO_2 emissions target.

Mathematical Formulation

The framework of hydrogen infrastructure planning is formulated as a multi-period spatially-explicit Mixed Integer Linear Programming (MILP) model based on the previous work of Efthymiadou et al. [8]. The objective is the minimisation of the total system cost TC as described by the Eq. (1). The total cost consists production capital cost PCC, storage capital cost SCC, transportation capital cost TCC, production operating cost POC, storage operating cost SOC, transportation operating cost TOC, carbon emissions cost CEC, international import cost IIC and renewable cost ReC.

$$TC = PCC + SCC + PLCC + POC + SOC + PLOC + CEC + IIC + ReC \tag{1}$$

Hydrogen energy balance is described by Eq. (2). In each region g, time period t, typical day c and hour h, the total production rate Pr_{pgtch} of production technology p, the flowrate $Q_{g'gtch}$ to region g, the rejected hydrogen from storage site s and the imported hydrogen Imp_{gtch} are equal to the flowrate $Q_{gg'tch}$ from region g, the hydrogen which is injected to storage site s Q^I_{gstch} and the total hydrogen demand TD_{gtch}.

$$\sum_{p\in P} Pr_{pgtch} + \sum_{l\in\{Pipe\}} \sum_{g'\in N^{pipe}_{g'g}} Q_{g'gtch} + \sum_{s\in GS_{gs}} Q^{R}_{gstch} + Imp_{gtch}$$
$$= \sum_{l\in\{Pipe\}} \sum_{g'\in N^{pipe}_{gg'}} Q_{gg'tch} + \sum_{s\in GS_{gs}} Q^{I}_{gstch} + TD_{gtch} \quad (2)$$
$$\forall g \in G, t \in T, c \in C, h \in H$$

The CO_2 mass balance is expressed by the Eq. (3). The right-hand side represents onshore CO_2 flowrate $\overline{Q}_{g'gtch}$ to region g from other regions g' and captured CO_2 which is equal to the hydrogen production rate Pr_{pgtch} multiplied by a CO_2 capture coefficient for each production technology type y^{c}_{pt}. The left-hand side represents the onshore CO_2 flowrate $\overline{Q}_{gg'tch}$ from region g to other regions g' and the offshore CO_2 flowrate $\overline{\overline{Q}}_{grtch}$ from region g to reservoir r.

$$\sum_{g'\in N_{g'g}} \overline{Q}_{g'gtch} + \sum_{p} y^{c}_{pt} Pr_{pgtch} = \sum_{g'\in N_{gg'}} \overline{Q}_{gg'tch} + \sum_{r\in GR_{gr}} \overline{\overline{Q}}_{grtch} \quad (3)$$
$$\forall g \in G, t \in T, c \in C, h \in H$$

In the context of heat decarbonisation, an CO_2 emissions target for hydrogen production is imposed for all 5-year bins t as in Eq. (4), where E_t stands for total CO_2 emissions from hydrogen production and e_t stands for CO_2 emissions target.

$$E_t \leq et_t \qquad \forall t \in T \quad (4)$$

Total emissions E_t depends on the production rate Pr_{pgtch} and it is calculated according to the following Eq. 5.

$$E_t = \sum_{p\in P} \sum_{g\in G} \sum_{c\in C} \sum_{h\in H} WF_c \cdot y^{e}_{pt} \cdot Pr_{pgtch} \qquad \forall t \in T \quad (5)$$

where y^{e}_{pt} is the emission coefficient for each production technology p.

The proposed mathematical framework includes detailed equations for all the aforementioned costs. Furthermore, it comprises of hydrogen production and storage as well as hydrogen and CO_2 pipeline capacity and availability equations. Production ramp up/down, storage inventory, electricity generation, import and CO_2 reservoir inventory constraints are included.

The resulting model is computationally intensive as its computational time is above 48 hours for optimality gap less than 5%. A tailored hierarchical solution approach is implemented to enhance solution performance, which comprises of two steps. In the first step, production and storage investments are determined while in the second step, pipeline and operating decisions are defined.

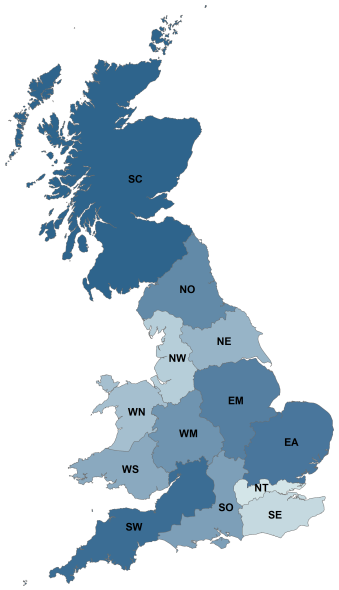

Figure 1: Regional representation of Great Britain

Case Study

The applicability of the spatial explicit multi-period model is demonstrated on a case study for hydrogen infrastructure planning towards heat decarbonisation in Great Britain (GB). As shown in Fig. 1, GB is divided into 13 regions according to local gas distribution zones (LDZ) of the incumbent natural gas network. In the context of model

size reduction, the total heat demand and renewable technologies availability hourly data are clustered using k-means clustering techniques.

Regarding the temporal resolution of the case study, we consider 5-year time steps from 2035 to 2050 to determine investment decisions and representative days with hourly resolution for operational decisions, such as hydrogen production and storage rates.

The investigated case study takes into account hydrogen production, storage and transmission technologies and a carbon capture and storage (CCS) system. Production technologies include Steam Methane Reforming (SMR), Auto-thermal Reforming (ATR), Biomass Gasification (BG) and Water Electrolysis (WE). Gas and biomass based technologies are coupled with CCS to reduce the carbon footprint. Moreover, the electricity required for water electrolysis is generated from renewable sources including wind and solar energy.

Two type of storage technologies are considered including medium and high storage pressure vessels as well as underground caverns. Concerning regional hydrogen transmission, it takes place though pipelines. In addition, CO_2 system consists of CO_2 pipelines and reservoirs located in North and East Irish sea.

The system-wide hydrogen demand for residential heat is obtained from National Grid ESO System Transformation scenario [15]. Emission targets are calculated according to Climate Change Committee residential emission targets [6].

Results & Discussion

The model is implemented in GAMS 41.5.0 and solved with Gurobi 9.5.2 using a Dell workstation with Intel® Core™ i9-10980XE CPU @ 3.00 GHz and 128 GB RAM. The multi-period model results present the optimal cost evolution of hydrogen infrastructure to meet hydrogen heat demand in the UK.

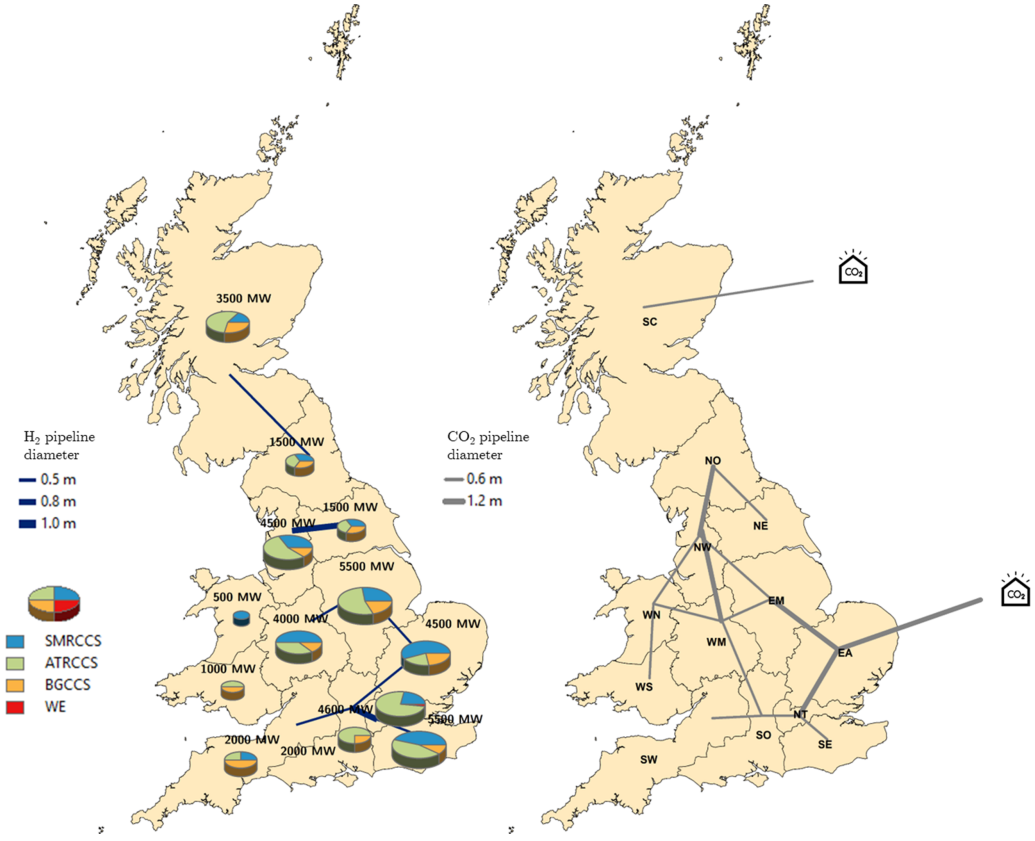

Figure 2: Production and pipeline investments in 2050

In Fig. 2, the production capacity expansion maps are illustrated. In 2050, a total of 40.6 GW hydrogen production capacity is commissioned. Reforming technologies (SMR and ATR with CCS) are mostly installed due to their lower production costs in comparison with the other technologies. Biomass

gasification with CCS production plants are installed in most regions as they play an important role in CO_2 emissions reduction because of their negative emissions carbon footprint. Moreover, 0.1 GW of water electrolysis for green hydrogen production is commissioned in North Thames while the electricity required for electrolysis is generated from wind onshore farms.

The regional transmission of hydrogen takes place through a pipeline network as depicted in Fig. 2. In 2050, the hydrogen network is expanded connecting most neighbouring regions in south GB. Moreover, CO_2 transmission takes place though pipelines which are commissioned between most GB regions. Scotland is the only region which is independent from the central CO_2 pipeline network. Two reservoirs are also established in north and south North Sea for CO_2 storage.

Hydrogen storage is a key element in hydrogen infrastructure strategy to meet peak heat demand. In 2050, a total storage capacity of 172 GW are commissioned mostly in medium pressure storage vessels.

The cost breakdown of the system is represented in 3. Production capital and operational expenditures make the most significant contributions in total system cost. Furthermore, gas and biomass, which are used as feedstock for gas reforming and biomass gasification technologies, have a great contribution in total cost. Hydrogen levelised cost is estimated 77 $/MWh$ taking into system expenditures.

The proposed model consists of 162,416 continuous and 776 discrete variables while total equations are 270,314. As mentioned in the previous Section, a hierachical approach is used to reduce CPU time and allow us to study more cases and introduce more features. More specifically, using the hierarchical approach, we achieve up to 85% CPU time reduction without significant compromise of the solution quality.

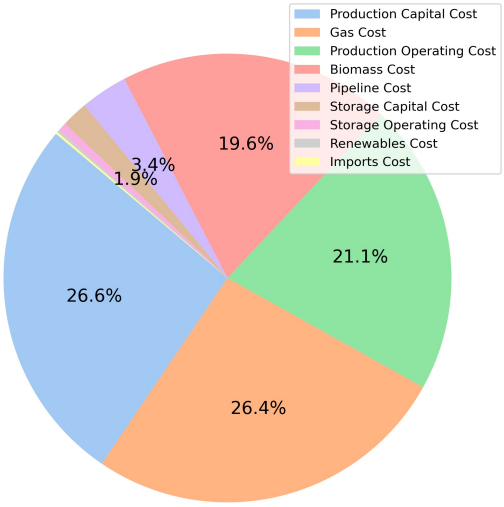

Figure 3: Cost breakdown of hydrogen system

Concluding Remarks

In this work, an optimisation-based framework has been proposed to facilitate the investigation of design and operating decisions in hydrogen infrastructure in the UK. Therefore, an insightful view for future hydrogen infrastructure investments is provided to achieve Net-Zero targets by 2050. From the results, we can conclude that reforming technologies with CCS constitute the most cost-effective low carbon alternative for hydrogen production. Moreover, hydrogen transmission is based on a pipeline network connecting most regions in GB network. Regarding CO_2 system, it plays a pivotal role in enabling low-carbon transition.

The introduction of uncertainty approaches in hydrogen supply chains is a future step for a risk averse infrastructure strategy, which explores the uncertainties of techno-economical data. Moreover, future research will include the exploration of new solution approaches and decomposition techniques. This step is important to deal with the high computational times and study case studies with more features and high spatio-temporal resolution.

Acknowledgements

Authors gratefully acknowledge the financial support from Engineering and Physical Sciences Research Council (EPSRC) under the project EP/T022930/1.

References

[1] P. Agnolucci, O. Akgul, W. McDowall, and L. G. Papageorgiou. The importance of economies of scale, transport costs and demand patterns in optimising hydrogen fuelling infrastructure: An

exploration with SHIPMod (spatial hydrogen infrastructure planning model). *International Journal of Hydrogen Energy*, 38:11189–11201, 8 2013.

[2] A. Almansoori and N. Shah. Design and operation of a future hydrogen supply chain: Multi-period model. *International Journal of Hydrogen Energy*, 34:7883–7897, 10 2009.

[3] A. Almansoori and N. Shah. Design and operation of a stochastic hydrogen supply chain network under demand uncertainty. *International Journal of Hydrogen Energy*, 37:3965–3977, 3 2012.

[4] A. O. Bique, L. K. K. Maia, I. E. Grossmann, and E. Zondervan. Design of hydrogen supply chains under demand uncertainty – a case study of passenger transport in germany. *Physical Sciences Reviews*, 6:000010151520200052, 8 2021.

[5] D. Camara, T. Pinto-Varela, and A. P. Barbósa-Povoa. Multi-objective optimization approach to design and planning hydrogen supply chain under uncertainty: A portugal study case. *Computer Aided Chemical Engineering*, 46:1309–1314, 1 2019.

[6] Climate Change Committee. Policies for the sixth carbon budget and net zero, 2020.

[7] L. Deben, K. Bell, N. Chater, M. Davies, P. Forster, P. Johnson, C. L. Quéré, and P. Betts. Progress in reducing emissions 2022 report to parliament, 2022.

[8] M. E. Efthymiadou, V. M. Charitopoulos, and L. G. Papageorgiou. Hydrogen infrastructure planning for heat decarbonisation in great britain. *Computer Aided Chemical Engineering*, 52:3025–3030, 1 2023.

[9] G. Guillén-Gosálbez, F. D. Mele, and I. E. Grossmann. A bi-criterion optimization approach for the design and planning of hydrogen supply chains for vehicle use. *AIChE Journal*, 56:650–667, 3 2010.

[10] G. He, D. S. Mallapragada, A. Bose, C. F. Heuberger, and E. Gencer. Hydrogen supply chain planning with flexible transmission and storage scheduling. *IEEE Transactions on Sustainable Energy*, 12:1730–1740, 7 2021.

[11] HM Government. Net zero strategy: Build back greener, 2021.

[12] A. Hugo, P. Rutter, S. Pistikopoulos, A. Amorelli, and G. Zoia. Hydrogen infrastructure strategic planning using multi-objective optimization. *International Journal of Hydrogen Energy*, 30:1523–1534, 12 2005.

[13] Industrial Strategy Committee. Decarbonising heat in homes seventh report of session 2021-22 report, 2022.

[14] M. Moreno-Benito, P. Agnolucci, and L. G. Papageorgiou. Towards a sustainable hydrogen economy: Optimisation-based framework for hydrogen infrastructure development. *Computers and Chemical Engineering*, 102:110–127, 2017.

[15] National Grid ESO. Future energy scenarios, 2022.

[16] G. S. Ogumerem, C. Kim, I. Kesisoglou, N. A. Diangelakis, and E. N. Pistikopoulos. A multi-objective optimization for the design and operation of a hydrogen network for transportation fuel. *Chemical Engineering Research and Design*, 131:279–292, 3 2018.

[17] S. Samsatli and N. J. Samsatli. The role of renewable hydrogen and inter-seasonal storage in decarbonising heat – comprehensive optimisation of future renewable energy value chains. *Applied Energy*, 233-234:854–893, 1 2019.

[18] N. Sunny, N. M. Dowell, and N. Shah. What is needed to deliver carbon-neutral heat using hydrogen and CCS? *Energy and Environmental Science*, 13:4204–4224, 11 2020.

[19] United Nations Framework Convention on Climate Change. Paris agreement, 2015.

Hydrogen storage in a continuous flow using benzyltoluene as liquid organic hydrogen carrier.

K. Alconada*[1], L. V. Barrio[1],

[1]School of Engineering (University of the Basque Country UPV/EHU), Plaza Ingeniero Torres Quevedo 1, 48013 Bilbao (Spain)

*kevin.alconada@ehu.eus

Introduction

In the transition towards a sustainable energy system, the use of renewable sources is proposed to be the key for energy sector decarbonization. The key hurdle for the integration of sustainable energy derived from these sources is their intermittent character. To overcome energy production/consumption mismatches, the production of green hydrogen as energy vector is positioned as a solution. Nowadays, compressed hydrogen is the most used storage technology, however, the low volumetric energy density of compressed H_2 has pushed the study of new hydrogen storage systems [1].

Liquid Organic Hydrogen Carriers (LOHCs) have been extensively studied during the recent years. These liquid organic compounds store H_2 through reversible hydrogenation/dehydrogenation reactions (Fig. 1). Since hydrogen is stored in molecules with a high boiling point, it can be stored and transported for long periods of time without boil-off losses. Additionally, due to the nature of these molecules the same distribution network of fossil fuels can be used. To date, many organic molecules based on heterocycles and homocycles compounds have been studied [2,3]. Among them, the benzyltoluene/perhydrobenzyltoluene system is a particularly interesting LOHC because of its low toxicity, high thermal stability, and reversibility [4].

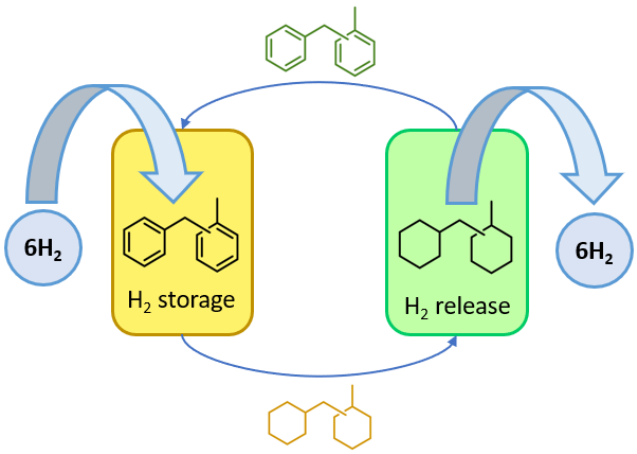

Figure 1. LOHC concept using Benzyltoluene/Perhydrobenzyltoluene system as hydrogen carrier.

* Corresponding author: kevin.alconada@ehu.eus

From the perspective of chemical equilibrium, the hydrogenation (H_2 storage) is favoured at high pressures and low temperatures, while the dehydrogenation (H_2 release) is favoured is favoured at low pressures and high temperatures. Both reactions are catalyzed by heterogeneous catalysts, and noble metal-based ones (Pd, Ru, Rh) have demonstrated to be particularly effective [5-7] . However, the high cost derived from the scarcity of noble metals impulse the development of new formulations to minimize their use.

In this work the application of nickel-based catalyst for benzyltoluene hydrogenation is studied. To evaluate the catalytic performance of Ni different monometallic Ni/Al_2O_3 catalyst were prepared and tested in a plug-flow type reactor. Additionally, the hydrogenation activity of these catalysts was compared with low-Pt doped (0.5 wt.%) nickel samples.

Methodology

Catalysts were prepared by wetness impregnation method. Afterwards, their physicochemical properties were characterized by ICP-OES, N_2-physisorption, H_2-TPR, NH_3-TPD and CO-pulse chemisorption.

The hydrogenation tests were carried out in a continuous flow reactor. The catalyst bed was established as 1 g of catalysts diluted 1:3 vol.: vol. with CSi. The reactant benzyltoluene (H0-BT) was feed (0.2 mL/min) using a peristaltic pump and the influence of pressure and temperature on the hydrogenation was evaluated at 30 bar, 40 bar and 50 bar, in a range of temperatures from 393 K to 453 K. To determine the hydrogenation activity and product composition, the liquid samples were analyzed by GC-MS.

Discussion

The activity results show that with increasing temperature and pressure conversion and selectivity to full hydrogenated perhydrobenzyltoluene (H12-BT) increased. Comparing the activity results of monometallic $25Ni/Al_2O_3$ catalyst with the bimetallic $0{,}5Pt25Ni/Al_2O_3$ sample, it can be observed that the conversion of H0-BT at low temperatures is enhanced with the incorporation of a low Pt content. At higher temperatures and pressures this difference was less significant, however, the selectivity towards H12-BT boosted with the Pt loading (Fig. 2). Analysis of the liquid phase composition revealed that the formation of H6-BT as a stable partially hydrogenated product. This result confirms the proposed reaction mechanism, wherein H0-BT is first hydrogenated to H6-BT, and then H6-BT is further hydrogenated to H12-BT (Fig. 3)

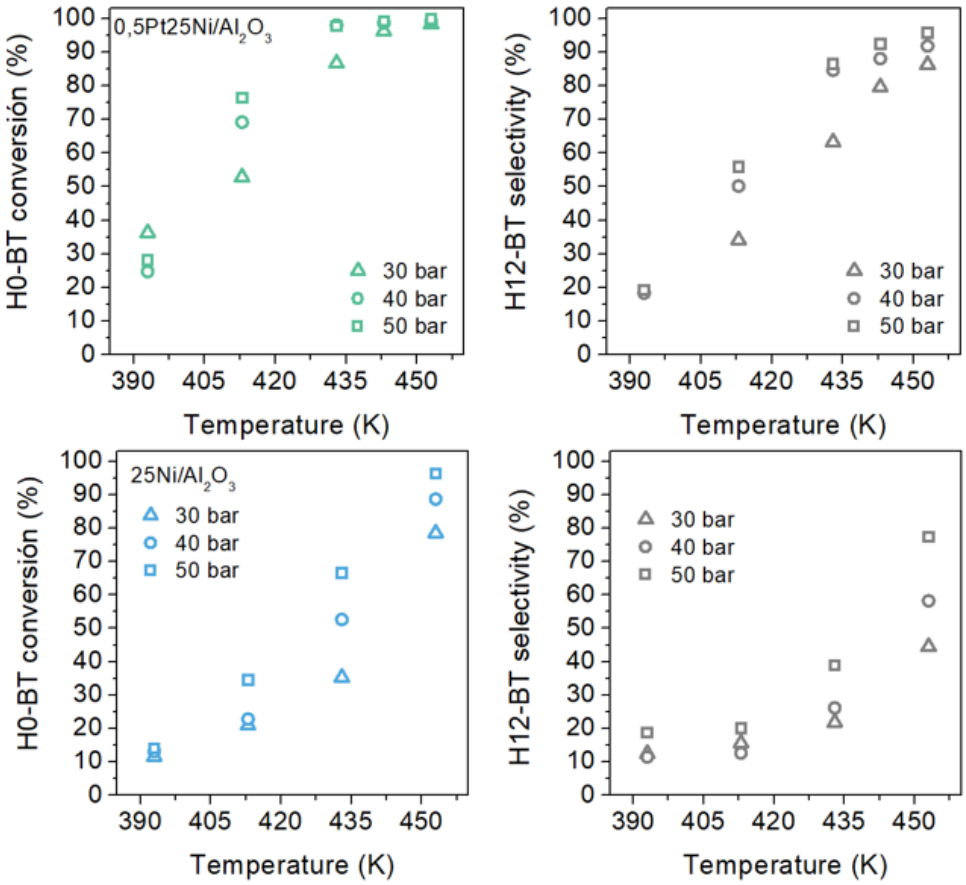

Figure 2. Benzyltoluene (H0-BT) conversion and selectivity to full hydrogenated perhydrobenzyltoluene (H12-BT). Up bimetallic 0,5Pt25Ni/Al_2O_3 and down monometallic 25Ni/Al_2O_3. WHSV = 12.9 h^{-1}; P = 30- 50 bar.

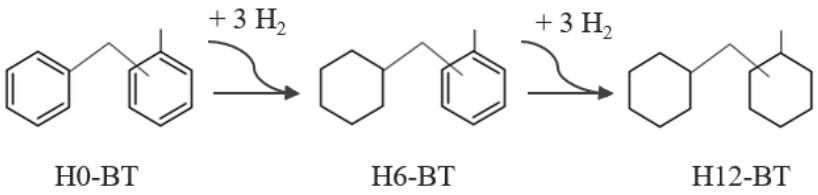

Figure 3. Reaction scheme of the benzyltoluene hydrogenation.

On the other hand, the number of by-products formed from non-desired side reactions was less than 0.6 %. Two type of by-product could be distinguised: the first group includes dicyclohexylmethane and cyclohexylmethyllbenzene, formed by hydrogenolisis and loss of a methyl group; the second group comprises perhydrophenantrene and s-octahydroanthracene, formed by C–C breaking and cyclization during hydrogenation. Based on these results, it can be concluded that Pt favours the product desorption, thereby minimizing by-product formation (Fig. 4).

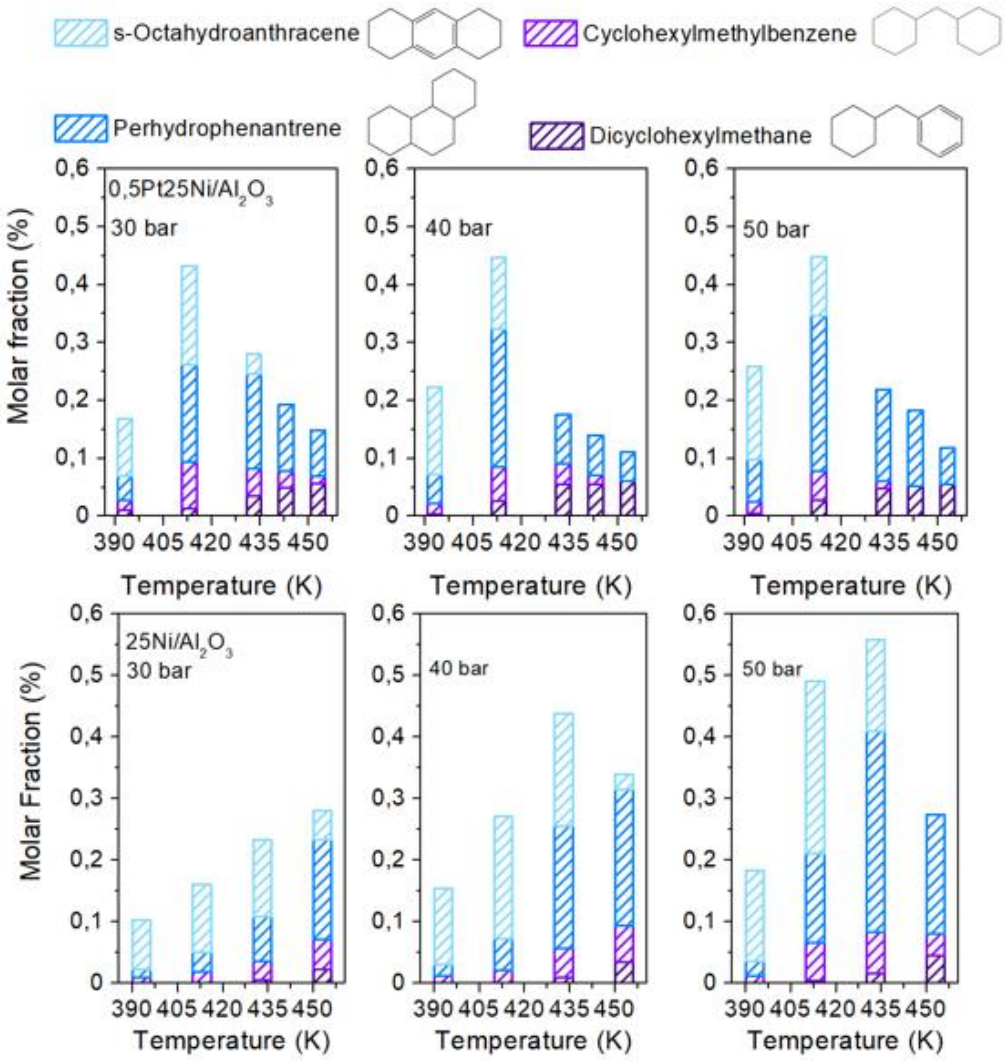

Figure 4. By-products identification for the hydrogenation reaction of monometallic $25Ni/Al_2O_3$ catalyst (up) and bimetallic $0,5Pt25Ni/Al_2O_3$ catalyst (down).

Conclusions

In this work the application of monometallic $25Ni/Al_2O_3$ and bimetallic $0,5Pt25Ni/Al_2O_3$ catalyst on benzyltoluene hydrogenation was studied. Activity results revealed that nickel-based catalyst is a suitable candidate for benzyltoluene hydrogenation. Operating at 50 bar and 453 K the H0-BT conversion was higher than 95% with a selectivity to full hydrogenated H12-BT higher than 77 %. Additionally, it was found that low Pt contents enhanced the activity at low temperatures and decreased the side-products formation.

Acknowledgements

This research was supported by the University of the Basque Country (UPV/EHU), Basque Government (Project: IT1554-22), and the Fuell Cells and Hydrogen 2 Joint Undertaking (now Clean Hydrogen Partnership) (grant agreement: 101007223). This Joint Undertaking receives support from the European Union's Horizon 2020 research and Innovation programme, Hydrogen Europe, and Hydrogen Europe research. Grant PID2020-112889RB-I00 funded by MCIN/AEI/ 10.13039/501100011033.

References

[1] C Chu, K Wu, B Luo, Q Cao, H Zhang. Hydrogen storage by liquid organic hydrogen carriers: Catalyst, renewable carrier, and technology – A review, Carbon resources conversion. 6 (2023) 334-351.

[2] PT Aakko-Saksa, C Cook, J Kiviaho, T Repo. Liquid organic hydrogen carriers for transportation and storing of renewable energy – Review and discussion, Journal of power sources. 396 (2018) 803-823.

[3] PM Modisha, CNM Ouma, R Garidzirai, P Wasserscheid, D Bessarabov, The Prospect of Hydrogen Storage Using Liquid Organic Hydrogen Carriers, Energy Fuels. 33 (2019) 2778.

[4] K Müller, K Stark, VN Emel'yanenko, MA Varfolomeev, DH Zaitsau, E Shoifet, et al. Liquid Organic Hydrogen Carriers: Thermophysical and Thermochemical Studies of Benzyl- and Dibenzyl-toluene Derivatives, Industrial & engineering chemistry research. 54 (1900) 7967-7976.

[5] H Jorschick, M Geißelbrecht, M Eßl, P Preuster, A Bösmann, P Wasserscheid. Benzyltoluene/dibenzyltoluene-based mixtures as suitable liquid organic hydrogen carrier systems for low temperature applications, International journal of hydrogen energy. 45 (2020) 14897-14906.

[6] A Leinweber, K Müller. Hydrogenation of the Liquid Organic Hydrogen Carrier Compound Monobenzyl Toluene: Reaction Pathway and Kinetic Effects, Energy technology (Weinheim, Germany). 6 (2018) 513-520.

[7] N Brückner, K Obesser, A Bösmann, D Teichmann, W Arlt, J Dungs, et al. Evaluation of Industrially Applied Heat-Transfer Fluids as Liquid Organic Hydrogen Carrier Systems, ChemSusChem. 7 (2014) 229-235.

Hydrothermal synthesis of earth-abundant electrocatalysts for PEM water electrolysis

N. Billiet*[1,2], D. De Sloovere[1,2], M. Safari [2,3], M. K. Van Bael[1,2], A. Hardy[1,2]

[1]UHasselt, Institute for Materials Research (imo-imomec) and Imec division imomec, DESINe, Agoralaan, building D, 3590 Diepenbeek, Belgium.
[2]EnergyVille, Thor Park 8320, 3600 Genk, Belgium.
[3]UHasselt, Institute for Materials Research (imo-imomec) and Imec division imomec, Electrochemical Engineering (EE), Wetenschapspark 1, 3590 Diepenbeek, Belgium.

Introduction

Hydrogen gas (H_2) has the potential to be a sustainable energy carrier, as it has a high energy density, does not release CO_2, and is a feedstock chemical in various industries. Unfortunately, H_2 is mainly produced from fossil fuels by steam methane reforming, naphtha reforming, and coal gasification.[1], [2] A promising alternative is water splitting through electrolysis, which produces H_2 and O_2 via the hydrogen evolution reaction (HER) and the oxygen evolution reaction (OER), respectively. As a major advantage, this method does not release CO_2 or other volatile by-products. Commercial water electrolysis methods are alkaline electrolysis and PEM (proton exchange membrane) electrolysis. The advantages of PEM electrolysis are higher energy efficiency, quick response, and scalability. However, the used catalysts for the HER and OER in PEM electrolysis are Pt and IrO_2, respectively, which are both expensive and low-abundance materials.[3]

Methodology

In the CLEANH2 project, we tackle these challenges. The aim of this PhD is to select, synthesize, characterize, and evaluate earth-abundant electrocatalysts for both HER and OER. The focus is on metal sulfides for HER and metal oxides for OER. Molybdenum disulfide (MoS_2) is a widely known alternative catalyst for the HER due to its high catalytic activity and high stability.[4] Other sulfides such as Fe sulfides, were also found to be active as HER catalysts.[5] This implies that a whole range of mixed metal sulfides may have a catalytic performance and stability that outperforms the more established materials. Finding an earth-abundant alternative for the OER is much more challenging. This is caused by the difficult kinetics of the OER and the strong oxidative and acidic environment on the OER side of PEM electrolyzer.[6] A material is needed that has good catalytic activity for the OER and is stable against oxidation in acidic environments. Therefore, metal oxides with more abundant metals were selected as replacements for IrO_2.

* Corresponding author: Naomi.billiet@uhasselt.be

Discussion

These materials were synthesized via hydrothermal synthesis routes. The synthesized materials were characterized using X-ray diffraction (XRD), Raman spectroscopy, and scanning electron microscopy (SEM) to investigate their morphology and crystal structure. The catalytic performances of the synthesized materials were evaluated with linear sweep voltammetry (LSV) using a three-electrode cell.

Conclusions

In our study, we have explored the potential of earth-abundant electrocatalysts for hydrogen production. Our initial choice of $Fe_2(MoO_4)_3$ for the oxygen evolution reaction did not yield the expected catalytic activity. Nevertheless, the synthesized Fe and Mo sulfides have demonstrated promising catalytic activity for the hydrogen evolution reaction. We will continue our search for alternative materials for the oxygen evolution reaction and further evaluate the stability and efficiency of these promising Fe and Mo sulfides. As we progress, we are optimistic about the potential impact of our research on the advancement of clean and sustainable energy technologies.

References

[1] J. D. Holladay, J. Hu, D. L. King, and Y. Wang, "An overview of hydrogen production technologies," *Catalysis Today*, vol. 139, no. 4. pp. 244–260, Jan. 30, 2009. doi: 10.1016/j.cattod.2008.08.039.

[2] D. A. J. Rand, "A journey on the electrochemical road to sustainability," *Journal of Solid State Electrochemistry*, vol. 15, no. 7–8. pp. 1579–1622, Jul. 2011. doi: 10.1007/s10008-011-1410-z.

[3] E. B. Agyekum, C. Nutakor, A. M. Agwa, and S. Kamel, "A Critical Review of Renewable Hydrogen Production Methods: Factors Affecting Their Scale-Up and Its Role in Future Energy Generation," *Membranes*, vol. 12, no. 2. MDPI, Feb. 01, 2022. doi: 10.3390/membranes12020173.

[4] R. Li *et al.*, "Recent advances in MoS2-based materials for electrocatalysis," *Chemical Communications*, vol. 58, no. 14, pp. 2259–2278, Feb. 2022, doi: 10.1039/d1cc04004a.

[5] D. Heift, "Iron sulfide materials: Catalysts for electrochemical hydrogen evolution," *Inorganics*, vol. 7, no. 6. MDPI Multidisciplinary Digital Publishing Institute, 2019. doi: 10.3390/INORGANICS7060075.

[6] X. K. Gu, J. C. A. Camayang, S. Samira, and E. Nikolla, "Oxygen evolution electrocatalysis using mixed metal oxides under acidic conditions: Challenges and opportunities," *Journal of Catalysis*, vol. 388. Academic Press Inc., pp. 130–140, Aug. 01, 2020. doi: 10.1016/j.jcat.2020.05.008.

Impact Analysis of Filament Wound Composite tanks for high-pressure hydrogen storage

Nazim Ali*[1], Wim Van Paepegem[1]

[1]Ghent University, Department of Materials, Textiles and Chemical Engineering

Introduction

In the contemporary era, sustainable and renewable energy is a necessity for mankind to meet the ever-growing energy demands of the commercial and domestic sectors, and to reduce the carbon footprint in the environment. Hydrogen, with its gravimetric energy density approximately three times higher than conventional fossil fuels (e.g. gasoline and diesel), can be proven as a game changer [1]. In the transportation sector, hydrogen is used as an input for fuel cells (FC) which generate electricity for the powering of vehicles and emit only hot air and water vapors. Therefore, the emission of greenhouse gases (GHGs) can be completely mitigated with the fuel-cell electric vehicles (FCEVs). Due to the lower volumetric energy density, hydrogen can be stored either in the compressed state of gaseous form at very high pressure or in the liquid state under cryogenic conditions. The storage of compressed hydrogen at 70MPa requires rigorous structures which cannot be achieved with the complete metallic structure because it leads to very heavy structures which are prone to hydrogen embrittlement. However, composite materials have the characteristic of high strength-to-weight ratio, and the required strength and reliability of the hydrogen storage systems can be achieved with lighter weight.

Pressure vessels are categorized into five types based on their design and the materials used in their construction, as indicated in Figure 1. A Type-I pressure vessel is entirely made up of steel while a Type-II pressure vessel has overwrapped composite laminate in the cylindrical region. Type-III and Type-IV pressure vessels are fully overwrapped with composite laminate and the primary distinction lies in the liner material. Type-III pressure vessels have a metallic liner whereas Type-IV pressure vessels utilize a polymer liner (typically Polyamide-6 or High-Density Polyethylene). Lastly, a Type-V pressure vessel is liner-less and entirely composed of composite laminate and metallic end fittings. In this paper, the entire focus is to estimate the mechanical behavior of type-IV pressure vessels under impact loading using finite element methods (FEM).

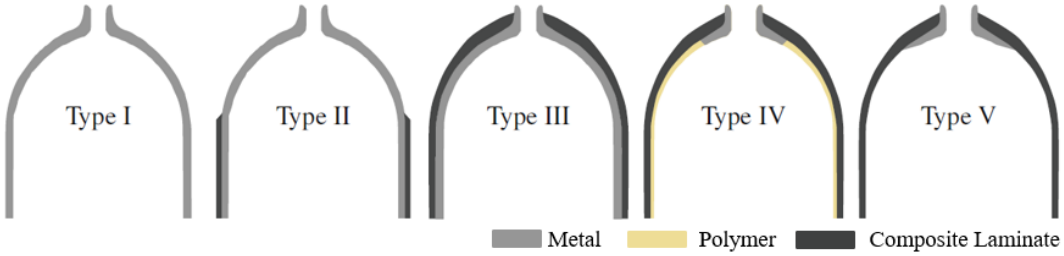

Figure 1: Types of pressure vessels (PVs) [2]

The qualification of type-IV pressure vessels requires the accurate prediction of the strength of pressure vessels under various loading conditions. Regulation No. 79[3] and Regulation No. 134[4] mandate the drop (impact) test as a requirement for the acceptance and qualification of

* Corresponding author: Nazim.Ali@UGent.be

composite overwrapped pressure vessels (COPV). As per regulations, the drop test for COPV must be performed in four different orientations to assess the mechanical response in various regions, as highlighted in Figure 2. This study focuses on finite element (FE) simulations for test IV orientation of COPV to analyze stresses in the dome and cylinder to dome transition region.

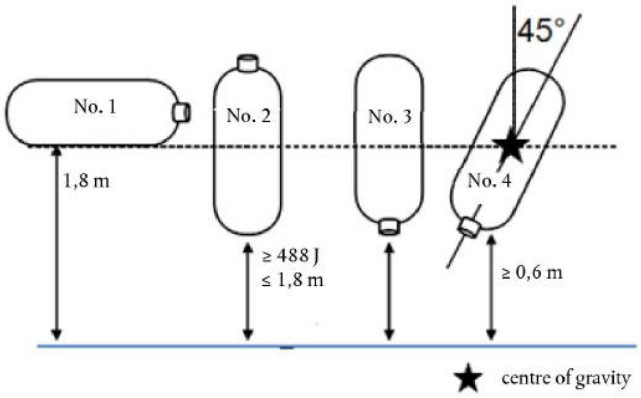

Figure 2: Orientations of COPV in drop tests [4]

Currently, most industries fully rely on experimentation to assess the mechanical response of composite overwrapped pressure vessels under dynamic loadings. The assessment of mechanical behavior using experimentation is not only expensive but also slows down the design modification process. During the preliminary design stages, utilizing finite element methods for assessing mechanical behavior of COPV can reduce the experimentation cost and leads to rational design modifications. Thus, a methodology is developed by utilizing outstanding features of multiple CAD/CAE tools for the modelling and analysis of composite overwrapped pressure vessels.

Methodology

Modelling of composite overwrapped pressure vessels (COPV) is performed in ComposicaD which is used for modelling, analysis, and manufacturing of composite pressure vessels, and exported to finite elements. The cross-sectional view of a half model of the composite overwrapped pressure vessel (COPV) is illustrated in Figure 3.

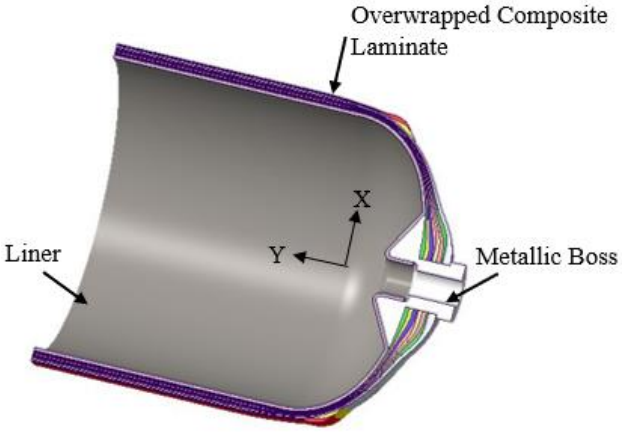

Figure 3: Geometry of type-IV pressure vessel

In order to evaluate all the stress components, a solid elements-based mesh model of the overwrapped composite laminate is generated.

Modelling the complete COPV assembly will have millions of solid elements, leading to a drastic increase in computational time and cost. Therefore, a methodology is developed to simulate the drop test of the COPV with a reduced model, and appropriate boundary and loading conditions. In the reduced model of the COPV, the mass and moments of inertia are maintained same as those of the full scale COPV, ensuring similar kinetic energy before touchdown. This method is first utilized and verified for steel vessels because it is very easy to assign the isotropic material property in ABAQUS.

Discussion

During the drop test, the stresses are higher in the touchdown region due to the impulsive forces. Therefore, the stresses in the critical region can be analyzed more efficiently by reducing the model size to the touch down region. Figure 4 shows the half vessel with steel properties, and the inertial properties of the excluded segment of the vessel are incorporated by using a reference point placed at the center of gravity of the excluded segment.

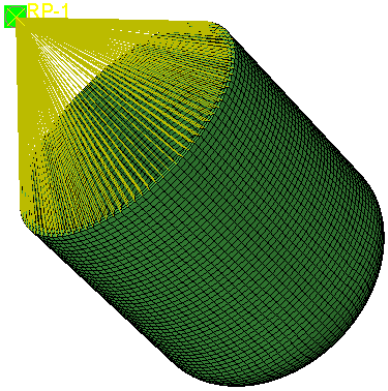

Figure 4: Point mass coupling with half vessel

This technique ensures that the reduced model has inertial properties similar to the full-scale model. Figure 5 illustrates the Von-Mises stress distribution in the full and half vessel with the incorporation of inertial properties of excluded segment. The stress distribution is very similar in full and half vessels with negligible difference in the maximum value of stress. The results for both models are comparable, but the computational time is nearly 50% less compared to that of full-scale model. It is important to mention that the stresses highlighted in Figure 5 are not indicative of realistic values, and they are just provided for the solely purpose of comparing the full-scale and reduced models. This methodology is validated with the steel vessels but the same will be applicable for composite overwrapped pressure vessels.

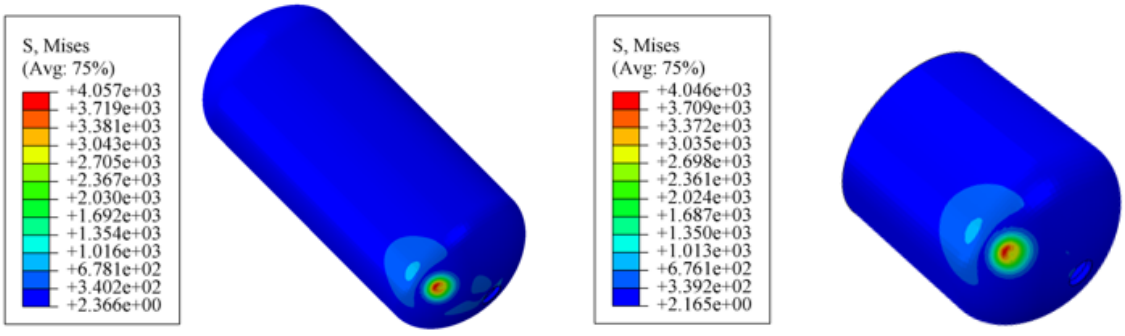

(a) **(b)**

Figure 5: Von-Mises stress distribution (a) Full Vessel (b) half vessel

Conclusion

Due to the impulsive forces in the touch-down region, the normal stress (S_3) and interlaminar shear stresses (S_{13} and S_{23}) would be higher. The higher values of interlaminar shear stresses will lead to the delamination in the overwrapped composite laminate. Therefore, the assessment of interlaminar shear stresses and delamination under the dynamic loading conditions can lead to a better design of overwrapped composite laminate which will enhance the overall structural integrity and reliability of the composite overwrapped pressure vessels.

Acknowledgment

We would like to express our sincere gratitude to Plastic Omnium for providing ComposicaD software for the modelling of composite overwrapped pressure vessels (COPV). Furthermore, the invaluable technical and financial support from Plastic Omnium is highly appreciable throughout this research work.

References

[1] HFCT, "Hydrogen Storage," *Energy.gov*, 2023. https://www.energy.gov/eere/fuelcells/hydrogen-storage (accessed Jul. 28, 2023).

[2] M. Nebe, *In Situ Characterization Methodology for the Design and Analysis of Composite Pressure Vessels*. in Werkstofftechnische Berichte | Reports of Materials Science and Engineering. Wiesbaden: Springer Fachmedien Wiesbaden, 2022. doi: 10.1007/978-3-658-35797-9.

[3] EU, *Approval of hydrogen-powered motor vehicles, and amending Directive 2007/46/EC*. [Online]. https://eurlex.europa.eu/LexUriServ/LexUriServ.do?uri=OJ:L:2009:035:0032:0046:en:PDF

[4] UN/ECE, *Regulation No 134 of the Economic Commission for Europe of the United Nations (UN/ECE) — Uniform provisions concerning the approval of motor vehicles and their components with regard to the safety-related performance of hydrogen-fuelled vehicles (HFCV) [2019/795]*, vol.129.2019.Accessed:Jul.28,2023.[Online]. Available:http://data.europa.eu/eli/reg/2019/795/oj/eng

Impact of differential diffusion on the ignition by a concentrated source

R. Carmona*, C. Jiménez, V. Kurdyumov

[1]CIEMAT, Avda. Complutense 40, 28040 Madrid, Spain.

Introduction

Igniting a combustible mixture is a fundamental step in many technological processes, even if accidental ignition is also an issue for the safety of combustion devices, as well as in fuel storage and transport. Ignition can occur, or be forced, in a variety of ways, and one of the most common is through the application of a localized source of thermal energy. Although research on the ignition of mixtures can be traced back to more than seventy years ago [1–3], only when numerical methods of analysis were applied to this problem it became possible to clarify many details of this process [4–8]. Considerable attention has been paid since to the numerical study of ignition processes using concentrated and local heat sources, as well as to the determination of the minimum energy required for a successful ignition, as for example in [9-10].

Methodology

In the present work, the ignition of a combustible mixture by the application of an instantaneous or finite in time concentrated heat source is studied. The study is carried out by numerical simulation of the temperature and fuel mass fraction conservation equations, using irreversible Arrhenius kinetics.

Discussion

Changes in the critical values of the energy source intensity for successful ignition will be first presented, as a function of the Lewis number, showing that for very small Lewis numbers, as in the case of lean hydrogen/air mixtures, the energy needed for ignition is very small. We will then study the effects of the initial curvature of the flame kernel on the minimum ignition energy

Conclusions

This study shows the effect of differential diffusion on the minimum energy required for ignition. It is relevant for safety issues in the sense of preventing accidental ignition of hydrogen at different equivalence ratio or in blends with other fuels.

* Corresponding author: email@example.com

References

[1] R. S. Silver, The ignition of gaseous mixtures by hot particles, Philos. Mag. J. Sci. 23 (156) (1937) 633–657.

[2] H.P. Stout, Mechanism of ignition by local sources of heat, Nature 166 (1950) 28–29.

[3] B. Lewis, G. von Elbe, Combustion, flames and explosions of gases, 2. Auflage, Academic Press Inc, New York and London, 1961.

[4] G. Dixon-Lewis, I. G. Shepherd, Some aspects of ignition by localized sources, and of cylindrical and spherical flames, Proc. Combust. Inst. 15 (1975) 1483–1491.

[5] G. Dixon-Lewis, Effect of core size on ignition energy by localized sources, Combust. Flame 33 (1978) 319–321.

[6] Kalkasanath, E. Oran, J. Boris, A theoretical study of the ignition of premixed gases, Combust. Flame 47 (1982) 173–190.

[7] P. S. Tromans, R. M. Furzeland, An analysis of Lewis number and flow effects on the ignition of premixed gases, Proc. Combust. Inst. 21 (1988) 1891–1897.

[8] A. Frendi, M. Sibulkin, Dependence of minimum ignition energy on ignition parameters, Combust. Sci. Technol. 73 (1990) 395–413.

[9] V. Kurdyumov, J. Blasco, A.L. Sánchez, A. Liñán, On the calculation of the minimum ignition energy, Combust. Flame 136 (2004) 394–397.

[10] V. Kurdyumov, C. Jiménez, M. Sánchez-Sanz, Flame initiation near a cold isothermal wall: Ignition by an instantaneous thermal dipole, Combust. Flame 234 (2021) 111643.

Implementation of a tool investigating the lifetime of a PEM electrolysis cell

J. Iliev[*1], D. Boychev[2], G. Borisov[3], E. Slavcheva[4]

[1,2,3,4]Institute of electrochemistry and energy systems "Academician Evgeni Budevski" – BAS, Acad. Georgi Bonchev Str., Block 10, 1113 Sofia, Bulgaria

Introduction

The challenge with harnessing renewable energy sources for hydrogen production lies in their intermittent nature. This characteristic contributes to decreased efficiency and the emergence of accelerated degradation (reduced lifespan) [1]. Among the most promising technologies for hydrogen production from renewables are PEMWEs. They offer rapid startup, swift dynamic response, and ability to operate at high current densities, making them well-suited for compatibility with renewable energy sources [2]. The proton transport through the polymer membrane swiftly adapts to power fluctuations, enabling testing of PEMWEs by altering the characteristics of electromotive signals (including amplitude, shape, and frequency) [3].

To enhance the efficiency and reliability of the PEMWE operation, there is a need to improve the entire system effectiveness. This encompasses both the electrolysis module itself and the peripheral components, such as the power supply and the management and control system. Therefore, it is crucial to explore system performance under varying power profiles, temperatures, and pressures [3], as these factors directly impact the PEMWE lifespan [4]. In a recent study [5] the duration of transient processes has been precisely measured and it has been proven that these measurements are invaluable in designing the power profile regulator, particularly for managing the cell current. Furthermore, they facilitate the calculation of essential regulator components, including integration constants, proportional coefficients, and differential constants. These values are particularly significant when immediate changes in current reference and dynamic operation modes need to be set.

The core objective of this study is to investigate how the cell operating parameters (cell voltage, temperature, and pressure) affect PEMWE performance, to determine the critical values of these parameters causing onset of degradation processes of the membrane electrode assembly (incl. the electrodes and/or the polymer membrane), and based on these experimental data to design electronic system for controlling and stabilizing the current through the electrolysis cell. By controlling the power profile of the PEMWE under stationary and dynamic profiles, analyzing volt-ampere characteristics, and identifying optimal operating modes this system will ensure the prediction and prevention of degradation processes and will increase PEMWE durability.

* Corresponding author: joiliev@iees.bas.bg

Methodology

To achieve our goal, a current generator has been designed (Figure 1) relying on a microprocessor control system from the PIC family [6] which handles logic and arithmetic functions. This system allows for adjustment of current density and operational modes, whether stationary or dynamic. Additionally, a relay protection mechanism has been integrated to cut off power supply upon detecting deviations from the set boundary operating parameters (cell voltage, temperature, and pressure). A block diagram of the system is shown in Figure 1.

The current generator consists of two primary functional modules: a processor and a digital-to-analog converter (*DAC*). Together, they constitute the *task generator* for the *electronic regulator*. The "reference assignment" (generated by the task generator) is encoded and stored within the processor. The electronic regulator conducts a comparison between the controlled variable, which is the current flowing through the *electrolytic cell*, and the control signal derived from the reference assignment.

A *measuring amplifier* is employed to amplify the signal, which is directly proportional to the load current at the required amplitude. The load current is then governed through the use of an *output amplifier*.

On the structural diagram, it can be observed that the connection between the electrolysis cell and the task generator is established through a feedback loop, implemented using analog-to-digital converters (*ADC*) for the parameters under study. This feedback loop represents the core component of the current regulator.

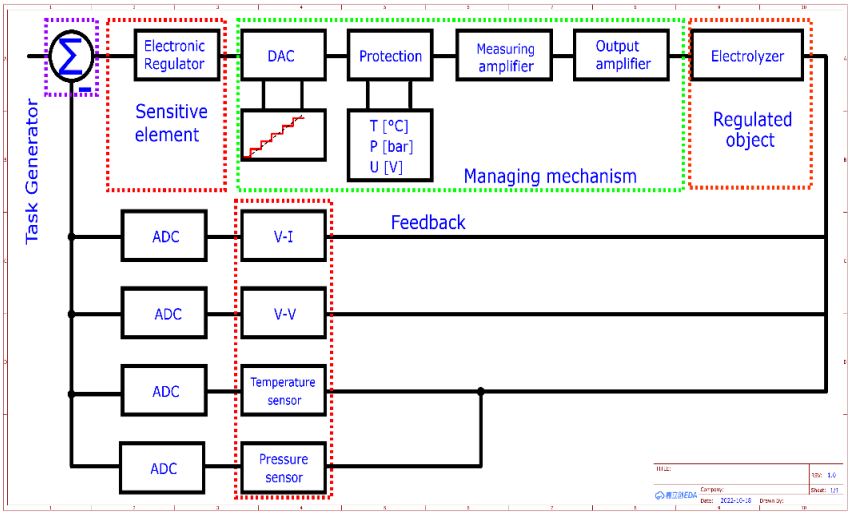

Figure 1: Block diagram of a system for automatic regulation of a control object (electrolysis cell)

An additional feature integrated into the system is the real-time transmission of data acquired from the Analog-to-Digital Converter (ADC) unit, along with the relay protection system status, individually to a Windows 10 program executing on a computer system . This functionality is achieved by harnessing the serial communication module within the PIC processor, facilitating the smooth data transmission to the computer program. The program has the ability to save the captured data in a text file, which makes the data relevant for processing in graphics software. Up to now the current generator has

undergone successful testing the serial communication module and has shown reliable operation (Figure 2).

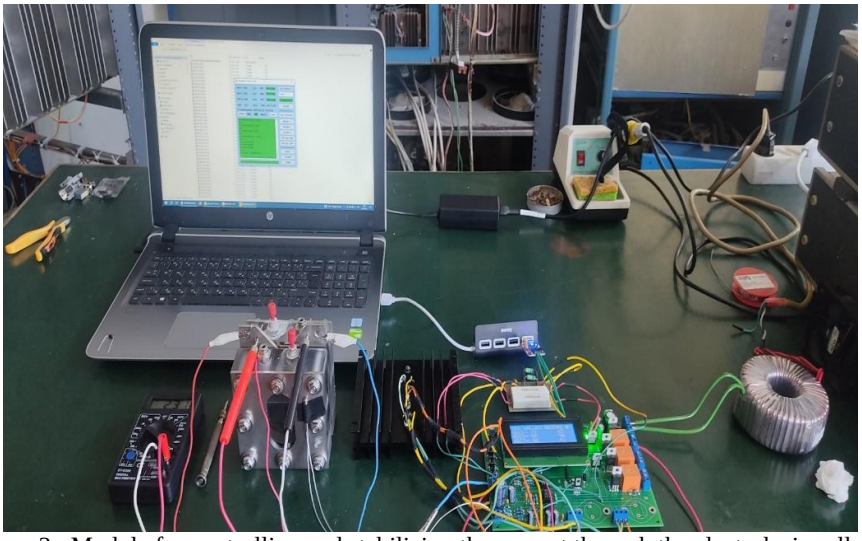

Figure 2: Module for controlling and stabilizing the current through the electrolysis cell.

Discussion

The emergence of degradation processes results in an increase in the operating voltage of an individual cell and subsequently affects the entire system. Continuous measurement of operating voltage allows for the easy detection of general deterioration in the performance of the cell, but the identification of processes responsible for this deterioration remains impossible. Consequently, linear and cyclic voltammetry will be employed to characterize the performance and degradation of PEMWE [7]. Such experiments are in progress using a self-designed single electrolysis cell (Fig.3).

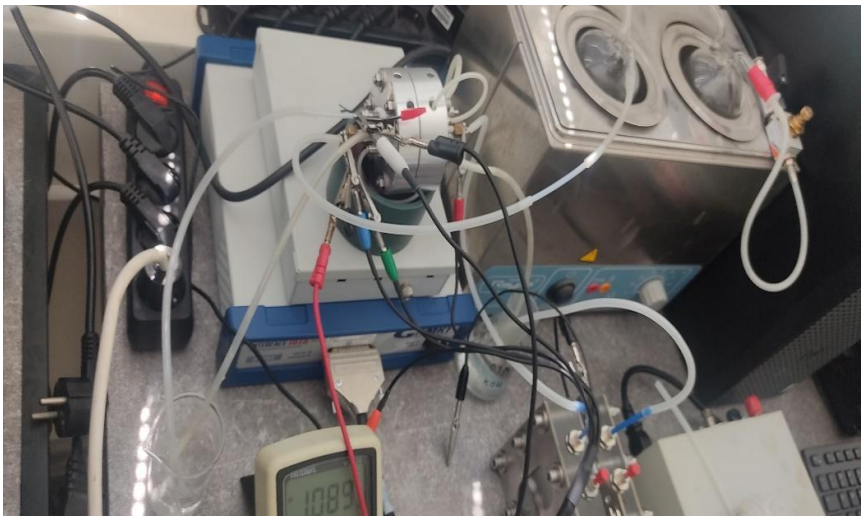

Figure 3: PEM electrolysis cell test bench.

The next steps are to carry out tests on the electrolysis cell at varying temperatures. To uphold the cell's temperature within the prescribed range, software algorithms will impose

an 80°C upper limit on the electrolysis process. Temperature values surpassing this threshold give rise to heightened water vapor pressure and the potential for corrosion instability in electrode materials. Precise temperature regulation will be achieved through the use of thermal insulation, actively monitored by thermocouples in both anode and cathode compartments.

At high pressures, ongoing experiments are focused on creating a pressure regulation system using a jump vessel configuration. This is necessary during water electrolysis because uneven gas buildup can disrupt the balance in the cathode and anode compartments, potentially causing damage to the proton exchange membrane and allowing gas crossover between the gas spaces [8]. The goal will be to identify the pressure level at which the most significant reduction in water decomposition voltage occurs. This test bench will be used also in real environment to observe potential degradation processes [9] during electrolytic decomposition of water under pressure in a hermetically sealed electrolysis cell.

By rationally selecting an appropriate operational power profile, maximum current utilization and decrease in water decomposition voltage will be ensured.

Conclusions

A current regulator for electrolysis cell has been developed. Relay protection (for cell voltage, temperature, and pressure) has been integrated into this regulator to ensure that in the event of an emergency situation, the power circuit undergoes mechanical disconnection.

Due to the utilization of processor control in the designed current regulator, optimizing parameters governing reversible degradation processes becomes possible.

References

[1] “CONTROL AND ENERGY EFFICIENCY OF PEM WATER ELECTROLYZERS IN RENEWABLE ENERGY SYSTEMS”, doi: 10.1016/j.ijhydene.2017.10.056
[2] “SIMPLE PEM WATER ELECTROLYSER MODEL AND EXPERIMENTAL VALIDATION”, doi: 10.1016/j.ijhydene.2011.09.027
[3] “HYDROGEN PRODUCTION FROM WATER ELECTROLYSIS: CURRENT STATUS AND FUTURE TRENDS”, doi: 10.1109/JPROC.2011.2156750.
[4] “DEVELOPMENT AND APPLICATION OF FLEXIBLE INTEGRATED MICROSENSOR AS REAL-TIME MONITORING TOOL IN PROTON EXCHANGE MEMBRANE WATER ELECTROLYZER”, doi: 10.1016/j.renene.2019.05.071
[5] “TRANSIENT BEHAVIORS AND MATHEMATICAL MODEL OF PROTON EXCHANGE MEMBRANE ELECTROLYZER”, doi: 10.1016/j.jpowsour.2022.231757
[6] “MICROCONTROLLER-BASED EMULATION OF A PEM FUEL CELL”, doi: 10.1016/j.ijhydene.2019.10.034
[7] “A REVIEW OF TESTING PROCEDURES FOR PROTON EXCHANGE MEMBRANE ELECTROLYZER DEGRADATION”, doi: 10.1016/j.jpowsour.2022.232569

[8] “IMPACT OF CLAMPING PRESSURE AND STRESS RELAXATION ON THE PERFORMANCE OF DIFFERENT POLYMER ELECTROLYTE MEMBRANE WATER ELECTROLYSIS CELL DESIGNS”, doi: 10.1016/j.ijhydene.2019.07.075
[9] “PRESSURIZED PEM WATER ELECTROLYSIS: EFFICIENCY AND GAS CROSSOVER”, doi: 10.1016/j.ijhydene.2013.09.013

Influence of mechanical contact pressure on performance and gas purity of an alkaline zero-gap water electrolysis cell

Lukas Ritz[*1], Martin Müller[1], Anna K. Mechler[2,3,4], Felix Lohmann-Richters[1]

[1] Institute of Energy and Climate Research, Electrochemical Process Engineering (IEK-14), Forschungszentrum Jülich GmbH, Jülich/Germany;
[2] Electrochemical Reaction Engineering (AVT.ERT), RWTH Aachen University, Aachen/Germany;
[3] Institute of Energy and Climate Research, Fundamental Electrochemistry (IEK-9), Forschungszentrum Jülich GmbH, Jülich/Germany;
[4] JARA-ENERGY, Aachen/Germany

Introduction

Alkaline water electrolysis offers high potential for the production of hydrogen from renewable energy sources. The development of the technology is focused on increasing efficiency and reducing costs. Classic alkaline electrolysis cells usually featured a gap between the electrodes and the separator. In more recent zero-gap cells the electrodes are directly placed on the separator. Using a zero-gap setup, the ohmic resistance of the cell can be reduced by 30 % compared to a 2 mm gap [1]. To ensure a zero-gap assembly of the electrodes, they must be mechanically pressed against the separator. The research question is how this mechanical contact pressure affects cell performance and product gas quality.

Methodology

A special contact pressure cell (CPC) was developed to investigate the cell behavior at different contact pressures. In this cell, an adjustment screw allows to apply a force only to the active cell area of the electrodes. The correlation between the torque of the adjustment screw and the resulting force was calibrated with a pressure-sensitive foil. Figure 1 shows the electrode configuration of the CPC. The stamp is used to apply the force of the adjustment screw homogeneously over the active cell surface. The flow field (in this case a porous Ni-foam flow field) and electrode are located on top of the stamp.

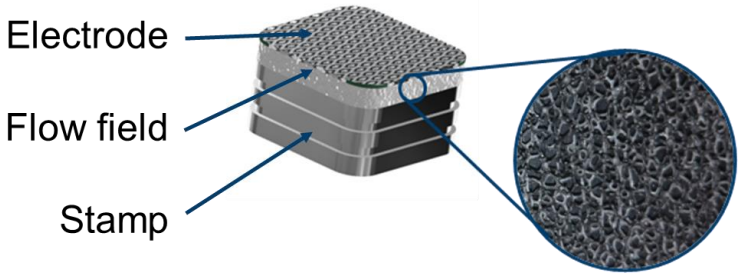

Figure 1: Electrode configuration of the CPC

The influence of contact pressure on performance and gas quality was investigated for two different cell configurations. In the first setup, the internal components were welded together. In that case no contact pressure dependent contact resistances were present. In the second setup, the components were only loosely stacked on top of each other and connected

[*] Corresponding author: l.ritz@fz-juelich.de

only by the applied force. In four compression cycles the cell was exposed to contact pressures ranging from 0.3 MPa to 3.1 MPa. Repeatable cell performance was observed from the third compression. For the experiment a Zirfon UTP500 separator, nickel foam electrodes and potassium hydroxide as electrolyte (30 wt. % and 80°C) were used.

Discussion

Figure 1 shows the current density in the third compression at a cell voltage of 2.2 V for the stacked and the welded configuration. The current density decreases with increasing contact pressure by 24 % (welded electrodes) and 17 % (stacked electrodes). Overall, higher current densities can be achieved by eliminating contact resistance in the welded setup.

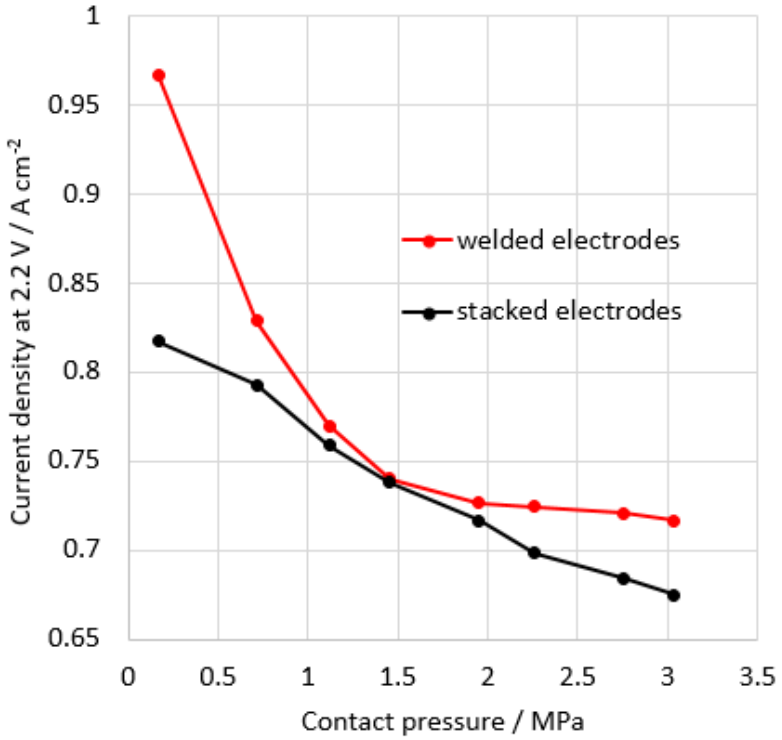

Figure 2: Current density at 2.2 V for different contact pressures during the third compression of the cell

Conclusions

The mechanical contact pressure in the active cell area can influence the behavior of a cell. Compressing the internal components can change their properties. For example, higher contact pressures lead to a deformation of the flow field or the electrodes and affect mass transfer, but it can also influence their electrical contact resistances. A compression of the porous separator can also change its properties, e.g., thickness, ionic conductivity, or diffusion coefficient.

The experimental results show that the lowest possible contact pressure should be selected for efficient operation of an alkaline electrolysis cell. In further experiments, we found that increasing contact pressure also increases the product gas contamination (H_2 in O_2).

Acknowledgement

The presented research is funded by the German Federal Ministry of Economic Affairs and Climate Action and the project "NextH2 - Next generation of powerful and efficient alkaline electrolyzers for regenerative H2 generation" (Reference 03EI3011A-C). Project partners include Agfa, TK nucera, De Nora and Forschungszentrum Jülich GmbH.

References

[1] “Minimising the ohmic resistance of an alkaline electrolysis cell through effective cell design”, doi: 10.1016/j.ijhydene.2017.07.184.

Integration of Solid Oxide Electrolysis and Enhanced Ammonia Synthesis for Green Ammonia Production: A Techno-economic Analysis

V. Verde[1,2] , A. Saker[*2], A. Berrady[2], A. Ramirez Santos[2], P. Olivier[2], F. Gallucci[1]

[1]*Inorganic Membranes and membrane Reactors, Sustainable Process Engineering, Chemical Engineering and Chemistry, Eindhoven Univeristy of Technology, Eindhoven, 5612 AZ, The Netherlands*
[2] *ENGIE Lab CRIGEN, ENGIE, Stains, 93240, France*

Introduction

Nowadays, ammonia is one of the most produced chemicals especially as precursor for fertilizers production. Ammonia production process is responsible of about 1% of global CO_2 emission and 15-20% of the chemical sector CO_2 emissions [1]. These emissions are mostly related to the upstream hydrogen production process necessary to run the synthesis reaction, based for several decades on steam methane reforming and coal gasification. There is a big interest in hydrogen production trough electrolysis process which, using renewable energy, allows for the decarbonization of ammonia production process. There are already several industrial projects involving electrolysis technologies for ammonia synthesis applications (e.g. YARA and HyEX projects [6],[7]]), mostly based on low-temperature electrolysis technologies, but the high temperature ones, especially Solid oxide Electrolytic Cells, have a more ever-growing interest.
Solid Oxide Electrolytic Cells (SOECs) seems to be one of the most promising electrolysis technology: due to higher operation temperature (650 °C-850 °C,[4]), higher efficiencies can be achieved (>84% LHV basis [5]) with respect to traditional electrolysis technologies, with the possibility of heat integration. Among the main advantages of SOECs, one of the most important is the possibility to use Nickel as catalyst instead of Platinum Group Metals (PGMs) like Pt and Ir, considered critical materials due to their low availability and high cost: this translates is a stronger supply chain. As the electrochemistry at cell level has a quick response [8], Solid Oxide Electrolysers could be suitable for renewable energy utilisation, thanks to specific adaptation at system level, especially to address thermal gradient issue .
Due to the intermittent nature of renewable energy and the constraints for the operation of electrolysis and ammonia synthesis units, the integration between hydrogen production and ammonia synthesis processes often requires an intermediate hydrogen storage, which size increases with high variation and low availability heads, having a non-negligible impact on CAPEX [2]. Literature presents few studies on Power-to-ammonia systems based on SOEC but no techno-economic studies based on dynamic operation have been carried out, especially for systems that include novel ammonia separation technologies. In this work, an SOECs system dynamic model including a hydrogen storage section has been developed to evaluate the integration of electrolysis and an enhanced ammonia synthesis process based on a novel ammonia separation method based on absorption. Compared to traditional separation method based on condensation, the mentioned method has the main advantage to lower system operating pressure with a reduction of system cost associated [9] and higher scaling factors which suggest that the process is more suited for small-scale applications [10], thus distributed ammonia production.
The model has been developed in the context of ARENHA project activities and is used as tool for the investigation on the impact that system flexibility and renewable energy input have on Levelized Cost of Ammonia (LCOA). Two renewable energy power profile have been used for this study: a wind only and a hybrid PV/wind, corresponding to a 42.5% and 63.8% capacity factor respectively. Results show that depending on flexibility of ammonia synthesis unit, oversizing renewable energy input is not always the best solution in terms of cost, since there is a trade-off between electrolyser utilisation, stack substitution, and capital expenditure of renewable energy system and hydrogen storage. However, further optimization is still possible with heat integration of ammonia synthesis unit with SOEC in dynamic operation.

Methodology

This study is based on process modelling, with the aim to obtain models that allow for the estimation of performances of each sub-system, and their operation under flexibility constraints (e.g. ammonia synthesis admittable load range). With model output data such as energy expenditures and production and trough equipment cost data and correlation for each sub-system, a discounted cash flow analysis can be carried out to calculate levelized cost of hydrogen and thus ammonia produced.

* Corresponding author: assia.saker@engie.com

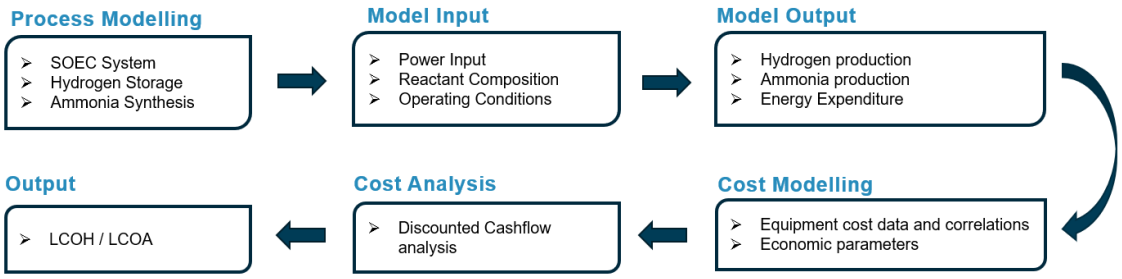

Figure 1. Study Methodology.

Solid Oxide Electrolyser is the core of the Power-to-Ammonia system. A lumped parameter model for SOEC stack has been developed in Aspen Custom Modeler and validated with experimental data from project partners. Each SOEC stack includes a set of Solid Oxide Cells which perform the water electrolysis according to the following chemical reaction:

$$H_2O_{(l)} \rightarrow H_{2(g)} + \frac{1}{2}O_{2(g)} \qquad \Delta G^0 = +237.22\ \frac{kJ}{mol}$$

Having a positive Gibbs free energy variation, energy is required to drive the reaction. This is done within the cell through both electrical and thermal energy. Electrochemical reactions involved at electrodes are:

$$\text{Cathode:} \quad H_2O_{(g)} + 2e^- \rightarrow H_{2(g)} + O^{2-}$$

$$\text{Anode:} \quad O^{2-} \rightarrow \frac{1}{2}O_{2(g)} + 2e^-$$

Cell voltage is the main parameter for the estimation of cell performance and is calculated as sum of open circuit voltage, activation overpotentials, ohmic overpotential and concentration overpotentials:

$$V_{cell} = V_{rev} + \eta_{cath}^{act} + \eta_{anod}^{act} + \eta_{Ohm} + \eta_{cath}^{conc} + \eta_{anod}^{conc}$$

Open circuit voltage is dependent on temperature, pressure and average reactant composition and is calculated trough Nernst equation:

$$V_{rev} = \frac{\Delta \bar{g}_0}{z_e F} + \frac{RT}{z_e F}\, ln \frac{P_{O_2}^{g\,1/2} \cdot P_{H_2O}}{P_{H_2O}}$$

Where z_e is the number of electrons exchanged in the reaction and F the Faraday constant. Activation overvoltage expresses the voltage spent to activate electrochemical reactions and it is dependent on stack operating condition, characteristic of electrodes and catalyst quality. Its formula is retrieved from Butler-Volmer equation, very common in literature, which links electrode voltage and current [11]:

$$i_{act} = i_{0,a/c}\left(e^{\alpha \frac{z_e F \eta_{a/c}^{act}}{RT}} - e^{-(1-\alpha)\frac{z_e F \eta_{a/c}^{act}}{RT}}\right)$$

Where α is a charge transfer coefficient that can be assumed 0.5 leading to activation overvoltage equation:

$$\eta_{a/c}^{act} = \frac{RT}{z_e F} arcsinh\left(\frac{i}{2i_{0,a/c}}\right)$$

Activation losses are dependent on exchange current density which physical meaning is the electrode capability of exchange current in no current flow conditions (electrodes forward and backward reactions are equal).

Correlations of anodic and cathodic exchange current densities in function of temperatures, activation energies and concentration at electrode three phase boundary are retrieved in literature [12],[13]:

$$i_{0,a} = B \cdot \left(\frac{p_{O_2}}{p_{ref}}\right)^{r} \cdot \exp\left(-\frac{Eact_{an}}{RT}\right)$$

$$i_{0,c} = A \cdot \left(\frac{p_{H_2}}{p_{ref}}\right)^{m} \cdot \left(\frac{p_{H_2O}}{p_{ref}}\right)^{n} \cdot \exp\left(-\frac{Eact_{cat}}{RT}\right)$$

Where A,B are pre-exponential factors depending and r, m and n experimental exponents. These parameters and activation energy are used as fitting parameters for model validation. Concentration losses, related to reactant diffusion into the electrode depend on gas diffusivities, temperature and electrode structure and are expressed as:

$$\eta^{conc} = \frac{RT}{z_e F} ln \prod_m \left(\frac{c_m^*}{c_{m,0}}\right)^{v}$$

Where $c_{m,0}$ is the bulk concentration of m-th specie and c_m^* is the concentration of m-th specie at three-phase boundary, the electrode reaction site. c_m^* is calculated for each specie considering both Knudsen and binary diffusion coefficients. For a cathode supported cell the effect of diffusion in the anode has been neglected due to the very low thickness. Ohmic losses are strictly dependent on cell materials conductivity and are expressed as:

$$\eta_{Ohm} = i\left(\frac{\tau_a}{\sigma_a(T)} + \frac{\tau_e}{\sigma_e(T)} + \frac{\tau_c}{\sigma_c(T)} + R_{cc}\right)$$

Where $\sigma_a, \sigma_e, \sigma_c$ and τ_a, τ_e, τ_c are respectively conductivities (ionic or electronic depending on the material) and thicknesses of anode, electrolyte, and cathode. Correlations for materials related to electrolyte and fuel electrode supported solid oxide cells have been retrieved from literature. R_{cc} is additional resistance related to interconnector conductivity and additional contact resistances and is used as fitting parameter for model validation as well as pre-exponential factors, experimental exponents and activation energies of activation polarization equation. Finally, a heat balance equation has been implemented:

$$C_{th} \cdot \frac{dT_{stack}}{dt} = P_{anode} + P_{cathode} + W_{el} - \dot{Q}_{loss}$$

Being the model 0D lumped, a stack thermal capacity C_{th} value is assumed while temperatures, pressures and concentrations are average between inlet and outlet conditions.

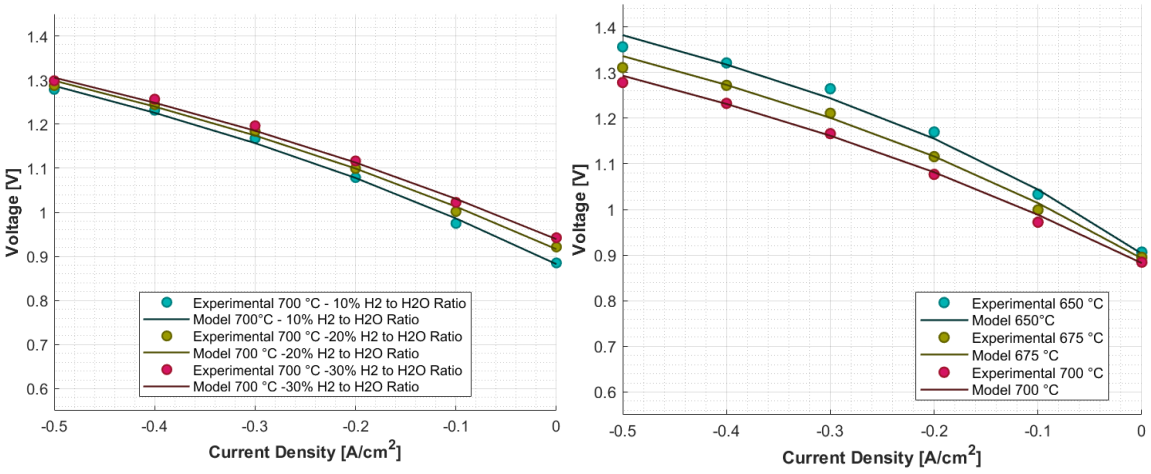

Figure 2. Electrochemical cell experimental data validation.

Imported in an Aspen Plus flowsheet including the balance of plant and a hydrogen compression and storage section, SOEC model has been exported in Aspen Plus Dynamics environment where a control strategy has been implemented to allow the dynamic operation of the system. Dynamic model of enhanced ammonia synthesis is in development, thus cost functions and energy consumption data have been assumed from literature according to [9],[10] assuming ammonia synthesis efficiency constant with load variation. The latter seems a reasonable assumption since ammonia synthesis electricity consumption, mainly based on feed an recycle compression accounts only for a small fraction of electrical energy consumption in Power-to-Ammonia systems [9]. The intermediate hydrogen storage, necessary for electrolysis and ammonia synthesis mass integration, is sized in the simulation depending on renewable energy power profile used as input, to meet system constraints which are mainly related to electrolysis and ammonia synthesis unit flexibility capability and compressor operation. In this study two power profiles from Fiennes (France) have been considered as input for the system: the first one is a 15 MW wind only, the second one is a hybridization of the first one with PV energy, with a nominal power ratio PV/wind equal to 4. When renewable energy is not available, energy is taken from the grid to guarantee the electrolyser minimum load (10% in this study) with a 100 €/MWh electricity cost, while on the other hand, excess of energy is curtailed and is considered to be sold with a very low price (20 €/MWh).

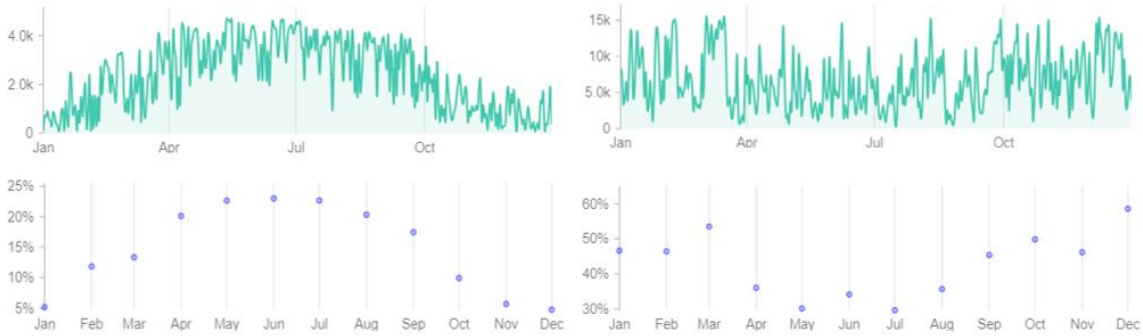

Figure 3. Daily average power (up) and monthly average capacity factor (down) for 16 MW PV (Left) and Wind (Right) systems located in Fiennes (France).

The picture below depict the simplified process flow diagram of the system under study:

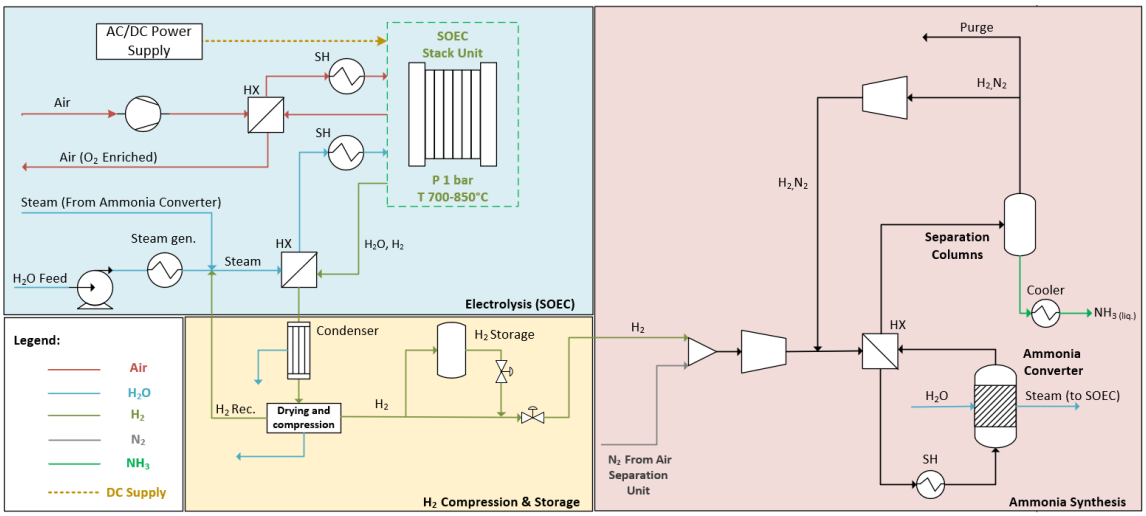

Figure 4. Power-to-Ammonia system layout.

Results and discussion

The electrolyser hydrogen production, the hydrogen flowrate to Haber-Bosch loop and the hydrogen storage level curves can be computed with the model. The Haber-Bosch loop is supposed to work on different levels in terms of percentage of nominal flowrate: for this reason, the hydrogen flowrate to ammonia synthesis unit has been automated, as simulation constraint, considering trigger levels as points for operation switch (*Figure 5*). The

maximum ramp rate value is a constraint related to the Haber-Bosch reactor operation and has been assumed to ± 20% F_{nom}/h in this study.

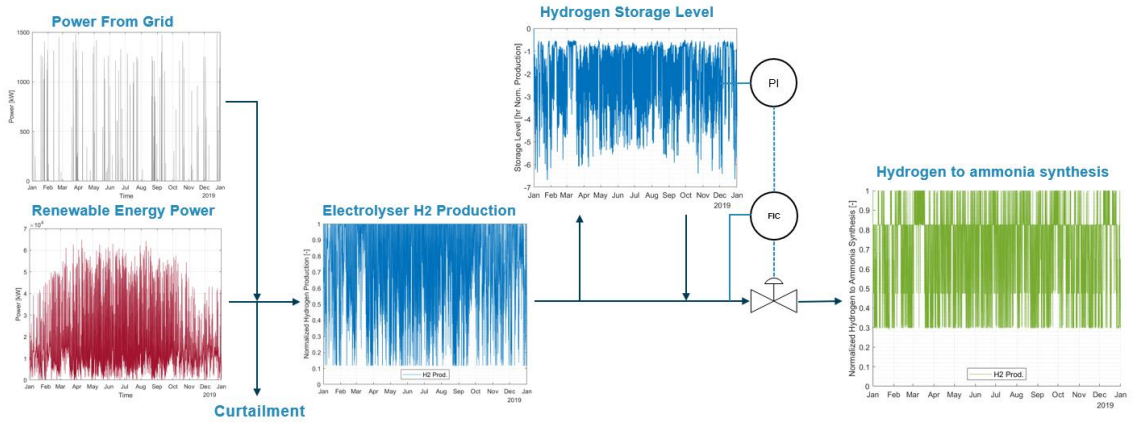

Figure 5. Simulation main input and outputs.

The effect of ammonia synthesis flexibility on storage size has been investigated. Using the wind only power profile and considering a 15 MW electrolysis power, leading to a ~55 t/d nominal ammonia production, a sensitivity analysis on ammonia synthesis flexibility has been done in order to study its effect on hydrogen storage size, thus levelized cost. A 90% maximum flexibility has been used for the sensitivity analysis since concepts of flexible ammonia synthesis loop with 10% minimum load with acceptable losses in efficiencies are already present [3]. From results it can be noticed that passing from 30% to 90% flexibility is possible to reduce storage size by a factor of 48 reducing LCOA by 26%. The "rigid" Power-to-Ammonia case would require 8 days of production storage compared to less than 4 hours of the highest turndown case which result in a 950.3 €/t_{NH3}. These results are strictly dependent on the "quality" of power profile in input to the system, since no battery storage is used for the electrolyser operation.

Finally, a comparison between 4 scenarios has been done: wind only and hybrid profiles with respectively 70% and 90% ammonia synthesis flexibility. From results in **Errore. L'origine riferimento non è stata trovata.** it can be noticed how, the hybrid power input implies a higher electrolyser capacity factor, thus lower cost associated to electrolyser operation and lower cost for hydrogen storage, but higher cost related to renewable energy system. However, the wind only power case implies lower costs related to renewable energy system, but higher cost of electrolyser related to lower capacity factor (production) and higher cost for hydrogen storage for lower flexibility values. It important to notice that having a high ammonia synthesis flexibility lead to a drastic reduction of cost associated to hydrogen storage for wind only scenario, which LCOA became slightly lower than the high-flexible hybrid case.

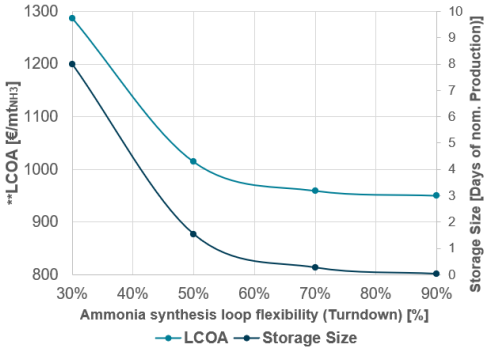

Figure 6. LCOA and storage size dependence with ammonia synthesis flexibility **Levelized Cost of Ammonia calculated for a ~55 t/d_{NH3} system, 60 €/MWh electricity cost, 1200 €/kW electrolyser cost, 7% WACC, 30 years plant lifetime.

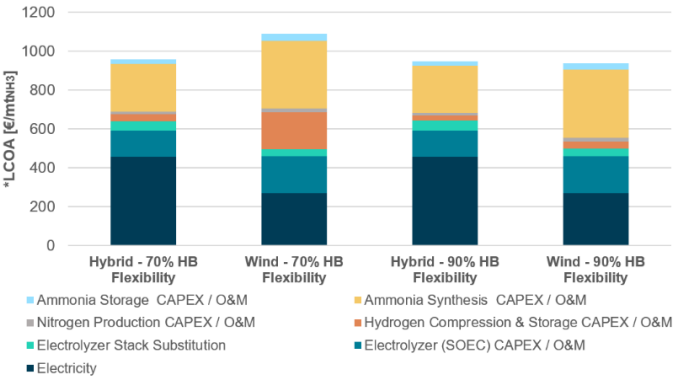

Figure 7. Levelized Cost of Ammonia calculated for a ~55 t/d_{NH3} system, 60 €/MWh electricity cost, 1200 €/kW electrolyser cost, 7% WACC, 30 years plant lifetime. *Cost function for ammonia synthesis loop from M. J. Palys et al. (2018) [14].

Conclusions

A dynamic model has been developed for a Solid Oxide Electrolysis Cells system. The model includes a control strategy to manage renewable energy integration which inevitably involves a load variability in the system. A hydrogen storage section has been modelled for the integration of ammonia synthesis operation which, depending on renewable energy input, is sized to meet the Power-to-Ammonia system constraints. Ammonia synthesis unit cost and energy indicator have been assumed using data from literature. A wind only and a hybrid with a 4 PV/ratio power profiles from Fiennes (France) have been considered in this study. A sensitivity analysis on ammonia unit load flexibility has shown how is possible to drastically reduce hydrogen storage size, thus its cost. Comparing the two scenarios is possible to obtain 950 €/t -1100 €/t levelized cost of ammonia with high ammonia synthesis flexibilities (70-90%), values inside the range of current ammonia production cost indicated by IEA [15]. However, the potential of integration of heat produced by ammonia converter with solid oxide electrolyser has not been shown. In the next steps, the dynamic thermal integration between electrolysis and ammonia synthesis unit will be pointed out, focusing on the model of enhanced ammonia synthesis based on absorption separation technology and the possible further cost reduction. The model of the complete system will constitute a consolidated tool for characterising the performance of power to ammonia systems, as well as a sizing tool for the hydrogen storage required, a tool for the development of control and management strategies, and will open the path to predictive control studies for cost optimization.

Acknowledgments

This project has received funding from the European Union's Horizon 2020 research and innovation programme under grant agreement No 862482.

References

[1] IRENA and AEA (2022), Innovation Outlook: Renewable Ammonia, International Renewable Energy Agency, Abu Dhabi, Ammonia Energy Association, Brooklyn.
[2] G. Genova, S. Panza (June 2022) , Casale flexible green ammonia plant, the economically viable green production"
[3] US9463983B2 - Method for load regulation of an ammonia plant (Patent)
[4] Godula-Jopek, A. (2015). Hydrogen production : By Electrolysis. John Wiley & Sons
[5] https://www.bloomenergy.com/wp-content/uploads/bloom-energy-electrolyzer-datasheet-march-2023.pdf Last visit: 09/05/2023
[6] https://engie.com.au/yuri Last visit: 09/05/2023
[7] https://tractebel-engie.fr/fr/references/green-ammonia-production-hyex-project Last visit: 09/05/2023
[8] Bloom Energy (January 2023), SOEC: Ammonia Energy Association Discussion.
[9] L. Bosong et al. (2020), "Performance of a Small-Scale Haber Process: A Techno-Economic Analysis"
[10] Matthew J. Paly et al. (2018), "Modeling and Optimal Design of Absorbent Enhanced Ammonia Synthesis"
[11] G. Herz, N. Müller, P. Adam, S. Megel, E. Reichelt, and M. Jahn, "High Temperature Co-Electrolysis as a Key Technology for CO2 Emission Mitigation – A Model-Based Assessment of CDA and CCU," Chemie-Ingenieur-Technik, vol. 92, no. 8, pp. 1044–1058, 2020, doi: 10.1002/cite.202000012.
[12] J. Laurencin, D. Kane, G. Delette, J. Deseure, and F. Lefebvre-Joud, "Modelling of solid oxide steam electrolyser: Impact of the operating conditions on hydrogen production," J. Power Sources, vol. 196, no. 4, pp. 2080–2093, 2011, doi: 10.1016/j.jpowsour.2010.09.054.
[13] P. Costamagna, A. Selimovic, M. Del Borghi, and G. Agnew, "Electrochemical model of the integrated planar solid oxide fuel cell (IP-SOFC)," Chem. Eng. J., vol. 102, no. 1, pp. 61–69, 2004, doi: 10.1016/j.cej.2004.02.005.
[14] Matthew J. Palys, Alon McCormick, E. L. Cussler and Prodromos Daoutidis – "Modeling and Optimal Design of Absorbent Enhanced Ammonia Synthesis", 2018
[15] IEA, Indicative production costs for ammonia via electrolysis in selected regions compared to current references, IEA, Paris https://www.iea.org/data-and-statistics/charts/indicative-production-costs-for-ammonia-via-electrolysis-in-selected-regions-compared-to-current-references, IEA. Licence: CC BY 4.0

International trade of green hydrogen: Implications and challenges for potential exporting countries

Müller, Viktor Paul[1,2,*]

[1] Fraunhofer Institute for Systems and Innovation Research ISI, Breslauer Straße 48, 76139 Karlsruhe, Germany
[2] Copernicus Institute of Sustainable Development, Utrecht University, Utrecht, 3584 CB, The Netherlands

Introduction

Especially in industrialized nations such as Germany, the import of hydrogen is seen as an important pillar of energy supply in a decarbonized energy system in the medium to long term. For this purpose, a large number of studies and peer-reviewed papers have investigated the techno-economic potential for green hydrogen production in different countries [1–3]. This is often done from the perspective of potential importing countries to assess how their future needs can be met in the most cost-effective way. Thus, many studies of potential exporting countries focus on estimating production and transportation costs based on existing resources and assumptions about future technological developments. In contrast, other aspects of green hydrogen production for exporting countries are only superficially considered. However, in the face of global climate change, it is important to examine the perspectives and concerns of exporting countries in more detail in order to take them into account when planning and implementing hydrogen production and trade. Various social, political, and economic aspects are relevant for the successful and sustainable development of an export-oriented hydrogen and Power-to-X (PtX) industry.

Methodology

Global energy trade is expected to change significantly in the coming years. While global demand for fossil fuels such as oil and natural gas will decrease in the medium term, green hydrogen and downstream products could become important new foreign trade commodities [4, 5]. However, these changes will not only have a direct impact on energy trade but also indirectly on a wide range of other products. This will be particularly relevant for future producing countries. In addition to export revenues, there are other economic aspects associated with the export of green hydrogen and downstream products. New local value creation in the PtX industry could create additional jobs and generate tax revenues. However, the question arises how to ensure that the development of an export-oriented PtX industry does not slow down the local energy transition and thus only relocates global emissions rather than reducing them? The aim of this thesis is to investigate the aforementioned aspects of trade in green hydrogen and downstream products from the perspective of potential exporting countries based on the following research question.

"What are the implications and challenges arising from international trade of green hydrogen and downstream products from the perspective of potential exporting countries?"

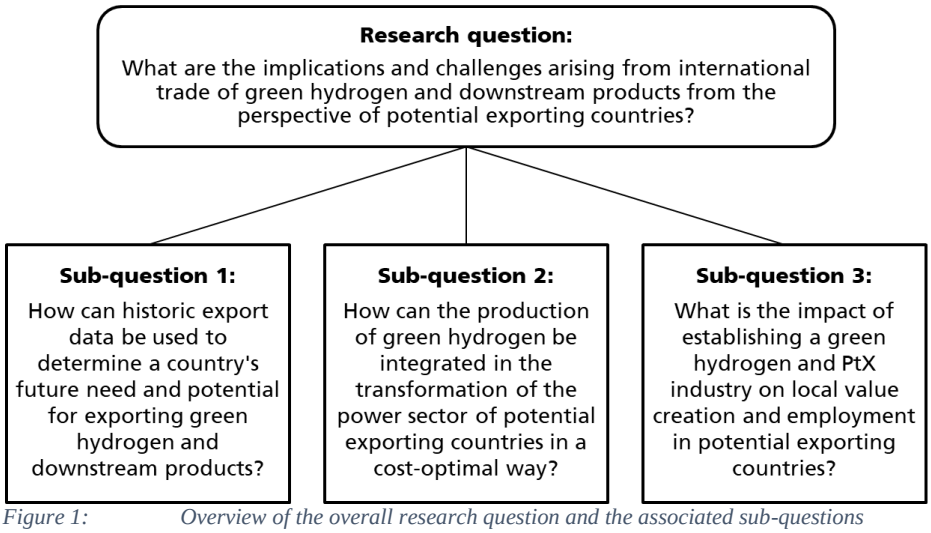

Figure 1: Overview of the overall research question and the associated sub-questions

To address the overall research question, three sub-questions are formulated, which are investigated using diferent quantitative and qualitative methods. The three sub-questions listed in Figure 1 and the applied methodology are presented in more detail below.

Discussion

Sub-question 1: How can historic export data be used to determine a country's future need and potential for exporting green hydrogen and downstream products?

Key idea

The historical global trade data of products between countries is an extensive dataset that contains information on the specialization and diversification of national economies. With increased attention on the trade of green hydrogen and downstream products, it therefore seems interesting to conduct a global analysis of trade data focusing on hydrogen-related products. The objective is to identify those countries that have a particular interest in the trade of green hydrogen and downstream products based on their historical trade data. It also seems worthwhile to take a closer look at the trade data of countries that have been identified in previous studies as promising exporting countries due to their geographical characteristics.

Paper 1 published in Renewable and Sustainable Energy Reviews:

Müller, V. P.; Eichhammer, W. (2023): Economic complexity of green hydrogen production technologies - a trade data-based analysis of country-specific industrial preconditions. In: Renewable and Sustainable Energy Reviews, 182, p. 113304.

Abstract

“Countries with high energy demand but limited renewable energy potential are planning to meet part of their future energy needs by importing green hydrogen. For potential exporting countries, in addition to sufficient renewable resources, industrial preconditions are also relevant for the successful implementation of green hydrogen production value chains. A list of 36 “Green H2 Products” needed for stand-alone hydrogen production plants was defined and their economic complexity was analyzed using international trade data from 1995 to 2019. These products were found to be comparatively complex to produce and represent an opportunity for countries to enter new areas of the product space through green diversification.

Large differences were revealed between countries in terms of industrial preconditions and their evolution over time. A detailed analysis of nine MENA countries showed that Turkey and Tunisia already possess industrial know-how in various green hydrogen technology components and perform only slightly worse than potential European competitors, while Algeria, Libya, and Saudi Arabia score the lowest in terms of calculated hydrogen-related green complexity. These findings are supported by statistical tests showing that countries with a higher share of natural resources rents in their gross domestic product score significantly lower on economic and green complexity. The results thus provide new perspectives for assessing the capabilities of potential hydrogen-producing countries, which may prove useful for policymakers and investors. Simultaneously, this paper contributes to the theory of economic complexity by applying its methods to a new subset of products, and using a dataset with long-term coverage."

Sub-question 2: How can the production of green hydrogen be integrated in the transformation of the power sector of potential exporting countries in a cost-optimal way?

Key idea

From a global perspective, trading green hydrogen and downstream products is only viable if the production of the electricity-based hydrogen is renewable and does not impede the transformation of the local energy system in the producing country. Especially for countries with currently high shares of fossil fuels in the electricity mix, it is therefore crucial to develop an understanding of what it means to simultaneously transform local electricity generation and provide additional renewable electricity for the export-oriented production of green hydrogen. The objective is therefore to carry out a scenario-based, cost-optimal expansion planning of electricity generation for one or more selected potential export countries. For the scenarios, different assumptions (e.g. technology cost, policy measures, efficiency improvements) are considered.

The proposed methodology to conduct case studies for selected countries generally consists of the following five steps:

(1) Implementation of the national energy system based on historical energy balances in the "Low Emissions Analysis Platform" (LEAP) [6]
(2) Scenario development for projections of future energy demand based on assumptions (e.g. population growth, GDP growth, energy efficiency measures, fuel switch)
(3) Implementation of different transformation modules including technical (e.g. efficiency, life time) and economic (e.g. CAPEX, fix & variable OPEX) parameters
(4) Implementation of time-resolved demand and generation curves for different technologies (in particular fluctuating RES)
(5) Least-cost optimized expansion planning of transformation modules for different scenarios using the "Next Energy Modeling system for Optimization" (NEMO) [7]

Sub-question 3: What is the impact of establishing a green hydrogen and PtX industry on local value creation and employment in potential exporting countries?

Key idea

The production of green hydrogen and downstream products creates added value in the producing country. In addition to trade revenues, the development of an export oriented PtX

industry thus has further positive effects on the local economy. The extent to which the local economy benefits depends on the share of the entire value chain that can be realized locally. For this purpose, the individual steps of the PtX value chain will be examined in more detail to identify the potential for economic growth, value and job creation for the respective countries. While there are several peer reviewed papers using input-output models to investigate the value-added and job effects of renewable energy for electricity generation (e.g. [8–11]), there are so far only a few studies related to green hydrogen and downstream products. The objective is therefore to carry out an input-output model based analysis of the value added and job affects associated by the implementation of an export oriented PtX industry in a selected country.

Input-output analyses allow predictions on how changes in one sector will directly and indirectly affect other sectors of an economy. However, since usually only aggregated data from several sectors is available, it should be noted that the level of detail of the analysis of specific technologies is limited [11]. To account for this, the costs of the examined technology can be allocated proportionally to sectors listed in the I-O tables. Table 1 provides a proposed cost distribution for five different renewable power plant technologies, taken from Dell'Anna [11].

Table 1: Allocation of cost shares for different renewable power plant technologies to the product sectors listed in the I-O table [11]

Costs distribution for RES technologies (Oliveira et al., 2013; Pereira Da Silva et al., 2013; Tourkolias and Mirasgedis, 2011; Tourkolias et al., 2009).

Products sectors	Wind		PV		Hydro		Geothermal		Biomass	
	Ci	O&M	Ci	O&M	Ci	O&M	Ci	O&M	Ci	O&M
Mines and quarries products							17.5%			
Rubber and plastic products	12%	5%								
Metal products, excluding machines and systems	12%		14%		2%		16%		5%	
Electrical machinery	6%	15%	14%	15%	5%	15%	5%	15%	10%	5%
Mechanical and equipment	37%	30%	49%	15%	23%	35%	33.5%	35%	40%	15%
Construction work	26%	2%	20%		60%		20%		40%	
Trade services										30%
Land transport and pipeline transport services	1%	1%	0.5%		1%				0.5%	40%
Accommodation and restaurant services	0.5%									
Financial services	0.5%	17%	0.5%	50%	1.5%	20%	1.5%	20%	0.5%	10%
Real estate services	5%	30%	2%	20%	7.5%	30%	6.5%	30%	4%	

Ci = Investment cost.
O&M = Operational and maintenance.

This method can be extended to other technologies such as electrolysers or ammonia and methanol synthesis and used to draw conclusions about the number of new jobs created and the associated economic impact of the introduction of certain PtX industries and their entire value chain. Scenarios can be used to vary different factors, such as the share of local manufacturing, in order to estimate possible ranges.

Conclusions

In summary, the work is intended to help broaden the view of the international trade in green hydrogen and PtX products and to illuminate it from different perspectives. In particular, the often prevailing euphoria of potential demand countries towards the production of hydrogen in emerging and developing countries is critically discussed in order to point out possible difficulties. At the same time, the industrial and socio-political opportunities for potential producer countries are examined, which could go beyond mere export revenues and thus represent an opportunity for sustainable economic development.

References

[1] B. Lux, J. Gegenheimer, K. Franke, F. Sensfuß, and B. Pfluger, “Supply curves of electricity-based gaseous fuels in the MENA region,” *Computers & Industrial Engineering*, vol. 162, p. 107647, 2021, doi: 10.1016/j.cie.2021.107647.

[2] J. Armijo and C. Philibert, “Flexible production of green hydrogen and ammonia from variable solar and wind energy: Case study of Chile and Argentina,” *International Journal of Hydrogen Energy*, vol. 45, no. 3, pp. 1541–1558, 2020, doi: 10.1016/j.ijhydene.2019.11.028.

[3] S. Touili, A. Alami Merrouni, A. Azouzoute, Y. El Hassouani, and A. Amrani, “A technical and economical assessment of hydrogen production potential from solar energy in Morocco,” *International Journal of Hydrogen Energy*, vol. 43, no. 51, pp. 22777–22796, 2018, doi: 10.1016/j.ijhydene.2018.10.136.

[4] A. Michaelowa and S. Butzengeiger, “Breakthrough of hydrogen technologies until 2030: chances and risks for Gulf countries, international policy implications,” doi: 10.5167/UZH-175363.

[5] T. van de Graaf, I. Overland, D. Scholten, and K. Westphal, “The new oil? The geopolitics and international governance of hydrogen,” *Energy research & social science*, vol. 70, p. 101667, 2020, doi: 10.1016/j.erss.2020.101667.

[6] Stockholm Environmental Institute (SEI), *LEAP: Introduction.* [Online]. Available: https://leap.sei.org/default.asp?action=introduction (accessed: Oct. 7 2021).

[7] Stockholm Environmental Institute (SEI), *NEMO: Next Energy Modeling system for Optimization.* [Online]. Available: https://github.com/sei-international/NemoMod.jl (accessed: Oct. 7 2021).

[8] H. Garrett-Peltier, “Green versus brown: Comparing the employment impacts of energy efficiency, renewable energy, and fossil fuels using an input-output model,” *Economic Modelling*, vol. 61, pp. 439–447, 2017, doi: 10.1016/j.econmod.2016.11.012.

[9] M. Kamidelivand, C. Cahill, M. Llop, F. Rogan, and B. O'Gallachoir, “A comparative analysis of substituting imported gas and coal for electricity with renewables – An input-output simulation,” *Sustainable Energy Technologies and Assessments*, vol. 30, pp. 1–10, 2018, doi: 10.1016/j.seta.2018.08.003.

[10] D. Keček, D. Mikulić, and Ž. Lovrinčević, “Deployment of renewable energy: Economic effects on the Croatian economy,” *Energy Policy*, vol. 126, pp. 402–410, 2019, doi: 10.1016/j.enpol.2018.11.028.

[11] F. Dell’Anna, “Green jobs and energy efficiency as strategies for economic growth and the reduction of environmental impacts,” *Energy Policy*, vol. 149, p. 112031, 2021, doi: 10.1016/j.enpol.2020.112031.

Interpretation of electrochemical impedance spectra in AEM-water electrolysis

M. Ranz*[1], G. Djordjic[1], F. de Pauli[1], B. Grabner[1], H. Wegleiter[2], B. Schweighofer[2], A. Trattner[1,3]

[1]HyCentA Research GmbH, Graz, Austria
[2]Institute of Electrical Measurement and Sensor Systems, Graz University of Technology, Austria
[3]Institute of Thermodynamics and Sustainable Propulsion Systems, Graz University of Technology, Austria

Introduction

Anion exchange membrane water electrolysis (AEM-WE) is one promising way of producing hydrogen from renewable energy and has the potential to combine the advantages of both predominant low-temperature electrolysis technologies, alkaline (AEL) and proton exchange membrane (PEM) water electrolysis. Like PEM-WE, AEM-WE allows a compact cell design and the operation under differential pressure; however, paired with non-precious metal catalysts in mild alkaline environment. Still, AEM-WE faces many challenges, such as short lifetime or low current densities, to become an industrially relevant electrolysis system. Advanced measurement methods have to be applied to optimize each component in the cell, in particular the membrane, catalysts and electrode structure [1].
Fig. 1 depicts the wide range of dynamic processes, loss mechanisms and ageing effects in electrochemical cells. Different measurement tools can be used to characterize, separate and quantify these processes. While time domain-based measurements access slow processes like degradation effects and changes in catalytic properties, frequency domain-based measurements e.g., electrochemical impedance spectroscopy (EIS), deconvolute phenomena in the order of 10^{-6}-10^{2} s.

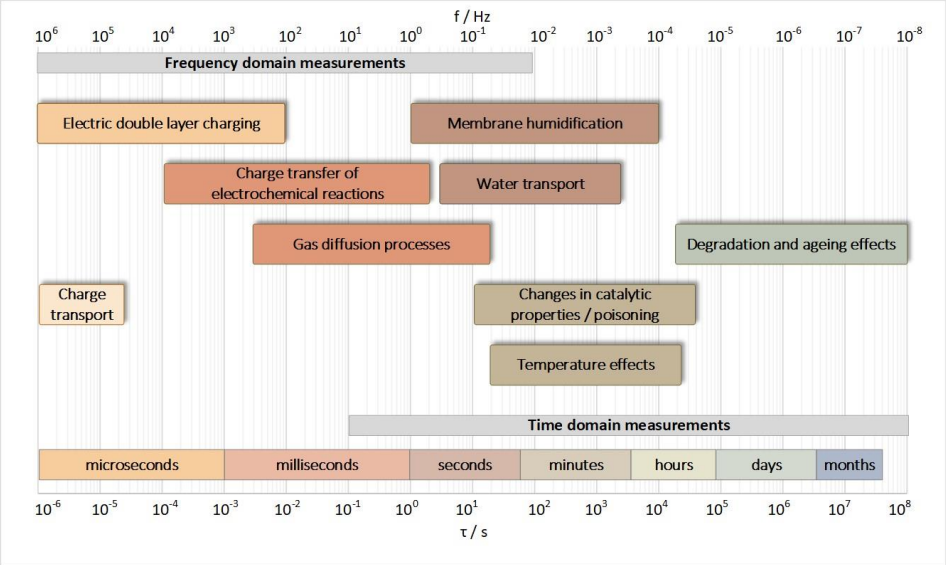

Figure 1: Overview of the wide range of dynamic processes in electrochemical cells. (Adopted from [5])

* Corresponding author: ranz@hycenta.at

EIS constitutes an excellent in-situ, non-destructive diagnostic tool for electrochemical cells. Hereby, AC-impedance analysis is used to separate the contribution of different loss mechanisms influencing the performance of an electrochemical process [2]. EIS allows to discern between the various phenomena on the basis of the different relaxation times of the single processes upon a change in the operating parameters such as potential, current density, temperature and membrane electrode assembly (MEA) characteristics [3]. Therefore, the change of impedance due to external working conditions can be used to analyze loss mechanisms and assign processes to their physical origin in order to optimize the electrochemical device [5].

Methodology

Results of EIS measurements are commonly presented as Nyquist or Bode plots. The shape of the Nyquist plot allows to distinguish between different diffusion processes and the deviation of the double-layer capacity from ideal behavior, i.e., constant phase element behavior [5]. However, interpretation of the data is often complex and not directly accessible.
One possible method to describe impedance spectra is equivalent circuit model fitting (ECM). Fig. 2 depicts the most common equivalent circuit describing the frequency response of an electrolyser with two charge transfer resistances parallel to constant phase elements (CPE) and a series resistance (R_S) [5]. A parallel circuit of constant phase element (CPE) and a resistor (R) describes the double layer capacitance and charge transfer resistance of an electrode, respectively. This structure is associated with a characteristic relaxation time $\tau = R \cdot C$ and appears as depressed half-circle in the Nyquist plot.
From fig. 2 it becomes apparent that at high frequencies the constant phase elements (CPE_1 & CPE_2) become conducting and the impedance of this circuit is dominated by the series resistance (R_S) also called high frequency resistance (HFR). Therefore, the value of the R_S can be measured at the intercept of the Nyquist plot with the abscissa at high frequencies and is interpreted as the sum of ionic and electrical resistance within the cell [6].
A second intercept with the abscissa may appear at sufficiently low frequencies at steady state comprising the sum of all resistances. The low frequency resistance (LFR) corresponds to the local inclination of the polarization curve [2]. The difference of LFR and HFR describes the polarization of the electrodes due to charge transfer of electrochemical reactions or mass transport losses.

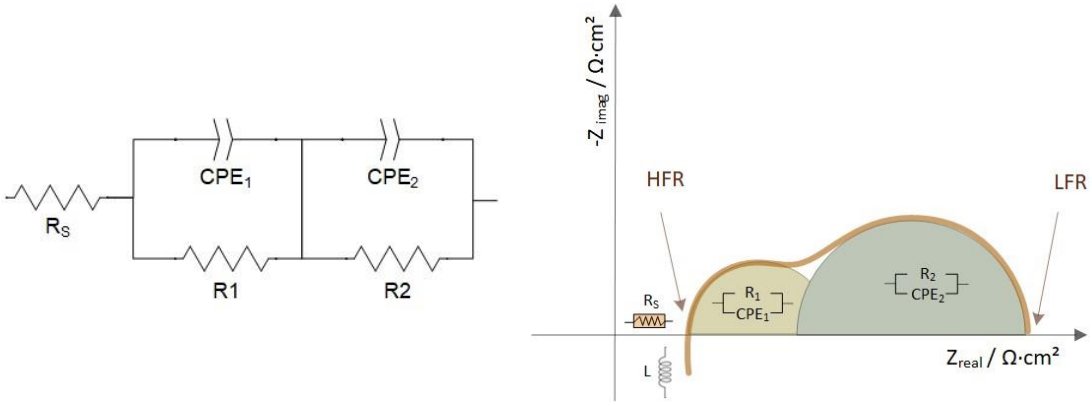

Figure 2: Standard equivalent circuit model (left) and exemplary Nyquist plot with two characteristic frequencies (right).

The ECM method provides a quick and easy possibility to separate the ohmic series resistances from polarization resistances [3]. However, further analysis and quantitative interpretation with ECM of EIS data requires prior knowledge of the equivalent circuit especially concerning the number and size of the polarization processes. Fig. 3 shows the impedance analysis of an AEM-WE cell with ECM method. An equivalent circuit with 3 R-CPE parallel circuits and one series resistance was used for this analysis. The result yields the magnitude of 3 different resistances in dependence on the current density, but gives no further insight on the origin or characteristics of these loss mechanisms.

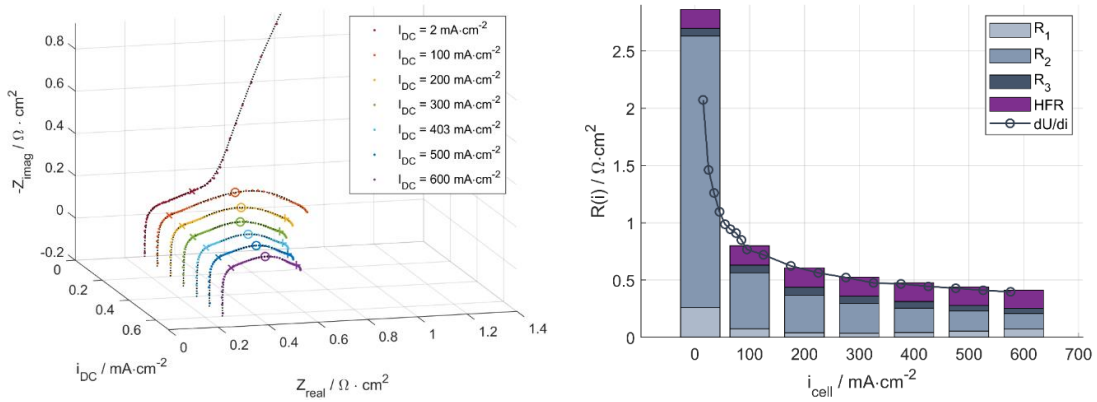

Figure 3: Nyquist plot at AEM-WE cell at varying current densities (left) and corresponding analysis with ECM method (right).

Another possibility to analyse EIS spectra is to transfer the data into the time domain and characterize the different mechanisms by their relaxation time constants. The distribution of relaxation times (DRT) $\gamma(\ln\tau)$ is extracted from the model impedance using eq. (1).

$$Z_{model}(\omega) = R_S + \int_{-\infty}^{\infty} \frac{\gamma(\ln\tau)}{1+i\omega\tau} dln\tau \qquad (1)$$

Eq. 1 describes a resistance (R_S) in series with an infinite number of serially connected RC parallel elements [8]. From a mathematically point of view eq. (1) describes a Fredholm integral of the first kind, known as an 'ill-posed inverse problem'. One solution to this problem is given by ridge or Tikhonov regularisation with the introduction of a regularisation parameter [9].

Different electrochemical systems have been analysed using DRT-methods in literature including solid oxide fuel cells (SOFC), PEM fuel cells (PEM-FC), PEM-WE and AEM fuel cells (AEM-FC). Fig. 4 illustrates the conclusions of different research groups in the field of electro chemistry. They have analysed electrochemical cells with DRT methods and attributed occurring loss mechanisms to the origin of: water transport, gas transport, charge transfer of the oxygen evolution reaction (CT of OER), charge transfer of hydrogen evolution reaction (CT of HER) and ion-, H^+-, OH^--transport in the catalyst layer. For fuel cells the according electrochemical reactions are the hydrogen oxidation reaction (HOR) and the oxygen reduction reaction (ORR).

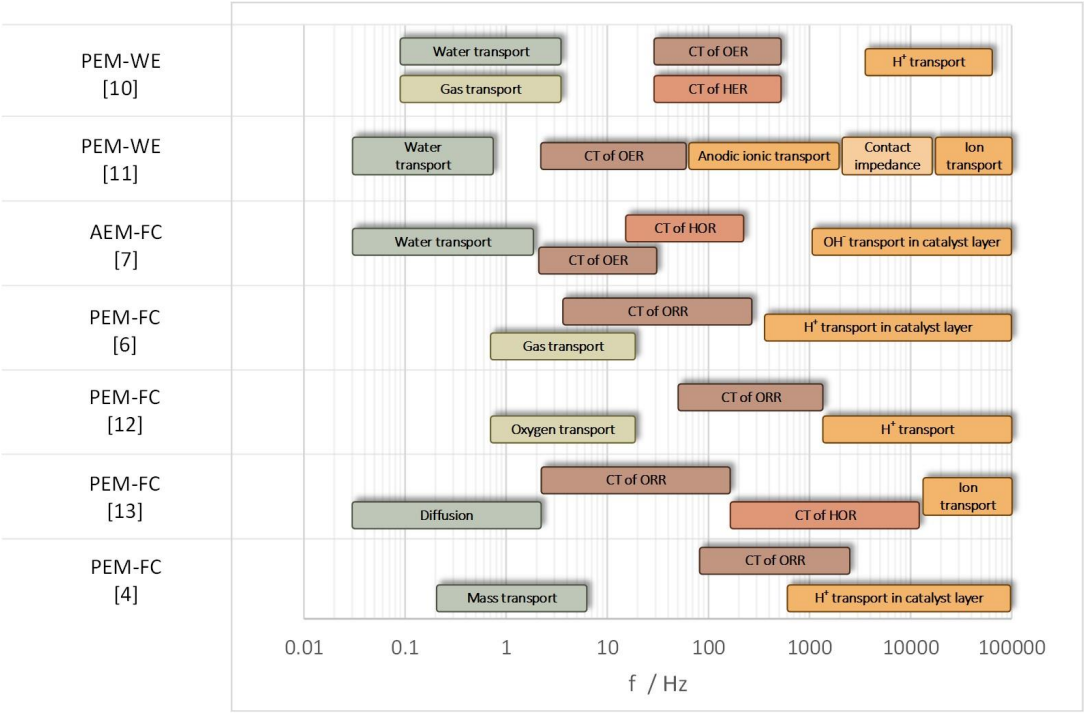

Figure 4: Literature review on relaxation processes in different electrochemical applications.

In fig. 4 a consent in literature about the characteristic frequencies of different loss mechanisms seems to exist:

1. There are three main loss mechanisms in electrochemical systems: Mass transport, charge transfer of electrochemical reactions and ion transport.
2. Mass transport appears in the frequency range of 0.05 – 10 Hz and can be further separated into water transport and gas transport. Water transport is considered to be the slower mechanism.
3. Charge transfer appears in the frequency range of 5 – 1000 Hz and can be split into the half-cell reaction OER and HER or ORR and HOR for electrolysers and fuel cells, respectively. The OER includes the transfer of four electrons and is therefore considered the more challenging and slower reaction in comparison to the HER [10].
4. Characteristic frequencies above 1000 Hz are often interpreted as ion transport phenomena in the catalyst layer. Dependent on the technology used, this may be proton (H^+) transport or anion (OH^-) transport. Different from ion transport through the membrane, modelled as series resistance, ion transport in the catalyst layer exhibits a capacitive portion which is expressed as polarization resistance in the high-frequency part of the spectrum.

Discussion

Electrochemical impedance spectroscopy is an excellent in-situ, non-destructive diagnostic tool for AEM-WE cells. Different methods of evaluation like ECM or DRT analysis have been applied extensively to EIS results to gain deeper understanding of the underlying physical processes. While the ECM model requires prior knowledge of the electrochemical process at hand, the DRT method offers a tool to analyze spectra regardless of further assumptions. However, an optimization parameter has to be chosen in order to restrict the resolution of the appearing characteristic frequencies.

Characteristic frequencies of electrochemical processes seem to be independent from the technical application to some extent. Therefore, results from PEM-WE, PEM-FC and AEM-FC can be transferred and compared to AEM-WE. To the best of the authors knowledge, no DRT analysis has been conducted on AEM-WE cells yet. This work strives to fill that gap.

Conclusions

AEM-WE cells are a promising alternative to the predominant electrolysis technologies PEM-WE and AEL. To further improve the technology readiness level and long-term stability of the cells, a profound understanding of loss and degradation mechanisms is necessary. EIS offers an in-situ diagnostic tool to characterize electrochemical devices. However, the interpretation of results is often difficult and an in depth understanding of the underlying phenomena is not entirely present in literature. Two possible methods are presented to interpret EIS spectra and their short cummings are discussed. The proposed methods shall be applied in the context of AEM-WE cells and the results will be compared to results in PEM-WE, PEM-FC and AEM-FC technology.

References

[1] Ranz, M.; Grabner, Bianca; Christine, Bandl; Kern, Wolfgang; Wegleiter, Hannes; Schweighofer, Bernhard; Trattner, Alexander (2023): AEM-Water Electrolysis – The Best of two Worlds, Conference: EFCF 2023: Low-Temp. Fuel Cells, Electrolysers & H2 Processing, Luzern Schweiz. https://www.efcf.com/2023

[2] Elsøe, K.; Grahl-Madsen, L.; Scherer, G. G.; Hjelm, J.; Mogensen, M. B. (2017): Electrochemical Characterization of a PEMEC Using Impedance Spectroscopy. In: J. Electrochem. Soc. 164 (13), F1419-F1426. DOI: 10.1149/2.0651713jes.

[3] Siracusano, Stefania; Trocino, Stefano; Briguglio, Nicola; Baglio, Vincenzo; Aricò, Antonino S. (2018): Electrochemical Impedance Spectroscopy as a Diagnostic Tool in Polymer Electrolyte Membrane Electrolysis. In: Materials (Basel, Switzerland) 11 (8). DOI: 10.3390/ma11081368.

[4] Wang, Haijiang; Yuan, Xiao-Zi; Li, Hui (Hg.) (2012): PEM fuel cell diagnostic tools. Boca Raton, London, New York: CRC Press (PEM fuel cell durability handbook). Online verfügbar unter https://www.taylorfrancis.com/books/9780429106255.

[5] Wagner, Norbert und Bauder, Alexander und Friedrich, Andreas (2011) Diagnostics of PEM fuel cells. 2nd International Workshop on Degradation Issues in Fuel Cells, 21.-23. Okt. 2011, Thessaloniki, Greek.

[6] Heinzmann, Marcel; Weber, André; Ivers-Tiffée, Ellen (2018): Advanced impedance study of polymer electrolyte membrane single cells by means of distribution of relaxation times. In: Journal of Power Sources

[7] Sediva, Eva; Bonizzoni, Simone; Caielli, Tommaso; Mustarelli, Piercarlo (2023): Distribution of relaxation times as an accessible method to optimize the electrode structure of anion exchange membrane fuel cells. In: Journal of Power Sources 558, S. 232608. DOI: 10.1016/j.jpowsour.2022.232608.

[8] Wan, Ting Hei; Saccoccio, Mattia; Chen, Chi; Ciucci, Francesco (2015): Influence of the Discretization Methods on the Distribution of Relaxation Times Deconvolution: Implementing Radial Basis Functions with DRTtools. In: Electrochimica Acta 184, S. 483–499. DOI: 10.1016/j.electacta.2015.09.097.

[9] Saccoccio, Mattia; Wan, Ting Hei; Chen, Chi; Ciucci, Francesco (2014): Optimal Regularization in Distribution of Relaxation Times applied to Electrochemical Impedance Spectroscopy: Ridge and Lasso Regression Methods - A Theoretical and Experimental Study. In: Electrochimica Acta 147, S. 470–482. DOI: 10.1016/j.electacta.2014.09.058.

[10] Li, Jiangtian (2022): Oxygen Evolution Reaction in Energy Conversion and Storage: Design Strategies Under and Beyond the Energy Scaling Relationship. In: Nano-micro letters 14 (1), S. 112. DOI: 10.1007/s40820-022-00857-x.

[11] Giesbrecht, Patrick K.; Freund, Michael S. (2022): Investigation of Water Oxidation at IrO 2 Electrodes in Nafion-Based Membrane Electrode Assemblies Using Impedance Spectroscopy and Distribution of

Relaxation Times Analysis. In: J. Phys. Chem. C 126 (42), S. 17844–17861. DOI: 10.1021/acs.jpcc.2c05104.

[12] Wang, Qing; Xu, Liangfei; Hu, Zunyan; Li, Jianqiu; Chen, Guangming; Dai, Wei; Ouyang, Minggao (2020 - 2020): Analysis of fuel cell impedance characteristics at high current density based on distribution of relaxation times. In: 2020 4th CAA International Conference on Vehicular Control and Intelligence (CVCI). 2020 4th CAA International Conference on Vehicular Control and Intelligence (CVCI). Hangzhou, China, 18.12.2020 - 20.12.2020: IEEE, S. 53–58.

[13] Wang, Haijiang; Yuan, Xiao-Zi; Li, Hui (Hg.) (2012): PEM fuel cell diagnostic tools. Boca Raton, London, New York: CRC Press (PEM fuel cell durability handbook). Online verfügbar unter https://www.taylorfrancis.com/books/9780429106255

Investigation and implementation of critical-raw-materials reduced catalysts for proton exchange membrane water electrolysis

Mafalda Pina*[1,2,3], Yury V. Kolen'ko[3], O. Salomé G. P. Soares[1,2]

[1]LSRE–LCM – Laboratory of Separation and Reaction Engineering – Laboratory of Catalysis and Materials, Faculty of Engineering, University of Porto, Rua Dr. Roberto Frias, 4200-465 Porto
[2]ALiCE – Associate Laboratory in Chemical Engineering, Faculty of Engineering, University of Porto, Rua Dr. Roberto Frias, 4200-465, Porto, Portugal
[3]Nanochemistry Research Group, International Iberian Nanotechnology Laboratory, Avenida Mestre José Veiga, 4715-330 Braga, Portugal

Introduction

Renewable H_2 is considered one of the key solutions to meet the 2050 climate neutrality goals of the EU Green Deal [1]. Unfortunately, vast majority of the current H_2 production in EU is based on steam reforming of fossil fuels that gives rise to a large emission of undesired greenhouse gases [2]. Hence, the implementation of efficient and low-cost water electrolysis for renewable H_2 generation is very important for decarburization of EU industries [3]. At the same time, current water electrolysis technologies are quite expensive in comparison with steam reforming. For example, one of the prominent technologies for renewable H_2 production is proton exchange membrane electrolysis (PEMEL), conducted in compact PEM electrolyzers with high power density [2]. Nevertheless, PEMEL is an expensive technology, and one of the reasons for this is the employment of platinum-group-metals (PGMs) as catalysts [4], which are rare and expensive plus belong to the EU Critical Raw Materials (CRMs) list [5]. Thus, reducing the PGMs usage in PEMEL is critical for widespread uptake of the technology for renewable H_2 generation.

PEM electrolyzer is a zero-gap stack of cells composed of a proton exchange membrane coupled to a catalyst and electrode on each side, anode and cathode [2]. Figure 1 shows a simplified scheme of the different layers that compose a PEMEL single cell. From top to bottom: (*i*) bipolar plate (BPP) – serves to conduct current and heat, and distribute water uniformly through the area of the cell, usually with flow fields; (*ii*) the porous transport layer (PTL) – mediates the passage of reactants/products and also function as an electrical current connector between the catalyst layer and the BPP; (*iii*) anode catalyst to promote the oxygen evolution reaction (OER); (*iv*) proton exchange membrane (PEM) – allows the permeation of protons (H^+) from the anode to the cathode side; (*v*) cathode catalyst promotes the hydrogen evolution reaction (HER); and again (*vi*) a PTL and (*vii*) a BPP at the cathode side with the same functions as the anode ones. The membrane, besides the obvious proton exchange mediator, also serves as a physical separator/barrier between the reaction products and is an electronic insulator between the anode and cathode [6]. Currently, state-of-the-art PEMEL cell performance is 2 A/cm^2 at 2 V, and it can operate with high pressure of around 50 bar [7].

* Corresponding author: mafalda.pina@inl.int

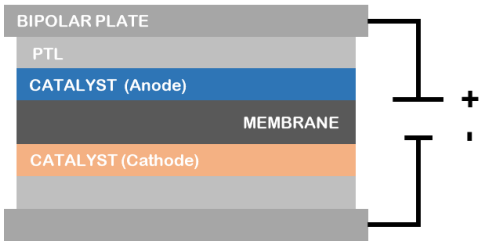

Figure 1: Scheme of a PEMEL single cell.

In PEMEL, conductive carbon supported Pt is the state-of-the-art cathode catalyst, efficiently and stably driving the HER, with typical loading of 0.4 mg/cm^2 [8] in commercial systems. The best anode catalysts for the OER in acidic conditions of PEM are oxides based on Ir and Ru, with loading between 0.8 and 2 mg/cm^2. Pt, Ir, and Ru are scarce and expensive PGMs (Pt in less extent), and simultaneously, they are considered CRMs in the EU with high economic importance and supply risk [9]. Evidently, a drastic reduction and/or elimination of PGM catalysts is urgently needed to enable prevalent implementation of PEMEL, and this is the main objective of the current study.

In this work, new earth abundant catalysts are prepared – PGM-free HER catalyst and IrO_x with reduced loading as OER catalyst. Synthesized materials are first studied individually, focusing on materials structural and morphological characterization, as well as their electrochemical HER and OER behavior using three-electrode configuration. Characterization will include different techniques to assess materials morphology, composition, electrochemical activity, and stability. The best-performing catalysts are tested in single-cell PEMEL and the obtained results are discussed.

Methodology

Powder X-ray diffraction (XRD) was performed on a X´Pert PRO diffractometer (PANalytical) set at 45 kV and 40 mA while using a Cu K_α radiation source (λ = 1.541874 Å). Half-cell electrochemical characterization in a three-electrode assembly was conducted using a Biologic VMP-3 potentiostat/galvanostat. For HER, as counter and reference electrodes, a platinum wire and a saturated calomel electrode (SCE) were used, respectively, in 0.5 M H_2SO_4 electrolyte. The working electrode was catalyst-coated carbon paper with an area of 1 cm^2 and a loading of 1 mg/cm^2. For OER, a glassy carbon rod with 3 mm diameter was coated with the catalyst ink, wherein the catalyst loading was 0.1 mg/cm^2. Catalysts ink preparation was very similar for both half-cell reactions. For HER catalyst the ink was prepared by mixing in an ultrasound bath 5 mg of the catalyst powder, 750 µL deionized water, 250 µL ethanol and 10 µL of Nafion ionomer solution (5% v/v Nafion solution), for more than 1 h before drop casting the ink into the carbon paper with a micropipette. For OER, the only difference was the amount of catalyst powder weighted, only 2.5 mg. Cyclic voltammetry (CV) and linear sweep voltammetry (LSV) curves were obtained for all tested catalysts after an initial catalyst's activation for 20-50 cycles. For some samples, chronoamperometry (CP) was also performed. This test is important in the future for assessing catalysts stability over a longer period of time. All the electrochemical results are presented against the RHE potential and are 85% *iR*-corrected.

Cathodic HER current state-of-the-art catalyst is Pt supported on carbon. In the present work, total substitution of Pt is intended. The nature of the reaction allows the use of more earth abundant materials with good activity and stability results, without the need to deploy CRMs. First, transition metal phosphides (TMP) were prepared, adapting the procedure from Brito and co-workers [10]. Iron(III) nitrate nonahydrate (Alfa Aeser) was used as transition

metal precursor. Carbon black Vulcan XCmax 22 (CABOT) was used as conductive carbon support. Incipient wet impregnation method was used, adding an aqueous solution containing Fe dropwise onto the carbon support in an ultrasonic bath. After 1 h of sonication, the prepared materials were dried in an oven at 100 °C overnight. Weight loading tested were 15, 20, and 25% (wt. %) of Fe. The process was followed by a thermal treatment in a vertical furnace under nitrogen atmosphere for 1 h with subsequent reduction under hydrogen atmosphere at 400 °C for 3 h, with 100 cm^3/min gas flow. After cooling down to the room temperature under nitrogen flow, 0.3 g of the samples were transferred into a horizontal furnace where phosphorization takes place. Inside the same reactor, 0.25 g of red phosphorus was also placed, and it was heated to 500 °C for 1 h followed by a reduction of temperature to 250 °C for 12 h. Phosphorization was conducted under 100 cm^3/min nitrogen flow. Characterization of the prepared catalysts occurred before and after the phosphorization step, to confirm the phosphorization success and increased activity.

For the OER reaction, the initial studies focused on the synthesis of iridium oxide IrO_x through a wet method, with the intention to use this as base material to be supported on conductive oxide materials with higher surface area. For that, by adapting the reported procedure from Ruiz Esquius and co-works [11], iridium oxide was prepared. In a round bottom flask, 1 mmol of $IrCl_3$ and 8 mmol of Li_2CO_3 were dissolved in 25 mL of deionized water and stirred overnight at room temperature. The yellow solution was then refluxed for 3 h, and the obtained blue precipitate was centrifuged several times while washing with deionized water. Afterwards, it was left to dry at room temperature, and the obtained blue powder was crushed in a mortar and stored. Commercial conductive antimony-doped tin oxide (ATO) from Thermo Scientific was used as support, being added to the $IrCl_3$ and Li_2CO_3 solution prior to reflux, testing different wt. % ratios between the IrO_x and the ATO. Iridium(IV) oxide, Premion®, 99.99% (metals basis) from Alfa Aesar was used without any treatment or purification as reference to the as-prepared IrO_x.

For the single-cell PEMEL testing, a 4 cm^2 active area cell was used, connected to an in-house build support system. Initially, commercially available membrane electrode assembly (MEA) with state-of-the-art catalysts (QuinTech) is tested in this system. These results help to optimize the characterization protocol and serve as benchmarks for comparison reasons with MEAs having the synthesized catalysts.

Results

HER catalyst

The synthesized carbon-supported samples were analyzed by XRD for the 20% impregnated Fe catalysts before and after phosphorization, represented in

Figure 2a, in black and red, respectively. The black pattern indicates that the Fe/C is a phase mixture of metallic iron (ICDD no. 04-012-6482) and iron oxide (ICDD no. 00-006-0615). The red pattern indicates that the phosphorization was successful, confirming the formation of iron phosphide HER catalyst (ICDD no. 00-039-0809) supported on carbon (FeP/C).

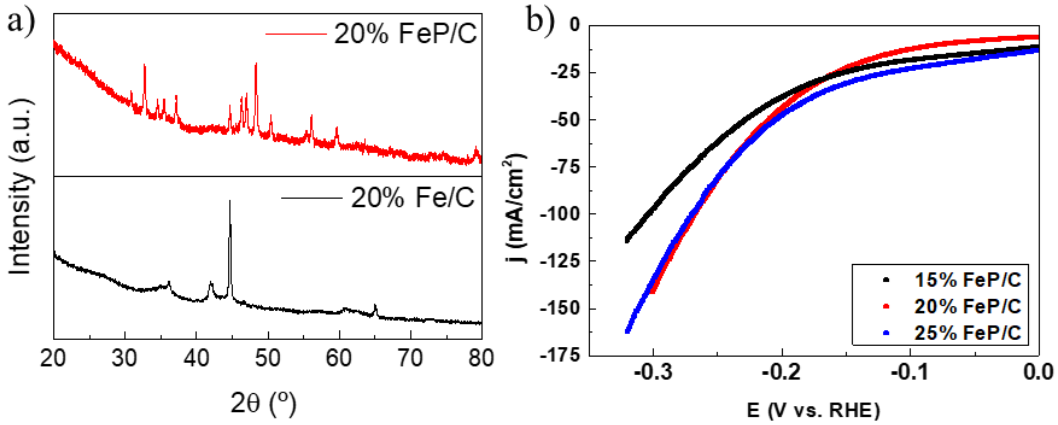

Figure 2. *a)* XRD patterns for 20% iron impregnated Fe/C precursor material (black pattern) and final iron phosphide FeP/C HER catalyst (red pattern) synthesized by phosphorization. b) HER cathodic polarization curves recorded for the synthesized FeP/C catalysts with different loadings. All polarization curves were 85% *iR*-compensated. Scan rate = 5 mV/s. Electrolyte = 0.5 M H_2SO_4.

For the electrochemical characterization, the LSV curves obtained for the different carbon-supported iron % catalysts were plotted against RHE reference value, in Figure 2b. The 15 % FeP/C is the less active catalyst with an overpotential at 100 mA/cm2 of 0.3 V. Both the 20 % and 25 % catalysts present a similar overpotential of 0.27 V.

OER catalyst

The prepared iridium oxide (IrO_x) was electrochemically tested and compared to commercial IrO_2 from Alfa Aeser (denoted as IrO_2_AA). The activity, Figure *3*Figure 3a, is superior for the synthesized catalyst compared to the commercial powder with a difference of overpotential at 10 mA/cm^2 between the catalysts of 120 mA/cm^2 (0.28 V and 0.4 V, respectively). This can be related to the phase of iridium present in each catalyst, since amorphous IrO_x has better activity than crystalline IrO_2 [12], but IrO_x can also have other amorphous phases still present from lithium, for example. Further studies and characterizations need to be performed to determine the real composition of the synthesized catalyst.

To assess the stability of the catalysts, chronoamperometry (CP) was performed in the same three electrode setup, at 10 mA/cm^2 for 2 h. In Figure 3b, IrO_x results show an increase of 50 mV of potential measured by the end of the 2 h. The stability for the commercial IrO_2_AA was also tested and, according to Xu and co-workers [12] it should be better, being more stable, with less potential increase (since it is crystalline). That was not the result obtained, as can be seen in the same graph. After 1.5 h the measurement was stopped to not damage the glassy carbon electrode, since the potential had already increased more than 100 mV and the tendency seemed to be increasing exponentially. This might be due to changes in the catalyst, having less active site, thus increasing the resistance. Detachment of the catalyst layer could also occur. There were no signs of such problem, but further testing should be carried out to understand what is really happening – analyzing the electrolyte after the measurement can give information about some catalyst material detaching or not.

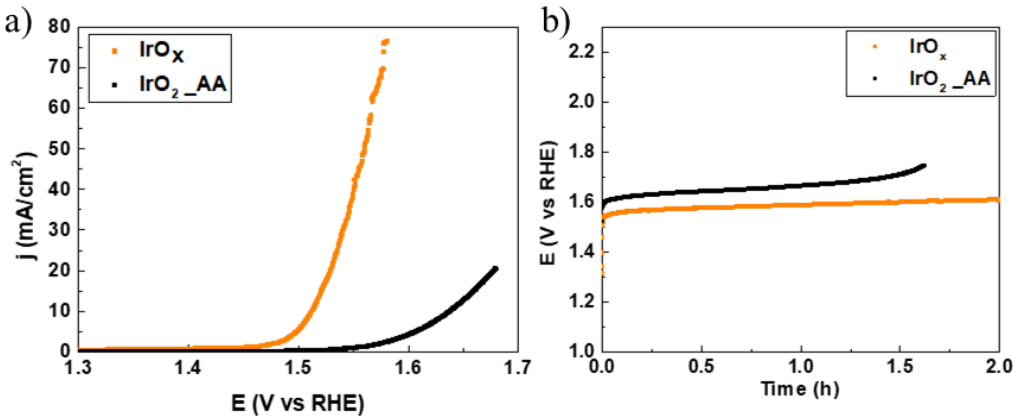

Figure 3. a) Catalytic activity and b) chronoamperometry at 10 mA/cm^2 results for the prepared IrO_x and commercial IrO_2 from Alfa Aeser (IrO_2_AA). All polarization curves are 85% *iR*-compensated. Scan rate = 5 mV/s. Electrolyte = 0.5 H_2SO_4.

The activity for the prepared IrO_x catalysts with ATO was measured through LSV, represented in Figure 4a. The current density obtained for the IrO_x is in accordance with the expected [11]. The overpotential at 10 mA/cm^2 for the IrO_x is around 270 mV, almost the same obtained for the catalyst 70%IrO_x/30%ATO. Further characterization of the latter sample is required to understand the increase in activity when compared to the other ATO supported catalysts. The catalysts with less content of IrO_x have lower activity and increased overpotential. The electrochemical stability for the ATO supported IrO_x catalysts was tested through CP, and the results are compared with the unsupported iridium catalysts in Figure 4b. As noted in the LSV, the necessary potential is superior for catalysts containing ATO, with similar stability between the unsupported and the 70% IrO_x containing catalysts. For the catalyst 50%IrO_x/50%ATO, the measurement had to be stopped before achieving the 2 h since the potential was increasing rapidly and could damage the glassy carbon electrode.

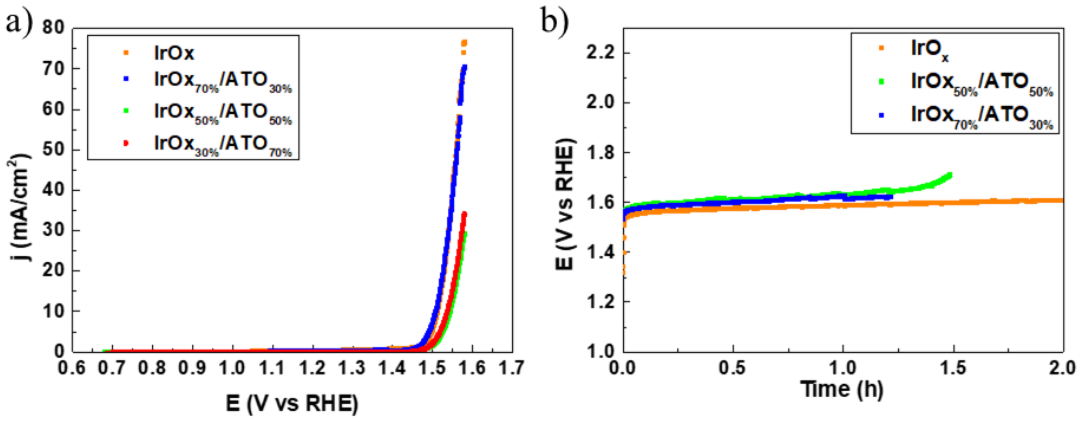

Figure 4. a) OER anodic polarization curves recorded for the synthesized IrO_x and ATO-supported catalysts. b) CP for the unsupported and ATO-supported IrO_x . Current applied = 10 mA/cm^2. All polarization curves are 85% *iR*-compensated. Scan rate = 5 mV/s. Electrolyte = 0.5 H_2SO_4.

Conclusions

The presented work is part of the PhD thesis of the corresponding author. Catalysts for both anode and cathode of a PEMEL have already been prepared, following current state-of-the-art and research on the topic. CRM free catalyst based on iron phosphide supported on carbon has been prepared for HER reaction. It is planned the functionalization of the carbon support and the implementation of other transition metals. For the anode catalyst the study started with the

synthesis of iridium oxide. Aiming for the reduction of CRM in the OER catalyst, ATO was added to the IrO_x synthesis as conductive supporting material. Further analysis of the prepared catalysts is required, namely the use of microscopy techniques and determination of the electrocatalytic surface area. One of the most important steps in the PhD work is the implementation of the best-performing catalysts in three-electrode configuration in the single-cell PEMEL testing.

Acknowledgments

This work was financially supported by LA/P/0045/2020 (ALiCE), UIDB/50020/2020, and UIDP/50020/2020 (LSRE-LCM), funded by national funds through FCT/MCTES (PIDDAC). Mafalda Pina acknowledges the PhD research grant from FCT (2021.08790.BD), funded by national funds and by the European Union (EU) through the European Social Fund (ESF). O.S.G.P.S. acknowledges FCT funding under the Scientific Employment Stimulus – Institutional Call CEECINST/00049/2018.

References

[1] European Commission, “European Green Deal.” [Online]. Available: https://commission.europa.eu/strategy-and-policy/priorities-2019-2024/european-green-deal_en

[2] M. Carmo, D. L. Fritz, J. Mergel, and D. Stolten, “A comprehensive review on PEM water electrolysis,” *International Journal of Hydrogen Energy*, vol. 38, no. 12. pp. 4901–4934, 2013. doi: 10.1016/j.ijhydene.2013.01.151.

[3] IEA, “The Future of Hydrogen,” 2019.

[4] A. Holland, “Green Hydrogen Production: Electrolyzer Markets 2023-2033,” 2023. [Online]. Available: www.IDTechEx.com/electrolyzer/research@IDTechEx.com

[5] European Comission, “Critical Raw Materials.”

[6] B. Bladergroen, H. Su, S. Pasupathi, and V. Linkov, “Overview of Membrane Electrode Assembly Preparation Methods for Solid Polymer Electrolyte Electrolyzer,” in *Electrolysis*, InTech, 2012. doi: 10.5772/52947.

[7] M. Chatenet *et al.*, “Water electrolysis: from textbook knowledge to the latest scientific strategies and industrial developments,” *Chem Soc Rev*, vol. 51, no. 11, pp. 4583–4762, May 2022, doi: 10.1039/D0CS01079K.

[8] M. Clapp, C. M. Zalitis, and M. Ryan, “Perspectives on current and future iridium demand and iridium oxide catalysts for PEM water electrolysis,” *Catal Today*, vol. 420, p. 114140, 2023, doi: 10.1016/j.cattod.2023.114140.

[9] R. J. Ouimet, J. R. Glenn, D. De Porcellinis, A. R. Motz, M. Carmo, and K. E. Ayers, “The Role of Electrocatalysts in the Development of Gigawatt-Scale PEM Electrolyzers,” *ACS Catalysis*. American Chemical Society, pp. 6159–6171, 2022. doi: 10.1021/acscatal.2c00570.

[10] J. Brito *et al.*, “Implementation of Transition Metal Phosphides as Pt-Free Catalysts for PEM Water Electrolysis,” *Energies (Basel)*, vol. 15, no. 5, Mar. 2022, doi: 10.3390/en15051821.

[11] J. Ruiz Esquius, D. J. Morgan, I. Spanos, D. G. Hewes, S. J. Freakley, and G. J. Hutchings, “Effect of Base on the Facile Hydrothermal Preparation of Highly Active IrOx Oxygen Evolution Catalysts,” *ACS Appl Energy Mater*, vol. 3, no. 1, pp. 800–809, Jan. 2020, doi: 10.1021/acsaem.9b01642.

[12] J. Xu *et al.*, “IrO x ·nH 2 O with lattice water-assisted oxygen exchange for high-performance proton exchange membrane water electrolyzers,” 2023. [Online]. Available: https://www.science.org

Investigation of hydrogen bubble growth in alkaline water electrolysis using an immersed boundary method

F. Khalighi[*1], Y. Tang[1,2], N.G. Deen[1,2], A.W. Vreman[1,2,3]

[1]Power and Flow Group, Department of Mechanical Engineering, Eindhoven University of Technology, Eindhoven, the Netherlands
[2]Eindhoven Institute for Renewable Energy Systems (EIRES), Eindhoven University of Technology, Eindhoven, the Netherlands
[3]Nobian Industrial Chemicals, Amersfoort, the Netherlands

Introduction

Today, global energy consumption has continuously increased due to population growth and lifestyle standards. In addition, with the increase of global warming and environmental pollution, the development of renewable energy sources has become more crucial. Hydrogen is one of the most promising clean and sustainable energy carriers since it can be produced and consumed without carbon emissions. Among the different methods of its production, the electrolysis of water has attracted significant attention because it is sustainable and renewable chemical technology [1]. A large area of research in water electrolysis is the development of active and robust electrocatalysts to improve the efficiency of water electrolysis reactions [2, 3, 4, 5]. Moreover, in order to design more efficient electrolyzers, it is important to obtain more understanding of the role of bubbles in the process. Bubbles can affect the efficiency of electrolysis in different ways, for instance by decreasing the active electrode surface or by increasing the cell resistance [6, 7, 8, 9]. Improved removal of bubbles is therefore expected to increase the efficiency of the electrolyzer. The bubble evolution behavior on the electrode surface has been studied by several theoretical and experimental methods. The bubble growth behavior is expected to be closely related to the mass transport caused by gradients of the dissolved hydrogen concentration, and also to coalescence [10]. So understanding the dynamics of bubble evolution and mass transport might aid in developing strategies to improve the efficiency of the water electrolyzers. In this study, we investigate how fast a bubble grows. Our approach is direct numerical simulation (DNS), for which we use a sharp immersed boundary method combined with an artificial compressibility method for pressure. Before presenting and discussing the results and summarizing our findings in the conclusions, details of the model and numerical methods are provided in the following sections.

Mathematical and numerical modelling

To simplify the complicated mathematical description of a bubble growing at an electrode in the presence of a surrounding flow, we make several assumptions in this paper: constant temperature, no evaporation of water and equal mass diffusivity coefficients of ions ($D_{K^+} = D_{OH^-}$). Due to these simplifications, no equation for the thermal energy is needed, and the equation for the electric potential remains relatively simple. Potassium hydroxide (KOH) is used as electrolyte. At the cathode, water molecules are reduced by electrons to hydrogen and hydroxide ions as follows:

$$2H_2O + 2e^- \rightarrow 2H_2 + 2OH^- \quad (1)$$

* Corresponding author: f.khalighi@tue.nl

Governing equations

In this study, we solve the 3D unsteady Navier Stokes equations for a viscous incompressible flow assuming constant density and viscosity:

$$\nabla \cdot \mathbf{u} = 0;\ \frac{\partial \mathbf{u}}{\partial t} + (\mathbf{u} \cdot \nabla)\mathbf{u} = -\frac{1}{\rho_f}\nabla p + \nu \nabla^2 \mathbf{u} \quad (2)$$

In these equations **u,** p, ν and ρ_f represent, respectively, the fluid velocity, the pressure relative to the ambient pressure, kinematic viscosity and the density of the fluid. The concentration transport equation using the Nernst-Planck equation is given by [11, 12, 13]:

$$\frac{\partial c_k}{\partial t} = -\nabla \cdot \mathbf{N}_k;\ \mathbf{N}_k = -z_k \frac{D_k}{R_u T} F c_k \nabla \phi - D_k \nabla c_k + c_k \mathbf{u} \quad (3)$$

$\mathbf{N}_k$, z_k, D_k, c_k are the flux vector, the charge, the mass diffusion coefficient and the molar concentration of species k, respectively. k can be H_2, H_2O, K^+, OH^- or KOH. $z_{K^+} = 1$, $z_{OH^-} = 1$, and $z_k = 0$ for other k. Here, F is Faraday's constant, R_u is the universal gas constant, T is the absolute temperature and ϕ is the electric potential. Formally, equation 3 is valid for dilute concentrations and they imply a variable density. For the sake of simplicity, we use these equations for all concentrations in combination with a velocity field based on constant density.

The electrical current density (**i**) in the solution is defined by Faraday's law as follows [11, 12]:

$$\mathbf{i} = F \sum_k z_k \mathbf{N}_k \quad (4)$$

Substituting Eq. 3 into Eq. 4, we obtain:

$$\mathbf{i} = -F^2 \nabla \phi \sum_k \frac{z_k^2 D_k}{R_u T} c_k - F \sum_k z_k D_k \nabla c_k + F \mathbf{u} \sum_k z_k c_k \quad (5)$$

The solution is electrically neutral, so the last term on the right side of the equation is zero. Electroneutrality provides the condition to express the ions (K^+ and OH^-) concentration as a single salt concentration ($c_{K+} = c_{OH-} = c_{KOH}$) [11, 12] . As already mentioned, in this research, $D_{K+} = D_{OH-}$ is considered. These conditions result in the second term on the right side of the equation being zero. This reduces Equation 6 to Ohm's law:

$$\mathbf{i} = -\kappa \nabla \phi;\ \kappa = F^2 \sum_k \frac{z_k^2 D_k}{R_u T} c_k = \frac{2F^2 D_{KOH}}{R_u T} c_{KOH} \quad (6)$$

where κ is the electrical conductivity. The charge balance in the electrolyte is satisfied by the following equation for the potential:

$$\nabla . \mathbf{i} = -\nabla \cdot (\kappa \nabla \phi) = 0 \quad (7)$$

By substituting Eq. 7 into the transport equation for K^+ or OH^- we obtain the transport equation for KOH:

$$\partial c_{KOH}/\partial t = D_{KOH} \nabla^2 c_{KOH} - \nabla \cdot (c_{KOH} \mathbf{u}) \quad (8)$$

where $D_{KOH} = D_{K+} = D_{OH-}$. The equivalent diffusion coefficient of the binary salt in the general case can be found in [11, 12].

To compute the bubble radius R the ideal gas law is used:

$$\frac{4}{3}\pi R^3 = m R_U T / P_g \quad (9)$$

where m represents the number of moles of hydrogen in the bubble and R represents the bubble radius. P_g is the absolute pressure of the gas inside the bubble which is equal to:

$$P_g = P_{\text{liquid}} + 2\gamma/R \quad (10)$$

where γ is the liquid-gas surface tension. The effects of inertia and viscosity in the gas phase are ignored. The pressure difference $2\gamma/R$ is the Laplace pressure. P_{liquid} is the average value of p over the bubble interface plus the ambient operating pressure (P).

The molar flux of hydrogen across the bubble surface (S) can be obtained using Fick's first law:

$$dm/dt = \int_S D_{H_2} \nabla c \cdot \mathbf{n} dS \quad (11)$$

where **n** is the unit normal vector of the bubble surface pointing to the liquid. A detailed description of the Initial and boundary conditions can be found in [15].

Numerical solution method

Direct numerical simulations are used to solve the system of equations on a three-dimensional Cartesian grid. The numerical method has been implemented in Fortran. The method is fully explicit using first order Euler. The spatial terms are discretized using second-order central differencing on a staggered grid. The solver is coupled with a sharp interface immersed boundary method [14], which enforces the no-slip condition for the velocity at the gas-liquid interface. Furthermore, an artificial compressibility method is used to solve the pressure in the Navier-Stokes equations. The mass continuity equation and Navier-Stokes equations are not solved inside the bubble.
In the present work, this method is extended for the mass transport and potential equation. Thus, the immersed boundary method enforces that the hydrogen concentration at the interface equals the hydrogen solubility concentration (equal to the hydrogen reference concentration). It is also employed to enforce that the current density and diffusion flux of water and electrolyte concentrations are equal to zero at the interface. Again, the mass transport and potential partial differential equations are not solved inside the bubble. In contrast to the velocity components, which are defined at staggered locations, all concentrations are defined at cell centers. In the following we describe the numerical method in more detail. A detailed description of the numerical method can be found in [15].

Results and discussion

The physical parameters for the base case are presented in the Table 1. The physical properties correspond to a 30 wt% KOH solution at 80 C° (typically used in industrial alkaline water electrolysis). The distance between electrode and membrane L is 100 μm. Such a narrow gap between electrode and membrane can occur in so-called zero gap electrolysis, in which the gap between electrode and membrane is often not exactly zero, see for example [16]. The value chosen for potential difference between electrode and membrane (ϕ_1) is such that a rather high current density is obtained, around 15 kA/m^2. The value for exchange current density (i_0)was used before [17] and is representative for a smooth Nickel surface without a catalytic coating. The number of grid cells is 96^3 in the simulations, the grid is uniform, and the time step corresponding to this grid is $\Delta t = 2.02 \times 10^{-4}$ s. The 3D configuration of the case study is shown in Figure 1.

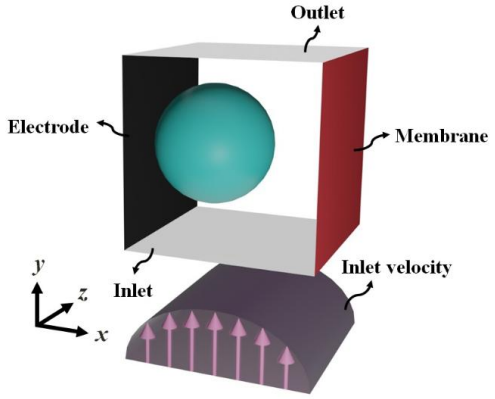

Figure 1: 3D configuration of the case study

Table 1: Physical parameters

L (μm)	100	υ (m^2/s)	6.7×10^{-7}
i_0 (A/m^2)	1	T (K)	353
P (Pa)	105	v_{inlet} (m/s)	0.67
σ (N/m)	7.7×10^{-2}	KOH (%)	30
ϕ (V)	-0.6	ρ_f (Kg/m^3)	1258
α_c	0.5	α_a	0.5

k	H_2	KOH	H_2O
D_k (m^2/s)	5.8×10^{-9}	3.2×10^{-9}	3.2×10^{-9}
$c_{k,0}$ (mol/m3)	0.16	6700	49000

Growing bubble

The bubble at the electrode grows due to the non-uniform concentration and the fact that the bubbles nucleate in areas with high supersaturation [18]. In the present study, we assume there is only one bubble (with an initial radius of 3 micrometers) on the cathode. However, in practice, new tiny bubbles do form adjacent to the bubble when the surrounding hydrogen concentration is high. Figure 2 shows snapshots of the hydrogen evolution during the growth of the bubble. Hydrogen is produced at the electrode surface, so hydrogen supersaturation at the electrode-liquid interface is greater than that in the bulk liquid.

In literature, different stages or regimes for bubble growth have been characterized by a power law: growth controlled by inertia ($R \propto t$), by diffusion ($R \propto t^{1/2}$) or by reaction ($R \propto t^{1/3}$) [19, 20]. The growth behavior $R(t) \propto t^{1/2}$ reflects a standard analytical solution for diffusive bubble growth [21, 22] The derivation is valid for a spherically symmetric concentration field, bubble radius much larger than the initial radius, constant solubility and, far away from the bubble, constant concentration and zero velocity. In our case, the concentration difference driving the bubble growth increases in time, because the hydrogen concentration averaged over the electrode increases in time. Therefore, even for a growth exponent larger than a half, the growth can be diffusion controlled. A logarithmic plot of the bubble growth rate from our simulation is shown in Figure 3. The growth between t = 0.005 s and t = 0.03 s is well described by $R(t) \propto t^{0.8}$. In a somewhat similar simulation, a case without flow over the bubble simulated using an axisymmetric method that was not an immersed boundary method, $t^{0.7}$ growth was observed [23].

Conclusions

A growing single hydrogen bubble was studied numerically. The proposed solver is verified by grid independence, mass, and momentum conversation. As the bubble behaves as a sink, the concentration of hydrogen around the bubble decreases. The simulations predict a stage with power law growth of the bubble radius ($R \propto t^{0.8}$) for a relatively large part of the total growth time. The effects of different bulk velocities and high pressure are discussed in the full paper [15]. The developed simulation tool is promising and can be used to answer fundamental questions about the bubble formation process in electrolysis processes.

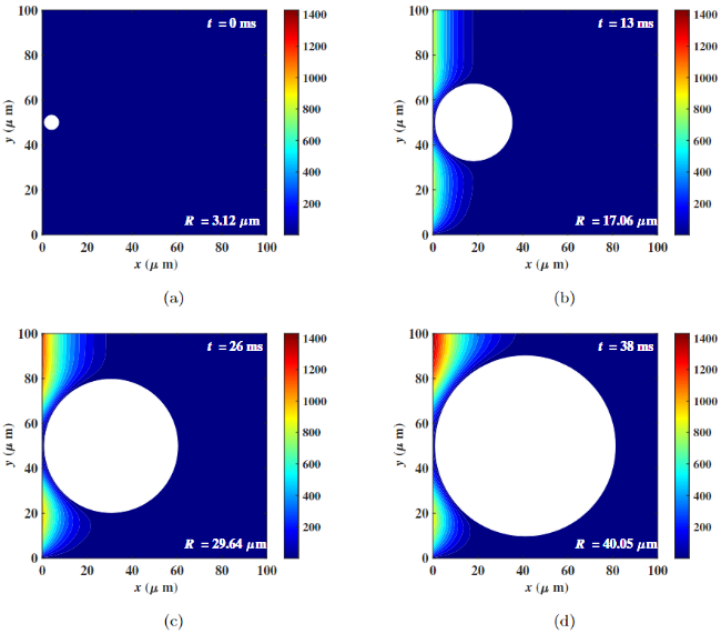

Figure 2: The dissolved hydrogen concentration normalized by $c_{H2,0}$ for a bubble growing in the x-y plane at $z/L = 0.5$ at different times.

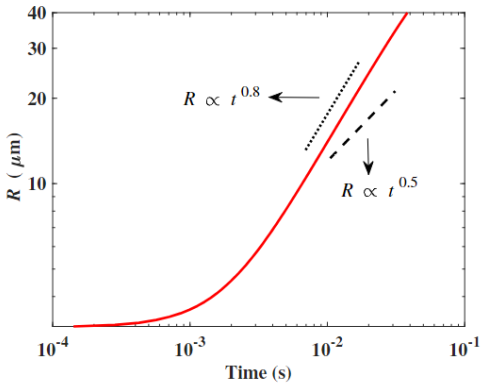

Figure 3: The growth of radius $R(t)$ versus time for a single bubble. The dotted and dashed lines refer to the power laws $R \propto t^{0.8}$ and $R \propto t^{0.5}$, respectively.

Acknowledgments

This research received funding from the Dutch Research Council (NWO) in the framework of the ENW PPP Fund for the top sectors [and from the Ministry of Economic Affairs in the framework of the PPS-toeslagregeling], grant number 741.019.201. Additionally, the research is funded by Shell, Nobian and Nouryon.

References

[1]“Hydrogen Generation by Water Electrolysis”, doi: 10.5772/intechopen.76814.

[2]“Highly Active and Durable Electrocatalytic Water Oxidation by a NiB0.45/NiOx Core-Shell Heterostructured Nanoparticulate Film”, doi: 10.1016/j.nanoen.2017.05.045.

[3]“Recent Progresses in Electrocatalysts for Water Electrolysis”, doi: 10.1007/s41918-018-0014-z.

[4]“Recent Progress in Bifunctional Electrocatalysts for Overall Water Splitting under Acidic Conditions”, doi: 10.1002/celc.201900507.

[5]“Recent Progress in Electrocatalysts for Acidic Water Oxidation”, doi: 10.1002/aenm.202000478.

[6]“Growth and Detachment of Single Hydrogen Bubbles in a Magnetohydrodynamic Shear Flow”, doi: 10.1103/PhysRevFluids.2.093701.

[7]“Recent advances in methods and technologies for enhancing bubble detachment during electrochemical water splitting”, doi: 10.1016/j.rser.2019.109300.

[8]“Gas Bubbles in Electrochemical Gas Evolution Reactions”, doi: 10.1021/acs.langmuir.9b00119.

[9]“Experimental Investigation on Bubble Growth and Detachment Characteristics on Vertical Microelectrode Surface Under Electrode-Normal Magnetic Field in Water Electrolysis”, doi: 10.1016/j.ijhydene.2021.08.164.

[10]“Review-Physicochemical Hydrodynamics of Gas Bubbles in Two Phase Electrochemical Systems”, doi: 10.1149/2.1161713jes.

[11]“Electrochemical Systems”, ISBN: 0471477567, 9780471477563.

[12]“Electrochemical Engineering”, ISBN: 978-1-119-00425-7.

[13]“Three-Dimensional Coupling Numerical Simulation of Two-Phase Flow and Electrochemical Phenomena in Alkaline Water Electrolysis”, doi: 10.1016/j.ijhydene.2021.08.101.

[14]“Immersed Boundary and Overset Grid Methods Assessed for Stokes Flow Due to an Oscillating Sphere”, doi: 10.3990/1.9789036547413.

[15]“Hydrogen Bubble Growth in Alkaline Water Electrolysis: An Immersed Boundary Simulation Study”, doi: 10.1016/j.ces.2022.118280.

[16]“Ohmic Resistance in Zero Gap Alkaline Electrolysis with a Zirfon Diaphragm”, doi: 10.1016/j.electacta.2020.137684.

[17]“The Influence of Attached Bubbles on Potential Drop and Current Distribution at Gas - Evolving Electrodes”, doi: 10.1149/1.2100456.

[18]“Microcavity Electrodes Used as Single-Nucleation Site Electrodes for the Electrolysis of Water”.

[19]“Growth kinetics of bubbles electrogenerated at microelectrodes”, doi: 10.1007/BF01059288.

[20]“Influence of Bubbles on the Energy Conversion Efficiency of Electrochemical Reactors”, doi: 10.1016/j.joule.2020.01.005.

[21]“Bubble Dynamics and Cavitation”, doi: 10.1146/annurev.fl.09.010177.001045.

[22]“On the Dynamics of Phase Growth”, doi: 10.1016/0009-2509(59)80019-1.

[23]“Bubble growth in alkaline electrolysis”, MSc thesis.

Justice in a H2 economy: a Green Energy Transition Led for and by the Citizens? The Law Speaks

Alba Forns Gomez[1*]

Rijksuniversiteit Groningen – Training for a Hydrogen Economy based Renewable Energy Society in the Anthropocene (THERESA) Marie Curie Doctoral Network

Introduction

In times of crisis, citizens are more keen on publicly formulating and sharing their concerns. Climate change and global warming are the nowadays crisis that is putting the existence of Planet Earth at stake. In reaction to that, the EU and its Member States have stressed the importance of reaching a green energy transition [1]. That means, decarbonising no later than 2050 the energy systems by adopting a green hydrogen economy as the alternative to fossil fuel markets [2].

Citizenry having a stake in the energy transition can have a facilitating effect on it succeeding. Society has shown that its concerns and worries go beyond that. Therefore, for a green energy transition to become reality, the EU regulator by including a justice dimension [3] acknowledges how crucial is the role that citizens can take in it.

While citizens are participating in the electricity sector through various forms and activities, their roles or possibilities to actively take part in the hydrogen energy sector is less clear. The willingness to actively participate in the implementation of a hydrogen economy might not be shared by all. Academia has shown that the reasons behind deciding whether to participate in an energy democracy differ depending on the personal background and values that define each individual [4]. This may lead to taking biased decisions only benefitting those who decided to take a proactive role in the decision-making process and perpetrate energy injustice instead.

Energy justice requires of a decision-making process that leaves no one behind, that is, takes into account all different views and ways of engaging in the hydrogen economy to prevent it from becoming benefit-exclusive [5]. From individual to collective action, either settled and new forms of participation (e.g. energy communities) in the decision-making process need to be inclusively considered to make the hydrogen economy happen.

It is in the hands of the EU and the national regulators to grant a fair decision-making process. Within the context of an emergent hydrogen economy, where a legal framework is still to be determined, this study will focus on determining to what extent the Aarhus Convention [6] and its national transpositions – with the Netherlands as the case study – are empowering equitably all societal groups and forms of participation in the decision-making process on the implementation of this new energy technology. To give answer to this question, an analysis of the two current regulatory frameworks on public participation by either individual or collective means, with special attention to energy communities, will be carried out.

[1*] a.forns.gomez@rug.nl

Methodology

Considering that the main question of this research aims to answer how the current legal framework on public participation at both the EU level and the national level treats the different forms of active participation for implementing hydrogen as the energy leading our future, the methodology needs to be focused on legal interpretation. Two legal research methodologies have been chosen to conduct the study: doctrinal and comparative research.

Applying a doctrinal methodology within legal research requires making use of the interpretative methods of law according to Savigny [7]: grammatical, systematic, historic and teleological interpretations. At first, a doctrinal approach of methodology will be taken, that is, interpretation of the laws applying to the specific topic: the Aarhus Convention at the EU level, and the Dutch transposition under the Environmental Protection Act (EPA) [8] and the General Administrative Law Act (GALA) [9]. This first step would cover the grammatical interpretation. To better understand the role given to individual and collective power in the decision-making process of implementing a hydrogen economy, other primary resources such as communications, roadmaps and strategies will be examined so as to cover the historic and systematic interpretations. Once these primary resources will have been analysed, the researcher will also take due account of the legal doctrine and proceed to do to some literature review of secondary sources to learn from the expertise of scholars in that line to also include a teleological approach that allows to envisage legal choices other than the ones taken in the aforementioned legally binding texts.

In order to reach potential conclusions stemming from this study, the second stage of the research will make use of a comparative legal research methodology. Due to the fact that the former stage of research based on a doctrinal methodology will have examined the legal framework of public participation within two different jurisdictions (EU and Dutch), a comparative methodology will contribute to determine the mismatches and coincidences between the two norms and the lessons that can be learned from one legal text to the other. The objective of comparing these two jurisdictions is to find out which of the two set of norms in place presents a framework that is a better fit to bring equitable and inclusive decision-making tools to adopt hydrogen as a key energy technology for our energy systems. What is more, the comparative legal research is intended to find the weaknesses of these public participation laws, to envisage the ways ahead to gran fair and just participation practices.

Discussion

This research is at the stage of interpreting the legal norms that centre the attention of the study: the Aarhus Convention and its transposition into the Dutch legal order. Based on a literature review, facts and data show that the Aarhus Convention must be regarded as an outdated norm that is no longer compatible with the context to which it applies. The Aarhus Convention dates of 1998. The thought back then of implementing a hydrogen economy as the key strategy to make Europe the first green and above all just energy market was nowhere near. The Dutch Environmental Protection Act (EPA) and the Dutch

General Administrative Law Act (GALA), both aimed at transposing the Aarhus Convention, follow similar outcomes as Aarhus itself.

Its outdate is also conditioned to the past trends of understanding that it is through equality how justice is brought into our democratic systems. Instead, following EU settled case law, we cannot treat different situations in the same way [10] If individuals enjoy at the kick-start of a public consultation procedure of different values and educational, economic, cultural, ethnic or religious backgrounds, the opportunities that they will have to have a say will differ from one individual to another. Scholars recommendations state that inserting equity into the formula contributes to balancing people's opportunities in the decision making process of implementing a hydrogen economy [11].

The challenge that this research faces is the determination whether the current norms both at the EU and national level on public participation treat differently individual and collective powers in the decision-making chain of energy policies for hydrogen. With new ways of collective power coming into scene, such as the case of energy communities, it is to be determined if individuals are treated differently when deciding to actively participate for the transition by themselves or as members of a community [12].

Conclusions

This is an ongoing study, therefore, no conclusions have been reached yet. On the course of the upcoming six months, the researcher envisions to have come up with conclusions prior to the 2024 European PhD Hydrogen Conference.

Yet, thanks to an interdisciplinary literature review that consists of law, sociology and environmental psychology expertise interacting with each other, it can be stated that the preliminary conclusions show that the current legislations will fail at providing the citizenry with inclusive mechanisms to participate in designing the hydrogen market. Therefore, vague laws bring in the population sentiments of fake participation and not trusting the process, which in the end, may rise the dissatisfaction once again of certain societal groups and communities that face a risk of being excluded of the decision-making chain.

Such conclusions will open the next phase of this research that would be directed to finding the alternatives to these mechanisms that are putting barriers to achieving a just transition within the hydrogen context.

References

[1] European Commission "The European Green Deal" (Communication) COM(2019) 640 final.
[2] European Commission " 'Fit for 55': delivering the EU's 2030 Climate Target on the way to climate neutrality" (Communication) COM(2021) 550 final.
[3] European Commission "The European Green Deal" […] page 15.
[4] L. Liu, G. Perlaviciute and L. Squintani "Opposing out loud versus supporting in silence: who wants to participate in decision-making about energy projects?" in *Environmental Research Letters* Volume 17, Number 11, 2022. doi: 10.1088/1748-9326/ac9f24

[5] G. Perlaviciute, L. Squintani, L. Liu "Contested climate policies and public participation: An equal-opportunities and values-based approach (EVA)", 2023, to be published.
[6] United Nations Organisation (UNO) "Convention on Access to Information, Public Participation in Decision-Making and Access to Justice in Environmental Matters", Aarhus, 1998.
[7] O. Ammann "The Interpretative Methods of International Law: What Are They, and Why Use Them?" in *Domestic Courts and the Interpretation of International Law*, 1st Edition, Development in International Law Volume 72, , Ed. Brill and Nijhoff, 2020, pp. 191-222, doi: 10.1163/9789004409873_008
[8] Ministerie van Infrastructuur en Milieu "Wet milieubeheer (WMB)" BWBR0003245, 1979, last modified 2023.
[9] Ministerie van Justitie en Veiligheid "Algemene wet bestuursrecht (Awb)" BWBR0005537, 1992, last modified 2023.
[10] European Court of Justice, Case C-344/04 IATA and ELFAA, 2006, paragraph 95. EUCLI:EU:C:2006:10.
[11] L. Squintani and G. Perlaviciute "The 4Ds Theory: Lessons learned from the Aarhus Convention, the Escazu Agreement and the Impact and Benefits Sharing Agreements (IBSA)", 2023, to be published.
[12] L. Diestelmeier "Citizen Energy Communities as a Vehicle for a Just Transition in the EU (Challenges for the Transposition)" in *Oil, Gas & Energy Law Intelligence*, Volume1 , 2021.

Large Eddy Simulations of hydrogen combustion in a reverse flow micro gas turbine burner

E. Stendardo*[1,2,4], M. M. Kamal[3,4], A. Coussement[3,4], A. Parente[3,4], J. Blondeau[1,4], L.Bricteux[2], K. Bioche[5]

[1]Thermo and Fluid Dynamics (FLOW), Vrije Universiteit Brussel (VUB), Pleinlaan 2, 1050 Brussels, Belgium
[2]Université de Mons (UMONS), Belgium
[3]Université Libre de Bruxelles (ULB), Belgium
[4]Brussels Institute for Thermal-fluid systems and clean Energy (BRITE), Vrije Universiteit Brussel (VUB) and Université Libre de Bruxelles (ULB), Belgium
[5]INSA Rouen Normandie, CORIA lab, France

Introduction

Hydrogen is gaining more and more interest in future power generation and heating systems. The current need for decarbonization of the energy sector indeed puts hydrogen forward as a suitable energy carrier [1]. However, the utilization of hydrogen in conventional combustion systems poses certain challenges due to its unique characteristics, including high molecular diffusivity and laminar flame speed. Besides, in comparison to natural gas, the use of hydrogen can lead to high temperatures and significant NO_x emissions [2]. The benefits, advancements, and difficulties of hydrogen mGTs are thoroughly covered by Deveriese et al. 2020 [3]. The aim of this research is to perform numerical simulations of the combustion process of H_2, H_2-derived fuels and their mixtures in innovative micro-Gas Turbines (mGT) combustors. Large Eddy Simulations (LES) are performed using YALES2 research code [4], in order to predict combustion efficiencies and pollutant emissions. Experimental data from a lab-scale reverse flow mGT combustion chamber will be used to validate the model. Reverse flow combustors, like the one under consideration, can also play an important role in reducing pollutant emissions from mGTs. The reverse flow of fuel and combustion gases within the combustion chamber allows for more complete combustion and better mixing of air and fuel, leading to reduced formation of nitrogen oxides NO_x, unburned hydrocarbons HC, and carbon monoxide CO [5]. The low-Mach number Navier - Stokes equations are solved using the variable-density low-Mach solver of YALES2. A first modelling step is used to solve the fuel mixing problem in a non-reacting flow, before moving on to the multi-species reacting flow. Having trustworthy computational models on hand for the combustion of H_2 and H_2-derived fuels will be beneficial during the development of advanced, decarbonized energy conversion systems.

Experimental setup

The mGT is one of the Université libre de Bruxelles(ULB) design details can be found in [6]. Its performances are currently being investigated in the ULB laboratory. The laboratory has two combustion chambers: an actual combustion chamber, and a copy that allows for optical access. The first chamber is enclosed in a casing that leads to the nozzle/exhaust. For simplicity and ease of measurement, the experiment related to combustion quality is being conducted in the equivalent chamber without the enclosure. Therefore, the simulations in this paper are being carried out on this exact unenclosed chamber as can be seen in Fig.2a that depicts the meshed computational domain.

The fuel and air are introduced through two separate concentric cylindrical ducts into a 213mm long quartz cylinder, which constitutes the combustor (see Fig.1b). The internal pipe introduces the fuel and the one surrounding it, the oxidizer (coflow). After the inlets, the mixing process begins. The combustor has an inner diameter of 118 mm and a wall thickness of 10 mm. A glow plug is used for ignition, and four support cylinders elevate the burner, leaving an opening (clearance) through which the exhaust gases escape. As the glow plug is removed from the combustion chamber after ignition, it will not be included in the mesh and the simulation.

*Corresponding author: elisa.stendardo@vub.be

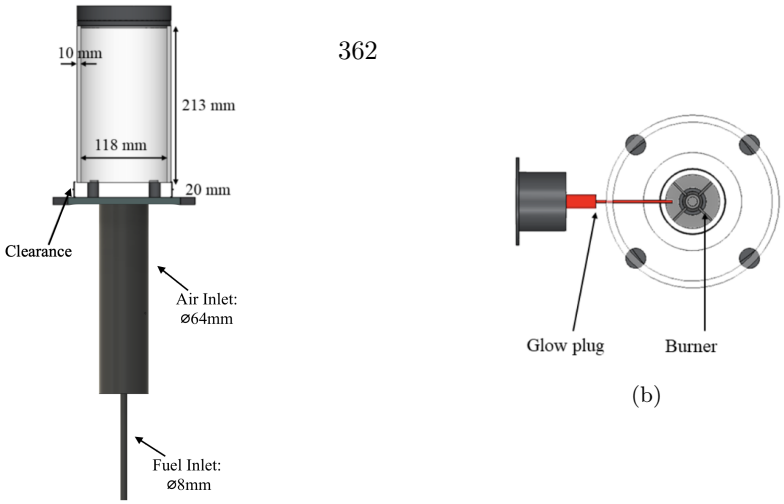

(a) (b)

Figure 1: a) CAD of Chamber, Fuel & Oxidizer inlet and b) Top view of the burner CAD model

Mesh Generation

The mesh was generated using the open-source software Gmsh, a three-dimensional finite element mesh generator with a build-in CAD engine and post-processor [7] The mesh generated is made of approximately 500K nodes and 3 million tetrahedral elements. The performed preliminary simulations indicate that it is suitable for capturing the flame structures.

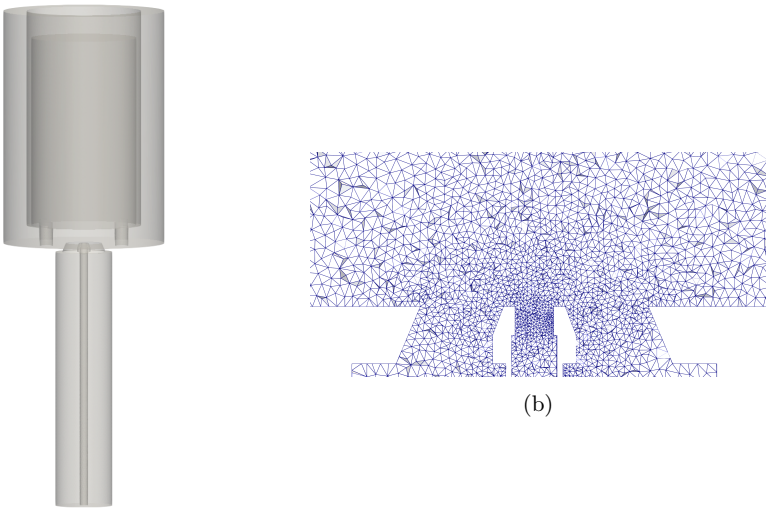

(a) (b)

Figure 2: a): Computational domain and b): Mesh at the inlet

Methodology

The simulation process has been split into two parts: the mixing of fuel with the oxidizer and combustion. We configured the boundary and initial conditions to replicate experiments conducted with a thermal input of 20 kW and an equivalence ratio of 0.4 at ambient temperature. Both steps, share the same boundary conditions. The final step of the pure-mixing simulation is used to initialize the reactive case. After the mixing is deemed complete, from the final fields of the mixing, the species and enthalpy are initialized. This way, the reaction is initialized by introducing species of the products.

Regarding the mixing part, YALES2 offers multiple options for the equation of state (EOS), one of which is the "Pure mixing" EOS. This EOS employs a linear interpolation method to determine fluid density and temperature from a tracer scalar field that is being transported in the domain. Specifically, the density (volume) and temperature are calculated as follows:

$$\rho^{-1} = (1 - Z)\,\rho_0^{-1} + Z\rho_1^{-1} \tag{1}$$

$$T = (1 - Z)\,T_0 + ZT_1 \tag{2}$$

The subscript '0' pertains to air properties, while the subscript '1' corresponds to fuel properties.

The LES simulations were performed using the YALES2 research code developed at the CORIA lab [4]. The low-Mach number Navier-Stokes equations are being solved using the variable-density low-Mach solver of YALES2. The solver uses a centered scheme, which is formally 4 th-order accurate on cartesian grids, for spatial discretization. The time integration scheme used in the solver is a hybrid of fourth order Runge-Kutta (RK4) and Taylor-Galerkin (TTG4A) [8], [9]. The Courant-Friedrichs-Lewy (CFL) is set to 0.4, and the Fourier limit has been set to a small value of 0.1.

Discussion

The Velocity profiles generated from the pure mixing simulation are shown in Fig.3 it can be seen that in the cold flow, the closed upper part of the combustion chamber favors a long recirculation zone that extends over the combustor. However, in the reacting case, we observe the impingement of the jet on a volume of stagnant gasses (probably combustion products) that occupy approximately half the volume of the combustor Fig.4. This leads to the formation of two recirculation zones (in 3D), a torus around the jet and a "ball" structure on top of it.

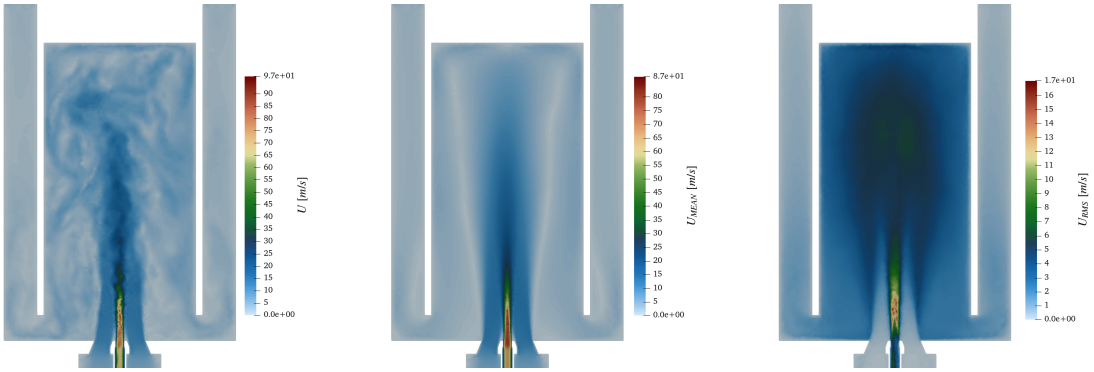

Figure 3: Velocity fields $[m/s]$ for the non-reacting fuel mixing problem

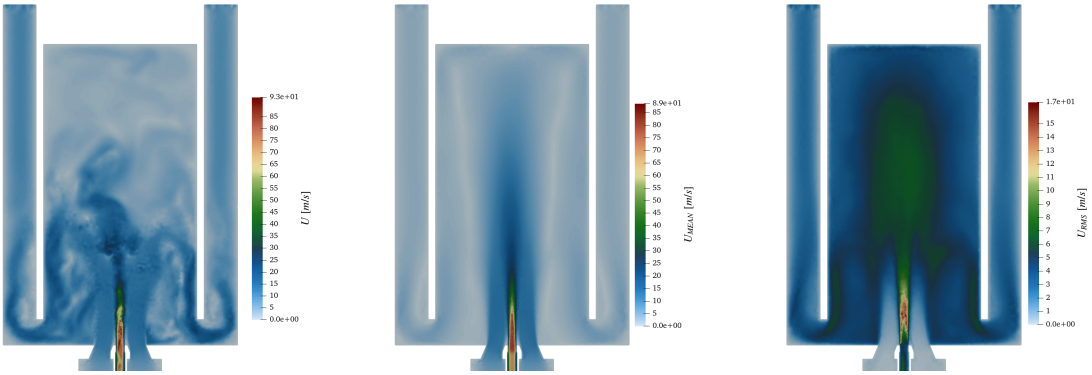

Figure 4: Velocity fields $[m/s]$ for the reacting case

This is also validated by inspecting the residence time in figure 5. We can conclude that the products of the combustion can not escape the chamber easily. From a total of 1.2 seconds of simulation time, the exhaust gases spend approximately 30% of the total time, trapped in the upper part of the combustor.

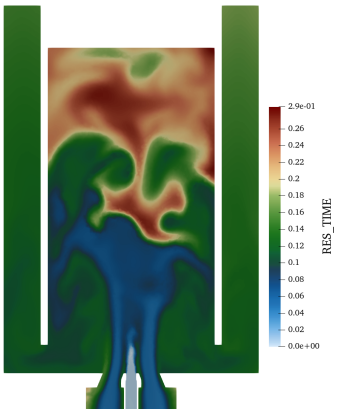

Figure 5: Residence time

The simulation results include a temperature profile in the combustion chamber expressed in Kelvin Fig.6. The difference in magnitude between the mean and the instantaneous field is due to the methodology of the two-step simulation. The stats of the velocity and temperature are not reset after the restart of the simulation, so the mean fields are affected by the statistics of the cold field. Commenting only on the instantaneous temperature field we can notice that the flame front is not evolving horizontally in the available vertical space and it seems that the recirculated products are not mixed with the incoming combustion air jet.

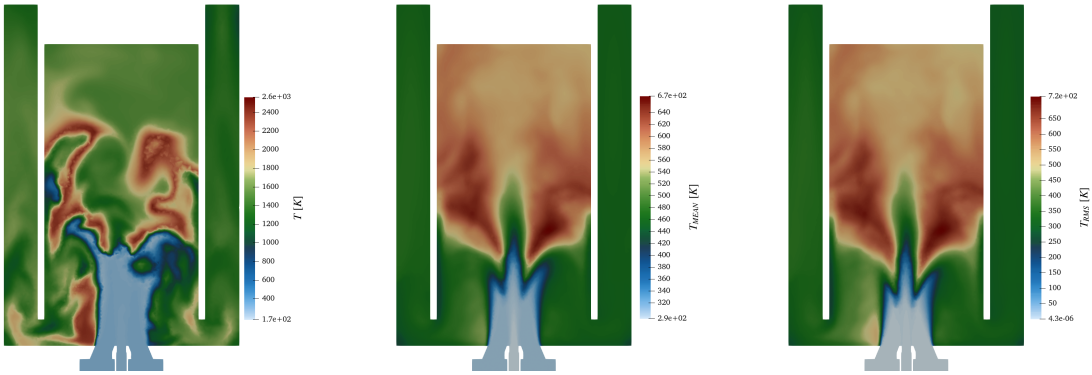

Figure 6: Temperature fields $[K]$ for the reacting case

Another important part of the problem under study are the thermal boundary conditions at the walls of the combustion chamber. Since experimental data are not available in the walls extra attention has to be paid. Regarding the treatment of the thermal boundary conditions, several approaches have been proposed that will affect the stability of the simulation. A comprehensive analysis can be found in [10], where the well-known PRECCINISTA burner is studied. The approaches in increasing order of complexity are:

1. Adiabatic wall: thermal flux $\dot{q}[W/s] = 0$ is zero for $\mathbf{x} \in \partial S$ where ∂S is the highlighted boundary of the chamber in figure 1b.
   This implies that there is no heat transfer through the boundary, an assumption done only for initial convenience. The conduction of the flow external to the chamber will play an important role in the study of the performance of the chamber.

2. The most common approach, is imposing a Dirichlet thermal boundary condition: $\forall \mathbf{x} = \mathbf{x}_0 \in \partial S,\ T(\mathbf{x}_0) = T_{wall}$ that is also the next that will be implemented for the present work. This approach has given promising results in predicting fundamental quantities in the PRECCINISTA case [11], but requires significant efforts in tuning this temperature. Also it might make the flame unstable [10].

3. Imposed local thermal resistance. In this approach, a heat resistance R is assumed for the material and the local thermal flux Φ_q is computed from the calculated temperature T_f near the wall and a reference temperature T_{ref}. In this approach a temperature is also assumed for the wall, but heat conduction through the boundary is also taken into account. $\Phi_f = (T_f - T_{ref})R$ [10]
4. The last and most reliable approach is to couple the LES simulation with a CHT (Conjugate Heat Transfer) solver for the solid parts [10]

Conclusion

While further validation of our models is still necessary to fully confirm their capabilities, the temperature and velocity profiles obtained from the simulation results appear to be well within a reasonable range considering the given conditions. We will pay particular attention to the mixing phenomenon, as the mixing of two substances with a significant density gradient can present numerical challenges. It is also essential to quantify the effect of the mixing within this chamber to assess how the high recirculation generated by the design itself impacts (mixing) the concentrations of the reactants. Consequently, upcoming post-processing efforts will be focused on this aspect. Additionally, imposing the correct thermal boundary conditions will provide us with a better understanding of the field, as compared to the thermal adiabatic assumptions. Beginning with a coarser mesh size, compared to references of the mesh sizes for LES simulations in the literature, can be advantageous in terms of computational cost. Subsequently, an adaptive mesh refinement algorithm will be implemented, to capture finer details, ultimately enhancing the accuracy of simulations and allowing for a more detailed analysis of turbulent phenomena. Finally, using experimental data for model validation is a critical step in ensuring the model's reliability and accuracy. This validation process is indispensable to establish confidence in the model's utility and assess its potential for future applications.

References

[1] David Parra, Luis Valverde, F. Javier Pino, and Martin K. Patel. A review on the role, cost and value of hydrogen energy systems for deep decarbonisation. *Renewable and Sustainable Energy Reviews*, 101:279–294, 3 2019.

[2] Zuohua Huang, Yong Zhang, Ke Zeng, Bing Liu, Qian Wang, and Deming Jiang. Measurements of laminar burning velocities for natural gas–hydrogen–air mixtures. *Combustion and Flame*, 146(1-2):302–311, 7 2006.

[3] Cedric Devriese, Rob Bastiaans, and Ward De Paepe. Opportunities, Advances and Challenges of Hydrogen micro Gas Turbines. 2020.

[4] CORIA-CFD.

[5] M. Graça, A. Duarte, P. J. Coelho, and M. Costa. Numerical simulation of a reversed flow small-scale combustor. *Fuel Processing Technology*, 107:126–137, 3 2013.

[6] Mitis.

[7] Christophe Geuzaine and Jean-François Remacle. Gmsh: a three-dimensional finite element mesh generator with built-in pre-and post-processing facilities. Technical report, 2009.

[8] Vincent Moureau, G. Lartigue, Y. Sommerer, C. Angelberger, O. Colin, and T. Poinsot. Numerical methods for unsteady compressible multi-component reacting flows on fixed and moving grids. *Journal of Computational Physics*, 202(2):710–736, 1 2005.

[9] Olivier Colin and Michael Rudgyard. Development of High-Order Taylor–Galerkin Schemes for LES. *Journal of Computational Physics*, 162(2):338–371, 8 2000.

[10] P. W. Agostinelli, D. Laera, I. Boxx, L. Gicquel, and T. Poinsot. Impact of wall heat transfer in Large Eddy Simulation of flame dynamics in a swirled combustion chamber. *Combustion and Flame*, 234:111728, 12 2021.

[11] P. Benard, G. Lartigue, V. Moureau, and R. Mercier. Large-Eddy Simulation of the lean-premixed PRECCINSTA burner with wall heat loss. *Proceedings of the Combustion Institute*, 37(4):5233–5243, 1 2019.

Leveraging offshore wind energy and green hydrogen: A techno-economic analysis for a floating liquefied green hydrogen plant

M. Delpisheh[1*], S.M. Alirahmi[2], H. Yui[2], M. Mamlouk[1]

[1] School of Engineering, Newcastle University, Newcastle upon Tyne NE1 7RU, United Kingdom
[2] Department of Chemistry and Bioscience, Aalborg University, Niels Bohrs Vej 8A, Esbjerg 6700, Denmark

Abstract

Having a variety of energy vectors in the overall energy basket is crucial to the UK's ambitious goal of achieving net-zero emissions by 2050 and transitioning to a low-carbon energy economy. As the UK enjoys a high capacity of offshore wind, this elicits attention to how it can be exploited to the maximum. Since high wind capacity occurs in areas further from shore and deeper waters, this causes a challenge of whether installing cables to shore is viable. Herein we implement a systems approach towards introducing and techoeconomic assessment of producing the hydrogen on an offshore platform, driven by electricity from windfarms. Thereafter, the hydrogen is liquefied in a liquefaction unit and transported to shore for user use via storage ships. The system incorporates different components, namely, offshore wind farm, reverse osmosis unit for seawater desalination, proton exchange membrane (PEM) electrolyzer, and hydrogen liquefaction unit.

Keywords

Green hydrogen; Offshore wind farms (OWF), Liquefied hydrogen; Technoeconomic analysis

* Corresponding author: m.delpisheh2@ncl.ac.uk

Introduction

Hydrogen is a rapidly emerging candidate to help decarbonize the economy through production, storage, distribution, and conversion. As per the green finance strategy, penned by the Department for Energy Security and Net Zero (DESNZ), Department for Environment, Food & Rural Affairs (Defra), and Department for Business, Energy & Industrial Strategy (BEIS), the UK aims at producing 10 GW of low carbon hydrogen production by 2030 [1] towards the plan of net zero by 2050 [2]. One avenue for producing green hydrogen is using electricity from wind turbines. Moreover, owing to a large coastline, the UK enjoys a high capacity from offshore wind, leading to the UK being the world's second-largest offshore wind market after China. To this end, the British Energy Security Strategy (BESS) has set to achieve 50 GW from offshore wind by 2030 [3], [4], currently having 13.9 GW of offshore wind fully commissioned [5] which contributes towards 13% of the UK's electricity basket [6]. Just recently, the Dogger Bank, as the world's largest offshore wind farm, was connected to the UK's national grid [7]. In this theme, to exploit the full offshore wind potential, the farms shall be situated further offshore in deeper waters. In this case, an alternative vector such as hydrogen could become the most attractive means of transporting the energy to shore [8]. In tandem with being a beneficial tool for integrating offshore wind, hydrogen is also gaining momentum as a low-carbon energy source to aid in decarbonizing challenging industries such as industrial heat, marine, trains, heavy-duty vehicles, chemicals, etc. [9]. The UK enjoys a high offshore wind capacity [10] as shown in **Figure 1**, and is the second leading producer of this renewable energy after China.

In this study, an offshore floating substation coupled to an offshore wind farm is proposed for green hydrogen production. A technoeconomic assessment is implemented to assess the configuration's viability.

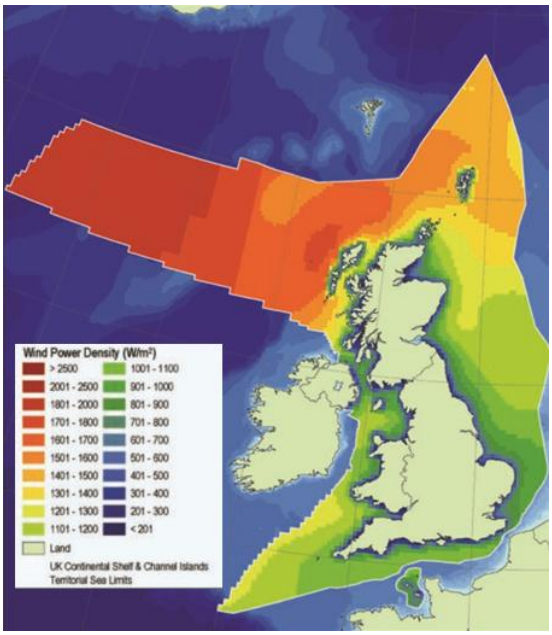

Figure 1: UK offshore ocwind energy capacity [10].

Methodology

The schematic of the proposed system is depicted in Figure 2. As shown, the electricity is transferred from the offshore floating platform to the substation. The electricity drives three components: a reverse osmosis (RO) desalination unit, a proton exchange membrane (PEM) electrolyzer, and a liquefaction unit. Initially, seawater is fed to the RO desalination unit and the resulting desalinated water (at the required purity level for succeeding sections) is fed to the PEM electrolyzer. Here, through electrolysis, the water is converted into hydrogen and oxygen. The oxygen is vented and the green hydrogen is transferred to the liquefaction unit. Finally, the liquefied hydrogen is transferred to the shore via specific storage ships.

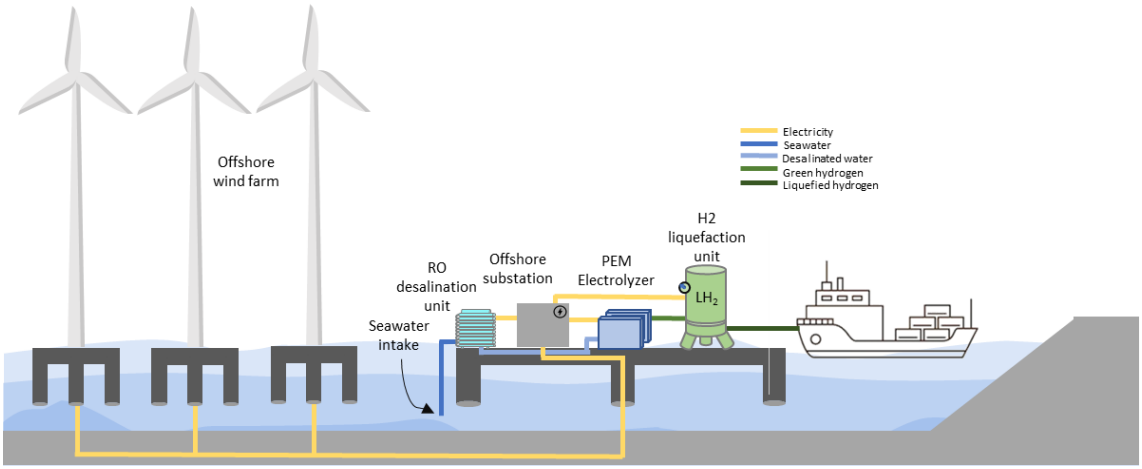

Figure 2: Schematic of the proposed system.

Offshore wind farm

The exergy of the flow stream in the wind turbine contains both kinetic energy and physical exergy [11]:

$$Ex_{\text{flow}} = Ex_{ph} + ke \tag{1}$$

Physical exergy is given as:

$$Ex_{ph} = \Delta H + \Delta S \tag{2}$$

where

$$\Delta H = \dot{m} c_p (T_2 - T_1) \tag{3}$$

$$I = T_0 \Delta S \tag{4}$$

$$\Delta S = \dot{m}\left(C_P \ln\left(\frac{T_2}{T_1}\right) - R\ln\left(\frac{P_2}{P_1}\right) - \frac{C_P\left(T_0 - T_{\text{ang}}\right)}{T_0}\right)$$

By inserting these we have:

$$Ex_{ph} = \dot{m}\left[c_p(T_2 - T_1) + T_0\left(C_P \ln\left(\frac{T_2}{T_1}\right) - R\ln\left(\frac{P_2}{P_1}\right) - \frac{C_P\left(T_0 - T_{\text{avg}}\right)}{T_0}\right)\right] \quad (5)$$

The kinetic energy is calculated by:

$$ke_{1\iota 2} = \frac{1}{2}\dot{m}v^2 \quad (6)$$

Whereby:

$$\dot{m} = \rho\pi r^2 v_1 \quad (7)$$

After calculating the exergy flow, the energy efficiency of the wind turbine (η) (the ratio of the highest amount of useful work being absorbed by the system per kinetic energy changes in the flow stream) and the exergy efficiency (Ψ) (the output power generated by the wind turbine per exergy of the wind flow passing through the system) are given as:

$$\eta = \frac{W_{\text{out}}}{\text{power of wind}} \quad (8)$$

$$\Psi = \frac{W_{\text{out}}}{Ex_{\text{flow}}} \quad (9)$$

PEM electrolyzer

Green hydrogen is produced in the PEM electrolyzer through the following water-splitting reaction; in the anode:

$$\mathrm{H_2O} \rightarrow 2\mathrm{H^+} + \frac{1}{2}\mathrm{O_2} + 2\mathrm{e^-} \quad (10)$$

In the cathode:

$$2\mathrm{H^+} + 2\mathrm{e^-} \rightarrow \mathrm{H_2} \quad (11)$$

Overall:

$$\mathrm{H_2O} \rightarrow \mathrm{H_2} + \frac{1}{2}\mathrm{O_2} \quad (12)$$

The produced hydrogen and oxygen flow rate can be calculated by:

$$\dot{N}_{H_2,\,\text{out}} = \frac{J}{2F} \quad (13)$$

$$\dot{N}_{O_2,\,\text{out}} = \frac{J}{4F} \tag{14}$$

whereby F and J are Faraday constant and current density. The equation below can be used to calculate the power consumption of a PEM electrolyzer:

$$\dot{W}_{PEM} = JV \tag{15}$$

where V is PEM electrolyzer voltage for each cell and determined by:

$$V = V_0 + V_{act,c} + V_{act,a} + V_{ohm} + V_{\text{conc}} \tag{16}$$

where $V_{act,c}$ and $V_{act,a}$ are the activation overpotentials of the cathode and anode respectively and V_{ohm} is the ohmic overpotential. The current density is below $10{,}000[\ \text{A/m}^2]$ and to this end the concentration overpotentials (V_{conc}) can be neglected. V_0 is the reversible potential and is calculated using the Nernst equation:

$$V_0 = 1.229 - 0.85 \times 10^{-3}(T_{PEM} - T_0) + \frac{RT_{PEM}}{2F} \ln \frac{P_{O_2}^{0.5} P_{H_2}}{a_{H_2O}} \tag{17}$$

here $a_{\text{H}_2\text{O}}$ is equal 1 for liquid water. The activation overpotentials of the anode and cathode can be expressed as:

$$V_{act,i} = \frac{RT}{F} \sinh^{-1}\left(\frac{J}{2J_{0,i}}\right), i = a, c \tag{18}$$

Herein $J_{0,i}$ is the exchange current density:

$$J_{0,i} = J_i^{ref} \exp\left(-\frac{E_{\text{act},i}}{RT}\right), i = a, c \tag{19}$$

In this equation j_i^{ref} and $E_{act,i}$ are pre-exponential factor and activation energy. Lastly, the Ohmic voltage is defined as:

$$V_{ohm} = JR_{PEM} \tag{20}$$

Whereby:

$$R_{PEM} = \int_0^L \frac{\mathrm{d}x}{\sigma[\lambda(x)]} \tag{21}$$

$$\sigma[\lambda(x)] = [0.5139\lambda(x) - 0.326]\exp\left[1268\left(\frac{1}{303} - \frac{1}{T_{PEM}}\right)\right] \tag{22}$$

$$\lambda(x) = \frac{\lambda_a - \lambda_c}{L} x + \lambda_c \tag{23}$$

RO desalination unit

In the RO desalination unit, the seawater experiences a pre-treatment entering the main RO system. The feed flow rate can be calculated by using the recovery ratio (RR) and the mass flow rate of desalinated water [12]:

$$M_{\text{feed}} = \frac{M_{\text{permeate}}}{RR} \tag{24}$$

The rejected brine and desalinated water salt concentrations, can be calculated through:

$$X_{\text{brine}} = \frac{M_{\text{feed}} X_{\text{feed}} - M_{\text{permeate}} X_{\text{permeate}}}{M_{\text{brine}}} \quad (25)$$

$$X_{\text{permeate}} = X_{\text{feed}} (1 - SR) \quad (26)$$

Here, SR is the salt rejection percentage and X is the salt concentration. The temperature correction factor (TCF) is given as:

$$TCF = \exp\left(2700\left(\frac{1}{T_{RO}} - \frac{1}{298}\right)\right) \quad (27)$$

The salt permeability (k_s) and membrane water permeability (k_w) is calculated as:

$$k_s = FF \times TCF \times 4.72 \times 10^{-7}\left(0.06201 - (5.31 \times 10^{-5} \times T_{RO})\right) \quad (28)$$

$$k_w = \frac{6.84 \times 10^{-8}\left(18.6865 - (0.177 X_{\text{brine}})\right)}{T_{\text{RO}}} \quad (29)$$

Herein, FF is fouling factor and it is assumed to be 0.85. The net osmotic pressure across the membrane and average osmotic pressure on the feed side are defined by:

$$P_{\text{net},RO} = P_{av,RO} - P_{\text{permeate}} \quad (30)$$

$$P_{av,RO} = 0.5(P_{\text{feed}} - P_{\text{brine}}) \quad (31)$$

whereby P_{permeate}, P_{feed}, and P_{brine} are osmotic pressure for desalinated product side, feed side and brine side, respectively, given as:

$$P_{\text{permeate}} = 75.84 X_{\text{permeate}} \quad (32)$$

$$P_{\text{feed}} = 75.84 X_{\text{feed}} \quad (33)$$

$$P_{\text{brine}} = 75.84 X_{\text{brine}} \quad (34)$$

Finally, the required power input to high-pressure pump and net pressure difference through the membrane is estimated by:

$$\dot{W}_{HP} = \frac{1000 \times \dot{m}_{\text{feed}} \times \Delta P}{3600 \times \rho_{\text{feed}} \times \eta_P} \quad (35)$$

$$\Delta P = \left(\frac{\dot{m}_{\text{permeate}}}{3600 \times TCF \times FF \times A_e \times n_e \times n_v \times k_w}\right) + P_{\text{net},RO} \quad (36)$$

Liquefaction unit

The liquefaction unit is comprised of the following components: compressor, heat exchanger, pump, mixer and separator, expansion valve, and a turbine expander. The pertinent equations for the mentioned equations are given in the table below [13].

Components	Energy equation	Exergy destruction	Exergy efficiency	Eq. No.

Compressor	$\dot{m}_o\ \mathrm{h}_o - \dot{m}_i\ \mathrm{h}_i = \dot{W}_{C,act}$	$I = e_i - e_o + W_c$	$\frac{e_i - e_o}{W_c}$	(37)
Heat exchanger	$\dot{m}_{i,1}\ \mathrm{h}_{i,1} + \dot{m}_{i,2}\ \mathrm{h}_{i,2} = \dot{m}_{o,3}\ \mathrm{h}_{i,3} + \dot{m}_{i,4}\ \mathrm{h}_{i,4}$	$I = (e_{i,1} + e_{i,2}) - (e_{o,3} + e_{o,4})$	$\frac{e_{e,3} + e_{o,4}}{e_{i,1} + e_{i,2}}$ $\frac{e_i - e_o}{W_p}$	(38)
Pump	$\dot{m}_o\ \mathrm{h}_o - \dot{m}_i\ \mathrm{h}_i = \dot{W}_{p,act}$	$I = e_i - e_o + W_p$	$\frac{e_0}{e_{in}}$	(39)
Mixer and separator	$\dot{m}_o\ \mathrm{h}_o = \dot{m}_i\ \mathrm{h}_i$	$I = e_i - e_o$	$\frac{e_0}{e_i}$	(40)
Expansion valve	$\mathrm{h}_o = \mathrm{h}_i$	$I = e_i - e_o$	$\frac{e_0}{e_i}$	(41)
Turbine expander	$\dot{m}_i\ \mathrm{h}_i - \dot{m}_o\ \mathrm{h}_o = W_{tur,act}$	$I = e_i - e_o + W_{tur}$	$\frac{e_i - e_o}{W_{tur}}$	(42)

Economic modeling

PEM electrolyzer

$$EC_{EL} = RC_{EL} \cdot P_{EL} \tag{43}$$

$$RC_{EL} = (k_0 + k \cdot p_{EL}^{\alpha-1}) \cdot \left(\frac{Y}{Y_0}\right)^{\beta} + RC_0 \tag{44}$$

Wind farm

$$IC_{WT} = \left(NL \cdot \left(\frac{2 \cdot DP_{WF}}{v} + t_{\text{load}}\right) + t_{\text{inst}} \cdot N_{WT}\right) \cdot \frac{DR}{24} \tag{45}$$

Offshore substation

$$EC_{PC} = RC_{PC} \cdot P_{PC} \tag{46}$$

$$EC_{PS} = RC_{PS} \cdot P_{WF} + UC_{PS} \cdot 10^3 \tag{47}$$

Desalination unit

$$CAPEX_{DS} = RC_{DS} \cdot \bar{V}_{H_2O} \tag{48}$$

$$\bar{V}_{\mathrm{H_2O}} = \dot{v}_{\mathrm{H_2O}} \cdot 0.8 \cdot P_{EL} \tag{49}$$

Discussion

Upon thermodynamic modeling of the system, this section will discuss the results of the thermodynamic and economic side of the project by addressing the CAPEX and OPEX of the system in operation.

Conclusions

The study concludes by addressing whether the proposed system is viable or not, and what circumstances and challenges can be expected if the system is implemented for operation.

References

[1] G. Shapps, J. Hunt, and T. Coffey, “Mobilising Green Investment - 2023 Green Finance Strategy,” Jul. 2023.
[2] K. Kwarteng, “Net Zero Strategy: Build Back Greener,” Apr. 2022.
[3] S. Hinkley Point C, “HM Government - British Energy Security Strategy,” Apr. 2022.
[4] R. H. G. Shapps MP, “Offshore Wind Net Zero Investment Roadmap: Leading the way to net zero,” Mar. 2023.
[5] “Offshore wind,” HM Government - Department of Business & Trade. Accessed: Oct. 21, 2023. [Online]. Available: https://www.great.gov.uk/international/content/investment/sectors/offshore-wind/
[6] C. Colombo, “United Kingdom Offshore Wind,” Feb. 2022. Accessed: Oct. 21, 2023. [Online]. Available: https://www.trade.gov/market-intelligence/united-kingdom-offshore-wind
[7] “World’s largest offshore wind farm Dogger Bank produces power for the first time - Equinor.” Accessed: Oct. 26, 2023. [Online]. Available: https://www.equinor.com/news/202310-dogger-bank
[8] A. Giampieri, J. Ling-Chin, and A. P. Roskilly, “Techno-economic assessment of offshore wind-to-hydrogen scenarios: A UK case study,” *Int J Hydrogen Energy*, Feb. 2023, doi: 10.1016/J.IJHYDENE.2023.01.346.
[9] P. Cavaliere, “Hydrogen Applications,” *Water Electrolysis for Hydrogen Production*, pp. 653–727, 2023, doi: 10.1007/978-3-031-37780-8_18.
[10] S. Cavazzi and A. G. Dutton, “An Offshore Wind Energy Geographic Information System (OWE-GIS) for assessment of the UK’s offshore wind energy potential,” *Renew Energy*, vol. 87, pp. 212–228, Mar. 2016, doi: 10.1016/J.RENENE.2015.09.021.
[11] A. Khanjari, E. Mahmoodi, and M. H. Ahmadi, “Energy and exergy analyzing of a wind turbine in free stream and wind tunnel in CFD domain based on actuator disc technique,” *Renew Energy*, vol. 160, pp. 231–249, Nov. 2020, doi: 10.1016/J.RENENE.2020.05.183.
[12] S. M. Alirahmi *et al.*, “Renewable-integrated flexible production of energy and methane via re-using existing offshore oil and gas infrastructure,” *J Clean Prod*, vol. 426, p. 139125, Nov. 2023, doi: 10.1016/J.JCLEPRO.2023.139125.
[13] S. Faramarzi, S. Gharanli, M. Ramazanzade Mohammadi, A. Rahimtabar, and A. J. Chamkha, “Energy, exergy, and economic analysis of an innovative hydrogen liquefaction cycle integrated into an absorption refrigeration system and geothermal energy,” *Energy*, vol. 282, p. 128891, Nov. 2023, doi: 10.1016/J.ENERGY.2023.128891.

Life cycle assessment of green ammonia production via renewable energy – a case study for Bulgaria

T.Madzharov*[1], D. Vladikova[1,2]

[1]Institute of Elctrochemistry and Energy Systems- BAS, 10 Acad. G. Bonchev St., 1113 Sofia, Bulgaria
[2]Institute for Sustainable Transition and Development – TrU, Student Campus, 6000 Stara Zagora, Bulgaria

Introduction

Bulgaria has established ambitious objectives for emissions reduction in the upcoming years, with the overall goal of attaining climate targets and mitigating the negative impacts of fossil fuels on public health and local ecosystems. The ammonia production sector which uses natural gas to produce hydrogen is among the various industries that ought to work towards decreasing their greenhouse gas emissions (GHG) while also increasing the production capacity of the current plants. The total ammonia-related hydrogen production capacity in the Member States is approximately 9,382 tonnes per day (Fig. 1) and the total demand for hydrogen by the ammonia industry in 2020 was 2.5 Mt [1].

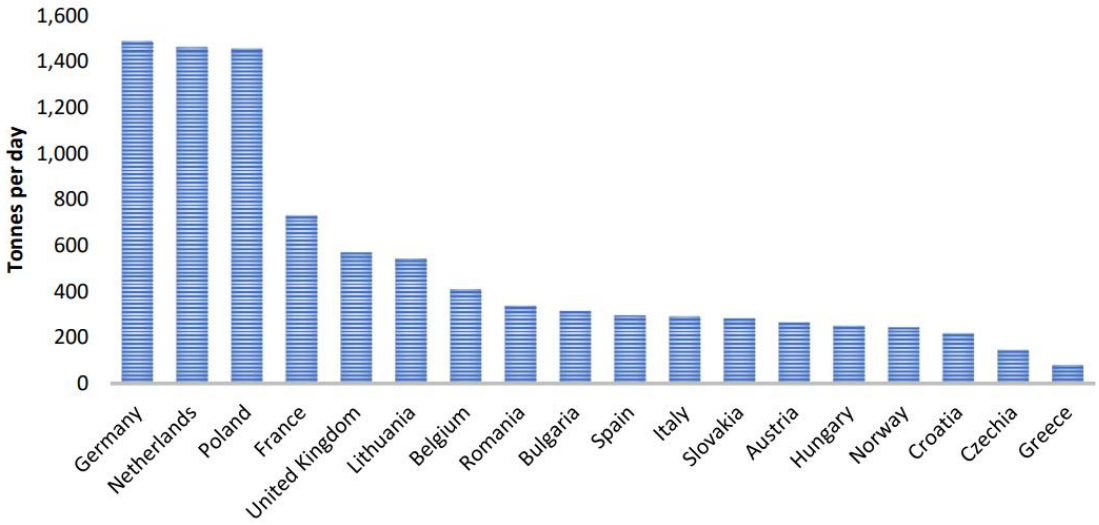

Figure 1. Hydrogen production capacity for ammonia plants by country

Transitioning away from non-renewable fuels as the primary source of hydrogen and instead adopting hydrogen derived from renewable sources like wind, solar, and hydro power is one of the routes toward achieving low-emission ammonia production [2]. There is an expanding body of literature on renewable hydrogen production driven by the imperative to mitigate climate change, reduce reliance on fossil fuels, and harness the economic and environmental potential of sustainable energy alternatives [3]. This growth is fuelled by increased global awareness, technological advancements, and supportive policy initiatives.

* Corresponding author: todor.madzharov@iees.bas.bg

In respect to industrial applications of renewable hydrogen in Bulgaria, one of the most urgent sectors for decarbonization is the ammonia production. For instance, NEOCHIM plant consumes yearly 55,000 t of hydrogen using reforming of natural gas. The corresponding CO_2 emissions are 503,000 t.
The method regarded as the most precise for quantifying and characterizing emissions from both renewable hydrogen and hydrogen produced by natural gas is known as Life Cycle Assessment (LCA). It offers a thorough comprehension of the environmental consequences of various hydrogen production methods, facilitating well-informed sustainability decisions and mitigating their adverse effects on the planet.
The aim of this study is to present the LCA of ammonia plant with a production capacity similar to the one of NEOCHIM ammonia plant in Bulgaria.

Methodology

The system under consideration for green ammonia production comprises of a renewable energy source (wind, solar and hydro), a solid-oxide electrolyzer (SOEL) and a Haber-Bosch reactor. The selection of the less mature SOEL technology for hydrogen production by electrolysis is motivated by the opportunity to reach higher energy efficiency due to heat utilization. Therefore, coupling a solid oxide electrolyzer with an ammonia production facility could significantly increase the efficiency of the whole system and dramatically reduce the emissions. For example, Cinti and Frattini (2016) reported electricity consumption of as low as 8.30 kWh/kg NH_3 and zero emissions of CO_2 in the case of combining SOEL with a Haber-Bosch reactor [4]. In addition, this technology is expected to have a quick large scale industrial deployment [5].
The goal of the study is to qualify and quantify the emissions of ammonia production with renewable hydrogen ($CO_2/kgNH_3$, $kWh_e/kgNH_3$, $kWh_{th}/kgNH_3$) and compare them with the emissions of ammonia production with hydrogen from natural gas.
The scope of this study is Cradle-to-grave, excluding post-life recycling or landfill. The functional unit is $CO_2/kgNH_3$. The software employed for conducting the analysis is open LCA 2.0 and the database under consideration is ecoinvent.
In this work the first results for renewable hydrogen production for ammonia plant via SOEL will be presented.

References

[1] „ 2022 Hydrogen Supply Capacity and Demand:Chapter 2“ FCHO Fuel Cells and Hydrogen Observatory, March 2022

[2] Dunn, S. (2002). Hydrogen futures: Toward a sustainable energy system. *International Journal of Hydrogen Energy*, *27*(3), 235–264. https://doi.org/10.1016/s0360-3199(01)00131-8

[3] Mayer, P., Ramirez, A., Pezzella, G., Winter, B., Sarathy, S. M., Gascon, J., & Bardow, A. (2023). Blue and green ammonia production: A techno-economic and life cycle assessment perspective. *iScience*, *26*(8), 107389. https://doi.org/10.1016/j.isci.2023.107389

[4] Cinti, G., Frattini, D., Jannelli, E., Desideri, U., & Bidini, G. (2017). Coupling solid oxide electrolyser (SOE) and ammonia production plant. *Applied Energy*, *192*, 466–476. https://doi.org/10.1016/j.apenergy.2016.09.026

[5] “Agenda Process for the European Research and Innovation Initiative on Green Hydrogen” https://www.bmbf.de/bmbf/shareddocs/downloads/files/SRIA_green_hydrogen.pdf?__blob=publicationFile&v=4

Life cycle assessment of hydrogen supply pathways for large transport vehicles

J. Wilkinson*[1,2], M. McManus[1,4,5], T. Mays[3,4]

[1]Department of Mechanical Engineering, University of Bath, UK
[2]Centre for Doctoral Training in Advanced Automotive Propulsion Systems, University of Bath, UK
[3]Department of Chemical Engineering, University of Bath, UK
[4]Centre for Sustainable Energy Systems, University of Bath, UK
[5]Institute for Sustainability, University of Bath, UK

Introduction

The motivation for this research is the urgent global climate challenge of preventing a global mean surface temperature increase of more than 1.5 °C compared to the pre-industrial average. The Intergovernmental Panel on Climate Change (IPCC) has warned of serious consequences to human health and societies of such a rise in global temperature [1]. We are already 80% of the way to this threshold: the global mean surface temperature for 2018-2022 was about 1.2 °C about the pre-industrial average [2].

Hydrogen is a promising fuel for road freight, shipping, and aviation because it can be used cleanly without producing any carbon dioxide at point of use [3]. However, about 95% of hydrogen is currently produced from fossil fuels, which results in significant carbon emissions even when carbon capture is implemented [4]. Previous reviews of the environmental impacts of hydrogen production have limited their scope to a subset of production technologies [5]-[7] or have only considered global warming potential (GWP) and acidification potential [8], [9] or a single environmental damage score [10].

Researchers and decision makers need a more comprehensive environmental comparison, incorporating techno-economic analysis, for the entire supply pathway to vehicles, including production, transport, and storage of hydrogen [4], [11]. It is also important to consider the impacts of decisions on the infrastructure and supply chains for competing or synergistic uses of hydrogen for producing ammonia, steel, and chemicals [12].

This project aims to expand knowledge of the absolute and relative environmental impacts and financial costs of pathways for producing, storing, and distributing hydrogen under various possible scenarios between now and 2050, considering the latest advancements in hydrogen technologies and renewable energy generation, and accounting for variations in infrastructure, geography, climate, level of investment in research and development, and the effects of decisions on competing uses of hydrogen. This project will produce as its outputs: a review of recent life cycle assessments (LCAs) of hydrogen [13]; a review of the most promising hydrogen technologies; a detailed LCA of hydrogen supply, from cradle to refilling station; recommendations for decision makers in the UK; and a user-friendly decision support tool to enable researchers, government officials and other interested parties to customise the LCA for their country, sector, or industry. Researchers will have full access to all the underlying data, research, and methodologies.

* Corresponding author: jw3503@bath.ac.uk

Methodology

Literature reviews have been carried out to answer the key research questions of this project. First, it was necessary to identify the most promising hydrogen supply technologies (production, storage, and transport) to assess in an LCA, and to identify the most important indicators (environmental and financial) to compare when assessing hydrogen supply scenarios. The decision has been made to use a prospective approach in formulating future scenarios, while assessing these scenarios using attributional LCA. In this way, the benefits of a prospective approach are realised while also facilitating the comparison of the results of the new LCA with those of other recent LCAs, nearly all of which are attributional LCAs [12]. Present day scenarios will be compared with future scenarios for 2035 and 2050. These years were chosen because 2050 is the target year for Net Zero for many countries including the UK [14], and 2035 is an intermediate milestone by which time key hydrogen technologies can mature and be rolled out at a large scale. Worst-case, base-case and best-case sub-scenarios will be formulated for 2035 and 2050, including parameters for electricity mix, rate and scale of technology adoption, costs of capital and key raw materials, and technological improvements including increased efficiencies and circularity of critical materials. When researching these technoeconomic factors, a literature review has been supplemented by elicitation interviews with experts from academia and industry, as described below.

For each literature review, the starting point was a systematic review of review articles, branching out to related papers via reference lists. Independent searches have also been made of relevant government, industry, and non-governmental reports. For hydrogen production technologies, a meta-analysis of methodological choices of recent LCAs led to the identification of mutually comparable studies, which were compared initially by GWP, then relatively low GWP scenarios (compared to the UK Low Carbon Hydrogen Standard [14]) were compared by cost and other indicators. The findings are summarised in the discussion section of this abstract, and the review has been published in a peer-reviewed journal [13].

After identifying the most significant gaps in the life cycle inventory (LCI) database, a selection of potential expert interviewees was identified, in collaboration with my advisors and subject experts at the University of Bath. The interview questions vary depending on the topic and level of specialisation, based initially on the questionnaire included in Delpierre *et al.* [15]. Interviews are being conducted mostly online, with some in person at the University of Bath.

For the LCA, my methodology follows the LCA framework established by the International Standards Organization in ISO 14040 [16], with reference to subsequent recommendations made in the ILCD handbook [17], FC-HyGuide [18], and recent published books and journal articles discussing best practice. LCA is an iterative process, so I started with a simple comparison of two hydrogen production scenarios – the incumbent steam methane reforming (SMR) technology, and PEM electrolysis powered by offshore wind energy – followed by refining scenarios and drilling into LCI data in increasing detail. From there, I have migrated from openLCA [19] to Brightway2 [20], because the latter facilitates rapid and flexible customisation and re-assessment of scenarios, including uncertainty and sensitivity analysis. The decision support tool will be implemented via a Jupyter notebook, where parameters can be edited in a web page, supported by an Excel workbook of key LCI data.

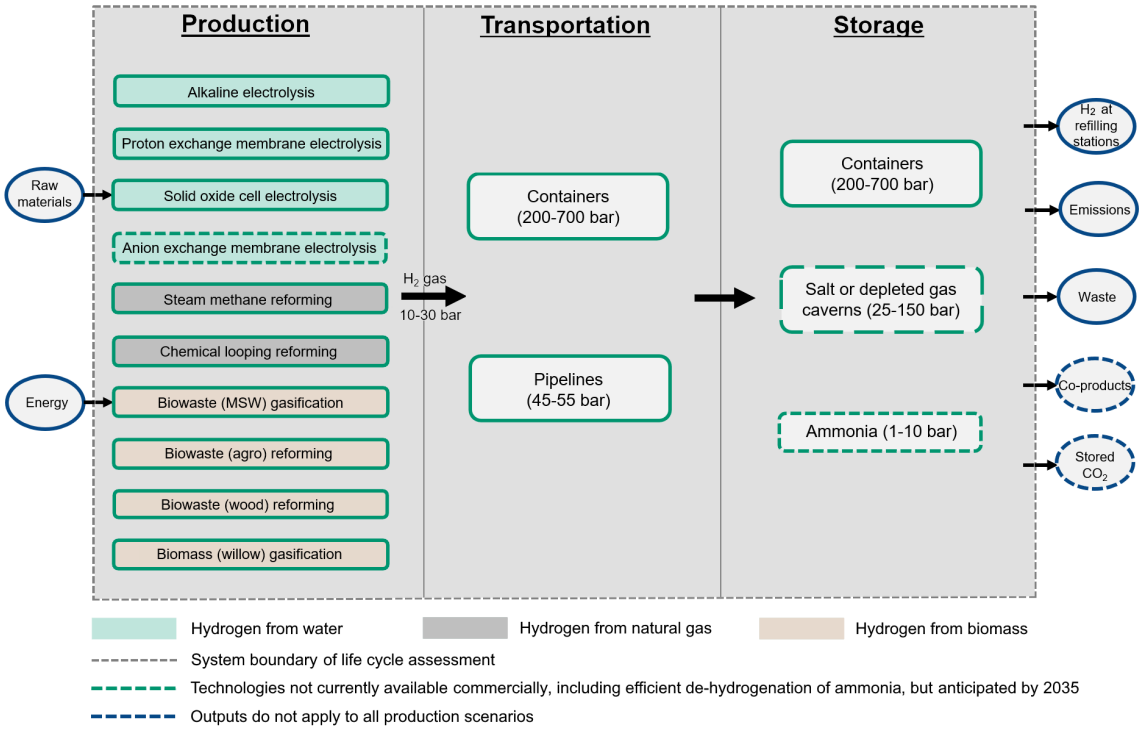

Figure 1 Overview and system boundary of the planned life cycle assessment of supplying hydrogen (H_2) to large transport vehicles. MSW = municipal solid waste, converted to refuse-derived fuel; agro = wheat straw and residue from agriculture; wood = post-consumer and sawmill waste; willow = cultivated short rotation coppice willow.

Discussion

The largest group of mutually comparable LCAs reviewed in [13] is the 56 studies with a cradle-to-gate scope (from raw materials to hydrogen, excluding the transport, storage, or use of hydrogen) where hydrogen is produced with a purity of at least 99.9%. Despite the significant uncertainties of the reviewed LCAs, collectively they show some striking differences in GWP between hydrogen production scenarios. Using fossil-based energy generally results in a significantly higher GWP than using nuclear or renewable energy. In fact, where hydrogen is produced using electrolysis powered by grid electricity, often the majority of GWP is due to electricity production. When comparing the GWP of renewable energy sources for the same production process, wind energy tends to perform better than a renewable mix that includes solar PV and/or hydro. Chemical looping reforming (CLR) with carbon capture and storage (CCS) is a potentially attractive alternative to the dominant production method of steam methane reforming of natural gas. Biomass gasification with CCS also shows potential for negative GWP, but biogenic emissions require careful accounting to assess longer-term sustainability.

A comparison of low-GWP methods shows that electrolytic methods, compared to dominant methods of producing hydrogen from fossil fuels, have a lower overall impact but are currently more expensive, while CLR may also have a lower overall impact and is potentially even cheaper. I am currently gathering LCI data for the hydrogen technologies shown in Figure 1. Where hydrogen is produced using electrolysis, scenarios will be assessed with different primary energy sources, while other scenarios will be assessed with and without CCS. Provided that sufficient LCI data can be obtained, I will include anion membrane exchange (AEM) electrolysis in future production pathways, because the consensus of expert interviewees is that this technology is expected to be ready to deploy at a large scale by the early 2030s. Transport options being assessed are pressurised containers carried by lorry or train, or a dedicated pipeline, while storage options being assessed are pressurised containers, ammonia, or potentially depleted salt or gas caverns where a very large volume and seasonal storage are desired.

Conclusions

Hydrogen is a carbon-free fuel with the potential to power road freight, shipping, and aviation. The technologies to produce, transport and store hydrogen are developing rapidly and there are significant uncertainties regarding technological progress in energy consumption, material usage, cost, environmental impacts, and scaling up the required infrastructure. This project is building realistic current and future scenarios to assess the cost and environmental impacts of potential hydrogen supply pathways, based on the published literature and interviews with experts in the field. By the time of EPHyC in March 2024, I expect to be able to present provisional LCA results for all pathways, including scenarios for the present day and the years 2035 and 2050, with uncertainty, sensitivity, and hotspot analysis. Future work will include providing a decision support tool for researchers and decision makers to customise the LCA.

References

[1] Intergovernmental Panel on Climate Change (IPCC), “Summary for Policymakers,” in *Climate Change 2021: The Physical Science Basis. Contribution of Working Group I to the Sixth Assessment Report of the Intergovernmental Panel on Climate Change*, V. Masson-Delmotte *et al.*, Eds., Cambridge, UK: Cambridge University Press, 2021, pp. 3–32, doi: 10.1017/9781009157896.

[2] Met Office, “HadCRUT5 analysis time series, Summary series, Global, Annual.” 23 Mar. 2023. Distributed by Met Office Hadley Centre. https://www.metoffice.gov.uk/hadobs/hadcrut5/data/current/analysis/diagnostics/HadCRUT.5.0.1.0.analysis.summary_series.global.annual.csv
[3] UK Government, “UK Hydrogen Strategy,” Department for Business, Energy and Industrial Strategy, London, UK, Aug. 2021.
[4] R.W. Howarth and M.Z. Jacobson, “How green is blue hydrogen?”, *Energy Sci. & Eng.*, vol. 9(10), pp. 1676–1687, Aug. 2021, doi: 10.1002/ese3.956.
[5] R. Bhandari, R., C.A. Trudewind, and P. Zapp, “Life cycle assessment of hydrogen production via electrolysis – a review,” *J. Clean. Prod.*, vol. 85, pp. 151–163, Dec. 2014, doi: 10.1016/j.jclepro.2013.07.048.
[6] O. Kanz, K. Bittkau, K. Ding, U. Rau, and A. Reinders, A., “Review and Harmonization of the Life-Cycle Global Warming Impact of PV-Powered Hydrogen Production by Electrolysis,” *Front. Electron.*, vol. 2, Sep. 2021, doi: 10.3389/felec.2021.711103.
[7] M. Buffi, M. Prussi, and N. Scarlat, “Energy and environmental assessment of hydrogen from biomass sources: Challenges and perspectives,” *Biomass Bioenergy*, vol. 165, Art. no. 106556, Oct. 2022, doi: 10.1016/j.biombioe.2022.106556.
[8] C. Acar and I. Dincer, “Comparative assessment of hydrogen production methods from renewable and non-renewable sources,” *Int. J. Hydrogen Energy*, vol. 39(1), pp. 1–12, Jan. 2014, doi: 10.1016/j.ijhydene.2013.10.060.
[9] M. Ji and J. Wang, “Review and comparison of various hydrogen production methods based on costs and life cycle impact assessment indicators,” *Int. J. Hydrogen Energy*, vol 46(78), pp. 38612-38635, Nov. 2021, doi: 10.1016/j.ijhydene.2021.09.142.
[10] S.Z. Baykara, “Hydrogen: A brief overview on its sources, production and environmental impact,” *Int. J. Hydrogen Energy*, vol 43(23), pp. 10605-10614, Jun. 2018, doi: 10.1016/j.ijhydene.2018.02.022.
[11] C. Cluzel *et al.* 2021, “Low Carbon Hydrogen Well-to-Tank Pathways Study,” Zemo Partnership, London, UK, Aug. 2021.
[12] A. Valente, D. Iribarren, and J. Dufour, “Life cycle assessment of hydrogen energy systems: a review of methodological choices," The International Journal of Life Cycle Assessment, vol. 22(3), pp. 346-363, Jun. 2017, doi: 10.1007/s11367-016-1156-z.
[13] J. Wilkinson, T. Mays, and M. McManus, “Review and meta-analysis of recent life cycle assessments of hydrogen production,” *Cleaner Env. Syst.*, vol. 9, Art. no. 100116, Jun. 2023, doi: 10.1016/j.cesys.2023.100116.
[14] Department for Energy Security & Net Zero (DESNZ), “UK Low Carbon Hydrogen Standard Version 2,” DESNZ, London, UK, Apr. 2023.
[15] M. Delpierre, J. Quist, J. Mertens, A. Prieur-Vernat, and S. Cucurachi, “Assessing the environmental impacts of wind-based hydrogen production in the Netherlands using ex-ante LCA and scenarios analysis,” *J. Clean. Prod.*, vol. 299, Art. no. 126866, doi: 10.1016/j.jclepro.2021.126866.
[16] *Environmental Management – Life Cycle Assessment – Principles and Framework*, ISO 14040, Geneva, Switzerland, 2006.
[17] M. Hauschild *et al.*, “ILCD handbook. Recommendations for Life Cycle Impact Assessment in the European context - based on existing environmental impact assessment models and factors,” European Union, Luxembourg, 2011.
[18] A. Lozanovski, O. Schuller, and M. Faltenbacher, “FC-HyGuide: Guidance Document for performing LCAs on Fuel Cells and H_2 Technologies,” European Commission, Brussels, Belgium, 2011.
[19] *openLCA* (2022). GreenDelta. Accessed: 31 Aug. 2023. [Online]. Available: https://www.openlca.org/
[20] *Brightway2* (2023). Python Software Foundation. Accessed: 31 Aug. 2023. [Online]. Available: https://pypi.org/project/brightway2/

Loading and boil-off analyses of liquid hydrogen into a specified cryogenic tank

S. M. Yahya*[1], U. Desideri[2], L. Ferrari[3], A. Baccioli[4]

[1]A. Department of Energy, Systems, Territory and Construction Engineering, University of Pisa, Pisa, Italy by cooperation with Gas & Heat Company.
[1]B. Mechanical Power Department, Faculty of Engineering, Tanta University, Egypt.

Introduction

The quest for sustainable and clean energy solutions has led to a renewed interest in hydrogen as a promising fuel source and energy carrier. Hydrogen offers zero-emission combustion so it can serve as a clean fuel for heating, power generation, and as a reducing agent in various chemical processes [1].

Hydrogen storage is a critical component of the pursuit of clean and sustainable energy solutions. As a lightweight and energy-dense fuel, hydrogen holds immense potential for various applications, including fuel cells and transportation. Efficient and safe storage methods are essential to harness hydrogen's benefits. Recent advancements are explored in hydrogen storage technologies, ranging from traditional methods like compression and liquefaction to emerging technologies such as solid-state and chemical storage [2-5].

Liquid hydrogen (LH_2) is interesting phase because of its versatility. It can be employed in various sectors, including transportation, industry, and power generation. As a fuel for fuel cell vehicles, liquid hydrogen offers zero-emission mobility, addressing the environmental impact of the transportation sector. Its high energy density ensures longer driving ranges for hydrogen-powered vehicles, making it a practical solution for both short and long-haul transportation [6]. In addition to transportation, liquid hydrogen finds applications in industrial processes. It can serve as a clean fuel for heating, power generation, and as a reducing agent in various chemical processes. The adoption of liquid hydrogen in industry contributes to reducing carbon footprints and promoting sustainable practices [7].

Liquid hydrogen storage is considered as the main point of the current work. Liquid hydrogen storage is a great challenge as it is stored at extremely low temperatures to maintain it in a liquid state, as hydrogen transitions from a gas to a liquid at temperatures below -252.8 degrees Celsius. The storage of liquid hydrogen involves several considerations to ensure safety, efficiency, and practicality [8]. Liquid hydrogen is stored in cryogenic tanks specifically designed to handle the extremely low temperatures required. These tanks are typically double-walled with a vacuum between the walls and highly insulated to minimize heat transfer. The materials used in cryogenic tanks must withstand low temperatures and the structural stresses associated with the expansion and contraction of the stored liquid. Inner tank materials are often stainless steel or other alloys designed to resist embrittlement at cryogenic temperatures [9,10]. The insulation helps to reduce the boil-off rate, where hydrogen returns to its gaseous state due to heat exposure. Effective insulation, such as multilayered thermal insulation, helps maintain the low temperatures and reduce heat ingress [9,11].

Boil-off is a natural occurrence in liquid hydrogen storage, where some of the liquid hydrogen vaporizes into gas. Managing boil-off is essential to prevent pressure buildup

* Corresponding author: saeed.yahya@phd.unipi.it

within the storage tank. Boil-off can be utilized, for example, as fuel for other processes or can be reliquefied and returned to the storage system [12]. Safety is also a parameter in liquid hydrogen storage. Cryogenic tanks must meet stringent safety standards to prevent leaks, ruptures, or any compromise in structural integrity. Emergency venting systems are in place to release excess pressure and avoid over-pressurization [9,13].

The loading and the off-loading process of a liquid hydrogen storage tank is also considered one of the great challenges in this field. Because of the extremely low boiling value of LH_2, a huge amount of LH_2 is lost during the loading process and needed to be re-liquified and re-feed. Therefore, the present work is focusing on studying the time estimated, the heat transfer and thermodynamic analysis, and the handling of the loading process.

Methodology

The current work will be performed on Amesim software before applied on a predefined tank which will be used to store liquid hydrogen as shown in Fig. 1. The liquid hydrogen tank consists of inner vessel storing (LH_2), outer jacket encasing the inner vessel, insulation system, and support elements. The elements of the liquid hydrogen tank will be designed according to ISO 13985 and ISO 21029-1 codes [14,15]. 316L stainless steel is recommended for the tanks' material because of its low susceptibility to hydrogen embrittlement and excellent toughness at cryogenic temperatures. Stainless steel has a low carbon content and a thermal conductivity of approximately 10 W/ (m. K) at 20 K in contact with LH_2 and approximately 16 W/ (m. K) in contact with the air at room temperature [9].

The insulation system is consisted of high degree of vacuum besides a perfect insulation material to configure a high performance of insulation between the two tanks. the applied insulation materials are preferred to be with a high thermal performance at vacuum pressure. for the current work, it is recommended to use the multi-layer insulation (MLI) because of its lower thermal conductivity than the other common materials as shown in Fig. 2 [16]. The current work is planned to be applied on predefined tank as a case study with dimensions as mentioned in Table 1.

Before initiation of loading LH_2 inside the tank, a preparation process should be carried out considering the precooling of the tank walls and the inside ambient volume of the tank to avoid the flashing phenomenon of LH_2 during the loading process. The preparation process consists of three steps. The first step is to precool the tank from 32 ℃ to -196 ℃ by using LN_2 as the precooling agent. The second step it to purge nitrogen gas from the inside volume by using hydrogen gas for this purpose. The third step is to continue cooling the tank walls from -196 ℃ to -252.8 ℃ by using LH_2 itself. The time estimation of the whole preparation process is considered the main point of study for the current work. It is also considered one the complicated studies in LH_2 storage. The reason of the aforementioned complexity is due to the action of the phase change of nitrogen or hydrogen from liquid to gas or the inverse during the cooling process. The action of the phase change definitely affects the overall heat transfer coefficients and as a sequence affects the estimated time of the preparation process.

For the present work, an appropriate model is prepared on Amesim software produced by Siemens to simulate the LH_2 storage tank and analyze its parameters during the loading, storage, transporting, and off-loading processes. The tank is discretized and divided into ten parts to study the distribution of the thermodynamic and heat transfer properties over the inside space of the tank and its walls. Fig. 3 shows only the first two parts of the tank as a first conception. Each part consists of various connected components to act a specific role. A constant temperature source is adjusted at 45 °C and connected to a thermal resistance

with 4 W/m^2. K air convection representing the outer ambient conditions. The inner and outer tanks are represented by two-thermal capacities considering the specifications mentioned in Table 1. A thermal radial resistance is connected between the two-thermal capacities to simulate the applied thermal insulation. For achieving high degree of insulation, the MLI insulation is performed beside a vacuum space and both are considered inside the radial resistance. From the fluid side, an adiabatic chamber with heat exchange is supported by a modulated mass and enthalpy flowrate source and are adjusted by the initial inner ambient conditions and the fluid specifications, respectively. The effect of the phase change can be controlled by adding a pilot thermal resistance and a generic sensor as an input and output to the adiabatic chamber. The sensor provides a high or low value of the heat transfer coefficient depending on the output phase of the fluid using the trigger and first order lag components. The same manner is followed for the remaining parts of the model.

Finally, the boil-off rate of LH_2 is estimated as it indicates the degree of performance of the LH_2 storage. The current work is also planned to be experimentally applied on site after achieving positive results from the modeling.

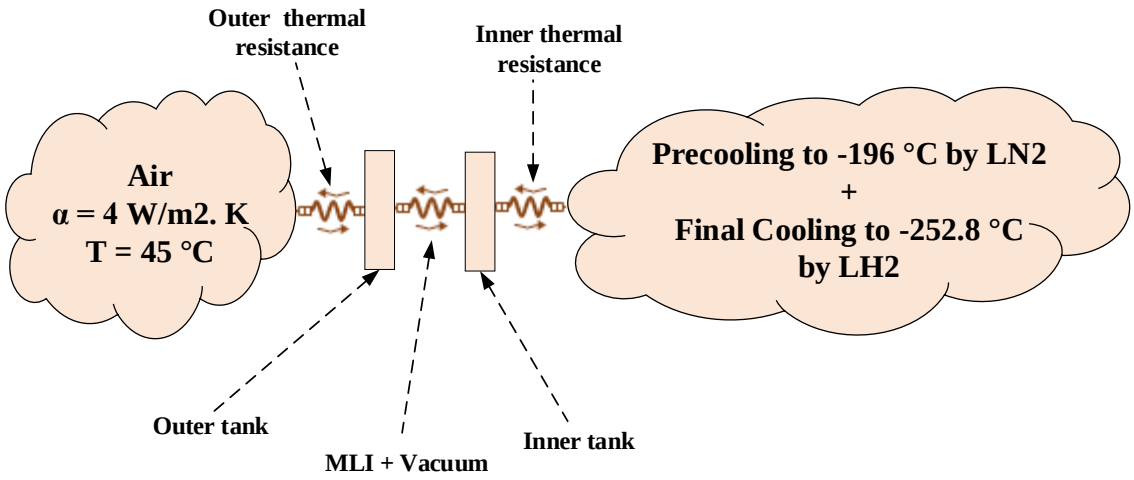

Figure 1: Configuration and conditions of Liquid hydrogen storage tank.

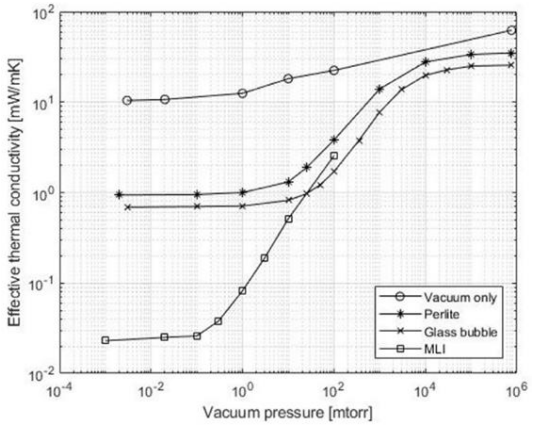

Figure 2: Effective thermal conductivity with cold vacuum pressure [16].

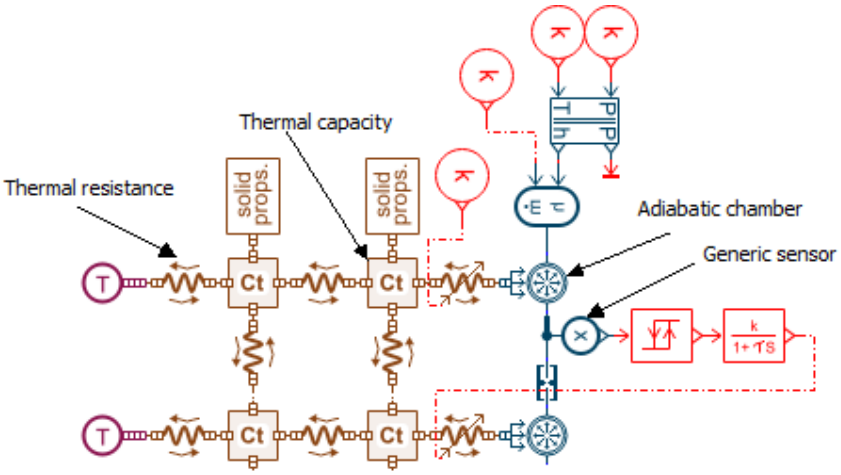

Figure 3: A first conception of the liquid hydrogen tank model on Amesim software for the first two parts only.

Table 1: Specifications of the tank case study.

Parameter	Inner tank	Outer tank
Material	316L stainless steel	316L stainless steel
Diameter (m)	11.5	12.2
Height (m)	31	32.984
Wall thickness (m)	0.021	0.015
Initial temperature (℃)	32	45
Final temperature (℃)	-252.8	___

Discussion

After preparing all the model components and adjusting the parameters with the design values, the model is activated to start the precooling run using the flowing of LN_2. Different mass flowrates of LN_2 between 0.4 to 2.2 kg/s are applied during the run. The temperature distribution and the precooling time can be estimated at the end of the run. Additional thermodynamic parameters of LN_2 can be estimated during the precooling process such as; specific enthalpy, density, and gas mass fraction at the output point of each part. The model can calculate the heat transfer rates to the tank as well. After that, nitrogen is purged away using hydrogen gas before continuing the cooling process. The purging process does not be simulated on Amesim, however, the purging time can be estimated by other simple ways like Excel. Then, the final cooling run is performed using LH_2 as the flowing fluid. The same calculated parameters of LN_2 can be done on LH_2. As a result, the overall loading time can be estimated. The other thermodynamic and heat transfer parameters are analyzed so they can present a first conception about what is happening during the preparation and the loading process. Finally, the boil-off rate is simulated under the same conditions and as a sequence, the performance of LH_2 storage can be expected. These analyses can lately be optimized to deduce the best recommended design parameters for a LH_2 storage tank.

Conclusions

Positive results are expected from performing such modeling on the LH_2 storage tank. Accurate time estimation of LH_2 loading process and relevant thermal analysis can be achieved. This can support the designers to optimize the best tank and insulation materials to put hands on the closest perfect design. In addition, the degree of safety can be developed across the gained analyses. The produced thermal and time analyses can also be a great guide to the manufacturers of the LH_2 tanks.

References

[1] Singh R, Altaee A, Gautam S. “Nanomaterials in the advancement of hydrogen energy storage. Heliyon”. 2020 Jul 1;6(7).

[2] Zhang F, Zhao P, Niu M, Maddy J. “The survey of key technologies in hydrogen energy storage. International journal of hydrogen energy”. 2016 Sep 7;41(33):14535-52.

[3] Zheng J, Liu X, Xu P, Liu P, Zhao Y, Yang J. “Development of high pressure gaseous hydrogen storage technologies. International journal of hydrogen energy”. 2012 Jan 1;37(1):1048-57.

[4] Satyapal S, Petrovic J, Read C, Thomas G, Ordaz G. “The US Department of Energy's National Hydrogen Storage Project: Progress towards meeting hydrogen-powered vehicle requirements. Catalysis today”. 2007 Feb 28;120(3-4):246-56.

[5] Hassan Q, Sameen AZ, Salman HM, Jaszczur M, Al-Jiboory AK. “Hydrogen energy future: Advancements in storage technologies and implications for sustainability”. Journal of Energy Storage. 2023 Nov 20; 72:108404.

[6] Scott RB, Denton WH, Nicholls CM, editors. “Technology and uses of liquid hydrogen”. Elsevier; 2013 Oct 22.

[7] Rondinelli S, Gardi A, Kapoor R, Sabatini R. “Benefits and challenges of liquid hydrogen fuels in commercial aviation”. International Journal of Sustainable Aviation. 2017;3(3):200-16.

[8] Valenti G. “Hydrogen liquefaction and liquid hydrogen storage”. In Compendium of hydrogen energy 2016 Jan 1 (pp. 27-51). Woodhead Publishing.

[9] Choi Y, Kim J, Park S, Park H, Chang D. “Design and analysis of liquid hydrogen fuel tank for heavy duty truck”. International Journal of Hydrogen Energy. 2022 Apr 15;47(32):14687-702.

[10] Gomez A, Smith H. “Liquid hydrogen fuel tanks for commercial aviation: Structural sizing and stress analysis”. Aerospace Science and Technology. 2019 Dec 1; 95:105438.

[11] Yatsenko EA, Goltsman BM, Novikov YV, Izvarin AI, Rusakevich IV. “Review on modern ways of insulation of reservoirs for liquid hydrogen storage”. International Journal of Hydrogen Energy. 2022 Dec 15;47(97):41046-54.

[12] Aziz M. “Liquid hydrogen: A review on liquefaction, storage, transportation, and safety”. Energies. 2021 Sep 17;14(18):5917.

[13] Kang D, Yun S, Kim BK. “Review of the liquid hydrogen storage tank and insulation system for the high-power locomotive”. Energies. 2022 Jun 15;15(12):4357.

[14] ISO 13985:2006 - Liquid hydrogen — Land vehicle fuel tanks.

[15] ISO 21029-1:2018 - Cryogenic vessels.

[16] Fesmire JE. “Standardization in cryogenic insulation systems testing and performance data”. Physics Procedia. 2015 Jan 1; 67:1089-97.

Long term and stability evaluation of Membrane electrode assembly of anion exchange water electrolyzer

Sepanta Dokhani[*1,2], Burak Koyuturk[2], Anders Lundblad[1,2], Amirreza Khataee[2], Göran Lindbergh[2]
[1]RISE, Research Institutes of Sweden AB
[2]KTH, Royal Institute of Technology

Introduction

As the world transitions from fossil fuels to renewable energy resources, there is a growing focus on hydrogen as an energy carrier. Yet, the production of clean green hydrogen remains a challenge, hindering its widespread use as an alternative to conventional fuels. One promising strategy to address this challenge involves the integration of renewable energy resources with electrochemical water electrolysis systems. Therefore, in recent years, anion exchange membrane water electrolysis (AEMWE) has gained significant attention due to its attractive features, combining low-cost materials with relatively high efficiency for hydrogen production. However, adopting AEMWE technology on a larger scale raises two key technical questions: the maturity of the technology and its long-term durability and stability.

Methodology

The Membrane Electrode Assembly (MEA) utilized in this study were prepared using commercial NiFeCo catalyst hand-painted on nickel fiber paper and $Ni_2Fe_2O_4$ on stainless steel fiber paper as the cathode and anode, respectively (Dioxide materials, USA). An Aemion$^+$ membrane from Ionomr Innovations was pressed between the catalysts layers in a zero-gap cell hardware (Dioxide Materials, USA), with an active surface area of 5 cm^2 at 2 Nm torque [1][2].

The test setup, as illustrated in Figure 1, consisted of separate tanks for the catholyte and anolyte to be fed into the cell, a four-channel peristaltic pump, two heating (heat exchange) bottles for the electrolytes, temperature probes, and the electrolyzer cell equipped with two heating jackets.

The system temperature was maintained at 55°C utilizing two heating (heat exchange) bottles for the electrolytes, temperature probes as a temperature controllers, and heating jackets for the cell. A 1M KOH electrolyte was cycled through a peristaltic pump at 1 ml/min during the measurement. To maintain a constant pH, DI water was added to the catholyte tank. Before running the test, electrolyte at the required temperature was pumped through the cell for 1 hour.

* Corresponding author: email address sepanta.dokhani@ri.se (S. Dokhai).

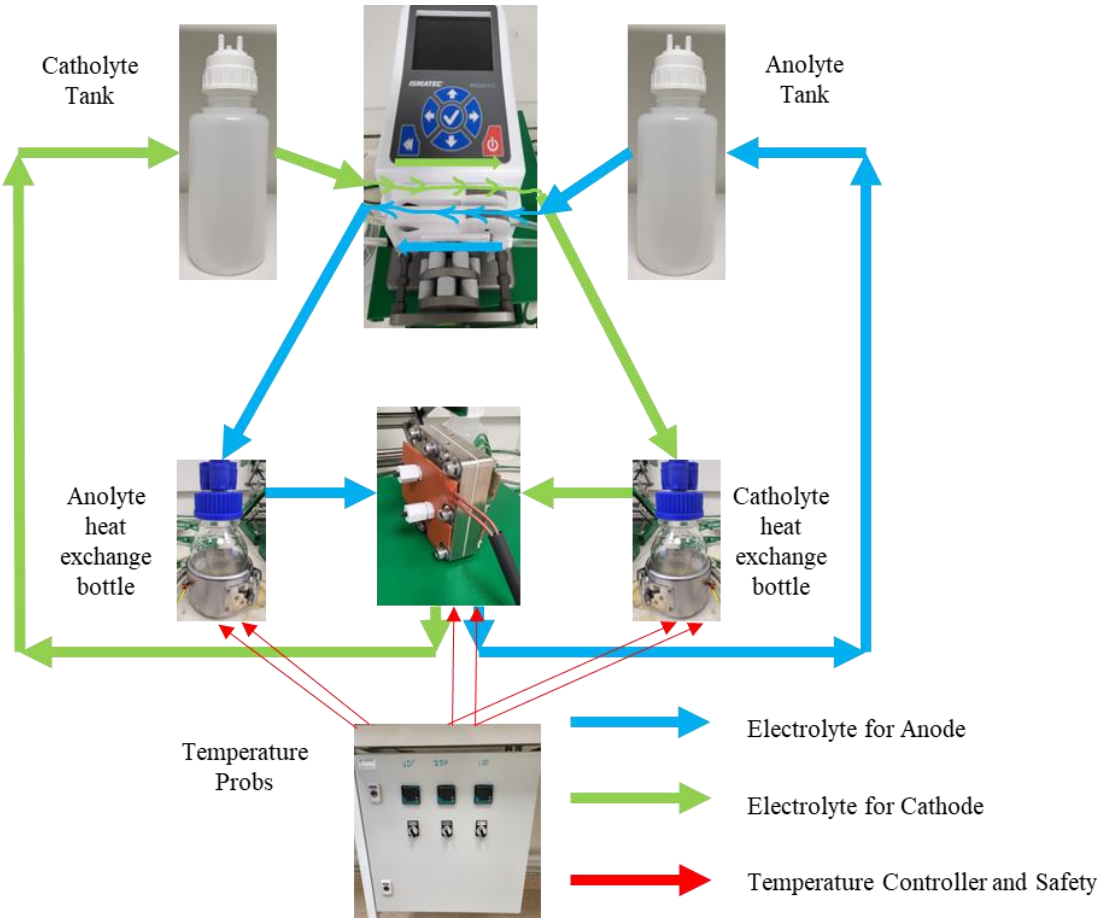

Figure 1: AEMWE lab build up testing bench.

The test protocol, which is shown in Figure 2, has two modes of operation:

- The cell will be held at galvanostatic mode at 1 A/cm² for 100 h and then electrochemical characterizations such as EIS measurement and polarization curve will be performed.
- Then a dynamic mode (i.e. accelerated stress test, AST) consisting of maintaining 0.2 A/cm² for 18 s and then 1A/cm² for 18 s and these two steps are repeated 10 000 times which adds up to 100 h of dynamic ageing, and after that electrochemical characterizations will be performed again. [3]

Results and discussion

It must be mentioned that we are in the early stage of our work for comparing benchmark testing result with the newly developed MEAs from other groups of the PUSH Research Center in Sweden. Below, you can find the benchmark results which is going to be compared with new MEAs.

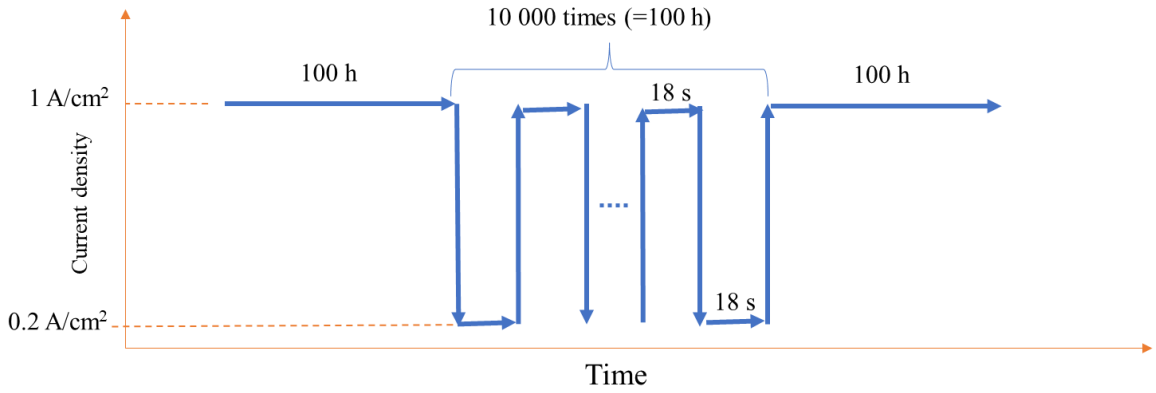

Figure 2: Designed test protocol for each cycle.

The test results will be discussed in three parts. It's important to note that due to experimental issues, the cell was subjected to operation at 0.1 A/cm² and room temperature (15-20°C) after 700 hours for 24 hours. These conditions yielded interesting results in terms of stability, impedance, and polarization curve performance.

- Regarding galvanostatic stability and AST. As can be seen in Figure 3, the electrolyzer has shown acceptable stability during the 2500 h test. As was mentioned, after 700 h, the cell were held at low current and temperature which surprisingly improved the performance of the cell in terms of cell voltage. However, this improvement might be an artefact (due to, for example, hydrogen crossover) and should be further investigated when ending the experiment. After 700 h the performance was not significantly changed even up to 2500 h

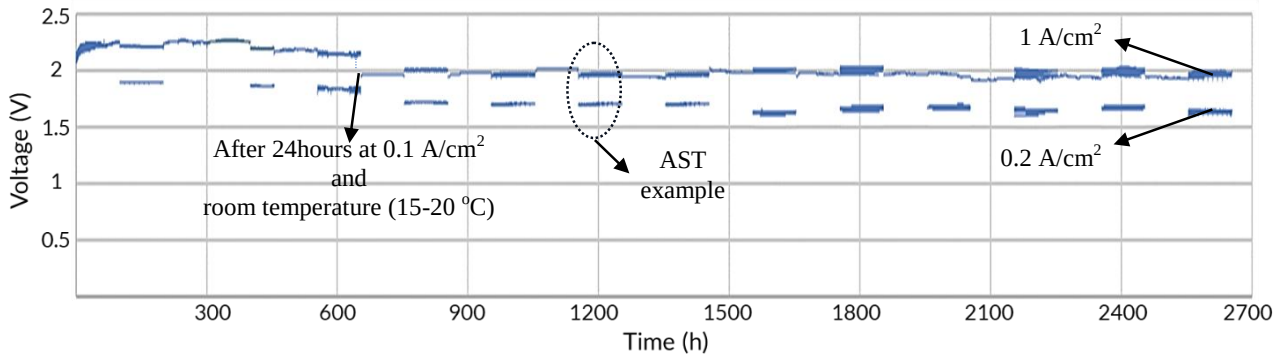

Figure 3: Galvanostatic stability and AST testing at 1000 and 200 mA/cm^2.

- When it comes to impedance, a relatively stable high frequency resistance (HFR) was observed. However, variations in low frequency semi-circle diameter were observed throughout the testing. This phenomenon is presented in Figure 4.

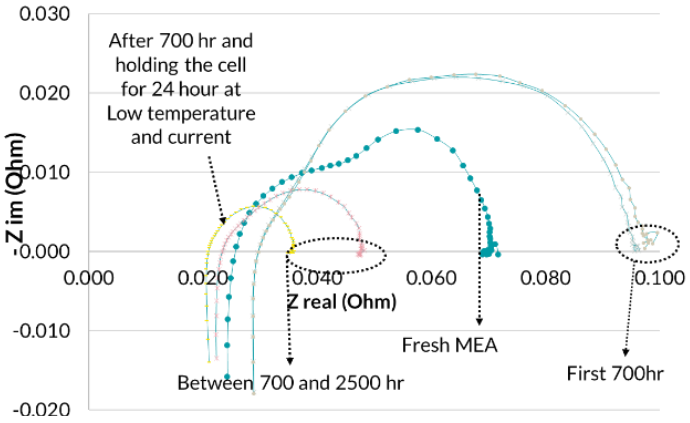

Figure 4: EIS analysis at different cycles.

- After subjecting the cell to 0.1 A/cm² and room temperature (15-20°C), we observed an improvement in the polarization curves (see Fig. 5). However, it is worth noted that low currents were observed at voltage levels below the standard potential of electrolysis, and we were unable to explain this phenomenon.

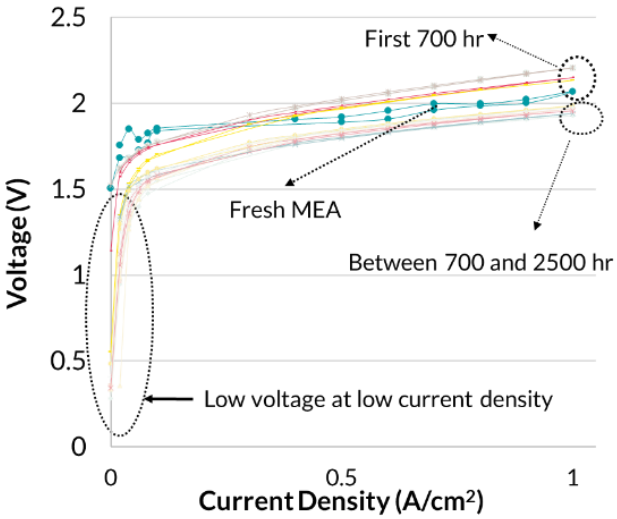

Figure 5: Polarization curve for different cycles.

Conclusions

The MEA exhibits robust stability, demonstrating continuous performance over 2500 hours. Notably, subjecting the cell to low current density and reduced temperature at the 700-hour mark seemingly enhances the cell's efficiency. Further investigation into the cause behind the voltage drop below the standard potential for electrolysis during low current conditions is needed. It's worth noting that during the final conference presentation, these findings will be contrasted with the results of lifetime tests and AST conducted on MEAs developed by other partners within the PUSH Research Center in Sweden.

References

[1] I.V. Pushkareva, A.S. Pushkarev, S.A. Grigoriev, P. Modisha, D.G. Bessarabov,Comparative study of anion exchange membranes for low-cost water electrolysis,International Journal of Hydrogen Energy,Volume 45, Issue 49,2020,Pages 26070-26079,ISSN 0360-3199,https://doi.org/10.1016/j.ijhydene.2019.11.011.

[2] Zengcai Liu, Syed Dawar Sajjad, Yan Gao, Hongzhou Yang, Jerry J. Kaczur, Richard I. Masel,The effect of membrane on an alkaline water electrolyzer, International Journal of Hydrogen Energy,Volume 42, issue 50,2017,Pages 29661-29665,ISSN 0360-3199,https://doi.org/10.1016/j.ijhydene.2017.10.050.

[3] ANIONE, Cor. “Milestone 8 Achieved: Improved MEA Electrochemical Durability| June 2022.” ANIONE, June 30, 2022. https://anione.eu/milestone-8-achieved-improved-mea-electrochemical-durability-june-2022/.

Low temperature synthesis of ammonia by a chemical looping process based on metal imides as nitrogen carrier

Antoine Dechany[*1] *, Lukas Buelens* [2]*, Vladimir Galvita*[2]*, Kevin Van Geem*[2]*, Joris Proost*[1] *and Christophe Detavernier*[3]

[1] Université catholique de Louvain (UCLouvain), Division of Materials and Process Engineering, Place St. Barbe 2, Louvain-la-Neuve, Belgium

[2] Universiteit Gent, Laboratory for Chemical Technology, Technologiepark 125, B-9025, Ghent, Belgium

[3]Universiteit Gent, Department of Solid State Sciences, Krijgslaan 281/S1, Ghent, Belgium

Introduction

While global warming becomes more and more tangible, joint efforts to decarbonize all human activities are intensifying. Among the sector that would benefit from carbon mitigation, the chemical industry holds a significant position. Beyond the fact it was responsible for 4.2% of the global CO_2 emissions in 2019, 1.2% are attributable to the production of ammonia alone, making it one of the largest CO_2 emitters of the chemical industry [1, 2]. The main reason behind this considerable contribution is the fossil-based Steam Methane Reforming process (SMR) used to produce hydrogen, which is then fed to the Haber-Bosch (HB) process for NH_3 synthesis. Furthermore, it is worth noting that half of the world's food production currently relies on fertilizers produced with synthetic ammonia through this method, making it a critical challenge to tackle [3]. Several alternative technologies have already been proposed and are currently being studied [4]. Among them is the electrification of the H_2 production, replacing SMR with electrolysis, which will have several implications on the process and will inevitably lead to new challenges [5]. However, such a solution revolves only around the replacement of the SMR. Transitioning to a lower operating conditions process such as alkaline water electrolysis (60-90°C & 1-30 bar) can lead to the entire process being rethought, including the well-established Haber-Bosch technique (350-500°C & 150-300 bar). In this work, a novel technique is investigated to fully replace the HB process with a low temperature and pressure chemical looping process.

Introduced in the early 20th century for hydrocarbon fuel conversion, the principle of chemical looping is based on the decoupling of a catalytic reaction in sub-reactions supported on a catalyst that passes through an intermediate state and is then regenerated in a loop. Nowadays, chemical looping emerges as a promising technology for various applications, including low-temperature and pressure ammonia synthesis [6, 7]. Among the recent studies on the subject, one demonstrated unparalleled NH_3 production rates at mild conditions using Ni-BaH_2/BaNH as a catalyst via reaction (1) and (2) [8].

$$4BaH_{2(s)} + 2N_{2(g)} = 4BaNH_{(s)} + 2H_{2(g)} \quad (1)$$

$$2BaNH_{(s)} + 4H_{2(g)} = 2BaH_{2(s)} + 2NH_{3(g)} \quad (2)$$

Ammonia started forming at ambient pressure and temperatures as low as 100°C, with the synthesis rate reaching 3125 µmol g^{-1} h^{-1} at 300°C. Within the context of electrifying ammonia production, such low conditions would better match with alkaline water electrolysis.

* Corresponding author: antoine.dechany@uclouvain.be

The present work provides an in-depth analysis of the behavior of Ni-BaH_2 during nitridation (reaction (1)) under isothermal conditions. Parallel experiments were conducted on both N_2 Temperature-Programmed Reaction (N2-TPR) and time-resolved in situ X-Ray Diffraction (XRD) to observe reaction (1) at 5 distinct temperatures ranging from 180°C to 300°C.

Methodology

Material synthesis

Ni-BaH_2 was prepared with a loading of 50% Ni nanopowder (Merck, <100 nm, 99%) and 50% BaH_2 (Strem) grinded by hand with an agate mortar and pestle inside an Ar-filled Jacomex P(BOX) glove box. The sample studied in this work was prepared by grinding 850mg of each powder for 1h, in 4 periods of 15minutes. 1mL of acetone was added each time after 15, 30 and 45min to improve homogeneity and prevent adherence to the edges of the mortar.

Experimental methods

N2-TPR measurements were carried out on a Micromeritics Autochem II 2920 setup connected to a Thermal Conductivity Detector (TCD) and the outlet gas composition was analyzed with a Mass Spectrometer (MS) detector. 200mg of Ni-BaH_2 was loaded in a quartz reactor and heated at 90°C/min in a He flow at atmospheric pressure (30 ml min^{-1}) to the target temperature, monitored by a thermocouple directly placed in the sample. After reaching the isothermal regime, the gas flow was switched manually to a N_2 flow at atmospheric pressure (30 ml min^{-1}). After 15min, the reactor was cooled down to room temperature. The sample was then retrieved from the reactor in an Ar-filled glove box.

Powder diffraction and time-resolved in situ XRD experiments were both conducted on a Bruker-AXS D8 Discover apparatus (Cu Kα radiation of 0.154 nm). 50mg of the sample was disposed on a silicon wafer, placed on a heating plate and enclosed in a home-built reaction chamber. Vacuum was progressively applied until a pressure of $5*10^{-2}$ mbar was reached. The chamber was then filled with He until atmospheric pressure. In situ XRD collects series of measurements at regular time intervals (10 seconds) in restricted angular ranges (2θ = 19° – 38°) and allows the analysis of samples in reaction conditions. In this case, it was set to follow the same temperature and gas protocol as the N2-TPR. The sample was heated to the target temperature at 90°C/min under He at atmospheric pressure (1000 ml min^{-1}). As the preset temperature provided to the program corresponds to that of the heating plate, a deliberate adjustment of +10°C was applied to account for heat losses. Upon reaching the target temperature, gas flow was then manually switched to a N_2 flow at atmospheric pressure (1000 ml min^{-1}). The sample was cooled down to room temperature after 15min.

Discussion

N2-TPR

The nitridation of Ni-BaH_2 as detailed in reaction (1) was tested by N2-TPR on 5 temperatures (180°C, 210°C, 240°C, 270°C and 300°C). The resulting signals are displayed on Figure 1. As expected from reaction (1), H_2 is produced during N2-TPR, as can be seen on Figure 1a & 1b (green section). Despite it being expressed in arbitrary units, the signal appears to be increasing with temperature, which confirms the increasing yield demonstrated in previous studies [8, 9]. However, the signal is decreasing again at 300°C.

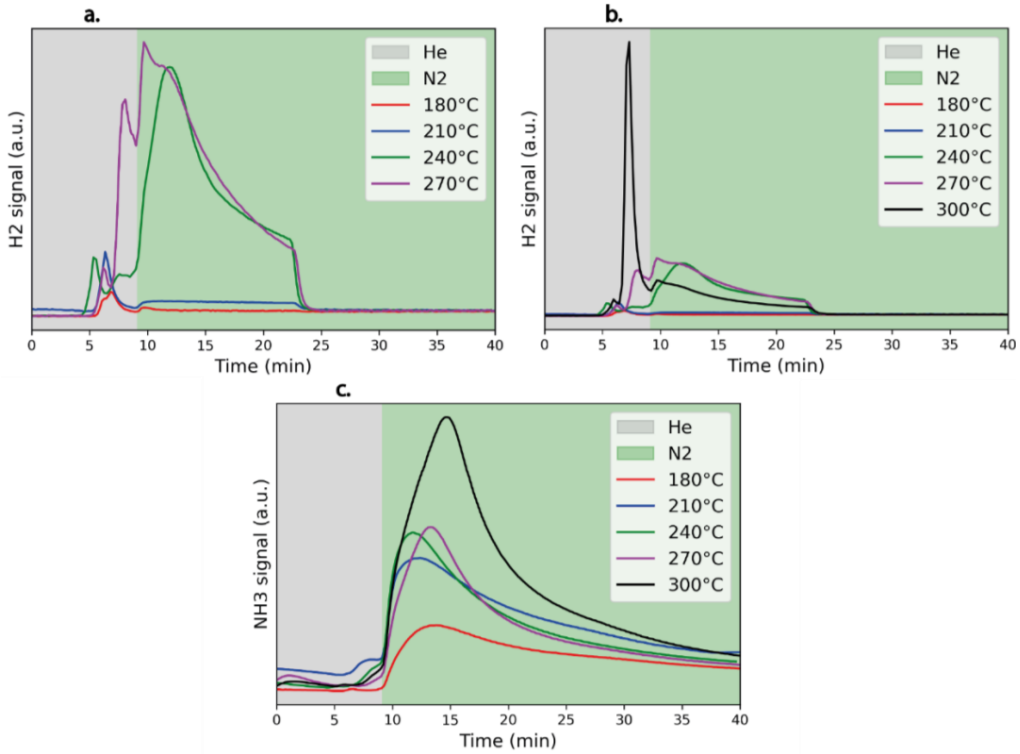

Figure 1: N2-TPR profiles of Ni-BaH_2. **a & b** H_2 signal through time for 180°C, 210°C, 240°C, 270°C (**a**) and 300°C (**b**) isothermals. **c.** NH_3 signal through time for the 5 isothermal experiments. (a.u.) = arbitrary units.

Hydrogen seems to be released even before N_2 is fed to the reactor, during the heating-up under He flow, indicating that a dehydrogenation reaction is taking place. This phenomenon was studied by Guan et al. in 2022 [9]. They first noticed a dehydrogenation happening under an Ar flow starting from 300°C, and then demonstrated that a pretreatment under argon at that same temperature would be beneficial for the later N_2 fixation, thanks to H vacancies being formed. Here however, the H_2 signal starts as low as 50°C as shown on Figure 2a, with an apparent maximum reached around 150°C. During the 2 highest isothermal experiments (270°C and 300°C), a second dehydrogenation mechanism seems to take place, starting from 210-230°C. On Figure 2b, one can notice that a second maximum is achieved around 275°C for both these isothermals. It is also noticeable as a second peak showing on Figure 2b. This 2-step dehydrogenation can be regarded as an indicator that 2 different hydrogen sites are at stake. The first (and weakest) dehydrogenation signal may be coming from a second hydride formed in lower quantity as a byproduct during the catalyst synthesis, such as Ni_2H. The second (and highest) dehydrogenation signal most certainly originates from BaH_2, the principal hydride of the sample.

Figure 1c shows that NH_3 is also produced during N2-TPR, which indicates that the second step of the chemical looping process, as detailed in reaction (2), is already taking place during the first nitridation step. This can also explain the decreased H_2 signal highlighted earlier at 300°C, as H_2 would be consumed to produce NH_3.

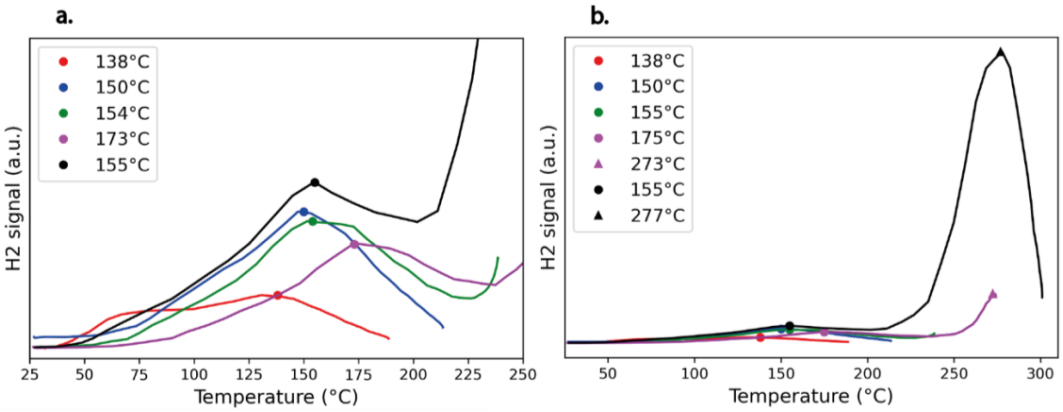

Figure 2: H_2 signal through temperature during heating-up for 180°C, 210°C, 240°C, 270°C (**a**) and 300°C (**b**) isothermals. (a.u.) = arbitrary units.

In-Situ XRD

Parallel to the N2-TPR, the same conditions were reproduced inside an in-situ XRD setup. Figure 3 displays the full diffraction pattern obtained after each isothermal N2-TPR, as well as the as-prepared sample. Some barium oxide ($BaO_{1.3}$) and nickel oxide (NiO) seem to have formed in the sample, as a result of the short exposure to the air when transferring the sample to the reaction chamber. It can be noted that the diffractograms do not vary after the first 3 isothermal experiments. However, changes appear clearly on the 280°C and 300°C isothermals.

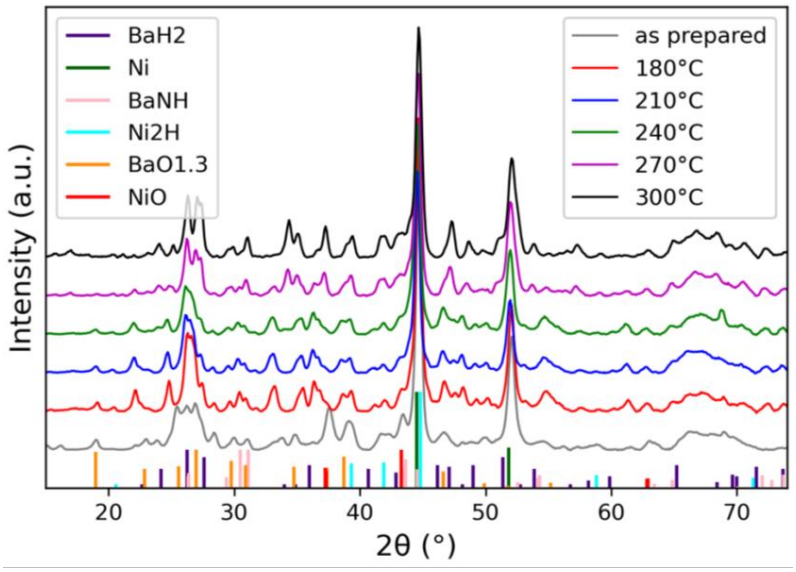

Figure 3: XRD patterns of the as-prepared sample and the sample after each isothermal experiments. (a.u.) = arbitrary units.

This is where in-situ XRD brings more detail to the measurements, as the sample was periodically scanned for the whole duration of the heating up and N_2 exposure. Figure 4 shows 3 diffraction patterns extracted from those measurements. The patterns are shown on a restricted angular range from 19° to 38° where the most prominent peaks for both BaH_2 and BaNH are located. On Figure 4.a, the initial state of the as-prepared sample can be seen. Figure

4.b and 4.c show the post-transition states at the corresponding temperatures where the transitions took place: 153°C and 275°C. Both these temperatures are very close to the ones observed earlier in the dehydrogenation steps during N2-TPR, and both

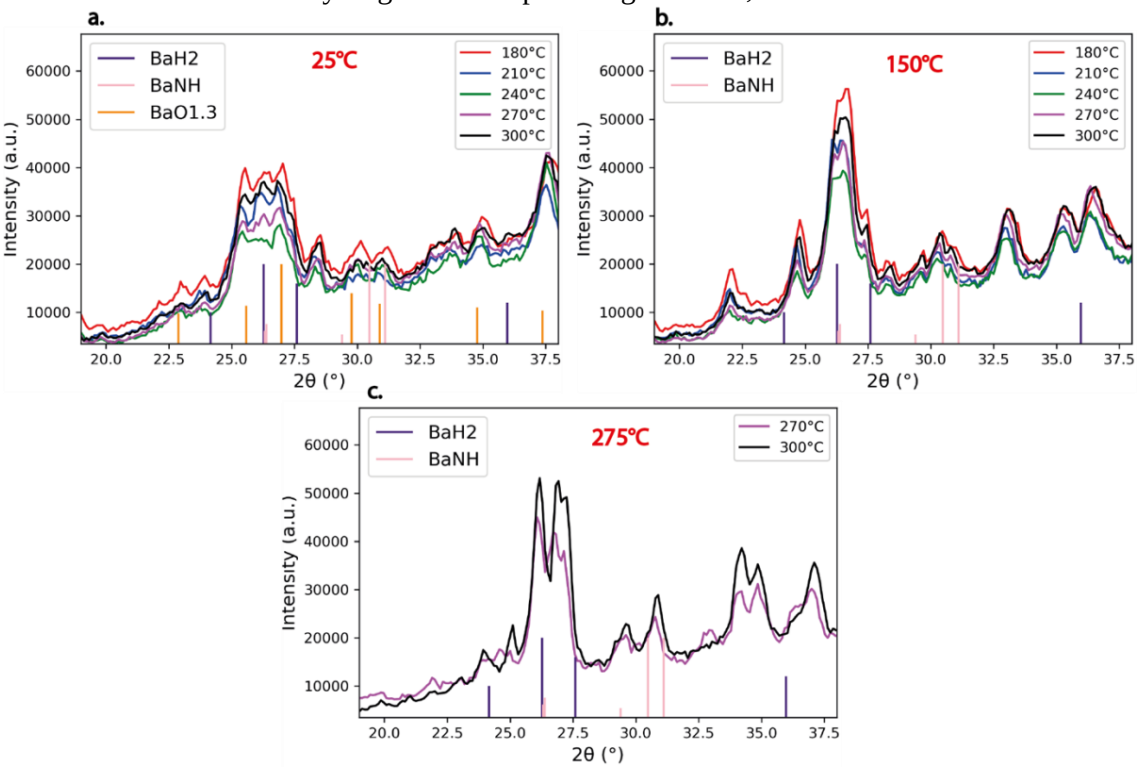

Figure 4: in-situ XRD patterns extracted at ambient temperature (**a**), 150°C (**b**) and 275°C (**c**) for each isothermal experiments. (a.u.) = arbitrary units.

happened during the heating-up under He. The 2-step dehydrogenation could then explain both transitions observed in the diffraction pattern. Furthermore, the idea that a secondary hydride Ni_2H is implied in one of the dehydrogenation mechanisms is supported by the presence of its peaks in the diffraction pattern on Figure 3. Finally, the last scan taken directly after the second transition (Figure 4.c) does not show a peak at 26.3° anymore. That specific diffraction peak is notably the strongest of BaH_2 and is associated to the (120) plane. This may be regarded as a shift in the diffraction plane following the appearance of H vacancies, especially given that they appear preferably on the (120) surface [9].

It is important to highlight that no variations took place during the nitridation step when the N_2 was flowed, showing no traces of BaNH whatsoever. The typical peaks around 2θ = 30-31° should have no link with BaNH as they were present before N_2 was flowed. Moreover, two $BaO_{1.3}$ peaks are also located in the same range and could very well be confused with BaNH.

Further work

In this work, the nitridation of Ni-BaH_2 could only be proven from the release of H_2 and NH_3 as observed during N2-TPR. However, no direct traces of BaNH have yet been highlighted. In subsequent research, more tests could be conducted using the same setups but with adapted parameters. For instance, it was shown that the nitridation increased with longer exposure to N_2 (40% of nitridation after 30 minutes of exposure to N_2 at 265°C) [8]. Another possibility

currently envisioned is the use of environmental Transmission Electron Microscopy (TEM) to observe the catalyst behavior in-situ on a submicron-scale under reaction conditions.

Conclusions

- Nitridation of Ni-BaH_2 was studied isothermally at five distinct temperatures (180°C, 210°C, 240°C, 270°C and 300°C).
- Hydrogen production during N2-TPR confirmed the nitridation process. Increased H_2 with increased temperature also confirmed literature results on the reaction yield.
- A two-step dehydrogenation was observed under helium flow during heating at 150°C and 275°C respectively.
- Ammonia production indicated the progression of the chemical looping process as the emitted hydrogen provides the reactant for the second reaction.
- Analysis of powder diffraction patterns revealed the formation of barium oxide ($BaO_{1.3}$) and nickel oxide (NiO) in the as-prepared sample, probably after a short exposure to air when transferring it to the in-situ XRD reactor chamber.
- The two-step dehydrogenation observed during N2-TPR experiments aligns with the changes in the diffraction pattern taking place at similar temperatures (153°C and 275°C).
- The presence of Ni_2H may indicate it is the second source of hydrogen acting in the dehydrogenation with BaH_2.

Acknowledgements

Funding from the Belgian Energy Transition Funds of the Federal Planning Service for Economy, S.M.E., Self-employment and Energy is gratefully acknowledged through the BE-HyFE project (Belgian Hydrogen Fundamental Expertise).

References

[1] IEA, *Energy Technology Perspectives 2020*. 2020. doi: 10.1787/ab43a9a5-en.
[2] IEA, "Global energy review: CO2 emissions in 2020." Accessed: Dec. 03, 2022. [Online]. Available: https://www.iea.org/articles/global-energy-review-co2-emissions-in-2020
[3] Our World in Data, "How many people does synthetic fertilizer feed?"
[4] F. B. Juangsa, A. R. Irhamna, and M. Aziz, "Production of ammonia as potential hydrogen carrier: Review on thermochemical and electrochemical processes," *Int J Hydrogen Energy*, vol. 46, no. 27, pp. 14455–14477, 2021, doi: 10.1016/j.ijhydene.2021.01.214.
[5] A. Dechany, K. Van Geem, and J. Proost, "Process implications of electrifying ammonia production," *Curr Opin Chem Eng*, vol. 40, no. 2, p. 100915, 2023, doi: 10.1016/j.coche.2023.100915.
[6] A. Joshi *et al.*, "Chemical looping-A perspective on the next-gen technology for efficient fossil fuel utilization," *Advances in Applied Energy*, vol. 3, no. March, p. 100044, 2021, doi: 10.1016/j.adapen.2021.100044.
[7] H. Poelman and V. V Galvita, "Intensification of Chemical Looping Processes by Catalyst Assistance and Combination," *Catalysts*, 2021.
[8] W. Gao *et al.*, "Production of ammonia via a chemical looping process based on metal imides as nitrogen carriers," *Nat Energy*, vol. 3, no. 12, pp. 1067–1075, 2018, doi: 10.1038/s41560-018-0268-z.
[9] Y. Guan *et al.*, "Transition-Metal-Free Barium Hydride Mediates Dinitrogen Fixation and Ammonia Synthesis," *Angewandte Chemie - International Edition*, vol. 61, no. 39, 2022, doi: 10.1002/anie.202205805.

Materials for hydrogen storage: synthesis, characterization and sorption properties

F. Garelli[1*], A.K. Patel[1], E. Dematteis[1], M. Baricco[1], P. Rizzi[1]

[1] Department of Chemistry and NIS, University of Torino, Italy
[*]Corresponding Author: francesca.garelli@unito.it

Introduction

According to the International Energy Association, the electricity consumption per capita at the global level increased by 58% in the last 30 years. On the other hand, thanks to the increase in use of renewable energies, the CO_2 emission production per capita raised much less at the global level (i.e., 14%). These values are very different considering different areas, as demonstrated by the difference between the energy consumption and the CO_2 emission in Europe (5.60 MWh/capita and 5.72 tCO_2/capita), Africa (0.57 MWh/capita and 0.98 tCO_2/capita) and Asia (6.04 MWh/capita and 8.58 tCO_2/capita). The difference in the CO_2 emission in different areas is following the diverse increment in renewable energy production [1].

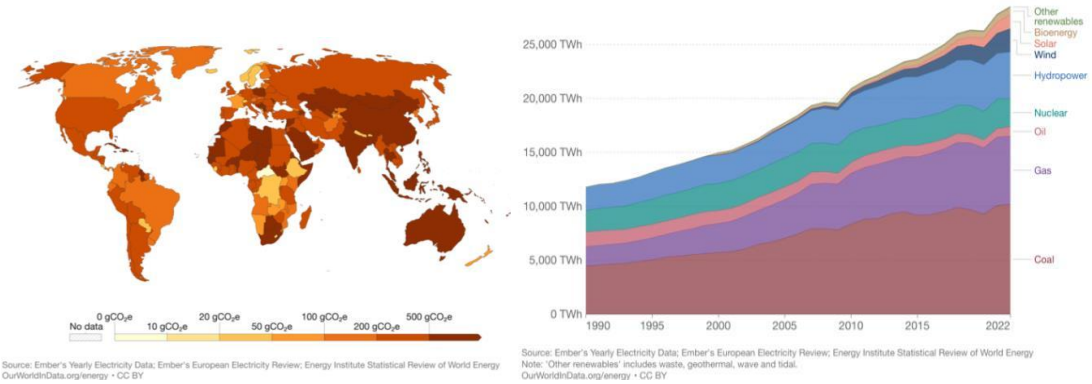

Figure 1: Carbon intensity of electricity 2022 (on the left) and World electricity production by source (on the right) [2], [3]

Renewable energies are highly considered as the alternative to fossil fuels, but their fluctuations in time and geography request the use of energy storage systems. The development of good, clean, and efficient technologies for energy storage is the key point for using only renewable energies. Thus, it is important to plan integrated systems at a large scale to store the excess energy to meet the future demand and utilization.

One alternative for electricity storage is using green hydrogen as a secondary energy vector producing it by electrolysis from water end excess electricity.
This option shows several advantages, such as hydrogen being unlimited, being stored for a long time and having higher energy-to-weight ratio compared to other fuels. On the other hand, for the energy- to-volume ratio, the situation is inverted. This is a drawback for hydrogen storage, and it can be fixed increasing energy density to limit system volume [4].
There are several possible hydrogen chains for energy communities based on the renewable source used or the different hydrogen storage method.

It should be noted that, in counting the benefits deriving from the use of hydrogen as an energy vector in the storage of excess electricity, the entire chain must be considered: the excess of renewable electricity used to produce hydrogen, hydrogen storage, generation of electricity from hydrogen, transport of electricity and final use [5].
A possible hydrogen chain is shown in Figure 2 and it could use excess solar or wind energy to produce hydrogen via electrolysis of water. Then the hydrogen produced is stored with the various methodologies existing today: compressed gas or liquid, solid state, underground storage. Finally, electricity is recovered from hydrogen using waste thermal energy and fuel cells. The electricity is fed into the grid, and it can be used in stationary or mobile applications [6].

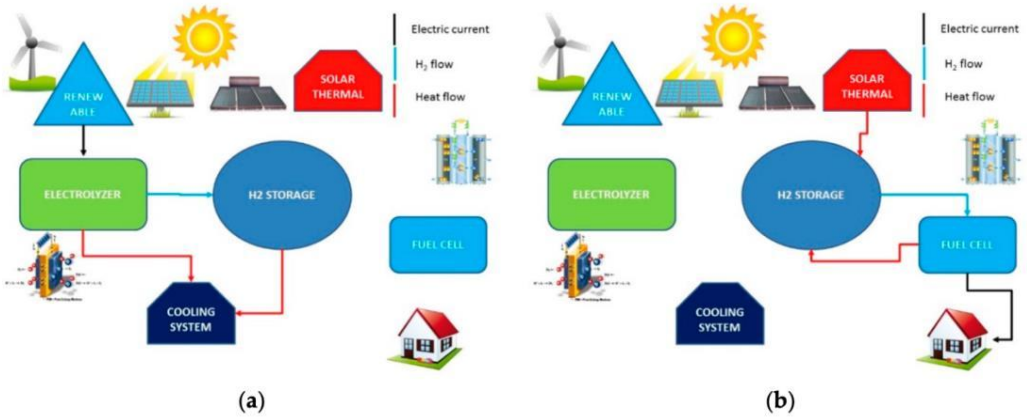

Figure 2: Possible hydrogen chain. Flow of hydrogen, heat, and electricity during hydrogen production (**a**) and use (**b**)

Among the several possible hydrogen storage methods, hydrogen carriers are a promising solution, since it is more affordable and allows large volumetric densities compared to compressed or liquid hydrogen. Moreover, handling hydrogen as hydride results safer than liquid and compressed gas.
A huge number of metal hydrides has been investigated and particularly interesting for hydrogen storage are hydrides based on intermetallic compounds A_2B, AB, AB_2, and AB_5. A is an element that forms stable hydrides, while B is an element that forms unstable hydrides, so that the resulting hydride has intermediate properties between A and B hydrides.
The most known AB compound for hydrogen storage application is TiFe and its modifications, obtained by substituting Ti or Fe with other metals [1]. This alloy stores hydrogen at low pressure and temperature and has a good cycle stability at low pressure. Furthermore, it is cheap and nontoxic, and the raw materials are abundant. The main obstacle in using TiFe is its hard activation, resulting in real applications being difficult and costly [4]. Therefore, either titanium (Ti) or iron (Fe) is replaced with other materials. The substitution of Fe or Ti aims to facilitate the activation process and influence the storage capacity of the alloy. Therefore, the project is directed towards the synthesis of alloys with varying amounts of substitutive elements, their characterization, and the investigation of their hydrogen absorption properties.

Methodology

The main objective of this project is to study the effects of substitutions in TiFe alloys in order to gather sufficient data to expand the machine learning technology database developed within the Ex MACHINA Project. Therefore, it is important to perform synthesis, chemical and structural characterization of the alloy (for example, through SEM and EDX analyses) and an investigation of the alloy's absorption properties (e.g., using a Sievert volumetric apparatus). The absorption results obtained can then be utilized to assess the temperatures and pressures for the alloy's hydrogen storage usage and potential real-world applications.

Discussion

Various Al substitutions were tested to check the properties of the produced alloys with respect to pure TiFe. The effect of aluminum substitution on the absorption kinetics and PCT curves was evident, with particularly steep plateaus indicating a higher quantity of secondary phases and alloy non-homogeneity. Moreover, the pressure required for hydrogen absorption was found to be higher. This effect has been attributed to the presence of aluminum in the alloy structure, leading to a variation in thermodynamic and kinetic properties of the system. However, it is important to note that the amount of aluminum and the production method may influence the severity of these effects.
Furthermore, it emerged that alloy synthesis through arc melting produced non-homogeneous samples, with composition variations in the matrix, which could have contributed to the appearance of unforeseen phases in ternary diagrams and the complexity of hydrogen activation, along with particularly steep plateaus.

The analysis of TiFe alloys with the addition of different elements such as chromium (Cr), cobalt (Co), and copper (Cu) revealed interesting findings about their structure and behavior. Regarding the TiFe-Cr alloy, the presence of the $Ti(Fe,Cr)_2$ phase and the oxide phase $Ti_4Fe_2O_{1-x}$ was detected. The $TiFe_{0.80}Cr_{0.20}$ phase also exhibited lattice expansion compared to stoichiometric TiFe.
In the case of the TiFe-Co alloy, two primary phases were identified: $TiFe_{0.80}Co_{0.20}$ and $Ti_4Fe_2O_{1-x}$. Cobalt partially replaces iron in this phase, causing lattice expansion compared to stoichiometric TiFe.
Lastly, for the TiFe-Cu alloy, primarily the $Ti_4Fe_2O_{1-x}$ phase was identified, with a small amount of the β-$Ti_{80}(Fe,Cu)_{20}$ phase, the latter only visible with XPD. In this case as well, lattice expansion compared to stoichiometric TiFe was observed.

In all three cases, the analysis demonstrated the presence of oxides in the alloy, suggesting that oxidation is an important process in these alloys. The obtained information is crucial for understanding the properties and potential applications of these alloys in various industrial contexts.

Conclusions

In conclusion, TiFe remains an intriguing alloy for hydrogen storage due to its low cost and significant capacity. However, it is worth noting that the binary compound has certain drawbacks that can be overcome through appropriate substitutions, significantly enhancing activation and kinetics. Nonetheless, thermodynamic and hydrogenation properties are also affected, often resulting in a decrease in capacity.

The analysis conducted on TiFe alloys with varying contents of aluminum, cobalt, copper, and chromium has revealed important findings regarding their chemical and structural characteristics, as well as their absorption properties. In general, lattice expansion compared to stoichiometric TiFe was observed for all these substituents. The secondary phases formed vary depending on the substituting element used, but in general, the formation of an oxide phase was observed for all elements studied, emphasizing the high importance of the oxidation process in these alloys.

The absorption properties are strongly influenced by the substituting element used, which can impact the activation process, plateau slope, the number of visible plateaus, storage capacity, and storage pressures, in addition to storage temperatures. The absorption kinetics are also often influenced by substitutions in the TiFe alloy.

Therefore, substitutions in TiFe alloys are of fundamental importance for tailoring the hydrogen absorption properties of the resulting alloy to one's preferences and can represent a viable solution for hydrogen storage. The information obtained is thus necessary for understanding the properties and potential applications of these alloys in various application contexts.

References

[1] Bhandari, R.; Trudewind, C.A.; Zapp, P. Life cycle assessment of hydrogen production via electrolysis– a review. *Journal of Cleaner Production* **2014**, *85*, 151-163, DOI: 10.1016/j.jclepro.2013.07.048
[2] IEA. Global Energy Review 2021—CO2 Emissions. Available online: https://www.iea.org/reports/global-energy-review-2021/co2-emissions (accessed on 26 June 2023).
[3] IEA. Global Hydrogen Review 2022. Available online: https://www.iea.org/reports/global-hydrogen-review-2022 (accessed on 26 June 2023).
[4] Dematteis, E.M.; Barale, J.; Corno, M.; Sciullo, A.; Baricco, M.; Rizzi, P. Solid-State Hydrogen Storage Systems and the Relevance of a Gender Perspective. *Energies* **2021**, *14*, 6158, DOI: 10.3390/en14196158
[5] Belmonte, N.; Staulo, S.; Fiorot, S.; Luetto, C.; Rizzi, P.; Baricco, M. Fuel cell powered octocopter for inspection of mobile cranes: Design, cost analysis and environmental impacts, *Applied Energy* **2018**, *215*, 556-565, DOI: 10.1016/j.apenergy.2018.02.072
[6] Costamagna, M.; Barale, J.; Carbone, C.; Luetto, C.; Agostini, A.; Baricco, M.; Rizzi, P. Environmental and economic assessment of hydrogen compression with the metal hydride technology. *International Journal of Hydrogen Energy* **2022**, *47*, 17, 10122-10136, DOI: 10.1016/j.ijhydene.2022.01.098

Mathematical Modeling of the Membrane Electrode Assembly Microstructure and its Influence on Thermal and Water Transport Properties in Polymer Electrolyte Fuel Cells

Arturo Sánchez-Ramos[1*1], Pablo A. García-Salaberri[1]

[1]Department of Thermal and Fluids Engineering, Universidad Carlos III de Madrid, 28911 Leganés, Spain

Introduction

The effect of water management on oxygen transport plays a critical role in the design of high-performance polymer electrolyte fuel cells (PEFCs) for the automotive industry, especially at low cathode platinum loading [1],[2]. In this regard, optimizing the hierarchical pore structure of the membrane electrode assembly (MEA) is crucial to alleviate cathode flooding while ensuring good membrane hydration [3]. However, this is a complicated task due to the small dimensions involved in the problem. Mathematical modeling has turned out to be a key tool to understand transport in the thin layered assembly used in PEFCs, including the catalyst layer (CL), microporous layer (MPL) and gas diffusion layer (GDL).

Methodology

In this work, a 1-dimensional mathematical model through the membrane electrode assembly (MEA) is developed. This model considers proton and electron, oxygen and hydrogen, thermal and water transport equations (either as vapor, liquid or dissolved in Nafion) and includes a detailed description of the MEA microstructure through pore size distributions of the CL, MPL and GDL, which is used to compute effectively properties such as local saturation or local permeability among others based on a bundle of capillary tubes approach. The model has also been prepared to compute thermal properties in a microscopic-detailed approach in the CL as this is the most relevant layer for fuel cell enhanced performance.

Discussion

The developed model polarization curves predictions are validated against previous experimental data from other authors [4] for various operating conditions and pore structures (Figure 1). The results offer precise information on the coupling between heat and water transport in both liquid and gas phases, and the impact of operating conditions and transport properties on the saturation distribution through the MEA layers. Then, the model is used to perform a parametric analysis focused on the obtention of optimal pore size distribution (PSD), which has influence on effective transport properties through pore size, porosity, tortuosity, hydrophilicity and hydrophobicity of the medium, etc. to produce improved MEA microstructures.

[1*] Corresponding author: artsanch@pa.uc3m.es

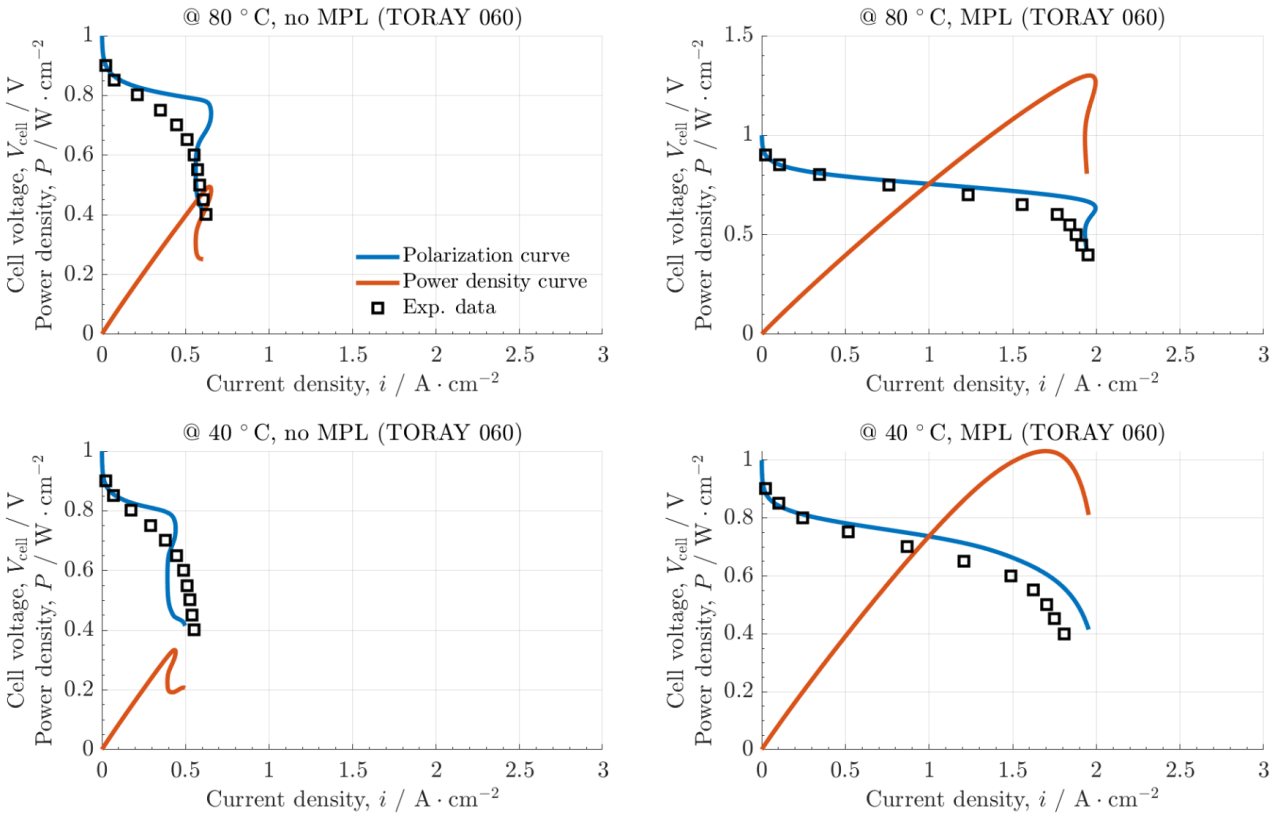

Figure 1: Validation of the MEA microscopic-detailed 1D model under different operating conditions and structure configurations: Temperatures of 80ºC in the upper subfigures vs 40ºC in the lower ones. Toray 060 without microporous layer (MPL) in the left ones vs Toray 060 with microporous layer in the right ones. Power density curves are also provided in red.

Conclusions

Due to the microscopic scale of polymer electrolyte fuel cell structures, a deep understanding in the physics involved is difficult without the use of tools such as mathematical models. In this work, the understanding of thermal and water transport dependencies on membrane electrode assembly (MEA) microstructure is studied through a 1D mathematical model. This model has been developed taking into account not only species, heat and water transport equations, but pore size distribution of the layers involved (catalyst layer, CL, microporous layer, MPL, and gas diffusion layer, GDL) and calculating effectively local properties such as saturation through a bundle of capillary tubes approach. The model has been validated in different operating conditions and structures and then has been used to perform a parametric study to determine optimum MEA microstructure parameters.

References

[1] A. Sánchez-Ramos, J. T. Gostick, and P. A. García-Salaberri, “Modeling the Effect of Low Pt loading Cathode Catalyst Layer in Polymer Electrolyte Fuel Cells: Part I. Model Formulation and Validation,” J. Electrochem. Soc., vol. 168, no. 12, p. 124514, Dec. 2021, doi: 10.1149/1945-7111/ac4456.

[2] A. Sánchez-Ramos, J. T. Gostick, and P. A. García-Salaberri, “Modeling the Effect of Low Pt Loading Cathode Catalyst Layer in Polymer Electrolyte Fuel Cells. Part II: Parametric Analysis,” J. Electrochem. Soc., vol. 169, no. 7, p. 074503, Jul. 2022, doi: 10.1149/1945-7111/ac811d.

[3] M. M. Gomaa et al., “Characterization and Modeling of Free Volume and Ionic Conduction in Multiblock Copolymer Proton Exchange Membranes,” Polymers, vol. 14, no. 9, Art. no. 9, Jan. 2022, doi: 10.3390/polym14091688.

[4] J. P. Owejan, J. E. Owejan, W. Gu, T. A. Trabold, T. W. Tighe, and M. F. Mathias, Water Transport Mechanisms in PEMFC Gas Diffusion Layers, J. Electrochem. Soc., vol. 157, no. 10, p. B1456, Aug. 2010, doi: 10.1149/1.3468615.

Mechanical Modeling of Carbon Fiber Paper Structures for PEM Gas Diffusion Layers Including Damage

F. Benz*[1]

[1]Forschungszentrum Jülich

Introduction

In Proton Exchange Membrane (PEM) fuel cells the simultaneous access of material and the eletrical contact to the electrodes is ensured typically by a GDL made of carbon fibers. The GDL is located at both sides between the flowfield and the Membrane Electrode Assembly (MEA) [1].

The GDL has to be porous to ensure mass transport as well as electrically conductive. It has to be rigid enough to avoid intrusion into the channels of the flowfield. The design and type of the GDL also sets a boundary for the mechanical stability of the membrane. While thin membranes are favorable in terms of the ionic resistance, the mechanical stability has to be respected in the fuel cell design. The GDL has to ensure the integrity of the membrane in the assembled cell. This gets more and more important, as the thickness of the membrane is decreased to enhance the performance of the cell.

To ensure a good electrical contact the system of layers is pressed together during the assembly process. As the GDL is the most compressible component inside the cell the majority of the deformation is governed by the mechanical properties of the GDL. While the macroscopic mechanical properties have been studied extensively in recent years, the influence of the microstructure on the deformation is still poorly understood. Deviations of the structure in the course of the production process might lead to extensive stress on the membrane or on poor mechanical and thus electrical contact in some regions. Even a homogeneous fabricated GDL will have a high local stress distribution due to the porosity and the randomly distributed fibers.

To ensure a good electrical contact and mechanical stability of the fuel cell components throughout the lifetime of the fuel cell, it is of essential importance for the GDL to maintain its elastic properties during the assembly and the operation of the cell. Large inelastic deformations of the GDL under compression have been reported in the literature e.g. by Carral et al.[2] and Hoppe et al. [5]. Even though a damaged GDL can have a significant effect on the performance of the cell [4], the causes for this and the mechanics of the damage to the GDL are still poorly understood. In the following a model is proposed to understand the inelastic deformations such as fiber breaking and binder damage and the effect on the mechanics of a GDL.

While several types of carbon fiber GDLs are available and used in PEM fuel cells, a paper type design is discussed in the following. A paper type GDL is made of straight horizontal carbon fibers with a random distribution in plane. During the production process carbonized straight PAN fibers are assembled in a plane in a papermaking technique and bound together with a binder.

Several models have been proposed to describe the elastic properties of the porous fiber structure of GDLs e.g. [7], [2]. These models give an analytical expression of the macroscopic elastic properties and deformations. However the individual fiber in the random structure is not considered or only given as a mean value. Other works such, e.g. from xiao et al. [11], aim to reconstruct the real microstructure of the fibers and binders. However this leads to high computational cost and limits the application of the model, when looking at e. g. the interaction with the membrane.

Microscopic fiber distribution models have been proposed for modeling physical quantities [9] and have been used to model porosities and flow through a membrane [3]. In the following a mechanical model is described which is able to predict the deformation of the random fiber structure for each fiber individually, while still having a low computational cost. The model includes inelastic contributions such as fiber breaking and binder damage.

*Corresponding author: f.benz@fz-juelich.de

Experimental Measurements

In order to obtain parameters and values for the simulation experimental compression tests were performed. The tests were performed with an ElektroForce DMA 3200. Single 1 cm diameter samples of a carbon fiber GDL were compressed and the force was measured up to a value of $P = 1.9\,\mathrm{MPa}$. This was repeated three times for each sample. A fourth cycle was performed up to $P = 3.8\,\mathrm{MPa}$. Figure 1b shows the mean displacement and the deviation from the mean. A total of 16 samples were measured.

CT measurements were taken for a GDL sample. An in plane slice is shown in figure 1a. The carbon fibers can be seen as straight lines with binder agglomerations inbetween. From the CT scan the density of fibers and binder is extracted. The mean extend of the binder field in between the fibers is estimated.

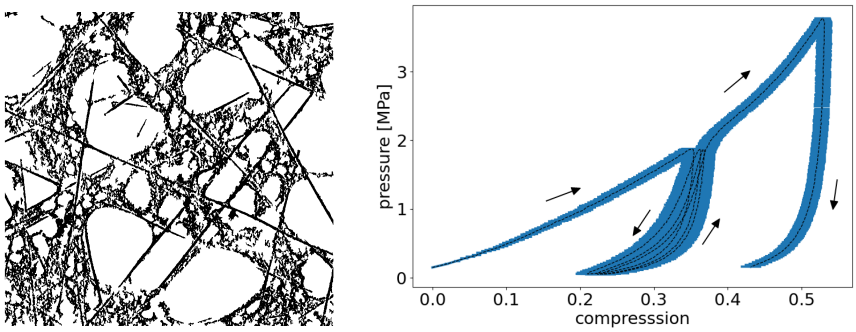

(a) (b)

Figure 1: (a) Slice from CT measurements of the paper structure. The binder accumulates at fiber crossings and at locations with high fiber density. (b) Experimental stress strain curve for a carbon paper GDL. Multiple stress cycles were performed.

Methodology

As described in [12] the fibers in a real carbon paper GDL have a broad azimutal angle distribution as well as a sharp polar angle distribution.

In the following model the random fiber structure is made of straight fibers in the x-y plane. A random fiber in the z-Plane is given by the angle in the plane ranging between 0^o and 180^o and the distance of the fiber to the origin ranging between 0 and the radius of the domain. These two values are evenly distributed. The fibers are evenly spaced in the z direction. Intersection of the fibers is possible if the fibers are close. Two fibers are considered touching if the crossing point lies within the domain, and the z distance is smaller than the fiber diameter d. The number of fibers in the structure is given by the fiber radius R_F and the fiber volume ratio V_F. This approach is similar to the one proposed by Thiedmann et al. [9] with the difference that fibers are not condensed in z planes, but are evenly distributed in z-direction.

Following the approach of Norouzifard et al. [7] the beam bending theory is used to model the deflection of the fibers. For high compressions the deflection of the beam is high enough for higher order terms to have a significant contribution. In case of second order the beam equation is given by:

$$\frac{d^2}{dx^2}\left(E_{fiber} I \frac{d^2\omega}{dx^2}\right) - \frac{3}{2} E_{fiber} A \left(\frac{d^2\omega}{dx^2}\right)\left(\frac{d\omega}{dx}\right)^2 = q(x)\ , \tag{1}$$

where x is the position along the beam, $\omega(x)$ is the deflection in z-direction, q is the force per length, E_{Fiber} is the elastic modulus of the beam, I is the second moment of area of the beam, and A is the beams cross section area.

At the crossing point x_c of two intersecting fibers i and j, the deflection of the two fibers is fixed:

$$\omega_i(x_c) = \omega_j(x_c) \tag{2}$$

As the major force inside a cell is perpendicuar to the GDL plane, the forces and the displacements in x-y direction are neglected.

On the side boundary a Neumann type boundary is used for the deflection, the top and bottom boundary are given by a Dirichlet type boundary for a fixed number of fibers on the top and bottom of the structure N_B:

$$\frac{\partial \omega}{\partial x} = 0 \qquad ; \qquad \omega = D_i \tag{3}$$

Where D_i is corresponds to the fixed compression of step i.

The paper type GDLs usually have additional binder present. Due to the geometry of the structure and the high sensitivity of the system to variations in the crossing density, the binder has an significant influence on the mechanical properties of the GDL. Different Binder materials have been used in GDLs. In the materials investigated a carbon based binder is used. During the production of the GDL the binder material is added to the carbonised fibers. The binder accumulates at fiber crossings, depending on the adhesion energy between the binder base material and the fibers.

In the following a model is discussed to include the binder in a beam model of paper GDLs.

The binder field acts on the vicinity of the fiber crossings. A fiber section i of length l_i is coupled via the binder to any fiber which is less than a maximum cutoff distance l_{max} away from the section i. The coupling takes place only between the section i of the first fiber and the section j of the second fiber, where j is determined by the condition that the position of segment j, i and the fiber crossing point form an isosceles triangle in the x-y plane. This takes the fibrous structure of the binder field, as seen in tomography images into account. Shear in the fiber field between neighbouring fiber strands is neglected.

If the displacements d_i and d_j are different, the fiber exerts a force F^i on the segments.

$$F^i = E_{binder} \frac{l_i b_{i,j}}{r_{i,j}} \Delta r_{i,j} \qquad , \tag{4}$$

with the distance $r_{i,j}$ between the segments in the undeformed configuration, $b_{i,j}$ the width of the binder between the segments and $\Delta r_{i,j}$ the distance variation in the deformed configuration.

Only the force and displacements in z direction are considered. The force in z direction is given by

$$F_z^i = F^i \cos(\theta) \tag{5}$$

with θ the angle between the segment connection and the z-axis.

The difference in the z-displacement $d_i - d_j$ and $\Delta r_{i,j}$ can be calculated with the z-position of the fibers z_i:

$$\Delta r_{i,j} \approx \frac{z_i - z_j}{r_{i,j}} (d_i - d_j) \tag{6}$$

The case of $z_i - z_j < d_i - d_j$, can be neglected if only the force in z-direction is considered.

The force in z direction is thus:

$$F_z^i = E_{binder} l_i b_{i,j} \frac{z_i - z_j}{(r_{i,j})^2} (d_i - d_j) \cos(\theta) \tag{7}$$

It is reported in the literature (e.g. [8]), that the binder field is not homogenous in the GDL. This is also seen in the CT scans. To account for the inhomogenous distribution a bimodal weighing function $B_{i,j}(z_{i,j}, l)$ is used for the thickness distribution depending on the z position of the two fibers and the fiber distance $r_{i,j}$:

$$B_{i,j} = \left[\left(\frac{z_{i,j}}{t/2} \right)^2 - \left(\frac{z_{ij}}{t/2} \right)^4 \right] (r_{max} - r_{i,j}) \tag{8}$$

with t the thickness of the GDL, r_{max} the maximum extend of the binder field and $z_{i,j}$ the distance between the mean position of the two fibers and the mid plane which corresponds to the point of minimal binder.

The width of the binder is assumed to be homogenous along the connection. The volume of all binder connections should be equal to the total binder volume V_{binder}.

$$\sum r_{i,j} b_{i,j} l_i = V_{binder} \tag{9}$$

The mechanical properties of the GDL are affected by inelastic deformations such as fiber breaking and damage in the binder. As can be seen in Figure 1b the majority of the damage occurs in the first

compression cycle, thus at the maximum point of stress. For the model a Brittle damage model is assumed and ductile components are neglected. As the fiber structure is compressed fibers which are not coupled before get into contact, thus the number of contact points is increasing with higher compression.

The stress in the binder field can be obtained from eq. (7). If the stress inside the binder exceeds the maximum stress, the elastic modulus of the binder at this point is set to 0.

The maximum stress inside a bend fiber occurs at the top and bottom side of the fiber. It is given by the elastic modulus E_{fiber}, the radius R of the fiber and the second derivative of the displacement:

$$\sigma_{max} = E_{fiber} R \frac{\partial^2 w}{\partial x^2} \tag{10}$$

If this stress exceeds the breaking point of the fiber the fiber will be considered broken at this point. The equations are modified in such a way, that the points i and $i+1$ are considered boundary points at a free end or a point force F. A point force boundary is given by:

$$\frac{\partial^3 w}{\partial x^3} = \frac{F}{E_{fiber} I} \quad \frac{\partial^2 w}{\partial x^2} = 0 \tag{11}$$

Each fiber is discretised into equidistant segments along the fiber direction.

The linearisation of the differential equations is done by calculating the difference quotient of the derivative at each point. The first order equation for a free bending segment at a point i can be discretised by:

$$E_{fiber} I \left(\frac{\omega_{i-2} - 4\omega_{i-1} + 6\omega_i - 4\omega_{i+1} + \omega_{i+2}}{\Delta x^4} \right) = q_i \tag{12}$$

This is the lowest order approximation with equidistant points possible for $m = 4$. Since this includes terms $i-2$ and $i+2$ the boundary consists of two points on each side of a beam.

To get a well defined breaking point, the second derivative is evaluated inbetween two discrete points i and $i+1$ at $x = x_i + 0.5\Delta x$ for calculating the maximum stress in a fiber.

In discretised form the maximal stress between point i and $i+1$ can be calculated by:

$$\sigma_{max} \approx E_{fiber} R \frac{4}{17} (w_{i-1} - w_i - w_{i+1} + w_{i+2}) / (\Delta x^2) \tag{13}$$

The resulting matrix equation is solved using the linalg package of scipy [10].

The elastic modulus of carbon fibers and of the carbon binder material depends on the production process. In this study it is assumed that $E_{fiber} = E_{binder} = 230\,\text{GPa}$ [6]. It was not possible however to confirm this value experimentally.

The fiber diameter for GDLs has been reported in several studies to be about $D_{fiber} = 7\mu\text{m}$ (e.g. [7]).

Due to the the complex binder structure, the binder cutoff distance is not a real physical value, but a model parameter. It was assumed to be $r_{max} = 20\,\mu\text{m}$

The maximum strain in a carbon fiber depends heavily on the production process and the precursor material [6]. Most GDLs are based on PAN fibers, in the scope of this study the maximum strain in the fibers and binders is assumed to be $\epsilon_{max} = 0.015$.

The porosity of the fiber structure can be determined using CT images. The fiber volume ratio is assumed to be $V_F = 0.1$, the binder volume ratio is assumed to be $V_{binder} = 0.02$.

A cylindrical domain with diameter $d_d = 600\,\mu\text{m}$ and a height of $h_d = 110\,\mu\text{m}$ is used for the simulation.

Discussion

Figure 2a shows the simulation result. The stress strain is simulated up to a compression of 0.27. After a compression of 0.09, 0.14 and 0.27 additional compression cycles were performed.

The stress strain curve of sample under first compression is subject to fluctuations. This stochastic nature of the material leads to various step functions in the elasticity as the material breaks. The area considered is small enough so the effects of individual major breaking points are not averaged out and can be seen in the resulting elasticity. No fluctuations can be seen in the stress strain curves the cycles at the points were the compression is below the maximal prevously applied compression. In this regions no damage is added.

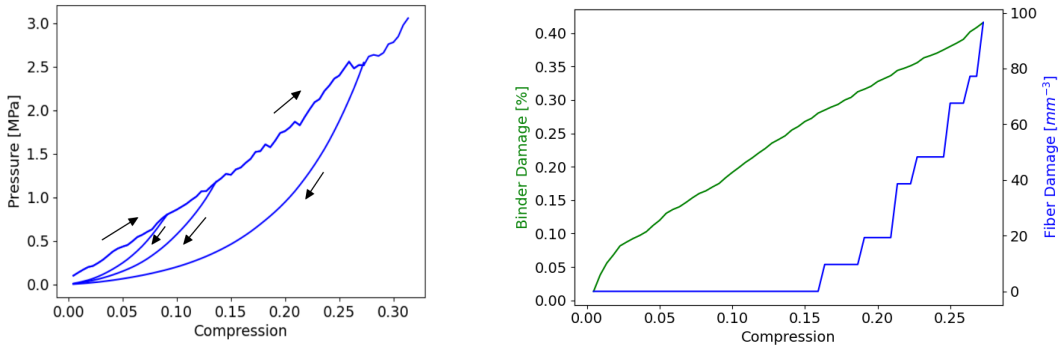

(a) (b)

Figure 2: (a) Results of the simulation. Three compression cycles with different maximum compressions are calculated. (b) Percentage of binder field broken and the density of fiber breaking points for different compressions.

The inelastic deformations during the compression lead to a lower mechanical resistance in the second cycle up to the point of maximum previously applied pressure. At the point of highest deformation of the first cycle the curves merge. After deformation the curve shows a steep stress strain behaviour.

The simulation shows a linear behaviour in the stress strain curve if only the first order terms are used in the beam equation. If higher orders are included there is a slight convex trend in the stress strain curve.

The additional cylces with damaged GDL material show similar inelastic behaviour as the experiment. However the inelastic deformation is not as pronounced in the simulation.

The increasing density of fiber crossings leads to an increase in the elastic modulus. This is counteracted by fiber breaking and damage to the binder structure. For small deformations the damage of the structure is governed by damage to the binder field. Figure 2b shows the percentage of the broken binder and the density of fiber break points for different compressions in the simulation. Parts of the binder field exceed the maximum stress and inelastic deformations occurs at small compressions $\epsilon < 0.01$. The binder tends to break at locations were the two connected fibers are far apart. Binder connecting fibers horizontally is more apt to break than vertical binder connections. The fiber breaking occurs at higher displacements of $\epsilon > 0.16$.

Conclusions

It was shown that it is necessary to include effects of the binder as well as damage when modeling the mechanics of carbon paper GDLs. An approach to include these effects into a simple 1D discretisation finite element framework was proposed. Randomly distributed fibers are modeled as bending beams with displacement coupling at fiber intersections. A spring model was added to include binder effects. Both fibers and binder were allowed to break if the respective yield strain was reached.

The simple model allows the simulation of complex fiber/binder structures at low computational cost. It was possible to simulate length scales above 0.5 mm on a single core within a time scale of several days.

Due to the stochastic nature of the material the resulting is not a straight line, but is fluctuating under the presence of damage. The compression under which the first fibers start to break was calculated for a random set of fibers. A comparison of the binder and the fiber damage shows, that the damage of the binder starts almost at zero deformations and dominates in the small deformation regime. Above $\epsilon > 0.16$ there is a significant contribution of the fiber damage to the total damage of the structure.

References

[1] F. Barbir. *PEM fuel cells: theory and practice*. Academic press, 2012.

[2] C. Carral and P. Mélé. A constitutive law to predict the compression of gas diffusion layers. *International Journal of Hydrogen Energy*, 43(42):19721–19729, 2018.

[3] D. Froning, G. Gaiselmann, U. Reimer, J. Brinkmann, V. Schmidt, and W. Lehnert. Stochastic aspects of mass transport in gas diffusion layers. *Transport in porous media*, 103(3):469–495, 2014.

[4] T. Ha, J. Cho, J. Park, K. Min, H.-S. Kim, E. Lee, and J.-Y. Jyoung. Experimental study on carbon corrosion of the gas diffusion layer in polymer electrolyte membrane fuel cells. *International journal of hydrogen energy*, 36(19):12436–12443, 2011.

[5] E. Hoppe, H. Janßen, M. Müller, and W. Lehnert. The impact of flow field plate misalignment on the gas diffusion layer intrusion and performance of a high-temperature polymer electrolyte fuel cell. *Journal of Power Sources*, 501:230036, 2021.

[6] S. A. Mirdehghan. 1 - fibrous polymeric composites. In M. Latifi, editor, *Engineered Polymeric Fibrous Materials*, The Textile Institute Book Series, pages 1–58. Woodhead Publishing, 2021.

[7] V. Norouzifard and M. Bahrami. Analytical modeling of pem fuel cell gas diffusion layers deformation under compression: Part 1 - linear behaviour region. *ECS Transactions*, 61(11):1–12, aug 2014.

[8] S. Odaya, R. Phillips, Y. Sharma, J. Bellerive, A. Phillion, and M. Hoorfar. X-ray tomographic analysis of porosity distributions in gas diffusion layers of proton exchange membrane fuel cells. *Electrochimica Acta*, 152:464–472, 2015.

[9] R. Thiedmann, F. Fleischer, C. Hartnig, W. Lehnert, and V. Schmidt. Stochastic 3d modeling of the gdl structure in pemfcs based on thin section detection. *Journal of the Electrochemical Society*, 155(4):B391, 2008.

[10] P. Virtanen, R. Gommers, T. E. Oliphant, M. Haberland, T. Reddy, D. Cournapeau, E. Burovski, P. Peterson, W. Weckesser, J. Bright, S. J. van der Walt, M. Brett, J. Wilson, K. J. Millman, N. Mayorov, A. R. J. Nelson, E. Jones, R. Kern, E. Larson, C. J. Carey, İ. Polat, Y. Feng, E. W. Moore, J. VanderPlas, D. Laxalde, J. Perktold, R. Cimrman, I. Henriksen, E. A. Quintero, C. R. Harris, A. M. Archibald, A. H. Ribeiro, F. Pedregosa, P. van Mulbregt, and SciPy 1.0 Contributors. SciPy 1.0: Fundamental Algorithms for Scientific Computing in Python. *Nature Methods*, 17:261–272, 2020.

[11] L. Xiao, Z. Yin, M. Bian, N. Bevilacqua, R. Zeis, J. Yuan, and P.-C. Sui. Microstructure reconstruction using fiber tracking technique and pore-scale simulations of heterogeneous gas diffusion layer. *International Journal of Hydrogen Energy*, 47(46):20218–20231, 2022.

[12] A. G. Yiotis, M. E. Kainourgiakis, G. C. Charalambopoulou, and A. K. Stubos. Microscale characterisation of stochastically reconstructed carbon fiber-based gas diffusion layers; effects of anisotropy and resin content. *Journal of Power Sources*, 320:153–167, 2016.

Microscopic Behaviour Of Hydrogen And Hydrides In Atom Probe Tomography of Pure Zirconium

A. Diagne*[1], L. Rigutti[1]

[1] Univ Rouen Normandie, INSA Rouen Normandie, CNRS, Groupe de Physique des Matériaux UMR 6634, F-76000 Rouen, France

Introduction

Because of its importance as an energy vector, hydrogen has become the focus of many scientific and environmental studies. It also plays a role in determining the structural properties of metals and interacts with functional defects in semiconductors. Understanding the mechanisms involving hydrogen, from its location to its quantification, remains important. This is why Atom Probe Tomography (APT) is required for this study, because it is an analysis technic that can detect single atoms and locate them within a nanometric volume. However, there are many problems with hydrogen, because it is generally present in the analysis chamber in its gaseous form (H_2). This gas polarises near the field emitter, can dissociate at the surface of the emitter and be ionised by the field applied to the surface or by the laser pulses that trigger the evaporation of ions from the matrix. Hydrogen also takes part in surface reactions, leading to the formation of new species such as hydrides (Figure 1). This can degrade the chemical sensitivity of the analysis.

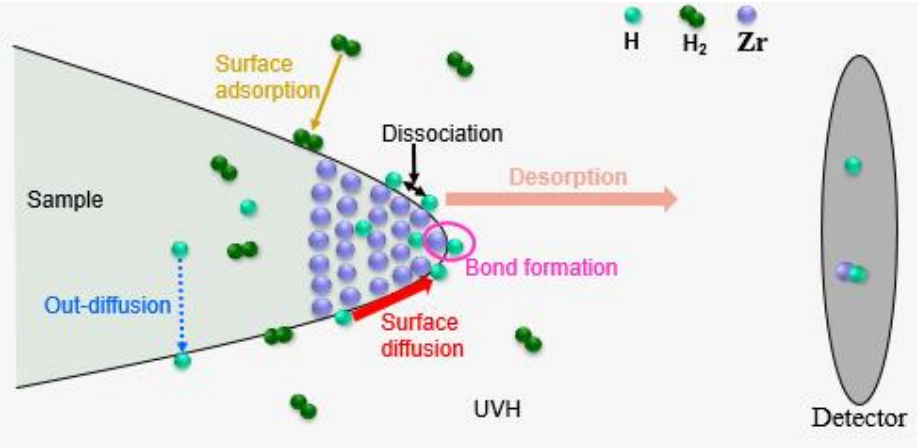

Figure 1 : Possible behavior of hydrogen at the surface of a material subjected to an electric field

This parasitic hydrogen also distorts the quantity of hydrogen detected when a material contains it. It is therefore important to be able to discriminate between chamber hydrogen and material hydrogen for clearer quantification.

To achieve this, several parameters could be used to study and understand the behaviour of hydrogen at the surface of the material (surface field, evaporation flux, temperature, laser energy, etc.) [1], [2], [3].

The objectives of our study are therefore to develop complementary approaches targeting the quantification of hydrogen, its localisation, and also the temporal study of phenomena

* Corresponding author: aissatou.diagne1@univ-rouen.fr

involving chemical reactions, to apply these technics to the study of hydrogen-containing systems of interest, and finally to extend the field of use of these techniques to materials for storing hydrogen in solid form and to the study of surface chemical interactions under high-field conditions.

Methodology

The instrument used is a laser-assisted tomographic atom probe, ideal for analysing semiconductor and metallic materials. The classic analysis carried out on this machine consists of applying a DC voltage to a fine tip and, with the contribution of laser pulses (thermal input), ionising and then tearing off the atoms from the surface of the material and projecting them towards a position- and time-sensitive detector (Figure 2). This type of analysis is carried out at a constant detection rate. Other parameters such as laser energy, temperature and pulse frequency remain fixed.

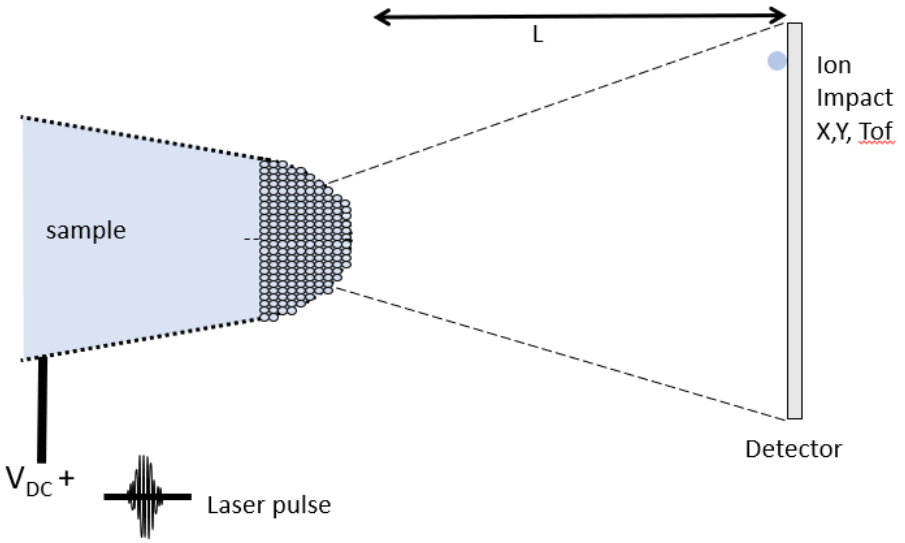

Figure 2: Principle of Atom Probe Tomography (APT): L = length of flight, Tof = time of flight

Our studies are carried out on pure zirconium (Zr) analysed by laser-assisted atom probe tomography. This is complex, because the hydrogen detected during the analysis could come from the analysis chamber (parasitic hydrogen) or from the material (hydrogen contained in the material). For the time being, this system is being analysed in the conventional way to see if the field has an influence on the formation of hydride species and the interactions that can take place between hydrogen and Zr.

Other analyses with more specific conditions, such as the introduction of gas into the chamber during the analysis, are planned. This procedure will give an idea of the effect of the field on the formation of hydrogen ions, the effect of the partial pressure of hydrogen on the material, and the interactions between hydrogen in the chamber and the material. To do this, the instrument is equipped with a gas bottle (H_2), linked to the analysis chamber, which allows hydrogen to be introduced, increasing the pressure from around 10^{-11} mbar to 10^{-9} mbar.

Once the behaviour of parasitic hydrogen is understood (evolution with the field, the chemical reactions in which it is involved), it will be possible to put in place strategies to discriminate it from the hydrogen contained in the material for better quantification and a better understanding of its behaviour within materials.

Discussion

Zr is a transition metal with 5 isotopes (Table 1).

Zr isotopes	Natural abundances (%)
^{90}Zr	51.45
^{91}Zr	11.22
^{92}Zr	17.15
^{94}Zr	17.38
^{96}Zr	2.80

Table 1: Zirconium isotopes and their natural abundances

Analysis of this material gives results showing the formation of hydrogen ions and hydride species. The hydrides appear overlapping the Zr isotopes, with which they have the same mass/charge ratios (Figure 3).

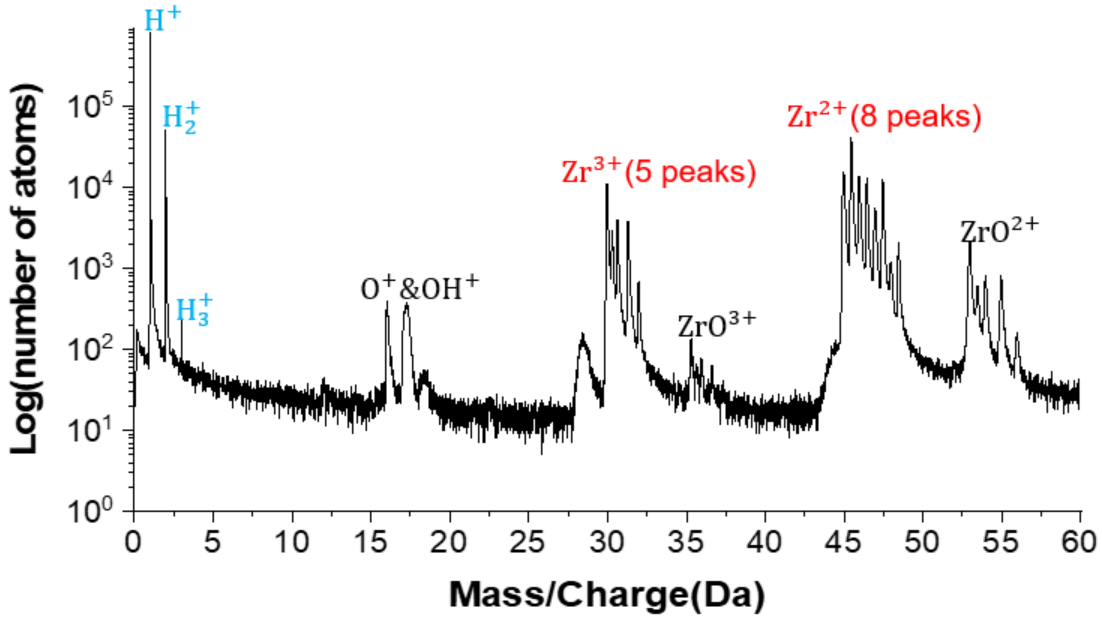

Figure 3: Zirconium mass spectrum

This phenomenon is only observed with the Zr^{2+} species, which distorts the abundance of the isotope peaks. In addition, new peaks containing only hydrides appeared. Only the peak of the first isotope (^{90}Zr) does not contain hydrides.
For the Zr^{3+} species, there was no formation of hydrides overlapping the isotopes and no new peaks of hydrides appeared. The isotopic abundances measured throughout the experiment were maintained.
To assess the influence of the field on the species formed, the field strength was estimated from the Charge State Ratio of Zr^{3+}/Zr^{2+} [CSR(Zr)] This field estimate allows us to assign values of the order of V/nm to the electric field, based on Kingham's post-ionization theory [4], and to see how it varies with the sample surface. An increase in the field strength was observed as a

function of depth (Figure 4). This is different from the evolution of the field observed on semiconductor materials (the field decreases with depth) [1]. However, the influence of the field on the formation of hydrogen ions can be seen here: H^+ is formed at high fields and H_2^+ at low fields (Figure 4).

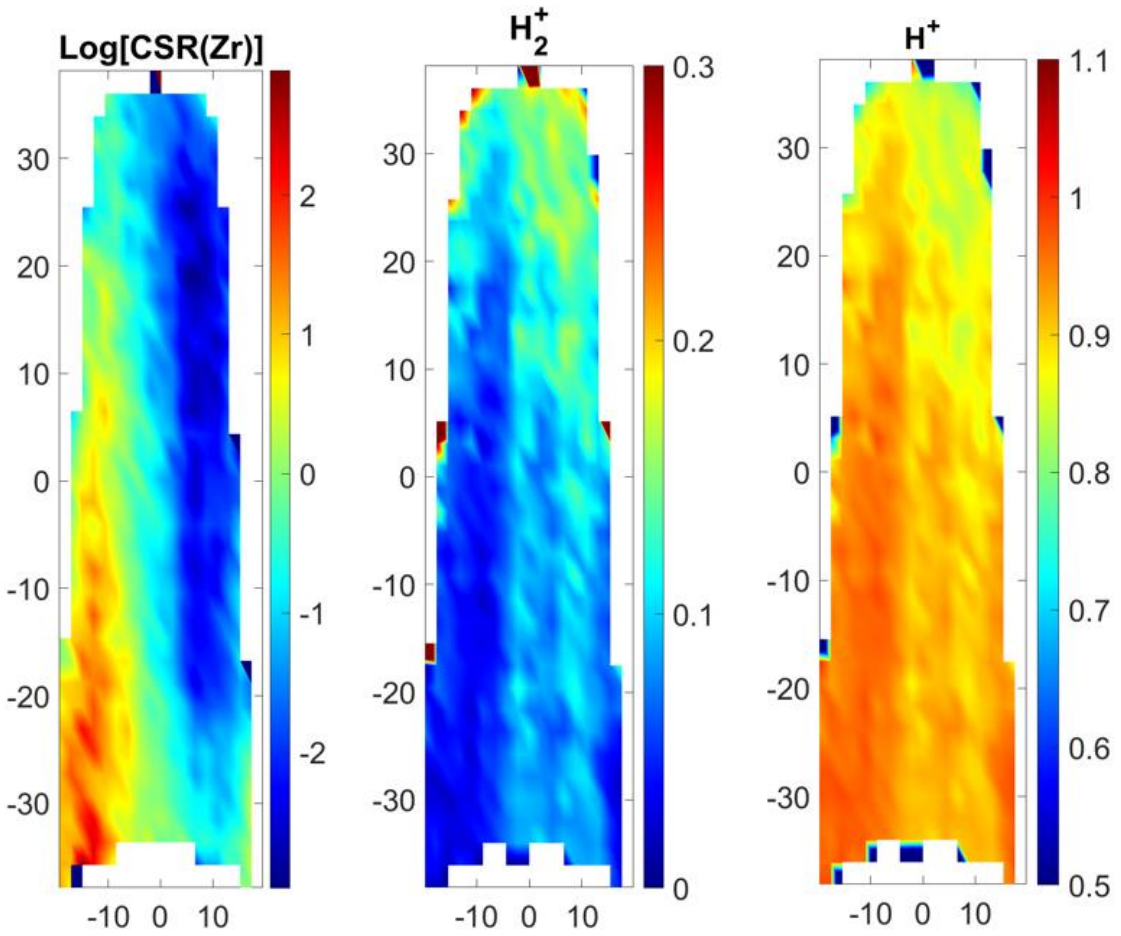

Figure 4: Sections along the volume of a pure zirconium sample showing the ratio of the charge states of Zr and the relative abundances of the H^+ and H_2^+ species.

As far as the hydrides are concerned, their superposition on the Zr isotopes makes it difficult to locate them precisely on the sample and to study the evolution of their formation as a function of the surface field. However, if we look at the distribution in detector space of the 3 peaks (46.5Da, 47.5Da and 48.5Da) containing only hydrides (figure 5), there is a correlation between the pole and the distribution of these species. Exploiting this crystallographic lead could help us to identify the preferred zones for hydride formation in the material, so that we can better study overlapping hydrides.

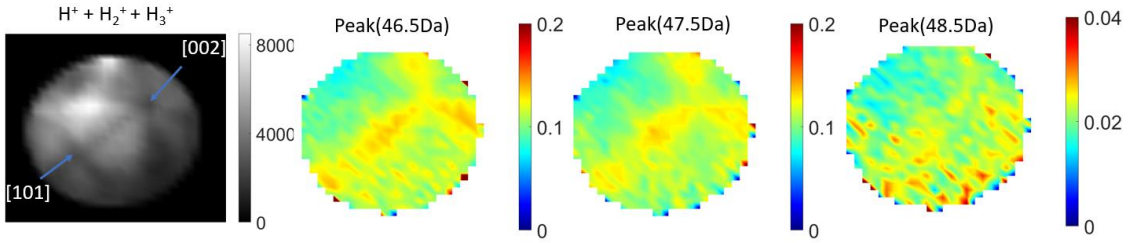

Figure 5: 2D map of hydrogen ion density and relative abundances of peaks containing only hydrides at 46.5Da, 47.5Da and 48.5Da in detector space.

Conclusions and Outlook

We investigate the microscopic behavior of hydrogen species H^+, H_2^+, H_3^+ and hydrogen-containing species formed on the surface of pure Zr samples by hydrogen in the analysis chamber in laser-assisted atom probe tomography. The formation of these species occurs at field strengths between 30-33 V/nm. This shows that the relative abundances of hydrogen species depend on the electric field. But for hydrides overlapped by isotopes, the study of their field-dependence remains to be explored. A decomposition of peaks containing Zr and hydrides remains to be carried out to estimate the quantity of hydrides formed and their location on the sample.

In perspective, other parameters that could influence hydride formation during evaporation, such as temperature applied to the sample, laser energy, partial pressure of hydrogen in the analysis chamber, etc., are also of interest. A particular interest would be represented by studies on systems that have a high affinity with H, such as Titanium and Magnesium-based materials, in order to elucidate the interactions between hydrogen and the constituent atoms of these materials, which may also be used for hydrogen storage.

References

[1] L. Rigutti *et al.*, « Surface Microscopy of Atomic and Molecular Hydrogen from Field-Evaporating Semiconductors », *J. Phys. Chem. C*, vol. 125, nº 31, p. 17078-17087, août 2021, doi: 10.1021/acs.jpcc.1c04778.

[2] M. S. Meier, M. E. Jones, P. J. Felfer, M. P. Moody, et D. Haley, « Extending Estimating Hydrogen Content in Atom Probe Tomography Experiments Where H2 Molecule Formation Occurs », *Microsc. Microanal.*, vol. 28, nº 4, p. 1231-1244, août 2022, doi: 10.1017/S1431927621012332.

[3] S.-H. Yoo, S.-H. Kim, E. Woods, B. Gault, M. Todorova, et J. Neugebauer, « Origins of the hydrogen signal in atom probe tomography: case studies of alkali and noble metals », *New J. Phys.*, vol. 24, nº 1, p. 013008, janv. 2022, doi: 10.1088/1367-2630/ac40cd.

[4] D. R. Kingham, North-Holland Publishing Company (1982)

Microstructural and hydrogen permeation characterization of CoCrCuFeMnNi High Entropy Alloy

O. Gordo-Burgoa*[1], L. Castrillejo[2], Y. Bilbao[2], I. Vicario[3], E. Mardaras[4], G. Plata[1], G. Arruebarrena[1], I. Hurtado[1]

[1]Mechanical and Manufacturing Department, Mondragon University, Arrasate-Mondragon, Spain
[2]Department of Mining & Metallurgical Engineering and Materials Science, Faculty of Engineering of Bilbao (UPV/EHU), Bilbao, Spain
[3]Metal processing platform, TECNALIA, Basque Research and Technology Alliance (BRTA), Derio, Spain
[4]Azterlan, Basque Research and Technology Alliance (BRTA), Durango, Spain

Introduction

Hydrogen industry is growing as a good choice among those available to deal with the high demand for energy. At present, much effort is being spent to use the existing gas pipelines to transport blended, or even pure, hydrogen all over Europe, considering topics such as pressure and temperature. Nevertheless, it is well known that certain metallic materials in contact with hydrogen show irreversible damage, i.e., hydrogen embrittlement (HE) of steels [1]. In order to overcome this problem, the study of new materials to be in contact with gaseous Hydrogen is becoming widespread.

High Entropy Alloys (HEAs), materials known because of their good mechanical properties even at cryogenic temperatures, are being analyzed to be used in contact with hydrogen. The renowned Cantor introduced by B. Cantor [2] is recognized as being one of the best known HEAs, composed of five metallic elements in atomic percentage varying from 5 to 35% and a single-phase solid solution structure. Moreover, this HEA presents an improvement in its ductility and strength resistance when in contact with hydrogen [3]. However, despite the amount of research found about mechanical properties of this kind of material, there is few information about its behavior regarding to hydrogen damage.

In this work, a modification of the CANTOR alloy will be explored with respect to its behaviour in contact with Hydrogen. In spite of its Cr content, Mn determinates the oxidation behavior of the CANTOR alloy, forming fast growth rate oxides at high temperatures. Some authors have completely replaced Mn for Cu in the alloy looking for a more oxide resistant material [4]. In this alloy, a two-phase microstructure was observed owing to the precipitation of a secondary FCC, Cu richer, in the primary FCC structure [4]. Since copper presents a low permeation with respect to hydrogen [5], the present work explores the possibility of a partial substitution of the Mn with Cu in the CANTOR alloy keeping a single FCC structure and, thus, controlling the oxidation problematic.

Methodology

The CAPHAD method is used to determinate the composition of the target alloy to be casted and analyzed. The balance between the amount of Mn and Cu is explored to get a FCC single-phase solid solution composition window. However, at present, CALPHAD databases have scarce data available for new HEAs compositions and, instead, extrapolations of other well stablished databases, i.e., those for steels or Ni, are being used. Experimental characterization

* O. Gordo-Burgoa: ogordo@mondragon.edu

of the obtained material is, thus, crucial. the software available for this study has not any specific database for that kind of new materials so an extrapolation in obtained results will be necessary. After several calculations using the software FactSage and a steel database the following chemical composition has been defined, Table I, that presents a single FCC phase window between 1000 and 1200 ℃, figure 1. Once quenched from a temperature within this window, the FCC phase could be retained at room temperature.

Table 1: Proposed target alloy composition

	Co	Cr	Cu	Fe	Mn	Ni
% at.	20	20	8	20	12	20
% wt.	20.76	18.32	8.95	19.67	11.61	20.68

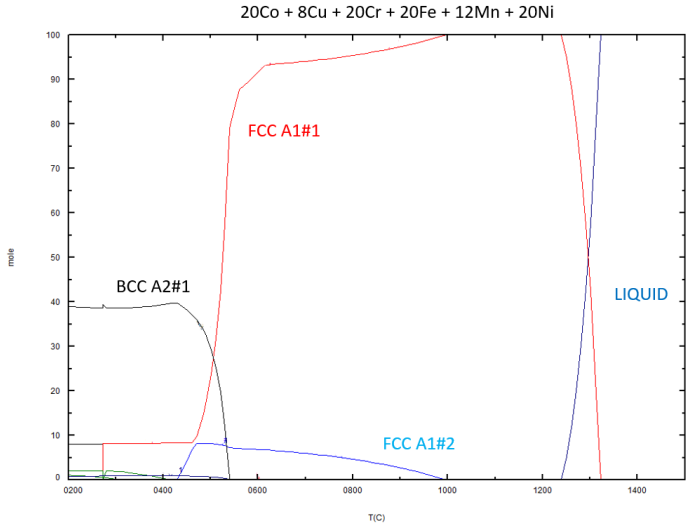

Figure 1. Calculated phase amounts during the equilibrium cooling of the target alloy. FactSage software with a Steel database has been used.

Once the composition of the alloy has been defined, the casting process to manufacture the HEA has been done using an induction oven INDUCTOTHERM and under argon gas atmosphere, figure 2. To obtain a high purity alloy, raw pure metals (purity > %99.5) have been used. For the purpose of reducing Manganese oxide formation during the casting process, Co, Cr, Fe, and Ni were first melted and then the liquid temperature was reduced and, Mn and Cu were added.

Figure 2. Oven used to produce the target CoCrCuFeMnNi alloy under Ar atmosphere.

After homogenization, alloy was cast in a pre-heated (300℃) stair-shape-mold, manufactured in H13 steel. This mold allows to study the evolution of the morphology of the alloy as it solidifies with different velocities due to the difference in stair thickness.

The material was then microstructurally characterized using a Field Emission Scanning Electron Microscope (SEM), its thermophysical properties were measured with Differential Scanning Calorimeter (DSC), and the characterization of hydrogen permeation characteristics were obtained making use of a Devanathan-Stachursky electrochemical cell. This cell, is principally composed of a testing specimen between two cells, one working as cathod, and the other anodic, figure 3.

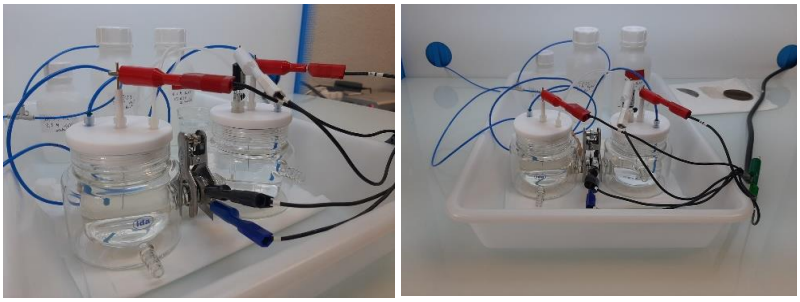

Figure 3. Devanathan-Stachursky electrochemical cell used in this work.

The hydrogen permeation test has been carried out following the ASTM G148-97 standard which helps to evaluate hydrogen uptake, permeation, and transport. As mentioned before, this test is driven by a DS cell which works through an electrochemical process where the reaction of reduction-oxidation of the material is caused by an electrical sourse or vice versa. Apart from the two cells and a testing specimen, this cell has a reference electrode (Ag/AgCl), two axiliar electrode and a working electrode (which is the same as the testing specimen). For the electrolite, different disolution have been tested.

Discussion

The microstructural characterization has started using optical microscopy. All as-cast samples show a dendritic structure, figure 4. That vary with the velocity of the solidification process. It is possible to difference two types of dendrites: primary solidified dendrites, which seem to be the ones which nucleates and grows first; and secondary solidified dendrites which are finer

and are formed between the first ones. The sample that belongs to the thickest stair has higher SDAS values compared with the sample that belongs to the thinnest stair.

In this material, two principal phases are expected: FCC#1 and FCC#2. FCC#1 should have a similar composition to the calculated one, however, FCC#2 is expected to have a copper-richer composition. Consecuently, a study of the composition has been done using SEM Energy Dispersive X-ray Spctroscopy (EDS) to visualise the distribution of different alloys' compounds, figure 5.

The map results shows a Cu-rich interdendritic structure. Moreover, presence of Mn in interdendritic areas is evident but in a lower amount compare to Cu. From the equilibrium solidification diagram it is known that FCC#2 phase is Cu-rich phase and, taking into account those maps results, FCC#2 phase could be the second solidifiying. Furthermore, a Electron Back-Scatterded Difraction (EBSD) study has been done in order to determinate the cristalographyc structure of dendrites and interdendrites. As a result, it is obtained that both of them have FCC structure.

For the porpuse of achiving a FCC single-phase solid solution alloy, a heat treatmen should be necessary to eliminate the FCC#2 phase and maintain FCC#1. Afteerward, the permeation characteristics of the alloy will be studied.

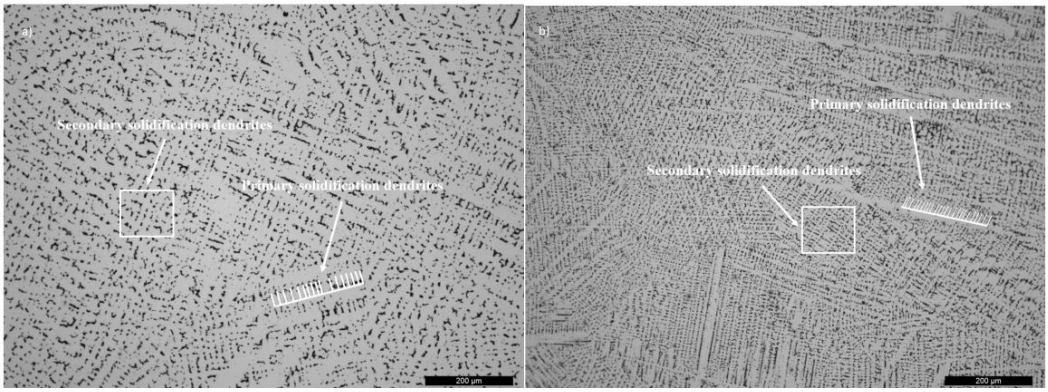

Figure 4. Optical microscope microstructure of the as-cast alloy.

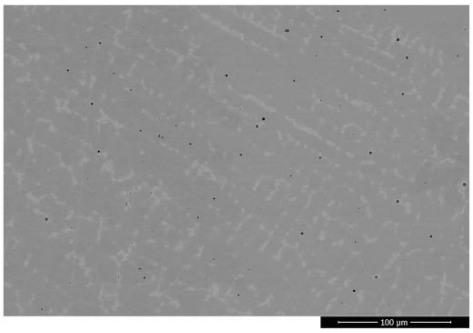

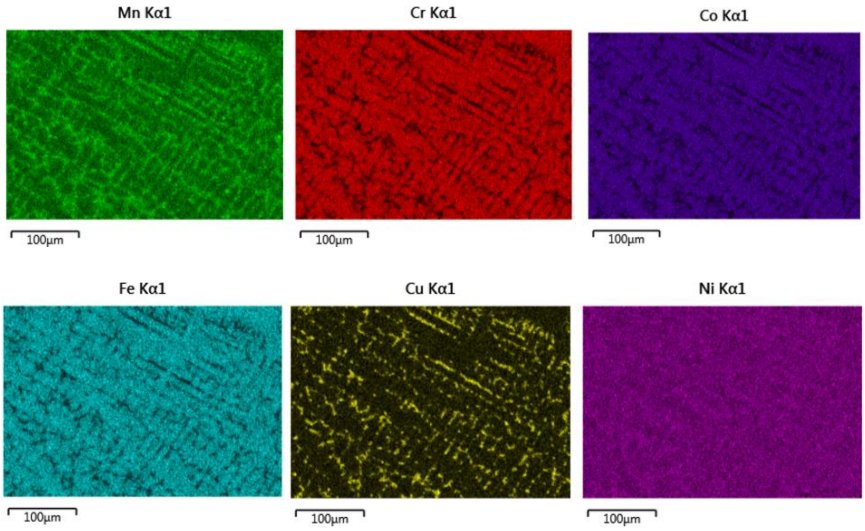

Figure 5. Energy Dispersive X-ray Spectroscopy (EDS) of the as-cast alloy.

Expectec results

According to the National Aeronautics and Space Administration (NASA) database, metals with a Face-Centered Cubic (FCC) crystallographic structure and low hydrogen solubility are those that present excellent resistance to hydrogen embrittlement [6]. HEAs with a FCC crystallographic structure such as CANTOR alloy presents a low hydrogen solubility since only can penetrate in a shallow depth [7]. In the same way, Cu and Cu-based alloys with FCC structure have shown good properties regarding the permeation of the hydrogen [8]. Moreover, commun stainless steels like AISI 4140 present an inprovement in hydrogen-permeation-rate when a Cu couted is applied [5]. Taking into account that, it is expected to achieve an HEA without any susceptibility or lower susceptibility to hidrogen embrittlement than nowadays materials. Furthermore, it is expectet to avoid the oxidation problems that Mn element causes and that could react with hydrogen.

Conclusions

In this study, microstructural and hydrogen-permeation study of a HEA were carried out. It is expected that:

- Two principal phases: FCC#1 and FCC#2. The second one with a copper-richer composition. Moreover, for the porpuse of achiving a FCC single-phase solid solution alloy, a heat treatmen should be necessary to eliminate the FCC#2 phase and maintain FCC#1.
- As happens with CANTOR alloy, it is expected an improvement in its ductility and strength resistance when in contact with hydrogen. Furthermore, copper presence could help in decreasing of hydrogen permeation.
- It is expectet to avoid the oxidation problems that Mn element causes

References

[1] M. Koyama, K. Ichii, and K. Tsuzaki, “Grain refinement effect on hydrogen embrittlement resistance of an equiatomic CoCrFeMnNi high-entropy alloy,” *Int J Hydrogen Energy*, vol. 44, no. 31, pp. 17163–17167, Jun. 2019, doi: 10.1016/j.ijhydene.2019.04.280.

[2] B. Cantor, I. T. H. Chang, P. Knight, and A. J. B. Vincent, “Microstructural development in equiatomic multicomponent alloys,” *Materials Science and Engineering A*, vol. 375–377, no. 1-2 SPEC. ISS., pp. 213–218, Jul. 2004, doi: 10.1016/j.msea.2003.10.257.

[3] T. Zhu *et al.*, “Influence of hydrogen behaviors on tensile properties of equiatomic FeCrNiMnCo high-entropy alloy,” *J Alloys Compd*, vol. 892, Feb. 2022, doi: 10.1016/j.jallcom.2021.162260.

[4] M. L. Bürckner, L. Mengis, E. M. H. White, and M. C. Galetz, “Influence of copper and aluminum substitution on high-temperature oxidation of the FeCoCrNiMn ‘Cantor’ alloy,” *Materials and Corrosion*, vol. 74, no. 1, pp. 79–90, Jan. 2023, doi: 10.1002/maco.202213382.

[5] J.-M. Chen and J.-K. Wu, “Hydrogen diffusion through copper-plated AISI 4140 Steel,” *Corros Sci*, vol. 33, no. 5, pp. 657–666, 1992.

[6] NASA, “Safety standard for hydrogen and hydrogen systems,” Washington DC, Feb. 1997.

[7] Z. Pu, Y. Chen, and L. H. Dai, “Strong resistance to hydrogen embrittlement of high-entropy alloy,” *Materials Science and Engineering A*, vol. 736, pp. 156–166, Oct. 2018, doi: 10.1016/j.msea.2018.08.101.

[8] H. S. Zhou *et al.*, “Deuterium permeation and retention in copper alloys,” *Journal of Nuclear Materials*, vol. 493, pp. 398–403, Sep. 2017, doi: 10.1016/j.jnucmat.2017.06.028.

MoS_2 catalysts for the WGS reaction: Optimization of activity, stability and characterization by spectroscopy and microscopy at atomic scale

S. Nouma*[1], A. Vimont[2], X. Portier[1], L. Oliviero[2]

[1] CIMAP
[2] LCS

Introduction

In the context of non-carbon energy production, hydrogen appears to be a relevant energy vector. One of the options for its production is to use biomass, a sustainable, carbon-neutral and abundant energy resource. Biomass emits less CO2 compared with conventional energy sources such as coal, oil or natural gas[1]–[3]. Processing biomass leads to the formation of synthesis gas (CO, H2), which cannot be used directly in industrial production. The water gas shift (WGS) reaction, which converts CO and H2O into CO2 and H2, is a key process for maximizing hydrogen production from biomass-derived syngas[4]–[6].

However, conventional metal oxide catalysts for the WGS reaction are easily deactivated by impurities containing sulfur, which are part of the biomass feedstock. It is therefore necessary to set up an efficient WGS catalytic process and to develop stable, high-performance catalysts capable to be adapted to the various properties of biomass, especially with the problem of sulfur poisoning[7]. Sulfides are considered to be good candidates for sulfur-tolerant WGS catalysts and also offer an economic advantage. This work focuses on molybdenum-based sulfide catalysts (MoS2), which exhibit excellent activity in the presence of H2S and have also been used in hydrotreating processes which aims to reduce the heteroatom content (sulfur, nitrogen and metals) of petroleum feedstocks[8]–[10].

Concerning these catalysts, most of the studies carried out until today have focused on their activity and stability by modifying the composition, but little work has been aimed at optimizing the results obtained. This can be explained by the difficulty of characterizing them due to their sensitivity to air[11]. In addition, the distinction between active edge sites of the material by microscopy has generally been limited to model catalysts[12], [13]. The adsorption of CO on sulfide-based catalysts for WGS has been studied by IR spectroscopy within my team at the LCS. This study led to the fact that the two different edges exposed by MoS2 nanosheets, the M (metal) and S (sulfur) edge sites, exhibit different WGS activity and stability as a function of time spent under the reaction feed. Mechanism studies have not been completed, but it was found that the S edge sites are the most stable active sites for this reaction[14]. The preparation of sulfide-based catalysts exposing more S-edge sites is therefore one of the aims of my thesis.

It has also been shown that the modification of the oxide support has an important role in the proportion of exposed sites. When moving from Al2O3 alumina to SiO2 silica, the S-edge/M-edge ratio increases due to the decrease in interactions between the MoS2 nanosheets and the support. However, the length of the sheet is also significantly increased, and the concentration of S-edge sites is not yet sufficient to enhance WGS activity[15], [16]. In addition to the effect of the support used and the type of edges mainly exposed, two other

* Corresponding author: saloua.nouma@ensicaen.fr

aspects are of interest: the effect of promoting agents and chelating agents. The role of a promoter is to improve catalytic activity[3]. A chelating agent is an organic additive capable of creating multiple bonds with the metal when it is impregnated onto the surface of the support. This prevents the metal from interacting strongly with the support surface and forming undesirable structures. In addition, sulfidation of the promoters will be optimally delayed until a significant proportion, or even almost all, of the MoS2 layers have been created[17].

Methodology

In the context of this thesis which mainly aims to improve the activity and stability of sulfide catalysts, and in order to supplement the studies carried out previously and try to optimize the results obtained, we will proceed on the basis of a methodology that combines indirect (infrared spectroscopy) and direct (transmission electron microscopy TEM) characterization of WGS catalysts. The effectiveness of this combination has been demonstrated by the information already obtained on this type of catalyst for hydrotreating processes. The adsorption of probe molecules (CO) followed by spectroscopy enables to determine indirectly the nature of the active sites, analyze the surface under conditions close to real conditions, and distinguish promoted and unpromoted Mo. Microscopy (TEM) gives more information about the morphology of sulfide catalysts, and helps to determine the dispersion of the different active sites. This compensates for the lack of detailed atomic-scale structural information on the catalysts resulting from characterization by the CO/IR method alone. The complementary nature of the two techniques should be highlighted, as it creates a link between what is observed; the average shape of the nanosheets, and the spectra obtained in IR. It can then be applied to different types of these catalysts (different promoters or supports, addition or absence of chelating agent, etc.)[15], [18], [19].

The strategy outlined presents an opportunity to obtain a quantitative and qualitative description of the edge sites. The work can be carried out in this order; firstly, optimizing the preparation of MoS2 on oxide supports (Al2O3, SiO2 or mixed) to obtain a high concentration of edge sites and a high proportion of S edge sites varying the nature and molar ratio of a chelating agent/metal use during the preparation. Decoration of MoS_2 catalysts by co-impregnation and selection of the best promoter (Co, Ni, Pt, etc.) to increase the activity and stability of the M edge under WGS conditions. Once the surface has been analyzed by IR spectroscopy, the most active sites (edge sites) can be characterized by HR-HAADF-STEM to determine the morphology of the nanosheets in terms of length and shape (S/M ratio), as well as verifying the edge decoration of the catalysts selected in the previous step. Evaluating the activity of the different catalysts by IR operando and understanding aspects of the mechanism is also a very important step in this study.

Results and Discussion

As expected, using IR spectroscopy, the interactions of CO with the sulfide phase as well as with the support (wavenumbers > 2130 cm^{-1}) in case of MoS_2/Al_2O_3 and MoS_2/ SiO_2 were observed. In the presence of the alumina support, M edges ($\simeq$2112 cm^{-1}) are more favored than S edges ($\simeq$2070 cm^{-1}). For silica as a support the dispersion of the sulfide phase is more complicated, this is illustrated by the weak signal of the Mo bands; S and M edges as well. (Figure 1)

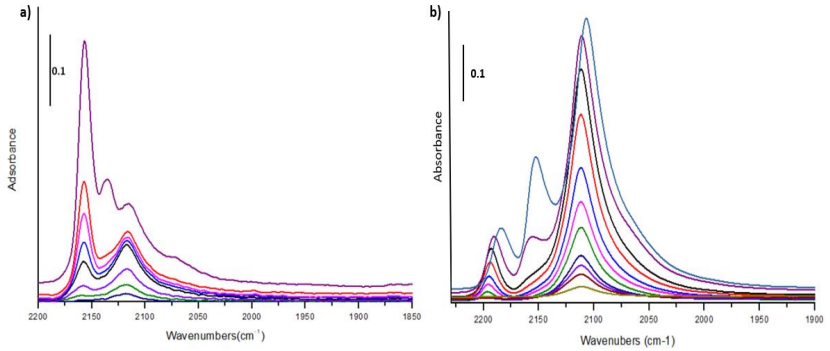

Figure 1 : IR spectra obtained after of increasing doses of CO up to saturation using equilibrium pressure (1Torr) on MoS_2 supported by a) SiO_2 b) Al_2O_3

At this level the use of chelating agents can be beneficial. The isopolymolybdate anion (Mo7O246-) used in the impregnation solution in order to incorporate the metal Mo into the support is stable in an acid medium and when it comes into contact with the support, acid-base reactions occur between the solution and the acid-base sites of the support. Simultaneous impregnation with the addition of the organic additive decomposes the anion into tetraoxomolybdenum (MoO4)2- which, after various protonation, condensation and complexation reactions, gives rise to powerful complex compounds, this inhibits direct metal-surface interactions and also the formation of unwanted structures[17]. Molar ratios of chelating agent to the metal of less than 1 are respected for the different agents chosen in order to avoid the presence of insoluble complexes. The metal dispersion was improved more by adding citric acid (AC) and nitrilotriacetic acid (NTA) than by adding ethylenediaminetetraacetic acid (EDTA). Regarding the type of edge that we aim to maximize in the structure (S edges), relevant results were obtained in the case of Mo/SiO_2 (AC/Mo=0.5) & (NTA/Mo=1). Figure 2.

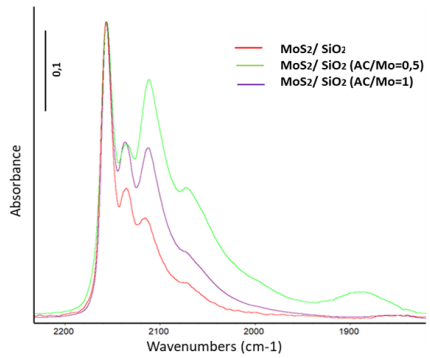

Catalyst	Mo/SiO_2	Mo/SiO_2 (AC/Mo=0.5)	Mo/SiO_2 (AC/Mo=1)
M-edge concentration	26	46	57
S-edge concentration	4	19	13
S/M ratio	0.16	0.42	0.05

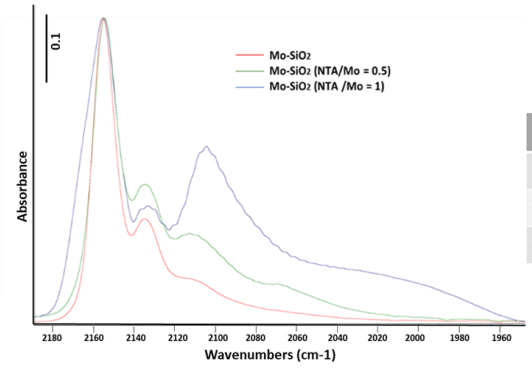

Catalyst	Mo/SiO_2	Mo/SiO_2 (NTA/Mo=0.5)	Mo/SiO_2 (NTA/Mo=1)
M-edge concentration	26	14	14
S-edge concentration	4	3	15
S/M ratio	0.15	0.21	1.07

Figure 2 : a) IR equilibrium spectra (1Torr of CO) normalized to 20 mg of MoS_2/SiO_2 (AC/Mo & NTA/Mo =0&0.5&1) b) Table of S & M edge concentrations and S/M ratios in the catalysts structure.

Conclusions

Comparing MoS_2 supported on alumina and silica, and in accordance with the structure-activity duality established in previous works, the WGS activity for MoS_2/Al_2O_3 is higher than for MoS_2/SiO_2 without organic additives (Figure 3), confirming the fact that S-edge sites is important but not yet sufficient to enhance WGS activity[15], [16].

Looking at the increase of S/M ratio after using chelating agents, or in other words, preparing sulfide-based catalysts MoS_2 exposing more S-edge, we expect promising results in terms of WGS activity also.

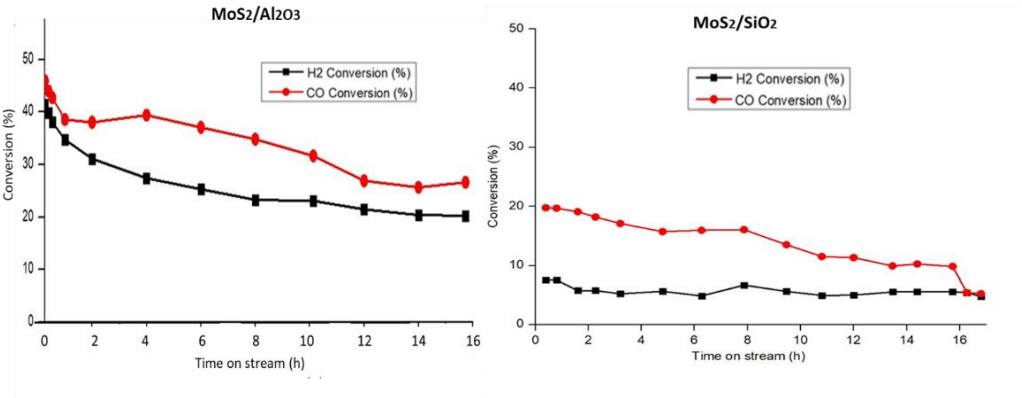

Figure 3 : CO & H2 conversion rate over MoS_2/SiO_2 and MoS_2/Al_2O_3 catalysts during WGS reaction $T_{sulfidation}$=623K & $T_{reaction}$= 573k

References

[1] A. Midilli, M. Ay, I. Dincer, and M. A. Rosen, 'On hydrogen and hydrogen energy strategies', *Renew. Sustain. Energy Rev.*, vol. 9, no. 3, pp. 255–271, Jun. 2005, doi: 10.1016/j.rser.2004.05.003.

[2] G. Nicoletti, N. Arcuri, G. Nicoletti, and R. Bruno, 'A technical and environmental comparison between hydrogen and some fossil fuels', *Energy Convers. Manag.*, vol. 89, pp. 205–213, Jan. 2015, doi: 10.1016/j.enconman.2014.09.057.

[3] J. Chen *et al.*, 'Hydrogen production by water-gas shift reaction over Co-promoted MoS2/Al2O3 catalyst: The intrinsic activities of Co-promoted and unprompted sites', *Int. J. Hydrog. Energy*, vol. 43, no. 15, pp. 7405–7410, Apr. 2018, doi: 10.1016/j.ijhydene.2018.02.194.

[4] G. J. Stiegel and M. Ramezan, 'Hydrogen from coal gasification: An economical pathway to a sustainable energy future', *Int. J. Coal Geol.*, vol. 65, no. 3–4, pp. 173–190, Jan. 2006, doi: 10.1016/j.coal.2005.05.002.

[5] C. Lang, 'Développement de catalyseurs pour la réaction de conversion du gaz à l'eau dans le cadre de la production d'hydrogène par vapogazéification de la biomasse', phdthesis, Université de Strasbourg, 2016. Accessed: Nov. 14, 2023. [Online]. Available: https://theses.hal.science/tel-01389458

[6] J. D. Holladay, J. Hu, D. L. King, and Y. Wang, 'An overview of hydrogen production technologies', *Catal. Today*, vol. 139, no. 4, pp. 244–260, Jan. 2009, doi: 10.1016/j.cattod.2008.08.039.

[7] D. B. Pal, R. Chand, S. N. Upadhyay, and P. K. Mishra, 'Performance of water gas shift reaction catalysts: A review', *Renew. Sustain. Energy Rev.*, vol. 93, pp. 549–565, Oct. 2018, doi: 10.1016/j.rser.2018.05.003.

[8] A. Travert *et al.*, 'CO Adsorption on CoMo and NiMo Sulfide Catalysts: A Combined IR and DFT Study', *J. Phys. Chem. B*, vol. 110, no. 3, pp. 1261–1270, Jan. 2006, doi: 10.1021/jp0536549.
[9] Q. H. Wang, K. Kalantar-Zadeh, A. Kis, J. N. Coleman, and M. S. Strano, 'Electronics and optoelectronics of two-dimensional transition metal dichalcogenides', *Nat. Nanotechnol.*, vol. 7, no. 11, pp. 699–712, Nov. 2012, doi: 10.1038/nnano.2012.193.
[10] E. Krebs, B. Silvi, and P. Raybaud, 'Mixed sites and promoter segregation: A DFT study of the manifestation of Le Chatelier's principle for the Co(Ni)MoS active phase in reaction conditions', *Catal. Today*, vol. 130, no. 1, pp. 160–169, Jan. 2008, doi: 10.1016/j.cattod.2007.06.081.
[11] H. Topsøe, B. S. Clausen, and F. E. Massoth, 'Hydrotreating Catalysis', in *Catalysis: Science and Technology*, J. R. Anderson and M. Boudart, Eds., in Catalysis-Science and Technology. , Berlin, Heidelberg: Springer, 1996, pp. 1–269. doi: 10.1007/978-3-642-61040-0_1.
[12] H. Topsøe, B. S. Clausen, R. Candia, C. Wivel, and S. Mørup, 'In situ Mössbauer emission spectroscopy studies of unsupported and supported sulfided Co□Mo hydrodesulfurization catalysts: Evidence for and nature of a Co□Mo□S phase', *J. Catal.*, vol. 68, no. 2, pp. 433–452, Apr. 1981, doi: 10.1016/0021-9517(81)90114-7.
[13] H. Topsoee, B. S. Clausen, N. Y. Topsoee, and E. Pedersen, 'Recent basic research in hydrodesulfurization catalysis', *Ind. Eng. Chem. Fundam.*, vol. 25, no. 1, pp. 25–36, Feb. 1986, doi: 10.1021/i100021a004.
[14] W. Zhao, F. Maugé, J. Chen, and L. Oliviero, 'Spectroscopic identification of active centers and reaction pathways on MoS2 catalyst for H2 production via water–gas shift reaction', *Chem. Eng. J.*, vol. 455, p. 140575, Jan. 2023, doi: 10.1016/j.cej.2022.140575.
[15] E. Dominguez Garcia, 'Effect of the support on the activity and morphology of hydrodesulfurization catalysts', These de doctorat, Normandie, 2017. Accessed: Nov. 14, 2023. [Online]. Available: https://www.theses.fr/2017NORMC258
[16] 'New insight into the support effect on HDS catalysts: evidence for the role of Mo-support interaction on the MoS2 slab morphology - ScienceDirect'. Accessed: Nov. 14, 2023. [Online]. Available: https://www.sciencedirect.com/science/article/pii/S0926337319307210
[17] L. Lukovicsová, 'Chelating agents in NiMo sulfided catalysts and the effect of nitrogen compounds on hydrodearomatization and hydrodenitrogenation reactions'.
[18] L. Zavala-Sanchez, X. Portier, F. Maugé, and L. Oliviero, 'High-resolution STEM-HAADF microscopy on a γ-Al2O3 supported MoS2 catalyst—proof of the changes in dispersion and morphology of the slabs with the addition of citric acid', *Nanotechnology*, vol. 31, no. 3, p. 035706, Oct. 2019, doi: 10.1088/1361-6528/ab483c.
[19] L. A. Zavala-Sanchez, X. Portier, F. Maugé, and L. Oliviero, 'Promoter Location on NiW/Al2O3 Sulfide Catalysts: Parallel Study by IR/CO Spectroscopy and High-Resolution STEM-HAADF Microscopy', *ACS Catal.*, vol. 10, no. 11, pp. 6568–6578, Jun. 2020, doi: 10.1021/acscatal.0c01092.

Modeling LPG reforming on SOEC Cathode: an innovative way to improve Power-to-Fuel efficiency

JH. Boilley[1,2], A. Berrady[1,*], E. Gürbüz[1], F. Gallucci[2]

[1] Hydrogen Lab ENGIE LAB CRIGEN, 4 rue Joséphine Baker, 93240, Stains, France
[2] Sustainable Process Engineering, Chemical Engineering and Chemistry, Eindhoven University of Technology, Eindhoven, The Netherlands

Introduction

Solar panels and wind turbines convert solar and wind energy respectively into renewable electricity. Due to its low carbon impact, this electricity produced is necessary to fight against global warming. Most sectors should use this energy in its electrical form following their electrification. Other sectors should use this electricity after its conversion into hydrogen to meet their energy demands. However, since hydrogen is a gas with a low energy density by volume, the heavy transportation sector, and especially aviation, will not be able, at least in the short term, to use this gas directly [1]. To achieve the ambitious goals of the Paris conference, they need to convert this energy a second time to produce molecules that can store a large amount of energy in a limited volume.

Among all the reactions to produce e-fuels, the Fischer-Tropsch synthesis seems to be the most relevant for air transport. Because Fischer-Tropsch process is exothermic, it could be interesting to combine this process with high temperature electrolysis to increase the global efficiency of the plant. Several studies already enlightened the benefits to combine this electrolyzer technology with Fischer-Tropsch process [2]. Moreover, it is possible thanks to Solid Oxide Electrolyzer Cell (SOEC) to produce directly a gas composed of H_2 and CO called syngas, this process is called co-electrolysis. This gas is the reactant of the hydrocarbons synthesis. Fischer-Tropsch produces a crude composed of alkanes with different molar masses, corresponding to different energy products with variable interest. Molecules heavier than the fractions of interest can be hydrocracked [3,4]. The lighter molecules, also known as liquefied petroleum gas (LPG), must be burned in order to provide the heat required for the process [5-9], or be reformed to improve the selectivity towards the heavier cuts [10]. Cinti et al [11] were the first to propose reforming the gases produced at the cathode, thus improving the energy efficiency of the process. The simulation of the SOEC proposed in their article consists in a 0D Gibbs reactor.

Co-electrolysis simulation is a hot topic, different models have been developed in recent years. Udagawa et al [12] proposed in 2007 a model of water electrolysis alone, including the limitations to the transfer of matter, the thermal management of the cell. In 2014, Aicart et al. [13] proposed a pseudo-2D model of co-electrolysis, this model took into account the production of CO by reverse water gas shift as well as by electroreduction and was updated later with kinetics of methane production by Bernadet [14].

A pseudo 2D model has been developed to simulate the co-electrolysis as well as the reforming of methane. The results have been verified on experimental polarization curves with regard to co-electrolysis. Tests in the presence of methane are in progress, including outlet gas composition analyses using micro-GC, and will be used to validate the rest of the model. The novelty of this model is to take into consideration the internal reforming of LPG. Moreover this model use kinetics of reforming and reverse water gas shift to estimate the Open Circuit Voltage (OCV) instead of thermodynamic equilibrium. Using OCV to predict methane reforming kinetics has already be done in context of methane fueled solid oxide fuel cell in

* Corresponding author: anass.berrady@engie.com

presence of a small amount of steam [15], but is from our knowledge a novelty concerning SOEC. After estimation and implementation of methane reforming kinetics in context of co-electrolysis, the interest of LPGs reforming was challenged with a simulation of the Power-to-Liquid process realized on Simulink.

Methodology

1. Power-to-Hydrocarbons process proposal

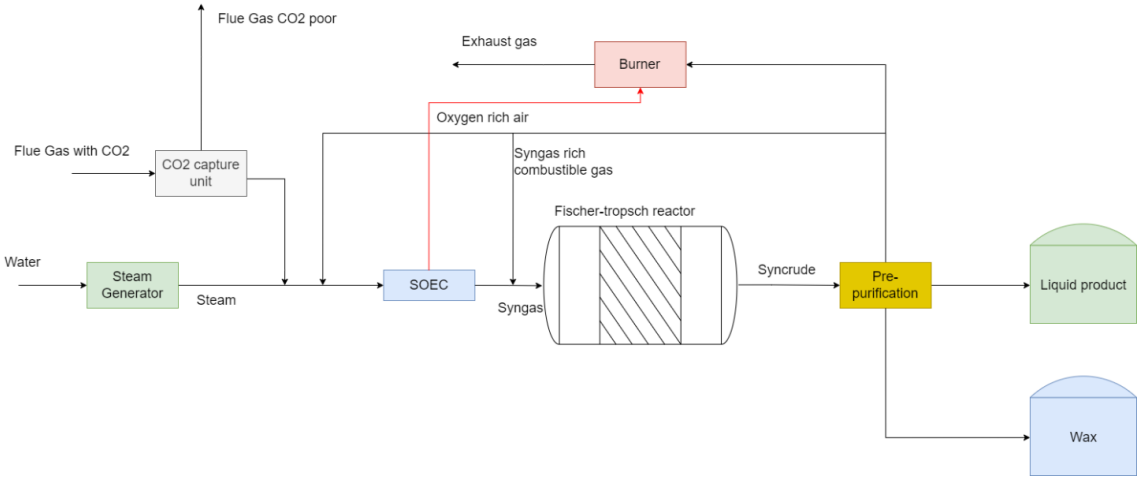

Figure 1 : Process Flow Diagram of the plant

The Power-to-Liquid process is made up of different bricks as schematically represented on the figure 1. The carbon dioxide used as a feedstock is firstly capture by CO_2 capture brick and then is heated to the temperature of the SOEC inlet. The water is vaporized in the steam generator, the heat required to produce the steam comes from the Fischer-Tropsch reactor, from the burner and the rest comes from an electric furnace. CO_2 and steam are mixed with gases from separation process and a fraction of the outlet of the SOEC to maintain some reducer, the gas is sent at the inlet of the electrolyzer to produce syngas. The outlet of the electrolyzer is cooled and then sent to the Fischer-Tropsch reactor where the hydrocarbons synthesis is realized. The hydrocarbons are then separated using flash separators, the gaseous fractions, composed of unreacted syngas or LPG, are sent either at the inlet of the Fischer-Tropsch reactor, at the inlet of the SOEC, or are purged and burned to supply the process with heat. The global process is simulated with Simulink.

2. SOEC modelling

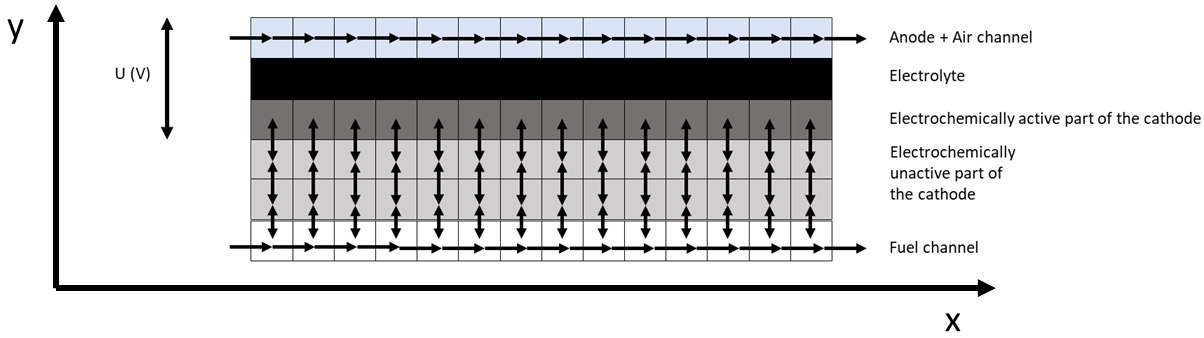

Figure 2 : Schematic representation of the model

The SOEC is simulated on Matlab, the pseudo-2D model is schematically represented on the figure 2. The different assumptions of the model are presented below.

- Discretization according to axis x (along the cell) and axis y (cell thickness), the gas composition is uniform on the width
- For chemical reactions, reaction sites are uniformly distributed in the cell
- For electrochemical reactions, reaction sites are uniformly distributed in the active part of the cathode
- Gases are ideal, flows are uncompressible
- Temperature is uniform throughout the cell
- H_2/H_2O CO/CO_2 are the only couples considered in the electrochemical reactions
- Carbon deposition is not considered
- Gases do not diffuse along x axis inside the cathode
- No diffusion limitation at anode (i.e. no discretization on the y axis for anode)
- No pressure loss
- Electric potential is specified at the outer boundaries of anode and active part of cathode as zero potential and working potential respectively
- Continuity of the equations close to the OCV on the fuel cell side

The chemical and electrochemical reactions are presented below :

- Electrochemical reaction occurring at anode
  - $2\,O^{2-} \leftrightarrow O_2 + 4e^-$
- Electrochemical reactions occurring in the active part of the cathode
  - $2\,H_2O + 4e^- \leftrightarrow 2\,H_2 + 2\,O^{2-}$
  - $CO_2 + 2e^- \leftrightarrow \mathrm{CO} + O^{2-}$
- Chemical reactions occurring in active and unactive part of the cathode
  - $CO + H_2O \leftrightarrow CO_2 + H_2$
  - $2CO + 2H_2 \leftrightarrow CH_4 + CO_2$
  - $CO + 3H_2 \leftrightarrow CH_4 + H_2O$

The modeling approach for electrochemical and chemical description of the co-electrolysis is taken from Aicart et al. and Bernadet [13, 14]. The differences with these models are the additions of the kinetics of light hydrocarbons reforming and the possibility to estimate OCV without considering thermodynamic equilibrium. The model takes into consideration the mass transfer according to the Dusty Gas Model as well as the chemical and electrochemical reactions. The model as simulated using the commercial software Matlab (R2023a), the cell is discretized using a finite difference method. The combination of chemical and diffusion reaction is solved using a loop. At each iteration kinetics, mass transfer and H_2O/CO_2 reduction currents are computed, then a new matrix of concentration is determined. The loop stops when the difference between the previous and the new matrix is below the tolerance ε.

3. Experimental

The experiments were conducted on a cathode supported cell provided by Elcogen at 800 °C and 750 °C. The cell was composed of a 10 µm thick air electrode, a dense electrolyte layer of 2 µm and a Ni-YSZ cathode with a thickness of 400 µm. The active area of the cell was 16 cm². The test bench presents a co-flow distribution of the gas.
The test campaign is divided into three parts,

- A first campaign providing polarization curves of the cell for steam and co-electrolysis, with different temperatures, flowrates and gas compositions.

- The objective of the second campaign is to test steam and dry reforming without current and to analyze exhaust gases with gas chromatography. The goal is to have a good understanding of the kinetics of steam reforming under co-electrolysis conditions. A good comprehension of the mechanism of steam reforming of hydrocarbons permits to be more reliant on the impact of LPG recycling on the efficiency of the electrolyzer.
- The next step is to test co-electrolysis and steam reforming together in order to understand the possible interactions between these reactions. In this campaign polarization curves, and gas analyses will be conducted.

Discussion

1. Comparison with experimental

The polarization curves produced were used to fit parameters of the model with a genetic algorithm. The following figure shows the experimental and simulated polarization curves.

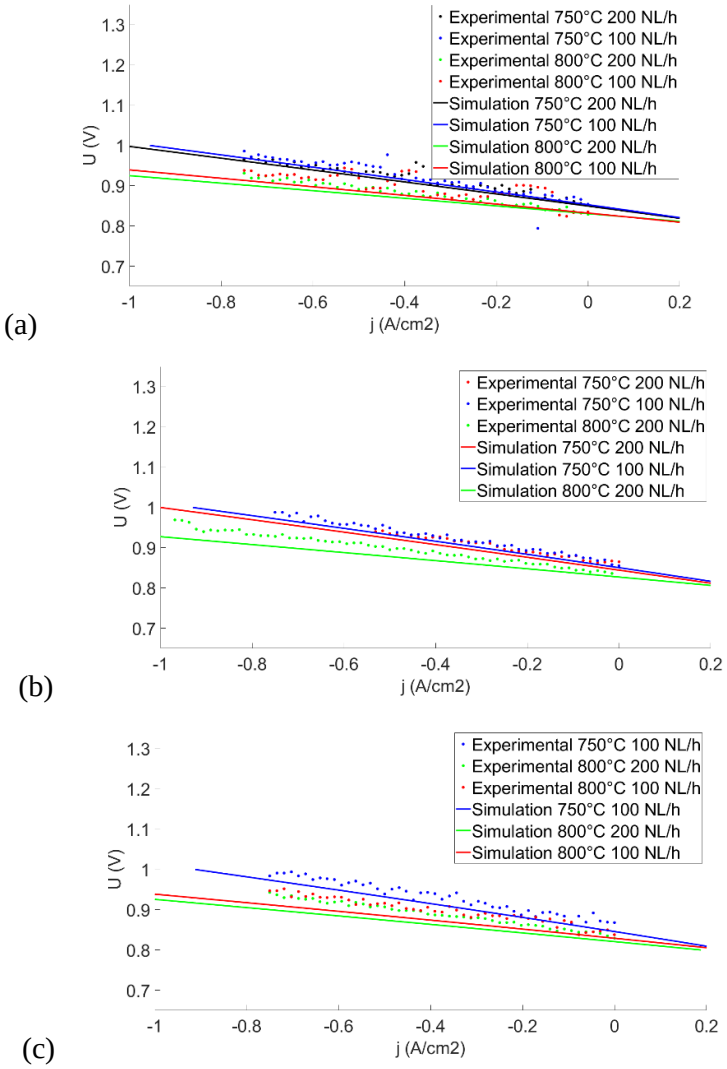

Figure 3.a : Experimental and simulated polarization curves with a gas composition of 60% H2O 30% CO2 and 10% H2 .b : Experimental and simulated polarization curves with a gas composition of 45% H2O 45% CO2 and 10% H2 3.c : Experimental and simulated polarization curves with a gas composition of 30% H2O 60% CO2 and 10% H2. Air flowrate is set equal to fuel flowrate

The result are presented in the figure 3. The model is still yet under development, but the simulated curves seem to fit well with the experimental ones. The gas composition simulated has to be challenged with the gas composition obtained with the µ-GC, and polarization curves has to be tested with presence of methane.

(a) Process efficiency

Energy balance	100% Burner	50% Burner – 50% Recycling	20% Burner – 80% Recycling
Outlet			
Lower Heating Value of product (MW)	4.10	5.11	5.95
Inlet			
Total Electric Need (MW)	7.96	8.43	9.10
Heat need (MW) (% total)	0.00 (0.00%)	0.35 (4.17%)	0.96 (10.54%)
SOEC Electric demand (MW) (% total)	7.00 (87.95%)	7.00 (83.33%)	7.00 (76.89%)
Electric need for Carbon Capture (MW) (% total)	0.29 (3.62%)	0.25 (2.95%)	0.24 (2.59%)
Compressors and pumps (MW) (% total)	0.67 (8.43%)	0.80 (9.56%)	0.91 (9.97%)
Efficiency			
Power to Liquid efficiency (%)	51.52	60.62	65.32
Carbon efficiency (%)	46.28	67.16	81.85

Table 1 : Efficiency of the Power-to-Liquid process

The table 1 above shows the energy efficiency of the process considering a total combustion (100% Burner) of the LPG, or considering different recycling rates to the stack. The recycling rate to the SOEC improve the efficiency from 51.52% to 65.32%, defined as the mass flow of fuel and wax produced by the process multiply by the mass energetic content divided by the power consumption the plant. It improves also the Carbon efficiency, defined as the quantity of carbons in the interest product divided by the carbon captured, from 46.28% to 81.85%.

Conclusions

Preliminary results show that experimental polarization curves and simulated ones are similar. However, gas compositions after reforming have to be challenged with experimental results. Process simulation shows an improvement of the process with gas recycling strategies both in terms of energetic efficiency and carbon efficiency. This process could be particularly interesting in order to produce e-Sustainable Aviation Fuel in compliance with the ReFuelEU initiative.

References

[1] Sharmina M, Edelenbosch OY, Wilson C, Freeman R, Gernaat DEHJ, Gilbert P, et al. “Decarbonising the critical sectors of aviation, shipping, road freight and industry to limit warming to 1.5–2°C.” Climate Policy 2021;21:455–74. https://doi.org/10.1080/14693062.2020.1831430.

[2] Markowitsch C, Lehner M, Maly M. “Evaluation of process structures and reactor technologies of an integrated power-to-liquid at a cement factory”. Journal of CO2 utilization 2023; 102449. https://doi.org/10.1016/j.jcou.2023.102449

[3] Gambaro C, Calemma V, Molinari D, Denayer J. “Hydrocracking of Fischer-Tropsch waxes: Kinetic modeling via LHHW approach”. AIChE Journal - Wiley Online Library n.d. https://aiche.onlinelibrary.wiley.com/doi/abs/10.1002/aic.12291

[4] Sun C, Luo Z, Choudhary A, Pfeifer P, Dittmeyer R. “Influence of the Condensable Hydrocarbons on an Integrated Fischer–Tropsch Synthesis and Hydrocracking Process: Simulation and Experimental Validation”. Ind Eng Chem Res 2017;56:13075–85. https://doi.org/10.1021/acs.iecr.7b01326.

[5] Adelung S, Maier S, Dietrich R-U. “Impact of the reverse water-gas shift operating conditions on the Power-to-Liquid process efficiency”. Sustainable Energy Technologies and Assessments 2021;43:100897. https://doi.org/10.1016/j.seta.2020.100897.

[6] Becker WL, Braun RJ, Penev M, Melaina M. “Production of Fischer–Tropsch liquid fuels from high temperature solid oxide co-electrolysis units”. Energy 2012;47:99–115. https://doi.org/10.1016/j.energy.2012.08.047.

[7] P. Kulkarni A, Hos T, V. Landau M, Fini D, Giddey S, Herskowitz M. “Techno-economic analysis of a sustainable process for converting CO 2 and H 2 O to feedstock for fuels and chemicals”. Sustainable Energy & Fuels 2021;5:486–500. https://doi.org/10.1039/D0SE01125H.

[8] König DH, Freiberg M, Dietrich R-U, Wörner A. “Techno-economic study of the storage of fluctuating renewable energy in liquid hydrocarbons”. Fuel 2015;159:289–97. https://doi.org/10.1016/j.fuel.2015.06.085

[9] Herz G, Reichelt E, Jahn M. “Techno-economic analysis of a co-electrolysis-based synthesis process for the production of hydrocarbons”. Applied Energy 2018;215:309–20. https://doi.org/10.1016/j.apenergy.2018.02.007.

[10] Pratschner S, Hammerschmid M, Müller FJ, Müller S, Winter F. “Simulation of a Pilot Scale Power-to-Liquid Plant Producing Synthetic Fuel and Wax by Combining Fischer–Tropsch Synthesis and SOEC”. Energies 2022;15:4134. https://doi.org/10.3390/en15114134

[11] Cinti G, Baldinelli A, Di Michele A, Desideri U. “Integration of Solid Oxide Electrolyzer and Fischer-Tropsch: A sustainable pathway for synthetic fuel”. Applied Energy 2016;162:308–20. https://doi.org/10.1016/j.apenergy.2015.10.053.

[12] Udagawa J, Aguiar P, Brandon N.P. “Hydrogen production through steam electrolysis: Model-based steady state performance of a cathode-supported intermediate temperature solid oxide electrolysis cell”. Journal of Power Sources 2007; 127-136; https://doi.org/10.1016/j.jpowsour.2006.12.081

[13] Aicart J, Laurencin J, Petitjean M, Dessemond L, “Experimental validation of Two-Dimensional H_2O and CO_2 Co-Electrolysis Modeling”, Fuel Cells 2014. https://doi.org/10.1002/fuce.201300214

[14] Bernadet L. “Étude de l’effet de la pression sur l’électrolyse de H2O et la co-électrolyse de H2O et CO2 à haute température” Université de Bordeaux 2016. NNT : 2016BORD0312. tel-01674502

[15] Wang B, Jiang Z, Lin Z. “A theoretical framework for multiphysics modeling of methane fueled solid oxide fuel cell and analysis of low steam methane reforming kinetics”. Applied Energy 2016; 1-11 https://doi.org/10.1016/j.apenergy.2016.05.049

Modeling of the catalyst degradation in PEM fuel cells

T. Uhlemayr*[1], J. Scholta[1]

[1]Zentrum für Sonnenenergie- und Wasserstoff-Forschung Baden-Württemberg (ZSW),
89081 Ulm, Germany

Introduction

The use of hydrogen in proton exchange membrane fuel cells (PEMFC) to generate electric power for motor vehicles is an environmentally friendly alternative to conventional combustion engines and reduces CO_2 emissions in the transport sector.
In mobile applications, many operational parameters such as temperature, humidity, mechanical stress and load cycling effect degradation mechanisms and the lifetime of the fuel cell. Degradation is among other things caused by mechanical or chemical processes that lead to failures of the cell components. Mechanical stress results in fractures in the bipolar plate (BPP), failure of the sealing gasket, deformation and thickness change of the gas diffusion layer (GDL) and crack and pinhole formation in the membrane. On BPP and GDL corrosion leads to thinning, conductivity loss and contact angle changes. Other chemical degradation processes are the dissolution of Platinum particle on the catalyst layer (CL) and contamination of reaction places in the membrane. [1] gives an overview on fuel cell degradation processes.
For better understanding of the degradation mechanisms and performance prediction over the lifetime, modeling is essential. This PhD project starts with developing a degradation model in Matlab, beginning with the chemical degradation process on the cathode CL.

Methodology

The electrochemical active surface area (ECSA) of the platinum particles on the catalyst layer is the parameter that gives an indication of the performance loss. There are four main chemical processes on the CL, which cause ECSA loss and degradation: Platinum oxidation, platinum dissolution, Ostwald ripening and particle loss to the membrane.
All of these reactions have an impact on the platinum particle size and distribution. In [2] Jahnke et.al. give an overview of these reactions with the associated reaction rate formulas and describes how the time dependent changes can be calculated.
The Platinum dissolution is described with three steps: a fast reversible oxidation step, a slower irreversible oxidation step and an irreversible reduction step. The change in the platinum oxide coverage is calculated from the reaction rates of the three mechanisms.
The progress of the platinum dissolution is divided into the direct dissolution and the oxide dissolution. Changes in radius are calculated out of the reaction rates of the dissolution processes.
For the simulation, the initial particle size distribution is determined and the initial ECSA calculated from it. The number of particles results from the platinum loading.

A 1D-Matlab model has been developed at ZSW, which is now being extended to include the degradation model. In this model, the fuel cell is divided into segments and it consists of three main steps: Computation of segment, cell voltage and time step. The cell voltage is calculated for each segment in all time steps.

* Corresponding author: theresa.uhlemayr@zsw-bw.de

The time-dependent changes in platinum oxide coverage and, based on this, the particle size changes are modeled as an ordinary differential equation (ODE) system with differential equations for each segment.

At each modeled time step, the total platinum oxide coverage is first calculated and, based on this, the changes in the individual particle size.
The ratio of the ECSA of the respective time step and the initial ECSA gives a degradation factor with impact to the activation overpotential.
In Figure 1 one can see the modelled total platinum oxide coverage at three different voltages over time.

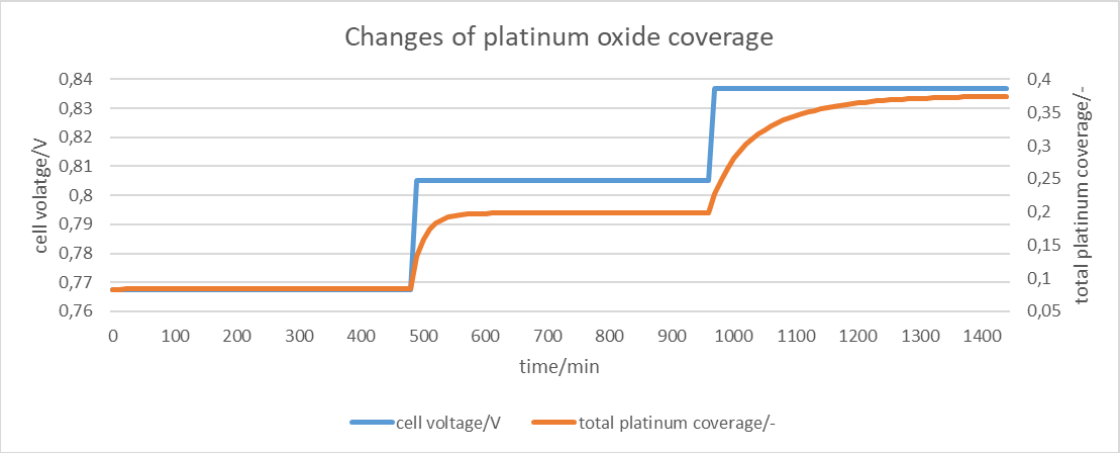

Figure 1: Total platinum oxide coverage

After adjusting some parameters in the Matlab model, this graph shows a good compliance with the course described in [2].
With the computed platinum coverage values, the radius changes are calculated, which leads to the ECSA at each time step.
Figure 2 shows the course of the rate ECSA/initial ECSA (ECSA factor) and voltage over time (2000 hours).
This graph shows decreasing cell voltage with decreasing ECSA over time and the change of the total oxide coverage.

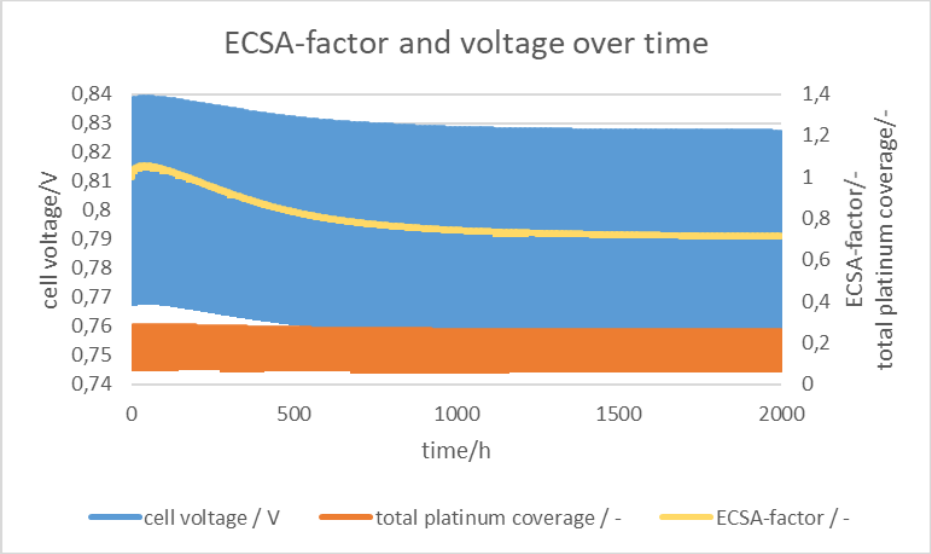

Figure 2: ECSA-factor and voltage over time (2000 hours)

Discussion

Since the project started only a few weeks ago, the aging model is at a more or less initial stage now.
So far, an initial model for the catalyst degradation has been developed and now needs to be optimized.
The current task is to adjust the curvature of the ECSA curve to match that describes by Jahnke in [2]. Furthermore, the decrease in the platinum concentration due to the particle loss to the membrane must be included in the model.
The model then will be tested with various operating conditions in order to optimize it with respect to the influencing parameters temperature, humidity, dwell time and load cycles.

Conclusions

In the last past week since the PhD project started, a lot of research work were done to get an overview of all degradation effects on the fuel cell components. The aim is to model the performance loss caused by the chemical processes. Starting with the software Matlab, a first model was built including the platinum particle size distribution and electrochemical active surface area changes.
In the further work the current model on the catalyst layer is optimized and validated. It is intended to include the other chemical degradation effects mentioned above.
In addition, another modeling software (AVL) is used to develop another 3D degradation model.

References

[1] H.L. Nguyen, J. Han, X.L. Nguyen, S. Yu, Y.-M. Goo, D.D. Le, Review of the Durability of Polymer Electrolyte Membrane Fuel Cell in Long-Term Operation: Main Influencing Parameters and Testing Protocols, Energies 14 (2021) 4048. https://doi.org/10.3390/en14134048.
[2] T. Jahnke, G.A. Futter, A. Baricci, C. Rabissi, A. Casalegno, Physical Modeling of Catalyst Degradation in Low Temperature Fuel Cells: Platinum Oxidation, Dissolution,

Particle Growth and Platinum Band Formation, J. Electrochem. Soc. 167 (2020) 13523. https://doi.org/10.1149/2.0232001JES.

Modeling hydrogen in the Spanish energy system through the TIMES model.

C. Mantilla*[1, 2], J. Dufour [2, 3],Y. Lechón[1]

[1]Energy Systems Analysis Unit. CIEMAT, Av. Complutense, 40, 28040 Madrid, Spain.
[2]Rey Juan Carlos University, Chemical and Environmental Engineering Group, 28933, Móstoles, Spain.
[3]IMDEA Energy, Systems Analysis Unit, 28935, Móstoles, Spain

Introduction

The European Union has three main priorities in its policies: ensuring energy security, maintaining competitiveness, and addressing climate change. While many have favored electrification as the primary means to reduce carbon emissions in various energy sectors, hydrogen has gained increasing attention, especially for those industries that are challenging to decarbonize, such as heavy-duty transportation, certain industrial processes, and the maritime and aviation sectors [1].

Numerous energy models have been developed to study the potential role of hydrogen in energy systems [2]. These models aim to explore how different energy sources and technologies can contribute to decarbonizing entire economies. However, these models often produce conflicting predictions use of hydrogen [3] [4]. The reasons for these disparities are not well understood. Hydrogen systems are complex, and the depth and breadth of their representation can vary significantly among models, especially when it comes to production technologies and the delivery and use of hydrogen.

Certain technical challenges, such as the specific pressure and purity requirements of hydrogen for various technologies, are addressed by only a limited number of models. Additionally, concerns have been raised about whether the assumptions regarding the cost and performance of hydrogen technologies in some models are accurate [1].

Spain's current energy and climate strategy is firmly rooted in ambitious 2050 objectives, including achieving national climate neutrality, sourcing 100% of electricity from renewables, and reaching a 97% renewable energy share in the overall energy mix. This strategy primarily revolves around significant developments in renewable energy, particularly solar and wind power, energy efficiency improvements, electrification, and the promotion of renewable hydrogen. These initiatives are viewed as opportunities to stimulate economic growth, create jobs, modernize industries, enhance competitiveness, provide support to vulnerable populations, bolster energy security, and drive research, development, and innovation.
To realize these targets, Spain has outlined its central roadmap in the National Energy and Climate Plan (NECP) for the 2021-2030 period. This comprehensive document details various policy actions spanning multiple sectors, all aimed at aligning the nation with its climate objectives. These actions encompass enhancing energy efficiency, expanding the use of renewables, and transforming the transport sector.
Currently, Spain is concentrating its efforts on the 2030 targets. Overall, Spain's NECP anticipates achieving a 48% renewable energy share in total energy consumption by 2030. This progress will be most pronounced in the power sector, where the plan envisions the installation

* Carlos Mantilla: carlos.mantilla@ciemat.es

of nearly 60 gigawatts (GW) of new renewable generation by 2030, led primarily by wind and solar sources. This substantial capacity expansion is expected to account for 81% of the total electricity generation in that year, firmly positioning Spain on the path to achieving its 2050 objective of sourcing 100% of its power from renewable sources, aligning with the nation's ultimate goal of carbon neutrality by 2050 [6].

Spain is poised to become a major European player in renewable energy generation, thanks to its favorable climate conditions and vast expanses of available land for the installation of renewable energy production facilities, both solar and wind energy. Leveraging this substantial potential, Spain is ambitiously positioning itself as a key producer of green hydrogen in Europe.

When we refer to green hydrogen, we mean hydrogen production by renewable energy sources, the more promising and likely method to take the lead in the coming years is power-to-hydrogen, which involves using zero-carbon electricity to produce hydrogen via water electrolysis. This approach is gaining prominence due to uncertainties surrounding the costs of CCUS and the ongoing reductions in renewable power generation and electrolyzer costs.
Spain's strategic focus on green hydrogen reflects its commitment to sustainable and environmentally friendly energy solutions, aligning with the broader European efforts to transition towards a greener and more carbon-neutral future [7].

The Spanish Hydrogen Roadmap considers renewable hydrogen as a key technology to increase the production of renewable electricity and renewable gases, targeting 4 GW of hydrogen electrolysis capacity in 2030[8]. This document shows how the Spanish energy strategy focuses on developing as a producer and exporter of green hydrogen to Europe.

Objectives

The primary objective is to integrate green hydrogen into Spain's energy system using the TIMES model. Using an adaptation of the Spanish TIMES-Sinergia model, various scenarios are explored to analyze market dimensions, assess production potential, evaluate utilization possibilities, and determine export viability and competitiveness.

Methodology

To incorporate green hydrogen into the Spanish energy system, a model from the TIMES family, representing the Spanish energy system will be employed. The TIMES model generator was developed by the Energy Technology Systems Analysis Program (ETSAP), which is one of the longest-running Technology Collaboration Programs under the International Energy Agency (IEA). This sophisticated tool, known as The Integrated MARKAL-EFOM System (TIMES) model generator, combines two distinct yet complementary approaches for modeling energy systems: a technical engineering approach and an economic approach.

TIMES is a technology-rich, bottom-up model generator that utilizes linear programming to create an optimized energy system. This system is designed to be the most cost-effective solution while adhering to various user-defined constraints, typically over medium to long-term timeframes. In essence, TIMES serves as a valuable tool for exploring potential energy futures by comparing different scenarios and their associated outcomes [9].
TIMES models encompass all the steps from primary resources through the chain of processes that transform, transport, distribute, and convert energy into the supply of energy services demanded by energy consumers [9]. The mathematical, economic, and engineering

relationships between these energy "producers" and "consumers" are the basis underpinning TIMES models.

All TIMES models are constructed from three basic entities [9]:
Technologies (also called processes) are representations of physical devices that transform commodities into other commodities. Processes may be primary sources of commodities or transformation activities.
Commodities (including fuels) are energy carriers, energy services, materials, monetary flows, and emissions; a commodity is either produced or consumed by some technology.
Commodity flows are the links between processes and commodities

These three entities are used to build an energy system that characterizes the country or region in question. All TIMES models have a reference energy system, which is a basic model of the energy system before it is substantially changed either for a particular region or for a particular scenario. The principle insights generated from TIMES are achieved through scenario analysis. A reference energy scenario is generated first by running the model in the absence of any policy constraints. A second scenario is then established by imposing policy constraints on the model and the model generates a different least-cost energy system with different technology and fuel choices. Once all the inputs, constraints, and scenarios have been put in place, the model will attempt to solve and determine the energy system that meets the energy service demands over the entire time horizon at least cost.

Recently, the IEA's Final Report published by Paul Dodds et al. has described in detail the modeling of hydrogen in different versions of TIMES, where eight national, one European, and one global model were included in the comparison. Modeling hydrogen is complex, the level of modeling detail for hydrogen technologies varies widely between models. Dodds et al. also establish best-practice guidelines for representing hydrogen in energy system models [1], which are going to be used in the implementation of hydrogen in the Spanish TIMES model.

In the current Spanish model, hydrogen is represented in a simplified and incomplete manner. As can be seen in Figure 1, the production part is described, although the production of green hydrogen is not detailed. However, distribution, storage, and also the final uses are not sufficiently precise.

This work aims to improve the hydrogen modeling in the Spanish model and generate scenarios to study the market dimensions, assess production potential, evaluate utilization possibilities, and determine export viability. All, essential aspects to position Spain as one of the main producers and exporters of renewable hydrogen in Europe.

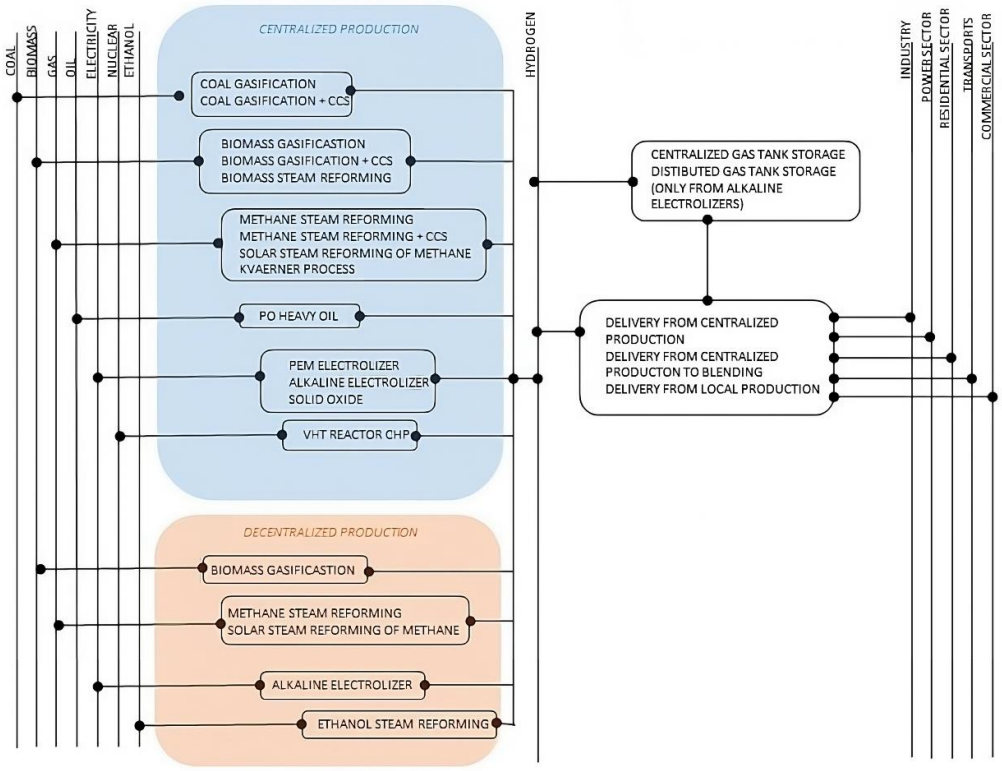

Figure 1: current hydrogen RES in Spanish TIMES model

Results and Discussion

This research is in progress since it is in an initial phase. The work is now in the information-gathering phase, to be able to characterize all the technologies, distribution and end uses, to obtain a detailed representation of the hydrogen in the reference energy system (RES). Both centralized and decentralized production will be represented in the RES and transportation, storage and distribution are also important and are going to be represented in detail since they have special complexities. A complete description of the end uses is also very important for the correct representation of the RES. This work proposes a more elaborate and complete RES that allows for studying a complete and detailed hydrogen energy system (Fig2).

This study incorporates green hydrogen into the framework. Additionally, it offers a comprehensive and in-depth exploration of various aspects, including end-use applications, distribution, storage, and production methods. Is recommended to start with demand-side options, then production technologies, and finally to choose an appropriate approach to delivery costs [1].

To ensure the reliability of our model and derive valuable insights into the energy system, we must integrate accurate data on costs, efficiencies, and production. Our work is based on the established TIMES-Sinergia energy model, and we are augmenting it with essential

information about hydrogen. This comprehensive approach encompasses every aspect of hydrogen, spanning production, distribution, storage, and consumption.

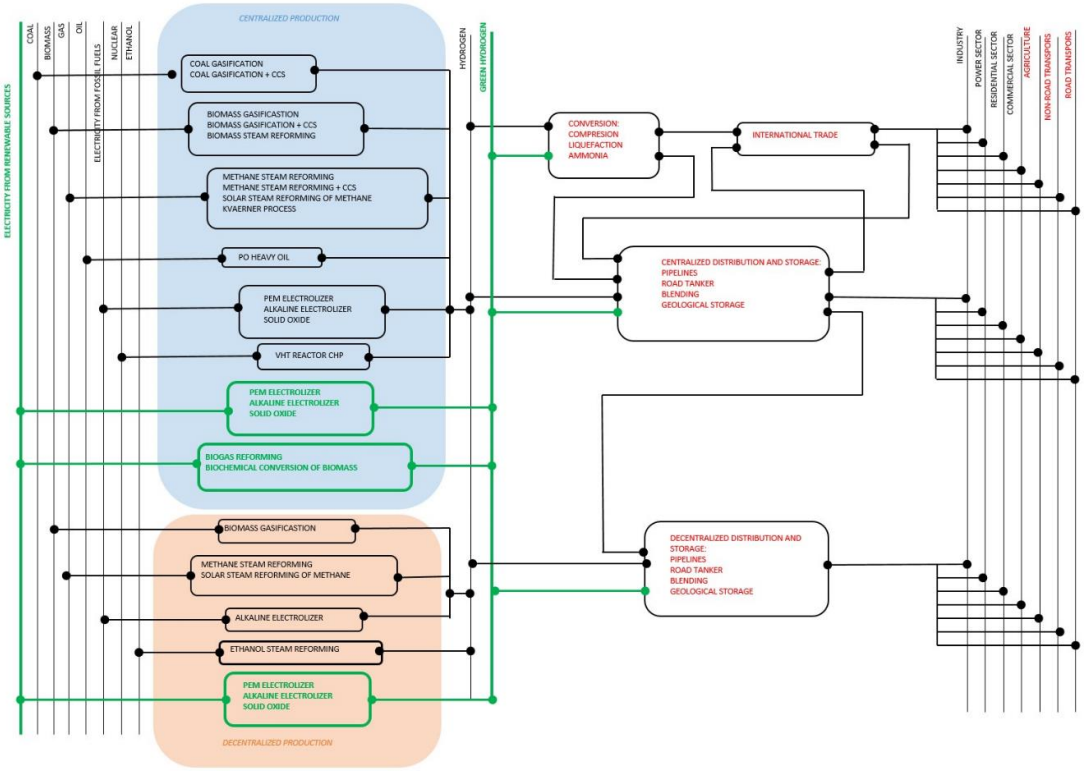

Figure 2: Proposal of the new hydrogen RES in the Spanish TIMES model. In green the green hydrogen RES and in red other elements added.

Furthermore, it is worth noting that ammonia derived from low-carbon hydrogen could emerge as a viable option for international trade and as a sustainable shipping fuel. Moreover, its potential extends beyond shipping, making it relevant for other facets of the energy system. It is also needed a detailed quantification of renewable resources available since they are the key factor for the production of renewable hydrogen.

The objective is to understand the surpluses of renewable energy that are destined for the production of green hydrogen to determine production potential. Use potential in the Spanish industrial, transport, and building sectors is also key to determining the green hydrogen export potential. Also other economic aspects such as technological maturity, the cost uncertainty related, and how learning curves influence costs and the competitiveness of all the green hydrogen sectors. Competitiveness is crucial if Spanish wants to place itself as a main producer and exporter of green hydrogen in Europe and all the technological and economic aspects have to be taken into account to create realistic scenarios so the model can make reliable predictions.

Conclusions

Being in a work-in-progress phase, there are many settings and factors to be adjusted to obtain a realistic and reliable model of the Spanish energy system, which allows for studying different penetration scenarios of green hydrogen.

In contrast to the well-established market for renewable electricity, a corresponding market for green hydrogen has yet to fully materialize. Currently, significant quantities of hydrogen are utilized in various industries; however, the majority of this hydrogen is derived from fossil fuels, resulting in elevated CO2 emissions [10].

To position hydrogen as a viable component within forthcoming low-carbon energy systems, it is imperative to showcase its capacity for achieving notably reduced carbon emissions. This paper embarks on an exploration of the definition of green hydrogen, delves into emerging initiatives for characterizing it as such, and underscores the primary hurdles that standards and guarantee of origin schemes must surmount to cultivate a market for green hydrogen.

The hydrogen economy is not a mere abstraction on the horizon; instead, the existing infrastructure and practices within the hydrogen economy are poised for expansion to meet the demands of the future.

References

1] Paul Dodds, Daniel Scamman, Kari Espegren 2022 Integrating Hydrogen into ETSAP Models. Final Report For the IEA/ETSAP Project (IEA Hydrogen TCP Task 41 Sub-task C).

[2] Energy Exemplar, GO 2 Power. Leveraging PLEXOS for a Variety of Energy Studies: Hydrogen Energy System Feasibility Studies. April.2023. Available at: https://www.energyexemplar.com/customers/go2-power.

[3] Quarton CJ, Tlili O, Welder L, Mansilla C, Blanco H, Heinrichs H, et al. The curious case of the conflicting roles of hydrogen in global energy scenarios. Sustainable Energy & Fuels. 2020;4:80-95.

[4] Hanley ES, Deane JP, Gallachóir BPÓ. The role of hydrogen in low carbon energy futures–A review of existing perspectives. Renewable and Sustainable Energy Reviews. 2018;82:3027-45.

[5] Staffell I, Scamman D, Velazquez Abad A, Balcombe P, Dodds PE, Ekins P, et al. The role of hydrogen and fuel cells in the global energy system. Energy & Environmental Science. 2019;12:463-91.

[6] National Energy and Climate Plan (NECP) for the 2021-2030

[7] Energy Policy Review Spain 202. The International Energy Agency (IEA)

[8] Spanish Hydrogen Roadmap 2020

[9] Loulou, R., Remne, U., Kanudia, A., Lehtila, A., Goldstein, G., 2005. Documentation for the TIMES Model - PART I 1–78.

[10]A. Velazquez Abad y P. E. Dodds. Green hydrogen characterization initiatives: Definitions, standards, guarantees of origin, and challenges. Energy Policy, vol. 138, p. 111300, mar. 2020, doi: 10.1016/j.enpol.2020.111300.

Modelling of Turbulent Hydrogen Combustion including Preferential Diffusion Effects for Gas Turbine Applications

S.N.J. Schepers*, R.J.M. Bastiaans, R.T.E. Hermanns, J.A. van Oijen

Eindhoven University of Technology

Abstract

Due to the global rise in temperatures, the need for clean and renewable energy sources is higher than ever. The irregular nature of energy generated by wind and photovoltaics poses challenges in establishing a stable electricity grid. Therefore, additional flexible power sources are necessary to stabilise the grid. A gas turbine is an example of such a flexible and reliable power source. However, the gas turbines currently in use operate generally on hydrocarbon-based fuels. A crucial step in decarbonising the power generation sector is to retrofit gas turbines to cope with green, renewable fuels, such as hydrogen. Hydrogen seems to be a viable solution due to the absence of carbon in its molecular structure. However, the combustion properties of hydrogen are vastly different relative to natural gas so design adaptations might be necessary. Efficient and accurate predictive CFD models are required to design combustion systems that operate on hydrogen.
This research is part of the EU HELIOS project, which is fully entitled: "Stable high hydrogen low NOx combustion in full-scale gas turbine combustor at high firing temperatures". This research mainly focuses on creating high-fidelity turbulent hydrogen combustion models for gas turbine applications. The combustion models will be based on the tabulated reduced chemistry method, the Flamelet Generated Manifold (FGM) method [1], and extended to take the large preferential diffusion effects of hydrogen into account. The interaction between turbulence and chemistry will be investigated by performing direct numerical simulation (DNS) of premixed hydrogen with detailed reaction mechanisms. The analyses of the DNS results will guide the development of the reduced order large eddy simulation (LES) turbulence model to come to an accurate and efficient FGM-LES tool [2]. The FGM-LES tool will be validated on experimental data obtained by laser-diagnostics measurements performed on a lab-scale model of a gas turbine combustor. When the tool is validated, phenomena such as flame stabilisation and flashback will be investigated to obtain a deep understanding of turbulent hydrogen combustion.
No specific results are there to be shown yet since the research project started in September 2023.

Acknowledgements

This project is supported by the Clean Hydrogen Partnership and its members.

References

[1] J. A. van Oijen and L. P. de Goey. Modelling of premixed laminar flames using flamelet-generated manifolds. *Combustion Science and Technology*, 161(1):113–137, 2000.

[2] J. A. van Oijen, A. Donini, R. J. Bastiaans, J. H. ten Thije Boonkkamp, and L. P. de Goey. State-of-the-art in premixed combustion modeling using flamelet generated manifolds. *Progress in Energy and Combustion Science*, 57:30–74, 2016.

*Corresponding author: s.n.j.schepers@tue.nl

Modelling of the Manufacturing Process Related Residual Stresses in Type 4 Pressure Vessels for Hydrogen Storage

B. Popiela[1], S. Günzel*[1], G. W. Mair[1], H. Seidlitz[2]

[1]Bundesanstalt für Materialforschung und -prüfung (BAM), Unter den Eichen 44-46, 12203, Berlin, Germany
[2]BTU Cottbus-Senftenberg, Konrad-Wachsmann-Allee 13, 03046, Cottbus, Germany

Introduction

Wide use of hydrogen technologies requires a rapid development of each link in the hydrogen value chain. In terms of the safety level and social acceptance of hydrogen technologies, hydrogen storage can be highlighted as one of the most important challenges. This project, within the BTU-BAM Graduate School "Trustworthy Hydrogen", focuses on hydrogen gas storage in pressure vessels. This method of hydrogen storage is widely used in the industry, transport, and on-board applications, mostly due to its technological maturity and energy efficiency [15].
According to the international standard ISO 11439 [7], there are four different types of pressure vessels for gas storage, schematically shown in Fig. 1.

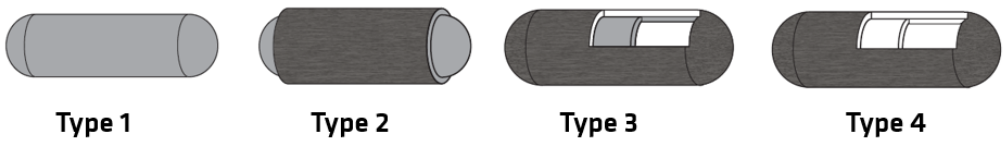

Figure 1: Pressure vessel types for gas storage [16]

Type 1 is a full-metal structure. Type 2 is characterized by a metal liner and hoop composite wrapping in the cylindrical section. In Type 3 vessels the metal liner is fully composite wrapped. Type 4 pressure vessels are also fully-wrapped structures, but their liner is non-load sharing and mostly made of plastic. Due to their weight-saving potential and capability to withstand high working pressures of up to 1000 bar, type 4 pressure vessels are particularly beneficial for on-board and transportation applications. Taking the type 1 pressure vessel as a reference, the weight-saving potential of up to 75% can be achieved, under the same working pressure and with the same vessel volume. This is even up to 25% more than the weight-saving potential of type 3 cylinders [1]. Therefore, this project focses only on type 4 pressure vessels.
Type 4 pressure vessels for hydrogen storage are typically manufactured in a filament winding process, which is characterized by a number of physical effects and process parameters. Those result in a residual stress state, which, if not controlled properly, can lead to an uneven stress distribution in operation.
The most important objective of the project is to deepen the understanding of how the residual stress impacts the operational safety of type 4 hydrogen pressure vessels. An additional goal is to develop methods to influence the residual stress distribution and the behaviour of a finished component by a targeted use of process parameters. As a starting point of the project, calculations of residual stresses in thin-walled filament wound structures based on the classical laminate theory (CLT) and finite element analyses (FEA) were carried out, and are discussed in this abstract. Those calculations were used to achieve a beneficial, uniform stress state in a 6.8 liter cylinder of type 4 with a nominal working pressure of 300 bar, which is being used as specimen within the scope of the project. The differing model assumptions for the analytical and FE calculations result in certain differences in the results, which are discussed in this abstract. An experimental study using the cylinders and defined process parameters is planned.

*Corresponding author: stephan.guenzel@bam.de

Methodology

In the filament winding process, the fibers are being placed under tension on a mandrel and, later, on the previously wound layers (see Fig. 2 (a)). To model the process for hoop layers in the most simplified way, it can be one dimensionally idealized as parallel strings, of which one is being elongated by the winding tension (see Fig. 2 (b)).

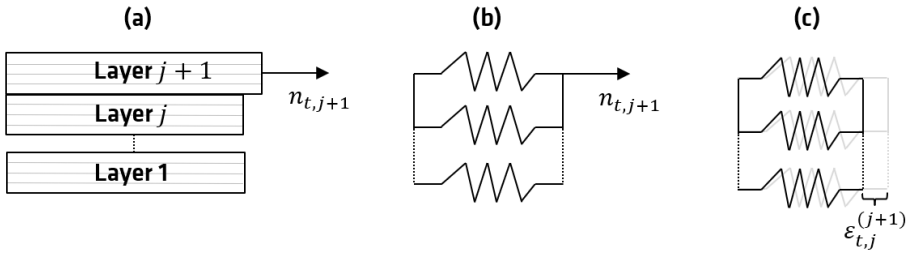

Figure 2: Idealization of filament winding as parallel springs

The spring constant corresponds with the fiber stiffness in the fiber direction. After the winding tension is removed, the behaviour of the parallel springs depends on the assumed friction between the layers. If no friction is assumed, the newly wound layer under pre-tension will not transfer the load to the previously wound layers and will go back to the unloaded state. If there is friction between the layers, the parallel springs are being compressed (see Fig. 2 (c)). On the other hand, the use of the internal pressure during winding causes expansion of the layers. The total strain change in a layer j after winding of the layer *j+1* considered with this simplified model can be calculated as:

$$\varepsilon_{p,j}^{(j+1)} = \frac{p^{(j+1)} r_m^{(j)}}{E_{ges}^{(j)} t_{ges}^{(j)}} - \frac{p^{(j+1)} r_m^{(j+1)}}{E_{ges}^{(j+1)} t_{ges}^{(j+1)}} \tag{1}$$

$$\varepsilon_{t,j}^{(j+1)} = \frac{n_{t,j+1}}{E_{ges}^{(j+1)} t_{ges}^{(j+1)}} \tag{2}$$

Hereby, $\varepsilon_{p,j}^{(j+1)}$ is the strain change in layer j due to the internal pressure $p^{(j+1)}$ used while winding the layer *j+1*. Further, $\varepsilon_{t,j}^{(j+1)}$ is the strain change due to the winding tension $n_{t,j+1}$ in layer *j+1*. The stiffness of the wound layers up to layer j is represented by the term $E_{ges}^{(j)} t_{ges}^{(j)}$. The total strain of layer j after the winding of the last layer n will be:

$$\varepsilon_j^{(n)} = \varepsilon_{t,j} - \frac{p^{(j)} r_m^{(j)}}{E_{ges}^{(j)} t_{ges}^{(j)}} + \sum_{i=j+1}^{n} (\varepsilon_{p,j}^{(i)} + \varepsilon_{t,j}^{(i)}) \tag{3}$$

where $\varepsilon_{t,j}$ is the initial winding tension of the layer.
However, for the analysis of a pressure vessel with a composite structure, consisting of multiple layers with different layer angles, the spring model is not sufficient anymore. Hence, a model based on the CLT was created. The assumption of a thin-walled cylinder is valid, since the ratio of the outer to inner radius is around 1,1 for the considered specimen [20, 9]. The cylindrical region of the pressure vessel is considered a shell element, as previously done in [20, 19, 13, 1]. Then, the strain change in layer j after winding of the layer *j+1* due to the used internal pressure and winding tension of the newly wound layer will be:

$$\{\varepsilon\}_{p,j}^{(j+1)} = [A]_{ges}^{-1^{(j)}} \cdot \{n\}_{p,j+1} - [A]_{ges}^{-1^{(j+1)}} \cdot \{n\}_{p,j+1} \tag{4}$$

$$\{\varepsilon\}_{t,j}^{(j+1)} = [A]_{ges}^{-1^{(j+1)}} \cdot \{n\}_{t,j+1} \tag{5}$$

where $[A]_{ges}^{(j)}$ is the shell stiffness matrix from the liner up to layer j. Moreover, $\{n\}_{p,j+1}$ as well as $\{n\}_{t,j+1}$ is the force flux due to the used internal pressure and winding tension of layer *j+1*, respectively. Details of how the shell stifnness is derived can be found in [17].
Furthermore, a strain change due to resin flow can modeled based on the Darcy's law, same as in the

models of *Cai* and *Lee* [4, 12]. However, for high fiber volume ratios after the resin bath, a negligible strain change is expected, due to the decreased permeability of the fiber sheet [4, 2].
Moreover, it is assumed that after the winding process a gelification occurs already at ambient conditions, before the curing in an oven. Due to that assumption, the reference temperature for the stress analysis is the room temperature and no additional thermal stresses in the finished component are expected. Nevertheless, thermal stresses can be also considered with the presented analytical model based on CLT, as discussed in [17].
Besides the analytical modelling, also FEA for obtaining the residual stress state were performed using ANSYS Mechanical 2023 R1. The FE model of the type 4 pressure vessel was created using ANSYS ACP Prep/Post, which is a dedicated tool for definition of composite layups. The geometry as well as the stacking sequence of the carbon fiber reinforced layers was derived from the investigated 6.8 liter type 4 cylinder. The material data used for the unidirectional carbon fiber reinforced ply is based on the data sheet of the fibers and resin, as well as experimental data from the literature [18, 3, 14]. For the unidirectional ply, the material data was obtained by rules of mixture according to [17] for the fiber volume ratio of 60% [8]. The material data for the liner was directly taken over from the data sheet [10]. All material data is summarized in Tab. 1. It is to be noted that the mechanical properties of the unidirectional ply refer to the cured state. For the winding process, a significantly different Young's Modulus perpendicular to the fiber direction is being used, calculated as discussed in [2]. Under the assumption of no resin flow or loss during the winding process, the Young's Modulus remains constant and can be calculated for 60% fiber volume ratio after the resin bath, which results in the value of 60 MPa for averagely well aligned fibers [6].

Component	**Material**	$E_{\parallel}$ **in MPa**	$E_{\perp}$ **in MPa**	$G_{\perp\parallel}$ **in MPa**	$\nu_{\perp\parallel}$
CFRP Ply	Teijin Tenax™ UTS50 LITESTONE® 3100E/2106H	151000	4380	3530	0.34
Liner	PET*	3600	-	1340	0.34

Table 1: Used material data. *-for PET liner as for an isotropic material, the values refer to all directions

Second order solid elements (SOLID186) were used to mesh the models, with one element layer per layer of the composite materials. Therefore, a 3D consideration of the stress state is possible. The boundary conditions involve only suppression of x and y displacement at the one boss part of the cylinder and all displacements at the other. The coordinate system and the meshed model are shown in Fig. 3.

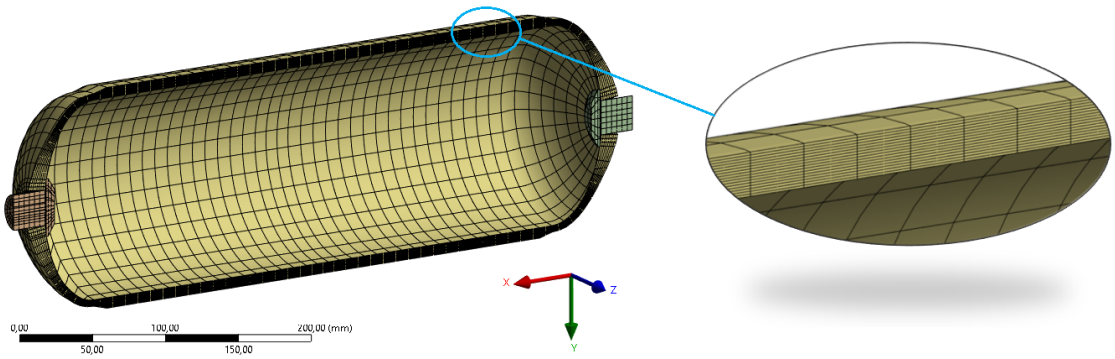

Figure 3: FE model of the investigated pressure vessel

To model the residual stress state after the winding process, the layers are being activated one-by-one in the following analysis steps by using the *birth and death* element control. After activating the layer, the temperature of the model is being reduced, what results in shrinkage of the newly wound layer on the previously wound structure. Hereby, the temperature change and the orthotropic coefficients of thermal expansion are defined in such a way, that the pressure on the previously wound layers is equal to the pressure resulting from the winding tension in filament winding process:

$$p^{(i)} = \frac{F_{t,i} cos^2 \phi_i}{r_i} \tag{6}$$

where $F_{t,i}$ is the winding tension force, ϕ_i is the angle of the currently wound layer i, and r_i is its radius. For each wound layer, a new internal pressure is being defined in the model to influence the residual stress state.

Discussion

Using the discussed models, the residual stresses resulting from the winding process of 6.8 liter type 4 cylinders were obtained. A winding tension force of 22.5 N was used. Two types of cylinders were modelled: type A with a constant internal pressure of 3 bar and type B with a defined internal pressure function (see Fig. 4).

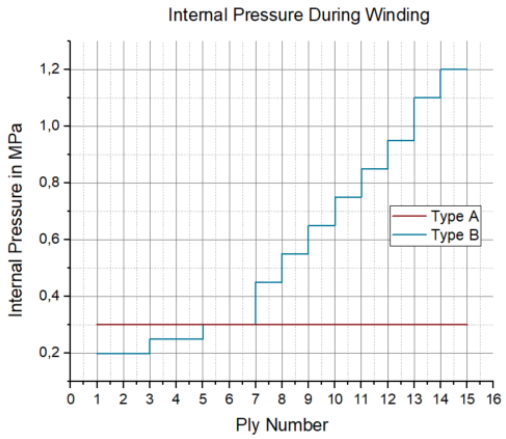

Figure 4: Internal pressure used during the filament winding process for type A and type B cylinders

There are two main goals for the internal pressure function. One is to achieve a more even residual stress state in the wound cylinder, focusing on the hoop layers. These are particularly important for the cylinder strength. On the other hand, the variable internal pressure should help avoid compressive stresses in the wound layers, which could increase the fiber waviness and have a negative impact on the quality of the pressure vessel.
For helical windings, only a relatively small increase in the internal pressure was defined with 0.5 bar per helical winding. During winding of the hoop layers, bigger steps of 1 bar per winding were used. For the last layers wound, an additional increase in the internal pressure was defined in order to decrease the fiber waviness, if occured in the following experimental study.

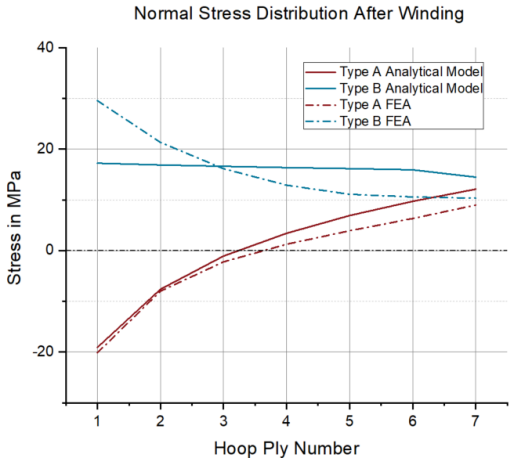

Figure 5: Normal stress distribution in fiber direction after the winding process for type A and type B cylinders

Fig. 5 shows the normal stress in fiber direction for each hoop layer after the winding process calculated by both, the analytical model based on the CLT and 3D FEA. For cylinders of type A, compressive

stresses in the first three hoop windings are expected. Those can be avoided in type B cylinders, wound with a variable internal pressure function. Also the stress distribution is more even in type B cylinders, although a different stress development through the thickness of the composite can be observed in the two models. Since the scattering between the different calculations for type A vessels is significantly lower, the interaction of the higher internal pressure with the relatively low Young's Modulus in the thickness direction of the fibers can be named as a possible reason.
In Fig. 6 the loaded state of the finished component is considered. Using the analytical model, the deviation from the average normal stress in hoop windings is shown in part (a). At 900 bar, the minimum burst pressure according to [5], the stress distribution for type B cylinders is nearly perfectly even. However, the maximum deviation for type A cylinders ranges from ca. -1.0% to 0.5%, so that no significant increase in burst pressures based on that result could be expected. Nevertheless, for lower pressures e.g., for the test pressure of 450 bar or nominal working pressure of 300 bar, the deviation from the average stress increases. Since the damage initiation, such as the first inter fiber failures, occurs at significantly lower pressures than the actual burst pressure, a delayed damage initiation could lead to a higher difference in burst pressures between cylinder types A and B [11].
In Fig. 6 (b) the stress distribution calculated with the analytical and FE model is compared. Although the investigated cylinder fulfils the literature criteria for consideration as a thin-walled structure, a significant stress gradient over the thickness can be observed in the 3D FEA. This effect leads to a stronger deviation of the calculated normal stresses from the average normal stress in hoop layers. Since an even stress state in the layers of type B pressure vessel after the winding process was achieved, the observed stress gradient leads to a more uneven distribution of the stresses under internal pressure loading, with the maximum deviation of ca. 3.3%.

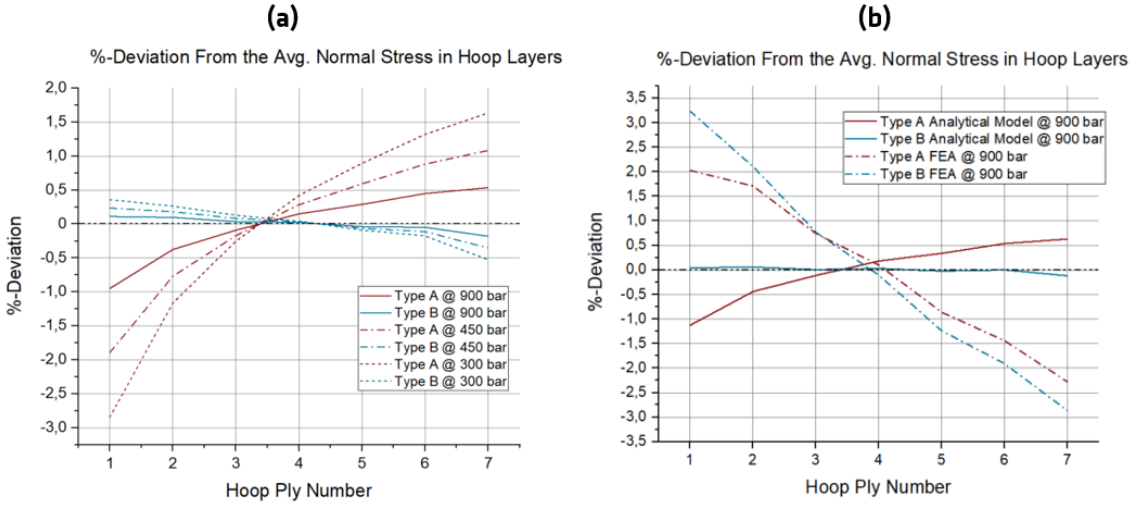

Figure 6: Percentage deviation from the avg. normal stress in the hoop windings according to (a) analytical model at different pressures and (b) analytical and FE model at the minimum burst pressure

Conclusions

To define the process parameters for the experimental study on filament-wound type 4 pressure vessels, analytical and FE models of the residual stress state were created. The analytical calculations of the residual stress state after the winding process are in agreement with the FE simulations. Both models show the possibility to influence the residual stress state in the wound cylinder by regulating the internal pressure. The results indicate not only the possibility to achieve a more even stress state in the finished component, but also to avoid compressive stresses during the winding process. The compressive stresses could otherwise lead to fiber waviness and a lower quality of the finished component. Even though the use of the internal pressure might not significantly decrease the peak stresses under the minimum burst pressures, the real burst pressures of the vessels wound with variable internal pressure could be higher than using constant internal pressure. This effect would be the result of the possible delayed damage initiation, such as inter fiber failure, which occurs at significantly lower pressures. Assumption of the

investigated structure as a thin-walled cylinder can have a significant impact on the calculated stress state under internal pressure loading, even though the literature criteria for a thin-walled structure are satisfied. The theoretical considerations are going to be validated and deepened in the experimental study on 6.8 liter type 4 cylinders.

References

[1] S. Anders. *Sensitivitätsanalyse des Eigenspannungszustandes eines Composite-Hybridhochdruckbehälters*. PhD thesis, TU Berlin, 2008.

[2] A. Banerjee, L. Sun, S. Matell, and D. Cohen. Model and experimental study of fiber motion in wet filament winding. *Composites: Part A*, 29A:251–263, 1998.

[3] R. Basan. *Untersuchung der intralaminaren Schubeigenschaften von Faserverbundwerkstoffen mit Epoxidharzmatrix unter Berücksichtigung nichtlinearer Effekte*. PhD thesis, TU Berlin, 2011.

[4] Z. Cai, T. Gutowski, and S. Allen. Winding and consolidation analysis for cylindrical composite structures. *Journal of Composite Materials*, 26:1374–1399, 1992.

[5] EN 12245:2022. Transportable gas cylinders – fully wrapped composite cylinders; german version, August 2022.

[6] T. Gutowski, Z. Cai, S. Bauer, D. Boucher, J. Kingery, and S. Wineman. Consolidation experiments for laminate composites. *Journal of Composite Materials*, 21:650–669, July 1987.

[7] ISO 11439:2013. Gas cylinders — high pressure cylinders for the on-board storage of natural gas as a fuel for automotive vehicles, June 2013.

[8] S. John. *Beitrag zur Analyse des Eigenspannungsverhaltens von Composite-Hochdruckspeichern mit metallischem Liner*. PhD thesis, TU Berlin, 2020.

[9] G. Knappstein. *Statik, insbesondere Schnittprinzip*, volume 4. Verlag Harri Deutsch, Europa-Lehrmittel, 2011.

[10] Kunststoffdreherei GmbH. Technisches Datenblatt PET, March 2016.

[11] A. Kupsch, V. Trappe, B. Müller, and G. Bruno. Evolution of cfrp stress cracks observed by in-situ x-ray refractive imaging. *IOP Conf. Series: Materials Science and Engineering*, 942(012035), 2020.

[12] S. Lee and G. Springer. Filament winding cylinders: I. process model. *Journal of Composite Materials*, 24:1270–1298, December 1990.

[13] J. Lifshitz and H. Dayan. Filament-wound pressure vessel with thick metal liner. *Composite Structures*, 32:313–323, 1995.

[14] Olin Corporation. Olin LITESTONE® Filament Winding System. LITESTONE 3100E Epoxy Resin, LITESTONE 2106H Hardener.

[15] E. Rivard, M. Trudeau, and K. Zaghib. Hydrogen storage for mobility: A review. *Materials*, 12, June 2019.

[16] M. Schulz. *Ein Beitrag zur Modellierung des Zeitstandverhaltens von Faserverbundwerkstoffen im Hinblick auf die Anwendung an Hochdruckspeichern*. PhD thesis, TU Berlin, 2013.

[17] H. Schürmann. *Konstruieren mit Faser-Kunststoff-Verbunden*. Springer-Verlag, Berlin Heidelberg, 2007.

[18] Teijin Carbon Europe GmbH. Tenax™ filament yarn. product data sheet., March 2022.

[19] J. Teply and W. Herbein. Failure modes for filament wound aluminium natural gas cylinders. In *Proceedings of the Fracture-Mechanism Program, Int. Con. and Exposition on Fatigue,*, Salt Lake City, 1985.

[20] S. Tsai. *Composites Design Third Edition*, volume 3. Think Composites, Dayton, Paris, Tokyo, 1987.

Modelling the Refuelling of Hydrogen Fuel-Cell Heavy-Duty Vehicles with Multiple Heterogenous Tanks.

N. Benvenuti[1,2], T. Guewouo[*1], M. Milhé[2], Q. Nouvelot [1],
J.L. Dirion[2], F. Baillon[2], C. Coquelet[2]

[1]Engie Lab CRIGEN, 4 Rue Joséphine Baker, 93240 Stains, France
[2]Université de Toulouse, IMT Mines Albi, UMR CNRS 5302, Centre RAPSODEE, Campus Jarlard, F-81013 Albi Cedex 09, France

Introduction

Road transport greenhouse gases (GHG) emissions accounts for over one fifth of global CO2 emissions in the EU. In Europe in recent years, road transport is the only sector whose emissions have unfortunately not stopped rising. This is particularly true for the heavy-duty mobility, such as trucks, city buses and long-distance buses, which account for over 25% of GHG emissions [1]. One of the most promising technologies to decarbonize heavy-duty transport (trucks, buses, trains, boats) is hydrogen fuel cell technology [2]. The development of this technology requires, besides the development of the vehicles, a parallel effort in the advance of hydrogen refuelling infrastructure and the related refuelling protocols.
In terms of vehicle development, the effort required to maintain a range similar to that of fossil-fuelled heavy-duty vehicles is significant. For this purpose, the fuel cell heavy-duty vehicles (FC-HDVs) need bigger onboard storage systems than fuel cell light-duty vehicles (FC-LDVs). To achieve the required hydrogen storage volume, automotive original equipment manufacturers (OEMs) have to exploit any available space in the vehicle by inserting multiple hydrogen storage tanks, often of different sizes, which is not the case for FC-LDVs.
This configuration of the on-board hydrogen storage system could have a significant impact on the derivation of parameters for advanced protocols (such as those defined in the European PRHYDE project [3]), as well as on the evaluation of the vehicle's instantaneous state of charge (SOC). Indeed, due to the different tank sizes of the FC-HDV storage system, the mass flow rate distribution between the tanks, the pressure evolution in each tank size and the temperature rise in the different tanks cannot easily be predicted. Thus, the models used to derive the parameters of FC-HDV refuelling protocols should therefore be updated to consider these effects. Moreover, fine modelling of the evolution of these parameters during refuelling would enable us to accurately estimate the thermodynamic state of each tank in the vehicle hydrogen storage system at the end of each refuelling session. Knowing this thermodynamic state will enable the automotive OEMs to know where to place the sensors needed to assess the vehicle's SOC.
The aim of this work is therefore to propose a thermodynamic model to simulate the refuelling of a hydrogen storage system for HDVs with multiple heterogeneous tanks.

Methodology

The model presented in this paper has been implemented in an internal tool at Lab H2 within CRIGEN called HyFill. HyFill is developed on MATLAB Simulink (R2021b) [4] from MathWorks® and allows to simulate the fast filling of fuel cell vehicle (FCV) hydrogen storage tanks at a hydrogen refuelling stations (HRS) from the dispenser to the vehicle (see Figure 1-a) to predict the final temperature and pressure reached by the hydrogen, as well as the total hydrogen mass transferred to the vehicle storage tanks.

* Corresponding author: thomas.guewouo@engie.com

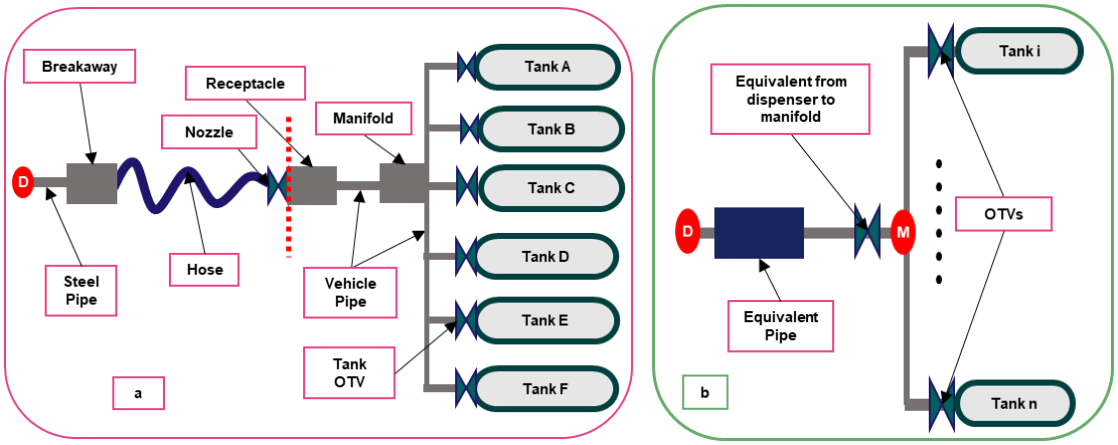

Figure 1 -Scheme of the refuelling station on the left (a) and its simplification on the right (b).

The modelling approach is pseudo-1D. It considers that the gas temperature is uniform at each instant in the tank. The heat transfer between the gas and the ambient is modelled by the unsteady one-dimensional radial heat conduction equation. To calculate the temperature, mass, and pressure of the gas in the tank, a system of three equations is solved at each time step during the whole filling or emptying simulation; these are the mass balance, the energy balance for a control volume and the equation of state here given by [5]:

$$\begin{cases} \dfrac{dm}{dt} = \dot{m}_{in} - \dot{m}_{out} \\ \dfrac{dmu}{dt} = \dot{m}_{in}h_{in} - \dot{m}_{out}h_{out} - \dot{Q}_{g-w} \\ \dfrac{P}{\rho} = ZRT \end{cases} \quad 1$$

In this equation system (Eq. 1), m is the hydrogen mass in the tank, $\dot{m}_{in}$ and $\dot{m}_{out}$ are the inlet and outlet mass flow rate respectively, u is the specific mass internal energy, h is the specific mass enthalpy, P, T and ρ are hydrogen pressure, temperature and density respectively, Z is the hydrogen compressibility factor depending on thermodynamic variables, R is the gas constant. The hydrogen compressibility factor as well as all other thermodynamic properties of hydrogen are calculated in HyFill using a fundamental equation of state (GERG-2008 equation of state [5]). The heat flow from the gas to the tank wall ($\dot{Q}_{g-w}[kW]$) is given by Eq. (2):

$$\dot{Q}_{g-w} = S_{in}H_{in}\left(T - T_{w_{r=r_{in}}}\right) \quad 2$$

Where S_{in} is the inner wall surface of the tank, H_{in} is the inner film mass heat transfer coefficient determined from the correlation for internal turbulent flow [7], $T_{w_{r=r_{in}}}$ is the temperature of the inner wall of the tank. It is obtained by solving the unsteady one-dimensional radial heat conduction equation (assuming azimuthal symmetry as the tank wall temperature is the same along its entire length for a given radius) given by [9], in Eq. (3):

$$\rho c_p \frac{\partial T}{\partial t} = \frac{\lambda}{r}\frac{\partial}{\partial r}\left(r\frac{\partial T_w}{\partial r}\right) \quad 3$$

Where c_P $[Jkg^{-1}K^{-1}]$ is the specific heat at constant pressure, and λ $[Wm^{-1}]$ is the thermal conductivity of the tank wall material. The boundary condition necessary to solve this equation is the mass heat flow from the outer tank wall to the ambient air:

$$\dot{Q}_{w-a} = S_{out}H_{out}\left(T_{w_{r=r_{out}}} - T_{amb}\right) + \varepsilon_w \sigma S_{out}(T^4_{w_{r=r_{out}}} - T^4_{amb}) \quad 4$$

where H_{out} is the outer film heat transfer coefficient considered constant (natural convection assumption), S_{out} is the outer wall surface of the tank, $T_{w_{r=r_{out}}}$ is the temperature of the outer wall of the tank, T_{amb} is the ambient temperature, ε_w is the emissivity of the external wall of the tank, σ is the Stefan-Boltzmann constant.

In HyFill the fuelling line is modelled in a separate Simulink block. The fuelling line is composed of stainless-steel pipe, breakaway, hose, nozzle, receptacle, on-tank valve (OTV) and it is modelled as a cylindrical pipe. The geometric model of the pipe conserves the fuelling line thermal mass. Distributed pressure drops along the pipe length are neglected and (hydrogen is not considered as compressible as the Mach number is lower than 0.3 in the piping ($Ma < 0.3$)), thus there is mass and momentum conservation between input and output of the pipe. To consider the effect of the thermal mass, the model consists of the energy balance of the gas in the pipe and of the pipe wall:

$$\begin{cases} \frac{dmu}{dt} = 0 = \dot{m}(h_{out} - h_{in}) + \dot{Q}_{g-w} \\ \frac{dU_{pipe}}{dt} = \dot{Q}_{w-a} + \dot{Q}_{g-w} \end{cases} \quad 5$$

Where $\dot{m}$ is the hydrogen mass flow rate the pipe, h_{out} and h_{in} are the mass enthalpy entering and exiting the pipe. U_{pipe} is the internal energy of the pipe wall. $\dot{Q}_{w-a}$ is the heat flux from the ambient to the pipe wall and it is calculated as Eq. 4. $\dot{Q}_{g-w}$ is the heat transfer from the pipe wall to the gas and it is estimated by assuming constant wall temperature along the pipe length. Consequently, the pipe transfers heat while maintaining a constant wall temperature along its length and radius. This can be motivated by the fact that the Biot number, defined as:

$$Bi = \frac{H_{in}}{\lambda_w / t_w} \quad 6$$

Where t_w is the wall thickness in first approximation the radial distribution of temperature can be neglected [9], thus $dT_w/dr = 0$. As seen in the experimental work by Kuroki et al [10], the temperature varies along the length only at he start of the refuelling, but the variation becomes smaller in the last part of the refuelling, therefore the longitudinal distribution of temperature can be negligeable, thus $dT_w/dx = 0$. The hydrogen properties along the pipeline are also considered as constant.

The refuelling is a process regulated with pressure, thus the mass flowing in the system depends on the pressure differential between the high-pressure storage of the station and the storage tanks of vehicle. On the other hand, the pressure drop depends on the gas mass and temperature in each tank, and both change depending on the mass flow rate. Thus, it is a complex problem determined by a non-linear equations system that must be solved simultaneously.

The system can be simplified as shown in the scheme in Figure 1-b, because two main hypotheses are applied:

- as the heat transfer is already considered in the pipe model, and the expansion through the valves is adiabatic, thus isenthalpic, the energy is conserved.
- The pressure drops of the piping section that share the same mass flow rate can be modelled as a single valve with a flow coefficient (k_V $[m^3 h^{-1}]$) representing the pressure drops of all the correspondent section. The distributed pressure drops are neglected.

Thus, the system can be described by associating a mass balance and the characteristic equation of each valve. The characteristic equation chosen is derived from the IEC 60534 standard [11]:

$$\dot{m} = \begin{cases} \rho_1 N k_v \frac{2}{3} \sqrt{\frac{P_1}{2\rho_1}} & if\ P_1 > 2\,P_2 \\ \rho_1 N k_v \left(1 - \frac{2}{3}\frac{P_1 - P_2}{P_1}\right) \sqrt{\frac{(P_1 - P_2)}{\rho_1}} & if\ P_1 \leqslant 2\,P_2 \end{cases} \quad 7$$

Where subscripts 1 and 2 refers respectively to upstream and downstream conditions, and N is a constant equal to 31.6.

Results and discussion

Generally, for a range of around 1000 km, the FC-HDV storage system needs to carry around 100 kg of hydrogen [12]. To maintain the same refuelling time as a diesel truck, it needs to be refuelled in around 10 minutes. For this reason, the model was tested in this study on a storage system with a total volume of around 2.5 m3, composed of Type IV tanks with a nominal working pressure of 70 MPa. This storage system is composed of two 500L tanks, four 300L tanks and three 100L tanks.

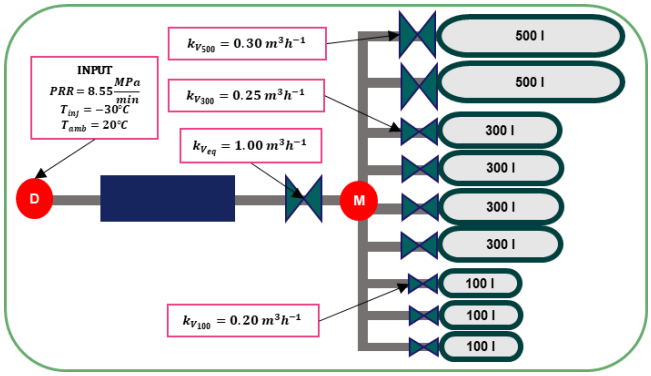

Figure 2 – Scheme of the model with the simulation inputs and parameters of the main components.

The refuelling simulation is performed at constant pressure ramp rate (PRR) of 8.55 MPa/min imposed at the dispenser. This PRR is calculated to satisfy 10 minutes refuelling from the lowest acceptable pressure (2 MPa) to the maximum operating pressure (MOP) of each tank (87.5 MPa). The equivalent flow coefficient (k_V) of the fuelling line is equal to 1 m^3h^{-1}.For the three tank sizes, the flow coefficients of the OTVs are 0.30, 0.25, 0.20 m^3h^{-1} respectively, in decreasing order of tank volume. As there is no thermodynamical difference in the tank parameters and input for each tank of the same size, only one tank for each size considered is simulated to evaluate temperature and pressure evolution, but all the tanks are considered in the total mass balance. The refuelling is simulated with ambient temperature set to 20°C, initial pressure of the tanks 2 MPa, initial thermal equilibrium between the system and the ambient. The initial gas temperature at the dispenser outlet is set at the ambient and it decreases linearly at -30°C in 30 seconds as recommended in the SAE J2601 protocol [13].

In Figure 3 are presented the results of the refuelling simulation considering different tank sizes. the top left graph presents the average gas temperature evolution in the in these conditions, none of the tanks reaches the critical temperature of 85°C. On the right the pressure is represented at different points of the station, it can be noted that the highest pressure drops are during the first part of the refuelling and are mainly concentrated in the fuelling line. On the bottom there is the mass flow rate on the left (total in black). The total mass flow rate does not excess the maximum value of 300 gs^{-1} allowed by the new protocols for FC-HVD refuelling [14]. In the graph only one curve I represented for each tank size not each tank has been simulated as identical tank have identical input conditions (with the applied hypothesis), thus the sum of the three curves do not add up to the total mass flowrate, as each curve should be multiplied for the correspondent number of tank. On the bottom right there is the SOC of each tank. The simulation ended when a SOC of 100% was reached in the smaller tank. From the results of the refuelling in Figure 3 we can see that temperature, pressure and mass flow rate evolve differently for the three tank types. More in detail, the larger the tank, the higher the mass flow rate. This could be explained by the higher-pressure difference and higher flow coefficient. The pressure increases faster in the smallest tanks even if it has lower mass flowrate when compared to the other tanks, this may be related to the low volume, as in small volume tanks the pressure increases more than in bigger tanks for the same amount of gas injected, ad

to the lower flow coefficient, which consents more mass flowrate to pass with a smaller pressure difference. It can also be noted that the temperature at the start is higher in the smallest size tank, due to the fastest compression, but by the end of the refuelling, it is the biggest tank the one with the highest temperature. This may be caused by the combined effects of the higher mass flow rate and the lower ratio of the internal surface over volume of the largest tank. This represents a first limiting factor when deriving the protocols, as the biggest tanks limit the refuelling speed. On the other hand, the state of charge (SOC) within small tanks increases faster than in bigger tanks, meaning that the smaller tanks will reach the maximum SOC earlier during the refuelling, thus imposing the premature end of the refuelling to avoid over pressures, even if the overall SOC is lower than 100%.

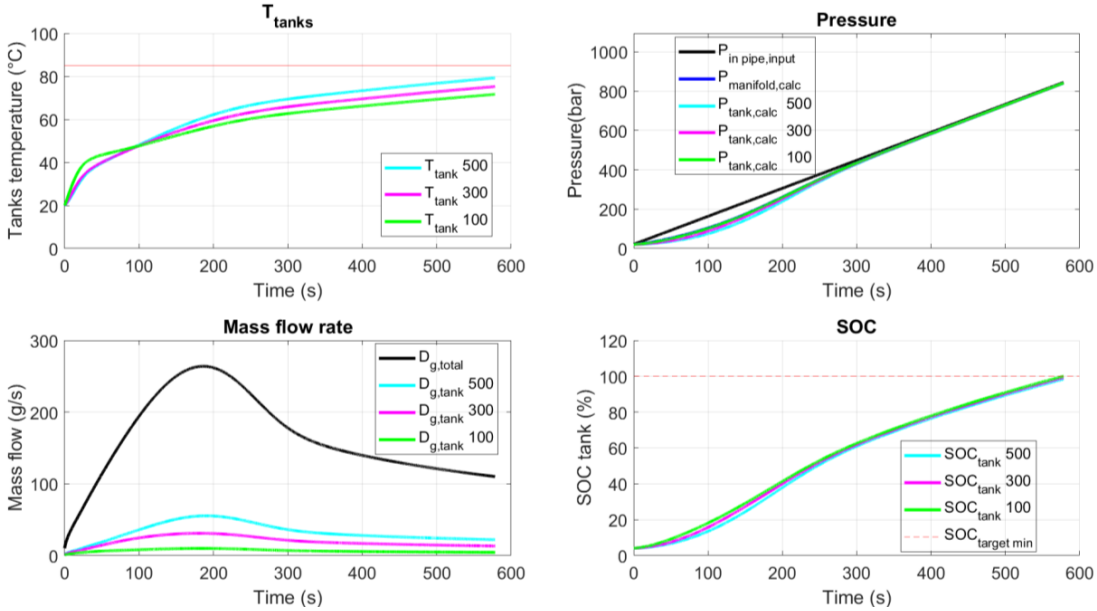

Figure 3 – Results of the refuelling simulation considering different tank sizes (light blue 500 l, pink 300 l, green 100 l) during the simulation. On the top left graphs presents the gas temperature inside the tank. On the right there the pressure is represented at different points of the station, in black is the pressure at the outlet of the dispenser, in blue the pressure at the manifold and then the pressure in the different tanks. On the bottom the mass flow rate on the left (total in black) and the SOC of each tank on the right.

Conclusions

A new model capable of predicting the behaviour of vehicle storage systems composed by multiple heterogeneous tanks during the refuelling, has been developed. This model can give a clear insight on the thermodynamical evolution of the gas in the hydrogen storage tanks system that will be commonly used in heavy-duty vehicles. A refuelling simulation has been conducted to analyse the evolution of the thermodynamical variables during the refuelling of a 100 kg storage system capacity.

Some critical aspects have been identified, such as the limitation to reach the complete filling of the system without exceeding the maximum allowable SOC of smaller tanks, and the correlation between the maximum tank size and final gas temperature that limits the refuelling time in the derivation of the protocol parameters. The identified behaviour shows trends in the refuelling of HDVs storage systems that can only be predicted by simulating all the tanks. Another consideration is that protocols with communication will need to communicate to the station pressure and temperature of the vehicle that in case of multiple heterogeneous tanks is not unique. From this first analysis, it seems that the correct pressure sensor to use is the one in the smallest tank, to avoid over pressure, while the correct temperature sensor is the one in

the biggest tank, to avoid overheating. The model could be used in the future to better define the sensors position.
Further perspectives to the work here presented are the experimental validation of the model and the integration of the distributed pressure drops in the fuelling line and in the pipe sections between the manifold and the tanks, alongside with a more precise estimation of the heat transfer between the hydrogen and the vehicle piping system. Once validated the model could be used to derive filling protocols adapted to vehicles with different tank sizes. As the model also gives information on the performances of the stations in terms of complete refuelling, it can be foreseen that this tool could be used in to test or compare stations designs, for example in terms of the cooling power required.

References

[1] 'CO2 emission standards for Heavy-Duty Vehicles', *European Commission - European Commission*. https://ec.europa.eu/commission/presscorner/detail/en/qanda_23_763 (accessed Aug. 28, 2023).

[2] A. Rinaldi, A. Syla, M. K. Patel, and D. Parra, 'Optimal pathways for the decarbonisation of the transport sector: Trade-offs between battery and hydrogen technologies using a whole energy system perspective', *Clean. Prod. Lett.*, vol. 5, p. 100044, Dec. 2023, doi: 10.1016/j.clpl.2023.100044.

[3] 'Protocol for heavy duty hydrogen refuelling | PRHYDE Project | Fact Sheet | H2020', *CORDIS | European Commission*. https://cordis.europa.eu/project/id/874997 (accessed Aug. 23, 2023).

[4] 'Simulink Version 10.4 (R2021b)'. The MathWorks, Inc., 2021.

[5] L. Ljung, T. Glad, and L. Ljung, *Modeling of dynamic systems*, Nachdr. in Prentice Hall information and system sciences series. Englewood Cliffs, N.J: PTR Prentice Hall, 2002.

[6] O. Kunz and W. Wagner, 'The GERG-2008 Wide-Range Equation of State for Natural Gases and Other Mixtures: An Expansion of GERG-2004', *J. Chem. Eng. Data*, vol. 57, no. 11, pp. 3032–3091, Nov. 2012, doi: 10.1021/je300655b.

[7] T. Kuroki *et al.*, 'Thermodynamic modeling of hydrogen fueling process from high-pressure storage tank to vehicle tank', *Int. J. Hydrog. Energy*, vol. 46, no. 42, pp. 22004–22017, Jun. 2021, doi: 10.1016/j.ijhydene.2021.04.037.

[8] M. M. Rathore and R. Kapuno, *Engineering Heat Transfer*. Jones & Bartlett Publishers, 2010.

[9] J. P. Holman, *Heat transfer*, 10. ed. in McGraw-Hill series in mechanical engineering. Boston, Mass.: McGraw-Hill Higher Education, 2010.

[10] T. Kuroki, N. Sakoda, K. Shinzato, M. Monde, and Y. Takata, 'Prediction of transient temperature of hydrogen flowing from pre-cooler of refueling station to inlet of vehicle tank', *Int. J. Hydrog. Energy*, vol. 43, no. 3, pp. 1846–1854, Jan. 2018, doi: 10.1016/j.ijhydene.2017.11.033.

[11] 'Industrial-process control valves Part 2-1: Flow capacity – Sizing equations for fluid flow under installed conditions'. 2011.

[12] H. Basma and F. Rodríguez, 'Fuel cell electric tractor-trailers: Technology overview and fuel economy'.

[13] Fuel Cell Standards Committee, 'Fueling Protocol for Gaseous Hydrogen Powered Heavy Duty Vehicles', SAE International. doi: 10.4271/J2601/2_202307.

[14] 'Refuelling Heavy Duty with very high flow Hydrogen | RHeaDHy Project | Fact Sheet | HORIZON', *CORDIS | European Commission*. https://cordis.europa.eu/project/id/101101443 (accessed Aug. 23, 2023).

Modelling PEMFC Degradation in Ships

A.E.Broer*[1], H. Polinder[1], L. Van Biert[1]

[1]Delft University of Technology — Department of Maritime and Transport Technology (MTT)

August 2023

Abstract

Switching to Proton Exchange Membrane Fuel Cell (PEMFC) systems can greatly reduce the environmental impact from the maritime industry. However, the limited durability of PEMFCs remains an obstacle for their implementation. Understanding fuel cell degradation is especially relevant for ships, as they typically operate for long periods and in isolated areas. Their energy systems therefore need to be exceptionally robust and reliable. In order to improve the design of maritime PEMFCs, we need to improve our understanding of degradation mechanisms induced by their use on a ship. Models can be a great tool to that end.

Many PEMFC models have been developed and used over three decades. They differ on various levels, from their spatial dimensions – one, two or three dimensional – to which processes are modelled and the detail to which they are described. Our previous review[1] shows that numerous processes contribute to degradation in a maritime context. These include more general processes, such as load induced damage, as well more specific ones for ships, such as sea salt contamination via the air inlet.

Currently, there is no modelling framework to quantify PEMFC degradation in a maritime environment specifically. The aim of this work is to propose such a framework, building on knowledge gained from previous modeling studies. It should integrate the additional degradation triggers such as salt contamination. We start out by analyzing existing PEMFC durability models. They are rated based on the coding complexity, computational costs, specificity and the possibility to incorporate both specific maritime as well as general degradation causes. Thereafter we analyze whether and how the models are validated and verified.

The proposed modeling framework can serve as a blueprint for future maritime PEMFC degradation models. These can facilitate vessel specific case studies, investigations to improve cell and stack design and explorations of altered ship operational profiles. The resulting insights will aid scientists, engineers and ship owners to improve PEMFC lifetime in maritime applications.

Introduction - Why do we need PEMFC degradation models for ships?

In a time of changing climate, fluctuating fossil fuel prices and ever growing international trade, innovations for sustainable shipping are urgently needed. Today, the maritime industry is responsible for about 3% of all anthropogenic greenhouse gas emissions worldwide, as well as 11% and 19% of all atmospheric sulfur and nitrogen oxide emissions within Europe [4, 3].

Hydrogen fuel cells (FCs) can greatly reduce the environmental impact of shipping as they have no polluting emissions. PEMFCs are amongst the most promising FCs types due to their ability to deal with fast fluctuating power demands, fast start-up, low operational temperature and high power density. Nevertheless, PEMFCs are also known for their limited lifetime compared to internal combustion engines and their sensitivity for contamination compared other fuel cell types. This is especially a risk as only few researchers have studied how the maritime environment will affect their performance and total lifetime.

Models have a great potential to advance PEMFC degradation research. Once developed, they can quickly provide results against low capital costs. These results can give insight in the working principles of fuel cells and the impact of operational conditions. It is therefore no surprise that many PEMFC models have been developed in the past decades, including ones that focus on degradation. However, to our knowledge, a dedicated maritime PEMFC degradation model has not been developed yet.

*Corresponding author: a.broer@tudelft.nl

[1]Review still under revision to be published. Abstract and conclusion are attached as the final page of this document.

Models vary widely in the applied approach and level detail. Spiegel et al ([7]) categorized the main model characteristics as: dimensions (zero to three dimensional); state (steady or dynamic); catalyst kinetics description; phases considered (liquid, gas or a mixture); mass transport description in the catalyst layer and membrane; inclusion of energy balances; and membrane swelling. On top of this, one can differentiate between empirical models that depend heavily on empirically obtained parameters and purely theoretical models. With this wide choice in models, it is challenging to select the effective and efficient approach.

Even if a suitable modeling approach is applied, models can still be worthless when they are not properly validated. Arif et al ([1]) pointed out that models can only be validated to a limited extent as various parameters cannot be independently measured in experiments. In addition the authors showed that most modeling studies only used one data set for model validation. Model verification is often not even mentioned in modeling studies. Nonetheless model verification is an important process to guarantee the correctness of model outcomes, even more when authors only have a limited amount of experimental data to initialize and validate the model.

The aim of this work is to propose a modelling framework for maritime PEMFC degradation simulations. It should conclude (i) which approach or approaches are most suitable for predicting performance decay caused by operation on a ship and (ii) a proper validation and verification plan. To reach this conclusion, we first define the model objective in more detail and provide a comprehensive overview of PEMFC degradation models. The latter are assessed on their coding complexity, computational costs, specificity and, most importantly, if they can be used to reach our main objective - maritime degradation modeling. Additionally, the validation and verification methods of each degradation model will be analyzed and compared to what is considered as 'sufficient' in dedicated validation and verification literature.

Background - PEMFC stack components and ensuring correct models

PEMFC components

Each PEMFC is composed of several layers as depicted in 1. The proton exchange membrane (PEM) is located in the center of the cell. Most PEMFCs use the commercial Nafion™, a perfluorosulfonic acid (PFSA) based membrane, for its adequate stability and good proton conductivity [2].

The membrane is flanked by an anodic and cathodic catalyst layer (CL). They are sometimes referred to as electrodes as the electrochemical reactions occur here. Each CL contains catalyst particles, a catalyst support and ionomer. Reactants and products are transported to and from the CLs via the pores in the gas diffusion layer (GDL), while freed electrons can exchange via its solid strands. Carbon based materials are often used, although metal based GDLs also occur.

The flow plates (i.e. current collectors) serve three main functions: conducting electrons to the external circuit, transporting reactants and products to and from the cell and providing structural support [5]. The layout of the flow-field can impact cell performance significantly. If the cell is part of a stack the flow plates are referred to as bipolar plates (BPs) as it has both an anodic and cathodic 'pole'. Finally, the cell is enclosed with two end plates (EPs), which compress the stack together and evenly distribute the pressure.

Most academic researchers test with single cells in order to save on capital costs and to limit confounding elements. However, in commercial applications these are stacked together in series. This way the overall potential difference increases, as does the output power.

Validation and verification

Model validation and verification are carried out to make sure the modeled outcomes are accurate and correct - at least, within the system boundaries for which it was designed. In model validation one checks if the outcomes are sufficiently accurate in comparison with an independent dataset of the modeled system. Aargent et al ([6]) summarize fourteen different validation techniques such as comparing modeled outcomes to outcomes of other, already validated models or using the model to predict the system behaviour.

Model verification concerns the correct implementation of code and overlap between the conceptual model and the computer model [6]. One should check if there are programming errors and if functions are implemented and initialized correctly. In general, more specialized and programming languages have a lower risk on programming mistakes.

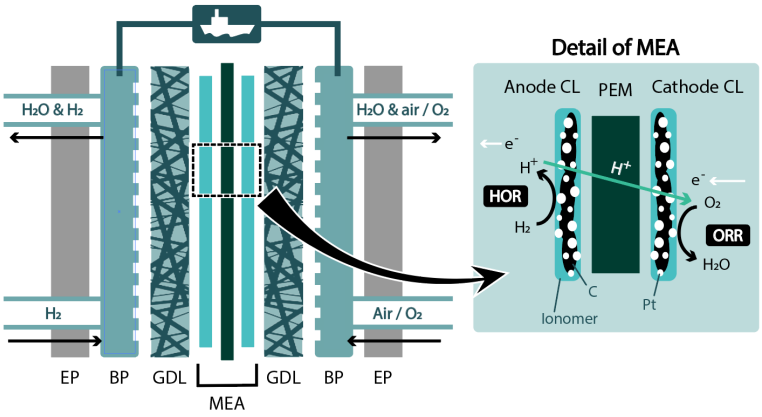

Figure 1: A schematic representation of a proton exchange membrane fuel cell (PEMFC). Its position in a stack (left) and a close up of the membrane electrode assembly (MEA, on the right) are indicated.

Methodology - Literature review, categorizing and framework outline

An initial set of literature will be collected via the Scopus search engine. Four search terms will be used: PEMFC, modeling, degradation and maritime. Maritime will be considered as an optional parameter, as we expect that there will be very few publications containing all four search terms. For each search term we try to improve our query by adding its synonyms, spelling variations and abbreviations. For example, the term PEMFC will be defined as *PEMFC, PEFC, "Proton exchange membrane fuel cell", "PEM fuel cell* or *"Polymer electrolyte fuel cell"* and modeling as *modeling, modelling, simulation, "theoretical model", "numerical model"* or *"computer model"*. The abstracts of the Scopus search results will be checked and relevant articles will be added to the literature list for this publication.

Discussion - code complexity, computational costs, specificity and maritime applicability

Expected outcome on types of PEMFC degradation models:

- Stack models or dedicated degradation models are scarce (most models focus on single PEMFCs or PEMFC components and aim to model performance at beginning of life (BoL))
- No dedicated maritime degradation models (most studies focus on automotive industry)

Expected outcome related to modeling approaches:

- Computational costs and model complexity go up with increasing dimensions and considering multiphase flows
- Model validation often occurs via comparison with one set of experimental data and only few describe the verification procedure

Conclusion - Most suitable modeling framework

Expected outcome:

- Two to three suitable model outlines for holistic modeling of maritime PEMFC stack degradation
- A validation and verification plan, using two sets of experimental data for validation and specific code checks for verification

References

[1] M. Arif, S. C. Cheung, and J. Andrews. Different Approaches Used for Modeling and Simulation of Polymer Electrolyte Membrane Fuel Cells: A Review. *Energy and Fuels*, 34(10):11897–11915, Oct. 2020. Number: 10 Publisher: American Chemical Society.

[2] A. Baroutaji, J. G. Carton, M. Sajjia, and A. G. Olabi. Materials in PEM Fuel Cells. In *Materials Science and Materials Engineering*. Elsevier, Jan. 2016.

[3] European Environment Agency. and European Maritime Safety Agency. *European maritime transport environmental report 2021.* Publications Office, LU, 2021.

[4] IMO. Fourth IMO Greenhouse Gas Study. Technical report, 2020.

[5] X. Li and I. Sabir. Review of bipolar plates in PEM fuel cells: Flow-field designs. *International Journal of Hydrogen Energy*, 30(4):359–371, 2005. Number: 4.

[6] R. G. Sargent. Verification and validation of simulation models - conference proceeding. Jan. 2011.

[7] C. Spiegel. *PEM fuel cell modeling and simulation using Matlab*. 2008.

Appendix - Related Unpublished Work

Review on Maritime PEMFC Degradation Causes and Research Gaps

Abstract

Marine fuel cell solutions need to be exceptionally robust and reliable. While degradation of PEMFCs is commonly studied in automotive applications, the maritime environment is seldomly considered. However, it may strongly affect the type and extent of damage. In this work we reviewed existing PEMFC durability research. We grouped external causes, mechanisms and monitoring options and created insightful visuals, showing the relations between them. This resulted in nine schematics of the thirteen different degradation causes considered in this review (an example is shown in 2). The causes were divided into three groups: contamination of the fuel and air inlet steams, vessel load profile and motions and vibrations. We categorized the mechanisms as damage to sulphonated polymers, carbon corrosion, catalyst inactivation and obstruction. Electrochemical impedance spectroscopy and analysis of the exhaust fluid were considered as promising in-situ analysis options. Post-mortem analysis mostly consists of imaging techniques. Our overview of PEMFC degradation and its focus on the maritime context provides input for possible mitigation procedures and improved cell and stack design. It could therefore aid engineers and ship owners to monitor different types of damage, and when possible adapt ship design and operation to enhance the PEMFC lifetime. To speed up PEMWE introduction in ships we suggest some areas for further research. contamination with low levels of sea salt, the influence of hydrogen carriers (including LOHCs and borohydrides) and the extent to which dynamic inclined operation affects performance and lifetime.

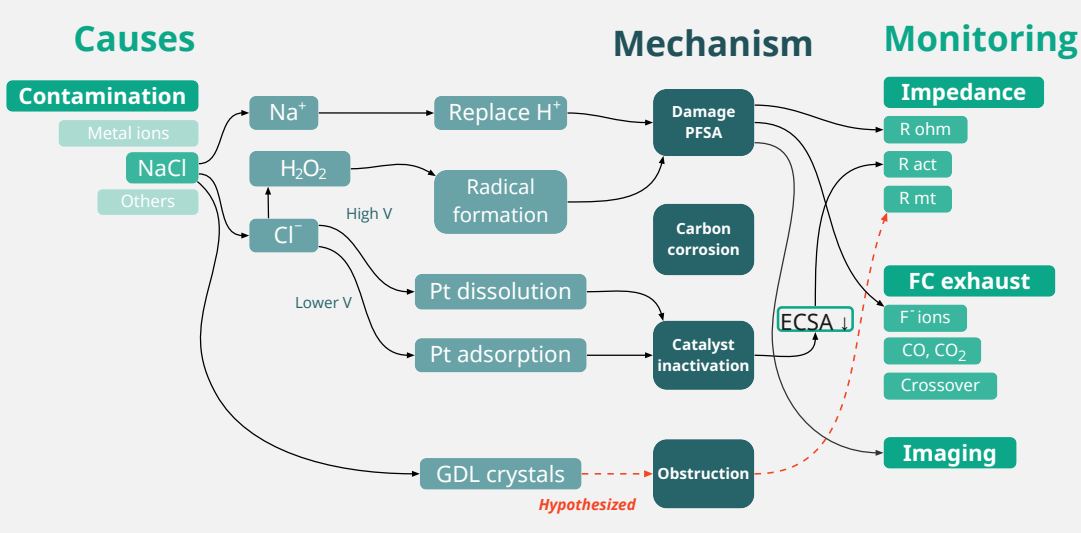

Figure 2: Schematic overview of degradation caused by NaCl contamination

Conclusion

PEMFCs are promising zero emission power sources for the maritime industry. Knowledge on their degradation in maritime applications is, however, limited. One field that requires particular attention is contamination with representative levels of atmospheric sea salt, as experiments up to now on average use 9×10^5 times higher NaCl concentrations compared to maritime air. Another interesting field is the influence of vessel motions and inclined operation. Finally it would be insightful to model the combined impact of different maritime degradation causes on PEMFC lifetime.

Modular Control for Hydrogen-based DC Shipboard Power Systems

T. Kopka*, A. Coraddu, H. Polinder

Department of Maritime and Transport Technology, Delft University of Technology, The Netherlands

Introduction

The transport and energy sectors are confronted with a series of challenges, pushing the industries to develop innovative and sustainable alternatives. The International Maritime Organization (IMO) has been prompted to define targets for the reduction of the carbon impact of ships [1], [2]. Hence, the maritime industry is under pressure to provide solutions for lowering its dependency on fossil fuels. Accordingly, more and more effort is put into research for zero emission ships (ZES) equipped with alternative power generation and storage technologies. With the SH2IPDRIVE project [3], a consortium has been brought to life that pursues the powering of the Dutch maritime sector with hydrogen. Produced from renewable energy sources (RESs), green hydrogen has the potential to serve as the main energy carrier in a ship. Hydrogen fuel cells (FCs) have emerged as the most prominent alternative as the main power supply in state-of-the-art applications [4], [5]. These are usually hybridized with energy storage systems (ESSs) due to their limited dynamic capabilities and specific operation characteristics [6]. Hence, FC-battery shipboard power systems (SPS) are a promising solution for decarbonizing the maritime transport in certain applications. A major challenge for fully exploiting the FC technology is the control of the electric power system and optimizing the coordination of the integrated energy resources, which is in the focus of this research.

A key development in the design of the SPS for FC-battery hybrid systems are the use of electric propulsion with an integrated power system (IPS) [7]. Moreover, the trend goes towards utilizing direct current (DC) distribution technology [8], [9], especially with many DC sources on board, e.g. FCs, batteries, and ultra-capacitor (UC). As identified in [10], state-of-the-art approaches for the control in hydrogen-based DC SPS focus on centralized solutions, typically for small systems with a single FC system and ESS. Examples involving a centralized controller computing the power references for the power sources are PI-control as in [11]–[13] and rule-based control as in [13]–[16]. Filter-based approaches can also commonly be observed in centralized control strategies in order to achieve a separation of load frequencies matching the differing characteristics of power supply and storage systems [17]–[19]. For the application in larger SPS that involve multiple parallel power supplies and ESS systems in a distributed fashion, centralized solutions are not feasible anymore.

Future SPS are expected to incorporate a wider variety of power supply and ESS technologies with differing characteristics [5]. All-electric ships (AES) with DC distribution technology and power electronics interfaces already offer a high degree of flexibility in the power system topology. This facilitates a simpler integration, extension and reconfiguration of the power system topology. Hence, components can be connected to the SPS in a modular fashion. This

*Corresponding author: t.kopka@tudelft.nl

research aims to develop control strategies for ZESs that also reflect this modularity in its power system control and energy management. A key part of this is to offer a plug-and-play (PnP) capability that minimizes the effort of integrating new technologies with unique characteristics into an existing power system topology. Moreover, a modular control framework can support the fault-tolerance and adaptation to changing circumstances, leading to a more resilient operation of the ship.

Methodology

This research aims to bring forward modular control strategies that can be implemented in real-time for the operation of an SPS with a DC distribution system. Specific interest lies in investigating zero-emission power supplies as an alternative to conventional fossil-fueled systems. With power electronics interfaced subsystems, the regarded SPS enable a high degree of controllability of power flows between power supplies, ESSs and loads. An exemplary FC-battery DC SPS is displayed in Fig. 1.

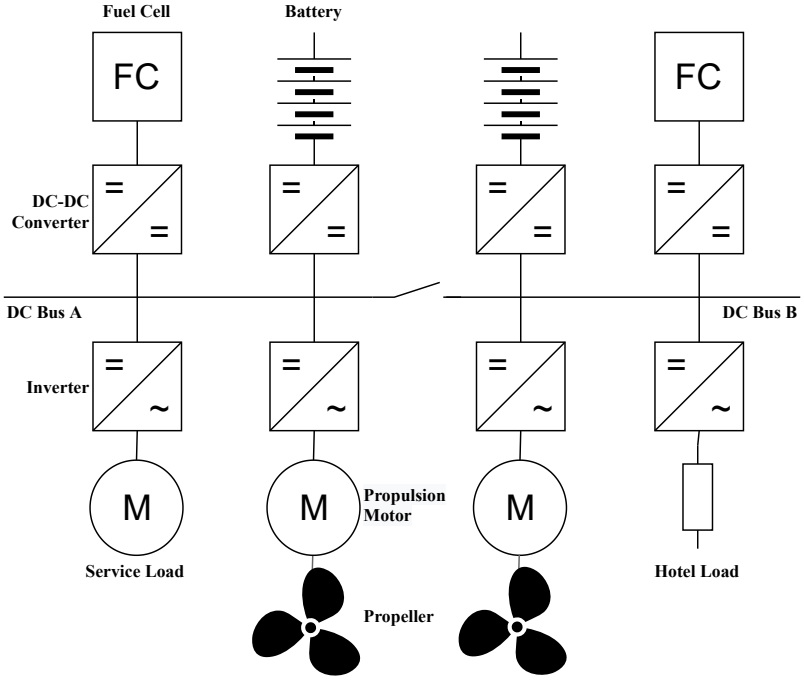

Figure 1: Exemplary DC SPS with FC-battery hybrid energy system

Whereas small, integrated power systems can be approached with a central controller computing all power references, more complex topologies also demand a higher control complexity. Figure 2 shows a generalized control hierarchy for power systems in which functionalities are distributed among local control, coordinated control, and high level control layers, typically with an increasing control bandwidth from top to bottom.

Each control functionality can be realized using a specific architecture, depending on the communication infrastructure used. Whereas current solutions on control for FC-battery SPS employ a centralized controller for the coordinated control, a decentralized or distributed architectures offers a more resilient and scalable alternative. Also, the high level control layer, including the energy management strategy (EMS), can in principle, be realized in a distributed or decentralized manner, which increases the modularity of the overall power system control. The three distinct control architectures are outlined in Fig. 3. Furthermore, the communication can be realized using either a high- or low-bandwidth network.

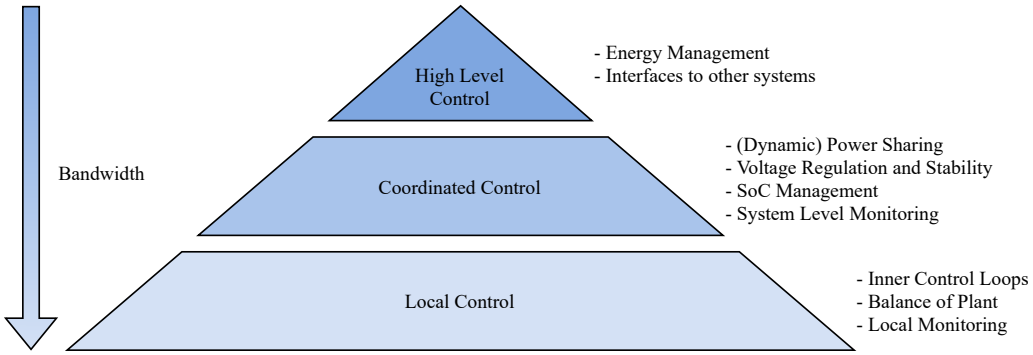

Figure 2: Control hierarchy for electric power systems on ships

In the context of a modular control framework, it is proposed to use standardized decentral controllers for the coordinated control, with parameters tuned depending on the devices' respective characteristics. A potential synergy between the control layer and physical system can be achieved by using common equipment, e.g., DCDC converters, for connections to the DC bus. This yields a unified, standardized hardware and control interface for connecting a wide variety of sources to the system. To stabilize the DC-bus voltage using FCs and batteries, droop-based approaches are investigated. In order to account for differing dynamic capabilities of subsystems, a bandwidth decoupling for different technologies is proposed, aiming at achieving an efficient dynamic power sharing. The scalability of this approach will be investigated by of extending the baseline FC-battery system, e.g., with additional parallel FC and battery modules. The addition of new technologies offers further opportunities to showcase the benefits of the PnP capability, where especially UCs as fast-response ESS and photovoltaic (PV) systems as RES offer promising features. A benefit of the approach also lies in the replacement of old components with riper technology at their end-of-life.

An additional power allocation and generation scheduling for power supplies can be realized via an EMS to enhance the overall system efficiency. In a FC-battery hybrid system, this encompasses the power split between main power supply and ESS and among parallel power supplies. A central aim of the EMS is the minimization of fuel consumption and component degradation. Using a centralized controller with low-bandwidth communication can be regarded as modular if all real-time computations are executed in the local controllers, while the central controller is merely used for information sharing and as an interface to other systems. In the first step, it is proposed to utilize a central controller and low-bandwidth communication to realize EMS functionalities via adaptive functions in the local controllers.

A further challenge for the operation of SPSs arises from uncertainties and changing condi-

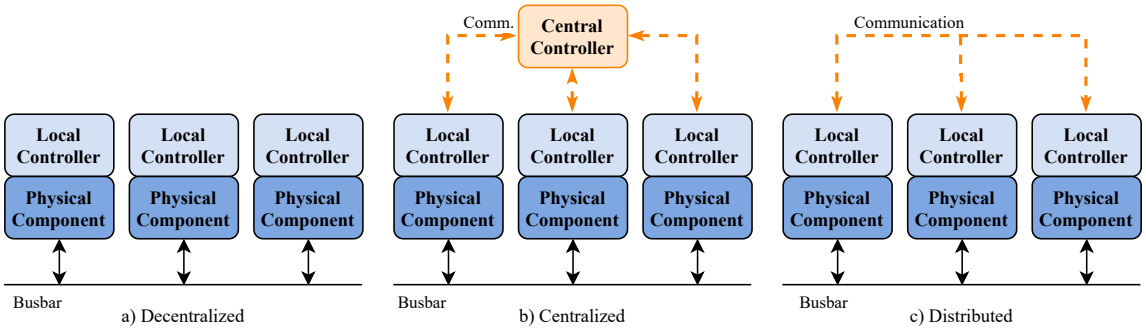

Figure 3: Generic control architectures for electric power systems

tions during a mission. Both component degradation and operational faults can alter the optimal conditions for system performance, affecting the availability of resources. The SPS shall be able to mitigate the effects of changing conditions and faults while maintaining power availability and an efficient operation of the system's resources. One focus point is the effect of altered parameters due to the degradation of components. Especially FCs and batteries show significant aging effects, which in turn influences the optimal operation of these systems. This issue will be addressed via adaptive functionalities in the (dynamic) power sharing, state of charge (SoC) management and EMS, so that system alterations are accounted for. The analysis and mitigation of effects from faults follows as a next step. The failure of a generation or storage component, the partial or total failure of an energy conversion device, and the failure of a communication link are of key interest to this research. The sudden discontinuation of power generation due to a component failure must be compensated. Hence, sufficient reserve must be maintained for stabilization, e.g., through virtual inertia provided by ESS, and the EMS shall be able to shift to a new efficient steady-state operation point. The proposed modular control approach will be extended to be able to reflect these faults in its coordinated control.

A library-based simulation environment is set up in Matlab/Simulink, including models of main and auxiliary power supplies, energy storages, power electronics converters, DC bus, and loads. This allows the modular configuration of power system topologies for the purpose of testing the developed control strategies on different systems. Real vessels and their measurements are used as reference designs, which can be virtually reconfigured and extended using the simulation environment. Finally, the proposed control strategies are aimed to be validated in a power hardware-in-the-loop (PHIL) test-bed, to prove their applicability and performance in real time.

Discussion

An initial study of the modular control approach for a FC-battery hybrid DC SPS has been conducted in [10]. This work describes a decentralized, virtual impedance-based strategy for the coordinated control covering dynamic power sharing, voltage control, and SoC management. Simulation results show that this architecture without communication links can achieve the same quality of power supply and load frequency separation as a centralized PI controller, given a proper tuning of the local controllers. Here, all components are parameterized so that they are utilized depending on their dynamic capabilities, which is especially beneficial for the operation of the FC. This approach has been extended by a modular EMS within a control hierarchy in [20]. The modularity of the approach is maintained by utilizing a low-bandwidth communication to enable information sharing among local controllers. A central controller is added to aggregate information while all key functionalities remain in the local controllers. This work showcases that a hierarchical control architecture can be realized using a modular approach. Furthermore, a central controller can contribute to facilitate awareness of global parameters and operator inputs while critical computations for the coordinated control remain decentralized.

Conclusions

The design of SPS is shifting from conventional diesel-driven topologies towards all-electric ships with an IPS, DC distribution, and zero-emission technologies. More components are integrated into future SPS, increasing their complexity and demanding for appropriate control strategies. This research proposes the development of a modular control framework facilitating the integration of a wide variety of differing power supply and storage technologies. Current contributions have shown that this modular approach can be used for both the coordinated control and energy management in a hierarchical control scheme for FC-battery systems.

In future investigations, the modular framework will be expanded to include further technologies and prove its effectiveness in dealing with a reconfiguration of the power system. A key challenge will be to deal with a multitude of power supplies and ESS with differing characteristics while maintaining an efficient operation of the power system. Furthermore, an analysis of system level faults and real-time adaptation to system alterations will be in the focus of research on this topic.

References

[1] T.-H. Joung, S.-G. Kang, J.-K. Lee, and J. Ahn, "The IMO initial strategy for reducing Greenhouse Gas(GHG) emissions, and its follow-up actions towards 2050," *Journal of International Maritime Safety, Environmental Affairs, and Shipping*, vol. 4, no. 1, pp. 1–7, Jan. 2020.

[2] "Fourth Greenhouse Gas Study 2020," https://www.imo.org/en/OurWork/Environment/Pages/Fourth-IMO-Greenhouse-Gas-Study-2020.aspx.

[3] "Sustainable Hydrogen Integrated Propulsion Drives (SH2IPDRIVE)," https://sh2ipdrive.com/.

[4] J. F. Hansen and F. Wendt, "History and State of the Art in Commercial Electric Ship Propulsion, Integrated Power Systems, and Future Trends," *Proceedings of the IEEE*, vol. 103, no. 12, pp. 2229–2242, Dec. 2015.

[5] C. Nuchturee, T. Li, and H. Xia, "Energy efficiency of integrated electric propulsion for ships – A review," *Renewable and Sustainable Energy Reviews*, vol. 134, p. 110145, Dec. 2020.

[6] N. Shakeri, M. Zadeh, and J. Bremnes Nielsen, "Hydrogen Fuel Cells for Ship Electric Propulsion: Moving Toward Greener Ships," *IEEE Electrification Magazine*, vol. 8, no. 2, pp. 27–43, Jun. 2020.

[7] S. Jayasinghe, L. Meegahapola, N. Fernando, Z. Jin, and J. Guerrero, "Review of Ship Microgrids: System Architectures, Storage Technologies and Power Quality Aspects," *Inventions*, vol. 2, no. 1, p. 4, Feb. 2017.

[8] M. Butcher, R. Maltby, and P. S. Parvin, "Compact DC power and propulsion systems - the definitive solution?" in *2009 IEEE Electric Ship Technologies Symposium*. Baltimore, MD, USA: IEEE, Apr. 2009, pp. 521–528.

[9] L. Xu, J. Guerrero, A. Lashab, B. Wei, N. Bazmohammadi, J. Vasquez, and A. Abusorrah, "A Review of DC Shipboard Microgrids—Part II: Control Architectures, Stability Analysis, and Protection Schemes," *IEEE Transactions on Power Electronics*, vol. 37, no. 4, pp. 4105–4120, Apr. 2022.

[10] T. Kopka, F. Mylonopoulos, A. Coraddu, and H. Polinder, "Decentralized Power Sharing with Frequency Decoupling for a Fuel Cell-battery DC Shipboard Power System," in *Modelling and Optimisation of Ship Energy Systems (MOSES)*, Delft, The Netherlands, Oct. 2023, in press.

[11] C.-L. Su, X.-T. Weng, and Ching-Jin Chen, "Power generation controls of fuel cell/energy storage hybrid ship power systems," in *2014 IEEE Conference and Expo Transportation Electrification Asia-Pacific (ITEC Asia-Pacific)*. Beijing, China: IEEE, Aug. 2014, pp. 1–6.

[12] H. Chen, Z. Zhang, C. Guan, and H. Gao, "Optimization of sizing and frequency control in battery/supercapacitor hybrid energy storage system for fuel cell ship," *Energy*, vol. 197, p. 117285, Apr. 2020.

[13] L. Balestra and I. Schjølberg, "Energy management strategies for a zero-emission hybrid domestic ferry," *International Journal of Hydrogen Energy*, vol. 46, no. 77, pp. 38 490–38 503, Nov. 2021.

[14] J. Han, J.-F. Charpentier, and T. Tang, "An energy management system of a fuel cell/battery hybrid boat," *Energies*, vol. 7, no. 5, pp. 2799–2820, 2014.

[15] A. M. Bassam, A. B. Phillips, S. R. Turnock, and P. A. Wilson, "Development of a multi-scheme energy management strategy for a hybrid fuel cell driven passenger ship," *International Journal of Hydrogen Energy*, vol. 42, no. 1, pp. 623–635, Jan. 2017.

[16] L. Zhu, J. Han, D. Peng, T. Wang, T. Tang, and J.-F. Charpentier, "Fuzzy logic based energy management strategy for a fuel cell/battery/ultra-capacitor hybrid ship," in *2014 First International Conference on Green Energy ICGE 2014*, Mar. 2014, pp. 107–112.

[17] Z. Jin, L. Meng, J. C. Vasquez, and J. M. Guerrero, "Frequency-division power sharing and hierarchical control design for DC shipboard microgrids with hybrid energy storage systems," in *2017 IEEE Applied Power Electronics Conference and Exposition (APEC)*, Mar. 2017, pp. 3661–3668.

[18] K. Kwon, D. Park, and M. K. Zadeh, "Load Frequency-Based Power Management for Shipboard DC Hybrid Power Systems," in *2020 IEEE 29th International Symposium on Industrial Electronics (ISIE)*, Jun. 2020, pp. 142–147.

[19] P. Xie, S. Tan, N. Bazmohammadi, Josep. M. Guerrero, Juan. C. Vasquez, J. M. Alcala, and J. E. M. Carreño, "A distributed real-time power management scheme for shipboard zonal multi-microgrid system," *Applied Energy*, vol. 317, p. 119072, Jul. 2022.

[20] T. Kopka, C. Loeffler, A. Coraddu, and H. Polinder, "Hierarchical Control Strategy for Fuel Cell-Battery Shipboard Power System Utilizing a Modular Control Architecture," in *IEEE Transportation Electrification Conference and Expo, Asia-Pacific (ITEC-AP)*, Chiangmai, Thailand, Nov. 2023, in press.

New PVA based PEMs for use in LTFCs

C. De Luca*[1], E. De Gregorio[2,3], A. Occhicone[2], G. Roviello[2], C. Ferone[2], V. Cigolotti[3], E. Jannelli[2], A. Pozio[3], O. Tarallo[1]

[1]University of Naples Federico II, Department of Chemical Sciences, Complesso Universitario di Monte Sant'Angelo, 80126 Naples, Italy

[2]University of Naples Parthenope, Department of Engineering, Centro Direzionale, Isola C4, 80143 Naples, Italy

[3]ENEA Italian National Agency for Energy, New Technologies and Sustainable Economic Development, Department of Energy Technologies and Renewable Sources, Laboratory of Energy Storage, batteries and Hydrogen Production and Use (TERIN PSU ABI), C.R. Casaccia, Rome, Italy;

Introduction

Fuel cells convert chemical energy to electrical energy via an electrochemical reaction. They are more efficient than traditional heat engine-based power systems and can have zero or near-zero emissions during operation. As a leading technology in alternative green energy, fuel cells are finding applications in many areas, including transportation, portable power, and stationary power generation [1]. These uses have driven development of several different types of fuel cell technologies. In this work we focus our attention on low-temperature proton exchange membrane fuel cells (LTPEMFCs).

A LTPEMFC consists of an anode and a cathode separated by a PEM, a solid electrolyte. These electrochemical power generators convert chemical energy to electrical energy, in a manner similar to that of batteries. This type of FC uses a proton conductive polymer membrane as electrolyte and operates at relatively low temperatures (60-90 °C), by electrochemically combining hydrogen fuel and oxygen to produce electricity, water, and heat [2]. Hydrogen fuel is oxidized at the anode to produce electrons and protons (eq. 1). The PEM acts to physically separate the two half-cell reactions and force electrons to pass throught an external circuit where they can do electrical work before returning to the cathode while the mobile protons pass through the membrane [1]. At the cathode, oxygen is reduced due its combination with the electrons and the mobile ions, completing the reaction and forming water as a waste product (eq. 2) [1].

$$H_2 \rightarrow 2H^+ + 2e^- \qquad \text{(eq. 1)}$$

$$\frac{1}{2}O_2 + 2H^+ + 2e^- \rightarrow H_2O \qquad \text{(eq. 2)}$$

Thus, the overall reaction is reported as (eq. 3).

$$H_2 + \frac{1}{2}O_2 \rightarrow H_2O \qquad \text{(eq. 3)}$$

This process continues producing electricity so long as fuel and oxidant are supplied to the cell, whereas in a battery, the fuel and oxidant are contained in the electrode materials themselves. Fuel cells are known for their high power density, compact size, and quick response to changes in power demand [3]. The most widely used solid electrolytes in LTFCs are solid sulfonated fluoropolymers (namely Nafion®). The fluoropolymer backbone of that material delivers a mechanically strong, chemically resistant structure while the sulfonic acid groups provide both hydrophilicity and surface acidity that facilitate proton conduction [3]. Despite Nafion® has

* Corresponding author: carlo.deluca@studenti.unina.it

been widely used as a benchmark material in LTPEMFCs due to its excellent properties [4], there are ongoing innumerable efforts to develop alternative PEM with improved performance, lower cost, and enhanced durability in respect to it.
Poly(vinyl alcohol), PVA, seems to be a promising candidate for use as a proton exchange membrane in LTFCs due to its good thermal and mechanical stability and low gas permeability [5]; however, it cannot be applied in this field because it is soluble in water and does not possess negatively charged groups that can transport protons. Nevertheless, in order to overcome this limitation, PVA polymer chains can be easily cross-linked and functionalized so that the material became water insoluble and capable of efficiently carrying mobile ions [6]. In this contribution we propose new PVA based membranes crosslinked with an alternative sulfonating and crosslinking agent, the 5-sulfoisophthalic acid (SIPA), characterized by good proton conductivity and water management together with good mechanical properties, and thermal stability.

Methodology

The PVA based membranes were obtained dissolving commercial PVA powder in deionized water for 6 h at 70 °C under magnetic stirring. After the PVA aqueous solution had become transparent, a given amount of SIPA, ranged between 10 and 40% by weight respect to PVA, was added dropwise to it, followed by stirring the PVA/SIPA solution at room temperature for further 12 h. After carrying out the chemical reaction for a given time, the membrane was then obtained by solution casting process, pouring the solution into a petri dish, and letting the water evaporate at room temperature in a hood. Finally, the obtained PVA/SIPA dried membranes were then peeled off from the substrate, heated at 120°C for 30 min to complete the crosslinking and then stored in a desiccator at 100% relative humidity until further testing. The membranes thickness of the cast membranes ranged between 100 and 150 μm, with a diameter of 10 cm. The overall reaction for the obtainment of the membranes with various grade of cross-linking agent is shown in Fig. 1.

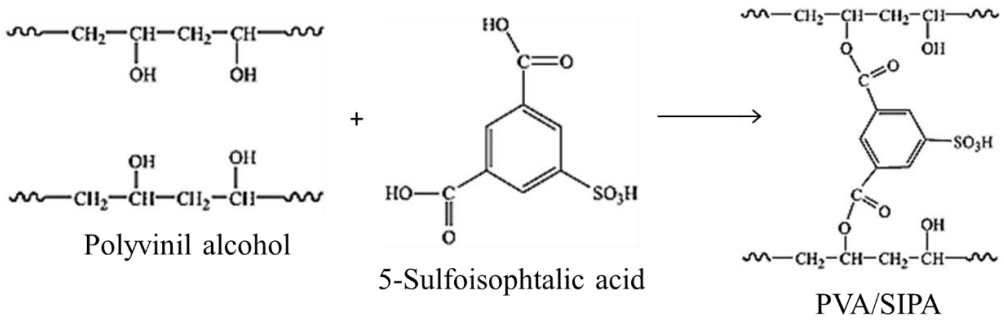

Fig. 1 - Chemical reaction between PVA and SIPA to form crosslinked/sulfonated PVA.

The obtained samples were characterized from a chemical and structural point of view by using Wide Angle X-Ray diffraction and Fourier Transform Infrared spectrophotometry. Thermal stabilities of PVA and the modified PVA membranes were examined by using a thermogravimetric analyzer (TGA). Measurements of water uptake (WU) values of crosslinked PVA membranes were conducted by immersing them into deionized water at 25°C for 24 h. After that, the swollen membranes were taken out, wiped with tissue paper, and immediately weighed. The water uptake values of the membranes were then calculated from (eq. 4).

$$W(\%) = \left[\left(W_{wet} - W_{dry}\right)/W_{dry}\right] \times 100 \qquad \text{(eq. 4)}$$

Where W_{wet} is the weight of the water swollen membrane and W_{dry} is the weight of the dried membrane [7].
Ion-exchange capacity (IEC) of the membranes was measured by a titration technique [8]. The membranes were immersed in 25 mL of 1 M HCl solution for 24 h to protonate all sites; subsequently, the membranes were washed with deionized water to remove excess acid and then immersed in 25 mL of 1 M NaCl solution for 24 h to promote the exchange between H^+ and Na^+. After that, the IEC value was determined by carrying out a titration of the solution with 0.01 M NaOH to evaluate the amount of exchanged protons. The IEC values of the membranes were calculated by using (eq. 5).

$$\mathrm{IEC\ (meq/g)} = (V_{NaOH} C_{NaOH} / W_{dry}) \qquad \text{(eq. 5)}$$

Where V_{NaOH} is the volume in mL of the added NaOH, C_{NaOH} is the concentration of NaOH and W_{dry} is the weight of the dried membrane [8].

Discussion

Fig. 2 show X-Ray diffraction (XRD) patterns of the developed membranes. All the samples exhibit a very similar diffraction pattern, with a main broad diffraction peak centered at about 2θ=20° thus indicating that, as expected, no significant structural modification has occurred in respect to pristine PVA film.
On the contrary, FTIR spectra of the crosslinked PVA/SIPA membranes differed significantly from that the pure PVA membrane (Fig. 3). A broad peak at wavenumber ranging between 3000 and 3600 cm^{-1}, representing the hydroxyl group of PVA can be observed [9]. In addition, five new peaks were noted at 1918, 1715, 1235, 1187 and 1043 cm^{-1} that could be attributed to the aromatic CH bending, the -CO-O- ester group, the O=S=O symmetric stretching, the O=S=O asymmetric stretching and the C-O-C acetal linkage, respectively [9]. In addition, the intensities of these bands increase as increasing the SIPA content.

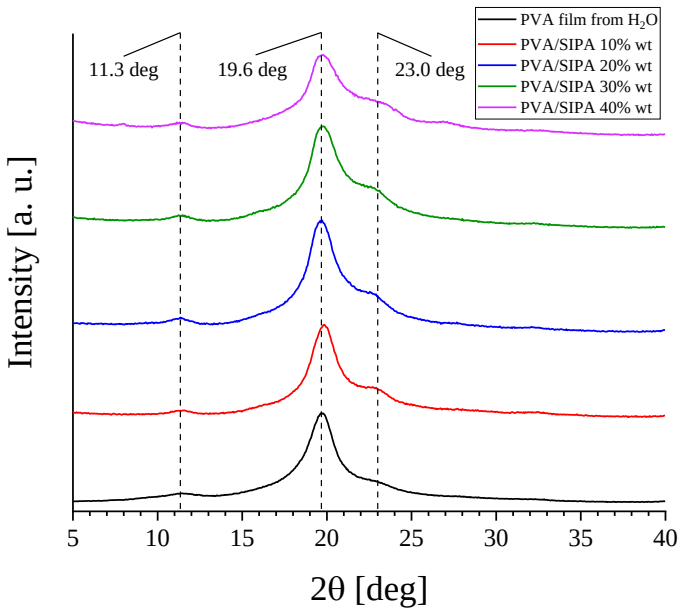

Fig. 2 - X-Ray diffraction pattern of PVA and PVA/SIPA membranes.

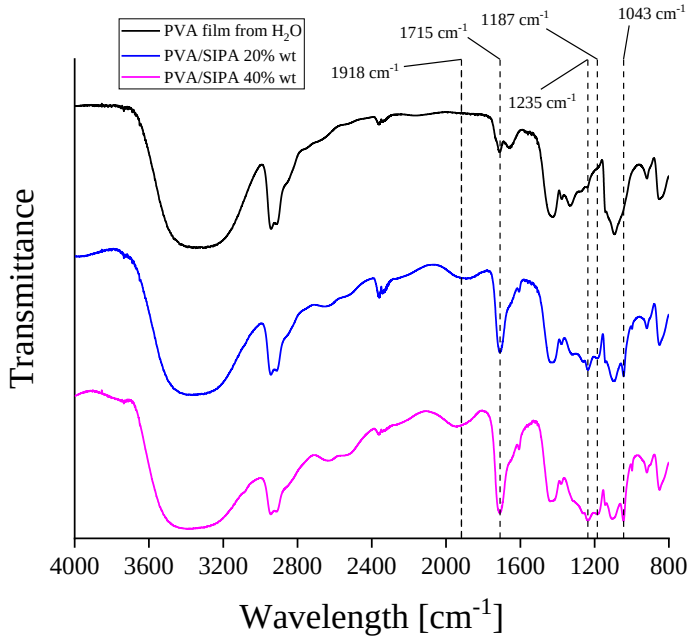

Fig. 3 – FTIR spectra of PVA and PVA/SIPA membranes.

Fig. 4 shows overlaid TGA thermograms of the pristine PVA and the modified membranes. For pristine PVA, the first weight loss occurred at approximately 100 °C from the removal of adsorbed water. The second weight loss (approximately 63%) between 230 and 350 °C is associated with the dehydration of hydroxyl groups between intra- or inter-chains in the PVA polymer [10]. The last weight loss appeared after 400 °C and is mainly correlated to the decomposition of the PVA chains. In terms of thermal stability for PVA/SIPA samples, there are three consecutive weight loss steps. The first weight loss from 60 to 160 °C could be ascribed to the removal of adsorbed water and water generated from the esterification process. The second weight loss occurred between 190 and 290 °C could be related to the desulfonation and dissociation of the ester bonds [11]. Finally, the third weight loss occurred after 400 °C and is related to the degradation of the polymer backbones in the crosslinked membranes. In addition, the residual amounts of PVA/SIPA were higher than pristine PVA, suggesting that PVA/SIPA is more thermally stable than PVA and the thermal stability increases with an increasing content of SIPA.

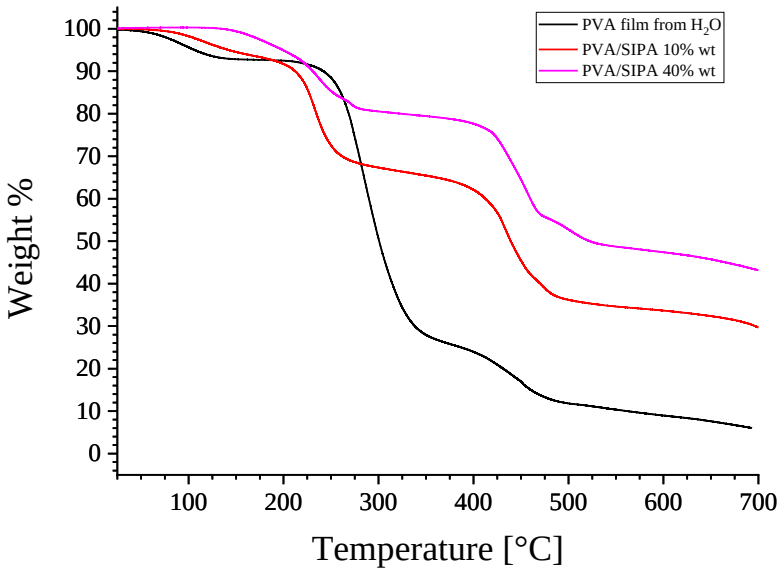

Fig. 4 – Overlaid TGA thermograms of PVA and PVA/SIPA membranes.

Tab. 2 show the water uptake values of the PVA/SIPA membranes. Compared to the pristine PVA membrane, the crosslinked ones do not dissolve in water and show a water content that decreases as the amount of SIPA increases, as would be expected from the ever-increasing crosslinking between the PVA chains. Tab. 2 also shows the IEC values of the membranes containing 20 and 40% wt. of SIPA. For the PVA membrane crosslinked with 40% wt. of SIPA, an IEC value of 1.56 meq/g was achieved, significantly higher than that of Nafion®, which has an IEC value of approximately 0.95 meq/g.

Tab. 2 – WU and IEC values of crosslinked PVA membranes.

Sample	**Water uptake [%]**	**Ion-exchange capacity (meq/g)**
PVA/SIPA 10 % wt.	181	/
PVA/SIPA 20 % wt.	160	0.873
PVA/SIPA 30 % wt.	139	/
PVA/SIPA 40 % wt.	118	1.56

Conclusion

Crosslinked proton exchange PVA/SIPA membranes were successfully obtained through solution casting procedure and seem to be promising for FCs applications. Preliminary results show that the chemical and physical properties of these membranes seem to be significantly enhanced with increasing the concentration of the crosslinking agent. Further studies are in progress to improve the chemical, physical and mechanical properties of the newly developed membranes and to complete the chemical, physical and electrochemical characterization of the obtained membranes. After having completed the thermal and electrochemical characterizations, a MEA will be produced and tested in an operational cell.

References

[1] Barbir, F. (2006). PEM fuel cells. In Fuel cell technology: reaching towards commercialization. Springer, London. (pp. 27-51). DOI: 10.1007/1-84628-207-1_2

[2] Daud, W. R. W., Rosli, R. E., Majlan, E. H., Hamid, S. A. A., Mohamed, R., & Husaini, T. (2017). PEM fuel cell system control: A review. Renewable Energy, 113, 620-638. DOI: 10.1016/j.renene.2017.06.027

[3] Gold, S. A. (2012). Low-temperature fuel cell technology for green energy. Handbook of Climate Change Mitigation, 1657-1702. DOI: 10.1007/978-1-4419-7991-9

[4] Collette, F. M., Thominette, F., Mendil-Jakani, H., & Gebel, G. (2013). Structure and transport properties of solution-cast Nafion® membranes subjected to hygrothermal aging. Journal of membrane science, 435, 242-252. DOI: 10.1016/j.memsci.2013.02.002

[5] Sau, S., Pandit, S., & Kundu, S. (2021). Crosslinked poly (vinyl alcohol): structural, optical and mechanical properties. Surfaces and Interfaces, 25, 101198. DOI: 10.1016/j.surfin.2021.101198

[6] Gautam, L., Warkar, S. G., Ahmad, S. I., Kant, R., & Jain, M. (2022). A review on carboxylic acid cross-linked polyvinyl alcohol: Properties and applications. Polymer Engineering & Science, 62(2), 225-246. DOI: 10.1002/pen.25849

[7] Zheng, Y., Ash, U., Pandey, R. P., Ozioko, A. G., Ponce-González, J., Handl, M., ... & Dekel, D. R. (2018). Water uptake study of anion exchange membranes. Macromolecules, 51(9), 3264-3278. DOI: 10.1021/acs.macromol.8b00034

[8] D'Epifanio, A., Navarra, M. A., Weise, F. C., Mecheri, B., Farrington, J., Licoccia, S., & Greenbaum, S. (2010). Composite nafion/sulfated zirconia membranes: effect of the filler surface properties on proton transport characteristics. Chemistry of Materials, 22(3), 813-821. DOI: 10.1021/cm901486t

[9] Hummel, D.; & Scholl, F., (1971). IR Analysis of Polymers, Resins and Additives, An atlas. Wiley-Interscience, Volume 1 Part 1.

[10] Shi, W., Li, H., Zhou, R., Qin, X., Zhang, H., Su, Y., & Du, Q. (2016). Preparation and characterization of phosphotungstic acid/PVA nanofiber composite catalytic membranes via electrospinning for biodiesel production. Fuel, 180, 759-766. DOI: 10.1016/j.fuel.2016.04.066

[11] Rachipudi, P. S., Kariduraganavar, M. Y., Kittur, A. A., & Sajjan, A. M. (2011). Synthesis and characterization of sulfonated-poly (vinyl alcohol) membranes for the pervaporation dehydration of isopropanol. Journal of Membrane science, 383(1-2), 224-234. DOI: 10.1016/j.memsci.2011.08.040

Next generation of conductive and stable electrocatalysts for CO_2 conversion

Digvijay Ghogare*[a,b], An Hardy[a], Marlies van Bael[a], Deepak Pant[b]

[a] Hasselt University, Campus Diepenbeek, Diepenbeek 3590, Belgium
[b] Flemish Institute of Technological Research (VITO), Mol 2400, Belgium

Introduction

Excessive CO_2 emissions from human activities significantly intensified global climate change. To achieve net zero emissions, these CO_2 emissions must be balanced by CO_2 utilization and sequestration. The electrochemical CO_2 reduction (eCO_2R) reaction is a promising technology for valorizing anthropogenic CO_2 emissions and storing energy for intermittent renewable sources like wind and solar. It can be carried out at ambient temperature and pressure, producing various products like formic acid, carbon monoxide, methane, methanol, and ethylene. However, the stability of CO_2 and the possibility of multiple products present challenges in energy efficiency and product selectivity. Electrocatalytic materials enhance CO_2 reduction by lowering activation barriers and reducing energy inputs, leading to faster kinetics for product generation. Recent efforts have improved electrocatalyst activity and selectivity, but electrocatalyst deterioration hinders eCO_2R's technology readiness for industrial applications. [1-4]

We have explored Tin oxide (SnO_2) nanoparticles as electrocatalysts for selective eCO_2R to formic acid, a promising hydrogen energy carrier with low toxicity and acceptable flammability. [5,6] Sn-based electrocatalysts have been extensively studied due to their high selectivity towards formic acid, low toxicity, non-noble nature, and ecological and inexpensive properties. A variety of Sn-based electrocatalysts, including bulk Sn, nanoparticles, alloys, oxides, sulfides, and carbon-supported catalysts, have been reported for eCO_2R reaction. [7] Despite their advanced morphology and composition, Sn-based electrocatalysts are more susceptible to degradation due to more new degradation mechanisms during eCO_2R reaction. [8] Therefore, obtaining prolonged electrocatalyst stability is crucial to maintain their enhanced activity and selectivity over long-term operation. Thus, Sn-based electrocatalyst stability remains insufficient as degradation processes during eCO_2R reaction inhibit the long-term electrocatalytic activity of these catalysts. Developing new catalyst architectures requires a better understanding of performance and challenges with existing electrocatalysts, which will be discussed through SnO_2 nanoparticles. Later, new Sn-based electrocatalysts with core-shell morphology, which can minimize most degradation processes through particle confinement, will be produced and compared to the performance of SnO_2 nanoparticles. [9,10]

Methodology

SnO_2 nanoparticles were synthesized using the polyol method reported by Soltan *et al.* [11] The choice of the polyol method was based on the advantageous functionalities such as chelating properties of the polyols for controlling particle size, particle growth, and agglomeration, yielding high-quality nanoparticles. SnO_2 nanoparticles were characterized with a set of

* Corresponding author: digvijay.ghogare@uhasselt.be

techniques. X-ray diffraction (XRD), Raman and Transmission electron microscopy (TEM) were used to investigate the material composition and morphology of SnO_2 nanoparticles.

All electrochemical CO_2 reduction experiments were conducted using a three-electrode system connected to an electrochemical workstation (BioLogic VMP3) in a gas-tight two-compartment H-cell separated by Nafion 117 membrane at room temperature (298 K) and atmospheric pressure. SnO_2 nanoparticles coated on Toray carbon paper are used as the working electrode and placed in the cathodic chamber alongside the reference electrode. Platinum wire is used as the counter electrode. Linear sweep voltammetry (LSV, scan rate 5 mV s^{-1}) and cyclic voltammetry (scan rate 50 mV s^{-1}) were performed before and after chronoamperometry tests at different potentials. Gaseous and liquid products generated during chronoamperometry measurements were quantified by gas chromatography (GC) and high-performance liquid chromatography (HPLC), respectively. The electrochemical active surface area (ECSA) for the working electrodes was determined using electrochemical double-layer capacitance measurement. All working electrode potentials are reported with respect to reversible hydrogen electrodes (RHE).

Discussion

The study investigates the performance of SnO_2 nanoparticles synthesized using the polyol method for electrocatalytically reducing CO_2 to HCOOH in aqueous electrolyte (0.5 M $KHCO_3$). The eCO_2R reaction competes with the H_2 evolution reaction (HER), with the standard equilibrium potential values being -0.12 V for CO_2 to HCOOH and 0.0V for HER. Linear Sweep Voltammetry (LSV) experiments were conducted to investigate electrocatalyst selectivity towards the eCO_2R reaction over HER. The early onset of increasing current density in CO_2 saturated electrolyte over Argon saturated electrolyte suggests SnO_2 nanoparticles have better selectivity toward the eCO_2R reaction [see Figure 1(a)]. Chronoamperometric measurements were conducted to evaluate the product selectivity of the eCO_2R reaction at various applied potentials [see Figure 1(b)]. The faradaic efficiency of different products was calculated, with formate first detected at -0.7V. The efficiency increased to >80% at -0.8 V and -1.2 V [see Figure 1(c)]. Faradaic efficiency for the two gaseous side products (CO and H_2) remained small at low-to-medium overpotentials. The partial current density for formate increased with increasing applied potential, reaching a maximum of 25 mA/cm^2 at -1.2 V [see Figure 1(d)].

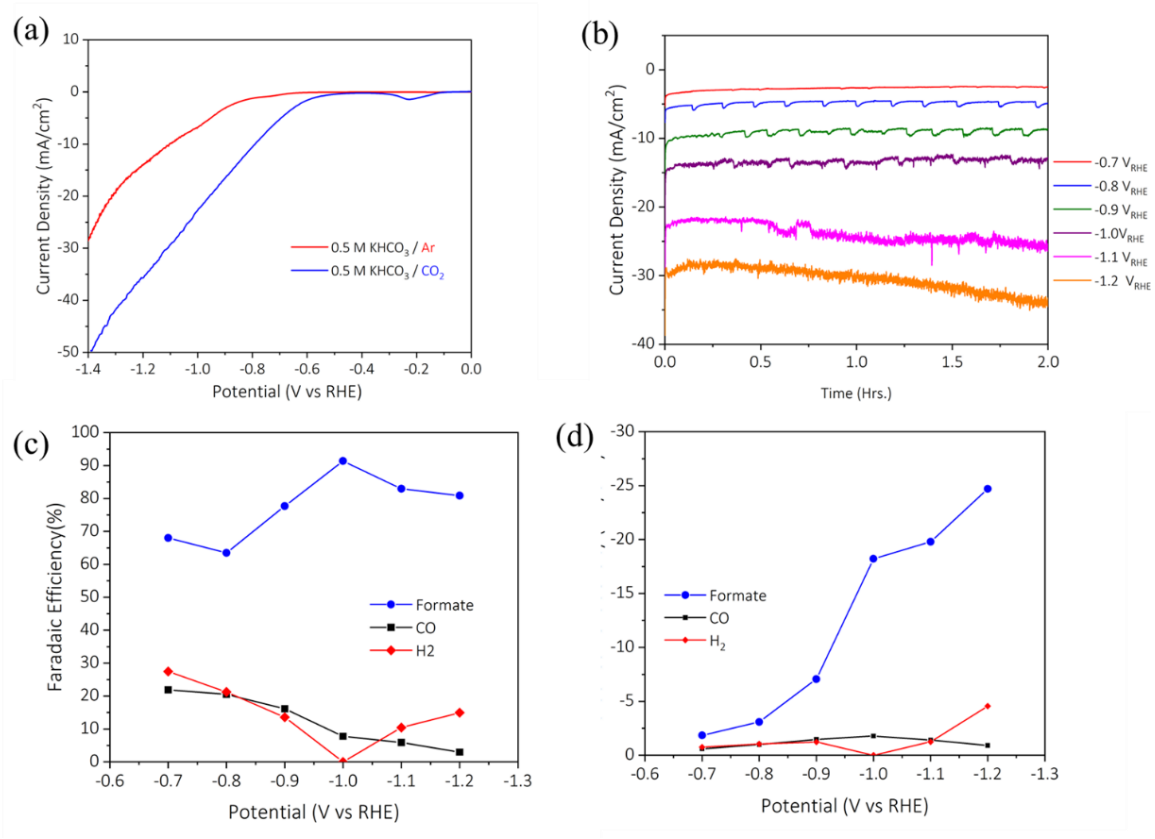

Figure 1(a) Linear sweep voltammetry (scan rate 5 mV/s) in 0.5 M Argon-saturated $KHCO_3$ (blue trace) and 0.5 M CO_2-saturated $KHCO_3$ (red trace), (b) Chronoamperometry measurements for over 2 h of reaction at each given potential (c) Faradaic efficiency and (d) partial current density of formate, CO, and H_2 at different applied potentials

SnO_2 nanoparticles showed selective CO_2 to formate conversion in H-cell testing. However, electrocatalysts often undergo degradation processes, leading to the loss of active sites. Analyzing ECSA values before and after chronoamperometric measurements revealed a decrease in C_{dl} correlated with increased applied potential, suggesting detachment to agglomeration [see Figure 2(a)]. The complete reduction of SnO_2 suppressed redox features associated with SnO_2, indicating overall restructuring of the electrocatalyst [see Figure 2(b)]. [12] These structural changes and decreased surface area resulted in active site losses, which reduced the performance of the SnO_2 electrocatalyst, evidenced by decreased current density from LSV [see Figure 2(c)].

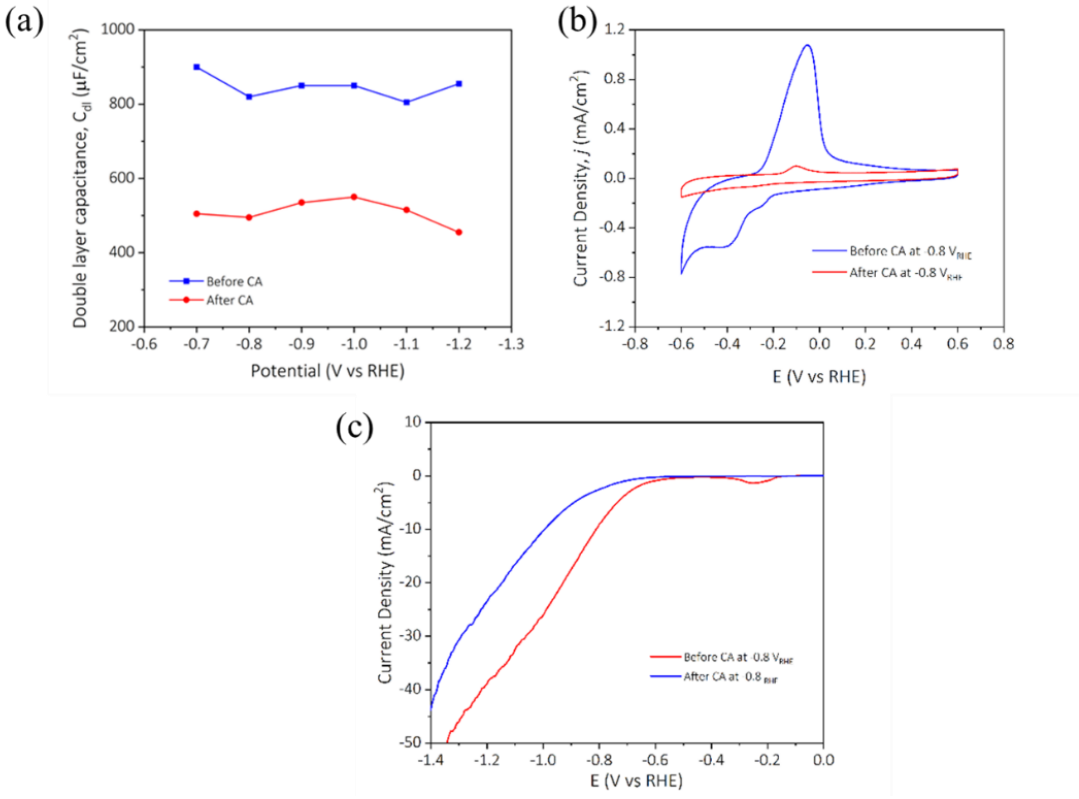

Figure 2(a) C_{dl} measurements before and after chronoamperometric tests at different applied potentials and (b) cyclic voltammetry demonstrating changes in peak size observed before and after chronoamperometric tests at -0.8V (c) LSV before and after chronoamperometric tests at -0.8V.

Conclusions

Evaluation of SnO_2 nanoparticles as electrocatalysts for eCO_2R reaction in H-cell configuration provided mechanistic insight like catalyst restructuring during eCO_2R and surface area losses using fundamental electrochemical descriptors. These electrochemical descriptors are essential in understanding ways of catalyst degradation during electrochemical measurements, thus allowing the identification of the steps and conditions that control electrocatalyst performance. This analysis can help us compare the electrochemical performance subsequently developed by the proposed electrocatalyst with SnO_2 nanoparticles and serves as the standard baseline for observing performance enhancements arising from structural modifications.

References

[1] S. Nitopi *et al.*, "Progress and perspectives of Electrochemical CO_2 reduction on copper in aqueous electrolyte," *Chemical Reviews*, vol. 119, no. 12, pp. 7610–7672, 2019. doi:10.1021/acs.chemrev.8b00705

[2] R. Kortlever, J. Shen, K. J. Schouten, F. Calle-Vallejo, and M. T. Koper, "Catalysts and reaction pathways for the electrochemical reduction of carbon dioxide," *The Journal of Physical Chemistry Letters*, vol. 6, no. 20, pp. 4073–4082, 2015. doi:10.1021/acs.jpclett.5b01559

[3] B. Khezri, A. C. Fisher, and M. Pumera, “CO_2 reduction: The quest for electrocatalytic materials,” *Journal of Materials Chemistry A*, vol. 5, no. 18, pp. 8230–8246, 2017. doi:10.1039/c6ta09875d
[4] S. Zhao *et al.*, “Advances in Sn-based catalysts for electrochemical CO_2 reduction,” *Nano-Micro Letters*, vol. 11, no. 1, 2019. doi:10.1007/s40820-019-0293-x
[5] M. Pérez-Fortes, J. C. Schöneberger, A. Boulamanti, G. Harrison, and E. Tzimas, “Formic acid synthesis using CO_2 as raw material: Techno-Economic and Environmental Evaluation and market potential,” *International Journal of Hydrogen Energy*, vol. 41, no. 37, pp. 16444–16462, 2016. doi:10.1016/j.ijhydene.2016.05.199
[6] A. S. Agarwal, Y. Zhai, D. Hill, and N. Sridhar, “The electrochemical reduction of carbon dioxide to formate/formic acid: Engineering and economic feasibility,” *ChemSusChem*, vol. 4, no. 9, pp. 1301–1310, 2011. doi:10.1002/cssc.201100220
[7] Q. Li *et al.*, “Energy storage through CO_2 electroreduction: A brief review of advanced sn-based electrocatalysts and electrodes,” *Journal of CO_2 Utilization*, vol. 27, pp. 48–59, 2018. doi:10.1016/j.jcou.2018.07.004
[8] K. Van Daele *et al.*, “Sn-based electrocatalyst stability: A crucial piece to the puzzle for the electrochemical CO_2 reduction toward formic acid,” *ACS Energy Letters*, vol. 6, no. 12, pp. 4317–4327, 2021. doi:10.1021/acsenergylett.1c02049
[9] B. Vanrenterghem *et al.*, “Increase of electrodeposited catalyst stability via plasma grown vertically oriented graphene nanoparticle movement restriction,” *Chemical Communications*, vol. 53, no. 67, pp. 9340–9343, 2017. doi:10.1039/c7cc05828d
[10] S. Popović *et al.*, “Stability and degradation mechanisms of copper-based catalysts for Electrochemical CO_2 Reduction,” *Angewandte Chemie*, vol. 132, no. 35, pp. 14844–14854, 2020. doi:10.1002/ange.202000617
[11] W. B. Soltan *et al.*, “Effect of hydrolysis ratio on structural, optical and electrical properties of SnO_2 nanoparticles synthesized by Polyol method,” *Optical Materials*, vol. 58, pp. 142–150, 2016. doi:10.1016/j.optmat.2016.05.001
[12] Y. Chen and M. W. Kanan, “Tin Oxide Dependence of the CO_2 reduction efficiency on tin electrodes and enhanced activity for tin/tin oxide thin-film catalysts,” *Journal of the American Chemical Society*, vol. 134, no. 4, pp. 1986–1989, 2012. doi:10.1021/ja2108799

Next-generation *in-situ* Sensors for Oxygen Concentration Measurements in PEM Fuel Cells

Mehran Afra*[1], Joe Fleming [1], Simon Shepherd [1], Oliver Curnick [1]
[1] Centre for Advanced Low Carbon Propulsion Systems, Coventry University
FEV UK Ltd.

Introduction

Proton Exchange Membrane Fuel Cells (PEMFCs) hold promise for clean power generation in a range of applications including aerospace, marine, heavy duty automotive and stationary power. The electrochemical reactions of hydrogen and oxygen responsible for power generation in PEMFCs take place at the surface of electrodes with geometric surface areas of several hundred cm² [1]. The distribution of the electrochemical reactions across each electrode is not uniform, giving rise to significant spatial variation in critical operating parameters such as temperature, current density, and reactant concentrations [2]. Local oxygen starvation at the cathode catalyst layer (CL) can result in poor performance and accelerated degradation [3] (see Figure 1).

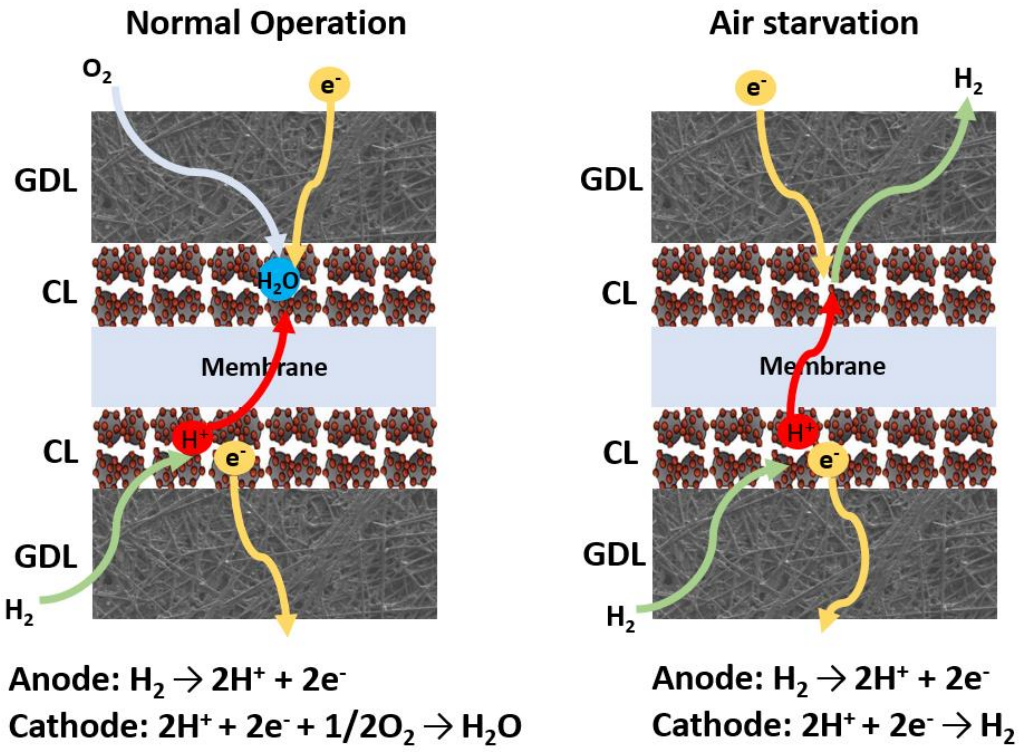

Figure 1: (a) Normal operation, (b) Air starvation

* Corresponding author: afram@uni.coventry.ac.uk

As a result, maintaining a uniform oxygen concentration is important for maximizing PEMFCs' performance and extending their lifetime. Techniques for direct, spatially-resolved measurement of oxygen concentration have not received as much attention as current or temperature. At present, there are no direct means to make spatially-resolved measurements of oxygen concentration across the plane (in plane) of PEMFC electrodes, particularly at the interface of the CL and membrane (CL/PEM).

Methodology

The goal of this research is to develop *in-situ* sensors and instrumentation to measure and map oxygen concentration inside a 250 cm² PEMFC. Prior to conducting *in situ* measurements, it is required to perform *ex situ* measurements only for the purpose of validating the concept. Micrometer platinum (Pt) wire was implemented for developing the oxygen sensors for *ex situ* measurements (see Figure 2).

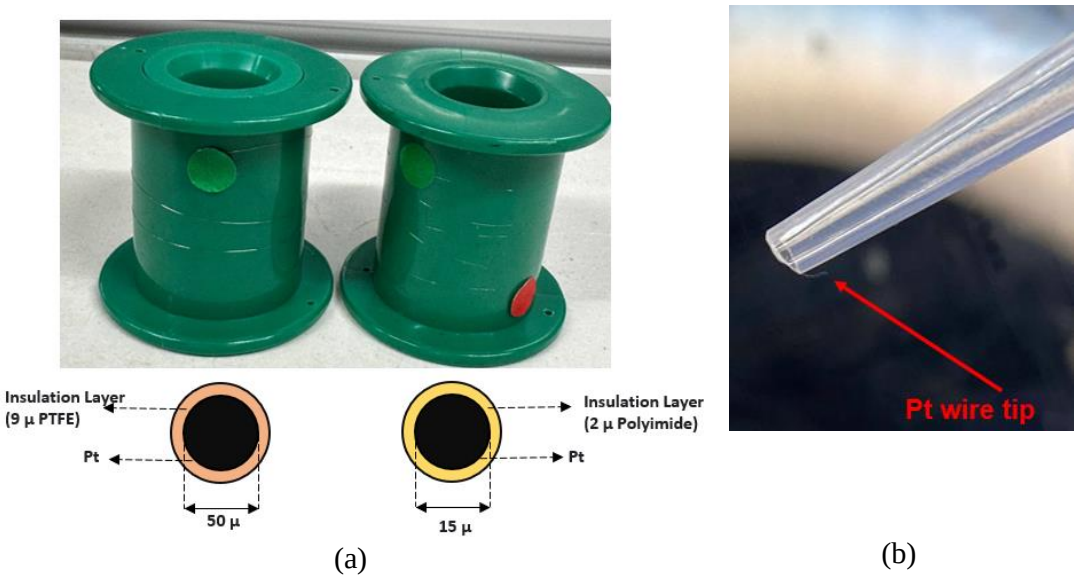

Figure 2: (a) Two different sizes of the Pt wire, (b) tip of the 15 µm Pt wire

Initially, the developed oxygen sensor was evaluated using a three-electrode cell and liquid electrolyte (0.1 M Perchloric acid). The three-electrode system consists of a Reference electrode (RE), a Counter electrode (CE), and a Working electrode (WE) (see Figure 3).

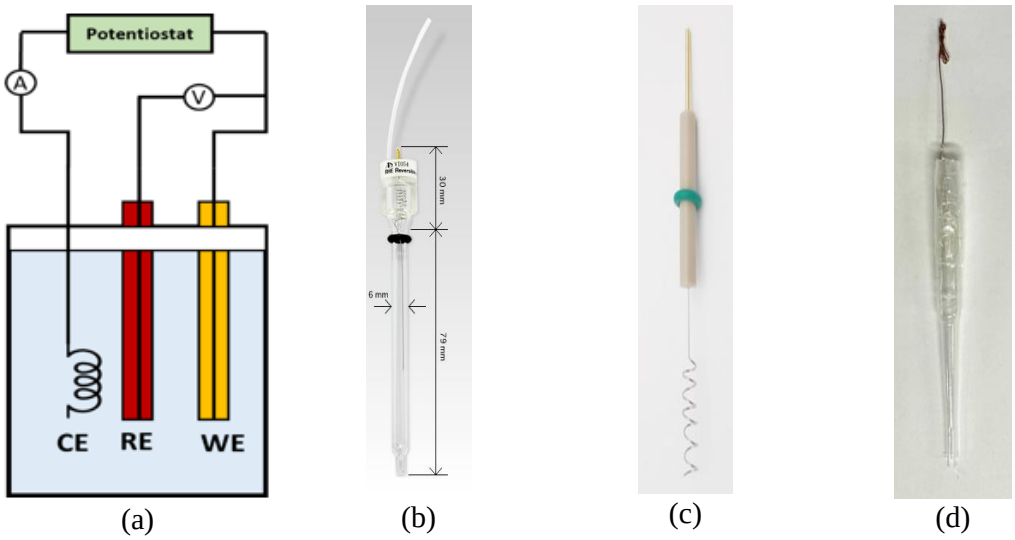

Figure 3: (a) Three electrode system, (b) RE (reversible hydrogen electrode), (c) CE (Pt coil), (d) WE (Pt wire as an oxygen sensor)

Electrochemical techniques including cyclic voltammetry and chronoamperometry were applied to characterise the sensor elements and evaluate their performance for oxygen concentration measurement. After confirming the proof of concept, *in-situ* measurements will be conducted by designing and printing an array of oxygen sensors onto a membrane layer and then inserting them at the interface of the CL/PEM, as shown in Figure 4. An inkjet printer will be utilized to create the sensor array.

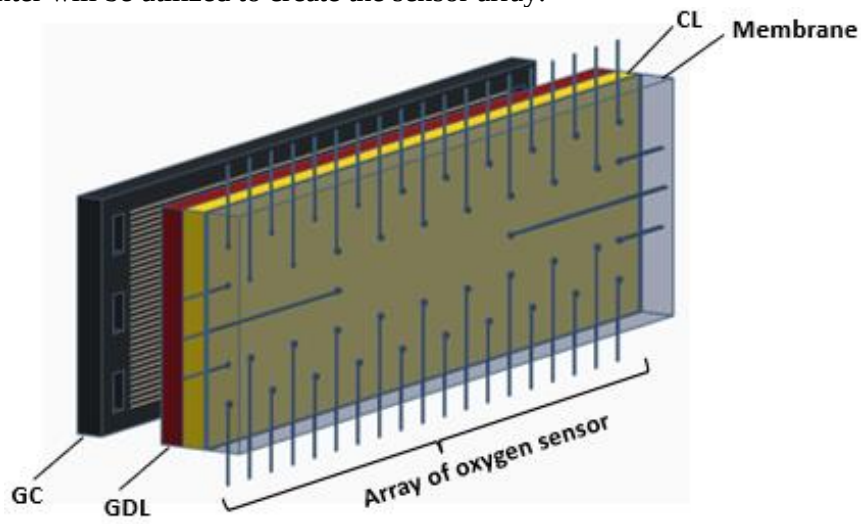

Figure 4: 3D schematic of an array of developed oxygen sensors at the interface of the CL/PEM

Discussion

Chronoamperometry measurements were conducted for *ex situ* experiment using three known oxygen concentrations at constant applied potential (0.4 V) in the mass transport-limited regime. To guarantee a baseline measurement free from oxygen disturbance, the experiments started with nitrogen purging (zero current). The obtained results showed an appropriate response of the developed oxygen sensor to the oxygen concentration changes

in the electrolyte solution. As depicted in Figure 4, when 20.9% oxygen was introduced into the cell, the oxygen reduction reaction (ORR) current transitioned from zero to a value of -7.27 × 10^{-8} A. Upon reducing the oxygen concentration to 4%, the ORR current showed a drop, reaching -1.36×10^{-8} A. Subsequently, it further decreased to -3.44×10^{-9} A when the oxygen concentration reached 1% (see Figure 5).

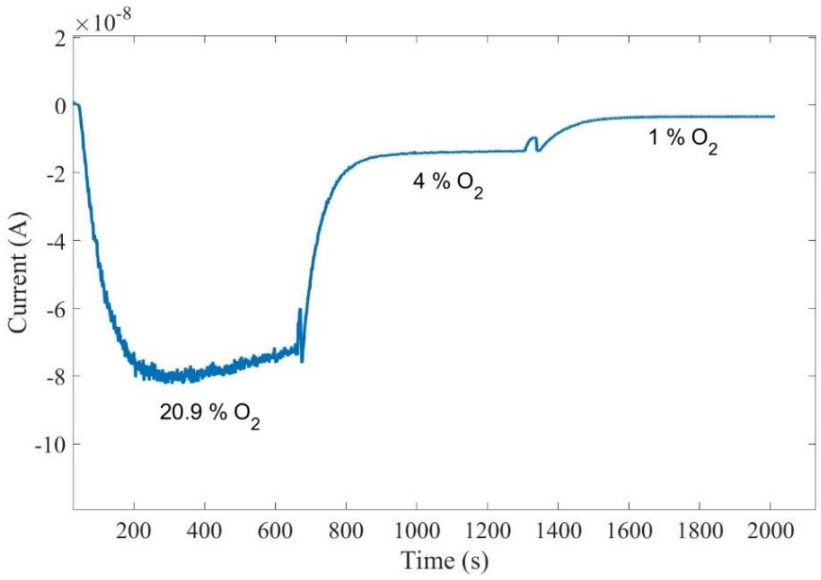

Figure 5: Response of the developed oxygen sensor to changes in oxygen concentrations from 0 % to 20.9 %, 4% , and 1%.

Steady-state ORR current is proportional to oxygen concentration. The obtained results were used to create a calibration curve for determining oxygen concentration based on the measured current, with an accuracy of ±1% (see Figure 6).

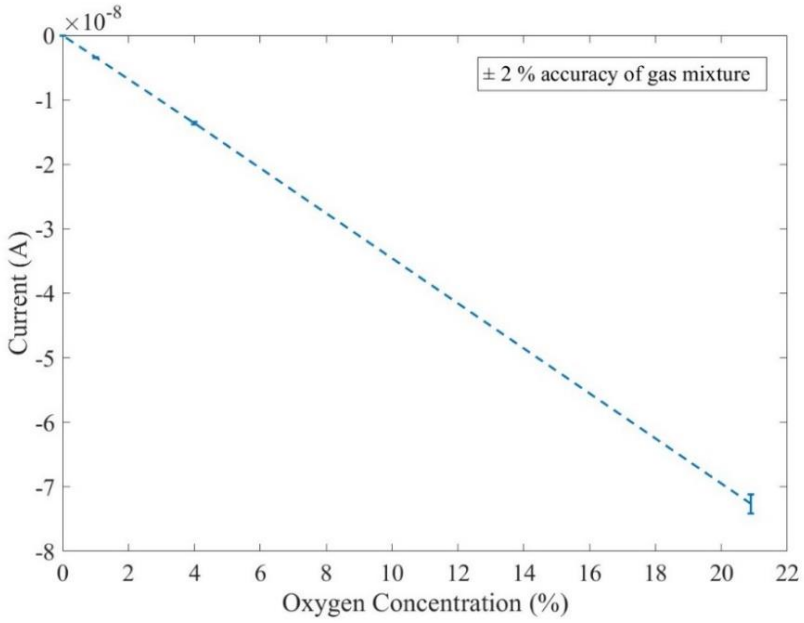

Figure 6: Calibration curve

Conclusions

The primary objective of this study is to map and measure oxygen concentration at the interface of CL/PEM in a 250 cm ^{2} PEM fuel cell. To validate the concept of oxygen concentration measurement, an *ex situ* experiment was conducted. The subsequent phase involves designing and printing an array of oxygen sensors and conducting spatially-resolved measurements. The outcomes of this research could be utilized to optimize flow field designs and improve stack durability and performance.

References

[1] P. Sharma and O. P. Pandey, Proton exchange membrane fuel cells: fundamentals, advanced technologies, and practical applications. INC, 2022. doi: 10.1016/b978-0-12-823708-3.00006-7.

[2] K. Takanohashi *et al.*, "Simultaneous visualization of oxygen partial pressure, current density, and water droplets in serpentine fuel cell during power generation for understanding reaction distributions," *J. Power Sources*, vol. 343, pp. 135–141, 2017, doi: 10.1016/j.jpowsour.2017.01.047.

[3] N. Yousfi-Steiner, P. Moçotéguy, D. Candusso, and D. Hissel, "A review on polymer electrolyte membrane fuel cell catalyst degradation and starvation issues: Causes, consequences and diagnostic for mitigation," *J. Power Sources*, vol. 194, no. 1, pp. 130–145, 2009, doi: 10.1016/j.jpowsour.2009.03.060.

Non-Gray Gas Radiation Model for Pure Water in Hydrogen MILD Combustion

Endeshaw A. Bekele[1*], Andrzej Szlęk[1], Sławomir Sładek[1]

[1]Department of Thermal Technology, Silesian University of Technology, Konarskiego 18A, 44-100, Gliwice, Poland

Abstract

A novel weighted-sum-of-gray-gases model (WSGGM) is proposed to estimate the non-gray radiative properties of water in a hydrogen combustion chamber. The line-by-line (LBL) method will employ the HITEMP 2010 (High-Temperature Molecular Spectroscopic) database to compute the total emissivity of H_2O. Based on the total emissivity benchmark from LBL, new correlation coefficients for the weighted sum of gray gas models (WSGGM) will be fitted for a given gas temperature, partial pressure, path length, and number of gray gases. The accuracy and effectiveness of the new WSGGM will be verified against the LBL results and previously developed WSGGM in the literature. The developed model will be applied to 1D and 3D benchmark hydrogen combustion simulations using CFD to solve the heat flux distribution and heat source within the combustion chamber, employing the radiative transport equation (RTE) in non-isothermal and non-homogeneous conditions.

Introduction

Combustion modelling plays a crucial role in understanding and optimizing industrial processes. In recent years, the focus has been on cleaner fuel alternatives because of climate change impacts and rising global energy demand. Hydrogen plays a vital role in de-carbonizing various sectors such as industry, transport, power generation, and building in countering the challenges of climate change, fluctuating energy costs, energy dependability, and global political dynamics [1-3]. Due to its high energy content, rapid flame propagation, and zero greenhouse gas emissions, hydrogen combustion is promising for achieving a greener future. However, hydrogen poses difficulties for combustion technology due to its strong reactivity and fast flame speed [4-5]. Burning hydrogen in MILD (Moderate or Intense Low Oxygen Dilution) combustion offers a viable advantage in terms of combustion efficiency, fuel consumption, heat transfer, flame stability, and emissions reduction [6-7]. Hydrogen combustion predominantly relies on radiative heat transfer due to high flame temperatures. Accurate prediction of radiative heat transfer in hydrogen combustion systems is challenging

[1*] Corresponding author: ebekele@polsl.pl

because of the drastic and rapid change of the radiative properties of the reacting gases in the entire spectrum. The modeling of gas radiation is crucial to predict flame structure and temperature distribution, as well as to enhance the heat transfer in the system [8]. Several approaches have been employed to model gas radiation in combustion chambers, like spectral line-by-line, spectral band, and global models. The weighted sum of gray gases (WSGG) model is commonly used due to its simplicity, accuracy, and computational efficiency [9]. In this work, a new WSSGM model will be developed to estimate the non-gray radiative properties of water in hydrogen combustion through the HITEMP2010 database and line-by-line approach at different temperatures and path lengths. Developing accurate and computationally efficient radiation models is crucial to optimizing combustion systems and achieving cleaner and more efficient combustion processes.

Methodology

The HITEMP 2010 (High-Temperature Molecular Spectroscopic) database will be utilized within the line-by-line (LBL) method to precisely compute the total emissivity of H_2O [10]. A new weighted-sum-of-gray-gases model (WSGGM) correlation coefficient of H_2O will be fitted using the LSQCURVEFIT algorithm with the emissivity from the LBL benchmark. The WSGGM polynomial coefficients are estimated using multivariate regression for a gas temperature range of 400- 2500K and pressure-path length product between 0.01 and 60 atm.m. Four gray gases ($N_g = 4$) with one transparent gas is employed, and the total pressure of the gas is kept at 1 atm.

Line-by-line absorption coefficient estimation

A line-by-line approach has been used to calculate the spectral absorption coefficient with a uniform spectral spacing. The absorption coefficient depends on the types of molecules, the number of waves, the temperature, the gas's partial pressure, and the gas mixture's total pressure [11].

The spectral absorption coefficient at a specific wave number can be computed by integrating contributions from all transition lines through the Lorentz profile.

$$K_\eta = N(p,T)\sum_i \left(S_i(T) f_i(\eta - \eta_i)\right)$$

Where the parameter, K_η is the spectral absorption coefficient at wave number η, N is the number density of the absorbing molecules of the participating gases (H_2O), S_i is the integrated intensity of the i[th] transition line, η is the wave number location, η_i is the spectral line location, and $f_i(\eta - \eta_i)$ is the line shape function at the wavenumber η.

The line intensity at the i[th] spectral line for a given temperature can be calculated as:

$$S_i(T) = S_i(T_{ref})\left(\frac{Q(T_{ref})}{Q(T)}\right)\left(\frac{exp\left(-\frac{C_2E_i}{T}\right)\left(1-exp\left(-\frac{C_2\eta_i}{T}\right)\right)}{exp\left(-\frac{C_2E_i}{T_{ref}}\right)\left(1-exp\left(-\frac{C_2\eta_i}{T_{ref}}\right)\right)}\right)$$

Where $S_i(T_{ref})$ is the line intensity at a reference temperature, E_i is the lower state energy of the i[th] transition line, Q represents the total internal partition sums and, $C_2 = 1.43877\ cmK$ is the second Plank's constant.

The normalized Lorentz line profile is used to evaluate the line shape function, $f_i(\eta - \eta_i)$. It describes the broadening of the spectral lines which is caused by the collisions between the molecules.

$$f_i(\eta - \eta_i) = \frac{1}{\pi}\left(\frac{\left(\left(\frac{T_{ref}}{T}\right)^{n_{air}}\left[\gamma_{air}(P_t - P_a) + \gamma_{self}P_a\right]\right)}{\left(\left(\frac{T_{ref}}{T}\right)^{n_{air}}\left[\gamma_{air}(P_t - P_a) + \gamma_{self}P_a\right]\right)^2 + (\eta - \eta_i)^2}\right)$$

Where, γ_{air} and γ_{self} are the air-broadened and self-broadened line half-widths, n_{air} is a temperature-dependent coefficient, P_t the total pressure and $T_{ref} = 296$ K. The parameters of the spectral line $Q, \eta_l, S_i(T_{ref}), E_I, \gamma_{air}, \gamma_{self},$ and n is obtained from the HITEMP 2010 databases [10].

Based on the spectral absorption coefficients, the total emissivity of the gas medium is estimated line-by-line as follows.

$$\varepsilon_{LBL} = \frac{\int_{\eta=0}^{\infty} I_{b\eta}(T)\left[1 - \exp\left(-k_\eta L\right)\right]d_\eta}{\frac{\sigma T}{\pi}}$$

Where, $I_{b\eta}$ is the spectral blackbody intensity at wavenumber η, which is calculated by Plank's law.

$$I_{b\eta} = \frac{C_1 \eta^3}{\left[e^{\frac{C_2 \eta}{T}} - 1\right]}$$

Where, $C_1 = 2\pi h c_o^2$ and $C_2 = \frac{h c_o}{k_B}$, c_o is the speed of light in a vacuum ($2.998 \times 10^8 \frac{m}{s}$), h is the Planck's constant (6.626×10^{-34}Js), k_B is Boltzmann's constant (1.3807×10^{-23}J/K), σ is the Stefan Boltzmann constant $5.67X\ 10^{-8} \frac{W}{m^2 K^4}$, and T is the local temperature of the gas.

WSGGM-based total emissivity estimation

The WSGGM represents the spectrum of transparent windows and a few gray gases with uniform pressure absorption coefficients and specific temperature weighting factors [12]. It assumes that the absorption coefficient is independent of the gas temperature; however, each gray gas's weighting factors are temperature-dependent.

Based on the spectral absorption coefficient, the total emissivity of a H_2O is calculated by.

$$\varepsilon = \sum_{i=0}^{N_g} a_i(T_g)\left(1 - e^{-k_i P_{(H_2O)} L}\right)$$

Where, a_i is the temperature-dependent emissivity weighting factor for i^{th} gray gas, T_g is the gas temperature, N_g is the number of gray gases, k_i is the pressure absorption coefficient, $P_{(H_2O)}$ is the participating gas's partial pressure in combustion chambers, and L is the beam length.

The absorption coefficient of each gray gas is estimated as.

$$k_i = \sum_{k=0}^{N_g} d_{i,k}\, M_r^k$$

Where M_r^k is a molar ratio of k^{th} gray gas in gas mixture.

$$\begin{cases} a_i(T_g) = \sum_{j=0}^{4} b_{i,j} \left(\frac{T_g}{T_{ref}}\right)^j, \quad a_i > 0, \quad b_{i,j} = \sum_{k=0}^{4} C_{i,j,k} M_r^k \\ K_0 = 0, \ a_0(T_g) = 1 - \sum_{i=0}^{N_g} a_i \ \ a_0 > 0 \text{ spectral windows between the absorption bands} \\ T_{ref} = 1200 \text{ K, and P is the partial pressure of water} \end{cases}$$

Discussion

The expected outcome of this research is to develop a novel non-gray gas-radiation model based on the Weighted Sum of Gray Gas Model (WSGGM) to enhance the understanding of radiative heat transfer in hydrogen combustion environments. The estimated emissivity will be verified against established models and data from the literature, ensuring its accuracy and applicability under non-isothermal and non-homogeneous conditions.

Conclusions

Accurately predicting radiative heat transfer is crucial for preventing local overheating, managing combustion temperature, reducing emissions, and enhancing the performance of hydrogen combustion chambers. This proposed work will develop a novel WSGG model to estimate the radiative properties of non-gray gas within a hydrogen combustion chamber using the most accurate emissivity calculation spectral LBL model and the HITEMP 2010 database. The developed model will be applied to 1D and 3D benchmarks of hydrogen combustion simulations using CFD to solve for the heat flux distribution and heat source within the combustion chamber, employing the radiative transport equation (RTE) in non-isothermal and non-homogeneous conditions.

References

[1] The Future of Hydrogen. OECD, 2019. doi: https://doi.org/10.1787/1e0514c4-en.

[2] D. Hauglustaine, F. Paulot, W. Collins, R. Derwent, M. Sand, and O. Boucher, "Climate benefit of a future hydrogen economy," Communications Earth & Environment, vol. 3, no. 1, Nov. 2022, doi: https://doi.org/10.1038/s43247-022-00626-z.

[3] S.Nižetić, F. Barbir, and N. Djilali, "The role of hydrogen in energy transition," International Journal of Hydrogen Energy, vol. 44, no. 20, pp. 9673–9674, Apr. 2019, doi: https://doi.org/10.1016/j.ijhydene.2019.02.174.

[4] H. L. Yip et al., "A Review of Hydrogen Direct Injection for Internal Combustion Engines: Towards Carbon-Free Combustion," Applied Sciences, vol. 9, no. 22, p. 4842, Nov. 2019, doi: https://doi.org/10.3390/app9224842.

[5] A. Onorati et al., "The role of hydrogen for future internal combustion engines," International Journal of Engine Research, vol. 23, no. 4, pp. 529–540, Mar. 2022, doi: https://doi.org/10.1177/14680874221081947.
[6] A. Parente and M. de Joannon, "Editorial: MILD Combustion: Modelling Challenges, Experimental Configurations, and Diagnostic Tools," Frontiers in Mechanical Engineering, vol. 7, Oct. 2021, doi: https://doi.org/10.3389/fmech.2021.726633.
[7] A. Cavaliere and M. de Joannon, "Mild Combustion," Progress in Energy and Combustion Science, vol. 30, no. 4, pp. 329–366, Jan. 2004, doi: https://doi.org/10.1016/j.pecs.2004.02.003.
[8] S. Mazumder and S. P. Roy, "Modeling Thermal Radiation in Combustion Environments: Progress and Challenges." Energies, vol. 16, no. 10, p. 4250, 2023, doi: 10.3390/en16104250.
[9] S. Zheng, R. Sui, Y. Sun, Y. Yang, and Q. Lu, "A Review on the Applications of Non-gray Gas Radiation Models in Multi-dimensional Systems." ES Energy & Environment, 2021, doi: 10.30919/esee8c423.
[10] L. Rothman, "HITEMP, the high-temperature molecular spectroscopic database." Journal of Quantitative Spectroscopy and Radiative Transfer, vol. 111, no. 15, pp. 2139-2150, 2010, doi: 10.1016/j.jqsrt.2010.05.001.
[11] Modest, M.F.; Mazumder, S. Radiative Heat Transfer, 4th ed.; Academic Press: New York, NY, USA, 2021.
[12] Hottel HC, Sarofim AF. Radiative transfer. New York: McGraw-Hill; 1967.
[13] M. Alberti, R. Weber, and M. Mancini, "Re-creating Hottel's emissivity charts for water vapor and extending them to 40 bar pressure using HITEMP-2010 database." Combustion and Flame, vol. 169, pp. 141-153, 2016, doi: 10.1016/j.combustflame.2016.04.013.

Norwegian Offshore Wind Farms: Pioneering Green Hydrogen for a Sustainable Energy Shift

T. Gogiyev*[1], S.K. Condon[1], M.D.B. Watanabe[1], F. Cherubini[1]

[1] Industrial Ecology Program, Department of Energy and Process Engineering, Norwegian University of Science and Technology (NTNU), Trondheim, Norway

Introduction

The urgency of the energy transition in the face of climate change has never been more pronounced. Among global greenhouse gas (GHG) emissions, those related to energy constitute the largest share, surging by 0.9% to a new high of over 36.8 billion metric tons of CO2 in 2022 [1]. However, energy plays a vital role in driving socio-economic progress, and the expansion of both the global population and the economies of developing nations in recent decades has resulted in a rapid surge in energy demand [2]. This upward trajectory in energy needs is projected to persist throughout the century due to ongoing socio-economic advancement [3, 4]. Thus, the imperative for a transition towards environmentally sustainable energy sources and technological advancements is unavoidable in order to address climate change and fulfill the escalating demands of a growing population.

Crucially, tackling this issue should not be approached with a one-size-fits-all mindset. Quite the opposite, a range of diverse energy sources ought to be taken into account to attain the ambitious goal of achieving net zero emissions by 2050 [5]. Hydrogen and hydrogen-based fuels, given their vast versatility, are poised to assume a potential role in addressing this challenge. Hydrogen finds applications across various facets of the energy sector and is projected to experience a sixfold increase from current levels, aiming to constitute 10% of total final energy consumption by 2050 [6]. Given its status as one of the fastest-growing renewable energy sources globally, offshore wind holds tremendous potential for integration with hydrogen [7]. This has paved the way for a potential strategy, which entails generating hydrogen through offshore electrolyzes situated alongside offshore wind farms. This would streamline distribution to Norway and enable exportation to Europe. Additionally, this work investigates the environmental impact of hydrogen leakage throughout the value chain. The widely employed 100-year global warming potential (GWP100) metric falls short in capturing the true warming potential of short-lived gases like hydrogen over shorter timeframes [8].

The main objective of this work is to investigate the potential and opportunities for producing offshore hydrogen from wind farms located off the coast of Norway. While there have been numerous studies conducting life cycle assessment (LCA) on comparable offshore hydrogen production scenarios, this endeavor seeks to offer a more comprehensive perspective by introducing novel value chains and incorporating assessments of the environmental impact stemming from hydrogen losses.

Methodology

This study establishes a baseline and defines three alternative scenarios for producing and distributing hydrogen derived from offshore wind farms. In all four scenarios, proton exchange membrane (PEM) electrolysis at 30 bar is employed for green hydrogen production. Furthermore, each scenario encompasses stages such as electricity generation, hydrogen

* Corresponding author: teymur.gogiyev@ntnu.no

production, compression, storage, as well as intermediate and final transportation of hydrogen for consumption. Additionally, this involved upscaling the operations to mirror the conditions and demands of a commercial setting.

Comprehensive life cycle inventories were compiled for every phase within both the baseline and alternative scenarios. Given that GHG emissions were presumed to be primarily attributable to material usage and fuel consumption during installation, these aspects were the main points of the inventory. The LCA was a cradle-to-gate study spanning the energy generation for electrolysis to final use distribution. The ReCiPe Midpoint (H) method was selected for impact assessment, placing primary emphasis on GWP100.

Discussion and Conclusions

During the conference, we will showcase a comprehensive comparison between the baseline and alternative scenarios, taking into account the influence of hydrogen leakage. Our first findings indicate that the best-case scenario involves bottom-fixed offshore wind turbines, demonstrating a lower environmental footprint in comparison to floating offshore wind turbines for energy generation. Moreover, the results suggest that the salt cavern storage method is the preferred option over compression and tank storage in terms of emission quantities. Finally, this study emphasizes the vital importance of considering hydrogen leakage, as it cannot be overlooked in the environmental assessment of the entire hydrogen value chain.

References

[1] IEA, "CO2 Emissions in 2022," Paris 2023. [Online]. Available: https://www.iea.org/reports/co2-emissions-in-2022

[2] S. Bilgen, "Structure and environmental impact of global energy consumption," (in English), *Renew Sust Energ Rev,* vol. 38, pp. 890-902, Oct 2014, doi: 10.1016/j.rser.2014.07.004.

[3] J. Rogelj *et al.*, "Scenarios towards limiting global mean temperature increase below 1.5 degrees C," (in English), *Nat Clim Change,* vol. 8, no. 4, pp. 325-+, Apr 2018, doi: 10.1038/s41558-018-0091-3.

[4] B. J. van Ruijven, E. De Cian, and I. S. Wing, "Amplification of future energy demand growth due to climate change," (in English), *Nat Commun,* vol. 10, Jun 24 2019, doi: ARTN 2762 10.1038/s41467-019-10399-3.

[5] D. Gielen, F. Boshell, D. Saygin, M. D. Bazilian, N. Wagner, and R. Gorini, "The role of renewable energy in the global energy transformation," (in English), *Energy Strateg Rev,* vol. 24, pp. 38-50, Apr 2019, doi: 10.1016/j.esr.2019.01.006.

[6] IEA, "Global Hydrogen Review 2021," 2021. Accessed: 04/10/2023. [Online]. Available: https://iea.blob.core.windows.net/assets/5bd46d7b-906a-4429-abda-e9c507a62341/GlobalHydrogenReview2021.pdf

[7] IEA, "Global Energy Review 2021," Paris, 2021. [Online]. Available: https://www.iea.org/reports/global-energy-review-2021

[8] I. B. Ocko and S. P. Hamburg, "Climate consequences of hydrogen emissions," (in English), *Atmos Chem Phys,* vol. 22, no. 14, pp. 9349-9368, Jul 20 2022, doi: 10.5194/acp-22-9349-2022.

Novel test and diagnostic methods for membrane electrolysis technologies

O. Mogg*[1], B. Grabner[1], A. Trattner[1,2]

[1]HyCentA Research GmbH, Graz, Austria
[2]Institute of Thermodynamics and Sustainable Propulsion Systems, Graz University of Technology, Graz, Austria

Introduction

Water electrolysis is a key technology for the conversion of electricity from fluctuating renewable sources to hydrogen and forms the backbone of future energy systems. Hydrogen can be stored unlimited and subsequently converted back into electricity or employed in various sectors, such as transportation and industry [3][6]. Therefore, water electrolysis serves as an integrative element connecting sectors like electricity, heating, and mobility within the context of power-to-liquid and power-to-gas concepts [6]. Various types of water electrolysis exist, differing in their operational temperature and electrolyte composition. Among these, membrane-based electrolysis technologies, such as Proton Exchange Membrane (PEM) and Anion Exchange Membrane (AEM), show great promise [4][5][6]. They meet all the criteria necessary for hydrogen production from renewable energy sources or grid stabilization, including short response times, a wide current density range, high efficiency, and the ability to operate under differential pressure conditions [1][4][5].

Despite the relatively high Technology Readiness Level (TRL) of PEM technology, both PEM and AEM technologies still confront several challenges, including a) reducing overall costs, b) minimizing the demand for critical raw materials, c) enhancing efficiency and d) increasing durability [4][5].

Electrolysis stacks coupled with renewable energy sources face dynamic and intermittent power supply, leading to new challenges such as accelerated aging when compared to steady-state operation. The degradation rate depends on multiple factors including the corrosive electrical environment, operating conditions, materials used in components, and more [1]. Usually, degradation of electrolysis systems is studied ex-situ employing a posteriori chemical analysis of key components (membrane, catalytic layers, bipolar plate, …) or in small single cell setups [2]. However, the methods and techniques employed are not representative for stacks and large active cell areas required for scaling up green H_2 production. Challenges such as thermal management, pressure distribution, uniform water supply, and electrode contact become significantly more complex as cell area increases, and these factors have a substantial impact on aging processes. The lack of appropriate testing facilities underscores the urgent need for further research in this area.

To address these issues, it is essential to transition characterization and measurement techniques from single-cell and small-scale stack testing to the required large-scale applications, including IV-characteristic curves and electrochemical impedance spectroscopy (EIS).

* Corresponding author: mogg@hycenta.at

As durability testing comes with high costs, there is also a significand demand in the development and definition of accelerated stress tests (ASTs), to minimize testing durations [7]. Furthermore, establishing standardized testing procedures and a Design-Verification and -Validation Plan (DVP) is crucial to contribute to the standardization and commercialization of membrane electrolysis stacks.

Methodology

To gain a deeper understanding of aging and degradation mechanism of large-scale electrolysis stacks, considering realistic operation conditions, a full-size stack testbench will be set up, which will feature novel diagnostic methods and is able to test membrane electrolysis stacks in different performance classes up to 1 600 cm² active cell areas. The novel test bench will be equipped with cutting-edge measurement technology and can simulate various operating states. It will be highly flexible in its setup to be able to test various units under testing (UUTs). The main features are listed below:

- Possibility to test PEM and AEM stacks
- Current densities up to 4 A/cm^2
- Stack voltage up to 80 V
- Overall power range up to 160 kW
- Temperature ranges from 40 – 80 °C
- Anode pressure up to 10 bar, cathode pressure from 20 – 50 bar
- Cell voltage monitoring measurements
- Long-term testing (new durability insights).

Besides the possibility to analyze stack performance, efficiency and the behavior in variable operating ranges, the utilization of the new testbench enables the exploration of innovative methodologies and analytical strategies concerning both in-situ and ex-situ degradation monitoring techniques.

Electrochemical characterization methods such as IV-curves, EIS and CV (cyclic voltammetry) measurements will also be part of the measurement activities on the 160 kW testbench. Illustrated in Figure 1 are sample outcomes obtained through EIS measurements conducted on the pre-existing 15 kW stack testbench at HyCentA Research GmbH.

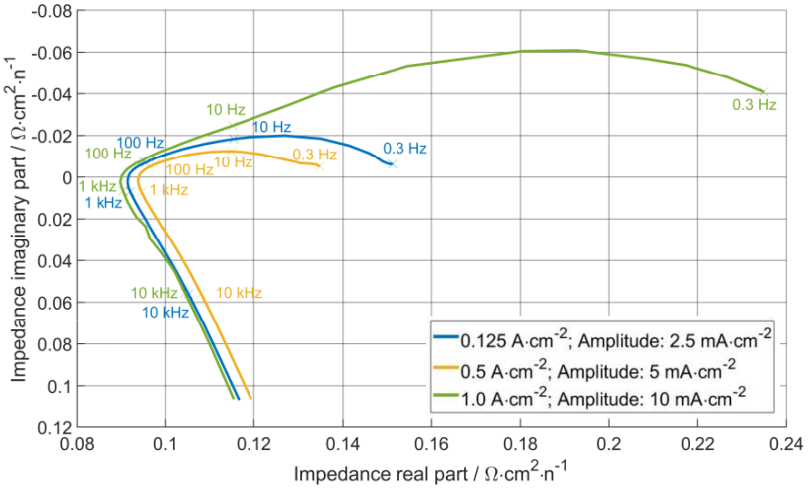

Figure 1: Nyquist plot for an electrolysis stack at different current density levels

Complementary to electrochemical characterization methods chemical analyses, such as electrolyte analysis, mixed bed resin analysis, fluoride monitoring, product gas analysis etc. will aid in gaining an understanding of aging processes. Correlations between gas, electrolyte or resin compositions and degradation mechanism as well as electrolysis stack performance parameters (faraday efficiency, current density, energy consumption) will be investigated.

In addition to moderate operating conditions reflecting long-term operation, tests shall also be performed under increased pressure, temperature and current load in order to accelerate aging processes. The scalability of existing AST protocols from single cell level to large scale stacks will be evaluated and the feasibility of replicating the accelerated stress conditions will be assessed. After defining appropriate acceleration factors and stressing conditions considering the big variety of stack designs AST protocols for large scale membrane electrolysis stacks will be developed and tested.

To identify approaches that effectively mitigate degradation the efficacy of various mitigation strategies will be examined. This thesis places a strong emphasis on optimizing operational parameters with the ultimate objective of minimizing degradation to the greatest extent possible. Through the application of novel methodologies and analyses, this research aims to enhance our comprehension and practical handling of degradation processes.

Subsequently standardized test protocols and procedures for stack testing, including performance evaluation, durability assessment, and safety testing will be developed, incorporating relevant international standards, guidelines and best practices to provide a common framework for stack assessment. A standardized DVP for membrane electrolysis stacks, outlining the necessary steps and requirements for design, verification, and validation will be defined. The DVP will include performance targets, test procedures, and acceptance criteria for each stage of the DVP (design validation, prototype testing, and product certification).

Through the whole research process and all work packages systematic literature research on the current state of the art will be conducted.

Discussion

The research presented in this study addresses critical issues in the field of membrane electrolysis stacks, which play a pivotal role in the conversion of renewable energy to hydrogen, a versatile and sustainable energy carrier. The study's primary objective is to comprehensively investigate the degradation mechanisms and performance optimization of these stacks under various operating conditions. The challenges associated with membrane electrolysis stacks, including degradation, cost reduction, and performance enhancement, are thoroughly discussed. Notably, these challenges are exacerbated when stacks are subjected to dynamic and intermittent power supply, making accelerated aging a significant concern.

By transitioning the techniques used for characterizing and measuring single-cell and small-scale stack testing to large-scale applications, the advancement of membrane electrolysis on a megawatt scale are expected to reach a higher level. The introduction of the new testbench, along with innovative diagnostic capabilities, offers the potential to test

various types of stacks across different performance categories and operating conditions. As a result, the following research outcomes related to membrane electrolysis are anticipated:

- Enhanced insights into the mechanisms of membrane and electrode degradation
- Novel approaches for real-time degradation monitoring
- Improved stack longevity and efficiency
- Development of test cycles and ASTs that accurately replicate real-world operational modes
- Reduction in overall costs

The development of ASTs is expected to prove as an effective strategy for reducing test duration while simulating extreme conditions, thereby contributing to more efficient research and development efforts. Furthermore, the development of standardized testing protocols, procedures, and a DVP is expected to promote the standardization and commercialization of membrane electrolysis stacks.

Conclusions

The establishment of a full-size stack testbench equipped with beyond state-of-the-art measurement technology signifies a significant leap forward, enabling comprehensive testing and analysis of these stacks under real-world operating conditions.

The primary research objectives involve the in-depth exploration of degradation mechanisms, the optimization of stack performance, and the investigation of mitigation strategies. By focusing on both in-situ and ex-situ degradation monitoring techniques, this study aims to make substantial contributions to the development of more durable and efficient membrane electrolysis stacks.

Moreover, the development of standardized testing protocols, procedures, and a DVP holds the potential to facilitate the standardization and commercialization of membrane electrolysis stacks. This holistic approach aligns with the broader objectives of advancing clean energy technologies and promoting the widespread adoption of hydrogen as a sustainable energy carrier.

In conclusion, this research represents a significant step toward achieving cleaner and more sustainable energy solutions, with membrane electrolysis technology playing an important role in this transformative journey. Expected outcomes include advancements in stack performance, durability, and cost-effectiveness, contributing to the overall goals of a greener and more sustainable energy future.

References

[1] Zhang, Liang, Wang, Sun, Wang, Xie, Wu, Bai, Hamdy, Chen, Zou, "Status and perspectives of key materials for PEM electrolyzer", Nano Research Energy, 2022, 1: e9120032.

[2] S. Boulevard, J. J. A. Kadjo, A. Thomas, B. Grondin Perez, S. Martemianov, "Characterization of Aging Effects during PEM Electrolyzer Operation Using Voltage Instabilities Evolution", Russian Journal of electrochemistry, 2022, Volume 58, No. 4, pp. 258-270.

[3] Feng, Zi Yuan, Liu, Wei, Zhang, Li, Wang, " A review of proton exchange membrane water electrolysis on degradation mechanisms and mitigation strategies ", Journal of Power Sources, 2017, 366 (2017) 33-55.

[4] Miller, Bouzek, Hnat, Loos, Bernäcker, Weißgärber, Röntzsch, Meier-Haack, "Green hydrogen from anion exchange membrane water electrolysis: a review of recent developments in critical materials and operating conditions", Sustainable Energy Fuels, 2020, 4, 2114–2133.

[5] Grigoriev, Fateev, Bessarabov, Millet, "Current status, research trends, and challenges in water electrolysis science and technology", international journal of hydrogen energy, 2020.

[6] Klell M., Eichlseder H., Trattner A., " Wasserstoff in der Fahrzeugtechnik: Erzeugung, Speicherung, Anwendung ", Springer Fachmedien Wiesbaden GmbH, Edition 4, 2018, ISBN: 978-3-658-20447-1.

[7] Kuhnert, Hacker, Bodner, " A Review of Accelerated Stress Tests for Enhancing MEA Durability in PEM Water Electrolysis Cells ", International Journal of Energy Research, Volume 2023, Article ID 3183108, 23 p.

Optimization methodology of hydrogen supply chain at the scale of an industrial cluster

N. C. Tano*[1,2,3], A. Zoughaib[1], S. Le Bourdiec[2], L. M. Malbec [3]

[1]Mines Paris – Université PSL, Centre d'Efficacité Energétique des Systèmes, 5 rue Léon Blum, 91120 Palaiseau, France.
[2]EDF R&D, Avenue des Renardières, 77250 Moret-Loing-et-Orvanne, France.
[3]IFP Energies Nouvelles, 1-4 Avenue du Bois Préau, 92852 Rueil-Malmaison, France.

Introduction

For several years now, plans to deploy hydrogen to decarbonize the economy have been multiplying around the world. In its Net Zero by 2050 scenario, the International Energy Agency (IEA) estimates an increase in hydrogen demand from 70 Mt in 2020, 96% of which comes from fossil sources, to 530 Mt in 2050, 75% of which will be produced outside of industrial sites and will therefore have to be transported while more than 90% of this production will have to be low carbon (**Figure 1**) [1]. These figures provide insight into the dual challenge of low-carbon hydrogen production and the deployment of delivery infrastructures. These infrastructures are still largely non-existent, and their deployment will largely depend on local initiatives at the regional, departmental or city level. It is therefore essential to optimize the hydrogen infrastructure at the local scale, with an integrated approach covering the issues of production, storage, transport, and distribution, as well as uses and demand. The literature proposes many case studies, but they are very often at the country level, and do not consider the whole hydrogen value chain or all available technologies.

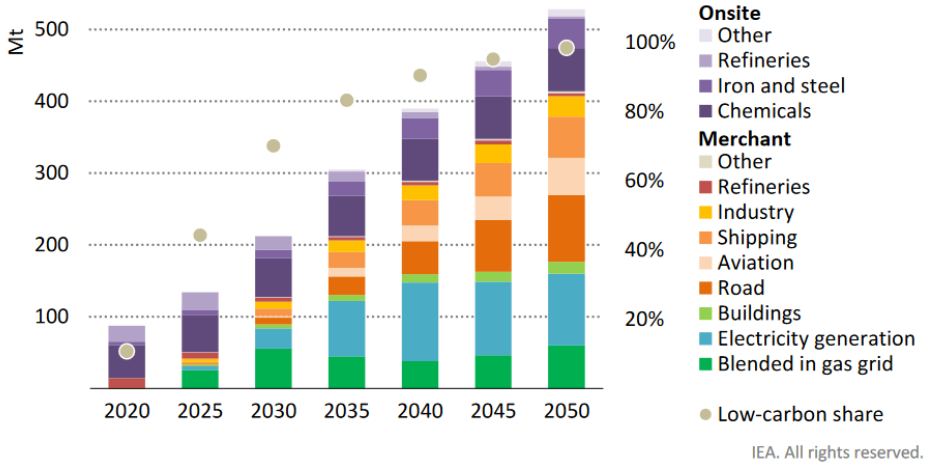

Figure 1: World hydrogen production by 2050 according to the Net Zero scenario of IEA [1]

As described in the literature, hydrogen value chain design is a strategic and tactical problem in the context of supply chain management. It is a complex problem that usually requires mathematical optimization approaches. In this context, several decision-support tools have been developed in recent years. These tools are often classified into three categories according to their spatial coverage and, above all, the main purpose of their modeling [2]. The first category includes Energy System Optimization Models (ESOMs), which model in detail every

* Corresponding author: n-guessan-charles.tano@minesparis.psl.eu

component within the energy system, including those related to hydrogen. The second are Geographically Explicit Optimization Models (GEOMs), focusing on the entire hydrogen supply system, usually used for local-level value chain. And finally, the third family, called Refueling Station-locating Optimization Models (ReSOMs), consists of models for optimizing the location of refueling stations for hydrogen-powered vehicles. Given their significance in assessing the entire hydrogen supply system, the first two categories of models appear to be the most relevant.

However, due to their intrinsic characteristics, the ESOMs and GEOMs are very often limited regarding the optimal design of the hydrogen value chain in a context of global decarbonization of the economy. These limitations are the exogeneity of spatio-temporal hydrogen demand and the inadequate modeling of transport and distribution infrastructures for GEOMs and ESOMs, respectively. To overcome these, a hybrid approach is strongly recommended since each of these model family address the limitation of the other one. In fact, one of the fundamental characteristics of energy system model is that both supply and demand are integrated, implying that one automatically adjusts as the other changes. As for geographically explicit model, spatial constraints are explicitly considered which allows appropriate modeling of transport and distribution. In the literature consulted so far, only Rosenberg et al. [3] adopt such a hybrid approach, which indicates the necessity for additional investigation in this particular field. Furthermore, regarding the development of the models in particular, improvements can be made based on the current state of the art. On one hand, for ESOMs, it seems appropriate to consider the studied energy system as part of a global one by taking into account the interconnections with other regions, as opposed to the approach proposed in the work of Rosenberg et al. [3]. Moreover, the integration of other end uses in addition to transport, such as industry, is strongly encouraged. Such models already exist in the literature. Some good examples are JRC-EU-TIMES [4] and MIRET-EU [5]. On the other hand, regarding GEOMs, the development of multi-energy and multi-material models that could take into account hydrogen-related value chains such as those of synthetic fuels, the raw materials and energy supply system and the co-products valorization from hydrogen production processes, seems essential. In the literature of GEOMs for hydrogen supply chain optimization, only a few works consider such systemic approach [[6], [7]]. This type of method is more common in the literature of eco-industrial park design, with some good examples being the works of Ghazouani [8] and Wissocq [9]. If they are well adapted, they could be extremely relevant for supply chain optimization, especially for hydrogen. Finally, to the best of our knowledge, there is no research work covering simultaneously all the aforementioned aspects. Thus, the aim of the current research is to address this existing gap.

Methodology

The main objective of this doctoral research thesis is to propose a generic methodology framework in order to optimize the hydrogen value chain at a local scale. The specific characteristics of this methodology are as follow:

- Hybrid optimization tool resulting from the combination of an energy system model and a geographically explicit model.
- Optimization will be globally deterministic and mono objective. Uncertainties will be taken into consideration through sensitivity analysis.
- The overall performance measure will be economic with environmental and technical constraints.
- Multi-period modeling will be considered to take into account prospective scenarios.

- The hybridization structure will be based on the generalized strategy used in the work of Rosenberg et al. [3]. This is shown in **Figure 2**. Briefly, from given techno-economic data of the hydrogen infrastructure, the ESOM will optimize the overall energy system and thus, give the hydrogen demand profile of the studied area. This parameter will be used as an input for the GEOM. The latter will then optimize in detail the hydrogen infrastructure according to the demand profile received and subsequently, update the techno-economic specification in the energy system model. These steps will iterate until convergence: the convergence criterion being the equality between the demand profiles of the iteration i and the iteration i-1.

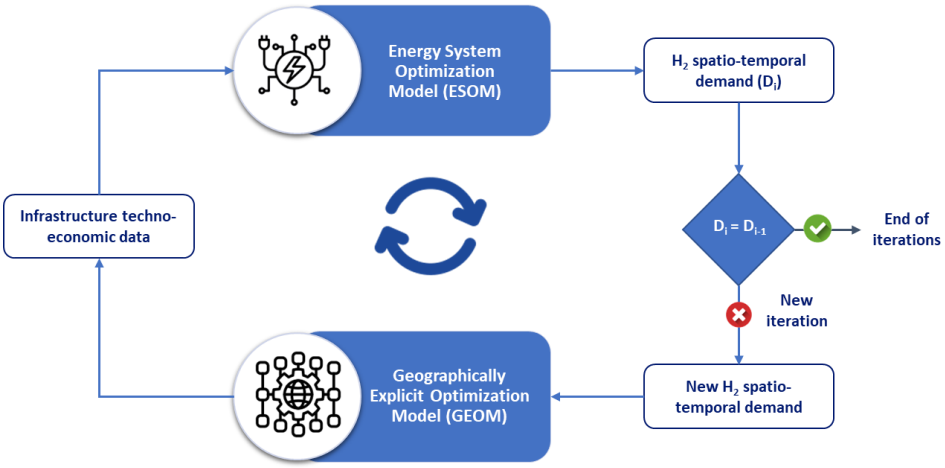

Figure 2: Generalized structure of the hybridization of ESOM and GEOM

- Regarding the ESOM, MIRET-EU will be used. It is a multiregional and inter-temporal optimization model of the European energy system developed by IFP Energies Nouvelles [5], based on the TIMES model generator. The benefit of using this model resides in the fact that the overall European system is considered with the different connection between the countries of the system. However, further development will be needed in the context of this work for the purpose of representing a local energy system within the overall perimeter.
- As for GEOM, PHOENIX, an optimization tool resulting from a partnership between EDF and Mines Paris – PSL will be used. This tool is based on MILP (Mixed Integer Linear Programming) algorithms developed in the works of Ghazouani [8] and Wissocq [9] that allow multi-material and multi-energy integration within a single industrial process or an industrial cluster. For this thesis, specific aspects of the hydrogen value chain, such as truck transport and the refinement of hydrogen production technologies, will be modelled.

An overview of the resulting methodology is presented in **Figure *3***. Overall, based on prospective decarbonization scenarios at the European scale and data collection, the hybrid optimization tool will propose an optimized hydrogen value chain for the study area. Dunkirk, one of the main French industrial regions, will be used as a case study. The infrastructure that will be developed will make it possible to meet the demand for hydrogen in the transport and

industrial sectors by 2050. In addition, all sources of hydrogen will be considered, the aim being to be able to propose optimal solutions without any initial preconceptions.

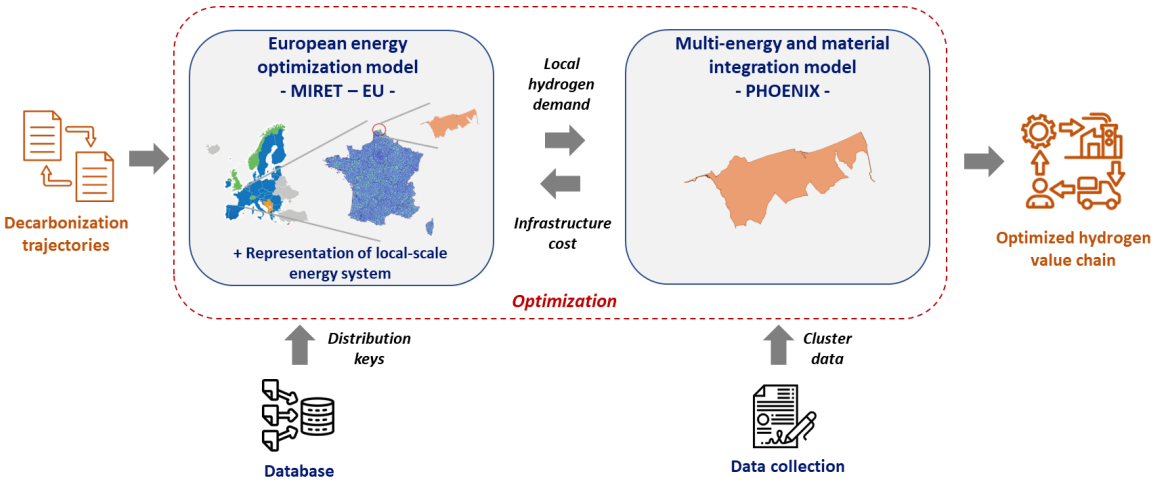

Figure 3: Proposed methodology

Expected Results

At the end of this work, the overall expected results are the validation of the proposed methodological framework for hydrogen value chain optimization, the proposal of an optimized hydrogen value chain in one of the major French industrial territories according to European and national decarbonization scenarios, and finally, an assessment of the limitations of these scenarios in terms of territorial resource availability.

References

[1] IEA, "Net Zero by 2050: A Roadmap for the Global Energy Sector," International Energy Agency, 2021. [Online]. Available: https://www.iea.org/reports/net-zero-by-2050

[2] P. Agnolucci and W. McDowall, "Designing future hydrogen infrastructure: Insights from analysis at different spatial scales," *International Journal of Hydrogen Energy*, vol. 38, no. 13, pp. 5181–5191, May 2013, doi: 10.1016/j.ijhydene.2013.02.042.

[3] E. Rosenberg, A. Fidje, K. A. Espegren, C. Stiller, A. M. Svensson, and S. Møller-Holst, "Market penetration analysis of hydrogen vehicles in Norwegian passenger transport towards 2050," *International Journal of Hydrogen Energy*, vol. 35, no. 14, pp. 7267–7279, Jul. 2010, doi: 10.1016/j.ijhydene.2010.04.153.

[4] S. Simões *et al.*, *The JRC-EU-TIMES model - Assessing the long-term role of the SET Plan Energy technologies*. 2013. doi: 10.2790/97596.

[5] G. S. Seck *et al.*, "Hydrogen and the decarbonization of the energy system in europe in 2050: A detailed model-based analysis," *Renewable and Sustainable Energy Reviews*, vol. 167, p. 112779, Oct. 2022, doi: 10.1016/j.rser.2022.112779.

[6] Y. Ibrahim, D. M. Al-Mohannadi, and P. Linke, "Modelling and Optimization of Hydrogen Production in an Industrial Cluster Accounting for Economic Cost and Environmental Impact," *Chemical Engineering Transactions*, vol. 88, pp. 439–444, Nov. 2021, doi: 10.3303/CET2188073.

[7] Y. Ibrahim and D. M. Al-Mohannadi, “Optimization of low-carbon hydrogen supply chain networks in industrial clusters,” *International Journal of Hydrogen Energy*, vol. 48, no. 36, pp. 13325–13342, Apr. 2023, doi: 10.1016/j.ijhydene.2022.12.090.
[8] S. Ghazouani, “Modèles linéaires d’optimisation pour la conception simultanée de réseaux de matière et de chaleur d’un écoparc industriel,” Ph.D. dissertation, Ecole nationnale des Mines de Paris - Université PSL, France, 2016.
[9] T. Wissocq, “Méthodes d’optimisation pour la conception d’éco-parcs industriels en considération de la dynamique temporelle,” Ph.D. dissertation, Ecole nationnale des Mines de Paris - Université PSL, France, 2021.

Optimization of Heat Treatment in Ni-Cr-Mo Wrought Steel for Hydrogen Environment

A. Mento*[1], A. Donato[2], M. Buccioni[2], E. Proverbio[1]

[1]Department of Engineering, University of Messina, Contrada di Dio, 98166 Messina, Italy
[2]Materials & Processes Engineering, Baker Hughes, Via Felice Matteucci 2, 50127 Firenze, Italy

Introduction

The energy transition process requires energy production through the management of non-polluting sources in line with what is foreseen in the Hydrogen Roadmap Europe [1]. To make the European system more sustainable in the long term through the decarbonization of all sectors, it is necessary to adopt solutions based on renewable and sustainable sources such as hydrogen, in line with the European Strategy [2]. Given the impossibility of replacing the current natural gas transport networks and related energy production plants for economic and safety reasons, blended hydrogen and natural gas transport methods are currently proposed [3]. However, the future aim is to use 100% pure hydrogen, especially produced from renewable energy sources. In this context, it is essential to solve the problems arising from the interaction of hydrogen with metal alloys. Hydrogen can damage the metal structure and, in some cases, induce brittle behavior. This phenomenon is called hydrogen embrittlement (HE) and it can be manifested in different mechanisms, such as hydrogen enhanced decohesion (HEDE) [4] [5], hydrogen enhanced localized plasticity (HELP) [6] and adsorption induced dislocation emission (AIDE) [4] [7]. It has been shown that these mechanisms can also act simultaneously [8]. In view of using hydrogen instead of natural gas, it is necessary to clarify the interaction mechanisms between the microstructure of metals deriving from manufacturing process, especially from heat treatment, and hydrogen in turbomachinery applications. The main materials used in turbomachines and gas pipelines are austenitic, ferritic, and martensitic steels and metal alloys such as nickel-based one [9].

From this perspective, a high-strength Ni-Cr-Mo martensitic steel has been selected for this research study because of the promising combination of high tensile properties, toughness, and microstructure features. This class of steels is widely selected for various mechanical components subjected to high stress, such as shafts, discs, gears, axles, bolting, and others [10]. Currently, there are few studies about the interaction of hydrogen with these steels [11] [12]. Studies have been conducted on the possible effect of hydrogen embrittlement in martensitic steels [13] caused by microstructural characteristics such as type of martensite, prior austenite grain size, presence of impurities. However, some of them are conflicting and the effect of these factors needs further investigation. It is known that the interaction of hydrogen with the microstructure of martensitic steels is strongly dependent on the density and type of lattice imperfections such as dislocations, grain boundaries, vacancies but also on the presence of alloy elements and carbides [14] [15] [16]. These factors act as hydrogen trap sites influencing the diffusivity and solubility of hydrogen in the martensitic matrix. Therefore, it is important to understand the type of interaction between microstructural features and hydrogen.

* Corresponding author: adriana.mento@unime.it

Considering that the microstructure is a direct consequence of the heat treatment, the aim of the present research project is to study how the mechanical and microstructural properties, obtained from a specific heat treatment, influence the alloy behavior in air and hydrogen environment. In this work it is proposed an optimization of heat treatment, for a good combination of mechanical properties and hydrogen embrittlement resistance. To achieve this objective, the tempering curves, mechanical properties, microstructural and fractographic characterization have been investigated.

Methodology

Materials

The Ni-Cr-Mo grade object of this study has been produced by steelmaking, bottom pouring, vacuum arc remelting and forging process. Forging dimensions consisted in 400mm of external diameter and 80 mm of thickness. The chemical composition (according to BS EN 10083-3:2006 standard [17]), in weight percentage, is reported in Table 1.

Table 1 Chemical composition of Ni-Cr-Mo forged steel

Element	**C**	**Mn**	**P**	**S**	**Si**	**Ni**	**Cr**	**Mo**
wt.%	0.29	0.54	0.005	0.003	0.21	3.43	1.51	0.43

The forging disk was delivered as austenitized at 850°C with a holding time of 600 minutes and quenched in water. Then, it was tempered at 565°C with a holding time of 750 minutes, followed by air cooling. It has been identified as in HT1 condition.

By constructing the tempering curve, it is possible to study the effect of the tempering treatment on the selected steel, therefore the variation of the properties in air and in hydrogen environment as a function of the tempering temperature. For this purpose, the selected temperatures have been 545°C, 585°C, 605°C and 625°C and material has been identified as in condition HT2, HT3, HT4, HT5 respectively.

Beside the experimental characterization, the phase transformations that occur in this steel grade, the type of secondary phases, the critical cooling rates and the start and finish martensitic temperatures, have been studied by JMatPro® software. In fact, this tool allows to obtain plot of step temperatures, Time-Temperature-Transformation (TTT) and Continuous-Cooling-Transformation (CCT).

Characterization in air environment

The Ni-Cr-Mo steel mechanical characterization in air environment has been conducted at room temperature. The steel in HT1 condition has been subjected to a tensile test with a Universal testing machine Shenck according to ASTM E8/E8M-22 standard [18]. The standard type 3 specimen has been tested in strain control mode with strain rate of 0.015 mm/mm/min. To evaluate the impact toughness, Charpy V notch impact test has been conducted as per ASTM E23-23a standard [19], using the Zwick Roell Charpy impact machine (maximum energy of 450J). Brinell hardness 187.5/2.5 has been measured by Universal hardness tester of Innovatest and following the instructions reported in ASTM E10-23 standard [20]. Finally, a set of fracture toughness with compact tension (CT) specimens 25 mm thick, has been carried out according to the ASTM E399-22 standard [21]. Specimen has been machined out as per C-R orientation from figure 1c of the same

standard. The same testing campaign has been conducted on the other HT2, HT3, HT4, HT5 conditions.

Characterization in hydrogen environment

The Ni-Cr-Mo steel characterization in hydrogen started from the physical properties measurement. Plates with a thickness of 0.5 mm, have been subjected to permeation test in hydrogen environment at room temperature and at 200°C according to the BS EN ISO 17081-2014 standard [22], to estimate the hydrogen diffusion coefficient. The thermal desorption spectroscopy (TDS) has been conducted on pre-charged plates of 0.5 mm thickness at 70 bar pressure of hydrogen and 200°C, to estimate the hydrogen binding energies, the desorbed diffusible hydrogen, and the total desorbed hydrogen. From this test, binding energies have been associated with the possible trap sites (lattice defects and precipitates) to understand how they influence the diffusivity and solubility of hydrogen in the lattice. Such result could help in defining the microstructural features responsible for reversible and irreversible hydrogen trapping.

Ni-Cr-Mo steel in HT1 condition has been subjected to Slow Strain Rate Test (SSRT) at 70 bar of hydrogen (purity grade 6.0), at room temperature, 80°C and 150°C using notched specimen. Test according to the ASTM G142-98 standard [23] with a displacement rate of $2x10^{-5}$ mm/s, to estimate the Notch Tensile Strength (NTS) in hydrogen. The SSRT of all other HT conditions has been conducted at the temperature associated with the highest HE obtained in the HT1 condition. SSRT in air environment has been conducted to compare results with the ones in hydrogen. The most relevant parameter to evaluate the embrittlement rate was Notched Tensile Strength Ratio (NTSR) (Eq. 1) [24].

$$NTSR = \frac{NTS_{H_2}}{NTS_a} \quad (1)$$

In which NTS_{H_2} is the NTS in the hydrogen environment and NTS_a the same value in the air one.

Microstructural and fractographic characterization

The microstructure and fractographic characterization of all the samples consisted of optical microscopy with Leica DFC 450, Scanning Electron Microscopy (SEM) with Tescan AmberX and Electron BackScattered Diffraction (EBSD) with Aztec 5.0 software. The metallographic characterization was carried out using the metallographic microscopy Leica M 6000M on chemically etched samples. By coupling the microstructural analyses, it has been possible to obtain a complete characterization of the microstructure through the identification and distribution of the phases, characterization of the grain boundaries, crystallographic orientation. The fractography characterization led to the observation of change in the fracture mode in steels moving from air to hydrogen because of the susceptibility to hydrogen embrittlement of martensitic steels.

Conclusions

This research project has been able to provide a complete characterization, both mechanical and microstructural, of Ni-Cr-Mo steel when subjected to different tempering treatments both in air and in hydrogen environment. A correlation has been proposed between the

mechanical properties and the microstructural features of the steel, as a result of the applied heat treatment, and the embrittlement level they promoted. The influence of alloying elements on hydrogen trapping has been studied as well. The heat treatment for the best combination of mechanical properties in air and hydrogen environment has been proposed.

References

[1] "A sustainable pathway for the European energy transition", *Publication Office*, 2016.

[2] "A hydrogen strategy for a climate-neutral Europe", *European Commission*, 2020.

[3] M. W. Melaina, O. Antonia e M. Penev, "Blending Hydrogen into Natural Gas Pipeline Networks: A review of Key Issues", National Renewable Energy Laboratory, Golden, 2013.

[4] R. A. Oriani, "A Mechanistic Theory of Hydrogen Embrittlement of Steels", *Berichte der Bunsengesellschaft für physikalische Chemie*, vol. 76, pp. 848-857, 1972.

[5] S. Lynch, "Hydrogen embrittlement phenomena and mechanisms", *Corrosion Reviews*, vol. 30, pp. 105-123, 2012.

[6] C. D. Beachem, "A new model for hydrogen-assisted cracking (hydrogen "embrittlement")", *Metallurgical Transactions*, vol. 3, pp. 441-455, 1972.

[7] I. M. Robertson, "The effect of hydrogen on dislocation dynamics", *Engineering Fracture Mechanics*, vol. 68, n. 6, pp. 671-692, 2001.

[8] A. Traidia, E. Chatzidouros e M. Jouiad, "Mechanisms of hydrogen assisted cracking- A review", in *International Conference on Hydrogen Effects on Material Behaviour and Corrosion Deformation Interactions*, Moran, 2033.

[9] E. Stefan, B. Talic., Y. Larring, A. Gruber e T. A. Peters, "Materials challenges in hydrogen-fuelled gas turbines", *International Materials Reviews* , pp. 1-26, 2021.

[10] R. Branco, J. D. Costa, F. V. Antunes e S. Perdigão, "Monotonic and Cyclic Behavior of DIN 34CrNiMo6 Tempered Alloy Steel", *Metals*, vol. 6, p. 98, 2016.

[11] A. Kuduzović, M. C. Poletti, C. Sommitsch, M. Domankova, S. Mitsche e R. Kienreich, "Investigations into the delayed fracture susceptibility of 34CrNiMo6 steel, and the opportunities for its application in ultra-high-strength bolts and fasteners", *Materials Science & Engineering: A*, vol. 590, pp. 66-73, 2014.

[12] A. K. B. A. M. Polyanskiy, V. A. Polyanskiy, C. Sommitsch e Y. A. Yakovlev, "Multichannel diffusion vs TDS model on example of energy spectra of bound hydrogen in 34CrNiMo6 steel after a typical heat treatment", *International Journal of Hydrogen Energy* , vol. 41, pp. 8627-8634, 2016.

[13] W. M. Garrison e N. R. Moody, "Hydrogen embrittlement of high strength steels", in *Gaseous Hydrogen Embrittlement of Materials in Energy Technologies*, Elsevier, 2021, pp. 421-492.

[14] J. Xu, X. Z. Yuan, X. K. Sun e B. M. Wei, "Hydrogen permeation and diffusion in a 0.2C-13Cr martensitic stainless steel", *Scripta metallurgica et materialia*, vol. 29, pp. 925-930, 1993.

[15] H. J. Seo, Y.-U. Heo, J. N. Kim, J. Lee, S. Choi e C. S. Lee, "Effect of V/Mo ratio on the evolution of carbide precipitates and hydrogen embrittlement of tempered martensitic steel", *Corrosion Science*, vol. 176, 2020.

[16] S. A. Golovanenko, V. N. Zikeev, E. B. Serebryanaya e L. V. Popova, "Effect of alloying elements and structure on the resistence of structural steels to hydrogen embrittlement", *Metal Science and Heat Treatment*, vol. 20, p. 3.14, 1978.

[17] BS EN 10083-3:2006, "Steels for quenching and tempering. Part 3: Technical delivery conditions for alloy steels", British Standard, 2008.

[18] ASTM E8/E8M-22 , "Standard Test Methods for Tension Testing of Metallic Materials", ASTM International, 2022.

[19] ASTM E23-23a, "Standard Test Methods for Notched Bar Impact Testing of Metallic Materials", ASTM International, 2023.

[20] ASTM E10-23, "Standard Test Method for Brinell Hardness of Metallic Materials", ASTM International, 2023.

[21] ASTM E399-22, "Standard Test Method for Plane-Strain Fracture Toughness of Metallic Materials", ASTM International, 2022.

[22] BS EN ISO 17081:2014, "Method of measurement of hydrogen permeation and determination of hydrogen uptake and transport in metals by an electrochemical technique", BSI Standards Publication, 2014.

[23] ASTM G142-98, "Standard Test Method for Determination of Susceptibility of Metals to Embrittlement in Hydrogen Containing Environments at High Pressure, High Temperature, or Both", ASTM International, 2022.

[24] ASTM G129-21, "Standard Practice for Slow Strain Rate Testing to Evaluate the Susceptibility of Metallic Materials to Environmentally Assisted Cracking", ASTM International, 2021.

Optimization of storage and compression for hydrogen refueling stations

S. Jottrand*[1,2] and P. Hendrick[1,2]

[1]Aero-Thermo-Mechanics, Ecole polytechnique de Bruxelles, Université libre de Bruxelles
[2]BRITE, Brussels Institute for Thermal-Fluid Systems and Clean Energy

Introduction

The development of Fuel Cell Electric Vehicles (FCEV) requires infrastructure to increase the availability of hydrogen and lower its cost. Hydrogen Refueling Stations (HRS) are the core of the success of such vehicles. The cost of hydrogen is mainly due to his production, but the operational costs of the HRS itself are non-negligible.

When inspecting the different elements related to LCOH (Levelized Cost of Hydrogen), the compression has a very large impact on the final price of hydrogen. In Hydrogen Refueling Stations (HRS), the current standard is to estimate a compression cost of $1\$/kg_{H_2}$. To be competitive with gasoline, the goal is to reach a final hydrogen price of 4$/kg, with a split of 2$/kg for the production and 2$/kg for the delivery [6]. Of course this depends mainly on the final pressure of storage and many other aspects as will be presented later, but this number is a good mean value to understand the challenge of hydrogen compression. This cost is divided into two main categories, called CAPEX (capital costs) and OPEX (operational costs). In capital costs are included the cost of the compressor and the cost of additional features related to compression like intermediate pressure storage tanks or intercooling. In operational costs are included the cost of energy to power the compressors, the maintenance costs, hydrogen leakage and personnel. This is known for HRS, but can of course be generalized to other applications where hydrogen is compressed. The main difference will be the pressure and mass flow rate orders of magnitude.

In a typical HRS providing hydrogen at 350 bar, the CAPEX due to the compressor is almost 19% of the total CAPEX of the HRS [10]. In this case, diaphragm compressor with a discharge pressure of 450 bar is operating. This is a very important part of the CAPEX, knowing that this station also uses an electrolyser on site to produce its hydrogen, costing only twice as much as the compressor. The operations and maintenance (O&M) costs are also substantially higher for compressors (8% of CAPEX) than for any other components of a HRS [5].

In HRS today, the compressors used are all reciprocating. The principle used to compress the hydrogen is to reduce its volume, therefore increasing the pressure of the gas. There are multiple types of reciprocating compressors, the main ones used for hydrogen are the mechanically driven compressor, the hydraulically driven compressor and the diaphragm compressor.

Mechanically driven compressors are used extensively in the industry for gas compression. They can be of various size depending on the mass flow rate of gas to be compressed. Many problems particular to hydrogen still exist in those industrial compressors, due in a majority of cases to valve failures [1, 2].

Without lubrication, these compressors can provide a discharge pressure of ... bar, and with lubrication a pressure of ... bar. However, lubricant mixed with hydrogen can cause damages to the piston chamber, due to the high speed of sound of hydrogen compared to other gases.

For HRS, reciprocating compressors used follow approximately the following price law [5]:

$$\mathrm{CAPEX}_{\mathrm{HRS,comp}}[\mathrm{EUR}] = 36079 * \dot{W}^{0.6038} \tag{1}$$

Hydraulically-driven compressors are using a liquid and a pump to move the pistons into the chambers. This allows a larger possible discharge pressure, very useful for HRS compression stations. This technology is for example used by Resato in some HRS. Compared to mechanically driven compressors, the mass flow rate achievable is however lower.

*Corresponding author: samuel.jottrand@ulb.be

Diaphragm compressors aim to solve the same problems as hydraulically-driven compressors, with the advantage of ensuring no contamination of the hydrogen[12]. This type of diaphragm is already used in HRS compression, mainly as last stage compressor, preceded by more conventional and cheaper mechanical compressors. The main drawback of this compressor is the low mass flow rate achievable, mainly limited by the flexibility of the metallic membrane used. Another drawback is the low service life of such compressors, which for very high pressure operations may be usable for only a few hundred hours [12]. Another main problem encountered in HRS is the high rate of failure due to the very intermittent usage of these compressors[7]. The shape of the diaphragm is a very important parameter for the clearance volume, and therefore the mass flow rate through the volumetric efficiency. However, this shape must also sustain the forces on the diaphragm, and therefore a trade-off between structural strength and compression efficiency must be found [3].

Methodology

Using existing cost functions and correlations of efficiency of compressors, the goal is to optimize the arrangement and choice of compressors by minimizing the total cost of the HRS. Two main types of cost are to be defined: capital costs (CAPEX) and operational costs (OPEX). The CAPEX corresponds to the price of the different elements present on the HRS, like the compressors, the valves, the tanks and the different pipes. The OPEX is a sum of the maintenance costs of the different elements, the labour cost of the people working on the station, and the cost of energy required for the operation of the HRS. This last element will be the most expensive one, as the energy cost of the compression of hydrogen is known as being a very important factor in its final price.

The optimization of gas compression and storage has already been studied for natural gas [11, 4]. In this study, the objective is to focus on hydrogen, requiring other ranges of pressure and mass flow rates.

Mixed Integer Non-Linear Programming (MINLP) is often used for optimization of gas storage, and also more particularly for nonconvex problems [8]. The presence of integers in the optimization process is important to describe some aspects like the presence or not of an element (tank, compressor, valve, ...). The optimization contains many non-linear equations, like the equation of the compressor power, or the correlations used to determine the isentropic efficiency of the compressor in changing conditions.

The typical design of a HRS can be schematized as on figure 1. The important element to understand is that the use of multiple pressures of storage in the station reduces the operational cost of the station. Indeed, fueling a tank that arrives at 100 bar with a storage tank at 900 bar is highly inefficient compared to a fueling at 300 bar. Using intermediate pressure allows to compress a gas at a lower pressure, requiring therefore less power.

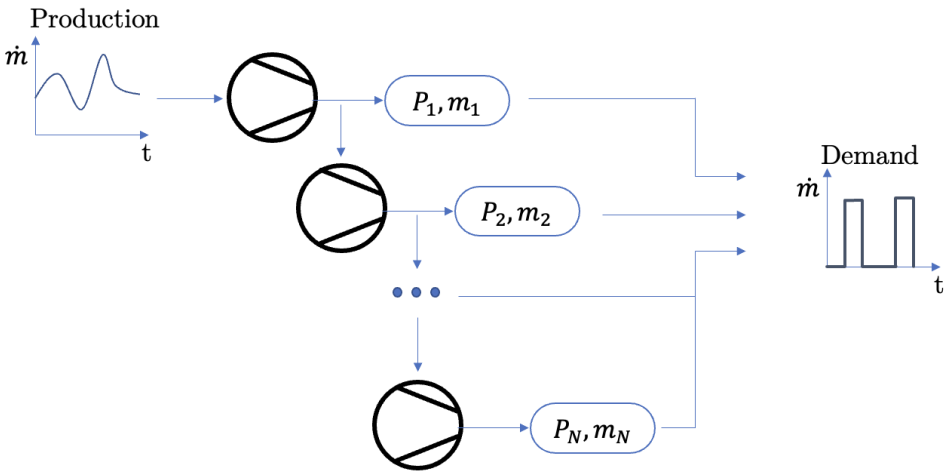

Figure 1: Design of a HRS

The basic equation of power of a compressor stage derive directly from the first principle of thermodynamics:

$$\dot{W}_{is} = \dot{m}\frac{\gamma}{\gamma - 1} RT_{in}\left(\left(\frac{p_{out}}{p_{in}}\right)^{\frac{\gamma-1}{\gamma}} - 1\right) \tag{2}$$

This equation is only true in an isentropic case, where no heat is exchanged with the surroundings, and for a reversible process. In the real case, the isentropic efficiency must be known for the compressor in the conditions considered to have a more precise idea of the power consumed. Isentropic efficiency correlations exist for reciprocating compressors, for example, in [9]:

$$\eta_{is} = 0.1091\kappa^3 - 0.5247\kappa^2 + 0.8577\kappa + 0.3727 \tag{3}$$

with $\kappa = \ln\left(\frac{p_{out}}{p_{in}}\right)$

The function to optimize is

$$\min \sum_{i=1}^{N_{\text{comp,i}}} C_{\text{comp,i}} + \sum_{j=1}^{N_{\text{tank,j}}} C_{\text{tank,j}} + \int_{T_0}^{T_f} \dot{W}(t) C_{\text{e}}(t) dt \tag{4}$$

With $C_{\text{e}}(t)$ the cost of energy fluctuating with time.

Results and discussion

A first step towards the optimization of the choice of pressure tanks and compressors is to be able to simulate the operation of a HRS. Here is an example for a three tanks and three compressors design. The first tank operates here at a maximum pressure of 400 bar, the second one at 650 bar and the last one at 900 bar. A standard scheme of vehicles refueling was chosen, and simulation is made over a full working day.

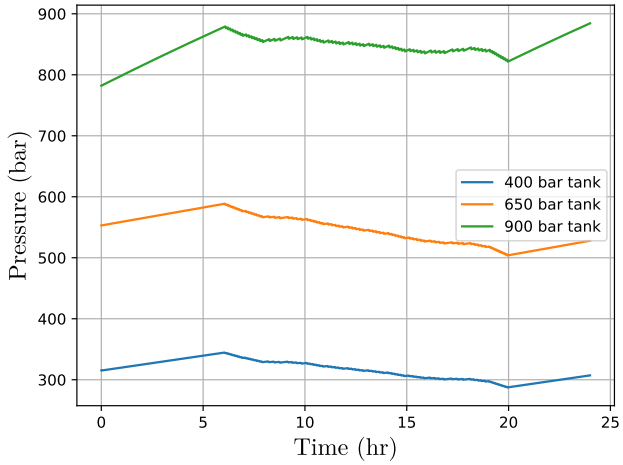

Figure 2: Pressure in the different tanks

In a second step, the goal is to use this simulation model to determine which design is the most efficient in terms of power consumed. Therefore, a parametric study was made to determine such a design. For example, if the intermediate pressures are variable, we can plot the following results, where each line represents a pressure of the first stage, going from 150 bar to 300 bar:

It has to be noted that the CAPEX of the tanks and compressors is not taken into account in the study for now. Even if the lowest pressure tank does not seem to be the best solution in terms of power, it might be so because of a reduced capital cost. Capital costs of hydrogen tanks of new generations must still be estimated to complete this study, as well as for hydrogen compressors. We can also expect a lot of changes in the price of this type equipment, due to the development and investment put in hydrogen technologies in general.

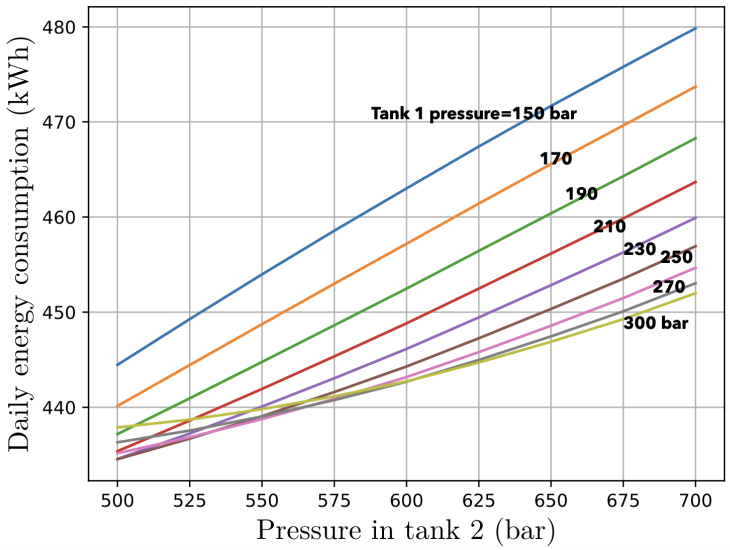

Figure 3: Energy consumption in function of intermediate storage pressures

Conclusions

The objective of this study is to optimize the design of a hydrogen refueling station by minimizing the cost over a period of time. This is done through capital cost estimation of the different elements linked to compression and storage, and through the computation of the compression powered required. To have a more precise model, the efficiency of the compressor must also be estimated in function of the operating conditions, this is done with correlations. The simulation of a defined HRS gives us the power used through, but also the state of filling of the different tanks. With this simulation tool, optimization can be made by varying parameters and minimizing the total cost.

References

[1] P. Białek and P. Bielawski. Failure analysis of refinery hydrogen reciprocating compressors. *Diagnostyka*, 19:83–92, Mar. 2018.

[2] M. Fouladivanda and M. A. Heidary. A study into the impact of chloride ions on the make-up hydrogen compressors. *IOP Conference Series. Materials Science and Engineering*, 1180(1), 2021. Place: Bristol, United Kingdom Publisher: IOP Publishing.

[3] X. Jia, Y. Zhao, J. Chen, and X. Peng. Research on the flowrate and diaphragm movement in a diaphragm compressor for a hydrogen refueling station. *International Journal of Hydrogen Energy*, 41:14842–14851, Sept. 2016.

[4] C. Kagiri, L. Zhang, and X. Xia. Optimization of a compressed natural gas station operation to minimize energy cost. *Energy Procedia*, 142:2003–2008, Dec. 2017.

[5] A. Perna, M. Minutillo, S. Di Micco, and E. Jannelli. Design and Costs Analysis of Hydrogen Refuelling Stations Based on Different Hydrogen Sources and Plant Configurations. *Energies*, 15(2):541, Jan. 2022.

[6] K. Reddi, A. Elgowainy, N. Rustagi, and E. Gupta. Impact of hydrogen refueling configurations and market parameters on the refueling cost of hydrogen. *International Journal of Hydrogen Energy*, 42(34):21855–21865, Aug. 2017.

[7] A. Rohatgi, N. Karri, and A. Soulami. III.10 Investigation of H2 Diaphragm Compressors to Enable Low-Cost Long-Life Operation. page 4, 2014.

[8] D. Rose, M. Schmidt, M. C. Steinbach, and B. M. Willert. Computational optimization of gas compressor stations: MINLP models versus continuous reformulations. *Mathematical Methods of Operations Research*, 83(3):409–444, June 2016.

[9] R. Smith. Chemical Process Design and Integration.

[10] L. Viktorsson, J. Heinonen, J. Skulason, and R. Unnthorsson. A Step towards the Hydrogen Economy—A Life Cycle Cost Analysis of A Hydrogen Refueling Station. *Energies*, 10(6):763, May 2017.

[11] M. Warchol, K. Świrski, N. wirski, B. Ruszczycki, and K. Wojdan. The method for optimisation of gas compressors performance in gas storage systems. *International Journal of Oil, Gas and Coal Technology*, 17:12, Jan. 2018.

[12] J. Zhang. Improvement of Performance for Superhigh Pressure Diaphragm Compressor. page 11.

Optimization of the Liquid Organic Hydrogen Carrier (LOHC) dehydrogenation selectivity by support acidity tuning: The case of Methylcyclohexane conversion over Ni-based catalysts.

P. Fernandez [1, *], E. Farah [1], E. Kantarelis [1,]

[1] KTH Royal Institute of Technology, Department of Chemical Engineering, Stockholm, Sweden

Introduction

The current climate change strategy urges to decarbonize the industry with green hydrogen considered as a sustainable energy carrier. However, due to its very low volumetric energy density, the development and implementation of storage and distribution systems is problematic. The chemical fixation of hydrogen in liquid organic molecules (LOHCs) that allow reversible hydrogen uptake and release is a promising alternative, because it offers the possibility of reusing the current oil infrastructure. [1] Nevertheless, the core of the technology relies on catalysts that enable efficient cyclic (de)hydrogenation which are currently not fully optimized. [2] While conventional dehydrogenation catalysts are Pt-based on γ-Al_2O_3, the acidity of the support influences the selectivity and facilitate unwanted C-C cleavage reactions. In view of this, the present study investigates the gas-phase dehydrogenation of methylcyclohexane (MCH) using non-noble metal (Ni)-based catalysts supported on materials of tuned acidity aiming at enhancing the C-H bond cleavage.

Methodology

The dehydrogenation of methylcyclohexane is investigated over Ni/γ-Al_2O_3 and Ni/$MgAl_2O_4$. Commercial grade (Sasol, Puralox NGa150) γ-Al_2O_3 was used as acidic support while Mg spinel was synthetized by a co-precipitation method. In the method, an aqueous solution containing $Mg(NO_3)_2$. 6 H_2O and $Al(NO_3)_3$. 9 H_2O, in a ratio Mg/Al = 0.5 and total metal ions 1.05M, was precipitated on a 0,35 M Na_2CO_3 aqueous solution, while adjusting the pH to 10 ± 0.5 by adding NaOH 2.0 M. The precipitate was washed, ground to fine powder and dried at 80 °C for 2 h and calcined at 900 °C for 5h with a ramp rate of 3 °C/min. The Nickel was added by wet-impregnation and calcined at 500 °C for 5 h. [3] The produced catalysts were characterized by BET, XRD, NH_3-TPD and Chemisorption.

The catalytic dehydrogenation was studied in a fixed bed reactor at a temperature of 270 – 350 °C and a pressure of 1.0 barg. (Figure 1) Both N_2 and MCH were co-fed in an evaporator with 3.0 mm glass beads, which was pre-heated at 150 °C. The resulting gas mixture was sent to the tubular reactor with an inner diameter of 15 mm. The tested catalysts were placed in the isothermal zone of the reactor supported by a ceramic monolith and a stainless-steel mesh. For each run, 500 mg of catalyst were loaded together with 3.0 g of silicon carbide (grit 120). The H_2 reduction of the catalyst, e.g from NiO/γ-Al_2O_3 to Ni/γ-Al_2O_3, was carried out on the reactor before the experiments in the reactor at 550 °C for 2 h with a H_2/N_2 flow on a ratio 1/9. [4] The reactor outflow was discharged on a vapor-liquid separator at of 7 °C. The selectivity towards toluene was determined by collecting the condensed liquids every 15 min for later analysis in GC/MS (Agilent Technologies 7890B), while the gaseous fraction was analyzed on-line by GC-FID/TCD (Perkin Elmer, Clarus 500).

* Corresponding author: Pol Fernandez i Reixach polfir@kth.se

Discussion

The prepared catalyst, Ni/γ-Al_2O_3 and Ni/ $MgAl_2O_4$, have been characterized by BET and the results show they both exhibit similar surface areas, 143 m^2/g and 120 m^2/g respectively. The NH_3-TPD analysis confirm the acidities assumed for the supports (Figure 2), while the XRD results validate the formation of the $MgAl_2O_4$ phase.

The analysis of the condensed liquid solutions are speculated to show reaction intermediates and the dehydrogenated LOHC form, toluene (TOL). For the acidic support, the solutions are also estimated to contain higher proportion of C-C cleavage products, e.g benzene, cyclohexane. The analysis of the gas released is presumed to display traces of vaporized products e.g MCH, TOL, along with molecules produced by C-C scission e.g methane. For the $MgAl_2O_4$-based catalysts, the gas is presumed to contain lower amount of impurities.

Conclusions

The outcomes of the study hope for certifying the viability of nickel-based catalysts for H_2 release from LOHCs. This could open the path to cost reduction of the technology and reduce the reliance on noble metals, benefiting other competing emerging technologies.

Acknowledgements.

The work is a part of Production, Use and Storage of Hydrogen research center (PUSH), which is financed by the Swedish Foundation for Strategic Research (SSF).

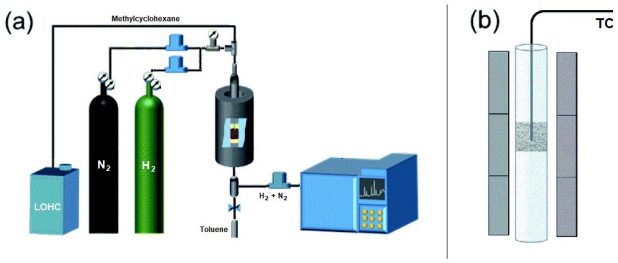

Figure 1a) Experimental set up b) catalytic fixed bed detail

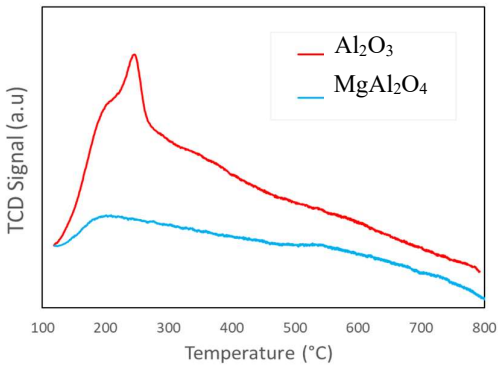

Figure 2. Acidity expressed by NH_3-TPD for supports

References

[1] M. Niermann, S. Timmerberg, S. Drünert, M. Kaltschmitt; "Liquid Organic Hydrogen Carriers and alternatives for international transport of renewable hydrogen", *Renewable and Sustainable Energy Reviews*, Vol. 135, p. 110171, Jan 2021.

[2] Faisal Alhumaidan, Dimos Tsakiris, David Cresswell, Arthur Garforth ; "Hydrogen storage in liquid organic hydride: Selectivity of MCH dehydrogenation over monometallic and bimetallic Pt catalysts", *International Journal of Hydrogen Energy*, Vol. 38, Is. 32, p. 14010-14026, Oct. 2013.

[3] Dalin Li, Miaomiao Lu, Yunbing Cai et al.; "Synthesis of high surface area MgAl2O4 spinel as catalyst support via layered double hydroxides-containing precursor", *Applied Clay Science*, Vol. 132–133, p. 243-250, Nov. 2016

[4] G. Poncelet, M.A. Centeno, R. Molina, "Characterization of reduced α-alumina-supported nickel catalysts by spectroscopic and chemisorption measurements", *Applied Catalysis A: General*, Vol. 288, Is. 1-2, p. 232-242, Jul. 2005

OPTIMIZED CARBON SUPPORTS FOR DURABLE AND HIGH PERFORMANCE PEMFC ELECTRODES

B. Carré[*1], B. Karaman[1] , A. Léonard[1], N. Job[1]

1 Department of Chemical Engineering - NCE (Nanomaterials, Catalysis, Electrochemistry), University of Liège, 4000 Liège, Belgium

Introduction

The Proton Exchange Membrane Fuel Cell (PEMFC) is a device capable of delivering electricity through the oxidation of hydrogen and reduction of oxygen, with only H_2O and heat as by-products. When combined with zero-emission green hydrogen, this type of device represents a sustainable way of producing electricity. However, the slow kinetics of the reactions involved lead to the necessary use of a catalytic layer. In this type of layer, catalyst nanoparticles are supported on a carbon structure, typically carbon blacks, and are covered by a proton-conducting ionomer.

Carbon xerogels (CX) are support materials that could serve as cost-effective substitutes to carbon blacks used in PEMFC. Carbon gels are amorphous materials made of covalently-bonded carbon nodules. Unlike carbon blacks, the size of the nodules is controllable by selecting the appropriate values of reaction variables, enabling a good adjustment of the carbon pore texture [1]. However, carbon xerogels do suffer from the same issue as carbon blacks, namely a relatively poor resistance to corrosion, both carbons being very disordered at their surface.

Nevertheless, recent researches show that both performance and durability could be improved by adjusting the carbon surface properties. As an example, the surface of carbon xerogels can be covered by a graphitic carbon layer through chemical vapor deposition (CVD) [2], which should provide better resistance to corrosion. In a second step, this surface could be doped with nitrogen, which in turn increases the interaction forces between the catalytic metal (Pt) nanoparticles and the support, producing long-lasting active layers.

Regarding the choice of catalyst, Pt and Pt-M (M being a transition metal) catalyst nanoparticles can be deposited onto these modified carbon xerogels. To do so, an impregnation method using formic acid reduction was used [3]. Our research thus turns toward the combination of those various approaches to obtain catalysts with high reactivity and long lifetime.

Methodology

Carbon xerogel are used as a carbon support material. Their synthesis entails the drying and pyrolysis of a resorcinol-formaldehyde gel in presence of sodium carbonate (Na_2CO_3), a pH regulator. The pore size of the xerogel can be tailored via the resorcinol/formaldehyde ratio, R/F, the resorcinol/sodium carbonate ratio, R/C, as well as the dilution ratio, D (solvent/(resorcinol + formaldehyde)). These ratios were taken accordingly to have a material with proper porosity for an application in PEMFC.

* Corresponding author: bryan.carre@uliege.be

To perform the xerogel synthesis, the mixture was put in a flask that was sealed and placed in an oven at 85 ºC to ensure gelling and ageing of the xerogel. The drying of the material was then performed under vacuum at 60 ºC : the flask was opened and the pressure was decreased at 20 mPa. The obtained organic xerogel was then crushed with a planetary mill and sieved so as to obtain a fine powder. It was subsequently pyrolyzed into carbon xerogel via a thermal treatment at 800 ºC under N_2 flow.

A chemical vapor deposition treatment was performed at 670 ºC in a stainless-steel tubular oven, in presence of ethylene, so as to cover the carbon xerogel surface with a graphite-like layer [2]. Ethylene was flowed inside the oven for different durations, ranging from 5 to 30 min.

The synthesis of Pt/CX catalysts was then performed through the reduction of a platinum salt precursor on the carbon xerogel surface with formic acid [3]. Briefly, carbon xerogel was mixed with a solution of formic acid 2 M. The suspension was then heated and a solution of $H_2PtCl_6.6H_2O$ was added dropwise to the suspension. The mixture was then stirred for 1 h, filtered and washed with ultrapure water. Finally, the obtained Pt/CX was dried at 50 ºC in an oven under air overnight.

A comprehensive assessment of the catalyst performances and durability before and after surface modification of the support was subsequently performed on rotating disk electrode (RDE) in H_2SO_4 0.5 M. To this end, cyclic voltammetries under argon, oxygen and CO atmospheres have been performed. Moreover, accelerated stress tests (AST) were performed both on the Pt/CX catalyst and a commercial catalyst reference (Vulcan® XC 72 carbon black). The procedure consisted in (1) measuring the initial performances (beginning of life, BoL), (2) measuring the performances after 5,000 AST cycles between 0.6 and 1.0 V vs. RHE (middle of life, MoL), and (3) measuring the performances after 20,000 AST cycles between 0.6 and 1.0 V vs. RHE (end of life, EoL).

Discussion

The textural properties of the carbon xerogel before and after CVD treatment were assessed using nitrogen adsorption, mercury porosimetry and helium pycnometry. Procedures can be found elsewhere [4]. The carbon xerogel used in this work has a median pore size of 53 nm, a bulk density of 1.27 $g.cm^{-3}$ and a skeletal density of 1.93 $g.cm^{-3}$. The BET surface area initially stands at 670 $m^2.g^{-1}$ for the pristine carbon xerogel and then decreases down to 120 $m^2.g^{-1}$ after 30 min of CVD treatment. N_2 isotherms show that CVD treatment results in the covering of the micropores with the deposition of a carbon layer (Figure 1), as expected [2]. Nevertheless, the size of the meso/macropores is not affected by that carbon layer.

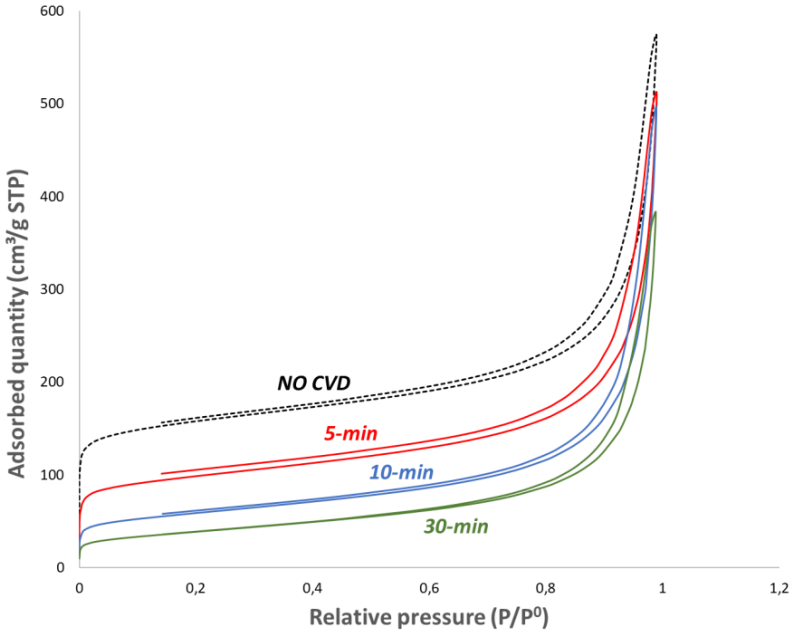

Figure 1: Nitrogen adsorption isotherms on carbon-coated xerogels with different CVD duration.

The platinum nanoparticles deposited onto the carbon support range from 2 to 6 nm in diameter, as shown on TEM micrographs (Figure 2). Nanoparticles deposited onto the CVD-treated carbon xerogel tend to be bigger with a higher standard deviation. As a consequence, the arithmetic average nanoparticle size goes from 3.7 to 4.7 nm on non-CVD and CVD-treated carbon xerogels, respectively. However, both particle sizes remain in the requested range for PEMFC applications [5].

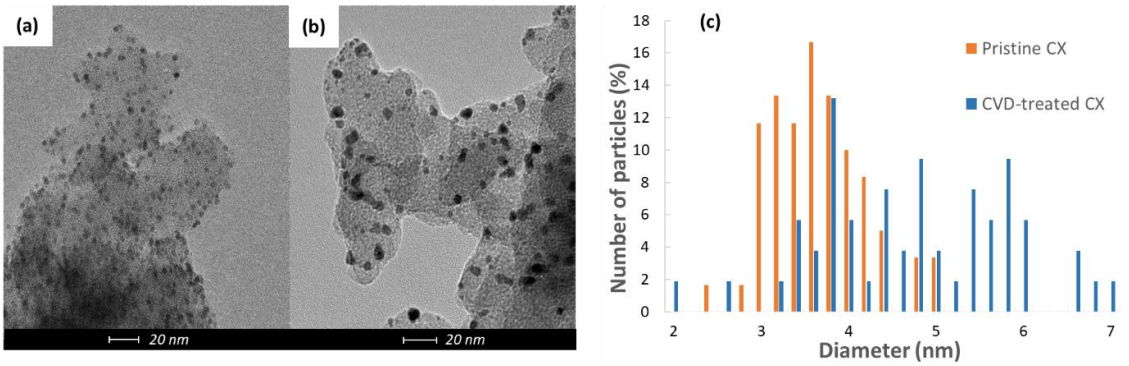

Figure 2: TEM photographs of Pt/CX (a) without and (b) with CVD treatment performed prior to catalyst deposition and (c) the Pt particle size distribution histogram.

Key parameters such as the Surface Activity (SA) and Mass Activity (MA) of the catalyst or the ElectroChemically active Surface Area (ECSA) of platinum were determined through cyclic voltammetry curves. These measurements were used to compare the catalytic activity to those of commercial platinum deposited on carbon black.

Cyclic voltammetry curves measured under argon atmosphere display a lower capacitive current between 0.3 and 0.7 V vs. RHE after CVD treatment, due to lower microporous surface area. This feature can also be observed on CO stripping curves (Figure 3a). CO stripping curves

display a shift of the Pt oxidation peak around 0.8 V vs. RHE to a lower voltage. This reflects the increase of particle size as already observed on TEM micrographs.

The ECSA was found to slightly decrease from 129 $m^2.g_{Pt}^{-1}$ on CX with no CVD treatment to 98 $m^2.g_{Pt}^{-1}$ on CVD-treated CX. This remains an appropriate value for final application in PEMFC, as the ECSA for commercial catalyst was measured at 63 $m^2.g_{Pt}^{-1}$. No major discrepancies were observed for ORR curves between untreated and CVD-treated CX (Figure 3b). Furthermore, the SA and MA show promising values as they increase from 0.114 $A.m_{Pt}^{-2}$ to 0.165 $A.m_{Pt}^{-2}$ for SA and from 13.6 $A.g_{Pt}^{-1}$ to 15.8 $A.g_{Pt}^{-1}$ for MA on CVD-treated CX. Previous studies [3] indicated the same range of values for Pt/CX with no CVD treatment with 0.109 $A.m_{Pt}^{-2}$ and 7.2 $A.g_{Pt}^{-1}$ for SA and MA respectively and 110 $m^2.g_{Pt}^{-1}$ for the ECSA.

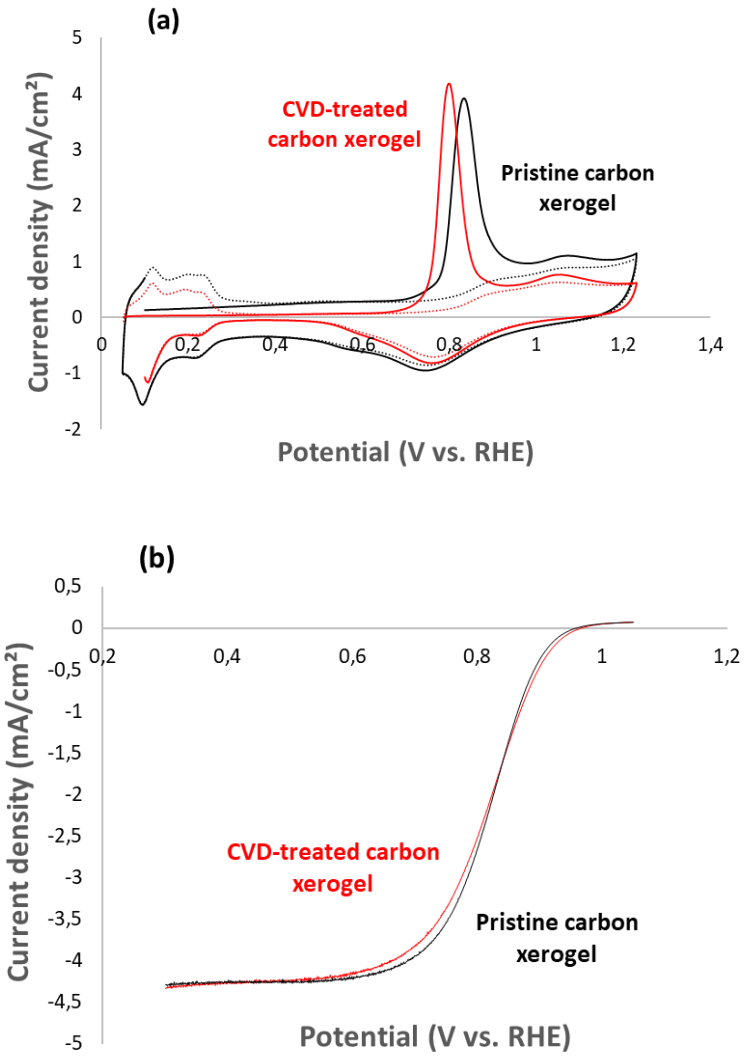

Figure 3: Cyclic voltammograms measured in 0.5M H_2SO_4 (a) CO stripping at a sweep rate of 20 $mV.s^{-1}$. (b) under oxygen atmosphere at a sweep rate of 1 $mV.s^{-1}$ and an electrode rotation of 1600 rpm

Measurements before and after AST show that the ECSA decreases from 129 to 65 $m^2.g_{Pt}^{-1}$ for Pt/CX catalyst with 50.4 % of the initial ECSA being retained (Figure 4a). Meanwhile for the commercial catalyst, the ECSA goes from 62 to 31 $m^2.g_{Pt}^{-1}$, with 50 % of ECSA remaining.

This indeed shows that both catalysts do suffer the same ageing issues. SA and MA activities were also determined (Figure 4b) and results indicate that the particle size increase is somewhat compensated by the appearance of larger Pt crystalline facets that are more active than the edges or corners.

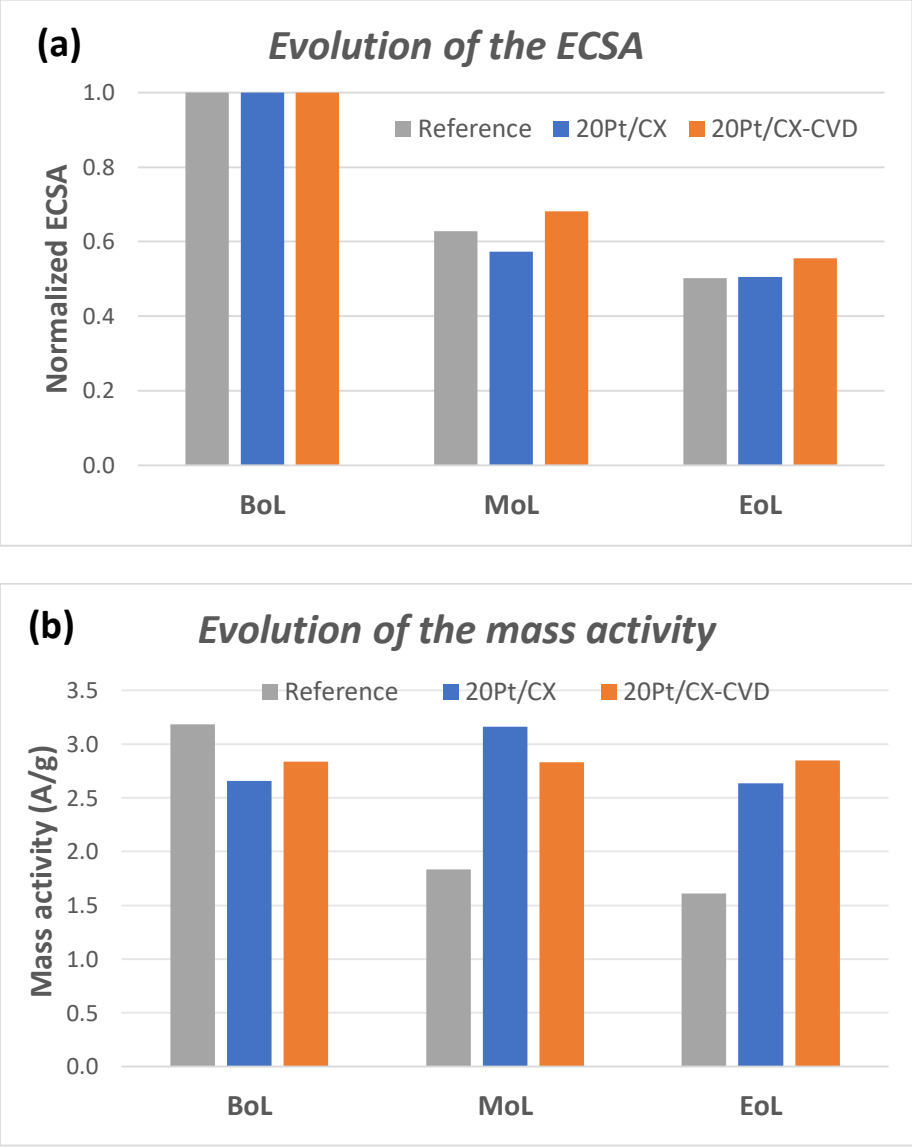

Figure 4: Evolution during Accelerated Stress Tests of (a) the Normalized ElectroChemically active Surface Area of platinum and (b) the catalyst mass activity at 0.95 V vs. RHE.

Conclusions

Carbon xerogels were synthesized via a sol-gel reaction followed by drying and pyrolysis. The carbon material obtained was used as a support for Pt nanoparticles in PEMFC but it still remains flawed with regards to durability given its disordered surface structure. To mitigate those issues, the carbon xerogel was coated with a graphitized carbon layer through Chemical Vapor Deposition (ethylene cracking) so as to obtain a more resilient surface.

Both uncovered and covered materials, onto which Pt nanoparticles were deposited, had their catalytic performances tested via a rotating disk electrode. No performances losses were observed. The Pt/CX catalysts were also submitted to Accelerated Stress Tests (AST) in RDE configuration to assess their resistance to degradation and corrosion

In the next step, the catalyst layers will be doped with nitrogen and tested in RDE setup. Eventually, the most promising catalysts will be assembled in Membrane-Electrode Assembly (MEA) to test their performance in a more realistic electrochemical setup.

References

[1] N. Job et al., "Carbon xerogels as catalyst support for PEM fuel cell cathode", *Energy Conversion and Management*, vol. 49, pp. 2461-2470, 2008. Doi:10.1016/j.enconman.2008.03.025

[2] M-L. C. Piedboeuf et al., "How do the micropores of carbon xerogels influence their electrochemical behavior as anodes for lithium-ion batteries", *Microporous and Mesoporous Materials*, vol. 275, pp. 278-287, 2019. Doi:10.1016/j.micromeso.2018.08.029

[3] A. Zubiaur et al., "Streamlining of the synthesis process of Pt/Carbon xerogel electrocatalysts with high Pt loading for the oxygen reduction reaction in proton exchange membrane fuel cells applications", *Applied Catalysis B.*, vol. 225, pp. 364-378, 2018. Doi: 10.1016/j.apcatb.2017.11.059

[4] N. Job et al., "Porous carbon xerogels with texture tailored by pH control during sol-gel process", *Carbon*, vol. 42, pp. 619-628, 2004. Doi: 10.1016/j.carbon.2003.12.072

[5] Kinoshita K. et al., "Particle size effects for oxygen reduction on highly dispersed platinum in acid electrolytes", *Journal of the Electrochemical Society*, vol. 137, pp. 845, 1990. Doi: 10.1149/1.2086566

PEM electrolysis dynamic operation optimization for affordable green hydrogen

Hassan Sayed-Ahmed*[1], Árpad I. Toldy[1], Annukka Santasalo-Aarnio[1]

[1]Research group of energy conversion and systems, School of Engineering, *Aalto University*, *Finland*

Introduction

Reducing the cost of green hydrogen is a must to defossilize the energy sector. Currently, the high cost of green hydrogen has been an obstacle in upscaling Power-to-X technologies, since green hydrogen cost is the main contributor of the levelized cost of different e-fuels. E-methanol is estimated to be about two times more expensive than fossil-based methanol [1].

Electricity prices are the main contributor to the levelized cost of green hydrogen [2]. Producing hydrogen when intermittent renewable energy is available and electricity prices are low can have a huge effect in reducing green hydrogen costs. Moreover, it can help stabilize the electricity grid and encourage the transition to a 100% renewable energy sector by increasing the electricity grid's flexibility and reliability. In addition to using green hydrogen to produce e-fuels, green hydrogen can be used for mid- and long-term energy storage and for short-term demand response in the electricity balancing markets [3].

However, producing green hydrogen only when low electricity prices are available increases the contribution of electrolysis plant capital cost to the levelized cost of green hydrogen. This happens due to the partial loading, load fluctuations, input power quality, and frequent switching between on and off cycles [4,5]. These effects can increase the levelized cost of green hydrogen produced. Therefore, dynamic optimization between the efficiency and durability of electrolyzer, the electrolysis plant capital cost, the electricity costs, and possible extra revenue from other activities (selling heat energy to district heating networks or nearby industrial facilities and providing demand response in electricity balancing market) is needed to efficiently produce green hydrogen with the lowest possible costs.

In this research, the focus is on optimizing the dynamic operation of proton exchange membrane (PEM) electrolysis. PEM electrolyzers have a faster response time when compared with other direct water splitting technologies (alkaline electrolysis and solid oxide electrolysis), which allows PEM electrolysis to be operated dynamically in connection with fluctuating power [6].

* Corresponding author: hassan.sayedahmed@aalto.fi

Methodology

A holistic data-driven approach is taken to model and optimize the PEM electrolysis dynamic operation. Machine learning algorithms are used to simulate PEM electrolysis performance, predict their long term degradation, and optimize their dynamic operation by considering different interconnected variables. In long term prediction of PEM electrolyzer degradation, the voltage will be used to measure the degradation of the PEM electrolyzer over time. Different conventional and more sophisticated machine learning algorithms for time series prediction will be considered, such as Autoregressive Integrated Moving Average (ARIMA), Long Short-Term Memory (LSTM), Gated Recurrent Units (GRU), and Temporal Convolutional Network (TCN). The accuracy and computational cost of each algorithm will be compared and the more suitable algorithm for predicting the degradation will be determined. Besides, regression models will be used to simulate the PEM electrolyzer performance under different operating current, temperature, and pressure.

Figure 1 summarizes the main interconnected variables to be considered in the dynamic operation optimization, where the effect of dynamic operation actions and operating parameters on efficiency and degradation will be taken into account with respecting the safety limits of operating the PEM electrolyzer. Moreover, extra revenue from providing demand response to the electricity balancing market and selling the produced heat energy to the district heating network will be considered in the optimization model. Moreover, Aspen Plus® is used for the heat integration of the PEM electrolysis plant.

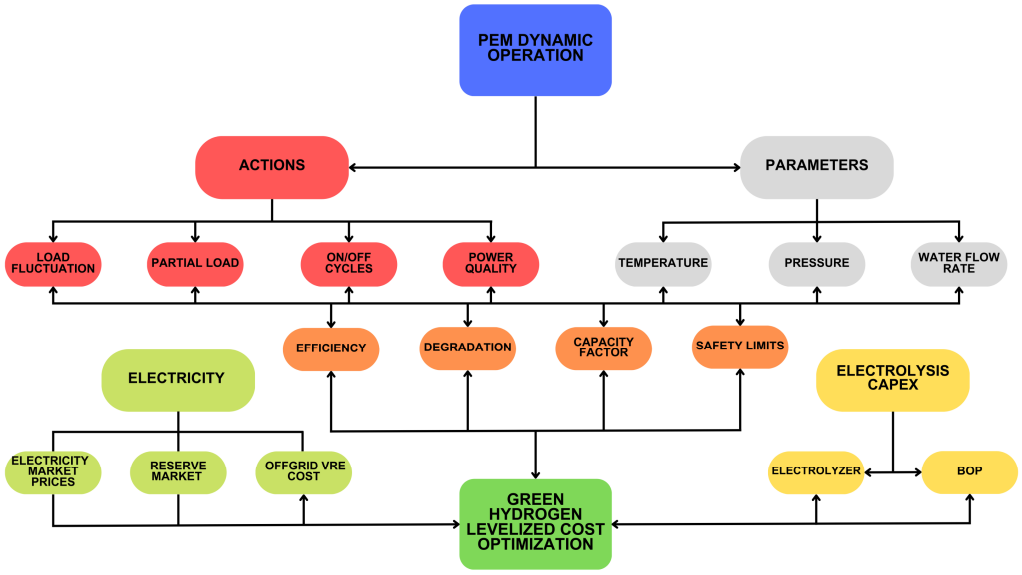

Figure 1: Interconnected variables to be considered in PEM electrolysis dynamic operation optimization [5]

In the perliminary results that will be presented in this abstract, the levelized cost of green hydrogen is calculated under lower and higher boundary assumptions. The lower boundary assumes plant capital costs of 625 Eur/kW, a lifetime of 9 years, and a system electricity consumption of 50 kWh/kg_H_2, while the higher assumes plant capital costs of 1250 Eur/kW, a lifetime of 6 years, and a system electricity consumption of 83 kWh/kg_H_2 [7].

Results

As perliminary results, the levelized cost of green hydrogen is calculated in constant and dynamic operation modes using electricity prices in Finland from 2020 to the first half of 2023. The comparison period interval between constant and dynamic operation modes is six months. Figure 2 shows the electricity prices in Finland from 2020 to the first half of 2023, where the second half of 2022 has the highest electricity prices and variability of prices, while the first half of 2020 has the lowest electricity prices and variability.

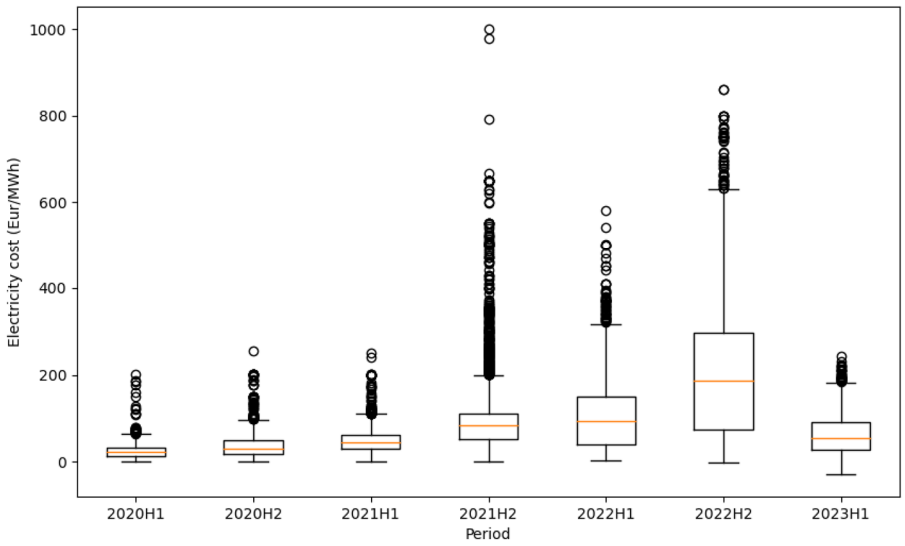

Figure 2: Electricity prices in Finland 2020-2023, data from [8]

Figure 3 shows the levelized cost of green hydrogen in contant and dynamic operation modes in each time interval (half a year). As can be seen , the dynamic operation can reduce the levelized cost of green hydrogen by up to 50% compared to constant operation. The highest reduction in green hydrogen cost was observed in the second half of 2022, a period which exhibited the highest electricity prices and the largest variation of electricity prices. Moreover, the added value to the levelized cost of green hydrogen that results from the dynamic operation of the PEM electrolyzer is the lowest at the first half of 2020 and the highest at the second half of 2022.

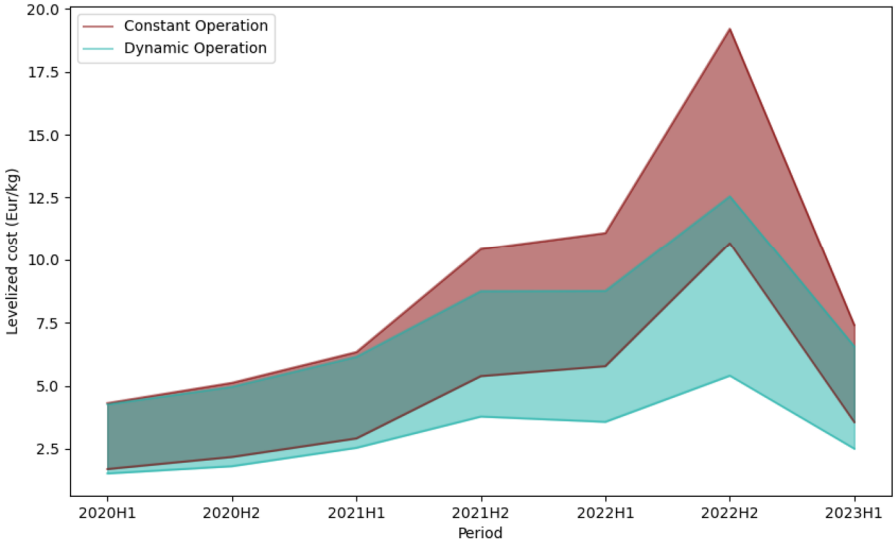

Figure 3: Levelized cost of green hydrogen in constant and dynamic operation modes

Therefore, the statistical features of electricity prices affecting the cost savings (expressed as percentage where the cost in constant operation is considered as 100%) between constant and dynamic operation are examined to find the most important feature of electricity prices affecting the cost savings. The mean, median, and standard deviation of electricity prices have a very strong positive correlation with cost savings, while skewness and kurtosis of electricity prices have a moderate negative correlation with cost savings. However, due to the very strong correlation between mean, median, and standard deviation in this dataset, another approach was taken to determine the most important feature affecting the cost savings. F-value and p-value of each electricity prices statistical feature dataset against cost savings are computed using f_regression() function provided by scikit-learn in Python. It was found that standard deviation, which represents the variation of electricity prices, is the most important feature affecting the cost savings.

In the next phase of the research, the degradation of the PEM electrolyzer, revenue from providing demand response in electricity balancing market, and revenue from selling heat to district heating netwok will all be included in the model. Although the extra degradation due to the dynamic operation is expected to increase the levelized cost of produced green hydrogen, the extra revenue from electricity balancing market and district heating market is expected to have a higher impact on the levelized cost of green hydrogen than the increase in degradation, which will further decrease the levelized cost of the green hydrogen when compared with the perliminary results.

Conclusion

Dynamic operation of PEM electrolysis can reduce the levelized cost of the produced green hydrogen and increase its economic feasibility. However, due to the large number of interconnected variables affecting the levelized cost of green hydrogen, a holistic optimization approach is needed to ensure the economic added value to the green hydrogen cost. In addition, the variability of the electricity prices, which is expected to increase in the future with connecting more intermittent renewable energies to the electricity grid, have the highest impact on decreasing the levelized cost of green hydogen in dynamic operation, when compared with constant operation. Therefore, as the share of intermittent renewable energies connected to the electricity grid increases, the need for optimizied dynamic operation of green hydrogen production increases.

References

[1] J. Nyári, M. Magdeldin, M. Larmi, M. Järvinen, and A. Santasalo-Aarnio. Techno-economic barriers of an industrial-scale methanol CCU-plant. *Journal of CO2 Utilization*, 2020.

[2] Department for Business, Energy & Industrial Strategy. Hydrogen Production Costs 2021. Technical Report, United Kingdom, 2021. [Online]. Available: https://www.gov.uk/government/publications/hydrogen-production-costs-2021

[3] J. Burre, D. Bongartz, L. Brée, K. Roh, and A. Mitsos. Power-to-X: Between Electricity Storage, e-Production, and Demand Side Management. *Chemie Ingenieur Technik, 2019*. doi: 10.1002/cite.201900102.

[4] S. M. Alia, S. Stariha, and R. L. Borup. Electrolyzer Durability at Low Catalyst Loading and with Dynamic Operation. *Journal of The Electrochemical Society, 2019*. doi: 10.1149/2.0231915jes.

[5] H. Sayed-Ahmed, Á. I. Toldy, and A. Santasalo-Aarnio. Dynamic operation of proton exchange membrane electrolyzers —Critical review. *Renewable and Sustainable Energy Reviews*, 2024.

[6] A. Buttler and H. Spliethoff. Current status of water electrolysis for energy storage, grid balancing and sector coupling via power-to-gas and power-to-liquids: A review. *Renewable and Sustainable Energy Reviews*, 2018.

[7] International Renewable Energy Agency. Green Hydrogen Cost Reduction: Scaling up Electrolysers to Meet the 1.5 ^{0}C Climate Goal. Technical Report, Abu Dhabi, 2020.

[8] European Network of Transmission System Operators for Electricity (ENTSO-E) Transparency Platform, 2023 [Online]. Available: https://transparency.entsoe.eu/

Potential use of hydrogen and carbon dioxide for the synthesis of industrially relevant renewable carbon-based fuels

E. Bernad*[1], J. Sanchez-Lainez[1], V. Gil[1,2]

[1]Aragon Hydrogen Foundation, Parque Tecnológico Walqa Ctra. N-330ª, km. 566, 22197 Cuarte, Huesca (Spain)

[2]Fundación ARAID, Avda. De Ranillas 1-D, 50018 Zaragoza (Spain)

Introduction

Carbon dioxide has a negative impact in our atmosphere. This has led numerous countries to commit to achieving net zero emissions. Improving energy efficiency, electrifying the economy, and utilizing renewable energies are seen as effective strategies to reach these goals. Additionally, hydrogen will play a pivotal role in this energy transition, enabling the decarbonization of end uses where these successful approaches are less mature, or less competitive, such as the heavy road transport, shipping and maritime, heavy industry and energy storage.

But…What if we could transform our CO_2 emissions (waste) into valuable products with the support of green H_2?

The production of alternative fuels and sustainable chemicals from CO_2 and H_2 as feedstocks always begins with the generation of renewable hydrogen through electrolysis. In order to make this happens in a sustainable manner, we need electricity from renewable resources. Subsequently, green H_2 reacts with a carbon source at high pressure and temperature to create drop-in hydrocarbons used as fuels, as well as other organic products of interest, such as methane, methanol, gasoline, diesel, plastics, or aviation fuels.

The Power to X technology for synthesizing liquid fuels and organic products involves three main steps. Producing synthesis gas or syngas (a CO/H_2 mixture of several ratios) from organic matter, using preferably green hydrogen from renewable sources. Afterward, transforming the syngas into hydrocarbons through the Fischer-Tropsch (FT) reaction, influenced by several parameters such as temperature or pressure. Finally, the purification product quality through various upgrading processes (such as methanation, isomerization, aromatization, distillation) to meet specific requirements.

Unfortunately, conventional technologies often suffer from low selectivity and control conversion while lacking energy efficiency [1]. Therefore, new technology solutions are required, in which the rational design of catalytic materials is a must.

Methodology

The objective of this work, situated within the core of the chemical engineering, is to design and commission an intensified process capable of integrating various innovative chemical reactions (i.e. electrochemical, thermal and biomimetic reactions) within a single cascade

* Corresponding author: ebernad@hidrogenoaragon.org

reactor, comprised of modules that achieve high yields under milder operating conditions compared to the state-of-art [1].This approach significantly enhances the energy efficiency of the overall process bringing technology to a larger scale of technological readiness level.

As part of the 4AirCRAFT project [2], a test rig has been developed to explore the proof of concept for producing sustainable aviation fuels from renewable H_2 and CO_2. This is achieved through the rational design of catalysts and adjustments to the catalytic environment using hierarchical catalytic scaffolds. The current work will elucidate the engineering design and assembly process of the test bench prepared for the assessment of various modules within the cascade reactor. It will demonstrate the system's proficiency in testing these modules, as well as their coupling for cascade operation. This collaborative work studies the joint use of advanced catalysts and catalytic supports that have been previously tested separately. In this way, the synergistic coupling of their properties is achieved to improve the efficiency of the process. The testing, for the first time, of these catalysts in cell-type configurations or on a larger scale in their appropriated reactor, faces the challenge of scaling up or increasing the Technology readiness level (TRL) to TRL3 of the process.

The initial module of the reactor comprises an electrochemical cell with the capability to convert H_2 and CO_2 streams into syngas. To accomplish this, a novel system based on Layered Double Hydroxide (LDH), developed by Hokkaido University, will be tested. This system is capable of performing the electroreduction of CO_2 using non-critical raw material for the production of the electrodes [3]. Within the cell, there is also an inorganic Anion Exchange Membrane (AEM), manufactured by the Institute of Nanoscience and Materials of Aragón (INMA). Figure 1 presents a basic schematic of the zero-gap electrolytic cell used in the proof of concept.

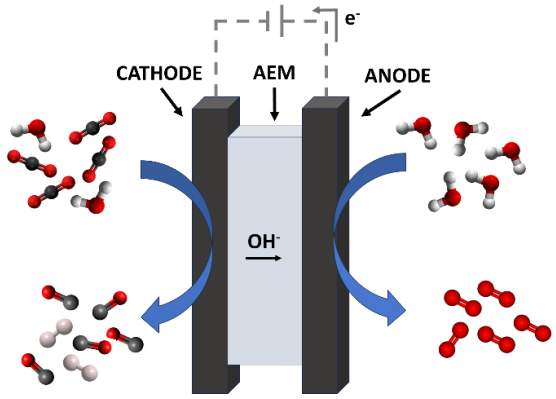

Fig 1. Basic schematic of the tested zero-gap electrochemical cell

In parallel, another module of the cascade reactor is based on a chemo-catalytic module developed by INMA and integrating biomimetic catalysts, whose synthesis and composition has been investigated by Bielefeld University, and Metal Organic Frameworks (MOFs) to increase catalysts stability. This innovative approach enables to obtain alkenes under mild temperature conditions (150 ºC, at 1 bar) and further upgrading to $C_{8\text{-}16}$. To study this process, the design and construction of a laboratory-scale test bench has been carried out in order to lay the foundations and knowledge prior to its subsequent scale-up.

Discussion

The system designed (see figure 2) for the first module of the cascade reactor allows the testing of electrochemical cells, feeding CO_2 streams that can replicate pure or air-captured CO_2 streams, at the time the reaction is monitored by a Gas Chromatograph (GC) System, Agilent 8890 GC, featured with Thermal Conductivity Detector (TCD) and Flame Ionization Detector (FID) analyser for online gas products analysis and off-line analysis for liquid products, featured automatic liquid sampler. The GC-FID-TCD is equipped with capillary columns for Jet Fuel analysis and permanents as 10 m DB-1 low polarity, 30 m HP-PLOT Q for separation of targeted nonpolar and polar compounds, 30 m HP-PLOT Molesieve, 50 m HP-FFAP, 30 m GS-GASPRO.

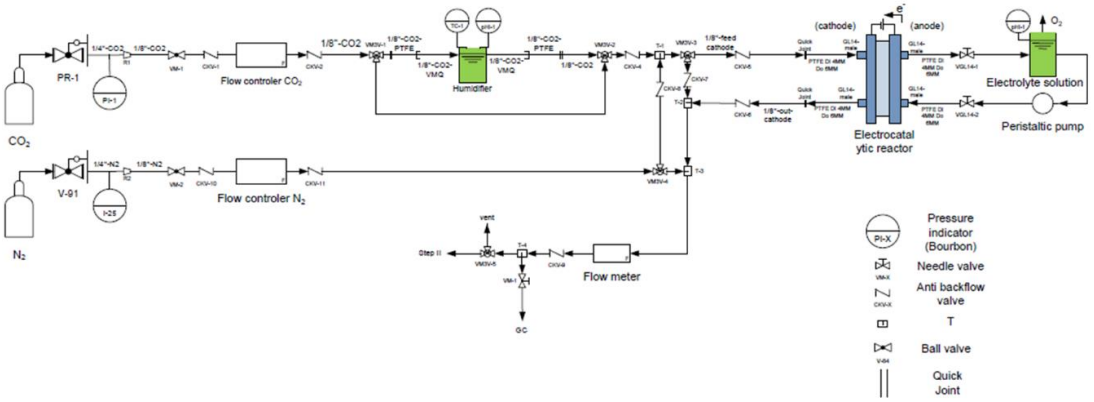

Fig 2. Test bench for the proof-of-concept of the electrochemical module.

During the presentation, the first results obtained from the electrochemical step will be shown. The results to be presented will cover the structure and conformation of the electrochemical cell designed to carry out the electroreduction of CO_2 to CO, incorporating the membrane electrolyte assembly (MEA). Among the results to be shown are the evolution of the voltage of the electrochemical module as a function of time, and the variation of Faradaic Efficiency (EF) with respect to time. At the same time, a comparison will be made between the results obtained by studying the isolated catalyst and the results obtained in a catalytic hierarchical environment with supports, which simulate operating conditions close to reality provided by the test bench.

On the other hand, the design of the test bench, which incorporates biomimetic catalysts, will be presented, along with the initial results obtained. This will be accompanied by the first results obtained from the conversion and selectivity of the reaction carried out at 150°C.

Conclusions

In the quest to convert carbon dioxide into energy-dense fuels, the conversion of carbon dioxide into carbon monoxide followed by its reaction with hydrogen is a critical process.

This endeavour sets out to tackle the formidable task of electro-reducing CO_2 to CO with exceptional Faradic Efficiency by employing cutting-edge inorganic catalysts devoid of precious metals. It also encompasses the subsequent stages that facilitate the synthesis of extended hydrocarbon chains.

This project has received funding from the European Union's Horizon 2020 research and innovation programme under grant agreement No 101022633. This work is supported by Japan Science and Technology Agency (JST) (Grant Agreement No JPMJSC2102) and São Paulo Research Foundation (FAPESP) (Grant number 2022/04751-0). Financial support from the T13-23R (the Aragón Government) is also gratefully acknowledged.

References

[1] M. Shahabuddin, M. T. Alam, B. B. Krishna, T. Bhaskar, y G. Perkins, «A review on the production of renewable aviation fuels from the gasification of biomass and residual wastes», *Bioresour. Technol.*, vol. 312, p. 123596, sep. 2020, doi: 10.1016/j.biortech.2020.123596.

[2] «Home - 4AIRCRAFT». Accessed: 29 June 2023. [Online]. Available at: https://4aircraft-project.eu/

[3] N. Yamaguchi *et al.*, «Electrocatalytic property of Zn-Al layered double hydroxides for CO2 electrochemical reduction», *J. Asian Ceram. Soc.*, vol. 11, n.º 3, pp. 406-411, 2023, doi: 10.1080/21870764.2023.2236441.

Pre-Chamber Ignition of Ammonia and Hydrogen Fuels for Marine Engines

Ducduy Nguyen*[1], James W.G Turner[2], Eilif Pedersen[1], David Emberson[1]

[1]Department of Marine Technology, NTNU, 7491 Trondheim, Norway
[2]Clean Combustion Research Center, KAUST, Thuwal 23955-6900, Saudi Arabia

Introduction

Global greenhouse emissions have been a matter of concern for many decades with the largest contribution coming from the combustion product of fossil fuels. Among the major sectors where the emissions come from, almost three-quarter come from energy consumption, especially transportation, which account for 16.2% of the global greenhouse gas emissions [1]. Greenhouse gas emissions from transportation primarily come from combustion of fossil fuel used in cars, trucks, ships, trains, and airplanes. Over 94% of the fuel used for transportation is petroleum based, which includes primarily gasoline and diesel [2]. Several experimental works have reported the feasibility of using ammonia as an alternative for internal combustion engines (ICE). Nevertheless, due to the properties of ammonia such as high auto ignition temperature and low laminar burning velocity, there are challenges in maintaining sufficient combustion of ammonia [3]. However, it is possible to achieve satisfactory combustion by using some type of combustion promoter. Common fuels used in ICEs such as gasoline and diesel, as well as alternative fuels like hydrogen, biodiesel, methanol can be used as combustion promoters [4]. To ensure efficient and complete combustion, hydrogen is considered the best promoter because it has characteristics that are opposite to and complement those of ammonia. Hydrogen possesses a rapid combustion rate, low ignition energy, and an extensive range of flammability [5, 6].

Although, the combination of ammonia and hydrogen results in a stable combustion, significant emissions of NOx and low combustion efficiency have been observed [7]. The implementation of a pre-chamber is a promising method to enhance the combustion quality, as demonstrated in conventional engines [8]. Simulation results show that a SI engine with a pre-chamber installed operating under lean conditions provides higher indicated thermal efficiency compared to the normal SI mode [9]. Adding hydrogen to a single cylinder engine with a pre-chamber increased the efficiency, gross work, and indicated mean effective pressure, while also improving combustion quality and reducing emissions by 20% and 15% [10]. While the pre-chamber has shown promising results, it is a relatively new concept for ammonia that requires further investigation to fully understand its potential benefits and limitations.

The study will focus on the ignition processes when an ammonia and hydrogen mixture is burnt inside an internal combustion. The main objective of the work will be to develop a suitable pre chamber which achieve lean burn combustion of ammonia and low emissions of nitrogen oxides and nitrous oxide. To meet the objectives a mixture of experimental and numerical work will be conducted. The project will be used to develop new engines and support new numerical models describing combustion of the fuel mixture.

*Corresponding author: duc.d.nguyen@ntnu.no

Methodology

To fully understand the combustion of ammonia and hydrogen mixtures in marine engines, this study will first develop a detailed computational fluid dynamics model to fundamentally understand in-cylinder combustion processes with different energy share ratios in a pre-chamber ignited marine engine. The effectiveness of hydrogen in improving combustion quality with ammonia fuelling will be assessed over the in-cylinder pressure-temperature domain using chemical kinetics modelling. Furthermore, for the experimental campaign, active pre-chambers with various geometry designs will be developed to investigate their effects on combustion and performance in ICEs.

Numerical Methodology

The LOGE software package will be used as a reaction kinetics solver to perform simulations such as ignition delay and laminar flame speed calculation. A closed, constant volume homogeneous 0-D batch reactor with adiabatic and chemically inert walls is used to calculate the ignition delay time of the air-fuel mixture, representing the in-cylinder trapped charge under engine pressure and temperature conditions. Additionally, the combustion and chemical kinetics simulations will be performed to predict NOx emission levels. Furthermore, a multidimensional, computational fluid dynamics simulation model using Converge CFD Software will be developed to predict the spray and combustion characteristics of hydrogen and ammonia mixtures inside a pre-chamber and in-cylinder under various conditions.

Experimental Activity

For all tests, the pre-chamber with various geometry and nozzle designs will be employed as an ignition system. Figure 1. illustrates the design of the pre-chamber with a 6-holes coaxial arrangement of nozzle and its cross section. It has been reported that the small pre-chamber concept (volume is usually less than 5% of the engine clearance volume) proposed by Gussak [11] is one of the most investigated concepts in recent years. Inspired by Hydrogen Assisted Jet Ignition system [12] a new pre-chamber unit was designed to be installed into a constant volume combustion chamber (CVCC) and optical accessible compression ignition chamber (OACIC) without significant modifications. In order to capture the turbulent jet from the pre-chamber, high speed imaging will be utilised to capture the spray images as the jet enters the main chamber.

To capture full images of the jet and spray angle and characteristics of the pre-chamber, a CVCC with optical imaging techniques will be utilised. The chamber consisting of an air supplying system to introduce a mixture of O_2, N_2 and CO_2; these gases will be mixed using a mixing fan to form a homogeneous mixture. A Bosch gasoline direct injection (HDEV5) will supply hydrogen, hydrogen/nitrogen or hydrogen/ammonia mixtures into the pre-chamber. A spark-plug type pressure transducer will be installed in the chamber for combustion measurement and pressure trace recording. Figure 2. shows a 3D CAD drawing of a CVCC with a pre-chamber on the top and the nozzle location when viewing from the front of the chamber.

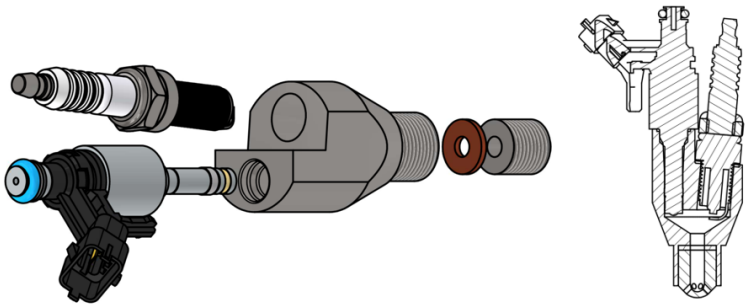

Figure 1: The design of a pre-chamber for hydrogen gas jet ignition system and its cross-section.

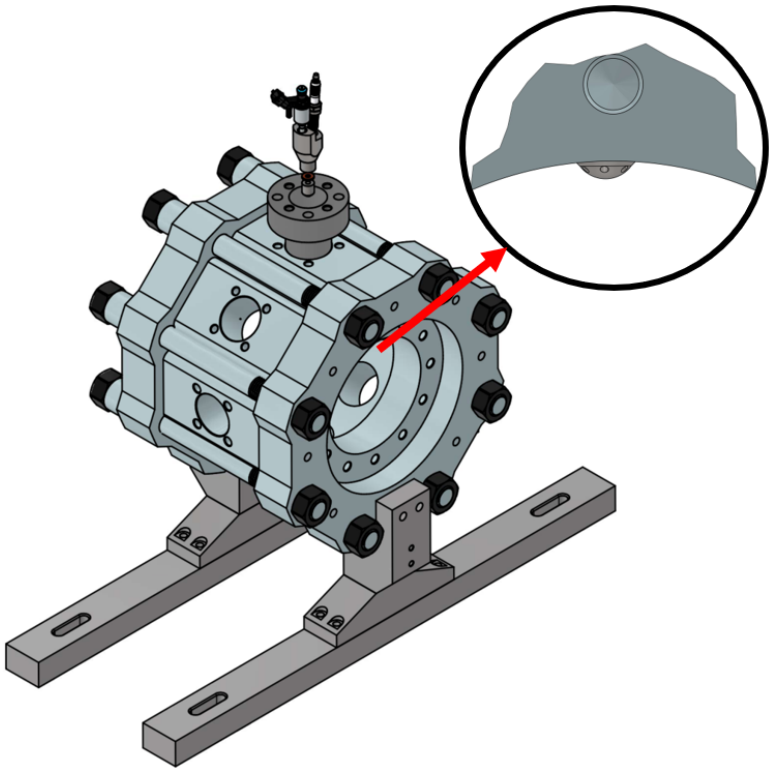

Figure 2: 3D CAD model of a constant volume combustion chamber (CVCC) with a pre-chamber on top. The nozzle location is shown from the front view of the chamber.

To conduct the experiment under engine conditions, the same pre-chamber system will be installed into an OACIC [13], the specifications of the engine are reported in Table 1. The pre-chamber has a volume of 4.2 cc which is 3.3% of the engine clearance volume. Figure 3. shows the cylinder head of the engine with the pre-chamber system mounted on the side. The optical engine allows capturing of the pre-chamber ignition event during engine operation. Furthermore, various engine parameters such as performance and emissions will be recorded and the combustion event will be captured from the optical window on the side. Figure 4. illustrates a cross section of the cylinder head and the view from the side of the cylinder.

Table 1: Engine specifications

Engine type	4-stroke, single cylinder
Bore/Stroke	130/140 mm
Displacement volume	1.85 L
Compression ratio	15.93:1
Compression ratio with pre-chamber	15.41:1

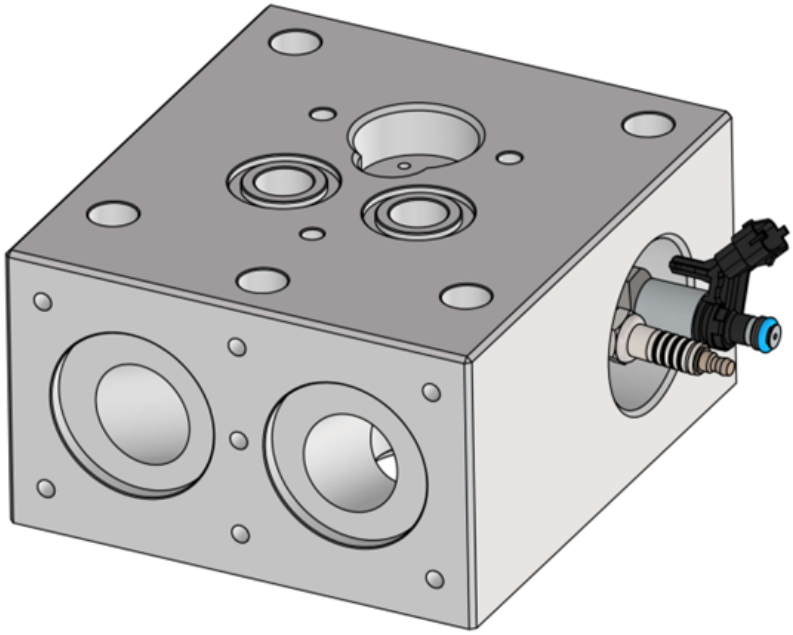

Figure 3: The cylinder head of the engine with the pre-chamber system mounted on the side.

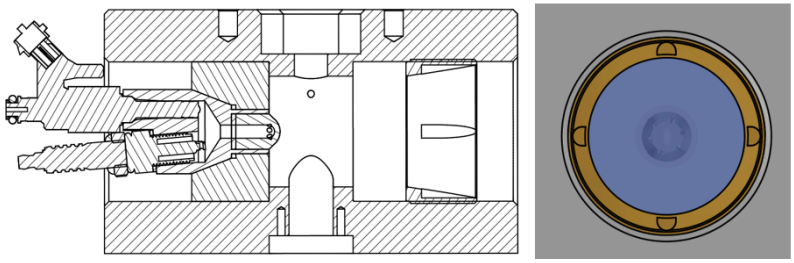

Figure 4: Cross-section of the cylinder head showing the interior view from the side of the cylinder. The pre-chamber system is visible mounted on the cylinder wall.

Expected results

This study aims to provide comprehensive results of utilising ammonia and hydrogen blends as a fuel for marine engines. The computational modelling will further improve the fundamental of the in-cylinder combustion processes and kinetics involved when using ammonia and hydrogen as the fuel. The effectiveness of hydrogen as a combustion promoter for ammonia is expected to be quantified across a range of operating conditions. The CFD simulations are anticipated to predict the spray, combustion, and emissions characteristics of the fuel blends. The experimental work will demonstrate the feasible of pre-chambers as an ignition system for ammonia-hydrogen fuels. Optical diagnostics will capture the ignition and combustion events, validating the computational models. Ultimately, the findings are expected to highlight the potential of ammonia-hydrogen blends to serve as a decarbonised, renewable fuel option for the maritime sector. The data will showcase the operational feasibility and benefits of ammonia/hydrogen mixture over conventional fossil fuels.

Acknowledgements

This publication has been produced with support from the HYDROGENi Research Centre (hydrogeni.no), performed under the Norwegian research program FMETEKN. The authors acknowledge the industry partners in HYDROGENi for their contributions and the Research Council of Norway (333118).

References

[1] Hannah Ritchie, Pablo Rosado, and Max Roser. Emissions by sector. *Our World in Data*, 2020. https://ourworldindata.org/emissions-by-sector.

[2] Priyadarshi R Shukla, Jim Skea, Raphael Slade, A Al Khourdajie, R Van Diemen, D McCollum, M Pathak, S Some, P Vyas, R Fradera, et al. Climate change 2022: Mitigation of climate change. *Contribution of working group III to the sixth assessment report of the Intergovernmental Panel on Climate Change*, 10:9781009157926, 2022.

[3] E. S. Starkman, H. K. Newhall, R. Sutton, T. Maguire, and L. Farbar. Ammonia as a spark ignition engine fuel: Theory and application. In *1966 Automotive Engineering Congress and Exposition*. SAE International, feb 1966.

[4] Aliasghar Mozafari-Varnusfadrani. Predictions and measurements of spark-ignition engine characteristics using ammonia and other fuels. 1988.

[5] Meng-Choung Chiong, Cheng Tung Chong, Jo-Han Ng, Syed Mashruk, William Woei Fong Chong, Nor Afzanizam Samiran, Guo Ren Mong, and Agustin Valera-Medina. Advancements of combustion technologies in the ammonia-fuelled engines. *Energy Conversion and Management*, 244:114460, 2021.

[6] Stefano Frigo, Roberto Gentili, and Franco De Angelis. Further insight into the possibility to fuel a si engine with ammonia plus hydrogen. In *SAE/JSAE 2014 Small Engine Technology Conference Exhibition*. SAE International, nov 2014.

[7] Charles Lhuillier, Pierre Brequigny, Francesco Contino, and Christine Mounaïm-Rousselle. Experimental study on ammonia/hydrogen/air combustion in spark ignition engine conditions. *Fuel*, 269:117448, 2020.

[8] Elisa Toulson, Harold J. Schock, and William P. Attard. A review of pre-chamber initiated jet ignition combustion systems. In *SAE 2010 Powertrains Fuels Lubricants Meeting*. SAE International, oct 2010.

[9] Carlos Eduardo Castilla Alvarez, Giselle Elias Couto, Vinícius Rückert Roso, Arthur Braga Thiriet, and Ramon Molina Valle. A review of prechamber ignition systems as lean combustion technology for si engines. *Applied Thermal Engineering*, 128:107–120, 2018.

[10] Alireza Kakoee, Younes Bakhshan, Sattar Motadayen Aval, and Ayat Gharehghani. An improvement of a lean burning condition of natural gas/diesel rcci engine with a pre-chamber by using hydrogen. *Energy Conversion and Management*, 166:489–499, 2018.

[11] LA Gussak, VP Karpov, and Yu V Tikhonov. The application of lag-process in prechamber engines. *SAE Transactions*, pages 2355–2380, 1979.

[12] Neil Glasson, Grant Lumsden, Robert Dingli, and Harry Watson. Development of the haji system for a multi-cylinder spark ignition engine. *SAE Transactions*, 105:1463–1469, 1996.

[13] Karl Oskar Pires Bjørgen, David Robert Emberson, and Terese Løvås. Combustion and soot characteristics of hydrotreated vegetable oil compression-ignited spray flames. *Fuel*, 266:116942, 2020.

Printing the Future of Hydrogen Generation: The 3D Printed PEC Standardized Test Reactor

R. Jacops*[1,2], M. De Rop[2], K. Van Daele[2], N. Daems[2], M. Van Bael[1], A. Hardy[1], T. Breugelmans[2]

[1] Institute for Materials Research and imec division imomec, Materials Chemistry, DESINe group, Hasselt University, UHasselt (Diepenbeek, Belgium)
[2] Faculty of Applied Engineering, ELCAT, University of Antwerp

Introduction

To reach the EU goal of being climate neutral by 2050, the energy network needs to be decarbonized. This raises a need for a sustainable method to store and transport large amounts of renewable energy. Green hydrogen is one of the key elements for the transition to renewable energy storage. Splitting water to form hydrogen gas is a way to convert renewable energy to a chemical that can be used for energy storage and transport or as a building block for other chemicals. Photoelectrochemical (PEC) water-splitting technology is an interesting alternative to conventional electrolysis for hydrogen generation. The concept of PEC water splitting is to directly convert incident sunlight to electrical energy and split water to form hydrogen and oxygen gas. One of the challenges for this technology is to develop a standardized lab scale PEC test reactor to screen PEC photoelectrode materials and assess their performance. [1, 2]
Efforts have previously been undertaken to standardize protocols and methods for testing photoelectrode materials. Nevertheless, there persists a lack of consistency across research groups and publications, where varying procedures and the absence of optimized reactors are prevalent. [1, 3-6]
In this study, our primary objective is to introduce a standardized Photoelectrochemical (PEC) reactor, meticulously engineered to address the inherent challenges and requirements of PEC testing. Our approach centers on the application of an engineering process. Notably, the reactor is predominantly fabricated through 3D printing technology, with the exception of the electrodes. This design choice ensures that the same reactor can be reproduced within different research groups, fostering the ability to evaluate diverse materials in an identical reactor setup. This standardization mitigates inconsistencies, facilitating meaningful material comparisons.
Key considerations for an effective PEC testing reactor encompass versatility, leak prevention, user-friendliness, minimized energy losses, and optimized performance. Another vital design criterion is the facilitation of easy 3D printing and the reduction of material consumption during the manufacturing process.

Methodology

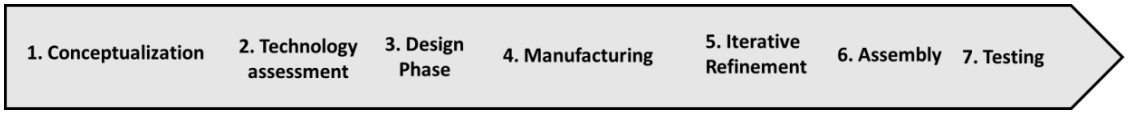

Figure 1: Engineering timeline

To outline the methodology employed in designing, manufacturing, and testing the PEC reactor, an "engineering timeline" is proposed (see Figure 1).[7, 8] The fundamental idea behind this timeline is to guide the progression from a basic concept to a functional reactor. Following each step in the design process ensures that any idea can be systematically developed into a functional reactor. The timeline consists of the following steps:

1. **Conceptualization**: Begin by forming a general idea of what the reactor should look like and what capabilities it should possess.
2. **Technology Assessment:** Examine existing techniques and evaluate which are most suitable for designing and producing the reactor. Select the techniques that align with the project's goals.
3. **Design Phase**: Utilize design tools while considering manufacturing constraints to create detailed designs for all reactor components.
4. **Manufacturing**: Execute the manufacturing process for all parts using the chosen techniques, ensuring precision and adherence to design specifications.

* Corresponding author: Robbe.jacops@Uhasselt.be/Robbe.jacops@Uantwerp.be

5. **Iterative Refinement**: Based on identified flaws or issues, make necessary iterations and improvements to the reactor's components.
6. **Assembly**: Perform the final assembly of the reactor, ensuring that all parts fit together seamlessly.
7. **Testing**: Evaluate the reactor's performance using standardized testing techniques, verifying its functionality and efficiency

This engineering timeline provides a structured approach, allowing for the systematic development of the PEC reactor from its initial concept to a fully operational system.
It's important to recognize that the engineering process isn't always a linear path. Depending on the problems encountered or new requirements that arise, it may be necessary to revisit previous steps and make adjustments. Additionally, it's worth noting that a reactor is never truly "finished." Even after initial construction, there's room for continuous improvement, and new parts or design iterations can be implemented at later stages of development. This flexibility allows for ongoing refinement and optimization.

Discussion

The reactor's conceptual framework draws inspiration from the stacked electrochemical reactors designed and constructed at ELCAT for CO_2 reduction.[9-11] Distinguishing itself from commercial reactors, this design exhibits superior versatility, accommodating both multi-chambered and single-chamber configurations. Photoelectrodes can be effortlessly replaced, accommodating various sizes, and the reactor demonstrates adaptability to a range of electrolytes. Leak prevention is integral to the reactor's design, while its internal structure minimizes potential losses and optimizes light absorption by reducing internal volume. Additionally, the internal configuration facilitates the circulation of liquid electrolyte and gas.

Throughout the technology assessment phase, manufacturing techniques are systematically categorized into three groups: formative manufacturing, subtractive manufacturing, and additive manufacturing.[12] For this reactor, 3D printing (additive manufacturing) is the preferred method for most parts, while CNC milling (subtractive manufacturing) is employed for graphite and copper electrodes. These selections prioritize rapid iteration and cost-effectiveness, making them suitable for low production volumes. The 3D printing technologies used are: filament extrusion (for prototyping) and vat polymerization (for the final product). Additional components like tubing connectors are procured and installed. Autodesk Inventor is the software used for designing all reactor components.

During the design phase, ideas are meticulously translated into individual parts within 3D design software, always mindful of manufacturing constraints. The 3D printing handbook [12] provides valuable guidance for the 3D printing process, while the expertise of the research group guides the milling process.

Parts are subsequently manufactured using the appropriate techniques, followed by post-processing to ensure impeccable quality and dimensional accuracy. Iterative refinement comes into play after manufacturing, allowing for adjustments due to fit issues or further iterations during reactor testing. The objective is to ensure that all components function impeccably and fit seamlessly. The final step involves assembling the electrodes, reactor compartments, and commercial parts into a complete unit.

Subsequently, the reactor undergoes rigorous testing in a PEC setup. First, it is scrutinized for liquid and gas leaks, after which it is deployed for photoelectrochemical testing of diverse photoelectrode materials. Various (photo)electrochemical analysis techniques are employed, including LSV analysis, CA analysis, CV analysis, and Mott-Schottky measurements. Benchmark photoelectrodes (TiO_2, $BiVO_4$) and new photoelectrodes (Bi_2WO_6, $CuBi_2O_4$) are tested to establish performance standards for the reactor. [13]

Conclusions

The "Engineering Timeline" methodology is used to transform a concept into a practical photoelectrochemical reactor that meets predefined criteria. This reactor has several noteworthy attributes: it effectively prevents leaks, offers straightforward operation, accommodates various electrode configurations (including dual and single chamber setups), and adequately addresses the essential functional requirements for testing PEC materials in a photoelectrochemical setup.

Moreover, the reactor employs an advanced design approach, featuring a primarily 3D-printed structure, with the exception of precision-milled copper and graphite electrodes. This innovation positions the reactor as a standardized design for evaluating PEC photoelectrode materials.

References

[1] X. Shi, L. Cai, M. Ma, X. Zheng, and J. H. Park, "General characterization methods for photoelectrochemical cells for solar water splitting," *ChemSusChem*, vol. 8, no. 19, pp. 3192-3203, 2015.

[2] Z. Chen, H. N. Dinh, and E. Miller, *Photoelectrochemical water splitting*. Springer, 2013.

[3] Z. Xing, X. Zong, J. Pan, and L. Wang, "On the engineering part of solar hydrogen production from water splitting: photoreactor design," *Chemical Engineering Science*, vol. 104, pp. 125-146, 2013.

[4] N. A. Kelly and T. L. Gibson, "Design and characterization of a robust photoelectrochemical device to generate hydrogen using solar water splitting," *International Journal of hydrogen energy*, vol. 31, no. 12, pp. 1658-1673, 2006.

[5] T. Lopes, L. Andrade, H. A. Ribeiro, and A. Mendes, "Characterization of photoelectrochemical cells for water splitting by electrochemical impedance spectroscopy," *international journal of hydrogen energy*, vol. 35, no. 20, pp. 11601-11608, 2010.

[6] L. J. Minggu, W. R. W. Daud, and M. B. Kassim, "An overview of photocells and photoreactors for photoelectrochemical water splitting," *International journal of hydrogen energy*, vol. 35, no. 11, pp. 5233-5244, 2010.

[7] Y. Haik, S. Sivaloganathan, and T. M. Shahin, *Engineering design process*. Cengage Learning, 2015.

[8] N. Cross, *Engineering design methods: strategies for product design*. John Wiley & Sons, 2021.

[9] K. Van Daele *et al.*, "Sn-based electrocatalyst stability: a crucial piece to the puzzle for the electrochemical CO2 reduction toward formic acid," *ACS Energy Letters*, vol. 6, no. 12, pp. 4317-4327, 2021.

[10] B. De Mot, J. Hereijgers, M. Duarte, and T. Breugelmans, "Influence of flow and pressure distribution inside a gas diffusion electrode on the performance of a flow-by CO2 electrolyzer," *Chemical Engineering Journal*, vol. 378, p. 122224, 2019.

[11] M. Duarte, B. De Mot, J. Hereijgers, and T. Breugelmans, "Electrochemical reduction of CO2: effect of convective CO2 supply in gas diffusion electrodes," *ChemElectroChem*, vol. 6, no. 22, pp. 5596-5602, 2019.

[12] B. Redwood, F. Schffer, and B. Garret, *The 3D printing handbook: technologies, design and applications*. 3D Hubs, 2017.

[13] K. Sivula and R. Van De Krol, "Semiconducting materials for photoelectrochemical energy conversion," *Nature Reviews Materials*, vol. 1, no. 2, pp. 1-16, 2016.

Production of green molecules at sea using the concept of energy island

Siavash Asiaban*[1,2], Nezmin Kayedpour[1,2], Dimitar Bozalakov[1,2], Lieven Vandevelde[1,2]

[1]Department of Electromechanical, Systems & Metal Engineering, Faculty of Engineering & Architecture, Ghent University, Tech Lane Ghent Science Park—Campus Ardoyen, Technologiepark-Zwijnaarde 131, B-9052 Ghent, Belgium
[2]FlandersMake@UGent—Corelab MIRO, Flanders Make, B-9052 Ghent, Belgium

Introduction

In recent years, renewable energy sources (RESs) have seen an increase in power generation capacity. Despite the fact that direct electrification is the best way to maximise the efficiency of using RESs, multiple challenges arise when a high share of RESs is integrated into the power system, assessed thoroughly in [1]. In some cases, such as when there are power transmission limitations or a surplus of energy from RESs, the extra power can be converted into green molecules, like hydrogen [2].

Owing to its distinctive characteristics, hydrogen has garnered escalating attention in recent years as an effective energy carrier. The two major pathways to produce hydrogen are fossil fuels and RESs. Having said that, the former emits carbon dioxide (CO_2) as a by-product, resulting in RESs being more desirable for sustainable hydrogen production. The green hydrogen produced from RESs is of use for several applications, including the production of syngases and bio-fuels, heating purposes, transportation, etc. There are numerous ongoing Power-to-X projects in the world, employing various technologies with different end-products such as methane, methanol, and dimethyl ether [3, 4].

In the context of this study, the end-product is aimed to be methanol due to its advantageous properties, including being liquid under atmospheric conditions, high gravimetric and volumetric hydrogen storage capacity and low transportation costs [5]. To synthesise methanol from hydrogen, a source of CO_2 is essential for the chemical reaction. This can be achieved through direct air capture (DAC) to reduce the atmospheric CO_2 concentration or by extracting CO_2 from seawater, where the CO_2 concentration is 125 times higher than in air [6, 7].

The rest of the article is structured as follows: The second section delves into the methodology to be employed throughout the study. Additionally, the proposed configuration for the offshore hydrogen production system is explained. Thereafter, the third section addresses the noteworthy challenges that merit exploration within the scope of this research. Lastly, the concluding remarks are presented in the final section, summarising the scope of this research.

Methodology

The aggregation of the required units for methanol production in close proximity presents an opportunity to leverage the concept of an energy island. Alongside the electrolyser for hydrogen production, a battery energy storage system (BESS) can be incorporated into the configuration of the island to explore the feasibility of the scheme. Furthermore, it is possible to integrate a chemical energy storage system (CESS) into the system to store the generated molecules. Moreover, to supply units such as electrolysers with direct current (DC), or convert the stored energy within the BESS to alternating current (AC), AC/DC/AC conversion units become necessary. Finally, any excess electricity, if available, as well as the produced hydrogen or methanol, can be either transported to the mainland or exported to neighbouring countries. A schematic of the proposed energy island, conceptualised to accumulate energy, capture CO_2, produce hydrogen, and ultimately synthesise methanol is shown in Fig. 1.

Employing an energy island offers a unique opportunity to utilise seawater for the electrolysis process. This approach effectively mitigates the concern associated with conserving fresh water for electrolysis, thereby addressing water scarcity issues. Nevertheless, owing to seawater impurities, the feed water needs some form of treatment. Generally, when opting for seawater as feedstock, two approaches for supplying

*Corresponding author: siavash.asiaban@ugent.be

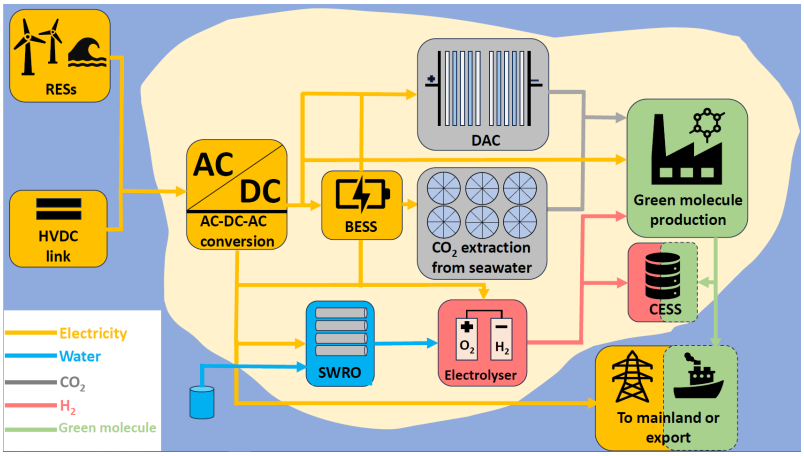

Figure 1: A schematic of the proposed energy island

electrolysers come into consideration, namely, direct seawater electrolysers (DSWE) and seawater electrolysis with upfront water treatment and purification. DSWE demands substantial re-designing of the currently available electrolysers as well as the development of new electrocatalysts for both conventional alkaline (AE) and proton exchange membrane (PEM) electrolysers, primarily due to the high concentration of corrosive chloride ions. Consequently, seawater with upfront treatment is the focus of this study. For this purpose, seawater reverse osmosis (SWRO) is considered due to its advantages, including producing high-quality water production and high energy efficiency [8].

In terms of selecting the appropriate type of electrolyser for the energy island, several conclusions have been drawn from existing literature. A recent study on seawater electrolysis technologies for hydrogen production at sea indicates that the differences between alkaline and PEM electrolysers are trivial [9]. Seeking the best current electrolysis technology to produce offshore hydrogen using marine energy, this study compared AE, PEM electrolyser, solid oxide (SO) electrolyser and direct seawater electrolysis where economic, environmental and social factors are considered as comparison criteria. Overall, this study concluded that both alkaline and PEM electrolysers are likely to play a major role in the sector of hydrogen production at sea, with the latter currently holding the best prospects of applicability. Nevertheless, this article suggests if AE makes sufficient progress, reducing its risk profile for offshore applications, it could become the more promising technology for hydrogen production at sea.

The authors in [10] see the desalination process comprising seawater reverse osmosis (SWRO) coupled with PEM electrolyser as the highest likelihood of being adopted in the near future. According to their findings, the aforementioned combination is a more practical immediate method for seawater electrolysis rather than investing in developing catalysts and systems for direct seawater electrolysis.

Discussion

When contemplating an energy island, several key aspects can be taken into account.

Synergies between offshore energy sources. The integration of offshore wind energy with wave or tidal energy presents an intriguing opportunity, benefiting from the time delay between these sources. For example, given the fact that waves are lagging with respect to wind, the synergy between these two sources is an area of interest. However, wave and tidal energy technologies are generally less mature and yield lower power compared to wind. Additionally, the synergy of the island with the onshore production is worth investigating.

Flexibility in low-inertia power systems. The ability of the energy island to provide flexibility in a low-inertia power system is of great significance. It can offer provision of ancillary services across different time scales and provides flexibility both on the production and load sides.

Dynamic scheduling and control of the electrolyser. Examining the dynamic scheduling and control of the electrolyser, when coupled with intermittent RESs, is valuable. This can be implemented based on factors such as the dynamic response of the electrolyser in the presence of fluctuating RESs, hydrogen demand, electricity price, and available storage capacity both in chemical and electrical forms.

Optimised operation. Optimising the operation of the energy island is critical. This can be achieved by taking into account various objectives such as costs, CO_2 reduction and so forth.

Life cycle assessment (LCA). Conducting a comprehensive LCA study is of importance. This study can compare different molecules, such as hydrogen, methanol and methane, to evaluate their environmental impacts and sustainability throughout their entire life cycles.

Incorporating these considerations can lead to an effective design and operation of energy islands, facilitating their integration into the energy systems.

Conclusions

This article presented a scheme for the production of green molecules at sea. Since RESs exhibit a fluctuating output power, their intermittency could be effectively accommodated using electrolysers. This study focuses on the production of green molecules at sea, taking advantage of the benefits offered by the seawater. To this end, the feed water for the electrolyser needs to undergo desalination, and for this purpose, SWRO has been chosen to supply the water. Additionally, the primary end-product of the project is methanol, which is why two CO_2 capturing methods, i.e., DAC and CO_2 extraction from seawater have been incorporated into the configuration of the energy island. By the end of this study, the operation of multiple units integrated into the energy island is going to be examined. This will include the interaction between the available, flexibility provision of the island, scheduling and control of the electrolyser, optimising the operation of the island and LCA studies.

References

[1] Siavash Asiaban, Nezmin Kayedpour, Arash E Samani, Dimitar Bozalakov, Jeroen DM De Kooning, Guillaume Crevecoeur, and Lieven Vandevelde. Wind and solar intermittency and the associated integration challenges: A comprehensive review including the status in the Belgian power system. *Energies*, 14(9):2630, 2021.

[2] Arash E Samani, Anna D'Amicis, Jeroen DM De Kooning, Dimitar Bozalakov, Paolo Silva, and Lieven Vandevelde. Grid balancing with a large-scale electrolyser providing primary reserve. *IET Renewable Power Generation*, 14(16):3070–3078, 2020.

[3] Christina Wulf, Petra Zapp, and Andrea Schreiber. Review of Power-to-X demonstration projects in Europe. *Frontiers in Energy Research*, 8:191, 2020.

[4] Zaher Chehade, Christine Mansilla, Paul Lucchese, Samantha Hilliard, and Joris Proost. Review and analysis of demonstration projects on Power-to-X pathways in the world. *International Journal of Hydrogen Energy*, 44(51):27637–27655, 2019.

[5] Konstantin Räuchle, Ludolf Plass, Hans-Jürgen Wernicke, and Martin Bertau. Methanol for renewable energy storage and utilization. *Energy Technology*, 4(1):193–200, 2016.

[6] Ahmed Sodiq, Yasser Abdullatif, Brahim Aissa, Arash Ostovar, Nashaat Nassar, Muftah El-Naas, and Abdulkarem Amhamed. A review on progress made in direct air capture of CO_2. *Environmental Technology & Innovation*, page 102991, 2022.

[7] Hongwei Li, Zhigang Tang, Xiao Xing, Dong Guo, Longpeng Cui, and Xian-zhong Mao. Study of CO_2 capture by seawater and its reinforcement. *Energy*, 164:1135–1144, 2018.

[8] Jungbin Kim, Kiho Park, Dae Ryook Yang, and Seungkwan Hong. A comprehensive review of energy consumption of seawater reverse osmosis desalination plants. *Applied Energy*, 254:113652, 2019.

[9] Rafael d'Amore Domenech, Oscar Santiago, and Teresa J Leo. Multicriteria analysis of seawater electrolysis technologies for green hydrogen production at sea. *Renewable and Sustainable Energy Reviews*, 133:110166, 2020.

[10] MA Khan, Tareq Al-Attas, Soumyabrata Roy, Muhammad M Rahman, Noreddine Ghaffour, Venkataraman Thangadurai, Stephen Larter, Jinguang Hu, Pulickel M Ajayan, and Md Golam Kibria. Seawater electrolysis for hydrogen production: a solution looking for a problem? *Energy & Environmental Science*, 14(9):4831–4839, 2021.

Public Participation in the decision-chain of hydrogen

Ruben Rehage[*1]
University of Groningen: Groningen Centre for Energy Law and Sustainability and the Department for Environmental Psychology

Introduction

To achieve the climate targets they have set themselves, the European Union and the member states must significantly increase the production of hydrogen in the coming years [1, p. 16]. It is the scientific consensus that various industrial processes (e.g. the production of steel) can hardly be decarbonised without the use of hydrogen [2].
Today, the development of a hydrogen economy in Europe is still at the initial stages of policy plans and programmes, e.g. [3], [4], [8]. However, a lack of public acceptance could significantly hinder progress or even cease the development of a hydrogen economy entirely.
While acceptance of an abstract renewable energy policy is often high, research (and experience) shows that acceptance tends to be significantly lower at the project level [5]. One reason for this acceptance gap is that citizens are often dissatisfied with how participation is organised in the decision-chain of an energy project, e.g. [6]. In particular, one issue that causes discontent is that a decision made at the macro-level (at the beginning of the decision-chain) can no longer be deviated from at the micro-level (at the end of the chain) [7].
The aim of this PhD project is to investigate the question of whether giving citizens engaging in public participation more leeway in deviating from macro-level decisions at project level leads to higher acceptance of the project. The overarching research question of this PhD project hence reads as follows:
How does giving citizens engaging in public participation more leeway at project level to deviate from decisions made at the macro-level of the decision-chain affect the acceptance gap between hydrogen as an energy technology and a concrete hydrogen project?
To answer this question, the research project is divided into four parts, each of which in itself answers individual research questions that add to the overall project.

Paper A: Public Participation in the hydrogen decision-chain in Germany

Governments across Europe are working to create the legal framework for the development of a hydrogen economy, e.g. [3], [4], [8]. Understandably, national governments try to design a legal framework that allows the hydrogen economy to develop as quickly as possible, [8, p. 4] and [4, p. 4]. However, when citizens feel excluded from the decision-making process or perceive the participation process as unfair, they might, for example, oppose individual hydrogen projects at the local level and hence slow down or even halt the development of individual projects [6]. This research project intends to legally investigate public participation in the decision-chain of the hydrogen core network in Germany.
A reform of the Energy Industry Act, which is currently at the final stages of the legislative process, sets out the procedure for the Transmission System Operators (TSOs) to come to a hydrogen core network, [10, section 28r]. The hydrogen core network shall be approved by the Bundesnetzagentur, the respective pipelines shall be “necessary and urgent in terms of the

* Corresponding author: r.m.k.rehage@rug.nl
[1] Note: The author has just begun his PhD in September 2023, and even though the theoretical basis of the project is already well developed, no results have been published yet. This may change by the date of the conference.

energy industry and (…) are in the overriding public interest" [10, section 28r (8), p. 25]. Such a qualification might potentially have extensive implications for further public participation at the later stages of the decision-chain, as, for example, the precise location of the pipelines will already be decided at this point.
The question that follows from this is how such a decision by the Federal Network Agency on the hydrogen core network according to section 28r (8) EnWG-E will affect further public participation exactly - and whether the legal character of the respective decision by the Federal Network Agency justifies that in the public participation during the planning approval procedure substantial questions have already been completely decided and are no longer open for debate (potentially making public participation largely pointless). The research question hence reads as follows:

How does the decision of the Bundesnetzagentur on a hydrogen core network according to section 28r (8) EnWG relate to the public participation procedure in the approval planning process?

Methodology
This paper's methodology employs a multifaceted approach, combining the legal comparison method and the legal dogmatic research method with doctrinal constructivism. The legal comparison method involves a systematic examination of the pertinent legal frameworks both for hydrogen and for public participation to identify similarities, differences, and underlying principles. Simultaneously, the legal dogmatic research method delves into the doctrinal aspects within the legal frameworks, analyzing statutory provisions, case law, and legal doctrines. Additionally, doctrinal constructivism critically engages with legal concepts to understand how legal doctrines are constructed and interpreted within specific contexts.
By integrating these methodologies, the research aims to provide a comprehensive analysis of the legal framework of public participation within the hydrogen decision-chain with a special focus on how the decision by the Bundesnetzagentur according to section 28r (8) EnWG-E affects public participation on the later stages of the planning approval procedure.

Paper B: The acceptance gap in the decision chain of hydrogen

It is undisputed that public acceptance of an energy technology is essential for its large-scale implementation. Consequently, it exists a large quantity of research on this topic, e.g. [12], [13]. One essential finding is that while acceptance of an abstract renewable energy policy is often high, research shows that acceptance tends to be significantly lower at the project level.[5] However, it is unclear whether this finding also holds true for hydrogen as an energy technology.
In this paper, it will be investigated whether it exists a gap between the acceptance towards the abstract idea of a hydrogen economy in general and the acceptance towards a concrete hydrogen project at the local level. While hydrogen acceptance is generally high [14, p. 10545], it remains to be researched whether this acceptance level remains similar when the decision-chain reaches project-level – or whether, comparable to other energy projects, an acceptance gap exists between hydrogen policy and hydrogen projects. The research question for this paper hence reads as follows:

Does an acceptance gap exist between hydrogen as an energy technology in general and concrete hydrogen projects at the local level?

Hydrogen can be transported and stored in a variety of ways [15], hence when discussing hydrogen projects at the local level, different possible technologies need to be considered. In the case of hydrogen storage, for example, Scovell notes that the various forms of hydrogen storage "have unique attributes that may influence acceptance" [14, p. 10454]. The author

points out that research has shown that some people for example might have concerns about storing hydrogen underground or might be less supportive of large-scale hydrogen infrastructure [14, p. 10454]. Building on these fundamental insights, in this paper it will be investigated how acceptance relates between the macro level of the decision-chain and the local level when differentiating between the different relevant hydrogen technologies of the hydrogen core-network, namely large-scale transport infrastructure (pipelines), underground storage and storage facilities for ammonia.

Methodology
To describe behaviors and to gather people's perceptions of a certain issue, survey studies with a standardized questionnaire are one suitable method [16, p. 7]. Steg and de Groot also point out that questionnaires are widely used to establish relationships between two or more variables. In this case, a representative image of people's acceptance of hydrogen shall be established. Furthermore, it shall be investigated how the acceptance of hydrogen as an energy technology relates to the respective concrete hydrogen projects at the local level. The aim is to find out whether it exists an acceptance gap between hydrogen as an energy technology in general and the relevant technologies of the hydrogen core network – or if, for example, such a gap only exists in the case of certain technologies, for example underground storage.

Paper C: Acceptance and engagement in the decision-chain of hydrogen

The hydrogen economy is still at the beginning of its development. As a result, there is a lack of experience in the realisation of hydrogen projects, including with regard to the role of citizens in public participation. Although there is a rich body of literature on public participation in wind and solar projects [17] [6], it has not yet been investigated whether these scientific findings can be transferred to hydrogen.
In this paper, it will hence be investigated whether and if so how citizens want to participate in the decision chain of hydrogen. The question is at what point in the decision chain citizens want to participate, whether this desire differs for the various technologies and how much and in what way citizens want to have influence on, e.g., the location, choice of technology etc. The respective research question hence reads as follows:

Do and if so how do citizens want to participate in the decision-chain of hydrogen?

To the author's best knowledge, the literature is still scarce in this field. For wind and solar, it is well established that while citizens want to participate in the decision-chain once a project becomes concrete at the local level, at the same time they also want to have influence on major decisions [18]. Furthermore, it is well established that the lower the level of acceptance for a (wind) project, the higher the willingness to participate in the decision-chain [19]. However, it must still be investigated whether these findings also hold true in the case of hydrogen as an energy technology. It must also still be established if citizens want to participate in the decision chain of hydrogen at all – and if there are differences between the respective technology and the willingness to participate.

Methodology
Again (see above), to describe behaviors and to gather people's perceptions of a certain issue, questionnaire studies are one suitable method [16, p. 7]. Steg and de Groot also point out that questionnaires are widely used to establish relationships between two or more variables. In this case, a representative image of people's desire to participate in the decision-chain of hydrogen shall be established. Furthermore, it shall be investigated how the level of acceptance of hydrogen as an energy technology in general and the respective technologies in particular

relative to the desire to participate in the decision-chain – and if citizens wish to participate is stronger in the case of certain technologies, e.g. underground storage.

Paper D: Public participation in the decision chain of hydrogen

While acceptance of an abstract renewable energy policy is often high, research shows that acceptance tends to be significantly lower at the project level [5]. One reason for this "acceptance gap" is that citizens are dissatisfied with how participation is organised in the decision-chain of an energy project, e.g. because they feel excluded from the decision-making process or perceive the participation process as unfair [7]. In particular, one issue that causes discontent is that at the level of the decision-chain at which participation takes place, citizens' possibilities for influence are often very limited. A decision, for example, that was made at the macro-level (at the beginning of the decision-chain) can normally no longer be deviated from at the micro-level (at the end of the chain) [7].
The aim of this paper is to investigate the question of whether giving citizens engaging in public participation more leeway in deviating from macro-level decisions at project level leads to higher acceptance of the project – and in turn leads to a decreased acceptance gap.
The overarching research question hence reads as follows:

> *How does giving citizens engaging in public participation more leeway at project level to deviate from decisions made at the macro-level of the decision-chain affect the acceptance gap between hydrogen as an energy technology in general and a concrete hydrogen project?*

Methodology
The idea of this paper is to test the effect it would have to give citizens more leeway in the participation process on the acceptance of a hydrogen project in an experimental setup. The chosen methodology for this paper is that of an experimental survey. Such an experimental setup enables the establishment of causal relationships between variables [16, p. 8]. In an experimental design, the variable that is thought to be essential for the outcome of a process (i.e. the independent variable) is manipulated to see if the change will lead to differences in the outcome variable of interest (i.e. the dependent variable) [20]. In this case, the independent variable is the level of leeway to deviate from macro-level decisions that citizens have during the public participation for a hydrogen project. The dependent variable therefore is citizens' acceptance of the respective project. The question of interest that follows from this is whether acceptance for a concrete hydrogen project at the local level increases (i.e., the acceptance gap decreases) when citizens' leeway in public participation increases as well.

References

[1] International Renewable Energy Agency (IRENA), "Global hydrogen trade to meet the 1,5°C climate goal," 2022, Accessed: Nov. 21, 2023, available: https://www.irena.org/-/media/Files/IRENA/Agency/Publication/2022/Jul/IRENA_Global_hydrogen_trade_part_1_2022_.pdf

[2] T. Fleiter et al., "METIS 3- Study S5 – The impact of industry transition on a CO2-neutral European energy system," Fraunhofer Inst. for Syst. and Innov. Res., 2023, Accessed: Nov. 21, 2023, available: https://op.europa.eu/en/publication-detail/-/publication/72954c87-327a-11ee-83b8-01aa75ed71a1

[3] European Commission, "REPowerEU Plan," 2022, COM(2022) 230 final

[4] Ministerio para la Transición Ecológica y el Reto Demográfico (MITERD), “Hoja de Ruta del hidrógeno,” 2020, accessed: Nov. 21, 2023, available: https://energia.gob.es/es-es/Novedades/Documents/hoja_de_ruta_del_hidrogeno.pdf

[5] S. Batel and P. Devine-Wright, “A critical and empirical analysis of the national-local ‘gap’ in public responses to large-scale energy infrastructures,” 2015, J. of Env. Pla. and Man., Vol. 58, Iss. 6, pp. 1076–1095

[6] L. Liu et al., “Public participation in decision making, perceived procedural fairness and public acceptability of renewable energy projects,” 2020, En. and Cl. Ch., Vol. 1

[7] G. Perlaviciute and L. Squintani: “Public Participation in Climate Policy Making: Toward Reconciling Public Preferences and Legal Frameworks,” 2020, One Ea. Persp., Vol. 2, Iss. 4

[8] Ministerium für Wirtschaft und Klimaschutz (BMWK), „Fortschreibung der Nationalen Wasserstoffstrategie,“ 2023, accessed: Nov. 21, 2023, available: https://www.bmbf.de/SharedDocs/Downloads/de/2023/230726-fortschreibung-nws.pdf?__blob=publicationFile&v=1

[9] G. A. Reigstad et al., “Moving toward the low-carbon hydrogen economy: Experiences and key learnings from national case studies,” 2022, Ad. in Ap. En., Vol. 8

[10] Bundesrat, Gesetzentwurf der Bundesregierung, „Entwurf eines Gesetzes zur Anpassung des Energiewirtschaftsrechts an unionsrechtliche Vorgaben und zur Änderung weiterer energierechtlicher Vorschriften,“ Drucksacke 230/23, 2023, accessed: 16.10.2023, available: https://dserver.bundestag.de/brd/2023/0230-23.pdf

[11] FNB Gas, „Wasserstoffnetz 2030: Aufbruch in ein klimaneutrales Deutschland,“ 2023, accessed: Nov. 21, 2023, available: https://fnb-gas.de/wasserstoffnetz/h2-netz-2030/

[12] R. Wüstenhagen et al., “Social acceptance of renewable energy innovation: An introduction to the concept,” 2007, En. Pol., Vol. 35, Iss. 5

[13] N. M. A. Huijts et al., “Psychological factors influencing sustainable energy technology acceptance: A review-based comprehensive framework,” 2012, Ren. and Sus. En. Rev., Vol. 16, Iss. 1

[14] M. D. Scovell, “Explaining hydrogen energy technology acceptance: A critical review,” 2022, Int. Jou. of Hyd. En., Vol. 47, pp. 10441-10459

[15] H. Frey et al., Energieträger Wasserstoff, Wiesbaden, Germany: Springer Vieweg, 2023

[16] L. Steg and J. de Groot, Environmental Psychology – An Introduction, 2nd. Ed., Hoboken, NJ : Wiley, 2019

[17] G. Perlaviciute et al., “At the Heart of a Sustainable Energy Transition – The Public Acceptability of Energy Projects,” 2018, IEEE Pow. & En. Mag., Vol. 16, No. 1

[18] G. Perlaviciute, “Contested climate policies and the four Ds of public participation,” 2022, Wiley Int. Rev.: Cl. Ch., Vol. 13, Iss. 1

[19] L. Liu et al., “Opposing out loud versus supporting in silence: who wants to participate in decision-making about energy projects?,” 2022, Env. Res. Let., Vol. 17, No. 11

[20] S. Schneider, “Experimental and Quasi-Experimental Designs in Behavioral Research: On Context, Crud, and Convergence,” 2011, in: *The SAGE Handbook of Social Science Methodology*, W. Outhwaite and S. P. Turner (ed.), London, UK: SAGE Publications

Radio Frequency Sputtering deposition of MoS_2 electrocatalyst thin films for Anion Exchange Membrane Water Electrolysis

G. Di Gregorio*[1,2], N. B. Laidani[1], M. Testi[1], M. Miola[2]

[1] Fondazione Bruno Kessler, Via Sommarive, 18, 38123 Povo (TN), Italy

[2] Enphos, Via Giuseppe Zorzi 7, 37138 Verona, Italy

The kinetics of the hydrogen evolution reaction (HER) in anion exchange membrane water electrolysis (AEMWE) can be significantly enhanced by carefully controlling the synthesis of electrocatalysts. Sputtering techniques offer numerous advantages over traditional catalyst fabrication methods, including the ability to deposit a large number of motifs while enabling precise control of the composition, microstructure, thickness, and load. Herein, we present a versatile method for fabricating ionomer-free molybdenum disulfide (MoS_2) electrocatalysts onto graphite laminate substrates using Radio Frequency Magnetron sputtering. Characterization of the as-sputtered thin films was conducted by X-ray photoelectron spectroscopy (XPS), X-ray Diffraction (XRD), and Scanning Electron Microscopy (SEM) to evaluate the influence of sputtering operating parameters. The as-sputtered samples will be incorporated into a 25 cm^2 Membrane Electrode Assembly (MEA) and tested as cathode electrodes, alongside commercial anodes and anion exchange membranes. The results will provide new insights into the capability of sputtering to regulate the electrochemical properties of HER electrocatalysts, thereby contributing to the advancement of AEMWE technology.

Introduction

The global pursuit of achieving carbon neutrality by 2050 has ushered in a new era for hydrogen as a critical energy source. Despite this, the prevailing and economically efficient method for hydrogen production remains steam-methane reforming, regrettably leading to substantial carbon emissions. Water electrolysis has thus emerged as a sustainable alternative, enabling the production of "green hydrogen" by utilizing electricity generated from renewable sources to split water into hydrogen and oxygen.

Among various water electrolysis technology, the anion exchange membrane water electrolysis (AEMWE) has recently gained widespread recognition. This technology preserves the advantages of proton exchange membrane water electrolysis (PEMWE) by employing solid electrolyte membranes. However, its principal merits stem from the use of non-corrosive liquid feeds, such as pure water or mild alkaline solutions. This mitigates challenges associated with carbonate formation prevalent in alkaline water electrolysis (AWE) operating with highly corrosive alkaline electrolytes, and increases compatibility with low-cost raw materials. Indeed, electrocatalysts for AEMWE can be made from platinum metal group (PGM)-free materials, such as nickel (Ni), cobalt (Co), iron (Fe), molybdenum (Mo), and copper (Cu) in the form of mixed-metal alloys, oxides, chalcogenides, nitrides, phosphates, carbides and composites/hybrids [1-2]. This results in cost reductions compared to PEMWE, which requires expensive corrosion-resistant components like platinum (Pt) for the hydrogen evolution reaction (HER).

Molybdenum disulfide (MoS_2) emerges as a promising alternative to Pt for the HER catalysis due to its stability and cost-effectiveness. In acidic conditions, crystalline MoS_2 exhibits catalytic activity primarily at its active edge sites, while the atomic basal planes have

* Corresponding author: gdigregorio@fbk.eu

limited reactivity towards HER [3]. However, in alkaline media, MoS_2 demonstrates slow dynamics of water adsorption and dissociation due to its intrinsic structural characteristics. It has been proved that amorphous MoS_2 offers abundant active sites and structural defects, resulting in enhanced hydrogen-evolution activity [4]. However, amorphous MoS_2 has low electronic conductivity, which can be overcome by combining it with highly conductive carbon-based supports [5]. To enhance the alkaline catalysis of MoS_2, various surface modifications involving the introduction of functional groups or molecules with a high affinity for water have been explored [6]. These entities attract and hold water molecules, promoting their adsorption near the catalyst's active sites. Another strategy involves incorporating first-row 3d transition metals, such as Co, Ni, or Fe, into MoS_2 to modulate its intrinsic electronic structure [7]. Despite these advancements, the catalytic activity of MoS_2 in alkaline conditions still remains unclear, and further research is needed to comprehend the reaction mechanisms.

In the realm of developing MoS_2 as electrocatalysts for AEMWE, careful selection of the proper composition and structure is thus crucial. Determining the most effective processing procedure for incorporating the catalyst into the membrane electrode assembly (MEA) is equally vital. Traditional multi-stage fabrication techniques, which involve the use of powders, binders/ionomers, and painting/spraying processes, have limitations in controlling the composition and structure of electrocatalysts. This can hinder scalability to larger areas with uniformity, and may result in the formation of hazardous by-products. Recently, physical vapor deposition (PVD), particularly sputtering, has garnered significant attention as catalyst fabrication technique due to its numerous advantages [8-11], including its reproducibility, scalability, and environmental friendliness. Sputtering techniques permit the deposition of a wide variety of materials onto different type of supports, including porous transport layers and membranes. Precise control over the properties of the deposited catalyst is achievable, allowing for tailoring the composition of the material, optimizing its microstructure, and controlling the loading and thickness on the substrate. Furthermore, by selecting the optimal operational parameters, such as sputtering targets, sputtering power, working gas composition, substrate temperature, and deposition geometry, it becomes possible to obviate many steps required by other techniques, thereby depositing the electrocatalyst layer in one step.

The capabilities of sputtering as catalyst fabrication technique for AEMWE have been previously demonstrated by López-Fernández et al. [12], who prepared nickel-based anodes for AEMWE with different chemical formulations, namely metallic Ni, oxide NiO, and oxyhydroxide $NiO_x(OH)_y$ layers, by changing the working gas composition from Ar, to Ar/O_2, and $Ar/O_2/H_2O$. Meanwhile, the film microstructure was precisely controlled by using the magnetron sputtering at oblique deposition angles (MS-OAD) technique, which allows the fabrication of porous nanocolumnar layers with higher electrocatalytic activity than compact films prepared at normal configuration. In another study [13], the authors demonstrated that MS can also avoid the need to mix ionomers with catalysts during the membrane electrode assembly (MEA) preparation, enabling the development of self-supported electrocatalysts. A nickel sputtering target with a specific number of iron stripes was used to fabricate an optimized ionomer-free Ni/Fe bimetallic thin film. This film exhibited outstanding electrochemical response as the anode in an AEMWE cell.

In this paper, we present a one-step method for fabricating ionomer-free MoS_2 electrocatalysts onto graphite laminate substrates using radio frequency magnetron sputtering. A preliminary ex-situ screening of the functional properties was conducted to evaluate the influence of sputtering operating parameters, using X-ray photoelectron spectroscopy (XPS), X-ray Diffraction (XRD), Scanning Electron Microscopy (SEM), and contact angle measurements. The samples will be incorporated into a 25 cm^2 AEMWE cell setup and tested as cathode electrodes at various pressures, temperatures and operating current densities. MEAs

demonstrating successful in-situ performance will be considered for inclusion in short stacks, after scaling up to the required geometric area.

Methodology

MoS_2 thin films were deposited at room temperature onto commercially available graphite laminate substrates (AvCarb®MGL370, FuelCellStore) using radio frequency (13.56 MHz) magnetron sputtering in the planar configuration. The deposition process occurred within a vacuum chamber, comprising a cathode serving as the target material and an anode holding the substrate. The working distance between the cathode and the anode was fixed at 25 cm. Before each deposition, the chamber was evacuated to reach a base pressure of approximately 3 x 10^{-6} mbar, achieved using a combination of a rotary pump and a turbo molecular pump. Subsequently, pure argon gas was introduced into the chamber to establish a working pressure of about 6 x 10^{-2} mbar with a constant flow rate at 21 sccm. A commercially available MoS_2 disc (99.95% purity, 50.8 mm diameter x 4 mm thick, Testbourne) served as the sputtering target. Prior to deposition, the MoS_2 target underwent a pre-sputtering step for 15 minutes to remove any surface contaminations. The deposition process was conducted by varying the deposition time and the sputtering power.

To enhance the compatibility of MoS_2 electrocatalysts with alkaline electrolytes, an additional treatment will be applied. After deposition, the samples will be treated with RF oxygen and argon plasma (Colibrì, by Gambetti) with variations in treatment time. This approach aims to improve the electrocatalytic performance of MoS_2 thin films by introducing a large number of defects that can facilitate the interaction with water molecules, thereby enhancing the alkaline HER catalysis. Furthermore, RF co-sputtering will be employed to fabricate Co-doped MoS_2 electrocatalysts, involving the simultaneous deposition of Co and MoS_2 targets. The presence of cobalt is expected to enhance the catalytic activity of the MoS_2 thin films, making them more effective in promoting the HER in alkaline media.

A thorough ex-situ physico-chemical characterization was conducted in order to elucidate the impact of sputtering fabrication parameters onto the structural, chemical, surface, and morphology properties of electrocatalysts. A profilometer was used to measure the thickness and surface roughness of the sputtered thin films. X-ray photoelectron spectroscopy (XPS) was performed for qualitative and quantitative surface characterization. X-ray diffraction (XRD) analysis determined the crystallographic structure of the thin films. Scanning electron microscopy (SEM) was employed to examine the surface morphology, size, shape, and homogeneity of the sputtered samples. Contact angle measurements were performed to evaluate the wettability and surface energy of the electrocatalyst thin films. By comparing the ex-situ analysis results before and after electrochemical operation, valuable insights will be obtained regarding the behavior and evolution of the electrocatalysts during electrochemical reactions.

The Membrane Electrode Assembly (MEA) will be prepared based on the configuration used in the NEWELY project, focused on advancing AEMWE technologies. This MEA possesses an area of 25 cm^2, and its design incorporates a patented hydraulic cell compression system, ensuring proper contact between components. For the anode, a commercially available product manufactured by Dioxide Materials is employed, while the anion exchange membrane is the FUMATECH FAA-50, known for its excellent ion conductivity and long-term stability. By incorporating commercial anodes and membranes, the MEA setup establishes a reliable performance baseline. Thus, a comprehensive system is created for evaluating the electrocatalytic activity and performance of the as-sputtered electrocatalysts.

The experiments will be carried out at a reference temperature ranging from 50 to 70 °C, using KOH feeding solutions with concentrations ranging from 0.1 to 1 M, while the pressure will be set between 8 and 11 bar. The protocol for characterizing the electrocatalysts in the single-cell configuration will entails a series of conductivity tests. In this test, the anion exchange membrane is replaced with a stainless steel foil to assess the ohmic resistance of the system in the absence of the membrane. A current ranging from -2 A to 2 A will be applied, with the corresponding voltage measurements recorded. Using Ohm's law, the ohmic resistance can be calculated. Furthermore, linear sweep voltammetry (LSV) analyses will be executed, spanning from open circuit voltage (OCV) to 2.1 V while recording the resulting current. This technique enables the construction of a polarization curve (IV curve), thereby providing insights into the electrochemical activity, reaction kinetics, and polarization behavior of the electrocatalyst. In addition, electrochemical impedance spectroscopy (EIS) will be performed at three different voltages: the OCV, 1.7 V, and 2.1 V. A small sinusoidal voltage perturbation with an amplitude of 20 mV will be applied, and the frequency range will be set between 100 kHz and 0.1 Hz.

Discussion

In order to understand the functional properties of the sputtered MoS_2 thin films, it is worth noting that the thickness of the catalyst film plays a crucial role in influencing its electrochemical behavior. Therefore, understanding the relationship between film thickness and functional properties is essential for optimizing the performance of MoS_2 thin films. A representative SEM image of a generic sample of MoS_2 deposited on AvCarb®MGL370 (Figure 1) clearly demonstrates the laminated nature of the substrate, which posed challenging in accurately measuring the film thickness. To overcome this limitation, we have devised a strategy that involves fabricating films with controlled and uniform thicknesses on flat silicon substrates. By using flat silicon substrates as a platform for studying film thickness, we have been able to make more precise measurements and comparative analyses among different samples. This approach provided us with a standardized metric, known as "equivalent thickness," which serves as a reference for evaluating and discussing film thickness across our experiments. By calculating the deposition rate, we can produce samples with identical thickness but varying the sputtering power during the deposition process. This approach will allow us to isolate the effect of film thickness on the electrochemical properties of the electrode.

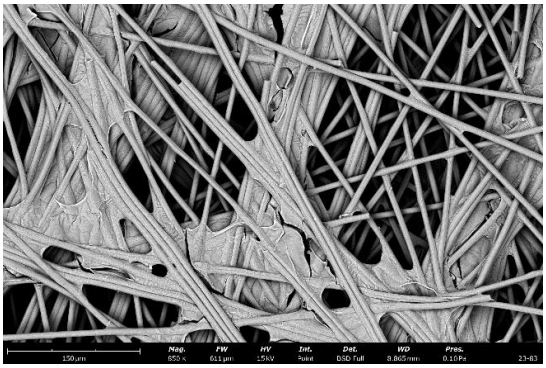

Figure 1. SEM image of amorphous MoS_2 deposited on AvCarb®MGL370

The structural properties of the deposited thin films were investigated through XRD analyses. The results showed that the MoS_2 films had an amorphous structure, as no XRD peaks were detected. Further XRD investigations will be conducted to explore potential phase

transformations or alterations in the film structure resulting from the electrochemical operations. By analyzing the evolution of the film structure, valuable insights are expected to be obtained into the correlation between the structural properties and electrochemical behavior exhibited by these films. This endeavor will undoubtedly contribute to our overall understanding of the intricate relationship between film structure and electrochemical performance.

In addition, XPS was conducted to analyze the chemical composition and surface states of the MoS_2 samples deposited on AvCarb®MGL370 substrate. The fitting software utilized for the XPS spectra analysis is based on R Studio. The XPS spectra were fitted with a Gaussian-Lorentz peak shape, after a Shirley-type background subtraction. Figure 2 presents the typical XPS core line spectra of S2p and Mo3d obtained for the amorphous MoS_2 samples.

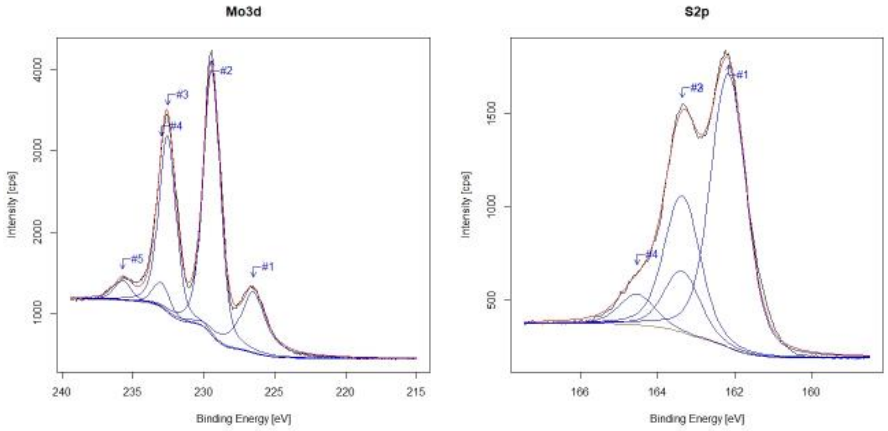

Figure 2. Mo3d and S2p core spectra of amorphous MoS2 deposited on AvCarb®MGL370

In the core spectrum of Mo3d, we have observed five distinct peaks. The lowest energy peak, which is a singlet, arises at 226.5 eV. This peak is attributed to the overlapping of sulfur signals in the Mo3d binding energy region and is associated with the S2s core level. The remaining four peaks correspond to two different doublet Mo3d peaks. To ensure accurate analysis, we have fitted the Mo3d spectra with proper constraints. The spin orbit splitting was fixed at 3.13 eV, and the area ratio between $Mo3d_{5/2}$ and $Mo3d_{3/2}$ was maintained at 3:2. The most intense doublet peaks occur at 229.4 eV and 232.6 eV, representing the $Mo3d_{5/2}$ and $Mo3d_{3/2}$ states, respectively. These peaks are associated with MoS_2, representing the Mo^{4+} oxidation state. On the other hand, the higher energy peaks at 233 eV and 235.7 eV correspond to MoO_3 (Mo^{6+}). Moving on the S2p core spectrum, we observe four distinct peaks, suggesting the presence of two different sulfur species in the amorphous MoS_2 samples. The intense peaks at higher binding energies (163.3 eV and 164.5 eV) correspond to bridging S_2^{2-} and/or apical S^{2-} $S2p_{3/2}$ and $S2p_{1/2}$ components, while the peaks at lower binding energies (162.1 eV and 163.3 eV) indicate the presence of unsaturated S^{2-} species. To ensure accurate analysis, also the S2p spectra were fitted with appropriate constraints. The spin orbit splitting was fixed at 1.18 eV, and the area ratio of $S2p_{3/2}$ and $S2p_{1/2}$ is maintained at 2:1. Furthermore, we are conducting a systematic analysis of the MoS_2 samples by varying the fabrication parameters. By gaining insights into the relationship between deposition conditions and the resulting characteristics of the MoS_2 films, we aim to optimize their electrochemical properties.

Our ongoing efforts involve the systematic acquisition of relevant measurements to elucidate key electrochemical characteristics. We will assess the ohmic resistance of the amorphous MoS_2 electrocatalysts through a comprehensive series of conductivity tests. It's crucial to note that the absence of the catalyst film resulted in an ohmic resistance of 25.53 mOhm. These preliminary findings inform our ongoing research, as we continue to explore and

improve the electrical conductivity of these electrocatalysts. Moreover, we will conduct in-situ measurements on the chosen samples to determine the potential suitability of the sputtered amorphous MoS_2 samples as high-performance electrocatalysts for the HER in AEMWE. Specifically, we aim to achieve a current density of at least 1 A/cm^2, aligning our research goals with the significant advances seen in the NEWELY project.

Conclusions

This study will contribute to the advancement of AEMWE technology by demonstrating the capability of Radio Frequency Magnetron sputtering to regulate the electrochemical properties of MoS_2 catalysts. The research findings will shed light on the potential of MoS_2 as a cost-effective alternative to Pt for HER catalysis in alkaline environments. By improving the understanding of MoS_2-based catalysts and their fabrication techniques, this work paves the way for the development of more sustainable and efficient methods for hydrogen production.

References

[1] Miller, Hamish Andrew, et al. "Green hydrogen from anion exchange membrane water electrolysis: a review of recent developments in critical materials and operating conditions." Sustainable Energy & Fuels 4.5 (2020): 2114-2133.

[2] Liu, Jiangjin, et al. "Elucidating the role of hydroxide electrolyte on anion-exchange-membrane water electrolyzer performance." Journal of The Electrochemical Society 168.5 (2021): 054522.

[3] Benck, Jesse D., et al. "Catalyzing the hydrogen evolution reaction (HER) with molybdenum sulfide nanomaterials." Acs Catalysis 4.11 (2014): 3957-3971.

[4] Ting, Louisa Rui Lin, et al. "Catalytic activities of sulfur atoms in amorphous molybdenum sulfide for the electrochemical hydrogen evolution reaction." Acs Catalysis 6.2 (2016): 861-867.

[5] Li, Dong Jun, et al. "Molybdenum sulfide/N-doped CNT forest hybrid catalysts for high-performance hydrogen evolution reaction." Nano letters 14.3 (2014): 1228-1233.

[6] Tao, Li, et al. "Plasma-engineered MoS2 thin-film as an efficient electrocatalyst for hydrogen evolution reaction." Chemical communications 51.35 (2015): 7470-7473.

[7] Inocêncio, Carlos VM, et al. "Taking advantage of teamwork: unsupported cobalt molybdenum sulfide as an active HER electrocatalyst in alkaline media." Journal of The Electrochemical Society 169.5 (2022): 054524.

[8] Liang, Jie, et al. "Magnetron sputtering enabled sustainable synthesis of nanomaterials for energy electrocatalysis." Green Chemistry 23.8 (2021): 2834-2867.

[9] López-Fernández, Ester, et al. "Recent advances in alkaline exchange membrane water electrolysis and electrode manufacturing." Molecules 26.21 (2021): 6326.

[10] de Lucas-Consuegra, Antonio, et al. "A novel sputtered Pd mesh architecture as an advanced electrocatalyst for highly efficient hydrogen production." Journal of Power Sources 321 (2016): 248-256.

[11] Alexeeva, O. K., and V. N. Fateev. "Application of the magnetron sputtering for nanostructured electrocatalysts synthesis." International journal of hydrogen energy 41.5 (2016): 3373-3386.

[12] López-Fernández, Ester, et al. "Chemistry and electrocatalytic activity of nanostructured nickel electrodes for water electrolysis." ACS Catalysis 10.11 (2020): 6159-6170.

[13] López-Fernández, Ester, et al. "Ionomer-Free Nickel-Iron bimetallic electrodes for efficient anion exchange membrane water electrolysis." Chemical Engineering Journal 433 (2022): 133774

Real scale safety investigations of hydrogen jet flames at high pressure

Christopher Bernardy*[1], Karim Habib[1], Alessandro Orchini [2]

[1] Bundesanstalt für Materialforschung und -prüfung (BAM), Berlin
[2] Chair of Nonlinear Thermo-Fluid Mechanics, Technical University of Berlin

Introduction

In order to reduce the human footprint of CO2 emissions and limit global warming effects hydrogen combustion is becoming increasingly important. To enable fuel cells and gas turbines to operates this carbon free fuel, unprecedently large amounts of hydrogen need to be produced and safely transported and stored. The investigation of the effects of accidents involving hydrogen is therefore becoming of outmost importance. Since hydrogen is usually stored and transported under pressure, one scenario to be considered is the release of hydrogen from a leakage with subsequent ignition. The resulting jet flame must be characterized with respect to the thermal radiation emitted into the environment to define safety regulations. Various models that characterize the resulting flame shape and radiation already exist in the literature, but these are mainly based on empirical data from hydrocarbon jet flames.[1-4] To verify these models, a H2 Jet Flame project conducted at BAM, is investigating the safety of momentum driven hydrogen jet flames. For this purpose, large-scale tests are carried out at the Test Site Technical Safety (BAM-TTS). The object of the investigations is to assess the effects of real scale release scenarios regarding flame geometry and the thermal radiation emitted. Parameters such as release angle, leakage diameter (currently 1 mm to 10 mm), pressure (currently up to max. 250 bar) and mass flow (up to max. 0.5 kg/s) are varied. In addition, influences such as the type of ignition, ignition location as well as delayed ignition can also be investigated. The gained knowledge will be compared with existing jet flame models, to validate these and identify a possible need for further development. In particular, the focus will be laid on the thermal radiation of hydrogen flames. The challenge here is the visualization and characterization of the flame geometry in an open environment. Visualization is performed using infrared (IR) camera systems from at least two viewing angles. Measurements of the heat radiation of jet flames, which can be found in the literature, are mostly based on unsteady outflow conditions.[5-11] The experimental setup used here allows for the generation of a steady-state outflow for several minutes and thus a direct comparability with existing (steady-state) models. Furthermore, the tests can be carried out for comparative measurements with hydrocarbons (methane, etc.) as well as mixtures of hydrogen and hydrocarbons.

Methodology

For large scale investigations a jet-flame test stand was constructed on the BAM-TTS. To ensure the requested steady state outflow with a constant mass flow over several minutes, a hydrogen storage of 90 kg at 300 bar is installed.

* Corresponding author: christopher.bernardy@bam.de

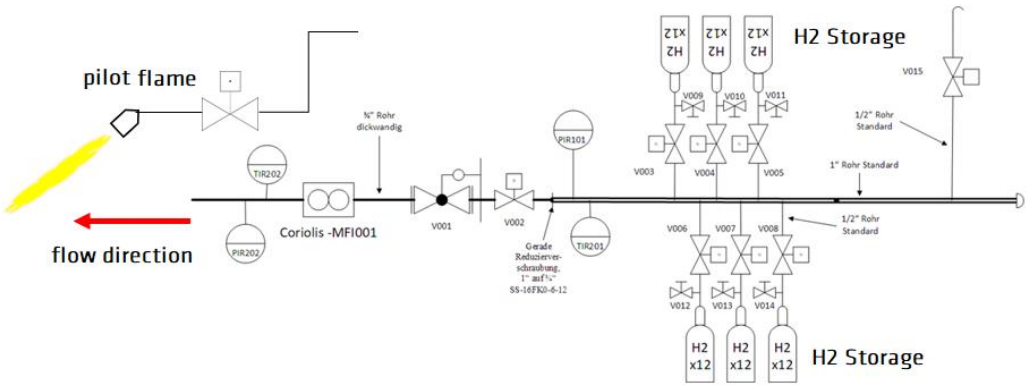

Figure 1: Flow chart and overview of jet flame test stand with used measurement equipment

The evaluation of the jet flame geometry is performed using infrared cameras. Two infrared camera systems are directed at the flame from two different angles. To evaluate the thermal radiation of the jet flame, four heat radiation sensors are used.

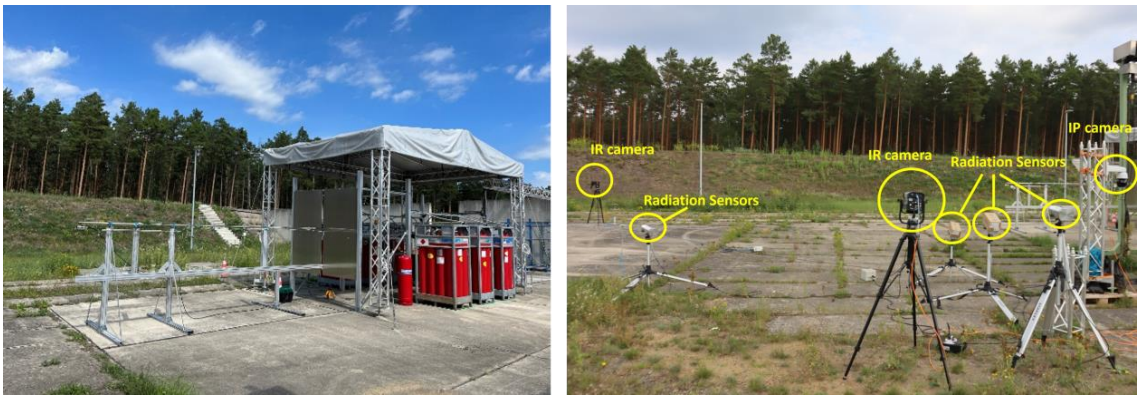

Figure 2: Jet Flame test area at the BAM-TTS, Dimensions of Jet-Flame Test Stand 18 m x 5 m x 4 m (length x wide x height) (left) and position of heat sensors and IR/IP CAM (right)

Three thermal radiation sensors are used to measure the thermal radiation at different distances from the flame and one thermal radiation sensor is used to measure the background radiation of the environment. With the help of these heat radiation sensors, the surface emissive power (SEP) of the jet flame can be determined. The SEP is an important value for hazard assessment purposes as it is the dominating value for calculating the radiation emitted to the surroundings in case of a fire. The mass flow is controlled remotely via an adjustable control valve. Monitoring takes place with the aid of a Coriolis mass flow meter.

Discussion

Since the experimental investigation and a full characterization of all operating conditions is still ongoing, only partial results are presented.
Figure 3 shows the shape of the hydrogen jet flame for the highest released mass flow (up to now) of $\dot{m}$=7.2 kg/min out of an orifice of 7.8 mm diameter at an absolute pressure before nozzle exit of p=50.3 bar (cf. Figure 1 – PIR 202). The flame shown in Figure 3 has an average length of l=9.1 m and an average diameter of d=1.6 m.

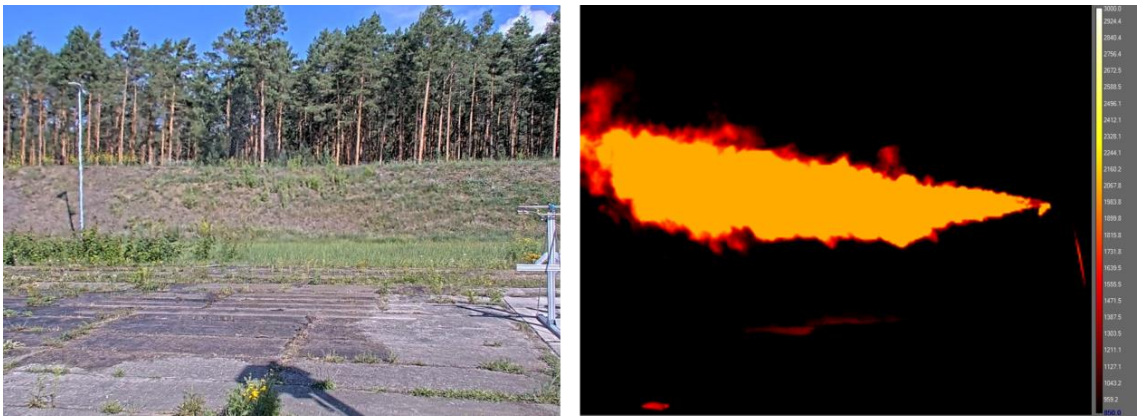

Figure 3: Comparison view on hydrogen flame with normal visible camera (left) and with IR Cam (right), mass flow of hydrogen $\dot{m}$= 7.2 kg/min, pressure before nozzle p=50.3 bar

The hydrogen flame is not emitting visible light (cf. Figure 3 – left). Only by using the IR camera, the flame can be visualized. The IR-Cam in Figure 3 – right is set to a temperature range from T=850 °C to T=2000 °C with a conservatively assumed emissivity of ε=1. The choice of the temperature limits in the IR camera is crucial as it determines the limits of the flame shape and therefore the size of the flame (Length, diameter and surface) which are directly linked to the SEP calculation.

The measured thermal heat radiation at each sensor is used to calculate the SEP. From the relative position in space of the sensor and the flame, the shape and size of sensor and flame, a so-called view factor is calculated. The choice of the view factor has a high impact on the SEP. After determining the geometric boundary conditions, atmospheric conditions have to be taken into consideration. The aspects are summarized by the atmospheric transmissivity factor. [12, 13]

In the following this study presents and discusses exemplary the results of one single test, as most of the obtained results show a similar behavior. A comparison of the SEP of a hydrogen and a methane jet flame each for a mass flow of $\dot{m}$=4 kg/min and an outlet diameter of 1/2" (outlet pressure p=10.0 bar for methane and p=27.1 bar for hydrogen) was carried out (cf. Figure 4). The advantage of using the same mass flow is that the combustion energy (and the resulting radiation energy) can be directly compared for both jet flames. The combustion energy Q in MW [12] is calculated according to:

$$Q = \dot{m} H_c \tag{1}$$

with $\dot{m}$ the mass flow in kg/s and H_c the lower heating value in MJ/kg. The lower heating value of methane is 50.31 MJ/kg and of hydrogen is 120 MJ/kg.[14] For the released mass flows the combustion energy of the methane jet flame is 3.35 MW and of the hydrogen jet flame is 8 MW. The radiation energy Q_{rad} in MW emitted by a flame is calculated according to

$$Q_{rad} = X_{rad} \dot{m} H_c \tag{2}$$

with the unitless radiative fraction of the combustion energy X_{rad}.[7] If we assume that the radiative fraction for hydrogen and methane is the same, the hydrogen jet flame would have a 2.4 times higher radiation energy than the methane jet flame. In literature, smaller radiative fractions for hydrogen in comparison to hydrocarbons were observed. Reported radiative fractions for hydrogen between 0.05 and 0.15.[10, 15, 16] with an average value of 0.1 can be

found. For methane the radiative fractions reported showed a range between 0.1-0.25 [2, 16, 17] with an average radiative fraction in the range of 0.2. In the experiment the SEP's of the jet flames were determined based on the measured heat radiation values in 8 m, 10 m and 12 m distance, resulting in 12 kW/m² for methane and 15 kW/m² for hydrogen (cf. Figure 4). The ratio between the hydrogen SEP to the methane SEP is 1.25, which is in good agreement with the theoretical predictions and in concordance with the observations from literature that a hydrogen flame has much lower radiative fraction than a methane flame.

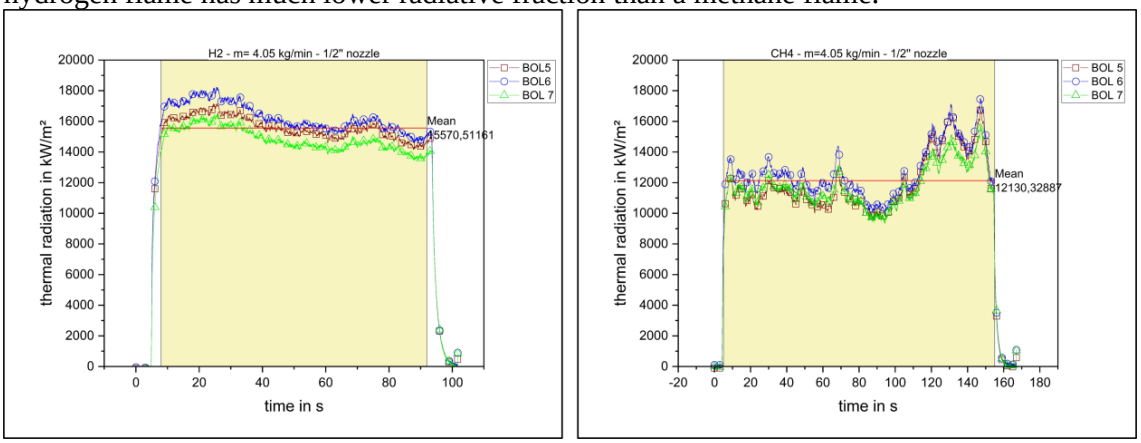

Figure 4: Comparison of Surface Emissive Power data from hydrogen jet flame (left) and methane jet flame (right), mass flow of m ̇=4.05 kg/min, nozzle diameter ½" (7.8 mm), pressure before nozzle for hydrogen p=27.1 bar, pressure before nozzle for methane p=10 bar

These values are significantly lower compared to the SEP's found in literature. Values found there cover the range of 201 – 208 kW/m² SEP for methane[2], 60 kW/m² for propane[18] or 419 kW/m² for LNG fires.[19]

Mostly in literature, SEP in W/m² were determined using Stefan-Boltzmann Law based on the flame temperature. [19-21]

$$SEP = \varepsilon \, \sigma \, T^4 \tag{3}$$

with T the temperature in K, σ the Stefan-Boltzmann constant in W/(m²K⁴) and ε the unitless emissivity. The challenge is to define the correct value of the flame temperature. In literature, the adiabatic combustion temperature is often assumed as the uniform jet flame temperature. Applying this to the experiment the resulting SEP's would be 1.375 MW/m² for methane and 1.81 MW/m² for hydrogen with an adiabatic flame temperature of T=2222 K for methane and T=2380 K for hydrogen and an emissivity of 1.[22]

In literature it can be found, that the emissivity for hydrogen flames is 0.1 [21], resulting in an SEP of 181 kW/m². From the documented SEP's for methane flames in literature of around 210 – 250 kW/m² it can be deduced that the emissivity of methane is around 0.2, resulting in a calculated SEP of 275 kW/m².[2] In reality the adiabatic combustion temperature is not reached, and the flame has no uniform temperature distribution (cf. Figure 5). Therefore a "mean flame temperature" has to be determined. To assess the sensitivity of the Stefan-Boltzmann Law to different temperatures, a mean temperature of only 90% of the adiabatic combustion temperature (1999 K for methane and 2140 K for hydrogen) is assumed. This leads to SEP's of 180 kW/m² for methane and 119 kW/m² for hydrogen with the respective emissivity's of 0.2 and 0.1. It can be seen that a reduction of the (adiabatic) flame temperature by 10% leads to a reduction of the SEP by nearly 40%. Since the Stefan-Boltzmann law is so sensitive towards temperature fluctuation and the determination of the flame temperature is not obvious especially since it has to be done for each time step, in this work the calculation of the SEP is done using equation (2).

Conclusions

The following findings can be determined as preliminary conclusions on the current status of the investigation:

1. Different flame shape of hydrogen flames compared to hydrocarbon flames:
These flame geometry investigations are systematically continued in order to establish a statistical database. On this basis, flame models can be developed further and adjusted to achieve a better prediction accuracy.
2. Differences in ignition behavior:
Hydrogen could be ignited without any problems at all pressure levels and all nozzle diameters. In the case of methane, it was observed that, above a pressure of p>30 bar and a nozzle diameter of 7.8 mm (at a mass flow of 12.5 kg/min), after turning off the pilot flame, the flame was not self-sustaining and blew itself out. Reason for this could be the low flame speed of methane especially compared to exit velocity. Depending on the pressure ratio the underexpanded jet can reach Ma>1 after nozzle exit.
3. Heat radiation values:
First results from the release of hydrogen and methane with the same mass flow show that the radiative fraction of hydrogen flame is significantly lower than that of methane, which is in good agreement with the observations found in literature.[8, 14, 17]

As an outlook, a systematic investigation of different scenarios with regard to pressure levels, mass flows, outlet geometries, outlet angles will be carried out. On the basis of these data, existing jet flame models will be evaluated towards their prediction accuracy and possible needs for further development.

References

[1] H. A. Becker, D. Liang, and C. I. Downey, "Effect of burner orientation and ambient airflow on geometry of turbulent free difussion flames," *Symposium (International) on Combustion,* vol. 18, no. 1, pp. 1061-1071, 1981/01/01/ 1981, doi: https://doi.org/10.1016/S0082-0784(81)80110-5.

[2] G. A. Chamberlain, "Developments in design methods for predicting thermal radiation from flares," (in English), vol. 65:4, 1987-07-01 1987, doi: https://doi.org/
Journal Name: Chem. Eng. Res. Des.; (United Kingdom); Journal Volume: 65:4.

[3] G. Kalghatgi, "Lift-off Heights and Visible Lengths of Vertical Turbulent Jet Diffusion Flames in Still Air," *COMBUSTION SCIENCE AND TECHNOLOGY,* vol. 41, pp. 17-29, 09/01 1984, doi: 10.1080/00102208408923819.

[4] A. D. Johnson, H. M. Brightwell, and A. J. Carsley, "A Model for predicting the thermal radiation hazards from large scale horizintally released natural gas jet fires," *Shell Internationale Research Maatschappij B.V.*, 1994.

[5] V. Molkov, D. Makarov, and M. Bragin, "Physics and modelling of under-expanded jets and hydrogen dispersion in atmosphere," *Physics of Extreme State of Matter 2009,* pp. 143-145, 01/01 2009.

[6] V. Molkov and J.-B. Saffers, "Hydrogen jet flames," *International Journal of Hydrogen Energy,* vol. 38, no. 19, pp. 8141-8158, 2013/06/27/ 2013, doi: https://doi.org/10.1016/j.ijhydene.2012.08.106.

[7] I. W. Ekoto, A. J. Ruggles, L. W. Creitz, and J. X. Li, "Updated jet flame radiation modeling with buoyancy corrections," *International Journal of Hydrogen Energy*, vol. 39, no. 35, pp. 20570-20577, 2014/12/03/ 2014, doi: https://doi.org/10.1016/j.ijhydene.2014.03.235.

[8] R. W. Schefer, W. G. Houf, T. C. Williams, B. Bourne, and J. Colton, "Characterization of high-pressure, underexpanded hydrogen-jet flames," *International Journal of Hydrogen Energy*, vol. 32, no. 12, pp. 2081-2093, 2007/08/01/ 2007, doi: https://doi.org/10.1016/j.ijhydene.2006.08.037.

[9] R. W. Schefer, W. D. Kulatilaka, B. D. Patterson, and T. B. Settersten, "Visible emission of hydrogen flames," *Combustion and Flame*, vol. 156, no. 6, pp. 1234-1241, 2009, doi: 10.1016/j.combustflame.2009.01.011.

[10] C. Proust, D. Jamois, and E. Studer, "High pressure hydrogen fires," *International Journal of Hydrogen Energy*, vol. 36, no. 3, pp. 2367-2373, 2011/02/01/ 2011, doi: https://doi.org/10.1016/j.ijhydene.2010.04.055.

[11] J. E. Hall, P. Hooker, L. O'Sullivan, B. Angers, A. Hourri, and P. Bernard, "Flammability profiles associated with high-pressure hydrogen jets released in close proximity to surfaces," *International Journal of Hydrogen Energy*, vol. 42, no. 11, pp. 7413-7421, 2017/03/16/ 2017, doi: https://doi.org/10.1016/j.ijhydene.2016.05.113.

[12] V. Gesellschaft, *VDI Heat Atlas*. Springer Berlin Heidelberg, 2010.

[13] F. D. Wayne, "1991 An economical formula for calculating atmispheric infrared transmissivities.pdf>," *Shell Research Ltd., Thornton Research Centre, PO, Box 1, Chester, CH1 3 SH, UK*, 1991.

[14] D. Miller, "New model for predicting thermal radiation from flares and high pressure jet fires for hydrogen and syngas," *Process Safety Progress*, vol. 36, no. 3, pp. 237-251, 09// 2017, doi: 10.1002/prs.11867.

[15] E. S. Fishburne and H. S. Pergament, "The dynamics and radiant intensity of large hydrogen flames," *Symposium (International) on Combustion*, vol. 17, no. 1, pp. 1063-1073, 1979/01/01/ 1979, doi: https://doi.org/10.1016/S0082-0784(79)80102-2.

[16] W. Houf and R. Schefer, "Predicting radiative heat fluxes and flammability envelopes from unintended releases of hydrogen," *International Journal of Hydrogen Energy*, vol. 32, no. 1, pp. 136-151, 2007, doi: 10.1016/j.ijhydene.2006.04.009.

[17] R. W. Schefer, W. G. Houf, B. Bourne, and J. Colton, "Spatial and radiative properties of an open-flame hydrogen plume," *International Journal of Hydrogen Energy*, vol. 31, no. 10, pp. 1332-1340, 2006/08/01/ 2006, doi: https://doi.org/10.1016/j.ijhydene.2005.11.020.

[18] B. Zhang, Y. Liu, D. Laboureur, and M. S. Mannan, "Experimental Study on Propane Jet Fire Hazards: Thermal Radiation," *Industrial & Engineering Chemistry Research*, vol. 54, no. 37, pp. 9251-9256, 2015/09/23 2015, doi: 10.1021/acs.iecr.5b02064.

[19] H. C. Hardee, D. O. Lee, and W. B. Benedick, "Thermal Hazard from LNG Fireballs," *Combustion Science and Technology*, vol. 17, pp. 189-197, 1978.

[20] A. Molina, R. Schefer, and W. G. Houf, "Radiative fraction and optical thickness in large-scale hydrogen-jet fires," *Proceedings of The Combustion Institute - PROC COMBUST INST*, vol. 31, pp. 2565-2572, 01/31 2007, doi: 10.1016/j.proci.2006.08.060.

[21] T. Mogi, H. Nishida, and S. Horiguchi, "Flame Characteristics of high-pressure hydrogen gas jet," 2005.

[22] C. S. Uwe Riedel, Jürgen Warnatz, Jürgen Wolfrum, *Grundlagen der Verbrennung: Wärmefreisetzung und adiabatische Flammentemperaturen*. Physik Online: De Gruyter, 2018.

Regeneration of iron-oxides powder: closing the iron fuel cycle

N.C. Stevens*[1], G. Finotello [1,2] , N.G. Deen, [1,2]

[1] Department of Mechanical Engineering, Power&Flow group, Eindhoven University of Technology, The Netherlands

[2] Eindhoven Institute for Renewable Energy Systems (EIRES), Eindhoven University of Technology, The Netherlands

Introduction

As an effect of climate change, extreme weather events take place more often all over the world [1]. The main cause of this development is the emission of greenhouse gasses, of which CO2 is a large contributor. The impact of climate change has been acknowledged and countries across the world are introducing policies to reduce the emissions [2]. Electrification is seen as a promising solution to the transition towards sustainable energy. However, the operation of the electricity network, is disrupted by intermittency of these sustainable energy sources [3]. Therefore stockpiled fuels are needed to deal with supply disruptions and variability of these clean sources. One of these storable energy sources is metal, that can be used as a recyclable dense energy carrier of green energy. Metals like iron can be burnt with air or react with water to release its chemical energy even up to industrial scale with a high power output. The thermal energy which is released during this process provides heat to high energy- and emission- intense industries. After combustion the generated metal oxides are captured and reduced back to metal. It is also possible to export the metal over long distances, or store it indefinitely with minimal loss [4]. Feasibility studies of the cycle showed that replacing coal plants with iron is realistic [5,6]. The main issue is that our scientific knowledge to support the metal fuel combustion/regeneration cycle is largely missing and needs to be developed. While the oxidation element of the cycle is a widely studied part of the metal fuel cycle, the regeneration of the energy carrier is still in a starting point of development. Study of the reduction process is essential for the future success of the metal fuel cycle. One application which can be used for reduction is the fluidized bed. The fluidization of particles depends on the type of gas, gas pressure and gas density, as well as solids characteristics, such as bed porosity, particle size and particle density. The porosity of the iron particles changes due to reduction of iron ore with hydrogen, having a large impact on density and flow properties. We investigated the impact of cyclic combustion-reduction on material properties, with the specific focus on the reduction of iron oxides using hydrogen under fluidization conditions.

Methodology

The powder is combusted and reduced over 3 cycles under the same conditions. Afterwards the properties of the powder and the reaction conversion are characterized. The physical techniques used for size and shape analysis include laser diffraction particle size analysis and

* Corresponding author: n.c.stevens@tue.nl

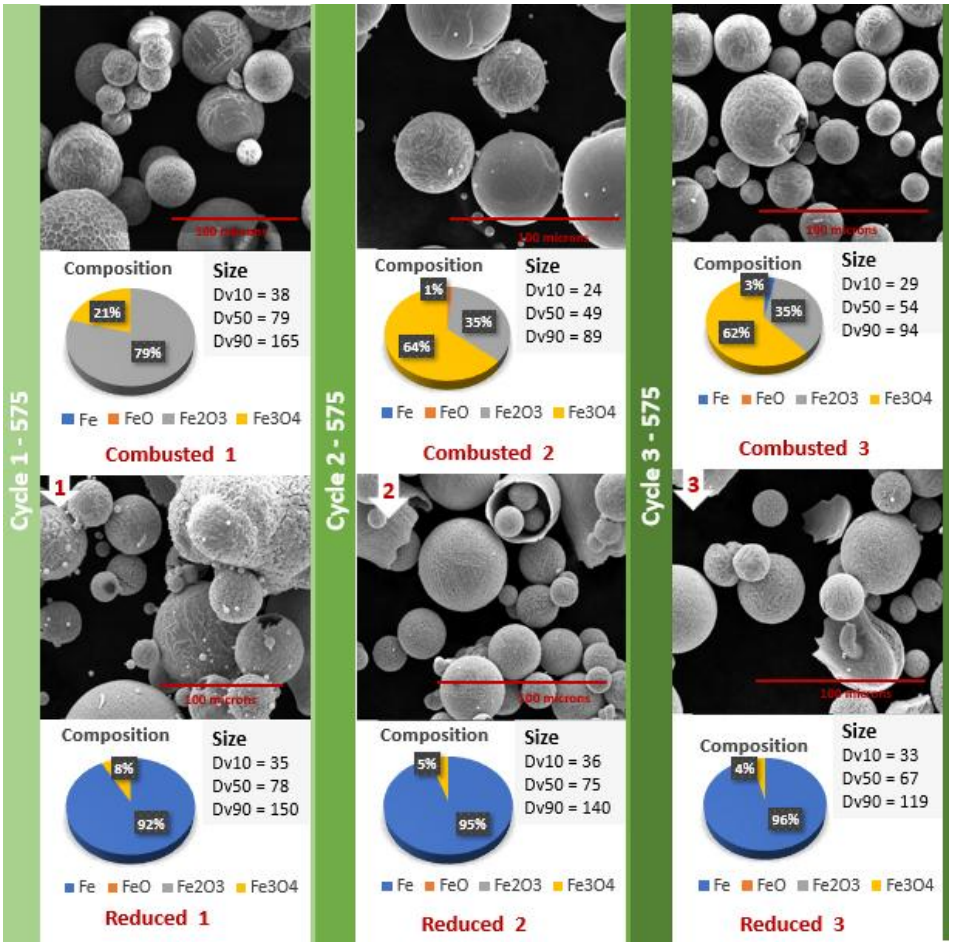

scanning electron microscopy (SEM). For structure and chemistry, X-ray diffraction (XRD) and energy dispersive X-ray (EDX) analysis are also employed.

Figure 1: overview of average particle sizes (Dv10, Dv50, Dv90), composition of the powder and a SEM image of the powder after partial cycle of reduction or combustion for the experiments performed with a reduction temperature of 575°*C*.

Discussion

Based on the results obtained from the particle size analysis, it appears that sticking is present after reduction of the powder. Previous studies on reduction of iron oxides in fluidized beds showed some technical issues with agglomeration of particles due to sintering at elevated temperature, causing de-fluidization of the bed [7,8]. The phenomenon of sticking is present after each cycle and is even visible on the SEM images (Figure 1, reduced 2), where a cluster of particles is visible. Another indication of sticking is the higher average particles sizes (Dv50) which shifted from +/- 50 microns towards +/- 70 microns. The Dv90, also visualizes the presence of large particle, which shows that 10% of the measured particles has a higher value than 140 microns for the second cycle and 119 microns for the third cycle. The higher Dv90 is also visible for the first combustion, where large agglomerates were formed due to particles melting together during combustion. These agglomerates were crushed before the

second cycle to be able to distribute the powder into the burner system. These agglomerates are from the second cycle no longer visible.

The measured composition of the powder showed a high reduction degree, more than 92% iron composition, for all cycles. The composition after combustion also showed almost full oxidation of the iron to iron-oxides. Overall, the presence of sticking shows that there is space for improving the operation conditions for reduction as well combustion on minimizing the sticking behavior and stimulating the stability of the particle size over multiple cycles.

Conclusions

We observe that the particle size distribution remains relatively stable over multiple cycles in both experiments, only a slight increase is visible after the first cycle. The results suggest that the powder can be effectively utilized in the iron fuel cycle without requiring additional intermediate treatments, such as grinding and sieving after each cycle. This aspect highlights the potential feasibility and simplicity of implementing the cyclic combustion-reduction process for practical applications of iron powder as an energy carrier.

References

[1] IPCC, 2014. Climate change 2014 synthesis report summary chapter for policymakers.

[2] Nachmany, M., Setzer, J., 2018. Policy brief global trends in climate change legislation and litigation: 2018 snapshot.

[3] Thoubboron, K., 2022. Advantages and disadvantages of renewable energy.

[4] Bergthorson, J.M., 2018. Recyclable metal fuels for clean and compact zero-carbon power. Progress in Energy and Combustion Sci

[5] Kuhn, C., Dull, A., Rohlfs, P., Tischer, S., B ¨ ornhorst, M., Deutschmann, O., 2022. Iron as recyclable energy carrier: Feasi- ¨ bility study and kinetic analysis of iron oxide reduction. Applications in Energy and Combustion Science 12, 100096. URL: https://linkinghub.elsevier.com/retrieve/pii/S2666352X22000395, doi:10.1016/j.jaecs.2022.100096.

[6] Bergthorson, J., Goroshin, S., Soo, M., Julien, P., Palecka, J., Frost, D., Jarvis, D., 2015. Direct combustion of recyclable metal fuels for zero-carbon heat and power. Applied Energy 160, 368–382. URL: https://linkinghub.elsevier.com/retrieve/pii/S0306261915011071, doi:10.1016/j.apenergy.2015.09.037.

[7] Spreitzer D., Schenk J. Iron ore reduction by hydrogen using a laboratory scale fluidized bed reactor: Kinetic investigation—experimental setup and method for determination. Metall. Mater. Trans. B, 50 (5) (2019), pp. 2471-2484

[8] Zhang X., He S., Sun H., Zhu Q., Li J., Li H. Mechanism of surface morphology evolution in the reduction of fine iron ore in a conical fluidized bed reactor. Chem. Eng. Sci., 220 (2020), Article 115468

Review of Printing Methodologies as a Key Enabling Technology for the Membrane Electrode Assembly of Hydrogen Fuel Cells

Guilherme Paixão da Costa[1], Diogo Garcia[1], Van Nguyen[1], Paul Lacharmoise[1], and Claudia Delgado[1*]

[1*]Eurecat - Centre Tecnológic de Catalunya, Functional Printing and Embedded Devices Unit, Av. Ernest Lluch 36, 08302 Mataró, Spain

*Corresponding author: claudia.delgado@eurecat.org

Introduction

In the coming years, driven significantly by initiatives such as the European Green Deal, the energy landscape is in position for a notable transition, in which renewable energy sources such as solar and wind are expected to play a dominant role. This transition towards sustainability and carbon neutrality is closely associated with the utilization of green hydrogen gas (H_2) as a prominent energy vector. [1],[2] In this context, proton exchange membrane (PEM) technology has emerged as highly advantageous, particularly in the domain of fuel cells designed for mobility applications. It's worth noting that experts anticipate that PEM technology will play a major role in the water electrolysis and fuel cell market by the year 2030. [3],[4],[5] Nevertheless, the broad integration of PEM technology is currently encountering considerable cost-related hurdles. As a result, extensive research efforts are underway to explore substitutes for noble metal catalysts and halogenated membrane materials. It's worth noting that manufacturing and assembling the Membrane Electrode Assembly (MEA) presently account for approximately 61% of the total cost associated with fuel cell systems. [5],[6] An additional strategy for cost reduction involves simplifying the complexity of the assembly processes, thus facilitating scalability through high-throughput manufacturing techniques. In this context, printing methodologies have emerged as a promising approach for PEM technology, largely due to their cost-effectiveness and capacity for high-throughput production. Some of these methodologies, such as spray coating, have been widely utilized for catalyst layer deposition, but exhibit broader applicability encompassing various other MEAs components. [7] Recent investigations on spray coating, inkjet printing, and screen printing have demonstrated their usefulness in depositing catalyst layers and membranes for PEM fuel cells. [8], [9] This comprehensive review provides a detailed analysis of the applications and outcomes achieved thus far.

Methodology

This comprehensive study is oriented towards a thorough exploration and analysis of the current state-of-the-art applications of printing methodologies in the fabrication of different MEA components within the PEM technology for fuel cells. The investigation covers the use of different printing methodologies, such as spray coating, screen-printing, and inkjet printing, to manufacture vital components of MEAs, such as gas diffusion layers, catalyst layers, and membranes, as seen in Figure 1, and compares the performance of these partially printed MEAs with conventional ones. The analytical scope includes a wide spectrum of parameters, including the domains of application, materials employed, specific printing methodologies applied in the manufacturing processes, classification of device types, and the resulting performance characteristics. Additionally, a meticulous examination of the electrochemical performance and stability of partially printed MEAs, both in singular cell configurations and within cell stacks, was conducted, allowing for comparative insights with traditionally assembled MEAs.

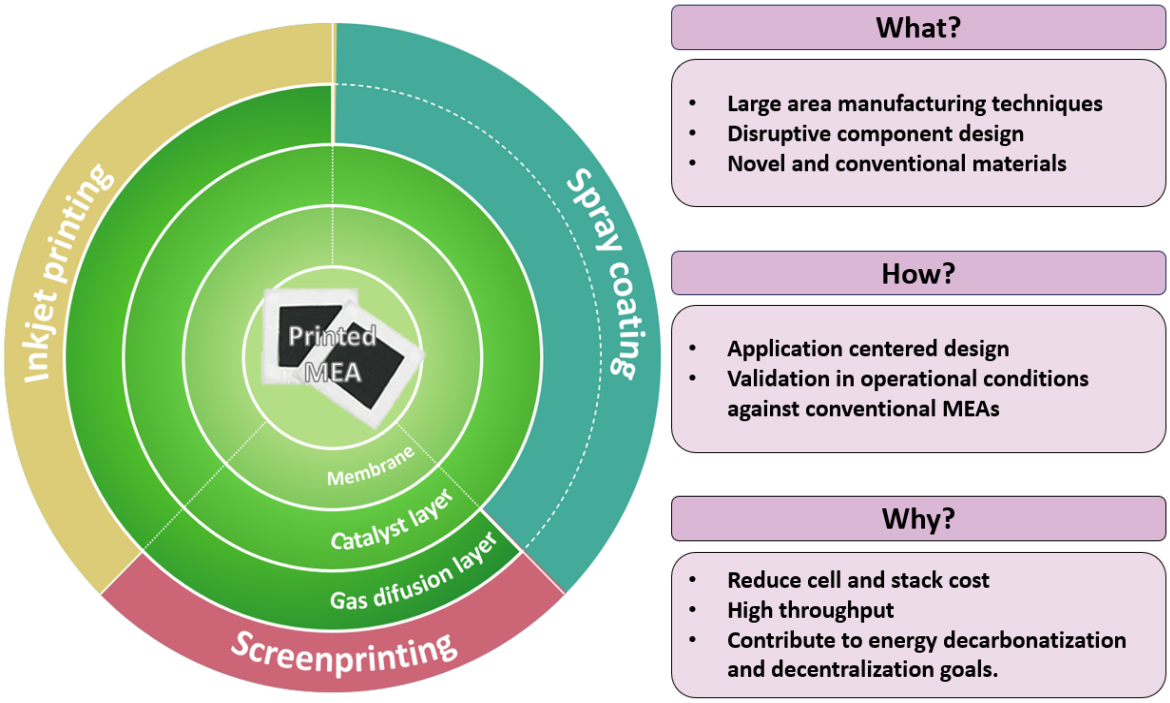

Figure 1- Schematic representation of the research study.

Discussion

This review provides a detailed exploration of the fundamental principles underlying spray coating, screen printing, and inkjet printing as versatile methodologies for the fabrication of key components within MEAs for PEM fuel cells. This review has elucidated the intricacies of employing these techniques to manufacture critical MEA constituents, including gas diffusion layers, catalyst layers, and proton exchange membranes. Moreover, it surveys the current state of the art in each component's manufacturing process, highlighting advancements and key findings in the field. The state of the art in the manufacturing processes of these components reveals an emerging research field focused on improving the performance while reducing costs. For instance, advancements in GDL fabrication involve tailoring the porosity to enhance mass transport, while catalyst layer development increasingly explores earth-abundant materials as substitutes for expensive noble metals. Membrane materials are evolving toward non-halogenated alternatives to mitigate environmental concerns. An essential focus of this review is an in-depth comparative analysis of the electrochemical performance and stability of partially printed MEAs and their conventionally assembled counterparts, where the partially printed MEAs demonstrate performance metrics on par with those of their conventionally manufactured counterparts. This comprehensive evaluation provides invaluable insights into the potential of printing methodologies for advancing the PEM technology in the pursuit of sustainable energy solutions.

Conclusions

This investigation demonstrates the prospective application of partially printed MEAs in Proton Exchange Membrane Fuel Cells (PEMFCs). This evaluation relies on a comprehensive analysis, incorporating performance metrics, to draw comparisons between the electrochemical performance of partially printed MEAs operating at specific current densities (mA/cm^2) and their conventionally manufactured counterparts, all under similar attributes and operating conditions. Significantly, these findings revealed that partially printed MEAs exhibit performance metrics comparable with those produced by conventional methods. However, to fully unlock their potential, ongoing research and optimization of the MEAs' component printing processes are imperative.

References

[1] E. Union, EU Energy in Figures 2021, Publications Office Of The European Union, Luxembourg (2021)

[2] Cook, T. R., Dogutan, D. K., Reece, S. Y., Surendranath, Y., Teets, T. S., & Nocera, D. G. (2010). Solar Energy Supply and Storage for the Legacy and Nonlegacy Worlds. Chemical Reviews, 110(11), 6474–6502. https://doi.org/10.1021/cr100246c

[3] Guo, Y., Li, G., Zhou, J., & Liu, Y. (2019). Comparison between hydrogen production by alkaline water electrolysis and hydrogen production by PEM electrolysis. IOP Conference Series: Earth and Environmental Science, 371(4). https://doi.org/10.1088/1755-1315/371/4/042022

[4] Schmidt, O., Gambhir, A., Staffell, I., Hawkes, A., Nelson, J., & Few, S. (2017). Future cost and performance of water electrolysis: An expert elicitation study. International Journal of Hydrogen Energy, 42(52), 30470–30492. https://doi.org/10.1016/j.ijhydene.2017.10.045

[5] Thompson, S. T., James, B. D., Huya-Kouadio, J. M., Houchins, C., DeSantis, D. A., Ahluwalia, R., Wilson, A. R., Kleen, G., & Papageorgopoulos, D. (2018). Direct hydrogen fuel cell electric vehicle cost analysis: System and high-volume manufacturing description, validation, and outlook. *Journal of Power Sources*, *399*, 304–313. https://doi.org/10.1016/j.jpowsour.2018.07.100

[6] International Renewable Energy Agency, T. (2020). *GREEN HYDROGEN COST REDUCTION SCALING UP ELECTROLYSERS TO MEET THE 1.5°C CLIMATE GOAL H 2 O 2*. www.irena.org/publications

[7] Mayyas, A., & Mann, M. (2019). Emerging Manufacturing Technologies for Fuel Cells and Electrolyzers. Procedia Manufacturing, 33, 508–515. https://doi.org/10.1016/j.promfg.2019.04.063

[8] Breitwieser, M., Klose, C., Klingele, M., Hartmann, A., Erben, J., Cho, H., Kerres, J., Zengerle, R., & Thiele, S. (2017). Simple fabrication of 12 µm thin nanocomposite fuel cell membranes by direct electrospinning and printing. Journal of Power Sources, 337, 137–144. https://doi.org/10.1016/j.jpowsour.2016.10.094

[9] Lagarteira, T., Han, F., Morawietz, T., Hiesgen, R., Garcia Sanchez, D., Mendes, A., Gago, A., & Costa, R. (2018). Highly active screen-printed Ir Ti4O7 anodes for proton exchange membrane electrolyzers. International Journal of Hydrogen Energy, 43(35), 16824–16833. https://doi.org/10.1016/j.ijhydene.2018.02.179

Role of FID (Flame Ionization Detector) in the detection and control of hydrogen-methane flames.

M.A. Ravotti*[1], P. Canu[2]

[1]Department of Industrial Engineering, University of Padua, Padua, Italy.
[2]Department of Industrial Engineering, University of Padua, Padua, Italy.

Introduction

The European Union (EU) has set ambitious targets for the development and deployment of hydrogen as a clean and sustainable energy source. [1]. It is clear that on the way to the net-zero target, the energy sector and industry are encountering several challenges, starting from the production stage and ending with the development of technologies to ensure the safe use of hydrogen as a fuel [2].

When it comes to the installation of combustion monitoring and safety systems, a key aspect is to have a flame detection device with high reliability. For conventional fuels, flame presence detection and combustion control in major cases are based on the measurement of ionization current, also widely used in research studies involving methane and combustion products such as carbon dioxide [3], [4], [5].

The rapid development of hydrogen-fuelled devices involves ensuring safe and efficient combustion management, for which reliable flame detection is a clear and necessary step. The use of ultraviolet radiation detectors has been proposed as an alternative [6], however, the high cost of these detectors remains a major obstacle. While they represent a reliable alternative, at the same time there is a need for accessible sensors. Innovation and development of new devices are indeed a challenge, but it is also a question of testing whether persistent technology with this feature can be applied.

The prospects for extending the use of flame ionization current detection (FID) to hydrogen-enriched hydrocarbon flames are promising. However, more precise experimental data on the application of this technology is needed to establish applicability guidelines, detection limits, and recommendations for the design of devices or control systems incorporating FIDs.

In this framework, the present work aims to address the interrogation of the possibility of applying FIDs, which is a widely used technology for conventional fuel flames, and well-known for its cost-effectiveness, to hydrogen burners.

Experimental Methodology

The experimental setup comprises four primary components, including the fuel-oxidizer premixing device, the burner, the probe, and the signal reading circuit. The sonde positioned

* M.A. Ravotti: mariaagustina.ravotti@phd.unipd.it

downstream in proximity to the flame and the surface of the burner body together represents the electrode pair, which is linked to the electrical circuit.

This report will highlight the results of three of these models. Firstly, the initial device facilitated preliminary studies (Fig.1-a) and was instrumental in advancing further design modifications. The Burner 1 is a 7 mm diameter Bunsen burner with a 0,2 mm light mesh on top, capable of dealing with hydrogen content ranging from 0 to 75%.

Secondly, a multi-hole burner was designed (Fig.1-b) to replicate the technology utilized in industrial settings. Burner 2 is a cylindrical burner with a diameter of 2 cm and 0.9 mm holes arranged at 360° over the entire surface. The last burner (Fig. 1-c) has the capability for complete methane substitution (100% hydrogen), owing to the arrangement of holes not covering the circumference, which enhances the cooling mechanism. It consists of an 8 mm diameter tube, with 90 0,5 mm holes arranged in rows of approximately 3 cm in length.

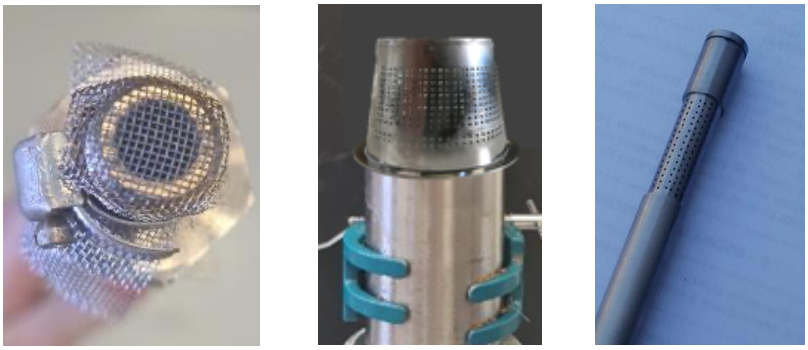

(a) (b) (c)

Figure 1: a) Burner 1 (Bunsen with mesh 0.2 mm). b) Burner 2 (conical multi-hole). c) Burner 3, (multi-hole 0.5 mm 90° d2).

The experimental campaign was structured in four stages:

1. Determination of the viability of using ionization current for methane-hydrogen flames detection: The evaluation was performed in burner 1. The probe was initially positioned within the blue cone of the flame, and then gradually moved away at a constant rate of 1,5 mm/min (45° angle, 7 mm from the surface). The volumetric flow rate of methane was maintained constant and equal to 200 mL/min. The experiments were conducted with a hydrogen concentration range of 0 to 60%.
2. Experimental verification of ionization current intensity in high hydrogen concentration flames: This experiment uses Burner 3, the experimental conditions considered H_2-rich fuel mixtures ranging from 86% to 100%. The volumetric flow of methane was fixed at 50 mL/min. The airflow was supplied to ensure stoichiometric conditions (ϕ =1). The electrode was positioned approximately 4 mm (perpendicular) from the burner surface in an area where a pronounced current signal was expected.
3. Verification of the feasibility of ionization for combustion control: The experiments were carried out in the second burner within a range of 0-67% hydrogen. The methane flow was fixed at 500 mL/min. Hydrogen supply varies according to the composition that is being analyzed, between 0 and 1000 mL/min (Pure CH_4 to 67% H_2). The ϕ ratio was varied

according to the airflow from stoichiometric conditions to leaner mixtures. The conditions of excess air were always maintained, as is the case at the industrial level. The electrode was positioned at z = 0,6 mm from the burner surface.

4. Feasibility of applying the principle of thermal conductivity for determining the methane/hydrogen ratio: For the test, TCD (Thermal Conductivity Detector) equipment was utilized, which functions by measuring the difference in thermal conductivity between a reference and the analytical gas mixture. Nitrogen was selected as the carrier gas.

Results and discussion

Figure 2 shows the ionization current intensity recorded at different electrode positions, with different hydrogen additions from 0 to 60%, varying the amount of air supplied, to maintain the stoichiometric ratio as the fuel mixture shifts its composition.

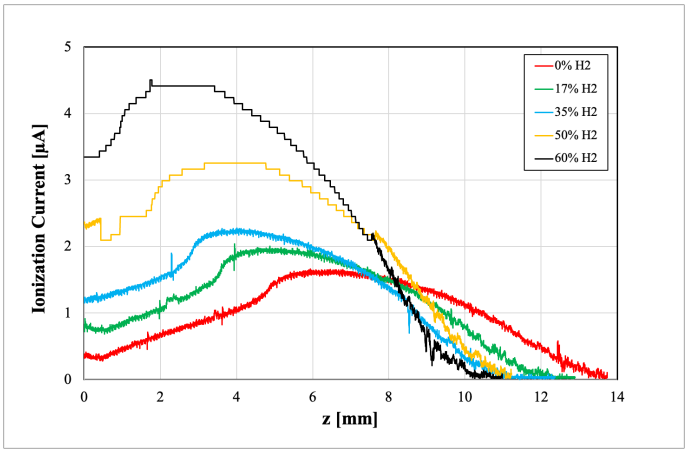

Figure 2: Ionization Current signal as a function of electrode position z, different fuel mixture composition, and λ =1; z=0 corresponds to the inside of the blue flame cone, (corresponding to t = 0).

It was observed that by placing the electrode close to the flame, the ionization current increases as the percentage of hydrogen increases, making the system suitable for flame detection with hydrogen-rich fuel. It is crucial to consider that this decline is partly because the flame height decreases as the hydrogen percentage increases. Figure 3 illustrates the change in flame height for 30% and 60% flames, the richer the fuel is in hydrogen, the shorter the flame (consistent with [7], [8]).

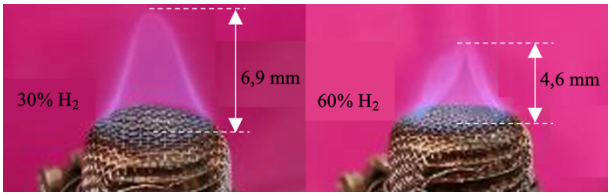

Figure 3: Flame shortening with increasing % hydrogen.

It was important to establish a limit for the instrument's applicability, especially for mixtures with a high percentage of hydrogen since they greatly deviate from the characteristics of pure methane for which its applicability has already been tested. Figure 4 displays the profiles of

the ionization current signal as the hydrogen percentage in the fuel evolved for two fixed positions. It was confirmed by this experimentation that the electrode can be utilized for flame detection up to 95% hydrogen content in the fuel mixture.

The obtained results are consistent with previous findings, which show that the addition of hydrogen can enhance the ionization of partially premixed flames by affecting the chemical ionization process [7]. In the range from 98% to total substitution, the results obtained are of the order of nA and are aligned with earlier studies that have noted that pure hydrogen flames can have very low ion concentrations. [9]

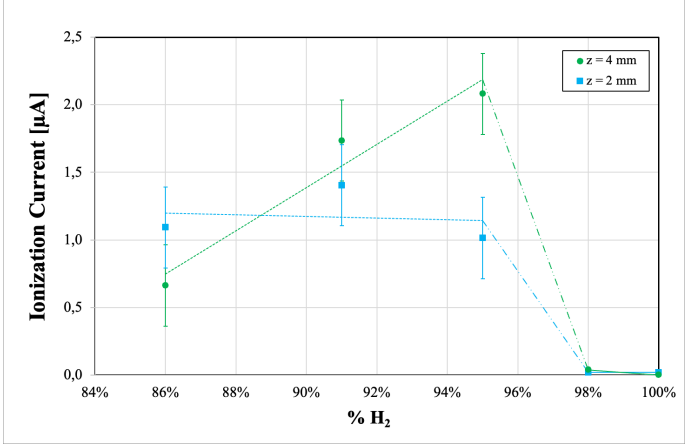

Figure 4: Ionization Current profile obtained with burner 3 at different hydrogen percentages, λ = 1, and at z = 2 mm y z = 4 mm.

In Figure 5, the ionization current, I [µA], was plotted in a master chart, including equivalence ratio ϕ, Airflow [L/h], Power [W], and CH_4-H_2 ratio. From the graph, it is observed that the same ionization current reading can correspond to four different curves. Ionization current could be used for combustion control if the system includes an upstream measurement point that records the CH_4-H_2 ratio, accompanied by flow meters that allow inferring the power released. Both values could be used as input for the selection of the correspondent parametrized curve.

Due to the promising results obtained regarding the utilization of the electrode in flame control and the necessity of measuring the composition as an additional datum for the control loop, the feasibility of adapting existing technology, such as TCD, for this application was tested. It was observed (Figure 6) that as the mixture is enriched in hydrogen, the thermal conductivity module increases. Moreover, a direct relationship between composition and voltage is observed, which confirms the feasibility of using TCD technology as part of combustion control for determining the composition of the fuel blend.

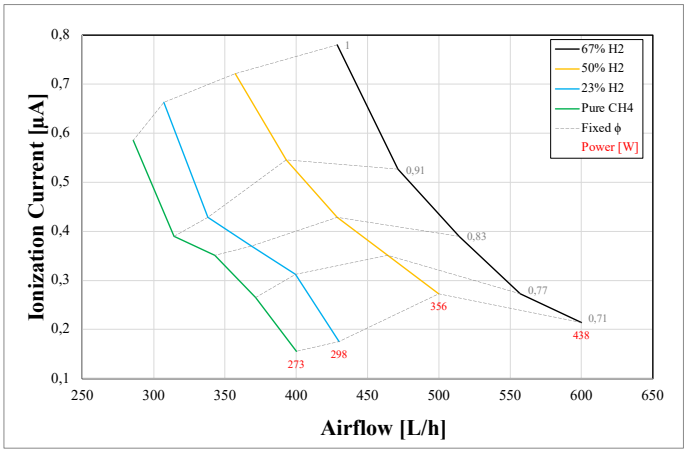

Figure 5: Ionization current profiles for H_2/CH_4 blends range from 0 to 67% H_2. Contour lines are plotted for ϕ. Electrode fixed at 0,6 mm from the burner surface. Burner 2 (multi-hole 0.9 mm 360°).

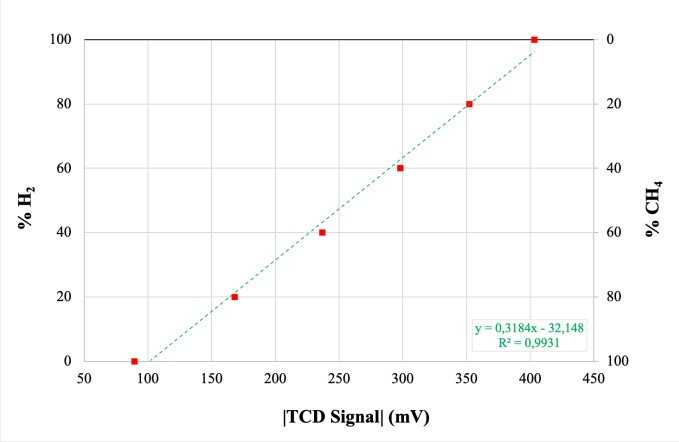

Figure 6: Sensitivity of the TCD signal (mV) to the changes in the hydrogen-methane ratio.

Conclusions

This work aimed to bring further information to the use of ionization current flame detection for mixtures of methane-hydrogen in the context of growing political and social interest in the use of hydrogen as fuel. It has been shown that flame ionization detection (FID) is a useful tool for hydrogen flame detection and that it can be part of the combustion control system, even for large hydrogen presence.

It was confirmed that the ionization current intensity rises close to the flame as the hydrogen percentage increases. Moreover, as the methane percentage in the fuel mixture drops, the optimum position of the electrode moves to the flame core. Furthermore, it was proven that the electrode is effective for flame detection of up to 95% hydrogen content in the fuel supply. Finally, deduced that by adding upstream measurement of fuel composition, for example using a thermal conductivity detector, and flow to calculate power [W], a control loop could be established.

Overall, it was confirmed that the ionization current varies according to the H_2/CH_4 ratio composition, ϕ, fuel and airflow rates, power, burner geometry, and electrode spatial arrangement. It is believed that the results obtained in this study could have significant implications not only on the design phase of future equipment but also in the adaptation of the existing ones currently using exclusively methane to run with hydrogen.

Acknowledgments

The authors would like to acknowledge the contributions of the K-inn Tech team, especially Arianna and Jessica, for their assistance in conducting the experiments.

Reference

[1] I. Maynard and A. Abdulla, 'Assessing benefits and costs of expanded green hydrogen production to facilitate fossil fuel exit in a net-zero transition', *Renew. Energy Focus*, vol. 44, pp. 85–97, 2023, doi: 10.1016/j.ref.2022.12.002.

[2] M. G. Rasul, M. A. Hazrat, M. A. Sattar, M. I. Jahirul, and M. J. Shearer, 'The future of hydrogen: Challenges on production, storage and applications', *Energy Convers. Manag.*, vol. 272, 2022, doi: 10.1016/j.enconman.2022.116326.

[3] H. He *et al.*, 'Study of hydrogen generation from heavy oil gasification based on ramped temperature oxidation experiments', *Int. J. Hydrog. Energy*, vol. 48, no. 6, pp. 2161–2170, Jan. 2023, doi: 10.1016/j.ijhydene.2022.10.095.

[4] M. J. van Rensburg, A. Botha, N. G. Ntsasa, J. Tshilongo, and N. Leshabane, 'Towards the simultaneous detection of the low nmol/mol range of CO, CH4 and CO2 in nitrogen using GC-FID', *Accreditation Qual. Assur.*, vol. 14, no. 12, pp. 665–670, 2009, doi: 10.1007/s00769-009-0580-1.

[5] P. Dagaut and A. Nicolle, 'Experimental and detailed kinetic modeling study of hydrogen-enriched natural gas blend oxidation over extended temperature and equivalence ratio ranges', *Proc. Combust. Inst.*, vol. 30, no. 2, pp. 2631–2638, Jan. 2005, doi: 10.1016/j.proci.2004.07.030.

[6] C. Lupan *et al.*, 'Nanosensors Based on a Single ZnO:Eu Nanowire for Hydrogen Gas Sensing', *ACS Appl. Mater. Interfaces*, vol. 14, no. 36, pp. 41196–41207, 2022, doi: 10.1021/acsami.2c10975.

[7] L. Guo, M. Zhai, Q. Shen, H. Guo, and P. Dong, 'Effect of hydrogen addition on the ionization of partially premixed methane flame', *Fuel*, vol. 285, p. 119141, Feb. 2021, doi: 10.1016/j.fuel.2020.119141.

[8] A. Aniello, T. Poinsot, L. Selle, and T. Schuller, 'Hydrogen substitution of natural-gas in premixed burners and implications for blow-off and flashback limits', *Int. J. Hydrog. Energy*, vol. 47, no. 77, pp. 33067–33081, Sep. 2022, doi: 10.1016/j.ijhydene.2022.07.066.

[9] A. Fialkov, 'Investigations on ions in flames', *Prog. Energy Combust. Sci.*, vol. 23, no. 5–6, pp. 399–528, 1997, doi: 10.1016/S0360-1285(97)00016-6.

Simulation of dual-fuel marine engines fueled by hydrogen or methanol

S. Parsa*[1], S. Verhelst[1,2]

[1] Ghent University
[2] Lund University

Introduction

Maritime transport contributed to 2.9% of anthropogenic global CO_2 emissions in 2018, emitting 1,076 million tons of CO_2. In the EU, maritime transport was responsible for 3-4% of total CO_2 emissions and emitted over 144 million tons of CO_2 in 2019. In order to reduce greenhouse gas emissions from maritime transport, the European Union has mandated a 2% reduction by 2025 and an 80% reduction by 2050 compared to 2020. One of the ways to achieve these targets is the use of renewable fuels such as hydrogen and methanol in marine engines [1, 2]. Due to the special combustion properties of these fuels, they can be used as the main fuel in internal combustion (IC) engines. Some of the combustion characteristics of hydrogen and methanol have been compared with those of diesel in Table 1.

Table 1 Comparison of various properties of hydrogen, methanol and diesel fuels [2, 3]

Property	Hydrogen	Diesel fuel	Methanol
Minimum ignition energy (mJ)	0.02	0.24	0.14
Lower heating value (MJ/kg)	120	42.5	20.09
Autoignition temperature in air (K)	858	453-593	738
Higher heating value (MJ/kg)	142	44.8	22.8
Stoichiometric air-to-fuel ratio (kg/kg)	34.2	14.5	6.5
Flammability limits in air (vol%)	4-75	0.6-5.5	1.81-36
Density at NTP (kg/m^3)	0.08	829	790
Mass diffusivity in air (cm^2 /s)	0.61	0.038	0.14
Quenching distance at NTP (mm)	0.64	-	1.85
Peak laminar flame velocity, NTP, m/s	2.65-3.25	0.3	0.42
Octane Number	>110	-	109
Latent Heat of vaporization (kJ/kg)	-	47.86	1100

Because of the high autoignition temperature of hydrogen and methanol, an ignition source is required to start their combustion in compression ignition (CI) engines. The Dual Fuel (DF) approach is an efficient way to use them [4, 5]. To add hydrogen into a CI engine, there are some techniques which have been investigated in literature [6-13]. The modification of conventional port fuel injected (PFI) to hydrogen can be achieved by replacement of the

* Corresponding author: somayeh.parsa@ugent.be

injection system (Fig. 1). The main challenges with the PFI method are pre-ignition, knock and backfiring due to the wide flammability range, low minimum ignition energy and low quenching distance of hydrogen. In addition, hydrogen displaces air in the intake and therefore limits the engine power density [14].

The most common methods of adding alcohol fuel to the engine are blending and fumigation. In the blending method, the alcohol fuel is mixed with diesel fuel before injection. Then the mixture of alcohol fuel and diesel fuel is injected directly into the cylinder. Although this method is considered the simplest way to use alcohol fuel in dual-fuel diesel engines, there are some serious problems when using some alcohols [15]. For example, to mix some alcohol fuels such as methanol with diesel fuel in all proportions and form a uniform blend, some additional additives would be required. Due to the very low cetane number of alcohols, the cetane number of alcohol-diesel blends decreases. Also, the hygroscopic nature of ethanol increases the possibility of corrosion of the injection system and fuel tank. The fumigation method is an efficient way to avoid these problems. In the fumigation method, alcohol fuel such as methanol is added to the intake air upstream of the manifold. There are different ways to add alcohol fuel to the air: Injection and carbureting [16, 17]. Although the fumigation technique is more effective than the blending method, there are still some challenges. Due to the low cetane number of alcohols, there is a probability of severe knocking under high load [18]. Due to the high evaporation heat of alcohols, the ignition is difficult at cold start, warming up and low load condition [19]. In addition, the amount of CO and THC (total unburned hydrocarbon) increase [20].

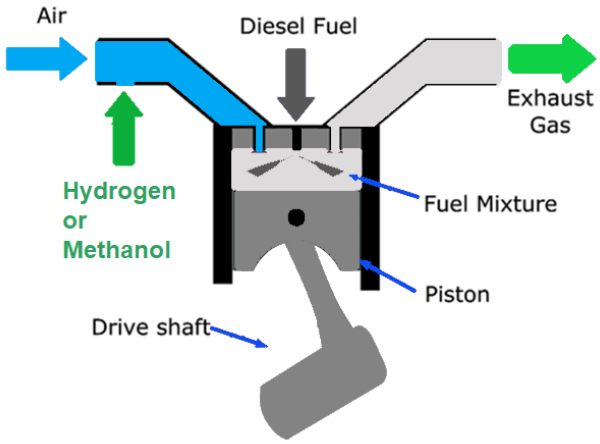

Figure 1 Dual fuel application of hydrogen and methanol

Thesis objective

In order to overcome the challenges and achieve the best operating conditions for engines running on hydrogen or methanol, the co-combustion of hydrogen/diesel and methanol/ diesel should be well understood. Therefore, the objective of this dissertation is to accurately simulate the co-combustion of hydrogen-diesel and methanol-diesel in marine engines. In dual-fuel applications, diesel fuel is injected into a premixed fuel-air mixture (Fig. 2). The cylinder mixture is therefore not homogeneous and there are different zones with different equivalence ratios from lean to rich [11]. The zones around the pilot injection are rich and

contain a high percentage of diesel fuel, while the zones far from it are lean and contain no or a lower percentage of diesel fuel. Thus, the different zones have different behavior, which should be taken into account when calculating the Ignition Delay (ID) and Laminar Burning Velocity (LBV) in the dual-fuel combustion simulation.

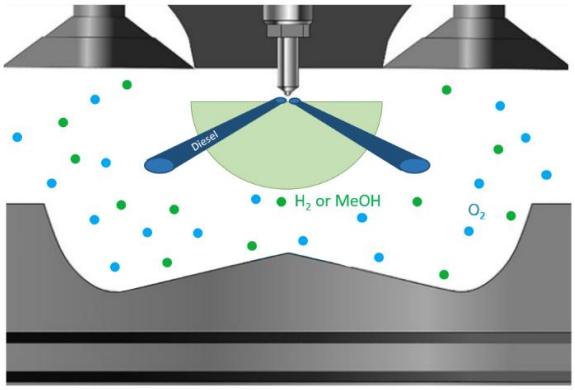

Figure 2 The schematic of in-cylinder mixture in dual fuel application

In the first stage of the PhD, the ignition delay of the pilot fuel and the laminar burning velocity of the premixed fuel have been calculated, since an accurate calculation of ID and LBV is required to model the combustion. The result of the first step shows that the premixed hydrogen has no significant effect on the ID of the pilot fuel, unless the proportion of hydrogen in the premixed fuel is very high. However, the ID of the pilot fuel is strongly influenced by the premixed methanol. In terms of LBV, it can be seen that the pilot fuel has a significant effect on the LBV in the rich area of the two premixed fuels - methanol and hydrogen [21]. Then, ID and LBV were calculated for different operating conditions and now the data retrieval will be optimized by neural network methods. In the next step, the data will be used for dual combustion simulation. Abnormal combustion phenomena will also be investigated to determine the causes and ways to avoid them. Various simulation tools are used, including Cantera, Python, and GT-POWER.

References

1. Verhelst, S., *Recent progress in the use of hydrogen as a fuel for internal combustion engines.* international journal of hydrogen energy, 2014. 39(2): p. 1071-1085.
2. Verhelst, S., et al., *Methanol as a fuel for internal combustion engines.* Progress in Energy and Combustion Science, 2019. 70: p. 43-88.
3. Zhen, X. and Y. Wang, *An overview of methanol as an internal combustion engine fuel.* Renewable and Sustainable Energy Reviews, 2015. 52: p. 477-493.
4. Lilik, G.K., et al., *Hydrogen assisted diesel combustion.* International Journal of Hydrogen Energy, 2010. 35(9): p. 4382-4398.
5. Saravanan, N., et al., *Combustion analysis on a DI diesel engine with hydrogen in dual fuel mode.* Fuel, 2008. 87(17-18): p. 3591-3599.
6. Bose, P.K. and D. Maji, *An experimental investigation on engine performance and emissions of a single cylinder diesel engine using hydrogen as inducted fuel and diesel as injected fuel with exhaust gas recirculation.* International journal of hydrogen energy, 2009. 34(11): p. 4847-4854.
7. Karagöz, Y., et al., *Effects of hydrogen and methane addition on combustion characteristics, emissions, and performance of a CI engine.* international journal of hydrogen energy, 2016. 41(2): p. 1313-1325.
8. Köse, H. and M. Ciniviz, *An experimental investigation of effect on diesel engine performance and exhaust emissions of addition at dual fuel mode of hydrogen.* Fuel processing technology, 2013. 114: p. 26-34.

9. Masood, M., M. Ishrat, and A. Reddy, *Computational combustion and emission analysis of hydrogen–diesel blends with experimental verification.* International Journal of Hydrogen Energy, 2007. 32(13): p. 2539-2547.
10. Rocha, H.M.Z., et al., *Experimental investigation of hydrogen addition in the intake air of compressed ignition engines running on biodiesel blend.* International Journal of Hydrogen Energy, 2017. 42(7): p. 4530-4539.
11. Sharma, P. and A. Dhar, *Compression ratio influence on combustion and emissions characteristic of hydrogen diesel dual fuel CI engine: Numerical Study.* Fuel, 2018. 222: p. 852-858.
12. Yilmaz, I., A. Demir, and M. Gumus, *Effects of hydrogen enrichment on combustion characteristics of a CI engine.* International Journal of Hydrogen Energy, 2017. 42(15): p. 10536-10546.
13. Yip, H.L., et al., *A Review of Hydrogen Direct Injection for Internal Combustion Engines: Towards Carbon-Free Combustion.* Applied Sciences, 2019. 9(22): p. 4842.
14. Fayaz, H., et al., *An overview of hydrogen as a vehicle fuel.* Renewable and Sustainable Energy Reviews, 2012. 16(8): p. 5511-5528.
15. Garcia, A.F.L., *Effect of alcohol fumigation on diesel engine*, in *Departamento de Ingeniería Mecánica*. 2014.
16. Can, Ö., I. Celikten, and N. Usta, *Effects of ethanol addition on performance and emissions of a turbocharged indirect injection diesel engine running at different injection pressures.* Energy conversion and Management, 2004. 45(15-16): p. 2429-2440.
17. Imran, A., et al., *Review on alcohol fumigation on diesel engine: a viable alternative dual fuel technology for satisfactory engine performance and reduction of environment concerning emission.* Renewable and Sustainable Energy Reviews, 2013. 26: p. 739-751.
18. Havemann HA, R.M., Nalaragan A,Narasimban TL., *Alcohol in diesel engines.* Automobile Engineer, 1954. 44: p. 256-262.
19. Zhang, Z., et al., *Effect of fumigation methanol and ethanol on the gaseous and particulate emissions of a direct-injection diesel engine.* Atmospheric Environment, 2011. 45(11): p. 2001-2008.
20. Imran, A., et al., *Review on alcohol fumigation on diesel engine: a viable alternative dual fuel technology for satisfactory engine performance and reduction of environment concerning emission.* Renewable and Sustainable Energy Reviews, 2013. 26: p. 739-751.
21. Parsa, S. and S. Verhelst, *Numerical Investigation of the Ignition Delay and Laminar Flame Speed for Pilot-Ignited Dual Fuel Engine Operation with Hydrogen or Methanol*. 2023, SAE Technical Paper.

Simulation-based optimization of a SOEC system for co-electrolysis operation

S. Beringer*[1], K. Treusch[1], B. Grabner[1], A. Trattner[1,2]

[1]HyCentA Research GmbH, Graz, Austria
[2] Institute of Thermodynamics and Sustainable Propulsion Systems, Graz University of Technology, Graz, Austria

Introduction

The EU's planned switch from fossil to renewable energy sources by 2050 poses crucial challenges for the energy sector. Generating electricity from renewable sources inherently brings significant fluctuations in production, adding strain to the already stretched grid capacities [3]. For this reason, in addition to the conversion of energy production to renewable, its distribution and storage is a major focus of current efforts. This is where high-temperature SOEC (solid oxide electrolysis cell) technology for the production of green hydrogen as an energy carrier comes in. Due to the high-temperature level of typically 600 – 850 °C, efficiencies of over 80 % can be achieved with this technology, which represents the highest of current electrolysis systems [1,2]. In addition to SOEC-steam electrolysis, SOEC is also an important technology for use as a co-electrolyser. One important application, for example, is the electrochemical splitting of steam and carbon dioxide into hydrogen and carbon monoxide, which will be investigated in this dissertation. Depending on the composition of the product gas, it can be used as feedstock for numerous downstream industrial processes or the production of synthetic fuels [6]. In addition, SOEC can be used to buffer peak loads of electricity through the possibility of a reversible mode of operation by reconverting hydrogen in fuel cell operation [1]. The same could be done with PCCE (Proton Conducting Ceramics Electrolysis), another emerging HTEL (High-Temperature Electrolysis) method. Despite lagging behind SOEC development, this technology demonstrates performance and efficiencies similar to SOEC, albeit at temperatures 200 – 300 °C lower. This is attributed to the reduced activation energy needed for protonic transport [5]. For this reason, PCCE technology is also analyzed in this dissertation.

Despite the great potential, significant problems still need to be solved for the commercial application of SOEC systems. One of the main challenges of this technology is the severe degradation caused by high temperatures. Thus, in comparison to other electrolysis technologies, only limited lifetimes can be achieved [8]. In addition to the temperature-related high degradation and the associated comparatively short lifetime, the lack of system-level investigations is another major issue of SOEC technology. To date, research has shown a high potential for HTEL, but this is mostly limited to the cell and stack level and little is known about the behavior in real operation. To implement this electrolysis technology cost-effectively on a large scale, it appears to be essential to integrate it with industrial processes, gas turbine plants, or other exothermic processes to optimize heat utilization [4]. Within the scope of this work, therefore, a virtual system for the optimization of operating strategies and BoP (Balance of plant) components is to be developed, which should increase the efficiency of the overall system and ensure the avoidance of lifetime-reducing operating modes for various application scenarios.

* Corresponding author: beringer@hycenta.at

Methodology

In the course of this dissertation, on the one hand, the lifetime of high-temperature and co-electrolysis as a central challenge of this technology shall be investigated and increased. On the other hand, the efficiency of the overall HTEL system is to be improved using numerical simulation and suitable operating strategies are to be derived. Currently, there is very little research in the field of HTEL beyond the cell and stack level, which is why this dissertation is intended to provide estimates of the overall efficiency and the development of operating strategies to improve it.

In the first step, a comprehensive literature review provided a basic comparison of different HTEL methods concerning their degradation behavior, lifetime, performance, efficiency, and suitability for use as co-electrolyzer. Therefore, we placed particular emphasis on SOEC and PCCE technology to analyze the overall potential of both technologies. Based on the findings, we plan to create a matrix of HTEL technologies to establish a foundational understanding for future studies.

The main focus of this dissertation is the development of a numerical simulation model from cell to system level. Based on the experimental results of a modified HTEL cell, an existing simulation model is currently being adapted for use in co-electrolysis operation. The model will focus on simulating the electrochemical reactions and diffusion processes of the reactants occurring within the cell, tailored to specific product gas compositions. This will generate an IV characteristic curve to estimate cell efficiency and product gas mass flow, factoring in the impact of degradation. For the overall system simulation, the main focus lies on the development of a virtual BoP design and its components to optimize efficiency. To achieve this, the components are analyzed in well-defined submodels and integrated into the overall virtual system environment. Figure 1 shows an example BoP architecture of an SOEC system which serves as a basis for the work within this dissertation.

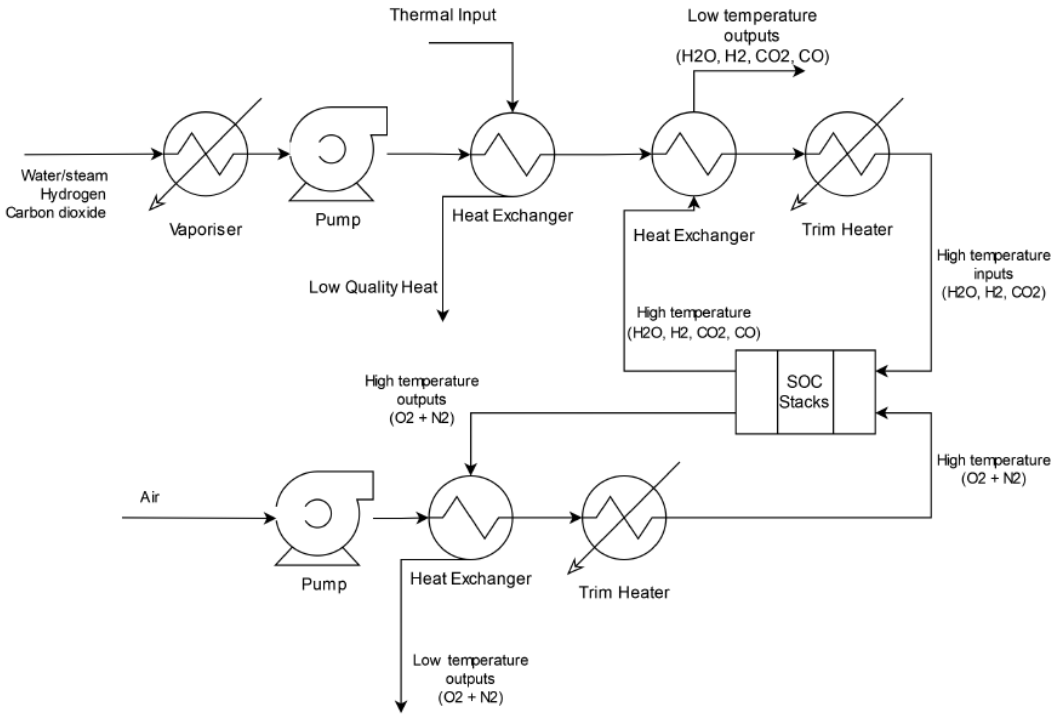

Figure 1: Exemplary BoP architecture of an SOEC system. Image taken from [7]

The creation of the submodels, as well as the virtual overall system, will be done with the software *Matlab-Simulink*. For all fluid mechanical processes of both the reactant and product flow inside the cell, as well as the BoP components, the *Ansys Fluent* fluid simulation software is utilized. The validation of the cell submodel in an experimental setup will be conducted cooperatively with the Institute of Thermal Engineering of the Graz University of Technology.

For a better understanding of long-term testing with a special focus on degradation mechanisms, the development of test methods, protocols, and diagnostic tools is another important task of this work. Therefore, specific tools such as EIS (Electrochemical Impedance Spectroscopy) will be further investigated and applied for stack characterization, performance evaluation, and state of health monitoring to build solid expertise for future research.

Discussion

The expected outcome of this work is a profound knowledge of the main degradation issues of SOEC technology and the definition of an optimized system layout, operation strategy, and BoP design for various application scenarios. The developed virtual system environment will be built modularly, facilitating the integration of different submodels like a stack model and BoP models. Therefore, the simulation model should be applicable to simulate different application scenarios and preferred feedstocks in the case of co-electrolysis. Data validation will be conducted collaboratively with industrial and scientific partners.

A key task in the dissertation is to improve thermal management by optimizing BoP size and physical positioning to account for heat flows and reduce thermal losses. According to the current state of the literature, little effort has been put into optimizing the thermal management of BoP components as well as the coupling with heat transport flows of industrial processes, why its optimization offers great potential to increase the overall plant efficiency. In addition to improving thermal efficiency, optimized heat flows will aid to increase service life by identifying and improving or eliminating the main degradation mechanisms.

The improvement and development of optimized operation strategies of SOEC and co-electrolysis systems in a virtual environment is another essential point of this work. Different application scenarios and feed gases have to be considered. The development of optimized operating strategies will also include degradation-promoting operations like highly dynamic load profiles to understand the grid connectivity of SOEC. The virtual system environment will provide the possibility of scale-up and serve to investigate

a) Effects of temperature distributions
b) Shutdown behaviour and thermal-cycling
c) Degradation behaviour and maintenance intervals of cell and BoP components

Finally, agreed on non-objectives of this dissertation are:

- System development and implementation into a specific real-life operation scenario
- Design and setup of a stack and module on the testbed
- Coupling of a SOEC and co-electrolysis system into an overall renewable power system

Conclusions

Within the scope of this dissertation, SOEC technology in the co-electrolysis operation mode is to be investigated and optimized. For this purpose, a virtual environment with numerous submodels is to be developed, which, depending on the application scenario, is suitable for predicting decisive operating parameters and lifetime issues. To accomplish this dissertation, the following summarized research methodology should be employed:

- Extensive literature review of the current state of the art
- Creation of a technology matrix of HTEL systems to compare critical operating characteristics
- Definition of system boundaries for each submodel
- Extension and creation of single models to represent co-electrolysis using SOEC on cell and stack level by validation with experimental tests
- Creation of single models for BoP component thermal simulation to improve thermal management, optimized component design and favourable overall system layout
- Creation of a virtual overall system and integration of submodels
- Development and optimization of suitable operating strategies for different application scenarios
- Development and selection of suitable analysis tools and test methods for the characterization of long-term behaviour with a focus on degradation

References

[1] Hauch, A., Küngas, R., Blenhow, P., Hansen, A.B., Hansen, J.B., Mathiesen, B.V., Mogensen, M.B.: "*Recent advances in solid oxide cell technology for electrolysis*", Science, Volume 370, Issue 6513, 2020, doi: 10.1126/science.aba6118.

[2] HTW Editorial Team: "*World's largest SOEC electrolyzer achieves record efficiency*", Hydrogen Tech World, 2022, retrieved from: https://hydrogentechworld.com/worlds-largest-soec-electrolyzer-achieves-record-efficiency on 29.08.2023.

[3] European Commission: "*Communication from the commission to the European Parliament, the Council, the European Economic and Social Committee and the Committee of the Regions. A hydrogen strategy for a climate-neutral Europe*", COM(2020) 301 final, 2021, EUR-Lex - 52020DC0301 - EN - EUR-Lex (europa.eu), Retrieved on 03.11.2023.

[4] Klell, M., Eichlseder, H., Trattner, A.: "*Wasserstoff in der Fahrzeugtechnik: Erzeugung, Speicherung, Anwendung*", Springer Fachmedien Wiesbaden GmbH, Edition 4, 2018, ISBN: 978-3-658-20447-1.

[5] Le, L.Q., Meisel, C., Hernandez, C.H., Huang, J., Kim, Y., O'Hayre, R.O., Sullivan, N.P.: "*Performance degradation in proton-conducting ceramic fuel cell and electrolyser stacks*", Journal of Power Sources, Volume 537, 2022, doi: 10.1016/j.jpowsour.2022.231356.

[6] Schmidt, O., Gambhir, A., Staffel, I., Hawkes, A., Nelsen, J., Few, S.: "*Future cost and performance of water electrolysis: An expert elicitation study*", International Journal of Hydrogen Energy, Volume 42, 2017, doi: 10.1016/j.ijhydene.2017.10.045, pages 30470-30492

[7] Spekreijse, A.: "*Steady State Modelling of Solid Oxide Cells*", Master Thesis, 2022.

[8] Su, H., Hu, Y.H.: "*Degradation issues and stabilization strategies of protonic ceramic electrolysis cells for steam electrolysis*", Energy Science and Engineering, Volume 10, 2021, doi: 10.10.1002/ese3.1010.

Simultaneous electrochemical production of hydrated lime and valuable gases in a three-phase hybrid electrolyzer

R.Rouxhet*[1], M.Loudèche[1], J.Proost [1]

[1] Division of Materials and Process Engineering (IMAP), UCLouvain

Introduction

Lime plays a vital role in various industries, including steel production, environmental applications, construction, and chemicals production. However, traditional lime production methods emit substantial CO_2, contributing to environmental concerns. Efforts to reduce carbon emissions in the lime industry are underway, including carbon capture and alternative production methods.

In response to the growing environmental challenges associated with traditional lime production, a novel electrochemical approach was introduced by Ellis et al. in 2019 [1]. This process takes place in a hybrid electrolyzer that operates with solid, liquid, and gaseous phases. It involves the dissolution of limestone in the anodic chamber, followed by the precipitation of calcium hydroxide in the cathodic chamber, driven by a pH gradient created during water electrolysis. This new route is compared to the conventional way and the four key steps of the process are explained in Figure 1.

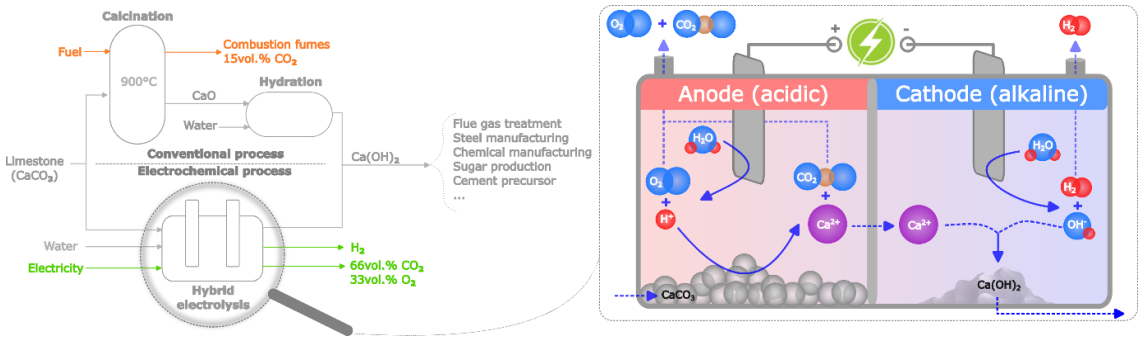

Figure 1: Comparison between thermal and electrochemical production of Ca(OH)2 and a simplified reaction scheme of the hybrid electrolyzer.

The operation of the hybrid electrolyzer in a two-compartment cell is thoroughly examined at various applied currents. Each step in the process, from neutral water electrolysis to hydroxide precipitation, is analyzed. Transport number is introduced to assess the establishment of the pH gradient and calcium migration. The study also addresses the effect of precipitation on membrane fouling and a strategy to minimize it.

* Corresponding author: remy.rouxhet@uclouvain.be

Methodology

Experiments at different current applied were performed in a 1-liter capacity glass H-cell. Both compartments of the cell were subjected to magnetic stirring at 400 revolutions per minute.
Calcium carbonate, with a purity exceeding 99.0% was introduced into the anode compartment. Electrodes with dimensions of 65x25x2mm were used, featuring a pure nickel cathode and a DSA-coated anode with mixed metal oxide on both sides. A cation exchange membrane, Nafion N115 served as the separator between the two compartments.
The experimental setup included a potentiostat and a double-junction pH electrode supplied by Metrohm. Sampling was conducted in each compartment during the experiments to determine pH and calcium ion concentration through ICP-AES analyses. XRD analysis was performed using a Bruker D8 Advanced device equipped with LYNXEYE detectors and a cobalt source to analyze the precipitate obtained. All experiments were conducted at room temperature.

Discussion

As can be seen in Figure 2, a perfect faradic efficiency for the first step, water electrolysis, has been obtained by using $NaClO_4$ or $Ca(ClO_4)_2$ as electrolytes. With $NaNO_3$ electrolyte, the preferential reduction of nitrate ions hinders the production of hydrogen. Electrodes used are DSA (Ti coated with IrO2) for the anode and nickel for the cathode. The establishment of a pH gradient inside the cell has also been highlighted thanks to the use of these neutral electrolytes.

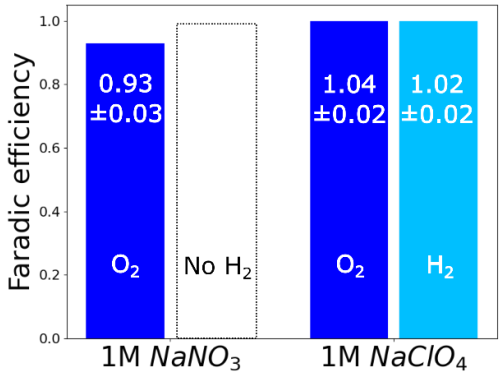

Figure 2: Faradic efficiencies obtained for both electrolytes tested with a DSA anode and nickel cathode.

The next step, the dissolution, follows the stoichiometry expected regardless of the current applied. Indeed, the slope of the linear fit ($5.12 \pm 0.07 \cdot 10^{-6}$ mol/C) shown in Figure 3 is close to the $5.18 \cdot 10^{-6}$ mol/C expected by the stoichiometry. It has to be noticed that with a higher applied current, kinetics limitations could appear.

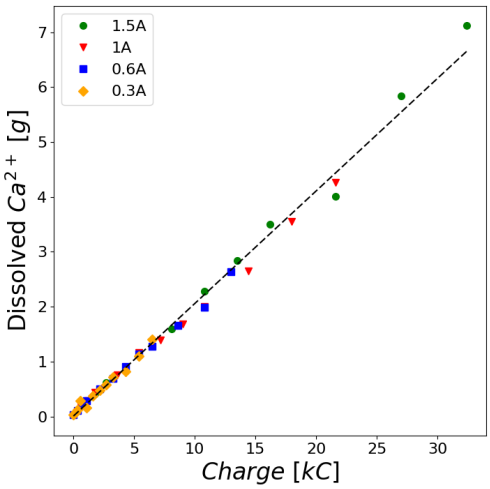

Figure 3: Quantity of calcium dissolved as a function of the charge applied

The efficiency of the calcium ions migration was understood thanks to the use of the transfer number, i.e. the fraction of current carried by an ionic species i.

$$\text{Transport number} \equiv t_i = \frac{I_i}{I} = \frac{z_i \mu_i [i]}{\sum_k z_k \mu_k [k]} \tag{6}$$

To respect the stoichiometry, the calcium ions transport number should reach one. Then, to maximize it, a cationic membrane and a calcium-based electrolyte in the anodic chamber must be used to prevent other ions from driving the current. Inevitably, the Ca^{2+} migration efficiency decreases with the pH value in the anodic compartment due to H^+ migration. As illustrated in Figure 4, the pH in the anodic compartment must be kept above 2.45 to obtain a transport number higher than 99%. Thanks to those insights, the linear fit performed on Figure 5 shows a migration efficiency of 96% compared to the stoichiometry expected.

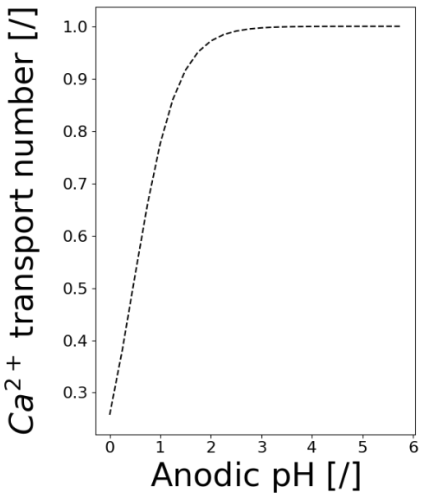

Figure 4: Ca^{2+} transport number as a function of the pH in the anodic chamber

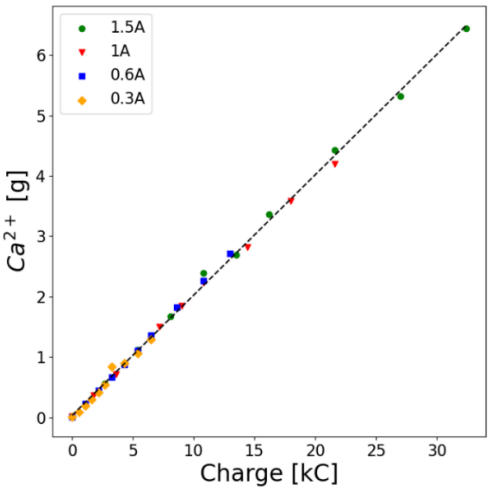

Figure 5: Quantity of migrated calcium ions as a function of the charge applied

Finally, the DRX and SEM analysis of the precipitates obtained, presented on Figure 6, proved the production of calcium hydroxide. Fouling of the membrane due to the precipitation has been highlighted. As illustrated on Figure 7, the fouling can be reduced, but not suppressed, by $CaCO_3$ batch additions that allow the choice of a lower working pH in the anodic compartment. A lower working pH implies also a decrease of the transport number and so, a decrease of the migration efficiency. A compromise must then be found.

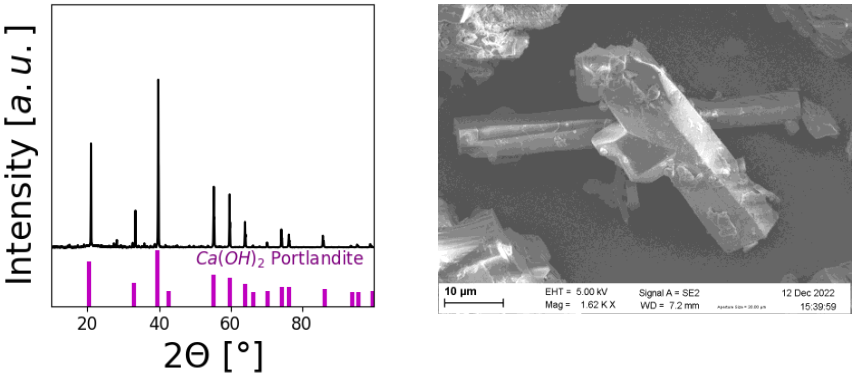

Figure 6: (A) DRX and (B) SEM analysis of the calcium hydroxide precipitates obtained by electrochemical way

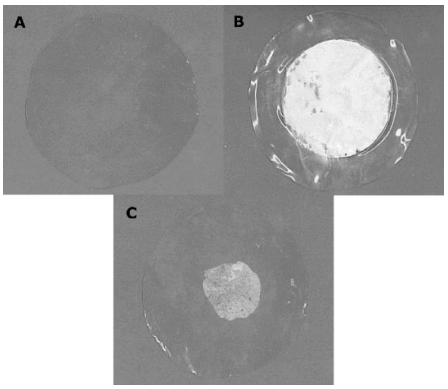

Figure 7: Pictures of membranes at the end of 6h experiments with different operating cases: A) Without $CaCO_3$; B) With an excess of $CaCO_3$; C) With batches of $CaCO_3$ to stay at a pH between 1.5 and 2

Conclusions

In summary, this study has highlighted critical aspects to maintain the stoichiometry of the four steps: water electrolysis, limestone dissolution, calcium ion migration and hydrated lime precipitation. Thoughtful choices of electrolytes and electrodes have led to notable efficiencies in water electrolysis. The dissolution stage showed no speed limitation regardless of the current tested. Calcium ion migration was also investigated emphasizing the importance of the transport number for optimal efficiency. Lastly, the analysis of precipitates proved the formation of calcium hydroxide and associated fouling issues. These findings contribute to the understanding of this novel electrochemical process for further industrial application.

References

[1] L. D. Ellis, A. F. Badel and M. L. Chiang, "Toward electrochemical synthesis of cement," *PNAS,* vol. 117, no. 23, pp. 12584-12591, 2019.

Sodium Borohydride as Alternative Fuel for Maritime Vessels

M.C. van Benten* [1], J.T. Padding[2], D.L. Schott[1]

[1]Maritime and Transport Technology, Faculty of Mechanical, Maritime and Materials Engineering, Delft University of Technology, 2628CD, the Netherlands
[2]Process and Energy, Faculty of Mechanical, Maritime and Materials Engineering, Delft University of Technology, 2628CD, the Netherlands

Introduction

Greenhouse gas emissions are responsible for global warming [1], and this could lead to significant and irreversible damage to the natural ecosystem and human society. As the maritime sector accounts for approximately 3% of the global emissions [2], the International Maritime Organization (IMO) posed restrictions on the emissions of the maritime sector to pursue a decrease of emissions of 40% by 2030, and 70% by 2050, with respect to 2008 [3]. This could be achieved by increasing the efficiency of maritime vessels [4], e.g. by designing modular power plants for maritime vessels [5]. Another option is to switch to alternative fuels such as hydrogen [6]. Traditionally, hydrogen is compressed and stored as a gas, liquefied, or cryo-compressed (liquefied under high pressure). However, each of these methods has drawbacks such as high pressures, low volumetric density, high energy requirements, and thick (insulated) walls. To overcome these disadvantages, alternative methods to store hydrogen are increasingly researched. Alternative methods, where hydrogen is stored in a carrier material, can be sorted into two different categories: liquid hydrogen carriers and solid hydrogen carriers. There are multiple viable hydrogen carriers, but the solid hydrogen carrier sodium borohydride ($NaBH_4$), which is a granular material, is particularly promising [7]. It is non-flammable, can be stored at ambient conditions (pressure and temperature), and has a relatively high volumetric energy density [8–10] compared to traditional hydrogen storage. When using $NaBH_4$ as fuel for maritime vessels, it reacts with water inside a reactor to produce hydrogen and a reaction product (spent fuel). The latter has to be stored for the remainder of the voyage and can be regenerated onshore. Both the $NaBH_4$ and its spent fuel are granular materials that can be classified as granulate or powder, depending on the size of their particles. While Lensing [11], Nievelt [12], and Düll et al. [13] investigated the use of $NaBH_4$ and other solid hydrogen carriers for maritime vessels, they did not discuss their mechanical characteristics which are required to design suitable storage and handling equipment.

This paper aims to identify the required mechanical characteristics of $NaBH_4$ and its spent fuel, to be able to design equipment for handling and storage using the Discrete Element Method (DEM). First, a circular bunkering process will be discussed, providing insight into the required storage and handling equipment. Then, a methodology to determine the required mechanical characteristics of $NaBH_4$ and its spent fuel is presented. Finally, a conclusion is given, and how the empirically determined data can be used for modelling equipment with DEM is discussed.

*Corresponding author: M.C.vanBenten@tudelft.nl

Circular Bunkering Process

In Figure 1, the required circular bunkering process to bunker multiple vessels simultaneously is shown. First, the fuel ($NaBH_4$), is stored in the port storage, from where it can be transported to the onboard fuel storage of the vessels when moored along the quay. During vessel operation, $NaBH_4$ is mixed with water and fed to the reactor, where it is converted into hydrogen (H_2), and a reaction product (spent fuel), conform Equation 1 [14]:

$$NaBH_4 + (2 + x)H_2O \rightarrow NaBO_2 \cdot xH_2O + 4H_2 \qquad \text{for } x \in [0, 2, 4] \tag{1}$$

While the obtained hydrogen is used to power the vessel, the spent fuel ($NaBO_2 \cdot xH_2O$) has to be stored. First, the spent fuel, also known as sodium metaborate, is separated by crystallisation from the unreacted fuel and water, where after it can be stored in the vessel's spent fuel storage. When the vessel receives new fuel, the spent fuel has to be transported to the port storage to be able to execute a new mission. At the port, the spent fuel can be regenerated into the fuel, as shown in Equation 2 [15, 16]:

$$NaBO_2 \cdot xH_2O + (2 + x)MgH_2 \rightarrow NaBH_4 + (2 + x)MgO + (2x)H_2 \quad \text{for } x \in [0, 2, 4] \tag{2}$$

where MgH_2 and MgO denote magnesium hydride, magnesium oxide, and magnesium, respectively. The design, configuration, and capacity of vessels' and port storage facilities and handling equipment for both the fuel and the spent fuel depends on numerous factors, such as the number of vessels N, the type of vessels, and the behaviour of the materials. The latter can be quantified by measuring the mechanical characteristics of the materials, which will be discussed in the next section.

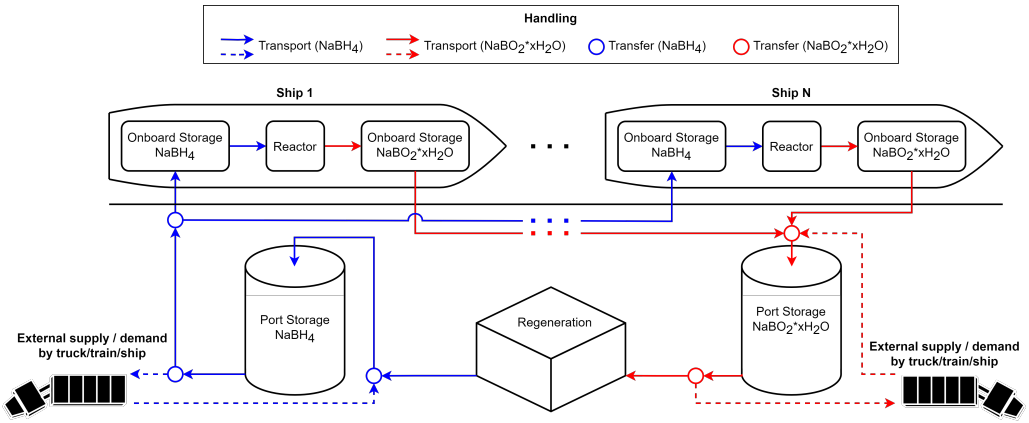

Figure 1: Circular Bunkering Process

Mechanical Characteristics of Bulk Materials

In a previous paper, we defined three categories of mechanical characteristics [17]: bulk material characteristics, interface characteristics, and particle characteristics. The former describes the characteristics of the bulk material and the interaction with itself, such as bulk density, particle size distribution, internal friction and cohesion, while the interface characteristics describe the interaction of the bulk material with the equipment, such as the wall friction or adhesion. The last category, particle characteristics, focuses on the individual particles, e.g. their density, size, and shape. Furthermore, these mechanical characteristics are not fixed but are affected

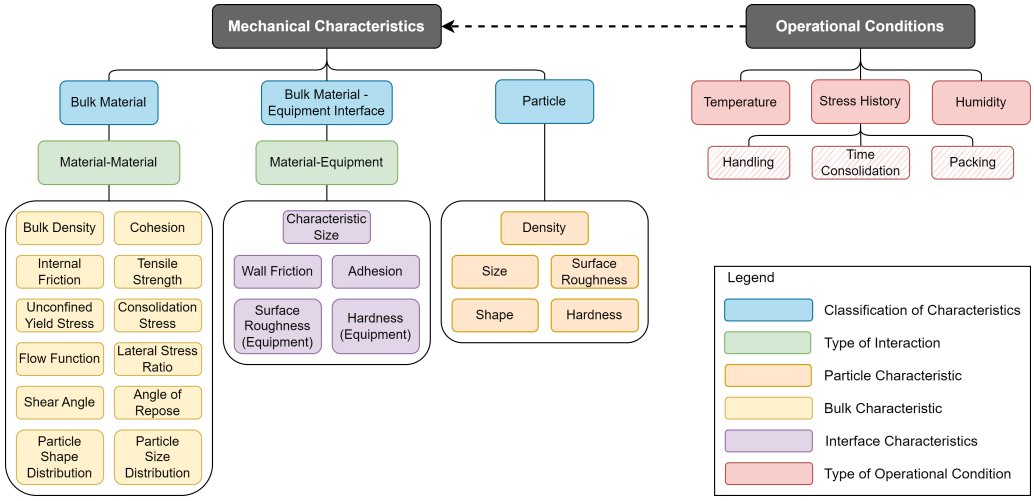

Figure 2: Mechanical Characteristics and Operation Conditions [17]

by operational conditions such as temperature, stress history, and humidity. Temperature and humidity affect the moisture content of bulk materials, which in turn affect their cohesion and adhesion through capillary forces [18]. Next to this, temperature changes can result in the expansion or contraction of individual particles [19], effectively altering the particle size, bulk density, and other characteristics. Stress history, including handling, time consolidation, and packing, affects the mechanical characteristics mainly due to prolonged and varying stresses applied to the particles. Handling could result in changing particle size and shape distributions due to attrition and breakage of particles [20], which in turn affect other characteristics such as cohesion and internal friction. Time consolidation may lead to deformations of the particles, effectively enlarging the contact area of particles with their neighbours and the equipment, such that cohesion and adhesion increase [21]. Packing describes the orientation of particles with respect to each other, hence a change in the packing can result in a change of characteristics such as internal friction, bulk density, cohesion, and adhesion. A visualisation of the different mechanical characteristics and the operational conditions is shown in Figure 2.

Methodology

To understand the behaviour of bulk materials, empirical data is required. Therefore, an experimental plan has been developed and shown in Table 1. It specifies the determined mechanical characteristics and the considered operational conditions for each experiment. Using this plan, the behaviour of the fuel and the spent fuel is quantified, such that the gathered data can be used to calibrate, verify, and validate material models in a DEM environment. These models will be used to provide guidelines for the design of storage and handling equipment.

Discussion

Ring shear tests, sieve analysis and imaging, but also individual particle strength tests showed that $NaBH_4$ is a free flowing material, unless it is consolidated over time or the moisture content exceeds a certain level. Furthermore, dynamic vapour sorption tests indicated a threshold for the relative humidity of the environment above which $NaBH_4$ starts to attract water from the air. Surprisingly, this threshold differs from the 19% RH found in the work of Murtomaa [22], Li [23], and Beaird [24]. Lastly, once moisture has been absorbed by $NaBH_4$, it could not simply be removed by drying the material, as the material would cake together and form a single large

Experiment	Mechanical Characteristics	Operational Conditions
Ring Shear Tester	• Bulk Density • Cohesion • Internal Friction • Tensile Strength • Unconfined Yield Stress • Consolidation Stress • Flow Function • Lateral Stress Ratio • Wall Friction • Adhesion	• Time Consolidation • Handling • Temperature[1] • Relative Humidity[1]
Sieve	• Particle Size (Distribution)	• Time Consolidation • Handling
Imaging	• Particle Size (Distribution) • Particle Shape (Distribution)	-
Individual Particle Strength Test	• Particle Strength	-
Dynamic Vapour Sorption Test	• Moisture Uptake[2]	• Relative Humidity
Moisture Depth Test	• Moisture Penetration (Rate)[2]	• Handling
Ledge Test	• Angle of Repose	• Time Consolidation • Temperature[1] • Relative Humidity[1]
Draw Down Test	• Angle of Repose • Shear Angle • Discharging Time	• Time Consolidation • Temperature[1] • Relative Humidity[1]
Equipment Test[3]	• T.B.D.	• T.B.D.

Table 1: Determined Mechanical Characteristics with Experiments

1: Depends upon the availability of a climate chamber
2: Moisture is not a mechanical characteristic, but it greatly affects them and is categorised as such
3: An experiment with real-life equipment is required to validate the developed DEM models

mass. These first results indicate that handling and storage equipment for $NaBH_4$ has to be designed such that no moisture can be absorbed by the material, but how time consolidation will affect the design is not yet clear.

Conclusions

$NaBH_4$ holds great promise as an alternative fuel for the maritime industry, and a circular bunkering process has been proposed which shows the required storage and handling equipment for both port and vessel operations. As the design of storage and handling equipment strongly depends on the mechanical characteristics of the fuel and the spent fuel, which are currently unknown, an experimental plan has been proposed to determine the relevant mechanical characteristics under various operational conditions. Preliminary results showed that an increase in moisture content in combination with time consolidation alters their behaviour indicating the importance of taking into account the storage and handling conditions on the vessel and at the port. DEM simulations are expected to provide insight into the behaviour of the materials, such that efficient equipment can be designed and $NaBH_4$ can be used as fuel for maritime vessels.

This research is supported by the project Sustainable Hydrogen Integrated Propulsion Drives (SH2IPDRIVE), which has received funding from RvO (reference number MOB21013), through the RDM regulation of the Ministry of Economic Affairs and Climate Policy.

References

[1] *Taking the lead on climate change*. URL: https://www.consilium.europa.eu/en/eu-climate-change/ (visited on 11/18/2022).

[2] *Klimaschutz report 2020*. 2020. URL: www.bdl.aero/wp-content/uploads/2021/03/klimaschutzreport2020_final-1.pdf (visited on 11/18/2022).

[3] *IMO's work to cut GHG emissions from ships*. URL: https://www.imo.org/en/MediaCentre/HotTopics/Pages/Cutting-GHG-emissions.aspx (visited on 11/18/2022).

[4] Birudula Anil Kumar et al. "A Coordinated Control Strategy for a Diesel-Electric Tugboat System for Improved Fuel Economy". In: *IEEE Transactions on Industry Applications* 56.5 (Sept. 2020). Conference Name: IEEE Transactions on Industry Applications, pp. 5439–5451. ISSN: 1939-9367. DOI: 10.1109/TIA.2020.3010779.

[5] M.C. van Benten, N. Kougiatsos, and V. Reppa. "Mission-oriented Modular Control of Retrofittable Marine Power Plants: 16th International Naval Engineering Conference and Exhibition incorporating the International Ship Control Systems Symposium, INEC/iSCSS 2022". In: *Proceedings of the International Ship Control Systems Symposium* 16.20 (2022). ISSN: 2631-8741. DOI: 10.24868/10721.

[6] O.B. Inal, J.F. Charpentier, and C. Deniz. "Hybrid power and propulsion systems for ships: Current status and future challenges". In: *Renewable and Sustainable Energy Reviews* 156 (Mar. 2022), p. 111965. ISSN: 1364-0321. DOI: 10.1016/j.rser.2021.111965. URL: https://www.sciencedirect.com/science/article/pii/S1364032121012302.

[7] E. van Rheenen et al. *A review of the potential of hydrogen carriers for zero emission, low signature ship propulsion systems*. preprint. Meeting Name: International Naval Engineering Conference. Oct. 2022. DOI: 10.24868/10649. URL: https://library.imarest.org/record/10649.

[8] Ç. Çakanyildirim and M. Gürü. "The Production of NaBH $_4$ from Its Elements by Mechanochemical Reaction and Usage in Hydrogen Recycle". In: *Energy Sources, Part A: Recovery, Utilization, and Environmental Effects* 33.20 (July 2011), pp. 1912–1920. ISSN: 1556-7036, 1556-7230. DOI: 10.1080/15567030903503175. URL: http://www.tandfonline.com/doi/abs/10.1080/15567030903503175.

[9] Y. Nagar et al. "Modeling the mechanical behavior of sodium borohydride ($NaBH_4$) powder". In: *Materials & Design* 108 (Oct. 2016), pp. 240–249. ISSN: 02641275. DOI: 10.1016/j.matdes.2016.06.077. URL: https://linkinghub.elsevier.com/retrieve/pii/S0264127516308334.

[10] P. Brack, S.E. Dann, and K.G.U Wijayantha. "Heterogeneous and homogenous catalysts for hydrogen generation by hydrolysis of aqueous sodium borohydride (NaBH $_4$) solutions". In: *Energy Science & Engineering* 3.3 (May 2015), pp. 174–188. ISSN: 20500505. DOI: 10.1002/ese3.67. URL: https://onlinelibrary.wiley.com/doi/10.1002/ese3.67.

[11] D. Lensing. "A study on the integration of a novel NaBH4 fuelled hybrid system for a small inland vessel". Apr. 2020.

[12] F.M. Nievelt. "Maritime application of sodium borohydride asan energy carrier". Feb. 2019.

[13] A. Düll et al. “Performance Evaluation of KBH $_4$ as Energy Carrier for Shipping Applications”. In: *Chemie Ingenieur Technik* 94.5 (May 2022), pp. 747–759. ISSN: 0009-286X, 1522-2640. DOI: 10.1002/cite.202100193. URL: https://onlinelibrary.wiley.com/doi/10.1002/cite.202100193.

[14] Y. Zhu et al. “Closing the Loop for Hydrogen Storage: Facile Regeneration of NaBH $_4$ from its Hydrolytic Product”. In: *Angewandte Chemie* 132.22 (May 2020), pp. 8701–8707. ISSN: 0044-8249, 1521-3757. DOI: 10.1002/ange.201915988. URL: https://onlinelibrary.wiley.com/doi/10.1002/ange.201915988.

[15] W. Chen et al. “Hydrolysis and regeneration of sodium borohydride (NaBH4) – A combination of hydrogen production and storage”. In: *Journal of Power Sources* 359 (Aug. 2017), pp. 400–407. ISSN: 0378-7753. DOI: 10.1016/j.jpowsour.2017.05.075. URL: https://www.sciencedirect.com/science/article/pii/S0378775317307267 (visited on 10/02/2023).

[16] H.X. Nunes et al. “Rehydrogenation of Sodium Borates to Close the NaBH4-H2 Cycle: A Review”. In: *Energies* 14.12 (Jan. 2021). Number: 12 Publisher: Multidisciplinary Digital Publishing Institute, p. 3567. ISSN: 1996-1073. DOI: 10.3390/en14123567. URL: https://www.mdpi.com/1996-1073/14/12/3567.

[17] M.C. van Benten, J.T. Padding, and D.L. Schott. “Towards Hydrogen-Fuelled Marine Vessels using Solid Hydrogen Carriers”. In: *The 14th International Conference on Bulk Materials Storage, Handling and Transportation*. Wollongong, Australia, July 2023.

[18] D. Schulze. *Powders and bulk solids: behavior, characterization, storage and flow*. OCLC: ocn166372537. Berlin ; New York: Springer, 2008. ISBN: 978-3-540-73767-4.

[19] Zhigang Cao et al. “Thermal Effects on Shear Characteristics of Unbound Granular Materials under Drained Conditions”. In: *Journal of Geotechnical and Geoenvironmental Engineering* 149.4 (Apr. 2023). Publisher: American Society of Civil Engineers, p. 04023012. DOI: 10.1061/JGGEFK.GTENG-10803. URL: https://ascelibrary.org/doi/10.1061/JGGEFK.GTENG-10803 (visited on 06/21/2023).

[20] H Kalman. “Particle Breakage and Attrition”. In: *KONA Powder and Particle Journal* 18 (2000), pp. 108–120. DOI: 10.14356/kona.2000017.

[21] Mingyang Chen et al. “Amorphous and humidity caking: A review”. In: *Chinese Journal of Chemical Engineering* 27.6 (June 2019), pp. 1429–1438. ISSN: 10049541. DOI: 10.1016/j.cjche.2019.02.004. URL: https://linkinghub.elsevier.com/retrieve/pii/S1004954118308747.

[22] M. Murtomaa et al. “On effects of ambient humidity on sodium borohydride powder”. In: *Powder handling & processing* Vol. 11.No. 1 (Jan. 1999).

[23] P. Li et al. “Deliquescence of NaBH4 from Density Functional Theory and Experiments”. In: *Industrial & Engineering Chemistry Research* 52.38 (Sept. 2013). Publisher: American Chemical Society, pp. 13849–13861. ISSN: 0888-5885. DOI: 10.1021/ie401742u. URL: https://doi.org/10.1021/ie401742u.

[24] A.M. Beaird, T.A. Davis, and M.A. Matthews. “Deliquescence in the Hydrolysis of Sodium Borohydride by Water Vapor”. In: *Industrial & Engineering Chemistry Research* 49.20 (Oct. 2010). Publisher: American Chemical Society, pp. 9596–9599. ISSN: 0888-5885. DOI: 10.1021/ie100244v. URL: https://doi.org/10.1021/ie100244v.

Structure-activity relation of Pt nanoparticles and Pt thin film deposited on Ni for electrocatalysis

S. Pahlavan*[1,2,3], S. Wodarz[1,3], R. Rupp[1,3], P. M. Vereecken[1,2,3]

[1] imec, Kapeldreef 75, 3001 Leuven, Belgium
[2] KU Leuven, M²S, cMACS, Celestijnenlaan 200F, 3001 Leuven, Belgium
[3] EnergyVille, Thor Park 8320, 3600 Genk, Belgium

Introduction

Catalyst particles which are used in water electrolysis and fuel cells are normally supported on high surface area materials, usually carbon, to increase their electrochemically active surface area [1], [2]. Catalytic materials possess different intrinsic catalytic activity; nevertheless, some physical characteristics of the catalysts can also deeply influence their catalytic activity, such as the shape, morphology of the Pt nanoparticles, and interparticle spacing [3]. There are a lot of studies in the literature dealing with this topic in electrolysis [4], [5], [6]. These characteristics can be used to tune the nanoparticles electrocatalytic activity [7].

Research perspective in designing the catalyst layer for fuel cell and water electrolysis applications is directed towards ordered controllable structures rather than the conventional carbon-supported disordered ones [8]. Recently, the potential use of high surface area nanomesh electrodes, possessing the surface area enhancement of 100x, is manifested in water electrolysis and CO_2 electroreduction applications [9], [10]. These nanomesh electrodes can be directly made of catalyst materials. Bearing in mind that the high surface area nanomesh electrodes intrinsically render high surface area without any need to make catalyst nanoparticles, one may argue if nanoparticles would give a higher catalytic activity in this type of ordered supports. The current dissertation aims to answer to this question, comparing the catalytic activity of Pt nanoparticles and Pt thin films, deposited on Ni substrates, for hydrogen evolution reaction (HER), oxygen evolution reaction (OER), and oxygen reduction reaction (ORR).

Methodology

Pt nanoparticles (NPs) and a Pt thin film were deposited on physical vapour deposited (PVD) Ni using a Teflon cell and three-electrode technique. The PVD Ni substrates were used as working electrodes together with a reference electrode (RE) and a platinized titanium mesh as counter electrode (CE). The bath used for the deposition was 3 mM K_2PtCl_4 + 0.5 M NaCl + 1 mM $HClO_4$. The nanoparticles were deposited at a given charge density of 5 mC/cm^2, at different current densities of -0.010, -0.025, -0.050, -0.100 mA/cm^2 for 500, 200, 100, and 50 s, respectively. Thin films of Pt were deposited using a technique known as Pt electrochemical atomic layer deposition (EALD)[11] by applying the potential of -0.8 V for 200 s for 4 cycles; the substrate was rinsed with deionised water in between the cycles. Characterisation of the nanoparticles was done using scanning electron microscopy (SEM) and hydrogen adsorption and desorption peaks analysis[12].

To electrochemically characterise the catalytic behaviour of the samples, an inverted rotation disk electrode (IRDE) tool was used. Electrochemical activity of the samples was thus compared for HER, OER, and ORR. A reversible hydrogen electrode (RHE) and a Pt mesh were respectively used as RE and CE. The working electrode potential was swap from its open circuit potential (OCP) up/down to the onset of HER, OER, or ORR. The scan was continued

* Corresponding author: sohrab.pahlavan@imec.be

until the absolute value of 50 mA/cm^2 is reached for the current density. The experiments were done in 1 M solution of KOH, and the solution was respectively purged with N_2, O_2, and O_2 again for the onsets of HER, OER, and ORR.

Discussion

Figure 1 shows the SEM images of the studied samples: blank PVD Ni, Pt nanoparticled Ni samples, and Pt EALD sample. It is seen that the deposited Pt NPs are almost equal in size in diameter, but the island density increases with increasing the applied current density. The surface area and the island density of the nanoparticles and the thin-film Pt is analysed by image analysis and by electrochemical methods.

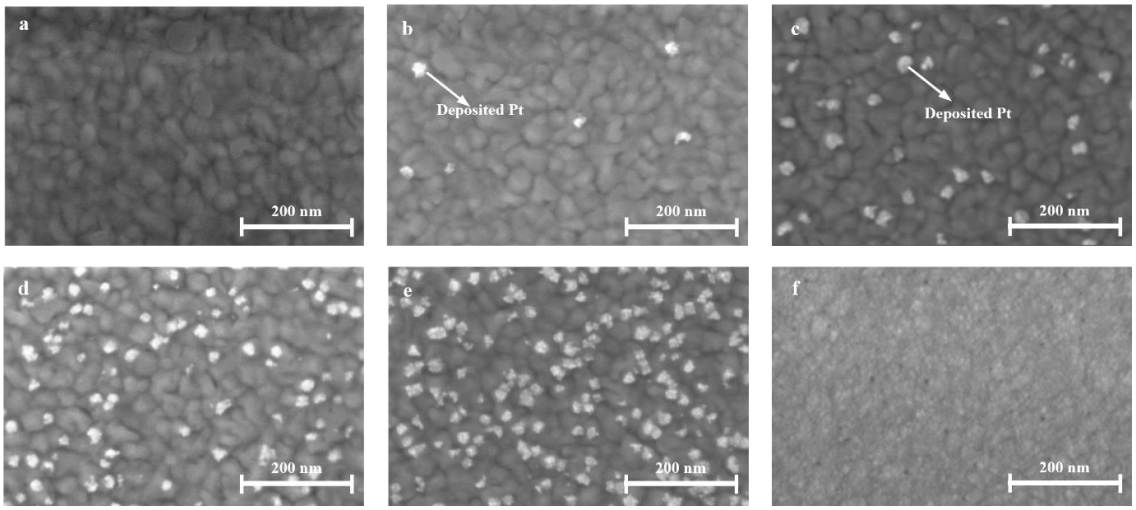

Figure 1: SEM image of a) blank PVD Ni and Pt NPs deposited at b) -0.010 mA/cm^2 for 500 s, c) -0.025 mA/cm^2 for 200 s, d) -0.050 mA/cm^2 for 100 s, e) -0.100 mA/cm^2 for 50 s, and f) Pt EALD.

The expected outcome is work is to study if there is a trend between the catalytic activity of Pt with the way it is deposited as nanoparticles or thin films. The rest of the work will involve measuring the onset of HER, OER, and ORR on the above-mentioned samples and normalization of the current density to the surface area or circumference of the Pt nanoparticles or thin film. Herewith the answer to the question is sought.

Conclusions

Pt nanoparticles were deposited on PVD Ni substrate by galvanostatic polarization. Pt EALD technique was also used to coat PVD Ni with a thin film of Pt. Comparing the catalytic performance of these substrates and exploring if there is a relation between the surface area or circumference of the Pt nanoparticles or thin film will be a way to find out how catalytic activity of highly porous ordered catalyst layers such as nanomesh electrodes, may be affected by nanoparticles.

References

[1] E. Antolini, “Carbon supports for low-temperature fuel cell catalysts,” *Appl Catal B*, vol. 88, no. 1–2, pp. 1–24, Apr. 2009, doi: 10.1016/J.APCATB.2008.09.030.

[2] Y. Yang, K. Chiang, and N. Burke, “Porous carbon-supported catalysts for energy and environmental applications: A short review,” *Catal Today*, vol. 178, no. 1, pp. 197–205, Dec. 2011, doi: 10.1016/J.CATTOD.2011.08.028.

[3] E. Antolini, “Structural parameters of supported fuel cell catalysts: The effect of particle size, inter-particle distance and metal loading on catalytic activity and fuel cell performance,” *Applied Catalysis B: Environmental*, vol. 181. Elsevier, pp. 298–313, Feb. 01, 2016. doi: 10.1016/j.apcatb.2015.08.007.

[4] T. O. Schmidt *et al.*, “Elucidation of Structure–Activity Relations in Proton Electroreduction at Pd Surfaces: Theoretical and Experimental Study,” *Wiley Online Library*, vol. 18, no. 30, Jul. 2022, doi: 10.1002/smll.202202410.

[5] M. Nesselberger *et al.*, “The effect of particle proximity on the oxygen reduction rate of size-selected platinum clusters,” *Nature Materials 2013 12:10*, vol. 12, no. 10, pp. 919–924, Jul. 2013, doi: 10.1038/nmat3712.

[6] L.-J. Yuan *et al.*, “Electrocatalysis Mechanism and Structure–Activity Relationship of Atomically Dispersed Metal-Nitrogen-Carbon Catalysts for Electrocatalytic Reactions,” *Small Methods*, vol. 7, no. 3, p. 2201524, Mar. 2023, doi: 10.1002/SMTD.202201524.

[7] J. Huang, J. Zhang, and M. H. Eikerling, “Particle Proximity Effect in Nanoparticle Electrocatalysis: Surface Charging and Electrostatic Interactions,” *Journal of Physical Chemistry C*, vol. 121, no. 9, pp. 4806–4815, Mar. 2017, doi: 10.1021/acs.jpcc.6b10842.

[8] M. Chen, C. Zhao, F. Sun, J. Fan, H. Li, and H. Wang, “Research progress of catalyst layer and interlayer interface structures in membrane electrode assembly (MEA) for proton exchange membrane fuel cell (PEMFC) system,” *eTransportation*, vol. 5. Elsevier B.V., Aug. 01, 2020. doi: 10.1016/j.etran.2020.100075.

[9] N. Plankensteiner *et al.*, “Freestanding µm-thin nanomesh electrodes exceeding 100x current density enhancement for high-throughput electrochemical applications,” *Mater Today Energy*, vol. 30, Dec. 2022, doi: 10.1016/j.mtener.2022.101172.

[10] N. Plankensteiner *et al.*, “Competitive enhancement of CO2 reduction reactions versus hydrogen evolution for high surface area electrodes: A comparative study for Cu and Ag nanomesh,” *Electrochim Acta*, vol. 474, p. 143495, Jan. 2024, doi: 10.1016/J.ELECTACTA.2023.143495.

[11] Y. Liu, C. M. Hangarter, D. Garcia, and T. P. Moffat, “Self-terminating electrodeposition of ultrathin Pt films on Ni: An active, low-cost electrode for H2 production,” *Surf Sci*, vol. 631, pp. 141–154, Jan. 2015, doi: 10.1016/J.SUSC.2014.06.002.

[12] R. Sharma, S. Gyergyek, and S. M. Andersen, “Critical thinking on baseline corrections for electrochemical surface area (ECSA) determination of Pt/C through H-adsorption/H-desorption regions of a cyclic voltammogram,” *Appl Catal B*, vol. 311, p. 121351, Aug. 2022, doi: 10.1016/J.APCATB.2022.121351.

Storage needs for integration of renewable hydrogen production with industrial processes

S. Pekkinen*[1], A. Santasalo-Aarnio[1]

[1]Department of Mechanical Engineering, School of Engineering, Aalto University

Introduction

The human society is facing an unprecedented challenge in anthropogenic climate change, mainly due to the massive greenhouse gas emissions from fossil fuels used in energy production and industry. Industry accounts for nearly 40% of the global energy consumption, mainly sourced from fossil fuels such as coal and natural gas [1]. Hydrogen has been identified as a potential feedstock that can be used a feedstock in oil refining, iron reduction or ammonia production. Hydrogen is already being used especially in chemical industry, produced from natural gas through steam methane reforming. Replacing this grey hydrogen with green hydrogen produced through water electrolysis with renewable electricity could reduce significantly industrial emissions globally. [2] However, renewable energy production is reliant on weather conditions while industrial processes are quite inflexible, meaning a balancing component is required in the system in the form of a hydrogen storage.

There are many known technologies to store hydrogen, either as a pure substance or bonded with different chemical compounds. Storing pure hydrogen as a compressed gas is the most used option currently, with high-pressure storage vessels being an already commercial technology. However, compressing low-density hydrogen gas to high pressures consumes energy and hydrogen-specific vessels can be costly. [3] Another method to store hydrogen gas is to use underground geological caverns that have non-permeable material on the surface to prevent leakages. Open spaces carved into salt deposits are already used to store hydrogen and show good capability of containing hydrogen gas. [4] However, these salt formations are not present everywhere in the world, for example in Scandinavia. Therefore, other solutions are required and hollowed out caverns could be lined with other materials, such as steel [5].

As industries are looking into green hydrogen as a means of decarbonization, more knowledge is required on what are the storage needs and what are the costs associated with them. Energy systems have been modeled extensively, including hydrogen systems, but many of them lack in-depth understanding of the storage technology in the system and often represent it only by energy capacity. This study aims at developing a model that includes the fundamental thermodynamic characteristics of compressed hydrogen gas in a large-scale storage system. Another aim is to quantify the storage capacities required when decarbonizing industrial hydrogen supply.

Methodology

To evaluate the hydrogen storage capacities required, a model has been developed where hydrogen is produced from renewable electricity and consumed in an industrial process. The model uses hourly data sets of renewable energy production, which is used to calculate hydrogen production with an electrolyzer. For every hour, hydrogen balance is calculated, resulting in hydrogen streams in the energy system. The state variables of hydrogen gas, most

* Corresponding author: simo.pekkinen@aalto.fi

importantly pressure and temperature are calculated, along with the compressibility factor to account for non-ideal behavior under high pressures. The model also includes the energy consumption of a hydrogen compressor used to charge the storage. Annual renewable energy data sets are used in the model to evaluate both daily and seasonal variance in hydrogen production and its impact on storage needs.

The annual hydrogen demand is assumed as 140 000 tons delivered with a constant stream throughout the year, corresponding to the annual industrial hydrogen consumption in Finland. The system is assumed to be located in Finland, with wind power as the primary renewable energy source. Solar power is considered to have a complementary role in the system as the two energy sources complement each other on a seasonal level. The power plants are dedicated to hydrogen production without grid connection. Additionally, alternative storage methods are considered to investigate the effect of storage technology on volume, costs and compression work required.

Results and Discussion

In this study, we present a model of hydrogen streams in a storage system with dedicated renewable energy production and constant industrial demand. Producing the annual demand of 140 000 tons of hydrogen with water electrolysis consumes 7.8 TWh of electricity, equaling nearly 10% of the total annual electricity consumption in Finland.

The storage capacity required is estimated in a dedicated wind-to-hydrogen system using wind power data from 2022. A total of 2 818 MW of wind power capacity is required to cover the annual hydrogen demand, equaling half of the wind capacity of Finland at the end of 2022. To ensure a steady hydrogen stream throughout the year, a storage with a capacity of 13 576 tons is required, equaling almost 10% of the annual demand. The hourly hydrogen streams in this case are presented in Figure 1.

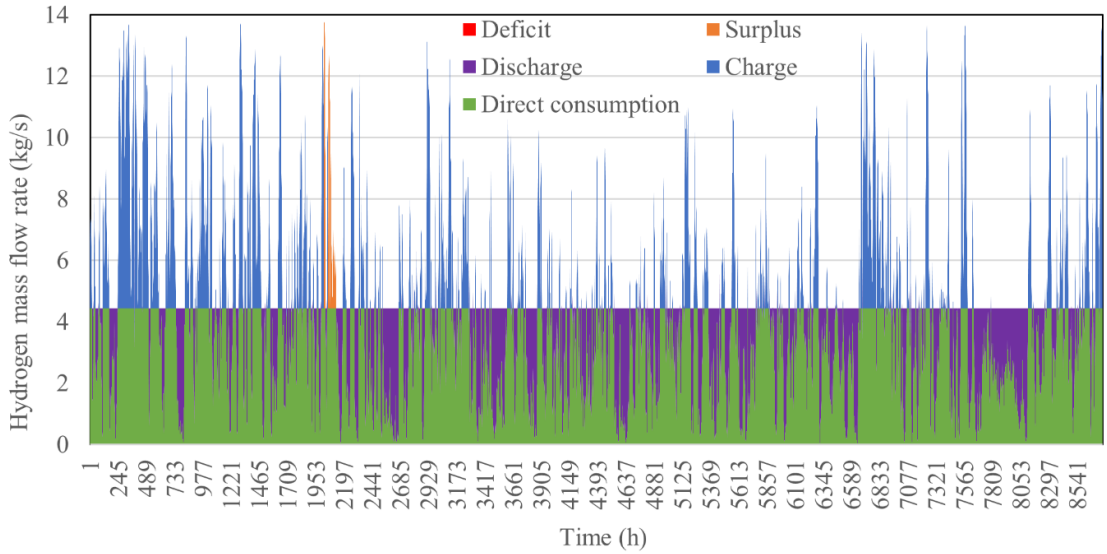

Figure 1: Hourly hydrogen streams in the dedicated wind-to-hydrogen system during 2022. Green: direct consumption of hydrogen without storage, blue: charging the storage, purple: discharging the storage, orange: surplus hydrogen stream if the storage is full, red: hydrogen deficit if the storage is empty. The solid line formed in the graph represents the constant hydrogen demand.

The storage is needed to balance seasonal variance in wind power production, with high production during winter and fall, and low production during the summer. This is highlighted in Figure 2, showing that the storage level increases during the winter and begins to fall after that towards until the end of the year.

Figure 2: Hydrogen storage level profile during 2022 coupled with a wind power farm located in Vaasa, western Finland.

A sensitivity analysis is carried out where the effects of additional wind capacity, addition of solar power, electrolyzer capacity and amount of cushion gas are analyzed. Preliminary results show that additional power production reduced the required storage capacity significantly, while reducing the electrolyzer capacity and increasing share of cushion gas in the storage increases the storage size.

Comparison of different storage technologies show significant differences in actual storage volume required and the investment costs associated with them. The volume in practical solutions vary significantly with the storage technology and especially the maximum pressure associated with them. The effect of considering the real behavior of hydrogen gas under pressure with the compressibility factor proves to be a significant factor in terms of the storage volume. Different technologies have varying characteristics and restrictions, most importantly investment costs and in terms of undergrounds storages, geological attributes of the area. Additionally, the storage pressure depending on the technology has a major impact on the electricity consumption of hydrogen gas compression.

Conclusions

Replacing industrial use of grey hydrogen produced from fossil fuels with green hydrogen has been identifies as a significant area of emissions reduction. However, coupling intermittent renewable energy sources with stable industrial processes requires a balancing hydrogen storage to ensure a steady stream of hydrogen feedstock. This study set out to quantify the needs for hydrogen storages in decarbonization of industries in the context of Finland and investigate the factors affecting the storage sizing and practical implementation.

The results show that a significant portion of current renewable energy capacity and production would be required for green hydrogen production with a large-scale storage in a dedicated wind-to-hydrogen scenario. Additionally, the choice of storage technology proved to be significant in terms of the actual storage volume, cost, and compression cost.

References

[1] IEA, "World Energy Outlook 2021," 2021. Accessed: Aug. 19, 2022. [Online]. Available: https://iea.blob.core.windows.net/assets/4ed140c1-c3f3-4fd9-acae-789a4e14a23c/WorldEnergyOutlook2021.pdf

[2] IEA, "The Future of Hydrogen," 2019. Accessed: Aug. 19, 2022. [Online]. Available: https://iea.blob.core.windows.net/assets/9e3a3493-b9a6-4b7d-b499-7ca48e357561/The_Future_of_Hydrogen.pdf

[3] A. M. Elberry, J. Thakur, A. Santasalo-Aarnio, and M. Larmi, "Large-scale compressed hydrogen storage as part of renewable electricity storage systems," *International Journal of Hydrogen Energy*, vol. 46, no. 29. Elsevier Ltd, pp. 15671–15690, Apr. 26, 2021. doi: 10.1016/j.ijhydene.2021.02.080.

[4] N. S. Muhammed, B. Haq, D. Al Shehri, A. Al-Ahmed, M. M. Rahman, and E. Zaman, "A review on underground hydrogen storage: Insight into geological sites, influencing factors and future outlook," *Energy Reports*, vol. 8. Elsevier Ltd, pp. 461–499, Nov. 01, 2022. doi: 10.1016/j.egyr.2021.12.002.

[5] J. Zheng, X. Liu, P. Xu, P. Liu, Y. Zhao, and J. Yang, "Development of high pressure gaseous hydrogen storage technologies," *Int J Hydrogen Energy*, vol. 37, no. 1, pp. 1048–1057, Jan. 2012, doi: 10.1016/j.ijhydene.2011.02.125.

Strategic Synthesis of Mixed Metal Oxides for the Oxygen Evolution Reaction

Faiz Sultan[1,2], Margarita Sánchez-Domínguez[3], Marcelo Videa[1], Dulce M. Morales*[2], Jorge L. Cholula-Díaz*[1]

[1]School of Engineering and Sciences, Tecnológico de Monterrey, Av. Eugenio Garza Sada 2501, 64849, N.L., México.
[1]Engineering and Technology institute Groningen (ENTEG), Faculty of Science and Engineering, University of Groningen, Nijenborgh 4, 9747 AG, Groningen, The Netherlands

[3]Centro de Investigación en Materiales Avanzados SC, Subsede Monterrey, Alianza Norte 202, Apodaca 66628, NL, México

Introduction

The increasing emission of greenhouse gasses into the atmosphere is a cause of global concern. Moreover, with the rising demand of energy alongside the limited amount of natural resources, current research has been driven towards the search for alternative, clean, and sustainable energy sources [1]. Hydrogen (H_2) is currently regarded as the most promising alternative to fossil fuels. Among various methods to produce H_2, water electrolysis powered by renewable energy is the most sustainable and eco-friendly approach [2]. There are two main reactions that take place during the water electrolysis process, the hydrogen evolution reaction (HER) at the cathode ($2H_2O + 2e^- \rightarrow 2OH^- + H_2$), and the oxygen evolution reaction (OER) at the anode ($4OH^- \rightarrow 2O_2 + 2H_2O + 4e^-$) [3]. HER is a two-electron transfer process, whereas the OER involves the transfer of four electrons. This makes the later a more sluggish reaction leading to large overpotentials, which renders the OER one of the major obstacles for the applicability of water electrolysis devices [4]. Therefore, the development of affordable and efficient electrocatalysts for the OER is crucial to achieve sustainable hydrogen production through water electrolysis. Precious metal-based materials such as iridium and ruthenium oxides are considered benchmark OER catalysts for water electrolysis, however, their widespread use is impeded by their scarcity and high cost [5].

To overcome this challenge, our aim is to synthesize electrocatalysts based on earth abundant transition metals by employing simple and cost-effective synthesis methods. OER electrocatalysts based on 3d metal oxides have gained significant attention not only due to their low cost and high abundance but also due to their suitable catalytic properties, structural stability and favorable redox chemistry. In particular, bimetallic oxide systems involving Ni, Co and Fe have demonstrated high performance for oxygen electrocatalysis in terms of both activity and stability [6]. For instance, spinel ferrites, denoted by the formula MFe_2O_4 (where M can be Ni^{2+}, Co^{2+}, or any other divalent metal), exhibit cubic, tightly-packed arrangements of oxygen atoms, with M^{2+} and Fe^{3+} ions occupying either tetrahedral or octahedral sites [7]. The coexistence of both M and Fe ions in these ferrites (MFe_2O_4) may facilitate a more diverse range of redox reactions compared to an individual metal oxide. These distinctive features distinguish them as promising candidates over the costly metals as OER electrocatalysts [8]. The bicontinuous microemulsion method is a simple and cost-effective method that offers high yield and control over particle size [9],

*Corresponding authors: J.L. Cholula jorgeluis.cholula@tec.mx, and D.M. Morales d.m.morales.hernandez@rug.nl

and can be effectively used to synthesize mixed metal oxides. Recently, Sanchez-Dominguez *et al*. reported the bicontinuous microemulsion method to synthesis Pt nanoparticles to be used as efficient electrocatalysts for the HER reaction [10]. Pt-Co_3O_4 nanomaterials were also synthesized by the same method, and used as OER electrocatalyst with promising results [3]. Alternatively, the hydrothermal method has been used for the preparation of bimetallic oxides, offering the advantages such as good control on composition, porosity, morphology, and particle size by adjusting autoclaving time, concentration, and temperature [11]. There are several reports on the synthesis of nanomaterials, simple oxides, complex oxides and heterostructures for various applications by hydrothermal method [12]. Recently, Muhammad *et al.*, synthesized active and stable RuO_2/MoO_3 bimetallic oxides by hydrothermal method for the oxygen evolution reaction [13].

Herein, we firstly followed the bicontinuous microemulsion approach to synthesize $CoFe_2O_4$ and $NiFe_2O_4$ and evaluated these materials towards the OER in alkaline media. In our ongoing work, we explore the hydrothermal synthesis method with the aim of comparing the performance of the resulting materials with those of the aforementioned method.

Methodology

In the first approach, $CoFe_2O_4$ and $NiFe_2O_4$ were prepared as nanoparticles (NPs) via a bicontinuous microemulsion method. Cobalt(II) 2-ethylhexanoate 65% ($C_{16}H_{30}CoO_4$), Nickel(II) 2-ethylhexanoate 78% ($C_{16}H_{30}NiO_4$), 2,2,4-trimethylpentane 99.5% (C_8H_{18}), tetramethylammonium hydroxide (TMAH) ≥97% ($C_4H_{13}NO$) and Synperonic^{TM} 91/5 ($C_{19}O_6H_{40}$) were used as starting materials. For the synthesis of $CoFe_2O_4$ NPs, a bicontinuous microemulsion containing water as an aqueous phase, 2,2,4-trimethylpentane as an oil phase and Synperonic as a surfactant, was prepared at a specific temperature. A second bicontinuous microemulsion was prepared with the same composition but TMAH was used as aqueous phase at a specific temperature. Once the microemulsions are formed, the TMAH containing microemulsion was added to the precursor containing microemulsion under constant magnetic stirring and pH was controlled between 11.5 and 12. The system was kept under constant stirring at the specific temperature for 24 h. A dark brown precipitation was achieved and the samples were washed vigorously and calcined for 5h at 600°C. The same procedure was followed to achieve the $NiFe_2O_4$ NPs.

Structural characterization by XRD was conducted using a PANalytical Empyrean diffractometer equipped with CuKα radiation operating in continuous scanning mode from 10 to 70^o of 2θ with a step size of 0.001°.

Electrochemical activity evaluation was done by using PalmSense4 potentiostat using a 3-electrode configuration electrochemical cell. The setup involved a Ag|AgCl|KCl (3 M) as reference electrode, a Pt wire as counter electrode, a catalyst-modified glassy carbon electrode (3 mm diameter) as a working electrode, and 1 M KOH solution as electrolyte. Linear sweep voltammetry was conducted at a scan rate of 5 mV/s in the potential range between 0 and 0.8 V vs Ag|AgCl. The measured current was normalized by the geometric area of the electrode and the measured potentials were converted to the reversible hydrogen electrode (RHE) scale according to equation 1.

$$E_{\text{meas,RHE}} = E_{\text{meas,Ag|AgCl}} + E_{\text{ref°,Ag|AgCl}} + 0.059(pH) \qquad (1)$$

The OER overpotential was calculated from the resulting voltammograms as the difference between the potential required to reach a current density of 10 mA cm^{-2} and the standard potential 1.23 V. Electrochemical impedance spectroscopy was conducted in the frequency

range from 10 to 10^5 Hz with a DC potential of 1.65 V vs RHE and an amplitude of 10 mV (RMS).
In the second approach, NiCOx mixed oxides were synthesized by hydrothermal method. Metal nitrates ($Ni(NO_3)_2.6H_2O$ and $Co(NO_3)_2.6H_2O$) were used with 1:1 and 1:2 molar ratios, and urea $CO(NH_2)_2$ was added as a crystallization agent. Structural and electrochemical characterization of the resulting materials is ongoing.

Discussion

Synthesis and characterization
In a first approach, two bimetallic oxides were strategically designed as electrocatalytic materials for the OER. Firstly, $CoFe_2O_4$ and $NiFe_2O_4$ were prepared as nanoparticles (NPs) using a bicontinuous microemulsion as nanoreactors. This method was strategically selected as it offers the advantages that (1) it is inexpensive, (2) offers good control over particle size and (3) gives high yield.
X-ray diffraction (XRD) was performed to determine the structural properties and phase purity of the prepared samples. The observed XRD peaks, as depicted in Fig 1(a), were indexed to the crystallographic planes (111), (220), (311), (400), (422), (511), and (440) of cubic $NiFe_2O_4$ (JCPDS#86-2267) and $CoFe_2O_4$ (JCPDS#22-1086), confirming that the samples consist of partially inverse spinel-type, pure phase structures. Further physicochemical characterization is ongoing, and will be valuable to observe the morphology, shape, electronic structure, surface area and elemental composition of the prepared ferrites samples, which can later be correlated to the catalytic properties of the samples.

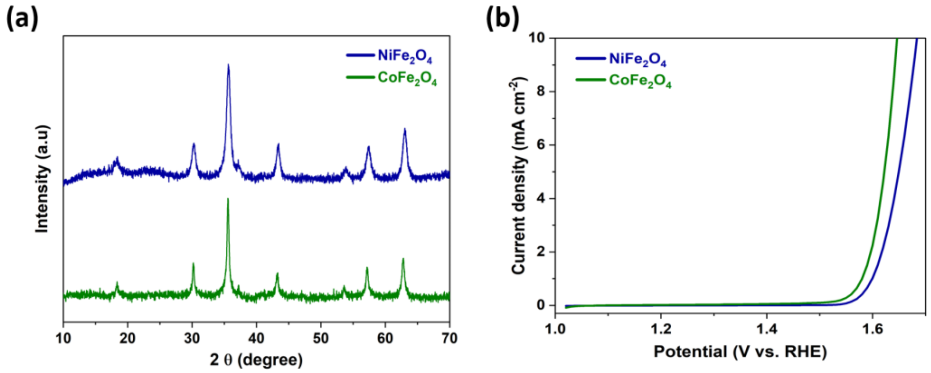

Figure 1: (a) XRD patterns and (b) LSV curves of MFe_2O_4 (M= Ni, Co) NPs.

Evaluation of the OER performance
The evaluation of the electrocatalytic performance of the samples towards the OER was carried out in a three-electrode configuration electrochemical cell using 1 M KOH aqueous solution as electrolyte. The activity of $CoFe_2O_4$ and $NiFe_2O_4$ was evaluated in terms of overpotential and current density by linear sweep voltammetry (Fig 1(b)). $CoFe_2O_4$ demonstrated relatively higher OER catalytic activity than $NiFe_2O_4$, requiring an overpotential of 410 mV to achieve a current density of 10 mA cm^{-2}, while $NiFe_2O_4$ exhibited an overpotential of 450 mV at the same current density. The superior performance of $CoFe_2O_4$ is ascribed to smaller particle size, higher electrochemically active surface area,

and lower charge transfer resistance according to electrochemical impedance spectroscopy analysis.

Conclusion

$CoFe_2O_4$ and $NiFe_2O_4$ nanoparticles were successfully synthesized via bicontinuous microemulsion method. XRD analysis was used to confirm the crystal structure, and electrochemical measurements were carried to test the OER performance of the ferrites NPs. Our investigation revealed the partially inverse spinel phase for both the prepared samples. In terms of OER activity, $CoFe_2O_4$ NPs showed a lower overportential (at a current density of 10 mA cm^{-2}) compared to its counterpart $NiFe_2O_4$. The bicontinuous method, can be used to synthesize a variety of metal oxides with different size, shape and morphology. We currently develop analogous materials with a different synthesis approach, and the physical and electrochemical characterization are work in progress that will involve their evaluation in terms of stability under industry-relevant conditions. Integrating our findings in these two synthesis approaches might provide opportunities to synthesize non-precious, active, and stable metal oxides as electrocatalysts for different applications including oxygen evolution reaction.

References

[1] "POWER-TO-HYDROGEN AND HYDROGEN-TO-X ENERGY SYSTEMS FOR THE INDUSTRY OF THE FUTURE IN EUROPE," doi: 10.1016/J.IJHYDENE.2023.01.194.

[2] "MINI REVIEW ON H_2 PRODUCTION FROM ELECTROCHEMICAL WATER SPLITTING ACCORDING TO SPECIAL NANOSTRUCTURED MORPHOLOGY OF ELECTROCATALYSTS", doi: 10.1016/J.FUEL.2021.122048.

[3] "Pt-Co_3O_4 SUPERSTRUCTURES BY ONE-POT REDUCTION/PRECIPITATION IN BICONTINUOUS MICROEMULSION FOR ELECTROCATALYTIC OXYGEN EVOLUTION REACTION", doi: 10.3390/CATAL10111311.

[4] "RECENT ADVANCES IN NON-PRECIOUS METAL-BASED ELECTRODES FOR ALKALINE WATER ELECTROLYSIS", doi: 10.1002/CNMA.202000010.

[5] "ENHANCING ELECTROCATALYTIC ACTIVITY THROUGH LIQUID-PHASE EXFOLIATION OF NIFE LAYERED DOUBLE HYDROXIDE INTERCALATED WITH METAL PHTHALOCYANINES IN THE PRESENCE OF GRAPHENE", doi: 10.1002/CPHC.201900577.

[6] "Fe/Co/Ni MIXED OXIDE NANOPARTICLES SUPPORTED ON OXIDIZED MULTI-WALLED CARBON NANOTUBES AS ELECTROCATALYSTS FOR THE OXYGEN REDUCTION AND THE OXYGEN EVOLUTION REACTIONS IN ALKALINE MEDIA", doi: 10.1016/j.cattod.2019.02.047

[7] "SUPERSPIN GLASS STATE IN $MnFe_2O_4$ NANOPARTICLES", doi: 10.1016/J.JMMM.2010.05.007.

[8] "HIERARCHICALLY POROUS $CoFe_2O_4$ NANOSHEETS SUPPORTED ON NI FOAM WITH EXCELLENT ELECTROCHEMICAL PROPERTIES FOR ASYMMETRIC SUPERCAPACITORS", doi: 10.1016/J.APSUSC.2017.04.067.

[9] "BICONTINUOUS MICROEMULSIONS FOR HIGH YIELD, WET SYNTHESIS OF ULTRAFINE NANOPARTICLES: A GENERAL APPROACH", doi: 10.1039/C5FD00004A.

[10] "FROM NANO TO MACRO: HIERARCHICAL PLATINUM SUPERSTRUCTURES SYNTHESIZED USING BICONTINUOUS MICROEMULSION FOR HYDROGEN EVOLUTION REACTION", doi: 10.1016/J.ELECTACTA.2020.136608.

[11] “METAL–FERRITE NANOCOMPOSITES FOR TARGETED DRUG DELIVERY”, doi: 10.1016/B978-0-12-813741-3.00032-7

[12] “HYDROTHERMAL SYNTHESIS OF NANOMATERIALS”, doi: 10.1155/2020/8917013

[13] “BOOSTED UP STABILITY AND ACTIVITY OF OXYGEN VACANCY ENRICHED RuO_2/MoO_3 MIXED OXIDE COMPOSITE FOR OXYGEN EVOLUTION REACTION”, doi: 10.1016/j.ijhydene.2020.04.101

Strategy or Improvisation? Uncovering the Determinants of Hydrogen Trade Partner Selection in Germany, the Netherlands, and Belgium

Marie Dejonghe*[1] and Tim Haesebrouck[1]

[1] Ghent Institute for International and European Studies (GIES), Ghent University

Introduction

Clean hydrogen is considered to be one of the key building blocks to achieve carbon neutrality by 2050. This ambition has prompted nations worldwide to formulate and publish national hydrogen strategies [1]. Notably, within these strategies, certain countries have positioned themselves as prospective hydrogen importers, exemplified by countries like Germany, Japan, Belgium, and the Netherlands, while others have positioned themselves as potential exporters, as exemplified by Morocco, Norway, Namibia, and Chile [2]. Against the backdrop of this burgeoning hydrogen trade landscape, numerous countries have embarked on what is commonly referred to as "hydrogen diplomacy." This diplomatic endeavor involves the launch of feasibility studies, the establishment of memorandums of understanding (MOUs), and the initiation of bilateral cooperation between future hydrogen trade partners [3].

Given the heightened awareness of energy commodity dependencies and associated vulnerabilities in the wake of the 2022 energy crisis, questions concerning how and whether countries at all should engage in bilateral hydrogen trade arise increasingly. To delve further into these questions, this study undertakes an in-depth assessment of the selection of future hydrogen trade partners in Belgium, Germany, and the Netherlands. At present, a considerable degree of heterogeneity exists among these countries regarding their respective hydrogen diplomacy. For instance, both the Netherlands and Germany have actively scrutinized agreements with more than ten prospective hydrogen trade partners, whereas Belgium has thus far explored collaboration with only five potential counterparts. Furthermore, differences manifest in terms of the types of agreements entered, encompassing feasibility studies, MOUs, or bilateral cooperative arrangements. Finally, variations are discernible concerning the selection of specific future hydrogen trade partners in terms of geography [2]–[4].

Considering these different dynamics, the primary objective of this study is to elucidate the determinants that affect the selection of future hydrogen trade partners in the aforementioned European countries. More specifically, we will build on Qualitative Comparative Analysis to uncover which conditions or guiding principles underpin the choices made regarding hydrogen trade partners and how they vary between the different countries. Insights derived from this research are anticipated to yield valuable insights and guidance in shaping national strategies and determining the evolving landscape of nascent hydrogen interdependencies.

* Corresponding author: marie.dejonghe@ugent.be

Methodology & research plan

Methodologically, our study will apply QCA, a configurational comparative method that allows to explain why an outcome (i.e. a hydrogen partnership) occurs in some cases, but not in others. In the present study, the cases are country dyads of the three selected import countries (Belgium, Germany, and the Netherlands) and potential export partners. We consider a country to be a potential export partner if it has concluded an agreement with at least one of the three import countries. Importer-exporter dyads that have concluded a hydrogen partnership are included as positive cases, i.e. cases in which the outcome is present; dyads the have not concluded a partnership are included as negative cases. With our analysis, we aim to uncover the (combinations of) conditions that consistently lead to the conclusion of a hydrogen partnership or to the absence of such a partnership in an importer-exporter dyad.

The first stage of our research will be the selection of potential explanatory conditions, among which the following seem particularly relevant:

- Bilateral trade flows importer-exporter dyad
- Official development aid from importer to potential exporter
- Development cooperation
- Agreements between importer and exporter during COP or other multilateral summits
- The involvement of national companies (e.g. the port of Antwerp, port of Rotterdam) of the importer country in the exporter country.

The second step of our study consists of the operationalization of our conditions and our outcome and the collection of the required data.

Finally, we analyze our data with QCA's analytical techniques, which build on truth tables and logical minimization. An important feature of QCA is that research is considered to be an iterative process, in which researchers regularly need to reconsider previous steps of their study based on information gained in later steps. So, if we do not find a consistent pattern in our data, we will reconsider the case selection, the selection of the explanatory conditions, and the operationalization of these conditions and our outcome. After several rounds of going back-and-forth between the initial theoretical expectations and the empirical data, QCA can be expected to allow to identify the combinations of conditions that explain the pattern of hydrogen partnerships. If no consistent pattern is uncovered, this might suggest that the pattern of hydrogen partnerships is the result of improvisation rather than of a clear strategy, a conjecture that we can further test with elite-interviews and process tracing.

Conclusions

Given the early stage of this research, there ae no conclusions yet in this paper.

References

[1] World Energy Council, “National Hydrogen Strategies,” 2021. Accessed: Jan. 24, 2023. [Online]. Available: https://www.worldenergy.org/assets/downloads/Working_Paper_-_National_Hydrogen_Strategies_-_September_2021.pdf

[2] IRENA, *Geopolitics of the energy transformation: the hydrogen factor*. 2022. [Online]. Available: https://www.irena.org/-/media/Files/IRENA/Agency/Publication/2022/Jan/IRENA_Geopolitics_Hydrogen_2022.pdf

[3] M. Dejonghe, “Seeking Reliable Partners: Assessing Hydrogen Partnerships Established by EU Member States,” *Sustainability* , under review.

[4] IRENA, *GLOBAL HYDROGEN TRADE TO MEET THE 1.5°C CLIMATE GOAL PART I TRADE OUTLOOK FOR 2050 AND WAY FORWARD*. 2022. [Online]. Available: www.irena.org/publications

Study of up-to-date hydrogen production costs and the effect of key parameter variations

J. Walton*[1], R. Steinberger-Wilckens[1]

[1]University of Birmingham, Birmingham, United Kingdom

Introduction

The worldwide effort to mitigate climate change has seen a growing number of companies, institutions and countries set net zero emissions targets for the mid-term future [1]. Yet thorough decarbonisation presents a great challenge, with global energy-related CO_2 emissions reaching a record high of 36.8 Gt in 2022 [2]. A major problem is that of energy storage, which is conventionally provided in the form of fossil fuels and critical to balance supply with demand. Hydrogen could form part of the solution, being a versatile fuel that is essentially clean at the point of use.

Ironically, the majority of hydrogen consumed at present is still 'grey', having been produced from natural gas without carbon capture and thus responsible for considerable greenhouse gas releases [3]. Even 'blue' hydrogen, the result of adding carbon utilisation and storage (CCUS), cannot achieve zero emissions. Ideally, hydrogen should be 'green', for which water electrolysis using renewable electricity is the most common production method.

Hydrogen with improved climate credentials is often linked with a higher internal cost. In the literature, green hydrogen is generally considered to be more expensive to produce than both grey and blue hydrogen at present, albeit with the possibility of becoming a cheaper option in the perhaps not-so-distant future [4-6]. However, high natural gas prices over the past two years suggest that green hydrogen may already be competitive, while the associated volatility of global natural gas prices implies that grey and blue hydrogen production costs should be given in terms of the natural gas price on which they are based. The latter will depend upon the nature in which natural gas is purchased, whether it is predominantly through long term contracts, the spot or futures market, or a supply owned by the hydrogen producer.

Methodology

The objective of this work is to investigate up-to-date hydrogen production costs and their sensitivity to key parameters, with a focus on the United Kingdom. To this end, a cost model is being developed to calculate the levelised cost of hydrogen (LCOH) for different production methods, where the LCOH can be defined as the total lifetime cost per unit of hydrogen supplied [7], to be adjusted to allow for profit. The sensitivity of the LCOH to different parameters can then be analysed by adjusting the value of the corresponding model input. Key considerations include the effect of natural gas price and carbon cost on the LCOH for grey and blue hydrogen; electricity price, operating strategy, and the cost and efficiency of electrolysers on the LCOH for green hydrogen; as well as the additional cost of CCUS for blue hydrogen, which will depend upon the project location and technology of carbon capture. Relative changes predicted by the model will be compared to those observed in the markets during past years, where possible.

* Corresponding author: jjw692@student.bham.ac.uk

Discussion

It can be shown that green hydrogen produced from recent renewable energy projects is competitive with grey and blue hydrogen under conditions of high feedstock cost. Notoriously volatile natural gas prices therefore link grey hydrogen with future commercial risk, making green hydrogen even more attractive. The reliance of blue hydrogen upon CCUS adds cost and exacerbates the risks already inherent in grey hydrogen.

Conclusions

Green hydrogen has the potential to play an important role in a low carbon future. Thus far, uptake has been limited by production costs that are higher than those of other 'colours' of hydrogen, but recent events suggest that green hydrogen can be immediately competitive, depending on natural gas market developments. In response, this work will present an up-to-date estimate of the LCOH for different production methods, including its sensitivity to key parameters. This will contribute towards the direction of future work and help identify the commercial prospects for green hydrogen deployment.

This work is supported by the Engineering and Physical Sciences Research Council (via the Sustainable Hydrogen Centre for Doctoral Training and University of Birmingham, School of Chemical Engineering).

References

[1] J. Rogelj, O. Geden, A. Cowie, and A. Reisinger, "Net-zero emissions targets are vague: three ways to fix," *Nature*, 591 (2021) 365-368, doi: 10.1038/d41586-021-00662-3.

[2] IEA, "CO2 Emissions in 2022," *International Energy Agency*, Paris, 2023. Available: https://www.iea.org/reports/co2-emissions-in-2022 [Accessed Sept. 12, 2023].

[3] IEA, "Global Hydrogen Review 2022," *International Energy Agency*, Paris, 2022. Available: https://www.iea.org/reports/global-hydrogen-review-2022 [Accessed Sept. 12, 2023].

[4] M. Newborough and G. Cooley, "Developments in the global hydrogen market: The spectrum of hydrogen colours," *Fuel Cells Bulletin*, 11 (2020) 16-22, doi: 10.1016/S1464-2859(20)30546-0.

[5] A. Ajanovic, M. Sayer, and R. Haas, "The economics and the environmental benignity of different colors of hydrogen," *International Journal of Hydrogen Energy*, 47 (2022) 24136-24154, doi: 10.1016/j.ijhydene.2022.02.094.

[6] T. Longden, F.J. Beck, F. Jotzo, R. Andrews, and M. Prasad, "'Clean' hydrogen? – Comparing the emissions and costs of fossil fuel versus renewable electricity based hydrogen," *Applied Energy*, 306 (2022) 118145, doi: 10.1016/j.apenergy.2021.118145.

[7] Q.V. Dinh, V.N. Dinh, H. Mosadeghi, P.H. Todesco Pereira, and P.G. Leahy, "A geospatial method for estimating the levelised cost of hydrogen production from offshore wind," *International Journal of Hydrogen Energy*, 48 (2023) 15000-15013, doi: 10.1016/j.ijhydene.2023.01.016.

Sub-national hydrogen policy-making in multi-level systems: The case of hydrogen in Germany

L. Flath*[1]

[1]Technical University Darmstadt, Institute of Political Science

Introduction

The subnational level represents an important but still underexplored setting for the analysis of hydrogen policies. Hydrogen market development is likely to emerge from local and regional clusters, where initial demand corresponds with supply without the need for extensive transport infrastructure. The transition to a hydrogen economy offers regional entities an opportunity for economic development and encourages the introduction of regional policies to propel the shift towards a hydrogen economy. While regions can become catalysts for innovation, different regional interests might lead to divergent and, perhaps, contradictory hydrogen policies [1]. This paper takes up on that and examines: a) which determinants lead to different hydrogen strategic goals at the sub-national level, and b) whether such differences lead to incoherent policies. The study focuses on Germany, which can be considered a crucial case, as it is, on one hand, a frontrunner in hydrogen policy and, on the other hand, a federal country in which all the states (Länder) pursue their own hydrogen strategies. The analytical framework to explain subnational hydrogen policy-making is composed of classical policy research theories (partisan theory and institutionalism), but it also specifically includes the role of the multi-level system and how interdependencies between levels are addressed. With reference to multi-level governance theory, the paper concludes by discussing the extent to which effective multi-level hydrogen governance for a coherent policy framework could be conceptualized.

Methodology

The paper follows a qualitative approach in analyzing the hydrogen strategies and policies of the 16 states. First, all hydrogen strategy and policy documents are identified based on research in official journals and press releases databases. Then, the documents are categorized by their targets and policy types, which are used to assess their overall coherence or fragmentation. Data for the explanation is partly based on publicly available information (e.g., partisan affiliation of responsible persons, institutional setting, socioeconomic structure) as well as on interviews. The interviews were conducted with representatives of the sub-national governments responsible for hydrogen, primarily to gather information about the multi-level processes related to hydrogen and to validate the assessment of strategies and policies. Based on the gathered information, a comparative case study is conducted to evaluate which factors determine hydrogen strategies and policies at the sub-national level.

Discussion

To be conducted.

* Corresponding author: flath@pg.tu-darmstadt.de

References

[1] Ekins, P. and Hughes, N. (2010) 'The prospects for a hydrogen economy (2): hydrogen transitions', Technology Analysis & Strategic Management, 22(1), pp. 1–17. doi: 10.1080/09537320903438013.

Support Mechanisms for Hydrogen: Interactions and Distortions of Different Instruments

Alexander Hoogsteyn[1,2], Kenneth Bruninx[3,1], Jelle Meus[1,2], Erik Delarue *[1,2]

[1]KU leuven, Division of Applied Mechanics and Energy Conversion, Belgium
[2]Energyville, Belgium
[3]Delft University of Technology, Faculty of Technology, Policy, and Management, The Netherlands

Introduction

Hydrogen and further derived molecules generated through electrolysis can serve as energy carriers in a climate-neutral society. Such CO_2 neutral molecules can make a remarkable contribution to the climate neutrality of the material and chemical industry by the middle of this century. They allow emission-free production of fertilisers and steel, facilitate innovative processes in the chemical industry and may be the basis of sustainable synthetic fuels for shipping and aviation.

Many governments have announced ambitious hydrogen strategies, and therefore want to accelerate the deployment of renewable production and end-use applications. Since the zero-carbon hydrogen production technologies are not yet competitive with the traditional hydrogen production route, governments wish to support the needed technologies to produce hydrogen sustainably and enable a carbon-neutral industry.

Some academic literature exists on the effects of hydrogen subsidy mechanisms [7] and the possible interactions it may cause with existing climate policy, such as carbon prices [6]. Little research dedicated to the design of hydrogen subsidy mechanisms currently exists. However, it is known from previous research that has studied the implementation of subsidy mechanisms for renewable electricity generation that such interventions in energy markets may lead to distortions in the dispatch of generation assets [4, 8] and distortions in technology choice [9, 3, 5].

To investigate the impact of hydrogen subsidy mechanisms on energy markets and cap-and-trade systems, we extend the state-of-the-art long-term equilibrium model that captures the interactions between hydrogen, electricity and emission markets developed by [2] which can be used to simulate the effect of different hydrogen support mechanisms. We compare capacity-based subsidy mechanisms (EUR/MW) with three quantity-based mechanisms (EUR/MWh): A tradable certificate system (QT), a fixed-premium (FP) and hydrogen contract for difference (CfD).

Methodology

To address our research questions we will employ an equilibrium model presented as a mixed complementary problem. The model comprises three different markets:

- An electricity market in which investors in gas-fired generation, wind, solar, and nuclear compete and optimize their operation considering the variable generation of renewables and demand for electricity.
- A hydrogen market in which investors in different renewable hydrogen production technologies compete with each other and with the traditional steam methane reforming (SMR) technology. Two electrolysis technologies are considered, i.e., a highly efficient (low OPEX, high CAPEX) and low efficient variant (high OPEX, low CAPEX), as well as SMR with carbon capture and storage (CCS) and hydrogen import.
- A cap-and-trade system for CO_2 emissions in which the fossil-based electricity actors compete with SMR technology and a competitive fringe. The fringe has to decide to buy emission permits or bear the abatement cost, which is modelled as a quadratically increasing function of abatement. This actor represents the remainder of the industrial demand for emission allowances. Emission permits are bankable between all compliance years 2020-2050 and borrowing is prohibited.

*Corresponding author: erik.delarue@kuleuven.be

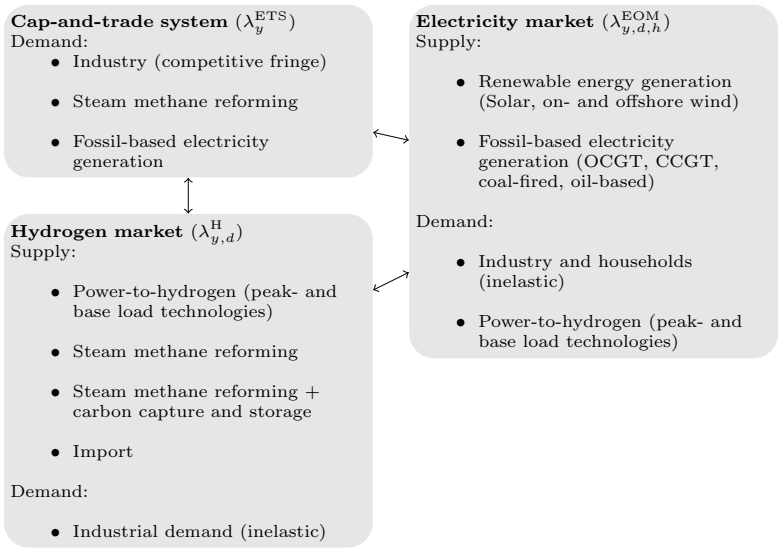

Figure 1: Block diagram model

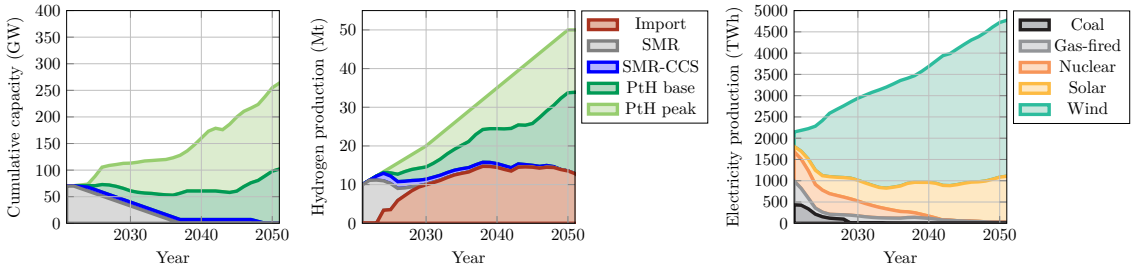

Figure 2: Hydrogen production, hydrogen production capacity investments and source of electricity production in the reference case

We solve the equilibrium model using the distributed Alternating Direction Method of Multipliers (ADMM) [1] which links the different markets: electricity, emissions and hydrogen through a set of coupling constraints in which the actions of the different actors are combined to find the equilibrium prices. As such, the interactions between the different markets can be studied. An overview of the actors in these markets and the interactions between them is provided in Figure 1. We conduct a case study using a power system inspired by the European system, recent electrolyser cost estimates, and a cap-and-trade system that is inspired by EU-ETS. The cap-and-trade model is implemented following [2] without considering the Market Stability Reserve.

Results

In Figure 2 the results of the multi-year equilibrium model are given in the reference case, which does not consider any hydrogen support mechanisms. In the hydrogen sector, no new investments in SMR occur and SMR-based hydrogen production is gradually phased out in favor of import and electrolytic hydrogen. By 2030 8.6 Mt is produced by PtH out of the 10 Mt domestic hydrogen production. SMR equipped with CCS contributes 1.3 Mt in 2030. We observe that, similarly to power systems, an optimal mix of low-CAPEX high-efficient and high-CAPEX low-efficient PtH techologies arises. In the power sector, 2416 TWh is supplied by solar and wind, and 522 TWh by non-renewable generation in 2030.

In Figure 3 a load duration curve of the hydrogen production is shown, which shows the dispatch of the peak and base PtH technology. Each value represents one hour and they are sorted from high to low profit margin. Their profit margin (i.e. operation profit) is given by the difference between the hydrogen and electricity prices during that hour, considering the efficiency of the considered technology variant. It can be observed that technologies are fully dispatched when it is economical. During the hours that the technologies are partially dispatched, they are price-setting in the electricity market. This can be seen by

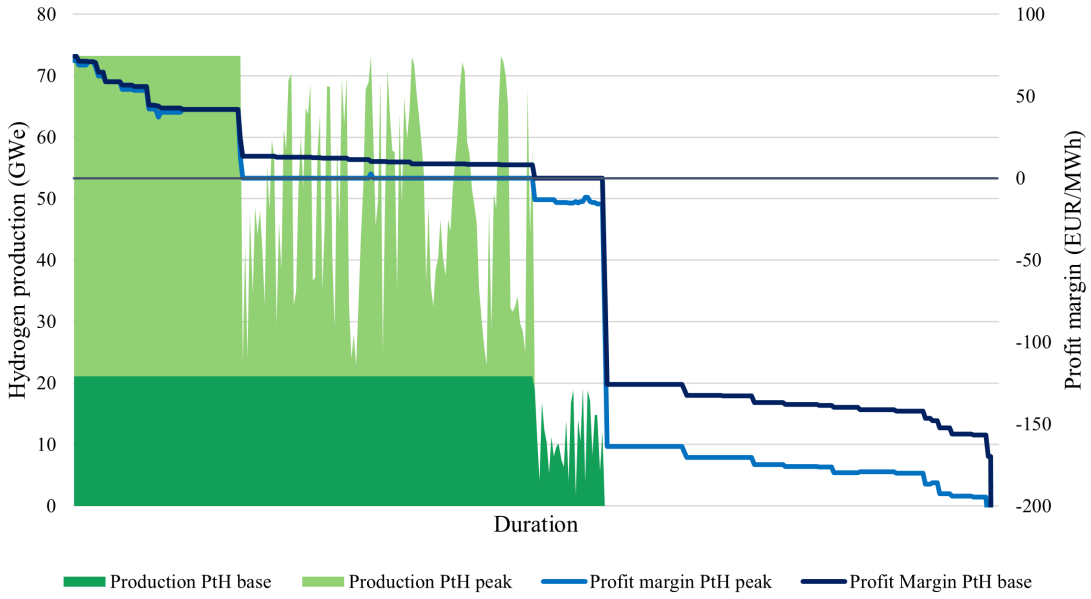

Figure 3: Hydrogen production duration curve of the hydrogen sector that shows the dispatch of the peak and base PtH technology as well as their profit margin.

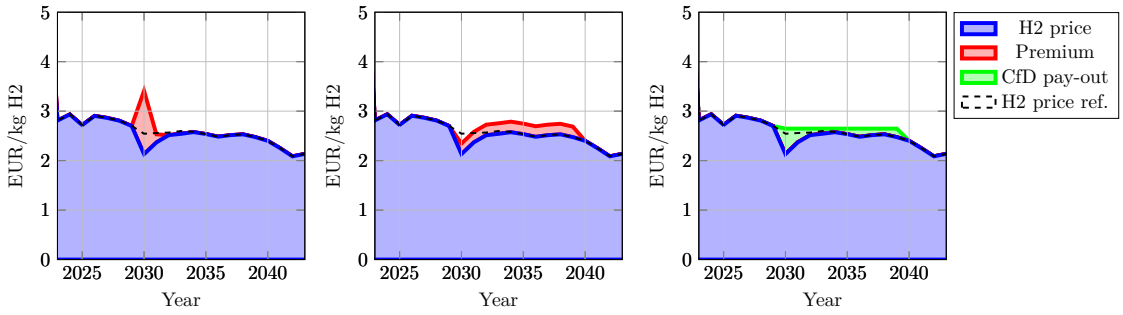

(a) Quantity target (b) Fixed premium (c) H2 CfD

Figure 4: Hydrogen market revenue and policy subsidy in the case of (a) a quantity target attained through a tradable certificate system, (b) an auctioned fixed premium and (c) an auctioned hydrogen contract for difference; that achieve 10 Mt electrolytic hydrogen target

the fact that they have a zero profit margin during these hours. This occurs during a significant number of operating hours.

In Figure 4 it is visualised how such multi-year instruments are different from a quantity target attained through a tradable certificate system (QT), and what the difference is between a FP and CfD. In the case of a quantity target the premium is determined each year such that the 10 Mt target is met in every year from 2030 onwards. Therefore, support is concentrated in the years when total hydrogen demand is low and the target is therefore strict. In the case of a FP the support is divided uniform over the duration of the contract.

In Figure 5, four different policies are shown that all achieve 10 Mt of electrolytic hydrogen production. While the capacity target produces the imposed 10 Mt of electrolytic hydrogen from the peak and base load technology at roughly the same proportion as the quantity target, it does install more peak capacity than the quantity target. This indicates that this policy has a selection bias towards the cheaper peak unit, which was expected.

In Figure 6, the impact on the power system is shown. In the left figure, the changes in production source are shown compared to the reference scenario without a target. Reaching the 10 Mt target of electrolytic hydrogen requires an additional 72 TWh electricity in case of a capacity target, 59 TWh in case of a quantity target, 62 TWh in case of a FP or CfD; these differences can be explained by the choice

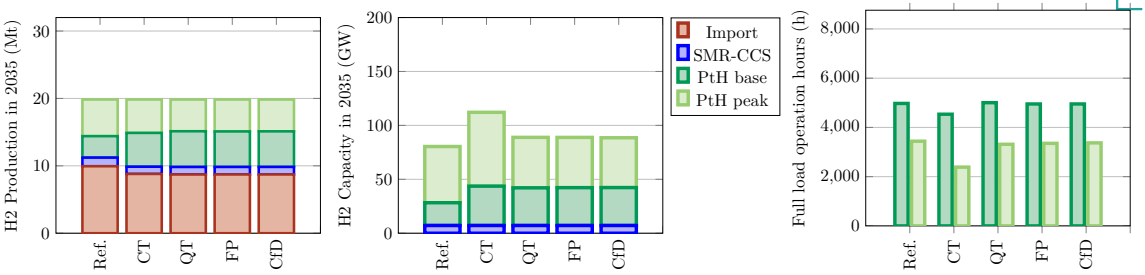

Figure 5: Impact of capacity target (CT), quantity targets (QT), fixed premium (FP) and hydrogen contract for difference (CfD) on hydrogen production and capacity investment in the hydrogen sector.

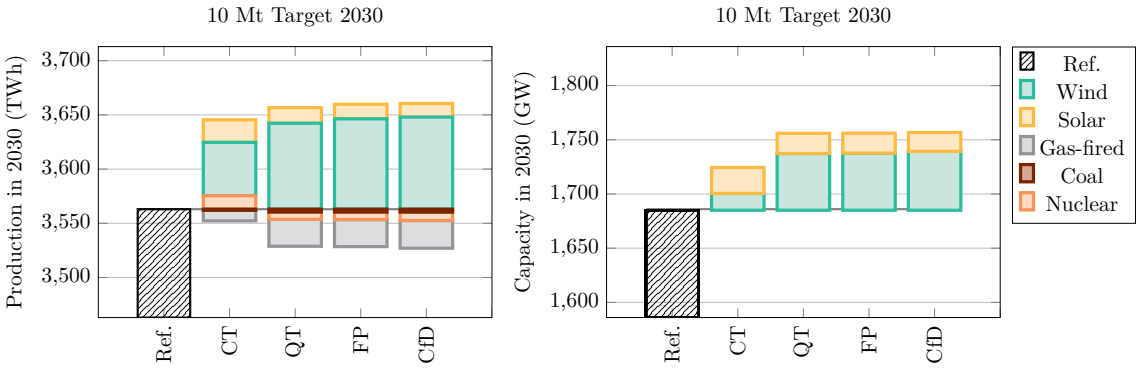

Figure 6: Impact of capacity target (CT), quantity targets (QT), fixed premium (FP) and hydrogen contract for difference (CfD) on electricity production and capacity investment in the power sector, compared to no target

of the peak PtH technology which has a lower efficiency and hence increases electricity demand. In the right figure, the changes in investment decisions are shown. Here it can be seen that a capacity target can obtain 10 Mt of electrolytic hydrogen with less renewables than the quantity target, which can be explained by less curtailment that occurs because electricity can be consumed by producing hydrogen. It can be observed that the PtH targets decrease production of gas-fired generation, this can be explained by the increased attractiveness of renewables when dispatchable load PtH is added to the system. The effect is more prominent for quantity targets than for capacity targets, due to the fact that a QT requires more installed capacity in renewables, which leads to more renewable electricity generation during peak hours, when PtH do not operate.

Discussion

Economic justifications for hydrogen subsidization go beyond climate damages and can be grounded in learning effects and the inability of risk averse investors to transfer their risk to parties that can take on the risk efficiently. Hydrogen markets in particular are still nascent and limited hedging possibilities exist. They typically take either the form of a capacity-based payment (EUR/MW) or quantity-based (EUR/MWh), examples of both approaches exist although there seems to be a trend towards quantity-based mechanism. The two most prominent mechanisms to date, the US Inflation Reduction Act and the EU hydrogen bank, employ quantity-based hydrogen support.

When comparing the mechanisms for their impact on energy markets, we did not find strong distortions to the operational decisions of the actors involved. It became apparent that achieving the 10 Mt target through a CT, requires less investment into renewables, since the higher peak PtH capacity allows the PtH facilities to capture more renewable energy and curtail less. All subsidy mechanisms tend to decrease fossil-based electricity generation because investment into renewables becomes more attractive when more dispatchable load is added to the system.

Conclusion

To conclude, we investigated the impact of hydrogen subsidy mechanisms on energy markets and cap-and-trade systems using a long-term equilibrium model that captures the interactions between hydrogen, electricity and emission markets. We compare capacity-based subsidy mechanisms with three quantity-based mechanisms: a tradable certificate system (QT), a fixed-premium (FP) and a hydrogen contract for difference (CfD). We observed that the choice of the mechanism has implications on the renewable capacity and displacement of gas-fired generation in the power sector.

In the full paper, we will focus on system costs as well as a metric to compare the different subsidy mechanisms. We suspect FP and CfD to offer better risk mitigation than a QT, to study that we plan to look into modelling under uncertainty.

References

[1] S. Boyd. Distributed Optimization and Statistical Learning via the Alternating Direction Method of Multipliers. *Foundations and Trends® in Machine Learning*, 3(1):1–122, 2010.

[2] K. Bruninx, M. Ovaere, and E. Delarue. The long-term impact of the market stability reserve on the EU emission trading system. *Energy Economics*, 89:104746, June 2020.

[3] N. May. The impact of wind power support schemes on technology choices. *Energy Economics*, 65:343–354, June 2017.

[4] J. Meus, S. De Vits, N. S'heeren, E. Delarue, and S. Proost. Renewable electricity support in perfect markets: Economic incentives under diverse subsidy instruments. *Energy Economics*, 94:105066, Feb. 2021.

[5] M. Pahle, W.-P. Schill, C. Gambardella, and O. Tietjen. Renewable Energy Support, Negative Prices, and Real-time Pricing. *The Energy Journal*, 37(01), Sept. 2016.

[6] M. Roach and L. Meeus. An energy system model to study the impact of combining carbon pricing with direct support for renewable gases. *Ecological Economics*, 210:107855, Aug. 2023.

[7] D. Schlund and M. Schönfisch. Analysing the impact of a renewable hydrogen quota on the European electricity and natural gas markets. *Applied Energy*, 304:117666, Dec. 2021.

[8] J. Schmidt, G. Lehecka, V. Gass, and E. Schmid. Where the wind blows: Assessing the effect of fixed and premium based feed-in tariffs on the spatial diversification of wind turbines. *Energy Economics*, 40:269–276, Nov. 2013.

[9] J. Winkler, A. Gaio, B. Pfluger, and M. Ragwitz. Impact of renewables on electricity markets – Do support schemes matter? *Energy Policy*, 93:157–167, June 2016.

Sustainable H_2 Production in Biorefineries: Coupling Steam Reforming and CO_2 Capture for Zero Emissions

A. Vega*[,1], F. Rubiera[1], C. Pevida[1], M.V. Gil[1]

[1]Instituto de Ciencia y Tecnología del Carbono (INCAR), CSIC. Francisco Pintado Fe 26, 33011 Oviedo, Spain

Introduction

A sustainable energy system is key in a society where the energy supply must be guaranteed. The environmental benefit associated with hydrogen relies on its production from renewable sources such as water and biomass [1]. The multiple possibilities for converting biomass into biofuels and energy carriers have driven the development of biorefineries, where hydrogen is essential for the conversion of synthesis gas, bio-oils or biogas into liquid biofuels.

The search for new pathways to hydrogen production has recently gained increasing attention towards the sorption-enhanced steam reforming (SESR) process. The fundamental principle of this technology is the multifunctional reactor, in which the reforming, water-gas shift and CO_2 removal reactions are integrated in a single step over a mixture of reforming catalyst and CO_2 acceptor. Hydrogen yield and purity are expected to improve by shifting the thermodynamic equilibrium toward hydrogen production through in situ CO_2 removal. One of the notable advantages of SESR technology over other hydrogen production processes is its great flexibility with respect to the feedstock used. The inlet biomass can be in the gas phase (e.g., biogas from anaerobic digestion of organic waste or syngas from biorefineries), liquid (bioethanol) and solid (raw lignocellulosic waste).

This work studies hydrogen production by catalytic steam reforming with integrated CO_2 capture (sorption-enhanced steam reforming, SESR) of gas streams produced inside a biorefinery. The effect of syngas composition on biohydrogen production has been evaluated using different gas mixtures (H_2/CO/CH_4/CO_2) representative of those commonly encountered in the outlet gas streams from thermochemical biomass conversion processes.

Methodology

The experiments were conducted in a Microactivity Reference equipment (PID Eng&Tech) using a fluidized bed reactor. A simulated syngas stream with a composition of 30 vol.% H_2, 30 vol.% CH_4, and CO concentrations ranging from 10 to 40 vol.% (balanced with CO_2) was the feedstock. To carry out the SESR experiments, a bed of Arctic dolomite (purity of 98.5% of $CaMg(CO_3)_2$) as a CO_2 sorbent blended with a hydrotalcite-derived catalyst (composition 1%Pd/20%Ni-20%Co) was used [2]. SESR experiments, which involve the steam reforming reaction with integrated CO_2 capture, have three stages commonly referred to as pre-breakthrough, breakthrough, and post-breakthrough. During the pre-breakthrough stage, the sorbent has the ability to capture the CO_2 produced from the reforming and WGS reactions, shifting the equilibrium of the reactions toward the product side. This stage is characterized by a high concentration of H_2 and low concentrations of other gases (CH_4, CO, and CO_2). However, when the sorbent becomes saturated, the CO_2 concentration starts increasing at the same time as the H_2 concentration decreases (breakthrough). Once the sorbent no longer captures more CO_2, a new steady state is established, corresponding to the

* Corresponding author: alejandra.vega@incar.csic.es

reforming and WGS reactions (post-breakthrough). At this stage, conventional steam reforming (SR) process occurs. In the present work, the post-breakthrough stage was allowed to study the SR process for comparison. The steam reforming (SR) process is similar to SESR but without integrated CO_2 capture.

Discussion

Gas mixtures typically produced from the thermochemical conversion of biomass in refineries contain varying amounts of CO [3]. Therefore, this work focuses on addressing the effect of different CO compositions on the performance of the SESR process. The objective is to evaluate the production of H_2 with variable CO concentrations in the inlet syngas stream. The results obtained from the SESR process show that the yield and purity of H_2 (Figure 1) remain constant regardless of the CO concentration. Moreover, the H_2 purity values are very close to those predicted by thermodynamic equilibrium. It indicates that the sorbent removes all CO_2 in the syngas from the gas phase, favoring the syngas conversion for the different CO concentrations studied, and shows the versatility of the process for hydrogen production from syngas.

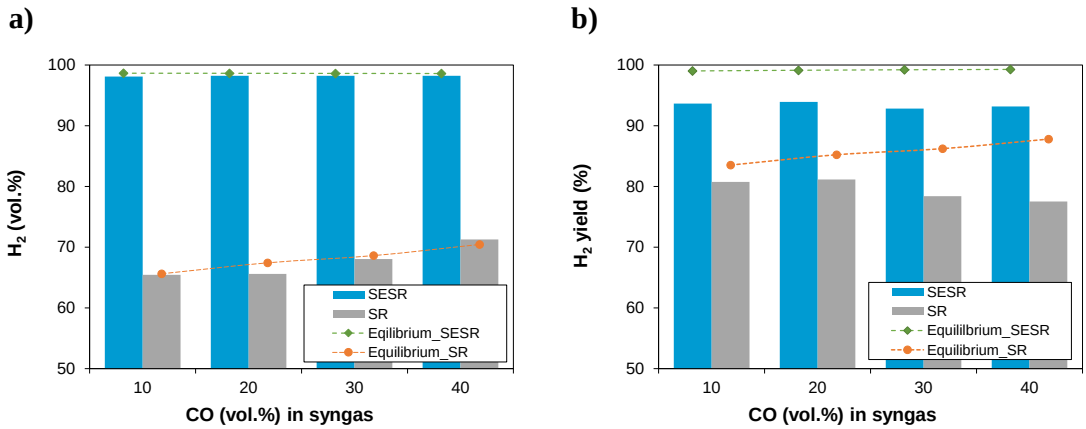

Figure 1: Effect of CO concentrations in syngas on the H_2 purity (a) and H_2 yield (b) from the SESR process. Conditions: T= 600 °C; space velocity= 2.4 L(CO+CH_4)/h g_{cat}; sorbent/catalyst = 20 g/g; syngas = 30H_2/30CH_4 %vol (CO_2 balance) with varying concentrations of CO.

The chemical reactions involved in the SESR process are the steam reforming of a biorefinery by-product, such as syngas (here represented as $C_nH_mO_k$), (Eq. (1)) and the water gas shift (WGS) reaction (Eq. (2)).

$$C_nH_mO_k + (n-k)H_2O \leftrightarrow nCO + \left(n + \frac{m}{2} - k\right)H_2 \quad (1)$$

$$CO + H_2O \leftrightarrow CO_2 + H_2 \quad (2)$$

These reactions are reversible, meaning that they are limited by thermodynamic equilibrium. Thus, removing of one of the products from the reaction medium shifts the chemical equilibrium to the product side, following Le Chatelier's principle. During the SESR process, CO_2 can be retained using solid sorbents, achieving this effect even at high temperatures. For this purpose, sorbents based on calcium oxides are mainly used in sorption enhanced processes, as they are able to remove CO_2 from the reaction medium through the carbonation reaction (Eq. (3)), generating $CaCO_3$. This reaction is also reversible so that

once exhausted, the sorbent can be regenerated by the calcination reaction, releasing the previously retained CO_2.

$$CaO + CO_2 \leftrightarrow CaCO_3 \quad (3)$$

In the case of the conventional reforming SR process without CO_2 capture, the purity of H_2 increases with the CO concentration in the syngas due to the decrease in CO_2 concentration. It favors the water gas shift and reforming reactions (1-2).

Conclusions

The sorption-enhanced steam reforming process is considered as an efficient alternative route for producing renewable H_2 from biomass. Diverse biomass-derived compounds have been promisingly demonstrated to produce high-purity and high-yield hydrogen. SESR of biomass-derived compounds compared to conventional reforming becomes highly attractive for biomass conversion to fuels due to advantages such as the simplicity of the process, flexibility in feedstock, high hydrogen yield, purity and energy efficiency and low cost.

When studying the performance of the SESR process with varying CO contents in the feed syngas, the purity and yield of H_2 remain constant for the evaluated range of CO concentrations because the CO_2 capture takes place during SESR, which means that all added CO_2 (regardless of its concentration) is removed by the sorbent. Therefore, H_2 yield and purity are increased compared to the conventional SR process. In addition to the increased H_2 purity and yield values, the SESR process brings an environmental benefit by reducing CO_2 emissions to the atmosphere.

These results demonstrate the flexibility of the sorption-enhanced steam reforming process, which allows the conversion of syngas with different compositions produced from a wide range of biomass conversion processes. Therefore, the SESR process can be considered a promising technology for in-situ hydrogen production within biorefineries.

Acknowledgments

This work was carried out with financial support from the Spanish MICINN through Grant PID2020-119539RB-I00, funded by MCIN/ AEI /10.13039/501100011033, and from the Gobierno del Principado de Asturias (PCTI, Ref. IDI/2021/000060). A. Vega acknowledges a fellowship awarded by the Spanish MICINN FPI program through Grant PRE2021-098782, funded by MCIN/AEI/ 10.13039/501100011033 and by "ESF Investing in your future". M.V. Gil acknowledges support from the Spanish AEI through the Ramón y Cajal Grant RYC-2017-21937 funded by MCIN/AEI/ 10.13039/501100011033 and by "ESF Investing in your future".

References

[1] J. Fermoso, L. He, and D. Chen, "SORPTION ENHANCED STEAM REFORMING (SESR): A DIRECT ROUTE TOWARDS EFFICIENT HYDROGEN PRODUCTION FROM BIOMASS-DERIVED COMPOUNDS," *Journal of Chemical Technology and Biotechnology*, vol. 87, no. 10. pp. 1367–1374, 2012. doi: 10.1002/jctb.3857.

[2] J. Fermoso, M. V. Gil, F. Rubiera, and D. Chen, "MULTIFUNCTIONAL PD/NI-CO CATALYST FOR HYDROGEN PRODUCTION BY CHEMICAL LOOPING COUPLED WITH STEAM REFORMING OF ACETIC ACID," *ChemSusChem*, vol. 7, no. 11, pp. 3063–3077, Nov. 2014, doi: 10.1002/cssc.201402675.

[3] L. He and D. Chen, "SINGLE-STAGE PRODUCTION OF HIGHLY CONCENTRATED HYDROGEN FROM BIOMASS-DERIVED SYNGAS," *ChemSusChem*, vol. 3, no. 10, pp. 1169–1171, 2010, doi: 10.1002/cssc.201000167.

Synergies between Direct Air Capture and Solar Hydrogen and Fuel Production

Enric Prats-Salvado[*1,2], Nathalie Monnerie[1], Christian Sattler[1,2]

[1]German Aerospace Center (DLR), Institute of Future Fuels, Linder Höhe, Cologne, Germany
[2] RWTH Aachen University, Chair for Solar Fuel Production, Templergraben 55, Aachen, Germany

Introduction

Climate change could increase the average temperature on Earth by 2.7 °C by 2100 if left unaddressed, with devastating effects on virtually all of Earth's ecosystems [1, 2]. To address one of the greatest challenges currently facing humanity, a technological leap is needed to phase out the burning of fossil fuels, which are responsible for the majority of greenhouse gas emissions [3, 4]. In this work, we explore two of the most important technologies that can drive the energy transition: direct air capture of CO_2 and solar thermochemical cycles.

Direct air capture of CO_2 (DAC) has gained interest because of its ability to remove diluted carbon dioxide from the atmosphere. The CO_2 captured can either be stored or used as feedstock for the so-called "carbon capture and utilization" (or CCU) industry [5]. DAC is expensive compared to other carbon dioxide sources, but it has no apparent biophysical limits (present with biogenic sources) and can produce carbon-neutral CO_2 when powered with the appropriate energy (as opposed to point source carbon capture) [6–8].

Solar thermochemical cycles aim to produce fuels such as hydrogen directly from heat. This capability contrasts with commercial approaches to hydrogen production that rely on electricity, and results in a potentially higher overall efficiency [9, 10]. Another advantage of solar thermochemical cycles is the ability to produce hydrogen and carbon monoxide simultaneously from water and carbon dioxide [11, 12]. The mixture of hydrogen and carbon monoxide is often referred to as synthesis gas and is an excellent feedstock for the production of liquid fuels such as methanol or kerosene [13, 14].

Considering the characteristics of these two technologies, it seems logical to aim for integrated operation of DAC in a solar fuel plant in the near future. However, most research in this area has focused on improving the technology readiness of each technology separately. This work attempts to fill this knowledge gap by identifying and evaluating the synergies between DAC and solar fuel production.

Methodology

There are several types of solar thermochemical cycles, but in this study, we focus on a technology called redox cycles, in which a metal oxide (e.g., cerium dioxide) is reduced at high temperature to create oxygen vacancies in its lattice. The metal oxide is then re-oxidized at a lower temperature by water vapor or carbon dioxide to produce hydrogen or carbon monoxide, respectively. Once this second step is complete, the cycle begins again without any loss of metal oxide [15, 16].

[*] Corresponding author: enric.pratssalvado@dlr.de

Currently, there is a broad portfolio of DAC technologies, but only two are considered in this study: liquid and solid DAC (often referred to as L-DAC and S-DAC, respectively). L-DAC uses a liquid solvent that reacts with atmospheric CO_2 and requires elevated temperatures for regeneration, while S-DAC uses a solid sorbent that binds with carbon dioxide molecules and can be regenerated at low temperatures [5, 17, 18].

Since there are multiple ways to integrate these technologies, we have defined 4 scenarios, each with a different configuration of DAC and solar fuel production [19, 20]. Scenarios A and B are based on L-DAC, with Scenario A incorporating a new concept of L-DAC powered entirely by solar energy. Scenario B, on the other hand, is based on the commercial L-DAC concept of oxyfuel combustion of natural gas. Scenarios C and D use S-DAC, but in Scenario C this system is centralized and powered by waste heat from the vacuum system and Rankine cycle (both required for solar fuel production). In contrast, in Scenario D, the S-DAC is decentralized and CO_2 is captured from the heating, ventilation, and air conditioning (HVAC) systems of buildings in urban areas near the plant. An overview of the different scenarios is shown in Figure 1.

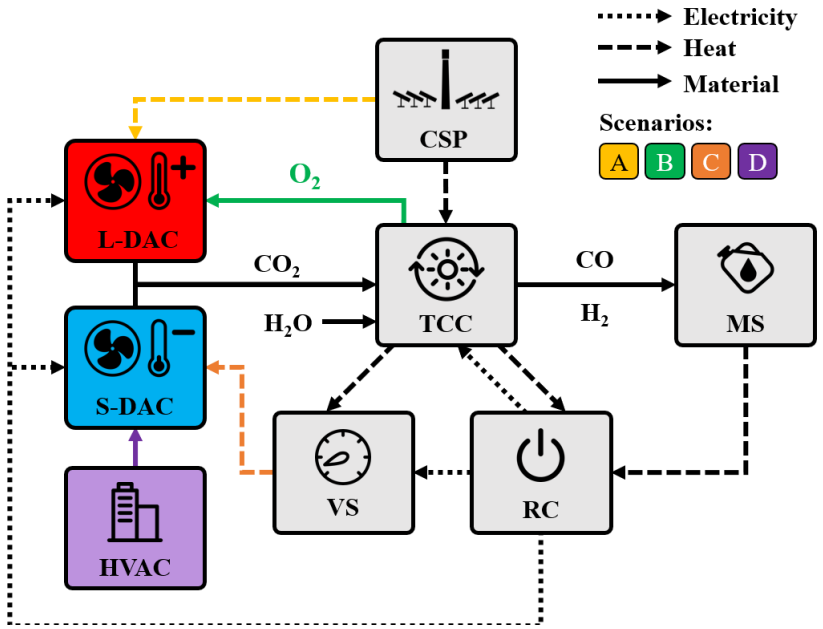

Figure 1: Schematic overview of the different scenarios. The abbreviations in the figure stand for: "L-DAC" = liquid direct air capture; "S-DAC" = solid direct air capture; "HVAC" = heating, ventilation, and air conditioning; "CSP" = concentrated solar power; "TCC" = thermochemical cycle; "MS" = methanol synthesis; "VS" = vacuum system; and "RC" = Rankine cycle. Adapted from [20].

Simulations were then built for each relevant part of the process. For the thermochemical cycle, the methanol synthesis, the vacuum system and the Rankine cycle, a model was built in Aspen Plus® , while the concentrated solar field was simulated with the DLR software HFLCAL VH13 [21]. The data related to the DAC were extracted from the relevant literature, except for scenario A, since it used an innovative solar L-DAC approach that had to be modeled in Aspen Plus®. The location considered was Riyadh, in Saudi Arabia, and was relevant to the study because of (1) the locally available solar irradiance (provided with hourly resolution by Meteonorm® software) and (2) the regional data used for the techno-economic and environmental assessments.

For the techno-economic assessment, the capital expenditure (CAPEX) was calculated with the results of the simulations and a combination of available correlations for mature process equipment [22] and cost estimation techniques from existing studies for non-standard units [23]. In addition, operational expenditure (OPEX) was determined by considering fixed (i.e., maintenance and insurance) and variable costs (i.e., local labor and raw materials). Utilities were not considered because the systems were designed to be autonomous. The Rankine cycle, which converts high-temperature waste heat into electricity, was the primary power source, with a photovoltaic and battery system acted as a backup. Finally, the levelized cost of the fuel (LCOF) was calculated from the OPEX and the annualized CAPEX (which considers the regional weighted average cost of capital or WACC [24]).

The environmental analysis consists of a cradle-to-grave life cycle assessment (LCA) that accounts for the production, transportation and combustion of the methanol. The database used is ecoinvent 3.7.1 with the openLCA® software and the ReCiPe Midpoint 2016 impact assessment methodology. The contribution of equipment not available in the database or in the literature was quantified using similar processes as proxies. From the obtained results, the climate change impact category (measured in kg of CO_2 equivalents per functional unit) was used as the main indicator of the carbon-neutrality of the fuel.

Discussion

The methodology described was applied to each of the scenarios and to a baseline consisting of a methanol production process without any integration with CO_2 capture via DAC. The main results of the techno-economic assessment are shown in Figure 2. As the reader will notice, it is safe to state that all scenarios with integrations between DAC and solar fuels production show a cost reduction compared to the baseline cost. Among all the scenarios studied, Scenario C stands out as the most cost-effective due to its lower initial investment and superior efficiency. This analysis is in the process of being improved through the determination of the confidence interval of the results.

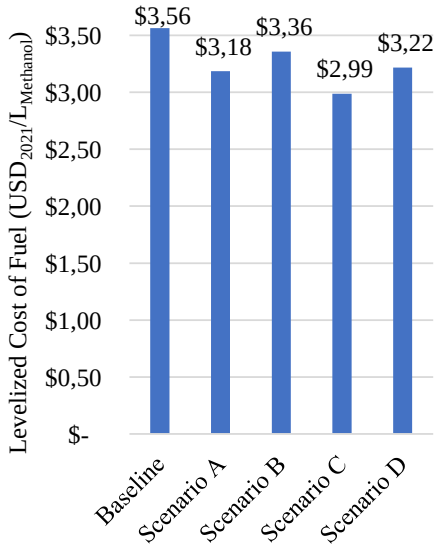

Figure 2: Levelized cost of fuel for each scenario and the baseline. Adapted from [20].

The preliminary data of the LCA show a similar trend with notable improvements over the baseline, led by Scenario C and closely followed by Scenario D. Compared to methanol

produced with hydrogen from commercial alkaline water electrolysis, the solar pathway has a lower cradle-to-grave carbon footprint. In addition, the results will be further discussed with a sensitivity analysis to identify hotspots in the process design phase.

Conclusions

The potential for integration between DAC and fuel production is explored in this work, with a particular focus on the solar thermochemical pathway. The results show that there are significant synergies in the design and operation of synthetic fuel plants without neglecting the supply of carbon-neutral CO_2 from DAC. At the current state of the art, S-DAC is recommended over L-DAC as it offers more integration opportunities with a lower initial investment. The study concludes with the possibility of solar hydrogen and its derivatives becoming economically and environmentally competitive in the coming years.

References

[1] United Nations Environment Programme, "Emissions Gap Report 2021: The Heat Is On - A World of Climate Promises Not Yet Delivered," Nairobi, Kenya.

[2] J. Blunden and D. S. Arndt, "State of the Climate in 2019," *Bulletin of the American Meteorological Society*, vol. 101, no. 8, S1-S429, 2020, doi: 10.1175/2020BAMSStateoftheClimate.1.

[3] D. Lüthi *et al.*, "High-resolution carbon dioxide concentration record 650,000-800,000 years before present," *Nature*, vol. 453, no. 7193, pp. 379–382, 2008, doi: 10.1038/nature06949.

[4] G. N. PLASS, "The Carbon Dioxide Theory of Climatic Change," *Tellus*, vol. 8, no. 2, pp. 140–154, 1956, doi: 10.1111/j.2153-3490.1956.tb01206.x.

[5] International Energy Agency (IEA), "Direct Air Capture: A key technology for net zero," France, 2022.

[6] R. Hanna, A. Abdulla, Y. Xu, and D. G. Victor, "Emergency deployment of direct air capture as a response to the climate crisis," *Nature Communications*, vol. 12, 2021, doi: 10.1038/s41467-020-20437-0.

[7] K. Madhu, S. Pauliuk, S. Dhathri, and F. Creutzig, "Understanding environmental trade-offs and resource demand of direct air capture technologies through comparative life-cycle assessment," *Nat Energy*, vol. 6, no. 11, pp. 1035–1044, 2021, doi: 10.1038/s41560-021-00922-6.

[8] S. Deutz and A. Bardow, "Life-cycle assessment of an industrial direct air capture process based on temperature–vacuum swing adsorption," *Nat Energy*, vol. 6, no. 2, pp. 203–213, 2021, doi: 10.1038/s41560-020-00771-9.

[9] Y. Lua, L. Zhua, C. Agrafiotis, J. Vieten, M. Roeb, and C. Sattler, "Solar fuels production: Two-step thermochemical cycles with cerium-based oxides," *Progess in Energy and Combustion Science*, vol. 75, 2019, doi: 10.1016/j.pecs.2019.100785.

[10] C. Agrafiotis, M. Roeb, and C. Sattler, "4.18 Solar Fuels," in *Comprehensive energy systems*, I. Dincer, Ed., Amsterdam, Netherlands: Elsevier, 2018.

[11] D. Marxer, P. Furler, M. Takacs, and A. Steinfeld, "Solar thermochemical splitting of CO2 into separate streams of CO and O2 with high selectivity, stability, conversion, and efficiency," *Energy Environ. Sci.*, vol. 10, pp. 1142–1149, 2017, doi: 10.1039/c6ee03776c.

[12] E. Rytter *et al.*, "Process concepts to produce syngas for Fischer–Tropsch fuels by solar thermochemical splitting of water and/or CO2," *Fuel Processing Technology*, vol. 145, pp. 1–8, 2016, doi: 10.1016/j.fuproc.2016.01.015.

[13] *Liquid fuels from concentrated sunlight: An overview on development and integration of a 50 kW solar thermochemical reactor and high concentration solar field for the SUN-toLIQUID project*, 2019.

[14] Manuel Romero *et al., Eds., Solar-Driven Thermochemical Production of Sustainable Liquid Fuels from H2O and CO2 in a Heliostat Field*, 2019.

[15] B. Bulfin, J. Vieten, C. Agrafiotis, M. Roeb, and C. Sattler, "Applications and Limitations of Two Step Metal Oxide Thermochemical Redox Cycles; A Review," *Journal of Materials Chemistry*.

[16] M. Pein *et al.*, "Redox thermochemistry of Ca-Mn-based perovskites for oxygen atmosphere control in solar-thermochemical processes," *Solar Energy*, vol. 198, pp. 612–622, 2020, doi: 10.1016/j.solener.2020.01.088.

[17] M. Fasihi, O. Efimova, and C. Breyer, "Techno-economic assessment of CO2 direct air capture plants," *Journal of Cleaner Production*, vol. 224, pp. 957–980, 2019, doi: 10.1016/j.jclepro.2019.03.086.

[18] National Academies of Sciences, Engineering, and Medicine, "Negative Emissions Technologies and Reliable Sequestration: A Research Agenda," 2019, doi: 10.17226/25259.

[19] E. Prats-Salvado, N. Monnerie, and C. Sattler, “Synergies between Direct Air Capture Technologies and Solar Thermochemical Cycles in the Production of Methanol,” *Energies*, vol. 14, no. 16, p. 4818, 2021, doi: 10.3390/en14164818.
[20] E. Prats-Salvado, N. Monnerie, and C. Sattler, “Techno-Economic Assessment of the Integration of Direct Air Capture and the Production of Solar Fuels,” *Energies*, vol. 15, no. 14, p. 5017, 2022, doi: 10.3390/en15145017.
[21] P. Schwarzbözl, R. Pitz-Paal, and M. Schmitz, Eds., *Visual HFLCAL - A Software Tool for Layout and Optimisation of Heliostat Fields*, 2009.
[22] M. S. Peters, K. D. Timmerhaus, and R. E. West, *Plant design and economics for chemical engineers*, 5th ed. Boston, London: McGraw-Hill, 2003.
[23] D. S. Remer and L. H. Chai, *Process Equipment, Cost Scale-up*. New York: Marcel Dekker, Inc., 1993.
[24] N. Ameli *et al.*, “Higher cost of finance exacerbates a climate investment trap in developing economies,” *Nature Communications*, vol. 12, no. 1, p. 4046, 2021, doi: 10.1038/s41467-021-24305-3.

Tailoring Polyaniline Bipyridine-Doped Fe–N–C Materials for High-Performance PEMFC Cathodes

G. Charalampopoulos[1], M. K. Daletou[*2]

[1]Ph.D. Candidate in Chemistry
[2] Principal Researcher FORTH/ICE-HT

[2] Corresponding author, Phone: +30 2610965213, e-mail: riadal@iceht.forth.gr

Introduction

Fuel cells have emerged as a sustainable energy technology with diverse applications, from transportation to stationary power generation. Proton Exchange Membrane Fuel Cells (PEMFCs) are particularly promising due to their high efficiency and low environmental impact. However, the widespread adoption of PEMFCs is hindered by the high cost of platinum-based catalysts, especially at the cathode. This research focuses on the development of non-platinum group metal (PGM) cathode electrocatalysts to address this cost barrier. Specifically, we investigate the synthesis, characterization, and electrochemical performance of Fe–N–C materials as alternative catalysts for the oxygen reduction reaction (ORR) in PEMFCs. Fuel cells are at the forefront of sustainable energy technologies, offering clean and efficient power generation with a variety of applications. Among them, Proton Exchange Membrane Fuel Cells (PEMFCs) hold great promise, particularly for applications such as transportation and stationary power generation. However, one of the primary challenges impeding the widespread adoption of PEMFCs is the high cost associated with platinum-based catalysts, which are used to facilitate the oxygen reduction reaction (ORR) at the cathode [1]–[4]. The need for alternative, non-PGM cathode catalysts is evident, especially as PEMFCs aim for higher power densities, longer lifespans, and cost competitiveness in the energy market. In response to this challenge, this research delves into the synthesis and evaluation of Fe–N–C materials as promising candidates for non-PGM cathode electrocatalysts in PEMFCs.

Methodology

The methodology employed in this study revolves around the rational design and synthesis of Fe–N–C materials with potential as cathode electrocatalysts. Key steps in the synthesis process include the use of halloysite nanoclay as a sacrificial template, the polymerization of aniline (PANI) in the presence of the template, and the addition of iron (II) chloride tetrahydrate as the iron source and 2,2-bipyridine as an additional organic dopant to modify the surface chemistry of the final catalyst. Pyrolysis of the composite under controlled conditions, including variations in temperature and atmosphere (argon or ammonia), plays a pivotal role in tailoring the resulting catalysts. Subsequent removal of the silica-based template is achieved using hydrofluoric acid, leaving behind a porous catalyst structure. These steps are carefully executed to explore the influence of synthesis parameters on the catalyst's properties and performance.

[*] M. K. Daletou: riadal@iceht.forth.gr

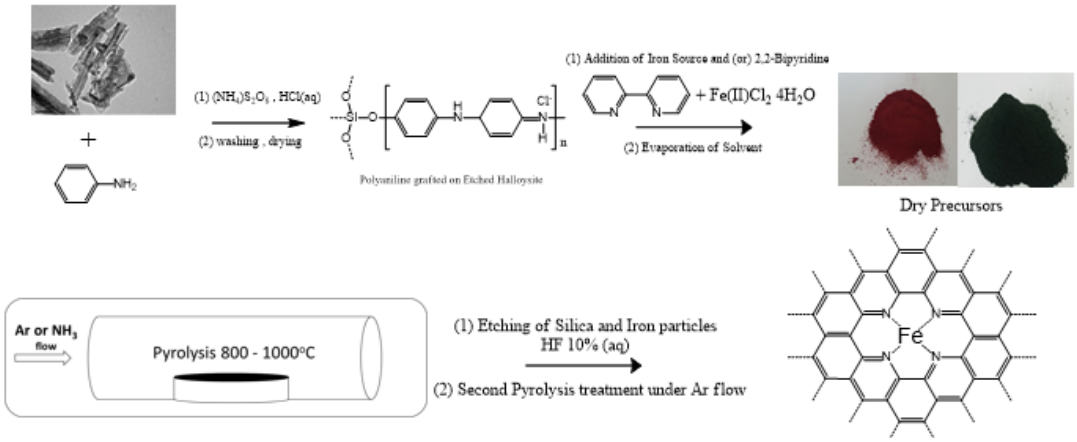

Figure 1: General synthetic procedure for all catalysts.

Discussion

The comprehensive characterization of the synthesized Fe–N–C catalysts provides valuable insights into their structural, physicochemical, and electrochemical properties.

To analyze the crystalline structure of the catalysts, X-ray diffraction (XRD) spectra were obtained. Notably, broad diffraction peaks at 26 and 44 deg confirmed the presence of amorphous hexagonal graphitic carbon. For the catalysts without 2,2-bipyridine no metallic phases were detected. However, iron carbide phases were detected for all catalysts containing 2,2-bipyridine in the precursor under Ar flow [5]. If the pyrolysis is done under NH_3 flow, no metallic iron phases can be detected and we also observe at 26 deg a sharp peak which is attributed to highly graphitized carbon. However, XRD can only detect crystalline phases with a scattering region larger than 2 nm [6]–[8].

TEM images revealed the presence of disordered and randomly oriented graphitic domains. Iron nanoparticles were detected for the catalyst with 2,2-bipyridine pyrolized under Ar flow, not however for the same precursor pyrolyzed under NH_3 flow. No significant Fe-based clusters or nanoparticles were observed for every other catalyst.

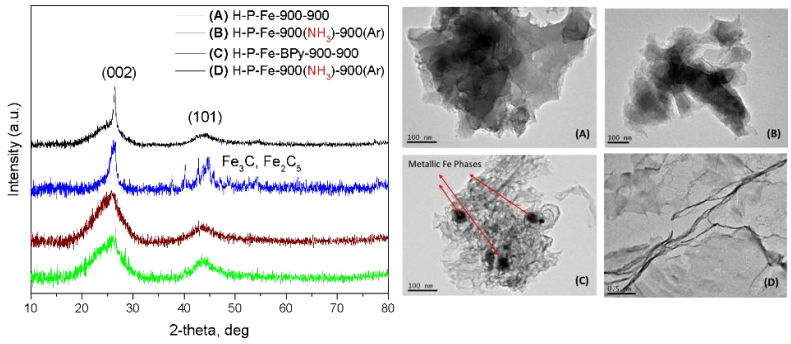

Figure 2: (Left) X-ray diffraction spectra of the different catalysts, (right) TEM images of the same catalysts A to D.

X-Ray photoelectron spectroscopy was performed to find a correlation between the catalytic activity of the catalysts and surface chemistry. For all samples higher pyrolysis temperature in Ar results in an increase of “graphitic” nitrogen species at the expense of pyridinic and

pyrrolic N. Here we showcase an example of this, and an increase of graphitic N from 26 % at 800 °C to 38 % at 900°C .Second heat treatment decreased the signal of surface carbides. As can be seen from the iron spectra. The presence of 2,2-bipyridine resulted in samples with higher Py and pyrrolic nitrogen, despite the similar overall N/C ratio.

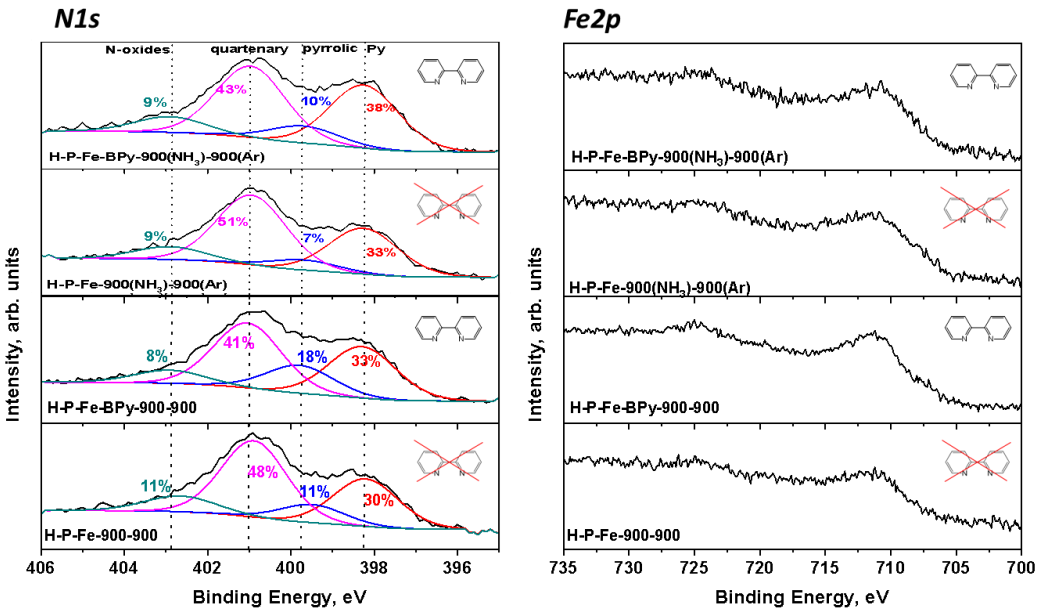

Figure 3: (Left) XPS spectra for N1s and (right) for Fe2p for the final catalysts after the second heat treatment.

The specific surface area and pore volume of the catalysts are crucial factors influencing their electrochemical activity. Nitrogen adsorption/desorption isotherms provide insights into these properties. Notably, the BET surface area and total pore volume exhibit sensitivity to the pyrolysis temperature, highlighting the significance of optimizing this parameter. A second heat treatment step is introduced to further enhance porosity and surface area, yielding promising results.

Catalyst		Iron Carbides (XRD)	Surface area (m^2/g)	Total pore volume (cc/g)	ICP-MS (Fe)wt%
No Bipyridine	900-900		865	0.606	0.94
	900(NH_3)-900(Ar)		730	0.542	1.10
Bipyridine	900-900	✓	492	0.600	5.1
	900(NH_3)-900(Ar)		780	0.866	1.11

Table 1: Surface area and total pore volume for the different catalysts, as assessed by BET analysis and Iron wt% content as assessed by Inductively coupled plasma mass spectrometry (ICP-MS).

Electrochemical testing employing the Rotating Disk Electrode (RDE) method offers a detailed evaluation of the catalysts' performance in the oxygen-saturated 0.5 M H_2SO_4 electrolyte and catalyst loading of 0.6 mg/cm^2. The focus is on the half-wave potential ($E_{1/2}$) as a key indicator of ORR activity. The results reveal notable differences among the synthesized catalysts. A second heat treatment is performed under Ar flow at the same conditions to eliminate impurities and stabilize the carbon structure. Second heat treatment under Ar atmosphere further enhances catalytic activity. In particular, the H-P-Fe-BPy-900(NH_3) catalyst, synthesized under ammonia atmosphere, exhibits $E_{1/2}$=0.834 V approaching the D.O.E. target for 2025 of 0.85 V (which is set for catalyst loading of 0.6-0.8 mg/cm^2), signifying superior ORR activity as well as, remarkable stability after accelerated stress test in O_2 saturated 0.5 M H_2SO_4 electrolyte. This outcome underscores the impact of synthesis parameters on electrocatalyst performance and suggests a promising avenue for further exploration.

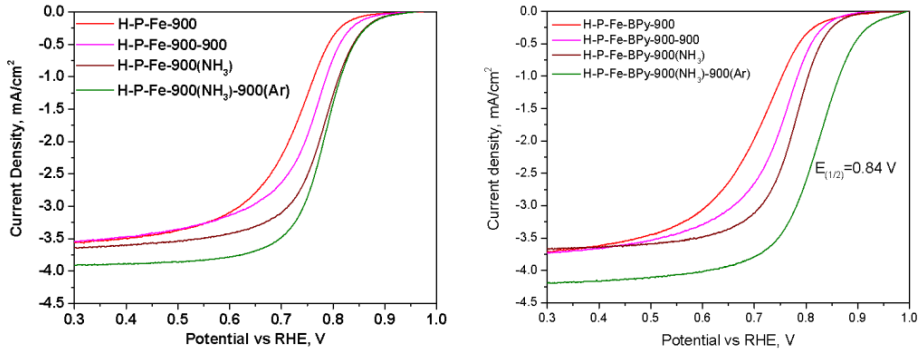

Figure 4: Polarization curves in oxygen saturated 0.5 M H_2SO_4 at 900 rpm, at room temperature and a scan rate of 1 mV/s. Electrode diameter 0.55 cm and catalyst loading 0.6 mg/cm^2.

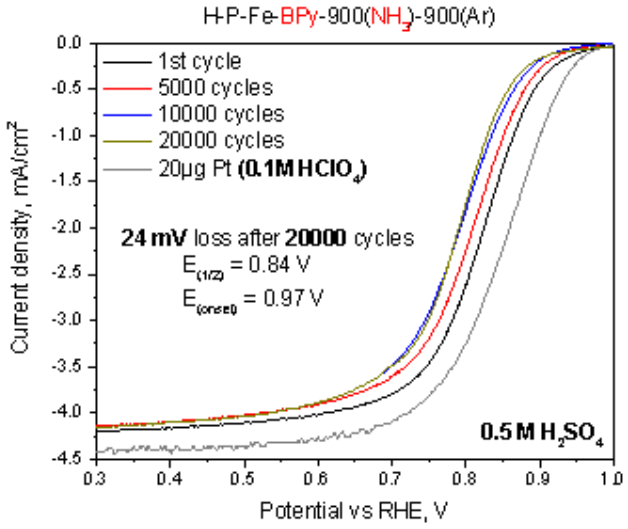

Figure 5: Polarization curves in oxygen saturated 0.5 M H_2SO_4 at 900 rpm, at room temperature and a scan rate of 1 mV/s of the best performing catalyst before and after the accelerated stress test. Electrode diameter 0.51 cm and catalyst loading 0.6 mg/cm^2.

Conclusions

This extended abstract encapsulates our research efforts aimed at developing non-PGM cathode electrocatalysts for PEMFCs. The high cost of platinum-based catalysts necessitates the exploration of alternative materials to enable cost-effective and sustainable fuel cell technology. The synthesis, characterization, and electrochemical evaluation of Fe–N–C materials reveal their potential as efficient ORR catalysts, particularly when synthesized under ammonia atmosphere. These findings underscore the importance of tailoring synthesis parameters to optimize catalyst performance. Further investigations into the template influence, and iron content are ongoing, with the goal of contributing to the advancement of PEMFCs.

References

[1] A. Chandan *et al.*, "High temperature (HT) polymer electrolyte membrane fuel cells (PEMFC)–A review," *Journal of Power Sources*, vol. 231, pp. 264–278, 2013.
[2] Y. Wang *et al.*, "Advanced electrocatalysts with single-metal-atom active sites," *Chemical reviews*, vol. 120, no. 21, pp. 12217–12314, 2020.
[3] Y. Wang, D. F. R. Diaz, K. S. Chen, Z. Wang, and X. C. Adroher, "Materials, technological status, and fundamentals of PEM fuel cells–a review," *Materials today*, vol. 32, pp. 178–203, 2020.
[4] R. Haider *et al.*, "High temperature proton exchange membrane fuel cells: progress in advanced materials and key technologies," *Chemical Society Reviews*, vol. 50, no. 2, pp. 1138–1187, 2021.
[5] D. Guo, S. Han, J. Wang, and Y. Zhu, "MIL-100-Fe derived N-doped Fe/Fe3C@ C electrocatalysts for efficient oxygen reduction reaction," *Applied Surface Science*, vol. 434, pp. 1266–1273, 2018.
[6] L. Osmieri, "Transition metal–nitrogen–carbon (M–N–C) catalysts for oxygen reduction reaction. Insights on synthesis and performance in polymer electrolyte fuel cells," *ChemEngineering*, vol. 3, no. 1, p. 16, 2019.
[7] Y. He, S. Liu, C. Priest, Q. Shi, and G. Wu, "Atomically dispersed metal–nitrogen–carbon catalysts for fuel cells: advances in catalyst design, electrode performance, and durability improvement," *Chemical Society Reviews*, vol. 49, no. 11, pp. 3484–3524, 2020.
[8] S. Gupta, S. Zhao, O. Ogoke, Y. Lin, H. Xu, and G. Wu, "Engineering favorable morphology and structure of Fe- N- C oxygen- reduction catalysts through tuning of nitrogen/carbon precursors," *ChemSusChem*, vol. 10, no. 4, pp. 774–785, 2017.

Techno-economic Analysis of Concentrated Solar Heat Supported High-Temperature Electrolysis Process

T. Roeder[*1,2], K. Risthaus[1], N. Monnerie[1], C. Sattler[1,2]

[1] Deutsches Zentrum für Luft- und Raumfahrt – DLR/German Aerospace Center, Institute of Future Fuels, Linder Höhe, 51147 Cologne, Germany
[2] RWTH Aachen University, Faculty of Mechanical Engineering, Chair for Solar Fuel Production, 52062 Aachen, Germany

Introduction

Reducing greenhouse gas emissions is one of the greatest challenges faced by society today. Renewable hydrogen production as a chemical feedstock is needed to replace the use of fossil fuels. Among water electrolysis technologies, solid oxide cell reactor systems can operate at the highest electrical efficiencies by using thermal energy and thereby substituting electrical energy partly [1]. This requires temperatures of about 800°C. Concentrated solar thermal energy can be used to meet the high heat requirements of high-temperature electrolysis (HTE) cost-efficiently. Since the price of electricity is the major driver of product cost development, large-scale hydrogen production using solar energy and HTE promises low H_2 production costs. However, the intermittent availability of solar energy requires an appropriate energy storage system. A possible system is depicted in Figure 1. Furthermore, in this study an approach is used that considers the cost and stack degradation development goals of the European Commission for future electrolyser systems.

When operating a high-temperature electrolysis system, the thermal energy supply in standby mode is also important. Therefore, it makes sense to provide sufficient heat for as long as possible. In addition, the process lifetime must be aligned with the planned operating hours. The process lifetime is often defined by the component with highest durability and therefore the longest component life time. Other components, e.g. the HTE, have a short expected lifetime and replacement of such components are needed during the total process life time. Due to the limited lifetime of an electrolyzer, it makes economic sense to avoid replacement close to the end of the total process lifetime. The investment in an HTE system and the cost of stack replacement can be one of the major cost drivers. HTE using solid oxide cells is currently at lower technology readiness levels (TRL) than polymer electrolyte membrane (PEM) and alkaline (AEL) electrolysis. As a result, significant cost reductions and lifetime extensions are still to be expected. To consider these aspects and compare a solar supported HTE with competing electrolyser technologies, a detailed process analysis is performed here to investigate the cost impact of a high temperature thermal energy storage (TES) system to further reduce electrical energy demand.

[*] Corresponding author: timo.roeder@dlr.de

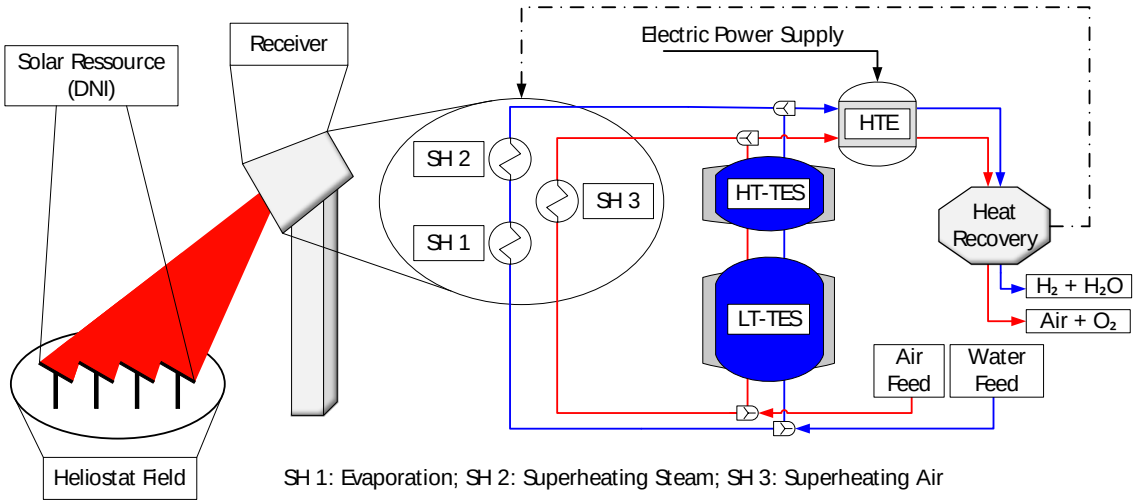

Figure 1: Process configuration of a concentrated solar heat supported high temperature electrolysis (HTE) process. The figure shows a process configuration with a high temperature (HT) and low temperature (LT) thermal energy storage (TES) unit.

Methodology

A process model of the solar supported HTE including a low- and high-temperature storage as shown in Figure 1 has been sat up. For the solar resources, a location in Morocco was chosen and the solar power input was calculated. To address the economics, different assumptions had to be made. For the solar thermal subcomponent, the lifetime is assumed to be 25 years [2]. State of the art solid oxide cell electrolysers achieve a maximum lifetime in the range of 20,000 to 30,000 full load hours [3–6]. Some studies are more optimistic about the current state and consider a life of 40,000 full load hours [7–9]. However, we conservatively assume the lower end here. By 2050, an increased life expectancy of over 80,000 full load hours is expected [3–6], which we also considered for the exchange of stacks. For example, for a planned process with yearly full load hours of 4000 or 8000, the stack would have to be replaced for the first time after 5 or 2.5 years respectively. Thus, the replacement of the HTE will take place during the plant lifetime. Therefore, a linear cost degradation to the future cost outlook and a linear component lifetime improvement is considered. During the lifetime of a stack, the electrical power demand increases linearly and is increased by 10% at the end of the lifetime. This takes into account the degradation rate of the stack. In addition, the cost of electricity and heat is assumed to be 100 €/MWh and 50 €/MWh, respectively. An electrical energy demand of 7% of the electrolysis power during hot standby operation is assumed for the HTE [11]. In addition to the economics, the integration and operation of the storage must also be investigated.

Discussion

The process integration of a thermal energy storage system into a high-temperature electrolysis process must be able to provide both thermal energy for the evaporation of water to steam and high temperatures for isothermal operation at about 800°C. Since the HTE requires both a steam and an air supply, both media can be used to charge the TES system. The use of steam flow as the heat transfer medium is advantageous as steam has a higher heat capacity compared to air. This allows for lower flow velocities and consequently a lower pressure drop in the process. Moreover, water can be pumped in liquid form with less

(electrical) energy input than air. In case of evaporation at higher pressure (8-10bar) during the day, condensation heat can be stored in the LT-TES storage and extracted at lower pressure (<2bar) during the night. Either steam or an air stream can be used to discharge the HT-TES unit. The LT-TES unit is discharged with a low-pressure water stream. This minimizes the total electrical energy demand of the process to be as close as possible to the electrical energy demand of the electrolyzer for the water splitting reaction.
From an economic point of view, the reduction of the electrical energy demand is mandatory, since the price of electrical energy has the largest impact on the operational expenditure (OPEX) of H_2 production. The second largest impact comes from the capital expenditure (CAPEX) of the electrolysis system and the required stack replacement. Figure 2 shows the evolution of replacement times for a process reaching 4000 and 8000 full load hours compared to no life time improvement. In addition, the cost evolution is shown compared to no cost reduction. Thus, the HTE system cost depends on the number of replacements, which will depend on the continuing developments. The total HTE system cost can be defined as the sum of the stack replacement costs and the initial HTE system cost. This results in total HTE system costs of 2955.2 €/kW and 3810.2 €/kW for 4000 and 8000 full load hours respectively. However, the H_2 production cost will be different for the two scenarios due to the different annual H_2 production capacity resulting from the process full load hours. In addition, the lifetime of the project must be considered. For a project life of 25 years, the end of life of the last stack installed may not be reached depending on the process full load hours. Care must be taken to ensure that the full load hours are consistent with the project life to be achieved.

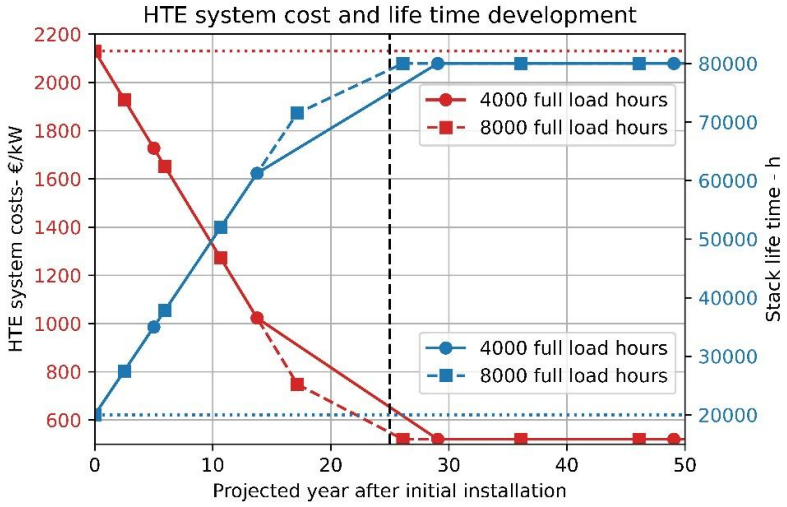

Figure 2: HTE system cost and life time development for 4000 and 8000 full load hours. Additionally, no cost reduction and no stack life time improvement are displayed as dotted lines. The markers indicate the time of replacement for the 4000 and 8000 full load hours operation.

The presented calculation of the total cost of the electrolyser system is also applicable to the other electrolyser technologies (PEM and AEL). Thus, the cost evolution of the HTE system can be compared with the development targets of PEM and AEL. Therefore, the targets of the European Commisions Strategic Research and Innovation Agenda (EU-SRIA) [10] are used for each technology. Figure 3 compares the levelized costs of hydrogen ($LCOH_2$) for the three technologies for a wide range of process full load hours and a development target within 20 years. For the selected cost reduction and lifetime improvement of the EU-SRIA,

costs below 7.50 €/kg are achievable with all three technologies. At low process full load hours, AEL and PEM perform better than HTE due to the HTE system investment cost and its electrical energy demand during hot stand-by operation. However, at about 4000 full load hours and above, HTE technology outperforms PEM due to the lower electrical energy requirement per amount of H_2 produced. The peaks within the plotted lines are caused by additional stack replacements due to the achievable process full load hours. An additional stack replacement increases the total CAPEX and has a negative impact on the $LCOH_2$ because the production rate does not increase much initially. As more process full load hours are achieved, the increased H_2 production rate becomes profitable and reduces the $LCOH_2$.

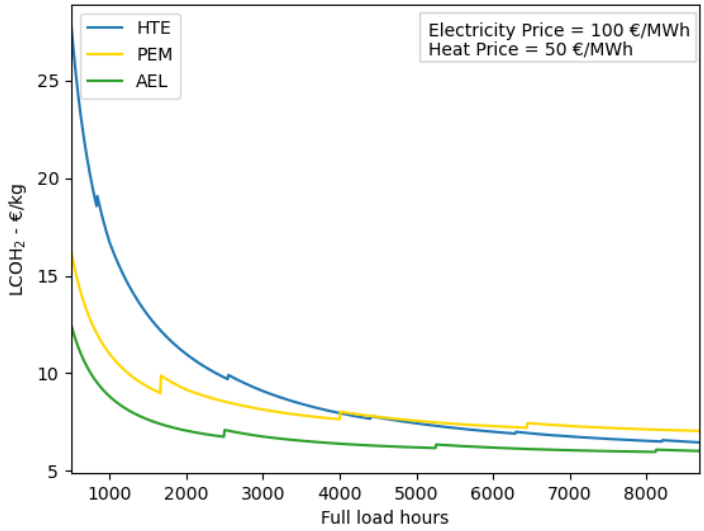

Figure 3: Levelized costs of hydrogen ($LCOH_2$) for the three main H_2O electrolysis technologies. The system comparison considers the European Commission's cost development targets for the three main technologies.

Conclusions

Concentrated solar thermal energy can reach temperatures of about 800°C for isothermal HTE operation. Thermal energy storage for overnight hydrogen production is important to achieve high process full-load operating hours. Although the thermal energy demand of high temperature heat is comparatively low, the use of high temperature energy storage is necessary to achieve the lowest electrical energy demand for the process. Thus, an HTE process with a concentrated solar thermal system can achieve cost-competitive green hydrogen production. However, the process needs to be optimized in terms of full load hours. In addition, rapid development of HTE cost reduction and reduced cell degradation is necessary for low H_2 production costs in general. With the current cost targets of the European Commission, HTE is already cost competitive with PEM and close to AEL technologies as long as heat is available at low cost, which can be achieved by concentrating solar energy systems.

References

[1] F. Petipas, A. Brisse, and C. Bouallou, "Benefits of external heat sources for high temperature electrolyser systems,", *International Journal of Hydrogen Energy*, vol. 39, no. 11, pp. 5505–5513, 2014, doi: 10.1016/j.ijhydene.2014.01.179.

[2] Jürgen Dersch, Simon Dieckmann, Klaus Hennecke, Robert Pitz-Paal, Michael Taylor, and Pablo Ralon, "LCOE reduction potential of parabolic trough and solar tower technology in G20 countries until 2030,", *AIP Conference Proceedings*, no. 2303, 2020.
[3] The International Renewable Energy Agency (IRENA), "Green hydrogen cost reduction: Scaling up electrolysers to meet the 1.5C climate goal,".
[4] N. Gerloff, "Economic analysis of hydrogen production in Germany with a focus on green hydrogen, considering all three major water electrolysis technologies,", *Sustainable Energy Fuels*, vol. 7, no. 8, pp. 1893–1907, 2023, doi: 10.1039/D3SE00073G.
[5] O. Schmidt, A. Gambhir, I. Staffell, A. Hawkes, J. Nelson, and S. Few, "Future cost and performance of water electrolysis: An expert elicitation study,", *International Journal of Hydrogen Energy*, vol. 42, no. 52, pp. 30470–30492, 2017, doi: 10.1016/j.ijhydene.2017.10.045.
[6] Tom Smolinka *et al.*, "Studie IndWEDe Industrialisierung der Wasser-elektrolyse in -Deutschland: -Chancen und -Herausforderungen für nachhaltigen Wasserstoff für Verkehr, Strom und -Wärme,".
[7] M. G. Rasul, M. Hazrat, M. A. Sattar, M. I. Jahirul, and M. J. Shearer, "The future of hydrogen: Challenges on production, storage and applications,", *Energy Conversion and Management*, vol. 272, p. 116326, 2022, doi: 10.1016/j.enconman.2022.116326.
[8] J. C. Restrepo, D. Luis Izidoro, A. Milena Lozano Násner, O. José Venturini, and E. Eduardo Silva Lora, "Techno-economical evaluation of renewable hydrogen production through concentrated solar energy,", *Energy Conversion and Management*, vol. 258, p. 115372, 2022, doi: 10.1016/j.enconman.2022.115372.
[9] H. Nami, O. B. Rizvandi, C. Chatzichristodoulou, P. V. Hendriksen, and H. L. Frandsen, "Techno-economic analysis of current and emerging electrolysis technologies for green hydrogen production,", *Energy Conversion and Management*, vol. 269, p. 116162, 2022, doi: 10.1016/j.enconman.2022.116162.
[10] European Commission - Clean Hydrogen Joint Undertaking, "Strategic Research and Innovation Agenda 2021 – 2027,", European Commission - Clean Hydrogen Joint Undertaking, Feb. 2022. Accessed: Feb. 8, 2023. [Online]. Available: https://www.clean-hydrogen.europa.eu/knowledge-management/sria-key-performance-indicators-kpis_en
[11] M. Tomberg, M. P. Heddrich, S. A. Ansar, and K. A. Friedrich, "Operation strategies for a flexible megawatt scale electrolysis system for synthesis gas and hydrogen production with direct air capture of carbon dioxide,", *Sustainable Energy Fuels*, vol. 7, no. 2, pp. 471–484, 2023, doi: 10.1039/D2SE01473D.

Technologies and energy strategies for the production and utilization of green hydrogen in the industrial sector

Ludovico Linzi*[1], Anna Stoppato[2], Francesca Mazzolini[3], Cristina Cavinato[4], Graziano Tassinato[5]

[1]University of Padova, Department of Industrial Engineering, Via Venezia, 1, 35131 Padova PD
[2]University of Padova, Department of Industrial Engineering, Via Venezia, 1, 35131 Padova PD
[3]University Ca' Foscari of Venice, Department of Environmental Sciences, Computer Science and Statistics, Via Torino 155, 30172, Venezia
[4]University Ca' Foscari of Venice, Department of Environmental Sciences, Computer Science and Statistics, Via Torino 155, 30172, Venezia
[5]Green Propulsion Laboratory Veritas spa, Via della Geologia, 31 / 1, 30176 Venezia VE

Introduction

The urgency of transitioning to sustainable energy sources in the face of escalating environmental concerns and depleting fossil fuel reserves has never been more acute. My Ph. D. project, situated within this critical context, aims to propose a solution to harness the untapped potential of organic waste and wastewater as sources of green energy. Spearheaded by VERITAS Spa, a leader in integrated water services and waste treatment, the project aims to transform the conventional approach to waste management and energy production.

The "MODel of Saving electric ENergy from organic waste fermentation (MODSEN)" project emerges as a strategic response to this challenge. Specifically, the project involves the study of a process for the energy valorization of sludge and organic waste through their conversion into hydrogen. At industrial sites, this process can be combined with the better-known production of hydrogen through electrolysis powered by photovoltaic panels. Different ways of storing the hydrogen produced are also proposed and studied, with the aim of making hydrogen production and use mutually independent in time. Solutions that are applicable in industrial sites, with regard to aspects of safety, cost, land occupancy, and that guarantee the highest possible values of efficiency are considered. In particular, the conversion of hydrogen into metal hydrides will be studied and tested, as well as the synthesis of metal organic frameworks (MOFs) designated specifically for hydrogen storage at low pressures, due to their tunable porous structure and high surface area suitable for gas adsorption. Finally, different technologies will be analyzed and proposed for the use of hydrogen at the industrial site itself for the production of electricity for self-consumption, in particular fuel cell technology, with a comparison between proton-exchange membrane fuel cells (PEMFC) and Solid Oxide fuel cell (SOFC).

The anticipated outcomes include the development of a viable, scalable process for hydrogen production, advancements in hydrogen storage and purification technologies, and a comprehensive assessment of environmental impacts, positioning the project at the forefront of renewable energy research.

The project is anchored in the concept of the circular economy, reimagining waste as a resource rather than a byproduct. By converting waste activated sludge and organic waste into hydrogen, the project not only provides a renewable energy source but also reduces waste volume and mitigates greenhouse gas emissions.

* Corresponding author: ludovico.linzi@phd.unipd.it

Specific Objectives

The specific objectives of the MODSEN project are multi-fold, reflecting the complexity and interdisciplinary nature of the research. The primary goal is to develop and validate a pilot-scale process for the conversion of organic waste into hydrogen. This involves exploring the potential of Dark Fermentation, a process that produces hydrogen from organic matrices like waste activated sludge and organic waste, independently of light. The project also aims to study the integration of this process with hydrogen production from photovoltaic-powered electrolysis, thereby enhancing the overall efficiency of hydrogen generation.

Another key objective is to explore and optimize various hydrogen storage methods, with a particular focus on Metal Hydrides and Metal Organic Frameworks (MOFs). These materials offer promising avenues for efficient and safe hydrogen storage, potentially overcoming some of the major challenges associated with hydrogen as an energy carrier, such as high energy demand related to gas compression in cylinders.

Additionally, one of the main goals is to consistently produce over 20 liters of hydrogen per kg of TVS (Total Volatile Solids) treated, with a purity level of 95%. The project also aims to convert 50% of the produced hydrogen into electric energy and enhance methane production by 15-20% compared to traditional fermentation methods. Moreover, the final goal is to integrate previous technologies on a pilot scale, i.e., verifying the potential of the system by realizing a line with a treatment capacity of 60 kg/day of waste. These objectives are not only technologically challenging but also critical for establishing the feasibility and scalability of the proposed solutions.

Methodology

The experimental phase of the project is focused on designing and optimizing processes for hydrogen purification and storage with a special attention to Metal Hydrides and the synthesis of innovative materials called Metal Organic Frameworks and metal hydrides for hydrogen storage.

In parallel, the project undertakes the development of an energetic model of the entire hydrogen production and utilization system. This model will consider various operational scenarios and configurations, enabling the team to assess the energy efficiency and environmental impact of different approaches. The modeling work is complemented by a Life-Cycle Assessment (LCA) to evaluate the environmental impact of the project. The LCA focuses on key indicators such as Cumulative Energy Demand and Carbon Footprint, providing a holistic view of the project's sustainability.

The first test was conducted in a two-stage anaerobic co-digestion system with waste activated sludge (WAS) and anaerobic sludge as inoculum. Dark fermentation was carried out in batch tests in co-digestion with a substrate/sludge ratio of 1:1 (based on VS). The batch tests were set with an organic load (OL) range from 10 to 25 kgVSfeed/m^3 using serum bottles at 39°C. A semi continuous reactor was then set up with pH control (5.2-5.5), using an organic loading rate of 12 kgVSfeed/m^3d and a hydraulic retention time (HRT) of 3.

The substrates were collected at a local vegetables market. Before using, the substrates were chopped and stored at -20°C. The sludge and the inoculum were collected from the local wastewater treatment plant. Standard Methods were followed for measuring TS and VS content, tCOD and sCOD, total nitrogen (TKN), and total alkalinity (TA). The ammonia content was measured using an ISE

electrode. The pH was measured with a pH-meter HANNA. VFAs were analyzed using high-performance liquid chromatography (HPLC) by means of an Agilent Technologies 1100 series equipped with a UV-Vis detector and an Acclaim™ Organic Acid 5µm 4x150mm column. A 1 mM CH_3SO_3H water solution was used as a mobile phase at a flow rate of 1 mL/min. Batch fermentation tests were carried out in triplicate using a Nautilus-AnaeroTechnology equipment to evaluate the biochemical hydrogen potential (BHP) of different substrates at different OL. The same equipment was used for the BMP test of the DF effluent at F/M of 0.3 conditions carried out in duplicate. The biogas composition was measured when a sufficient gas production was detected. The semi-continuous test was carried out using a 4L CSTR reactor with an automatic control system (RES Italia s.r.l) and hydrogen was measured daily with a portable analyser (ETG s.r.l). Liquid samples were collected every day for the chemical parameters' determinations.

Discussion

Dark fermentation for hydrogen production involves the anaerobic degradation of organic substrates by microbes in the absence of light. This process results in hydrogen as a byproduct of fermentation, leveraging organic residues as the material source. Dark fermentation, facilitated predominantly by bacteria such as Clostridium, Bacillus, Enterobacter, Klebsiella, and Eubacterium, commences with the hydrolysis of complex organic compounds, including proteins, carbohydrates, and lipids, into simpler substances like amino acids, sugars, and fatty acids. Extracellular enzymes secreted by these bacteria orchestrate the hydrolytic process. Subsequently, fermentative bacteria metabolize hydrolysis products, resulting in the production of hydrogen gas, carbon dioxide, and organic acids. Maintaining an optimal pH level between 5.5 and 6.5 is crucial to prevent the formation of undesired byproducts. Temperature control, with an optimum at 37°C, is also imperative. Despite its potential, dark fermentation confronts challenges, including low hydrogen yields and the generation of gaseous byproducts such as methane, carbon dioxide, and volatile fatty acids. [4]

The efficiency of the dark fermentation process is comparatively lower than that of alternative hydrogen production methods, influenced by factors such as the type of organic waste, waste composition, microbial population, and operating conditions. The inefficiency stems from incomplete degradation of organic matter, substrate losses to secondary reactions, and the inhibition of microbial populations by toxic compounds such as ammonia and volatile fatty acids.

Nonetheless, dark fermentation presents several merits over other hydrogen production methods. Firstly, it can effectively harness a wide array of organic wastes, including those unsuitable for alternative biomass conversion methods like lignocellulosic biomass. Secondly, the process exhibits simplicity and does not necessitate sophisticated equipment. Lastly, dark fermentation is operable at low temperatures and atmospheric pressure, resulting in reduced energy consumption and production costs.

The quantity of organic waste or biomass required to produce a specific quantity of hydrogen through dark fermentation varies depending on multiple factors such as waste composition, microbial population and operating conditions. The typical yield of hydrogen from dark fermentation ranges from 0.5 to 3.0 moles of hydrogen per mole of glucose consumed.

For example, if the goal is to produce 1 kg of hydrogen gas through dark fermentation using food waste as a feedstock, the food waste composition might

approximate 20% protein, 50% carbohydrates, 10% lipids, with the remaining 20% comprising moisture and non-organic materials. The average energy content of food waste is approximately 16 MJ/kg.

Assuming an average yield of 1.5 moles of hydrogen per mole of glucose consumed and a glucose content of 50% in the food waste, we can estimate that approximately 100 kg of food waste would be required to produce 1 kg of hydrogen. However, this estimate on presupposes that all glucose in the food waste is entirely converted into hydrogen gas, which is not a realistic assumption. Factors such as incomplete organic matter degradation and substrate losses to secondary reactions result in a lower actual hydrogen yield from food waste compared to the theoretical yield.

Typically, dark fermentation processes span from several days to several weeks, with the retention time of the feedstock within the reactor serving as a critical parameter affecting process efficiency. The optimal retention time is contingent upon feedstock composition and microbial population.

Biogas, generated through anaerobic digestion of organic waste, sewage sludge, and biomass, constitutes a renewable energy source predominantly composed of hydrogen (H2), methane (CH4) and carbon dioxide (CO2), along with impurities such as hydrogen sulfide (H2S), which is a corrosive gas and therefore poses a threat to metal surfaces and fuel cell components. Thus, the presence of impurities in the biogas stream significantly impacts the performance, reliability, and longevity of fuel cell systems, particularly for PEMFCs that mandate purified hydrogen as a fuel source. [2][3]

The graph in figure 1 reports the hourly production during a steady-state week. The biogas production rate ranged from 5.5 to 9 NL/L-d (Normal liters per liters per day), while the Specific Gas Production (SGP) at steady state condition was 120 NL/kgVS (Normal Liters per kilogram of Volatile Solids) with about 30% hydrogen content. The Dark Fermentation effluent of the semi continuous process was characterized and investigated with Biochemical Methane Potential (BPM) test studying a Food to Microorganism (F/M) ratio of 0.3 to determine its biomethane production capacity. This condition obtains a maximum Specific Methane Output (SMO) of 0.590 m^3_{CH4}/kgVS on the eighth day of testing with an average percentage of CH_4 around 76%. The result demonstrates how the two processes could enhance the overall economy of the bioenergy production system from waste. The obtained results will be used for carrying forward the MODSEN project.

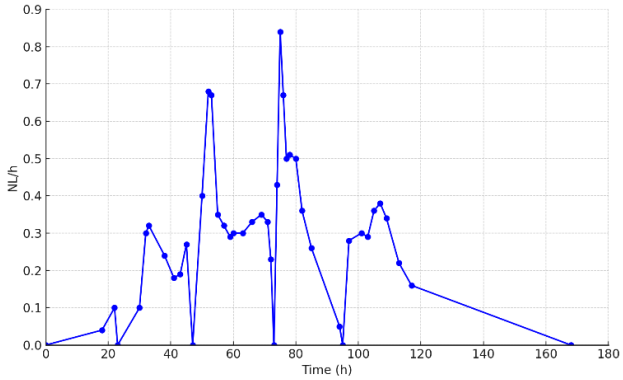

Figure 1: hourly biogas production rate during a steady-state week

Use of hydrogen for electricity generation

The generation of electricity using biogas involves diverse technologies, including combustion engines, gas turbines, and fuel cells. In this context, our objective is to assess the advantages of utilizing a Solid Oxide Fuel Cell (SOFC) compared to a Proton Exchange Membrane Fuel Cell (PEMFC) for the generation of electricity from biogas. SOFCs operate at elevated temperatures, typically ranging from 600 to 1000°C, affording them the flexibility to utilize diverse fuels, including natural gas, biogas, and hydrogen, without requiring an external reformer.

A paramount advantage of SOFCs is their exceptional efficiency, capable of reaching up to 60% under optimal conditions. This is primarily attributed to their ability to harness waste heat generated during the electrochemical process, which can be converted into additional electricity or utilized for other applications. SOFCs also exhibit low emissions, as the sole byproduct of the electrochemical reaction is water.

SOFCs offer a broad spectrum of potential applications, including stationary power generation, distributed energy systems, and transportation. Nevertheless, their high operational temperature presents commercialization challenges, such as material durability, thermal cycling, and startup time.

PEMFCs demand purified hydrogen as fuel, with impurities in the gas stream causing performance deterioration and potential harm to the fuel cell stack. Consequently, a purification step becomes imperative to eliminate impurities from the biogas stream before introducing it into a PEMFC. The purification process can be energy-intensive and costly, often necessitating chemical scrubbing or adsorption procedures to remove impurities like H2S.

In contrast, SOFCs exhibit greater tolerance for impurities in the fuel stream, encompassing CO, H2S and other impurities. The elevated operating temperature of SOFCs facilitates the catalytic conversion of impurities into less harmful species, such as H2O and CO2. As a result, SOFCs do not demand as extensive purification processes, thereby reducing the energy and cost associated with biogas conditioning [5].

The critical comparative analysis between the two fuel cell technologies is primarily focuses on evaluating the trade-offs between employing highly purified hydrogen in PEM cells versus the utilization of 'dirty' hydrogen in SOFCs. The objective is to ascertain the most efficient and cost-effective approach, considering both the energy output and the practicality of hydrogen purification processes. Over the coming months, experimentation will be conducted on these two types of fuel cells, providing vital empirical data. This data will support the theoretical framework and inform the decision-making process in the selection of the most suitable fuel cell technology, balancing efficiency and practicality in hydrogen utilization

During the period January 2023-July 2023 a research project was conducted in Denmark at the DTU Offshore laboratories, focusing on the synthesis of Metal-Organic Frameworks (MOFs) specifically designed for hydrogen storage. This work involved the synthesis of two Zirconium-based MOFs, namely UiO-66 and UiO-66-NH2 [6] [7] to acquire fundamental knowledge about the material's synthesis process. Subsequently, a novel organic linker, a derivative of 2,3-dihydroxy terephthalic acid with two exposed OH groups, was synthesized [8]. Utilizing this linker, a new Zr-MOF was successfully developed, demonstrating enhanced hydrogen absorption capabilities. This improvement is primarily attributed to the linker's ability to bind metal ions, thereby facilitating hydrogen

molecule chemisorption. The increased hydrogen absorption capacity of this Zr-MOF could lead to more efficient and compact hydrogen storage solutions, potentially making the use of hydrogen as a clean energy carrier more viable and cost-effective. Furthermore, this development could also contribute to the optimization of fuel cell performance, especially in systems where hydrogen purity and storage efficiency are crucial parameters.

Conclusions

In this work, the primary objective is to significantly influence the domain of green hydrogen production. This aligns with various national research programs that emphasize the development of novel energy technologies and services, with a specific focus on those that facilitate the shift to renewable energy and decarbonized gases. The project's outcomes are expected to contribute significantly to the efficiency and sustainability of multiutility services, presenting a clear trajectory towards green hydrogen utilization in industrial settings.

Acknowledgements

The research activity has been funded by MoDSEn project: “MODel of Saving electric ENergy from organic waste fermentation” CSEAB_00364, financed by Italian Minister of Economic Development, 20 September 2021, published on G.U.R.I. n.234, 30 September 2021. The Green Propulsion Laboratory of VERITAS S.p.a. is gratefully acknowledged for its support and hospitality.
The Ph.D research activity has been founded by PON doctoral grants on Green and Innovation topics.
The authors would like to express their sincere gratitude to the Department of Industrial Engineering at the University of Padua and the laboratories at DTU Offshore, Kongens Lyngby, Denmark.

References

[1] “A SUSTAINABLE PATHWAY FOR THE EUROPEAN ENERGY TRANSITION HYDROGEN ROADMAP EUROPE”, doi: 10.2843/249013.

[2] “BIO-HYTHANE PRODUCTION FROM FOOD WASTE BY DARK FERMENTATION COUPLED WITH ANAEROBIC DIGESTION PROCESS: A LONG-TERM PILOT SCALE EXPERIENCE”, doi:10.1016/j.ijhydene.2012.03.065

[3] “BOOSTING BUTYRATE AND HYDROGEN PRODUCTION IN ACIDOGENIC FERMENTATION OF FOOD WASTE AND SEWAGE SLUDGE MIXTURE: A PILOT SCALE DEMONSTRATION”, doi: https://doi.org/10.1016/j.jclepro.2023.136919

[4] “COUPLING MIXED CULTURE FERMENTATION AND PHOTO-FERMENTATION FOR BIO-H2 RECOVERY: PRELIMINARY ASSESSMENT OF THE FERMENTATION YIELDS AND PNSB GROWTH ON FERMENTATIVE BROTH” doi: 10.3303/CET2399008

[5] “SOLID OXIDE FUEL CELLS FUELLED WITH BIOGAS: POTENTIAL AND CONSTRAINTS” doi: https://doi.org/10.1016/j.renene.2018.11.028

[6] “NANOSIZE ZR-METAL ORGANIC FRAMEWORK (UIO-66) FOR HYDROGEN AND CARBON DIOXIDE STORAGE” doi:10.1016/j.cej.2012.01.104

[7] “CATECHOL REDOX COUPLE FUNCTIONALIZED METAL-ORGANIC FRAMEWORK UIO-66-NH2 AS AN EFFICIENT CATALYST FOR CHROMIUM ION SENSOR IN WATER SAMPLES” doi: https://doi.org/10.1039/C2CC35565E

[8] “CONTROL OF FRAMEWORK INTERPENETRATION FOR IN SITU MODIFIED HYDROXYL FUNCTIONALISED IRMOFS” doi: https://doi.org/10.1039/C2CC35565E

The Effect of Policy Instruments on the Diffusion of Renewable Hydrogen among Energy Intensive Industries: An Evolutionary Game Model of Complex Networks

Negar Namazifard[*1,2,3], Harrie Wigerinck[1], Jorge Andrés Moncada[1,2], Pieter Vingerhoets[2,3], Erik Delarue[1,2]

[1]Division of Applied Mechanics and Energy Conversion (TME), Department of Mechanical Engineering, KU Leuven, Celestijnenlaan 300 (box 2421), 3001 Leuven, Belgium
[2]EnergyVille, Thor Park 8310, 3600 Genk, Belgium
[3]Flemish Institute for Technological Research (VITO), Boeretang 200, B-2400 Mol, Belgium

Introduction

Renewable hydrogen is seen as a key element in the EU strategy to reduce the Greenhouse gas (GHG) emissions of various sectors, including industry. Europe is targeting 20 Mt clean hydrogen by 2030 for a hybrid and cross-sector green energy transition [1]. To achieve this ambitious goal, rapid infrastructure development is essential for large-scale hydrogen production, transportation, storage, and utilization [1]–[5].

However, the hydrogen market is still in its early stages of development, and there is a high degree of uncertainty surrounding its production and transport needs [6]. The absence of a clear regulatory framework and the lack of risk protection for investors are significant barriers to the development of investment plans for renewable hydrogen production, consumption, and transportation by both industries and gas operators, creating the well-known "chicken-egg problem". On one hand, without certain plans for hydrogen production and infrastructure, investments in the deployment of low-carbon hydrogen consumption processes by industries remain very risky. On the other hand, without any market interest, there will not be enough incentive for the deployment of a hydrogen network.

Although some gas Transmission System Operators (TSOs) in Europe such as Fluxys [7] and Gasunie [8] have already taken the first step and developed their national hydrogen backbone plans by identifying the potential market interest in different industrial zones within their respective countries, the progress in other European countries may differ. Therefore, there is a compelling need to analyze the factors and policy instruments that affect the diffusion of renewable hydrogen demand in heavy industries and its impact on the investment decisions of gas operators.

Peer effects play an important role in industrial innovation diffusion and financial decisions. When companies make decisions, especially in the context of incomplete information, industry competition, and government policies, they often look to their peers and competitors for guidance and opportunities [9]–[12]. In addition, the differential payoffs (e.g., income differences) are another deriving factor of the green technology diffusion among industries [13]–[15]. That is when, companies attempt to maximize their own profit with bounded rationality and imperfect information and their strategy could be greatly impacted if the peer enterprises achieve higher or lower benefits after adopting or rejecting green innovations, respectively.

* Corresponding author: negar.namazifard@vito.be

To address the above-mentioned factors, in recent years, researchers in energy and environment fields have shown increasing interest in building the so-called network-based evolutionary game models for analyzing the low-carbon or green product diffusion among enterprises that can potentially use various strategies. Evolutionary Game Theory (EGT) focuses on the dynamic behavior of decision-makers with bounded rationality over time and it usually assumes that all individuals can interact with each other randomly in a well-mixed manner that is not necessarily in line with reality. However, EGT in complex networks expands the traditional framework by considering network structures where interactions among individuals are defined under a determined typology [14]–[16]. There are several studies in the literature focusing on the diffusion behavior of the industries in the adoption of green or low-carbon innovations. Zhang et al. investigated the effect of Chinese low-carbon policies on the diffusion of green technologies among alliance-based manufacturers with complex network interactions. Fan et al. emphasize on the role of consistency pressure [†] among peer enterprises alongside the learning behavior in the diffusion of green innovation [14]. Shi et al. explore the evolution of the diffusion of low-carbon technology and products in both the supply and demand sides, respectively [17].

However, the dynamics of the investment decisions on the transmission network side and their corresponding effect on the green technology adoption rate of market participants (industries) which is highly important in the emerging markets (e.g., renewable hydrogen) is still missing and needs to be further investigated. Therefore, the purpose of this study is to develop a two-level EGT model and investigate the effect of policy instruments (e.g., carbon prices and, hydrogen subsidies) on the counter correlation of the renewable hydrogen diffusion among industries and the evolution of investment decisions by gas TSOs for the development of hydrogen networks.

Methodology

The model structure comprises two interacting layers: the industry layer and the gas TSO layer (see Figure 1). The industry layer holds the connection among the energy intensive industries (that can potentially adopt renewable hydrogen in their processes) through a complex network reflecting the possibility of interactions among the companies within the same subsector (among e.g., steel, fertilizers, refineries, glass, cement). The gas TSO layer is inhabited by the gas transmission operator as a regulated monopoly who can invest or not in renewable hydrogen pipelines contingent upon the market interest that they perceive from the industrial layer. The industries are represented as profit maximizers while, the gas TSO's objective is to recover their investment and operational costs by collecting tariffs from the connection points (industries).

Following the work of Fab et al. the interaction among industries can be based on both the 1) imitation effects due to the consistency pressure and 2) demonstration effects based on learning behaviors following the payoff differences (the difference between the profits of an industry who adopts green innovation and the one who did not adapt) [14]. In the imitation effect path, when the neighboring industries that adopt a certain strategy in the complex network reaches a specific threshold, the industry will experience the pressure of consistency and start to imitate the strategy based on equation (1) (inspired by the DeGroot model) [18].

(1)

$$p_i(t) = \frac{T_{ii}(t)G_i(t) + \sum_{j=1}^{m} T_{ij}(t)G_j(t)}{T_{ii}(t) + \sum_{j=1}^{m} T_{ij}(t)}$$

[†] Consistency pressure is a driving factor for the imitation behavior among peer enterprises. It makes enterprises take irrational decisions only due to imitating the choices of their surrounding peers in a complex network

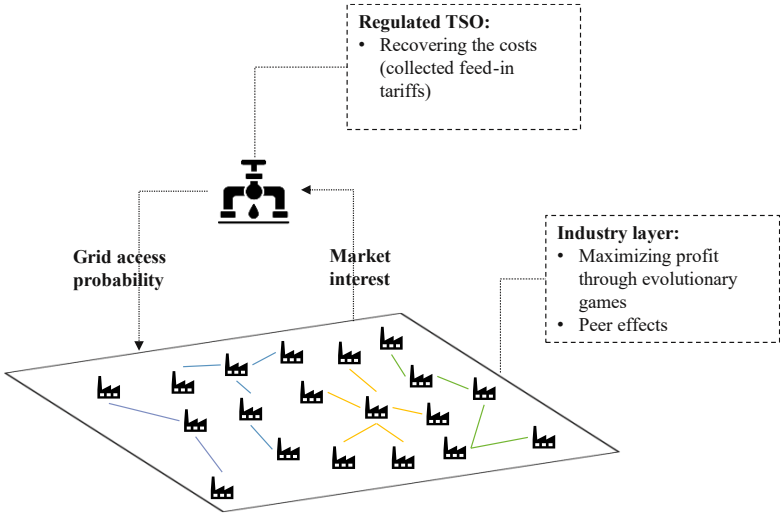

Figure 1 Model structure

Where, $T_{ij}(t)$ represents the weight or impact of industry j on industry i at time t and $G_i(t)$ represents the strategy taken by industry i at time t in terms of adopting or rejecting the green technology.

(2)

$$G_i(t) = \begin{cases} 1, Industry\ i\ adopts\ the\ green\ technology \\ 0, Industry\ i\ rejects\ the\ green\ technology \end{cases}$$

If $T_{ij}(t)$ is higher or lower than a certain threshold, then industry i will be directly affected by the imitation pressure for the next step's decision as shown in equation (3). Nevertheless, if $T_{ij}(t)$ is between the lower and upper bound, industry i will be affected only by demonstration effect for the next time step. An upper and lower bound represents the tendency of interconnected industries for adopting the green technology is high or low enough, respectively.

(3)

$$G_i(t+1) = \begin{cases} 1 & p_i \in [U, 1] \\ 0 & p_i \in [0, L] \\ P(i \to j) & p_i \in [L, U] \end{cases}$$

In the demonstration effect path, industry i starts to randomly select a peer company j among its interconnections in the complex network with probability formula represented in equation (4) meaning that the peer company with higher social influence (e.g., large companies with higher production capacities in this case) are more likely to be selected for the payoff comparison. If the two industries have different strategies in adoption of renewable hydrogen at time step t, the state of industry i may be updated based on the probability formula suggested by Wang and Zheng (2019). In this study, the grid access signal coming from the TSO layer is an external factor for the industries and may also affect the probability of their adoption strategy during the demonstration path. Therefore, we improve the evolutionary game formula

suggested by Wang and Zheng (2019) by considering a grid access coefficient (α) in the decision-making process of enterprises (equation 5). This coefficient can be considered as the probability of the investment by the gas grid operator. The larger the value of α, the stricter the TSO is in investing in hydrogen pipelines. $\alpha = 1$ means that the gas TSO will certainly invest on a hydrogen backbone in the future and industries will for sure have access to a hydrogen grid. In contrast, $\alpha = 0$ means that the TSO will have no plan and outlook for a hydrogen network across the country.

(4)

$$p_{ij} = \frac{A_{ij}(t)}{\sum_{k \in m} A_{ik}(t)}$$

(5)

$$P(i \to j) = \begin{cases} \alpha & U_i \le 0.5U_j \\ (U_j - U_i)a_t/U_i & 0.5U_j < U_i < U_j \\ 0 & U_i \ge U_j \end{cases}$$

Where, U_i and U_j are the payoffs (in this case, profits) of industry i and its peer j, respectively. Table 1 illustrates the payoff matrix of two industries which includes their revenues from selling their final products (π^a, π^r) the investments required for the new technologies (IC^a_{ht}), cost of purchasing renewable hydrogen and fossil gas fuel (VC^a_{hg}, VC^r_{fg}), hydrogen and natural gas grid tariffs (TR^a_{hg}, TR^r_{fg}) , carbon taxes (T^r) for the companies that rejected the green innovation and the revenues from selling the output products and, governmental fixed subsidies for the industries that adapt the green innovation.

Table 1 Payoff matrix of the industrial layer

		Industry 2	
		Adopt	Reject
Industry 1	Adopt	1) $\pi^a + S^a - IC^a_{ht} - VC^a_{hg} - TR^a_{hg}$; 2) $\pi^a + S^a - IC^a_{ht} - VC^a_{hg} - TR^a_{hg}$	1) $\pi^a + S^a - IC^a_{ht} - VC^a_{hg} - TR^a_{hg}$; 2) $\pi^r - T^r - VC^r_{fg} - TR^r_{fg}$
	Reject	1) $\pi^r - T^r - VC^r_{fg} - TR^r_{fg}$; 2) $\pi^a + S^a - IC^a_{ht} - VC^a_{hg} - TR^a_{hg}$	1) $\pi^r - T^r - VC^r_{fg} - TR^r_{fg}$; 2) $\pi^r - T^r - VC^r_{fg} - TR^r_{hg}$

From a TSO point of view, the external factor that affects the evolution of its investment decision on the construction of the hydrogen network is basically the level of market interest of the industrial consumers. In other words, higher renewable hydrogen adoption rates (β) in the industrial layer leads to higher probability of the investment (α) by the gas TSO in the future hydrogen network. These two variables of the model are correlated with each other by the share of collected tariffs by the gas TSO to the total requited initial investment for the development of the hydrogen backbone as represented in equation (6).

(6)

$$\alpha = \frac{\beta . N . TR^a_{hg}}{IC_{tso}}$$

In later stages, different potential government policy instruments are applied on both the industrial layer and TSO layer to analyze their effectiveness in promoting the diffusion of renewable hydrogen. These policies include carbon prices for the industries, inter-temporal cross-subsidies[‡], targets on the share of hydrogen consumption in industries set by the Renewable Energy Directive (RED III) [20], and green innovation subsidies.

Discussion

This study is still in the early stages of the model development. Nevertheless, the following results are expected from our analysis:

- The dynamics of renewable hydrogen diffusion in the industrial layer and investment decisions in the TSO layer throughout time taking into account their potential interactions;
- The evolution in the marginal effect of the "market interest" on the TSO layer and the "grid access" on the industrial layer;
- The effectiveness of different policies on the adoption rate exploring how one policy can overweigh the other in terms of increasing the diffusion of the renewable hydrogen;
- The correlation between incremental intensity of policies (e.g., subsides and carbon prices) and their marginal effectiveness;
- The extend in which the diffusion of renewable hydrogen is sensitive to the change of production capacities of various industries throughout time.

Conclusions

This study develops a novel agent-based model to analyze the dynamics of the investment decisions in both the industrial and TSO layers under the principles of evolutionary game theory in complex networks. Unlike existing studies, the bidirectional interactions of industries with the transmission system operator in an emerging market (renewable hydrogen) is integrated into this model to address the so-called "chicken-egg" problem as one of the main barriers of the future hydrogen market development. Without effective policy measures, industries may not have the motivation of adopting hydrogen infrastructure as they face additional costs compared to their baseline operations. Therefore, proactive policy implementation such as environmental taxes (carbon prices) and investment subsidies are crucial to create a supportive environment that encourages the adoption of renewable hydrogen among industries.

‡ To avoid undue and excessive cross-subsidies among first and future users of hydrogen networks, Member States may allow hydrogen network operators to spread network development costs over time, by ensuring that future users pay part of the initial costs [19]

References

[1] Commission staff working document implementing the repower eu action plan: investment needs, hydrogen accelerator and achieving the bio-methane targets. 2022. Accessed: Sep. 16, 2023. [Online]. Available: https://eur-lex.europa.eu/legal-content/EN/TXT/?uri=SWD%3A2022%3A230%3AFIN

[2] 'EHB-Analysing-the-future-demand-supply-and-transport-of-hydrogen-June-2021-v3.pdf'. Accessed: Aug. 24, 2023. [Online]. Available: https://www.ehb.eu/files/downloads/EHB-Analysing-the-future-demand-supply-and-transport-of-hydrogen-June-2021-v3.pdf

[3] 'ehb-report-220428-17h00-interactive-1.pdf'. Accessed: Aug. 24, 2023. [Online]. Available: https://www.ehb.eu/files/downloads/ehb-report-220428-17h00-interactive-1.pdf

[4] 'European-Hydrogen-Backbone-April-2021-V3.pdf'. Accessed: Aug. 24, 2023. [Online]. Available: https://www.ehb.eu/files/downloads/European-Hydrogen-Backbone-April-2021-V3.pdf

[5] '2020_European-Hydrogen-Backbone_Report.pdf'. Accessed: Aug. 24, 2023. [Online]. Available: https://www.ehb.eu/files/downloads/2020_European-Hydrogen-Backbone_Report.pdf

[6] 'Green hydrogen for industry: A guide to policy making', p. 68.

[7] 'Hydrogen: Preparing to build the network'. Accessed: Sep. 16, 2023. [Online]. Available: https://www.fluxys.com/en/about-us/energy-transition/hydrogen-carbon-infrastructure/hydrogen_preparing-to-build-the-network

[8] 'Dutch national hydrogen network launches in Rotterdam', Gasunie. Accessed: Sep. 16, 2023. [Online]. Available: https://www.gasunie.nl/en/news/dutch-national-hydrogen-network-launches-in-rotterdam

[9] M. T. Leary and M. R. Roberts, 'Do Peer Firms Affect Corporate Financial Policy?', The Journal of Finance, vol. 69, no. 1, pp. 139–178, 2014, doi: 10.1111/jofi.12094.

[10] M. Machokoto, D. Gyimah, and C. G. Ntim, 'Do peer firms influence innovation?', The British Accounting Review, vol. 53, no. 5, p. 100988, Sep. 2021, doi: 10.1016/j.bar.2021.100988.

[11] H. Xiong, D. Payne, and S. Kinsella, 'Peer effects in the diffusion of innovations: Theory and simulation', Journal of Behavioral and Experimental Economics, vol. 63, pp. 1–13, Aug. 2016, doi: 10.1016/j.socec.2016.04.017.

[12] S. Kelchtermans, D. Neicu, and P. Teirlinck, 'The role of peer effects in firms' usage of R&D tax exemptions', Journal of Business Research, vol. 108, pp. 74–91, Jan. 2020, doi: 10.1016/j.jbusres.2019.09.059.

[13] Y. Shi, Z. Wei, M. Shahbaz, and Y. Zeng, 'Exploring the dynamics of low-carbon technology diffusion among enterprises: An evolutionary game model on a two-level heterogeneous social network', Energy Economics, vol. 101, p. 105399, Sep. 2021, doi: 10.1016/j.eneco.2021.105399.

[14] R. Fan, Y. Wang, F. Chen, K. Du, and Y. Wang, 'How do government policies affect the diffusion of green innovation among peer enterprises? - An evolutionary-game model in complex networks', Journal of Cleaner Production, vol. 364, p. 132711, Sep. 2022, doi: 10.1016/j.jclepro.2022.132711.

[15] L. Zhang, L. Xue, and Y. Zhou, 'How do low-carbon policies promote green diffusion among alliance-based firms in China? An evolutionary-game model of complex networks', Journal of Cleaner Production, vol. 210, pp. 518–529, Feb. 2019, doi: 10.1016/j.jclepro.2018.11.028.

[16] R. Fan, L. Dong, W. Yang, and J. Sun, 'Study on the optimal supervision strategy of government low-carbon subsidy and the corresponding efficiency and stability in the small-world network context', Journal of Cleaner Production, vol. 168, pp. 536–550, Dec. 2017, doi: 10.1016/j.jclepro.2017.09.044.

[17] Y. Shi, Z. Wei, M. Shahbaz, and Y. Zeng, 'Exploring the dynamics of low-carbon technology diffusion among enterprises: An evolutionary game model on a two-level heterogeneous social network', Energy Economics, vol. 101, p. 105399, Sep. 2021, doi: 10.1016/j.eneco.2021.105399.

[18] Y. Dong, M. Zhan, G. Kou, Z. Ding, and H. Liang, 'A survey on the fusion process in opinion dynamics', Information Fusion, vol. 43, pp. 57–65, Sep. 2018, doi: 10.1016/j.inffus.2017.11.009.

[19] '08_CA_H2_EN.pdf'. Accessed: Sep. 19, 2023. [Online]. Available: https://www.europarl.europa.eu/meetdocs/2014_2019/plmrep/COMMITTEES/ITRE/DV/2023/02-09/08_CA_H2_EN.pdf

[20] 'Revision of the Renewable Energy Directive: Fit for 55 package'.

The impact of decarbonising the iron and steel industry on European power and hydrogen systems

Annika Boldrini*[1,2], Derck Koolen[2,3], Wina Crijns-Graus[1], Machteld van den Broek[4]

[1]Copernicus Institute of Sustainable Development, Utrecht University. Utrecht, Netherlands
[2]European Commission, Joint Research Centre, Directorate for Energy, Transport and Climate. Petten, Netherlands
[3]School of Economics, Utrecht University. Utrecht, Netherlands
[4]Faculty of Science and Engineering, University of Groningen. Groningen, Netherlands

Introduction

The transition of the power sector is widely regarded as a cornerstone pillar to achieve the ambition of the European Union (EU) to become climate neutral by 2050 [17]. Where most of the EU's energy demand is today met by using fossil fuels, the electrification of the industry, buildings and transport sectors in combination with an increased scaling- and speeding-up of renewable energy in the power sector reduces dependence on foreign energy sources and energy-related greenhouse gas (GHG) emissions. The industrial sector was responsible in 2021 for almost 21% of carbon dioxide (CO_2) emissions in the EU [20], of which almost a quarter derived from the iron and steel industry (ISI). Emissions in the sector are usually considered hard-to-abate, mainly due to the high heat requirements, using carbon as a process input, as well as low profit margins, high capital intensity, long asset life, and trade challenges [12]. While various technologies may help producers in increasing energy efficiencies and cutting CO_2 emissions, a deep decarbonisation of the sector is expected to rely on new technologies [8], mainly employing hydrogen (H_2) for the reduction of iron ore as substitute to carbon [14]. While offering great potential benefits in reducing ISI's process emissions, the H_2-based core processes has specific electricity use per tonne of steel 35 times higher than the traditional coal-based production methods [4].

The demand for electricity and H_2 by the ISI is likely to experience a significant increase by 2030. This rapid surge in electricity demand poses additional challenges for the transitioning power sector, still focusing on expanding and integrating renewable power generation. While the accelerated electrification of the ISI leads to reduced emissions within the industry, it also risks to be counter effective if not properly supported by an expansion of renewable power supply. If the additional demand for electricity and electrolytic H_2 is primarily supplied by fossil-based sources, it may result in an increase of indirect CO_2 emissions from the power system. Previous studies have either targeted the long-term transition of the ISI through high temporal resolution unit commitment and economic dispatch (UCED) models operating with large shares of renewable power capacities [15, 21], or examined the short-term transition of the ISI without conducting modelling analysis neither considering H_2 demand for steel [10, 2], thus without the updated decarbonisation targets of European steel manufacturers.

Therefore, this study aims at assessing the short-term decarbonisation of the European ISI and the effect on the power system through high-temporal resolution modelling, by answering to the following research question: *how does the short-term transition to a low-carbon ISI affect the European power system operations and its CO_2 emissions?*

Method

To answer the research question, this study first develops scenarios that reflect various levels of decarbonisation of the ISI in 2030 to define the energy demand and direct CO_2 emissions reduction. Second, it performs high temporal resolution power system modelling in 2030 to evaluate the impact of various level of decarbonisation of the ISI on indirect, power generated CO_2 emissions, and marginal electricity prices.

*Corresponding author: a.boldrini@uu.nl

Table 1: Assumptions applied to develop 2030 steel scenarios.

Scenarios	Share of secondary production	Deployment of low-carbon primary route	Fuel shift	Fuel for DRI
Base	45%	Reflecting operating pilots and approved projects [14]	33% of natural gas used for finalisation processes shifts to electricity	Natural gas and H_2
Pace	45%	Reflecting all announced projects [14]	33% of natural gas used for finalisation processes shifts to electricit	All H_2
Accelerated	47%	Reflecting the refurbishment needs of existing blast furnaces [7] assuming 25 years of lifetime [1] and CCUS projects applied to BF-BOF with timeframe beyond 2030	33% of natural gas used for finalisation processes shifts to electricit	All H_2

Table 2: Overview of sub-scenarios differentiated by (*i*) generation capacities as foreseen by the MIX-H2 – i.e., UCED problem – and with capacity expansion – i.e., UCED problem with capacity expansion – and (*ii*) low and high natural gas and *H_2 other supply* prices. All other parameters of the energy system are retrieved from the 2030 MIX-H2 scenario.

2030 MIX-H2		(*ii*) Low prices	(*ii*) High prices
(*i*)	UCED problem	*Reference* *Base* *Pace* *Accelerated*	*Reference_high* *Base_high* *Pace_high* *Accelerated_high*
(*i*)	UCED problem with capacity expansion	*Reference_EXP* *Base_EXP* *Pace_EXP* *Accelerated_EXP*	*Reference_high_EXP* *Base_high_EXP* *Pace_high_EXP* *Accelerated_high_EXP*

The scenario development is carried out by identifying decarbonisation pathways for the ISI in 2030, defined by the extent to which low-carbon steel technologies replace existing BF-BOF capacity, currently the most widely adopted but also most polluting production route. The scenarios take into account recent projects development documented by the Green Steel Tracker [14] and lifespan of existing assets. As many of the announcements are non-binding, the advancement of these projects have a certain degree of uncertainties that is reflected in our three scenarios. Table 1 summarises the assumptions applied for the scenarios development. Based on the steel production by manufacturing technology, the energy demand for electricity and H_2 is calculated by applying country and technology-specific energy intensities. For currently used technologies, energy intensities are derived following the method developed by Koolen and Vidovic [13]. Regarding new steel-making technologies, we apply values and assumptions from literature [19, 11, 23].

We build the analysis on the European energy system by using the electricity and H_2 demand per scenario and country as input for modelling. We use the METIS model to simulate the effect of the decarbonisation of the ISI on EU power system dynamics. *METIS* is a mathematical model simulating the electricity system operations at country-level through a UCED problem [18, 3]. We simulate the effect of the steel scenarios in 2030. The steel energy demand complements the MIX-H2 context developed by De Felice [6], whose parameters are use for all parts of the modelled energy system but the ISI. The results of our scenarios are compared to a *Reference* case that reflects a conservative decarbonisation pathway as foreseen by the POTEnCIA (Policy Oriented Tool for Energy and Climate Change Impact Assessment) Central Scenario [16].

Furthermore, we define a set of sub-scenarios to run sensitivity analyses on the following parameters: (*i*) the availability of renewable electricity generation and electrolyser capacity, which preliminary results have shown to be critical factors in delivering cost-effective renewable energy supply; and (*ii*) the prices of natural gas and H_2 for supply other than electrolysis, to reflect the price sensitivities of these carriers[1] observed in recent years in the European energy markets [9]. Table 2 reports an overview of all sub-scenarios.

Results

Steel production by technology and their energy demand in 2030 are shown in Figure 1 and 2, respectively. Compared to 2018, *Base* foresees an increment of electricity and H_2 demand of about

[1] H_2 is currently mainly produced from natural gas in the EU, thus we assume the price of H_2 as produced via steam methane reforming (SMR).

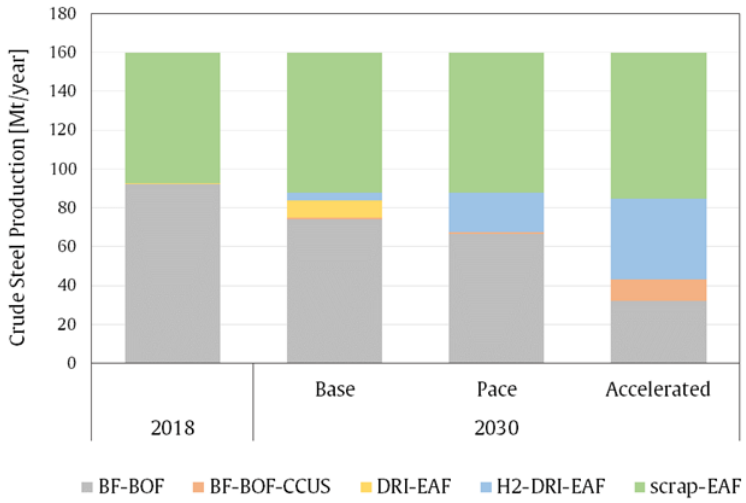

Figure 1: EU steel production by technology in 2018 and in 2030 as foreseen by the steel scenarios. Abbreviations: BF-BOF blast furnace basic oxygen furnace, BF-BOF-CCUS blast furnace basic oxygen furnace with carbon capture utilisation and/or storage, DRI-EAF natural gas-based direct reduction of iron and electric arc furnace, H2-DRI-EAF hydrogen-based direct reduction of iron and electric arc furnace, scrap-EAF recycled scrap steel processing in electric arc furnace.

11 and 8 TWh_{HHV}, respectively. *Pace* foresees a sharp increase in H_2 demand, almost five times larger than in *Base* and a 5% increase of electricity demand compared to *Base*. *Accelerated* further stretches the electricity demand by 15% and more than doubles the H_2 demand compared to *Pace*. If H_2 is produced via electrolysis, power demand further increases in all scenarios.

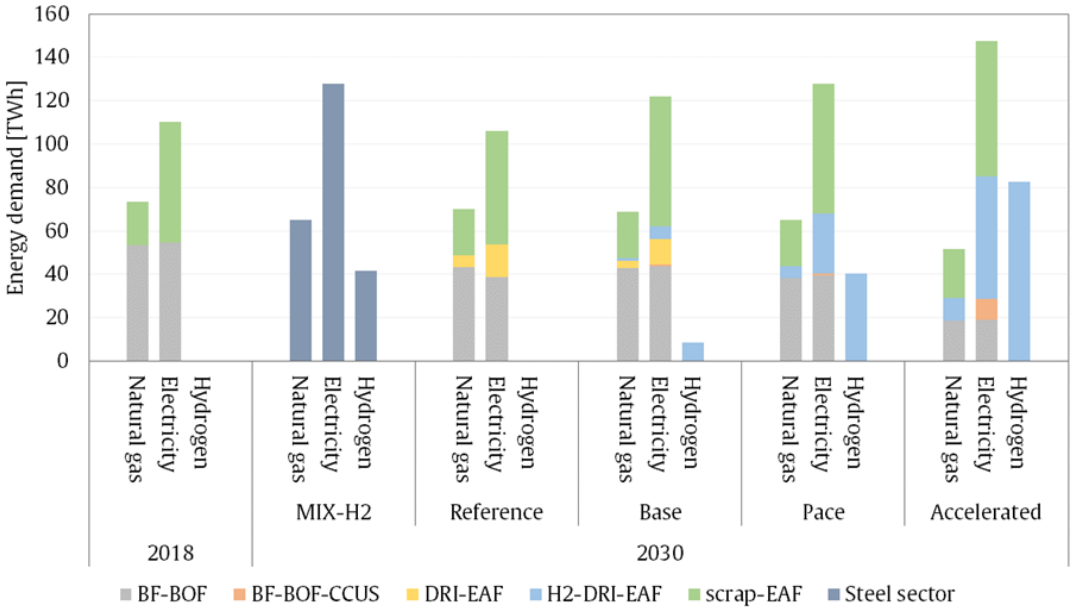

Figure 2: Energy demand of the EU ISI in 2018, MIX-H2, Reference and the steel scenarios. MIX-H2 is shown without differentiation among production route because the information is not available. Energy demand for natural gas and H_2 is expresses in higher heating value (HHV). Technologies abbreviations are reported under Figure 1.

For the sake of conciseness, we exclude from this abstract a details assessment of the power system operation to give focus on the net CO_2 emissions under all scenarios reported in Table 2. Figure 3 shows the absolute results of CO_2 emissions for all sub-scenarios and for 2018, together with the power system operational costs variation compared to *Reference*. As the full range of options to supply H_2 was not taken into account in this study, Figure 3 shows in patterned grey the CO_2 emission as if

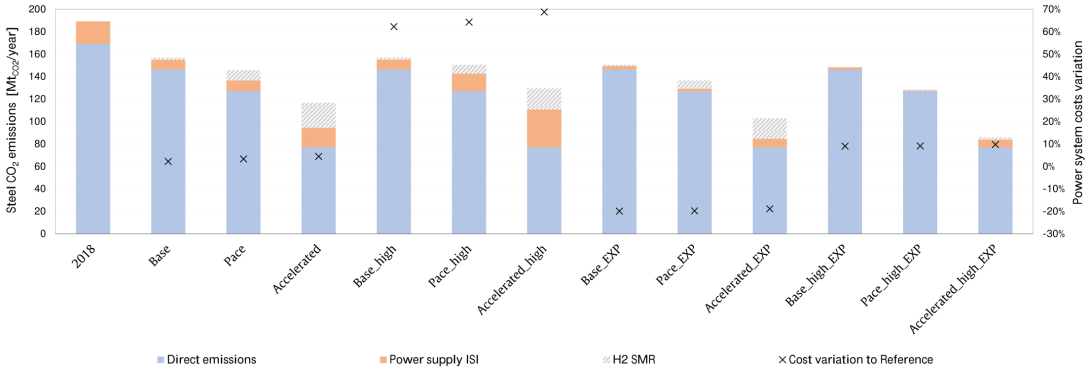

Figure 3: Direct and indirect CO_2 emission in the EU of steel scenarios compared to 2018, with and without capacity expansion. The secondary axis reports the variation of operational power system costs and annualised investment of the additional renewable and electrolyser capacities deployed in the capacity expansion scenarios, compared to Reference (97 *B€*).

H_2 was supplied via SMR. Other plausible options such as SMR with CCUS or imported green H_2 would have lower or null H_2 emissions, thus fitting within the range of the patterned grey stacked columns. All scenarios present an overall reduction of CO_2 emissions compared to 2018 mainly due to direct emissions reduction of 14%, 25% and 54% in *Base*, *Pace* and *Accelerated*, respectively. Without renewable capacity expansion, there is an increase in indirect as electricity demand grows from *Base* to *Accelerated*. However, the level of ISI indirect emissions remains below the values recorded in 2018 even while supplying more electricity for almost all sub-scenarios. This can be attributed to the already large deployment of renewable power generators foreseen by the MIX-H2 scenario. In *Accelerated_high*, high natural gas and *H_2 other supply* prices lead to a larger use of coal- and lignite-based power plants, resulting in indirect emissions in 2030 much almost 70% higher than in 2018. This also comes at the cost of almost 70% increase of power system costs. Overall, five countries are responsible for 74% of total EU indirect CO_2 emissions. These are, in order of contribution, Poland, Germany, Italy, Czech Republic and Romania. The indirect CO_2 emissions are largely and cost-effectively reduced by up to 96% in *_EXP* scenarios. Furthermore, system costs increase by a maximum of only 10% even when faced with *high prices* scenarios.

Discussion

This study assesses the results' robustness by running sub-scenarios that involve varying fuel prices, and renewable and electrolyser capacities. Nonetheless, the study presents limitations arising from the uncertainty encompassing numerous parameters related to the future of the European ISI, such as production and circularity levels in 2030. Examining our results in a broader context, *Accelerated_high_EXP* and *Pace_high_EXP* allocate 20 *GW* and 10 *GW* of electrolyser capacity to steel-making, which correspond to half and a quarter of total electrolyser capacity foreseen by MIX-H2 in 2030, respectively. With low gas prices, these numbers reduce to 9 *GW* and 4 *GW* for *Accelerated* and *Pace*. *Pace*, which is in line with MIX-H2, foresees 10% of the total MIX-H2 electrolyser capacity allocated to supply the ISI.

Since the energy crisis there has been a stronger push by the EU to move away from the dependency on foreign countries for natural gas by increasing the renewable energy targets and H_2 production and import. The price applied for non-electrolytic H_2 – e.g., imported, produced as grey or blue H_2 – is between 2 and 10 $€/kg_{H_2}$, which is in line with the price of green H_2 expected by currently developing H_2 hubs around the world [5]. Therefore, the study provides realistic insights into the competitiveness of future locally produced H_2. Lastly, in line with the study of Toktarova *et al.* [21], our findings puts into discussion the strategy of brownfield investments for new steelmaking technologies when affordable H_2 is not available or when the price of CO_2 allowances increases. However, as suggested by Vögele *et al.* [22], European steel-making is already among the most energy efficient and with lower CO_2 emissions globally. Therefore, relocation of production outside of the EU could potentially increase energy consumption and limit global CO_2 emissions reduction.

Conclusion

Decarbonising the ISI involves the application of direct or indirect electrification technologies – i.e., H_2 produced via electrolysis. As part of the ISI energy input electrifies, the impact on the power system becomes more pronounced. Many steel manufacturer plan to start the operation of new low-carbon technologies, such as H_2-based direct reduction of iron (H_2-DRI-EAF) by 2030. A this point in time, the power sector will not have fully transitioned to a low-carbon system. This study aims at assessing the consequences of a short-term increase of ISI electricity demand by developing nine scenarios that reflect various levels of decarbonisation, fuel prices, and renewable power and electrolyser capacities. Through modelling, this work evaluates the impact of the transformation of the ISI in 2030 on the European power and H_2 system in terms of generating technologies, marginal prices and CO_2 emissions.

The findings of this study indicate that the European power system, as foreseen by the MIX-H2 scenario for 2030, is capable of accommodating an advanced transition of the ISI, represented by our *Pace* scenario. In the *Pace* scenario, the ISI achieves a direct CO_2 emissions reduction of 25% compared to 2018, thanks to the adoption of electrified processes that increase electricity and H_2 demand, respectively, by 17 TWh and 40 TWh_{HHV} at EU-level. Nonetheless, indirect CO_2 emissions decrease by one-third to one-half compared to 2018, considering a range of fuel prices, despite the 16% increase in electricity demand. Electrolytic H_2 supply remains below 25% of demand, even when the price of alternative supplies - e.g., import, produced by steam methane reforming (SMR) - reaches 10 €/kg_{H_2}. On the other hand, an *Accelerated* transition of the European ISI, which results in a substantial 54% reduction of CO_2 direct emissions, can cause an increment of indirect emissions up to 69%. This increase occurs because the additional demand is mainly met by fossil-based power plants.

The study further demonstrates that a drastic reduction of indirect CO_2 emissions can be realised by combining the installation of dedicated renewable capacity alongside the transformation of the ISI. In the *Pace* scenario, 30 and 70 GW of renewable power generators, and 5 and 10 GW of electrolysers are installed with *low* and *high* fuel prices, respectively. That entails that a reduction of indirect CO_2 emissions of over 85%, together with 25% reduction of direct CO_2 emissions compared to 2018, can be achieved by deploying 1.2 and 2.7 GW of renewable power generators, and 200 and 400 MW of electrolysers for each million tonne of steel produced annually with low-carbon technologies. Establishing a cost-effective and low-carbon H_2 supply is crucial to decarbonise the ISI and to facilitate the competitiveness of European steel-makers on the global market. Additional renewable capacity that ensures green steel production is key to avoid CO_2 emissions spill-over and maintaining stable electricity prices.

References

[1] ArcelorMittal. Blast furnace relining has commenced. https://belgium.arcelormittal.com/en/blast-furnace-relining/, accessed on 25-04-2023.

[2] M. Arens, M. Åhman, and V. Vogl. Which countries are prepared to green their coal-based steel industry with electricity? - Reviewing climate and energy policy as well as the implementation of renewable electricity. *Renewable and Sustainable Energy Reviews*, 143:110938, 2021.

[3] R. Bardet, A. Bossavy, M. Chammas, L. Fournié, P. Khallouf, and B. Texier. METIS Technical Note T2 - METIS Power Market Models. Technical Report October, 2016.

[4] A. Boldrini, D. Koolen, W. Crijns-Graus, M. van den Broek, and E. Worrell. The Demand Response Potential in a Decarbonising Iron and Steel Industry: A Review of Flexible Steelmaking. 2023. 10.2139/SSRN.4472250 [Preprint].

[5] Clean Hydrogen Partnership and Mission Innovation. Hydrogen cost and sales prices. https://h2v.eu/analysis/statistics/financing/hydrogen-cost-and-sales-prices, accessed on 15-07-2023.

[6] M. De Felice. *Fit for 55 MIX scenario 2030 (JRC-FF55-MIX-2030) - input data for METIS context.* European Commission, Joint Research Centre (JRC) [Dataset] PID: http://data.europa.eu/89h/d4d59b89-89f7-4275-801a-45ea8957e973, 2022.

[7] Eurofer. European steel in figures - covering 2011-2020. Technical report, 2020.

[8] Z. Fan and S. J. Friedmann. Low-carbon production of iron and steel: Technology options, economic assessment, and policy. *Joule*, 2021.

[9] A. Gasparella, D. Koolen, and A. Zucker. *The Merit Order and Price Setting Dynamics in European Electricity Markets*. Publications Office of the European Union, 2023. JRC134300, 2023.

[10] L. Göransson, M. Lehtveer, E. Nyholm, M. Taljegard, and V. Walter. The Benefit of Collaboration in the North European Electricity System Transition—System and Sector Perspectives. *Energies 2019, Vol. 12, Page 4648*, 12(24):4648, 2019.

[11] S. Jackson and E. Brodal. A comparison of the energy consumption for CO2 compression process alternatives. In *IOP Conference Series: Earth and Environmental Science*, volume 167, 2018.

[12] J. Kim, B. K. Sovacool, M. Bazilian, S. Griffiths, J. Lee, M. Yang, and J. Lee. Decarbonizing the iron and steel industry: A systematic review of sociotechnical systems, technological innovations, and policy options. *Energy Research and Social Science*, 89:2214–6296, 2022.

[13] D. Koolen and D. Vidovic. Greenhouse gas intensity of the EU steel industry and its trading partners. Technical report, Publications Office of the European Union, 2022.

[14] Leadership group for industry transition (LEADIT). Green Steel Tracker. https://www.industrytransition.org/green-steel-tracker/, accessed on 15-03-2022.

[15] S. Lechtenböhmer, L. J. Nilsson, M. Åhman, and C. Schneider. Decarbonising the energy intensive basic materials industry through electrification – Implications for future EU electricity demand. *Energy*, 115:1623–1631, 2016.

[16] L. Mantzos, N.-A. Matei, E. Mulholland, M. Rózsai, M. Tamba, and T. Wiesenthal. *JRC-IDEES 2015*. European Commission, Joint Research Centre (JRC). [dataset]., 2018.

[17] K. Peng, K. Feng, B. Chen, Y. Shan, N. Zhang, P. Wang, K. Fang, Y. Bai, X. Zou, W. Wei, X. Geng, Y. Zhang, and J. Li. The global power sector's low-carbon transition may enhance sustainable development goal achievement. *Nature Communications 2023 14:1*, 14(1):1–14, 2023.

[18] K. Sakellaris, J. Canton, E. Zafeiratou, and L. Fournié. METIS – An energy modelling tool to support transparent policy making. *Energy Strategy Reviews*, 22(August):127–135, 2018.

[19] J. Somers. Technologies to decarbonise the EU steel industry. Technical report, Publications Office of the European Union, 2022.

[20] I. Tiseo. Carbon dioxide emissions from fossil fuel combustion in Europe in 2021, by sector, 2023. Statista. https://www.statista.com/statistics/206115/total-oecd-europe-carbon-dioxide-emissions-by-sector/.

[21] A. Toktarova, V. Walter, L. Göransson, and F. Johnsson. Interaction between electrified steel production and the north European electricity system. *Applied Energy*, 310(November 2021), 2022.

[22] S. Vögele, M. Grajewski, K. Govorukha, and D. Rübbelke. Challenges for the European steel industry: Analysis, possible consequences and impacts on sustainable development. *Applied Energy*, 264:114633, apr 2020.

[23] V. Vogl, M. Åhman, and L. J. Nilsson. Assessment of hydrogen direct reduction for fossil-free steelmaking. *Journal of Cleaner Production*, 203, 2018.

Thermal coupling of methanol steam reformer and high temperature proton exchange membrane fuel cell

Emilija Todorovski[1], Mihael Sekavčnik[1], Mitja Mori[1], Andrej Lotrič*[1]

[1]Faculty of Mechanical Engineering, University of Ljubljana

Introduction

Hydrogen, despite being the most abundant element on the Earth, presents a paradoxical challenge: it does not occur naturally in a free state that can readily serve as a clean energy source. Instead, it necessitates extraction and processing, which can be accomplished through a variety of means. On one hand, it can be sourced sustainably from renewable resources such as biomass and water, aligning with our commitment to minimizing environmental harm. On the other hand, hydrogen can also be derived from non-renewable sources like coal, natural gas, and hydrocarbons, which poses a more significant environmental concern due to their finite nature and associated emissions. The environmental impact varies significantly based on the specific production method [1].

Presently, global hydrogen production is predominantly reliant on fossil fuels, constituting approximately 82% of the total production [2]. This percentage underscores the need for continued research and development efforts to transition towards cleaner, more sustainable hydrogen sources.

Methanol (MeOH), as a hydrogen carrier fuel, presents an attractive solution for addressing key challenges in hydrogen integration within the energy sector. Its chemical structure has a favorable hydrogen-to-carbon ratio at 4:1. With a boiling point of 65 °C, it vaporizes at a temperature comparable to water [3]. Moreover, the absence of robust C-C bonds lowers conversion temperatures compared to other fuels, resulting in reduced energy consumption during hydrogen production. Notably, methanol's liquid state at standard environmental conditions and atmospheric pressure suggests compatibility with existing oil and gas infrastructure for transportation and storage. Producing hydrogen on-site when required can streamline logistical processes and decrease the necessity for high-pressure hydrogen storage [4]. This addresses a significant techno-economic concern associated with hydrogen adoption. Additionally, methanol can be derived from renewable and sustainable raw materials, including municipal solid waste, biomass, biogas from digesters, and captured CO_2 from industrial processes.

In summary, renewable methanol, as a hydrogen carrier, aligns with the broader objectives of achieving a Zero Net scenario and has gained interest for its applications in fuel cell technology.

The advancement of high-temperature proton exchange membrane fuel cells (HT PEMFC) represents a promising solution to address several challenges encountered in low-temperature proton exchange membrane fuel cells (LT PEMFC). HT PEMFCs exhibit the capability to operate at elevated CO concentrations, potentially reaching up to 5 %, which simplifies their usage by relaxing the constraints on the composition of the incoming gas. Consequently, it becomes feasible to directly supply HT PEMFCs with unprocessed

* Corresponding author: andrej.lotric@fs.uni-lj.si

hydrogen-rich reformats, including the product gas from methanol steam reforming, without the need for prior purification.
Furthermore, elevating the operational temperature of these cells raises the prospect of exploiting their exothermic properties, particularly in utilizing waste heat. The thermal integration of an exothermic HT PEMFC stack with an endothermic methanol steam reformer (MSR) and a methanol/water evaporator holds the potential to create a compact unit (figure 1). This unit could effectively utilize methanol/water as fuel while simultaneously generating electricity, marking a significant step toward more efficient and versatile portable energy systems.

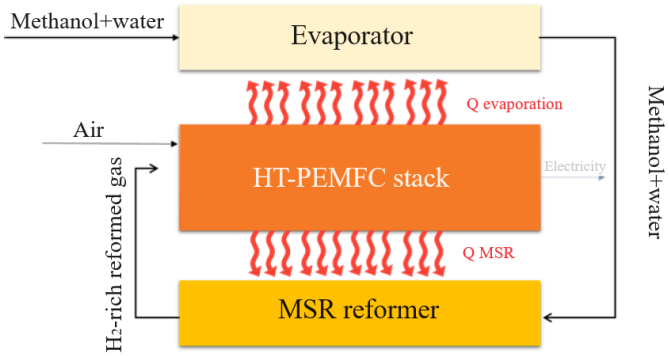

Figure 1: Graphical representation of an integrated system of HT PEMFC stack, MSR reactor and evaporator

Methodology

Theoretical background

The thermochemical processes for converting methanol into hydrogen include methanol steam reforming (MSR), partial oxidation (POM), autothermal reforming (ATRM), and thermal decomposition of methanol (MD). MSR is an endothermic process that employs steam as an oxidant. Among all methanol conversion reactions, MSR yields the highest concentration of hydrogen. The process occurs within a temperature range of 150-350 °C, and its primary reforming products are H_2 and CO_2, followed with the production of low concentrations of CO as well [5].

$$CH_3OH + H_2O = CO_2 + 3H_2 \qquad \Delta H^0_{298\,K} = +49{,}7\,\frac{kJ}{mol}$$

The composition of the reforming gas depends on the reactor's geometry and the catalyst employed. Catalysts utilized in MSR can be categorized into two groups: 1) copper-based catalysts and 2) group 8-10 metal catalysts.
The primary objectives, pursued when designing a MSR reactor, include producing a hydrogen-rich product gas with minimal CO content, achieving a high level of methanol conversion, all while operating at the lowest feasible temperatures.

HT PEMFCs have been developed to address specific challenges present in LT PEMFCs and operate in the temperature range of 120–200 °C. The lower temperature limit is to avoid

the appearance of any liquid water in the system while the upper limit is associated with pronounced degradation. To overcome issues related to humidity and temperature stability of the Nafion membrane, HT PEMFCs often employ a polybenzimidazole (PBI) membrane doped with phosphoric acid (PA) [6]. In this configuration, PA serves as the proton carrier, allowing for operation at higher temperatures. This higher temperature operation offers the advantage of accommodating higher CO content compared to LT PEMFCs, with CO resistance increasing to 3–5% (2000 times that of LT PEMFCs). This enables the use of locally produced reformate gas from MSR reaction, without any pre-cleaning step.

The genesis of the concept behind this work lies in the observed convergence of the operational temperature ranges of the MSR reactor, the HT PEMFC, and the methanol-water vaporizer (figure 2 (left)). The HT PEMFC's exothermic operation releases heat that can potentially fuel the endothermic MSR process. Furthermore, an adequate amount of heat can be generated to evaporate the methanol/water mixture prior to its entry into the MSR reactor.

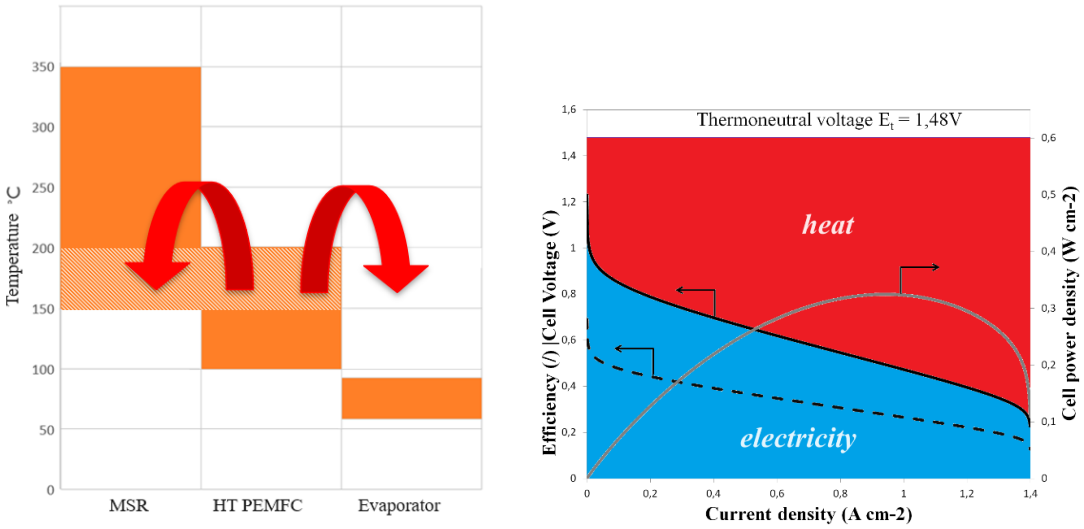

Figure 2: (left) Operating temperature ranges of MSR reactor, HT PEMFC, and evaporator, (right) the relationship between released heat and electricity production based on the polarization curve

The primary challenge we encounter here pertains to the trade-off between the efficiency and heat generated by the HT PEMFC stack. Figure 2 (right) illustrates the distribution of waste heat and electricity production along the polarization curve, power curve, and efficiency curve. The upper limit is represented by the thermoneutral voltage, signifying the total available energy (reaction enthalpy or in other words heating value of hydrogen). The portion of this energy - that can be converted into electricity - constitutes exergy or Gibbs free energy (the blue area on the graph), while the remaining part (the red area) represents anergy, denoting the released waste heat, which, in our case, is useful heat. The production of waste heat is directly correlated with polarization losses. It is now evident that increased voltage losses lead to greater heat generation.
Our objective is to identify the optimal operating range while maximizing the overall system efficiency.

Experimental setup

The experimental setup is depicted in figure 3. After the HT PEMFC/MSR/vaporizer system integration, a prepared mixture of MeOH and water will be introduced into the system using a syringe pump. For the gas reactants (air and H_2) mass flow controllers (MFCs) will be used. For the characterization of the HT PEMFC stack, an electronic load will be used to measure and analyze the stack's electrical performance and characteristics. For individual characterization of both cells, additional voltage measurements will be conducted for each of them. By comparing the online voltage measurements of both HT PEMFCs, it will be possible to determine if both cells are operating under similar conditions.

The system's startup and initial heating will be accomplished with the assistance of four electric heaters and the use of H_2/air for reactants. Initiating with pure H_2 aids in activating the HT PEMFC stack and the MSR catalyst. Once activated and heated to the desired temperature, the system will operate using a MeOH/water mixture and air.

All system components are integrated with the in-house developed LabView application. Achieving thermally self-sustained operation is a primary objective, and one of the key performance indicators involves monitoring the temperature profile inside the system, including the operating temperatures of all the reactors. Local temperature measurements will be conducted using thermocouple probes, while a thermal imaging camera will capture an entire system-level perspective. Aligning these temperatures with the calculated values, which will be modeled prior to experiment, is essential for achieving thermally self-sustained operation.

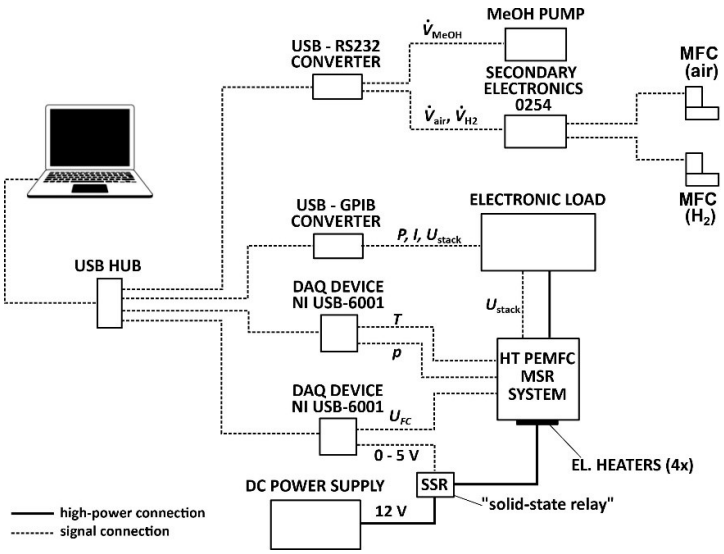

Figure 3: Scheme of the experimental setup

Future work

Evaporator

The introduction of the MeOH/water mixture into the system occurs in a liquid phase, necessitating the use of an evaporator. The temperature range for evaporating the mixture is

lower than operational temperature range of the HT PEMFC stack, and the excess heat will be utilized for this purpose. The system's geometry is determined by the surface area of the used membrane-electrode assemblies (MEAs). To optimize heat transfer via conduction and convection, the evaporator's geometry is constrained to match the contact area of the HT PEMFC stack. To address pressure pulsations in the system (discovered in previous experiments) porous material was introduced into the evaporation chamber. This was inspired by similar issues documented in the literature [7]. Currently, the reactor is in the testing phase, and significantly lower pulsations are experienced by this phase. The reactor is tested separately for its characterization and once the pulsations are acceptably low or completely gone it will be integrated into the system.

MSR reactor

The MSR reactor's design should include a sufficient surface area to enable convective heat transfer while maintaining an abundant volume to supply the HT PEMFC stack with the necessary hydrogen flow, thus enabling the cells to operate at the selected optimum operating point. Given that the upper temperature limit is defined by the HT PEMFC's operating temperature, which is 200 °C, there is a need for the MSR reaction to occur at lower temperatures. However, the literature review has highlighted the challenge of achieving this, as most referenced studies employ temperatures higher than 200 °C.
Lowering the temperature is possible by using catalysts that are active at lower temperatures. One of the most promising options is $Cu/Zn/GaO_x$ [8], [9].
The second idea for lowering the reaction temperature is implementing a membrane MSR reformer, which could enhance the system's overall performance by shifting the equilibrium state of the MSR reaction, following La Chatelier's principle. To achieve this, we intend to utilize a Pd-Ag membrane due to its favorable properties for hydrogen permeation at lower temperatures and commercial availability.

HT PEMFC stack

HT PEMFC stack is constructed from two cells, each with an active area of 12,9 cm^2. Characterization of the HT PEMFC stack is imperative, beginning with a polarization curve analysis to comprehend its primary characteristics. Subsequently, electrochemical impedance spectroscopy (EIS) analysis is anticipated, as it can provide supplementary insights, such as the impact of CO or unconverted methanol on the cell properties [10], [11]. This collective information will enable us to determine the desired operating point.

Conclusions

It is feasible to achieve thermal integration within the HT PEMFC-MSR system, where evaporation occurs within the system using the heat generated during the operation of the HT PEMFC stack [12]. Several research groups are actively pursuing this area; however, as far as we know, the integration of the evaporator into the same system has not been realized yet. The field offers significant room for system optimization [13]–[17].
Currently, our workflow is in the characterization phase of the manufactured evaporator, and the experimental test setup is in the preparatory stage. At the same time, the experimental work on EIS analysis for the HT PEMFC is in its initial stages. Our forthcoming efforts will concentrate on designing and optimizing the MSR reactor to meet the desired operating conditions.

References

[1] A. Lotrič, M. Sekavčnik, I. Kuštrin, and M. Mori, "Life-cycle assessment of hydrogen technologies with the focus on EU critical raw materials and end-of-life strategies," *Int J Hydrogen Energy*, vol. 46, no. 16, pp. 10143–10160, Mar. 2021, doi: 10.1016/J.IJHYDENE.2020.06.190.

[2] "IEA, Global hydrogen production by technology in the Net Zero Scenario, 2019-2030, IEA, Paris https://www.iea.org/data-and-statistics/charts/global-hydrogen-production-by-technology-in-the-net-zero-scenario-2019-2030, IEA. Licence: CC BY 4.0."

[3] "National Center for Biotechnology Information (2023). PubChem Compound Summary for CID 887, Methanol. Retrieved March 2, 2023 from https://pubchem.ncbi.nlm.nih.gov/compound/Methanol."

[4] S. Dutta, "A review on production, storage of hydrogen and its utilization as an energy resource," *Journal of Industrial and Engineering Chemistry*, vol. 20, no. 4, pp. 1148–1156, Jul. 2014, doi: 10.1016/J.JIEC.2013.07.037.

[5] G. Garcia, E. Arriola, W. H. Chen, and M. D. de Luna, "A comprehensive review of hydrogen production from methanol thermochemical conversion for sustainability," *Energy*, vol. 217, p. 119384, Feb. 2021, doi: 10.1016/J.ENERGY.2020.119384.

[6] R. E. Rosli *et al.*, "A review of high-temperature proton exchange membrane fuel cell (HT-PEMFC) system," *Int J Hydrogen Energy*, vol. 42, no. 14, pp. 9293–9314, Apr. 2017, doi: 10.1016/J.IJHYDENE.2016.06.211.

[7] J. Li *et al.*, "Over 10 kg m−2 h−1 Evaporation Rate Enabled by a 3D Interconnected Porous Carbon Foam," *Joule*, vol. 4, no. 4, pp. 928–937, Apr. 2020, doi: 10.1016/J.JOULE.2020.02.014.

[8] K. Rubin, A. Pohar, V. D. B. C. Dasireddy, and B. Likozar, "Synthesis, characterization and activity of CuZnGaOx catalysts for the water–gas shift (WGS) reaction for H2 production and CO removal after reforming," *Fuel Processing Technology*, vol. 169, pp. 217–225, Jan. 2018, doi: 10.1016/J.FUPROC.2017.10.008.

[9] A. Lotrič, M. Sekavčnik, A. Pohar, B. Likozar, and S. Hočevar, "Conceptual design of an integrated thermally self-sustained methanol steam reformer – High-temperature PEM fuel cell stack manportable power generator," *Int J Hydrogen Energy*, vol. 42, no. 26, pp. 16700–16713, Jun. 2017, doi: 10.1016/J.IJHYDENE.2017.05.057.

[10] C. Brunetto, A. Moschetto, and G. Tina, "PEM fuel cell testing by electrochemical impedance spectroscopy," *Electric Power Systems Research*, vol. 79, no. 1, pp. 17–26, Jan. 2009, doi: 10.1016/J.EPSR.2008.05.012.

[11] C. Brunetto, G. Tina, G. Squadrito, and A. Moschetto, "PEMFC diagnostics and modelling by electrochemical impedance spectroscopy," in *Proceedings of the 12th IEEE Mediterranean Electrotechnical Conference (IEEE Cat. No.04CH37521)*, 2004, pp. 1045-1050 Vol.3. doi: 10.1109/MELCON.2004.1348234.

[12] A. Lotrič and M. Sekavčnik, "Sistem sočasne proizvodnje toplote in električne energije z visokotemperaturnimi gorivnimi celicami s protonsko prevodnimi membranami," 2017. [Online]. Available: https://repozitorij.uni-lj.si/IzpisGradiva.php?lang=slv&id=96191

[13] P. Ribeirinha, G. Schuller, M. Boaventura, and A. Mendes, "Synergetic integration of a methanol steam reforming cell with a high temperature polymer electrolyte fuel cell," *Int J Hydrogen Energy*, vol. 42, no. 19, pp. 13902–13912, May 2017, doi: 10.1016/J.IJHYDENE.2017.01.172.

[14] P. Ribeirinha, M. Abdollahzadeh, A. Pereira, F. Relvas, M. Boaventura, and A. Mendes, "High temperature PEM fuel cell integrated with a cellular membrane methanol steam reformer: Experimental and modelling," *Appl Energy*, vol. 215, pp. 659–669, Apr. 2018, doi: 10.1016/J.APENERGY.2018.02.029.

[15] G. Schuller, F. V. Vázquez, W. Waiblinger, S. Auvinen, and P. Ribeirinha, "Heat and fuel coupled operation of a high temperature polymer electrolyte fuel cell with a heat exchanger methanol steam reformer," *J Power Sources*, vol. 347, pp. 47–56, Apr. 2017, doi: 10.1016/J.JPOWSOUR.2017.02.021.

[16] D. Wichmann, P. Engelhardt, R. Wruck, K. Lucka, and H. Köhne, "Development of a Highly Integrated Micro Fuel Processor Based on Methanol Steam Reforming for a HT-PEM Fuel Cell with an Electric Power Output of 30 W," *ECS Trans*, vol. 26, no. 1, p. 505, 2010, doi: 10.1149/1.3429023.

[17] J. Papavasiliou, C. Schütt, G. Kolb, S. Neophytides, and G. Avgouropoulos, "Technological aspects of an auxiliary power unit with internal reforming methanol fuel cell," *Int J Hydrogen Energy*, vol. 44, no. 25, pp. 12818–12828, May 2019, doi: 10.1016/J.IJHYDENE.2018.11.136.

Thermochemical oxygen pumps: A promising candidate to increase the efficiency of thermochemical fuel production

J. Keller*[1], M. Pein[1], N. Neumann[1], S. Brendelberger[1], C. Sattler[1,2]

[1]Institute of future Fuels, German Aerospace Center
[2]RWTH Aachen, Chair for Solar Fuel Production

Introduction

The thermochemical fuel production process is one of the most promising methods to convert solar energy into green hydrogen or syngas. The high temperature heat required for the underlying redox cycle is supplied by concentrated solar energy with the principal ability to utilize the whole solar spectrum. It is a two-step process: In a reduction step the heat is used to endothermally reduce a metal oxide at high temperatures. In a temperature swing the pre-reduced metal oxide is cooled down to lower temperature and exothermally re-oxidized by reacting with water/steam or carbon dioxide to form hydrogen and/or carbon monoxide. [1]

State-of-the-art materials for this process such as Ceria are hard to reduce even at the high temperatures employed. In order to increase the reduction extent during the reduction step, and thereby the cyclic yield of the process, it is necessary to provide a controlled reducing atmosphere with a low oxygen partial pressure. While conventional vacuum pumping remains to be the state-of-the-art, alternative methods such as thermochemical oxygen pumping (TCOP) exhibit great potential to increase the efficiency of the fuel production process with comparatively little energy consumption. [2] With TCOP a second two step thermochemical cycle is employed to reduce the oxygen partial pressure during the reduction step. [3]
In comparison to conventional vacuum pumps, a TCOP requires up to 90% less energy in a pressure range below 1 mbar and therefore has the ability to increase the overall efficiency of the thermochemical fuel production. This pumping process also utilizes redox metal oxides, which can be cycled at much lower temperatures than the splitting materials like Ceria. [4] Additionally, no mechanical components are required and recuperated heat from the thermochemical splitting cycle can be utilized to power the pumping cycle. [2]

* Corresponding author: jens.keller@dlr.de

The functional principle of a thermochemical hydrogen production process in combination with a TCOP is shown in Fig. 1.

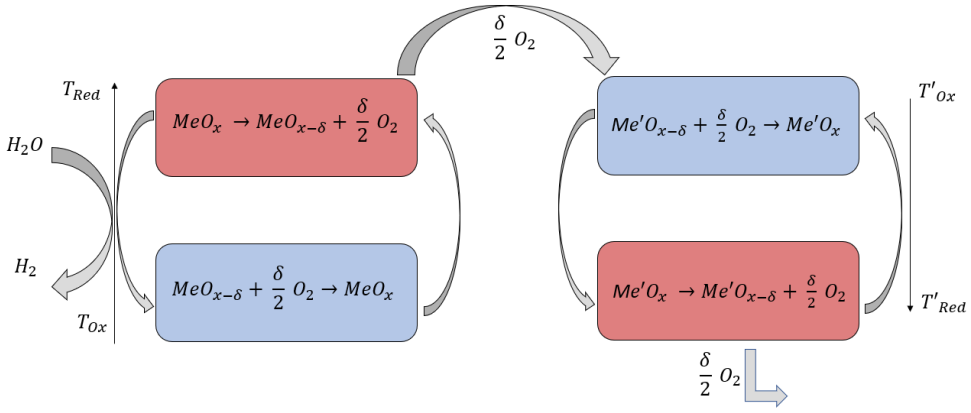

Figure 1: Functional principle of a two-step thermochemical cycle for splitting water in combination with a two-step thermochemical cycle to provide a reducing atmosphere during the reduction step of the thermochemical splitting cycle.

Methodology

While efforts were made to identify suitable TCOP materials [5] and the proof of concept has been demonstrated [2,4], further improvements are mandatory in order to enable thermochemical oxygen pumps for industrial scale applications. In this work a model is developed, which allows to determine the reduction extend of ceria during the TCOP process with the goal to identify suitable modes of operation for a TCOP with considerably high heat recuperation.

Discussion

Different use cases for thermochemical oxygen pumps as well as initial modeling results of TCOP reactor system will be outlined and discussed. Based on the developed model, the most promising operation modes are highlighted and presented here. An outlook is given on how to transfer these results to TCOP reactor with semicontinuous mode of operation.

Conclusions

Proper modelling of various operational modes as well as simulation of practical scale-up scenarios of TCOP is crucial in order to identify optimized operational parameters and suitable pumping materials. As part of ongoing work, a sophisticated modelling approach is outlined in this work and initial results are discussed in the context of solar fuel production.

References

[1] Y. Lu, L. Zhu, C.Agrafiotis, J. Vieten, M. Roeb, C. Sattler, “Solar fuels production: Two-step thermochemical cycles with cerium-based oxides”, *Progress in Energy and Combustion Science*, pp. 100785, 2019, DOI: 10.1016/j.pecs.2019.100785

[2] S. Brendelberger, Henrik von Storch, B. Bulfin, C. Sattler, “Vacuum pumping options for application in solar thermochemical redox cycles – Assessment of mechanical-, jet- and thermochemical pumping systems”, *Solar Energy*, pp. 91-102, 2017, DOI: 10.1016/j.solener.2016.11.023

[3] B. Bulfin, F. Call, M. Lange, O. Lübben, C. Sattler, R. Pitz-Paal, I. V. Shvets, “Thermodynamics of CeO2 Thermochemical Fuel Production”, *Energy Fuels*, pp. 1001-1009, 2015, DOI: 10.1021/ef5019912

[4] M. Pein, C. Agrafiotis, J. Vieten, D. Giasafaki, S. Brendelberger, M. Roeb, C. Sattler,” Redox thermochemistry of Ca-Mn-based perovskites for oxygen atmosphere control in solar-thermochemical processes ”, *Solar Energy*, pp. 612-622, 2020, DOI: 10.1016/j.solener.2020.01.088

[5] J. Vieten, B. Bulfin, P. Huck, M. Horton, D. Guban, L. Zhu, Y. Lu, K. A. Persson, M. Roeb, C. Sattler, “Materials design of perovskite solid solutions for thermochemical applications”, *Energy Environ. Sci.*, pp: 1369-1384, 2019, DOI:10.1039/C9EE00085B

Towards seawater electrolysis in alkaline media

Nathan Wauthy*[1], Renaud Delmelle[1], Joris Proost [1]

[1] Division of Materials and Process Engineering, Université catholique de Louvain (UCLouvain), Louvain-la-Neuve, Belgium

Introduction

The increase of renewable energy share is a key element to reach the goal of carbon neutrality by 2050. Offshore wind turbines are increasingly used in European countries. Thanks to better wind quality and larger suitable area, offshore wind turbines are also developed far from the coast [1]. However, the cost of connection to the mainland grid increases largely with distance and power [2].
A solution to limit transportation costs is to transport energy in chemical rather than electrical form using hydrogen [2]. Hydrogen is produced offshore by water electrolysis ($H_2O \rightleftarrows H_2 + ½\ O_2$) and is then transported to shore. The transport of chemical energy can be achieved in several ways, by conversion of produced hydrogen into e-fuel using existing petroleum infrastructure, or after compression by pipelines or ships. Furthermore, hydrogen can also be used to limit the intermittency of renewable energy by allowing energy storage. Nevertheless, a significant issue arises when utilizing water electrolysis in offshore conditions: the only steadily available water source is seawater, which contains numerous trace elements in addition to water. Some of these elements negatively impact the electrodes or separator, thereby diminishing the lifetime of the electrolyser and its efficiency [3].
There are two development paths to allow the use of seawater in water electrolysis. One involves development of new catalysts that are stable in the presence of these impurities. The other one entails implementing pre-treatment processes for seawater before electrolysis. The latter approach enables the use of industrial setups but necessitates a thorough examination of how trace impurities remaining after seawater treatment might impact the performance and lifetime.

There are currently two low temperature water electrolysis technologies industrially available: proton exchange membrane electrolysis (PEMEL) and alkaline electrolysis (AEL). Alkaline water electrolysis is widely recognized for its lower sensitivity to water quality compared to polymer electrolyte membrane electrolysis [4]. The use of an alkaline medium also avoids the formation of chlorine gas, but at the cost of the low solubility of magnesium and calcium hydroxides as shown in Table 1.

mmol/L	KOH	NaOH	$Ca(OH)_2$	$Mg(OH)_2$
water, 20°C	19.9e3	27.25e3	23.4	0.154
water, pH = 14, 25°C, based on Ks			5.62e-3	5.61e-9

Table 1: Solubility of different hydroxides.

Therefore, the main goal of this work is to understand the impact of different levels of impurities on the electrochemical performance of conventional alkaline water electrolyser to be able to determine the optimised water quality.
To know the range of study, the seawater composition must be known. In this work, seawater of different localisation around Europe is considered. Seawater composition

* Corresponding author: nathan.wauthy@uclouvain.be

depends on the localisation, but the range is the same except in Baltic sea as shown in Table 2. Thus, a standard can be used to produce synthetic seawater.

mmol/L	Na^+	Mg^{2+}	Ca^{2+}	K^+	Cl^-	SO_4^{2-}
Standard seawater	469	52.7	10.3	10.2	553	28.2
Atlantic	493	55.1	10.8	10.9	577	29.5
North sea	478	54.6	11.9	10.3	569	28.4
Baltic sea	99	10.5	2.6	2,17	116	5.99
Mediterranean sea	515	62.3	10	9.49	615	22.4

Table 2: Most prevalent ions of seawater in different localisations.

Methodology

The faradaic efficiency and the voltage change in the presence of different trace elements are studied in 1 M KOH electrolyte.
Firstly, the most prevalent anion in seawater (chloride) is investigated using KCl salts.
Concerning cations, sodium ions are the most prevalent cations in seawater, although they are usually already found in the KOH pellets used to prepare the solution. Hence, our investigation is focused on the second most commonly occurring cation in seawater, namely magnesium ions (Mg^{2+}).
Concerning the setup, 4 cm^2 industrial (Hydrogenics, Pt/IrO2 coated) electrodes and 3000 µm Nickel foam (Alantum) as spacer are used with Nickel bipolar plates and EPDM gaskets. Electrolyte is at room temperature and flow at 0.9 l/min using peristaltic pumps.
The schematic of the setup is illustrated in Figure 1.

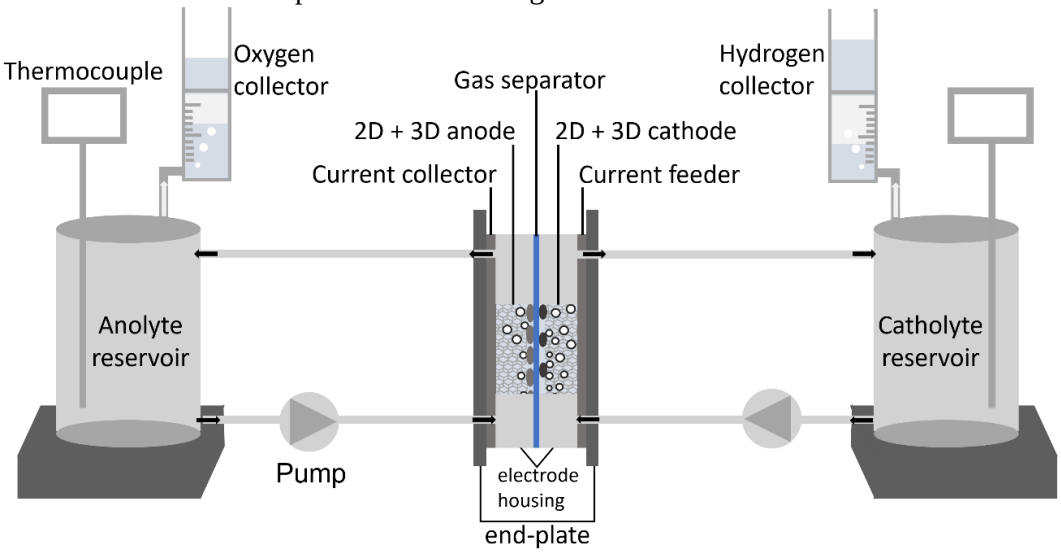

Figure 1: Schematic of the setup used.

To study the effect on the cell voltage, the following protocol is applied to the cell and is illustrated in Figure 2.

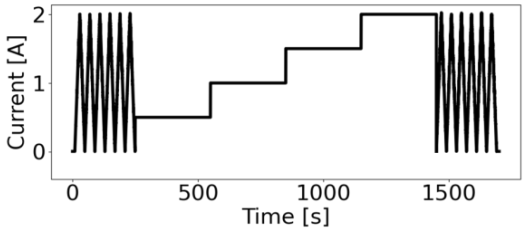

Figure 2: Applied current to compare cell voltage.

- Open circuit (10 s)
- 6 cyclovoltammetry 0 to 2 A (100 mA/s)
- 4 galvanostatic from 0,5 to 2 A with 0,5 A step (300 s each)
- 6 cyclovoltammetry 0 to 2 A (100 mA/s)
- Open circuit (10 s)

To study the faradaic efficiency, a galvanostatic at 2A is applied during the required time to perform three gas collections.
Each experiment is composed of one voltage and one faradaic efficiency study.
The effect of a given contaminant is studied with the same cell (no dismantling) for each concentration.
The study begins without additional impurity to have a voltage reference value and to ensure a perfect sealing (faradaic efficiency equal to 1). Afterwards 0.01 mM of the impurity is added, and a new experiment is performed. The experiment is repeated with a concentration increased by a factor 10 until an effect is observed or it reaches the seawater concentration.

Discussion

Potassium chloride (KCl)

The first element to study is KCl as chlorine is the most prevalent ion in seawater.
Figure 3 illustrates that no gaseous species are expected with chlorine as only Cl^- and ClO_4^- are present at pH = 14.

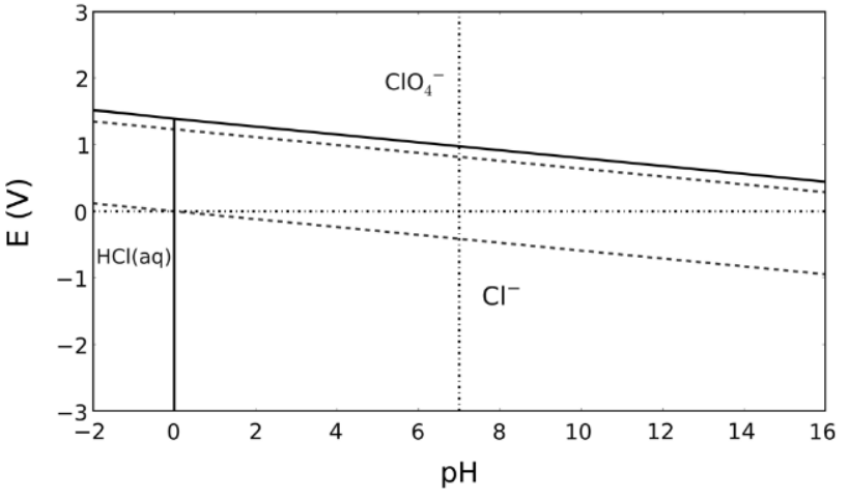

Figure 3: Pourbaix diagram of the chlorine-water system (aqueous species) [5].

However, the formation of ClO_4^- requires several steps as described below:

$Cl^- + 2\ OH^- \rightleftarrows ClO^- + H_2O + 2e^-$ (1)
$ClO^- + 2\ OH^- \rightleftarrows ClO_2^- + H_2O + 2e^-$ (2)
$ClO_2^- + 2\ OH^- \rightleftarrows ClO_3^- + H_2O + 2e^-$ (3)
$ClO_3^- + 2\ OH^- \rightleftarrows ClO_4^- + H_2O + 2e^-$ (4)

Overall equation: $Cl^- + 8\ OH^- \rightleftarrows ClO_4^- + 4\ H_2O + 8e^-$ (5)

ClO^- step is crucial to start the reaction because this reaction requires the largest potential (+0.89 V). Therefore, a metastable Pourbaix diagram (illustrated in Figure 4 with ClO4-, ClO3-, ClO2- excluded) can be considered.

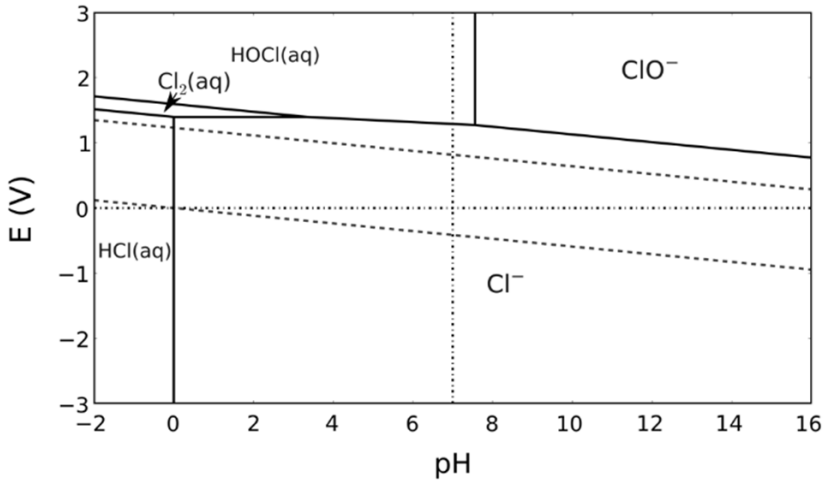

Figure 4: Pourbaix diagram of the chlorine-water system (aqueous species, considering ClO-) [5].

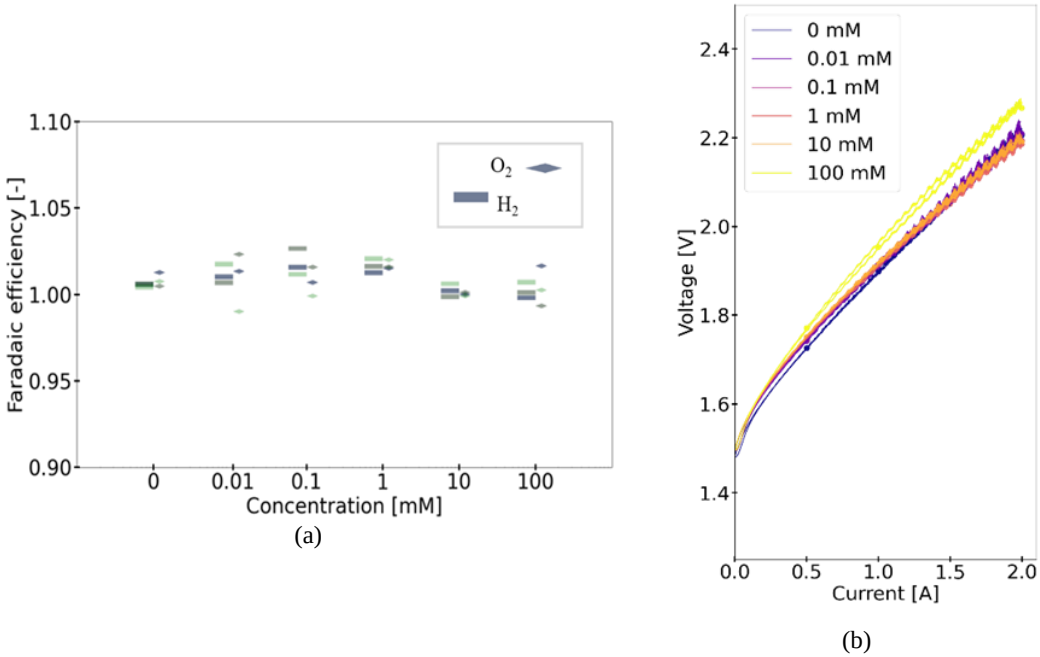

Figure 5: Effect of chlorine concentration on (a) faradaic efficiency (b) cell voltage.

Figure 5a shows that the faradaic efficiency is close to one. This means that no side reaction occurs whatever the concentration studied. If the ClO^- reaction had taken place, two electrons would have been consumed (eq. 1) without producing any gas leading to a Faradaic efficiency different to one.

Concerning the voltage change, an increase of cell voltage can be observed in Figure 5b with a concentration of 100 mM. An increase of the cell voltage leads to an increased energy consumption for a given amount of H_2 produced.100mM represents a fifth of the concentration in seawater. It means that seawater pre-treatment is required to perform industrial alkaline water electrolysis.

Magnesium sulfate ($MgSO_4$)

Another experiment was performed with $MgSO_4$.

As magnesium has a large negative overpotential, there is no risk of reduction at the cathode. However, as shown in the introduction, magnesium hydroxide has a low solubility which leads to potential precipitation. Concerning sulfate, the corresponding Pourbaix diagram is shown in Figure 6.

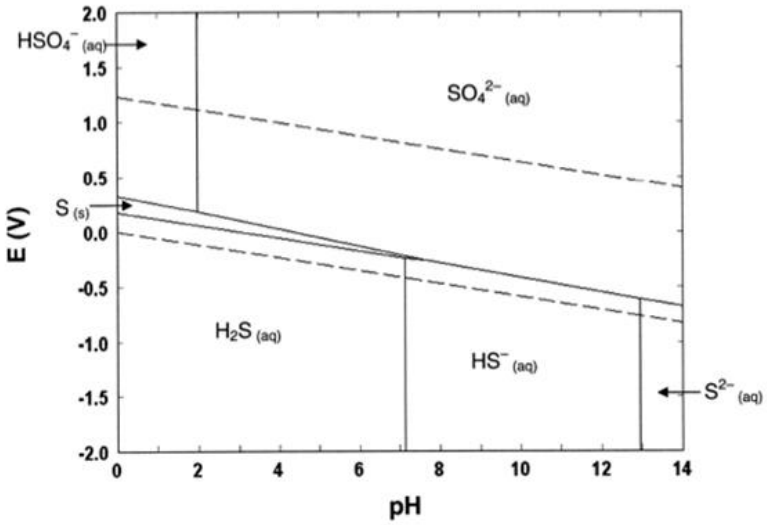

Figure 6: Pourbaix diagram of the sulfur-water system.

This figure shows that there is no side reaction at the anode as SO_4^{2-} is stable. However, it can react at the cathode to form S^{2-}. But this reaction requires 8 electrons ($SO_4^{2-} + 4H_2O + 8e^- \rightleftarrows S^{2-} + 8\ OH^-$) which is an important limitation.

The voltage and the faradaic efficiency are shown in Figure 7.

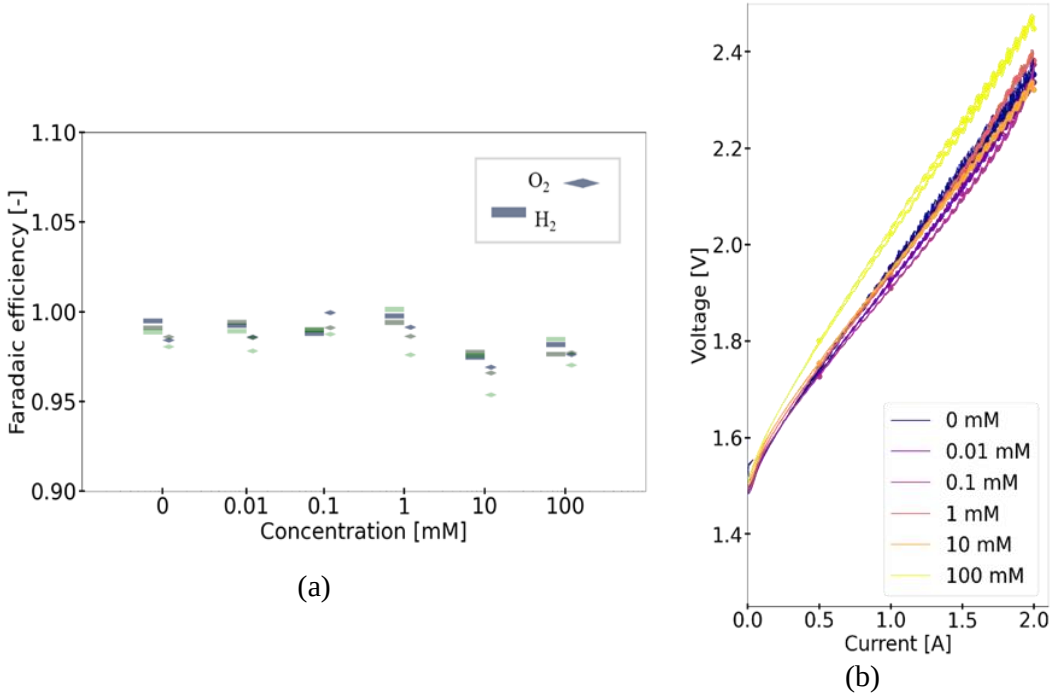

Figure 7: Effect of the magnesium sulfate concentration on the (a) faradaic efficiency (b)cell voltage.

Faradaic efficiency is also close to one meaning that no side reaction occurs. Concerning the voltage, there is an increase once again at a concentration of 100 mM. Nevertheless, 100 mM is above the concentration of magnesium and sulfate in seawater. But a precipitate is already observed at 10 mM (below the concentration of seawater). Precipitations is an issue as there is a risk of accumulation in the system leading to clogging.

Conclusions

This work explores the impact of different concentrations of KCl or $MgSO_4$ on the electrochemical performance of conventional alkaline water electrolyser. Preliminary results show that a direct electrolysis of seawater with an industrial setup can not be performed due to an increase of cell voltage with KCl. Therefore, a water pre-treatment is required before producing hydrogen with industrial alkaline electrolysers.
But this study must continue to ensure that no element impacts the performance of the electrolyser with a purified seawater containing less than 100 mM chloride. Therefore, most prevalent ions in seawater have to be studied. But even further development is required to know if the effect is dependent on the salt (NaCl vs KCl for example) and the presence of other elements (combined effect).

Acknowledgements

Funding from the Belgian Energy Transition Funds (ETF) of the Federal Planning Service for Economy, S.M.E., Self-employment and Energy is gratefully acknowledged through the MuSE project (Molecules at Sea).

References

[1] M. D. Esteban., J. J. Diez, J. S. López, V. Negro, “Why Offshore Wind Energy?, ”*Renew. Energy*, vol. 36, 444-450, Feb. 2011.

[2] O. S. Ibrahim, A. Singlitico, R. Proskovics, S. McDonagh, C. Desmond, J. D. Murphy, “Dedicated Large-Scale Floating Offshore Wind to Hydrogen: Assessing Design Variables in Proposed Typologies, ”*Renew. Sustain. Energy Rev.*, vol. 160, 112310, Mar. 2022.

[3] H. Xie, Z. Zhao, T. Liu, Y. Wu, C. Lan, W. Jiang, L. Zhu, Y. Wang, D. Yang, Z. Shao, ”A membrane-based seawater electrolyser for hydrogen generation, ”*Nature,* vol. 612, 673–678, Nov. 2022.

[4] M.A. Khan, T. Al-Attas, S. Roy, M. M. Rahman, N. Ghaffour, V. Thangadurai, S. Larter, J. Hu, P. M. Ajayan, M. G. Kibria, ”Seawater Electrolysis for Hydrogen Production: A Solution Looking for a Problem?, ”*Energy Environ. Sci.*, vol. 14, 4831–4839, Mar. 2021.

[5] R. K. B. Karlsson, A. Cornell, ”Selectivity between Oxygen and Chlorine Evolution in the Chlor-Alkali and Chlorate Processes, ”*Chem. Reviews*, vol. 116, 2982-3028, Mar. 2016.

Unlocking H_2 Storage Potential in Clathrate Hydrates at Mild Thermodynamic Conditions

Nithin B. Kummamuru*[1,2], Radu-George Ciocarlan[3], Geert Watson[4], Sammy W. Verbruggen[2,5], Pegie Cool[3], Pascal Van der Voort[4], Johan Martens[6]. Patrice Perreault[1,2,7]

[1] Laboratory for the Electrification of Chemical Processes and Hydrogen (ElectrifHy), University of Antwerp, Olieweg 97, 2020 Antwerpen, Belgium
[2] Sustainable Energy, Air & Water Technology (DuEL), Department of Bioscience Engineering, University of Antwerp, Groenenborgerlaan 171, 2020 Antwerpen, Belgium
[3] Department of Chemistry, University of Antwerp, Universiteitsplein 1, 2610 Wilrijk, Belgium
[4] Centre for Ordered Materials, Organometallics and Catalysis (COMOC), Department of Chemistry, Ghent University, Krijgslaan 281-S3, 9000 Ghent, Belgium
[5] NANOlab Center of Excellence, University of Antwerp, Groenenborgerlaan 171, 2020 Antwerpen, Belgium
[6] Centre for Surface Chemistry and Catalysis, NMRCoRe - NMR - XRAY - EM Platform for Convergence Research, Department of Microbial and Molecular Systems (M2S), KU Leuven, Celestijnenlaan 200F, 3001, Leuven, Belgium
[7] University of Antwerp, BlueApp, Olieweg 97, 2020 Antwerpen, Belgium

Introduction

Hydrogen (H_2) is considered a promising alternative to fossil fuels and a vital element in decarbonizing various industries, making it a pivotal component of future energy systems. However, establishing a sustainable H_2-based economy poses challenges related to safety, storage, and efficient transportation. Current storage methods include compression, cryogenic liquefaction, chemisorption in metal hydrides, or physisorption in nanoporous materials, each with its own advantages and drawbacks, making it challenging to meet cost, safety, and performance requirements[1]. To enable the H_2 economy, new storage technologies with high volumetric and gravimetric density and favorable thermodynamic conditions are essential. In this regard, the hydrate-based gas (clathrate hydrate) storage method has received widespread attention in recent times[2]. Clathrate hydrates are unique inclusion compounds where non-polar gas molecules (guest) are trapped within the hydrogen-bonded H_2O cages through van der Waals forces under specific thermodynamic conditions. The interaction between H_2O and different guest gases results in the formation of various cage-like structures such as the structure I (sI) hydrate unit cell, having two 5^{12} cages and six $5^{12}6^2$ cages, similarly, the structure II (sII) hydrate unit cell comprises sixteen 5^{12} cages and eight $5^{12}6^4$ cages[3]. Bulk, synthetic clathrates are typically formed at high-pressure and low temperatures. By confining H_2O in hydrophobic pores of activated carbon, methane (CH_4) clathrate formation was recently shown to be easier and reversible, occurring at much milder thermodynamic conditions than expected[4]. H_2 clathrates can also be obtained from bulk H_2O, but this process requires pressures above 200 MPa and temperatures below 248 K[5], limiting their practical application. Nevertheless, hydrophobic materials are expected to facilitate reversible, fast uptake of H_2 into clathrates, and enable stabilization at milder thermodynamic conditions, akin to CH_4 clathrates. Achieving this, however, still demands pressures of 200 - 300 MPa and temperatures between 240 K and 248 K to enable H_2 storage of 5.3 wt.%. The inclusion of larger-sized liquid-based molecules such as tetrahydrofuran (THF), 1,3-dioxolane (DIOX), 1,2-Epoxycyclopentane (ECP) as co-guest and promoters helps to form mixed H_2 clathrates under milder conditions (6 - 12 MPa and 278 K), at the expense of storage capacity (1 wt.%

* Corresponding author: NithinBharadwaj.Kummamuru@uantwerpen.be

H_2) as these larger molecules occupy the large cages ($5^{12}6^4$) of the sII structure[1]. Consequently, there exists a trade-off between synthesis conditions and maximizing H_2 storage capacities. On the other hand, there's been limited research on enhancing the kinetics in an unstirred packed (porous materials) bed reactor, which could offer the potential for advancing clathrate-based H_2 technology. Recent studies have demonstrated that within a hydrophobic environment, H_2O molecules try to minimize free energy by arranging themselves in a regular tetrahedral pattern, which enhances their mobility and boosts hydrate nucleation, compared to hydrophilic materials[6]. Inspired by these findings, this study utilizes CH_4 as a promoter rather than a liquid-based promoter, in a hydrophobic environment considering the ability of CH_4 to shift hydrate equilibrium to mild conditions compared to bulk pure H_2 hydrates, moreover, the smaller molecular size of CH_4, compared liquid promoters, might facilitate H_2 to compete/accommodate/exchange in both large and small cages, thereby enhancing the storage density of H_2. Meanwhile, any CH_4 molecules within the hydrate that remain unexchanged with H_2, can further serve as an additional energy medium, thereby enhancing the overall energy density, which contrasts with liquid promoters, that offer no such advantage. However, it is crucial to conduct preliminary investigations to comprehend several essential aspects. First, understanding the phase equilibrium of CH_4 hydrates is vital, as they provide the foundational medium for incorporating H_2 into the cages through a gas exchange mechanism. Second, evaluating the storage capacity and kinetics of CH_4 hydrate growth within interstitial spaces and hydrophobic porous materials. These evaluations determine the quantity of H_2 that can be stored. Third, analyzing the H_2 storage capacity within a binary H_2-liquid promoter hydrate influenced by hydrophobic porous materials establishes a baseline for the minimum storage capacity. Lastly, investigate the hypothesis that H_2 can be enclathrated in large or small cages of CH_4 hydrate through an exchange mechanism, thus enhancing H_2 storage density. Therefore, this study will address and explore all the aforementioned aspects.

Methodology

A schematic layout experimental setup is shown in Fig. 1.

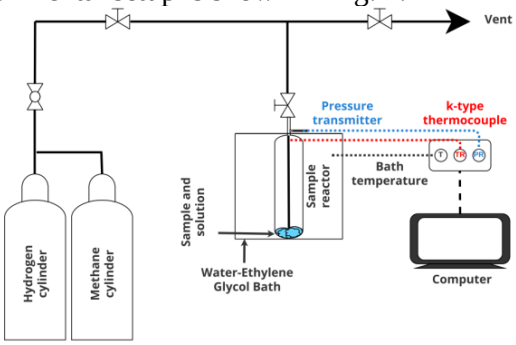

Fig. 1: Schematic layout of the experimental setup used in this study

Further information corresponding to all the experimental procedures for CH_4 hydrate investigation as mentioned in the introduction is outlined in earlier publication[7]. A similar methodology was followed for H_2 uptake experiments, except for pure H_2O, a stoichiometric amount of 5.56 mol% THF solution was added to the synthesized material based on complete pore volume saturation. Interstitial space between stainless steel beads (SSB) of different diameters and mesopores of hydrophobic porous materials were exploited to estimate CH_4 hydrate storage capacity and hydrate growth kinetics in an unstirred reactor. Detailed information on these materials' synthesis and characterization is presented in our

latest publication[7]. Unfortunately, additional details regarding the materials used for H_2 hydrates cannot be disclosed as they are currently undergoing review with a scientific publisher at the time of submitting this extended abstract. For the gas exchange experiments, a novel procedure was employed. After forming CH_4 hydrate within the hydrophobic porous material, the reactor's temperature was lowered to self-preservation temperature (268.15 K) of the CH_4 hydrate at 1 atm. At this point, the CH_4 gas in the reactor was rapidly removed, followed by multiple H_2 flushes to eliminate any remaining CH_4 gas in the reactor environment. Subsequently, H_2 gas was introduced into the reactor at 268.15 K to reach a desired pressure of 5 MPa. Thermal stimulation steps were then conducted by increasing the reactor's temperature from 268.15 K to 272 K and beyond, to partially melt the hydrate layers in porous media and facilitate H_2/CH_4 exchange within the cages. Throughout the replacement process, gas samples were extracted at different time periods (at the start of H_2 injection, after 24 hours of thermal stimulation to monitor changes in CH_4 and H_2 compositions in the gas phase, and after a sufficient time following further temperature elevation) and analyzed using a Quadrupole Mass Spectrometer (QMS). The gas sample volume was 1 mL, and any potential impact of the sampling process on the replacement process was disregarded in this study. Prior to gas analysis, the QMS was also calibrated with various H_2/CH_4 ratios in the gas phase. The amount of CH_4 or H_2 gas consumed during hydrate formation, the normalized gas uptake (NG_t) at any given time *t*, and the percentage of H_2O to hydrate conversion were estimated using different calculation methods as presented in one of our recent publications[7, 8]. However, a slight modification was applied to the percentage of H_2O to hydrate conversion in the case of H_2 hydrates with liquid promoter and is presented in 1 and 2.

$$WtH(\%) = \frac{\left(\Delta n_{H2,t} + \Delta n_{THF}\right) \times Hn}{n_{H2O}} \times 100 \quad (1)$$

$$\Delta n_{THF} = \Delta n_{H2,t} \times \frac{no.of\ large\ cages}{no.of\ small\ cages} \quad (2)$$

Here, $\Delta n_{H2,t}$ is moles of H_2 consumed at time *t*, n_{H2O} is moles of H_2O introduced into the reactor; Δn_{THF} is moles of THF consumed for hydrate formation, assuming that THF occupies solely $5^{12}6^4$ cages, and *Hn* is hydration number, which is 5.67.

Discussion

Gas hydrates have a vital role as a potential energy source, and their phase equilibrium (P-E) conditions are necessary for storage applications. To date, hydrate P-E conditions are determined from experiments, thermodynamic models, artificial intelligence algorithms, and empirical correlations. Among these, the first three approaches are subjected to high cost, sophisticated programming, long training time, and are not suitable for hand calculations. Whereas there exist significant advantages of using empirical correlations such as accuracy (within the range of its application) and simplicity in terms of requiring less input data such as pressure, temperature, molecular weight, and specific gas gravity. Considering this, a new generalized empirical correlation, as shown in 3, is proposed for predicting CH_4 hydrate P-E in pure H_2O applicable in the ranges of 273.2−303.48 K and 2.63−72.26 MPa.

$$T = a + bP + c/P \quad (3)$$

Here, *T* is the temperature in K, *P* is pressure in MPa, and *a, b, c* are correlation coefficients with values 288.0102, 0.2488, -45.0063, respectively. A total number of 260 equilibrium

data points were collected from the literature, out of which, 215 data points were employed to obtain the coefficient parameters by adopting a nonlinear regression technique, and the remainder data points were allotted to check the validity of the proposed correlation. Statistical error analysis showed that the new correlation has better performance (Fig. 2) compared to conventional empirical correlations in predicting P-E conditions. For further information into statistical error analysis, we direct the reader to refer to our recent publication[9].

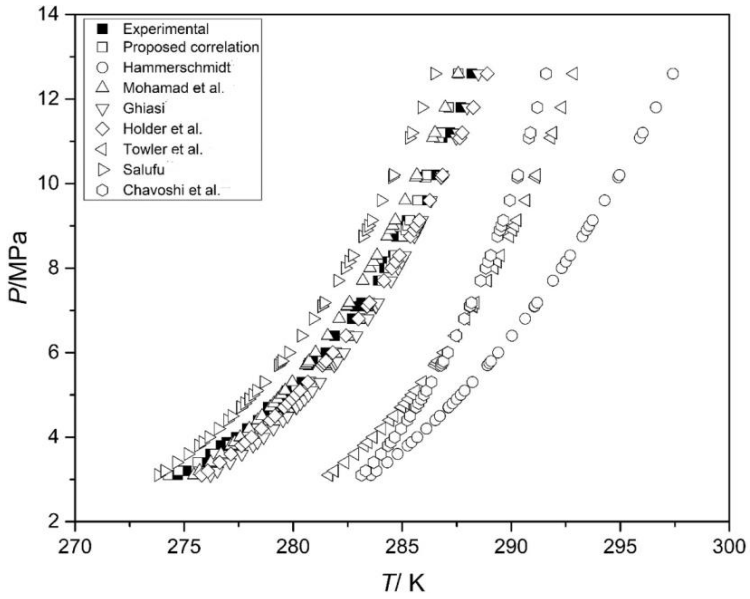

Fig. 2: P–T plot between experimental values and those calculated from the empirical correlations

For the second stage of the investigation, i.e., evaluating the CH_4 storage capacity and kinetics of hydrate growth in unstirred packed bed reactor, preliminary test was performed to exploit the interstitial space between SSB in a packed fixed-bed reactor, also considering that high thermal conductivity of SSB can potentially accelerate hydrate growth by rapidly removing hydrate heat from the reaction. Fig. 3a compares the hydrate formation at 6 MPa in 5 mm and 2 mm diameter SSB packing filled with 2.05 g H_2O. While both achieved similar maximum gas uptake, the 2 mm packing exhibited a higher CH_4 hydrate formation rate due to the availability of more interstitial space, offering more nucleation sites. Despite reaching approximately 0.14 mol CH_4/mol H_2O, a substantial 70% reduction in gas uptake was noted when increasing H_2O content from 2.05 g to 10.25 g (Figure 3b), resulting in very sluggish uptake kinetics. These outcomes clearly suggest significant mass transfer reduction and diffusion effects, attributed to a higher gas-liquid interface due to higher H_2O content, compared to the solid-gas-liquid interface observed with lower H_2O content. These findings emphasize that although SSBs are cost-effective, water-to-hydrate conversion relies on the water content-to-SSB ratio, favoring lower ratios, which might not be ideal for larger-scale setups.

CH_4 hydrates within hydrophobic porous materials (SBA-15 C8 and Ring PMO) were also studied under various conditions, including different pore-volume saturations and temperatures (269 K - 276 K) with an experimental pressure of 6 MPa. Both materials displayed rapid hydrate growth, making them favorable for CH_4 storage applications. However, SBA-15 C8 took longer than Ring-PMO to reach its peak storage capacity, regardless of the driving force applied. Optimal pore-volume saturations were found to be 130% for SBA-15 C8 and 200% for Ring-PMO. Beyond these values, a significant decrease in gas uptake was observed. At 269 K, the maximum storage capacity was 0.098 mol

CH_4/mol H_2O at 130% pore-volume saturation for SBA-15 C8 and 0.101 mol CH_4/mol H_2O at 200% pore-volume saturation for Ring-PMO (Fig. 4a). Compared to SSB, porous materials are advantageous due to their lighter weight, lower volume occupancy, higher surface area availability, making them ideal for large-scale hydrate-based energy storage. Both hydrophobic materials demonstrated favorable CH_4 storage as clathrate hydrates, with Ring-PMO showing a higher storage capacity as it can incorporate more H_2O, leading to substantially increased total dry weight storage capacities of 5.4 wt.% for SBA-15 C8 and 17.2 wt.% for Ring-PMO. For further into the kinetic modeling on gas uptake, we direct the reader to refer to our recent publication[7].

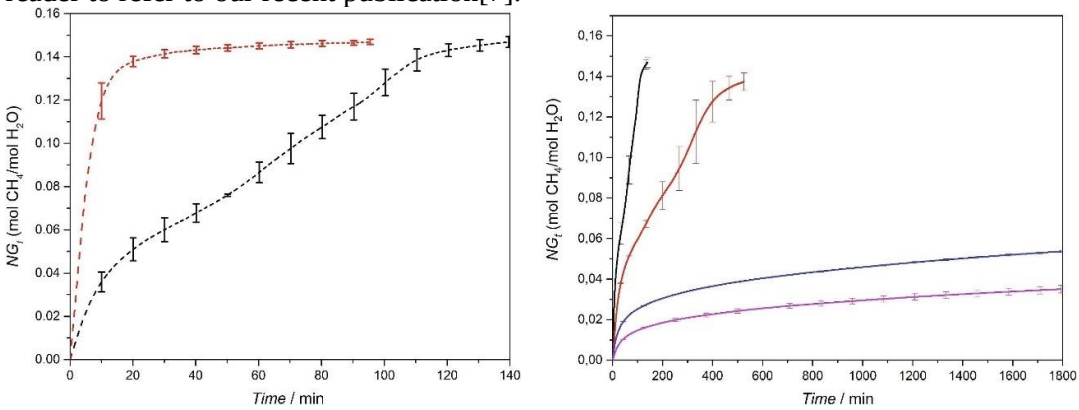

Fig. 3: ((a-left)) Normalized CH_4 uptake at 273.65 K in 5 and 2 mm SSB packed bed filled with 2.05g H_2O, ((b-right)) Normalized CH_4 uptake in 5 mm SSB in 2.05g and 10.25g H_2O. Black: (2.05g H_2O – 273.65 K), Red: (2.05g H_2O – 275.65 K), Blue: (10.25g H_2O – 273.65 K), Magenta: (10.25g H_2O – 275.65 K).

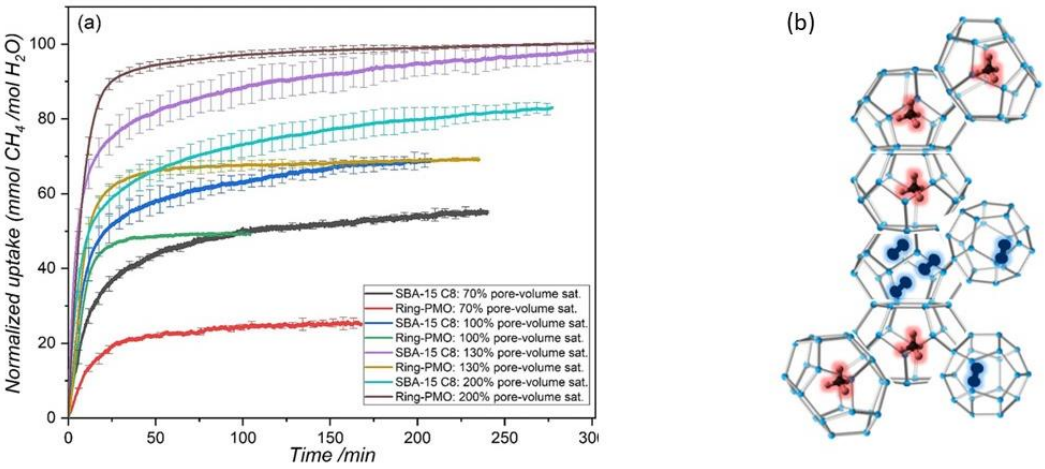

Fig. 4: (a) CH_4 uptake behavior in SBA-15 C8 and Ring-PMO at 269 K and 6 MPa; (b) Schematic of CH_4 and H_2 in sI unit cell after gas exchange in cages

Confirming that hydrophobic porous materials are efficient in terms of favorable CH_4 storage capacities, additional tests on silica-based hydrophobic porous materials using THF as a liquid-promoter molecule were performed to estimate maximum H_2 storage capacity, as these results establish a baseline for our hypothesis. However, detailed synthesis and characterization information, as well as specific figures, are undergoing review with a scientific publisher and cannot be disclosed at this time. The results showed that with 5.56 mol% THF in an aqueous phase, a maximum storage capacity of $\approx$ 46.77 mmoles H_2/mole H_2O can be achieved, translating to 0.52 wt.% of H_2 at 7 MPa and 262 K. At 268 K, a maximum of 0.16 wt.% can be achieved, demonstrating higher H_2 storage capacities

compared to the literature. This suggests that hydrophobic porous materials facilitate better mass transfer, enhancing H_2 enclathration within the pores, compared to bulk systems. Using the same hydrophobic silica-based material, we tested the hypothesis of using CH_4 as a thermodynamic promoter for H_2 enclathration via a gas exchange mechanism. Initially, a maximum storage capacity of 9.6 wt.% of CH_4 hydrates at 5 MPa and 272 K with 100% pore volume saturation with pure H_2O was obtained. Following the evacuation procedure, H_2 gas at 5 MPa was pressurized upon already formed CH_4 hydrates. After 24 hours and thermal stimulation to 272 K, a maximum storage capacity of 0.36 wt.% of H_2 was achieved, with 6.3 wt.% of CH_4 hydrates remaining in the system. This indicated a H_2/CH_4 exchange ratio of $\approx$ 0.4, where one H_2 molecule replaced one CH_4 molecule in each small cage and in two H_2 replaced one CH_4 in a large cage. Further temperature increases to 274 K led to a maximum H_2 storage capacity of 0.47 wt.%, with a H_2/CH_4 exchange ratio of $\approx$ 0.5, signifying the addition of one more H_2 in large cage. A schematic of CH_4 and H_2 molecules in sI hydrate unit cell is presented in Fig. 4b. It is also important to mention that these exchange ratios mentioned are purely based on theoretical calculations for sI hydrate. Further experiments via *in-situ* NMR are due to verify.

Conclusions

H_2 is a key player in decarbonization and future energy systems. However, challenges in safe storage and transportation persist highlighting the need for novel approaches that offer high storage density at favorable thermodynamic conditions. One promising method is the utilization of clathrate hydrates. In this study, we explored the potential of utilizing hydrophobic porous materials to enhance H_2 storage in clathrate hydrates via a gas exchange mechanism with CH_4. The results demonstrated the efficiency of hydrophobic porous materials in facilitating higher H_2 storage capacities (0.47 wt.%) compared to the literature at milder thermodynamic conditions (274 K and 5 MPa). Additionally, incorporating CH_4 as a promoter proved to be a promising strategy, resulting in improved H_2 storage density by enhancing the H_2/CH_4 exchange within the hydrate cages. Our findings emphasized the importance of understanding phase equilibrium, storage capacity, and kinetics of hydrate growth within different porous materials. Further investigation (*in-situ* NMR) is essential to validate and optimize these findings, potentially paving the way for practical and efficient H_2 storage solutions using clathrate hydrates.

References

[1] N. N. Nguyen, "Prospectand Challenges of Hydrate-Based Hydrogen Storage in the Low-Carbon Future," *Energy Fuels*, vol. 37, pp. 9771-9789, 2023.

[2] A. Gupta, G. V. Baron, P. Perreault, S. Lenaerts, *et al.*, "Hydrogen clathrates: Next generation hydrogen storage materials," *Energy Storage Mater.*, vol. 41, pp. 69-107, 2021.

[3] E. D. Sloan and C. A. Koh, *Clathrate hydrates of natural gases*, 3 ed. Boca Raton, FL: Taylor & Francis-CRC Press, 2008.

[4] M. E. Casco, J. S. Albero, A. J. Ramírez-Cuesta, F. Rey, *et al.*, "Methane hydrate formation in confined nanospace can surpass nature," *Nat. Commun.*, vol. 6, p. 6432, 2015.

[5] W. L. Mao, H. K. Mao, A. F. Goncharov, V. V. Struzhkin, *et al.*, "Hydrogen clusters in clathrate hydrate," *Science*, vol. 297, pp. 2247-2249, 2002.

[6] J. L. Wang, R. J. Wang, R. H. Yoon, and Y. Seol, "Use of hydrophobic particles as kinetic promoters for gas hydrate formation," *J. Chem. Eng. Data*, vol. 60, pp. 383-388, 2015.

[7] N. B. Kummamuru, G. Watson, R-G. Ciocarlan, S. W. Verbruggen, *et al.*, "Accelerated methane storage in clathrate hydrates using mesoporous (Organo-) silica materials," *Fuel*, vol. 354, p. 129403, 2023.

[8] N. B. Kummamuru, S. W. Verbruggen, S. Lenaerts, and P. Perreault, "Experimental investigation of methane hydrate formation in the presence of metallic packing," *Fuel*, vol. 323, p. 124269, 2022.

[9] N. B. Kummamuru, P. Perreault, and S. Lenaerts, "A New Generalized Empirical Correlation for Predicting Methane Hydrate Equilibrium Conditions in Pure Water," *Ind. Eng. Chem. Res.*, vol. 60, pp. 3474-3483, 2021.

Using H_2 for CO_2 activation on the way towards synthetic fuels

A. Rouxhet*[1], G. Léonard[1]

[1]Chemical Engineering, Université de Liège, Liège, Belgium

Introduction

Fighting global warming is probably one of the biggest challenges we must face this century. Therefore, the scientific community is exerting great efforts to reduce anthropogenic CO_2 emissions and decrease its concentration within the atmosphere. In 2022, the combined worldwide operational CO_2 capture plants prevented the emission of almost 50 Mt of CO_2. This capacity is expected to increase 6-fold by 2030, counting only the already planned projects [1]. It shows the companies' desire to limit their CO_2 emissions in the foreseeable future, especially in Europe where it is motivated by the increasing price for the emitted tonne of CO_2. Indeed, the cost of emitting one tonne of CO_2 on the European ETS market has increased from 25 €/tonne in early 2020 to 86 €/tonne in August 2023 [2]. Among the possible CO_2 utilization routes, the production of synthetic fuels by combining CO_2 with H_2 remains the leading option, mainly due to policy incentives. The European Union voted the ReFuelEU Aviation proposal as part of its "Fit for 55" package in April 2023, stating that the market share of synthetic aviation fuels should grow from 0.7% in 2030 to 28% in 2050 [3]. It is particularly interesting for long-freight transportation, namely ships and aircraft, for which hydrogen powering or electrification presents significant limitations. Hence, it would turn the long-haul transport industry into a defossilized, rather than decarbonized industry. Additionally, producing liquid fuels from CO_2 and H_2 offers an energy storage opportunity. Indeed, it is possible to store eight times more energy in traditional liquid fuels than in 700 bar hydrogen and even more when compared to Li-Ion batteries [4]. Those processes are generally referred to as Power-to-fuel processes, as the electricity generated from renewable energies is eventually stored in fuels. Once these fuels are burnt, the stored energy is released, and CO_2 is emitted, but once captured (e.g., by Direct Air Capture), it can be reused as an input of the process, creating a circular usage of carbon.

Practically, CO_2 must be hydrogenated to yield hydrocarbon chains, which can be further upgraded to the desired fuel. Ideally, the CO_2 conversion can be conducted with one reaction on a bifunctional catalyst, i.e. a catalyst capable of activating the highly inert CO_2 molecule and crossing the high C-C coupling barrier required for hydrocarbon chain growth. However, the yields and selectivities obtained from these catalysts are low and demand further improvements to be applicable in large-scale facilities. Therefore, the indirect synthesis is a suitable alternative in which CO_2 is activated in a first reactor, and then the polymerization reaction occurs in a second one. This work investigates principally the first reaction where CO_2 is transformed into CO, which is less stable and thus more adapted to yield complex hydrocarbons, through the reverse water-gas shift (rWGS) reaction:

$$CO_2 + H_2 \rightleftharpoons CO + H_2O \qquad \Delta H^0 = 41 \frac{kJ}{mol} \tag{1}$$

* Corresponding author: antoine.rouxhet@uliege.be

Objectives

This work focuses on three main objectives. First and foremost, the goal is to determine the best possible operating conditions for a specific study case and design an optimal rWGS unit accordingly. The discussions conducted in this paper focus on this first objective. The study case corresponds to the experimental installation that will be set up at the University of Liège (ULiège) and that consists in a small pilot-scale Power-to-kerosene process made up of a rWGS reactor followed by a Fischer-Tropsch (FT) reactor. The H_2 necessary for the reactions is produced by three water electrolysis cells, already operating at ULiège and having a combined peak production of 1.5 Nm^3/h of H_2. The reactor numerical model used to size this experimental installation will then be included in a complete process model to study process-related aspects. For instance, it will be possible to determine which recycling option for unreacted gases better suits a Power-to-kerosene process. Indeed, the process consists of a succession of two reaction units (rWGS and FT), bringing various recycling options, as testified by Figure 1. The recycling loop can be isolated around each reaction unit (options A and B), the outlet of the process can be recirculated at its inlet (option C) and additionally between the rWGS and FT units (option D). It is worth mentioning that the literature shows that recycling loops are generally used to intensify Power-to-kerosene processes. In many cases, the loop integrates a combustion unit which burns a fraction of the tail gases to provide heat for the rest of the process, especially for the rWGS reaction [5]–[7].

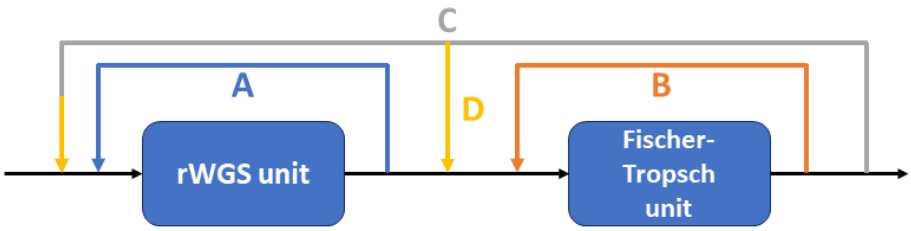

Figure 1 : Recyling loop possibilities between the rWGS and the Fischer-Tropsch units

Concerning the second objective, the scope is not only centred on kerosene production anymore. The aim is to investigate the production of other types of end products and to determine the impact of the end product nature on the rWGS unit design. In other words, the point will be to determine whether the optimal design developed for kerosene synthesis is also suitable for another product synthesis and, thus, whether it is possible to propose a standardized rWGS unit design. Among others, the targetted end products can be gasoline or diesel, which can also be synthesised through the Fischer-Tropsc reaction, methanol, ethanol, dimethyl ether, etc. The last objective of this work is to pass from the steady-state model developed for the first objective to a dynamic model. Indeed, it turns out that modelling of the rWGS reaction, and Power-to-X processes in general, lacks transient considerations. Thus, flexibility analysis is outlined as a crucial perspective in this field to counterbalance this scarcity [8]–[10]. The study of the transient behaviour of these processes is paramount as they rely on the utilisation of renewable energies, which are variable in nature.

Methodology

This thesis combines modelling and experimental work through the installation of the pilot facility at ULiège. The first utilization of the developed model is to design and determine the size of this actual installation. Therefore, the model should be sufficiently precise, which is the reason why the model accounts for the reaction kinetics. Nevertheless, the first developed

model is a simple Gibbs model, i.e. an equilibrium model, which enables the obtention of first insights regarding the influence of operating variables on reaction performance. It also helps to have a first idea of the operating conditions ranges and to compare them with the values found in the literature. The Gibbs model considers the rWGS reaction (see Equation (1)) and also two exothermic parallel methanation reactions, which appear along this one:

$$CO_2 + 4\,H_2 \leftrightarrow CH_4 + 2\,H_2O \qquad \Delta H^0 = -165\,\frac{kJ}{mol} \tag{2}$$

$$CO + 3\,H_2 \leftrightarrow CH_4 + H_2O \qquad \Delta H^0 = -206\,\frac{kJ}{mol} \tag{3}$$

In some simulation works, exothermic coking side reactions (Boudouard and Bosch equilibria, methane pyrolysis) are also included in the model. However, these reactions are generally neglected, given the high operating temperature required for the rWGS reaction [5], [6], [11]–[13]. Some results obtained from this equilibrium model are discussed in the following section.

In order to upgrade this equilibrium model, a complete kinetic model was developed in Aspen Custom Modeler (ACM) accounting for material, heat and momentum balances. The utilization of ACM as a simulation software offers some freedom in terms of reactor modelling compared to built-in reactor models from Aspen Plus but still keeps the advantage of the availability of the different Aspen Properties databases. The kinetics implemented in this model were designed for a 2 wt-% Ni/Al_2O_3 catalyst by Vidal Vázquez et al. [14] and were chosen for different reasons. The kinetic model structure of Vidal Vázquez et al. is based on the work of Xu and Froment [15], who developed a model for methane steam reforming, methanation and water-gas shift reactions, which has been used in numerous works in the past. Furthermore, Vidal Vázquez et al.'s kinetics have been presumably used to size a rWGS experimental installation whose size is similar to the one that will be set up at ULiège [16]. Finally, Vidal Vázquez et al. regressed their model with experimental data obtained in a wide range of temperatures (between 550 and 850°C) and pressures (between 1 and 30 bar). This latter point is worth mentioning as most of the rWGS kinetics accessible in the literature are based on experiments conducted at atmospheric pressure and lower temperatures [17]–[20].

Discussion

Table 1 gathers the rWGS reaction operating temperature and pressure referenced in various simulation works. This table comes from a review paper on the rWGS reaction, which is currently in preparation. The operating conditions are discussed in further detail in this future paper [21].

Table 1 - Operating conditions applied for the rWGS reaction in different simulation works

Temperature (°C)	Pressure (bar)	Reference	Temperature (°C)	Pressure (bar)	Reference
900	25	[5]	1000	30	[22]
550 – 950	1 – 25	[6]	950	25 – 30	[23]
900	30	[12]	900	4.2	[24]
665 – 750	1	[25]	1000 – 1200	1 – 30	[20]
350 – 940	1 – 30	[26]	980 – 1000	20	[16]
400 – 700	1	[27]	800	1	[28]

The main message emerging from this table is the high operating temperature required by the rWGS reaction. Although some of the referenced works studied it at a lower temperature, their conclusion regarding the optimal operating temperature is always towards the higher values of their considered range. The general conclusion drawn from these works reveals that the rWGS reaction should be operated above 700°C. There is not a straight conclusion that can be figured out from Table 1 regarding the operating pressure, which is discussed at the end of this section. Those trends are verified using the Gibbs reactor model mentioned previously. Figure 2 shows how the equilibrium composition obtained at the outlet of a Gibbs reactor varies for different operating temperatures. The methane curve justifies the high operating temperature required, as below 700°C, its proportion in the outlet stream starts increasing. Conversely, above this temperature, the amount of CH_4 becomes negligible, and the CO selectivity can be maximized.

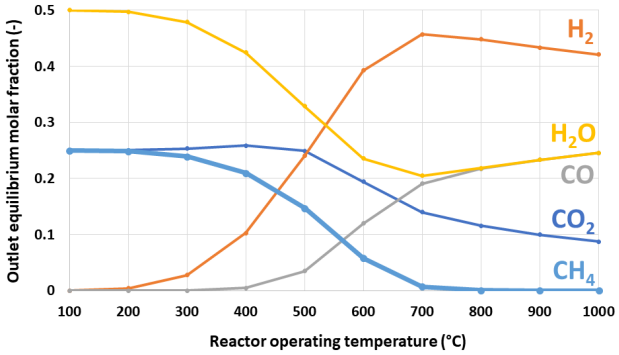

Figure 2 - Equilibrium composition obtained at the outlet of a Gibbs reactor for different operating temperatures at 1 bar and for an inlet $H_2/CO_2 = 2$

This decrease in the methane curve with temperature is explained by the exothermicity of methanation reactions (see Equations 2 and 3), while the selectivity of CO increases with temperature as the rWGS reaction is endothermic. This competing effect between the rWGS and the methanation reactions also explains the H_2 curve shape. The methanation reactions are favoured at low temperatures, leading to a significant H_2 consumption, induced by its stoichiometric coefficient in Equations 2 and 3. As the temperature rises, those reactions are less and less favoured, and H_2 is less consumed. At 700°C, the conditions start to be optimal for the rWGS reaction, and H_2 consumption is increased by this latter. Yet, the decline rate is slower as its stoichiometric coefficient is now 1 with respect to CO_2.

As mentioned in the previous section, coking side reactions are generally neglected in rWGS reactor models. In order to verify the validity of this assumption, the Gibbs reactor model can be used by comparing a simulation considering those side reactions (dashed line in Figure 3) and a simulation without them (solid line in Figure 3). The CO selectivity is barely impacted by the coking reactions, as depicted in the right-hand side graph, but CO_2 conversion is enhanced at low temperatures, which is explained by the exothermicity of this kind of reaction. However, at high temperatures, the effect of coking reactions is not visible anymore as they become negligible, and these graphs reinforce the assumption of neglecting these reactions in the model, as mentioned in the literature. Concerning the impact of the operating pressure, it turns out that in the range of operating temperatures for the rWGS reaction, the CO_2 conversion and CO selectivity are both favoured at atmospheric pressure. However, Table 1 shows a tendency in some works to operate the reaction at higher pressure. This discrepancy in the optimal pressure for the rWGS reaction comes from process considerations and not only reactor engineering aspects. Indeed, most reactions taking place after the rWGS unit in Power-to-X

processes are generally operated at high pressure. The selection of the optimal rWGS pressure is thus a trade-off between operating at low pressure to hinder side reactions and consequently favour the rWGS reaction or at high pressure to minimize the subsequent compression needs.

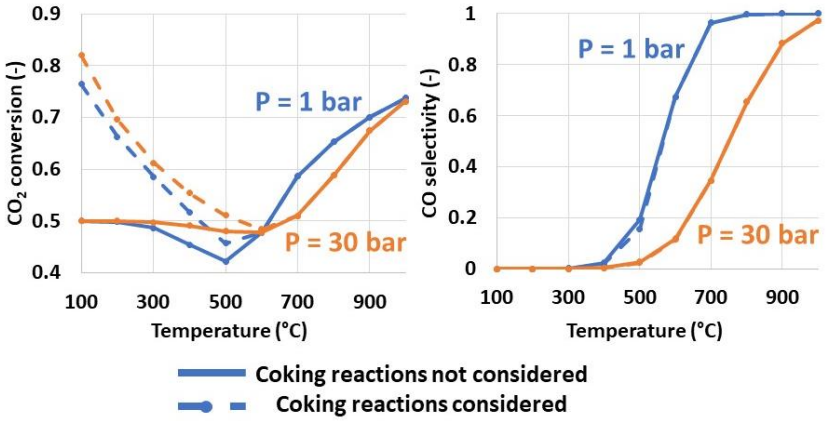

Figure 3 - Influence of temperature and pressure on CO_2 conversion (left) and CO selectivity (right) for a Gibbs reactor model (coking reactions considered or not)

Conclusions

This work investigates the rWGS reaction as an intermediate step in Power-to-X processes, especially to convert CO_2 into CO. This paper focuses on the first objective of this work, namely designing an optimal rWGS unit for integration in a Power-to-kerosene process. The reaction operating conditions referenced in the literature were compiled and validated with a Gibbs reactor model. It turns out that the reaction should be operated above 700°C to maximise CO selectivity, while the optimal pressure must be selected by considering additional process aspects. The kinetic reactor model is already implemented, but the results are discussed in another paper. The upcoming steps will be to use this kinetic model to design the ULiège experimental installation and to include it in a complete Power-to-kerosene process model.

References

[1] IEA, “CCUS Projects Explorer - Tracking CO2 capture, transport, storage, and utilisation projects worldwide.” Accessed: Sep. 03, 2023. [Online]. Available: https://www.iea.org/data-and-statistics/data-tools/ccus-projects-explorer?gclid=CjwKCAjw3dCnBhBCEiwAVvLcu1iG4lfrd5HrMZultEX75Ecl5uksp7eIV9Yxj6icM1PHQDCi9TzPyBoCIysQAvD_BwE

[2] EMBER, “Carbon Price Tracker.” Accessed: Sep. 03, 2023. [Online]. Available: https://ember-climate.org/data/data-tools/carbon-price-viewer/

[3] IEA, “CO2 Capture and Utilisation.” Accessed: Sep. 18, 2023. [Online]. Available: https://www.iea.org/energy-system/carbon-capture-utilisation-and-storage/co2-capture-and-utilisation

[4] G. Léonard, “Carbon capture and re-use: technological and other challenges,” Naples, May 24, 2023.

[5] D. H. König, N. Baucks, R.-U. Dietrich, and A. Wörner, “Simulation and evaluation of a process concept for the generation of synthetic fuel from CO2 and H2,” *Energy*, vol. 91, pp. 833–841, Nov. 2015, doi: 10.1016/j.energy.2015.08.099.

[6] S. Adelung, S. Maier, and R.-U. Dietrich, “Impact of the reverse water-gas shift operating conditions on the Power-to-Liquid process efficiency,” *Sustain. Energy Technol. Assess.*, vol. 43, p. 100897, Feb. 2021, doi: 10.1016/j.seta.2020.100897.

[7] G. Zang, P. Sun, H. E. Delgado, V. Cappello, C. Ng, and A. Elgowainy, “The Modeling of the Synfuel Production Process: Process models of Fischer-Tropsch production with electricity and hydrogen provided by various scales of nuclear plants,” Argonne National Lab. (ANL), Argonne, IL (United States), United States, ANL/ESD-22/8 175009, Apr. 2022. [Online]. Available: https://www.osti.gov/servlets/purl/1868524.

[8] V. Dieterich, A. Buttler, A. Hanel, H. Spliethoff, and S. Fendt, "Power-to-liquid *via* synthesis of methanol, DME or Fischer–Tropsch-fuels: a review," *Energy Environ. Sci.*, vol. 13, no. 10, pp. 3207–3252, 2020, doi: 10.1039/D0EE01187H.
[9] M. González-Castaño, B. Dorneanu, and H. Arellano-García, "The reverse water gas shift reaction: a process systems engineering perspective," *React. Chem. Eng.*, vol. 6, no. 6, pp. 954–976, 2021, doi: 10.1039/D0RE00478B.
[10] A. C. Ince, C. O. Colpan, A. Hagen, and M. F. Serincan, "Modeling and simulation of Power-to-X systems: A review," *Fuel*, vol. 304, p. 121354, Nov. 2021, doi: 10.1016/j.fuel.2021.121354.
[11] E. Schwab, A. Milanov, S. A. Schunk, A. Behrens, and N. Schödel, "Dry Reforming and Reverse Water Gas Shift: Alternatives for Syngas Production?," *Chem. Ing. Tech.*, vol. 87, no. 4, pp. 347–353, Apr. 2015, doi: 10.1002/cite.201400111.
[12] A. Wolf, A. Jess, and C. Kern, "Syngas Production via Reverse Water-Gas Shift Reaction over a Ni-Al_2O_3 Catalyst: Catalyst Stability, Reaction Kinetics, and Modeling," *Chem. Eng. Technol.*, vol. 39, no. 6, pp. 1040–1048, Jun. 2016, doi: 10.1002/ceat.201500548.
[13] M. Marchese, E. Giglio, M. Santarelli, and A. Lanzini, "Energy performance of Power-to-Liquid applications integrating biogas upgrading, reverse water gas shift, solid oxide electrolysis and Fischer-Tropsch technologies," *Energy Convers. Manag. X*, vol. 6, p. 100041, Apr. 2020, doi: 10.1016/j.ecmx.2020.100041.
[14] F. Vidal Vázquez, P. Pfeifer, J. Lehtonen, P. Piermartini, P. Simell, and V. Alopaeus, "Catalyst Screening and Kinetic Modeling for CO Production by High Pressure and Temperature Reverse Water Gas Shift for Fischer–Tropsch Applications," *Ind. Eng. Chem. Res.*, vol. 56, no. 45, pp. 13262–13272, Nov. 2017, doi: 10.1021/acs.iecr.7b01606.
[15] J. Xu and G. F. Froment, "Methane steam reforming, methanation and water-gas shift: I. Intrinsic kinetics," *AIChE J.*, vol. 35, no. 1, pp. 88–96, Jan. 1989, doi: 10.1002/aic.690350109.
[16] F. V. Vázquez *et al.*, "Power-to-X technology using renewable electricity and carbon dioxide from ambient air: SOLETAIR proof-of-concept and improved process concept," *J. CO2 Util.*, vol. 28, pp. 235–246, Dec. 2018, doi: 10.1016/j.jcou.2018.09.026.
[17] K. Ernst, C. T. Campbell, and G. Moretti, "Kinetics of the reverse water-gas shift reaction over Cu(110)," *J. Catal.*, vol. 134, no. 1, pp. 66–74, Mar. 1992, doi: 10.1016/0021-9517(92)90210-9.
[18] M. J. L. Ginés, A. J. Marchi, and C. R. Apesteguía, "Kinetic study of the reverse water-gas shift reaction over CuO/ZnO/Al2O3 catalysts," *Appl. Catal. Gen.*, vol. 154, no. 1–2, pp. 155–171, Jun. 1997, doi: 10.1016/S0926-860X(96)00369-9.
[19] T. Osaki, N. Narita, T. Horiuchi, T. Sugiyama, H. Masuda, and K. Suzuki, "Kinetics of reverse water gas shift (RWGS) reaction on metal disulfide catalysts," *J. Mol. Catal. Chem.*, vol. 125, no. 1, pp. 63–71, Oct. 1997, doi: 10.1016/S1381-1169(97)00080-0.
[20] R. B. Unde, "Kinetics and Reaction Engineering Aspects of Syngas Production by the Heterogeneously Catalysed Reverse Water Gas Shift Reaction," Universität Bayreuth, 2012.
[21] A. Rouxhet, M. E. A. Berchiche, and G. Léonard, "A Review of the Reverse Water-Gas Shift Reaction as an Intermediate Step in Power-to-Fuels Processes." unpublished.
[22] P. Kaiser, R. B. Unde, C. Kern, and A. Jess, "Production of Liquid Hydrocarbons with CO_2 as Carbon Source based on Reverse Water-Gas Shift and Fischer-Tropsch Synthesis," *Chem. Ing. Tech.*, vol. 85, no. 4, pp. 489–499, Apr. 2013, doi: 10.1002/cite.201200179.
[23] L. J. F. Comidy, M. D. Staples, and S. R. H. Barrett, "Technical, economic, and environmental assessment of liquid fuel production on aircraft carriers," *Appl. Energy*, vol. 256, p. 113810, Dec. 2019, doi: 10.1016/j.apenergy.2019.113810.
[24] E. Rezaei and S. Dzuryk, "Techno-economic comparison of reverse water gas shift reaction to steam and dry methane reforming reactions for syngas production," *Chem. Eng. Res. Des.*, vol. 144, pp. 354–369, Apr. 2019, doi: 10.1016/j.cherd.2019.02.005.
[25] R. M. Bown, M. Joyce, Q. Zhang, T. R. Reina, and M. S. Duyar, "Identifying Commercial Opportunities for the Reverse Water Gas Shift Reaction," *Energy Technol.*, vol. 9, no. 11, p. 2100554, Nov. 2021, doi: 10.1002/ente.202100554.
[26] O. Y. H. Elsernagawy *et al.*, "Thermo-economic analysis of reverse water-gas shift process with different temperatures for green methanol production as a hydrogen carrier," *J. CO2 Util.*, vol. 41, p. 101280, Oct. 2020, doi: 10.1016/j.jcou.2020.101280.
[27] F. Ghodoosi, M. R. Khosravi-Nikou, and A. Shariati, "Mathematical Modeling of Reverse Water-Gas Shift Reaction in a Fixed-Bed Reactor," *Chem. Eng. Technol.*, vol. 40, no. 3, pp. 598–607, Mar. 2017, doi: 10.1002/ceat.201600220.
[28] M. Wenzel, L. Rihko-Struckmann, and K. Sundmacher, "Thermodynamic analysis and optimization of RWGS processes for solar syngas production from CO_2," *AIChE J.*, vol. 63, no. 1, pp. 15–22, Jan. 2017, doi: 10.1002/aic.15445.